Design, synthesis and structural determination of antimicrobial peptides and peptidomimetics

Inaugural dissertation
of the Faculty of Science,
University of Bern

presented by

Hippolyte Personne

from Amiens, France

Supervisor of the doctoral thesis:
Prof. Dr. Jean-Louis Reymond

Department of Chemistry, Biochemistry and Pharmaceutical Sciences

Design, synthesis and structural determination of antimicrobial peptides and peptidomimetics

Inaugural dissertation
of the Faculty of Science,
University of Bern

presented by

Hippolyte Personne

from Amiens, France

Supervisor of the doctoral thesis:
Prof. Dr. Jean-Louis Reymond
Department of Chemistry, Biochemistry and Pharmaceutical Sciences

Accepted by the Faculty of Science.

Bern, 8th December 2023

The Dean,
Prof. Dr. Marco Herwegh

Acknowledgments

I would like to express here my gratitude to all the people who helped or supported me during the accomplishment of this PhD thesis. First of all, I deeply thank my PhD supervisor, **Prof. Dr. Jean-Louis Reymond** for giving me this opportunity. I am very thankful for all his guidance, ideas and discussions which drove to the success of the following work. I really appreciated the freedom I had on my projects and all the advice and support concerning my future career.

I thank **Prof. Dr. Ivan Huc** for accepting the terrible task to correct and evaluate this thesis; and **Prof. Dr. Robert Häner** who accepted to be the internal chairman of the PhD defense.

I deeply thank **Dr. Stéphane Baeriswyl**, **Dr Thissa Siriwardena**, **Dr. Xingguang Cai** and **Dr. Sacha Javor** for introducing me to all the knowledge and experiments I needed to conduct my thesis. Special thanks to **Prof. Dr. Achim Stocker** for all the help during crystallography experiments and useful discussions.

I am sincerely grateful to our collaborators from the University of Geneva **Dr. Thilo Kohler**, **Alexandre Lüscher**, **Lana Mazza** and **Prof. Dr. Christian van Delden** for all the help with MDR experiments in their lab and the fruitful discussions.

I would like to specially thank **Sofia Fulgencio** for all the great work she completed during her Bachelor project under my supervision.

I am thankful to all my colleagues I had the chance to work with for the fruitful projects and great science, namely **Dr. Alice Capecchi**, **Dr. Xingguang Cai**, **Dr. Sacha Javor**, **Dr. Thissa Siriwardena**, **Etienne Bonvin, Thierry Paschoud**, **Dr. Elena Zakharova** and **Dr. Bee Ha Gan**.

Many thanks to **Sandra Zbinden** who provide a huge administrative support.

On top of science, I met here real friends who supported me during good and bad times and with whom I created very strong relationships, and for that I am warmly thanking **David Kreutter**, **Thierry Paschoud**, **Etienne Bonvin**, **Kleni Mulliri**, **Samuel Yasmin, Yves Grandjean** and **Sacha Javor**. The success of this thesis is undoubtedly related to the endorsement they provide all along.

For all the good moments and nice atmosphere in the lab, I would like to mention and thank all the past and current group members not cited above with whom I really enjoyed to spend my four years in and outside the lab: **Céline**, **Geo**, **Jérémie**, **Leon**, **Başak**, **Andrea**,

Matheus, **Markus**, **Giorgio**, **Alice**, **Dina**, **Amol**, **Marc**, **Aline**, **Kris**, **Josep**, **Susanna**, **Elena**, **Kapila**, **Thissa**, **Mario**, **Kaishuai**, **Bee Ha**, **Maedeh**, **Xiaoling**, **Sven**, **Philippe**, **Daniel** and **Ye**.

To finish, I would like to thank my family and close friends, especially **Arthur Despois,** who supported me more generally along my studies and pushed me to the top.

This thesis is dedicated to my father Jean-François Personne who sadly passed away during the accomplishment of the present work.

General abstract

This thesis was guided by two major objectives. The first one, consisting in one global project, was the optimization and the structural determination of mixed-chirality α-helical antimicrobial peptides. To start with, I synthesized the fucosylated analogs of two antimicrobial peptides **ln65** (homochiral L-) and **ln69** (mixed-chirality) discovered in our group by Dr. Stéphane Baeriswyl. The addition of the sugar moiety aimed to obtain their X-ray structures by co-crystallization with lectin LecB. Therefore, I resolved the X-ray structure of both fucosylated **ln65** and **dln69**, the enantiomer of **ln69**, both showing a α-helical structure. This represents the first α-helix composed only of L- and D- natural amino acids. As **ln69** showed reduced hemolysis but similar antimicrobial activity compared to **ln65**, I explored the diastereomeric chemical space of **ln65** sequence by synthesizing 31 diastereomers. Through the biological assays and structural determination by circular dichroism, I highlighted a correlation between antimicrobial activity, hemolysis and α-helical structure. This study led to new potent and non-toxic mixed-chirality α-helical AMPs. The structural behaviour of these diastereomers was supported by X-ray crystallography and Molecular Dynamics. As a last investigation, I applied the **ln69** chirality pattern to reported α-helical peptides. The stereochemical modifications led to a disappearance of membrane-disruptive ability, underlining the sequence dependence of stereochemical optimization.

The second objective was to contribute to improving solid-phase synthesis methodology for peptides and peptidomimetics. This objective contained two subprojects. In the first one, I addressed the question of substituting piperidine, which is toxic, expensive, and regulated due to its use in illegal drug manufacturing, by a more benign reagent for 9-fluorenylmethoxycarbonyl (Fmoc) deprotection. In collaboration with Dr. Thissa Siriwardena, we screened a broad range of bases and identified dipropylamine (DPA) as a potential new Fmoc deprotection agent to replace piperidine in the context of high-temperature Solid-Phase Peptide Synthesis. The use of DPA on aspartimide-prone sequences showed significant decrease of aspartimide and related byproducts formation. In addition, DPA gave high yields for the syntheses of challenging therapeutical peptides and peptide dendrimers. This new Fmoc removal agent is cheaper, less malodorous than piperidine and non-regulated.

In the second project, I investigated how to improve the synthesis of inverse polyamidoamine (i-PAMAM) dendrimers, a new type of dendritic molecules developed in our group. The synthesis of i-PAMAMs employed iterative peptide coupling and deprotection of the very expensive *N*,*N*-bis(3-fluorenylmethoxycarbonyl-aminopropyl)glycine building block. I

designed a new method, inspired from the submonomer approach of peptoid synthesis in which dendrimer extension occurs by on-bead acylation of a free *N*-terminus with bromoacetic acid, followed by nucleophilic substitution of bromide by *N*,*N*-bis(3-trifluoroacetyl-aminopropyl)amine and finally trifluoroacetyl deprotection with aqueous piperidine. This method is less expensive and time-consuming compared to the previous i-PAMAMs synthesis. The effectiveness of this innovative synthesis was showcased through the successful obtention of i-PAMAMs of different sizes.

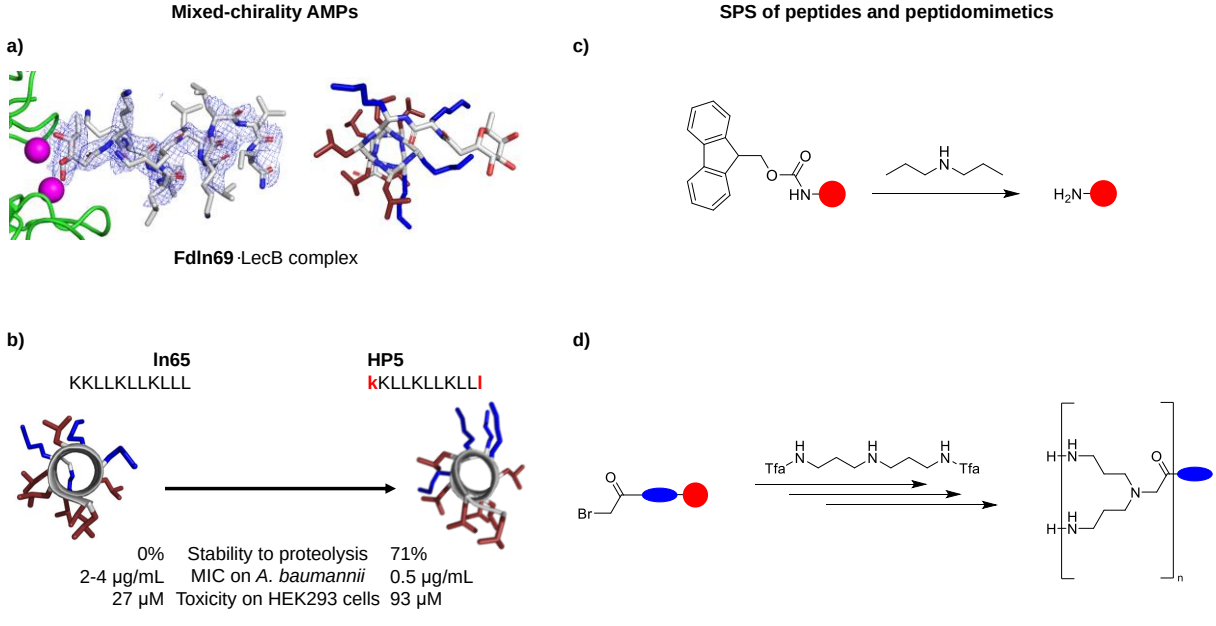

Figure 1: Thesis general graphical abstract. **(a)** X-ray structure obtained by co-crystallization of α-helical mixed-chirality fucosylated peptide **Fdln69** with lectin LecB. **(b)** Diastereomeric optimization of linear AMP **ln65**. **(c)** Fmoc deprotection with dipropylamine **(d)** Novel synthesis of inverse polyamidoamine dendrimers.

Table of Contents

Abbreviations

One letter and three letter codes of natural and unnatural L-amino acids used in this thesis. D-amino acids were written in lower case. Dendrimer branching residues were written in italics. The full list of used building blocks is presented in the following table.

Amino acid	Three letter code	One letter code
Alanine	Ala	A
Arginine	Arg	R
Asparagine	Asn	N
Aspartic acid	Asp	D
Cysteine	Cys	C
Glycine	Gly	G
Glutamine	Glu	Q
Glutamic acid	Glu	E
Histidine	His	H
Isoleucine	Ile	I
Leucine	Leu	L
Lysine	Lys	K
Norleucine	Nle	
Phenylalanine	Phe	F
Proline	Pro	P
Serine	Ser	S
Threonine	Thr	T
Tryptophane	Trp	W
Tyrosine	Tyr	Y
Valine	Val	V

AMBP	antimicrobial bicyclic peptide
AMP	antimicrobial peptide
Bag	*N*,*N*-bis(3-aminopropyl)glycyl
BOP	(benzotriazol-1-yloxy)tris(dimethylamino)phosphonium hexafluorophosphate
Cbz	benzylcarbonyl
CD	circular dichroism
DBU	1,8-diazabicyclo[5.4.0]undec-7-ene
DEA	diethylamine
DIBA	diisobutylamine
DIC	*N*,*N*-diisopropylcarbodiimide
DIPA	diisopropylamine
DMF	dimethylformamide

DODT	3,6-dioxa-1,8-octane-dithiol
DPA	dipropylamine
Dts	dithiasuccinoyl
ETFA	ethyl trifluoroacetate
Fmoc	9-fluorenylmethyloxycaronyl
h	hour
HF	hydrogen fluoride
HPLC	High-Performance Liquid Chromatography
HRMS	High Resolution Mass Spectrometry
i-PAMAM	inverse polyamidoamine
kDa	kilodalton
LB	Lysogeny Broth
LecB	Lectin B
MD	Molecular Dynamics
MDR	multidrug resistant
MH	Mueller-Hinton
min	minute
NBP	*N*-butylpyrrolidinone
ns	nanosecond
PAMAM	polyamidoamine
PDB	Protein Data Bank
PPR	piperidine
PyBOP	(benzotriazol-1-yloxy)tri(pyrrolidino)phosphonium hexafluorophosphate
PZ	piperazine
RMSD	Root Mean Square Deviation
SPS	Solid-Phase Synthesis
SPPS	Solid-Phase Peptide Synthesis
^{t}Bu	*tert*-butyl
TFA	trifluoroacetic acid
Tfa	trifluoroacetyl group
TFE	2,2,2-trifluroethanol
TIS	triisopropylsilane
XDR	extensively-drug resistant

1. General Introduction

1.1 Solid-Phase Peptide Synthesis

Natural and synthetic peptides gained interest these last decades as exemplified by the increasing number of therapeutic peptides approved for clinical use.[1,2] The main strategy to prepare such molecules is to use Solid-Phase Peptide Synthesis (SPPS), which consists in elongating a growing peptide chain, attached by its *C*- terminus to a polymeric resin used as solid-support, by adding amino acids to its *N*-terminus iteratively. First, the free peptide *N*-terminus is reacted with a solution containing an excess of an *N*-protected amino acid and a coupling reagent. The resin is then washed with solvent to remove unreacted excess reagents and coupling byproducts and treated with an *N*-deprotection reagent. After washing the excess reagents and byproducts, the growing peptide chain is ready for the next elongation cycle. (Figure 2). When the peptide sequence is fully assembled, cleavage from the resin and deprotection of side chains are simultaneously performed. Although widely used and automated, SPPS is still in constant improvement due to its environmentally detrimental process and hazardous chemicals. In this thesis, SPPS was used as a tool for the synthesis of antimicrobial peptides but also optimized for standard peptides and peptidomimetics synthesis. In this context, after an introduction on the principal breakthroughs since its discovery, we will focus on the recent advancements aiming for a greener and safer SPPS.

The term SPPS and its first methodology was introduced by Robert Bruce Merrifield in 1963,[3] using a polystyrene crosslinked with divinylbenzene solid-support, giving him the Nobel Prize of Chemistry in 1984. A hydrophobic tetrapeptide was successfully synthesized using the benzylocarbonyl (Cbz) protecting group for α-amines (Figure 3a). A few months later, Merrifield introduced the acid-labile *tert*-butyloxycarbonyl (Boc) as an amino protecting group for the synthesis of the larger peptide Bradykinin,[4] and optimized the procedure with milder conditions.[5] In 1967, Sakibara *et al* reported anhydrous hydrogen fluoride (HF) for the removal of several protecting groups,[6] which was further used for final cleavage during Boc SPPS. Afterwards, the major SPPS concept of orthogonal synthesis was brought to the community by George Barany after the design of dithiasuccinoyl (Dts) protecting group[7] which can be removed with a reducing agent and resisting mild and strong acidic conditions used in Boc SPPS allowing high selectivity between side chains deprotection. While being efficient, Boc synthesis required multiple acidolysis, by treatment with trifluoroacetic acid (TFA) during elongation and the final HF cleavage causing many complications and careful handling.[8,9]

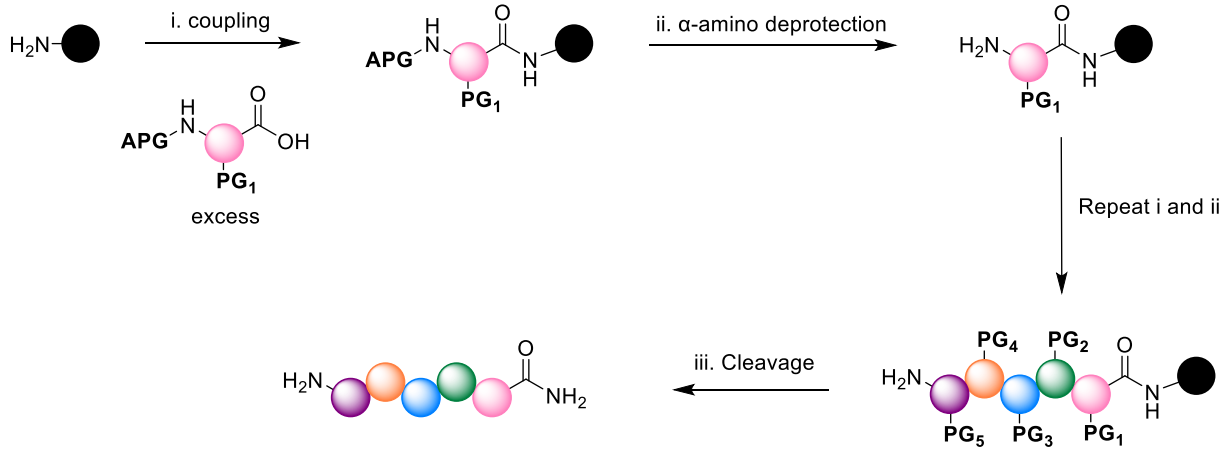

Figure 2: Overview of standard SPPS strategy in the case of a carbamide *C*-terminal sequence. AA = amino acid, APG = α-amino protecting group. PG_x = orthogonal protecting group. Synthesis on solid support leads to high yield of amino acid sequence by the iteration of (i) amino acid coupling using excess of reagents and (ii) deprotection of the α-amino group. Final peptide is obtained after (iii) simultaneous cleavage of orthogonal side chains protecting groups and of peptide from resin.

A new SPPS method was developed by Hoffmann-La Roche[10] using the base-labile 9-fluorenylmethoxycarbonyl (Fmoc) amino protecting group developed by Carpino and Han,[11] leading to the procedure used nowadays. This strategy used the *tert*-butyl (^{t}Bu) side chain protecting group that can be removed in acidic conditions, which avoided final HF cleavage. The standard procedure of Fmoc SPPS involved the anchoring of the first *C*-terminal Fmoc-protected amino acid on the solid support via ester of amide linkage, followed by Fmoc deprotection (usually using piperidine, Figure 3b) and is conducted in *N,N*-dimethylformamide (DMF).

The peptide sequence is built on the solid support through the repetition of (1) Fmoc-amino acid coupling with either a phosphonium salt as (benzotriazol-1-yloxy)tris(dimethylamino)phosphonium hexafluorophosphate (BOP)[12] or (benzotriazol-1-yloxy)tri(pyrrolidino)phosphonium hexafluorophosphate (PyBOP)[13] with 1-hydroxybenzotriazole (HOBt)[14] as an additive to reduce racemization and other base-catalysed side reactions, or more recently with a standard carbodiimide such as *N,N'*-diisopropylcarbodiimide (DIC) commonly mixed with ethyl cyanohydroxyiminoacetate (Oxyma)[15] (Figure 3c) and (2) Fmoc deprotection (Figure 3b). Finally, cleavage from the resin and removal of side chains protecting groups is performed usually by treatment with TFA in presence of scavengers such as triisopropylsilane (TIS)[16] or 3,6-dioxa-1,8-octane-dithiol[17] (DODT) to avoid reactions between deprotected amino acids and formed side-products (Figure 3d).

a) SPPS protecting groups

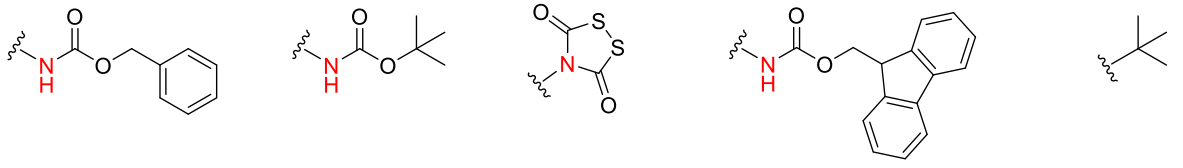

Cbz Boc Dts Fmoc ^{t}Bu

b) Fmoc deprotection agents

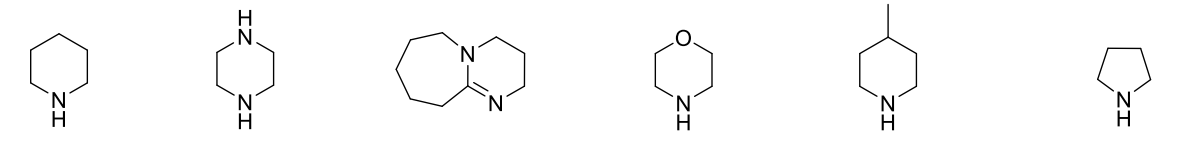

Piperidine Piperazine DBU Morpholine 4-methylpiperidine Pyrrolidine

c) Amide coupling agents

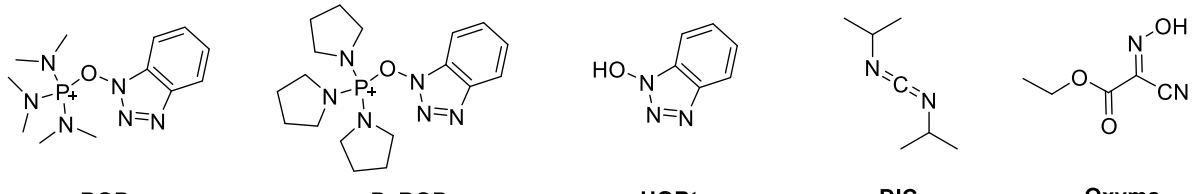

BOP PyBOP HOBt DIC Oxyma

d) Scavengers for TFA cleavage

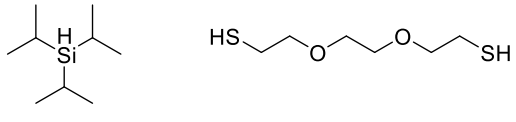

TIS DODT

e) SPPS solvents

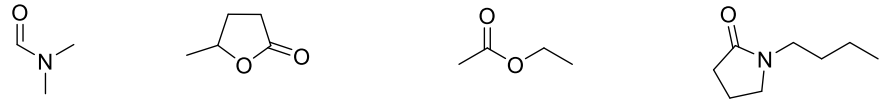

DMF γ-valerolactone Ethyl acetate NBP

Figure 3: SPPS protecting groups and reagents mentioned in the introduction.

Multiple orthogonal protecting groups[18] and coupling reagents[19,20] have been designed to tune SPPS. In addition, the various resins, chemical ligation strategies [21–23] and stapling / cyclization / bioconjugation methods[24,25] development facilitated the access to a broad range of complex peptide and peptide-based molecules including mono- and multicyclic peptides, peptide dendrimers and modified proteins for various applications.

During the last years, the chemical industry is facing ecological issues, and efforts have been concentrated on the development of new green and safe process. Focusing on peptide industry, this was exemplified recently in European Union by the near future regulation of DMF use.[26] Lately, reviews highlighted recent efforts made to reduce environmental impact of SPPS.[27,28] Among all research reported, the principal objective was to substitute DMF by a green solvent or solvent mixture suitable for Fmoc SPPS. Notably, γ-valerolactone[29], *N*-butylpyrrolidinone (NBP),[30] ethyl acetate[31,32] and various solvent mixtures[33] were extensively studied both in academia and in industry as very promising DMF alternatives (Figure 3e).

Secondly, amino acid coupling was shown to product toxic hydrogen cyanide (HCN) by side reaction between DIC and Oxyma.[34] As safer procedures, SPPS in a mixture of NBP and ethyl acetate were developed.[35,36] The elaboration of new carbodiimide also helped to reduce HCN formation when used together with Oxyma.[37]

Another aspect when thinking about safer SPPS is the replacement of piperidine for Fmoc deprotection as it is toxic, expensive, and regulated as a drug precursor. Furthermore, piperidine induces base-catalyzed side-reactions, especially aspartimide formation for aspartic acid containing peptides. The last ten years, piperazine / 1,8-diazabicyclo[5.4.0]undec-7-ene (DBU),[38] morpholine,[39] 4-methylpiperidine[40] and pyrrolidine[41] have been reported to replace piperidine (Figure 3b).

Finally, significant process changes have been published, importantly SPPS in aqueous media for suitable Fmoc and Boc strategies,[42,43] and new procedures for significant reduction of solvent consumption.[44,45]

1.2 Bacterial pathogens and antimicrobial resistance

Bacteria are classified in two different types: Gram-negative and Gram-positive, names acquired from the Gram staining test for which the result, negative or positive, differs depending on the bacterial morphology. Gram-negative pathogens possess two different membranes: an outer membrane mainly composed of phospholipids and negatively charged lipopolysaccharides (LPS), responsible for inflammation through its interactions with the immune system. The outer

wall also contains Gram-negative specific proteins named porins having a crucial role in bacterial infection and defense.[46] In addition, a thin peptidoglycan layer is present between the outer and the inner (cytoplasmic) membranes. On the other hand, Gram-positive bacteria are only surrounded by thick layers of peptidoglycan.[47] (Figure 4). As a result of a stronger protection from their environment, Gram-negative pathogens are more prone to develop resistance against various types of bactericidal drugs.[48,49]

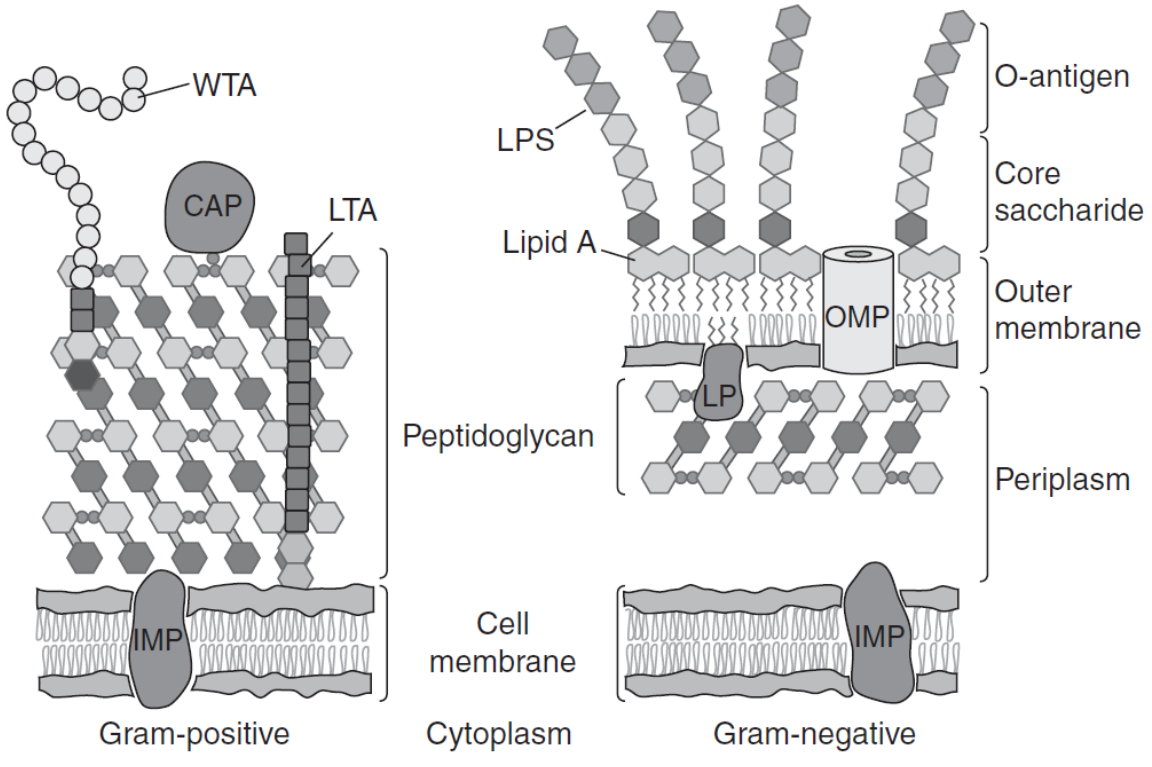

Figure 4: Structures of Gram-positive and Gram-negative membranes. WTA = wall teichoic acid, CAP = covalently attached protein, LTA = lipoteichoic acid, IMP = integral membrane protein, LPS = lipopolysaccharides, OMP = outer membrane protein, LP = lipoprotein. Figure taken from reference [47].

In 2019, 13.7 million deaths were related to infections, and 7.7 million were caused by only 33 bacterial pathogens,[50] representing around 14% of global deaths. These number are constantly increasing, due to the aptitude of bacteria to develop resistance to antibiotics after the overuse of classical molecules. A bacterial specie is defined as multi-drug resistant (MDR) if it is not susceptible to at least one antimicrobial agent in three or more categories. In addition, a new type of resistant bacteria appeared at the beginning of the 21st century, called extensively-drug resistant (XDR) pathogens,[51] for those almost no approved antibiotics are shown to be effective.[52] Resistance could be either intrinsic, meaning the resistance is always expressed by the bacteria; induced, for which the pathogen will express resistance mechanism by itself after exposure to drugs even if already present in its natural genome; or acquired, which signifies that the genetic material will mutate by transformation of its own genome or by acquisition of genetic

material from another specie.

Although bacterial resistance mechanisms can take multiple facets, four categories enclose all modes of action.[53] (1) The limitation of drug uptake; (2) the mutation of the specific drug-target inducing the absence of interactions necessary for the antimicrobial activity, including not only mutations of protein or RNA targets of antibiotics, but also the modification of membrane components, as observed with alteration of lipid A as a resistance mechanism against polymyxins;[54] (3) the inactivation of the antibiotic by degradation or chemical modification; and (4) the activation of drug efflux by overexpression of efflux pumps or by their modification to render them more effective.

In 2018, the World Health Organization listed bacterial species depending on their priority to be treated. In particular, six of them called ESKAPE (two Gram-positive strains: *Enterococcus faecium* and *Staphylococcus aureus*, and four Gram-negative: *Klebsiella pneumoniae*, *Acinetobacter baumannii*, *Pseudomonas aeruginosa* and *Enterobacter* species) particularly developed critical resistance mechanisms and caused a majority of the treated infections in hospitals. Since these pathogens are considered as "opportunistic", meaning they normally do not cause severe infections but induce serious pathogenic diseases if low efficiency of the immune system, development and design of new antibiotics were lately focused on these specific pathogens.

1.3 Antimicrobial peptides to tackle bacterial resistance

Antimicrobial peptides (AMPs) have emerged as a new class of antibiotics and have been intensively studied to counter antimicrobial resistance. Natural AMPs are present in all living organisms and are part of the immune system to defend the host against infections, which can be bacterial, fungal or viral;[55,56] therefore exhibiting a broad-range on Gram-negative bacteria, Gram-positive bacteria and other pathogens. AMPs can be either ribosomal, usually linear amino acids sequences that are further modified after translation, or non-ribosomal (NRPs), which are synthesized by non-ribosomal peptide synthetases incorporating moieties that are not limited to the 20 natural amino acids, such as D- amino acids or lipidic chains, but also can confer specific cyclized structures. Despite efforts made during the last century to identify such molecules, only ten NRPs have been clinically approved and marketed, notably gramicidin, polymyxin, colistin or vancomycin (Figure 5).[57]

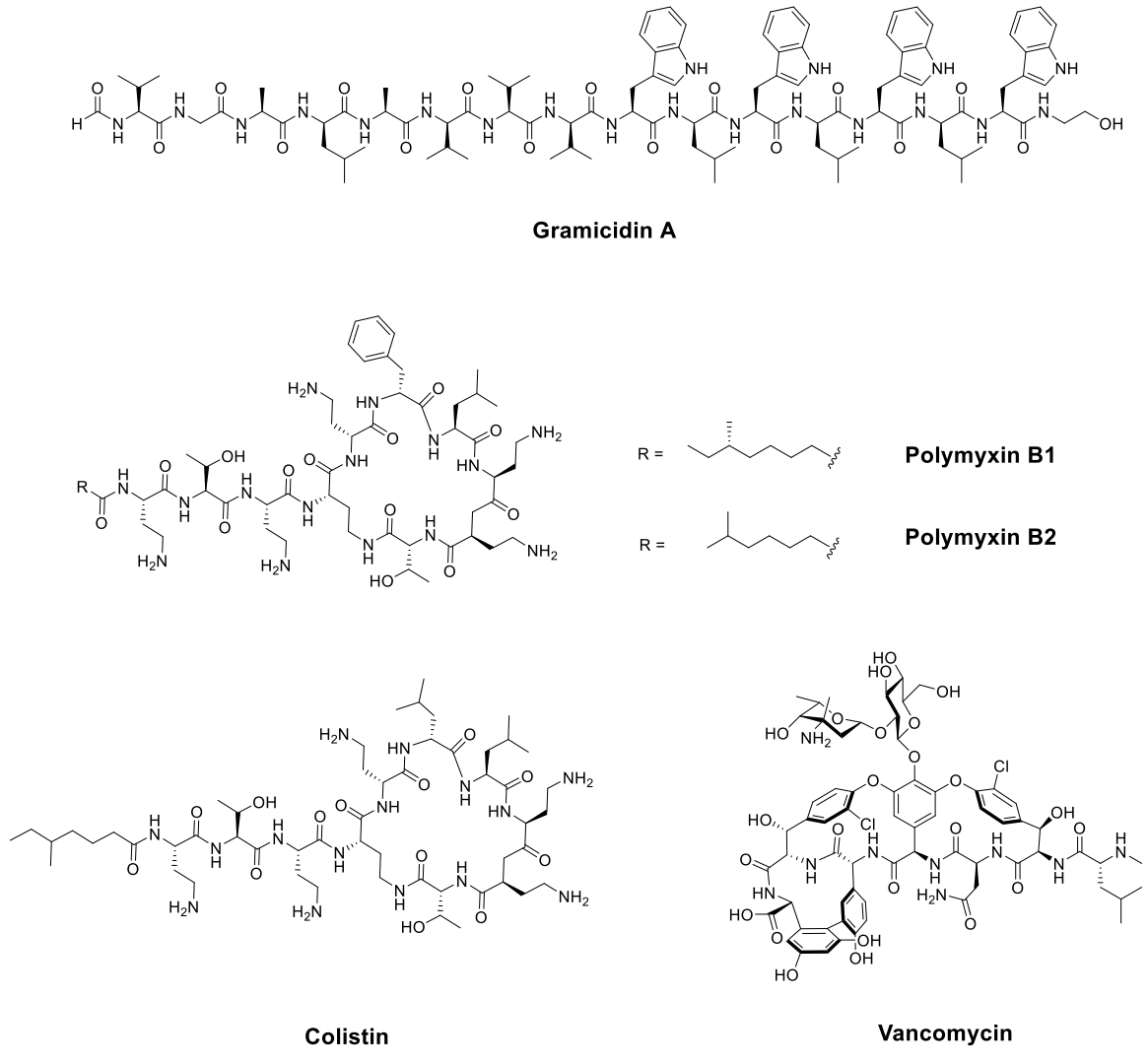

Figure 5: Structures of commercial non-ribosomal antimicrobial peptides.

However, the majority of developed AMPs are rather short linear peptides, constantly feeding the lately created databases with today thousands of reported sequences.[58,59] AMPs display different mode of actions:[57,60] via a direct action on bacteria by membrane targeting and disruption or by the inhibition of vital process via intracellular targeting; or by regulation of the host immune system. In the context of this thesis, we will focus on the mechanism of membrane-disruptive AMPs and on the recent developed strategies for AMPs enhancement.

Most of the membrane-disruptive AMPs are usually amphiphilic, *i.e.* presenting both hydrophobic and hydrophilic properties, feature necessary for their antibacterial behaviour, and generally present an α-helical structure observed in presence of a membrane-like environment but not in solution, and less frequently a β-sheet structure maintained with or without membrane component. The hydrophilic part is generally composed of cationic residues which interact with the negative charges of the bacterial membrane for a first adherence of the peptide on the

bacterial cell surface. Then, the hydrophobic part induces new interactions with membrane's lipids and / or aggregations via inter-peptides interactions. Three major models had been described to explain membrane-disruptive mechanisms of action. The carpet model in which peptides are covering membrane's surface and disrupting it in a "detergent" like mechanism (Figure 6a). The barrel-stave model, usually caused by amphiphilic α-helical peptides, induces the formation of helix bundles incorporated into the membrane, with the hydrophobic surface of peptides interacting with cell's lipids and the cationic residues pointing to the centre of the formed pore (Figure 6b). Finally, the toroidal model causes local curvature creating "torus-like" shape pore, disrupting membrane integrity (Figure 6c).

Due to the intrinsic difference in the lipid composition of bacterial and mammalian cells, with an overall more anionic envelop in case of bacteria,[61] the selectivity for bacterial cells targeting is possible. Note that cancer cells also present an increase of their membrane's net negative charge, conferring amphiphilic cationic AMPs anticancer properties.[62]

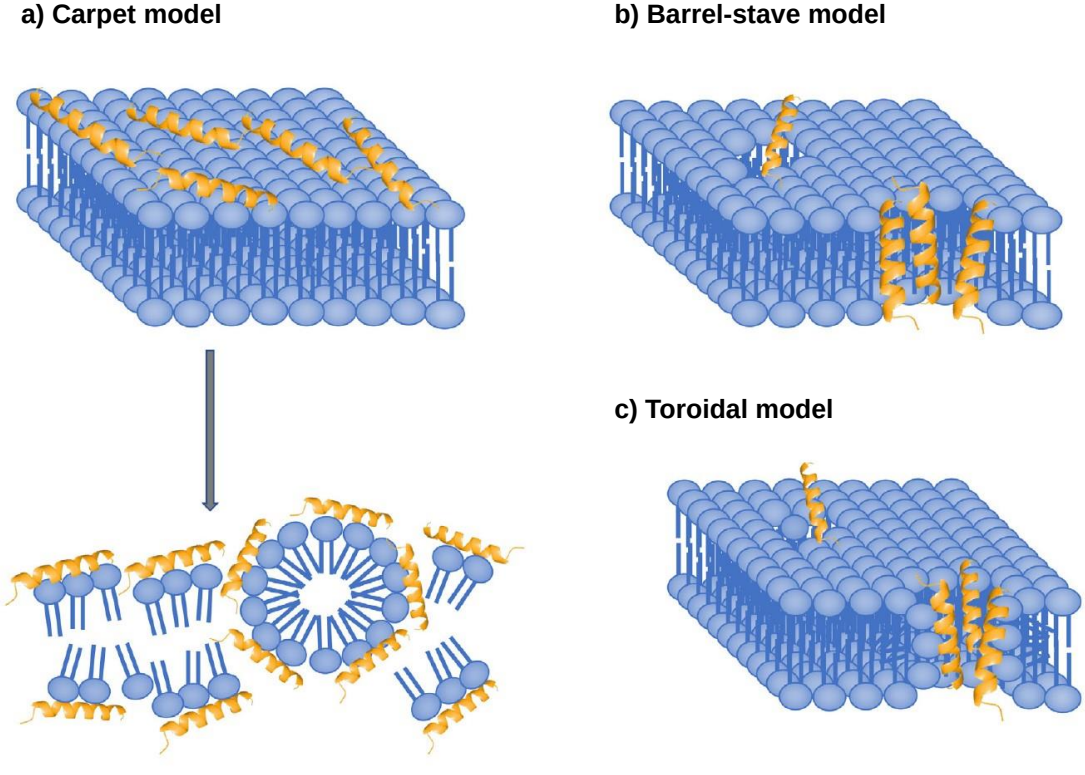

Figure 6: Principal membrane-disruptive models by AMPs. **(a)** Carpet-model **(b)** Barrel-stave model and **(c)** Toroidal model. Figure adapted from reference[56].

Although this type of AMPs showed high potency against a broad range of bacterial species, they are usually lacking selectivity between bacterial and eukaryotic cells, making impossible to enter further clinical development.[63] Furthermore, as they are mainly composed of natural amino acids, they are easily degraded by proteolysis. Improving AMPs properties to

balance their antibacterial activity, toxicity and stability have lately become the main priority in the field of AMPs design. Substitution of natural amino acids by their D- enantiomers or incorporation of other unnatural building blocks was shown to reduce toxicity and prevent AMPs from proteolytic degradation.[64–68] Same effect was observed in the case of the use of peptoid residues for which side chains are attached on the α-nitrogens.[69–72] Cyclization of AMPs via stapling methods also enhance stability in addition to maintaining the structure responsible for the antibacterial activity,[73–77] similarly to foldamers design.[78–80] On the top of experimental structural design, emerging computational tools showed efficiency to design AMPs sequences and predict their biological properties.[81–85]

1.4 Structural determination of antimicrobial peptide by X-ray crystallography

X-ray crystallography is a method to resolve the three-dimensional structure of very small to large molecules such as protein and nucleic acids with atomic resolution. It requires a periodic assembly within the crystal lattice of the target molecule able to create a diffraction pattern when submitted to X-rays. The relationship between atomic structure and the diffraction pattern was first discovered in the early 1910s by William Henry Bragg and his son William Lawrence Bragg, sharing the Nobel Prize in Physics in 1915.[86] The same year, W. H. Bragg first described the relationship between the X-ray diffraction pattern and the arrangement of atoms within the crystal using a mathematical Fourier transform operation. However, the resolution of the Fourier transforms to the molecular structure needs both amplitudes and phases, while X-ray only gives the amplitude: this is the "phase problem". To counter this lack of experimental information, one can use different strategies depending on the size of the molecule. For small molecules, direct methods where the phases can be mathematically constructed are preferred. In the case of larger molecules, as in structural biology, other approaches need to be employed as the molecule's flexibility is higher. Three major methods have been developed: isomorphous replacement and anomalous dispersion, for which phases can be obtained by the insertion of known perturbations; and molecular replacement, where a similar structure with known phases is used to approximate the unknown information.[87]

Two recent breakthroughs redefined the way to deal with biomolecules structural determination. The first one is cryo-electron microscopy (cryo-EM) that enables the access to biomacromolecules structures at very high resolution without requiring crystal assembly.[88] The biomolecules are frozen at very low temperature, trapping their conformations in amorphous ice. Through the analysis of the sample from multiple angles with electron microscopy, several two-

dimensional are obtained from which the three-dimensional structure can be determined at very high resolution. This tool is extremely powerful as the visualization of native protein conformation and their dynamics can be deciphered. Nevertheless, cryo-EM is not well-suited for proteins with a mass less than around 60 kDa; and despite the latest enhancements in cryo-EM techniques, the resolution achieved for protein structures remains inferior to that of X-ray determination.[89] Furthermore, in our case, the aim is to obtain a particular secondary structure of our AMPs, which are usually unfolded in water. The cryo-EM samples are frozen directly in aqueous solution and most of the peptide would not show any specific conformation. In addition, from our experience, α-helical structures of our AMPs are stabilized within the crystal by the formation of helix bundle, supposedly formed during the crystallization process.

The second is the lately development of AlphaFold,[90] which is an artificial intelligence's tool predicting protein structures with very high accuracy, as exemplified by the structural prediction of 98.5% of the human proteome.[91] However, the prediction of protein structure is limited by sequence's length and is not suitable for short peptide. Although the emergence of AlphaFold represents a huge scientific advance for various applications, it is still a prediction tool useless as we are looking for direct structural observations, which is currently only achievable by X-ray crystallography.

As X-ray crystallography was used in this thesis to obtain three-dimensional insights of AMPs using co-crystallization method with the bacterial protein lectin LecB from *Pseudomonas aeruginosa*, we will now focus on X-ray crystallography of proteins and on the method used to obtain the experimental data presented later.

Four major steps are needed to obtain the crystal structure of a protein: (1) to crystallize the biomolecule, (2) to obtain high quality diffraction pattern, (3) to computationally determine the electron-density map and (4) to build and refine the protein structure (Figure 7). Experimentally, the most widely used technique, also used in this thesis, is the vapor diffusion technique. A drop of the protein solution with precipitant is either sitting or hanging in a sealed compartment with a reservoir of pure precipitant condition. This technique is based on the equilibrium between the concentrations of the two solutions.[92] Once high-quality crystals are obtained, they are collected in specific cryogenic conditions, frozen and stored in liquid nitrogen until diffraction experiment. The record of X-ray diffraction is performed in a synchrotron, in our case at the Swiss Light Source (Paul Scherrer Institute, Villigen, Switzerland), by measuring diffraction patterns through different angles of the crystal. The electron-density map which allows to visualize the molecular shape is assembled computationally. The molecule is then built and refined until the atomic model satisfies the map for the obtention of the final crystal

structure.

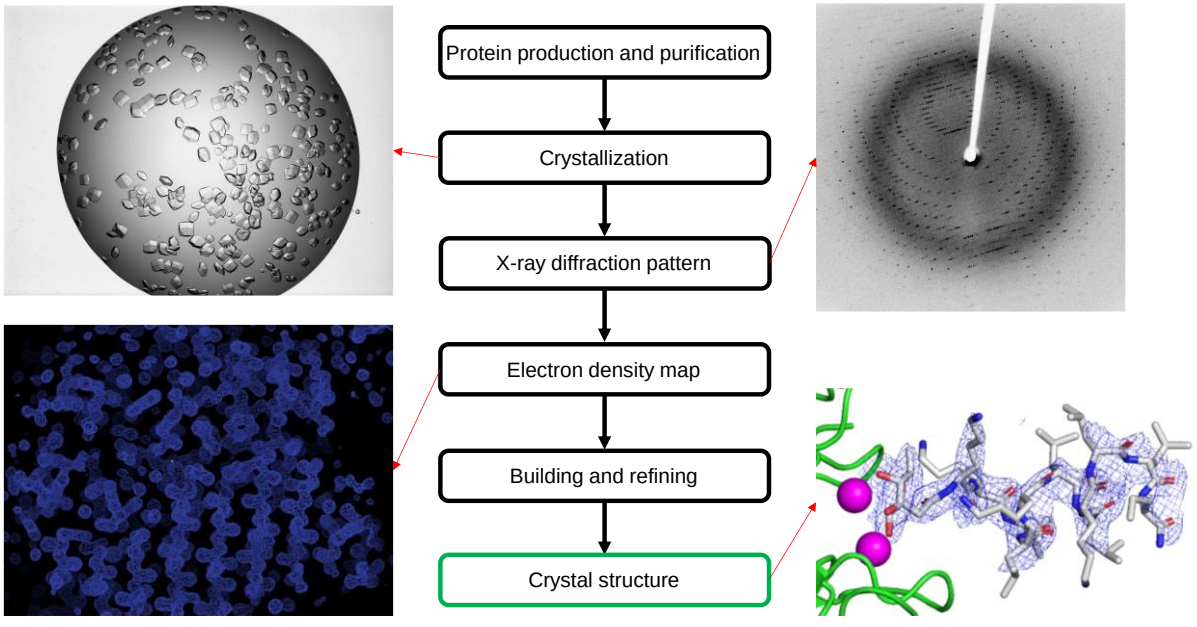

Figure 7: Workflow of the conventional protein crystallography process from protein production to final crystal structure.

While widely used for small molecules and biomacromolecules, X-ray crystallography is still getting poorly utilized for structural determination of small peptides due to their difficulty to crystallize. X-ray crystallography of peptides is limited by the difficulty to obtain high-quality crystals that are well-diffracting and the necessity of a large amount of materials. In the context of AMPs, getting insights into their structural properties would be of high interest for structure-based optimization.[93] In our lab, we developed a co-crystallization strategy to obtain snapshots of AMPs three-dimensional structures. The peptide of interest is first fucosylated at his *N*-terminus and mixed with LecB. Due to the high affinity of the LecB for fucosyl moiety, the peptide binds the protein and is effectively immobilized within the crystal structure. The robustness of this method has been shown with the structural insights of linear,[94] cyclic,[95] byclic[96] and dendritic peptides (Figure 8).[97] In the following chapters, the co-crystallization methodology has been successfully used for the resolution of α-helical mixed-chirality peptides.

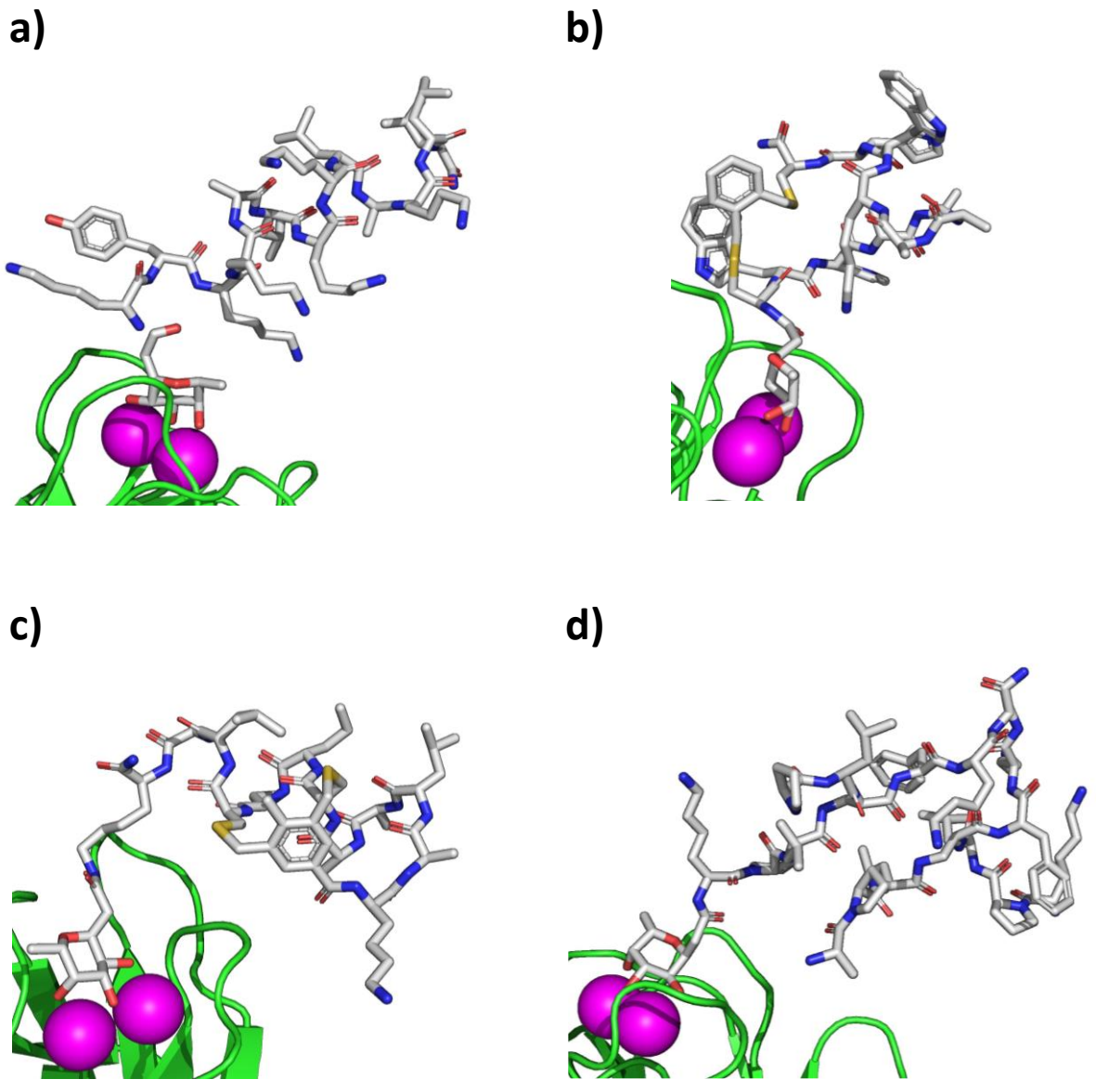

Figure 8: X-ray structures of antimicrobial peptides obtained via co-crystallization with lectin LecB. **(a)** linear AMP **SB4** (PDB 6Q86), **(b)** cyclic AMP **RH11o** (PDB 5NEY), **(c)** bicyclic peptide **bp71** (PDB 6Y0U) and **(d)** dendritic AMP **SBD8** (PDB 6S5S). LecB is represented in green cartoon and Ca^{2+} atoms in magenta.

2. Chapter 1: Structural study and optimization of mixed-chirality linear α-helical antimicrobial peptides

2.1 X-ray structure of a mixed-chirality short α-helical linear AMP

Work presented in this section was part of the following published study. It has been rewritten to show PhD candidate's contribution only.

S. Baeriswyl,* **H. Personne**,* I. Di Bonanventura, T. Köhler, C. van Delden, A. Stocker, S. Javor and J.-L. Reymond, A mixed chirality α-helix in a stapled bicyclic and a linear antimicrobial peptide revealed by X-ray crystallography, *RSC Chem. Biol.*, **2021**, 2, 1608-1617. https://doi.org/10.1039/D1CB00124H

* These authors contributed equally.

Abstract

The α-helical secondary structure of natural peptides is right-handed as composed of L- amino acids. The incorporation of D- amino acids usually disrupt the helix due to the induction of left-handed conformation. However, the helix can be maintained by stapling motifs or by introducing α-helix inducer. In this section, we report the X-ray crystal structures of a fucosylated α-helical mixed-chirality short linear peptide containing L- and D- enantiomers of natural amino acids obtained by co-crystallization with bacterial lectin LecB. The superimposition of mixed-chirality α-helices onto homochiral α-helices revealed almost identical backbone structures. Together with non-hemolytic and stability properties of the mixed-chirality sequence, this finding highlights the potential of mixed-chirality for bioactive α-helical L-peptides optimization.

Introduction

α-Helicity is one of the most common secondary structures of peptides and proteins involved in their interactions and activities. Naturally composed of L-amino acids, this conformation adopts a right-handed three-dimensional structure. Generally, incorporation of D-amino acids in these sequences results in the disruption of the helix.[98,99] Mixed-chirality peptides have been reported which form alternative conformations such as β-helices, exemplified by Gramicidin,[100–102] α-strands,[103] or supramolecular assemblies.[104–106] However, preserved α-helicity have been observed by X-ray crystallography in mixed-chirality peptides containing the α-helix inducer 2-aminoisobutyric acid residue.[107–111] α-helices were also observed in mixed-chirality macrocyclic and stapled peptides containing only one or two D-amino acids substitutions.[112–114] A systematic study published by Chen *et al.* on incorporation of a single D- residue in a 18-mer helical peptide showed helicity disruption in aqueous solution but not in a hydrophobic environment using circular dichroism.[115]

In the context of small amphiphilic α-helical AMPs, D-amino acid substitutions have been reported to prevent peptides from proteolytic degradation and reduce toxicity against red blood and mammalian cells while preserving antibacterial activity, however they were generally detrimental for helical folding.[65,116–124] This behaviour is supported by a so-called "carpet" model in which AMPs interact with the bacterial membrane through their hydrophobic part and act as detergents, in line with the absence of pore formation necessary for hemolysis.[125] Nevertheless, mixed-chirality seems to be generally incompatible with α-helical folding.

Starting from the antimicrobial bicyclic peptide (AMBP) **bp3** designed by chemical space guided approach,[126] optimization by adding a leucine at its *C*-terminus and switching L-lysines to their D- version led to AMBPs **bp65** and **bp69** and their linear analogs **ln65** and **ln69**.[96] Circular dichroism and molecular dynamics simulation in membrane-like environment suggested that all four compounds were α-helical. In this section, we obtained direct structural proof of α-helicity in these all L- and L-/D- mix linear sequences using co-crystallization strategy with lectin LecB, an approach to structural studies of short peptides previously reported for linear,[94] cyclic,[127] bicyclic[96,128] and dendritic peptides.[97] we obtained X-ray crystal structures of fucosylated analogs as complexes with LecB, establishing unequivocal proof of α-helical conformations and high structural similarity between homochiral and mixed-chirality helices.

Results and Discussion

Co-crystallization with lectin LecB

In the aim to get an insight into structural conformation of these peptides by co-crystallization with LecB protein, we prepared fucosylated analogs of **ln65**, **ln69** and their enantiomers **dln65** and **dln69**, respectively named **Fln65**, **Fln69**, **Fdln65** and **Fdln69** using SPPS and by coupling peracetylated α-L-fucosyl acetic acid moiety at the *N*-terminus (Scheme 1 and Table S1.1). Acetyl groups were removed before cleavage from the resin and purification with preparative HPLC.

These compounds, mixed to lectin LecB in a molar ratio of 5 peptides for 1 protein monomer, were screened over 192 different crystallization conditions. Among the 27 crystals obtained, two of them showed good diffraction and gave full peptide structures as lectin LecB complexes, one for the homochiral **Fln65** and one of mixed-chirality **Fdln69** (Table 1). **Fln65**·LecB complex structure (PDB 7NEF, 1.51 Å resolution, Table S1.2 and Figure S1.1) involved eight non-equivalent asymmetric units containing each one lectin monomer and one *N*-terminally fucosylated peptide, leading to eight complete **Fln65** structures. All of them presented amphiphilic α-helical conformation. In addition, the superimposition of crystallographically distinct peptides showed similar three-dimensional conformations (Figure 9A). The crystal structure was maintained by hydrophobic intermolecular interactions between leucines side chains of peptides forming a bundle composed of eight helices (Figure S1.1).

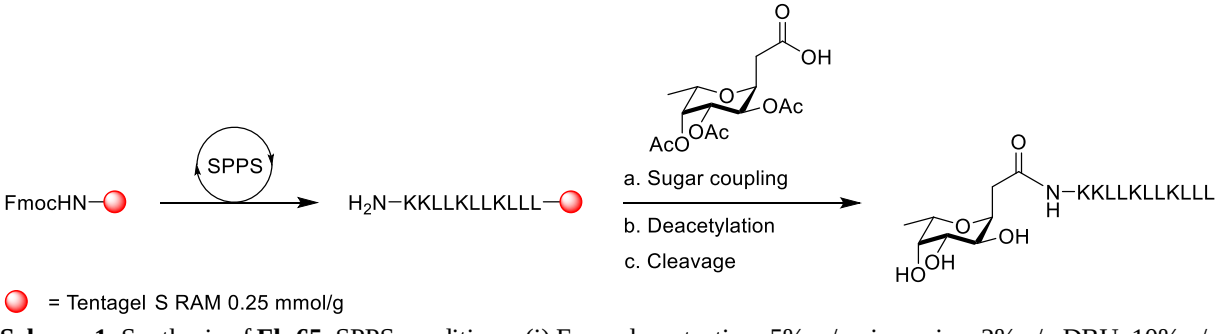

Scheme 1: Synthesis of **Fln65**. SPPS conditions: (i) Fmoc deprotection: 5% w/v piperazine, 2% v/v DBU, 10% v/v butanol in DMF, 60 °C, 1 and 4 min, (ii) Amino acid coupling: Fmoc-AA-OH (5 eq.), Oxyma (5 eq.), DIC (6 eq.) in DMF, 60 °C, 2 x 8 min; (a) Peracetylated α-L-fucosyl-acetic acid (3 eq.), Oxyma (3 eq.), DIC (3 eq.) in DMF, 50 °C, 30 min; (b) MeOH/NH_4OH (25%)/H_2O (8/1/1 v/v/v), r. t., overnight; (c) TFA/TIS/H_2O (94/5/1 v/v/v), r. t., 3 h. C-terminus is a carbamide.

Table 1: X-ray crystal structures of **Fln65** and **Fdln69**.

no.	Sequence[a)]	Conditions	PDB code	Res.	N[b)]
Fln65	*KKLLKLLKLLL	40 µM LecB, 200 µM peptide, 0.2 M Magnesium formate dihydrate (Crystal Screen D8)	7NEF	1.5 Å	8
Fdln69	*KKllKllKlll	40 µM LecB, 200 µM peptide, 0.2 M Sodium citrate, 0.1 M Sodium cacodylate pH 6.5, 30% v/v *i*-ProH (Crystal Screen A8)	7NEW	2.0 Å	2

[a)] One letter codes for amino acids, * = α-L-fucosyl-acetyl. The structural formulae of compounds are shown in the Supporting Information. [b)] N = number of crystallographically non-equivalent fully resolved structures.

Similarly, the crystal structure of **Fdln69** in complex with LecB (PDB 7NEW, 2.02 Å resolution, Table S1.3 and Figure S1.2) contained four asymmetric fucose-binding sites. Two of them showed full α-helices conformations after resolution (Figure 9B), whereas only the fucosyl group and the first amino acid were resolved for the two other asymmetric sites, indicating unfolded conformation (Figure S1.2). Interestingly, the exact mirror images of the two left-handed helical structures resolved in **Fdln69** X-ray structure were almost identical to the eight different structures obtained for the homochiral analog with RMSD values between the backbones < 0.9 Å (Figure 9B). These very small variations indicate that the incorporation of D- amino acids did not alter peptide folding.

Molecular dynamics of Fln65 bundles

The characteristic behaviour observed in small α-helical amphiphilic AMPs, as revealed by CD measurements for **ln65** and **ln69**,[96] includes folding in a membrane-mimicking environment and a complete unfolding in aqueous solutions. This observation was corroborated by MD simulations for a single peptide in the presence or absence of interactions with a DPC micelle.[96] However, in the X-ray crystal structure of **Fln65** in complex with LecB, the different copies of peptide **ln65** present in the asymmetric unit are not making significant binding with the lectin monomers apart from the fucosyl groups and are mainly surrounded by water. To investigate whether the helical conformation is due to interpeptide interactions as reported for other AMPs,[94] we removed sugar moieties from the peptides structures obtained for **Fln65** and performed molecular dynamics in aqueous physiological salted conditions (0.15 M NaCl) during 1000 ns for the complete bundle and for one of the obtained helices. The bundle's aggregation was maintained along the run by hydrophobic contacts showing folding ability in absence of membrane environment (Figure 10). In contrast, the single peptide rapidly unfolded after the beginning of the simulation. These results confirmed the ability of the intermolecular interactions within the bundle to maintain secondary structure of the peptides in aqueous

surroundings. Due to incomplete bundle in the case of **Fdln69** structure, the MD was not performed.

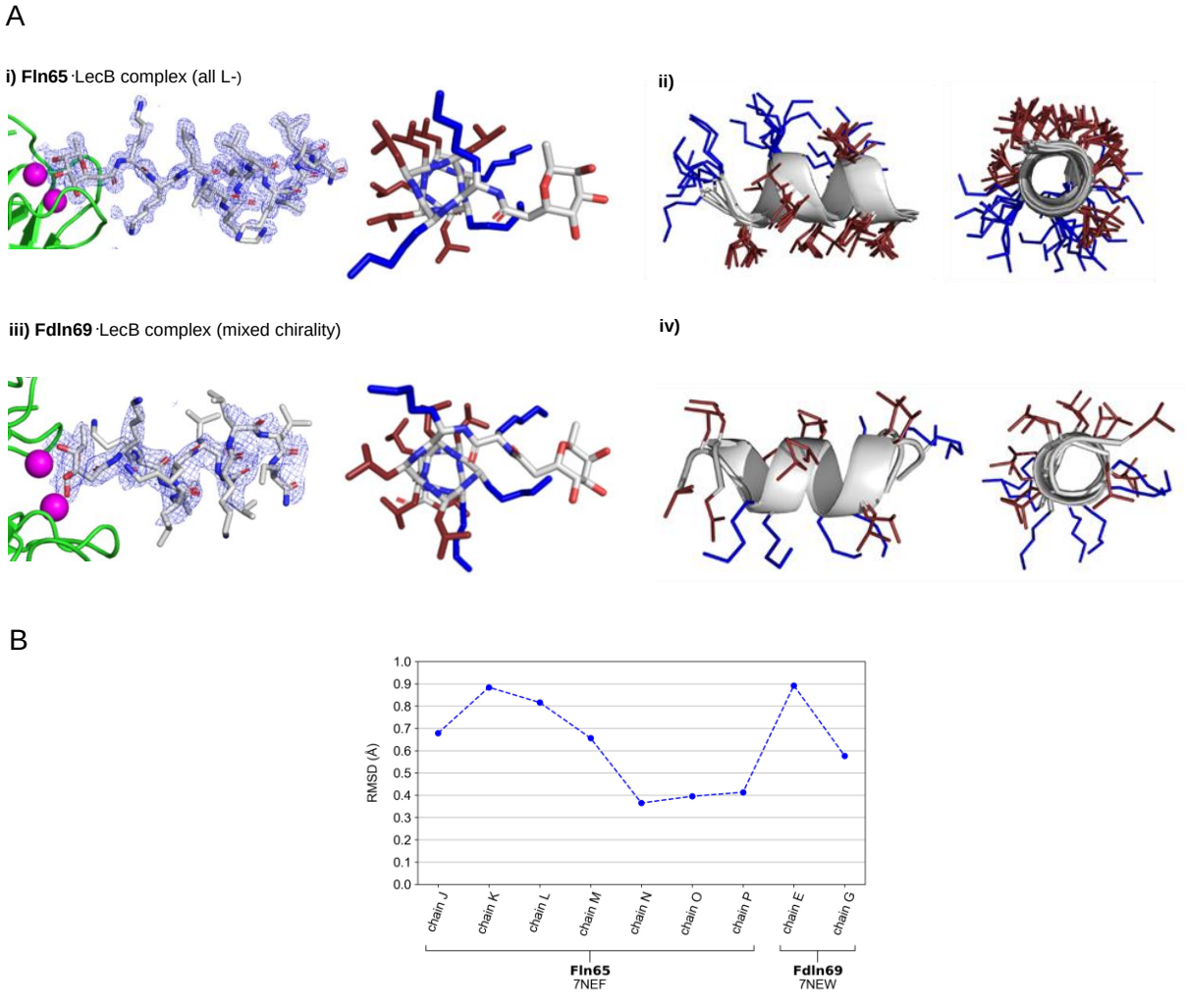

Figure 9: X-ray structures of **Fln65** and **Fdln69**. **(A) (i)** Left panel: X-ray structure of the **Fln65**·LecB complex. Electron density (blue mesh) for one of the eight distinct helices in PDB 7NEF. Peptide is represented as sticks, LecB monomer in green cartoon and Ca^{2+} atoms of the lectin binding site are represented by magenta spheres. Right panel: Stick model as observed in the crystal. Hydrophobic side chains are colored in red and cationic side chains in blue. **(ii)** Superimposition of all eight asymmetric peptides. Same color code as described before. **(B)** Same as (A) for **Fdln69**·LecB complex (PDB 7NEW). **(C)** RMSD calculated in PyMol between the backbone of **Fln65** (PDB 7NEF chain I) and the backbones of other non-equivalent helices (PDB 7NEF chains J, K, L, M, N, O and P) and **Fdln69** helices (PDB 7NEW chains E and G). Fucosyl groups were omitted for superimposition and RMSD calculations.

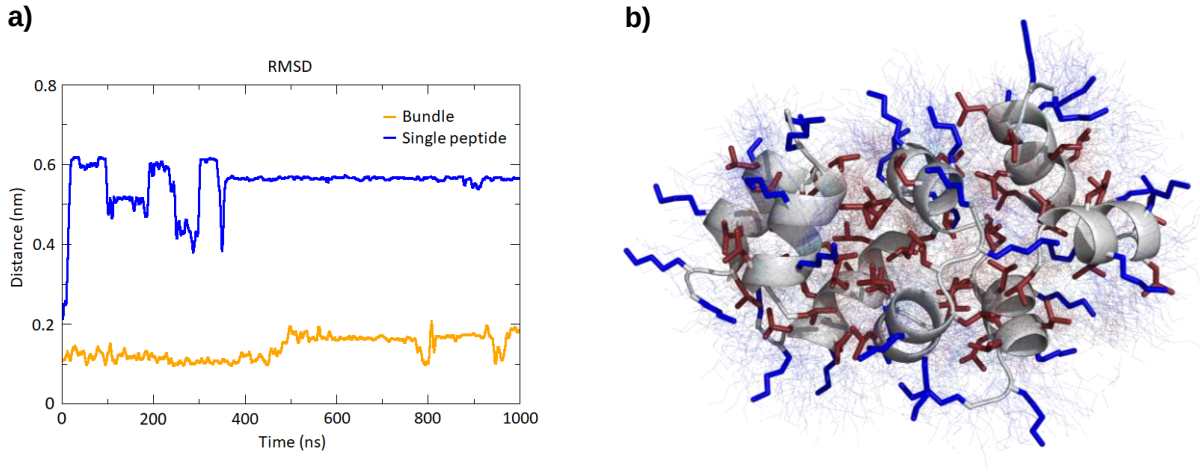

Figure 10: MD simulations of **ln65** obtained by X-ray crystallography. **(a)** Root mean square distances of the backbone atoms relative to the starting backbone conformation of a single peptide in the bundle (orange curve) compared to a single peptide in water (blue curve). **(b)** Overlay of 100 states over the 1000 ns run trajectory of the bundle in water. The average structure is shown as grey cartoon (backbone) and colored sticks (side chains). The 100 states are shown as thin lines. Hydrophophic side chains are colored in red and cationic side chains are colored in blue.

Conclusion

Starting from the discovery of homochiral (**ln65**) and mixed-chirality (**ln69**) linear sequences,[96] we investigated structural behaviour of their fucosylated analogs using co-crystallization with lectin LecB. X-ray crystal structures were obtained for homochiral **Fln65** and mixed-chirality **Fdln69** showing similar α-helical conformation. In addition, MD simulation of **Fln65** peptide bundle suggested a stable conformation in aqueous environment maintained by hydrophobic interactions.

This first direct observation of a mixed-chirality α-helix only composed of natural amino acids demonstrate the ability of a folded sequence to tolerate multiple D- residues incorporations, which should retain its amphiphilic structure and therefore its antibacterial activity. Taking together with the reduced toxicity and higher stability of these peptides, these results suggest mixed-chirality as an optimization method of L-bioactive α-helical peptides.

2.2 To Fold or Not to Fold: Diastereomeric Optimization of an α-Helical Antimicrobial Peptide

This work has already been published and the publication is reproduced hereafter. Authors contributions are detailed at the end of the section.

H. Personne, T. Paschoud, S. Fulgencio, S. Baeriswyl, T. Köhler, C. van Delden, A. Stocker, S. Javor and J.-L. Reymond, To Fold or Not to Fold: Diastereomeric Optimization of an α-helical Antimicrobial Peptide, *J. Med. Chem*, **2023**, 66(*11*), 7570-7583. https://pubs.acs.org/doi/10.1021/acs.jmedchem.3c00460

Abstract

Membrane disruptive α-helical antimicrobial peptides (AMPs) offer an opportunity to address multidrug resistance, however most AMPs are toxic and unstable in serum. These limitations can be partly overcome by introducing D-residues, which often confers protease resistance and reduces toxicity without affecting antibacterial activity, presumably due to lowered α-helicity. Here we investigated thirty-one diastereomers of the α-helical AMP KKLLKLLKLLL. Three diastereomers containing two, three and four D-residues showed increased antibacterial effects, comparable hemolysis, reduced toxicity against HEK293 cells, and excellent serum stability, while another diastereomer with four D-residues additionally displayed lower hemolysis. X-ray crystallography confirmed that high or low α-helicity as measured by circular dichroism indicated α-helical or disordered structures independently of the number of chirality switched residues. In contrast to previous reports, α-helicity across diastereomers correlated with both antibacterial activity and hemolysis and revealed a complex relationship between stereochemistry, activity, and toxicity, highlighting the potential of diastereomers for property optimization.

Introduction

Membrane disruptive antimicrobial peptides (AMPs), which occur naturally as part of the innate immune system, offer an opportunity to address multidrug resistant (MDR) bacteria because of their unspecific mechanism of action, against which resistance does not occur easily.[129–131] Such AMPs are however unstable in serum and most often toxic owing to their membrane disruptive amphiphilic and most often α-helical structure triggering their antibacterial effect. Their properties can be improved by sequence optimization,[132–135] whereby the most versatile approach consists in introducing non-natural structural elements[57] such as D-amino acids,[117,65,136–138] non-natural residues,[139] β- or γ-amino acids,[140,141] isopeptide bonds,[142] or entirely non-peptidic elements such as spermine[143] or fatty acids.[144,145] A complete redesign of AMPs is also possible in form of dimers,[146] cyclic or bicyclic staples,[126,147,148] small molecules,[149] peptoids,[150,151] foldamers,[152] or dendrimers.[153,154]

For α-helical AMPs and analogs, the toxicity reduction effect observed upon introducing D-residues or similar perturbations, often measured as lower hemolysis of red blood cells, is generally attributed to a reduced α-helical folding, which would block pore formation on the membrane surface as a trigger for hemolysis. On the other hand, coating and destabilization of the bacterial membrane, and therefore the antibacterial effect, would still be possible with the modified peptide in the absence of folding.[137,119,155,156] However, very little structural evidence or systematic studies support the hypothesis that reduced α-helical folding should generally preserve antibacterial activity while reducing toxicity.

In our own search for new antibacterial compounds, we have discovered several antimicrobial peptide dendrimers (AMPDs) with very low hemolysis and strong activity against Gram-negative bacteria including MDR clinical isolates.[157–160] By investigating stereorandomized sequences, which are obtained by solid-phase synthesis using racemic building blocks and consist of a mixture of all possible diastereomers, we found that stereorandomized (*sr*-) AMPDs also exhibit strong antibacterial effects and very low hemolysis, suggesting an intrinsically disordered bioactive conformation.[161,162] The same effect was observed with the intrinsically disordered AMP indolicidin[163] but not with α-helical linear AMPs such as DJK-5,[164] which lost their activity when stereorandomized.[161]

In a separate series of experiments with antimicrobial bicyclic peptides,[126,128] we discovered a short membrane disruptive antibacterial but somewhat hemolytic linear undecapeptide, KKLLKLLKLLL (**ln65**), which did not appear, even as partial sequence, in databases of AMPs,[165,166] proteins,[167] or ChEMBL (Figure 11).[168] The activity of this AMP was

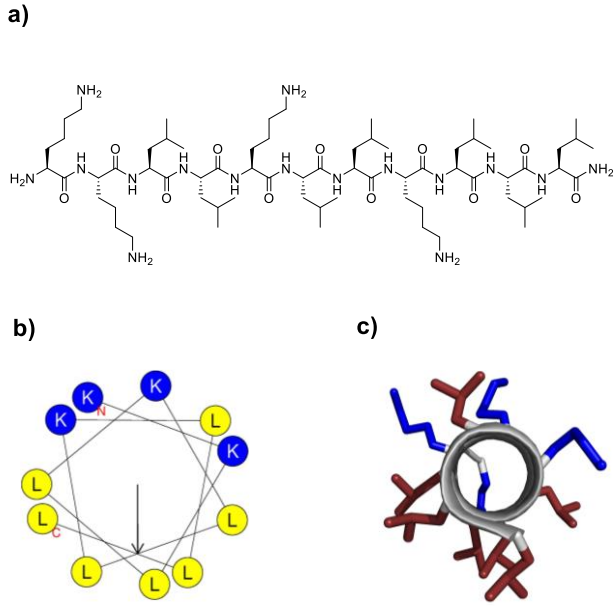

Figure 11: **(a)** Chemical structure of **ln65**. **(b)** Helix wheel of **ln65** sequence predicted by HeliQuest.[169] Blue and yellow indicate respectively cationic and hydrophobic residues. The arrow inside the helix wheel indicates the magnitude and direction of the hydrophobic moment. **(c)** Structure of **ln65** (PDB 7NEF, chain I) obtained by X-ray crystallography of a fucosylated analogs in complex with the bacterial lectin LecB. Cationic side chains are colored in blue and hydrophobic side chains are colored in red.

preserved upon inverting it's four lysine residues to D-enantiomers to form kkLLkLLkLLL (**ln69**), while its hemolysis was strongly reduced.[96] Strikingly, both the all-L sequence **ln65** and its diastereomer **ln69** were strongly α-helical as established by Circular Dichroism (CD) and X-ray crystallography, showing that in this case lowered hemolysis was not related to a reduced α-helical folding. Intrigued by this observation, we set out to prepare and test the stereorandomized version *sr*-**ln65** as well as multiple diastereomers of **ln65** in search for analogs with possibly improved activity and/or reduced toxicity. Systematic studies of multiple diastereomers have shown significant activity modulations in the case of short, non-helical arginine-tryptophan containing AMPs.[170–172]

Results and Discussion

Enantiomeric and stereorandomized sequences

We first investigated **dln65** and **dln69**, the enantiomers of **ln65** and its diastereomer **ln69**, to check that they displayed similar activities as expected for enantiomeric membrane disruptive AMPs (Table S2.1). CD spectra of **dln65** and **dln69** in aqueous phosphate buffer in the presence of either 5 mM dodecylphosphocholine (DPC) micelles mimicking a membrane environment,[173] or 20% trifluoroethanol (TFE) as folding inducer,[174,175] were mirror-images from those of the L-enantiomers and confirmed their α-helical folding (Figure 12a/b). The enantiomeric pair

ln65/**dln65** gave essentially the same minimal inhibitory concentrations (MICs) values against the five bacterial species used in this study (*Pseudomonas aeruginosa, Klebsiella pneumoniae*, *Acinetobacter baumannii, Escherichia coli* and methicillin resistant *Staphylococcus aureus*), as well as the same minimum hemolysis concentration (MHC) on human red blood cells indicating significant hemolysis (125 µg/mL, Table 2, Figure S2.1 and Table S2.2). In line with these activities, the membrane disruptive effects of both enantiomers on fluorescein loaded vesicles[176] made of the anionic egg yolk phosphatidyl glycerol (EYPG) mimicking bacterial membranes as well as on vesicle made of zwitterionic egg yolk phosphatidyl choline (EYPC) mimicking eukaryotic membranes was comparably strong (Table 2, columns 8 and 9 and Figure S2.2). The similar behavior of **ln65** and its enantiomer **dln65** was consistent with membrane disruption as the primary mechanism of action for these α-helical AMPs. On the other hand, despite the mirror image CD-spectra and comparable vesicle leakage activities of **ln69** and **dln69**, **dln69** was 4-fold more antibacterial and hemolytic than **ln69**, which might reflect an additional activity of **dln69** unrelated to its membrane activity.

To further probe if α-helical folding was required for activity, we prepared the fully stereorandomized sequence *sr*-**ln65**, a racemic mixture of the 1024 possible diastereomers, as well as *sr*-**ln65L^{6}** with pure L-leucine at position 6 of the sequence, containing all 1024 diastereomers with single chirality at position 6 such as to make a possible folding detectable by CD. Remarkably, both *sr*-**ln65** and *sr*-**ln65L^{6}** were as antibacterial as **ln65** but much less hemolytic, an effect comparable to our previous observation with AMPDs and *sr*-AMDPs suggesting that the antibacterial bioactive conformation of **ln65** might be disordered while the hemolytic bioactive conformation would be α-helical.[161,162] However, while CD spectra of *sr*-**ln65** were nearly flat as expected because the stereorandomized sequence is racemic, those of *sr*-**ln65L^{6}** showed approximately 17% α-helix content in 5 mM DPC or with TFE, suggesting that a significant fraction of the 1024 possible diastereomers of **ln65** might be α-helical (Figure 12c). Therefore, the activity of *sr*-**ln65** might also be explained by the presence of some highly active and α-helical diastereomers, such as **ln69**, mixed with inactive and possibly disordered diastereomers.

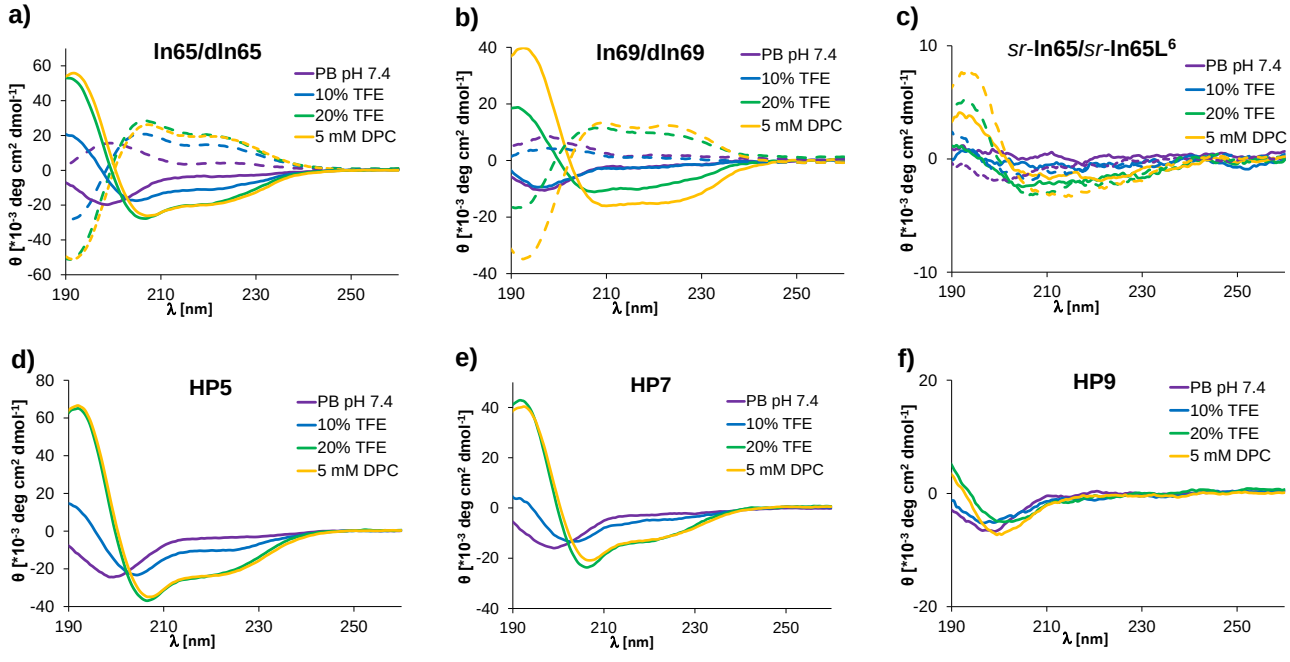

Figure 12: Determination of secondary structure by CD of **ln65**, **dln65**, **ln69**, **dln69**, *sr*-**ln65**, *sr*-**ln65L**^{6}, **HP5**, **HP7** and **HP9**. CD spectra in phosphate buffer at pH 7.4 with 10 and 20% v/v 2,2,2-trifluoroethanol and with 5 mM DPC of **(a) ln65** (full lines) and **dln65** (dashed lines), **(b) ln69** (full lines) and **dln69** (dashed lines), **(c)** *sr*-**ln65** (full lines) and *sr*-**ln65L**^{6} (dashed lines), **(d) HP5**, **(e) HP7** and **(f) HP9**.

Diastereomers and mutants of ln65

In view of these preliminary experiments, we set out to test a series of diastereomers of **ln65** for their α-helicity, antibacterial and hemolytic effects. From the 1024 possible diastereomers, 11 (0.1%) sequences are possible with a single inverted chirality residue, 55 (5.4%) with two, 165 (16.1%) with three, 330 (32.2%, including **ln69**) with four, and 462 (45.1%) with five inverted chirality residues. Balancing our interest to investigate diastereomers with multiple D-residues related to **ln69** with the expectation that α-helical folding was more likely to be preserved with only a few inverted chirality residues,[98,99] we selected 31 diastereomers **HP1** – **HP31**, one (3%) with a single D-residue, five (16%) with two D-residues, four (13%) with three D-residues, thirteen (42%) with four D-resides, and eight (26%) with five D-residues, distributing D-residues in groups or scattered, at *N*- or *C*-termini, or in the middle of the sequence (Table 2).

Table 2: Activity of linear AMPs.

Cpd.	Sequence[a)]	α-helix content	*E. coli* W3110	*P. aeruginosa* PAO1	*A. baumannii* ATCC19606	*K. pneumoniae* NCTC418	*S. aureus* COL MRSA	MHC[d)]	EYPG Vesicle leakage	EYPC Vesicle leakage
		(%)[b)]	MIC (μg/mL)[c)]					(μg/mL)	(%)[e)]	(%)[e)]
ln65	KKLLKLLKLLL	73	4	2-4	2-4	4	4	125	79	85
dln65	**kk**ll**k**ll**k**ll	67	2-4	2-4	4	4	2-4	125	82	90
ln69	**kk**LL**k**LL**k**LLL	61	4	8	2-4	8	16	1000	98	26
dln69	KK**ll**K**ll**K**lll**	59	0.5-1	2-4	2	4	2	250	94	24
sr-**ln65**	KKLLKLLKLLL	10	4	4	4	16-32	8	1000	90	22
sr-**ln65L[6]**	KKLLKLLKLLL	17	4	8	8	16-32	16	2000	91	12
Diastereomers of **ln65**										
HP1	K**k**LLKLLKLLL	73	2	4	4	4-8	2	< 15.6	73	87
HP2	**kk**LLKLLKLLL	69	4	4	4	2-4	4	< 15.6	70	87
HP3	K**k**LL**k**LLKLLL	69	2	4	2	8	2-4	< 15.6	90	55
HP4	K**k**L**l**KLLKLLL	46	2-4	2-4	2-4	2	2-4	< 15.6	74	83
HP5	**k**KLLKLLKLL**l**	90	0.5	2	0.5	2	2	62.5	64	39
HP6	KKLLK**ll**KLLL	29	2	8	4	64	16	500	90	9
HP7	**kk**LLKLLKLL**l**	60	0.5	2	0.5	4	2	125	90	28
HP8	K**ll**KLLKLLL	37	2	4	2-4	4	4	< 15.6	91	63
HP9	KKLL**ll**KLLL	10	8	64	> 64	> 64	> 64	31.3	59	5
HP10	**kk**LL**k**LLKLLL	90	2	4	2	4	2	< 15.6	82	54
HP11	K**ll**KL**l**KLLL	52	2	2-4	2	4-8	2	62.5	94	43
HP12	K**ll**K**l**LKLLL	17	2-4	4-8	8	8-16	4	250	97	34
HP13	KKLL**kll**kLLL	9	4-8	16-32	16-32	> 64	> 64	1000	42	8
HP14	KK**ll**K**ll**KLLL	13	2	8	4-8	> 64	16-32	1000	95	10
HP15	KK**l**L**k**L**l**KlLL	6	8	16	32-64	> 64	> 64	> 2000	34	3
HP16	KKL**l**kLL**kl**LL	8	4	32	32-64	8-16	> 64	125	50	2
HP17	K**kl**LKLLK**ll**L	16	8	16	32	32-64	32-64	1000	20	12
HP18	**kk**LLKLLKL**ll**	63	4-8	8	8	> 64	16-32	1000	61	11
HP19	**kk**LL**k**LLKLL**l**	55	2-4	8	4	16	8	1000	95	9
HP20	KK**ll**KLL**kl**LL	15	8	16	32-64	> 64	> 64	1000	58	12
HP21	K**kl**LK**l**LK**l**LL	11	4	8	32	16-32	16-32	> 2000	44	5
HP22	KK**ll**KL**l**K**l**L	23	2	8	8	> 64	16	> 2000	76	5
HP23	KKL**l**kLL**k**LL**l**	10	2	4-8	> 64	> 64	32	> 2000	51	10
HP24	K**kll**K**ll**KLLL	7	4-8	16	8	> 64	32	250	81	13
HP25	KK**ll**K**ll**K**l**LL	12	8-16	8-16	32	> 64	> 64	> 2000	70	4
HP26	**kk**LL**k**LLKL**ll**	41	4	4	16	> 64	32	> 2000	68	6
HP27	**kk**LL**k**LL**k**LL**l**	23	4	8	32	> 64	32	> 2000	31	5
HP28	**k**KLL**kll**KLL**l**	10	2-4	4	64	> 64	32	1000	29	3
HP29	KKL**l**k**ll**kLLL	7	2	4	8	64	32	250	53	6
HP30	K**k**L**l**K**l**L**k**L**l**L	7	8	8-16	32	> 64	64	> 2000	11	10
HP31	**k**K**l**L**k**L**l**K**l**L**l**	5	8	8	32	> 64	32	> 2000	22	9
Lys → Arg and Leu → Ile analogs of **ln65**/**ln69** and dimers										
HP32	RRLLRLLRLLL	62	4-8	8-16	4	4-8	4-8	15.6	30	99
HP33	**rr**LL**r**LL**r**LLL	63	4-8	4-8	4	4-8	2-4	125	85	56
HP34	KKIIKIIKIII	68	32	> 64	8-16	> 64	> 64	62.5	95	10
HP35	**kk**I**k**I**k**III	22	4	16	8	> 64	> 64	125	98	13
HP36	RRIIRIIRIII	60	16	64	8-16	16	16-32	62.5	99	39
HP37	**rr**I**r**I**r**III	50	8	4-8	8-16	32-64	8-16	250	98	8
2ln65	$(KKLLKLLKLLL)_2$	91	> 64	> 64	> 64	> 64	> 64	< 15.6	73	40
2ln69	$(\mathbf{kk}LL\mathbf{k}LL\mathbf{k}LLL)_2$	82	> 64	> 64	> 64	> 64	> 64	< 15.6	71	74

[a)] One letter for amino acids. D- amino acid are in lower case and bold and stereorandomized residues (ratio 1:1 of L and D) are underlined. [b)] Values are corresponding to data recorded by circular dichroism for the condition 5mM DPC in 7 mM PB buffer pH 7.4. Percentage of α-helix content were extracted from using Dichroweb[177] (Contin LL method, set 4[178]).[c)] Minimum Inhibitory Concentrations (MIC) were determined after incubation in Mueller-Hinton (MH) broth pH 7.4 for 16-20 h at 37 °C. Values represent two independent duplicates MIC determinations. [d)] Minimum Hemolytic Concentration (MHC) measured on human red blood cells in PBS (pH 7.4) after 4 h incubation at room temperature. [e)] Lipid vesicles made of EYPG or EYPC were suspended in buffer (10 mM TRIS, 107 mM NaCl, pH 7.4). After 45 s, the indicated compound was added at desired concentration and after 240 s, 30 μL of Triton X-100 1.2% was added for full fluorescein release. The percentage leakage observed with 10 μg/mL of compound is given. See Supporting Information for full curves.

Many of these diastereomers showed substantial α-helical folding in their CD spectra recorded in 5 mM DPC (Table 2, Figure 12d-f, Figure S2.1 and Table S2.2). The average α-helicity decreased with increasing D-residues from 73% for **ln65** and **HP1** (zero and one D-residues), to 61±24% for **HP2** – **HP6** (two D-residues), 49±34% for **HP7** – **HP10** (three D-residues), 23±20% for **HP11** – **HP23** (four D-residues) and 14±12% for **HP24** – **HP31** (five D-residues). Assuming that these average α-helicity values were representative of the average across all **ln65** diastereomers with the corresponding number of D-residues gave a predicted weighted average α-helicity of 26% for *sr*-**ln65L**^{6}, slightly above the measured 17%.

Diastereomers with one, two or three D-residues (**HP1** – **HP10**) generally showed activities comparable to the full L peptide **ln65** against the five bacterial strains (MIC = 0.5 – 8 μg/mL) but were slightly more hemolytic (MHC = 15.6 – 62.5 μg/mL) than **ln65**. Notable exceptions were **HP6**, which was less active than **ln65** against *K. pneumoniae* (MIC = 64 μg/mL) and MRSA (MIC = 16 μg/mL) and less hemolytic (MHC = 500 μg/mL), and **HP9**, which had much weaker antibacterial effects than **ln65** (MIC = 8 – >64 μg/mL) but was quite hemolytic (MHC = 31.3 μg/mL). **HP6** and **HP9** both had a relatively low α-helicity (29% and 10%). On the other hand, **HP5** (2 D-residues) and **HP7** (3 D-residues) stood out in this series as particular antibacterial (MIC = 0.5 – 4 μg/mL) although somewhat hemolytic (MHC = 62.5 – 125 μg/mL). Both peptides completely killed bacteria within one hour in the time-kill assay as expected for membrane disruptive compounds (Figure S2.3). Furthermore, EYPG vesicle leakage activities of **HP5** and **HP7** were strong in line with antibacterial effects. Except for the non-helical but hemolytic **HP9**, EYPC vesicle leakage activities varied in line with hemolysis, consistent with a membrane disruptive activity.

Diastereomers with four and five D-residues (**HP11** – **HP31**) were generally less active against bacteria, especially against *A. baumannii*, *K. pneumoniae* and MRSA, although they all kept significant EYPG vesicle leakage activities, reflecting the fact that vesicle leakage activity is often not sufficient for antibacterial effects to occur due to the much more complex nature of bacteria compared to lipid vesicles. Furthermore, these diastereomers mostly lost their hemolytic activity in proportion to their low EYPC vesicle leakage activities, except for **HP16**, **HP24** and **HP29**, which, like **HP9**, showed significant hemolysis despite of being non-helical and inactive on EYPC vesicles. The least active peptides were **HP13** with four D-residues and **HP25** with five D-residues. Both peptides retained some activity against *E. coli*, *P. aeruginosa* and *A. baumannii* (MIC = 4 – 32 μg/mL) but were inactive against *K. pneumoniae* and MRSA, were non-hemolytic, and were not α-helical (7 and 11% in 5 mM DPC). Gratifyingly, one peptide

with four D-residues, **HP19**, was as strongly antibacterial and low hemolytic as the previously identified **ln69** with four D-residues. Another peptide with four D-residues, **HP11** (MIC = 2-8 µg/mL), was even slightly more antibacterial than **ln69**, although slightly more hemolytic (MHC = 62.5 µg/mL). **HP11** and **HP19** were among the most α-helical in this set (52 – 55% in 5 mM DPC) although not as much as **ln69** (61%).

To compare the effects of diastereomeric changes with more classical sequence variations, we performed conservative mutations in **ln65** and **ln69** by mutating all lysines to arginines, all leucines to isoleucines, or both, preserving their chirality pattern. In this series, the Lys→Arg exchanges (**ln65→HP32** and **ln69→HP33**) preserved α-helicity, antibacterial activity and EYPG vesicle leakage, but increased hemolysis and EYPC vesicle leakage, which might be related to the better cell-penetrating properties of poly-arginines versus poly-lysines attributed to stronger binding to phospholipids.[179] On the other hand, Leu→Ile exchanges (**ln65→HP34**, **ln69→HP35**, **HP32→HP36**, **HP33→HP37**) led to reduced antibacterial effects and in part lower hemolysis, accompanied by slighted lower α-helicity as expected since Leu stabilizes and Ile destabilizes α-helices.[180] Surprisingly, dimerization of **ln65** to **2ln65** and **ln69** to **2ln69** gave peptides that were strongly α-helical and hemolytic but entirely inactive against bacteria. Vesicle leakage activities were generally high for EYPG vesicles and partially followed hemolysis trends for EYPC.

Taken together, these experiments showed that diastereomers of **ln65** featured new analogs with interesting activity profiles, while other simple modifications such as Lys→Arg, Leu→Ile mutations or dimerization were not as profitable. For further evaluation, we selected the most strongly antibacterial diastereomeric AMPs irrespective of their hemolytic properties, namely **ln65**, **ln69**, **dln69**, and all diastereomers **HP1** – **HP11** except **HP6** and **HP9**. These AMPs showed good activities (MIC = 2-8 µg/mL) against additional Gram-negative and Gram-positive bacteria including several drug resistant *P. aeruginosa* variants,[181] although none of them were active against *Burkholderia cenocepacia*, a Gram-negative bacterium which is naturally resistant to antimicrobial peptides like colicin (Table 3).[182] Furthermore, most diastereomers were much more stable against serum degradation than the full L-sequence **ln65** (Figure 13a). Interestingly, inverting the chirality of only the *N*- and *C*-terminus (**ln65 → HP5**) was sufficient to entirely stabilize the peptide in line with the non-recognition of D-amino acids by proteases preventing the proteolysis from peptide extremities. On the other hand, **dln69** with 7 D-leucine residues was entirely degraded due to proteolytic scission at the *N*-terminal L-lysine residue presumably from trypsin-like proteases (Figure S2.4).

Table 3. Antimicrobial activity of diastereomeric AMPs.

Cpd.	PA14[a)]	PA14 4.13 (*phoQ*)[a,b)]	PA14 4.18 (*pmrB*)[a,b)]	PA14 2P4 (*pmrB*)[a,b)]	ZEM-1A[a,c)]	ZEM9A[a,c)]	*K. pneumoniae* Oxa-48[a,c)]	*Enterobacter cloacae*[a,c)]	*Stenotrophomonas maltophilia*[a,c)]	*Burkolderia cenocepacia*[a,c)]	*Staphylococcus epidermis*[c,d)]	*S. aureus* Newman[d)]
ln65	2-4	4	32	32	4	4	2	2	2	> 64	2	2
ln69	2	4	16	32	2	8	4	4	2	> 64	4	8
dln69	1	2	8	16	4	8	8	4	2	> 64	4	1
HP1	2	4	32	64	2	4	8	2	4	> 64	2	2
HP2	2	4	32	64	2	4	2	2	2	> 64	2	2
HP3	4	8	32	32	2	8	4	4	4	> 64	4	2
HP4	2	4	32	64	2	4	2	2	2	> 64	2	2
HP5	2	4	16	32	2	4	2	2	2	> 64	2	2
HP7	2	4	16	16	1	4	4	2	2	> 64	2	4
HP8	2	4	16	32	2	8	4	4	2	> 64	4	4
HP10	2	4	16	32	2	4	2	2	2	> 64	2	2
HP11	1	2	8	16	2	8	4	4	4	> 64	4	2
Pol B	< 0.125	0.25	1	1	< 0.125	2	2	1	0.5	> 16	-	-
Vancomycin	-	-	-	-	-	-	-	-	-	-	0.5	0.5

[a)] Gram-negative strains. [b)] Strains carrying spontaneous mutations in the indicated genes, all leading to polymyxin B resistance. [c)] MDR strains. [d)] Gram-positive strains. [e)] Minimum Inhibitory Concentrations (MIC) were determined after incubation in Mueller-Hinton (MH) broth pH 7.4 for 16-20 h at 37 °C. Values represent two independent duplicate MIC determinations.

While most of these strongly antibacterial diastereomers were equally or more hemolytic than the full L-sequence **ln65**, they showed reduced cytotoxicity against human embryonic kidney HEK293 cells (Figure 13b). Diastereomer **HP7**, which was the most active AMP against bacteria, showed the lowest toxicity in the series (IC_{50} = 128±5 µM). Furthermore, diastereomers were generally toxic against A549 lung cancer cells, with **HP11** showing the strongest toxicity (IC_{50} = 3.6±0.1 µM), in line with the fact that many AMPs are often active against cancer cells (Figure S2.5 and S2.6).[183,184] The observed differences between diastereomers in hemolysis, toxicity against HEK293 cells or A549 lung cancer cells, are probably caused by diastereomeric interactions with the different membrane components of the different cell types and possibly proteins in the cell culture medium.[185]

X-ray crystallography

To establish whether the CD signal observed with diastereomeric AMPs was indeed caused by α-helical folding, we prepared derivatives with their *N*-termini acylated with an α-C-fucosylacetyl group for crystallization as complexes with lectin LecB,[186] an approach which we have successfully used for oligonucleotides,[187] cyclic,[95] bicyclic[96] and linear peptides,[94] as well as for peptide dendrimers.[97,188] We considered the nine most potent diastereomers detailed above, the Lys→Arg mutants **HP32** and **HP33**, and the inactive, alternating chirality diastereomers **HP30** and **HP31**. Crystallization screening provided good diffracting LecB crystals with well resolved ligand electron density for complexes with the fucosylated analogs

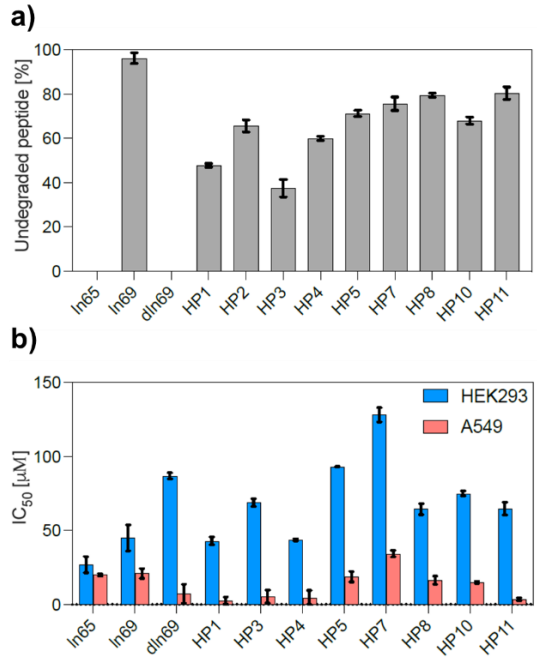

Figure 13: **(a)** Percentage of undegraded peptide after 24 h incubation in 12.5% human serum in TRIS buffer pH 7.4 at 37 °C. Data is presented in mean ± SD, n= 3. See supporting information for full curves. **(b)** Toxicity on HEK293 and A549 cells represented as the IC_{50} measured by Alamar blue assay after 24 h treatments with concentrations of peptide ranging from 0 to 200 µM. Data are presented as the mean ± SD, n = 3. See Supporting Information for all data and procedure.

Table 3. X-ray crystallography of mixed-chirality AMPs.

Cpd.	Sequence[a)]	Conditions	Composition	PDB ID
FHP5	(*)kKLLKLLKLLl	Crystal Screen G7	0.1 M HEPES pH 7.5, 20% v/v Jeffamine ® M-600 ®	8AN9
FHP8	(*)KkllKLLKLLL	Index Screen D8	0.1 M HEPES pH 7.5, 25% w/v polyethylene glycol 3,350	8ANO
FHP30	(*)KkLlKlLkLlL	Index Screen H4	0.2 M Ammonium citrate tribasic pH 7.0, 20% w/v polyethylene glycol 3,350	8ANR
FHP31	(*)kKlLkLlKlLl	Index Screen G8	0.2 M Ammonium acetate, 0.1 M HEPES pH 7.5, 25% w/v polyethylene glycol 3,350	8AOO

a) One letter code for amino acids. * = α-L-fucosyl-acetyl. Many high quality LecB crystals were also obtained in complex with fucosylated **ln65R** and **ln69r**, however in these two cases electron density only revealed the L-fucose and the adjacent two arginine residues.

FHP5, **FHP8**, **FHP30** and **FHP31** (Table 3).

In the X-ray crystal structure of the fucosylated **HP5** in complex with LecB, the undecapeptide was visible in full α-helical conformation in two of the four different fucose binding sites present in the asymmetric unit, while the other two fucose binding sites only showed electron density for the fucosyl group, probably due to a disordered conformation (PDB 8AN9, 1.3 Å resolution, Figure 14a, Table S2.3 and Figure S2.7). The two α-helices in the well-resolved binding sites are superimposable and interact through intermolecular hydrophobic interactions between leucine side chains (Figure 14b). We observed a similar situation for the

structure of fucosylated **HP8** in complex with LecB (PDB 8ANO, 1.3 Å resolution, Figure 14c/d, Table S2.4 and Figure S2.8). Both structures were very similar to the previously reported structure of fucosylated **dln69** with LecB.[96]

Although the inactive undecapeptides **HP30** and **HP31** with alternating L- and D-residues in their sequences had almost the same number of L- and D-residues, their flat CD spectra most likely indicated a disordered conformation considering that an excess of just one chiral residue was sufficient to indicate folding with *sr*-**ln65L^6**. Indeed, the structure containing two asymmetric units of the LecB complex with fucosylated **HP30** showed two different undefined structures, one forming a four members bundle maintained by H-bonds and hydrophobic interaction between the four symmetric peptide and the other one forming H-bonds with LecB (PDB 8ANR, 1.6 Å resolution, Figure 14e/f, Table S2.5 and Figure S2.9). A similar situation was observed in the LecB complex with fucosylated **HP31** containing four different asymmetric units. In this case, only two of them were completely resolved and showed unordered conformations interacting with LecB *via* H-bonds but also with symmetrical peptides (PDB 8AOO, 1.2 Å resolution, Table S2.6 and Figure S2.10).

Molecular Dynamics

To further investigate the α-helical folding of our diastereomers, we performed Molecular Dynamics (MD) simulations over 250 ns using GROMACS[189] starting from a pre-folded α-helical structure in water with or without a DPC micelle. For active diastereomers such as **HP5** in the presence of DPC micelles, the peptide first entered in contact with the micelle surface by salt bridges between lysine side chain ε-ammonium groups and phosphate groups of DPC, and later remained in an α-helical conformation at the micelle surface (Figure 15a/b). The peptide did not deviate significantly from the starting α-helical conformation (Figure 15d) and retained the full set of backbone H-bonds (Figure 15e).

In water by contrast, the α-helix of **HP5** completely and irreversibly unfolded to an unordered conformation (Figure 15c). This unordered conformation strongly differed from the starting α-helix (Figure 15a) with complete loss of backbone H-bonds (Figure 15b). Similar results were obtained for the other active compounds (**HP1**, **HP2**, **HP3**, **HP4**, **HP7**, **HP8, HP10 and HP11**, Figure S2.11 to S2.19). For the inactive, non-helical diastereomers **HP16** and **HP29** by contrast, the starting α-helical conformation rapidly unfolded to an unordered conformation with complete loss of backbone H-bonds even in the presence of the DPC micelle (Figures S2.20 and S2.21).

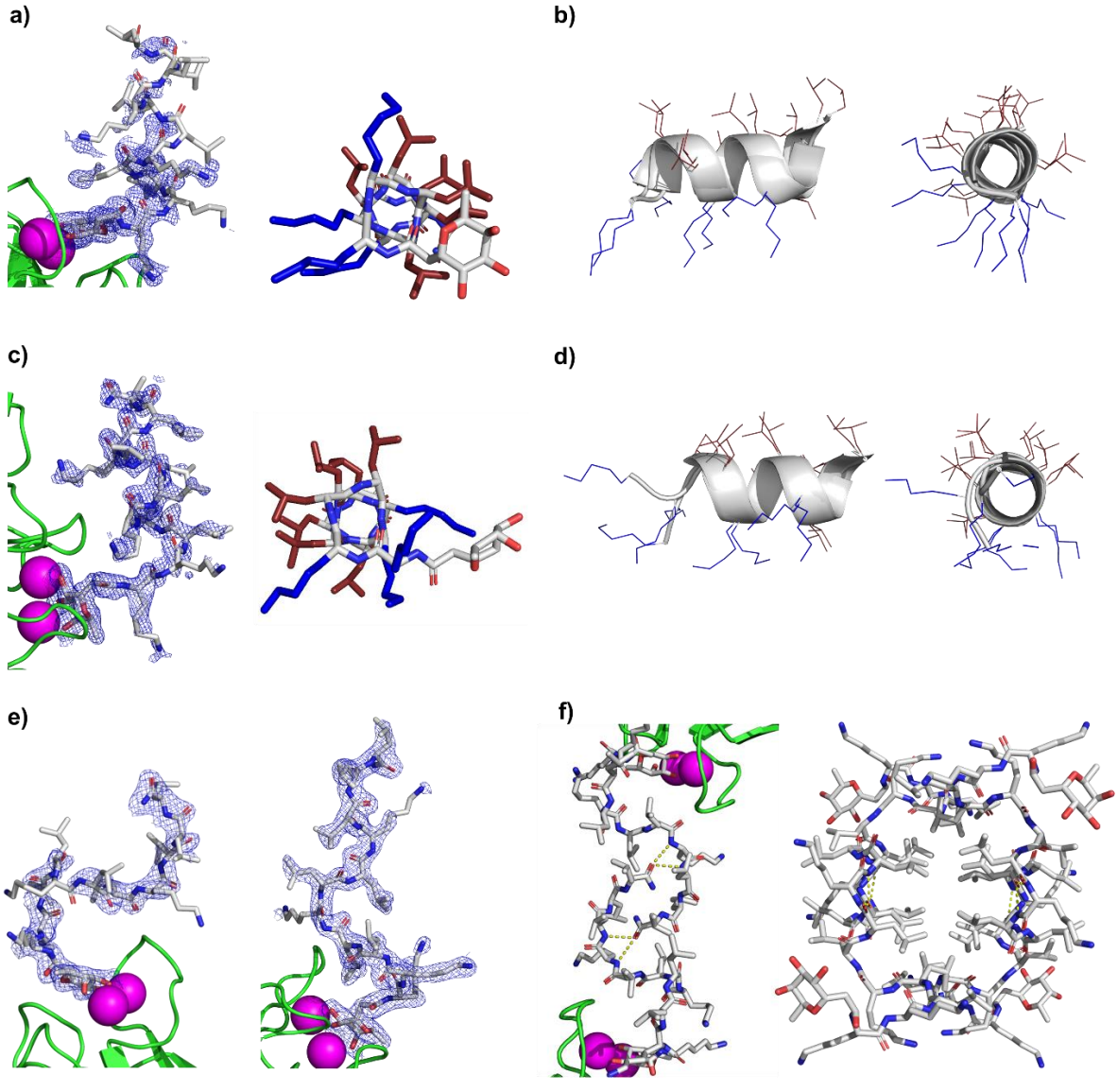

Figure 14: X-ray crystallography of mixed-chirality AMPs. **(a)** X-ray crystal structure of the **FHP5**·LecB complex (PDB 8AN9, chain E). Left panel: Peptide is represented in stick, Ca^{2+} atoms in magenta spheres and LecB in green cartoon. Blue mesh represents electron density (0.5σ level). Right panel: Stick model of the **FHP5** crystal structure, lysine side chains shown in blue and leucine side chains shown in red. **(b)** Superposition of the 2 complete non-equivalent peptides in the unit cell of PDB 8AN9. Fucose is omitted for more clarity. **(c)** Same as (a) for X-ray structure of the **FHP8**·LecB complex (PDB 8ANO, chain H). Electron density are shown for a 0.7σ level. **(d)** Same as (b) for the two complete non-equivalent peptides in the unit cell of PDB 8ANO. **(e)** X-ray structures of the two different asymmetric peptides in **FHP30**·LecB complex (PDB 8ANR). Same color code as in (a). Electron densities are shown for a 1.0σ level. **(f)** Left panel: H-bonds between two symmetrical **FHP30** chains. Right panel: full bundle of four symmetrical **FHP30** chains. Lectins monomers and calcium atoms were omitted for clarity in right panel. Same color code as in (a).

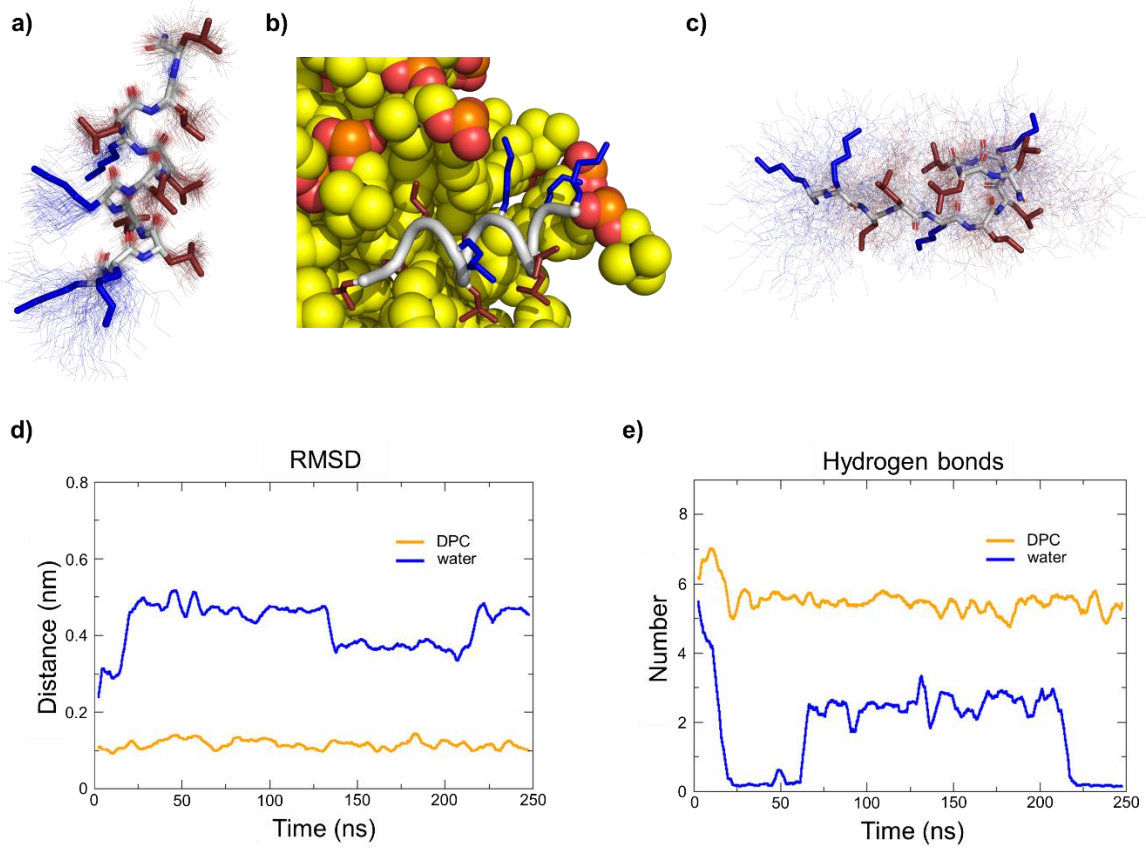

Figure 15: MD simulations of **HP5** with and without DPC micelle. **(a)** Average structure (stick model) in presence of DPC micelle over 100 structures sampled during the last 100 ns (thin lines). Hydrophobic side chains are colored in red and cationic side chains are colored in blue. DPC micelle was omitted for clarity. **(b)** Last frame of the 250 ns run with DPC micelle. Peptide backbone is in gray cartoon, cationic side chains are colored in blue, hydrophobic side chains are colored in red and DPC molecules are represented in spheres. **(c)** Same as (a) for run in water. **(d)** Comparison of root-mean square deviation of the peptide backbone relative to starting coordinates of the α-helix built in PyMol between run with DPC and run in water. **(e)** Comparison of the number of intramolecular backbone hydrogen bonds between run with DPC and run in water.

Statistical analysis

In view of the structural studies above showing in several cases that the degree of α-helicity of **ln65** diastereomers as measured by CD corresponded to an observable α-helix or structural disorder, we assumed that the CD-signal could be used as indication of folding across the entire series. Strikingly, increasing α-helicity (% in 5 mM DPC) was linearly correlated with increasing antibacterial activity measured as $\log_2$(MIC) against *K. pneumoniae* (r^2 = 0.57), *A. baumannii* (r^2 = 0.59) and MRSA (r^2 = 0.62), but to a lesser extent with activity against *P. aeruginosa* (r^2 = 0.41) and with hemolysis (r^2 = 0.37), and only quite poorly with activity against *E. coli* (r^2 = 0.29) against which most diastereomers were active (Figure 16a/b and Figure S2.22).

To gain an overview of the series, we performed principal component analysis of the complete dataset of antimicrobial activity, hemolysis and folding under the different conditions

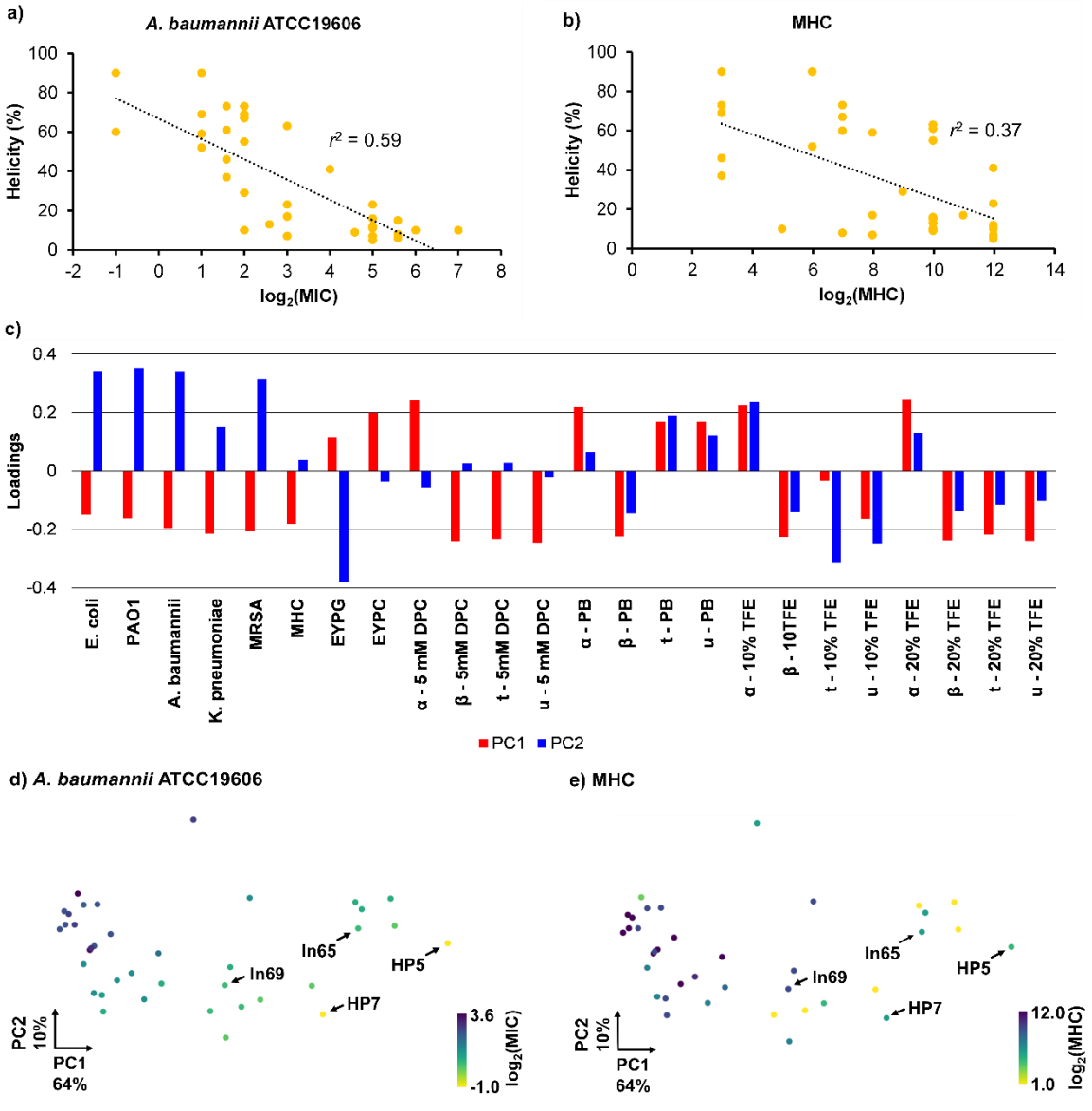

Figure 16: Statistical analysis of dataset measured on **ln65** derivatives. **(a)** Scatter plot of % helicity in 5 mM DPC against $\log_2$(MIC) for *A. baumannii* ATCC19606. **(b)** Same as (a) for $\log_2$(MHC). **(c)** Loadings analysis of principal components 1 and 2. α = α-helix, β = β-sheet, t = turn, u = unordered. Visualization of the (PC1, PC2) plane. Each point represents one compound and is colour coded depending on **(d)** activity on *A. baumannii* and **(e)** hemolytic activity.

measured. The first principal component PC1 covered 64 % of data variance and reflected the variation of antimicrobial activities, hemolysis and vesicle leakage activities with α-helicity measured in any of the four conditions (Figure 16c). The second principal component PC2 covered another 10% of data variance and reflected a modulation of antimicrobial activities with α-helicity and EYPG vesicle leakage independent of hemolysis and EYPC vesicle leakage. The distribution of the diastereomers on the (PC1, PC2) plane separated active from inactive compounds from right to left and separated the two most active diastereomers identified, **HP5** and **HP7**, from the majority of tested diastereomers (Figure 16d/e and Figure S2.23). Both

optimized AMPs stood out by their increased antimicrobial activity, which was particularly strong against *A. baumannii*, while keeping a moderate level of hemolysis, and reduced toxicity against HEK293 cells.

Conclusion

The above experiments with diastereomers of undecapeptide **ln65** supported by X-ray crystallography show that this α-helical AMP preserves folding and activity across many of its diastereomers. In contrast to previous studies of diastereomers focused on cases with reduction in toxicity and preservation of antibacterial effects, our study across a broad set of diastereomers shows that introducing D-residues in an α-helical AMP can affect antibacterial effects at least as much as toxicity as measured by hemolysis. Although these activities were correlated, sufficient variability was available to identify two diastereomers with improved properties, **HP5** and **HP7**, as two AMPs with increased antibacterial effects compared to the full L-AMP **ln65**, and moderate hemolysis and reduced toxicity against HEK293 cells.

In the present study, the preservation of folding and activity across many diastereomers of **ln65** was anticipated by characterizing its stereorandomized version *sr*-**ln65L**^{6}, which showed only modest reduction in antibacterial effects and significant α-helicity. Identifying active diastereomers might be more difficult for other α-helical AMPs if they lose their activity in stereorandomized form as reported for **DJK-5** (vqwrairvrvir) and **SB1** (KYKKALKKLAKLL).[161] Testing the stereorandomized sequence might therefore be the first step to address diastereomeric optimization of other AMPs.

Authors contributions statement.

H.P. designed the project and carried out peptide synthesis, microbiological, hemolysis, serum stability and vesicle leakage assays, CD spectroscopy, MD simulations, and X-ray crystallography and wrote the paper. T.P. performed cytotoxicity assay and wrote the paper. S.F. (bachelor student under the supervision of H.P.) and S.B. synthesized peptides, performed microbiology and hemolysis assays and CD spectroscopy. T.K. and C.v.D. supervised experiments with clinical and MDR strains. A.S. supervised X-ray crystallography experiment. S.J. supervised MD studies and wrote the paper. J.-L.R. designed and supervised the study and wrote the paper.

2.3 Mixed-chirality design of existing α-helical AMPs

Abstract

The major issues encountered in common development of membrane-disruptive α-helical amphiphilic AMPs are the lack of selectivity between bacterial and eukaryotic cells and the poor stability against proteolysis. L- to D- amino acid substitutions have been reported to minimize cell toxicity and drastically reduce degradation by proteases while still killing bacterial strains, but usually induce secondary structure disruption. Following our recently reported diastereomers of **ln65** sequence KKLLKLLKLLL, we used the chirality pattern of **ln69** (kkLLkLLkLLL), found to preserve α-helical conformation in this peptide, to modify other α-helical linear AMPs, aiming to test whether the chirality inversion pattern of **ln69** might preserve their conformational integrity and optimize their biological properties. These stereochemical modifications led to reduced toxicity on red blood cells but also to a loss of antibacterial activity and helicity. These results suggests that diastereomeric optimization of existing α-helical peptides is dependent to the amino acid sequence and therefore need complete investigations for each different AMP.

Introduction

Considering the raising of antimicrobial resistance and the exponential number of death cases related to multi-drug resistant strains, the development of new antibiotics is needed.[190–192] During the last years, membrane-disruptive antimicrobial peptides (AMPs) gained high interest due to low induction of resistance.[130,131] However, AMPs are susceptible to degradation by proteases and usually present poor selectivity between bacterial and eukaryotic cells. Optimization of these biological properties can be conducted by changing peptide stereochemistry.[65,136–138] In the case of small α-helical amphiphilic AMPs, modifying the chirality of some residues typically results in the disappearance of folding capacity on membrane surface. However, these mixed-chirality peptides sometimes preserve their antimicrobial activity, probably because they destabilize the bacterial membrane by a carpet mechanism but cannot form pores, a mechanisms requiring folding and associated with toxicity on mammalian cells.[119,137,155] Therefore, mixed-chirality appears to improve selectivity of the modified peptides for targeting bacteria. Nevertheless, no general rules on D- amino acids insertions have been found to systematically improve AMPs properties.

On the other hand, our recent optimization of bicyclic peptides showed that L- to D-amino acids switches can be tolerated by α-helical structure in the mixed-chirality AMP **ln69**, for which secondary structure was supported by X-ray crystallography.[96] Following this observation, we explored stereochemical space of that particular sequence by testing 31 diastereomers revealing mandatory helicity to act as antimicrobial.[193] In order to apply one specific stereochemical pattern to other linear α-helical AMPs, we chose **ln69** pattern which presented the best ratio between antimicrobial potency and reduced hemolysis. We used this pattern on four different reported α-helical AMPs and determined if these changes preserved secondary structure and activity while reducing toxicity. Although hemolytic activity was almost completely abolished, the mixed-chirality analogs were not anymore active on different bacterial strains and did not show any signal of α-helicity in CD spectra. These results suggest necessity of helical structure for these sequences to be active and more generally suppose that diastereomeric optimization of α-helical bioactive peptides is highly sequence dependent, appealing for a systematic diastereomers sequence exploration.

Results and Discussion

Design and synthesis of mixed-chirality analogs of α-helical AMPs based on ln69 chirality pattern

We set out to apply the **ln69** chirality pattern to other AMPs using two different approaches: (i) use the exact same chirality switches at position 1, 2, 5 and 8 in an 11-mer sequence; and (ii) invert the chirality of all cationic residues, as is the case in **ln69**. To begin with, we searched for documented peptide sequences that exhibited a wider range of amino acids, since **ln69** contains only lysines and leucines. We chose two 11-mer AMPs derived from natural compounds for the first approach: the amidated *C*-terminus version of **Decoralin**, a cationic AMP present in wasp venom,[194] and **W^{4,8}-GGN5**, an optimized sequence derived from Gaegurin 5, an antibiotic peptide isolated from Asian frog *Rana rugosa* skin.[195,196] to respectively obtain mixed-chirality compounds **HP38** and **HP39**. For the second approach, we selected **SB1,** first reported by Hancock et al.[197] and structurally determined in our group[94] (13 residues, lysines as cationic moieties) and the well-characterized D- enantiomeric peptide **DJK5**[164] (12 residues, arginines as cationic moieties) to give **HP40** and **HP41**, respectively the analogs of **SB1** and **DJK5** with D- cationic residues (Table 4).

All peptides, homochiral and mixed-chirality analogs, were synthesized using high-temperature synthesis at 60 °C leading to high yields (22-52%, Table 4). Characterization by analytical HPLC revealed slight decrease in the retention times between the homochiral parents and their mixed-chirality derivatives, a feature observed in almost all **ln65** diastereomers[193] and reported in the literature as the incorporation of D- amino acids reduces molecule's hydrophobicity, presumably resulting from amphiphilic secondary structure disturbance.[123,198–202] However, according to our data on **ln65** diastereomers, the decrease in hydrophobicity is not sufficient to predict compounds activity.

Table 4: Synthesis of linear AMPs.

Cpd.	Sequence[a)]	SPPS yield[b)]	MS analysis[c)]	Analytical HPLC[d)]
		mg (%)	calc./obs.	t_R (min)
Decoralin-NH$_2$	SLLSLIRKLIT	40.6 (31.1)	1255.84/1255.85	1.85
HP38	slLSlIRkLIT	39.8 (42.9)	1255.84/1255.85	1.60
W^{4,8}-GGN5	FLGWLFKWASK	52.8 (49.0)	1381.77/1381.78	1.65
HP39	flGWlFKwASK	55.6 (51.6)	1381.77/1381.78	1.63
SB1	KYKKALKKLAKLL	87.6 (44.7)	1544.07/1544.07	1.35
HP40	kYkkALkkLAkLL	78.0 (39.8)	1544.07/1544.07	1.27
DJK5	vqwrairvrvir	47.3 (21.8)	1550.98/1550.98	1.33
HP41	VQWrAIrVrVIr	64.3 (36.4)	1550.98/1550.98	1.26

[a)] One letter code for amino acid. D- amino acids in lower case. All C-termini are carboxamide. [b)] Yields given for RP-HPLC purified products. [c)] High-resolution electrospray ionization mass spectrometry (positive mode), the

calculated monoisotopic mass and the observed mass are given. [d] Retention time in analytical RP-HPLC (A/D = 100/0 to 0/100 in 3.5 min, λ = 214 nm).

D-amino acids insertions led to secondary structure disruption and loss of bioactivity

We first investigated whether the α-helical conformation was conserved in the mixed-chirality analogs. We used circular dichroism (CD) to experimentally determined secondary structure in phosphate buffer at physiological pH (7.4) in presence of 10 or 20% trifluoroethanol (TFE) known to promote secondary structure folding[203–205] and in 5 mM dodecylphosphocholine (DPC) mimicking a membrane-like environment[206] (Table 5, Figures 17 and S3.1 and Table S3.1). As reported, all homochiral peptides showed α-helicity signal both in presence of 20% TFE or DPC whereas they were completely unfolded in aqueous environment (Figures 17 and S3.1). α-Helices formed by the 11 residues peptides **Decoralin-NH_2** and **$W^{4,8}$-GGN5** were completely disrupted in their mixed-chirality counterparts **HP38** and **HP39** with respective reduction of 58 and 49% α-helical content in 5 mM DPC (Figure 17a/b, Table 5). The same phenomenon was observed for the D- cationic residues containing peptides **HP40** and **HP41** with 71 and 22% α-helicity reduction in membrane-like environment (Figure 17c/d, Table 5). In all cases, the loss of secondary structure also occurred in 20% TFE (17-60% reduction, Figure S3.1 and Table S3.1) indicating high disturbance of our modifications on peptide's folding ability.

Table 5: Activity of homochiral and mixed-chirality AMPs.

Cpd.	Sequence[a]	α-helix content (%)[b]	MIC (μg/mL)[c]					MHC[e] (μg/mL)	EYPG Vesicle leakage (%)[e]	EYPC vesicle leakage (%)[e]
			E. coli W3110	*P. aeruginosa* PAO1	*A. baumannii* ATCC19606	*K. pneumoniae* NCTC418	*S. aureus* COL MRSA			
Decoralin-NH_2	SLLSLIRKLIT	84	8	16	4	8	4	62.5	96	75
HP38	slLSlIRkLIT	26	32	64	64	> 64	32	1000	31	3
$W^{4,8}$-GGN5	FLGWLFKWASK	77	8	8-16	8	8	2-4	31.3	26	38
HP39	flGWlFKwASK	28	32	64	64	> 64	32	1000	32	5
SB1	KYKKALKKAKLL	78	0.5	1	1	64	> 64	> 2000	85	24
HP40	kYkkALkkAkLL	7	> 64	> 64	> 64	> 64	> 64	> 2000	51	1
DJK5	vqwrairvrvir	29	2	4	4	4	2	125	88	1
HP41	VQWrAIrVrVIr	7	> 64	> 64	> 64	> 64	> 64	> 2000	21	1

[a] One letter for amino acids. D- amino acid are in lower case. [b] Values are corresponding to data recorded by circular dichroism for the condition 5mM DPC in 7 mM PB buffer pH 7.4. Percentage of α-helix content were extracted from using Dichroweb[177] (Contin LL method, set 4[178]).[c] Minimum Inhibitory Concentrations (MIC) were determined after incubation in Mueller-Hinton (MH) broth pH 7.4 for 16-20 h at 37 °C. Values represent two independent duplicates MIC determinations. [d] Minimum Hemolytic Concentration (MHC) measured on human red blood cells in PBS (pH 7.4) after 4 h incubation at room temperature. [e] Lipid vesicles made of EYPG or EYPC were suspended in buffer (10 mM TRIS, 107 mM NaCl, pH 7.4). After 45 s, the indicated compound was added at desired concentration and after 240 s, 30 μL of Triton X-100 1.2% was added for full fluorescein release. The percentage leakage observed with 10 μg/mL of compound at 220 s is given. See Supporting Information for full curves.

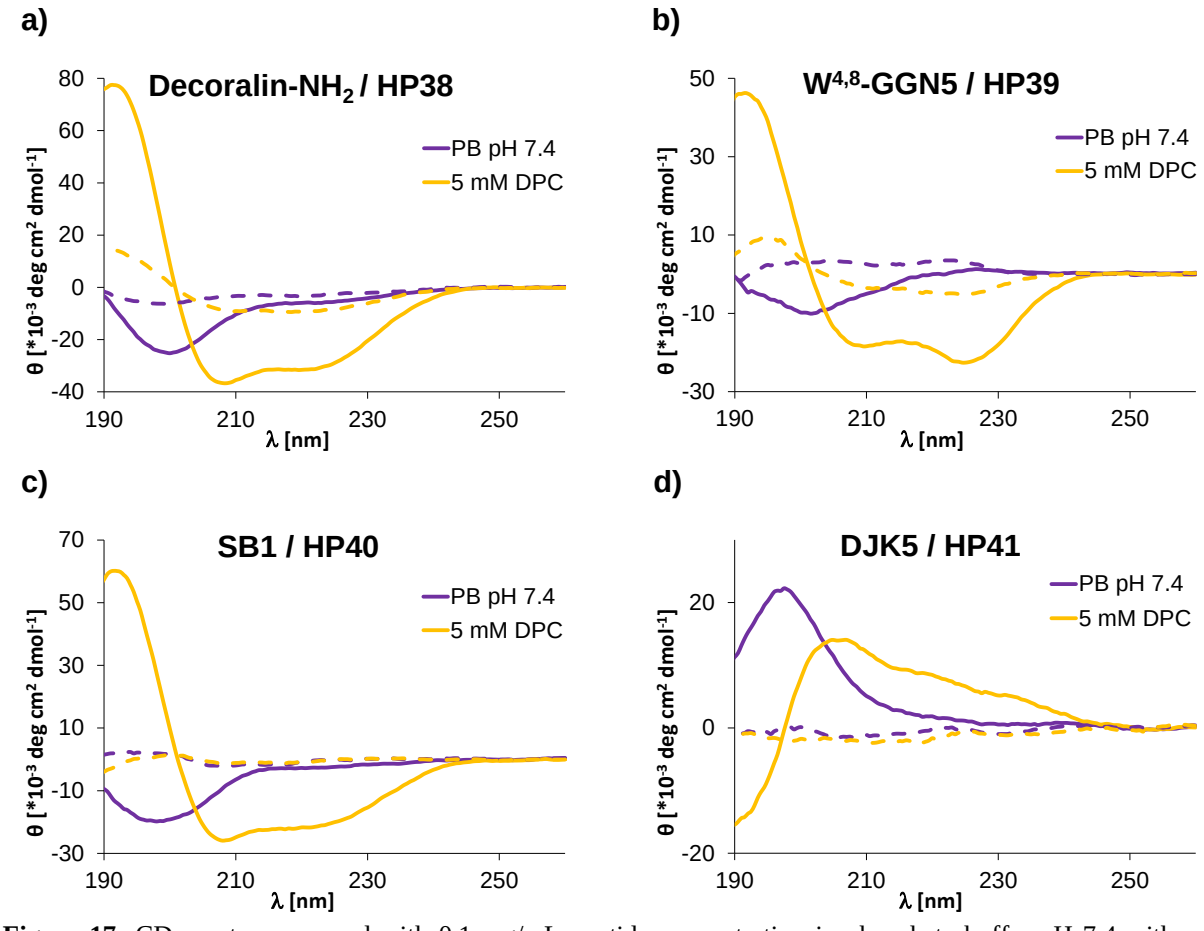

Figure 17: CD spectra measured with 0.1 mg/mL peptide concentration in phosphate buffer pH 7.4 with and without 5 mM DPC of **(a) Decoralin-NH$_2$** (full lines) and **HP38** (dashed lines), **(b) W^{4,8}-GGN5** (full lines) and **HP39** (dashed lines), **(c) SB1** (full lines) and **HP40** (dashed lines) and **(d) DJK5** (full lines) and **HP41** (dashed lines).

We then tested our compounds on different bacterial strains as sometimes preserved antibacterial activity was reported in case of unfolded mixed-chirality peptides.[118,120,123] We conducted antimicrobial assay on four Gram-negative pathogens (*E. coli* W3110, *P. aeruginosa* PAO1, *A. baumannii* ATCC19606 and *K. pneumoniae* NCTC418) and the Gram-positive methicillin-resistant *S. aureus* (MRSA). All homochiral peptides showed similar antimicrobial activities as the ones reported in original papers (Table 5).[94,164,194,195] **HP38** and **HP39** were 3 to 4-fold less active than their parent all-L sequences for all the tested strains, suggesting a mandatory folding to interact with bacterial membrane. Loss of activity was even more pronounced for **HP40** and **HP41** which were completely inactive (MIC > 64 µg/mL) against all strains, in line with the stronger α-helicity reduction observed by CD spectroscopy.

We next determined toxicity of our peptides by measuring their activities on human red blood cells (hRBCs). Apart from **SB1**, which was reported non-hemolytic,[94] homochiral peptides presented hRBCs degradation at low concentrations (< 125 µg/mL, Table 5). As

expected, all mixed-chirality sequences were not toxic against hRBCs (> 1000 μg/mL).

To correlate the absence of activity on bacterial and eukaryotic cells with a disappearance of membrane-disruptive effect, we next examined the capacity of our eight peptides to disrupt lipidic vesicles encapsulating carboxyfluorescein. We used two lipid types: egg yolk phosphatidyl glycerol (EYPG) and phosphatidyl choline (EYPC), mimicking respectively bacterial and eukaryotic membranes. (Figures 18 and S3.2). Homochiral peptides **Decoralin-NH_2**, **SB1** and **DJK5** exhibited significant EYPG leakage (> 85%) consistent with observed antimicrobial properties (Figure 18a, c and d). Surprisingly, **$W^{4,8}$-GGN5** only displayed only 26% EYPG vesicles lysis, suggesting a slow fluorescein release related to poor membrane activity (Figure 18b), consistent with the four hours needed for other analogs to kill bacteria in the original study.[195] Similar EYPG leakage was observed for its mixed-chirality analog **HP39** in line with low activity observed against *E. coli* and MRSA. In all other three cases, fluorescent signal was drastically reduced for the sequences containing D- residues (reduction of 34-67%, Table 5, Figure 18). Significant fluorescence signal was observed for **Decoralin-NH_2** and **$W^{4,8}$-GGN5** for EYPC leakage in line with their hemolytic effect, but surprisingly also for **SB1** (24%) similar to previous investigations.[94] Following the reduction of toxicity observed on hRBCs, mixed-chirality peptides exhibited no disruption of EYPC vesicles (< 5%).

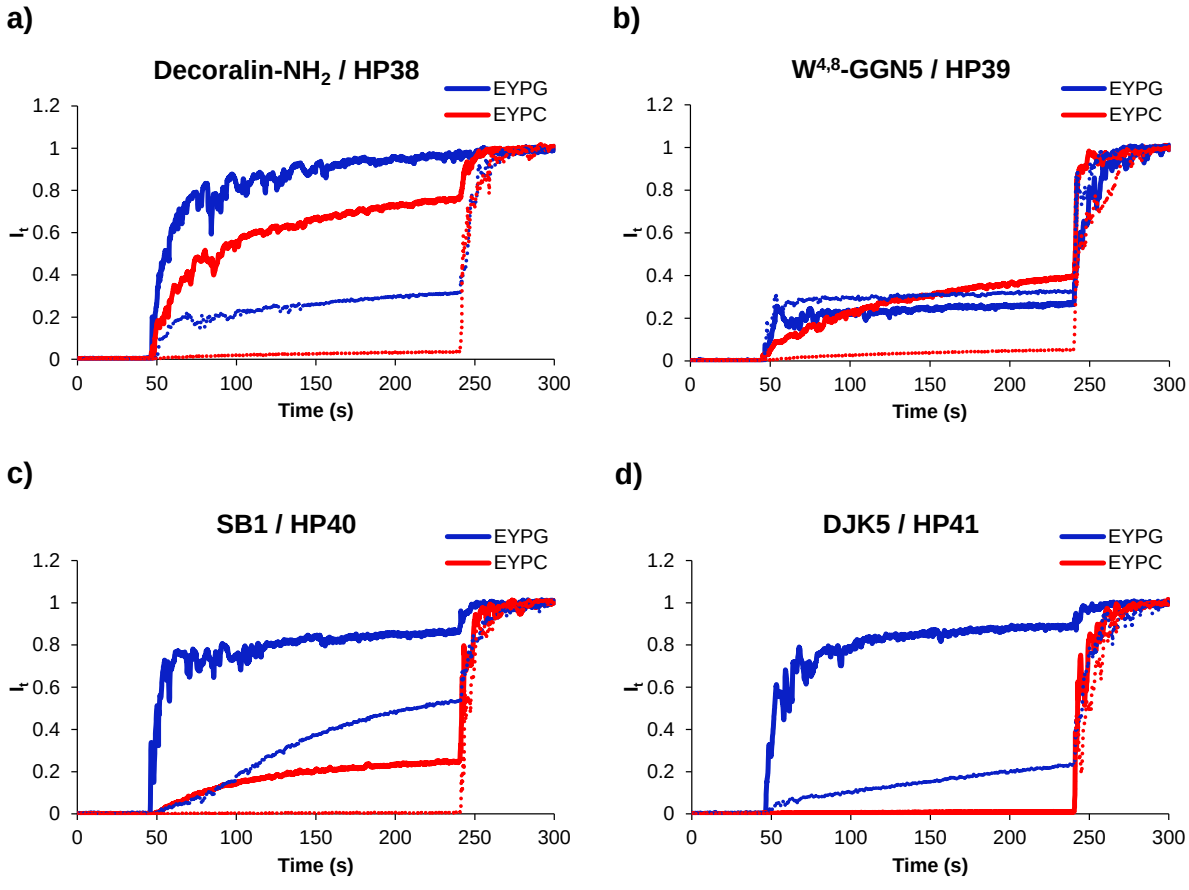

Figure 18: EYPG (blue) and EYPC (red) vesicle leakage measured at 10 µg/mL peptide concentration of **(a) Decoralin-NH_2** (full thick line) and **HP38** (thin dashed line), **(b) $W^{4,8}$-GGN5** (full thick lines) and **HP39** (thin dashed lines), **(c) SB1** (full thick lines) and **HP40** (thin dashed lines) and **(d) DJK5** (full thick lines) and **HP41** (thin dashed lines). Desired amount of compound was injected after 45 s measurement and 30 µL Triton X-100 was added after 240 s for full release of carboxyfluorescein.

Taking together, these results suggest that chirality modifications made on the four different reported α-helical peptides disrupt secondary structures for all sequences, which was necessary for biological membrane-disruptive activity.

Conclusion

Application of **ln69** chirality pattern on four different helical AMPs induced the loss of α-helical conformation and activity against bacterial and red blood cells. These results were strengthened by the absence of membrane disruption observed by vesicle leakage assay. First, this suggests that finding a general pattern to keep both folding ability and activity might be impossible. This suggest that diastereomeric investigations should be conducted for each peptide sequence. In addition, and in contrast to previous reports, these observations highlight a strong correlation between the helical conformation for antibacterial and more generally membrane-disruptive capability.

Absence of activity observed in mixed-chirality analogs of **SB1** and **DJK5** correlated

with disappearance of antimicrobial properties in their stereorandomized versions *sr*-**SB1** and *sr*-**DJK5** in our peptides stereorandomization study.[161] In contrast, the diastereomers mixture of **ln65** showed activity against a broad range of bacterial strains.[193] Therefore, these results represent further evidence to obtain active stereorandomized peptides prior to start diastereomers exploration for homochiral α-helical AMPs.

3. Chapter 2: Dipropylamine for 9-Fluorenylmethylcarbonyl (Fmoc) Deprotection with Reduced Aspartimide Formation in Solid-Phase Peptide Synthesis

This work has already been published and the publication is reproduced hereafter. Authors contributions are detailed at the end of the section.

H. Personne,* T. N. Siriwardena,* S. Javor and J.-L. Reymond, Dipropylamine for 9-Fluorenylmethylcarbonyl (Fmoc) Deprotection with Reduced Aspartimide Formation in Solid-Phase Peptide Synthesis, *ACS Omega*, **2023**, 8(*5*), 5050-5056. https://doi.org/10.1021/acsomega.2c07861

* These authors contributed equally.

Abstract

Herein, we report dipropylamine (DPA) as a fluorenylmethyloxycarbonyl (Fmoc) deprotection reagent to strongly reduce aspartimide formation compared to piperidine (PPR) in high-temperature (60 °C) solid-phase peptide synthesis (SPPS). In contrast to PPR, DPA is readily available, inexpensive, low toxicity, and non-stench. DPA also provides good yields in SPPS of non-aspartimide-prone peptides and peptide dendrimers.

Introduction

SPPS with Fmoc as α-amino protecting group for amino acid building blocks is currently the dominant synthesis method for peptide research and manufacturing. The Fmoc protecting group is removed by a base which triggers β-elimination of carbamic acid followed by the formation of an adduct with the dibenzofulvene (DBF) by-product (Figure 19a) with a nucleophile.[207] PPR is currently the most widely used Fmoc removal reagent. However, in addition to its toxicity and regulation, PPR induces the formation of aspartimide in some aspartic acid containing sequences, which can hydrolyze to α- or β-peptides, react again with the nucleophile to form peptide-base derivatives or induce an intramolecular formation of the terminating diketopiperazine by-product by nucleophilic attack of the deprotected amino group of the next amino acid (Figure 19b and c).[208–212]

PPR can be replaced by a mixture of piperazine (PZ) as nucleophile and 1,8-diazabicyclo[5.4.0]undec-7-ene (DBU) as base[38] or simply DBU without added nucleophile (Figure 19d),[213] however DBU is quite expensive and produces a considerable amount of aspartimide for aspartimide-prone sequences. One can also add weak acids such as formic acid or ethyl cyanohydroxyiminoacetate (Oxyma) to temper the basicity of the PPR solution to reduce aspartimide formation[214] However, this still does not solve the cost, stench and availability issues of PPR.

Alternative bases[215–218] or aspartate side chain protecting groups[219–222] have been reported to overcome the limitations of PPR or PZ/DBU, however none of them combines low cost and convenient use with low aspartimide and good yields. Here we searched for PPR alternatives in the context of a high temperature (60 °C) SPPS protocol with Oxyma and *N,N′*-diisopropylcarbodiimide (DIC) as coupling reagent[15] and *N,N*-dimethylformamide (DMF) as solvent, which in our hands works excellently for a variety of peptides, cyclic peptides, and peptide dendrimers.[96,161,223,224] We noted that diethylamine (DEA, b.p. 55 °C) has been used for Fmoc removal in process scale SPPS.[225] We therefore set out to test the less volatile dipropylamine (DPA, b.p. 110 °C), which is advantageously cheaper than both DEA and dibutylamine (DBA).

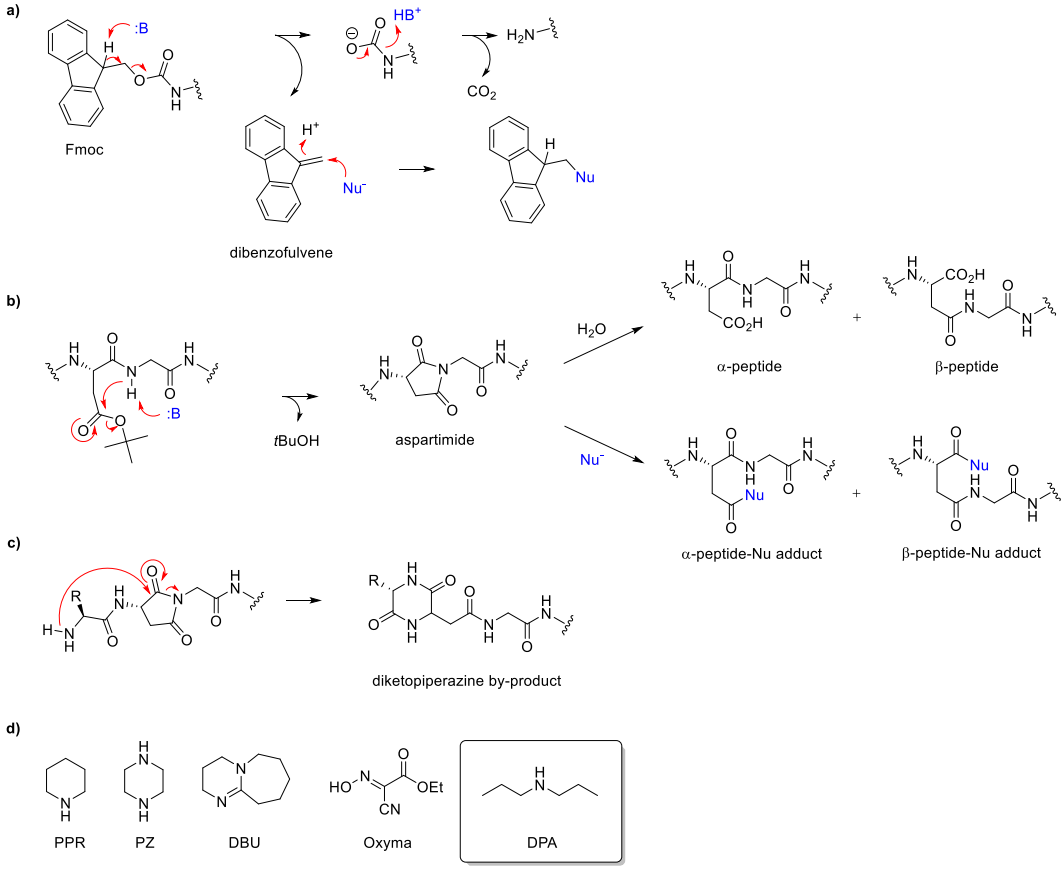

Figure 19. (a) Mechanism of Fmoc deprotection and trapping of dibenzofulvene. **(b)** Mechanism of aspartimide formation, its hydrolysis to α- or β-peptides and its ring opening by nucleophilic attack to α- or β-peptide-nucleophile adducts. **(c)** Mechanism of diketopiperazine by-product formation. **(d)** Structural formulae of reagents used for Fmoc removal.

Results and Discussion

Aspartimide-prone sequences.

Due to the lower basicity of DPA (pKa = 10.9) compared to PPR (pKa = 11.1) we investigated whether DPA might solve the issue of aspartimide formation in SPPS of aspartimide-prone sequences using the prototypical test case hexapeptide **1** (VKDGYI) and compared it to other Fmoc deprotecting reagents.

Aspartimide formation is catalyzed by relatively strong bases and lowering basicity allows to reduce the formation of this side product. For instance, the crude product of hexapeptide **1** synthesized using PPR for Fmoc removal contained 17% aspartimide. The results were even worse with DBU, which is a stronger base than PPR. In this case purity was only 52% due to 25% aspartimide and 23% by-products. Furthermore, using PZ/DBU only gave by-products (Table 6).

Table 6: Screening of deprotection conditions for low aspartimide formation in hexapeptide **1** (VKDGYI).

Fmoc deprotection reagent [a)]	Temperature, ° C	Crude yield [b)], %	Products ratio [c)], %
20% PPR	60	47	83 / 17 / 0
2% DBU	60	26	52 / 25 / 23
5% PZ + 2% DBU	60	0	0 / 0 / 100
25% DPA	60	53	96 / 4 / 0
25% DEA	60	46	89 / 8 / 3
25% DBA	60	52	93 / 4 / 3
20% PPR + 0.5 M Oxyma	60	17	93 / 6 / 1
5% PZ + 2% DBU + 0.5 M Oxyma	60	22	86 / 13 / 1
20% DPA + 0.5 M Oxyma	60	45	93 / 6 / 1
20% PPR	90	28	70 / 20 / 10
25% DPA	90	34	78 / 11 / 11

[a)] PPR = Piperidine, PZ = Piperazine, DBU = 1,8-diazabicyclo[5.4.0]undec-7-ene, DPA = Dipropylamine, DEA = Diethylamine, DBA = Dibutylamine. Percentages (%) are in w/v in case of PZ and in v/v otherwise. [b)] Crude yield is calculated as followed: (crude mass / molecular weight of desired peptide) / (mass of resin × resin loading) × % of desired product content in crude. [c)] Product ratio was determined by LC analysis and is given as follow: % desired product / % aspartimide / % other by-products. The main by-product observed was diketopiperazine terminating sequence (mass 576.3 Da), see HRMS data in Supporting Information.

By contrast, the crude product of hexapeptide **1** synthesized using DPA for Fmoc removal was 96% pure and contained only 4% aspartimide as the only detectable by-product. We obtained similar SPPS yields with hexapeptide **1** using the secondary aliphatic amines DEA and DBA for Fmoc removal, although some by-products were also observed, whereas sterically hindered diisobutylamine (DIBA) only gave by-products (Table S4.1). Furthermore, we did not detect any trace of the β-peptide of hexapeptide **1**, VKD(β)GYI, which can potentially be formed by reopening of the aspartimide, upon ^{1}H-NMR analysis in comparison with an independently synthesized β-peptide sample (Figure S4.1). Note that aspartimide formation was strongly reduced by adding 0.5 M Oxyma or hydroxybenzotriazole (HOBt) as weak acids to PPR (Tables 6 and S4.1), reproducing published results.[214] Adding Oxyma also allowed to obtain the product with PZ/DBU, however adding Oxyma to DPA did not reduce aspartimide formation further compared to DPA alone. When tested at 90 °C, SPPS of hexapeptide **1** with PPR gave 20% aspartimide in the crude, and only 11% with DPA for Fmoc removal, showing that DPA was also superior to PPR in terms of low aspartimide at high temperature (Table 6).

We further tested DPA on other aspartimide-prone sequences, hexapeptide **2**[212] and analogs of hexapeptides **1** and **2** with various Asp-X motives (Table 7). Aspartimide content was four-fold lower with DPA in contrast to PPR in the case of hexapeptide **2**. Substitution of glycine by arginine showed again a reduction of aspartimide formation and a yield increase using DPA with hexapeptides **3** and **4**. Substitution by a cysteine (hexapeptide **5**) gave similar results with both bases and almost no aspartimide was observed for the substitution with alanine

(hexapeptide **6**). Finally, we performed the synthesis of hexapeptide **7** bearing a glutamic instead of the aspartic acid to investigate glutarimide formation, but none was observed for all the conditions tested (Table S4.1).

Fmoc removal by DPA in solution.

Following the deprotection of the amino acid building block Fmoc-Lys(Boc)-OH in solution using HPLC confirmed the formation DBF as well as adduct formation with the base, according to the general deprotection mechanism (Figure 19). We found that 25% DPA in DMF rapidly released DBF with only a small amount of adduct formation (Figure 20, see Figure S4.2 for examples with Fmoc-Phe-OH and Fmoc-PEG-OH). Similar effects occurred with DEA and DBA consistent with hexapeptide **1** syntheses data (Table 6), while the hindered secondary amines diisopropylamine (DIPA) and DIBA gave only partial deprotection (Figure S4.2). By comparison, PZ/DBU and PPR led to the most adduct formation while DBU produced no adduct.Javor

Fmoc deprotection with linear peptides.

We next tested our DPA protocol with the linear peptide drugs **Afamelanotide** (13 residues) and **Bivalirudin** (20 residues). In both cases DPA performed well, independent of sequence length, with similar purities compared to PPR. We also observed excellent yields with both bases for **Bivalirudin**. We further tested **Bivalirudin** synthesis at 90 °C, which provided the desired product for both PPR and DPA, however with a comparable reduction in yield compared to the 60 °C protocol (Table 8).

Table 7: Aspartimide formation in other aspartimide-prone peptide sequences.

Cpd. Sequence [a)]	Fmoc deprotection reagent [b)]	Crude yield [c)], %	Products ratio [d)], %
Hexapeptide **2** GDGAKF	20% PPR	41	67 / 32 / 1
	25% DPA	49	84 / 8 / 8
Hexapeptide **3** VKDRYI	20% PPR	40	84 / 8 / 8
	25% DPA	43	90 / 4 / 6
Hexapeptide **4** GDRAKF	20% PPR	51	96 / 3 / 1
	25% DPA	63	99 / 0 / 1
Hexapeptide **5** VKDCYI	20% PPR	53	90 / 5 / 5
	25% DPA	48	88 / 4 / 8
Hexapeptide **6** VKDAYI	20% PPR	55	97 / 1 / 2
	25% DPA	51	96 / 1 / 3

[a)] One letter code for amino acids. *C*-termini are carboxamide. [b)] SPPS was carried at 60 °C. PPR = Piperidine, DPA = Dipropylamine. Percentages (%) are in v/v. [c)] Crude yield is calculated as explained in Table 6.[d)] Products ratio was determined by LC analysis and is given as follow: % desired product / % aspartimide / % other by-products.

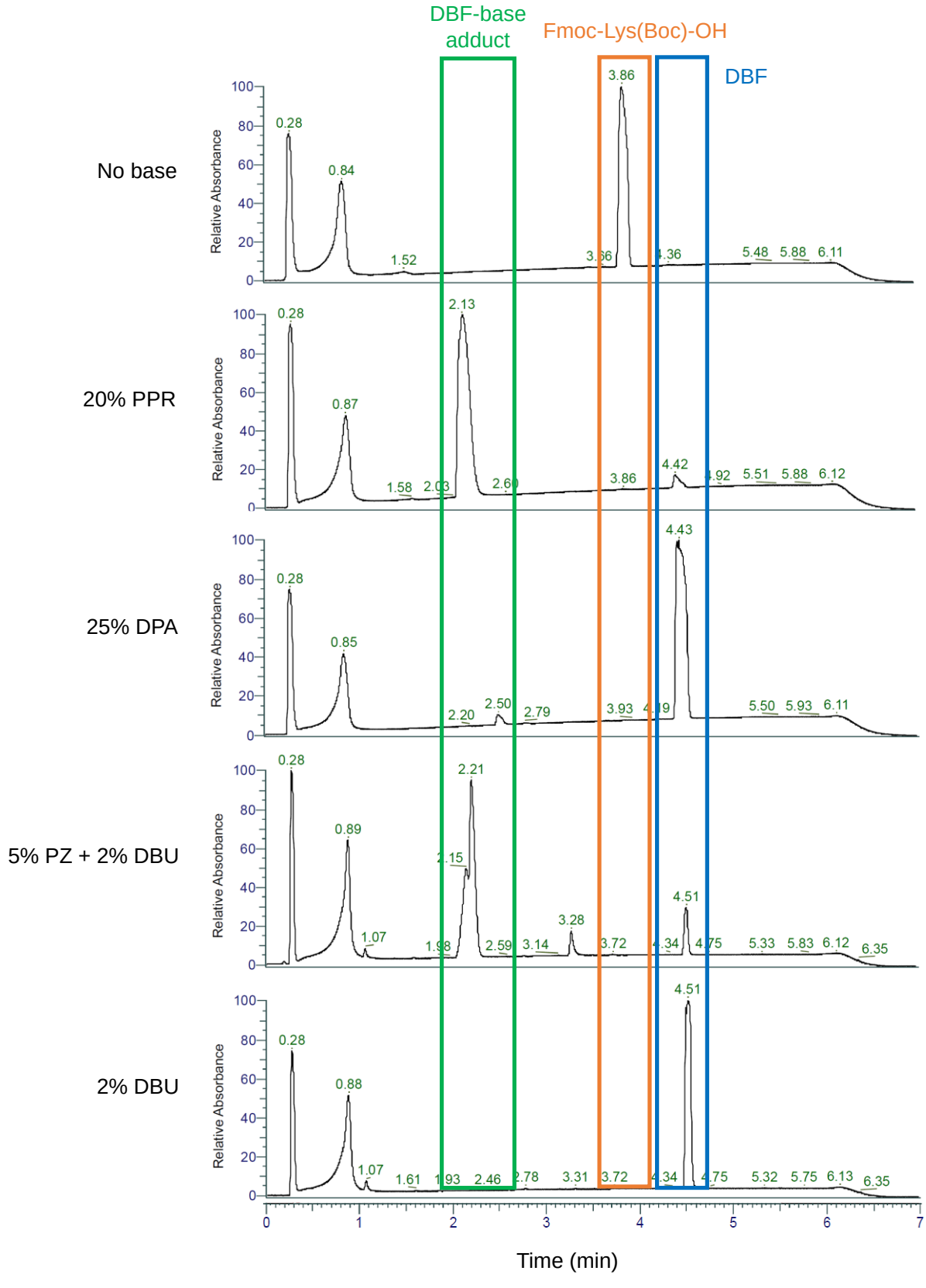

Figure 20: Liquid phase Fmoc deprotection of Fmoc-Lys(Boc)-OH in DMF at room temperature during 30 minutes analyzed by HPLC (λ = 214 nm). Fmoc-Lys(Boc)-OH (t_R = 3.86 min) and (b) Fmoc-Phe-OH (t_R = 3.85 min). DBF-PPR adduct (t_R = 2.13 min), DBF-DPA adduct (t_R = 2. 50 min), PZ-DBF adduct (t_R = 2.21 min) and DBF (t_R = 4.42-4.51 min) can be observed. DBF = dibenzofulvene, PPR = Piperidine, DPA = Dipropylamine, PZ = Piperazine, DBU = 1,8-diazabicyclo[5.4.0]undec-7-ene.

Table 8: Syntheses of peptide drugs using piperidine and dipropylamine as Fmoc removal agents.

Cpd. Sequence [a)]	Fmoc deprotection reagent [b)]	Temperature, °C	Crude yield [c)], %	Crude purity [d)], %	Isolated yield [e)], %
Afamelanotide	20% PPR	60	70	46	17
Ac-SYSNleEHfRWGKPV	25% DPA	60	45	50	10
Bivalirudin	20% PPR	60	n.d.	77	46
fPRPGGGGNGDFEEIPEEYL-OH	25% DPA	60	n.d.	77	39
	20% PPR	90	6.6	28	n.d.
	25% DPA	90	4.6	25	n.d.

[a)] One letter code for amino-acids, D- amino acids in lower case. C-terminus is carboxamide for **Afamelanotide** and carboxyl for **Bivalirudin**. Ac = acetyl group, Nle = norleucine. [b)] PPR = Piperidine, DPA = Dipropylamine. Percentages (%) are in v/v. [c)] Crude yield is calculated as explained in Table 6. [d)] The crude product after resin cleavage was precipitated, washed, dried, and analyzed by analytical HPLC to determine the percentage of desired product and other by-products [e)] Isolated yields were calculated after preparative RP-HPLC purification according to the amount of resin and its indicated loading. n.d. = not determined.

Fmoc deprotection in peptide dendrimers.

We finally investigated Fmoc deprotection with DPA and other deprotection agents for SPPS of peptide dendrimer **G1KL** at 60 °C, a prototypical first-generation peptide dendrimer (Table 9).[226] Dendrimer SPPS is an interesting test case for Fmoc deprotection because it requires simultaneous Fmoc removal at the lysine α- and ε-amino groups at the branching point. SPPS with PPR gave good crude purity (90%) and a crude yield of 73%. Crude purity was higher with PZ/DBU (97%), but the yield was much lower (26%). Using 25% DPA for Fmoc removal provided slightly lower crude purities (88%) and yields (65%) than with PPR but reducing DPA to 20% gave lower crude purities (78%) and yields (35%). Interestingly, adding 1% DBU to 20% DPA did not increase yields, but adding 1% DBU to the sterically hindered DIPA, which itself was unable to remove Fmoc, gave crude purities and crude yields comparable to 20% DPA, suggesting that DBU alone was triggering Fmoc removal with DIPA. DPA gave lower but still good crude yields compared to PPR even at room temperature in the case of the second generation dendrimer **G2KL**.[227] For the third generation dendrimer **G3KL**,[226] both high and room temperatures syntheses gave very poor yields with DPA, while PPR worked well at both temperatures. Note that DBU alone gave yields comparable to PPR in this case showing that the difficulty of DPA with peptide dendrimer synthesis is not related to the lack for DBF adduct formation.

Table 9: Syntheses of peptide dendrimers with various Fmoc deprotection conditions.

Cpd. Sequence [a)]	Fmoc deprotection reagent [b)]	Temperature [c)], °C	Crude yield [d)], %	Crude purity [e)], %
G1KL $(KL)_2KKL$	20% PPR	60	73	90
	5% PZ + 2% DBU	60	26	97
	20% DPA	60	35	78
	25% DPA	60	65	88
	20% DPA + 1% DBU	60	34	85
	20% DIPA	60	0	0
	20% DIPA + 1% DBU	60	36	86
G2KL $(KL)_4(KKL)_2KKL$	20% PPR	r.t.	65	79
	5% PZ + 2% DBU	r.t.	54	74
	20% DPA	r.t.	42	82
	25% DPA	r.t.	46	80
G3KL	20% PPR	60	47	74
$(KL)_8(KKL)_4(KKL)_2KKL$	20% PPR	r.t.	41	78
	25% DPA	60	N/A [f)]	N/A [f)]
	25% DPA	r.t.	12	29
	2% DBU	60	48	70

[a)] One letter code for amino-acids, K indicates branching L- lysine. C-termini are carboxamide. [b)] PPR = Piperidine, PZ = Piperazine, DBU = 1,8-diazabicyclo[5.4.0]undec-7-ene, DPA = Dipropylamine, DIPA = Diisopropylamine Percentages (%) are in w/v in case of PZ and in v/v otherwise. [c)] r.t. = room temperature. [d)] Crude yield is calculated as explained in Table 6. [e)] The crude product after resin cleavage was pre-cipitated, washed, and dried, and analyzed by analytical HPLC to determine the percentage of desired product and other by-products. [f)] Not applicable. Peak integration was not possible in case of G3KL, 25% DPA, 60 °C due to by-products / impurities in the crude but traces of desired compounds were observed by HRMS (see Supporting Information).

Conclusion

In summary, the experiments above documenting 56 individual SPPS runs with 11 different peptides (Tables 6, 7, 8, 9 and Table S4.1) provide strong evidence that DPA can be used as Fmoc removal reagent in high temperature SPPS. The key application for DPA is clearly the case of aspartimide-prone sequences, in which aspartimide and related by-product formation is considerably reduced, and yields are substantially increased compared to PPR. Although generally lower yielding than PPR for challenging syntheses, DPA gave reasonable purities and yields for therapeutic linear peptides and first and second-generation peptide dendrimers. Furthermore, DPA is unregulated, non-stench and much cheaper than PPR.

Authors contributions statement.

H. P. and T. N. S. conceived the project, performed experiments, analyzed the data and wrote the paper. S. J. analyzed the data and wrote the paper. J.-L. R. conceived and supervised the project and wrote the paper.

4. Chapter 3: Submonomer Synthesis of antimicrobial inverse polyamidoamines

This work is part of the following publication:

H. Personne, X. Hu, E. Bonvin, J. Reusser and J.-L. Reymond, Submonomer synthesis of inverse polyamidoamines (i-PAMAMs) antibacterials, *Helv. Chim. Acta*, **2024**, e202400041

https://onlinelibrary.wiley.com/doi/10.1002/hlca.202400041

Abstract

Polyamidoamines (PAMAMs) dendrimers, consisting of repeating $N(CH_2CH_2CONHCH_2CH_2)_2$ dendrons, have been investigated for diverse therapeutic applications. However, the β-alanine unit present in their dendron is susceptible to retro-Michael reaction, leading to degradation. Our group recently reported inverse polyamidoamines (i-PAMAMs) featuring a modified dendron $N(CH_2CH_2CH_2NHOCCH_2)_2$, which differs from the PAMAM dendron only by the position of the carbonyl group, such that the retro-Michael reaction cannot occur. i-PAMAMs can be prepared by solid-phase peptide synthesis from iterative coupling of *N*,*N*-bis(3-fluorenylmethoxycarbonyl-aminopropyl)glycine. To circumvent this relatively expensive building block, we developed a new solid-supported synthetic route to i-PAMAMs exploiting the sub-monomer strategy used to prepare peptoids. Our new procedure consists of acylation of *N*-termini with bromoacetic acid, followed by nucleophilic substitution of the bromacetyl group using *N*,*N*-bis(3-trifluoroacetylaminopropyl)amine and deprotection of the trifluoroacetyl groups with piperidine. This new synthetic route, which is more atom-economical than our previous approach, is exemplified with the synthesis of polycationic i-PAMAMs of different generation numbers and testing of their antibacterial effects.

Introduction

Dendrimers represent an emerging class of therapeutic molecules. Their intrinsic structure makes them very attractive for a broad range of applications due to their high degree of functionalization.[228–232] Among them, polyamidoamines (PAMAMs) have extensively studied, mainly because of their malleable structure and their simple construction.[233] PAMAM molecules showed high efficiency as nanocarrier for drug and gene delivery,[234–242] antimicrobial agents[243–245] as well as other technologies.[246–249] However, PAMAMs fundamentally undergo self-degradation by retro-Michael addition limiting their life-time.[250–253] Inverse polyamidoamines (i-PAMAMs), varying from PAMAMs by the position of the carbonyl group (Figure 21), were proved to be highly stable.[254] Moreover, their architecture is inclined to be constructed using a similar strategy to solid-phase peptide synthesis (SPPS), which enhances their appeal compared to PAMAMs counterparts.

A first i-PAMAM solid-phase synthesis (SPS) was introduced in 2013 by Kao *et al*,[255] based on the use of *N*,*N*-bis(*N*'-Boc-aminopropyl)-β-alanine dendron (Figure 22a). i-PAMAMs were then obtained by iterative building block coupling / Boc deprotection cycles on solid support, showing efficient synthesis of a seventh-generation dendrimer.[256]

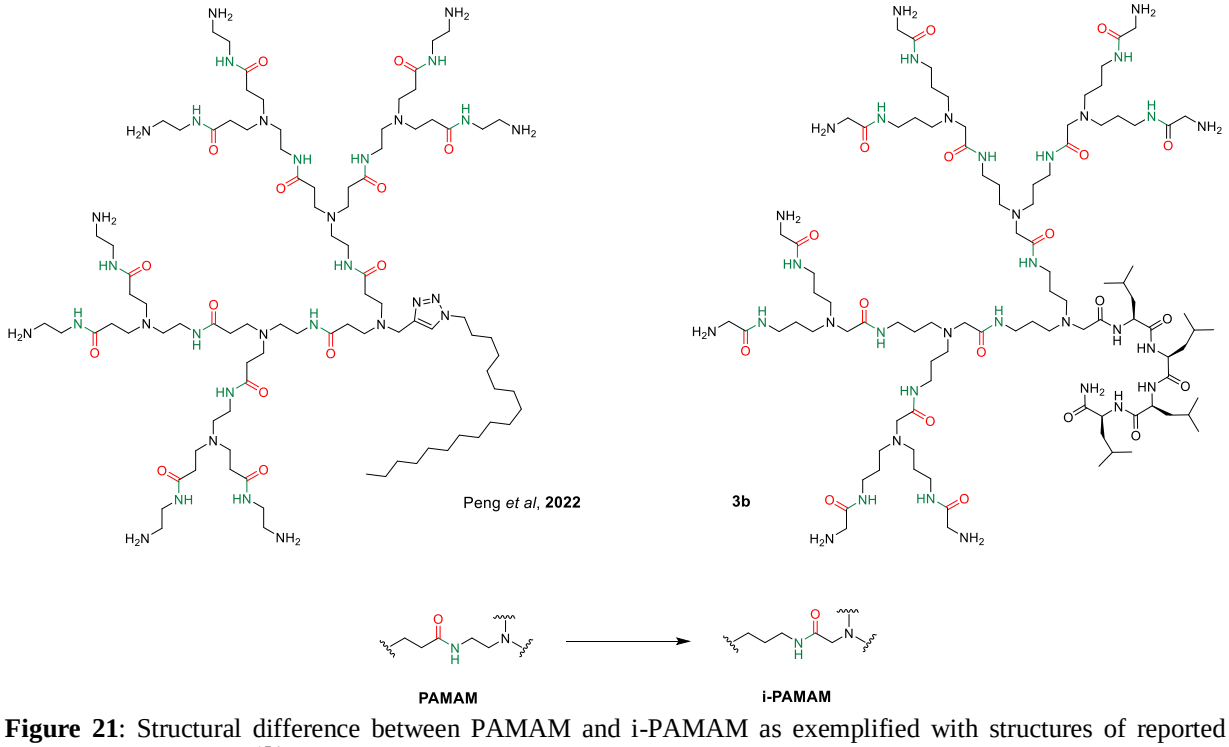

Figure 21: Structural difference between PAMAM and i-PAMAM as exemplified with structures of reported antimicrobial PAMAM[154] and *N*-terminal glycines i-PAMAM **3b**.

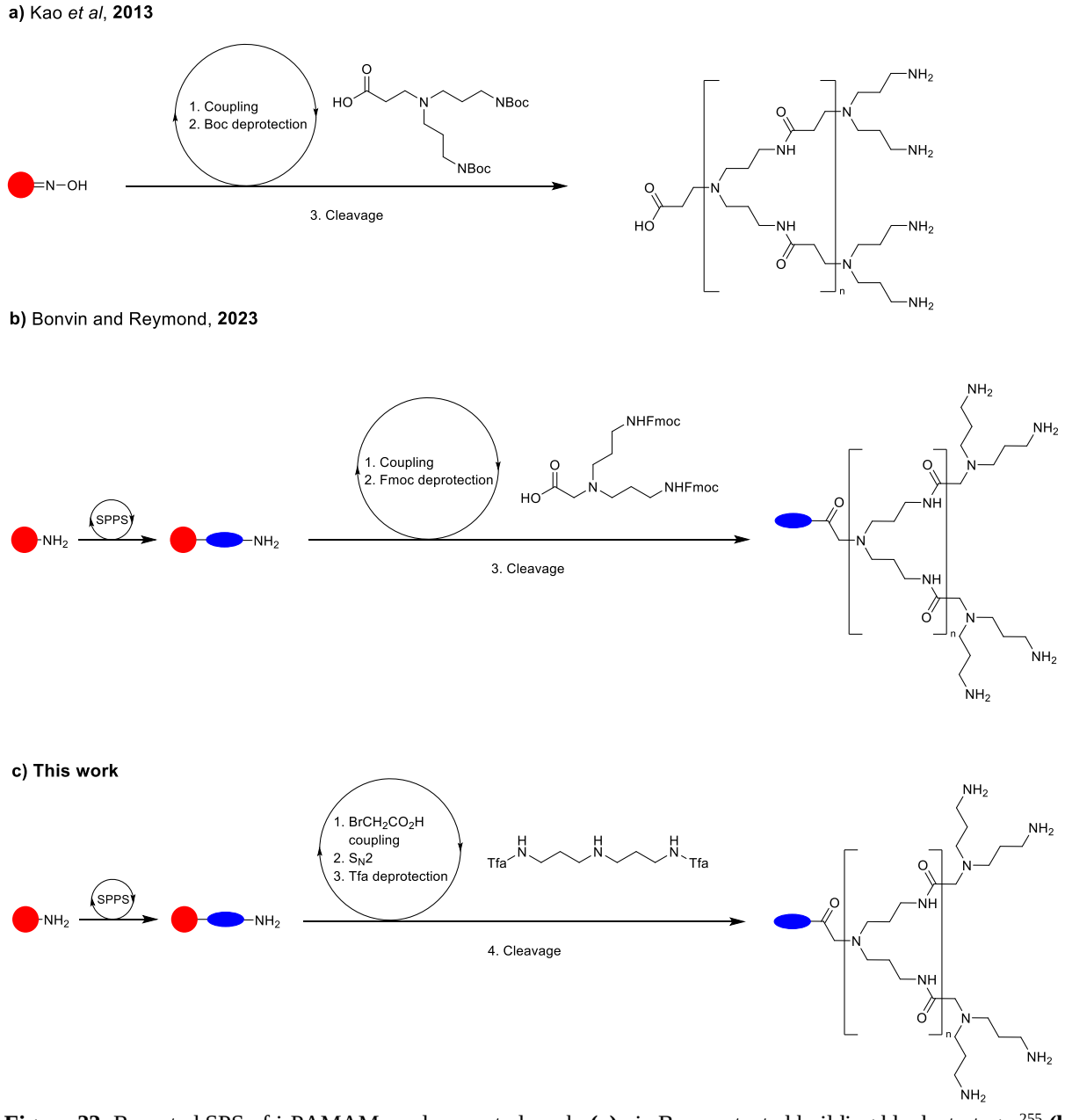

Figure 22: Reported SPS of i-PAMAMs and presented work. **(a)** via Boc-protected building block strategy,[255] **(b)** via Fmoc-protected building block strategy[254] and **(c)** current work: i-PAMAMs synthesis via key nucleophilic substitution of $BrCH_2CO_2H$. Red bead represents solid-support resin and blue oval represents peptide sequence.

However, the obtained dendritic structures retained the unstable β-alanine subunit of PAMAMs with their dendrons, implying that they would be similarly unstable. In this regard, our group recently developed a new strategy based on the repetitive coupling of the commercially available *N*,*N*-bis(*N*'-Fmoc-3-aminopropyl)glycine building block (Figure 22b).[254] This method was exemplified with the obtention of a new class of stable antimicrobial dendrimers.

Despite the effectiveness of the mentioned i-PAMAM synthetic methods, dendrons-based strategies are either time and chemical consuming in the case of the building block preparation due to a protection / deprotection synthesis, or expensive if conducted with

commercial building block. Here, we got inspired by peptoid synthesis approach[257] and developed a new cost-saving and time-effective SPS for the obtention of i-PAMAMs based on the formation of the *N,N*-bis(3-aminopropyl)glycyl motif directly during SPS. This novel method involves the preparation of trifluoroacetyl- (Tfa) protected *N,N*-bis(3-aminopropyl)amine which can provoke a S_N2 reaction on a bromine incorporated by the coupling of a bromoacetic acid ($BrCH_2CO_2H$) on the elongated chain (Figure 22c). Our new synthetic route was successfully used to obtain antimicrobial dendrimers up to the fourth generation. In addition, we synthesized the *N*-terminal glycine analogs respecting PAMAMs atomic skeleton by only switching the carbonyl bonds position to assess their antimicrobial properties.

Results and Discussion

Synthesis of *N,N*-bis(3-trifluoroacetylaminopropyl)amine

As a first step, we prepared our protected nucleophile with the reported reaction between *N,N*-bis(3-aminopropyl)amine with ethyltrifluoroacetate (ETFA, 2.1 eq.) in acetonitrile (ACN) (Scheme 2).[258] Reaction was stirred overnight at room temperature and ACN was evaporated. The final crude product was obtained in large scale (49.2 g) and analyzed by ^1H and ^{13}C NMR and HPLC-MS (Figures S5.1 to S5.3). To our delight, crude analyses showed high purity of the primary amines-protected product, with trisubstituted compound as the only side product. We therefore use the crude product without further purification.

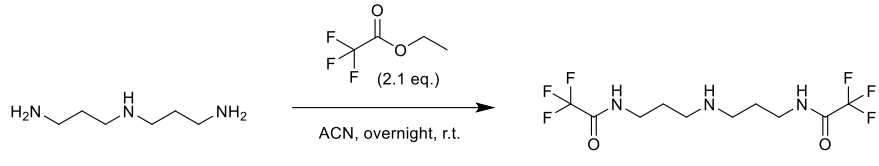

Scheme 2: Trifluoroacetyl protection of *N,N*-bis(3-aminopropyl)amine.

Screening of Tfa deprotection conditions

We then investigated the optimal deprotection conditions to remove both Tfa protecting groups during high-temperature SPS. In this aim, we tested deprotection conditions on a first-generation i-PAMAM. We first synthesized a linear tetra-leucine core using standard SPPS. We then used DIC-mediated amide bond formation to couple $BrCH_2CO_2H$ at the *N*-terminus. This coupling was performed with same conditions as standard amino acids, but without Oxyma as a coupling agent since bromoacetic acid is unable to racemize. Nucleophilic substitution of the bromide by

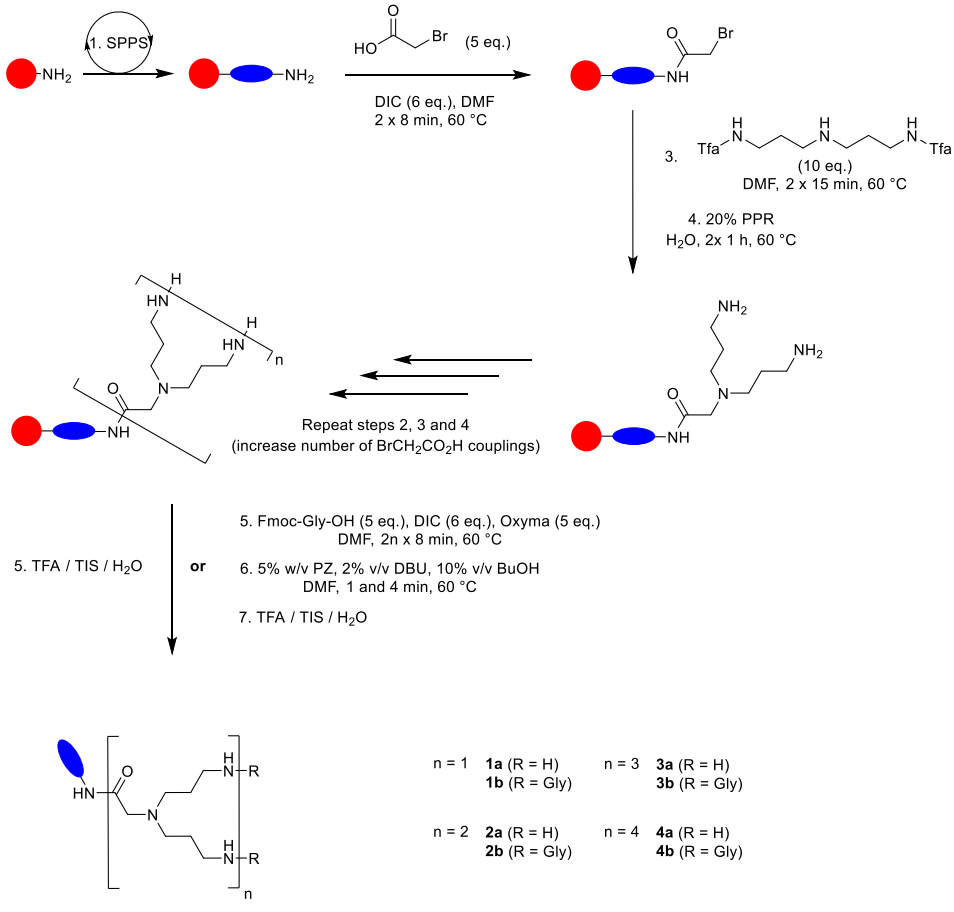

Scheme 3: Synthetic solid-phase strategy for i-PAMAMs. PPR = piperidine, PZ = piperazine, DBU = diazabicyclo[5.4.0]undec-7-ene, BuOH = butanol, TFA = trifluoracetic acid, TIS = triisopropylsilane. Red bead represents solid-support resin and blue oval represents leucines tail.

our Tfa-protected amine (10 eq.) was performed twice during 15 min at 60 °C (Scheme 3, steps 1, 2 and 3) to obtain a Tfa-protected *N*,*N*-bis(aminopropyl)glycyl motif (Bag). After the preparation of our on-beads Tfa-protected first generation i-PAMAM, we screened a total of fourteen conditions for Tfa deprotection (Table 10). We first tested sodium borohydride as reported in the literature for on-resin Tfa deprotection for the synthesis of *N*-methylated peptides and liquid phase peptide synthesis.[259,260] The reaction was first conducted at 60 °C for 10 min, and only 22% of fully deprotected compound were observed (Table 10 entry 1, Figure S5.4). Using the same concentration of $NaBH_4$, reaction was performed during 30 min at room temperature, giving 47% of desired product (Table 10 entry 2, Figure S5.5). No deprotected dendrimer was observed by the treatment with 0.2 M NaOH in DMF / H_2O and only 10% were detected by HPLC analysis in case of aqueous NaOH[261] (Table 10, entries 3 and 4, Figures S5.6 and S5.7), although 38% of mono-deprotection was observed. Similar results were obtained with 0.2 M LiOH, even by increasing reaction time (Table 10 entry 5, Figure S5.8).

Table 10: Screening of trifluoroacetamide deprotection conditions.

Entry	Conditions[a)]	Reaction time	Solvent	desired product (%)[b)]	mono-protected product (%)[b)]
1	2% w/v $NaBH_4$	10 min	EtOH / THF (1:1)	22	19
2	2% w/v $NaBH_4$ (r. t.)	30 min	EtOH / THF (1:1)	47	23
3	0.2 M NaOH	10 min	DMF / H_2O (1:1)	0	traces
4	0.2 M NaOH	10 min	H_2O	9	38
5	0.2 M LiOH	30 min	H_2O	18	37
6	20% PPR	10 min	DMF / H_2O (1:1)	0	traces
7	20% PPR	10 min	H_2O	27	39
8	20% PPR	30 min	H_2O	37	23
9	20% PPR	2 x 30 min	H_2O	65	10
10	20% PPR	3 x 30 min	H_2O	72	4
11	20% PPR	4 x 30 min	H_2O	100[c)]	0
12	20% PPR	2 h	H_2O	80	2
13	20% PPR	2 x 1 h	H_2O	100[c)]	0
14	20% EA	2 x 1 h	H_2O	9	25

[a)] All reactions were performed under nitrogen bubbling at 60 °C, except entry **2** for which the reaction was conducted at room temperature. PPR = piperidine. EA = ethanolamine [b)] Conversion calculated by integration of HPLC spectra. [c)] Monoprotected and fully protected products were not observed by HPLC-MS analysis. HPLC-MS spectra are shown in Supporting Information.

Furthermore, deprotection trials with NaOH and LiOH modified resin appearance, causing it to become more viscous, which made the nitrogen bubbling less efficient. Following previous reports on the use of aqueous piperidine (PPR) for Tfa deprotection in the case of proteins,[262–264] we assessed its suitability in our case. We first evaluated 20% PPR in DMF / H_2O and H_2O for 10 min. Similarly to NaOH, no Tfa removal was observed for the solvent mixture (Table 10 entry 6, Figure S5.9). However, aqueous PPR gave 27% fully deprotected and 39% mono-protected products (Table 10 entry 7, Figure S5.10), surpassing all previous tested conditions. Encouraged by this result, we increased deprotection time to 30 min and repeated the reaction two, three and four times (Table 10 entries 8 – 11, Figures S5.11 to S5.14). The amount of desired product increased with the number of repetitions, and complete Tfa deprotection was achieved after 4 x 30 min. Interestingly, only 80% conversion was reached for a continuous 2 h reaction, whereas two repetitions of one hour successfully removed all Tfa protecting groups (Table 10 entries 12 and 13, Figures S5.15 and S5.16), underlining the relevance of repetitive reactions. We finally sought to test ethanolamine (EA) to see whether its basic and nucleophilic capacities could increase reaction rate, but only 9% free amines product

were observed after 2 x 1 h (Table 10 entry 14, Figure S5.17). We chose to further use the 2 x 1 h treatment with 20% aqueous PPR for i-PAMAMs syntheses.

Synthesis and biological evaluation of i-PAMAMs library

We designed a library of eight compounds from first to fourth generation. Each compound contains a tetra-leucine linear peptide core to obtain amphiphilic dendrimers, a feature associated with antibacterial activity. For each generation, number of coupling repetitions for amide bond formation was increased (Table S5.1). Nucleophilic substitution of bromides was performed with 10 equivalents of protected bis(3-aminopropyl)amine relative to number of bromides during twice 15 min, independently from the number of branches. After Tfa deprotection using 20% aqueous PPR, iterations of $BrCH_2CO_2H$ coupling, S_N2 and Tfa deprotection were accomplished to obtain dendrimers with one to four consecutive Bag motifs (Scheme 3, compounds **1a**-**4a**). For each generation, we also performed the synthesis of *N*-terminal glycines analogs (Scheme 3, compounds **1b**-**4b**) to obtain strict PAMAM structure mimics with carbonyl groups switched to the other side of the amide nitrogens (Figure 21). After cleavage from the resin and reverse-phase high performance liquid chromatography (RP-HPLC) purification, all compounds were successfully obtained in high purity (Table 11). Increasing the number of generations was accompanied by lower yields (from 27% for first generation to 1% for fourth generation), as observed for previous reported third generation peptide dendrimers.[224,265,266] Lower retention times following increasing dendrimer sizes were observed by analytical RP-HPLC, consistent with the doubling of positively charged *N*-terminal amino groups. Same effect was shown between the absence and the presence of terminal glycines, in line with the higher polarity due to the presence of carbonyl groups.

Table 11: Synthesis of i-PAMAMs library.

Cpd.	Sequence[a)]	SPPS yield[b)]	MS analysis[c)]	Analytical HPLC[d)]
		mg (%)	calc./obs. (g/mol)	t_R (min)
1a	*Bag*LLLL	18.0 (27.8)	641.50/641.56	3.03
1b	G_2*Bag*LLLL	14.8 (20.4)	755.54/755.55	2.99
2a	*Bag*$_2$*Bag*LLLL	22.7 (19.3)	983.77/983.78	2.65
2b	G_4*Bag*$_2$*Bag*LLLL	11.5 (8.7)	1211.86/1211.87	2.61
3a	*Bag*$_4$*Bag*$_2$*Bag*LLLL	12.5 (5.6)	1667.32/1667.33	2.42
3b	G_8*Bag*$_4$*Bag*$_2$*Bag*LLLL	15.8 (6.2)	2124.49/2124.50	2.33
4a	*Bag*$_8$*Bag*$_4$*Bag*$_2$*Bag*LLLL	12.4 (2.9)	3038.42/3038.43	2.21
4b	G_{16}*Bag*$_8$*Bag*$_4$*Bag*$_2$*Bag*LLLL	6.1 (1.2)	3949.76/3949.78	2.13

[a)] One letter code for amino acids. Bag = bis(aminopropyl)amine glycyl. Italic case indicates branching point. All *C*-termini are carboxamide. [b)] Yields given for RP-HPLC purified products. [c)] High-resolution electrospray ionization mass spectrometry (positive mode), the calculated monoisotopic (+1) mass and the observed mass are given. [d)] Retention time in analytical RP-HPLC (A/D = 100/0 to 0/100 in 7.0 min, λ = 214 nm).

To investigate antimicrobial capacity of our compounds, we determined the Minimum Inhibitory Concentration (MIC) on four Gram-negative (*E. coli* W3110, *P. aeruginosa* PAO1, *A. baumannii* ATCC19606 and *K. pneumoniae* NCTC418) and the Gram-positive methicillin-resistant *S. aureus* COL (MRSA). MIC measurements were carried out using broth dilutions for concentrations between 0.25 and 32 μg/mL. These tests were conducted in full and 12.5% Mueller Hinton (MH) broth media, a condition known to enhance activity of proline-rich antimicrobial peptides.[267–269]. Furthermore, we explored the impact of pH variations by assessing two pH levels, 7.4 and 8.5. Basic pH have previously been shown to enhance the antimicrobial activity of cationic AMPs, peptide dendrimers and i-PAMAMs.[254,270]

Among the first and second-generation dendrimers (**1a-b** and **2a-b**) only compound **2a** which displayed modest activity against *E. coli* in 12.5% MH (MIC = 16-32 μg/mL, Table 3). However, third generation and fourth-generation compounds **3a** and **4a** were active on four out of five strains (MICs = 2-32 μg/mL). Remarkably, the activity of compound **4a** demonstrated high level of reproducibility with MIC measured for the dendrimer synthesized by the Fmoc dendron approach.[254] On the other hand, the addition of *N*-terminal glycines reduced the activity in the case of compounds **3b** and **4b** by 2 to 8-fold when compared to their glycine-free counterparts. Overall, the observed activity was predominantly noted in minimal medium at pH 8.5, while little to no activity was observed in full medium, regardless of the pH (Tables 12 and S5.2). Additionally, we assessed the toxicity of these compounds by determining the minimum hemolytic concentration (MHC) on human red blood cells. Importantly, none of them induced hemolysis at the tested concentration (Table 12, MHC > 1000 μg/mL), underscoring their selectivity for bacterial cells over eukaryotic cells.

Table 12: Antimicrobial and hemolytic activity of i-PAMAMs.

Cpd.	**MIC (μg/mL)[a)]**										**MHC[b)] (μg/mL)**
	P. aeruginosa PAO1		*K. pneumoniae* NCTC418		*A. baumannii* ATCC19606		*E. coli* W3110		*S. aureus* COL		
	pH 7.4	pH 8.5	pH 7.4	pH 8.5	pH 7.4	pH 8.5	pH 7.4	pH 8.5	pH 7.4	pH 8.5	
1a	>32	>32	>32	>32	>32	>32	>32	>32	>32	>32	>1000
1b	>32	>32	>32	>32	>32	>32	>32	>32	>32	>32	>1000
2a	>32	>32	>32	>32	>32	>32	32	16	>32	32	>1000
2b	>32	>32	>32	>32	>32	>32	>32	>32	>32	>32	>1000
3a	16	16	>32	>32	16	8	4	4	32	8	>1000
3b	32	>32	>32	>32	32	>32	4	16	>32	>32	>1000
4a	4	2-4	>32	16	8	4	4	2-4	16	2	>1000
4b	8	8-16	32	32	16	32	8	8	16	16	>1000
Pol B	1	0.5	0.5	1	0.5	0.5	0.5	0.5	8	2-4	n.d.
Vancomycin	>16	>16	>16	>16	>16	>16	>16	>16	0.25	0.25	n.d.

[a)] Minimum Inhibitory Concentrations were determined after incubation in 12.5% MH broth pH 7.4 and 8.5 for 16-20 h at 37 °C. Values represent two independent duplicates MIC determinations. Activity was only observed in full MH at pH 8.5 for **3a** (32 μg/mL against MRSA) and **4a** (16-32 and 32 μg/mL respectively against *E. coli* and MRSA), see Table S5.2.[b)] Minimum Hemolytic Concentration measured on human red blood cells in PBS (pH 7.4) after 4 h incubation at room temperature.

Conclusion

In the present work, we have introduced a new SPS to access i-PAMAMs dendritic molecules. In contrast to existing methods, which involve the sequential attachement of dendrons, our streamlined approach relies on iterative bromo acetic coupling and nucleophilic substitution by a Tfa-potected *N*,*N*-bis(3-aminopropyl)amine. This method offers significant advantages in terms of cost-effectiveness and time efficiency. Our research successfully resulted in the synthesis of amphiphilic i-PAMAMS of various sizes, tailored to the PAMAM carbonic structure. When these compounds were subjected to antibacterial testing, we observed significant activity from third-generation dendrimers, suggesting a size-dependent activity. However, the addition of glycyl moieties at the *N*-termini resulted in unactive molecules. Further investigations of the hydrophobic core will enhance i-PAMAM dendrimers bioactivity. Given the growing utility of dendritic molecules across diverse therapeutic applications, this work offers meaningful advancements in their synthesis.

5. General conclusions

Overall, this thesis aimed to enhance and structurally determined antimicrobial peptide properties by exploring the diastereomers of linear α-helical AMPs, and to develop new synthetic approaches for peptides and peptidomimetics solid-phase synthesis. I will now come back on the crucial highlights made in each study and discuss the results obtained.

Firstly, structural behaviours of L- homochiral AMP **ln65** and its mixed-chirality analog **ln69** designed by Dr. Stéphane Baeriswyl were deciphered by X-ray crystallography. Using co-crystallization strategy of fucosylated AMP with bacterial lectin LecB, the resolution of crystal structures revealed a perfect α-helical conformation for the homochiral peptide. Unexpectedly and in contrast to previous studies reported the inability of a mixed-chirality sequence to fold into a helical structure, the X-ray structure of **Fdln69** also showed a perfect α-helix. Despite the D- amino acids content, the mixed-chirality helix backbone was superimposable with the backbone of the homochiral counterpart. This X-ray study represents the first evidence of a mixed-chirality α-helical conformation. Together with the increased stability and reduced toxicity of the mixed-chirality sequence, this structural insight suggests that stereochemical switches, in addition to be tolerated by the α-helical folding, can be used for optimizing AMPs properties. Furthermore, the 8-helix bundle in the **Fln65** crystal structure was maintained through intermolecular hydrophobic interactions in aqueous solvent in MD simulations, showing the ability to fold not only in a membrane-like environment.

Knowing the possibility to tune this α-helical sequence with stereochemical changes to improve biological properties without altering the secondary structure, 31 diastereomers of **ln65** were investigated. α-Helicity and antimicrobial property were preserved for many diastereomers, highlighting a strong correlation between the secondary structure, the antimicrobial activity, and the hemolysis. More importantly, this study spotlighted two new compounds, **HP5** and **HP7**, showing activity on a broad range of bacterial strains including multi-drug resistant bacteria and clinical isolates. In addition, their toxicity towards HEK293 cells was dramatically reduced compared to the homochiral parent **ln65**. The ability of active diastereomers to fold into an α-helical structure was strengthened by the obtention of two high-resolution X-ray crystal structures of α-helical peptides and MD simulations in membrane-mimicking surroundings.

ln69 chirality pattern was then applied to reported natural and designed α-helical AMPs. Two approaches were tested: the strict application of the pattern on other 11 residues sequences;

and the chirality switch for cationic residues in other amphiphilic α-helical AMPs. In all cases, the modification of sequence's stereochemistry suppressed biological activities on bacterial and red blood cells, which was further demonstrated by the absence of membrane-disruptive ability as measured by vesicle leakage assay. Together with the results obtained on **ln65** diastereomers, these observations suggest a strong sequence dependence for a possible diastereomeric optimization. Furthermore, the stereorandomization of **ln65** and other helical AMPs sequences were tested,[161] underlining a correlation between activities of fully stereorandomized peptide and diastereomers. As a stereorandomized peptide is a mixture of all possible diastereomers, we could expect its antibacterial activity to be correlated with the amount of α-helical diastereomers. Therefore, evaluating stereorandomized analogs appears to be a trustable indication for a possible stereochemical optimization of active α-helical peptides.

The second chapter focused on the replacement of piperidine for Fmoc deprotection in the context of high-temperature SPPS. Jointly with Dr. Thissa Siriwardena, we first screened a total of eighteen different deprotection conditions on a model peptide sequence, hexapeptide **1** (VKDGYI), known to induce aspartimide formation. From these analyses, we identified 25% DPA as the best aspartimide-reducing condition with 13% less aspartimide compared to the standard 20% piperidine Fmoc deprotection. DPA was shown to be superior to piperidine for six other aspartimide-prone sequences. We then evaluated DPA as a Fmoc removal agent for arduous syntheses. High-yielding SPPS was realized for two therapeutic and commercial peptides, Afamelanotide and Bivalirudin, as well as for first- and second-generation peptide dendrimers. Efficient Fmoc deprotection was also observed in solution for single amino acid deprotection. However, DPA showed limitations for the synthesis of third-generation dendrimer when compared to piperidine and DBU, showing difficulty to simultaneously deprotect eight Fmoc groups. Together with its non-toxicity, its cost and its accessibility, these results highlighted dipropylamine as a promising alternative to piperidine for Fmoc SPPS, with an oriented use for aspartimide-prone and linear sequences.

The third and last chapter was dedicated to the development of a novel solid-phase synthetic route of inverse polyamidoamine dendrimers. Inspired by the solid-phase synthesis of peptoid polymers, we used a similar strategy to directly construct the dendritic molecules on-beads. First, we protected primary amines of *N*,*N*-bis(3-aminopropyl)amine using ethyl trifloroacetate to obtain *N*,*N*-bis(3-trifluoroacetylaminopropyl)amine. After the construction of a peptide core and the attachement at the *N*-termini of a bromoacetic acid using standard SPPS,

the non-protected secondary amine of *N*,*N*-bis(3-trifluoroacetylaminopropyl)amine was subsequently used to substitute the bromide, creating a first-generation i-PAMAM. Treatment of the trifluoroacteyl-protected dendrimer linked to the solid support with 20% aqueous piperidine during twice one hour was found to be the optimal Tfa deprotection condition. The iteration of bromoacetic coupling, nucleophilic substitution and Tfa removal allowed to successfully access i-PAMAM dendrimers up to fourth-generation. Nonetheless, yields obtained were low and decreased with the number of branching points, giving only 1% isolated yield for the biggest molecule. Further synthesis optimization, notably by reducing the resin loading using acetylation, will be conducted to increase i-PAMAM yields with this strategy. The obtained dendrimers were then assessed to antibacterial and hemolysis assays. While none was hemolytic, only the third- and fourth-generation dendrimers showed activity. Generally, antimicrobial properties were obtained in minimal medium and amplified at basic pH, conditions known to enhance proline-rich peptides activity. The analogs containing *N*-terminal glycines, identical to PAMAM dendrimers with a simple carbonyl position change, lost their antimicrobial abilities, suggesting a necessary linear alkyl spacer between *N*-terminal primary amines and the last amide bonds. Further investigations will be conducted to increase biological properties of i-PAMAMs through the modification of the lipid core. Our new approach provides a more efficient synthetic process compared to existing dendrons-based syntheses.

6. Experimental part

6.1 Material and reagents

DMF (*N*,*N*-dimethylformamide) was purchased from Thommen-Furler AG, Oxyma was purchased from SENN AG, DIC (N,N'-diisopropyl carbodiimide) was purchased from Iris BIOTECH GMBH, piperazine, butanol and DBU were purchased from Alfa Aesar; piperidine and bromoacetic acid were purchased from Acros Organics, triisopropylsilane and TFA (trifluoroacetic acid) were purchased from Fluorochem Ltd; dipropylamine, diisopropylamine, diethylamine, dibutylamine, diisobutylamine, DMAP, HOBt, DIPEA, DODT, ethyl trifluoroacetate, sodium borohydride ($NaBH_4$), lithium hydroxide (LiOH) and 2-aminoethanol were purchased from Sigma Aldrich. Amino acids were purchased from GL Biochem Shanghai Ltd or supplied by Shanghai Space Peptides Pharmaceuticals Co., Ltd except from Fmoc-Nle-OH which was purchased from Iris BIOTECH GMBH. Amino acids were used as the following derivatives: Fmoc-Leu-OH, Fmoc-(D)-Leu-OH, Fmoc-Lys(Boc)-OH, Fmoc-Lys(Fmoc)-OH, Fmoc-(D)-Lys(Boc)-OH, Fmoc-Ile-OH, Fmoc-Arg(Pbf)-OH, Fmoc-D-Arg(Pbf)-OH, Fmoc-Nle-OH, Fmoc-Val-OH, Fmoc-Asp(tBu)-OH, Fmoc-Asp-OtBu, Fmoc-Glu(tBu)-OH, Fmoc-Glu-OtBu, Fmoc-Gly-OH, Fmoc-Tyr(tBu)-OH, Fmoc-Ile-OH, Fmoc-Ser-OH, Fmoc-Nle-OH, Fmoc-His(Trt)-OH, Fmoc-D-Phe-OH, Fmoc-Phe-OH, Fmoc-Trp(Boc)-OH, Fmoc-Pro-OH, Fmoc-Cys(Trt)-OH and Fmoc-Asn(Trt)-OH. Tentagel S RAM resin was purchased from RAPP Polymer. Rink Amide AM LL resin was purchased from Novabiochem. Wang resin was purchased from Iris BIOTECH GMBH. *N*,*N*-bis(aminopropyl)amine was purchased from Fluka. Sodium hydroxide (NaOH) was purchased from Hänseler Swiss Pharma.

Analytical reverse-phase HPLC-MS was performed with an Ultimate 3000 Rapid Separation LC-MS System (DAD-3000RS diode array detector) using an Acclaim RSLC 120 C18 column (2.2 µm, 120 Å, 3×50 mm, flow 1.2 mL/min) from Dionex. The HPLC is directly linked to a Thermo Scientific LCQ-Fleet Ion-trap MS. Data recording and processing was done with Dionex Chromeleon Management System Version 6.80 (analytical RP-HPLC) and FreeStyle software. All RP-HPLC were using HPLC-grade acetonitrile and Milli-Q deionized water. The elution solutions were A: MilliQ deionized water containing 0.05% TFA; D: MilliQ deionized water/acetonitrile (10:90, v/v) containing 0.05% TFA. Preparative RP-HPLC was performed with a Waters automatic Prep LC Controller System containing the four following modules: Waters2489 UV/Vis detector, Waters2545 pump, Waters Fraction Collector III and Waters 2707 Autosampler. A Dr. Maisch GmbH Reprospher column (C18-DE, 100×30 mm,

particle size 5 μm, pore size 100 Å, flow rate 40 mL/min) was used. Compounds were detected by UV absorption at 214 nm using a Waters 248 Tunable Absorbance Detector. Data recording and processing was performed with Waters ChromScope version 1.40 from Waters Corporation. All RP-HPLC were using HPLC-grade acetonitrile and Milli-Q deionized water. The elution solutions were: A MilliQ deionized water containing 0.1% TFA; D MilliQ deionized water/acetonitrile (10:90, v/v) containing 0.1% TFA. MS spectra, recorded on a Thermo Scientific LTQ OrbitrapXL, were provided by the MS analytical service of the Department of Chemistry, Biochemistry and Pharmaceutical Sciences at the University of Bern (group PD Dr. Stefan Schürch).

6.2 Solid-Phase Peptide Synthesis

Standard Fmoc Solid-Phase Peptide synthesis

Peptides were synthesized manually using 300 to 400 mg of resin at 60°C under nitrogen bubbling. The needed amount of resin was swollen in DMF during 10 min. Double deprotections of Fmoc group were performed using a solution of 5% w/v piperazine / 2% DBU with 10% of butanol in DMF during 1 and 4 minutes. The resin was washed 5 times (5 x 8 mL DMF) after deprotection. Double couplings (2 x 8 minutes) were performed with 3 mL of amino acid (0.2 M), 2 mL of DIC (0.8 M) and 1.5 mL of Oxyma (0.8 M) in DMF. Resin was washed twice (2 x 8 mL DMF) between couplings, and 3 times (3 x 8 mL DMF) after second coupling. Reaction mixture was removed by filtration and the resin was washed with DMF and MeOH before cleavage.

Synthesis of fucosylated peptides

After normal Fmoc synthesis and deprotection of last amino group, peracetylated α-L-fucosyl-acetic acid (3 eq.), Oxyma (3 eq.) and DIC (3 eq.) were dissolved in 6 mL of DMF. Double coupling (2 x 1 hour) was performed at 50 °C under nitrogen bubbling on resin. Deacetylation of sugar was performed directly on-bead using a mixture of MeOH/H_2O/NH_3 (8:1:1, v/v/v). Reaction was stirred overnight at room temperature. Reaction mixture was removed by filtration and the resin was washed with DMF and MeOH before cleavage.

Cleavage from the resin

Cleavage was carried out by treating the compound-resin with 7 mL of a TFA/TIS/H_2O (94:5:1, v/v/v) mixture or TFA/TIS/DODT/H_2O (94:2.5:2.5:1, v/v/v/v) mixture in case of cysteine peptides for 3 hours at room temperature. Compounds were precipitated by adding 25 mL of

cold *tert*-butyl methyl ether and centrifuged for 10 min at 3500 rpm. Supernatant was discarded and the pellet was dried under argon.

Peptides purification

The dried crude was dissolved in water / acetonitrile mixture, filtered (pore size, 0.45 μm) and purified by preparative HPLC with various gradient depending on the peptide. The pure fractions were collected and analysed by analytical LC-MS. Finally pure products were obtained as white solids after lyophilization. The isolated yields were calculated for the obtained TFA salts.

6.3 Antimicrobial assay

Antimicrobial activity was determined for all peptides on *E. coli* W3110, *P. aeruginosa* PAO1, *A. baumannii* ATCC19606, *K. pneumoniae* NCTC418, methicillin-resistant *S. aureus* COL and for selected peptides on *P. aeruginosa* PA14 and the polymyxin B resistant derivatives PA14 4.13, PA14 4.18 and PA14 2P4 as well as the clinicakl isolates ZEM-1A and ZEM9A, *K. pneumoniae* OXA-48, *Enterobacter cloacae*, *Stenotrophomonas maltophilia*, *Burkholderia cenocepacia* and *Staphylococus epidermis*. To determine the Minimal Inhibitory Concentration (MIC), broth Microdilution method was used.[271] A colony of bacteria was grown in LB medium overnight at 37 °C and 180 rpm shaking. The compounds were prepared as stock solutions of 2 mg/mL in sterilized milliQ deionized water, added to the first well of 96-well sterile, polypropylene round bottom microtiter plates (TPP, untreated, Corning Incorporated, Kennebunk, USA) and diluted serially by ½. Concentration range tested was 0.5 - 64 μg/mL.The concentration of the bacteria was quantified by measuring absorbance at 600 nm and diluted to an OD_{600} of 0.022 in desired concentration of MH medium (Sigma Aldrich, Buchs, Switzerland). The sample solutions (150 μL) were mixed with 4 μL diluted bacterial suspension with a final inoculation of about 5×10^5 CFU. For each test, two columns of the plate were kept for sterility control (MH medium only), growth control (MH medium with bacterial inoculum, no compound). Positive control was done using either polymyxin B for Gram-negative or vancomycin for Gram-positive strains (starting with a concentration of 16 μg/mL) in MH medium. The plates were incubated at 37 °C for 16-20 h under static conditions. 15 μL of 3-(4,5-dimethylthiazol-2-yl)-2,5-diphenyltetrazolium bromide (MTT)[272] (1 mg/mL in sterilized milliQ deionized water) were added to each well and the plates were incubated at room temperature until MTT staining was completed. The minimal inhibitory concentration (MIC) was defined as the lowest concentration of the compound that inhibits the visible growth of the tested bacteria (yellow) with the unaided eye.

6.4 Hemolysis assay

To determine the minimal hemolytic concentration (MHC) stock solutions of 8 mg/mL of the peptide in PBS pH 7.4 were prepared and 50 µL were diluted serially by l/2 in 50 µL PBS pH 7.4 in 96-well plate (Costar or Nunc, polystyrene, untreated). Concentration range tested was 15.6 - 2000 µg/mL. Human red blood cells (hRBC) were obtained by centrifugation of 1.5 mL of whole blood, from the blood bank of Bern, at 3000 rpm for 15 min at 4 °C. Plasma was discarded and the pellet was re-suspended in a 15 mL Falcon tube in 5 mL of PBS. The washing was repeated three times and the remaining pellet was re-suspended in 10 mL of PBS. The hRBC suspension (50 µL) was added to each well and the plate was incubated at room temperature for 4 h. Minimal hemolytic concentration (MHC) end points were determined by visual determination of the wells after the incubation period. Controls on each plate included a blank medium control (50 µL PBS + 50 µL of hRBC suspension) and a hemolytic activity control (mQ-deionized water 50 µL + 50 µL hRBC suspension).

6.5 Circular Dichroism spectroscopy

CD experiments were measured on a Jasco J-715 spectropolarimeter. All the experiments were performed using Hellma Suprasil 110-QS 0.1 cm cuvettes. For each peptide, the measurements were performed in phosphate buffer (PB, pH 7.4, 7 mM), 10% TFE, 20% TFE, 5 mM DPC and 10 mM SDS. The buffer was degassed for 10 min under high vacuum before each set of experiments. The concentration of the peptides was 0.100 mg/mL and each sample was measured in one accumulation. The scan rate was 20 nm/min, pitch 0.5 nm, response 16 sec and bandwidth 1.0 nm. The nitrogen flow was kept > 8 L/min. After each measurement, the cuvettes were washed successively with milli-Q H_2O and PB pH 7.4. The baseline was recorded under the same conditions and subtracted manually. Primary CD spectra were analyzed using DichroWeb[177] and Contin-LL method (set 4).[273]

6.6 Vesicle leakage assay

5(6)-carboxyfluorescein (CF) was purchased from Sigma. Egg Yolk Phosphatidylcholine (EYPC), Egg Yolk Phosphatidylglycerol (EYPG) and a Mini-Extruder were purchased from Avanti Polar Lipids. Egg PC or Egg PG thin lipid layers were prepared by evaporating a solution of 100 mg EYPC or EYPG in 4 mL MeOH/$CHCl_3$ (1:1) on a rotary evaporator at room temperature and then dried in vacuo overnight. The resulting film was then hydrated with 2 mL CF buffer (50 mM CF, 10 mM TRIS, 10 mM NaCl, pH 7.4) for 30 min at room temperature

under stirring and then subjected to freeze-thaw cycles (7×) and extrusion (15×) through a polycarbonate membrane (pore size 100 nm). Extra vesicular components were removed by gel filtration (Sephadex G-50) with 10 mM TRIS, 107 mM NaCl, pH 7.4 buffer. Final conditions: ~ 2.5 mM PC or PG; inside: 50 mM CF, 10 mM TRIS, 10 mM NaCl, pH 7.4 buffer; outside: 10 mM TRIS, 107 mM NaCl, pH 7.4. PC or PG stock solutions (37.5 µL) were diluted to 3000 µL with a buffer (10 mM TRIS, 107 mM NaCl, pH 7.4) in a thermostated fluorescence cuvette (25 °C) and gently stirred (final lipid concentration ~31 µM). CF efflux was monitored at λ_{em} 517 nm (λ_{ex} 492 nm) as a function of time after addition of the desired volume of peptide from 2 mg/mL stock in mQ water at t = 45 s. 10 and 50 µg/mL were monitored for both EYPC and EYPG. Finally, 30 µL of 1.2% Triton X-100 was added to the cuvette (0.012% final concentration) at t = 240 s to reach the maximum intensity. Fluorescence intensities were then normalized to the maximal emission intensity using $I(t) = (I_t - I_0) / (I_\infty - I_0)$ where $I_0 = I_t$ at peptide addition, $I_\infty = I_t$ at saturation of lysis.

6.7 Time-killing assay

A single colony of *P. aeruginosa* PAO1 was picked and grown overnight with shaking (180 rpm) in LB (Sigma Aldrich, Buchs, Switzerland) medium 5 mL overnight at 37 °C. The overnight bacterial culture was diluted to OD_{600} 0.002 (2 x 10^6 CFU/mL) in fresh MH medium. Stock solutions of AMPs in sterilized milliQ water were prepared in 1 mg/mL and were diluted to two times more than required concentration in fresh MH (Sigma Aldrich, Buchs, Switzerland) medium at pH 7.4. 100 µL prepared bacteria solution in MH and 100 µL samples in MH were mixed in 96-well microtiter plate (TPP, untreated, Corning Incorporated, Kennebunk, USA). Untreated bacteria at 1 x 10^6 CFU/mL were used as a growth control. 96-well microtiter plates were incubated in 37 °C with shaking (180 rpm). Surviving bacteria were quantified at 0, 0.5, 1, 2, 3, 4, 5 and 6 hours by plating 10-fold dilutions of sample in sterilized normal saline on LB agar plates. LB agar plates were incubated at 37 °C for 10 hours and the number of individual colonies was counted at each time-point. The assay was performed in triplicate in the biosafety level 2 lab.

6.8 Serum stability assay

Human serum was diluted in 0.1 M filtered TRIS buffer pH 7.4 (25%, 1:3, v/v). Selected peptides were diluted in 0.1 M filtered TRIS buffer pH 7.4 to a concentration of 400 µM and 0.1 mg/mL 4- hydroxybenzoic acid was added as internal standard. Aliquots of peptide solution (50 µL) were added to aliquots of serum (50 uL) in sterile Eppendorf tubes, to reach a peptide

concentration of 200 μM during the assay. Samples were incubated at 37 °C under gentle stirring (350 rpm). Different samples (triplicates) were quenched at different time points (0/1/6/12/24 h) by precipitating serum proteins through the addition of (0.1 M) $ZnSO_4 \cdot 7\ H_2O$/ ACN (1:1) (0.1 M, 100 μL) and cooling in ice bath for 10 minutes. Protein precipitates were pelleted under centrifugation and supernatants were then sampled and analyzed by LC-MS. Experiment controls included two references, one known to be degraded and one known to be undegraded. Peaks corresponding to the internal standard and the undegraded peptides were integrated, with the ratio peptide/standard at t = 0 h as 100%.

6.9 Cytoxicity assay

Cell culture. The A549 human lung adenocarcinoma cells are derived from a patient and were kindly given to us by Dr. Georgia Konstatinidou (Pharmacology institute, Bern University). HEK293T cells were obtained from ATCC (CRL-11268). A549 and HEK293 were cultured in an incubator at 37°C and 5% CO_2 in RPMI-1640 (Gibco) and DMEM (Gibco) containing 10% fetal bovine serum (Thermo Fisher), 100 I.U./mL penicillin and 100 μg/mL streptomycin (Gibco).

Cell-viability assay. The viability of the cells was assessed with an AlamarBlue assay® (ThermoFisher). Cells were seeded into 96 well plates, 4000 cells/well (HEK293) and 8000 cells/well (A549), the day before the experiment. Cells were then treated with increasing concentration of the compound and incubated for 24 hours at 37 °C in the presence of 5% CO_2. The next day, the medium was removed and replaced by a 10 % AlamarBlue® solution in full growth medium (DMEM or RPMI-1640). The cells were incubated for 3-5 hours at 37 °C with 5% CO_2 in a humidified atmosphere. The fluorescence was then measured on a Tecan Infinite M1000 Pro plate reader at λ_{ex} 560 nm and λ_{em} 590 nm. The value was normalized according to the untreated cells.

6.10 Crystallography experiment and data acquisition

Suitable diffracting crystals were obtained via co-crystallization of the C-fucosylated derivatives with the bacterial lectin LecB. Sitting drop vapor diffusion method was used, screening 192 different conditions per compound The lyophilized protein was dissolved in milli-Q water (5 mg/ml) in the presence of salts (6 mM $CaCl_2$ and $MgCl_2$). The peptides were added to the protein at a 5:1 molar excess related to the LecB lectin monomer. Crystals were obtained within one to three months after mixing 1.5 μL of LecB ligand-complex with 1.5 μL of reservoir solution at

18 °C. All crystallization conditions were found in Index screens I/II (96 conditions) and Crystal Screen I/II (96 conditions) (Hampton Research, Laguna Niguel, CA, USA). Diffraction data were collected at the Paul Scherrer Institute (Villigen, Switzerland) on beamline X06DA PX-III using a DECTRIS PILATUS 2M-F detector and a multi-axis PRIGo goniometer. The structures were solved and visualized with the help of Phenix,[274] ccp4,[275] PyMol,[276] coot[277] and XDS.[278]

6.11 Molecular Dynamics

MD simulations were performed using GROMACS[189] software version 2018.1 and the GROMOS53a6 force field.[279] The starting topologies were built from Pymol. A dodecahedral box was created around the peptide 1.0 nm from the edge of the peptide and filled with extended simple point charge water molecules. Sodium and chloride ions were added to produce an electroneutral solution at a final concentration of 0.15 M NaCl. The energy was minimized using a steepest gradient method to remove any close contacts before the system was subjected to a two-phase position-restrained MD equilibration procedure. The system was first allowed to evolve for 100 ps in a canonical NVT (N is the number of particles, V the system volume, and T the temperature) ensemble at 300 K before pressure coupling was switched on and the system was equilibrated for an additional 100 ps in the NPT (P is the system pressure) ensemble at 1.0 bar.

MD in the presence of DPC micelle. MD simulations in the presence of a DPC (n-dodecylphosphocholine) micelle were performed as follows. Parameters and references for the DPC molecule for the GROMOS53a6 forcefield are given in the Supporting Information. Peptides were manually placed at a distance from the pre-equilibrated micelle (of 65 DPC molecules) equal to the diameter of said peptide. Box, solvation and NVT equilibration procedures were performed as explained previously. For each peptide/micelle system, 10 runs of 50 ns were generated to show the possibility for the peptide to either interact or diffuse away from the micelle. Then, runs of interest were extended up to 250 ns. Topology used for DPC molecules is described below.[280]

```
; Charge from Chiu et al.
; Chiu, S. W.; Clark, M.; Balaji, V.; Subramaniam, S.; Scott, H. L.; Jakobsson, E. Incorporation of surface tension into molecular dynamics simulation of an interface: a fluid phase lipid bilayer membrane. Biophys. J. 1995, 69, 1230-1245.
; Atom types from GROMOS53A6
; Oostenbrink, C.; Soares, T. A.; van der Vegt, N. F. A.; van Gunsteren, W. F. Validation of the 53A6 GROMOS force field. Eur. Biophys. J. 2005, 34, 273-284.

[ moleculetype ]
; Name   nrexcl
DPC         3

[ atoms ]
```

```
;   nr    type   resnr  residu    atom    cgnr        charge          mass
     1     CH3       1    DPC      C1       1         0.40  15.035  ; qtot: 0.25
     2     CH3       1    DPC      C2       2         0.40  15.035  ; qtot: 0.50
     3     CH3       1    DPC      C3       3         0.40  15.035 ; qtot: 0.75
     4      NL       1    DPC      N4       4         -0.5  14.0067 ; qtot: 0.75
     5     CH2       1    DPC      C5       5         0.30  14.027 ; qtot:  1.0
     6     CH2       1    DPC      C6       6         0.40  14.027 ; qtot: 1.0
     7      OA       1    DPC      O7       7        -0.80  15.999 ; qtot: 0.64
     8       P       1    DPC      P8       8          1.7  30.973 ; qtot : 1.63
     9      OM       1    DPC      O9       9         -0.8 15.999 ; qtot: 0.995
    10      OM       1    DPC     O10      10         -0.8 15.999 ; qtot: 0.36
    11      OA       1    DPC     O11      11         -0.7  15.999 ; qtot: 0.0
    12     CH2       1    DPC     C12      12          0.0   14.027  ; qtot: 0
    13     CH2       1    DPC     C13      13          0.0   14.027  ; qtot: 0
    14     CH2       1    DPC     C14      14          0.0   14.027  ; qtot: 0
    15     CH2       1    DPC     C15      15          0.0   14.027  ; qtot: 0
    16     CH2       1    DPC     C16      16          0.0   14.027  ; qtot: 0
    17     CH2       1    DPC     C17      17          0.0   14.027  ; qtot: 0
    18     CH2       1    DPC     C18      18          0.0   14.027  ; qtot: 0
    19     CH2       1    DPC     C19      19          0.0   14.027  ; qtot: 0
    20     CH2       1    DPC     C20      20          0.0   14.027  ; qtot: 0
    21     CH2       1    DPC     C21      21          0.0   14.027  ; qtot: 0
    22     CH2       1    DPC     C22      22          0.0   14.027  ; qtot: 0
    23     CH3       1    DPC     C23      23          0.0   15.035  ; qtot: 0


[ bonds ]
;  ai    aj funct           c0          c1          c2          c3

    1     4     2    gb_21
    2     4     2    gb_21
    3     4     2    gb_21
    4     5     2    gb_21
    5     6     2    gb_27
    6     7     2    gb_18
    7     8     2    gb_28
    8     9     2    gb_24
    8    10     2    gb_24
    8    11     2    gb_28
   11    12     2    gb_18
   12    13     2    gb_27
   13    14     2    gb_27
   14    15     2    gb_27
   15    16     2    gb_27
   16    17     2    gb_27
   17    18     2    gb_27
   18    19     2    gb_27
   19    20     2    gb_27
   20    21     2    gb_27
   21    22     2    gb_27
   22    23     2    gb_27

[ pairs ]
;  ai    aj funct
    1     6     1
    2     6     1
    3     6     1
    4     7     1
    5     8     1
    6     9     1
    6    10     1
    6    11     1
    7    12     1
    8    13     1
    9    12     1
   10    12     1
   11    14     1
;   12    15     1
;   13    16     1
;   14    17     1
;   15    18     1
;   16    19     1
;   17    20     1
;   18    21     1
;   19    22     1
;   20    23     1
```

```
[ angles ]
;  ai    aj    ak funct
   1     4     2     2    ga_13
   1     4     3     2    ga_13
   1     4     5     2    ga_13
   2     4     3     2    ga_13
   2     4     5     2    ga_13
   3     4     5     2    ga_13
   4     5     6     2    ga_15
   5     6     7     2    ga_15
   6     7     8     2    ga_26
   7     8     9     2    ga_14
   7     8    10     2    ga_14
   7     8    11     2    ga_5
   9     8    10     2    ga_29
  10     8    11     1    ga_14
   8    11    12     1    ga_26
  11    12    13     1    ga_15
  12    13    14     1    ga_15
  13    14    15     1    ga_15
  14    15    16     1    ga_15
  15    16    17     1    ga_15
  16    17    18     1    ga_15
  17    18    19     1    ga_15
  18    19    20     1    ga_15
  19    20    21     1    ga_15
  20    21    22     1    ga_15
  21    22    23     1    ga_15

[ dihedrals ]
;  ai    aj    ak    al funct
   1     4     5     6     1 gd_29
   4     5     6     7     1 gd_4
   4     5     6     7     1 gd_36
   5     6     7     8     1 gd_29
;
; define gd_20     0.000       5.09          2
; O-P-O- (dna, lipids)  1.2
   6     7     8     9     1 gd_20
   7     8    11    12     1 gd_27
   8    11    12    13     1 gd_29
  11    12    13    14     1 gd_1
  12    13    14    15     1 gd_34
  13    14    15    16     1 gd_34
  14    15    16    17     1 gd_34
  15    16    17    18     1 gd_34
  16    17    18    19     1 gd_34
  17    18    19    20     1 gd_34
  18    19    20    21     1 gd_34
  19    20    21    22     1 gd_34
  20    21    22    23     1 gd_34
```

Clustering of stable structures. To obtain a representative conformer for each SA-MD run, the last 100 ns (10001 frames) of each run were clustered using an RMSD cut-off adapted to get a good balance between the number of clusters and the size of the main cluster. Many clusters combined with a very large percentage of structures in the top cluster is an indication of the stability of the one main conformer in each case. The PyMol Molecular Graphics System, version 1.8 (Schrödinger, LLC), was used to create structural models.

7. References

(1) Wang, L.; Wang, N.; Zhang, W.; Cheng, X.; Yan, Z.; Shao, G.; Wang, X.; Wang, R.; Fu, C. Therapeutic Peptides: Current Applications and Future Directions. *Sig Transduct Target Ther* **2022**, *7* (1), 1–27. https://doi.org/10.1038/s41392-022-00904-4.

(2) Fetse, J.; Kandel, S.; Mamani, U.-F.; Cheng, K. Recent Advances in the Development of Therapeutic Peptides. *Trends in Pharmacological Sciences* **2023**, *44* (7), 425–441. https://doi.org/10.1016/j.tips.2023.04.003.

(3) Merrifield, R. B. Solid Phase Peptide Synthesis. I. The Synthesis of a Tetrapeptide. *J. Am. Chem. Soc.* **1963**, *85* (14), 2149–2154. https://doi.org/10.1021/ja00897a025.

(4) Merrifield, R. B. Solid Phase Peptide Synthesis. II. The Synthesis of Bradykinin. *J. Am. Chem. Soc.* **1964**, *86* (2), 304–305. https://doi.org/10.1021/ja01056a056.

(5) Merrifield, R. B. Solid-Phase Peptide Synthesis. III. An Improved Synthesis of Bradykinin*. *Biochemistry* **1964**, *3* (9), 1385–1390. https://doi.org/10.1021/bi00897a032.

(6) Sakakibara, S.; Shimonishi, Y.; Kishida, Y.; Okada, M.; Sugihara, H. Use of Anhydrous Hydrogen Fluoride in Peptide Synthesis. I. Behavior of Various Protective Groups in Anhydrous Hydrogen Fluoride. *BCSJ* **1967**, *40* (9), 2164–2167. https://doi.org/10.1246/bcsj.40.2164.

(7) Barany, G.; Merrifield, R. B. A New Amino Protecting Group Removable by Reduction. Chemistry of the Dithiasuccinoyl (Dts) Function. *J. Am. Chem. Soc.* **1977**, *99* (22), 7363–7365. https://doi.org/10.1021/ja00464a050.

(8) Kent, S. B. H.; Mitchell, A. R.; Engelhard, M.; Merrifield, R. B. Mechanisms and Prevention of Trifluoroacetylation in Solid-Phase Peptide Synthesis. *Proceedings of the National Academy of Sciences of the United States of America* **1979**, *76* (5), 2180–2184.

(9) Meienhofer, J. 3 - Peptide Synthesis: A Review of the Solid-Phase Method. In *Hormonal Proteins and Peptides*; Li, C. H., Ed.; Academic Press, 1973; pp 45–267. https://doi.org/10.1016/B978-0-12-447202-0.50009-0.

(10) Chang, C.-D.; Meienhofer, J. SOLID-PHASE PEPTIDE SYNTHESIS USING MILD BASE CLEAVAGE OF NαFLUORENYLMETHYLOXYCARBONYLAMINO ACIDS, EXEMPLIFIED BY A SYNTHESIS OF DIHYDROSOMATOSTATIN. *International Journal of Peptide and Protein Research* **1978**, *11* (3), 246–249. https://doi.org/10.1111/j.1399-3011.1978.tb02845.x.

(11) Carpino, L. A.; Han, G. Y. 9-Fluorenylmethoxycarbonyl Function, a New Base-Sensitive Amino-Protecting Group. *J. Am. Chem. Soc.* **1970**, *92* (19), 5748–5749. https://doi.org/10.1021/ja00722a043.

(12) Castro, B.; Dormoy, J. R.; Evin, G.; Selve, C. Reactifs de Couplage Peptidique I (1) - l'hexafluorophosphate de Benzotriazolyl N-Oxytrisdimethylamino Phosphonium (B.O.P.). *Tetrahedron Letters* **1975**, *16* (14), 1219–1222. https://doi.org/10.1016/S0040-4039(00)72100-9.

(13) Coste, J.; Le-Nguyen, D.; Castro, B. PyBOP®: A New Peptide Coupling Reagent Devoid of Toxic by-Product. *Tetrahedron Letters* **1990**, *31* (2), 205–208. https://doi.org/10.1016/S0040-4039(00)94371-5.

(14) König, W.; Geiger, R. Eine neue Methode zur Synthese von Peptiden: Aktivierung der Carboxylgruppe mit Dicyclohexylcarbodiimid unter Zusatz von 1-Hydroxy-benzotriazolen. *Chemische Berichte* **1970**, *103* (3), 788–798. https://doi.org/10.1002/cber.19701030319.

(15) Subirós-Funosas, R.; Prohens, R.; Barbas, R.; El-Faham, A.; Albericio, F. Oxyma: An Efficient Additive for Peptide Synthesis to Replace the Benzotriazole-Based HOBt and HOAt with a Lower Risk of Explosion[1]. *Chemistry – A European Journal* **2009**, *15* (37), 9394–9403. https://doi.org/10.1002/chem.200900614.

(16) Pearson, D. A.; Blanchette, M.; Baker, M. L.; Guindon, C. A. Trialkylsilanes as Scavengers for the Trifluoroacetic Acid Deblocking of Protecting Groups in Peptide Synthesis. *Tetrahedron Letters* **1989**, *30* (21), 2739–2742. https://doi.org/10.1016/S0040-4039(00)99113-5.
(17) Teixeira, A.; Benckhuijsen, W. E.; Koning, P. E. de; Valentijn, A. R. P. M.; Drijfhout, J. W. The Use of Dodt as a Non-Malodorous Scavenger in Fmoc-Based Peptide Synthesis. *Protein & Peptide Letters 9* (5), 379–385.
(18) Isidro-Llobet, A.; Álvarez, M.; Albericio, F. Amino Acid-Protecting Groups. *Chem. Rev.* **2009**, *109* (6), 2455–2504. https://doi.org/10.1021/cr800323s.
(19) El-Faham, A.; Albericio, F. Peptide Coupling Reagents, More than a Letter Soup. *Chem. Rev.* **2011**, *111* (11), 6557–6602. https://doi.org/10.1021/cr100048w.
(20) Albericio, F.; El-Faham, A. Choosing the Right Coupling Reagent for Peptides: A Twenty-Five-Year Journey. *Org. Process Res. Dev.* **2018**, *22* (7), 760–772. https://doi.org/10.1021/acs.oprd.8b00159.
(21) Agouridas, V.; El Mahdi, O.; Diemer, V.; Cargoët, M.; Monbaliu, J.-C. M.; Melnyk, O. Native Chemical Ligation and Extended Methods: Mechanisms, Catalysis, Scope, and Limitations. *Chem. Rev.* **2019**, *119* (12), 7328–7443. https://doi.org/10.1021/acs.chemrev.8b00712.
(22) Conibear, A. C.; Watson, E. E.; Payne, R. J.; Becker, C. F. W. Native Chemical Ligation in Protein Synthesis and Semi-Synthesis. *Chem. Soc. Rev.* **2018**, *47* (24), 9046–9068. https://doi.org/10.1039/C8CS00573G.
(23) Liu, H.; Li, X. Serine/Threonine Ligation: Origin, Mechanistic Aspects, and Applications. *Acc. Chem. Res.* **2018**, *51* (7), 1643–1655. https://doi.org/10.1021/acs.accounts.8b00151.
(24) Bechtler, C.; Lamers, C. Macrocyclization Strategies for Cyclic Peptides and Peptidomimetics. *RSC Med. Chem.* **2021**, *12* (8), 1325–1351. https://doi.org/10.1039/D1MD00083G.
(25) Lau, Y. H.; Andrade, P. de; Wu, Y.; Spring, D. R. Peptide Stapling Techniques Based on Different Macrocyclisation Chemistries. *Chem. Soc. Rev.* **2014**, *44* (1), 91–102. https://doi.org/10.1039/C4CS00246F.
(26) *News - ECHA*. https://echa.europa.eu/view-article/-/journal_content/title/9109026-58 (accessed 2023-10-04).
(27) Musaimi, O. A.; Torre, B. G. de la; Albericio, F. Greening Fmoc/tBu Solid-Phase Peptide Synthesis. *Green Chem.* **2020**, *22* (4), 996–1018. https://doi.org/10.1039/C9GC03982A.
(28) Martin, V.; Egelund, P. H. G.; Johansson, H.; Quement, S. T. L.; Wojcik, F.; Pedersen, D. S. Greening the Synthesis of Peptide Therapeutics: An Industrial Perspective. *RSC Adv.* **2020**, *10* (69), 42457–42492. https://doi.org/10.1039/D0RA07204D.
(29) Al Musaimi, O.; El-Faham, A.; Basso, A.; de la Torre, B. G.; Albericio, F. γ-Valerolactone (GVL): An Eco-Friendly Anchoring Solvent for Solid-Phase Peptide Synthesis. *Tetrahedron Letters* **2019**, *60* (38), 151058. https://doi.org/10.1016/j.tetlet.2019.151058.
(30) Lopez, J.; Pletscher, S.; Aemissegger, A.; Bucher, C.; Gallou, F. N-Butylpyrrolidinone as Alternative Solvent for Solid-Phase Peptide Synthesis. *Org. Process Res. Dev.* **2018**, *22* (4), 494–503. https://doi.org/10.1021/acs.oprd.7b00389.
(31) Jad, Y. E.; Acosta, G. A.; Govender, T.; Kruger, H. G.; El-Faham, A.; de la Torre, B. G.; Albericio, F. Green Solid-Phase Peptide Synthesis 2. 2-Methyltetrahydrofuran and Ethyl Acetate for Solid-Phase Peptide Synthesis under Green Conditions. *ACS Sustainable Chem. Eng.* **2016**, *4* (12), 6809–6814. https://doi.org/10.1021/acssuschemeng.6b01765.
(32) Pawlas, J.; Rasmussen, J. H. ReGreen SPPS: Enabling Circular Chemistry in Environmentally Sensible Solid-Phase Peptide Synthesis. *Green Chem.* **2019**, *21* (21), 5990–5998. https://doi.org/10.1039/C9GC02775K.
(33) Jadhav, S.; Martin, V.; Egelund, P. H. G.; Castro, H. J.; Krüger, T.; Richner, F.; Quement,

S. T. L.; Albericio, F.; Dettner, F.; Lechner, C.; Schönleber, R.; Pedersen, D. S. Replacing DMF in Solid-Phase Peptide Synthesis: Varying the Composition of Green Binary Solvent Mixtures as a Tool to Mitigate Common Side-Reactions. *Green Chem.* **2021**, *23* (9), 3312–3321. https://doi.org/10.1039/D1GC00604E.

(34) McFarland, A. D.; Buser, J. Y.; Embry, M. C.; Held, C. B.; Kolis, S. P. Generation of Hydrogen Cyanide from the Reaction of Oxyma (Ethyl Cyano(Hydroxyimino)Acetate) and DIC (Diisopropylcarbodiimide). *Org. Process Res. Dev.* **2019**, *23* (9), 2099–2105. https://doi.org/10.1021/acs.oprd.9b00344.

(35) Erny, M.; Lundqvist, M.; Rasmussen, J. H.; Ludemann-Hombourger, O.; Bihel, F.; Pawlas, J. Minimizing HCN in DIC/Oxyma-Mediated Amide Bond-Forming Reactions. *Org. Process Res. Dev.* **2020**, *24* (7), 1341–1349. https://doi.org/10.1021/acs.oprd.0c00227.

(36) Pawlas, J.; Rasmussen, J. H. Environmentally Sensible Organocatalytic Fmoc/t-Bu Solid-Phase Peptide Synthesis. *Org. Lett.* **2022**, *24* (9), 1827–1832. https://doi.org/10.1021/acs.orglett.2c00266.

(37) Manne, S. R.; Luna, O.; Acosta, G. A.; Royo, M.; El-Faham, A.; Orosz, G.; de la Torre, B. G.; Albericio, F. Amide Formation: Choosing the Safer Carbodiimide in Combination with OxymaPure to Avoid HCN Release. *Org. Lett.* **2021**, *23* (17), 6900–6904. https://doi.org/10.1021/acs.orglett.1c02466.

(38) Ralhan, K.; KrishnaKumar, V. G.; Gupta, S. Piperazine and DBU: A Safer Alternative for Rapid and Efficient Fmoc Deprotection in Solid Phase Peptide Synthesis. *RSC Adv.* **2015**, *5* (126), 104417–104425. https://doi.org/10.1039/C5RA23441G.

(39) Mthembu, S. N.; Chakraborty, A.; Schönleber, R.; Albericio, F.; de la Torre, B. G. Morpholine, a Strong Contender for Fmoc Removal in Solid-Phase Peptide Synthesis. *Journal of Peptide Science n/a* (n/a), e3538. https://doi.org/10.1002/psc.3538.

(40) Castañeda, J. E. G.; Galeano, C. F. V.; Monroy, Z. J. R.; Pérez, J. E. R. Efficient Synthesis of Peptides with 4-Methylpiperidine as Fmoc Removal Reagent by Solid Phase Synthesis. *Journal of the Mexican Chemical Society* **2014**, *58* (4). https://doi.org/10.29356/jmcs.v58i4.47.

(41) Egelund, P. H. G.; Jadhav, S.; Martin, V.; Johansson Castro, H.; Richner, F.; Le Quement, S. T.; Dettner, F.; Lechner, C.; Schoenleber, R.; Sejer Pedersen, D. Fmoc-Removal with Pyrrolidine Expands the Available Solvent Space in Green Solid-Phase Peptide Synthesis. *ACS Sustainable Chem. Eng.* **2021**, *9* (42), 14202–14215. https://doi.org/10.1021/acssuschemeng.1c04770.

(42) Jaradat, D. M. M.; Musaimi, O. A.; Albericio, F. Advances in Solid-Phase Peptide Synthesis in Aqueous Media (ASPPS). *Green Chem.* **2022**, *24* (17), 6360–6372. https://doi.org/10.1039/D2GC02319A.

(43) Raz, R.; Burlina, F.; Ismail, M.; Downward, J.; Li, J.; Smerdon, S. J.; Quibell, M.; White, P. D.; Offer, J. HF-Free Boc Synthesis of Peptide Thioesters for Ligation and Cyclization. *Angewandte Chemie International Edition* **2016**, *55* (42), 13174–13179. https://doi.org/10.1002/anie.201607657.

(44) Kumar, A.; Sharma, A.; Torre, B. G. de la; Albericio, F. In Situ Fmoc Removal – a Sustainable Solid-Phase Peptide Synthesis Approach. *Green Chem.* **2022**, *24* (12), 4887–4896. https://doi.org/10.1039/D2GC00963C.

(45) *Speciality Chemicals Magazine JAN / FEB 2022 | Seite 40*. Joomag. https://viewer.joomag.com/speciality-chemicals-magazine-jan-feb-2022/0923309001642110848?page=40 (accessed 2023-10-03).

(46) Galdiero, S.; Falanga, A.; Cantisani, M.; Tarallo, R.; Pepa, M. E. D.; D'Oriano, V.; Galdiero, M. Microbe-Host Interactions: Structure and Role of Gram-Negative Bacterial Porins. *Current Protein & Peptide Science 13* (8), 843–854.

(47) Silhavy, T. J.; Kahne, D.; Walker, S. The Bacterial Cell Envelope. *Cold Spring Harb*

Perspect Biol **2010**, *2* (5), a000414. https://doi.org/10.1101/cshperspect.a000414.
(48) Miller, S. I. Antibiotic Resistance and Regulation of the Gram-Negative Bacterial Outer Membrane Barrier by Host Innate Immune Molecules. *mBio* **2016**, *7* (5), 10.1128/mbio.01541-16. https://doi.org/10.1128/mbio.01541-16.
(49) Exner, M.; Bhattacharya, S.; Christiansen, B.; Gebel, J.; Goroncy-Bermes, P.; Hartemann, P.; Heeg, P.; Ilschner, C.; Kramer, A.; Larson, E.; Merkens, W.; Mielke, M.; Oltmanns, P.; Ross, B.; Rotter, M.; Schmithausen, R. M.; Sonntag, H.-G.; Trautmann, M. Antibiotic Resistance: What Is so Special about Multidrug-Resistant Gram-Negative Bacteria? *GMS Hyg Infect Control* **2017**, *12*, Doc05. https://doi.org/10.3205/dgkh000290.
(50) Ikuta, K. S. *et al.* Global Mortality Associated with 33 Bacterial Pathogens in 2019: A Systematic Analysis for the Global Burden of Disease Study 2019. *The Lancet* **2022**, *400* (10369), 2221–2248. https://doi.org/10.1016/S0140-6736(22)02185-7.
(51) Paterson, D. L.; Doi, Y. A Step Closer to Extreme Drug Resistance (XDR) in Gram-Negative Bacilli. *Clinical Infectious Diseases* **2007**, *45* (9), 1179–1181. https://doi.org/10.1086/522287.
(52) Magiorakos, A.-P.; Srinivasan, A.; Carey, R. B.; Carmeli, Y.; Falagas, M. E.; Giske, C. G.; Harbarth, S.; Hindler, J. F.; Kahlmeter, G.; Olsson-Liljequist, B.; Paterson, D. L.; Rice, L. B.; Stelling, J.; Struelens, M. J.; Vatopoulos, A.; Weber, J. T.; Monnet, D. L. Multidrug-Resistant, Extensively Drug-Resistant and Pandrug-Resistant Bacteria: An International Expert Proposal for Interim Standard Definitions for Acquired Resistance. *Clinical Microbiology and Infection* **2012**, *18* (3), 268–281. https://doi.org/10.1111/j.1469-0691.2011.03570.x.
(53) Reygaert, W. C. An Overview of the Antimicrobial Resistance Mechanisms of Bacteria. *AIMSMICRO* **2018**, *4* (3), 482–501. https://doi.org/10.3934/microbiol.2018.3.482.
(54) Ayoub Moubareck, C. Polymyxins and Bacterial Membranes: A Review of Antibacterial Activity and Mechanisms of Resistance. *Membranes* **2020**, *10* (8), 181. https://doi.org/10.3390/membranes10080181.
(55) Pasupuleti, M.; Schmidtchen, A.; Malmsten, M. Antimicrobial Peptides: Key Components of the Innate Immune System. *Critical Reviews in Biotechnology* **2012**, *32* (2), 143–171. https://doi.org/10.3109/07388551.2011.594423.
(56) Huan, Y.; Kong, Q.; Mou, H.; Yi, H. Antimicrobial Peptides: Classification, Design, Application and Research Progress in Multiple Fields. *Frontiers in Microbiology* **2020**, *11*.
(57) Gan, B. H.; Gaynord, J.; Rowe, S. M.; Deingruber, T.; Spring, D. R. The Multifaceted Nature of Antimicrobial Peptides: Current Synthetic Chemistry Approaches and Future Directions. *Chem. Soc. Rev.* **2021**, *50* (13), 7820–7880. https://doi.org/10.1039/D0CS00729C.
(58) Pirtskhalava, M.; Amstrong, A. A.; Grigolava, M.; Chubinidze, M.; Alimbarashvili, E.; Vishnepolsky, B.; Gabrielian, A.; Rosenthal, A.; Hurt, D. E.; Tartakovsky, M. DBAASP v3: Database of Antimicrobial/Cytotoxic Activity and Structure of Peptides as a Resource for Development of New Therapeutics. *Nucleic Acids Research* **2021**, *49* (D1), D288–D297. https://doi.org/10.1093/nar/gkaa991.
(59) Ramazi, S.; Mohammadi, N.; Allahverdi, A.; Khalili, E.; Abdolmaleki, P. A Review on Antimicrobial Peptides Databases and the Computational Tools. *Database* **2022**, *2022*, baac011. https://doi.org/10.1093/database/baac011.
(60) Zhang, Q.-Y.; Yan, Z.-B.; Meng, Y.-M.; Hong, X.-Y.; Shao, G.; Ma, J.-J.; Cheng, X.-R.; Liu, J.; Kang, J.; Fu, C.-Y. Antimicrobial Peptides: Mechanism of Action, Activity and Clinical Potential. *Military Medical Research* **2021**, *8* (1), 48. https://doi.org/10.1186/s40779-021-00343-2.
(61) Epand, R. M.; Walker, C.; Epand, R. F.; Magarvey, N. A. Molecular Mechanisms of Membrane Targeting Antibiotics. *Biochimica et Biophysica Acta (BBA) - Biomembranes*

2016, *1858* (5), 980–987. https://doi.org/10.1016/j.bbamem.2015.10.018.
(62) Gaspar, D.; Veiga, A. S.; Castanho, M. A. R. B. From Antimicrobial to Anticancer Peptides. A Review. *Front. Microbiol.* **2013**, *4*. https://doi.org/10.3389/fmicb.2013.00294.
(63) Kang, S.-J.; Park, S. J.; Mishig-Ochir, T.; Lee, B.-J. Antimicrobial Peptides: Therapeutic Potentials. *Expert Review of Anti-infective Therapy* **2014**, *12* (12), 1477–1486. https://doi.org/10.1586/14787210.2014.976613.
(64) Shai, Y.; Oren, Z. Diastereomers of Cytolysins, a Novel Class of Potent Antibacterial Peptides (∗). *Journal of Biological Chemistry* **1996**, *271* (13), 7305–7308. https://doi.org/10.1074/jbc.271.13.7305.
(65) Hong, J.; Oren, Z.; Shai, Y. Structure and Organization of Hemolytic and Nonhemolytic Diastereomers of Antimicrobial Peptides in Membranes. *Biochemistry* **1999**, *38* (51), 16963–16973. https://doi.org/10.1021/bi991850y.
(66) Pratap Verma, D.; Ansari, M. M.; Verma, N. K.; Saroj, J.; Akhtar, S.; Pant, G.; Mitra, K.; Singh, B. N.; Ghosh, J. K. Tandem Repeat of a Short Human Chemerin-Derived Peptide and Its Nontoxic d-Lysine-Containing Enantiomer Display Broad-Spectrum Antimicrobial and Antitubercular Activities. *J. Med. Chem.* **2021**, *64* (20), 15349–15366. https://doi.org/10.1021/acs.jmedchem.1c01352.
(67) Slingerland, C. J.; Kotsogianni, I.; Wesseling, C. M. J.; Martin, N. I. Polymyxin Stereochemistry and Its Role in Antibacterial Activity and Outer Membrane Disruption. *ACS Infect. Dis.* **2022**, *8* (12), 2396–2404. https://doi.org/10.1021/acsinfecdis.2c00307.
(68) Guo, X.; Yan, T.; Rao, J.; An, Y.; Yue, X.; Miao, X.; Wang, R.; Sun, W.; Cai, J.; Xie, J. Novel Feleucin-K3-Derived Peptides Modified with Sulfono-γ-AA Building Blocks Targeting Pseudomonas Aeruginosa and Methicillin-Resistant Staphylococcus Aureus Infections. *J. Med. Chem.* **2023**, *66* (2), 1254–1272. https://doi.org/10.1021/acs.jmedchem.2c01396.
(69) Chongsiriwatana, N. P.; Patch, J. A.; Czyzewski, A. M.; Dohm, M. T.; Ivankin, A.; Gidalevitz, D.; Zuckermann, R. N.; Barron, A. E. Peptoids That Mimic the Structure, Function, and Mechanism of Helical Antimicrobial Peptides. *Proceedings of the National Academy of Sciences* **2008**, *105* (8), 2794–2799. https://doi.org/10.1073/pnas.0708254105.
(70) Nielsen, J. E.; Alford, M. A.; Yung, D. B. Y.; Molchanova, N.; Fortkort, J. A.; Lin, J. S.; Diamond, G.; Hancock, R. E. W.; Jenssen, H.; Pletzer, D.; Lund, R.; Barron, A. E. Self-Assembly of Antimicrobial Peptoids Impacts Their Biological Effects on ESKAPE Bacterial Pathogens. *ACS Infect. Dis.* **2022**, *8* (3), 533–545. https://doi.org/10.1021/acsinfecdis.1c00536.
(71) Nyembe, P. L.; Ntombela, T.; Makatini, M. M. Review: Structure-Activity Relationship of Antimicrobial Peptoids. *Pharmaceutics* **2023**, *15* (5), 1506. https://doi.org/10.3390/pharmaceutics15051506.
(72) Bolt, H. L.; Eggimann, G. A.; Jahoda, C. a. B.; Zuckermann, R. N.; Sharples, G. J.; Cobb, S. L. Exploring the Links between Peptoid Antibacterial Activity and Toxicity. *Med. Chem. Commun.* **2017**, *8* (5), 886–896. https://doi.org/10.1039/C6MD00648E.
(73) Mourtada, R.; Herce, H. D.; Yin, D. J.; Moroco, J. A.; Wales, T. E.; Engen, J. R.; Walensky, L. D. Design of Stapled Antimicrobial Peptides That Are Stable, Nontoxic and Kill Antibiotic-Resistant Bacteria in Mice. *Nat Biotechnol* **2019**, *37* (10), 1186–1197. https://doi.org/10.1038/s41587-019-0222-z.
(74) Li, H.; Hu, Y.; Pu, Q.; He, T.; Zhang, Q.; Wu, W.; Xia, X.; Zhang, J. Novel Stapling by Lysine Tethering Provides Stable and Low Hemolytic Cationic Antimicrobial Peptides. *J. Med. Chem.* **2020**, *63* (8), 4081–4089. https://doi.org/10.1021/acs.jmedchem.9b02025.
(75) He, T.; Xu, L.; Hu, Y.; Tang, X.; Qu, R.; Zhao, X.; Bai, H.; Li, L.; Chen, W.; Luo, G.; Fu, G.; Wang, W.; Xia, X.; Zhang, J. Lysine-Tethered Stable Bicyclic Cationic Antimicrobial Peptide Combats Bacterial Infection in Vivo. *J. Med. Chem.* **2022**, *65* (15), 10523–10533.

https://doi.org/10.1021/acs.jmedchem.2c00661.
(76) Schouten, G. K.; Paulussen, F. M.; Kuipers, O. P.; Bitter, W.; Grossmann, T. N.; van Ulsen, P. Stapling of Peptides Potentiates the Antibiotic Treatment of Acinetobacter Baumannii In Vivo. *Antibiotics* **2022**, *11* (2), 273. https://doi.org/10.3390/antibiotics11020273.
(77) Selvarajan, V.; Tram, N. D. T.; Xu, J.; Ngen, S. T. Y.; Koh, J.-J.; Teo, J. W. P.; Yuen, T.-Y.; Ee, P. L. R. Stapled β-Hairpin Antimicrobial Peptides with Improved Stability and Activity against Drug-Resistant Gram-Negative Bacteria. *J. Med. Chem.* **2023**, *66* (13), 8498–8509. https://doi.org/10.1021/acs.jmedchem.3c00140.
(78) Yokoo, H.; Hirano, M.; Misawa, T.; Demizu, Y. Helical Antimicrobial Peptide Foldamers Containing Non-Proteinogenic Amino Acids. *ChemMedChem* **2021**, *16* (8), 1226–1233. https://doi.org/10.1002/cmdc.202000940.
(79) Mensa, B.; Kim, Y. H.; Choi, S.; Scott, R.; Caputo, G. A.; DeGrado, W. F. Antibacterial Mechanism of Action of Arylamide Foldamers. *Antimicrobial Agents and Chemotherapy* **2011**, *55* (11), 5043–5053. https://doi.org/10.1128/aac.05009-11.
(80) Tew, G. N.; Scott, R. W.; Klein, M. L.; DeGrado, W. F. De Novo Design of Antimicrobial Polymers, Foldamers, and Small Molecules: From Discovery to Practical Applications. *Acc. Chem. Res.* **2010**, *43* (1), 30–39. https://doi.org/10.1021/ar900036b.
(81) Juretić, D.; Vukičević, D.; Ilić, N.; Antcheva, N.; Tossi, A. Computational Design of Highly Selective Antimicrobial Peptides. *J. Chem. Inf. Model.* **2009**, *49* (12), 2873–2882. https://doi.org/10.1021/ci900327a.
(82) Capecchi, A.; Cai, X.; Personne, H.; Köhler, T.; Delden, C. van; Reymond, J.-L. Machine Learning Designs Non-Hemolytic Antimicrobial Peptides. *Chem. Sci.* **2021**, *12* (26), 9221–9232. https://doi.org/10.1039/D1SC01713F.
(83) Vishnepolsky, B.; Pirtskhalava, M. Prediction of Linear Cationic Antimicrobial Peptides Based on Characteristics Responsible for Their Interaction with the Membranes. *J. Chem. Inf. Model.* **2014**, *54* (5), 1512–1523. https://doi.org/10.1021/ci4007003.
(84) Aronica, P. G. A.; Reid, L. M.; Desai, N.; Li, J.; Fox, S. J.; Yadahalli, S.; Essex, J. W.; Verma, C. S. Computational Methods and Tools in Antimicrobial Peptide Research. *J. Chem. Inf. Model.* **2021**, *61* (7), 3172–3196. https://doi.org/10.1021/acs.jcim.1c00175.
(85) Kavousi, K.; Bagheri, M.; Behrouzi, S.; Vafadar, S.; Atanaki, F. F.; Lotfabadi, B. T.; Ariaeenejad, S.; Shockravi, A.; Moosavi-Movahedi, A. A. IAMPE: NMR-Assisted Computational Prediction of Antimicrobial Peptides. *J. Chem. Inf. Model.* **2020**, *60* (10), 4691–4701. https://doi.org/10.1021/acs.jcim.0c00841.
(86) Thomas, J. M. The Birth of X-Ray Crystallography. *Nature* **2012**, *491* (7423), 186–187. https://doi.org/10.1038/491186a.
(87) Cowtan, K. Phase Problem in X-Ray Crystallography, and Its Solution. In *Encyclopedia of Life Sciences*; John Wiley & Sons, Ltd, 2003. https://doi.org/10.1038/npg.els.0002722.
(88) Murata, K.; Wolf, M. Cryo-Electron Microscopy for Structural Analysis of Dynamic Biological Macromolecules. *Biochimica et Biophysica Acta (BBA) - General Subjects* **2018**, *1862* (2), 324–334. https://doi.org/10.1016/j.bbagen.2017.07.020.
(89) Renaud, J.-P.; Chari, A.; Ciferri, C.; Liu, W.; Rémigy, H.-W.; Stark, H.; Wiesmann, C. Cryo-EM in Drug Discovery: Achievements, Limitations and Prospects. *Nat Rev Drug Discov* **2018**, *17* (7), 471–492. https://doi.org/10.1038/nrd.2018.77.
(90) Jumper, J.; Evans, R.; Pritzel, A.; Green, T.; Figurnov, M.; Ronneberger, O.; Tunyasuvunakool, K.; Bates, R.; Žídek, A.; Potapenko, A.; Bridgland, A.; Meyer, C.; Kohl, S. A. A.; Ballard, A. J.; Cowie, A.; Romera-Paredes, B.; Nikolov, S.; Jain, R.; Adler, J.; Back, T.; Petersen, S.; Reiman, D.; Clancy, E.; Zielinski, M.; Steinegger, M.; Pacholska, M.; Berghammer, T.; Bodenstein, S.; Silver, D.; Vinyals, O.; Senior, A. W.; Kavukcuoglu, K.; Kohli, P.; Hassabis, D. Highly Accurate Protein Structure Prediction with AlphaFold. *Nature* **2021**, *596* (7873), 583–589. https://doi.org/10.1038/s41586-021-03819-2.

(91) Tunyasuvunakool, K.; Adler, J.; Wu, Z.; Green, T.; Zielinski, M.; Žídek, A.; Bridgland, A.; Cowie, A.; Meyer, C.; Laydon, A.; Velankar, S.; Kleywegt, G. J.; Bateman, A.; Evans, R.; Pritzel, A.; Figurnov, M.; Ronneberger, O.; Bates, R.; Kohl, S. A. A.; Potapenko, A.; Ballard, A. J.; Romera-Paredes, B.; Nikolov, S.; Jain, R.; Clancy, E.; Reiman, D.; Petersen, S.; Senior, A. W.; Kavukcuoglu, K.; Birney, E.; Kohli, P.; Jumper, J.; Hassabis, D. Highly Accurate Protein Structure Prediction for the Human Proteome. *Nature* **2021**, *596* (7873), 590–596. https://doi.org/10.1038/s41586-021-03828-1.

(92) Chayen, N. E.; Saridakis, E. Protein Crystallization: From Purified Protein to Diffraction-Quality Crystal. *Nat Methods* **2008**, *5* (2), 147–153. https://doi.org/10.1038/nmeth.f.203.

(93) Benedetti, E. X-Ray Crystallography of Peptides: The Contributions of the Italian Laboratories. *Peptide Science* **1996**, *40* (1), 3–44. https://doi.org/10.1002/(SICI)1097-0282(1996)40:1<3::AID-BIP2>3.0.CO;2-#.

(94) Baeriswyl, S.; Gan, B.-H.; Siriwardena, T. N.; Visini, R.; Robadey, M.; Javor, S.; Stocker, A.; Darbre, T.; Reymond, J.-L. X-Ray Crystal Structures of Short Antimicrobial Peptides as Pseudomonas Aeruginosa Lectin B Complexes. *ACS Chem. Biol.* **2019**, *14* (4), 758–766. https://doi.org/10.1021/acschembio.9b00047.

(95) He, R.; Bonaventura, I. D.; Visini, R.; Gan, B.-H.; Fu, Y.; Probst, D.; Lüscher, A.; Köhler, T.; Delden, C. van; Stocker, A.; Hong, W.; Darbre, T.; Reymond, J.-L. Design, Crystal Structure and Atomic Force Microscopy Study of Thioether Ligated D,L-Cyclic Antimicrobial Peptides against Multidrug Resistant Pseudomonas Aeruginosa. *Chem. Sci.* **2017**, *8* (11), 7464–7475. https://doi.org/10.1039/C7SC01599B.

(96) Baeriswyl, S.; Personne, H.; Bonaventura, I. D.; Köhler, T.; Delden, C. van; Stocker, A.; Javor, S.; Reymond, J.-L. A Mixed Chirality α-Helix in a Stapled Bicyclic and a Linear Antimicrobial Peptide Revealed by X-Ray Crystallography. *RSC Chem. Biol.* **2021**, *2* (6), 1608–1617. https://doi.org/10.1039/D1CB00124H.

(97) Baeriswyl, S.; Javor, S.; Stocker, A.; Darbre, T.; Reymond, J.-L. X-Ray Crystal Structure of a Second-Generation Peptide Dendrimer in Complex with Pseudomonas Aeruginosa Lectin LecB. *Helvetica Chimica Acta* **2019**, *102* (9), e1900178. https://doi.org/10.1002/hlca.201900178.

(98) Nanda, V.; DeGrado, W. F. Computational Design of Heterochiral Peptides against a Helical Target. *J. Am. Chem. Soc.* **2006**, *128* (3), 809–816. https://doi.org/10.1021/ja054452t.

(99) Shepherd, N. E.; Hoang, H. N.; Abbenante, G.; Fairlie, D. P. Left- and Right-Handed Alpha-Helical Turns in Homo- and Hetero-Chiral Helical Scaffolds. *J. Am. Chem. Soc.* **2009**, *131* (43), 15877–15886. https://doi.org/10.1021/ja9065283.

(100) Ketchem, R. R.; Hu, W.; Cross, T. A. High-Resolution Conformation of Gramicidin A in a Lipid Bilayer by Solid-State NMR. *Science* **1993**, *261* (5127), 1457–1460. https://doi.org/10.1126/science.7690158.

(101) Allen, T. W.; Andersen, O. S.; Roux, B. Structure of Gramicidin A in a Lipid Bilayer Environment Determined Using Molecular Dynamics Simulations and Solid-State NMR Data. *J. Am. Chem. Soc.* **2003**, *125* (32), 9868–9877. https://doi.org/10.1021/ja029317k.

(102) Takada, Y.; Itoh, H.; Paudel, A.; Panthee, S.; Hamamoto, H.; Sekimizu, K.; Inoue, M. Discovery of Gramicidin A Analogues with Altered Activities by Multidimensional Screening of a One-Bead-One-Compound Library. *Nat Commun* **2020**, *11* (1), 4935. https://doi.org/10.1038/s41467-020-18711-2.

(103) Zhou, P.; Hu, X.; Li, J.; Wang, Y.; Yu, H.; Chen, Z.; Wang, D.; Zhao, Y.; King, S. M.; Rogers, S. E.; Wang, J.; Lu, J. R.; Xu, H. Peptide Self-Assemblies from Unusual α-Sheet Conformations Based on Alternation of d/l Amino Acids. *J. Am. Chem. Soc.* **2022**, *144* (47), 21544–21554. https://doi.org/10.1021/jacs.2c08425.

(104) Clover, T. M.; O'Neill, C. L.; Appavu, R.; Lokhande, G.; Gaharwar, A. K.; Posey, A.

E.; White, M. A.; Rudra, J. S. Self-Assembly of Block Heterochiral Peptides into Helical Tapes. *J. Am. Chem. Soc.* **2020**, *142* (47), 19809–19813. https://doi.org/10.1021/jacs.9b09755.

(105) Fernandez-Lopez, S.; Kim, H.-S.; Choi, E. C.; Delgado, M.; Granja, J. R.; Khasanov, A.; Kraehenbuehl, K.; Long, G.; Weinberger, D. A.; Wilcoxen, K. M.; Ghadiri, M. R. Antibacterial Agents Based on the Cyclic D,L-α-Peptide Architecture. *Nature* **2001**, *412* (6845), 452–455. https://doi.org/10.1038/35086601.

(106) Kurbasic, M.; Garcia, A. M.; Viada, S.; Marchesan, S. Heterochiral Tetrapeptide Self-Assembly into Hydrogel Biomaterials for Hydrolase Mimicry. *Journal of Peptide Science* **2022**, *28* (1), e3304. https://doi.org/10.1002/psc.3304.

(107) Demizu, Y.; Yabuki, Y.; Doi, M.; Sato, Y.; Tanaka, M.; Kurihara, M. Conformations of Helical Aib Peptides Containing a Pair of L-Amino Acid and d-Amino Acid. *Journal of Peptide Science* **2012**, *18* (7), 466–475. https://doi.org/10.1002/psc.2418.

(108) Demizu, Y.; Yamashita, H.; Doi, M.; Misawa, T.; Oba, M.; Tanaka, M.; Kurihara, M. Topological Study of the Structures of Heterochiral Peptides Containing Equal Amounts of L-Leu and d-Leu. *J. Org. Chem.* **2015**, *80* (17), 8597–8603. https://doi.org/10.1021/acs.joc.5b01541.

(109) Demizu, Y.; Okitsu, K.; Doi, M.; Misawa, T.; Oba, M.; Tanaka, M.; Kurihara, M. Influence of L-Leu to D-Leu Replacement on the Helical Secondary Structures of L-Leu-Aib-Based Dodecapeptides. *ChemistrySelect* **2016**, *1* (18), 5805–5811. https://doi.org/10.1002/slct.201601493.

(110) Aravinda, S.; Shamala, N.; Desiraju, S.; Balaram, P. A Right Handed Peptide Helix Containing a Central Double D-Amino Acid Segment. *Chem. Commun.* **2002**, No. 20, 2454–2455. https://doi.org/10.1039/B207960G.

(111) Karle, I. L.; Gopi, H. N.; Balaram, P. Crystal Structure of a Hydrophobic 19-Residue Peptide Helix Containing Three Centrally Located d Amino Acids. *Proceedings of the National Academy of Sciences* **2003**, *100* (24), 13946–13951. https://doi.org/10.1073/pnas.2336106100.

(112) Partridge, A. W.; Kaan, H. Y. K.; Juang, Y.-C.; Sadruddin, A.; Lim, S.; Brown, C. J.; Ng, S.; Thean, D.; Ferrer, F.; Johannes, C.; Yuen, T. Y.; Kannan, S.; Aronica, P.; Tan, Y. S.; Pradhan, M. R.; Verma, C. S.; Hochman, J.; Chen, S.; Wan, H.; Ha, S.; Sherborne, B.; Lane, D. P.; Sawyer, T. K. Incorporation of Putative Helix-Breaking Amino Acids in the Design of Novel Stapled Peptides: Exploring Biophysical and Cellular Permeability Properties. *Molecules* **2019**, *24* (12), 2292. https://doi.org/10.3390/molecules24122292.

(113) Guardiola, S.; Seco, J.; Varese, M.; Díaz-Lobo, M.; García, J.; Teixidó, M.; Nevola, L.; Giralt, E. Toward a Novel Drug To Target the EGF–EGFR Interaction: Design of Metabolically Stable Bicyclic Peptides. *ChemBioChem* **2018**, *19* (1), 76–84. https://doi.org/10.1002/cbic.201700519.

(114) Xu, L.; Li, C.; An, L.; Dai, Z.; Chen, X.; You, Q.; Hu, C.; Di, B. Selective Apoptosis-Inducing Activity of Synthetic Hydrocarbon-Stapled SOS1 Helix with d-Amino Acids in H358 Cancer Cells Expressing KRASG12C. *European Journal of Medicinal Chemistry* **2020**, *185*, 111844. https://doi.org/10.1016/j.ejmech.2019.111844.

(115) Chen, Y.; Mant, C. T.; Hodges, R. S. Determination of Stereochemistry Stability Coefficients of Amino Acid Side-Chains in an Amphipathic α-Helix. *The Journal of Peptide Research* **2002**, *59* (1), 18–33. https://doi.org/10.1046/j.1397-002x.2001.10994.x.

(116) Huang, Y.; Huang, J.; Chen, Y. Alpha-Helical Cationic Antimicrobial Peptides: Relationships of Structure and Function. *Protein Cell* **2010**, *1* (2), 143–152. https://doi.org/10.1007/s13238-010-0004-3.

(117) Shai, Y.; Oren, Z. Diastereomers of Cytolysins, a Novel Class of Potent Antibacterial Peptides (∗). *J. Biol. Chem.* **1996**, *271* (13), 7305–7308.

https://doi.org/10.1074/jbc.271.13.7305.
(118) Oren, Z.; Hong, J.; Shai, Y. A Repertoire of Novel Antibacterial Diastereomeric Peptides with Selective Cytolytic Activity*. *Journal of Biological Chemistry* **1997**, *272* (23), 14643–14649. https://doi.org/10.1074/jbc.272.23.14643.
(119) Shai, Y.; Oren, Z. From "Carpet" Mechanism to de-Novo Designed Diastereomeric Cell-Selective Antimicrobial Peptides. *Peptides* **2001**, *22* (10), 1629–1641. https://doi.org/10.1016/S0196-9781(01)00498-3.
(120) Pag, U.; Oedenkoven, M.; Papo, N.; Oren, Z.; Shai, Y.; Sahl, H.-G. In Vitro Activity and Mode of Action of Diastereomeric Antimicrobial Peptides against Bacterial Clinical Isolates. *Journal of Antimicrobial Chemotherapy* **2004**, *53* (2), 230–239. https://doi.org/10.1093/jac/dkh083.
(121) Wang, P.; Nan, Y. H.; Yang, S.-T.; Kang, S. W.; Kim, Y.; Park, I.-S.; Hahm, K.-S.; Shin, S. Y. Cell Selectivity and Anti-Inflammatory Activity of a Leu/Lys-Rich α-Helical Model Antimicrobial Peptide and Its Diastereomeric Peptides. *Peptides* **2010**, *31* (7), 1251–1261. https://doi.org/10.1016/j.peptides.2010.03.032.
(122) Oren, Z.; Shai, Y. Cyclization of a Cytolytic Amphipathic α-Helical Peptide and Its Diastereomer: Effect on Structure, Interaction with Model Membranes, and Biological Function. *Biochemistry* **2000**, *39* (20), 6103–6114. https://doi.org/10.1021/bi992408i.
(123) Papo, N.; Oren, Z.; Pag, U.; Sahl, H.-G.; Shai, Y. The Consequence of Sequence Alteration of an Amphipathic α-Helical Antimicrobial Peptide and Its Diastereomers*. *Journal of Biological Chemistry* **2002**, *277* (37), 33913–33921. https://doi.org/10.1074/jbc.M204928200.
(124) Papo, N.; Shai, Y. A Molecular Mechanism for Lipopolysaccharide Protection of Gram-Negative Bacteria from Antimicrobial Peptides*. *Journal of Biological Chemistry* **2005**, *280* (11), 10378–10387. https://doi.org/10.1074/jbc.M412865200.
(125) Oren, Z.; Shai, Y. Mode of Action of Linear Amphipathic α-Helical Antimicrobial Peptides. *Peptide Science* **1998**, *47* (6), 451–463. https://doi.org/10.1002/(SICI)1097-0282(1998)47:6<451::AID-BIP4>3.0.CO;2-F.
(126) Di Bonaventura, I.; Baeriswyl, S.; Capecchi, A.; Gan, B.-H.; Jin, X.; Siriwardena, T. N.; He, R.; Kohler, T.; Pompilio, A.; Di Bonaventura, G.; van Delden, C.; Javor, S.; Reymond, J.-L. An Antimicrobial Bicyclic Peptide from Chemical Space Against Multidrug Resistant Gram-Negative Bacteria. *Chem. Commun.* **2018**, *54*, 5130–5133. https://doi.org/10.1039/c8cc02412j.
(127) He, R.; Bonaventura, I. D.; Visini, R.; Gan, B.-H.; Fu, Y.; Probst, D.; Lüscher, A.; Köhler, T.; Delden, C. van; Stocker, A.; Hong, W.; Darbre, T.; Reymond, J.-L. Design, Crystal Structure and Atomic Force Microscopy Study of Thioether Ligated D,L-Cyclic Antimicrobial Peptides against Multidrug Resistant Pseudomonas Aeruginosa. *Chem. Sci.* **2017**, *8* (11), 7464–7475. https://doi.org/10.1039/C7SC01599B.
(128) Bonaventura, I. D.; Jin, X.; Visini, R.; Probst, D.; Javor, S.; Gan, B.-H.; Michaud, G.; Natalello, A.; Doglia, S. M.; Köhler, T.; Delden, C. van; Stocker, A.; Darbre, T.; Reymond, J.-L. Chemical Space Guided Discovery of Antimicrobial Bridged Bicyclic Peptides against Pseudomonas Aeruginosa and Its Biofilms. *Chem. Sci.* **2017**, *8* (10), 6784–6798. https://doi.org/10.1039/C7SC01314K.
(129) Lakemeyer, M.; Zhao, W.; Mandl, F. A.; Hammann, P.; Sieber, S. A. Thinking Outside the Box—Novel Antibacterials To Tackle the Resistance Crisis. *Angew. Chem., Int. Ed. Engl.* **2018**, *57* (44), 14440–14475. https://doi.org/10.1002/anie.201804971.
(130) Magana, M.; Pushpanathan, M.; Santos, A. L.; Leanse, L.; Fernandez, M.; Ioannidis, A.; Giulianotti, M. A.; Apidianakis, Y.; Bradfute, S.; Ferguson, A. L.; Cherkasov, A.; Seleem, M. N.; Pinilla, C.; de la Fuente-Nunez, C.; Lazaridis, T.; Dai, T.; Houghten, R. A.; Hancock, R. E. W.; Tegos, G. P. The Value of Antimicrobial Peptides in the Age of

Resistance. *The Lancet Infectious Diseases* **2020**, *20* (9), e216–e230. https://doi.org/10.1016/S1473-3099(20)30327-3.
(131) Mookherjee, N.; Anderson, M. A.; Haagsman, H. P.; Davidson, D. J. Antimicrobial Host Defence Peptides: Functions and Clinical Potential. *Nat Rev Drug Discov* **2020**, *19* (5), 311–332. https://doi.org/10.1038/s41573-019-0058-8.
(132) Lakshmaiah Narayana, J.; Mishra, B.; Lushnikova, T.; Wu, Q.; Chhonker, Y. S.; Zhang, Y.; Zarena, D.; Salnikov, E. S.; Dang, X.; Wang, F.; Murphy, C.; Foster, K. W.; Gorantla, S.; Bechinger, B.; Murry, D. J.; Wang, G. Two Distinct Amphipathic Peptide Antibiotics with Systemic Efficacy. *Proc. Natl. Acad. Sci. U. S. A.* **2020**, *117* (32), 19446–19454. https://doi.org/10.1073/pnas.2005540117.
(133) Ouyang, X.; Li, B.; Yang, Y.; Ba, Z.; Zhang, J.; Zhang, T.; Chang, L.; Zhang, F.; Zhang, Y.; Liu, H.; Gou, S.; Ni, J. Improving the Antimicrobial Performance of Amphiphilic Cationic Antimicrobial Peptides Using Glutamic Acid Full-Scan and Positive Charge Compensation Strategies. *J. Med. Chem.* **2022**, *65* (20), 13833–13851. https://doi.org/10.1021/acs.jmedchem.2c01076.
(134) Li, B.; Ouyang, X.; Ba, Z.; Yang, Y.; Zhang, J.; Liu, H.; Zhang, T.; Zhang, F.; Zhang, Y.; Gou, S.; Ni, J. Novel β-Hairpin Antimicrobial Peptides Containing the β-Turn Sequence of -RRRF- Having High Cell Selectivity and Low Incidence of Drug Resistance. *J. Med. Chem.* **2022**, *65* (7), 5625–5641. https://doi.org/10.1021/acs.jmedchem.1c02140.
(135) Zhang, M.; Ouyang, J.; Fu, L.; Xu, C.; Ge, Y.; Sun, S.; Li, X.; Lai, S.; Ke, H.; Yuan, B.; Yang, K.; Yu, H.; Gao, L.; Wang, Y. Hydrophobicity Determines the Bacterial Killing Rate of α-Helical Antimicrobial Peptides and Influences the Bacterial Resistance Development. *J. Med. Chem.* **2022**, *65* (21), 14701–14720. https://doi.org/10.1021/acs.jmedchem.2c01238.
(136) Pratap Verma, D.; Ansari, M. M.; Verma, N. K.; Saroj, J.; Akhtar, S.; Pant, G.; Mitra, K.; Singh, B. N.; Ghosh, J. K. Tandem Repeat of a Short Human Chemerin-Derived Peptide and Its Nontoxic d-Lysine-Containing Enantiomer Display Broad-Spectrum Antimicrobial and Antitubercular Activities. *J. Med. Chem.* **2021**, *64* (20), 15349–15366. https://doi.org/10.1021/acs.jmedchem.1c01352.
(137) Ben Hur, D.; Kapach, G.; Wani, N. A.; Kiper, E.; Ashkenazi, M.; Smollan, G.; Keller, N.; Efrati, O.; Shai, Y. Antimicrobial Peptides against Multidrug-Resistant *Pseudomonas Aeruginosa* Biofilm from Cystic Fibrosis Patients. *J. Med. Chem.* **2022**, *65* (13), 9050–9062. https://doi.org/10.1021/acs.jmedchem.2c00270.
(138) Slingerland, C. J.; Kotsogianni, I.; Wesseling, C. M. J.; Martin, N. I. Polymyxin Stereochemistry and Its Role in Antibacterial Activity and Outer Membrane Disruption. *ACS Infect. Dis.* **2022**, *8* (12), 2396–2404. https://doi.org/10.1021/acsinfecdis.2c00307.
(139) Sandín, D.; Valle, J.; Chaves-Arquero, B.; Prats-Ejarque, G.; Larrosa, M. N.; González-López, J. J.; Jiménez, M. Á.; Boix, E.; Andreu, D.; Torrent, M. Rationally Modified Antimicrobial Peptides from the N-Terminal Domain of Human RNase 3 Show Exceptional Serum Stability. *J. Med. Chem.* **2021**, *64* (15), 11472–11482. https://doi.org/10.1021/acs.jmedchem.1c00795.
(140) Hayouka, Z.; Chakraborty, S.; Liu, R.; Boersma, M. D.; Weisblum, B.; Gellman, S. H. Interplay among Subunit Identity, Subunit Proportion, Chain Length, and Stereochemistry in the Activity Profile of Sequence-Random Peptide Mixtures. *J. Am. Chem. Soc.* **2013**, *135* (32), 11748–11751. https://doi.org/10.1021/ja406231b.
(141) Guo, X.; Yan, T.; Rao, J.; An, Y.; Yue, X.; Miao, X.; Wang, R.; Sun, W.; Cai, J.; Xie, J. Novel Feleucin-K3-Derived Peptides Modified with Sulfono-γ-AA Building Blocks Targeting Pseudomonas Aeruginosa and Methicillin-Resistant Staphylococcus Aureus Infections. *J. Med. Chem.* **2023**, *66* (2), 1254–1272. https://doi.org/10.1021/acs.jmedchem.2c01396.

(142) Wani, N. A.; Stolovicki, E.; Hur, D. B.; Shai, Y. Site-Specific Isopeptide Bond Formation: A Powerful Tool for the Generation of Potent and Nontoxic Antimicrobial Peptides. *J. Med. Chem.* **2022**, *65* (6), 5085–5094. https://doi.org/10.1021/acs.jmedchem.2c00061.

(143) Dewangan, R. P.; Verma, D. P.; Verma, N. K.; Gupta, A.; Pant, G.; Mitra, K.; Habib, S.; Ghosh, J. K. Spermine-Conjugated Short Proline-Rich Lipopeptides as Broad-Spectrum Intracellular Targeting Antibacterial Agents. *J. Med. Chem.* **2022**, *65* (7), 5433–5448. https://doi.org/10.1021/acs.jmedchem.1c01809.

(144) Koh, J. J.; Lin, H.; Caroline, V.; Chew, Y. S.; Pang, L. M.; Aung, T. T.; Li, J.; Lakshminarayanan, R.; Tan, D. T.; Verma, C.; Tan, A. L.; Beuerman, R. W.; Liu, S. N-Lipidated Peptide Dimers: Effective Antibacterial Agents against Gram-Negative Pathogens through Lipopolysaccharide Permeabilization. *Journal of medicinal chemistry* **2015**, *58* (16), 6533–6548. https://doi.org/10.1021/acs.jmedchem.5b00628.

(145) Topman-Rakover, S.; Malach, E.; Burdman, S.; Hayouka, Z. Antibacterial Lipo-Random Peptide Mixtures Exhibit High Selectivity and Synergistic Interactions. *Chem. Commun.* **2020**, *56* (80), 12053–12056. https://doi.org/10.1039/D0CC04493H.

(146) Li, W.; Lin, F.; Hung, A.; Barlow, A.; Sani, M.-A.; Paolini, R.; Singleton, W.; Holden, J.; Hossain, M. A.; Separovic, F.; O'Brien-Simpson, N. M.; Wade, J. D. Enhancing Proline-Rich Antimicrobial Peptide Action by Homodimerization: Influence of Bifunctional Linker. *Chem. Sci.* **2022**, *13* (8), 2226–2237. https://doi.org/10.1039/D1SC05662J.

(147) Mourtada, R.; Herce, H. D.; Yin, D. J.; Moroco, J. A.; Wales, T. E.; Engen, J. R.; Walensky, L. D. Design of Stapled Antimicrobial Peptides That Are Stable, Nontoxic and Kill Antibiotic-Resistant Bacteria in Mice. *Nat Biotechnol* **2019**, *37* (10), 1186–1197. https://doi.org/10.1038/s41587-019-0222-z.

(148) He, T.; Xu, L.; Hu, Y.; Tang, X.; Qu, R.; Zhao, X.; Bai, H.; Li, L.; Chen, W.; Luo, G.; Fu, G.; Wang, W.; Xia, X.; Zhang, J. Lysine-Tethered Stable Bicyclic Cationic Antimicrobial Peptide Combats Bacterial Infection in Vivo. *J. Med. Chem.* **2022**, *65* (15), 10523–10533. https://doi.org/10.1021/acs.jmedchem.2c00661.

(149) Teng, P.; Shao, H.; Huang, B.; Xie, J.; Cui, S.; Wang, K.; Cai, J. Small Molecular Mimetics of Antimicrobial Peptides as a Promising Therapy To Combat Bacterial Resistance. *J. Med. Chem.* **2023**, *66* (4), 2211–2234. https://doi.org/10.1021/acs.jmedchem.2c00757.

(150) Chongsiriwatana, N. P.; Patch, J. A.; Czyzewski, A. M.; Dohm, M. T.; Ivankin, A.; Gidalevitz, D.; Zuckermann, R. N.; Barron, A. E. Peptoids That Mimic the Structure, Function, and Mechanism of Helical Antimicrobial Peptides. *Proc. Natl. Acad. Sci. U. S. A.* **2008**, *105* (8), 2794–2799. https://doi.org/10.1073/pnas.0708254105.

(151) Nielsen, J. E.; Alford, M. A.; Yung, D. B. Y.; Molchanova, N.; Fortkort, J. A.; Lin, J. S.; Diamond, G.; Hancock, R. E. W.; Jenssen, H.; Pletzer, D.; Lund, R.; Barron, A. E. Self-Assembly of Antimicrobial Peptoids Impacts Their Biological Effects on ESKAPE Bacterial Pathogens. *ACS Infect. Dis.* **2022**, *8* (3), 533–545. https://doi.org/10.1021/acsinfecdis.1c00536.

(152) Yokoo, H.; Hirano, M.; Misawa, T.; Demizu, Y. Helical Antimicrobial Peptide Foldamers Containing Non-Proteinogenic Amino Acids. *ChemMedChem* **2021**, *16*. https://doi.org/10.1002/cmdc.202000940.

(153) Tam, J. P.; Lu, Y. A.; Yang, J. L. Antimicrobial Dendrimeric Peptides. *Eur. J. Biochem.* **2002**, *269* (3), 923–932.

(154) Dhumal, D.; Maron, B.; Malach, E.; Lyu, Z.; Ding, L.; Marson, D.; Laurini, E.; Tintaru, A.; Ralahy, B.; Giorgio, S.; Pricl, S.; Hayouka, Z.; Peng, L. Dynamic Self-Assembling Supramolecular Dendrimer Nanosystems as Potent Antibacterial Candidates against Drug-Resistant Bacteria and Biofilms. *Nanoscale* **2022**, 10.1039/D2NR02305A.

https://doi.org/10.1039/D2NR02305A.
(155) Di Grazia, A.; Cappiello, F.; Cohen, H.; Casciaro, B.; Luca, V.; Pini, A.; Di, Y. P.; Shai, Y.; Mangoni, M. L. D-Amino Acids Incorporation in the Frog Skin-Derived Peptide Esculentin-1a(1-21)NH2 Is Beneficial for Its Multiple Functions. *Amino Acids* **2015**, *47* (12), 2505–2519. https://doi.org/10.1007/s00726-015-2041-y.
(156) Hayouka, Z.; Bella, A.; Stern, T.; Ray, S.; Jiang, H.; Grovenor, C. R. M.; Ryadnov, M. G. Binary Encoding of Random Peptide Sequences for Selective and Differential Antimicrobial Mechanisms. *Angew. Chem., Int. Ed. Engl.* **2017**, *56* (28), 8099–8103. https://doi.org/10.1002/anie.201702313.
(157) Stach, M.; Maillard, N.; Kadam, R. U.; Kalbermatter, D.; Meury, M.; Page, M. G. P.; Fotiadis, D.; Darbre, T.; Reymond, J.-L. Membrane Disrupting Antimicrobial Peptide Dendrimers with Multiple Amino Termini. *MedChemComm* **2012**, *3* (1), 86–89. https://doi.org/10.1039/c1md00272d.
(158) Siriwardena, T. N.; Lüscher, A.; Köhler, T.; van Delden, C.; Javor, S.; Reymond, J.-L. Antimicrobial Peptide Dendrimer Chimera. *Helv. Chim. Acta* **2019**, *102* (4), e1900034. https://doi.org/10.1002/hlca.201900034.
(159) Gan, B.-H.; Siriwardena, T. N.; Javor, S.; Darbre, T.; Reymond, J.-L. Fluorescence Imaging of Bacterial Killing by Antimicrobial Peptide Dendrimer G3KL. *ACS Infect. Dis.* **2019**, *5* (12), 2164–2173. https://doi.org/10.1021/acsinfecdis.9b00299.
(160) Reymond, J.-L. Peptide Dendrimers: From Enzyme Models to Antimicrobials and Transfection Reagents. *Chimia* **2021**, *75* (6), 535–538. https://doi.org/10.2533/chimia.2021.535.
(161) Siriwardena, T. N.; Gan, B.-H.; Köhler, T.; van Delden, C.; Javor, S.; Reymond, J.-L. Stereorandomization as a Method to Probe Peptide Bioactivity. *ACS Cent. Sci.* **2021**, *7* (1), 126–134. https://doi.org/10.1021/acscentsci.0c01135.
(162) Cai, X.; Orsi, M.; Capecchi, A.; Köhler, T.; Delden, C. van; Javor, S.; Reymond, J.-L. An Intrinsically Disordered Antimicrobial Peptide Dendrimer from Stereorandomized Virtual Screening. *Cell Rep. Phys. Sci.* **2022**, *3* (12). https://doi.org/10.1016/j.xcrp.2022.101161.
(163) Falla, T. J.; Karunaratne, D. N.; Hancock, R. E. W. Mode of Action of the Antimicrobial Peptide Indolicidin. *J. Biol. Chem.* **1996**, *271* (32), 19298–19303. https://doi.org/10.1074/jbc.271.32.19298.
(164) de la Fuente-Núñez, C.; Reffuveille, F.; Mansour, S. C.; Reckseidler-Zenteno, S. L.; Hernández, D.; Brackman, G.; Coenye, T.; Hancock, R. E. W. D-Enantiomeric Peptides That Eradicate Wild-Type and Multidrug-Resistant Biofilms and Protect against Lethal Pseudomonas Aeruginosa Infections. *Chemistry & Biology* **2015**, *22* (2), 196–205. https://doi.org/10.1016/j.chembiol.2015.01.002.
(165) Wang, G.; Li, X.; Wang, Z. APD3: The Antimicrobial Peptide Database as a Tool for Research and Education. *Nucleic Acids Res.* **2016**, *44* (Database issue), D1087–D1093. https://doi.org/10.1093/nar/gkv1278.
(166) Gogoladze, G.; Grigolava, M.; Vishnepolsky, B.; Chubinidze, M.; Duroux, P.; Lefranc, M.-P.; Pirtskhalava, M. Dbaasp: Database of Antimicrobial Activity and Structure of Peptides. *FEMS Microbiol. Lett.* **2014**, *357* (1), 63–68. https://doi.org/10.1111/1574-6968.12489.
(167) Gasteiger, E.; Jung, E.; Bairoch, A. SWISS-PROT: Connecting Biomolecular Knowledge Via a Protein Database. *Curr. Issues Mol. Bol.* **2001**, *3* (3), 47–55. https://doi.org/10.21775/cimb.003.047.
(168) Mendez, D.; Gaulton, A.; Bento, A. P.; Chambers, J.; De Veij, M.; Félix, E.; Magariños, M. P.; Mosquera, J. F.; Mutowo, P.; Nowotka, M.; Gordillo-Marañón, M.; Hunter, F.; Junco, L.; Mugumbate, G.; Rodriguez-Lopez, M.; Atkinson, F.; Bosc, N.; Radoux, C. J.;

Segura-Cabrera, A.; Hersey, A.; Leach, A. R. ChEMBL: Towards Direct Deposition of Bioassay Data. *Nucleic Acids Res.* **2019**, *47* (D1), D930–D940. https://doi.org/10.1093/nar/gky1075.

(169) Gautier, R.; Douguet, D.; Antonny, B.; Drin, G. HELIQUEST: A Web Server to Screen Sequences with Specific α-Helical Properties. *Bioinformatics* **2008**, *24* (18), 2101–2102. https://doi.org/10.1093/bioinformatics/btn392.

(170) Strøm, M. B.; Haug, B. E.; Skar, M. L.; Stensen, W.; Stiberg, T.; Svendsen, J. S. The Pharmacophore of Short Cationic Antibacterial Peptides. *J. Med. Chem.* **2003**, *46* (9), 1567–1570. https://doi.org/10.1021/jm0340039.

(171) Albada, H. B.; Prochnow, P.; Bobersky, S.; Langklotz, S.; Bandow, J. E.; Metzler-Nolte, N. Short Antibacterial Peptides with Significantly Reduced Hemolytic Activity Can Be Identified by a Systematic L-to-d Exchange Scan of Their Amino Acid Residues. *ACS Comb. Sci.* **2013**, *15* (11), 585–592. https://doi.org/10.1021/co400072q.

(172) Albada, H. B.; Prochnow, P.; Bobersky, S.; Bandow, J. E.; Metzler-Nolte, N. Highly Active Antibacterial Ferrocenoylated or Ruthenocenoylated Arg-Trp Peptides Can Be Discovered by an L-to-D Substitution Scan. *Chem. Sci.* **2014**, *5* (11), 4453–4459. https://doi.org/10.1039/C4SC01822B.

(173) Townsley, L. E.; Tucker, W. A.; Sham, S.; Hinton, J. F. Structures of Gramicidins A, B, and C Incorporated into Sodium Dodecyl Sulfate Micelles,. *Biochemistry* **2001**, *40* (39), 11676–11686. https://doi.org/10.1021/bi010942w.

(174) Jasanoff, A.; Fersht, A. R. Quantitative Determination of Helical Propensities from Trifluoroethanol Titration Curves. *Biochemistry* **1994**, *33* (8), 2129–2135.

(175) Arunkumar, A. I.; Kumar, T. K.; Yu, C. Specificity of Helix-Induction by 2,2,2-Trifluoroethanol in Polypeptides. *Int. J. Biol. Macromol.* **1997**, *21* (3), 223–230. https://doi.org/10.1016/s0141-8130(97)00064-0.

(176) Hennig, A.; Gabriel, G. J.; Tew, G. N.; Matile, S. Stimuli-Responsive Polyguanidino-Oxanorbornene Membrane Transporters as Multicomponent Sensors in Complex Matrices. *J. Am. Chem. Soc.* **2008**, *130* (31), 10338–10344. https://doi.org/10.1021/ja802587j.

(177) Miles, A. J.; Ramalli, S. G.; Wallace, B. A. DichroWeb, a Website for Calculating Protein Secondary Structure from Circular Dichroism Spectroscopic Data. *Protein Science* **2022**, *31* (1), 37–46. https://doi.org/10.1002/pro.4153.

(178) Provencher, S. W.; Gloeckner, J. Estimation of Globular Protein Secondary Structure from Circular Dichroism. *Biochemistry* **1981**, *20* (1), 33–37. https://doi.org/10.1021/bi00504a006.

(179) Takechi, Y.; Tanaka, H.; Kitayama, H.; Yoshii, H.; Tanaka, M.; Saito, H. Comparative Study on the Interaction of Cell-Penetrating Polycationic Polymers with Lipid Membranes. *Chemistry and Physics of Lipids* **2012**, *165* (1), 51–58. https://doi.org/10.1016/j.chemphyslip.2011.11.002.

(180) Lyu, P. C.; Sherman, J. C.; Chen, A.; Kallenbach, N. R. Alpha-Helix Stabilization by Natural and Unnatural Amino Acids with Alkyl Side Chains. *Proceedings of the National Academy of Sciences* **1991**, *88* (12), 5317–5320. https://doi.org/10.1073/pnas.88.12.5317.

(181) Ben Jeddou, F.; Falconnet, L.; Luscher, A.; Siriwardena, T.; Reymond, J.-L.; van Delden, C.; Köhler, T. Adaptive and Mutational Responses to Peptide Dendrimer Antimicrobials in Pseudomonas Aeruginosa. *Antimicrobial Agents and Chemotherapy* **2020**, *64* (4), e02040-19. https://doi.org/10.1128/AAC.02040-19.

(182) Loutet, S. A.; Flannagan, R. S.; Kooi, C.; Sokol, P. A.; Valvano, M. A. A Complete Lipopolysaccharide Inner Core Oligosaccharide Is Required for Resistance of Burkholderia Cenocepacia to Antimicrobial Peptides and Bacterial Survival In Vivo. *J. Bacteriol.* **2006**, *188* (6), 2073–2080. https://doi.org/10.1128/JB.188.6.2073-2080.2006.

(183) Gabernet, G.; Müller, A. T.; Hiss, J. A.; Schneider, G. Membranolytic Anticancer

Peptides. *Med. Chem. Commun.* **2016**, *7* (12), 2232–2245. https://doi.org/10.1039/C6MD00376A.
(184) Zakharova, E.; Orsi, M.; Capecchi, A.; Reymond, J.-L. Machine Learning Guided Discovery of Non-Hemolytic Membrane Disruptive Anticancer Peptides. *ChemMedChem* **2022**, e202200291. https://doi.org/10.1002/cmdc.202200291.
(185) Greco, I.; Molchanova, N.; Holmedal, E.; Jenssen, H.; Hummel, B. D.; Watts, J. L.; Håkansson, J.; Hansen, P. R.; Svenson, J. Correlation between Hemolytic Activity, Cytotoxicity and Systemic in Vivo Toxicity of Synthetic Antimicrobial Peptides. *Sci. Rep.* **2020**, *10* (1), 13206. https://doi.org/10.1038/s41598-020-69995-9.
(186) Mitchell, E. P.; Sabin, C.; Snajdrova, L.; Pokorna, M.; Perret, S.; Gautier, C.; Hofr, C.; Gilboa-Garber, N.; Koca, J.; Wimmerova, M.; Imberty, A. High Affinity Fucose Binding of Pseudomonas Aeruginosa Lectin PA-IIL: 1.0 A Resolution Crystal Structure of the Complex Combined with Thermodynamics and Computational Chemistry Approaches. *Proteins* **2005**, *58* (3), 735–746. https://doi.org/10.1002/prot.20330.
(187) Roethlisberger, P.; Istrate, A.; Marcaida Lopez, M. J.; Visini, R.; Stocker, A.; Reymond, J. L.; Leumann, C. J. X-Ray Structure of a Lectin-Bound DNA Duplex Containing an Unnatural Phenanthrenyl Pair. *Chem. Commun.* **2016**, *52* (26), 4749–4752. https://doi.org/10.1039/c6cc00374e.
(188) Michaud, G.; Visini, R.; Bergmann, M.; Salerno, G.; Bosco, R.; Gillon, E.; Richichi, B.; Nativi, C.; Imberty, A.; Stocker, A.; Darbre, T.; Reymond, J.-L. Overcoming Antibiotic Resistance in Pseudomonas Aeruginosa Biofilms Using Glycopeptide Dendrimers. *Chem. Sci.* **2015**, *7* (1), 166–182. https://doi.org/10.1039/C5SC03635F.
(189) Abraham, M. J.; Murtola, T.; Schulz, R.; Páll, S.; Smith, J. C.; Hess, B.; Lindahl, E. GROMACS: High Performance Molecular Simulations through Multi-Level Parallelism from Laptops to Supercomputers. *SoftwareX* **2015**, *1–2*, 19–25. https://doi.org/10.1016/j.softx.2015.06.001.
(190) Bertagnolio, S.; Suthar, A. B.; Tosas, O.; Weezenbeek, K. V. Antimicrobial Resistance: Strengthening Surveillance for Public Health Action. *PLOS Medicine* **2023**, *20* (7), e1004265. https://doi.org/10.1371/journal.pmed.1004265.
(191) Limmathurotsakul, D.; Dunachie, S.; Fukuda, K.; Feasey, N. A.; Okeke, I. N.; Holmes, A. H.; Moore, C. E.; Dolecek, C.; van Doorn, H. R.; Shetty, N.; Lopez, A. D.; Peacock, S. J. Improving the Estimation of the Global Burden of Antimicrobial Resistant Infections. *The Lancet Infectious Diseases* **2019**, *19* (11), e392–e398. https://doi.org/10.1016/S1473-3099(19)30276-2.
(192) Murray, C. J. L.; Ikuta, K. S.; Sharara, F.; Swetschinski, L.; Aguilar, G. R.; Gray, A.; Han, C.; Bisignano, C.; Rao, P.; Wool, E.; Johnson, S. C.; Browne, A. J.; Chipeta, M. G.; Fell, F.; Hackett, S.; Haines-Woodhouse, G.; Hamadani, B. H. K.; Kumaran, E. A. P.; McManigal, B.; Achalapong, S.; Agarwal, R.; Akech, S.; Albertson, S.; Amuasi, J.; Andrews, J.; Aravkin, A.; Ashley, E.; Babin, F.-X.; Bailey, F.; Baker, S.; Basnyat, B.; Bekker, A.; Bender, R.; Berkley, J. A.; Bethou, A.; Bielicki, J.; Boonkasidecha, S.; Bukosia, J.; Carvalheiro, C.; Castañeda-Orjuela, C.; Chansamouth, V.; Chaurasia, S.; Chiurchiù, S.; Chowdhury, F.; Donatien, R. C.; Cook, A. J.; Cooper, B.; Cressey, T. R.; Criollo-Mora, E.; Cunningham, M.; Darboe, S.; Day, N. P. J.; Luca, M. D.; Dokova, K.; Dramowski, A.; Dunachie, S. J.; Bich, T. D.; Eckmanns, T.; Eibach, D.; Emami, A.; Feasey, N.; Fisher-Pearson, N.; Forrest, K.; Garcia, C.; Garrett, D.; Gastmeier, P.; Giref, A. Z.; Greer, R. C.; Gupta, V.; Haller, S.; Haselbeck, A.; Hay, S. I.; Holm, M.; Hopkins, S.; Hsia, Y.; Iregbu, K. C.; Jacobs, J.; Jarovsky, D.; Javanmardi, F.; Jenney, A. W. J.; Khorana, M.; Khusuwan, S.; Kissoon, N.; Kobeissi, E.; Kostyanev, T.; Krapp, F.; Krumkamp, R.; Kumar, A.; Kyu, H. H.; Lim, C.; Lim, K.; Limmathurotsakul, D.; Loftus, M. J.; Lunn, M.; Ma, J.; Manoharan, A.; Marks, F.; May, J.; Mayxay, M.; Mturi, N.;

Munera-Huertas, T.; Musicha, P.; Musila, L. A.; Mussi-Pinhata, M. M.; Naidu, R. N.; Nakamura, T.; Nanavati, R.; Nangia, S.; Newton, P.; Ngoun, C.; Novotney, A.; Nwakanma, D.; Obiero, C. W.; Ochoa, T. J.; Olivas-Martinez, A.; Olliaro, P.; Ooko, E.; Ortiz-Brizuela, E.; Ounchanum, P.; Pak, G. D.; Paredes, J. L.; Peleg, A. Y.; Perrone, C.; Phe, T.; Phommasone, K.; Plakkal, N.; Ponce-de-Leon, A.; Raad, M.; Ramdin, T.; Rattanavong, S.; Riddell, A.; Roberts, T.; Robotham, J. V.; Roca, A.; Rosenthal, V. D.; Rudd, K. E.; Russell, N.; Sader, H. S.; Saengchan, W.; Schnall, J.; Scott, J. A. G.; Seekaew, S.; Sharland, M.; Shivamallappa, M.; Sifuentes-Osornio, J.; Simpson, A. J.; Steenkeste, N.; Stewardson, A. J.; Stoeva, T.; Tasak, N.; Thaiprakong, A.; Thwaites, G.; Tigoi, C.; Turner, C.; Turner, P.; Doorn, H. R. van; Velaphi, S.; Vongpradith, A.; Vongsouvath, M.; Vu, H.; Walsh, T.; Walson, J. L.; Waner, S.; Wangrangsimakul, T.; Wannapinij, P.; Wozniak, T.; Sharma, T. E. M. W. Y.; Yu, K. C.; Zheng, P.; Sartorius, B.; Lopez, A. D.; Stergachis, A.; Moore, C.; Dolecek, C.; Naghavi, M. Global Burden of Bacterial Antimicrobial Resistance in 2019: A Systematic Analysis. *The Lancet* **2022**, *399* (10325), 629–655. https://doi.org/10.1016/S0140-6736(21)02724-0.

(193) Personne, H.; Paschoud, T.; Fulgencio, S.; Baeriswyl, S.; Köhler, T.; van Delden, C.; Stocker, A.; Javor, S.; Reymond, J.-L. To Fold or Not to Fold: Diastereomeric Optimization of an α-Helical Antimicrobial Peptide. *J. Med. Chem.* **2023**, *66* (11), 7570–7583. https://doi.org/10.1021/acs.jmedchem.3c00460.

(194) Konno, K.; Rangel, M.; Oliveira, J. S.; dos Santos Cabrera, M. P.; Fontana, R.; Hirata, I. Y.; Hide, I.; Nakata, Y.; Mori, K.; Kawano, M.; Fuchino, H.; Sekita, S.; Neto, J. R. Decoralin, a Novel Linear Cationic α-Helical Peptide from the Venom of the Solitary Eumenine Wasp Oreumenes Decoratus. *Peptides* **2007**, *28* (12), 2320–2327. https://doi.org/10.1016/j.peptides.2007.09.017.

(195) Won, H.-S.; Jung, S.-J.; Kim, H. E.; Seo, M.-D.; Lee, B.-J. Systematic Peptide Engineering and Structural Characterization to Search for the Shortest Antimicrobial Peptide Analogue of Gaegurin 5. *Journal of Biological Chemistry* **2004**, *279* (15), 14784–14791. https://doi.org/10.1074/jbc.M309822200.

(196) Park, J. M.; Jung, J. E.; Lee, B. J. Antimicrobial Peptides from the Skin of a Korean Frog, Rana Rugosa. *Biochemical and Biophysical Research Communications* **1994**, *205* (1), 948–954. https://doi.org/10.1006/bbrc.1994.2757.

(197) Zhang, L.; Parente, J.; Harris, S. M.; Woods, D. E.; Hancock, R. E. W.; Falla, T. J. Antimicrobial Peptide Therapeutics for Cystic Fibrosis. *Antimicrobial Agents and Chemotherapy* **2005**, *49* (7), 2921–2927. https://doi.org/10.1128/aac.49.7.2921-2927.2005.

(198) Munegumi, T. Hydrophobicity of Peptides Containing D-Amino Acids. *Chemistry & Biodiversity* **2010**, *7* (6), 1670–1679. https://doi.org/10.1002/cbdv.200900370.

(199) Lee, D. l.; Powers, J. p. s.; Pflegerl, K.; Vasil, M. l.; Hancock, R. e. w; Hodges, R. s. Effects of Single D-Amino Acid Substitutions on Disruption of β-Sheet Structure and Hydrophobicity in Cyclic 14-Residue Antimicrobial Peptide Analogs Related to Gramicidin S. *The Journal of Peptide Research* **2004**, *63* (2), 69–84. https://doi.org/10.1046/j.1399-3011.2003.00106.x.

(200) Rothemund, S.; Krause, E.; Beyermann, M.; Dathe, M.; Engelhardt, H.; Bienert, M. Recognition of α-Helical Peptide Structures Using High-Performance Liquid Chromatographic Retention Data for d-Amino Acid Analogues: Influence of Peptide Amphipathicity and of Stationary Phase Hydrophobicity. *Journal of Chromatography A* **1995**, *689* (2), 219–226. https://doi.org/10.1016/0021-9673(94)00909-S.

(201) Wessolowski, A.; Bienert, M.; Dathe, M. Antimicrobial Activity of Arginine- and Tryptophan-Rich Hexapeptides: The Effects of Aromatic Clusters, d-Amino Acid Substitution and Cyclization. *The Journal of Peptide Research* **2004**, *64* (4), 159–169.

https://doi.org/10.1111/j.1399-3011.2004.00182.x.
(202) Li, H.; Anuwongcharoen, N.; Malik, A. A.; Prachayasittikul, V.; Wikberg, J. E. S.; Nantasenamat, C. Roles of D-Amino Acids on the Bioactivity of Host Defense Peptides. *International Journal of Molecular Sciences* **2016**, *17* (7), 1023. https://doi.org/10.3390/ijms17071023.
(203) Rajan, R.; Balaram, P. A Model for the Interaction of Trifluoroethanol with Peptides and Proteins. *International Journal of Peptide and Protein Research* **1996**, *48* (4), 328–336. https://doi.org/10.1111/j.1399-3011.1996.tb00849.x.
(204) Roccatano, D.; Colombo, G.; Fioroni, M.; Mark, A. E. Mechanism by Which 2,2,2-Trifluoroethanol/Water Mixtures Stabilize Secondary-Structure Formation in Peptides: A Molecular Dynamics Study. *Proceedings of the National Academy of Sciences* **2002**, *99* (19), 12179–12184. https://doi.org/10.1073/pnas.182199699.
(205) Starzyk, A.; Barber-Armstrong, W.; Sridharan, M.; Decatur, S. M. Spectroscopic Evidence for Backbone Desolvation of Helical Peptides by 2,2,2-Trifluoroethanol: An Isotope-Edited FTIR Study. *Biochemistry* **2005**, *44* (1), 369–376. https://doi.org/10.1021/bi0481444.
(206) Beswick, V.; Guerois, R.; Cordier-Ochsenbein, F.; Coïc, Y.-M.; Huynh-Dinh, T.; Tostain, J.; Noël, J.-P.; Sanson, A.; Neumann, J.-M. Dodecylphosphocholine Micelles as a Membrane-like Environment: New Results from NMR Relaxation and Paramagnetic Relaxation Enhancement Analysis. *Eur Biophys J* **1998**, *28* (1), 48–58. https://doi.org/10.1007/s002490050182.
(207) Li, W.; O'Brien-Simpson, N. M.; Hossain, M. A.; Wade, J. D. The 9-Fluorenylmethoxycarbonyl (Fmoc) Group in Chemical Peptide Synthesis – Its Past, Present, and Future. *Aust. J. Chem.* **2019**, *73* (4), 271–276. https://doi.org/10.1071/CH19427.
(208) Nicolás, E.; Pedroso, E.; Girald, E. Formation of Aspartimide Peptides in Asp-Gly Sequences. *Tetrahedron Letters* **1989**, *30* (4), 497–500. https://doi.org/10.1016/S0040-4039(00)95238-9.
(209) Lauer, J. L.; Fields, C. G.; Fields, G. B. Sequence Dependence of Aspartimide Formation during 9-Fluorenylmethoxycarbonyl Solid-Phase Peptide Synthesis. *Lett Pept Sci* **1995**, *1* (4), 197–205. https://doi.org/10.1007/BF00117955.
(210) Luna, O. F.; Gomez, J.; Cárdenas, C.; Albericio, F.; Marshall, S. H.; Guzmán, F. Deprotection Reagents in Fmoc Solid Phase Peptide Synthesis: Moving Away from Piperidine? *Molecules* **2016**, *21* (11), 1542. https://doi.org/10.3390/molecules21111542.
(211) Dölling, R.; Beyermann, M.; Haenel, J.; Kernchen, F.; Krause, E.; Franke, P.; Brudel, M.; Bienert, M. Piperidine-Mediated Side Product Formation for Asp(OBut)-Containing Peptides. *J. Chem. Soc., Chem. Commun.* **1994**, No. 7, 853–854. https://doi.org/10.1039/C39940000853.
(212) Samson, D.; Rentsch, D.; Minuth, M.; Meier, T.; Loidl, G. The Aspartimide Problem Persists: Fluorenylmethyloxycarbonyl-Solid-Phase Peptide Synthesis (Fmoc-SPPS) Chain Termination Due to Formation of N-Terminal Piperazine-2,5-Diones. *Journal of Peptide Science* **2019**, *25* (7), e3193. https://doi.org/10.1002/psc.3193.
(213) Wade, J. D.; Bedford, J.; Sheppard, R. C.; Tregear, G. W. DBU as an N Alpha-Deprotecting Reagent for the Fluorenylmethoxycarbonyl Group in Continuous Flow Solid-Phase Peptide Synthesis. *Pept Res* **1991**, *4* (3), 194–199.
(214) Michels, T.; Dölling, R.; Haberkorn, U.; Mier, W. Acid-Mediated Prevention of Aspartimide Formation in Solid Phase Peptide Synthesis. *Org. Lett.* **2012**, *14* (20), 5218–5221. https://doi.org/10.1021/ol3007925.
(215) Chen, C.-C.; Rajagopal, B.; Liu, X. Y.; Chen, K. L.; Tyan, Y.-C.; Lin, F.; Lin, P.-C. A Mild Removal of Fmoc Group Using Sodium Azide. *Amino Acids* **2014**, *46* (2), 367–374.

https://doi.org/10.1007/s00726-013-1625-7.
(216) Rodríguez, V.; Pineda, H.; Ardila, N.; Insuasty, D.; Cárdenas, K.; Román, J.; Urrea, M.; Ramírez, D.; Fierro, R.; Rivera, Z.; García, J. Efficient Fmoc Group Removal Using Diluted 4-Methylpiperidine: An Alternative for a Less-Polluting SPPS-Fmoc/tBu Protocol. *Int J Pept Res Ther* **2020**, *26* (1), 585–587. https://doi.org/10.1007/s10989-019-09865-9.
(217) Martelli, G.; Cantelmi, P.; Palladino, C.; Mattellone, A.; Corbisiero, D.; Fantoni, T.; Tolomelli, A.; Macis, M.; Ricci, A.; Cabri, W.; Ferrazzano, L. Replacing Piperidine in Solid Phase Peptide Synthesis: Effective Fmoc Removal by Alternative Bases. *Green Chem.* **2021**, *23* (20), 8096–8107. https://doi.org/10.1039/D1GC02634H.
(218) Egelund, P. H. G.; Jadhav, S.; Martin, V.; Johansson Castro, H.; Richner, F.; Le Quement, S. T.; Dettner, F.; Lechner, C.; Schoenleber, R.; Sejer Pedersen, D. Fmoc-Removal with Pyrrolidine Expands the Available Solvent Space in Green Solid-Phase Peptide Synthesis. *ACS Sustainable Chem. Eng.* **2021**. https://doi.org/10.1021/acssuschemeng.1c04770.
(219) Mergler, M.; Dick, F.; Sax, B.; Weiler, P.; Vorherr, T. The Aspartimide Problem in Fmoc-Based SPPS. Part I. *Journal of Peptide Science* **2003**, *9* (1), 36–46. https://doi.org/10.1002/psc.430.
(220) Mergler, M.; Dick, F.; Sax, B.; Stähelin, C.; Vorherr, T. The Aspartimide Problem in Fmoc-Based SPPS. Part II. *Journal of Peptide Science* **2003**, *9* (8), 518–526. https://doi.org/10.1002/psc.473.
(221) Mergler, M.; Dick, F. The Aspartimide Problem in Fmoc-Based SPPS. Part III. *Journal of Peptide Science* **2005**, *11* (10), 650–657. https://doi.org/10.1002/psc.668.
(222) Neumann, K.; Farnung, J.; Baldauf, S.; Bode, J. W. Prevention of Aspartimide Formation during Peptide Synthesis Using Cyanosulfurylides as Carboxylic Acid-Protecting Groups. *Nat Commun* **2020**, *11* (1), 982. https://doi.org/10.1038/s41467-020-14755-6.
(223) Reymond, J.-L. Peptide Dendrimers: From Enzyme Models to Antimicrobials and Transfection Reagents. *CHIMIA* **2021**, *75* (6), 535–535. https://doi.org/10.2533/chimia.2021.535.
(224) Erzina, D.; Capecchi, A.; Javor, S.; Reymond, J.-L. An Immunomodulatory Peptide Dendrimer Inspired from Glatiramer Acetate. *Angewandte Chemie International Edition* **2021**, *60* (50), 26403–26408. https://doi.org/10.1002/anie.202113562.
(225) Frederick, M. O.; Boyse, R. A.; Braden, T. M.; Calvin, J. R.; Campbell, B. M.; Changi, S. M.; Coffin, S. R.; Condon, C.; Gowran, O.; McClary Groh, J.; Groskreutz, S. R.; Harms, Z. D.; Humenik, A. A.; Kallman, N. J.; Klitzing, N. D.; Kopach, M. E.; Kretsinger, J. K.; Lambertus, G. R.; Lampert, J. T.; Maguire, L. M.; Moynihan, H. A.; Mullane, N. S.; Murphy, J. D.; O'Mahony, M. E.; Richey, R. N.; Seibert, K. D.; Spencer, R. D.; Strege, M. A.; Tandogan, N.; Torres Torres, F. L.; Tsukanov, S. V.; Xia, H. Kilogram-Scale GMP Manufacture of Tirzepatide Using a Hybrid SPPS/LPPS Approach with Continuous Manufacturing. *Org. Process Res. Dev.* **2021**, *25* (7), 1628–1636. https://doi.org/10.1021/acs.oprd.1c00108.
(226) Stach, M.; Siriwardena, T. N.; Köhler, T.; van Delden, C.; Darbre, T.; Reymond, J.-L. Combining Topology and Sequence Design for the Discovery of Potent Antimicrobial Peptide Dendrimers against Multidrug-Resistant Pseudomonas Aeruginosa. *Angewandte Chemie International Edition* **2014**, *53* (47), 12827–12831. https://doi.org/10.1002/anie.201409270.
(227) Siriwardena, T. N.; Stach, M.; He, R.; Gan, B.-H.; Javor, S.; Heitz, M.; Ma, L.; Cai, X.; Chen, P.; Wei, D.; Li, H.; Ma, J.; Köhler, T.; van Delden, C.; Darbre, T.; Reymond, J.-L. Lipidated Peptide Dendrimers Killing Multidrug-Resistant Bacteria. *J. Am. Chem. Soc.* **2018**, *140* (1), 423–432. https://doi.org/10.1021/jacs.7b11037.
(228) Wu, L.; Ficker, M.; Christensen, J. B.; Trohopoulos, P. N.; Moghimi, S. M. Dendrimers

in Medicine: Therapeutic Concepts and Pharmaceutical Challenges. *Bioconjugate Chem.* **2015**, *26* (7), 1198–1211. https://doi.org/10.1021/acs.bioconjchem.5b00031.
(229) Espinar Buitrago, M. de la S.; Muñoz Fernández, M. Á. Chapter 10 - Dendrimers and Their Applications in Biomedicine: Dendrimer-Drug Interaction, a New Therapeutic Alternative. In *Dendrimer-Based Nanotherapeutics*; Kesharwani, P., Ed.; Academic Press, 2021; pp 163–182. https://doi.org/10.1016/B978-0-12-821250-9.00019-6.
(230) Turrin, C.-O.; Caminade, A.-M. Dendrimers as Transfection Agents. In *Dendrimers*; John Wiley & Sons, Ltd, 2011; pp 413–435. https://doi.org/10.1002/9781119976530.ch17.
(231) Fischer, M.; Vögtle, F. Dendrimers: From Design to Application—A Progress Report. *Angewandte Chemie International Edition* **1999**, *38* (7), 884–905. https://doi.org/10.1002/(SICI)1521-3773(19990401)38:7<884::AID-ANIE884>3.0.CO;2-K.
(232) Bosman, A. W.; Janssen, H. M.; Meijer, E. W. About Dendrimers: Structure, Physical Properties, and Applications. *Chem. Rev.* **1999**, *99* (7), 1665–1688. https://doi.org/10.1021/cr970069y.
(233) Lyu, Z.; Ding, L.; Huang, A. Y.-T.; Kao, C.-L.; Peng, L. Poly(Amidoamine) Dendrimers: Covalent and Supramolecular Synthesis. *Materials Today Chemistry* **2019**, *13*, 34–48. https://doi.org/10.1016/j.mtchem.2019.04.004.
(234) Li, X.; Ta, W.; Hua, R.; Song, J.; Lu, W. A Review on Increasing the Targeting of PAMAM as Carriers in Glioma Therapy. *Biomedicines* **2022**, *10* (10), 2455. https://doi.org/10.3390/biomedicines10102455.
(235) Wang, Y.; Luo, Y.; Zhao, Q.; Wang, Z.; Xu, Z.; Jia, X. An Enzyme-Responsive Nanogel Carrier Based on PAMAM Dendrimers for Drug Delivery. *ACS Appl. Mater. Interfaces* **2016**, *8* (31), 19899–19906. https://doi.org/10.1021/acsami.6b05567.
(236) Chanphai, P.; Bekale, L.; Sanyakamdhorn, S.; Agudelo, D.; Bérubé, G.; Thomas, T. J.; Tajmir-Riahi, H. A. PAMAM Dendrimers in Drug Delivery: Loading Efficacy and Polymer Morphology. *Can. J. Chem.* **2017**, *95* (9), 891–896. https://doi.org/10.1139/cjc-2017-0115.
(237) Esfand, R.; Tomalia, D. A. Poly(Amidoamine) (PAMAM) Dendrimers: From Biomimicry to Drug Delivery and Biomedical Applications. *Drug Discovery Today* **2001**, *6* (8), 427–436. https://doi.org/10.1016/S1359-6446(01)01757-3.
(238) Eichman, J. D.; Bielinska, A. U.; Kukowska-Latallo, J. F.; Baker, J. R. The Use of PAMAM Dendrimers in the Efficient Transfer of Genetic Material into Cells. *Pharmaceutical Science & Technology Today* **2000**, *3* (7), 232–245. https://doi.org/10.1016/S1461-5347(00)00273-X.
(239) Navarro, G.; Tros de ILarduya, C. Activated and Non-Activated PAMAM Dendrimers for Gene Delivery in Vitro and in Vivo. *Nanomedicine: Nanotechnology, Biology and Medicine* **2009**, *5* (3), 287–297. https://doi.org/10.1016/j.nano.2008.12.007.
(240) Kesharwani, P.; Banerjee, S.; Gupta, U.; Mohd Amin, M. C. I.; Padhye, S.; Sarkar, F. H.; Iyer, A. K. PAMAM Dendrimers as Promising Nanocarriers for RNAi Therapeutics. *Materials Today* **2015**, *18* (10), 565–572. https://doi.org/10.1016/j.mattod.2015.06.003.
(241) Li, J.; Liang, H.; Liu, J.; Wang, Z. Poly (Amidoamine) (PAMAM) Dendrimer Mediated Delivery of Drug and pDNA/siRNA for Cancer Therapy. *International Journal of Pharmaceutics* **2018**, *546* (1), 215–225. https://doi.org/10.1016/j.ijpharm.2018.05.045.
(242) Zhou, J.; Wu, J.; Hafdi, N.; Behr, J.-P.; Erbacher, P.; Peng, L. PAMAM Dendrimers for Efficient siRNA Delivery and Potent Gene Silencing. *Chem. Commun.* **2006**, No. 22, 2362–2364. https://doi.org/10.1039/B601381C.
(243) Holmes, A. M.; Heylings, J. R.; Wan, K.-W.; Moss, G. P. Antimicrobial Efficacy and Mechanism of Action of Poly(Amidoamine) (PAMAM) Dendrimers against Opportunistic Pathogens. *International Journal of Antimicrobial Agents* **2019**, *53* (4), 500–507.

https://doi.org/10.1016/j.ijantimicag.2018.12.012.
(244) Gholami, M.; Mohammadi, R.; Arzanlou, M.; Akbari Dourbash, F.; Kouhsari, E.; Majidi, G.; Mohseni, S. M.; Nazari, S. In Vitro Antibacterial Activity of Poly (Amidoamine)-G7 Dendrimer. *BMC Infectious Diseases* **2017**, *17* (1), 395. https://doi.org/10.1186/s12879-017-2513-7.
(245) Dhumal, D.; Maron, B.; Malach, E.; Lyu, Z.; Ding, L.; Marson, D.; Laurini, E.; Tintaru, A.; Ralahy, B.; Giorgio, S.; Pricl, S.; Hayouka, Z.; Peng, L. Dynamic Self-Assembling Supramolecular Dendrimer Nanosystems as Potent Antibacterial Candidates against Drug-Resistant Bacteria and Biofilms. *Nanoscale* **2022**, *14* (26), 9286–9296. https://doi.org/10.1039/D2NR02305A.
(246) Hussain, I.; Muhammad, N.; Subhani, Q.; Shou, D.; Jin, M.; Yu, L.; Lu, G.; Wen, X.; Intisar, A.; Yan, Z. A Review on Structural Aspects and Applications of PAMAM Dendrimers in Analytical Chemistry: Frontiers from Separation Sciences to Chemical Sensor Technologies. *TrAC Trends in Analytical Chemistry* **2022**, *157*, 116810. https://doi.org/10.1016/j.trac.2022.116810.
(247) Bahadır, E. B.; Sezgintürk, M. K. Poly(Amidoamine) (PAMAM): An Emerging Material for Electrochemical Bio(Sensing) Applications. *Talanta* **2016**, *148*, 427–438. https://doi.org/10.1016/j.talanta.2015.11.022.
(248) DeFever, R. S.; Geitner, N. K.; Bhattacharya, P.; Ding, F.; Ke, P. C.; Sarupria, S. PAMAM Dendrimers and Graphene: Materials for Removing Aromatic Contaminants from Water. *Environ. Sci. Technol.* **2015**, *49* (7), 4490–4497. https://doi.org/10.1021/es505518r.
(249) Diallo, M. S.; Christie, S.; Swaminathan, P.; Johnson, James H.; Goddard, W. A. Dendrimer Enhanced Ultrafiltration. 1. Recovery of Cu(II) from Aqueous Solutions Using PAMAM Dendrimers with Ethylene Diamine Core and Terminal NH2 Groups. *Environ. Sci. Technol.* **2005**, *39* (5), 1366–1377. https://doi.org/10.1021/es048961r.
(250) Peterson, J.; Allikmaa, V.; Tonis, P.; Lopp, M. Fragmentation of PAMAM Dendrimers in Methanol/Poluamidoamiini Dendrimeeri Metanooli Lahuses Lagunemise Uurimine. *Estonian Academy of Sciences: Chemistry* **2001**, *50* (3), 167–173.
(251) Peterson, J.; Allikmaa, V.; Subbi, J.; Pehk, T.; Lopp, M. Structural Deviations in Poly(Amidoamine) Dendrimers: A MALDI-TOF MS Analysis. *European Polymer Journal* **2003**, *39* (1), 33–42. https://doi.org/10.1016/S0014-3057(02)00188-X.
(252) Zhao, M.; Liu, Y.; Crooks, R. M.; Bergbreiter, D. E. Preparation of Highly Impermeable Hyperbranched Polymer Thin-Film Coatings Using Dendrimers First as Building Blocks and Then as in Situ Thermosetting Agents. *J. Am. Chem. Soc.* **1999**, *121* (5), 923–930. https://doi.org/10.1021/ja9825027.
(253) Xiao, Y.; Shao, L.; Chung, T.-S.; Schiraldi, D. A. Effects of Thermal Treatments and Dendrimers Chemical Structures on the Properties of Highly Surface Cross-Linked Polyimide Films. *Ind. Eng. Chem. Res.* **2005**, *44* (9), 3059–3067. https://doi.org/10.1021/ie048837g.
(254) Bonvin, E.; Reymond, J.-L. Inverse Polyamidoamine (i-PAMAM) Dendrimer Antimicrobials. *Helvetica Chimica Acta* **2023**, *106* (6), e202300035. https://doi.org/10.1002/hlca.202300035.
(255) Huang, A. Y.-T.; Tsai, C.-H.; Chen, H.-Y.; Chen, H.-T.; Lu, C.-Y.; Lin, Y.-T.; Kao, C.-L. Concise Solid-Phase Synthesis of Inverse Poly(Amidoamine) Dendrons Using AB2 Building Blocks. *Chem. Commun.* **2013**, *49* (51), 5784–5786. https://doi.org/10.1039/C3CC40661J.
(256) Kao, C.-L.; Huang, A. Y.-T.; Chen, H.-T. Solid-Phase Synthesis of a Seventh-Generation Inverse Poly(Amidoamine) Dendrimer: Importance of the Loading Ratio on the Resin. *Macromolecular Rapid Communications* **2017**, *38* (12), 1700062.

https://doi.org/10.1002/marc.201700062.
(257) Clapperton, A. M.; Babi, J.; Tran, H. A Field Guide to Optimizing Peptoid Synthesis. *ACS Polym. Au* **2022**, *2* (6), 417–429. https://doi.org/10.1021/acspolymersau.2c00036.
(258) Dioury, F.; Sylvestre, I.; Siaugue, J.-M.; Wintgens, V.; Ferroud, C.; Favre-Réguillon, A.; Foos, J.; Guy, A. Regioselectively N-Functionalised 14-Membered Azapyridinomacrocycles Bearing Trialkanoic Acid Side Chains as Ligands for Lanthanide Ions. *European Journal of Organic Chemistry* **2004**, *2004* (21), 4424–4436. https://doi.org/10.1002/ejoc.200400264.
(259) Turner, R. A.; Hauksson, N. E.; Gipe, J. H.; Lokey, R. S. Selective, On-Resin N-Methylation of Peptide N-Trifluoroacetamides. *Org. Lett.* **2013**, *15* (19), 5012–5015. https://doi.org/10.1021/ol402341u.
(260) Weygand, F.; Frauendorfer, E. N-Trifluoracetyl-aminosäuren, XXI. Reduktive Entfernung des N-Trifluoracetyl- und N-Trichloracetyl-restes durch Natriumborhydrid mit Anwendungen in der Peptidchemie. *Chemische Berichte* **1970**, *103* (8), 2437–2449. https://doi.org/10.1002/cber.19701030816.
(261) Weygand, F.; Csendes, E. N-Trifluoracetyl-Aminosäuren. *Angewandte Chemie* **1952**, *64* (5), 136–136. https://doi.org/10.1002/ange.19520640505.
(262) Ohno, M.; Eastlake, A.; Ontjes, D. A.; Anfinsen, C. B. Synthesis of the Fully Protected, Carboxyl-Terminal Tetradecapeptide Sequence of Staphylococcal Nuclease. *J. Am. Chem. Soc.* **1969**, *91* (24), 6842–6847. https://doi.org/10.1021/ja01052a051.
(263) Goldberger, R. F.; Anfinsen, C. B. The Reversible Masking of Amino Groups in Ribonuclease and Its Possible Usefulness in the Synthesis of the Protein. *Biochemistry* **1962**, *1* (3), 401–405. https://doi.org/10.1021/bi00909a005.
(264) Moroder, L.; Filippi, B.; Borin, G.; Marchiori, F. Studies on Cytochrome c. X. Synthesis of Nα-Benzyloxycarbonyl-[Thr107]-Dotetracontapeptide (Sequence 67–108) of Baker's Yeast Iso-1-Cytochrome c. *Biopolymers* **1975**, *14* (10), 2061–2074. https://doi.org/10.1002/bip.1975.360141007.
(265) Cai, X.; Capecchi, A.; Olcay, B.; Orsi, M.; Javor, S.; Reymond, J.-L. Exploring the Sequence Space of Antimicrobial Peptide Dendrimers. *Israel Journal of Chemistry n/a* (n/a), e202300096. https://doi.org/10.1002/ijch.202300096.
(266) Siriwardena, T. N.; Capecchi, A.; Gan, B.-H.; Jin, X.; He, R.; Wei, D.; Ma, L.; Köhler, T.; van Delden, C.; Javor, S.; Reymond, J.-L. Optimizing Antimicrobial Peptide Dendrimers in Chemical Space. *Angewandte Chemie International Edition* **2018**, *57* (28), 8483–8487. https://doi.org/10.1002/anie.201802837.
(267) Knappe, D.; Piantavigna, S.; Hansen, A.; Mechler, A.; Binas, A.; Nolte, O.; Martin, L. L.; Hoffmann, R. Oncocin (VDKPPYLPRPRPPRRIYNR-NH2): A Novel Antibacterial Peptide Optimized against Gram-Negative Human Pathogens. *J. Med. Chem.* **2010**, *53* (14), 5240–5247. https://doi.org/10.1021/jm100378b.
(268) Kolano, L.; Knappe, D.; Berg, A.; Berg, T.; Hoffmann, R. Effect of Amino Acid Substitutions on 70S Ribosomal Binding, Cellular Uptake, and Antimicrobial Activity of Oncocin Onc112. *ChemBioChem* **2022**, *23* (5), e202100609. https://doi.org/10.1002/cbic.202100609.
(269) Lai, P.-K.; Tresnak, D. T.; Hackel, B. J. Identification and Elucidation of Proline-Rich Antimicrobial Peptides with Enhanced Potency and Delivery. *Biotechnology and Bioengineering* **2019**, *116* (10), 2439–2450. https://doi.org/10.1002/bit.27092.
(270) Cai, X.; Javor, S.; Gan, B. H.; Köhler, T.; Reymond, J.-L. The Antibacterial Activity of Peptide Dendrimers and Polymyxin B Increases Sharply above pH 7.4. *Chem. Commun.* **2021**, *57* (46), 5654–5657. https://doi.org/10.1039/D1CC01838H.
(271) Wiegand, I.; Hilpert, K.; Hancock, R. E. W. Agar and Broth Dilution Methods to Determine the Minimal Inhibitory Concentration (MIC) of Antimicrobial Substances. *Nat*

Protoc **2008**, *3* (2), 163–175. https://doi.org/10.1038/nprot.2007.521.
(272) Berridge, M. V.; Herst, P. M.; Tan, A. S. Tetrazolium Dyes as Tools in Cell Biology: New Insights into Their Cellular Reduction. In *Biotechnology Annual Review*; Elsevier, 2005; Vol. 11, pp 127–152. https://doi.org/10.1016/S1387-2656(05)11004-7.
(273) Sreerama, N.; Woody, R. W. Estimation of Protein Secondary Structure from Circular Dichroism Spectra: Comparison of CONTIN, SELCON, and CDSSTR Methods with an Expanded Reference Set. *Analytical Biochemistry* **2000**, *287* (2), 252–260. https://doi.org/10.1006/abio.2000.4880.
(274) Liebschner, D.; Afonine, P. V.; Baker, M. L.; Bunkóczi, G.; Chen, V. B.; Croll, T. I.; Hintze, B.; Hung, L.-W.; Jain, S.; McCoy, A. J.; Moriarty, N. W.; Oeffner, R. D.; Poon, B. K.; Prisant, M. G.; Read, R. J.; Richardson, J. S.; Richardson, D. C.; Sammito, M. D.; Sobolev, O. V.; Stockwell, D. H.; Terwilliger, T. C.; Urzhumtsev, A. G.; Videau, L. L.; Williams, C. J.; Adams, P. D. Macromolecular Structure Determination Using X-Rays, Neutrons and Electrons: Recent Developments in Phenix. *Acta Cryst D* **2019**, *75* (10), 861–877. https://doi.org/10.1107/S2059798319011471.
(275) Winn, M. D.; Ballard, C. C.; Cowtan, K. D.; Dodson, E. J.; Emsley, P.; Evans, P. R.; Keegan, R. M.; Krissinel, E. B.; Leslie, A. G. W.; McCoy, A.; McNicholas, S. J.; Murshudov, G. N.; Pannu, N. S.; Potterton, E. A.; Powell, H. R.; Read, R. J.; Vagin, A.; Wilson, K. S. Overview of the CCP4 Suite and Current Developments. *Acta Cryst D* **2011**, *67* (4), 235–242. https://doi.org/10.1107/S0907444910045749.
(276) The PyMOL Molecular Graphics System, Version 2.0 Schrödinger, LLC.
(277) Emsley, P.; Cowtan, K. Coot: Model-Building Tools for Molecular Graphics. *Acta Cryst D* **2004**, *60* (12), 2126–2132. https://doi.org/10.1107/S0907444904019158.
(278) Kabsch, W. XDS. *Acta Cryst D* **2010**, *66* (2), 125–132. https://doi.org/10.1107/S0907444909047337.
(279) Oostenbrink, C.; Soares, T. A.; van der Vegt, N. F. A.; van Gunsteren, W. F. Validation of the 53A6 GROMOS Force Field. *Eur Biophys J* **2005**, *34* (4), 273–284. https://doi.org/10.1007/s00249-004-0448-6.
(280) Chiu, S. W.; Clark, M.; Balaji, V.; Subramaniam, S.; Scott, H. L.; Jakobsson, E. Incorporation of Surface Tension into Molecular Dynamics Simulation of an Interface: A Fluid Phase Lipid Bilayer Membrane. *Biophysical Journal* **1995**, *69* (4), 1230–1245. https://doi.org/10.1016/S0006-3495(95)80005-6.

8. Supporting Information

8.1 SI for X-ray structure of a short α-helical mixed-chirality AMPs

Peptide synthesis

Table S1.1: Synthesis of linear AMPs.

Cpd.	Sequence[a)]	SPPS yield[b)]	MS analysis[c)]	Analytical HPLC[d)]
		mg (%)	calc./obs.	t_R (min)
Fln65	*KKLLKLLKLLL	21.9 (11.0)	1510.07/1510.43	3.95
Fdln65	*kkllkllklll	9.8 (8.0)	1510.07/1510.50	3.95
Fln69	*kkLLkLLkLLL	38.2 (19.0)	1510.07/1509.89	3.45
Fdln69	*KKllKllKlll	12.9 (13.0)	1510.07/1510.08	3.45

[a)] One letter code for amino acid. D- amino acids in lower case. * = α-L-fucosyl acetyl moiety. [b)] Yields given for RP-HPLC purified products. [c)] High-resolution electrospray ionization mass spectrometry (positive mode), the calculated monoisotopic mass and the observed mass are given. [d)] retention time in analytical RP-HPLC (A/D = 100/0 to 0/100 in 7.0 min, λ = 214 nm).

Crystallography

Table S1.2: Data collection and refinement statistics for the X-ray structure of the **Fln65**·LecB complex.

Structural data	**Fln65·LecB**
Beam line	PSI PXIII
Wavelength(Å)	0.976
Resolution(Å)	48.6-1.5 (1.515-1.507)[a)]
Cell dimension	
Space group	4, P 1 2_1 1
Unit cell(Å)	a = 74.5, b = 64.3, c = 118.9; α = 90°, β = 94.9°, γ = 90°
Measured reflection / unique	1071279/336482
Average multiplicity	3.2 (2.4)
Completeness (%)	96.2 (89.8)
Average $I / \sigma(I)$	8.23 (1.23)
Correlation CC (1/2) (%)	99.7 (68.5)
R_{meas} (%)	11.7 (93.3)
Wilson B-factor (Å^2)	12.8
Refinement	
Resolution range (Å)	48.59-1.51
R_{work} (%)	18.21
R_{free} (%)	20.60
Average Biso (Å^2)	89.1
RMSD from ideality angles (°)	1.025
Bonds (Å)	0.008
Water molecules	1415
Ligand molecules	8
Protein Data Bank deposition code	7NEF

[a)] Values in brackets correspond to the outer shell.

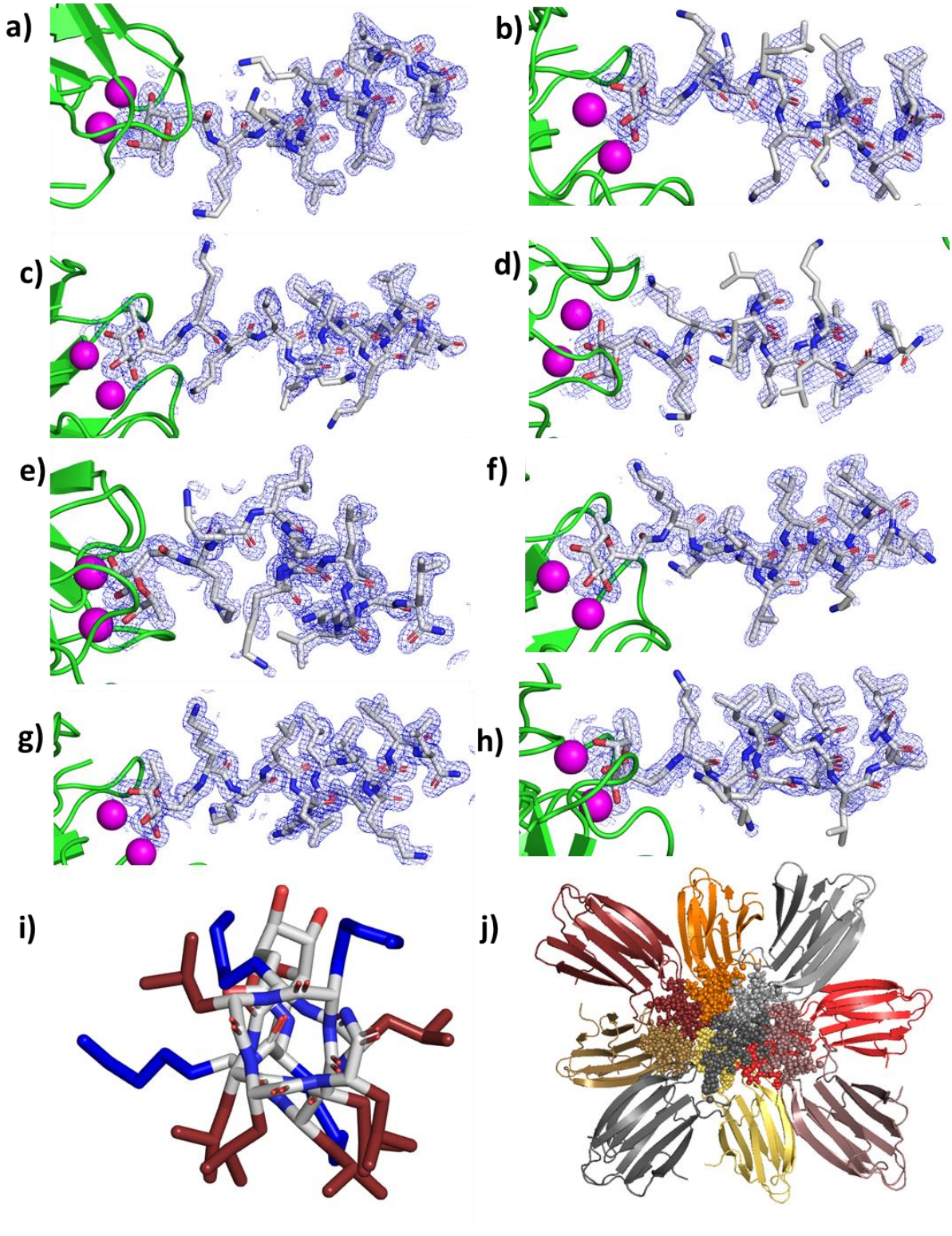

Figure S1.1: Details of the X-ray structure of the **Fln65**·LecB complex in P 1 2_1 1. (**a-h**) Asymmetric peptide entities with corresponding electron density map as blue mesh, with Ca^{2+} atoms shown as magenta spheres and the bound LecB monomer as green cartoon. (**i**) Amphiphilic arrangement of leucine and lysine residues along the α-helix. Amino acid side chains are color-coded. Red: leucine, blue: lysine. (**j**) View of the unit cell including LecB subunits and the bound peptides. Peptides are shown as spheres and bound lectin monomers are displayed as cartoon of the same color.

Table S1.3: Data collection and refinement statistics for the X-ray structure of the **Fdln69**·LecB complex.

Structural data	**Fdln69·LecB**
Beam line	PSI PXIII
Wavelength(Å)	0.976
Resolution(Å)	48.3-2.0 (2.027-2.017)[a)]
Cell dimension	
Space group	5, C 1 2 1
Unit cell(Å)	a = 130.6, b = 64.8, c = 73.6; α = 90°, β = 113.3°, γ = 90°
Measured reflection / unique	252919/71291
Average multiplicity	3.5 (3.5)
Completeness (%)	97.5 (96.1)
Average $I / \sigma(I)$	6.89 (1.01)
Correlation CC (1/2) (%)	99.5 (51.2)
R_{meas} (%)	16.7 (139.3)
Wilson B-factor (Å^2)	32.0
Refinement	
Resolution range (Å)	40.03-2.02
R_{work} (%)	20.70
R_{free} (%)	22.80
Average Biso (Å^2)	161.2
RMSD from ideality angles (°)	0.702
Bonds (Å)	0.003
Water molecules	236
Ligand molecules	4
Protein Data Bank deposition code	7NEW

[a)] Values in brackets correspond to the outer shell.

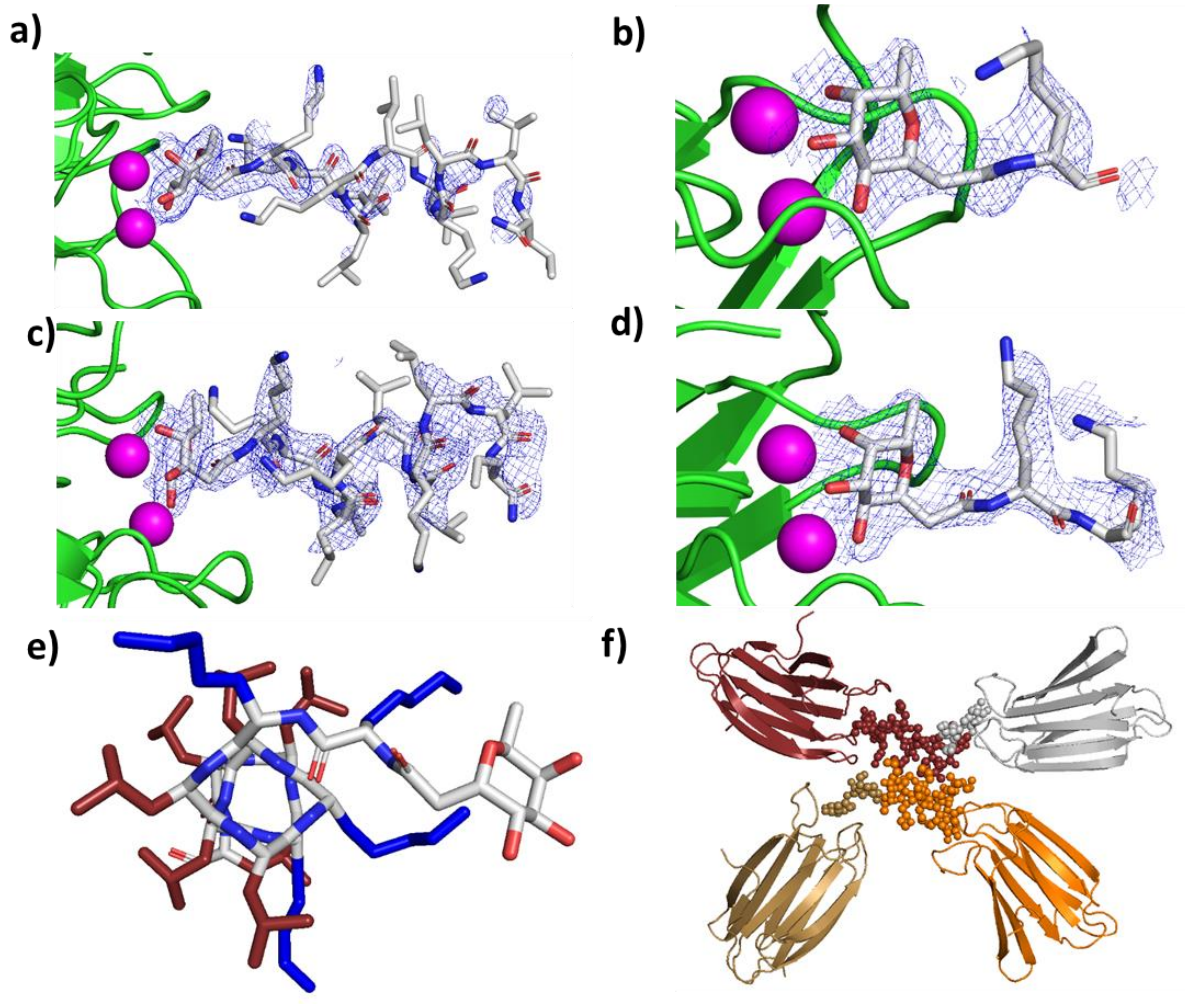

Figure S1.2: Details of the X-ray structure of the **Fdln69**·LecB complex in C 1 2 1. **a-d**) Asymmetric peptide entities with corresponding electron density map as blue mesh, with Ca^{2+} atoms shown as magenta spheres and the bound LecB monomer as green cartoon. **e**) Amphiphilic arrangement of leucine and lysine residues along the α-helix. Amino acid side chains are color-coded. Brown: leucine, blue: lysine. **f**) View of the unit cell including LecB subunits and the bound peptides. Peptides are shown as spheres and bound lectin monomers are displayed as cartoon of the same color.

HPLC and HRMS data

(*)KKLLKLLKLLL (Fln65) was obtained as foamy white solid after preparative RP-HPLC (21.9 mg, 11.0 %). * = α-L-fucosyl-acetyl group. Analytical RP-HPLC: t_R = 3.95 min (A/D 100:0 to 0:100 in 7.0 min, λ = 214nm). MS (ESI^+): $C_{74}H_{140}N_{16}O_{16}$ calc./obs. 1510.07/1510.43 Da $[M+H]^+$.

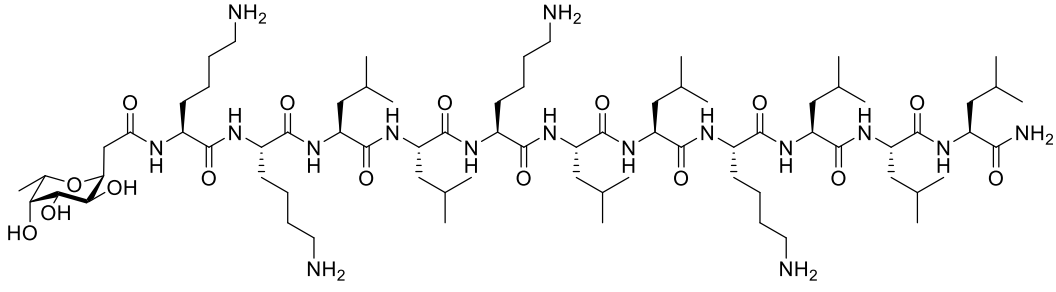

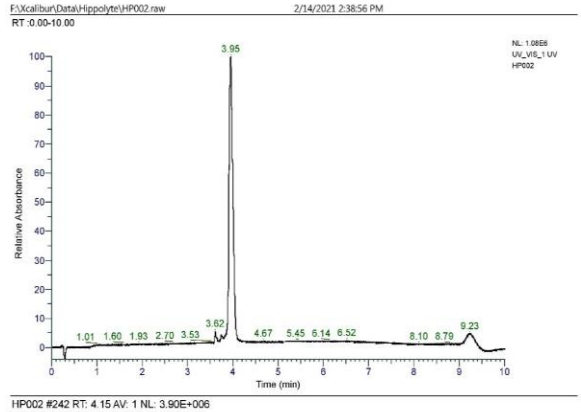

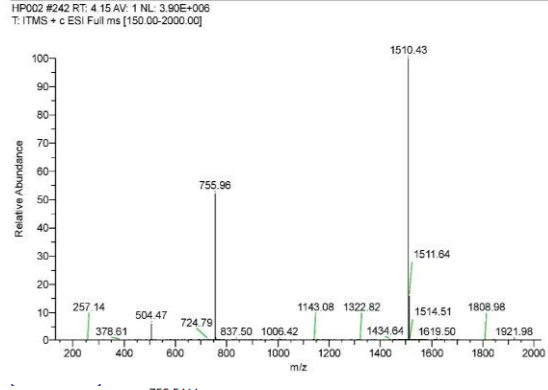

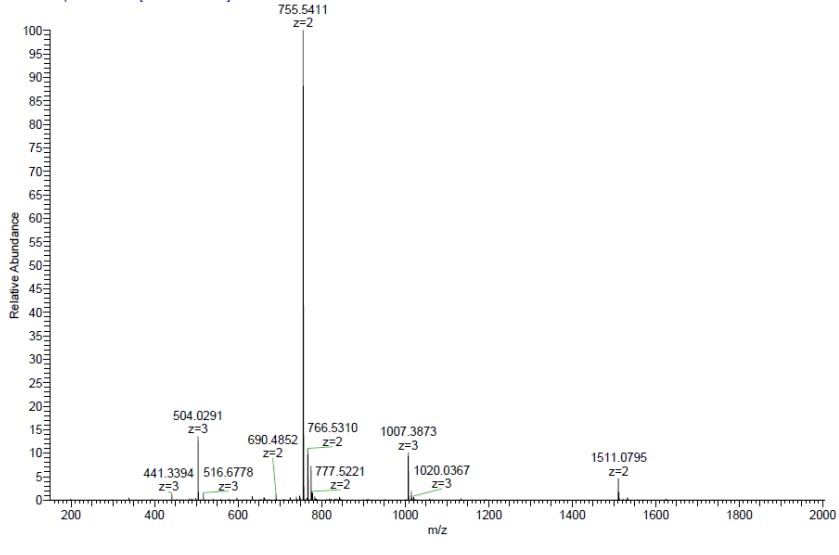

(*)kkllkllklll (Fdln65) was obtained as foamy white solid after preparative RP-HPLC (9.8 mg, 8.0 %). * = α-L-fucosyl-acetyl group. Analytical RP-HPLC: t_R = 3.95 min (A/D 100:0 to 0:100 in 7.0 min, λ = 214nm). MS (ESI$^+$): $C_{74}H_{140}N_{16}O_{16}$ calc./obs. 1510.08/1510.50 Da $[M+H]^+$.

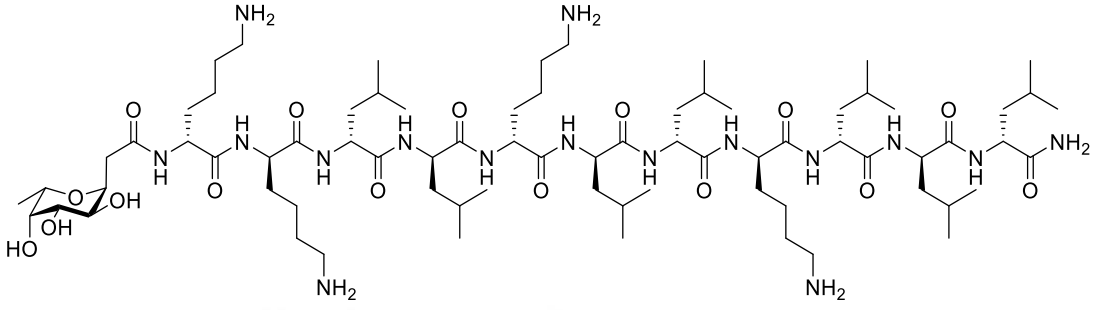

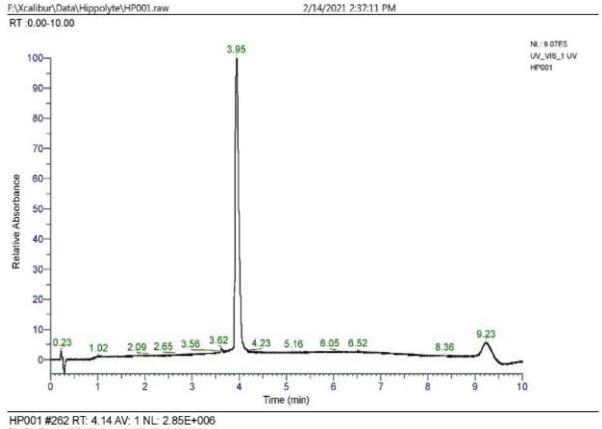

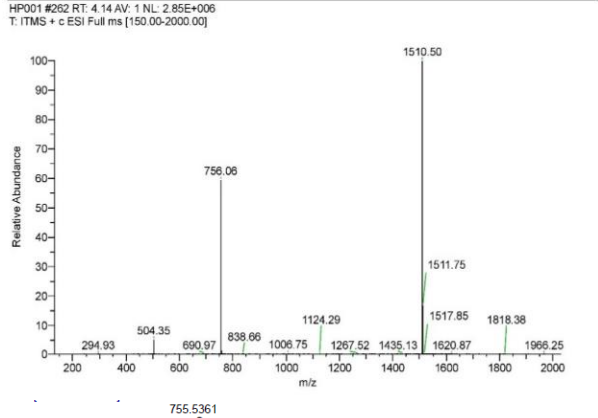

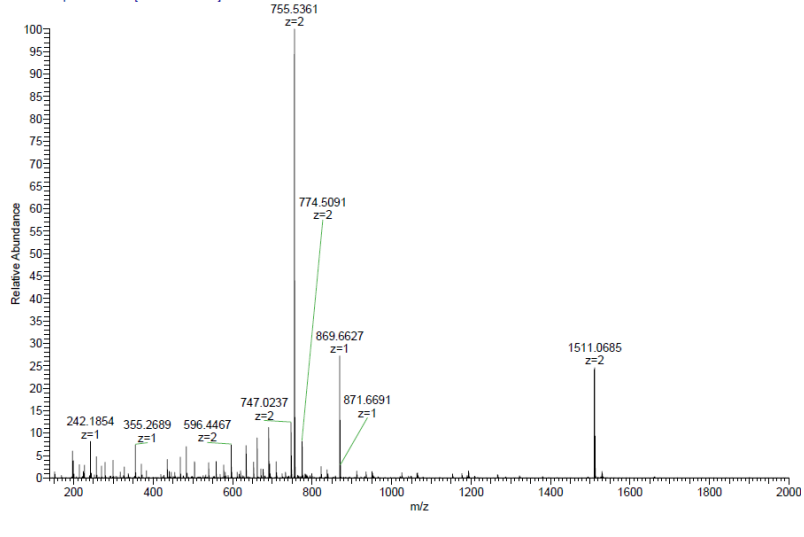

(*)kkLLkLLkLLL (Fln69) was obtained as foamy white solid after preparative RP-HPLC (38.2 mg, 19.0 %). * = α-L-fucosyl-acetyl group. Analytical RP-HPLC: t_R = 3.45 min (A/D 100:0 to 0:100 in 7.0 min, λ = 214nm). MS (ESI^+): $C_{74}H_{140}N_{16}O_{16}$ calc./obs. 1510.07/1509.89 Da $[M+H]^+$.

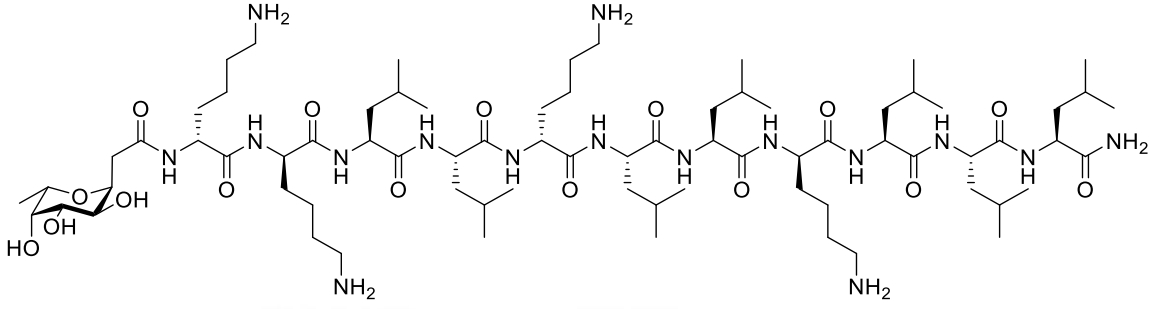

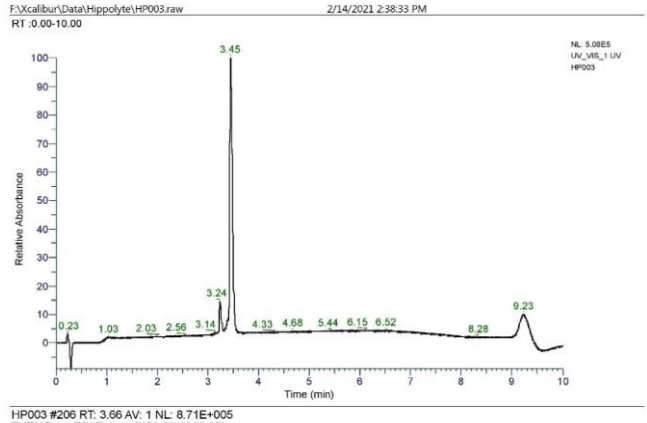

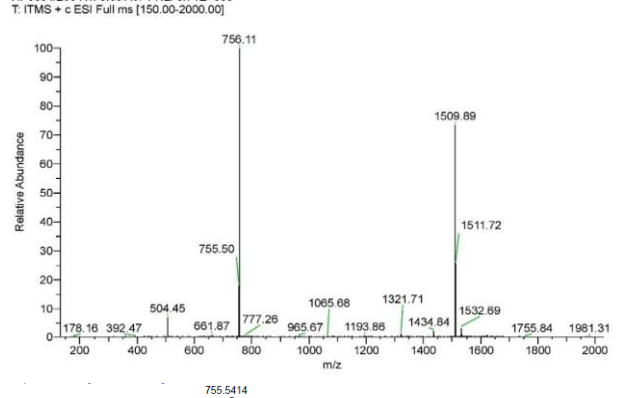

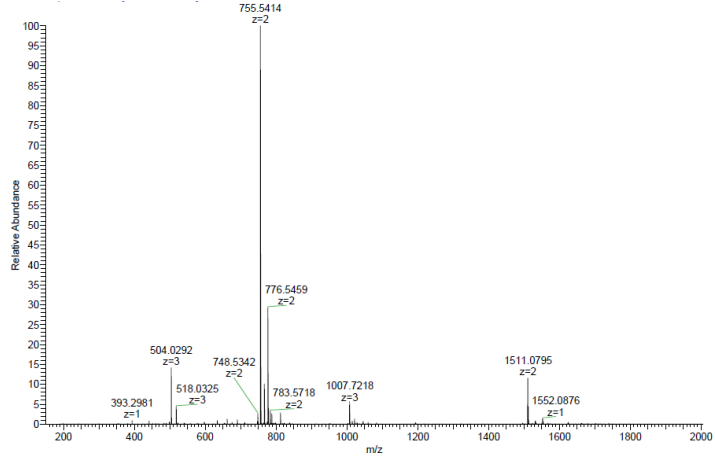

(*)KKllKllKlll (Fdln69) was obtained as foamy white solid after preparative RP-HPLC (12.9 mg, 13.0 %). * = α-L-fucosyl-acetyl group. Analytical RP-HPLC: t_R = 3.45 min (A/D 100:0 to 0:100 in 7.0 min, λ = 214nm). MS (ESI^+): $C_{74}H_{140}N_{16}O_{16}$ calc./obs. 1510.07/1510.08 Da $[M+H]^+$.

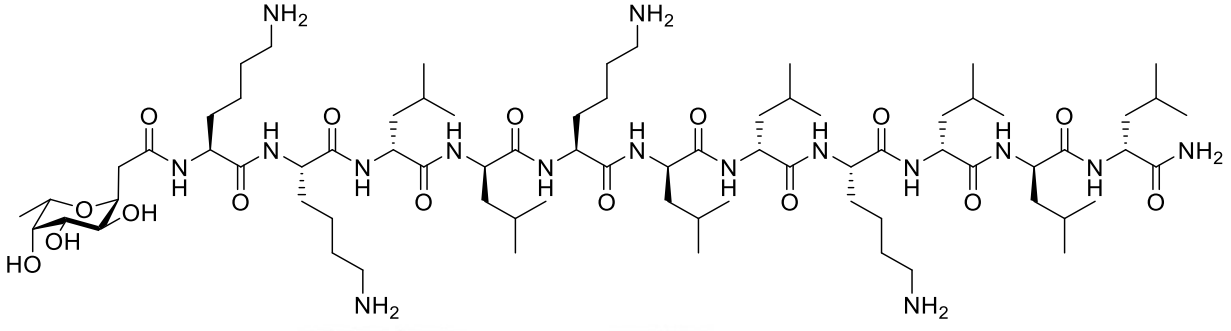

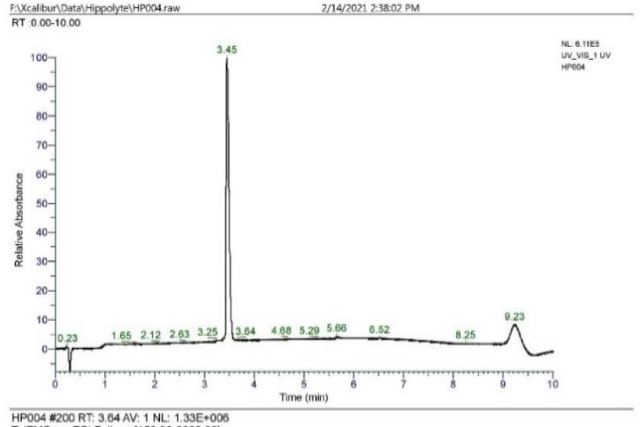

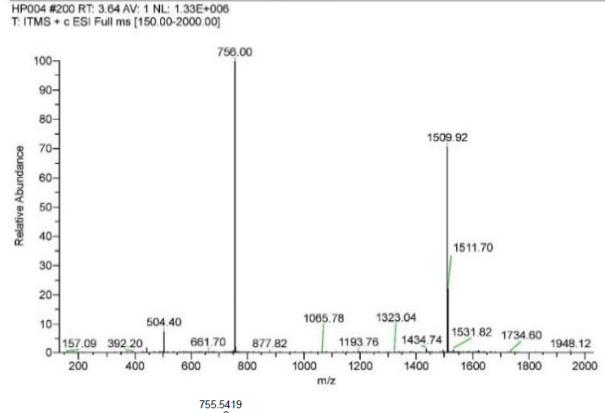

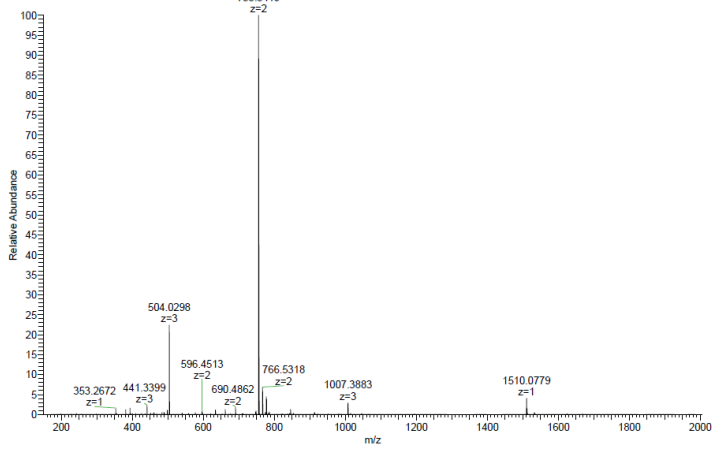

8.2 SI for To Fold or Not to Fold: Diastereomeric Optimization of an α-helical Antimicrobial Peptide

Peptide synthesis

Table S2.1: Synthesis of linear AMPs.

Cpd.	Sequence[a)]	SPPS yield[b)]	MS analysis[c)]	Analytical HPLC[d)]
		mg (%)	calc./obs.	t_R (min)
ln65	KKLLKLLKLLL	84.0 (58.0)	1320.99/1320.99	1.66
dln65	kkllkllklll	34.9 (24.1)	1320.99/1322.00	1.62
ln69	kkLLkLLkLLL	102.6 (70.9)	1320.99/1320.99	1.55
dln69	KKllKllKlll	69.7 (44.6)	1320.99/1322.00	1.52
***sr*-ln65**	KKLLKLLKLLL	64.6 (41.3)	1320.99/1321.00	1.58
***sr*-ln65L^6**	KKLLKLLKLLL	77.3 (49.4)	1320.99/1322.00	1.56
HP1	KkLLKLLKLLL	53.0 (47.7)	1320.99/1321.00	1.67
HP2	kkLLKLLKLLL	56.7 (51.0)	1320.99/1320.99	1.66
HP3	KkLLkLLKLLL	50.1 (45.1)	1320.99/1322.00	1.61
HP4	KkLlKLLKLLL	42.6 (38.3)	1320.99/1322.00	1.74
HP5	kKLLKLLKLLl	49.1 (44.2)	1320.99/1322.00	1.65
HP6	KKLLKllKLLL	49.3 (44.4)	1320.99/1322.00	1.53
HP7	kkLLKLLKLLl	60.6 (54.5)	1320.99/1322.00	1.62
HP8	KkllKLLKLLL	46.9 (42.2)	1320.99/1322.00	1.63
HP9	KKLLkllKLLL	63.9 (57.5)	1320.99/1322.00	1.52
HP10	kkLLkLLKLLL	50.0 (45.0)	1320.99/1322.00	1.60
HP11	KkllKLlKLLL	31.5 (35.4)	1320.99/1322.00	1.60
HP12	KkllKlLKLLL	26.8 (30.1)	1320.99/1322.00	1.60
HP13	KKLLkllkLLL	37.4 (42.1)	1320.99/1322.00	1.53
HP14	KKllKllKLLL	33.7 (37.9)	1320.99/1322.00	1.53
HP15	KKlLkLlKlLL	34.5 (38.8)	1320.99/1322.00	1.60
HP16	KKLlkLLklLL	16.0 (18.0)	1320.99/1322.00	1.59
HP17	KklLKLLKllL	29.0 (26.1)	1320.99/1322.00	1.61
HP18	kkLLKLLKLll	36.3 (32.7)	1320.99/1320.99	1.58
HP19	kkLLkLLKLLl	53.0 (47.7)	1320.99/1322.00	1.56
HP20	KKllKLLklLL	51.4 (46.3)	1320.99/1322.00	1.52
HP21	KklLKlLKlLL	64.2 (65.7)	1320.99/1322.00	1.60
HP22	KKllKLlKLlL	45.9 (46.9)	1320.99/1322.00	1.55
HP23	KKLlkLLkLLl	64.7 (66.2)	1320.99/1322.00	1.56
HP24	KkllKllKLLL	54.7 (49.2)	1320.99/1322.00	1.56
HP25	KKllKllKlLL	38.8 (34.9)	1320.99/1322.00	1.55
HP26	kkLLkLLKLll	52.6 (47.3)	1320.99/1322.00	1.57
HP27	kkLLkLLkLLl	53.7 (48.3)	1320.99/1322.00	1.54
HP28	kKLLkllKLLl	45.6 (41.0)	1320.99/1322.00	1.55
HP29	KKLlkllkLLL	59.3 (53.4)	1320.99/1322.00	1.58
HP30	KkLlKlLkLlL	35.7 (32.1)	1320.99/1322.00	1.57
HP31	kKlLkLlKlLl	45.3 (40.8)	1320.99/1322.00	1.57
HP32	RRLLRLLRLLL	32.5 (27.5)	1433.02/1434.03	1.64
HP33	rrLLrLLrLLL	44.3 (37.5)	1433.02/1434.03	1.52
HP34	KKIIKIIKIII	35.1 (31.6)	1320.99/1322.00	1.44
HP35	kkIIkIIkIII	29.3 (26.4)	1320.99/1322.00	1.36
HP36	RRIIRIIRIII	7.7 (6.5)	1433.02/1434.03	1.47
HP37	rrIIrIIrIII	38.7 (32.8)	1433.02/1434.03	1.68
2ln65	$(KKLLKLLKLLL)_2$	119.3 (38.3)	2624.96/2625.67	2.38
2ln69	$(kkLLkLLkLLL)_2$	85.8 (27.6)	2624.96/2625.97	1.85
FHP1	(*)KkLLKLLKLLL	2.9 (3.9)	1509.06/1511.07	1.76
FHP2	(*)kkLLKLLKLLL	0.6 (0.8)	1509.06/1510.07	1.73
FHP3	(*)KkLLkLLKLLL	4.5 (6.1)	1509.06/1510.07	1.67
FHP4	(*)KkLlKLLKLLL	4.5 (6.1)	1509.06/1510.07	1.74
FHP5	(*)kKLLKLLKLLl	4.3 (5.8)	1509.06/1510.07	1.66
FHP7	(*)kkLLKLLKLLl	3.4 (4.6)	1509.06/1510.07	1.63

FHP8	(*)KkllKLLKLLL	5.7 (7.7)	1509.06/1510.06	1.63
FHP10	(*)kkLLkLLKLLL	4.0 (5.4)	1509.06/1510.07	1.67
FHP11	(*)KkllKLlKLLL	16.9 (17.2)	1509.06/1510.07	1.63
FHP30	(*)KkLlKlLkLlL	9.0 (12.2)	1509.06/1510.06	1.62
FHP31	(*)kKlLkLlKlLl	5.7 (7.7)	1509.06/1510.07	1.62
FHP32	(*)RRLLRLLRLLL	5.7 (7.3)	1621.09/1621.09	1.79
FHP33	(*)rrLLrLLrLLL	2.5 (3.2)	1621.09/1621.09	1.62

[a)] One letter code for amino acid. D- amino acids in lower case. (*) = α-L-fucosyl acetyl moiety. [b)] Yields given for RP-HPLC purified products. [c)] High-resolution electrospray ionization mass spectrometry (positive mode), the calculated monoisotopic mass and the observed mass are given. [d)] retention time in analytical RP-HPLC (A/D = 100/0 to 0/100 in 3.5 min, λ = 214 nm).

Circular dichroism spectroscopy

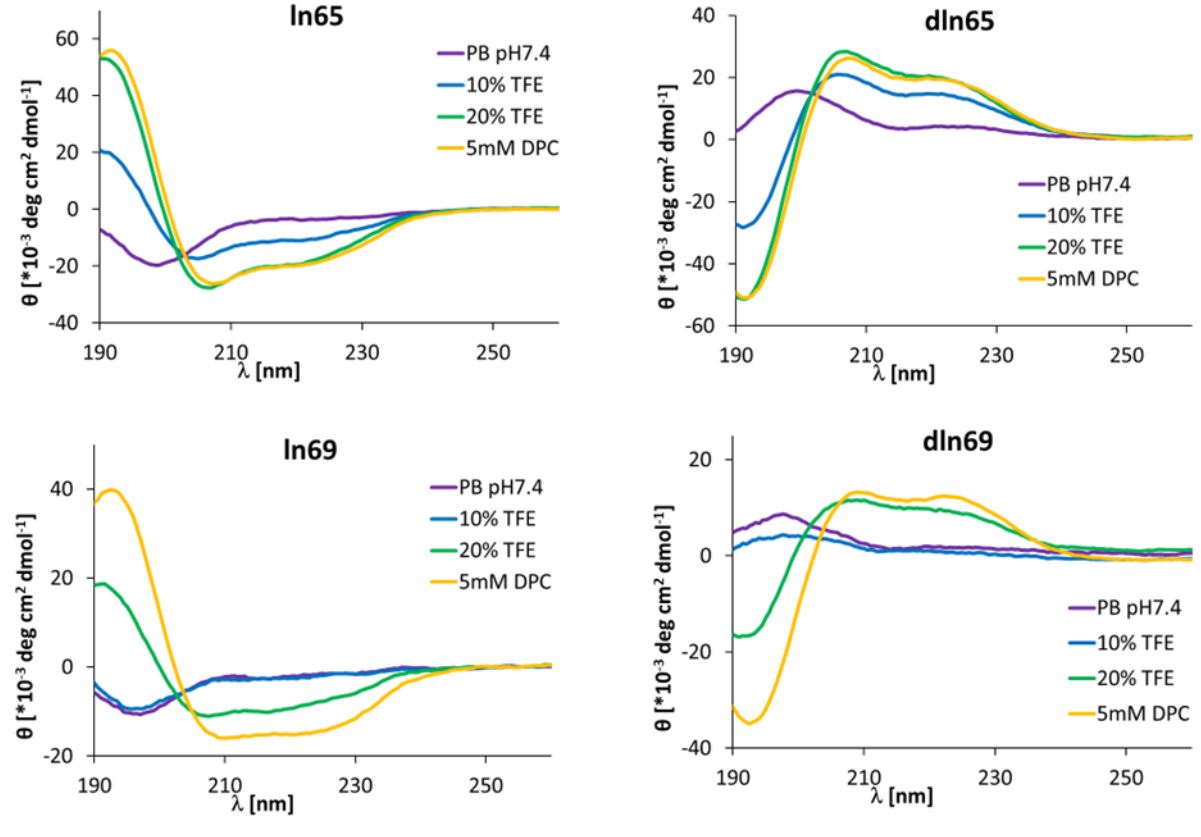

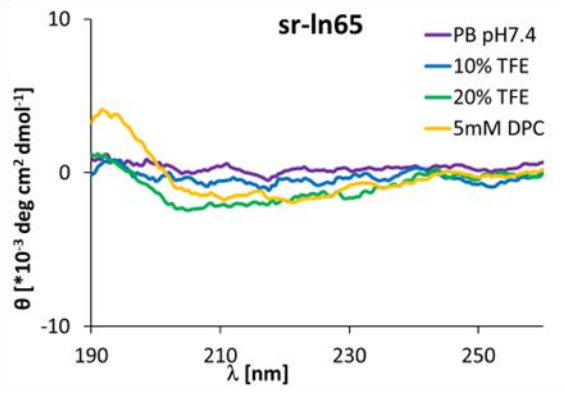
sr-ln65
PB pH7.4
10% TFE
20% TFE
5mM DPC
θ [*10-3 deg cm2 dmol-1]
λ [nm]

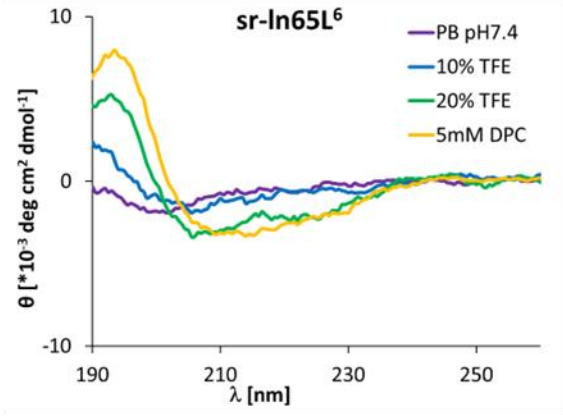
sr-ln65L6
PB pH7.4
10% TFE
20% TFE
5mM DPC
θ [*10-3 deg cm2 dmol-1]
λ [nm]

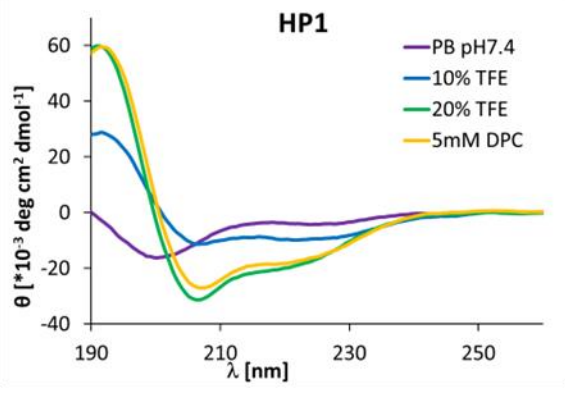
HP1
PB pH7.4
10% TFE
20% TFE
5mM DPC
θ [*10-3 deg cm2 dmol-1]
λ [nm]

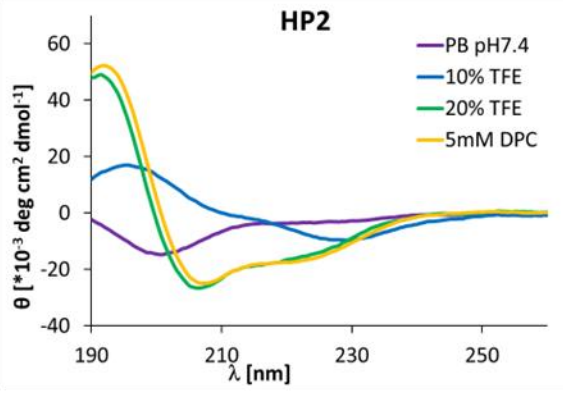
HP2
PB pH7.4
10% TFE
20% TFE
5mM DPC
θ [*10-3 deg cm2 dmol-1]
λ [nm]

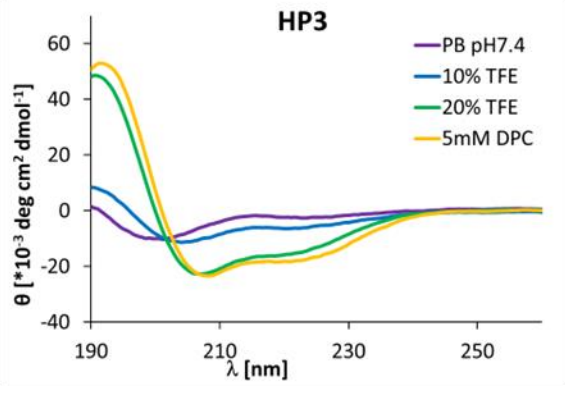
HP3
PB pH7.4
10% TFE
20% TFE
5mM DPC
θ [*10-3 deg cm2 dmol-1]
λ [nm]

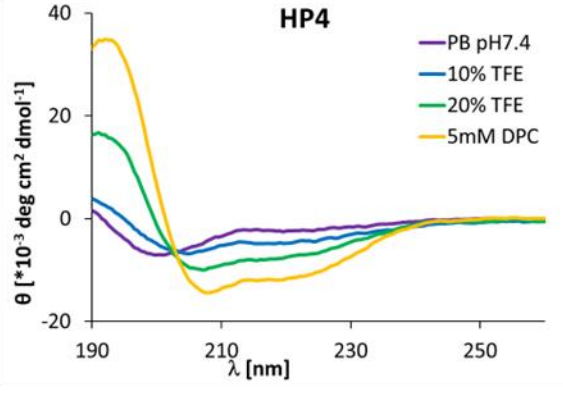
HP4
PB pH7.4
10% TFE
20% TFE
5mM DPC
θ [*10-3 deg cm2 dmol-1]
λ [nm]

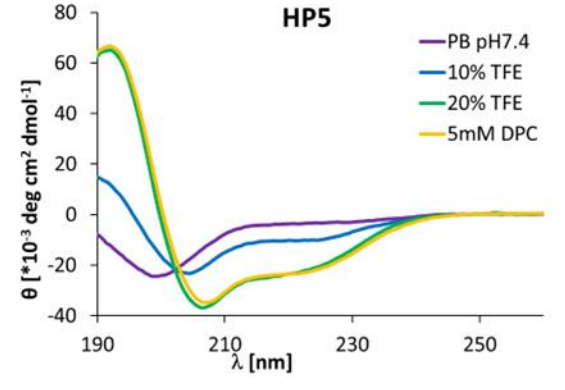
HP5
PB pH7.4
10% TFE
20% TFE
5mM DPC
θ [*10-3 deg cm2 dmol-1]
λ [nm]

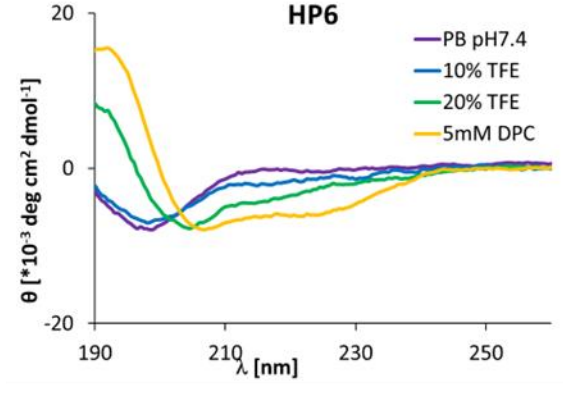
HP6
PB pH7.4
10% TFE
20% TFE
5mM DPC
θ [*10-3 deg cm2 dmol-1]
λ [nm]

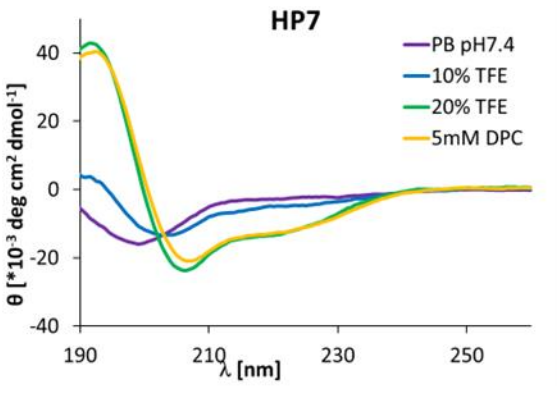
HP7
PB pH7.4
10% TFE
20% TFE
5mM DPC
θ [*10-3 deg cm2 dmol-1]
λ [nm]

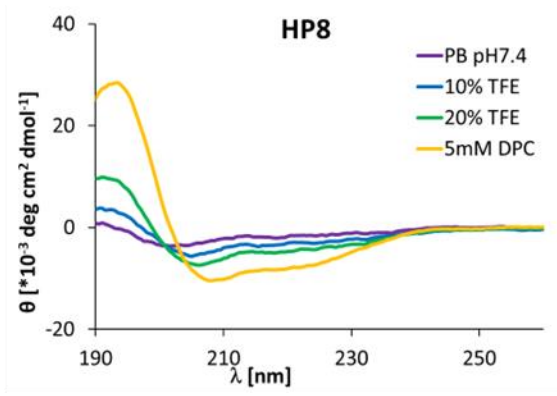
HP8
PB pH7.4
10% TFE
20% TFE
5mM DPC
θ [*10-3 deg cm2 dmol-1]
λ [nm]

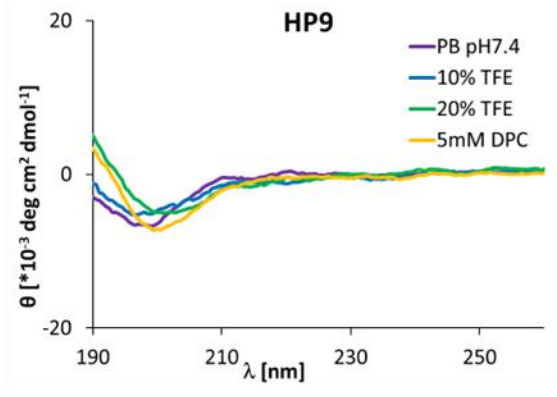
HP9
PB pH7.4
10% TFE
20% TFE
5mM DPC
θ [*10-3 deg cm2 dmol-1]
λ [nm]

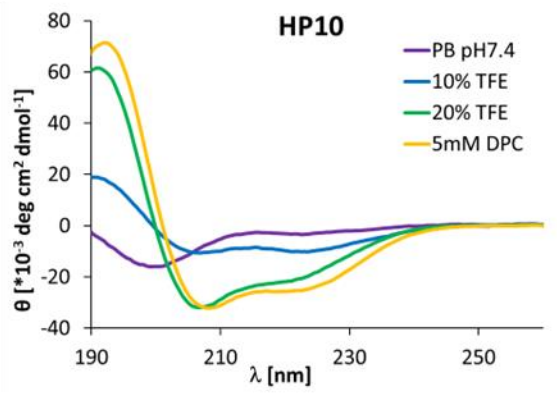
HP10
PB pH7.4
10% TFE
20% TFE
5mM DPC
θ [*10-3 deg cm2 dmol-1]
λ [nm]

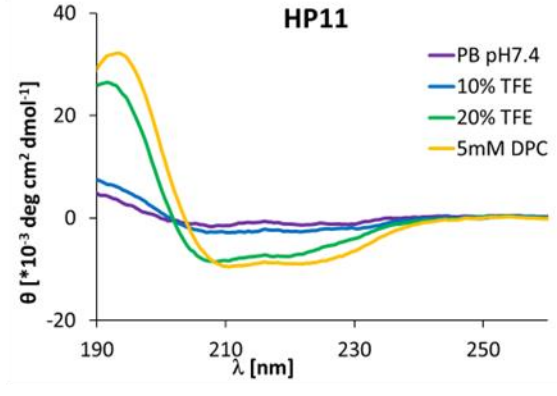
HP11
PB pH7.4
10% TFE
20% TFE
5mM DPC
θ [*10-3 deg cm2 dmol-1]
λ [nm]

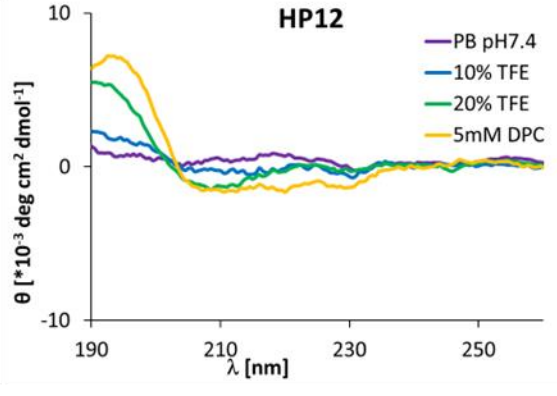
HP12
PB pH7.4
10% TFE
20% TFE
5mM DPC
θ [*10-3 deg cm2 dmol-1]
λ [nm]

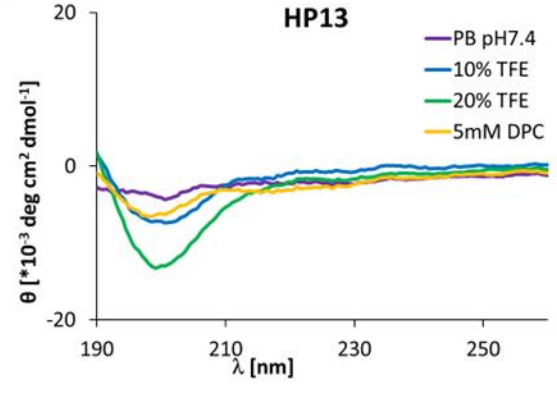
HP13
PB pH7.4
10% TFE
20% TFE
5mM DPC
θ [*10-3 deg cm2 dmol-1]
λ [nm]

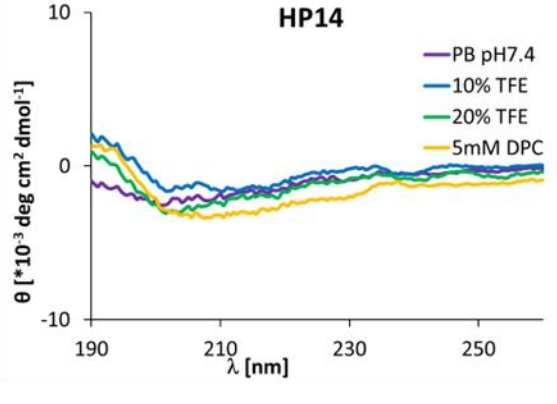
HP14
PB pH7.4
10% TFE
20% TFE
5mM DPC
θ [*10-3 deg cm2 dmol-1]
λ [nm]

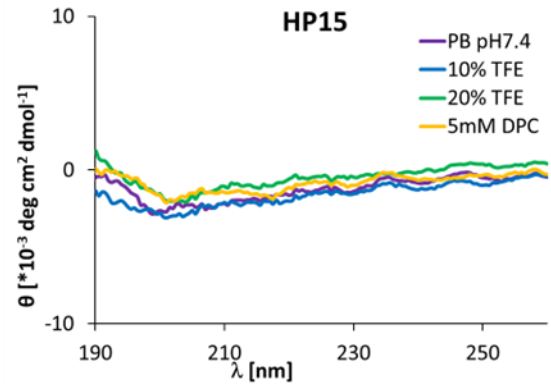
HP15
PB pH7.4
10% TFE
20% TFE
5mM DPC
θ [*10-3 deg cm2 dmol-1]
λ [nm]

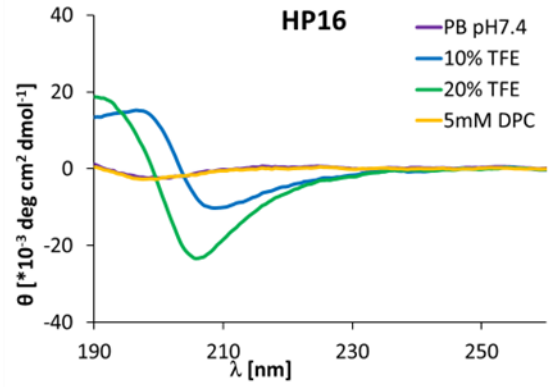
HP16
PB pH7.4
10% TFE
20% TFE
5mM DPC
θ [*10-3 deg cm2 dmol-1]
λ [nm]

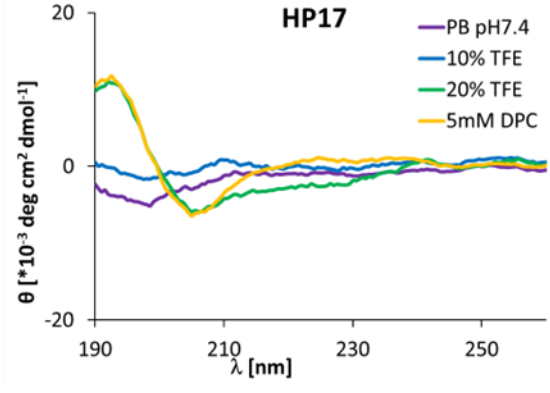
HP17
PB pH7.4
10% TFE
20% TFE
5mM DPC
θ [*10-3 deg cm2 dmol-1]
λ [nm]

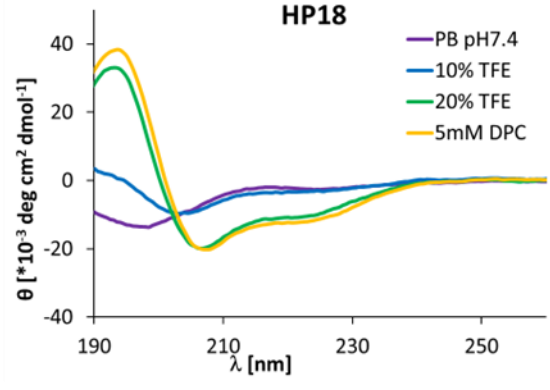
HP18
PB pH7.4
10% TFE
20% TFE
5mM DPC
θ [*10-3 deg cm2 dmol-1]
λ [nm]

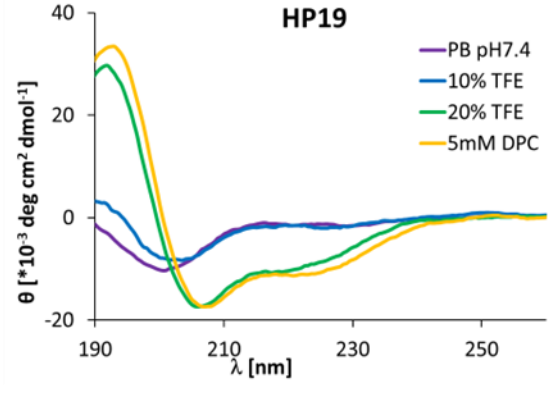
HP19
PB pH7.4
10% TFE
20% TFE
5mM DPC
θ [*10-3 deg cm2 dmol-1]
λ [nm]

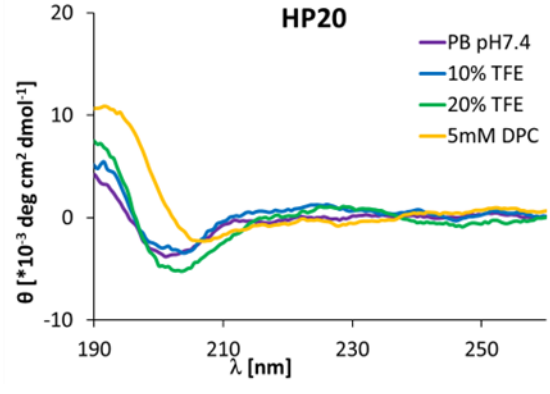
HP20
PB pH7.4
10% TFE
20% TFE
5mM DPC
θ [*10-3 deg cm2 dmol-1]
λ [nm]

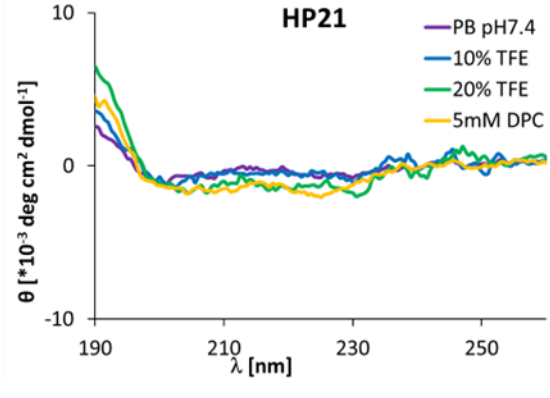
HP21
PB pH7.4
10% TFE
20% TFE
5mM DPC
θ [*10-3 deg cm2 dmol-1]
λ [nm]

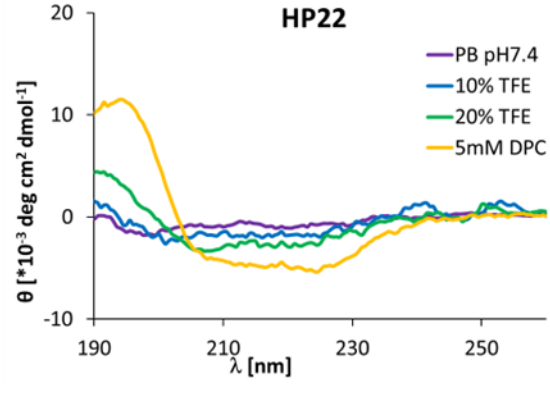
HP22
PB pH7.4
10% TFE
20% TFE
5mM DPC
θ [*10-3 deg cm2 dmol-1]
λ [nm]

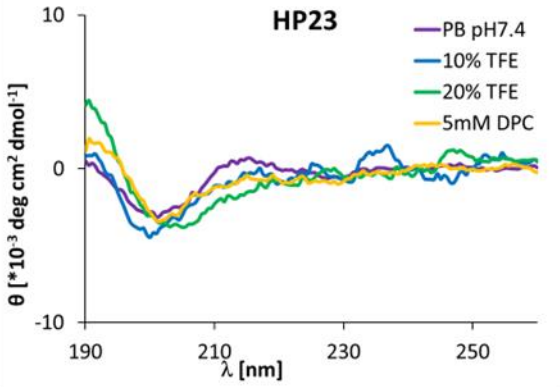
HP23
PB pH7.4
10% TFE
20% TFE
5mM DPC
θ [*10-3 deg cm2 dmol-1]
λ [nm]
10
0
-10
190
210
230
250

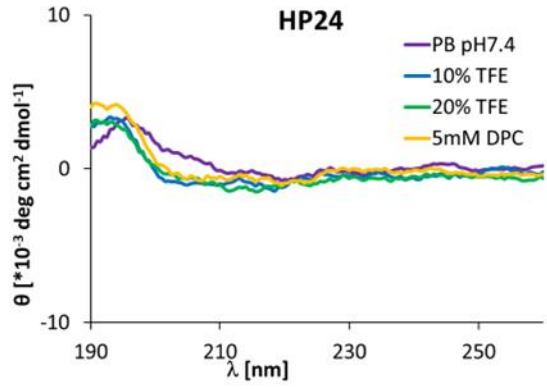
HP24
PB pH7.4
10% TFE
20% TFE
5mM DPC
θ [*10-3 deg cm2 dmol-1]
λ [nm]
10
0
-10
190
210
230
250

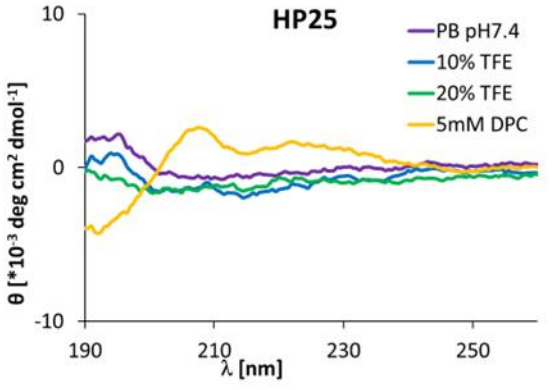
HP25
PB pH7.4
10% TFE
20% TFE
5mM DPC
θ [*10-3 deg cm2 dmol-1]
λ [nm]
10
0
-10
190
210
230
250

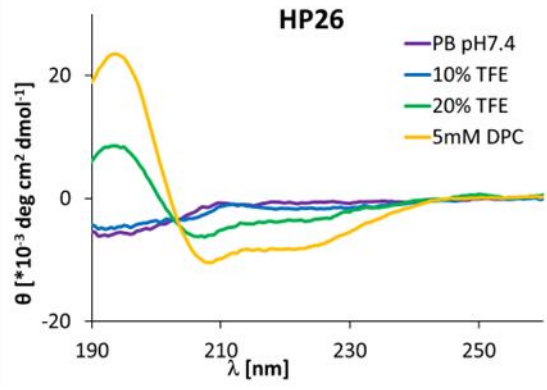
HP26
PB pH7.4
10% TFE
20% TFE
5mM DPC
θ [*10-3 deg cm2 dmol-1]
λ [nm]
20
0
-20
190
210
230
250

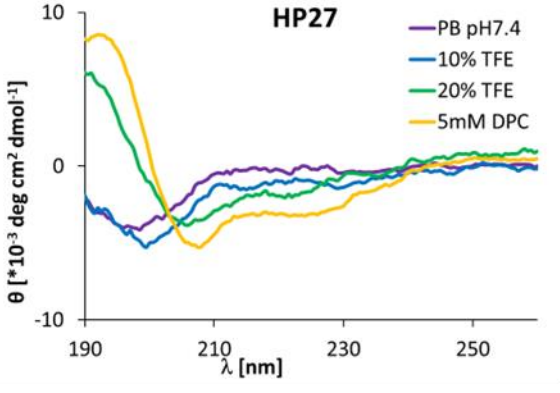
HP27
PB pH7.4
10% TFE
20% TFE
5mM DPC
θ [*10-3 deg cm2 dmol-1]
λ [nm]
10
0
-10
190
210
230
250

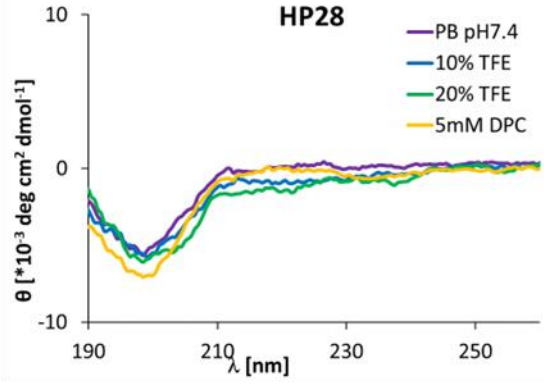
HP28
PB pH7.4
10% TFE
20% TFE
5mM DPC
θ [*10-3 deg cm2 dmol-1]
λ [nm]
10
0
-10
190
210
230
250

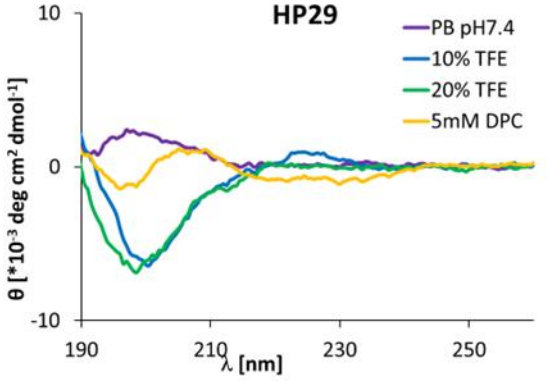
HP29
PB pH7.4
10% TFE
20% TFE
5mM DPC
θ [*10-3 deg cm2 dmol-1]
λ [nm]
10
0
-10
190
210
230
250

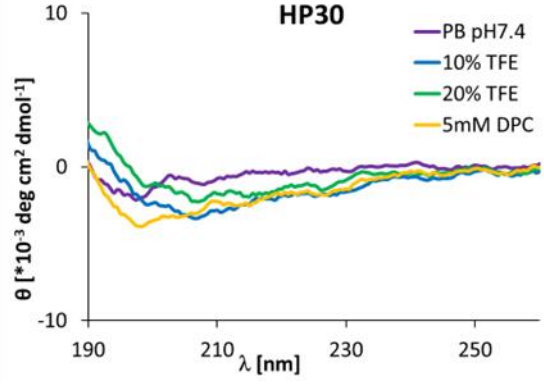
HP30
PB pH7.4
10% TFE
20% TFE
5mM DPC
θ [*10-3 deg cm2 dmol-1]
λ [nm]
10
0
-10
190
210
230
250

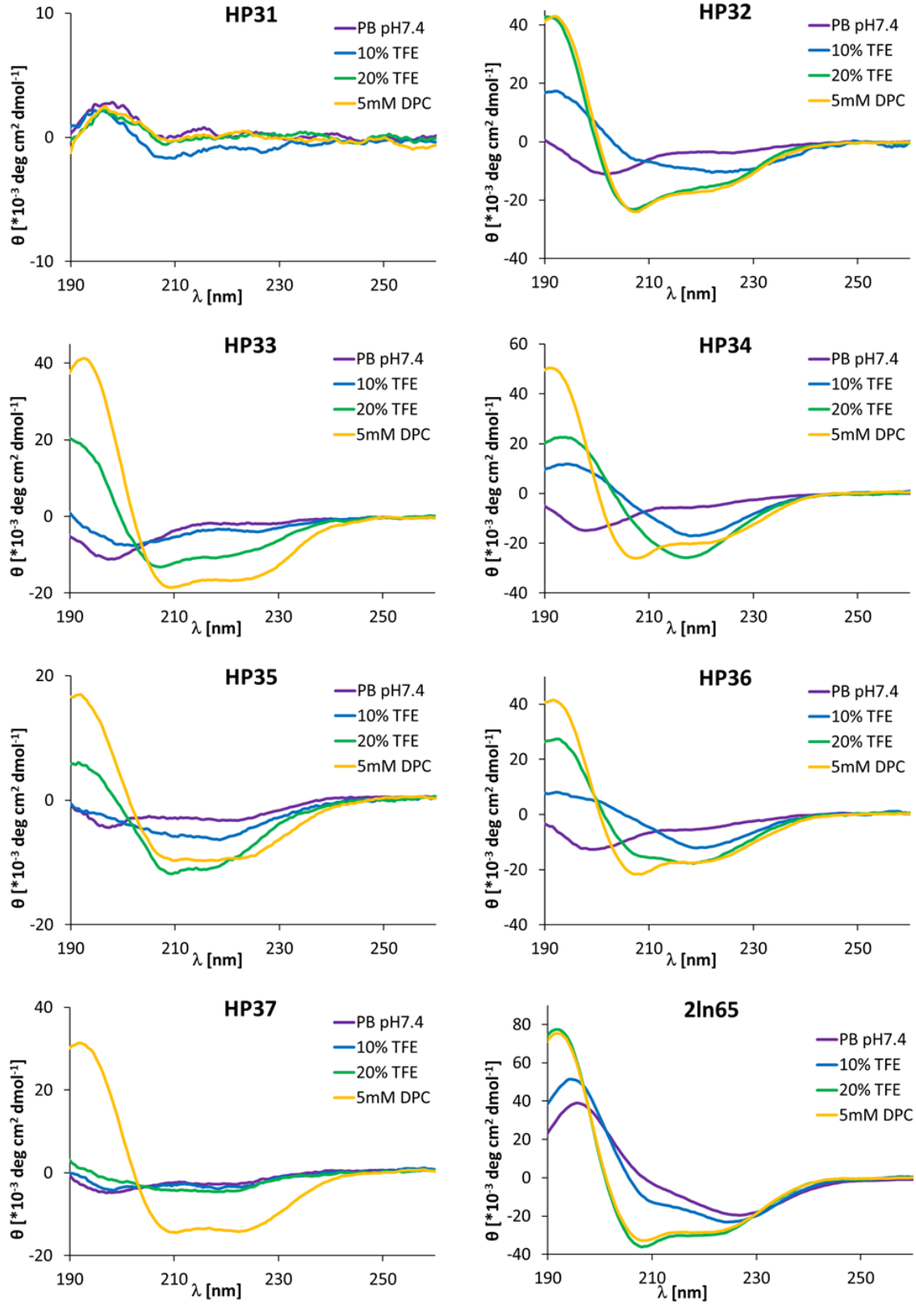
HP31
HP32
HP33
HP34
HP35
HP36
HP37
2ln65
PB pH7.4
10% TFE
20% TFE
5mM DPC
θ [*10⁻³ deg cm² dmol⁻¹]
λ [nm]

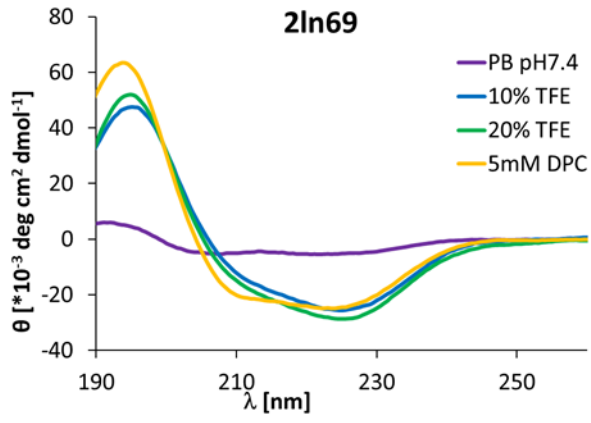

Figure S2.1: Circular dichroism spectra of linear peptides at 0.100 mg/mL in 7 mM phosphate buffer pH 7.4 with different amount of TFE and 5 mM DPC.

Table S2.2: Dichroweb analysis of linear peptides.

Cpd.	Sequence [a)]	CD α/β/t/u (%) [b)]			
		PB Buffer	10% TFE	20% TFE	5 mM DPC
sr-**ln65**	KKLLKLLKLLL	5/42/21/32	7/39/22/32	10/37/22/31	10/36/23/31
sr-**ln65L**[6]	KKLLKLLKLLL	9/35/24/32	11/36/23/31	17/30/22/31	17/32/22/29
ln65	KKLLKLLKLLL	14/24/27/35	37/12/24/27	64/3/17/16	73/2/15/10
dln65	kkllkllklll	11/18/24/37	45/9/20/26	61/3/16/20	67/2/14/17
ln69	kkLLkLLkLLL	11/30/24/35	10/30/25/35	34/20/20/26	61/6/16/17
dln69	KKllKllKlll	8/34/23/35	7/36/22/35	28/23/20/29	59/13/15/23
HP1	KkLLKLLKLLL	18/22/24/36	43/18/20/19	69/3/16/12	73/2/14/11
HP2	kkLLKLLKLLL	16/23/27/34	35/24/21/20	60/3/17/20	69/2/15/14
HP3	KkLLkLLKLLL	13/30/23/34	24/22/25/29	56/8/16/20	69/3/15/13
HP4	KkLkLLKLLL	11/33/23/33	15/31/24/30	27/25/21/27	46/17/16/21
HP5	kKLLKLLKLLl	16/19/28/37	40/7/23/30	84/0/12/4	90/0/10/0
HP6	KKLLKllKLLL	9/32/24/35	9/22/24/34	16/30/24/30	29/23/22/26
HP7	kkLLKLLKLLl	14/25/27/34	23/21/25/31	59/2/22/17	60/6/17/17
HP8	KkllKLLKLLL	9/36/23/32	16/33/23/28	22/28/23/27	37/22/19/22
HP9	KKLLkllKLLL	8/34/24/34	9/34/24/33	9/35/22/34	10/33/25/32
HP10	kkLLkLLKLLL	12/26/26/36	35/19/21/25	72/2/13/13	90/1/9/0
HP11	KkllKLlKLLL	14/32/22/32	18/31/21/30	38/22/18/22	52/15/14/18
HP12	KkllKlLKLLL	8/37/23/32	10/37/22/31	12/36/22/30	17/34/21/28
HP13	KKLLkllkLLL	11/31/26/32	6/37/22/35	11/30/24/35	9/34/24/33
HP14	KKllKllKLLL	7/37/23/33	5/40/23/32	8/37/24/31	13/33/23/31
HP15	KKlLkLlKlLL	9/35/23/33	8/36/25/31	6/41/21/32	6/39/23/32
HP16	KKLlkLLklLL	8/36/24/32	39/23/16/22	56/5/20/19	8/31/19/22
HP17	KklLKLLKllL	8/35/24/33	7/38/22/33	17/31/22/30	16/33/22/29
HP18	kkLLKLLKLll	13/24/27/36	18/26/23/33	56/4/21/19	63/3/17/17
HP19	kkLLkLLKLLl	13/29/25/33	16/28/24/32	44/13/21/22	55/6/20/19
HP20	KKllKLLklLL	7/38/23/32	8/38/23/31	9/35/25/31	15/37/20/28

HP21	KklLKlLKlLL	8/37/23/32	8/38/22/32	11/37/22/30	11/35/22/32
HP22	KKllKLlKLlL	8/37/23/32	8/36/22/34	13/34/22/31	23/30/19/28
HP23	KKLlkLLkLLl	10/35/23/32	8/36/23/33	11/36/23/30	10/35/24/31
HP24	KkllKllKLLL	7/39/22/32	7/39/23/31	8/38/23/31	7/39/22/32
HP25	KKllKllKlLL	6/39/22/33	5/40/21/34	5/40/21/34	12/34/22/32
HP26	kkLLkLLKLll	9/33/24/34	12/33/24/31	24/26/22/28	41/18/19/22
HP27	kkLLkLLkLLl	9/34/24/33	10/33/24/33	14/32/22/32	23/27/21/29
HP28	kKLLkllKLLl	8/35/23/34	10/32/24/34	10/33/25/32	10/33/24/33
HP29	KKLlkllkLLL	6/39/22/33	7/36/24/33	7/35/23/35	7/38/22/33
HP30	KkLlKlLkLlL	6/38/22/34	10/35/23/32	7/38/23/32	7/37/23/33
HP31	kKlLkLlKlLl	5/38/22/35	4/40/21/35	6/39/21/34	5/39/20/36
HP32	RRLLRLLRLLL	16/27/24/33	32/25/20/23	56/5/17/22	62/3/16/19
HP33	rrLLrLLrLLL	10/30/25/35	14/29/23/34	32/21/19/28	63/5/16/16
HP34	KKIIKIIKIII	12/26/27/35	16/32/20/32	21/29/20/30	68/3/15/14
HP35	kkIIkIIkIII	10/32/23/35	12/30/24/34	22/23/23/32	22/22/19/27
HP36	RRIIRIIRIII	12/27/26/35	14/33/20/33	39/16/18/27	60/4/18/18
HP37	rrIIrIIrIII	7/34/23/36	10/33/23/34	11/32/23/34	50/11/16/23
2ln65	$(KKLLKLLKLLL)_2$	58/14/18/10	68/3/9/10	94/1/5/0	91/1/7/1
2ln69	$(kkLLkLLkLLL)_2$	20/28/21/31	73/5/11/11	80/5/13/2	82/3/9/6

[a] One letter code for amino acids. D- amino acids are in lower case and stereorandomized residues are underlined. [b] CD spectra were recorded at 0.100 mg/mL in aqueous 7 mM phosphate buffer pH 7.4 with addition of 0, 10 and 20% TFE or 5 mM DPC. The primary CD spectra were analyzed using Dichroweb and the percentages of α-helical (α), β-sheet (β), turns (t) and unordered (u) signals were extracted. The Contin-LL method and reference set 4 were used.[178]

Vesicle leakage assay

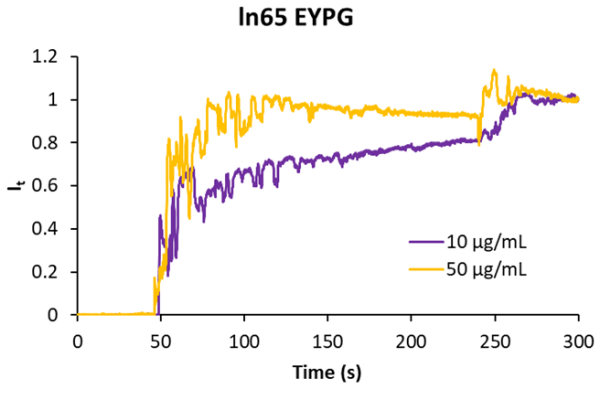

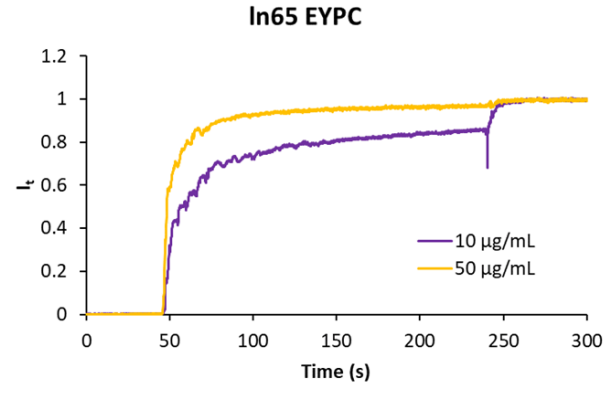

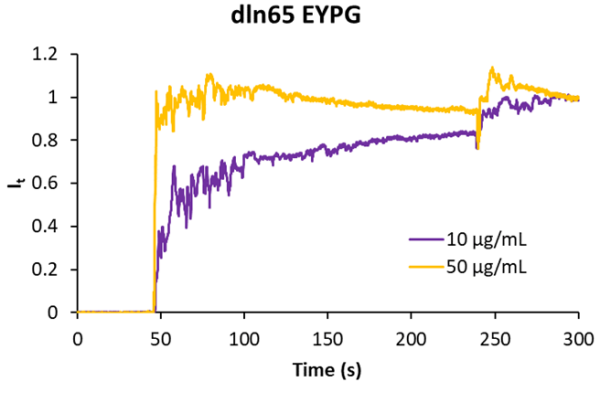

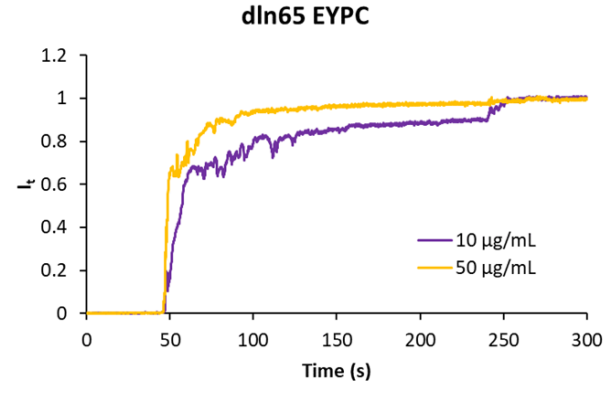

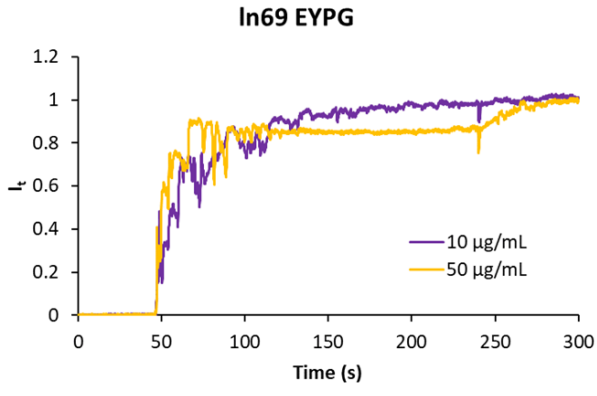

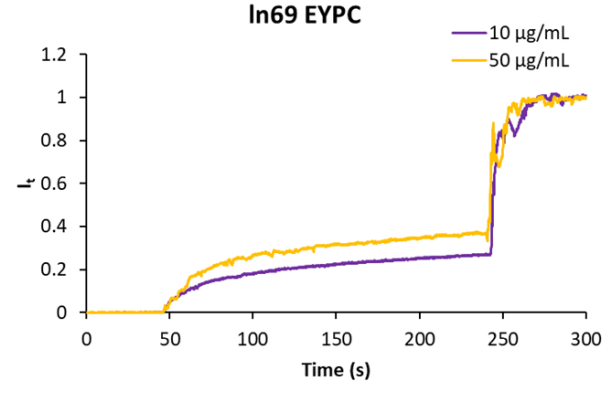

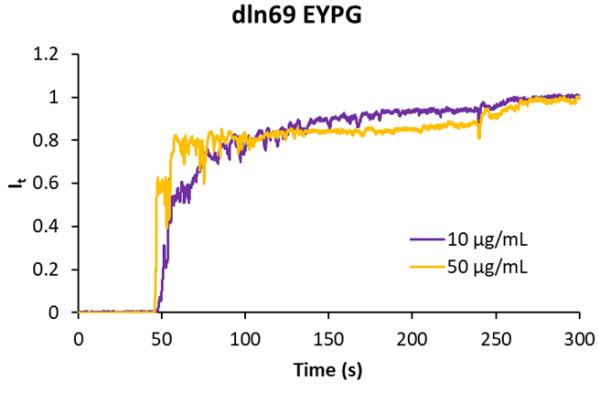

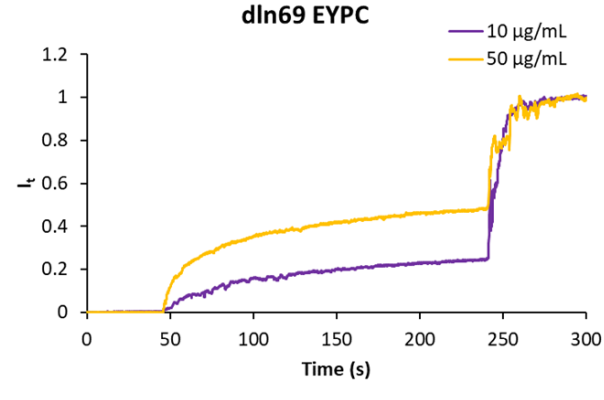

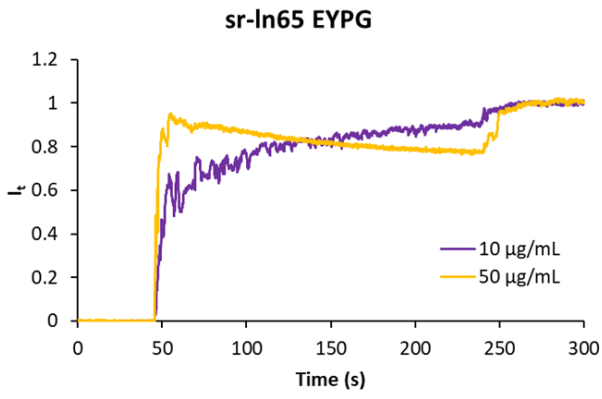
sr-ln65 EYPG
I_t
Time (s)
10 µg/mL
50 µg/mL

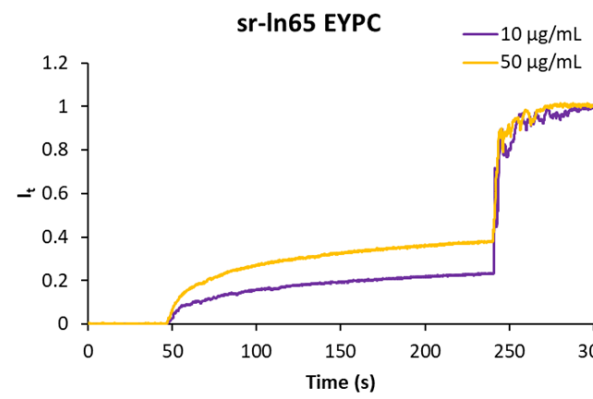
sr-ln65 EYPC
I_t
Time (s)
10 µg/mL
50 µg/mL

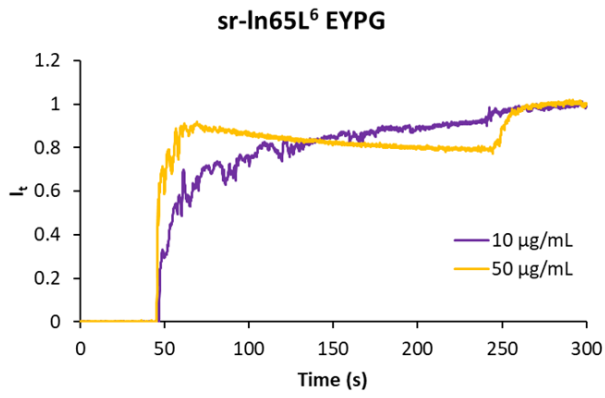
sr-ln65L^6 EYPG
I_t
Time (s)
10 µg/mL
50 µg/mL

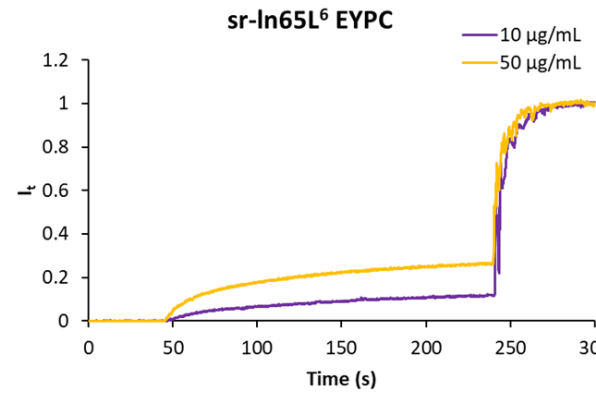
sr-ln65L^6 EYPC
I_t
Time (s)
10 µg/mL
50 µg/mL

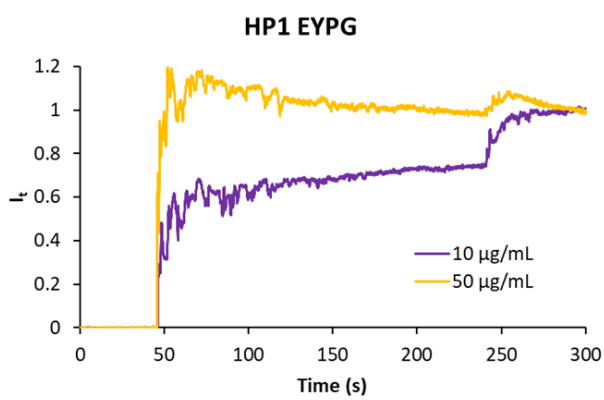
HP1 EYPG
I_t
Time (s)
10 µg/mL
50 µg/mL

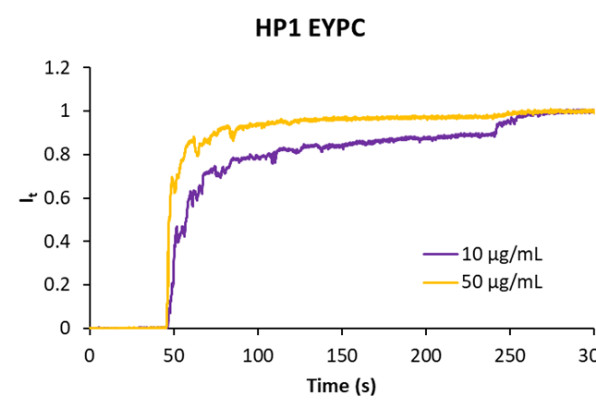
HP1 EYPC
I_t
Time (s)
10 µg/mL
50 µg/mL

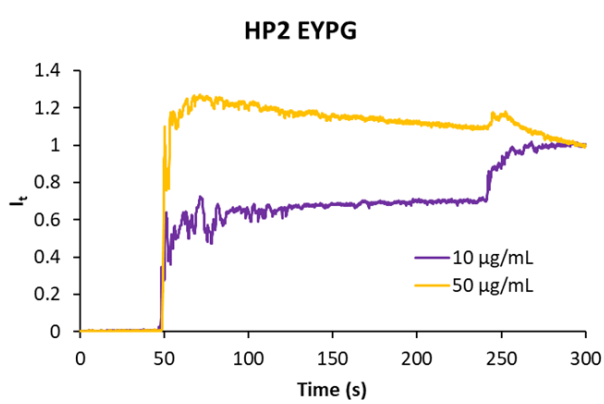
HP2 EYPG
I_t
Time (s)
10 µg/mL
50 µg/mL

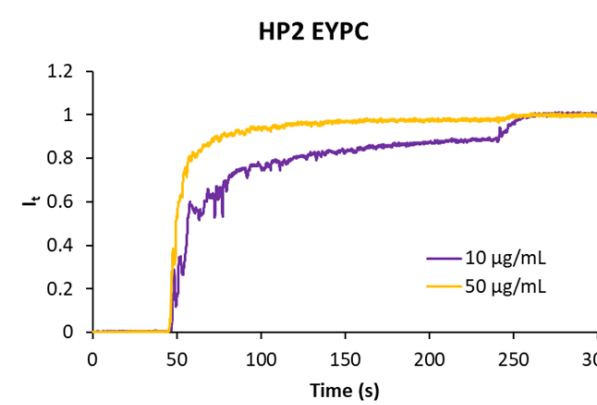
HP2 EYPC
I_t
Time (s)
10 µg/mL
50 µg/mL

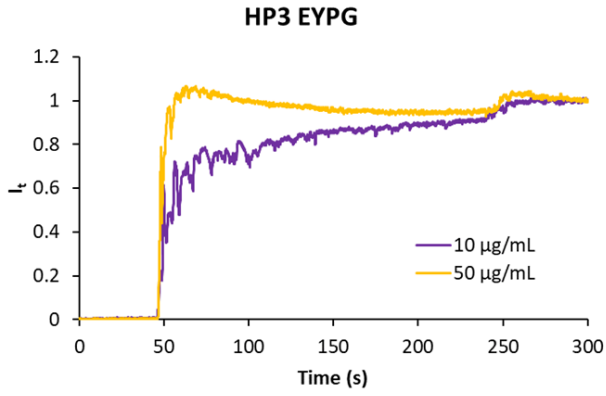
HP3 EYPG
1.2
1
0.8
0.6
0.4
0.2
0
I_t
0
50
100
150
200
250
300
Time (s)
10 µg/mL
50 µg/mL

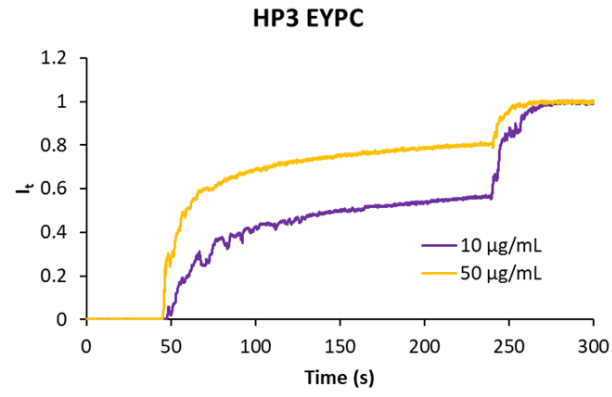
HP3 EYPC
1.2
1
0.8
0.6
0.4
0.2
0
I_t
0
50
100
150
200
250
300
Time (s)
10 µg/mL
50 µg/mL

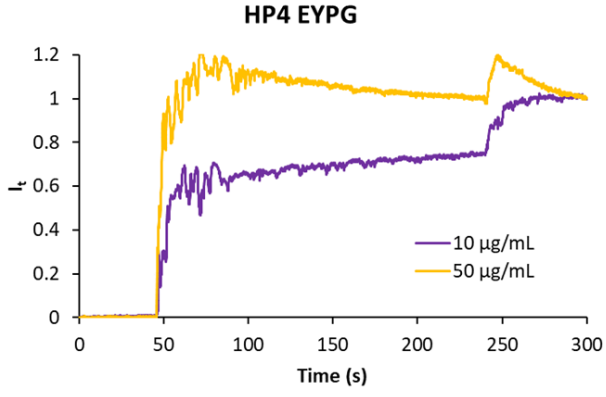
HP4 EYPG
1.2
1
0.8
0.6
0.4
0.2
0
I_t
0
50
100
150
200
250
300
Time (s)
10 µg/mL
50 µg/mL

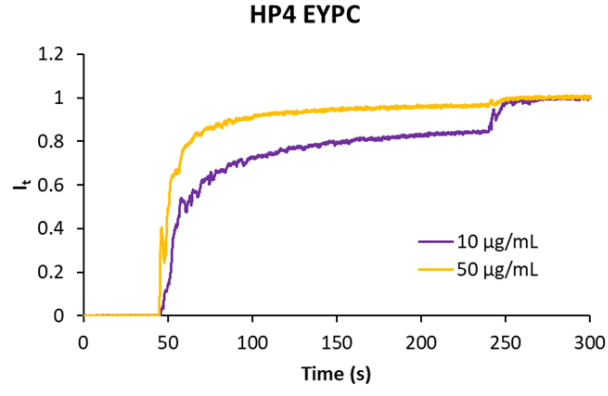
HP4 EYPC
1.2
1
0.8
0.6
0.4
0.2
0
I_t
0
50
100
150
200
250
300
Time (s)
10 µg/mL
50 µg/mL

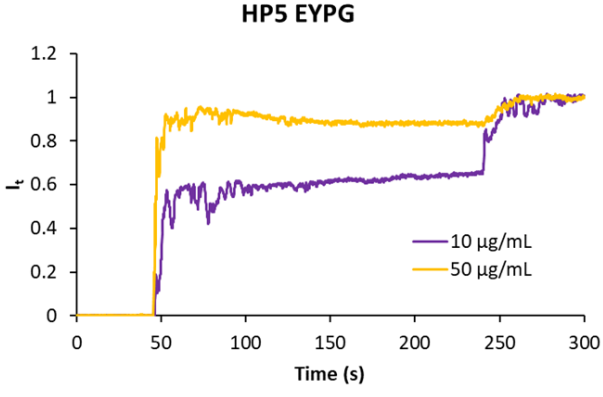
HP5 EYPG
1.2
1
0.8
0.6
0.4
0.2
0
I_t
0
50
100
150
200
250
300
Time (s)
10 µg/mL
50 µg/mL

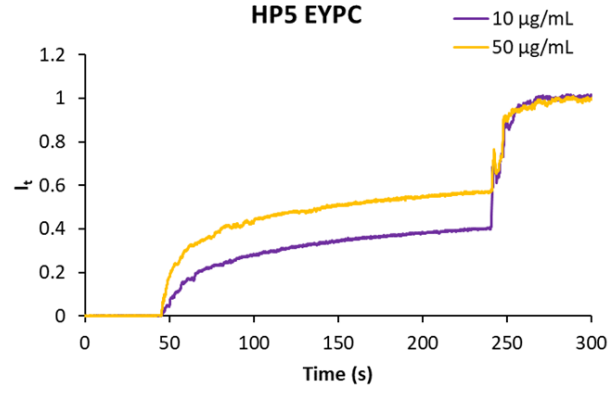
HP5 EYPC
1.2
1
0.8
0.6
0.4
0.2
0
I_t
0
50
100
150
200
250
300
Time (s)
10 µg/mL
50 µg/mL

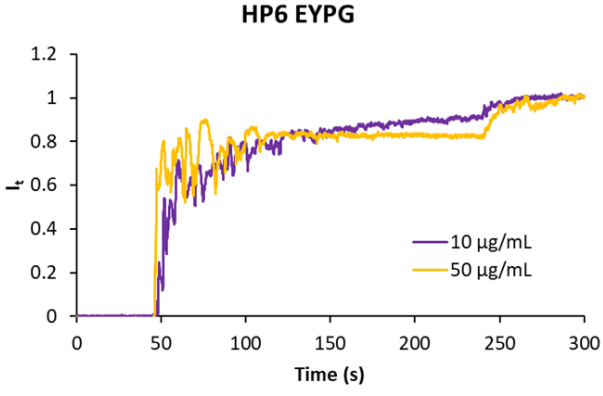
HP6 EYPG
1.2
1
0.8
0.6
0.4
0.2
0
I_t
0
50
100
150
200
250
300
Time (s)
10 µg/mL
50 µg/mL

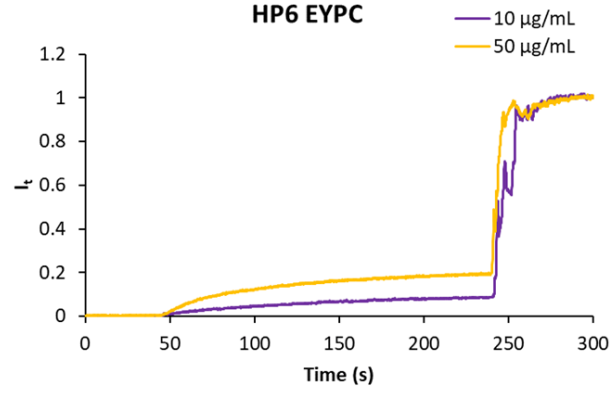
HP6 EYPC
1.2
1
0.8
0.6
0.4
0.2
0
I_t
0
50
100
150
200
250
300
Time (s)
10 µg/mL
50 µg/mL

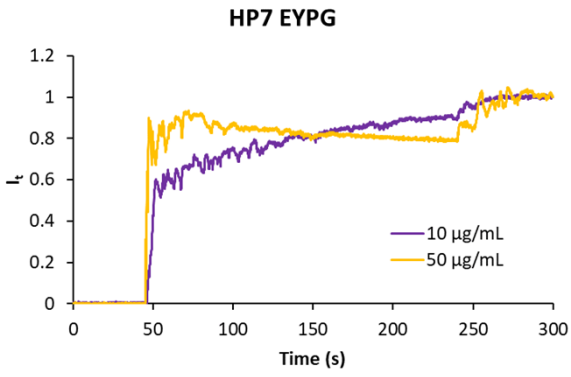
HP7 EYPG
1.2
1
0.8
0.6
0.4
0.2
0
I_t
0
50
100
150
200
250
300
Time (s)
10 µg/mL
50 µg/mL

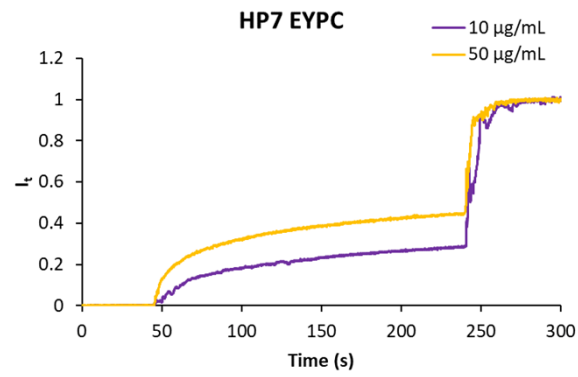
HP7 EYPC
10 µg/mL
50 µg/mL
1.2
1
0.8
0.6
0.4
0.2
0
I_t
0
50
100
150
200
250
300
Time (s)

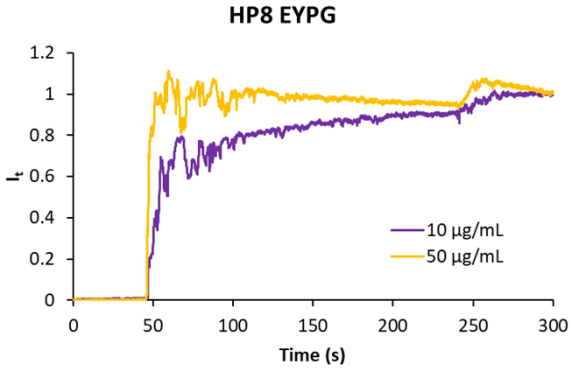
HP8 EYPG
1.2
1
0.8
0.6
0.4
0.2
0
I_t
0
50
100
150
200
250
300
Time (s)
10 µg/mL
50 µg/mL

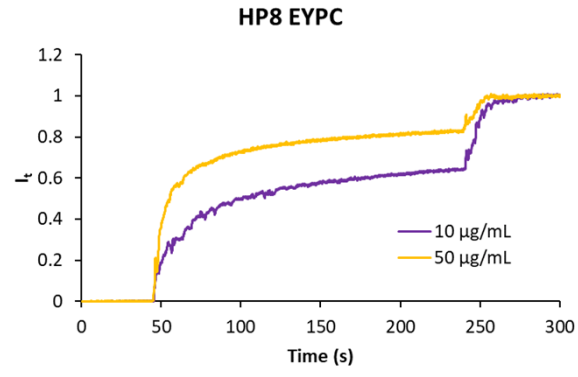
HP8 EYPC
1.2
1
0.8
0.6
0.4
0.2
0
I_t
0
50
100
150
200
250
300
Time (s)
10 µg/mL
50 µg/mL

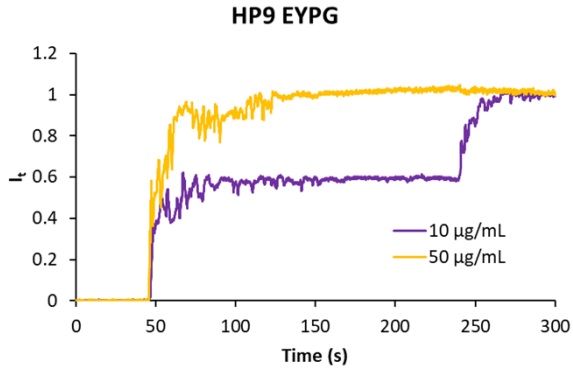
HP9 EYPG
1.2
1
0.8
0.6
0.4
0.2
0
I_t
0
50
100
150
200
250
300
Time (s)
10 µg/mL
50 µg/mL

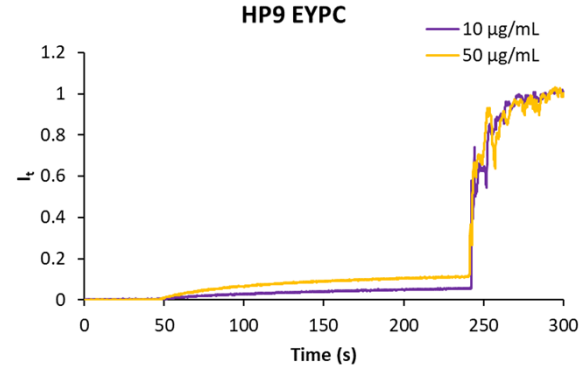
HP9 EYPC
10 µg/mL
50 µg/mL
1.2
1
0.8
0.6
0.4
0.2
0
I_t
0
50
100
150
200
250
300
Time (s)

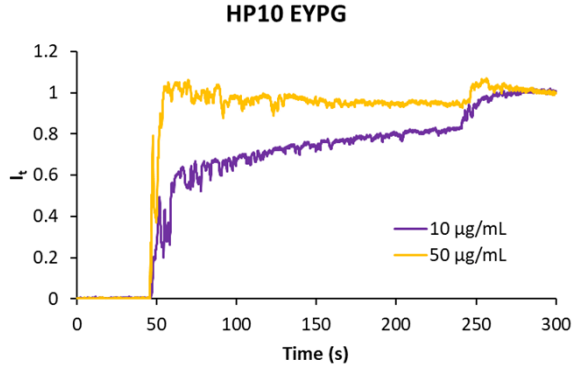
HP10 EYPG
1.2
1
0.8
0.6
0.4
0.2
0
I_t
0
50
100
150
200
250
300
Time (s)
10 µg/mL
50 µg/mL

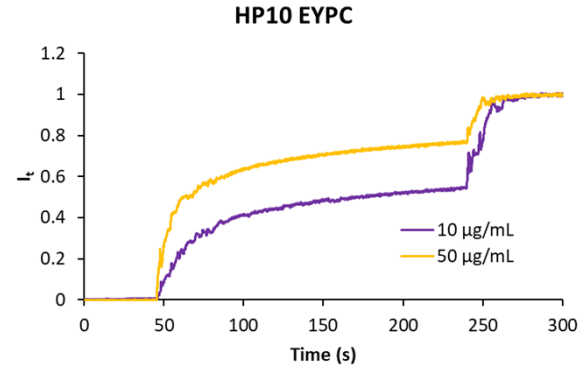
HP10 EYPC
1.2
1
0.8
0.6
0.4
0.2
0
I_t
0
50
100
150
200
250
300
Time (s)
10 µg/mL
50 µg/mL

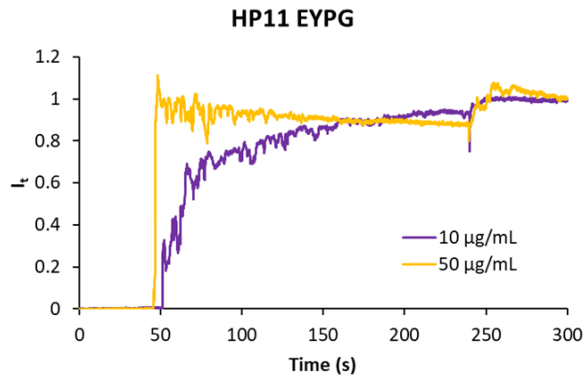
HP11 EYPG
1.2
1
0.8
0.6
0.4
0.2
0
I_t
0
50
100
150
200
250
300
Time (s)
10 µg/mL
50 µg/mL

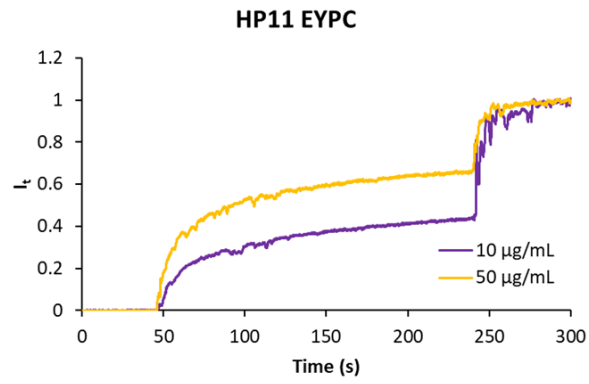
HP11 EYPC
1.2
1
0.8
0.6
0.4
0.2
0
I_t
0
50
100
150
200
250
300
Time (s)
10 µg/mL
50 µg/mL

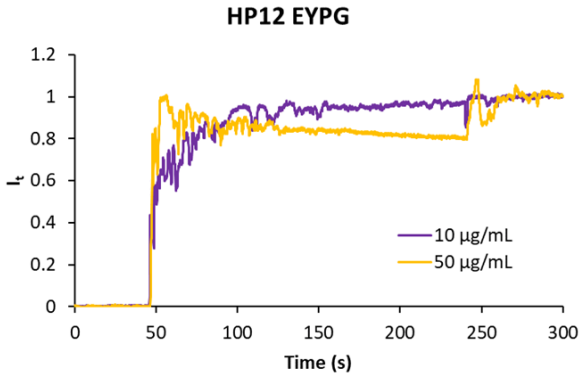
HP12 EYPG
1.2
1
0.8
0.6
0.4
0.2
0
I_t
0
50
100
150
200
250
300
Time (s)
10 µg/mL
50 µg/mL

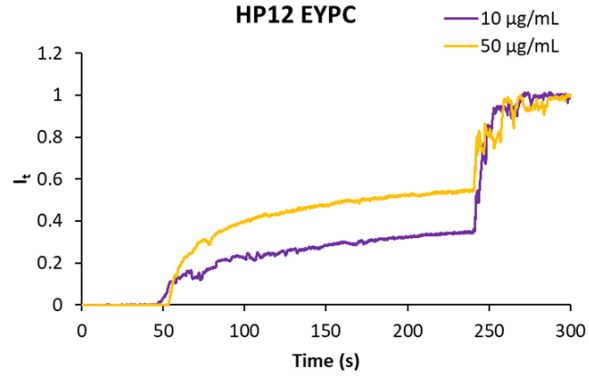
HP12 EYPC
1.2
1
0.8
0.6
0.4
0.2
0
I_t
0
50
100
150
200
250
300
Time (s)
10 µg/mL
50 µg/mL

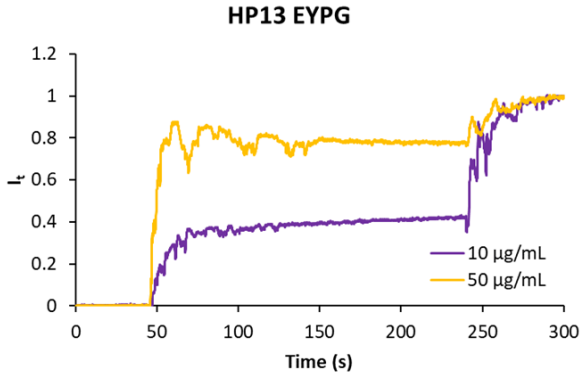
HP13 EYPG
1.2
1
0.8
0.6
0.4
0.2
0
I_t
0
50
100
150
200
250
300
Time (s)
10 µg/mL
50 µg/mL

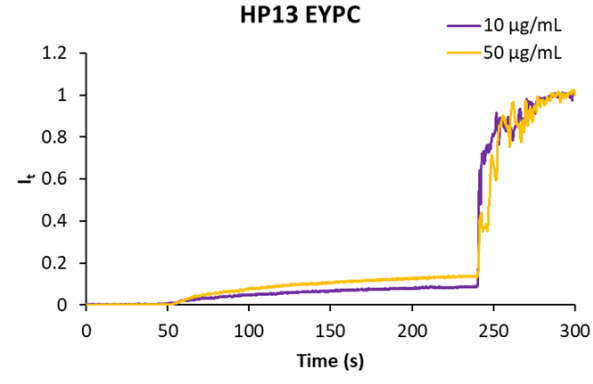
HP13 EYPC
1.2
1
0.8
0.6
0.4
0.2
0
I_t
0
50
100
150
200
250
300
Time (s)
10 µg/mL
50 µg/mL

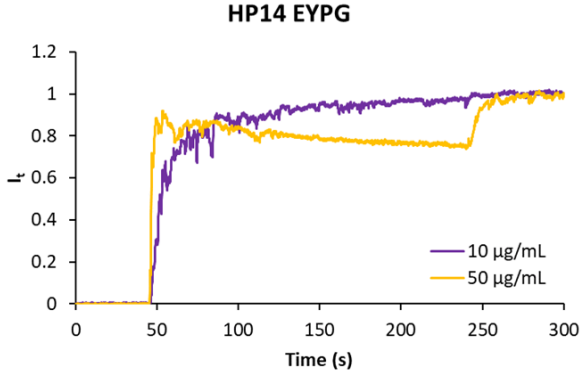
HP14 EYPG
1.2
1
0.8
0.6
0.4
0.2
0
I_t
0
50
100
150
200
250
300
Time (s)
10 µg/mL
50 µg/mL

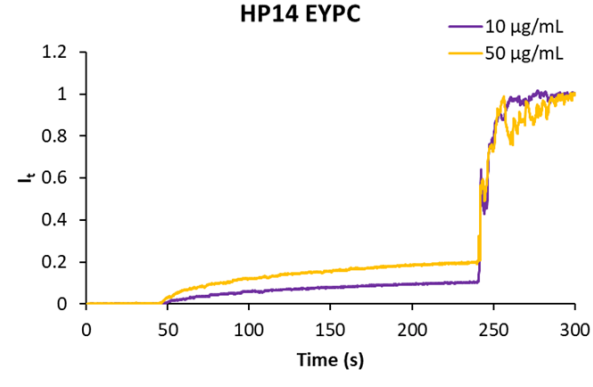
HP14 EYPC
1.2
1
0.8
0.6
0.4
0.2
0
I_t
0
50
100
150
200
250
300
Time (s)
10 µg/mL
50 µg/mL

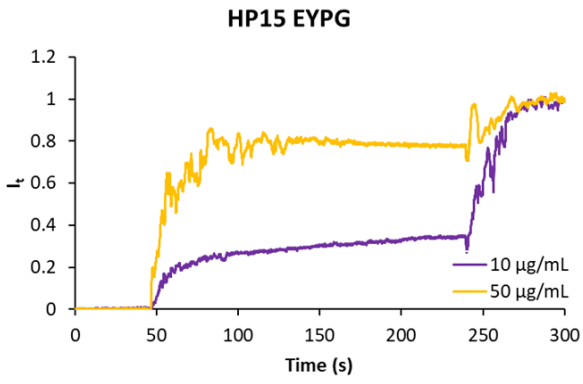
HP15 EYPG
1.2
1
0.8
0.6
0.4
0.2
0
I_t
0
50
100
150
200
250
300
Time (s)
10 µg/mL
50 µg/mL

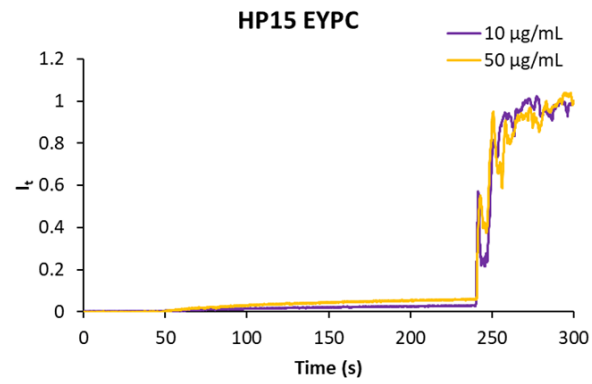
HP15 EYPC
10 µg/mL
50 µg/mL
1.2
1
0.8
0.6
0.4
0.2
0
I_t
0
50
100
150
200
250
300
Time (s)

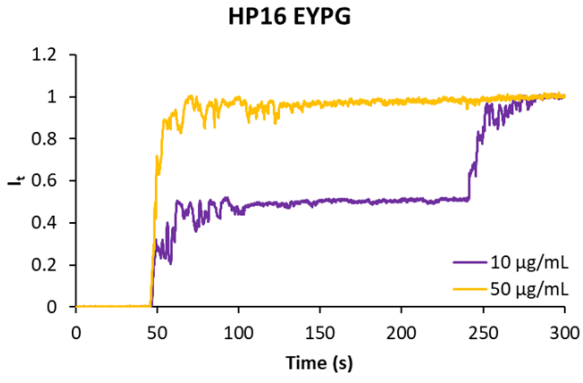
HP16 EYPG
1.2
1
0.8
0.6
0.4
0.2
0
I_t
0
50
100
150
200
250
300
Time (s)
10 µg/mL
50 µg/mL

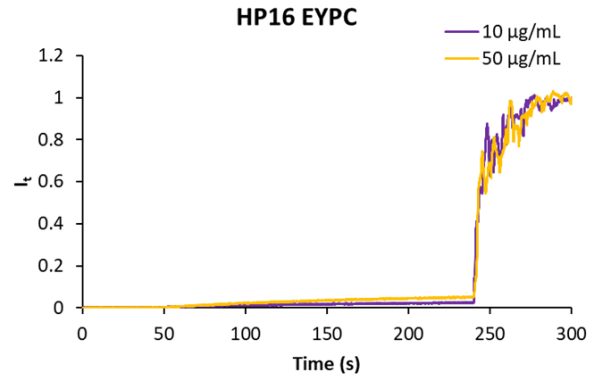
HP16 EYPC
10 µg/mL
50 µg/mL
1.2
1
0.8
0.6
0.4
0.2
0
I_t
0
50
100
150
200
250
300
Time (s)

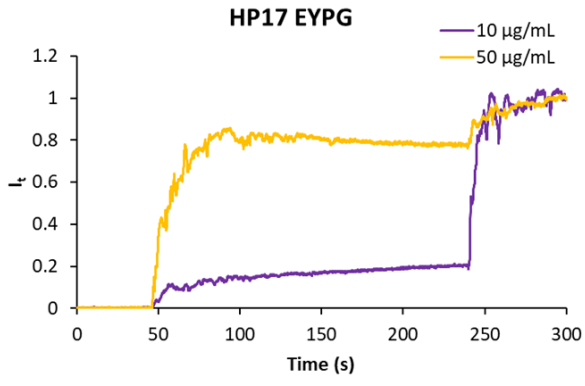
HP17 EYPG
10 µg/mL
50 µg/mL
1.2
1
0.8
0.6
0.4
0.2
0
I_t
0
50
100
150
200
250
300
Time (s)

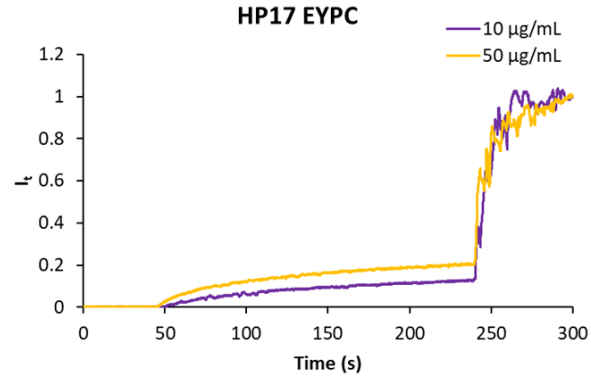
HP17 EYPC
10 µg/mL
50 µg/mL
1.2
1
0.8
0.6
0.4
0.2
0
I_t
0
50
100
150
200
250
300
Time (s)

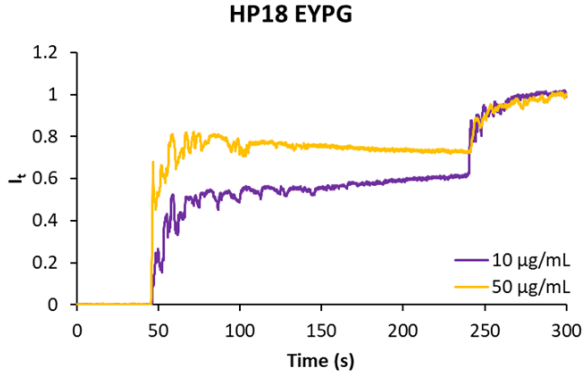
HP18 EYPG
1.2
1
0.8
0.6
0.4
0.2
0
I_t
0
50
100
150
200
250
300
Time (s)
10 µg/mL
50 µg/mL

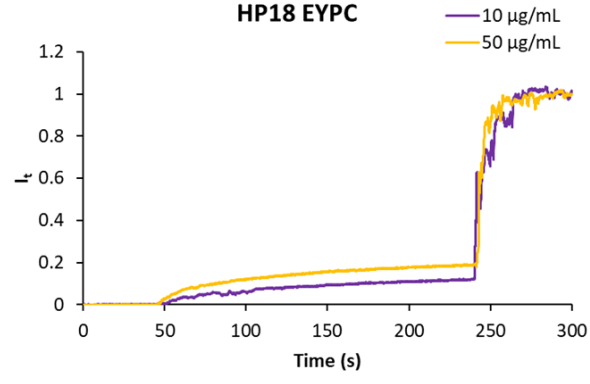
HP18 EYPC
10 µg/mL
50 µg/mL
1.2
1
0.8
0.6
0.4
0.2
0
I_t
0
50
100
150
200
250
300
Time (s)

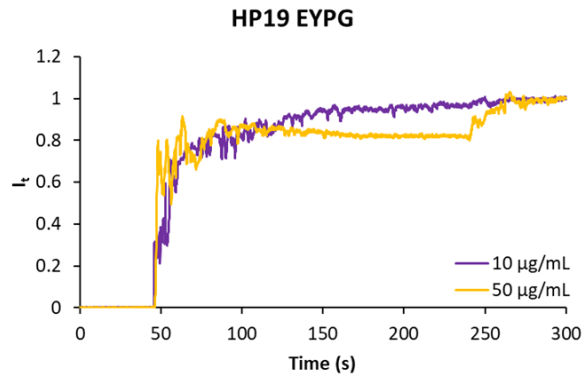
HP19 EYPG
1.2
1
0.8
0.6
0.4
0.2
0
I_t
0
50
100
150
200
250
300
Time (s)
10 µg/mL
50 µg/mL

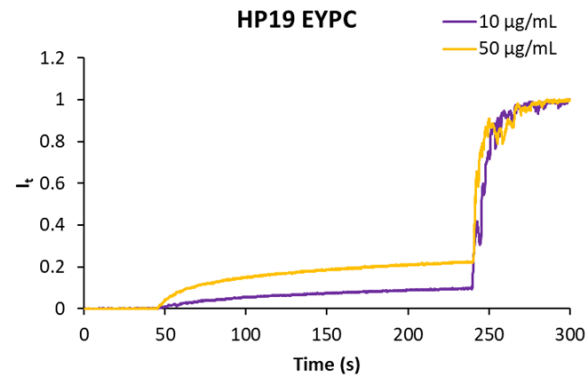
HP19 EYPC
10 µg/mL
50 µg/mL
1.2
1
0.8
0.6
0.4
0.2
0
I_t
0
50
100
150
200
250
300
Time (s)

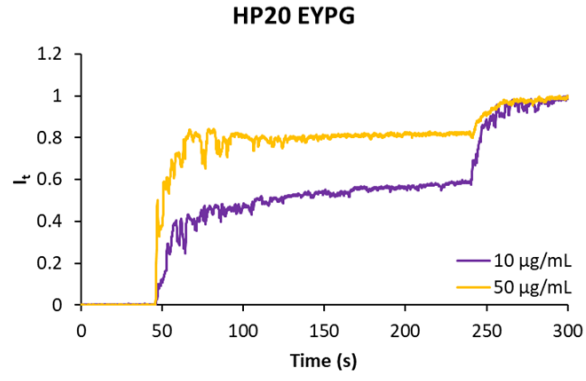
HP20 EYPG
1.2
1
0.8
0.6
0.4
0.2
0
I_t
0
50
100
150
200
250
300
Time (s)
10 µg/mL
50 µg/mL

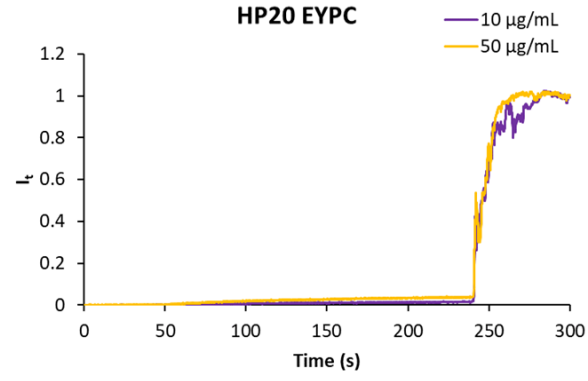
HP20 EYPC
10 µg/mL
50 µg/mL
1.2
1
0.8
0.6
0.4
0.2
0
I_t
0
50
100
150
200
250
300
Time (s)

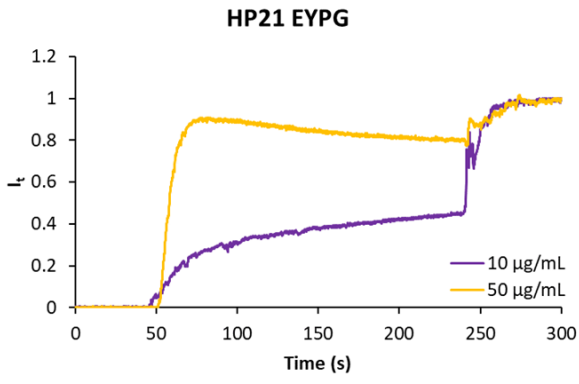
HP21 EYPG
1.2
1
0.8
0.6
0.4
0.2
0
I_t
0
50
100
150
200
250
300
Time (s)
10 µg/mL
50 µg/mL

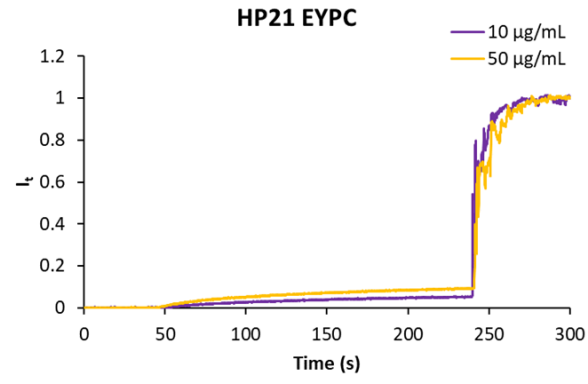
HP21 EYPC
10 µg/mL
50 µg/mL
1.2
1
0.8
0.6
0.4
0.2
0
I_t
0
50
100
150
200
250
300
Time (s)

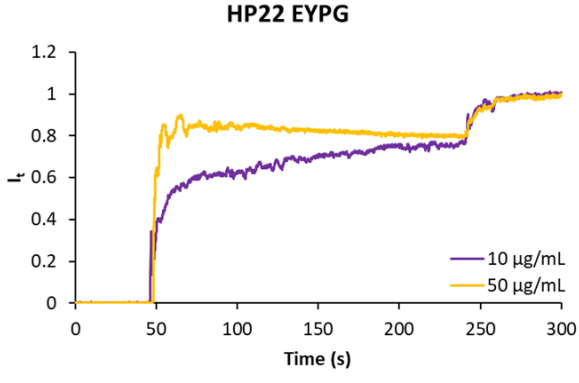
HP22 EYPG
1.2
1
0.8
0.6
0.4
0.2
0
I_t
0
50
100
150
200
250
300
Time (s)
10 µg/mL
50 µg/mL

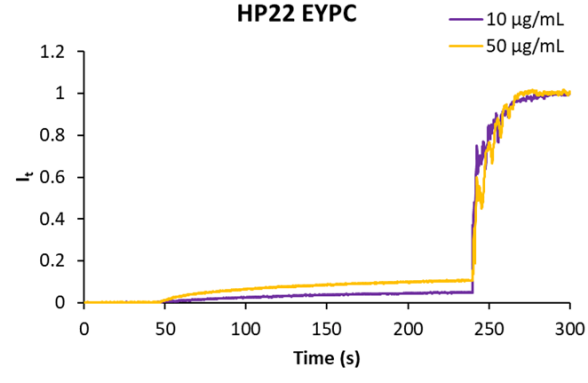
HP22 EYPC
10 µg/mL
50 µg/mL
1.2
1
0.8
0.6
0.4
0.2
0
I_t
0
50
100
150
200
250
300
Time (s)

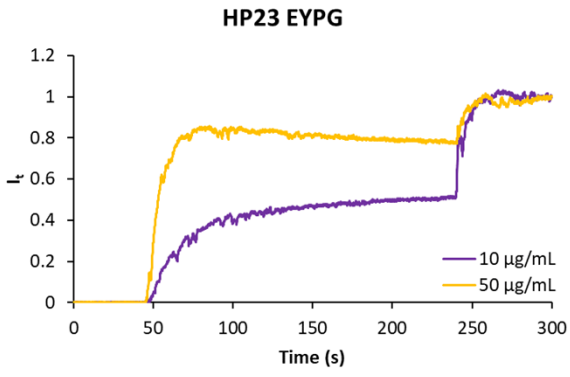
HP23 EYPG
I_t
Time (s)
10 µg/mL
50 µg/mL

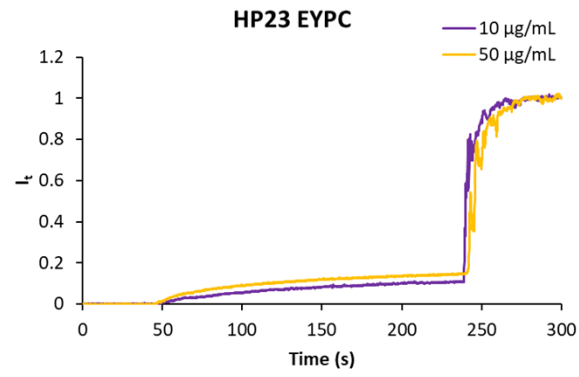
HP23 EYPC
I_t
Time (s)
10 µg/mL
50 µg/mL

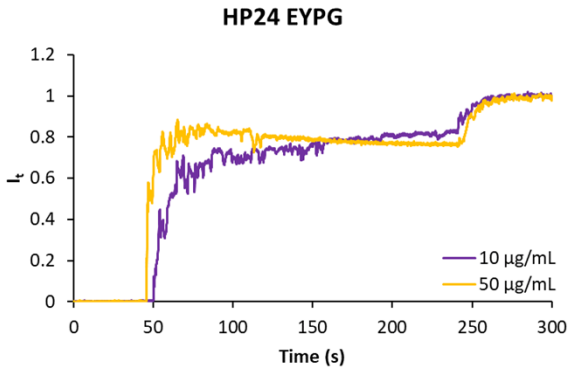
HP24 EYPG
I_t
Time (s)
10 µg/mL
50 µg/mL

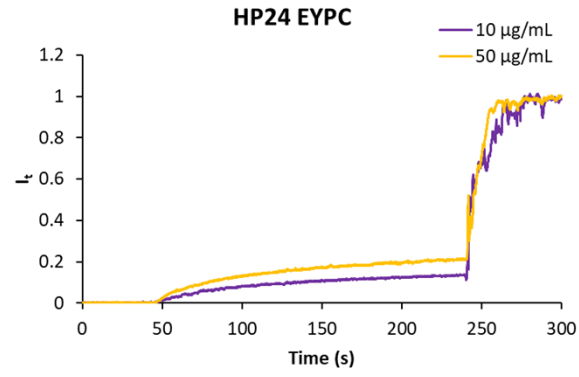
HP24 EYPC
I_t
Time (s)
10 µg/mL
50 µg/mL

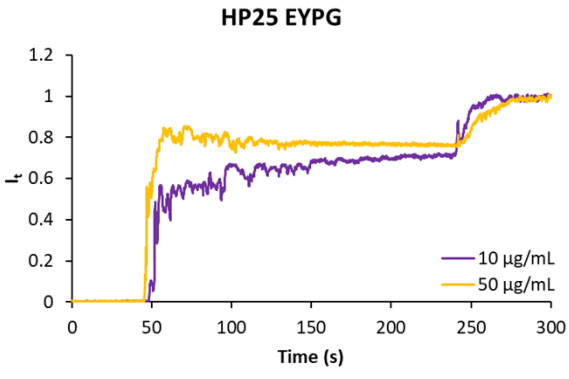
HP25 EYPG
I_t
Time (s)
10 µg/mL
50 µg/mL

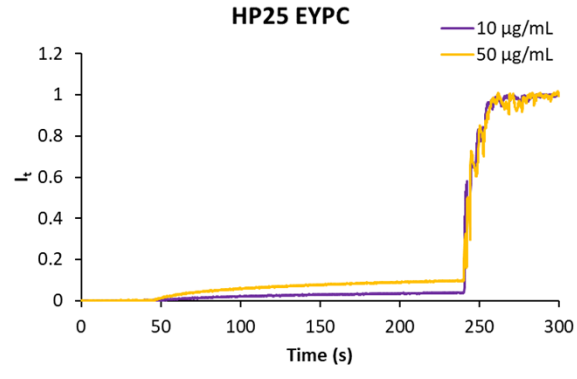
HP25 EYPC
I_t
Time (s)
10 µg/mL
50 µg/mL

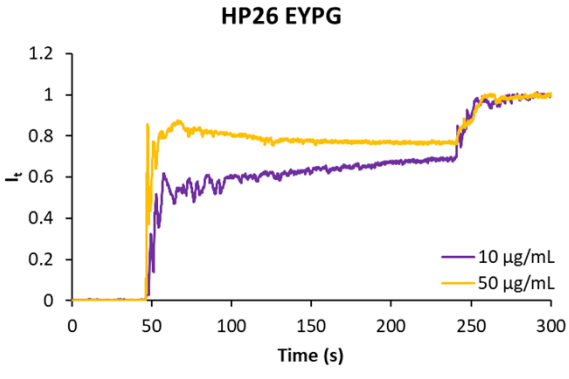
HP26 EYPG
I_t
Time (s)
10 µg/mL
50 µg/mL

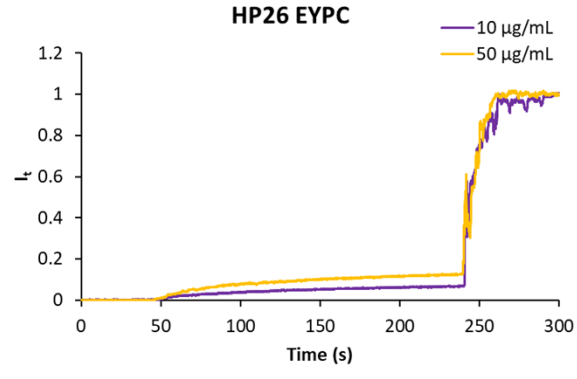
HP26 EYPC
I_t
Time (s)
10 µg/mL
50 µg/mL

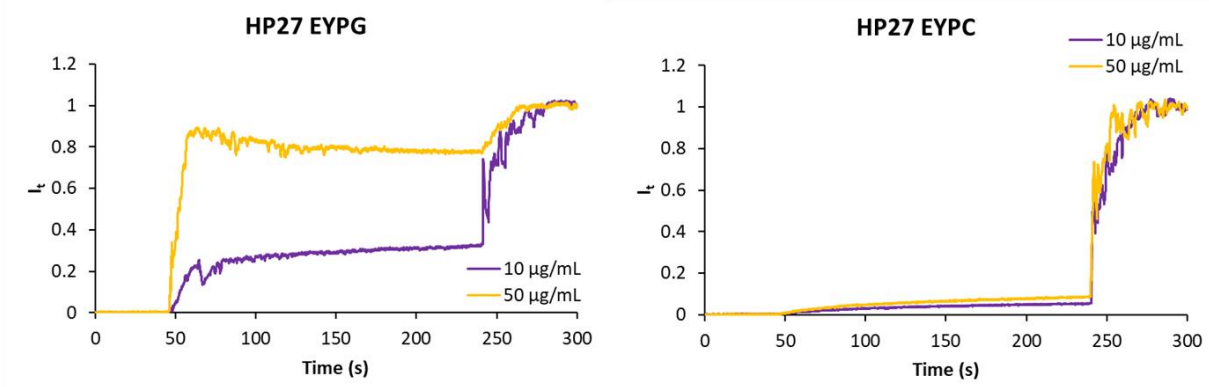
HP27 EYPG
HP27 EYPC
10 µg/mL
50 µg/mL
I_t
Time (s)

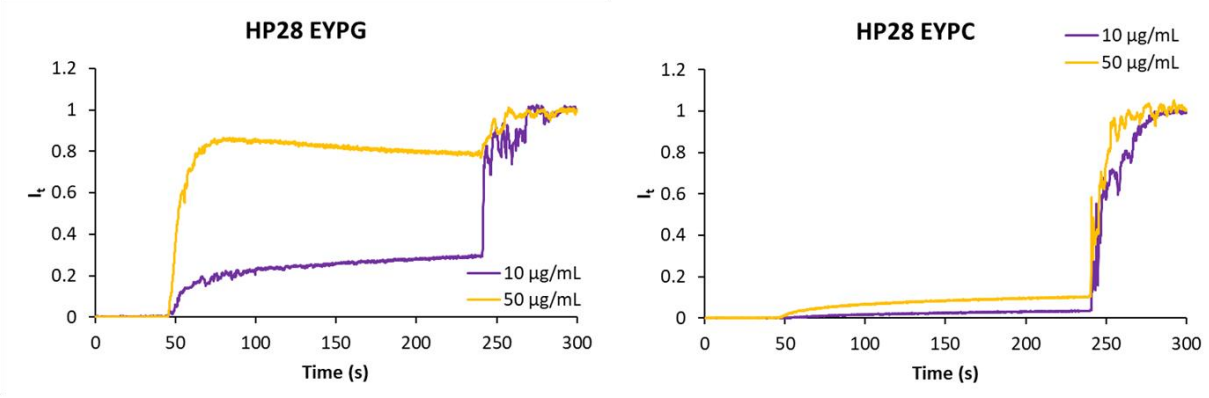
HP28 EYPG
HP28 EYPC
10 µg/mL
50 µg/mL
I_t
Time (s)

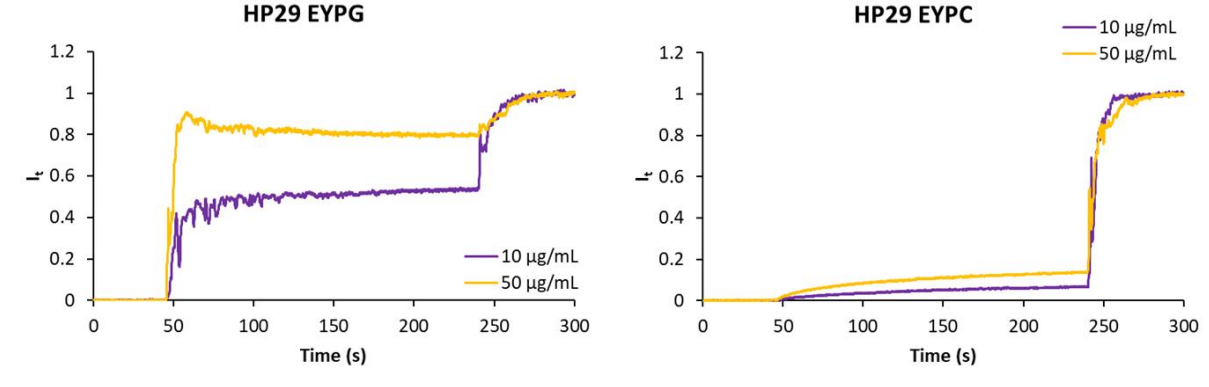
HP29 EYPG
HP29 EYPC
10 µg/mL
50 µg/mL
I_t
Time (s)

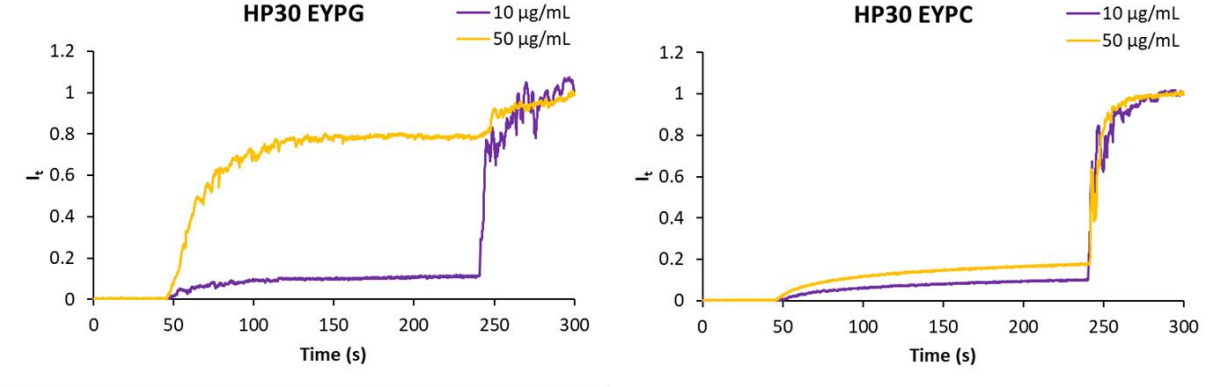
HP30 EYPG
HP30 EYPC
10 µg/mL
50 µg/mL
I_t
Time (s)

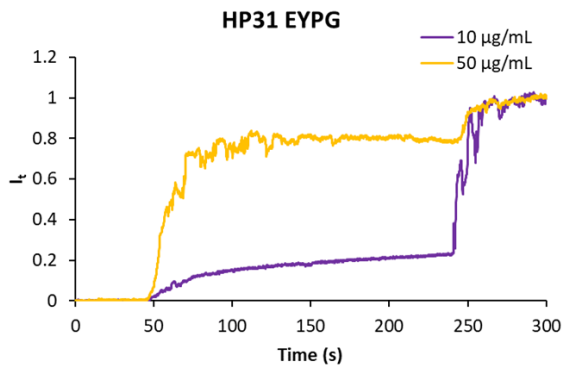
HP31 EYPG
10 µg/mL
50 µg/mL
I_t
Time (s)

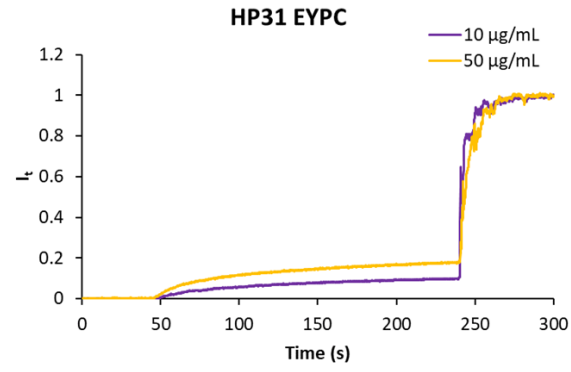
HP31 EYPC
10 µg/mL
50 µg/mL
I_t
Time (s)

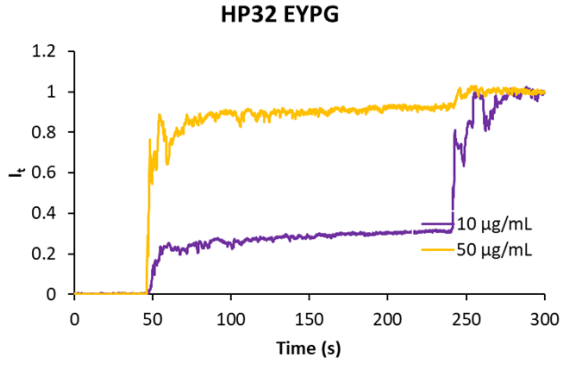
HP32 EYPG
10 µg/mL
50 µg/mL
I_t
Time (s)

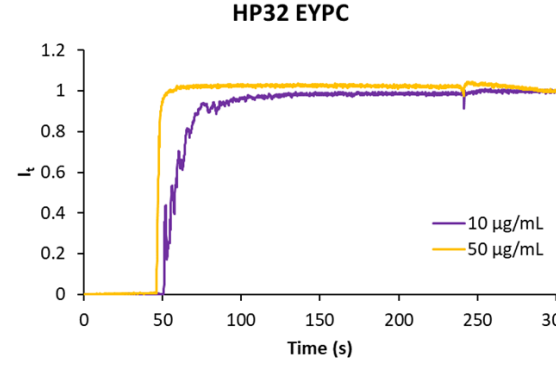
HP32 EYPC
10 µg/mL
50 µg/mL
I_t
Time (s)

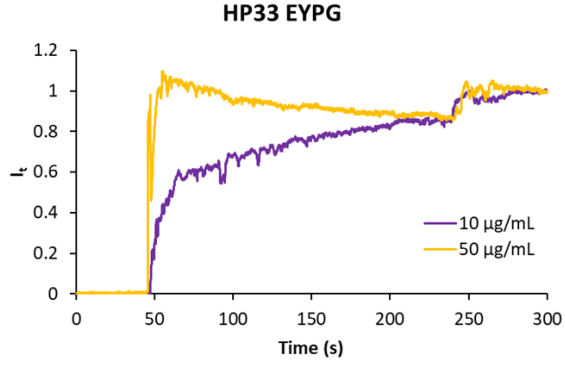
HP33 EYPG
10 µg/mL
50 µg/mL
I_t
Time (s)

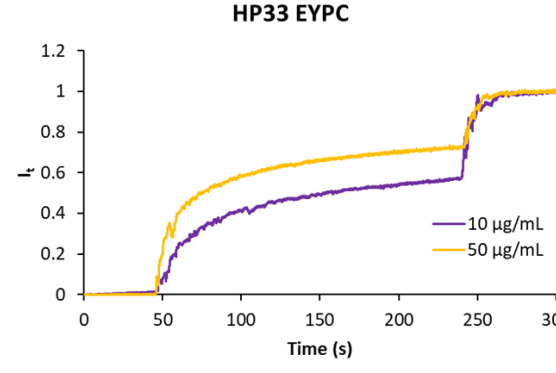
HP33 EYPC
10 µg/mL
50 µg/mL
I_t
Time (s)

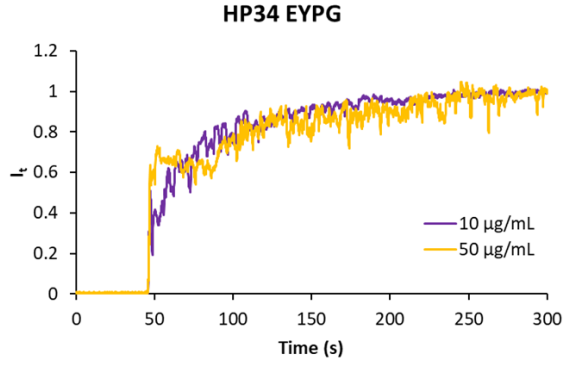
HP34 EYPG
10 µg/mL
50 µg/mL
I_t
Time (s)

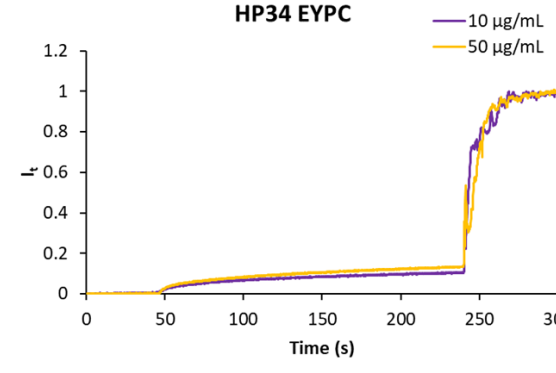
HP34 EYPC
10 µg/mL
50 µg/mL
I_t
Time (s)

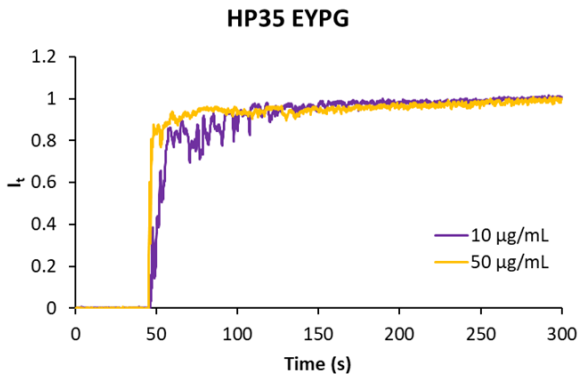
HP35 EYPG
I_t
Time (s)
10 µg/mL
50 µg/mL

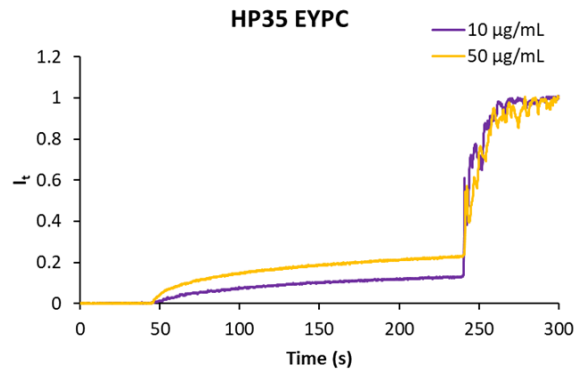
HP35 EYPC
I_t
Time (s)
10 µg/mL
50 µg/mL

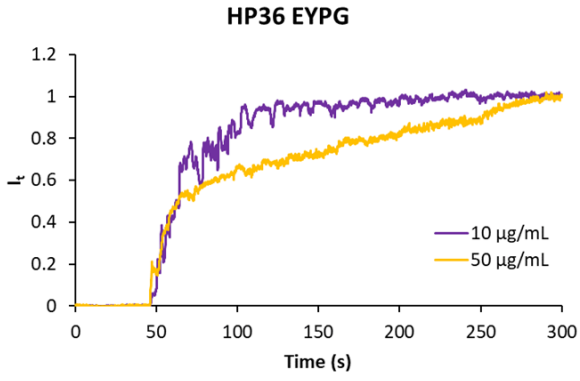
HP36 EYPG
I_t
Time (s)
10 µg/mL
50 µg/mL

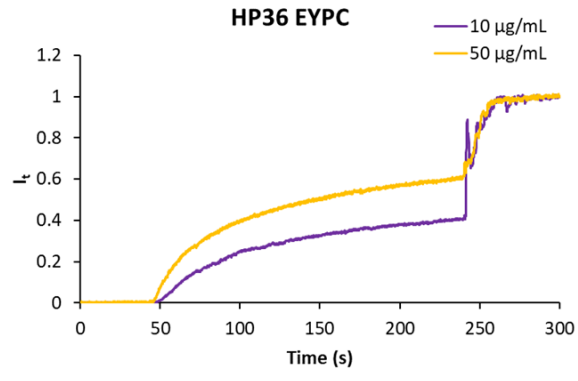
HP36 EYPC
I_t
Time (s)
10 µg/mL
50 µg/mL

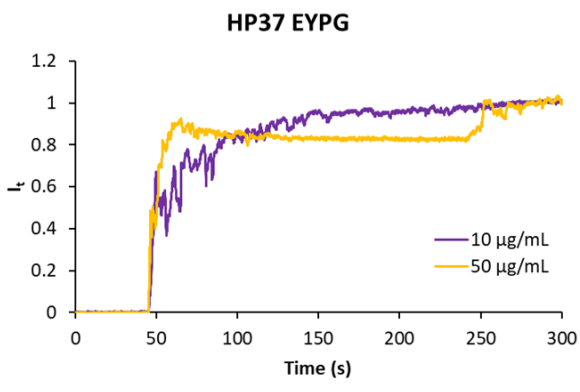
HP37 EYPG
I_t
Time (s)
10 µg/mL
50 µg/mL

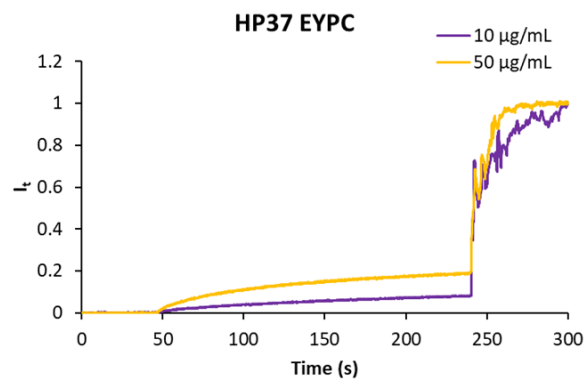
HP37 EYPC
I_t
Time (s)
10 µg/mL
50 µg/mL

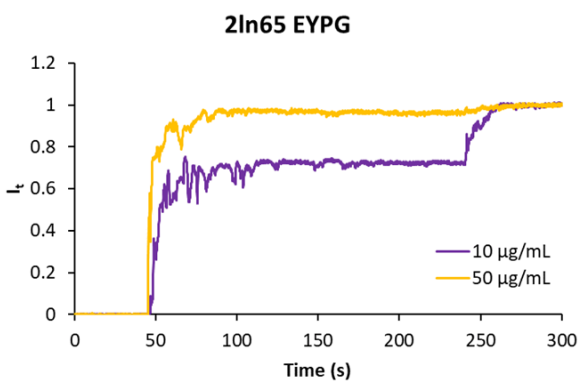
2ln65 EYPG
I_t
Time (s)
10 µg/mL
50 µg/mL

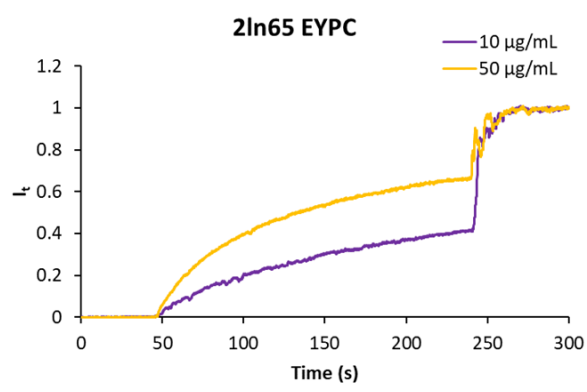
2ln65 EYPC
I_t
Time (s)
10 µg/mL
50 µg/mL

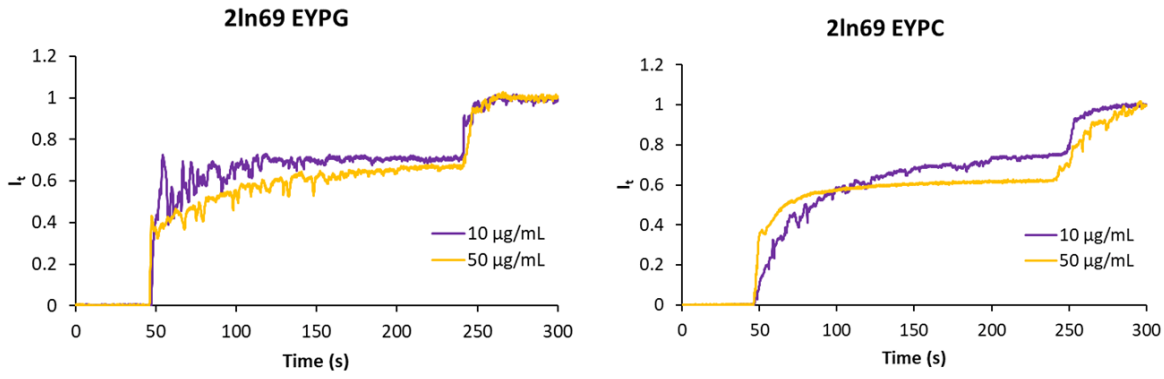

Figure S2.2: Vesicle leakage experiments using 5(6)-carboxyfluorescein induced by peptides. EYPG and EYPC vesicles were suspended in buffer (10 mM Tris, 107 mM NaCl, pH 7.4) and the indicated concentration of the compound was added after 45 seconds. After 240 seconds 30 µL of Triton X-100 1.2% was added for full release of the fluorescein.

Time kill kinetics assay

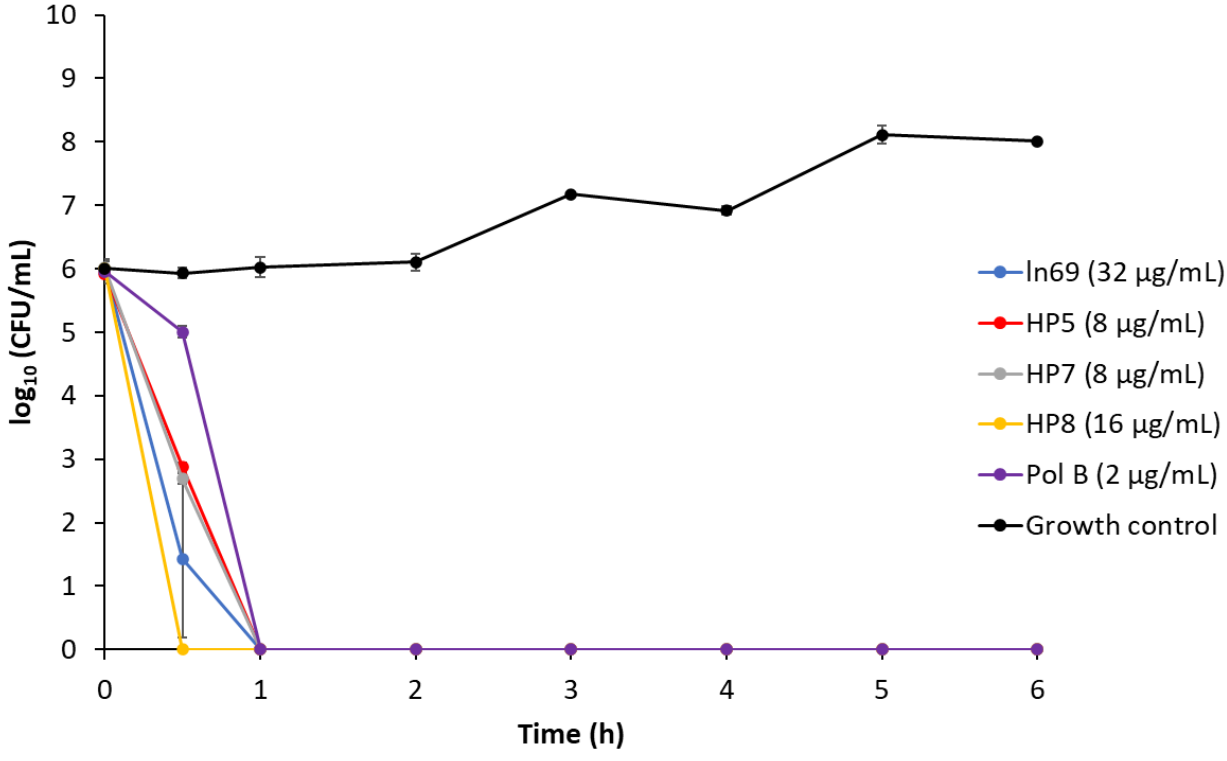

Figure S2.3: Bacteria killing assay at pH 7.4 against *P. aeruginosa* PAO1 at a concentration of 4 × MIC. Data are given as the mean ± SD, n = 3. A value of $\log_{10}$ of 0 means no colony was observed.

Serum stability assay

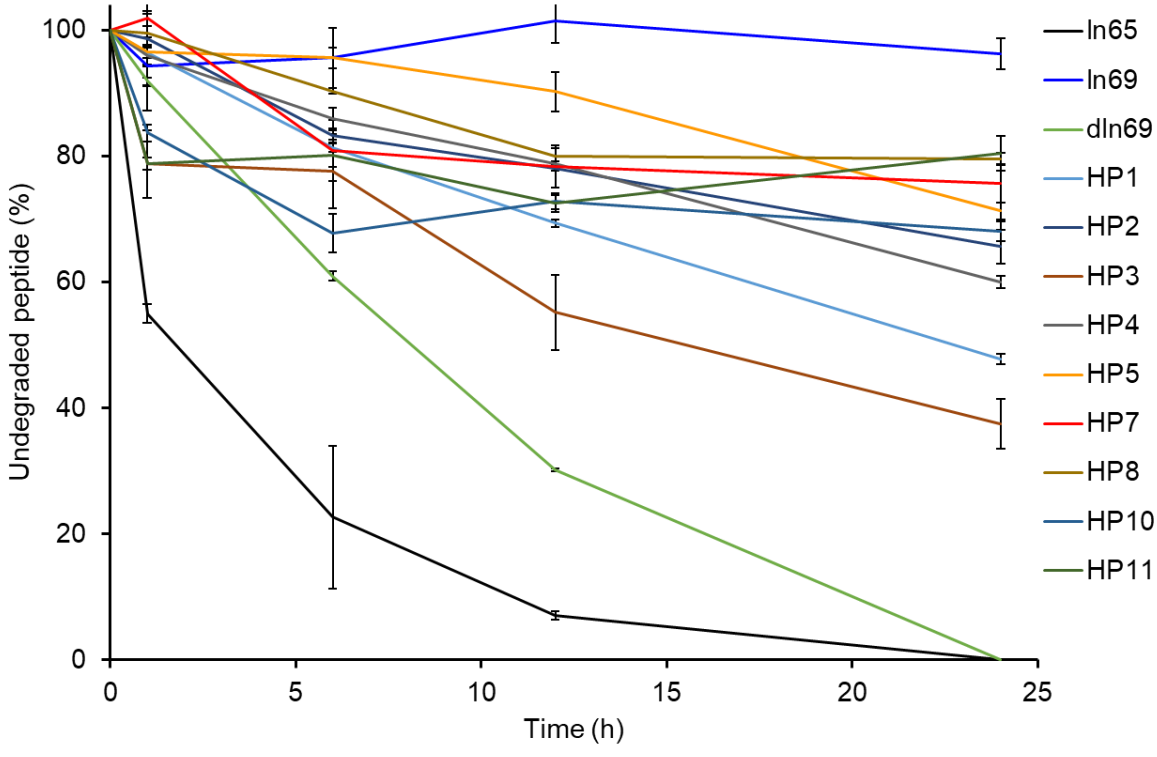

Figure S2.4: Serum stability of mixed-chirality peptides in 12.5% human serum in 0.1 M filtered TRIS buffer pH 7.4. Normalized undegraded peptides values were determined by RP-HPLC analysis using hydroxybenzoic acid as internal standard. Data from triplicate experiments.

Cytotoxicity assay

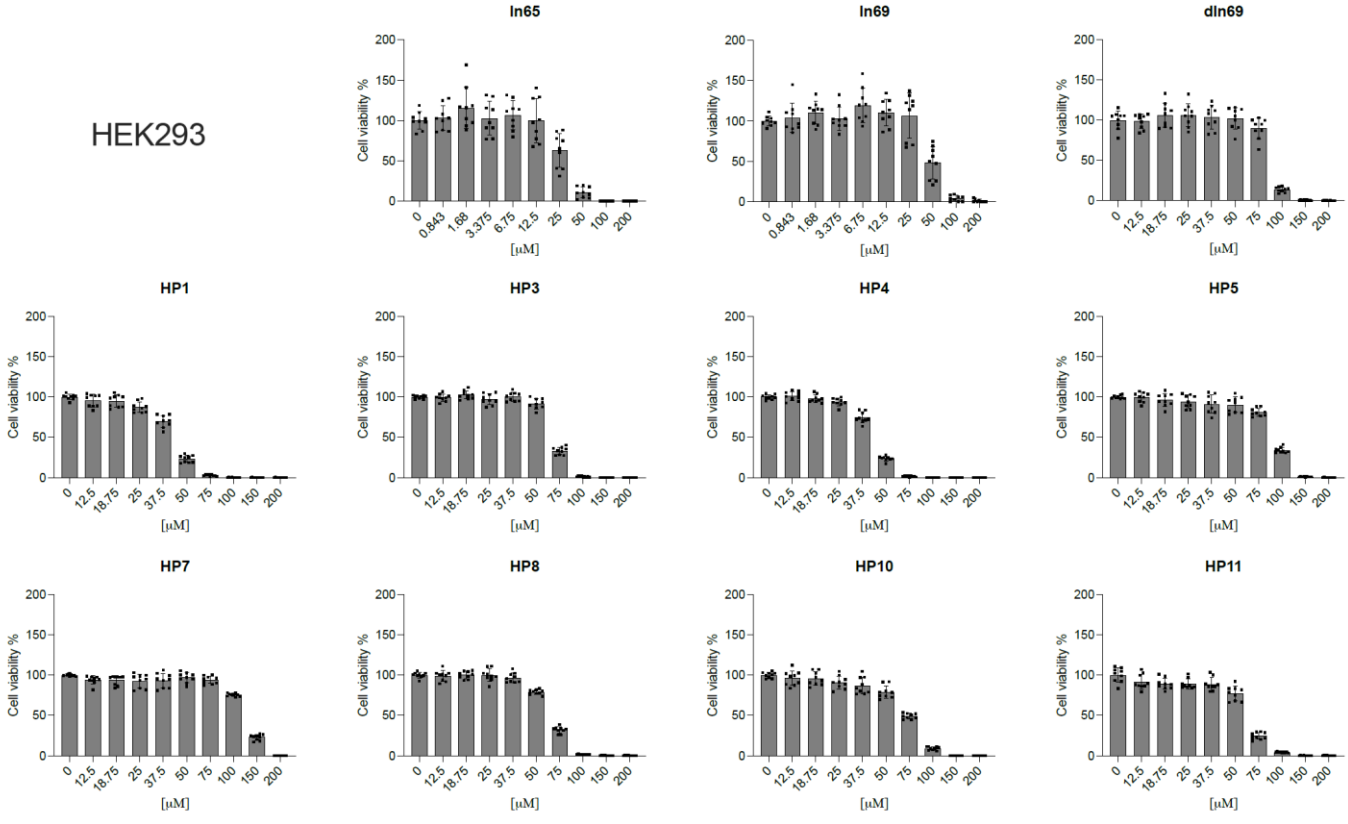

Figure S2.5: Cytotoxicity **ln65**, **ln69**, **dln69**, **HP1**, **HP3**, **HP4**, **HP5**, **HP7**, **HP8**, **HP10** and **HP11** on HEK293 cells. The data of three experiments with three replicates per sample were pooled and represented as barplots. The cells were treated with the desired concentration of compound for 24 h and their viability was measured with an Alamar Blue assay.

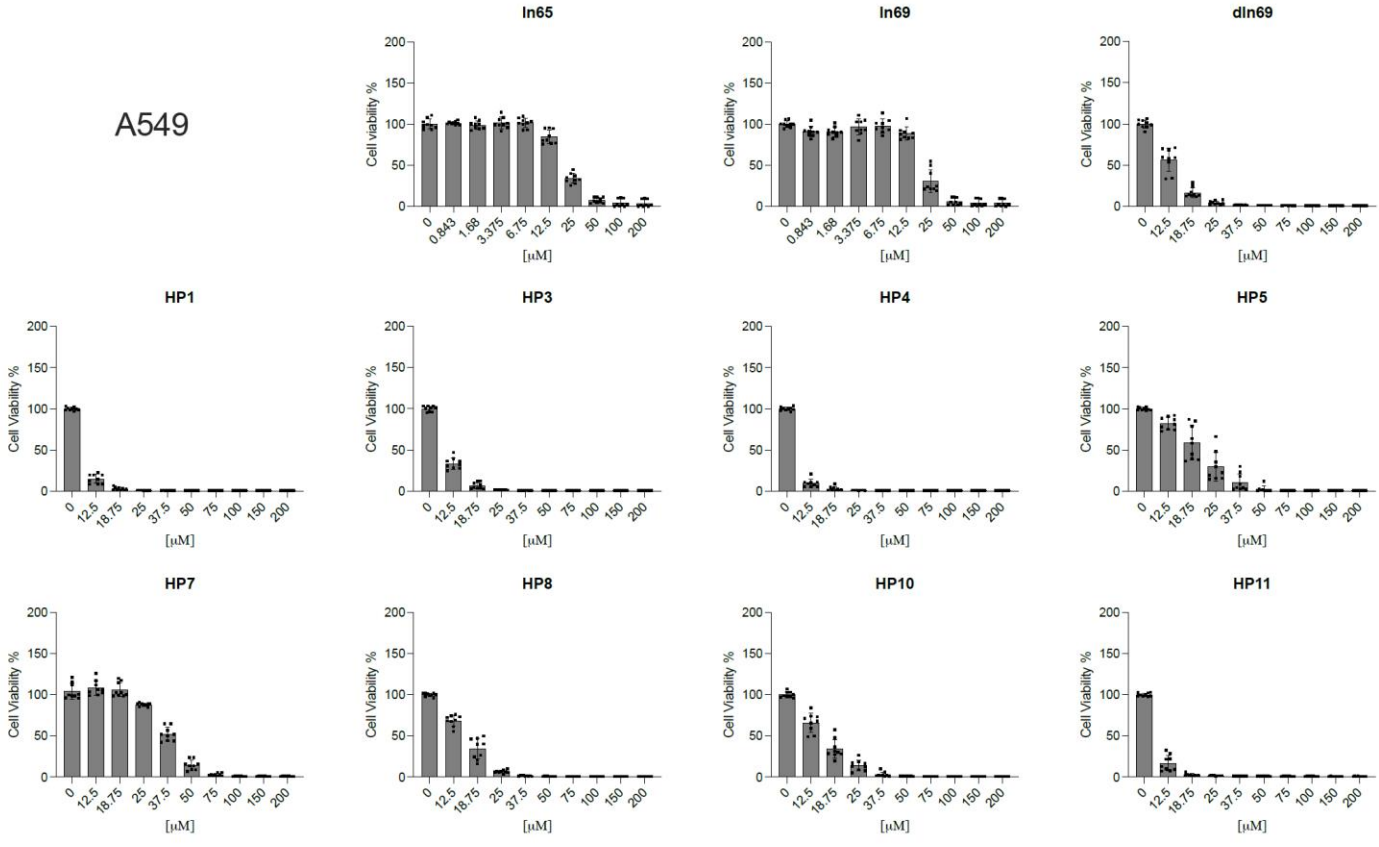

Figure S2.6: Cytotoxicity **ln65**, **ln69**, **dln69**, **HP1**, **HP3**, **HP4**, **HP5**, **HP7**, **HP8**, **HP10** and **HP11** on A549 cells. The data of three experiments with three replicates per sample were pooled and represented as barplots. The cells were treated with the desired concentration of compound for 24 h and their viability was measured with an Alamar Blue assay.

Crystallography

Table S2.3: Data collection and refinement statistics for the X-ray structure of the **FHP5**·LecB complex.

Structural data	**FHP5·LecB**
Beam line	PSI PXIII
Wavelength (Å)	1.000
Resolution (Å)	50.0-1.3 (1.35-1.27)[a)]
Cell dimension	
Space group	4, P 1 2_1 1
Unit cell (Å)	*a* = 52.8, *b* = 62.8, *c* = 64.2 α = 90.0°, β = 92.8°, γ = 90.0°
Measured reflection / unique	660242/211407
Average multiplicity	3.1 (2.4)
Completeness (%)	98.9 (92.4)
Average $I / \sigma(I)$	9.16 (1.08)
Correlation $CC_{1/2}$ (%)	99.8 (71.7)
R_{meas} (%)	6.9 (84.1)
Wilson β-factor (Å^2)	13.0
Refinement	
Resolution range (Å)	44.90-1.27
R_{work} (%)	16.27
R_{free} (%)	19.19
Average Biso (Å^2)	99.3
RMSD from ideal angles (°)	1.005
Bonds (Å)	0.007
Water molecules	492
Ligand molecules	4
Protein data Bank deposition code	8AN9

[a)] Values in brackets correspond to the outer shell.

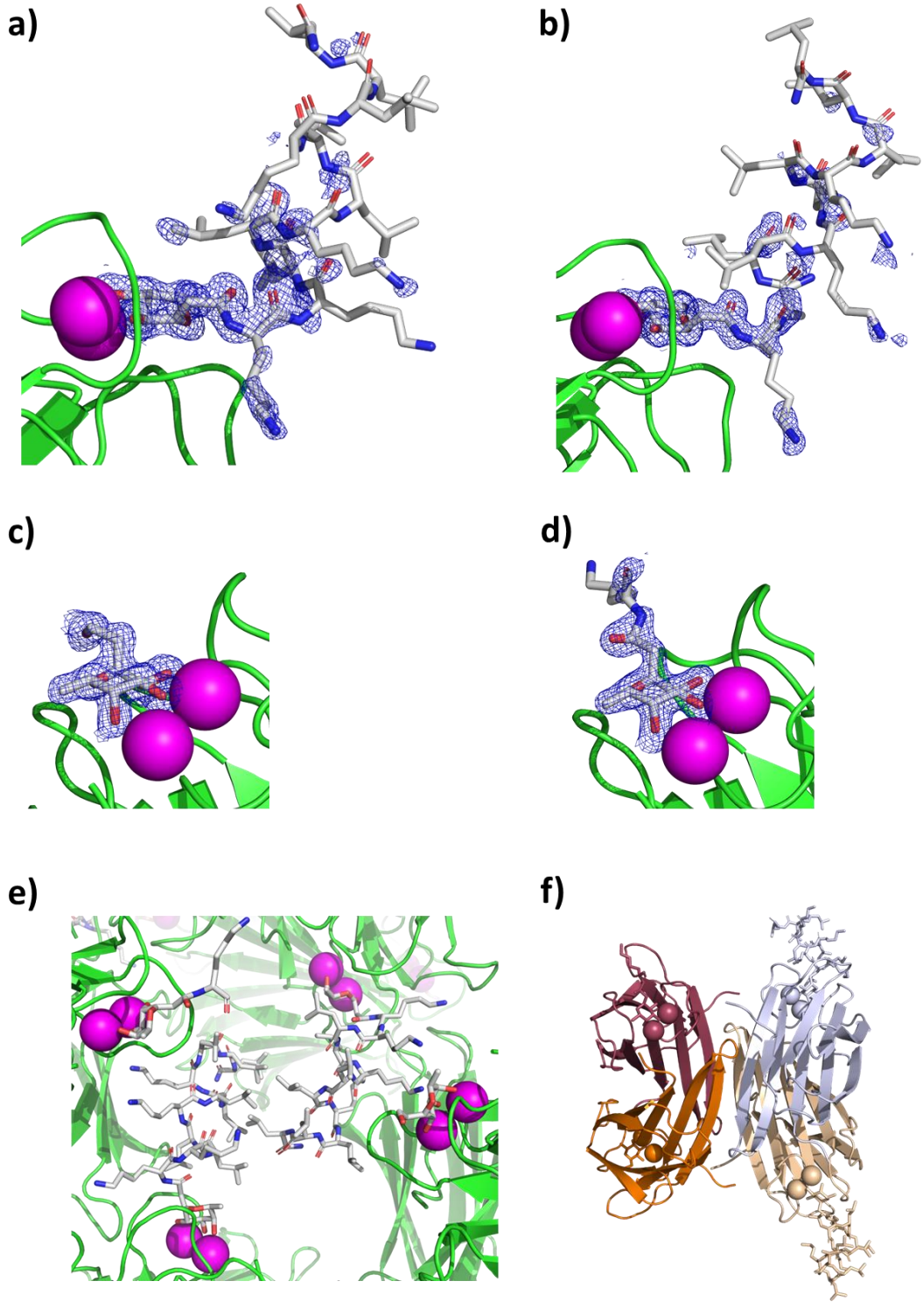

Figure S2.7: Details of the X-ray structure of the **FHP5**·LecB complex in P 1 2_1 1. **(a-d)** Asymmetric peptide entities with corresponding electron density map as blue mesh, Ca^{2+} atoms as magenta spheres and the bound LecB monomer as green cartoon. Electron density is shown for a 1.0σ level. **(e)** Incomplete bundles of four different asymmetric complete and incomplete peptides Same color code as in (a). **(f)** View of the unit cell including LecB subunits, Ca^{2+} atoms and the bound peptides. Peptides are shown as sticks, Ca^{2+} atoms as spheres and lectin monomers are displayed as cartoon of the same color.

Table S2.4: Data collection and refinement statistics for the X-ray structure of the **FHP8**·LecB complex.

Structural data	**FHP8·LecB**
Beam line	PSI PXIII
Wavelength (Å)	1.000
Resolution (Å)	50.0-1.3 (1.36-1.29)[a)]
Cell dimension	
Space group	4, P 1 2_1 1
Unit cell (Å)	a = 52.8, b = 62.9, c = 64.6 α = 90.0°, β = 92.9°, γ = 90.0°
Measured reflection / unique	660731/207353
Average multiplicity	3.2 (2.6)
Completeness (%)	99.0 (92.7)
Average $I / \sigma(I)$	8.08 (0.81)
Correlation $CC_{1/2}$ (%)	99.7 (81.0)
R_{meas} (%)	9.9 (143.3)
Wilson β-factor (Å^2)	10.7
Refinement	
Resolution range (Å)	45.00-1.29
R_{work} (%)	16.66
R_{free} (%)	20.17
Average Biso (Å^2)	83.8
RMSD from ideal angles (°)	1.225
Bonds (Å)	0.012
Water molecules	570
Ligand molecules	4
Protein data Bank deposition code	8ANO

[a)] Values in brackets correspond to the outer shell.

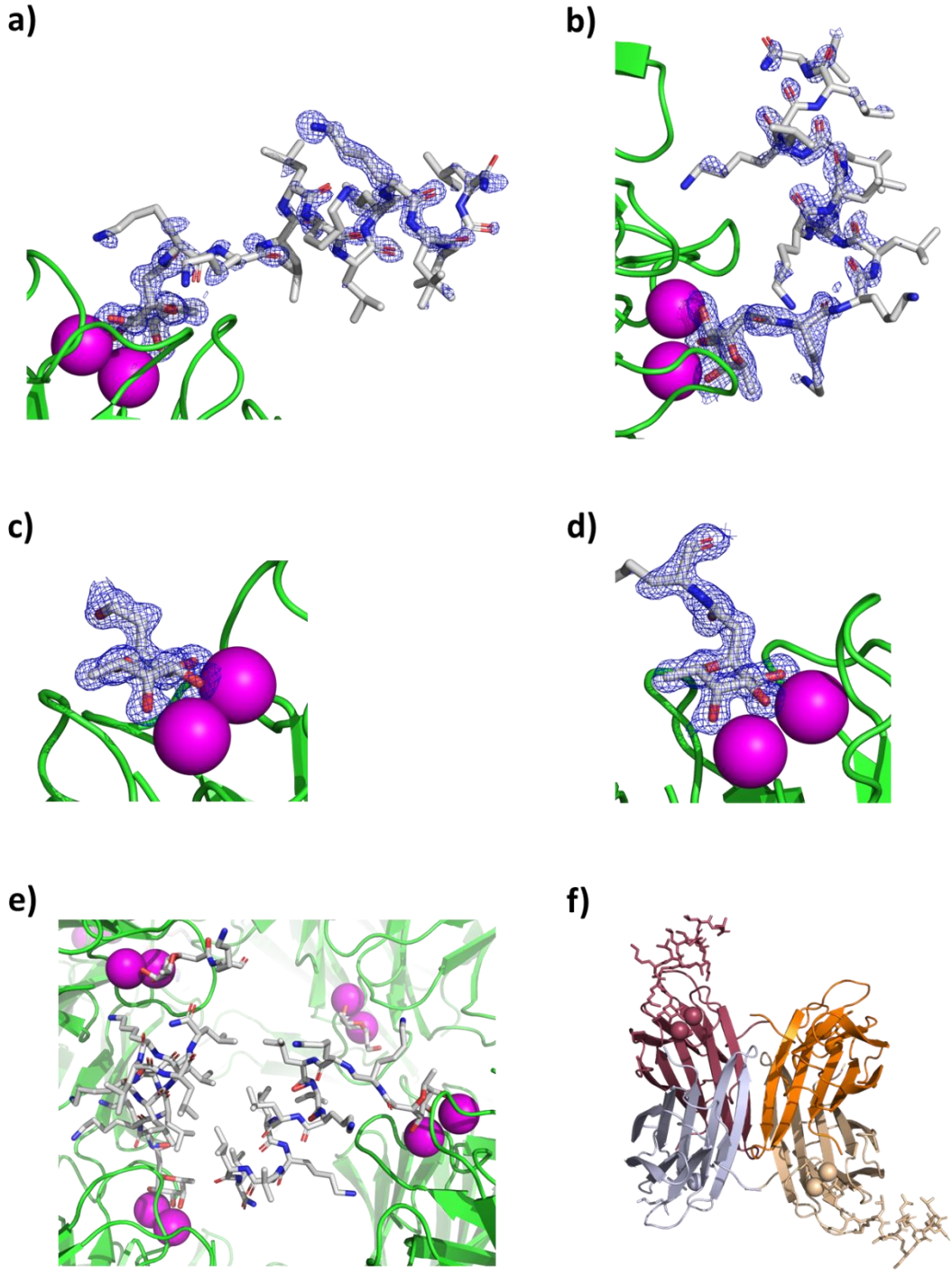

Figure S2.8: Details of the X-ray structure of the **FHP8**·LecB complex in P 1 2_1 1. **(a-d)** Asymmetric peptide entities with corresponding electron density map as blue mesh, Ca^{2+} atoms as magenta spheres and the bound LecB monomer as green cartoon. Electron density is shown for a 1.0σ level. **(e)** Incomplete bundles of four different asymmetric complete and incomplete peptides Same color code as in (a). **(f)** View of the unit cell including LecB subunits, Ca^{2+} atoms and the bound peptides. Peptides are shown as sticks, Ca^{2+} atoms as spheres and lectin monomers are displayed as cartoon of the same colour.

Table S2.5: Data collection and refinement statistics for the X-ray structure of the **FHP30**·LecB complex.

Structural data	**FHP30·LecB**
Beam line	PSI PXIII
Wavelength (Å)	1.000
Resolution (Å)	50.0-1.6 (1.72-1.62)[a)]
Cell dimension	
Space group	94, P 4_2 2_1 2
Unit cell (Å)	a = 70.7, b = 70.7, c = 103.4 α = 90.0°, β = 90.0°, γ = 90.0°
Measured reflection / unique	885904/63954
Average multiplicity	13.9 (13.4)
Completeness (%)	100.0 (99.9)
Average $I / \sigma(I)$	15.46 (0.98)
Correlation $CC_{1/2}$ (%)	99.9 (37.8)
R_{meas} (%)	15.2 (284.0)
Wilson β-factor (Å^2)	18.1
Refinement	
Resolution range (Å)	45.00-1.62
R_{work} (%)	14.82
R_{free} (%)	18.34
Average Biso (Å^2)	83.1
RMSD from ideal angles (°)	0.802
Bonds (Å)	0.005
Water molecules	266
Ligand molecules	2
Protein data Bank deposition code	8ANR

[a)] Values in brackets correspond to the outer shell.

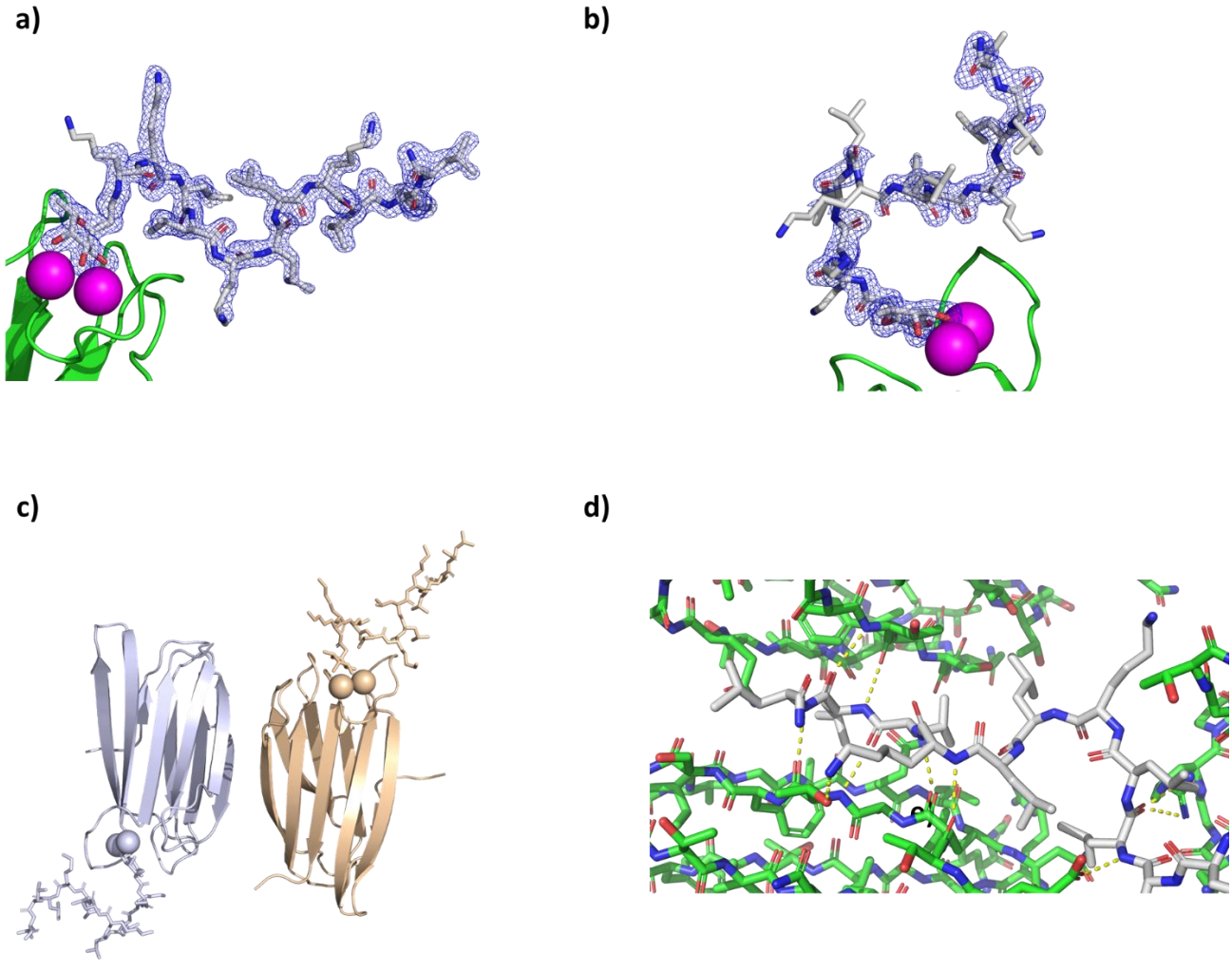

Figure S2.9: Details of the X-ray structure of the **FHP30**·LecB complex in P 4_2 2_1 2. **(a-b)** Asymmetric peptide entities with corresponding electron density map as blue mesh, Ca^{2+} atoms as magenta spheres and the bound LecB monomer as green cartoon. Electron density is shown for a 1.0σ level. **(c)** View of the unit cell including LecB subunits, Ca^{2+} atoms and the bound peptides. Peptides are shown as sticks, Ca^{2+} atoms as spheres and lectin monomers are displayed as cartoon of the same color. **(d)** Hydrogen bonds (yellow dashed lines) between lectin B monomers and **FHP30** (chain C).

Table S2.6: Data collection and refinement statistics for the X-ray structure of the **FHP31**·LecB complex.

Structural data	**FHP31·LecB**
Beam line	PSI PXIII
Wavelength (Å)	1.000
Resolution (Å)	50.0-1.2 (1.25-1.18)[a)]
Cell dimension	
Space group	4, P 1 2_1 1
Unit cell (Å)	a = 52.8, b = 62.7, c = 64.4 α = 90.0°, β = 93.2°, γ = 90.0°
Measured reflection / unique	714411/235325
Average multiplicity	3.0 (1.3)
Completeness (%)	90.1 (35.0)
Average $I / \sigma(I)$	20.70 (2.50)
Correlation $CC_{1/2}$ (%)	99.9 (81.2)
R_{meas} (%)	4.4 (46.5)
Wilson β-factor (Å^2)	9.4
Refinement	
Resolution range (Å)	44.88-1.18
R_{work} (%)	12.68
R_{free} (%)	15.14
Average Biso (Å^2)	60.1
RMSD from ideal angles (°)	1.196
Bonds (Å)	0.009
Water molecules	656
Ligand molecules	4
Protein data Bank deposition code	8AOO

[a)] Values in brackets correspond to the outer shell.

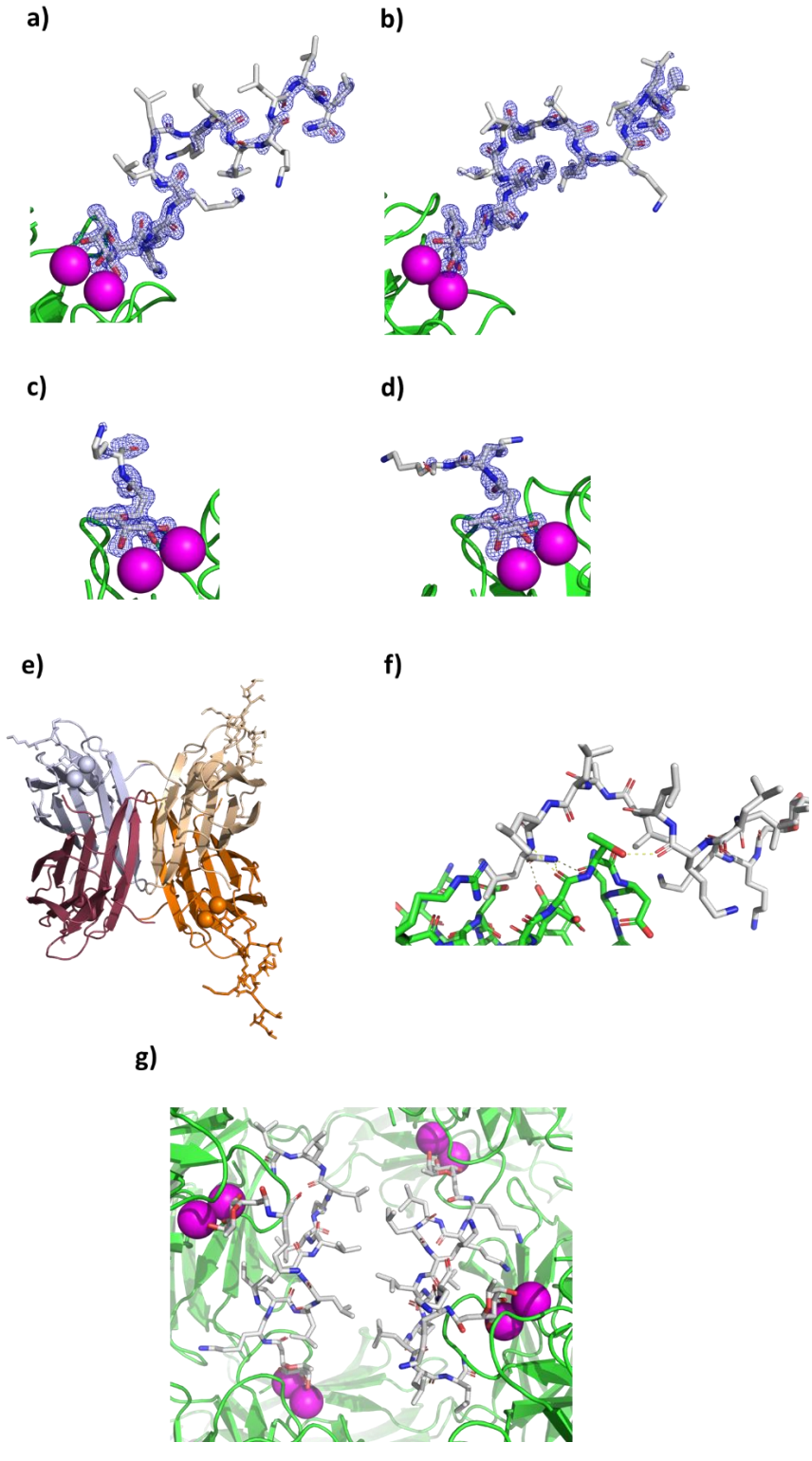

Figure S2.10: Details of the X-ray structure of the FHP31·LecB complex in P 1 21 1. (a-d) Asymmetric peptide entities with corresponding electron density map as blue mesh, Ca^{2+} atoms as magenta spheres and the bound LecB monomer as green cartoon. Electron density is shown for a 1.0σ level. **(e)** View of the unit cell including LecB subunits, Ca^{2+} atoms and the bound peptides. Peptides are shown as sticks, Ca^{2+} atoms as spheres and lectin monomers are displayed as cartoon of the same color. **(f)** H-bonds interaction (yellow dashed lines) between FHP31 (grey stick) and lectin monomer (green stick). (g) Incomplete bundle of four different complete and incomplete peptides. Same color code as in (a).

Molecular Dynamics

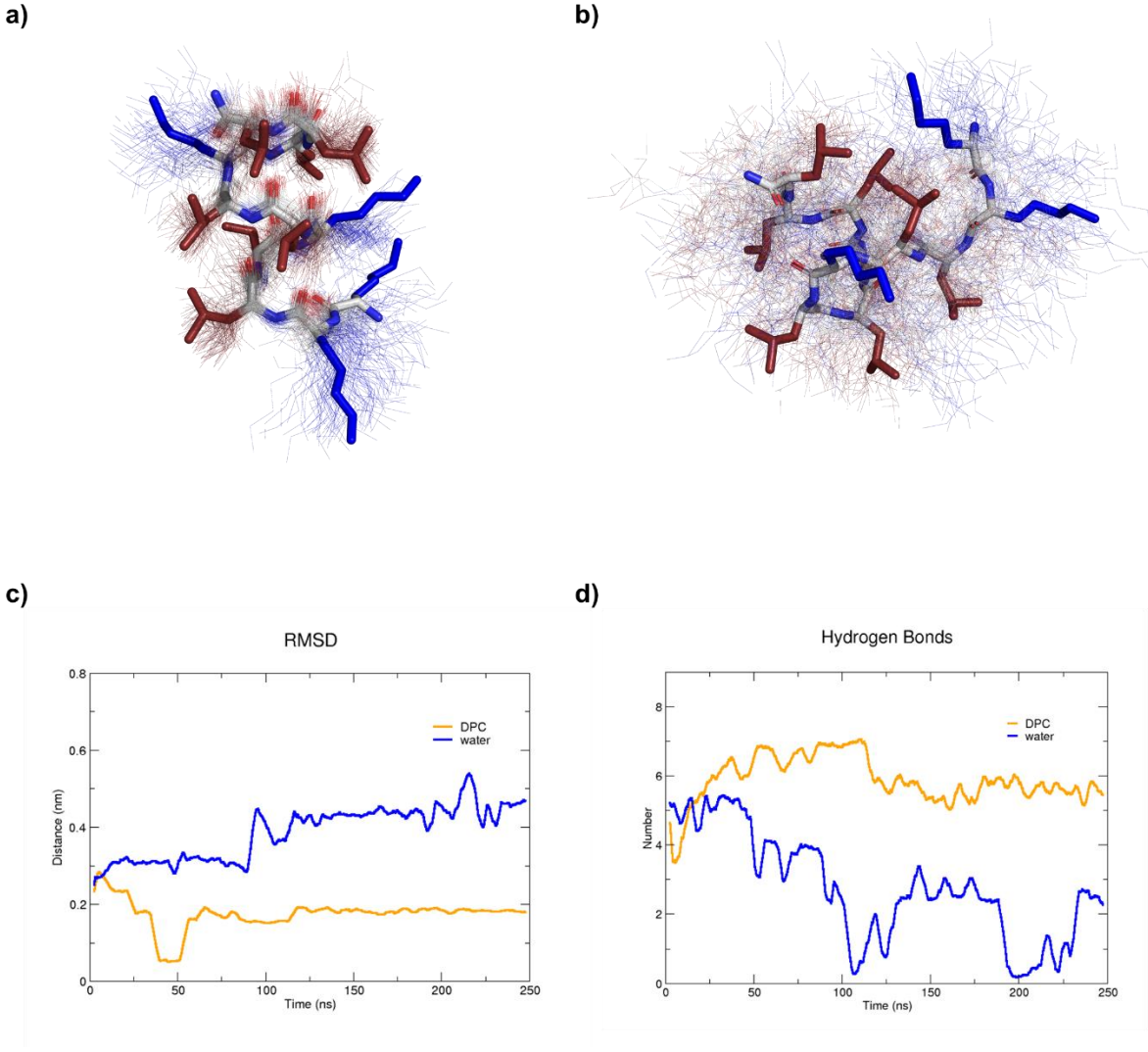

Figure S2.11: MD simulations of **dln69** with and without DPC micelle. **(a)** Average structure (stick model) in presence of DPC micelle over 100 structures sampled during the last 100 ns (thin lines). Hydrophobic side chains are colored in red and cationic side chains are colored in blue. **(b)** Same as (a) for run in water. **(c)** Comparison of root-mean square deviation of the peptide backbone relative to starting coordinates of the α-helix built in PyMol between run with DPC and run in water. **(d)** Comparison of the number of intramolecular backbone hydrogen bonds between run with DPC and run in water.

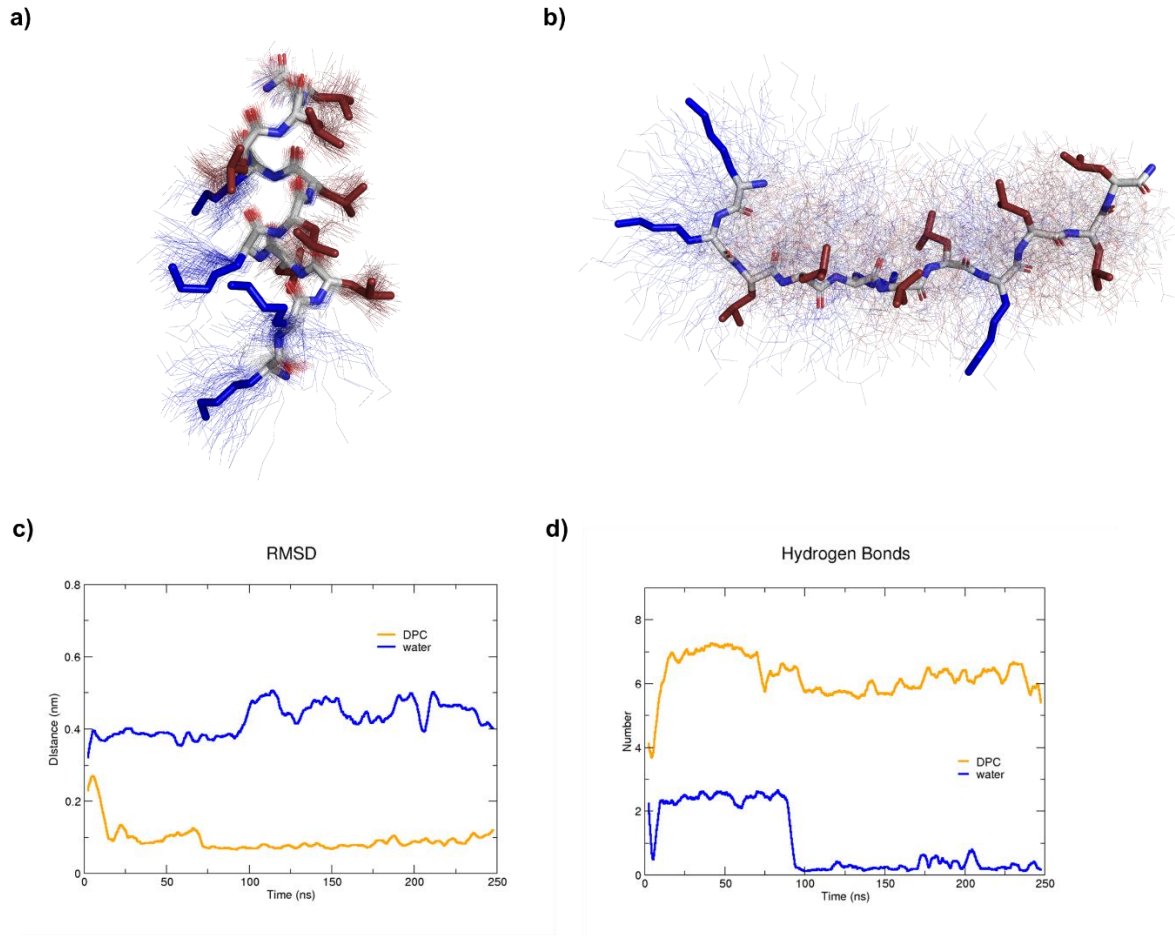

Figure S2.12: MD simulations of **HP1** with and without DPC micelle. **(a)** Average structure (stick model) in presence of DPC micelle over 100 structures sampled during the last 100 ns (thin lines). Hydrophobic side chains are colored in red and cationic side chains are colored in blue. **(b)** Same as (a) for run in water. **(c)** Comparison of root-mean square deviation of the peptide backbone relative to starting coordinates of the α-helix built in PyMol between run with DPC and run in water. **(d)** Comparison of the number of intramolecular backbone hydrogen bonds between run with DPC and run in water.

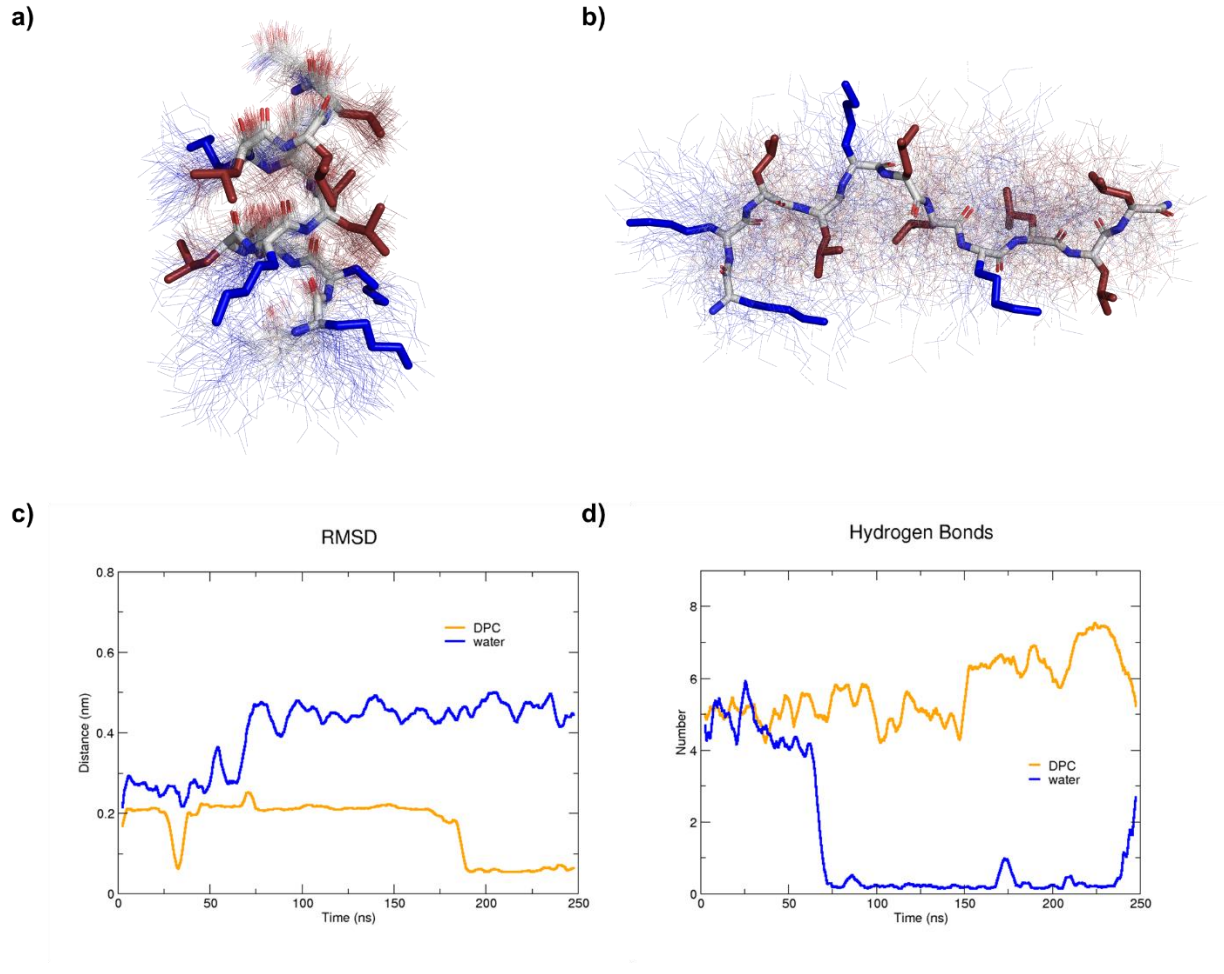

Figure S2.13: MD simulations of **HP2** with and without DPC micelle. **(a)** Average structure (stick model) in presence of DPC micelle over 100 structures sampled during the last 100 ns (thin lines). Hydrophobic side chains are colored in red and cationic side chains are colored in blue. **(b)** Same as (a) for run in water. **(c)** Comparison of root-mean square deviation of the peptide backbone relative to starting coordinates of the α-helix built in PyMol between run with DPC and run in water. **(d)** Comparison of the number of intramolecular backbone hydrogen bonds between run with DPC and run in water.

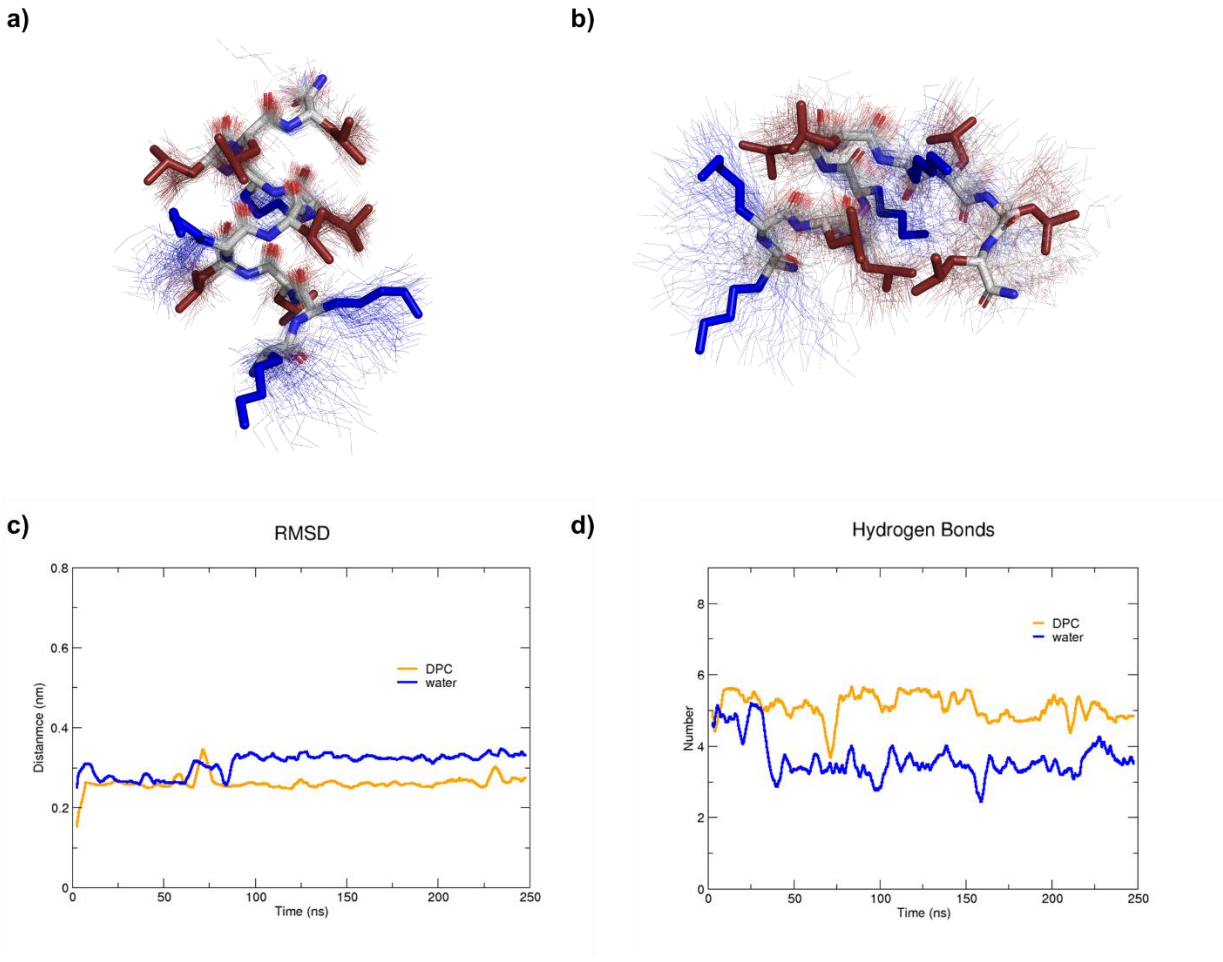

Figure S2.14: MD simulations of **HP3** with and without DPC micelle. **(a)** Average structure (stick model) in presence of DPC micelle over 100 structures sampled during the last 100 ns (thin lines). Hydrophobic side chains are colored in red and cationic side chains are colored in blue. **(b)** Same as (a) for run in water. **(c)** Comparison of root-mean square deviation of the peptide backbone relative to starting coordinates of the α-helix built in PyMol between run with DPC and run in water. **(d)** Comparison of the number of intramolecular backbone hydrogen bonds between run with DPC and run in water.

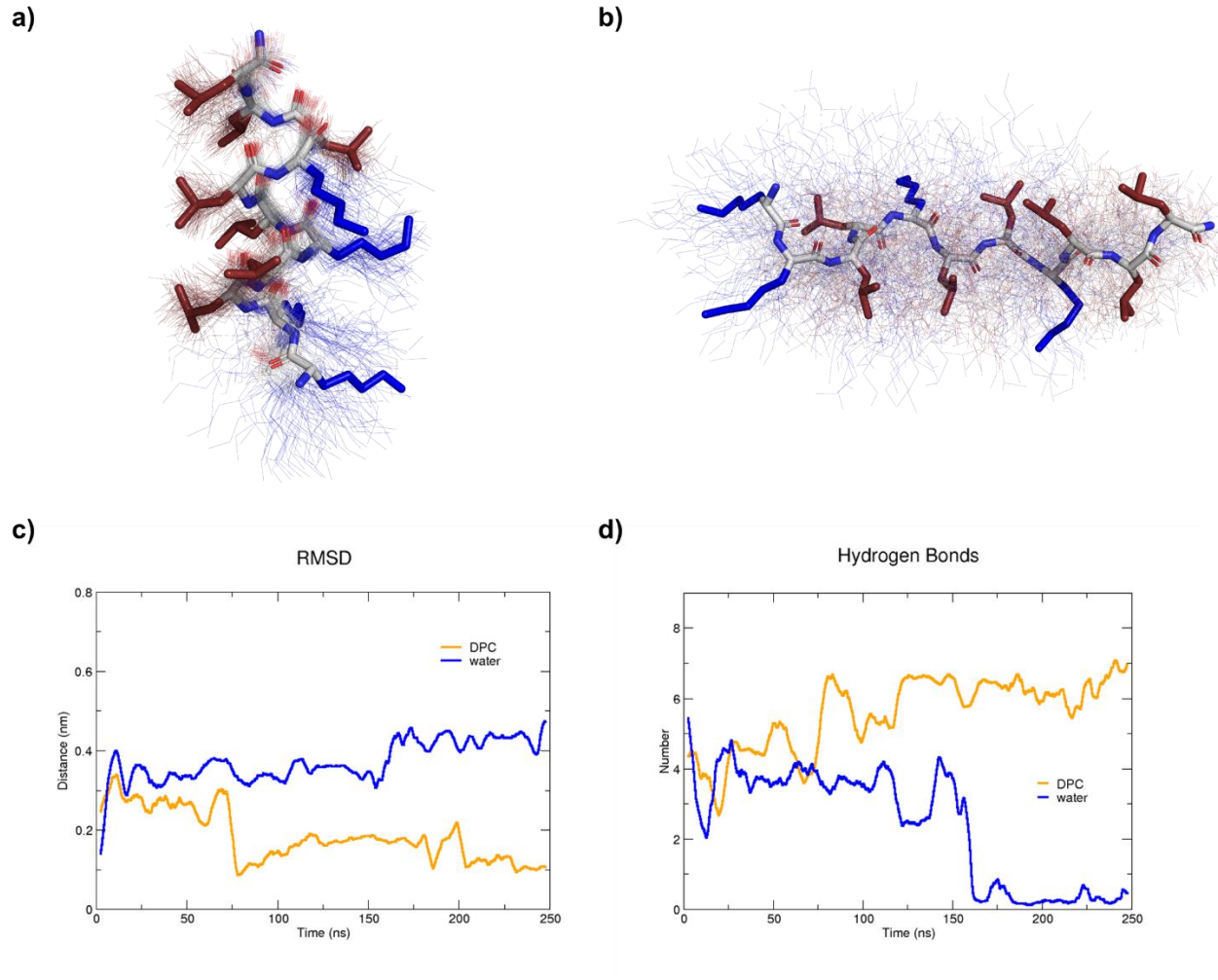

Figure S2.15: MD simulations of **HP4** with and without DPC micelle. **(a)** Average structure (stick model) in presence of DPC micelle over 100 structures sampled during the last 100 ns (thin lines). Hydrophobic side chains are colored in red and cationic side chains are colored in blue. **(b)** Same as (a) for run in water. **(c)** Comparison of root-mean square deviation of the peptide backbone relative to starting coordinates of the α-helix built in PyMol between run with DPC and run in water. **(d)** Comparison of the number of intramolecular backbone hydrogen bonds between run with DPC and run in water.

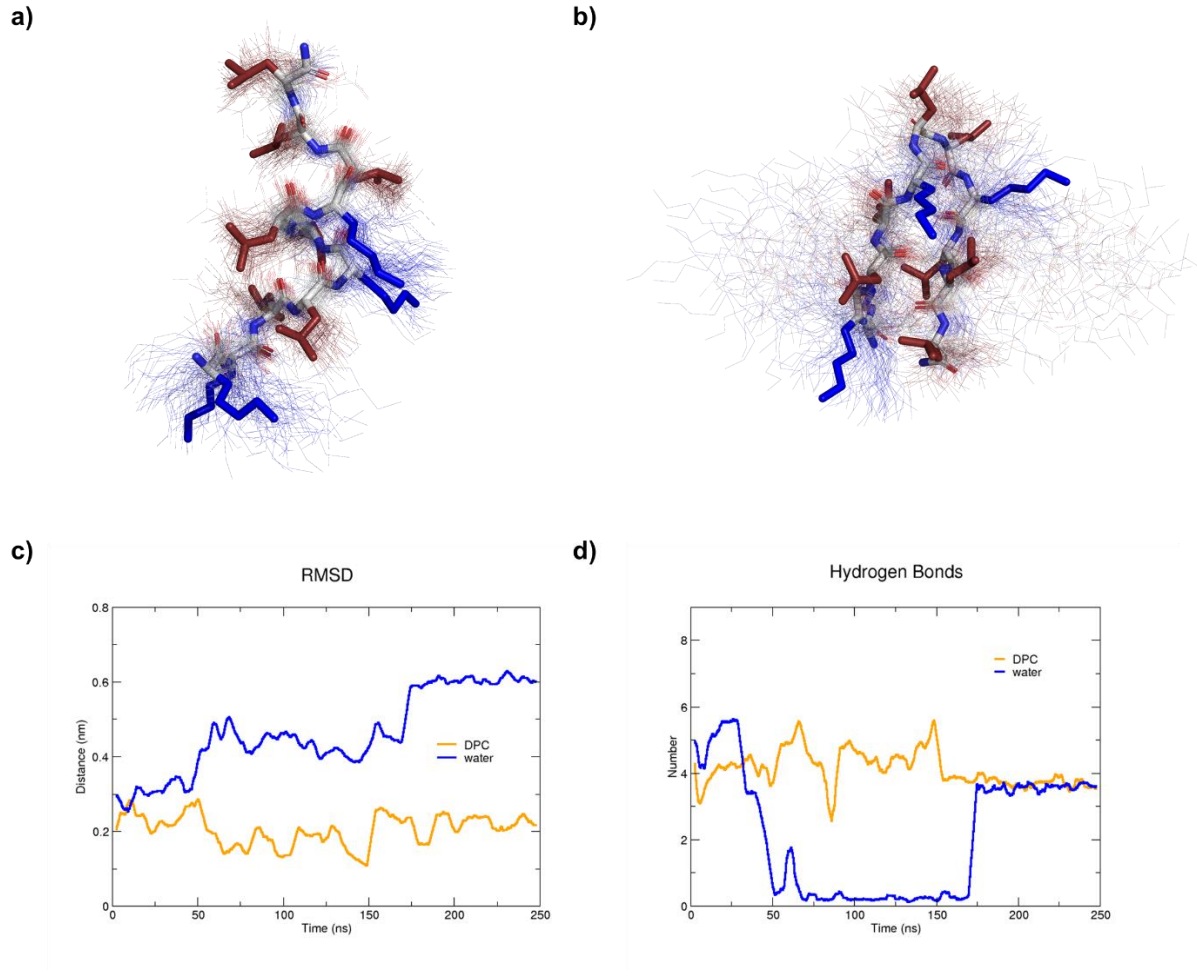

Figure S2.16: MD simulations of **HP7** with and without DPC micelle. **(a)** Average structure (stick model) in presence of DPC micelle over 100 structures sampled during the last 100 ns (thin lines). Hydrophobic side chains are colored in red and cationic side chains are colored in blue. **(b)** Same as (a) for run in water. **(c)** Comparison of root-mean square deviation of the peptide backbone relative to starting coordinates of the α-helix built in PyMol between run with DPC and run in water. **(d)** Comparison of the number of intramolecular backbone hydrogen bonds between run with DPC and run in water.

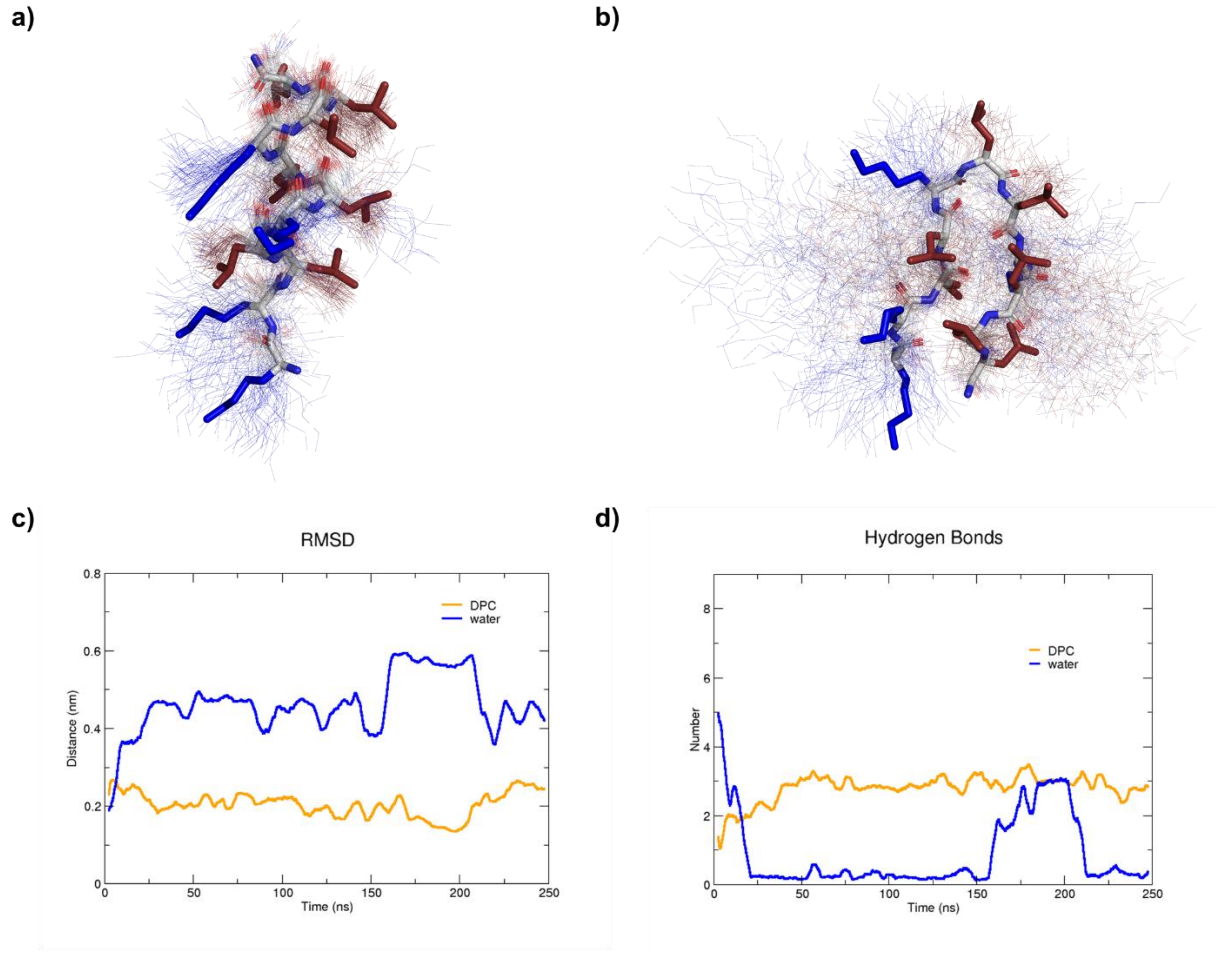

Figure S2.17: MD simulations of **HP8** with and without DPC micelle. **(a)** Average structure (stick model) in presence of DPC micelle over 100 structures sampled during the last 100 ns (thin lines). Hydrophobic side chains are colored in red and cationic side chains are colored in blue. **(b)** Same as (a) for run in water. **(c)** Comparison of root-mean square deviation of the peptide backbone relative to starting coordinates of the α-helix built in PyMol between run with DPC and run in water. **(d)** Comparison of the number of intramolecular backbone hydrogen bonds between run with DPC and run in water.

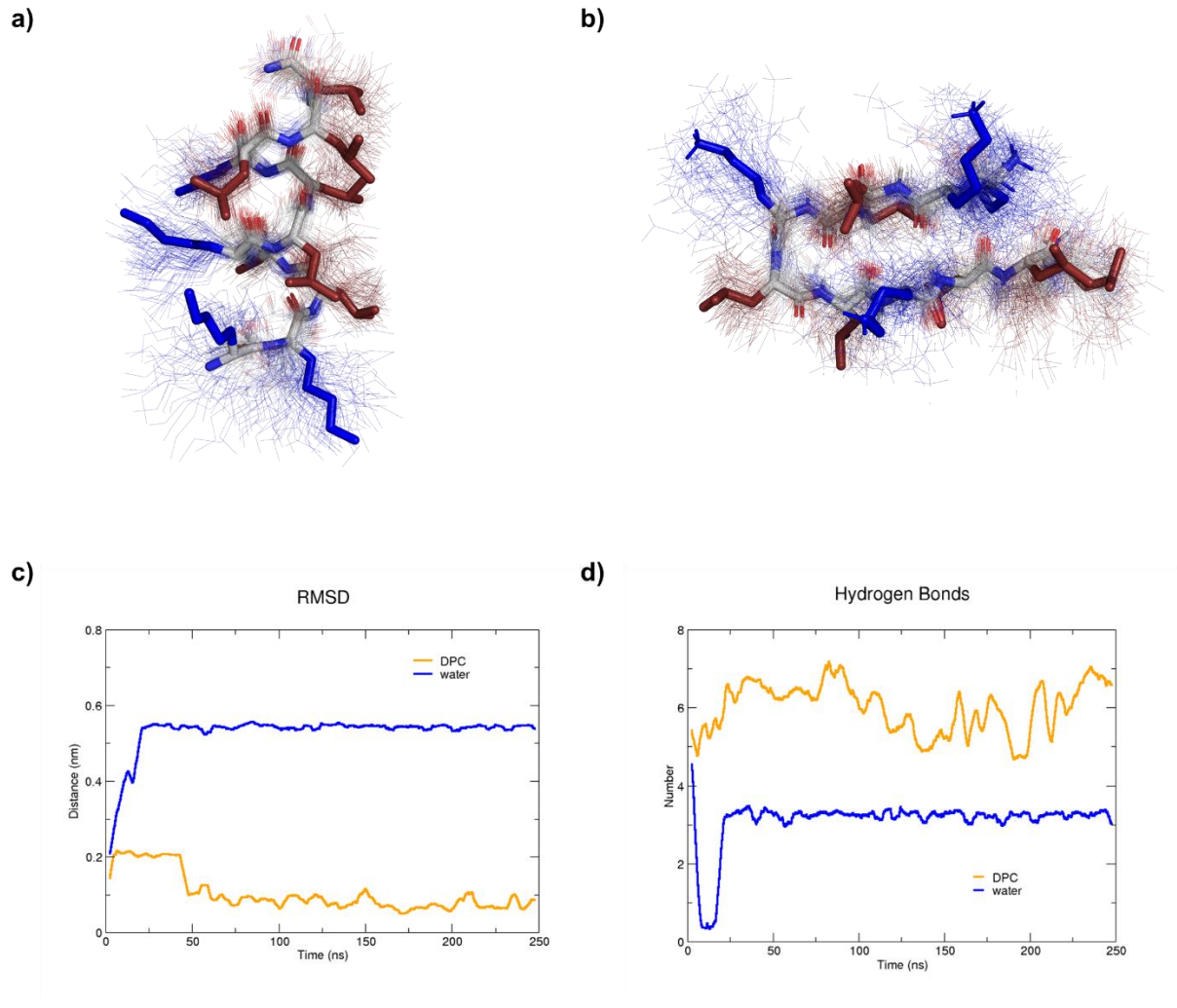

Figure S2.18: MD simulations of **HP10** with and without DPC micelle. **(a)** Average structure (stick model) in presence of DPC micelle over 100 structures sampled during the last 100 ns (thin lines). Hydrophobic side chains are colored in red and cationic side chains are colored in blue. **(b)** Same as (a) for run in water. **(c)** Comparison of root-mean square deviation of the peptide backbone relative to starting coordinates of the α-helix built in PyMol between run with DPC and run in water. **(d)** Comparison of the number of intramolecular backbone hydrogen bonds between run with DPC and run in water.

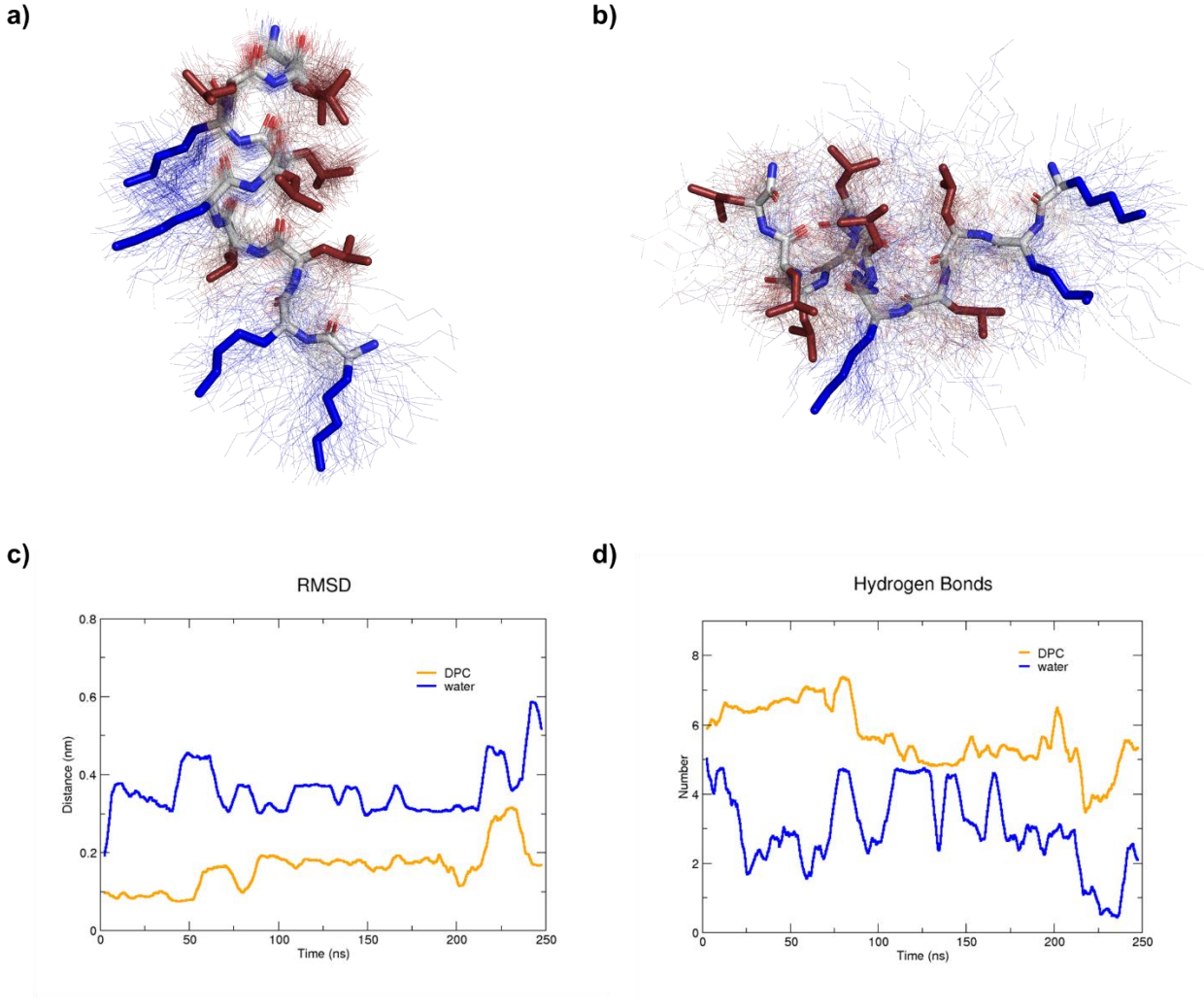

Figure S2.19: MD simulations of **HP11** with and without DPC micelle. **(a)** Average structure (stick model) in presence of DPC micelle over 100 structures sampled during the last 100 ns (thin lines). Hydrophobic side chains are colored in red and cationic side chains are colored in blue. **(b)** Same as (a) for run in water. **(c)** Comparison of root-mean square deviation of the peptide backbone relative to starting coordinates of the α-helix built in PyMol between run with DPC and run in water. **(d)** Comparison of the number of intramolecular backbone hydrogen bonds between run with DPC and run in water.

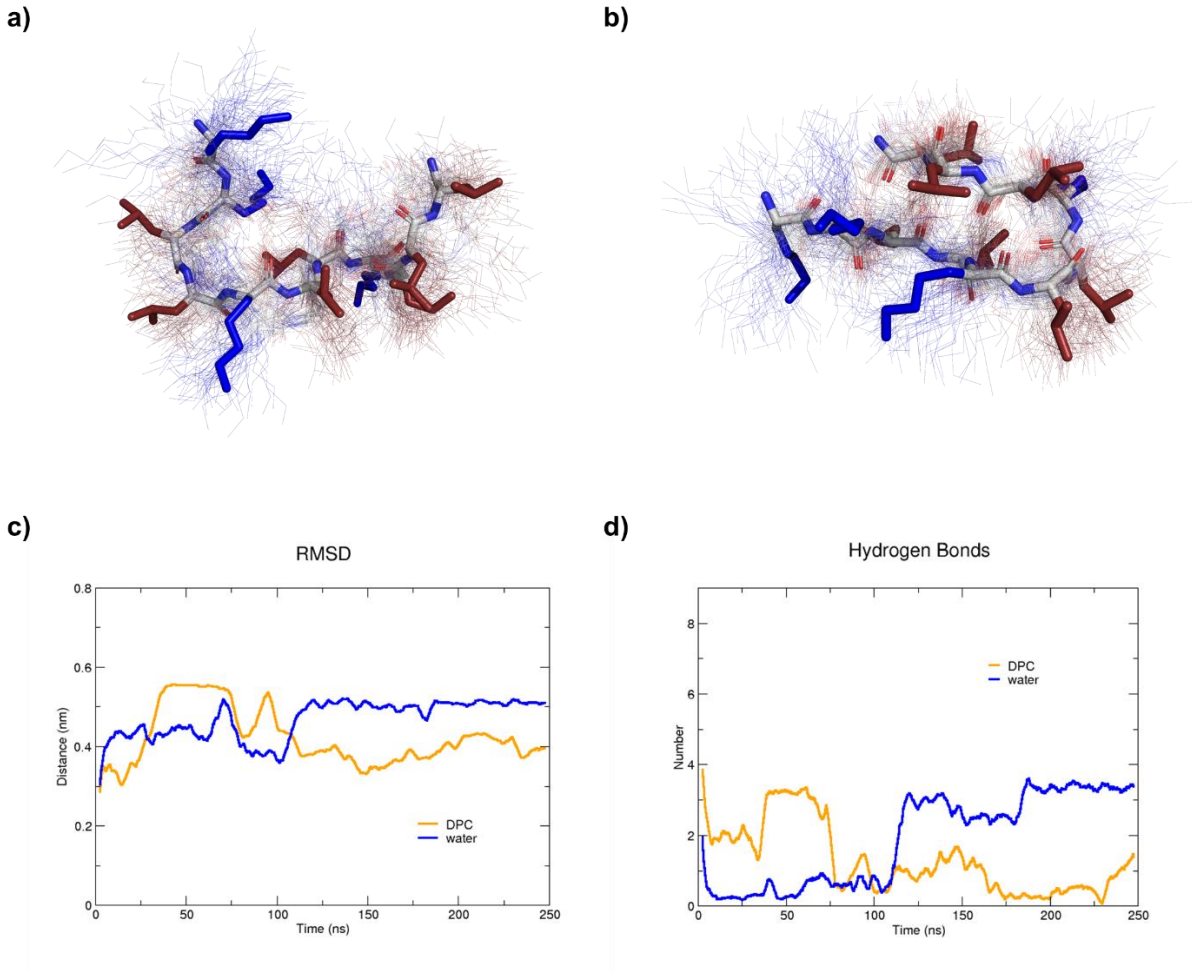

Figure S2.20: MD simulations of **HP16** with and without DPC micelle. **(a)** Average structure (stick model) in presence of DPC micelle over 100 structures sampled during the last 100 ns (thin lines). Hydrophobic side chains are colored in red and cationic side chains are colored in blue. **(b)** Same as (a) for run in water. **(c)** Comparison of root-mean square deviation of the peptide backbone relative to starting coordinates of the α-helix built in PyMol between run with DPC and run in water. **(d)** Comparison of the number of intramolecular backbone hydrogen bonds between run with DPC and run in water.

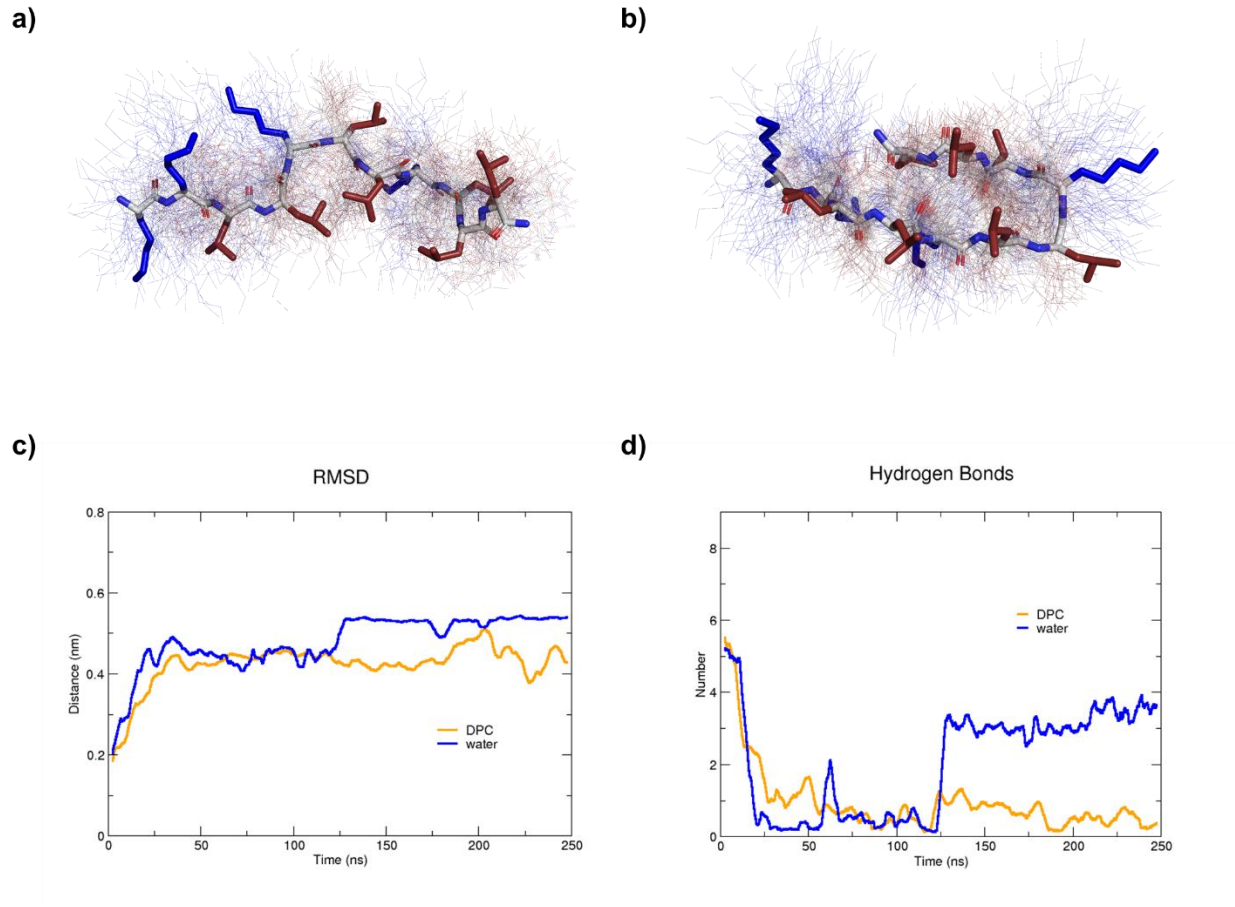

Figure S2.21: MD simulations of **HP29** with and without DPC micelle. **(a)** Average structure (stick model) in presence of DPC micelle over 100 structures sampled during the last 100 ns (thin lines). Hydrophobic side chains are colored in red and cationic side chains are colored in blue. **(b)** Same as (a) for run in water. **(c)** Comparison of root-mean square deviation of the peptide backbone relative to starting coordinates of the α-helix built in PyMol between run with DPC and run in water. **(d)** Comparison of the number of intramolecular backbone hydrogen bonds between run with DPC and run in water.

Statistical Analysis

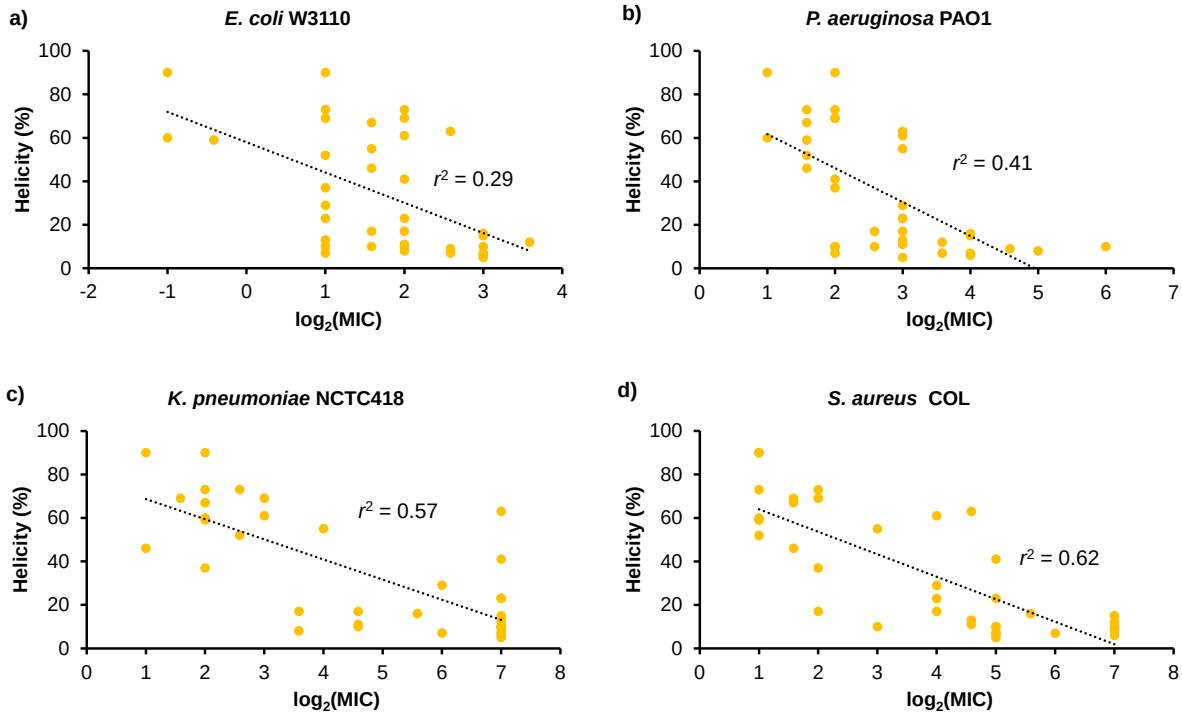

Figure S2.22: Scatter plot of % helicity in 5 mM DPC against $\log_2$(MIC) for (a) E. coli, (b) PAO1, (c) K. pneumoniae and (d) MRSA.

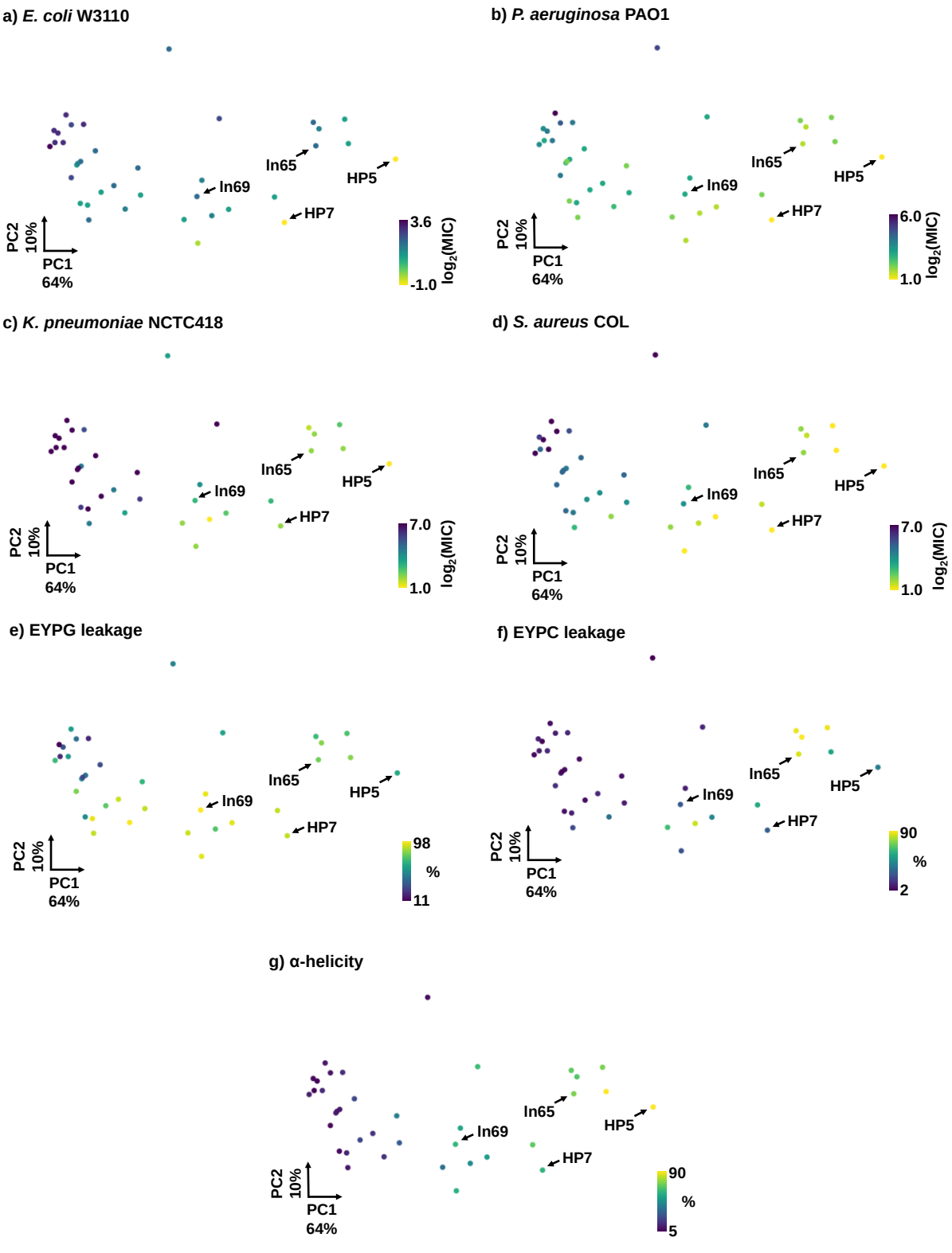

Figure S2.23: Principal Components Analysis visualization of dataset measured on **ln65** derivatives using Faerun Each point represents one compound and is colour coded depending on **(a)** activity on E. coli W3110, **(b)** activity on P. aeruginosa PAO1, **(c)** activity on K. pneumoniae NCTC418 **(d)** activity on S. aureus COL, **(e)** percentage of EYPG vesicles leakage, **(f)** percentage of EYPC vesicles leakage and **(g)** α-helicity in 5 mM DPC.

HPLC-MS and HRMS data

KKLLKLLKLLL (ln65) was obtained as white solid after preparative RP-HPLC (84.0 mg, 58.0%). Analytical RP-HPLC: t_R = 1.66 min (A/D 100:0 to 0:100 in 3.5 min, λ = 214 nm). MS (ESI+): $C_{66}H_{128}N_{16}O_{11}$ calc./obs. 1320.99/1320.99 Da [M].

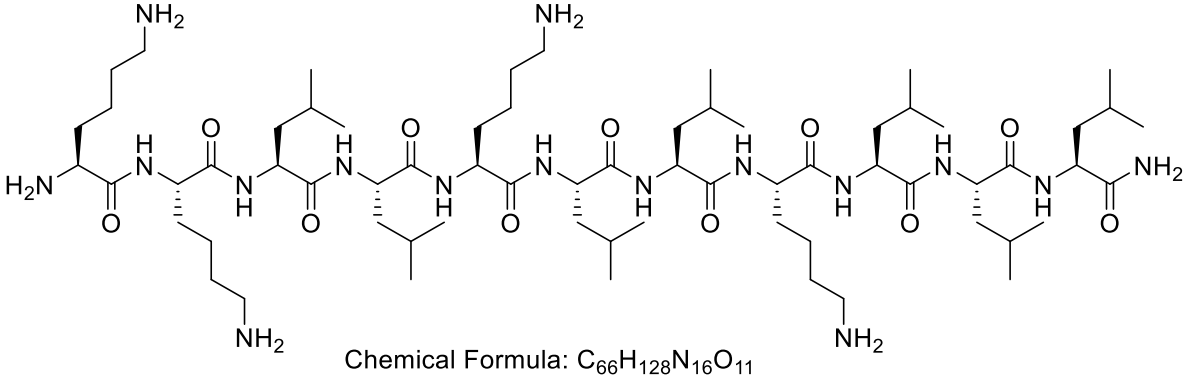

Chemical Formula: $C_{66}H_{128}N_{16}O_{11}$
Exact Mass: 1320.99
Molecular Weight: 1321.85

Analytical HPLC-MS data:

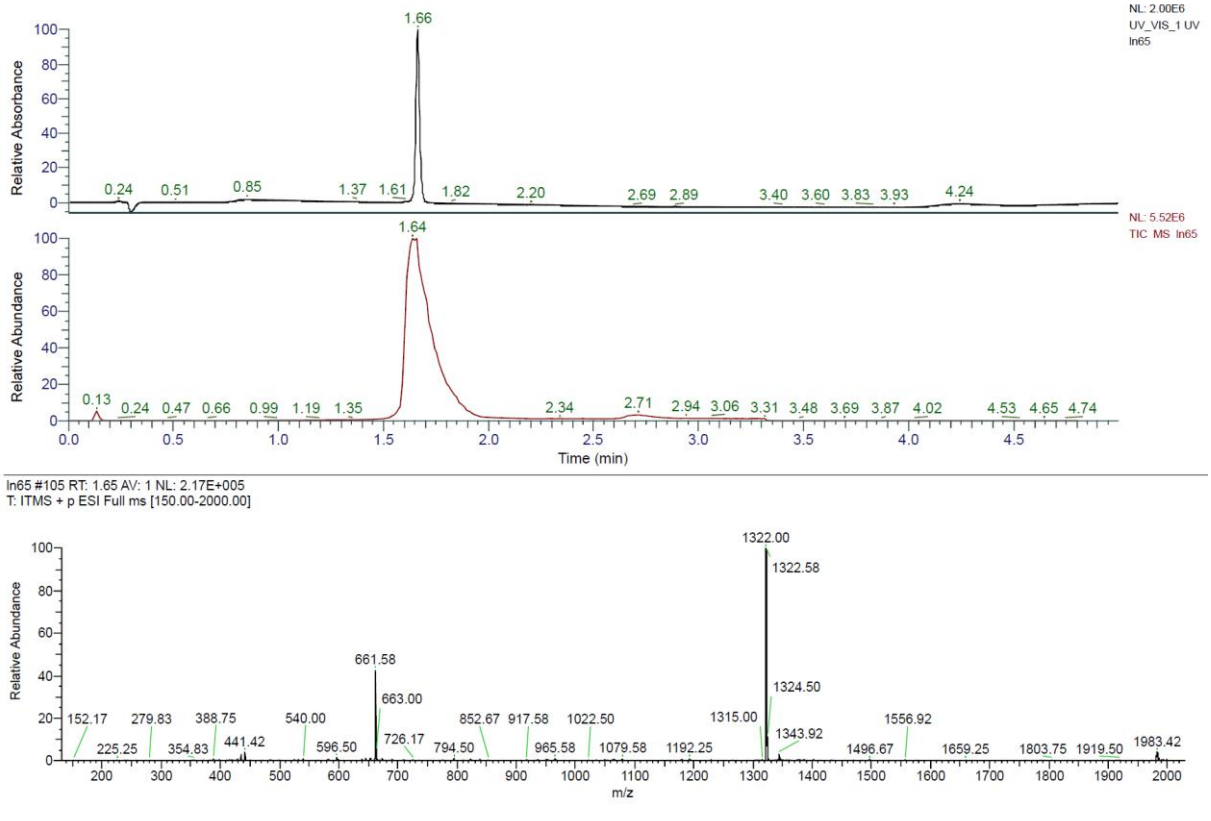

HRMS spectra:

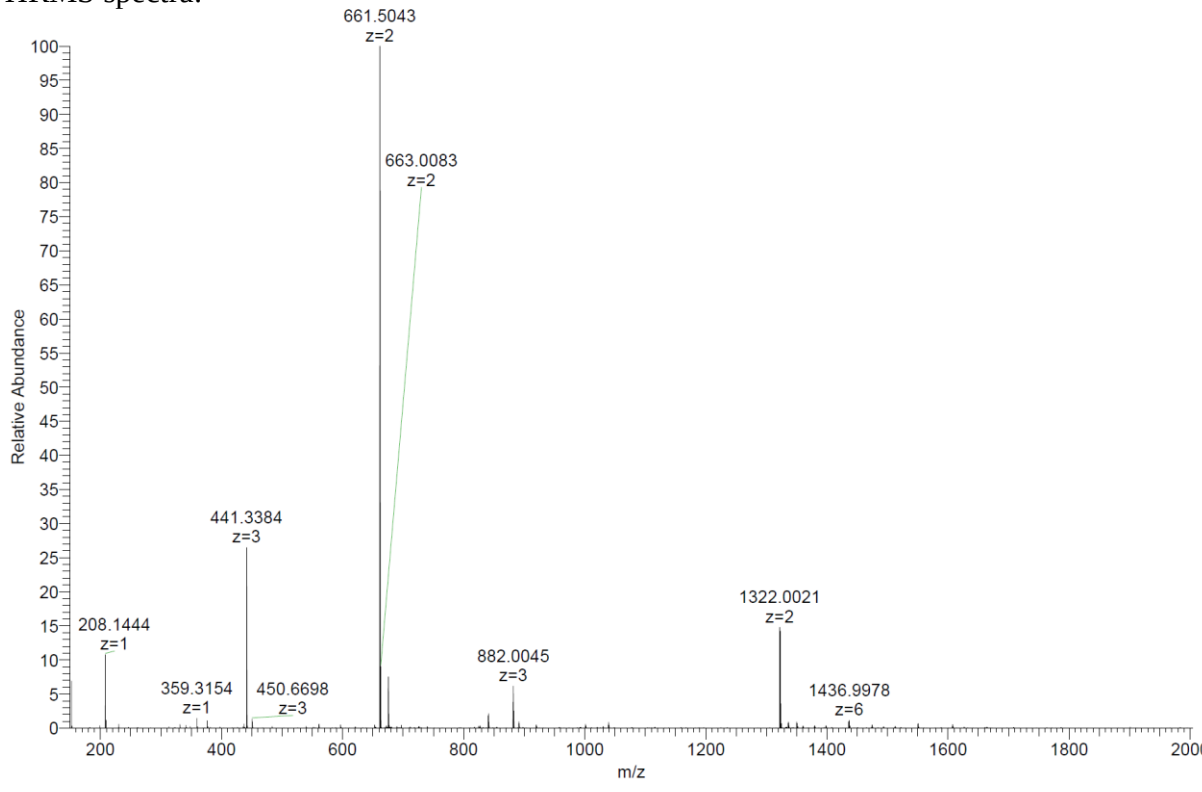

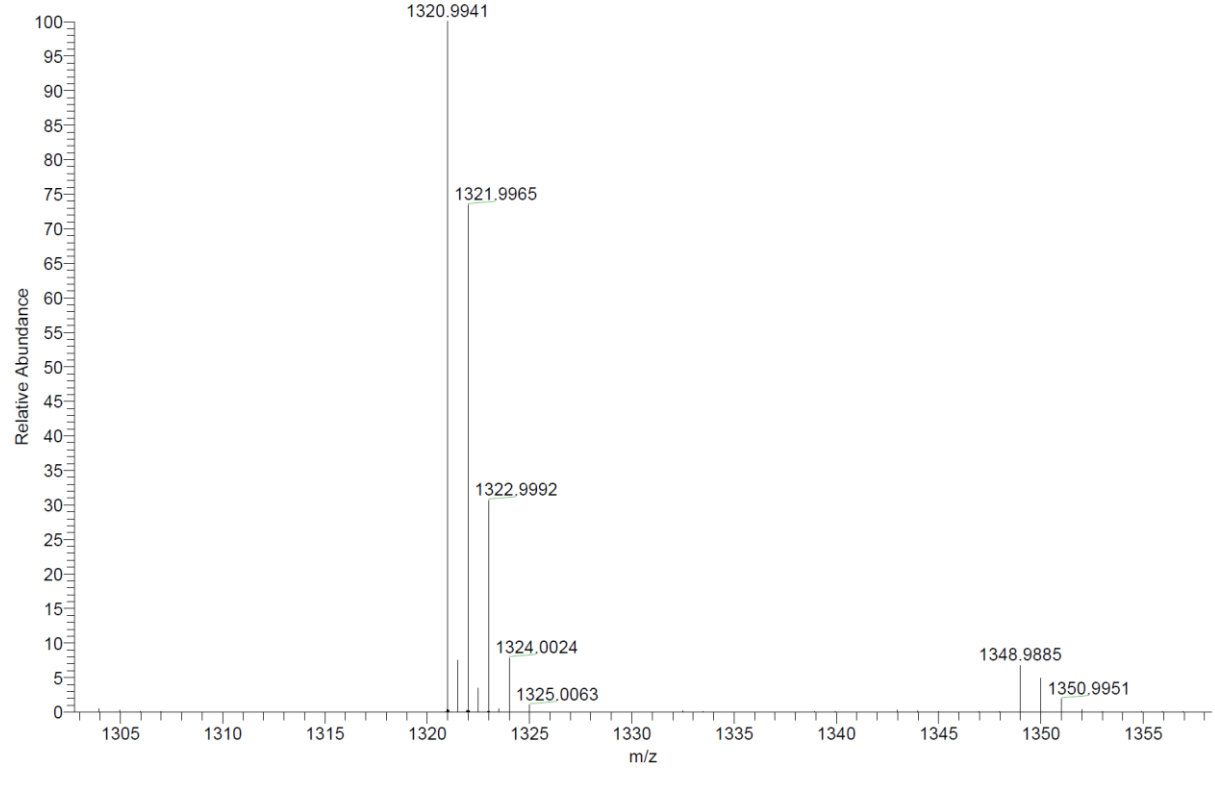

kkllkllkll (dln65) was obtained as white solid after preparative RP-HPLC (34.9 mg, 24.1%). Analytical RP-HPLC: t_R = 1.62 min (A/D 100:0 to 0:100 in 3.5 min, λ = 214 nm). MS (ESI+): $C_{66}H_{128}N_{16}O_{11}$ calc./obs. 1321.99/1322.00 Da $[M+H]^+$.

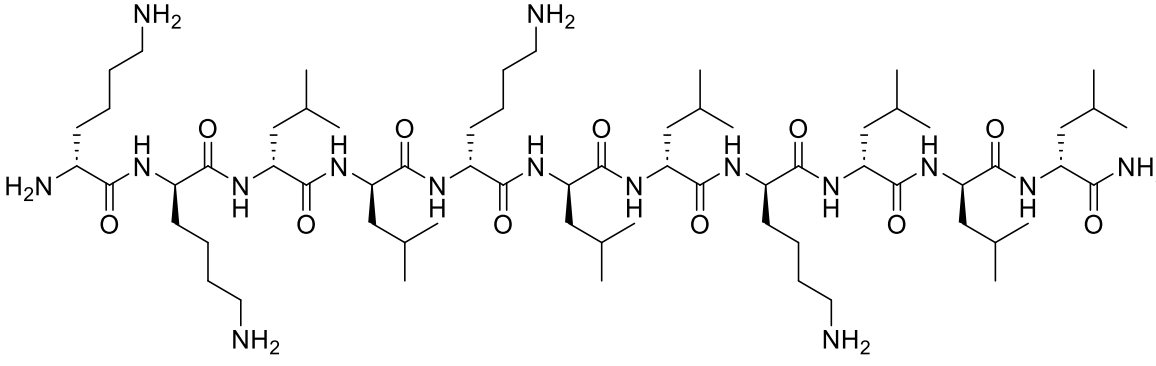

Chemical Formula: $C_{66}H_{128}N_{16}O_{11}$
Exact Mass: 1320.99
Molecular Weight: 1321.85

Analytical HPLC-MS data:

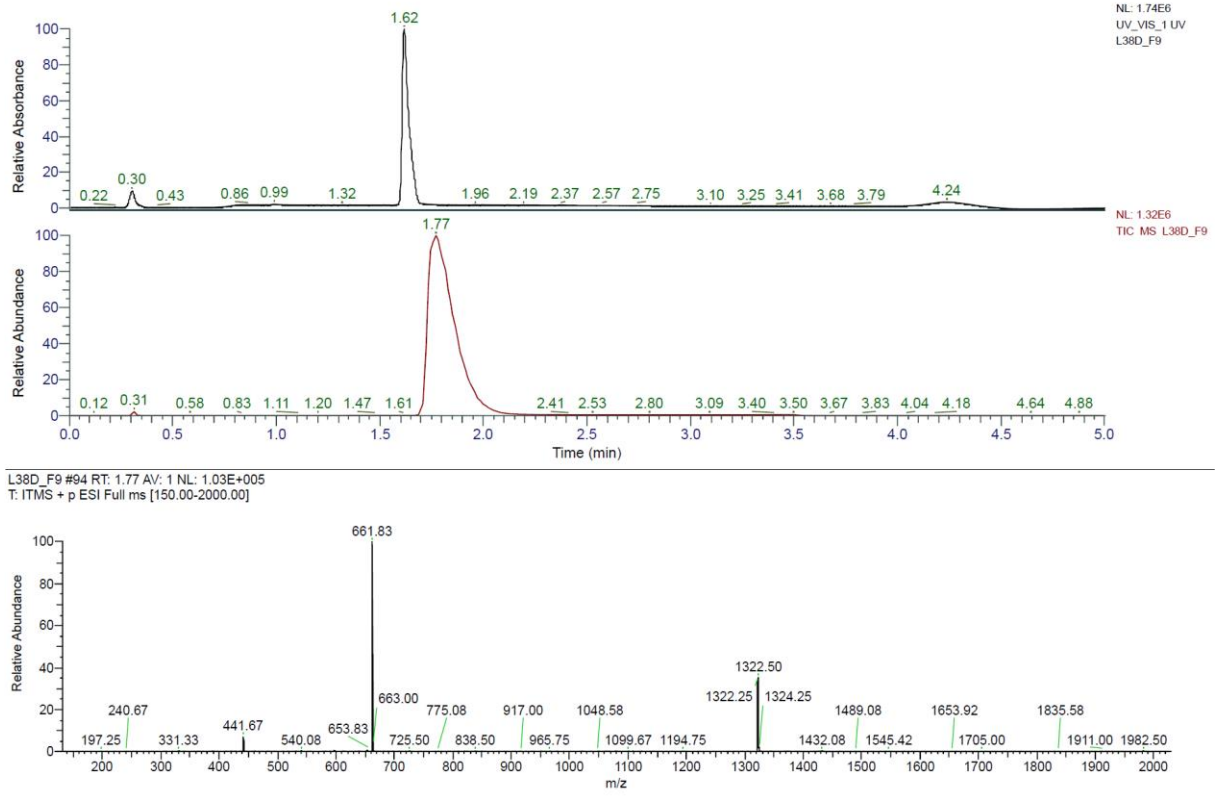

HRMS spectra:

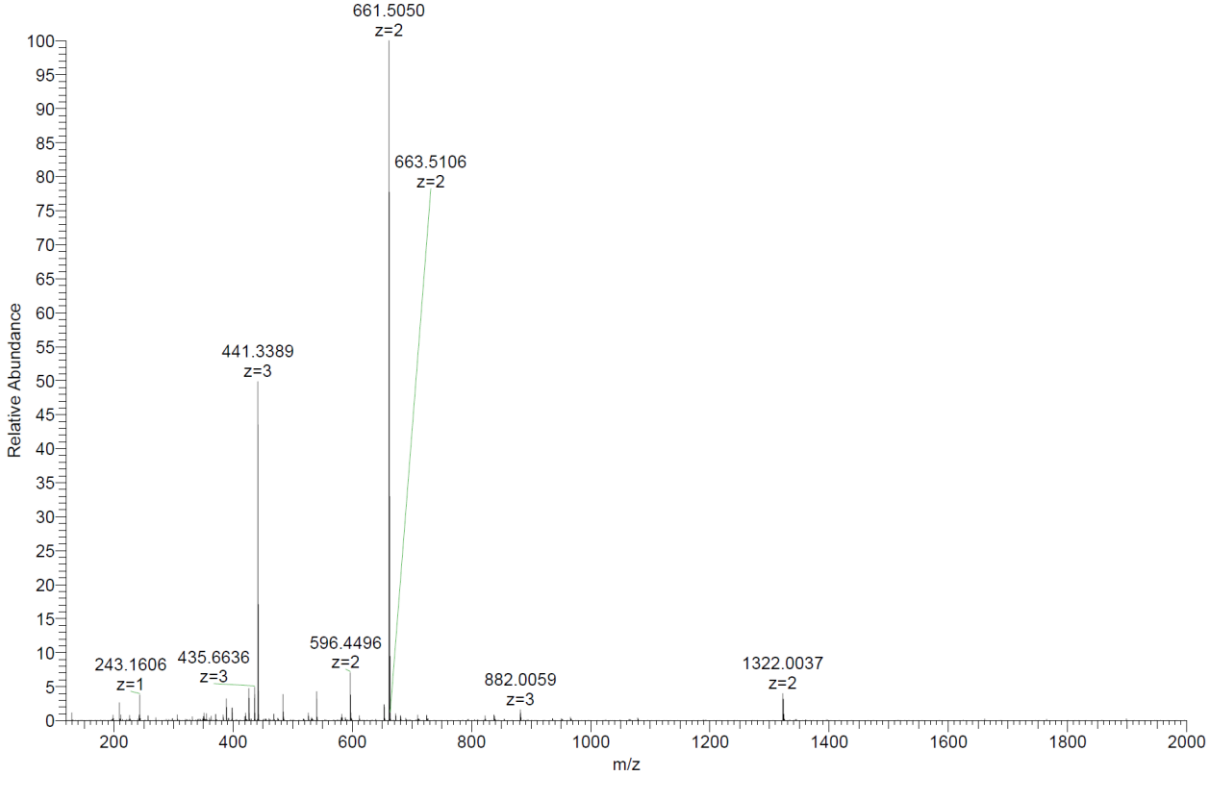

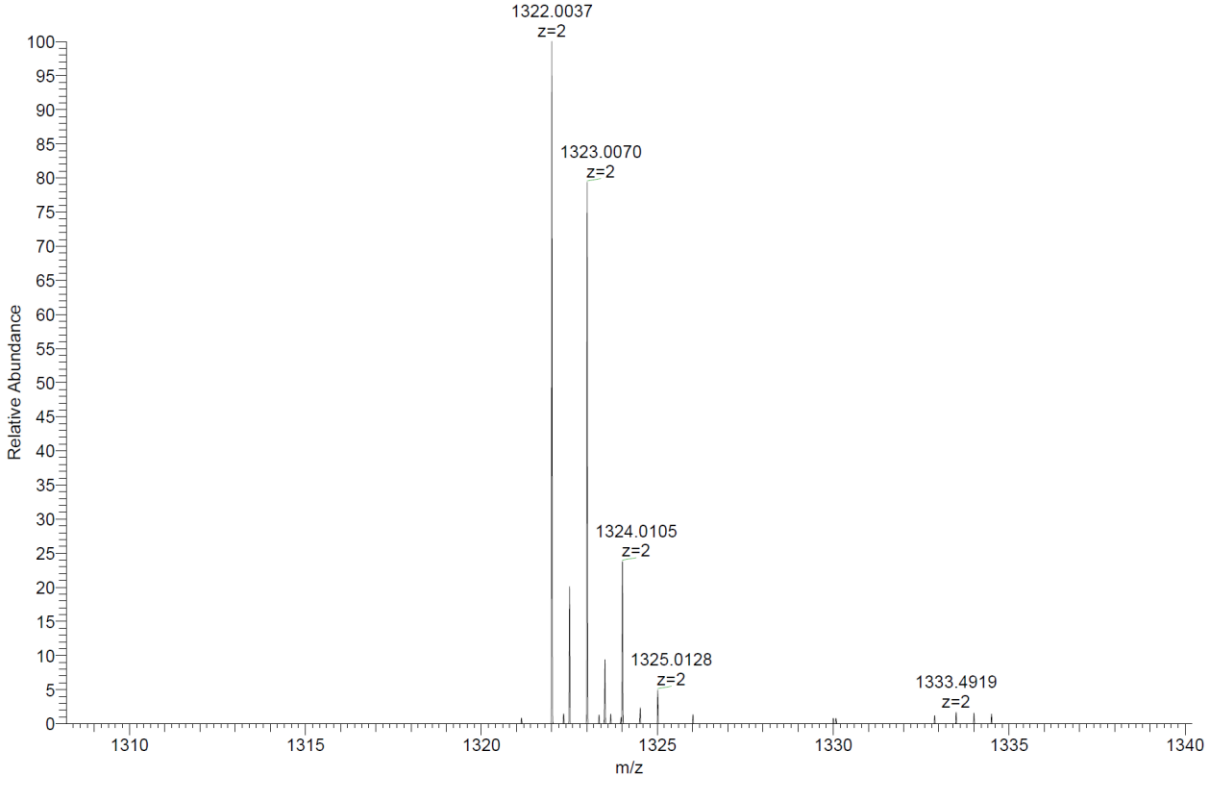

kkLLkLLkLLL (ln69) was obtained as white solid after preparative RP-HPLC (102.6 mg, 70.9%). Analytical RP-HPLC: t_R = 1.55 min (A/D 100:0 to 0:100 in 3.5 min, λ = 214 nm). MS (ESI+): $C_{66}H_{128}N_{16}O_{11}$ calc./obs. 1320.99/1320.99 Da [M].

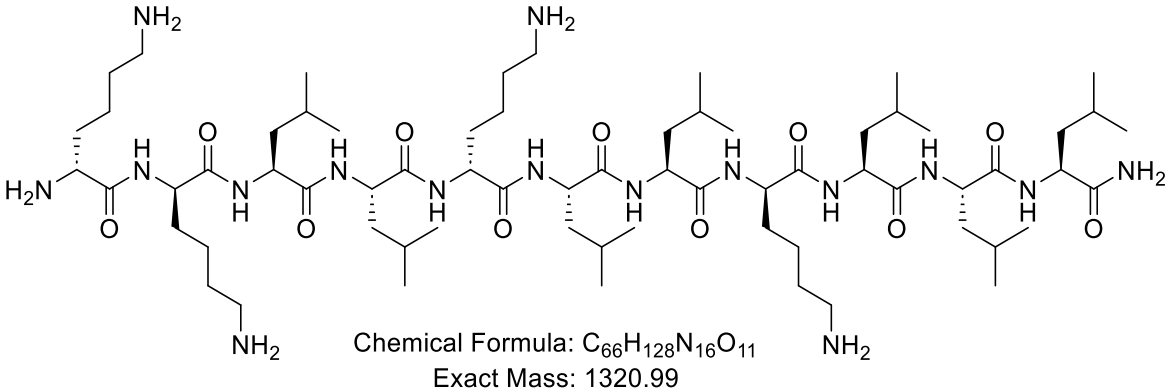

Analytical HPLC-MS data:

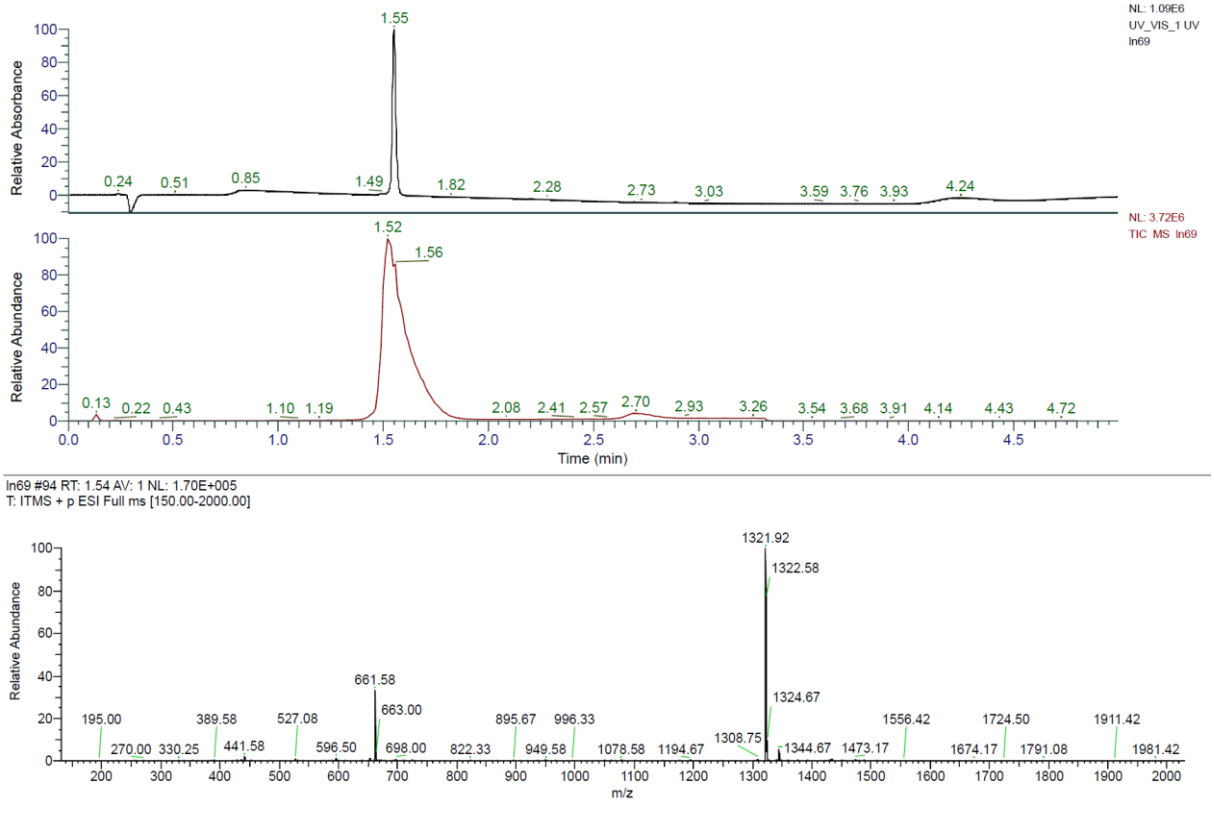

HRMS spectra:

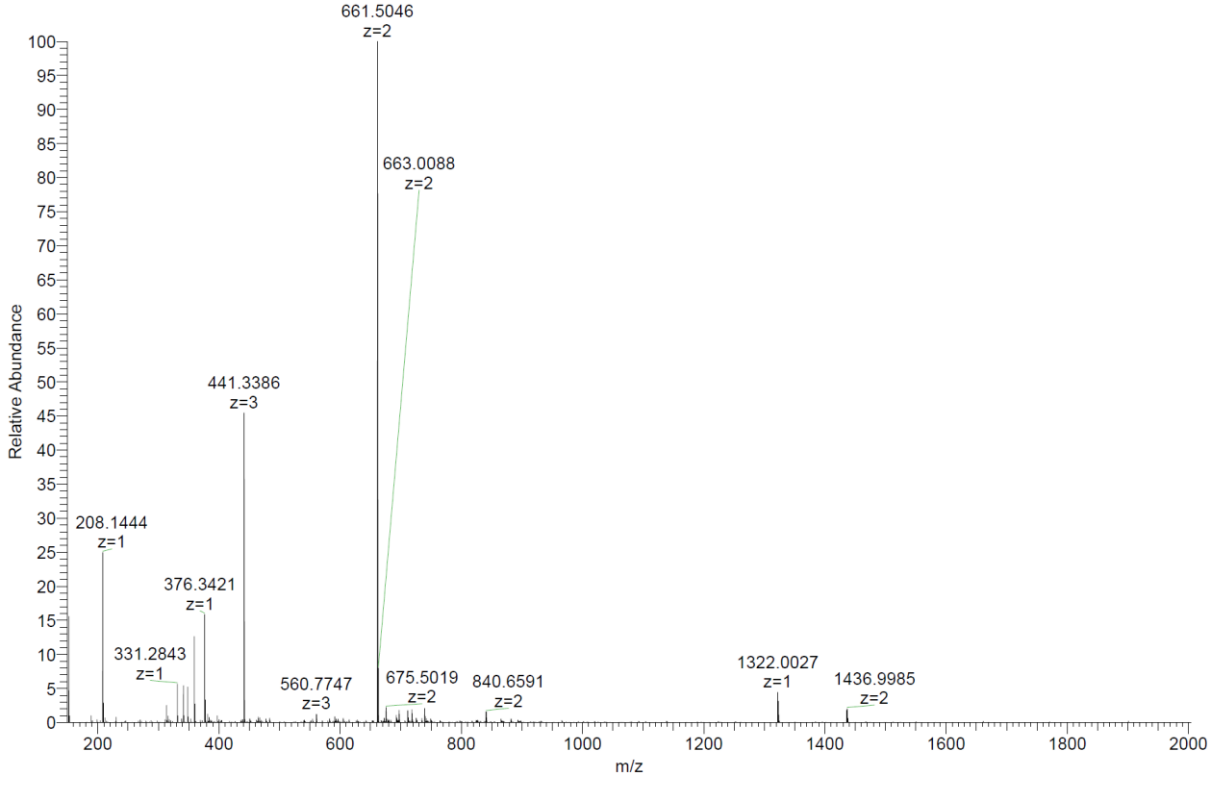

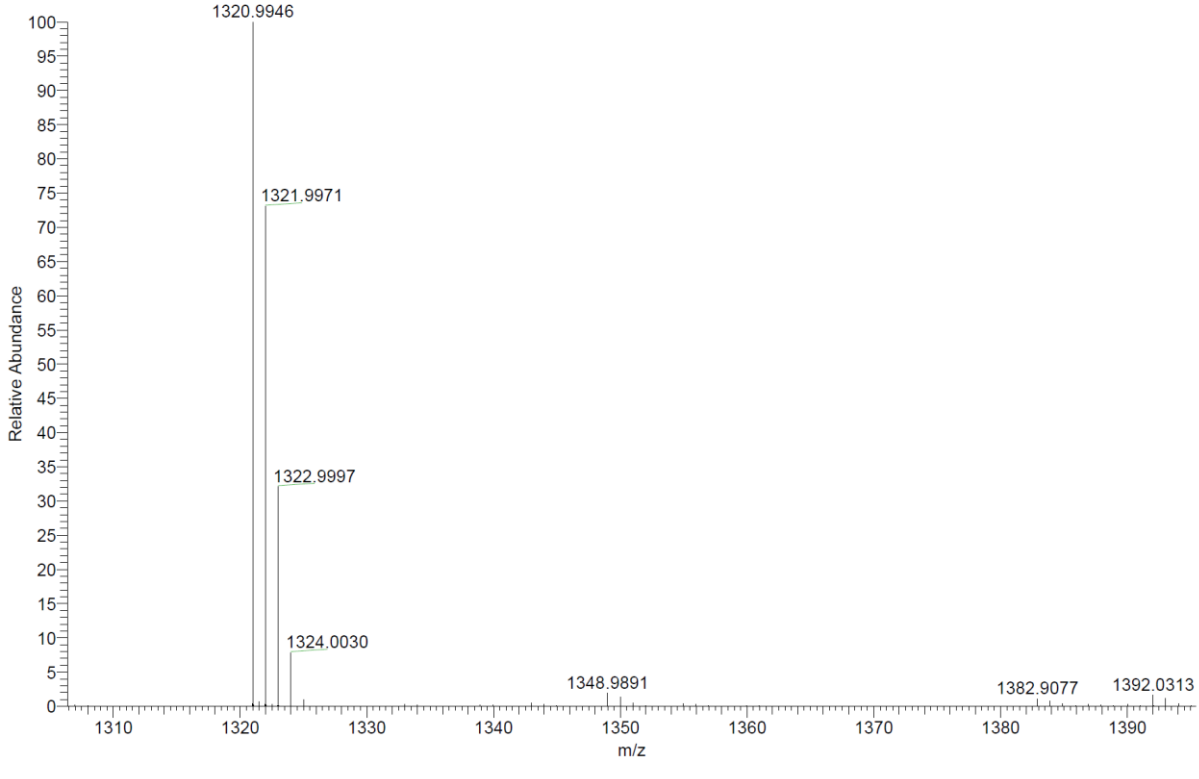

KKllKllKlll (dln69) was obtained as white solid after preparative RP-HPLC (69.7 mg, 44.6%). Analytical RP-HPLC: t_R = 1.52 min (A/D 100:0 to 0:100 in 3.5 min, λ = 214 nm). MS (ESI+): $C_{66}H_{128}N_{16}O_{11}$ calc./obs. 1321.99/1322.00 Da $[M+H]^+$.

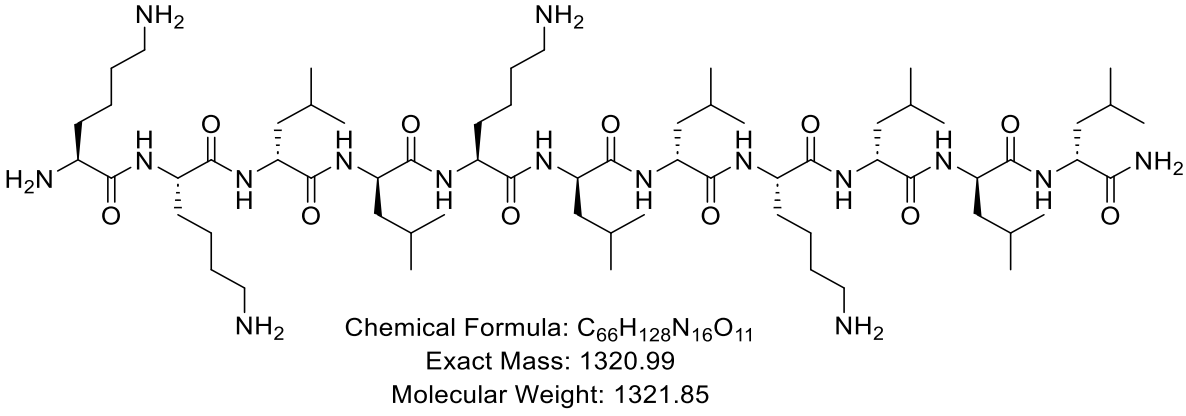

Analytical HPLC-MS data:

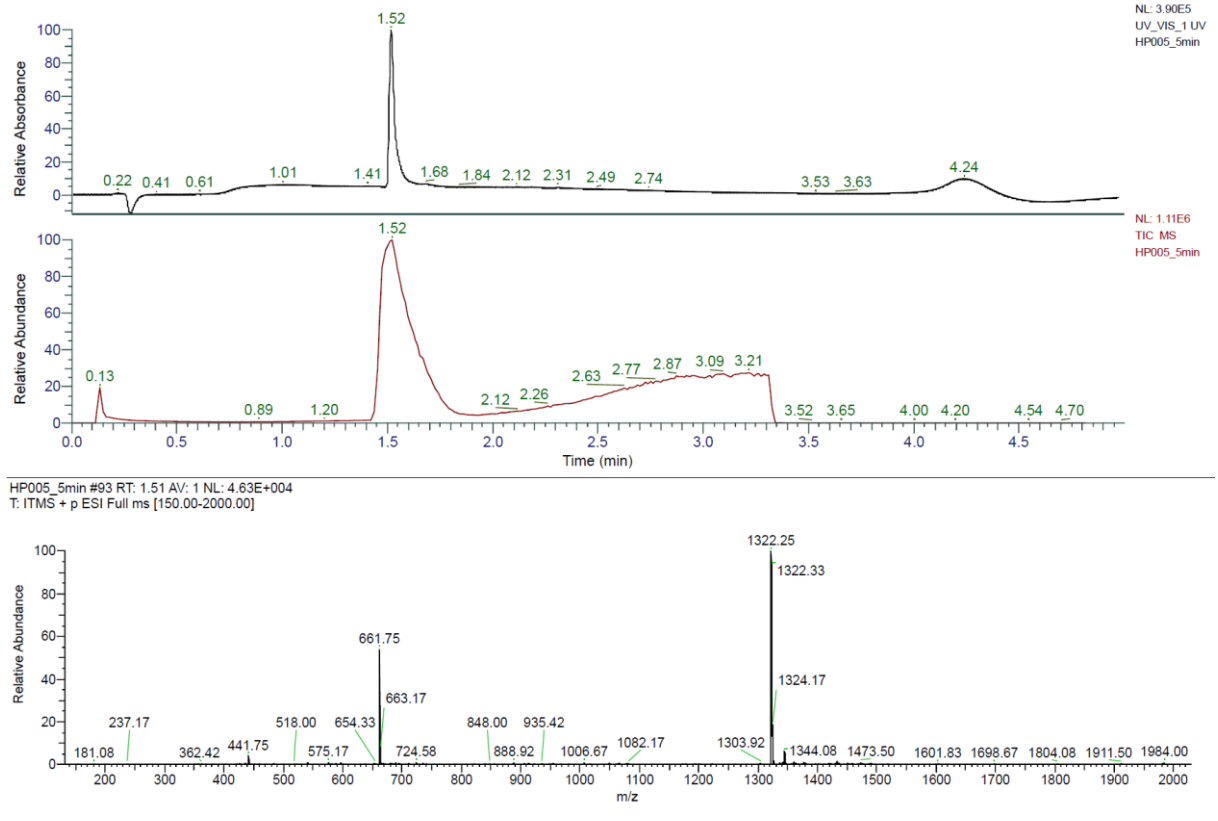

HRMS spectra:

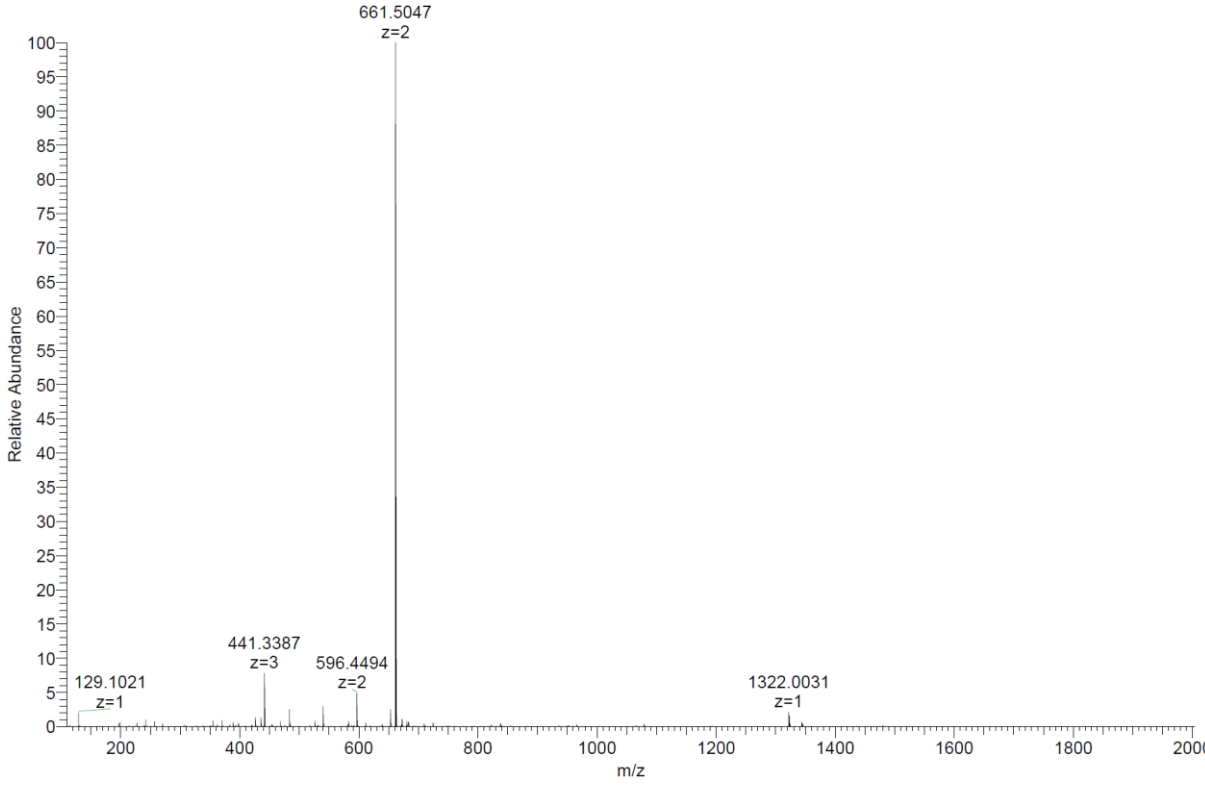

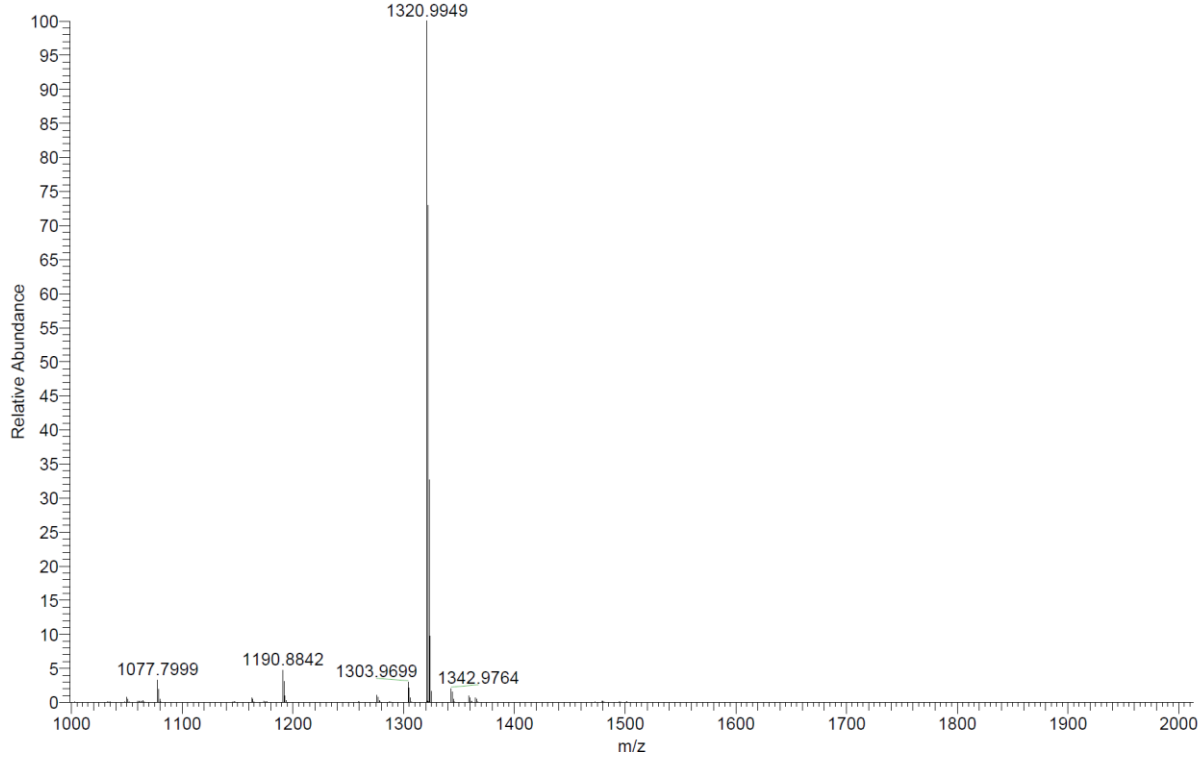

<u>KKLLKLLKLLL</u> (*sr*-ln65) was obtained as white solid after preparative RP-HPLC (64.6 mg, 41.3%). Analytical RP-HPLC: t_R = 1.58 min (A/D 100:0 to 0:100 in 3.5 min, λ = 214 nm). MS (ESI+): $C_{66}H_{128}N_{16}O_{11}$ calc./obs. 1320.99/1321.00 Da [M].

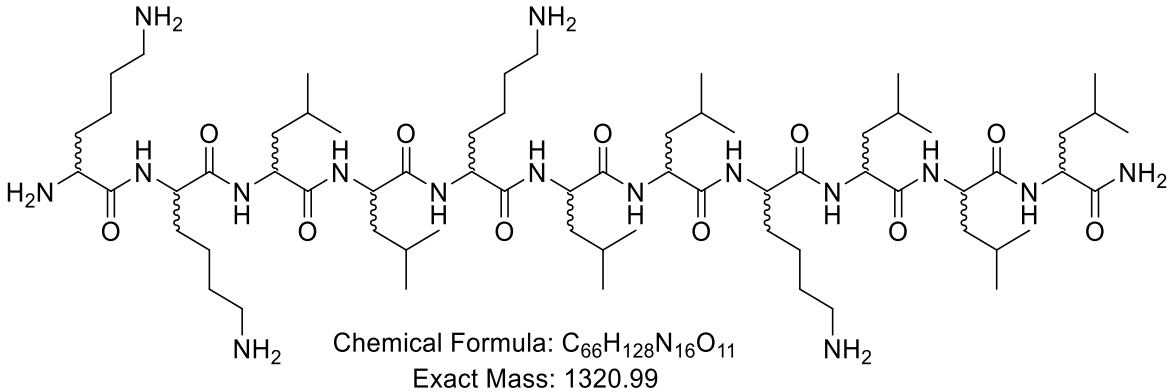

Analytical HPLC-MS data:

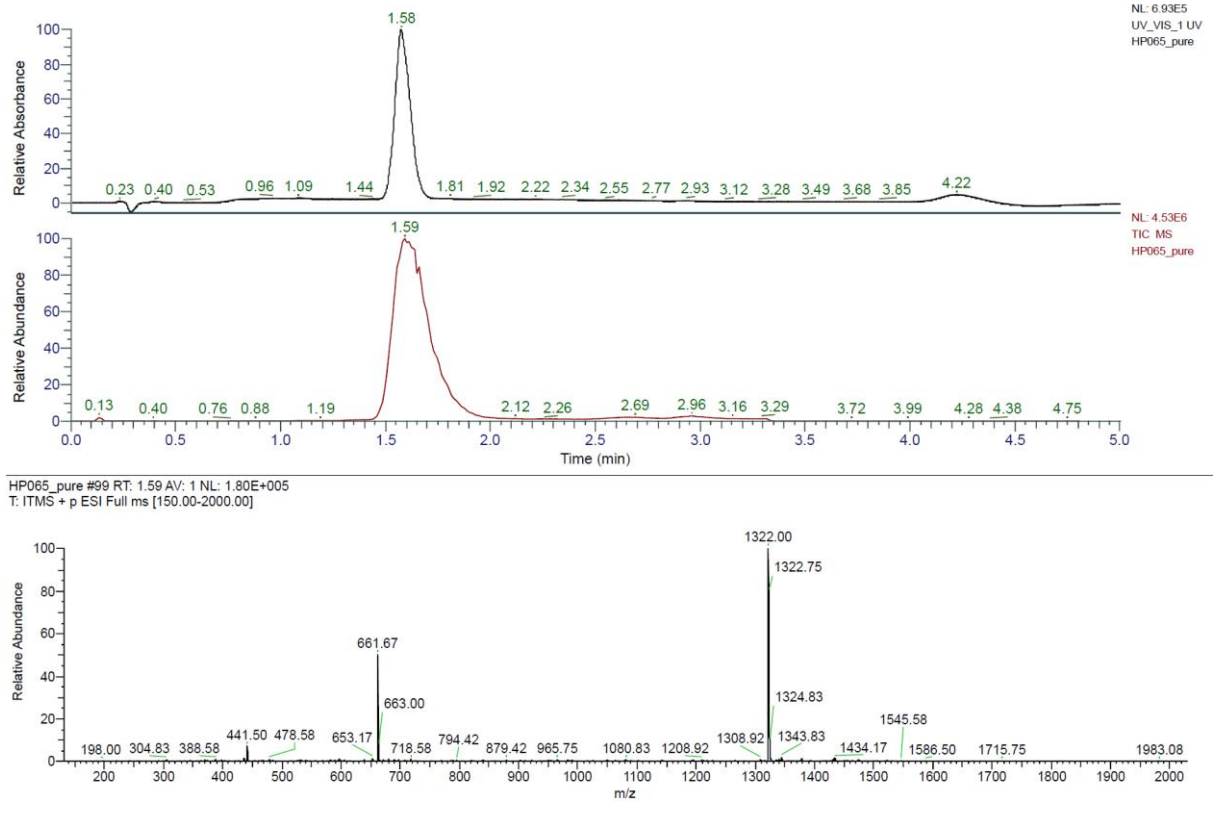

HRMS spectra:

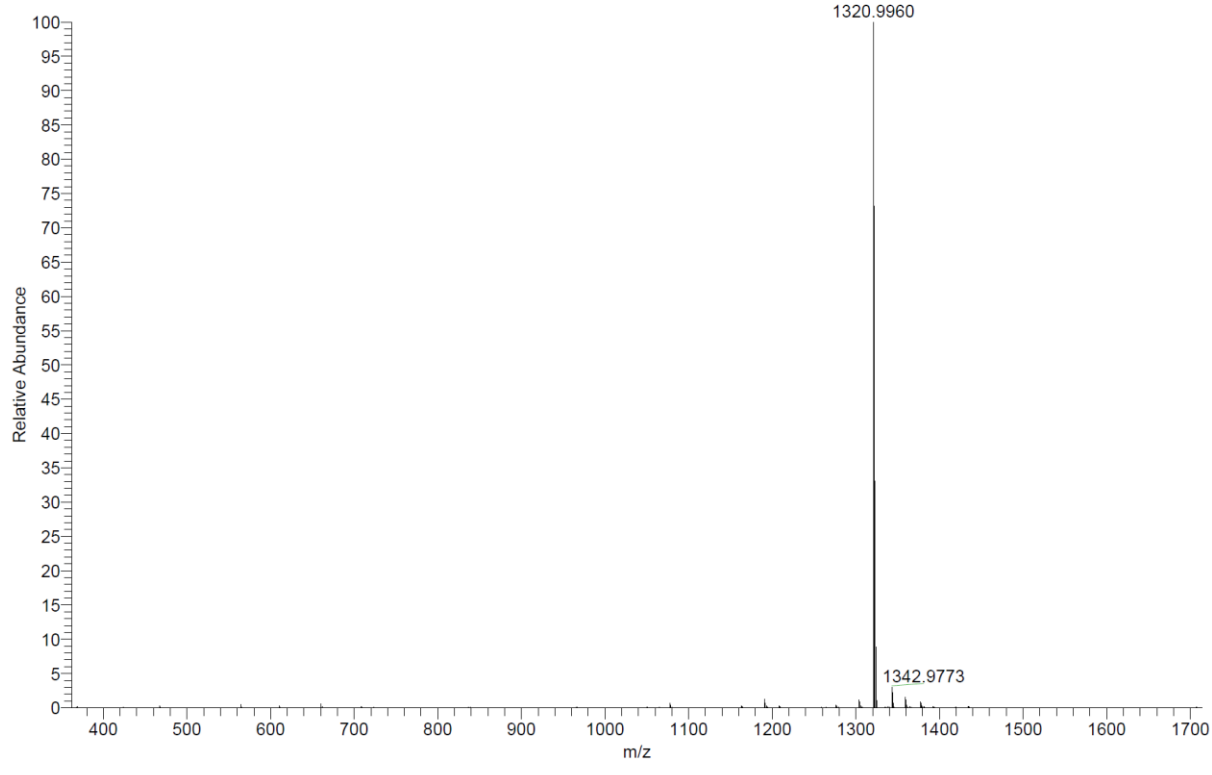

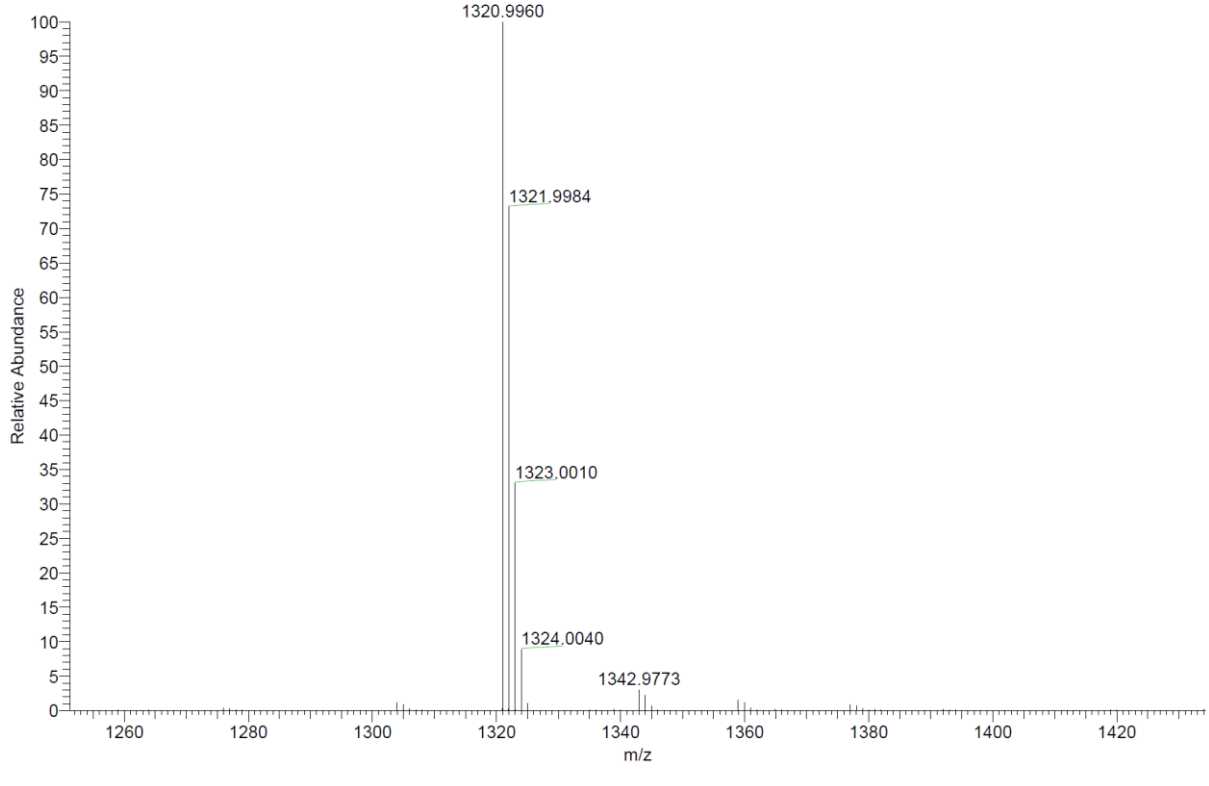

<u>KKLLKLLKLLL</u> (*sr*-ln65L^6) was obtained as white solid after preparative RP-HPLC (77.3 mg, 49.4%). Analytical RP-HPLC: t_R = 1.56 min (A/D 100:0 to 0:100 in 3.5 min, λ = 214 nm). MS (ESI+): $C_{66}H_{128}N_{16}O_{11}$ calc./obs. 1321.99/1322.00 Da $[M+H]^+$.

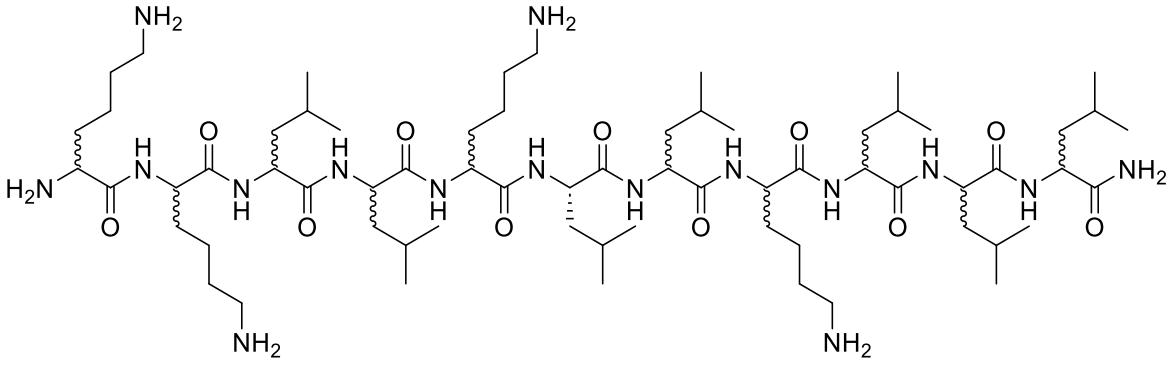

Chemical Formula: $C_{66}H_{128}N_{16}O_{11}$
Exact Mass: 1320.99
Molecular Weight: 1321.85

Analytical HPLC-MS data:

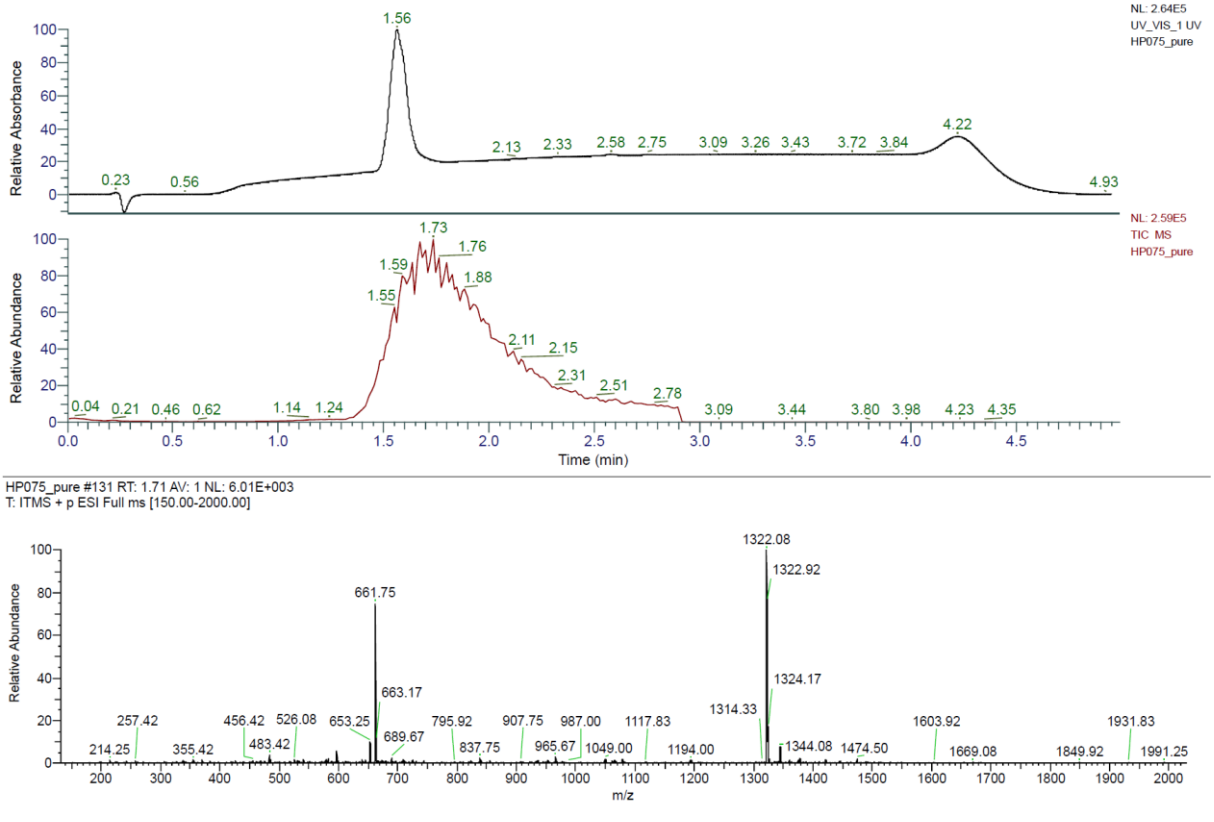

HRMS spectra:

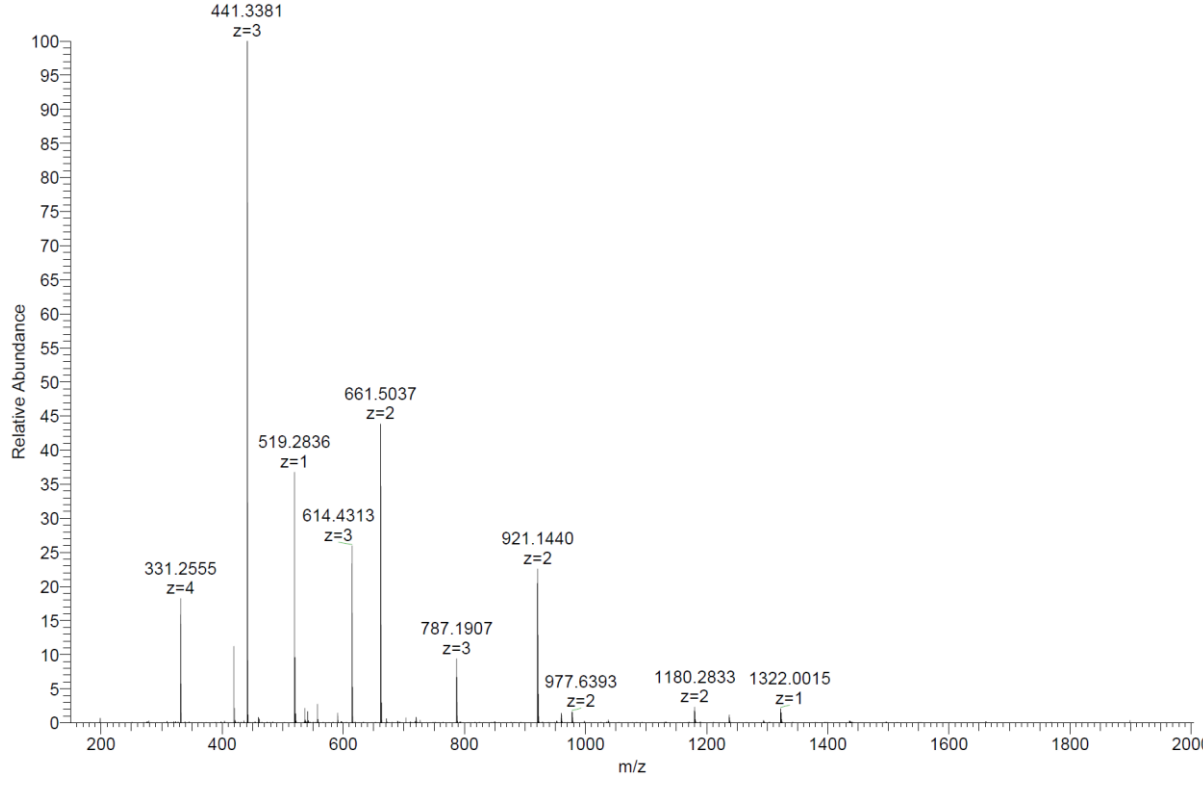

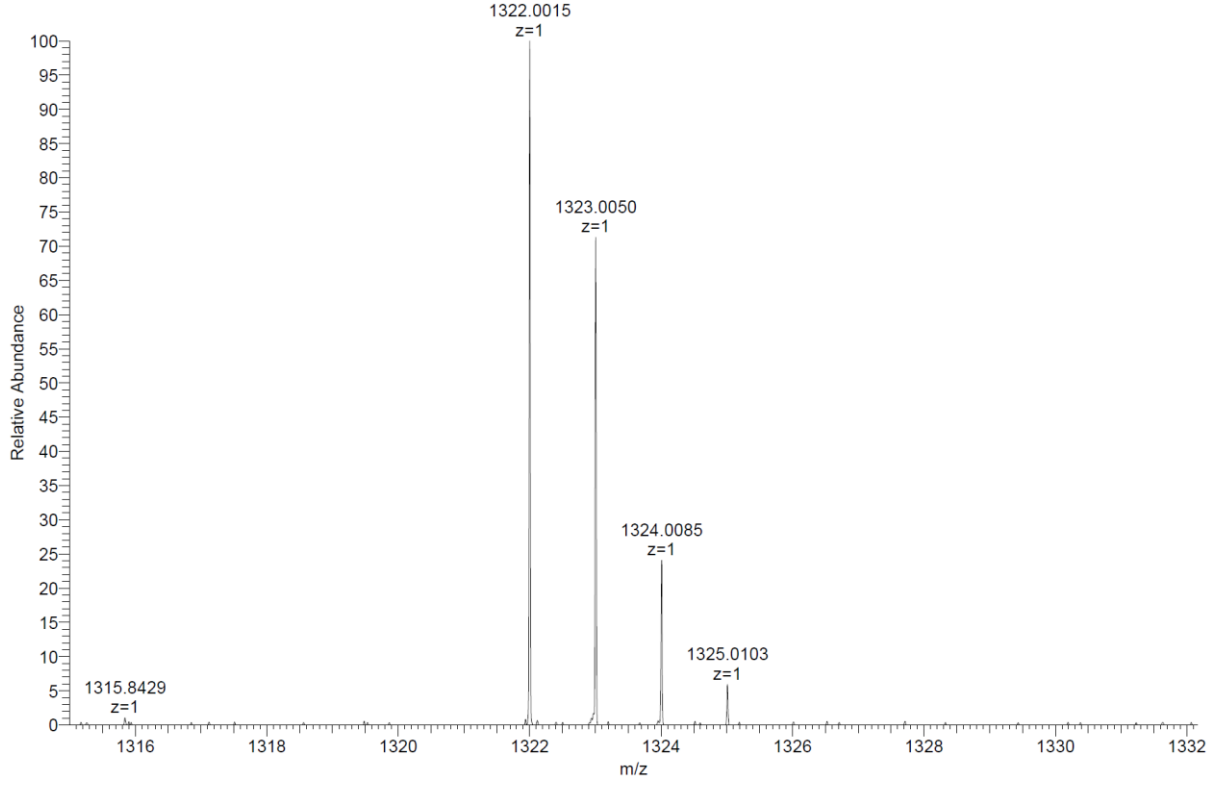

KkLLKLLKLLL (HP1) was obtained as white solid after preparative RP-HPLC (53.0 mg, 47.7%). Analytical RP-HPLC: t_R = 1.67 min (A/D 100:0 to 0:100 in 3.5 min, λ = 214 nm). MS (ESI+): $C_{66}H_{128}N_{16}O_{11}$ calc./obs. 1320.99/1321.00 Da [M].

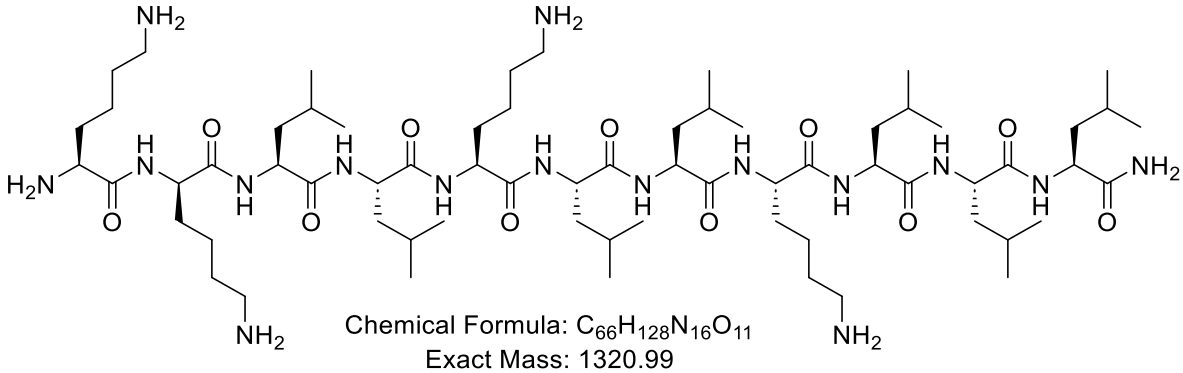

Analytical HPLC-MS data:

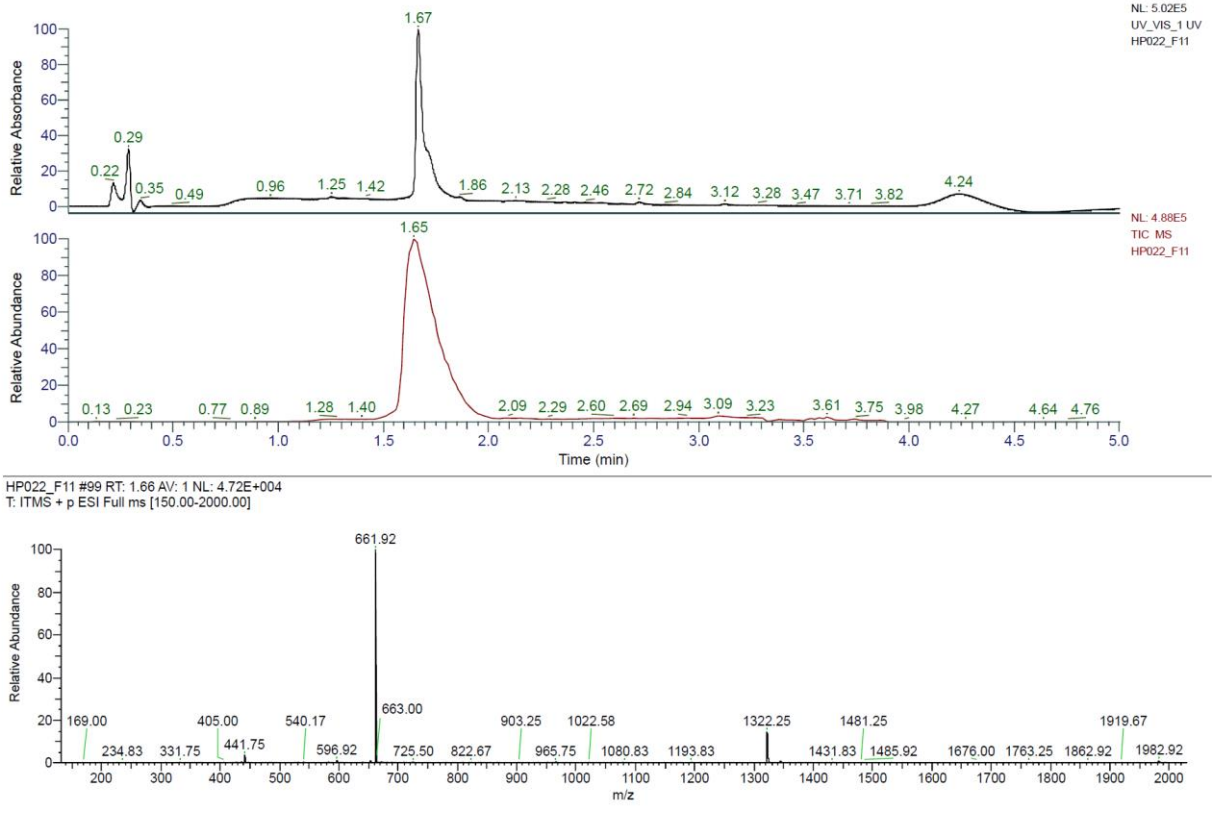

HRMS spectra:

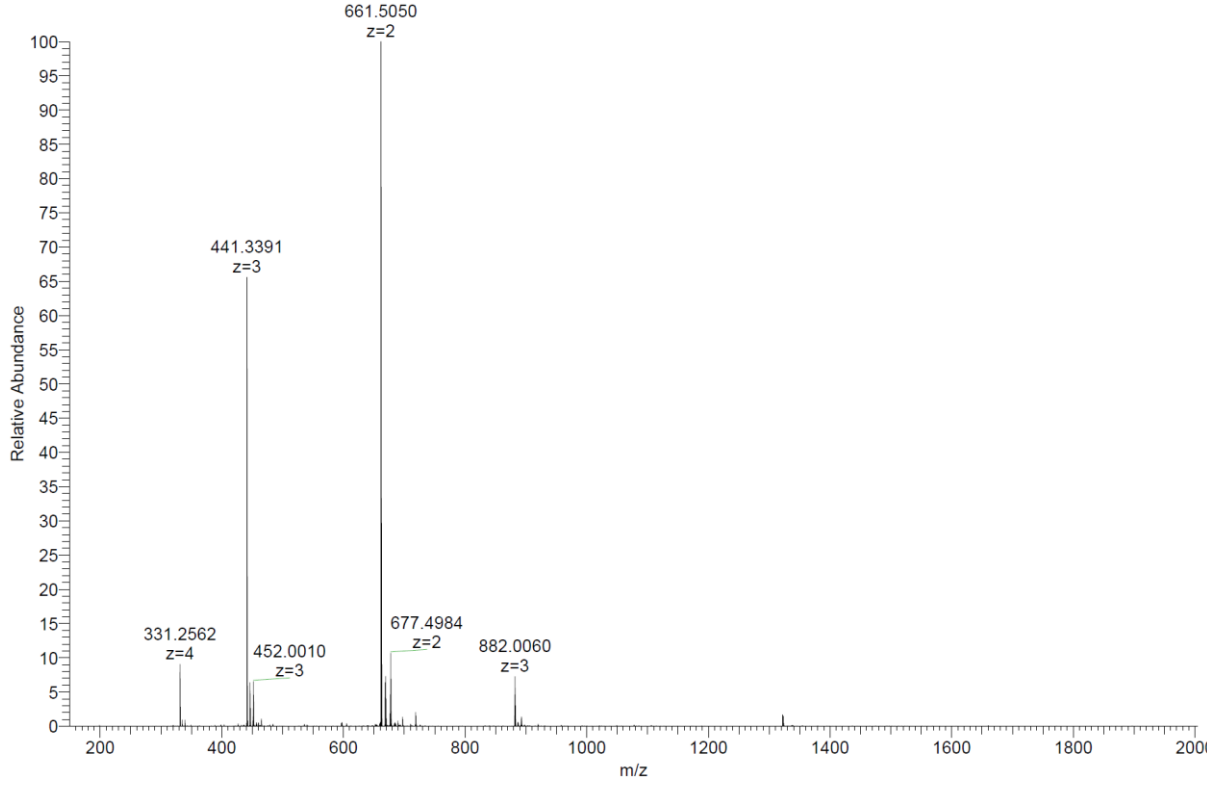

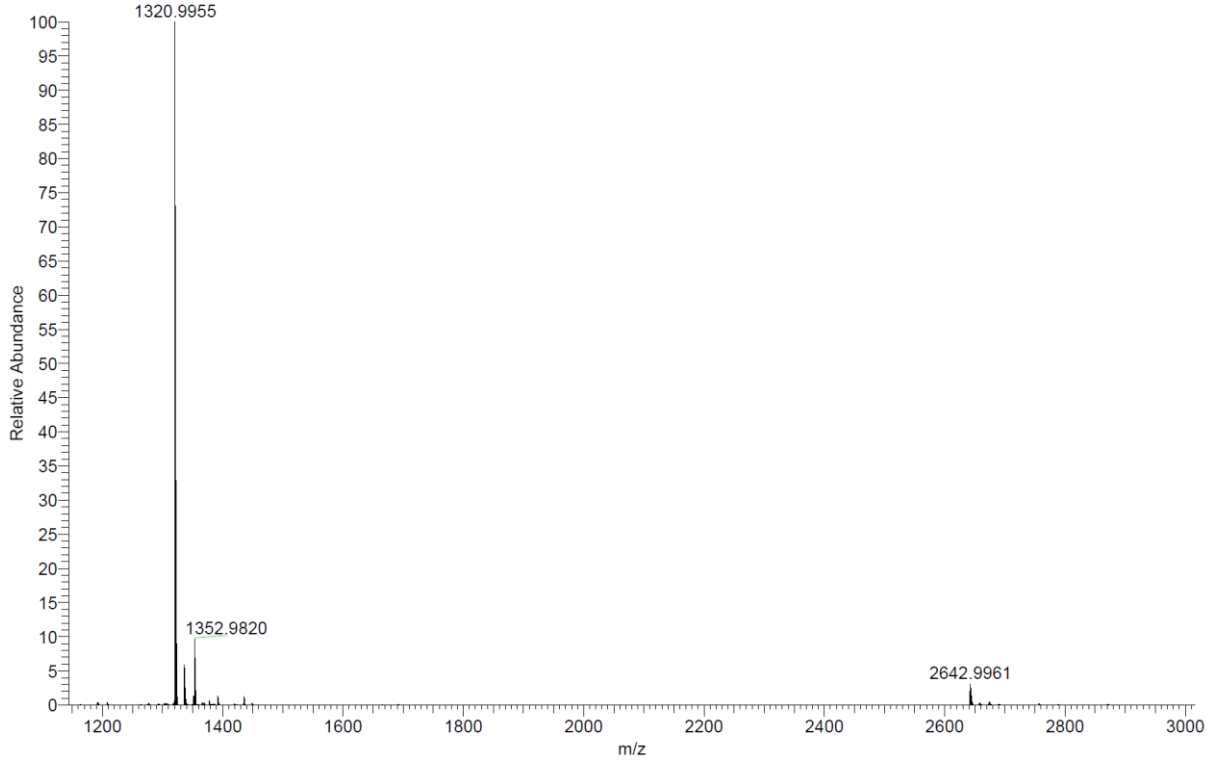

kkLLKLLKLLL (HP2) was obtained as white solid after preparative RP-HPLC (56.7 mg, 51.0%). Analytical RP-HPLC: t_R = 1.66 min (A/D 100:0 to 0:100 in 3.5 min, λ = 214 nm). MS (ESI+): $C_{66}H_{128}N_{16}O_{11}$ calc./obs. 1320.99/1320.99 Da [M].

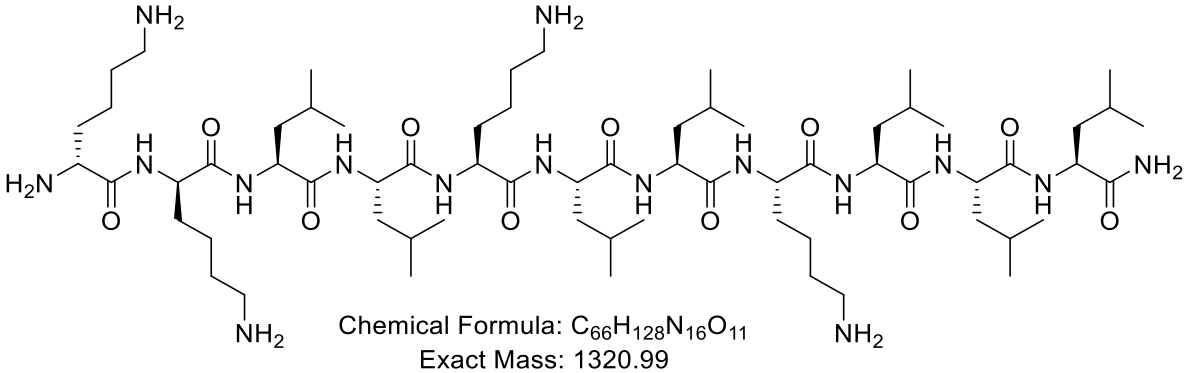

Analytical HPLC-MS data:

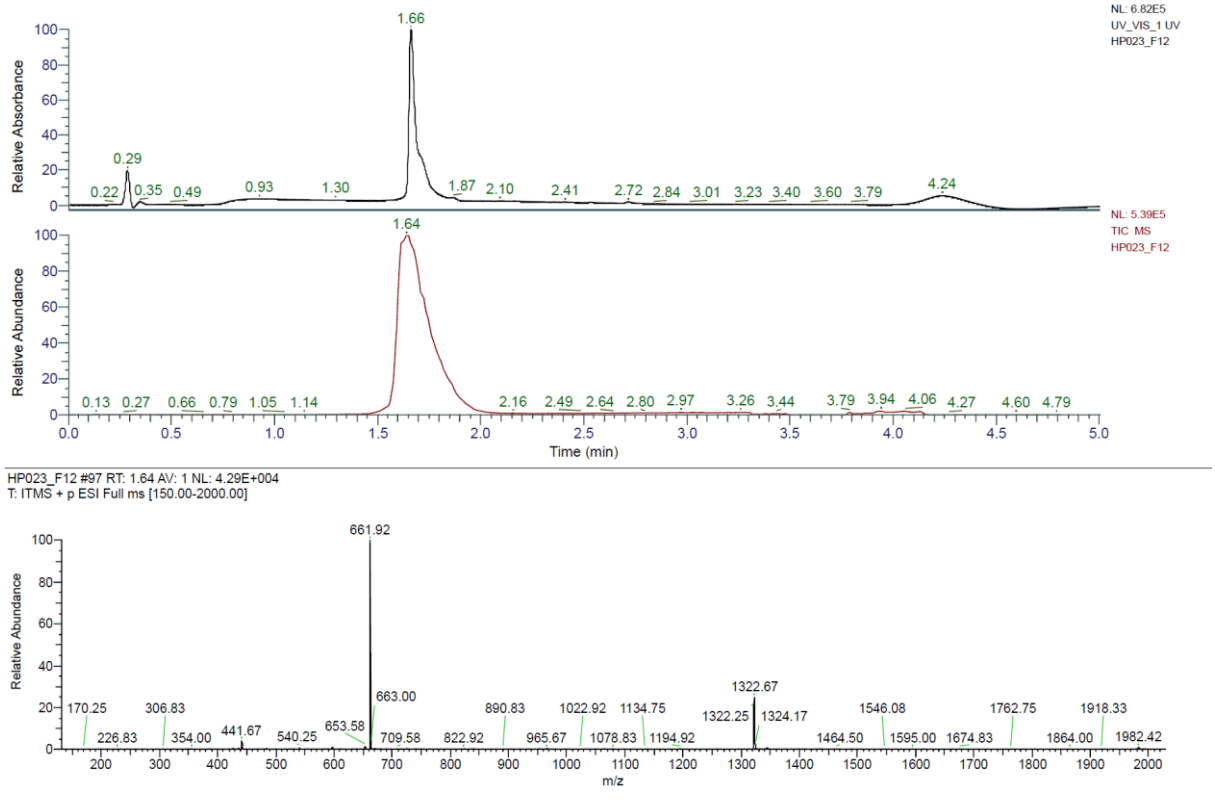

HRMS spectra:

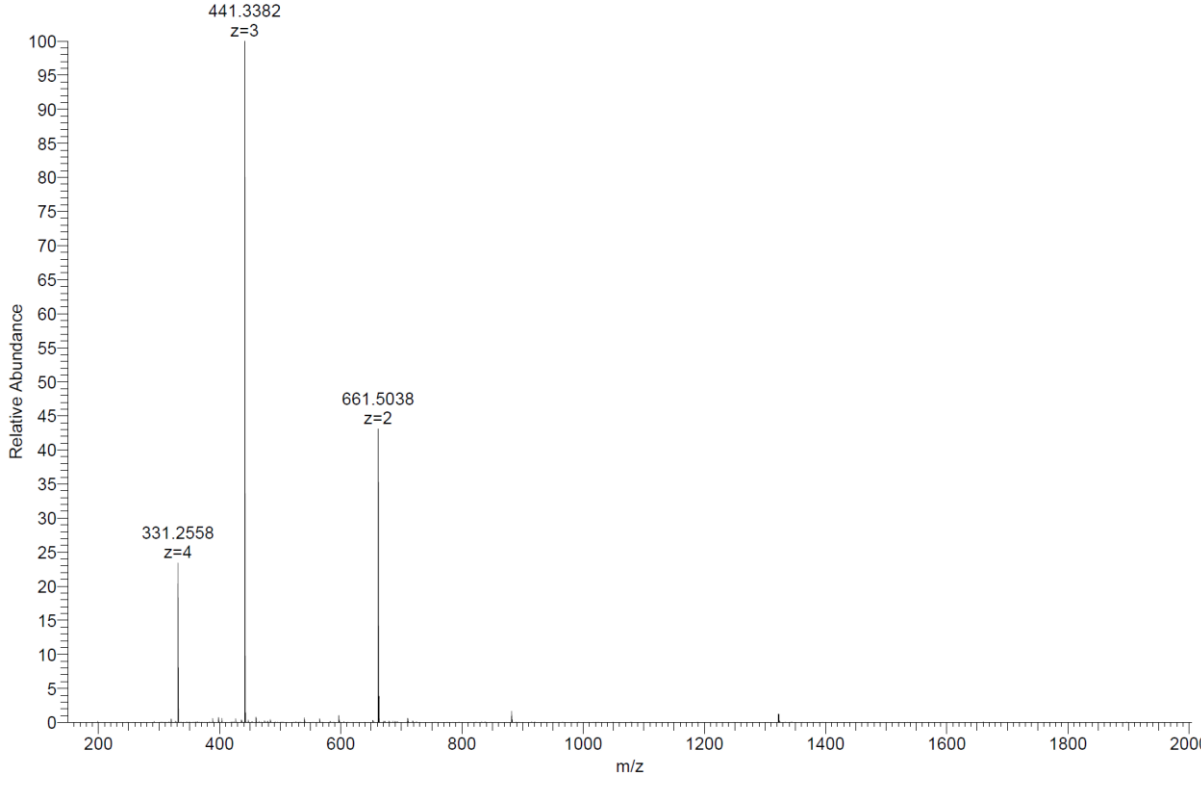

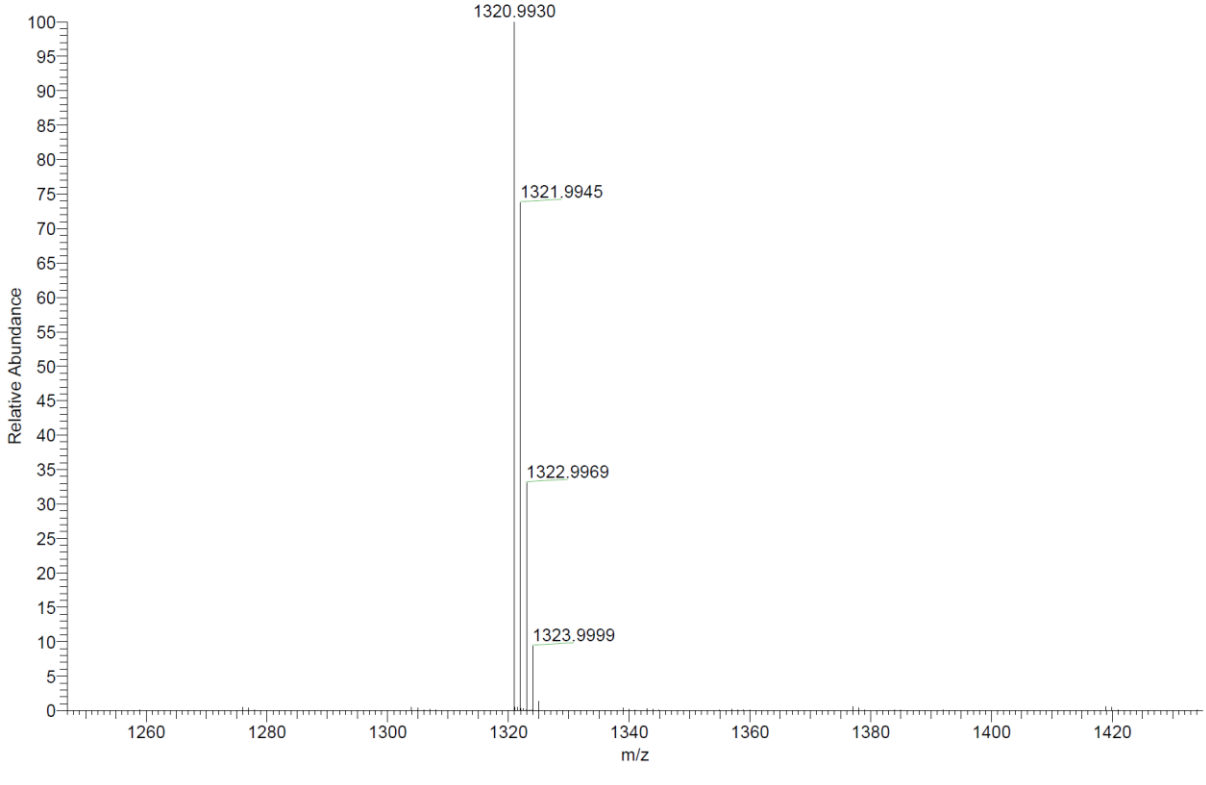

KkLLkLLKLLL (HP3) was obtained as white solid after preparative RP-HPLC (50.1 mg, 45.1%). Analytical RP-HPLC: t_R = 1.61 min (A/D 100:0 to 0:100 in 3.5 min, λ = 214 nm). MS (ESI+): $C_{66}H_{128}N_{16}O_{11}$ calc./obs. 1321.99/1322.00 Da $[M+H]^+$.

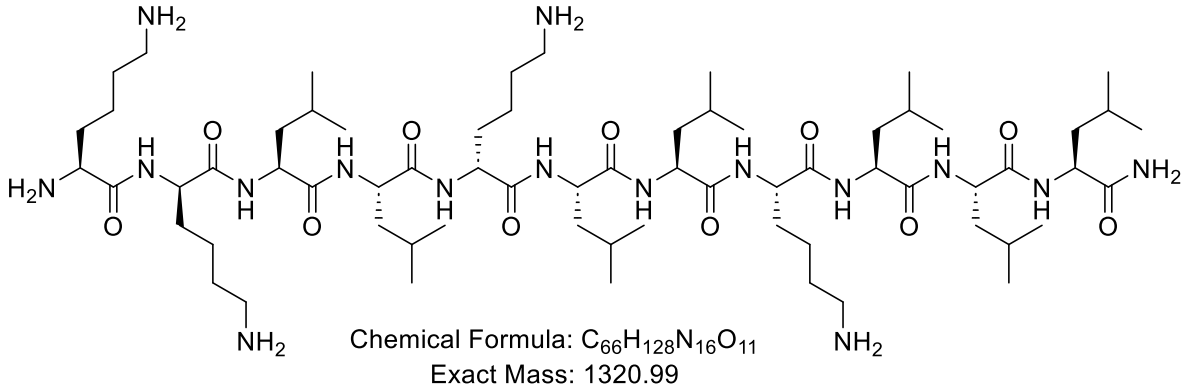

Analytical HPLC-MS data:

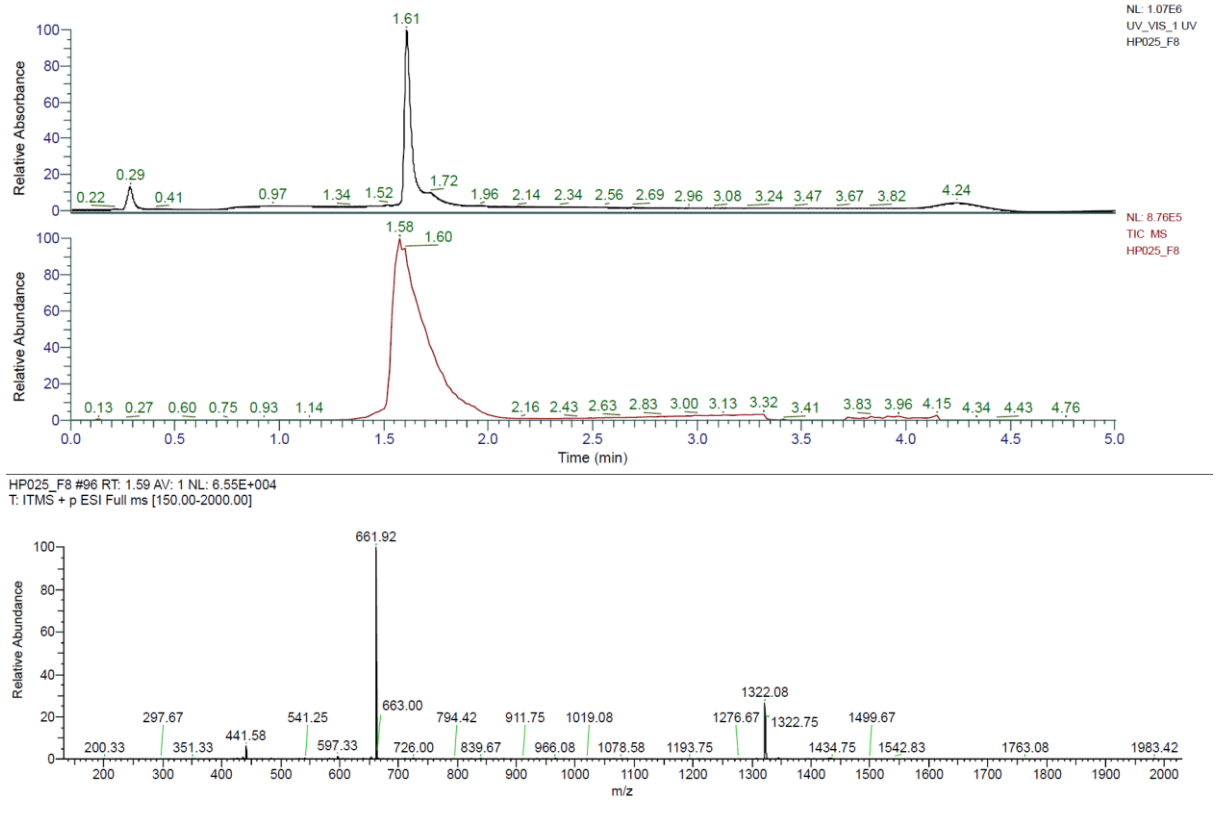

HRMS spectra:

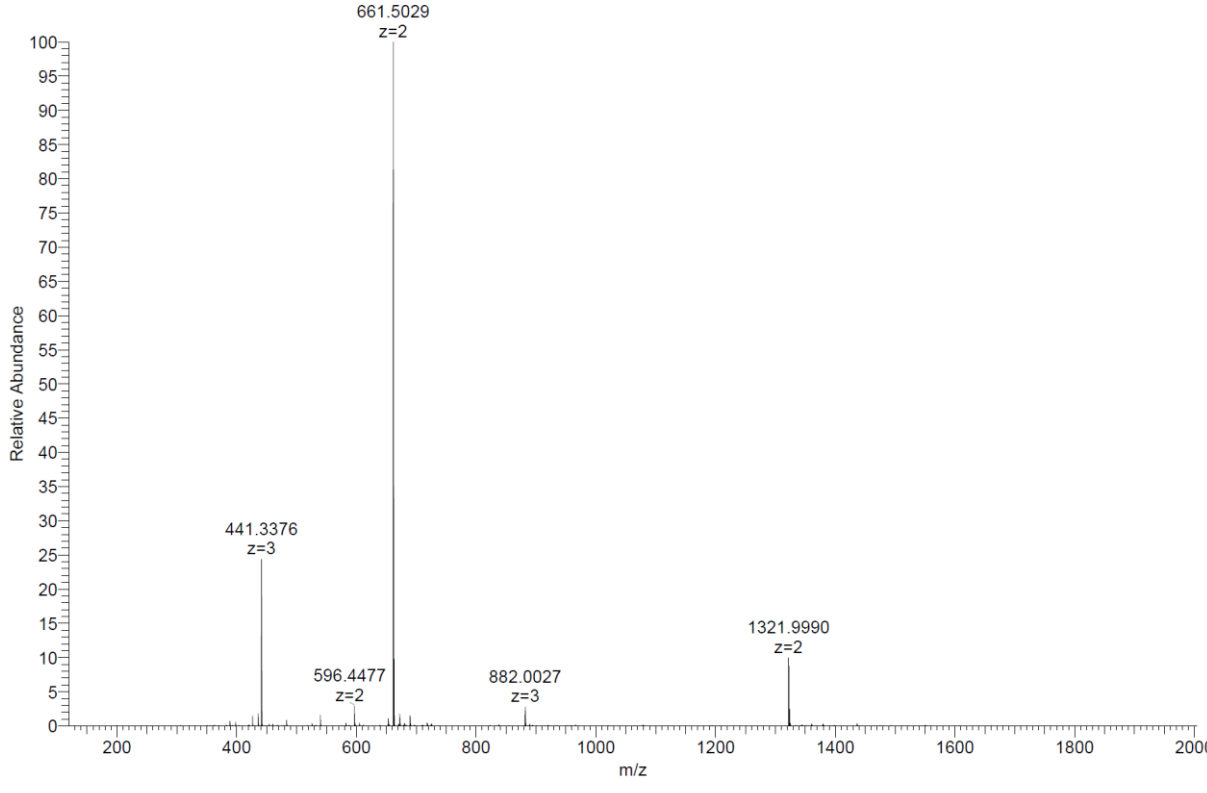

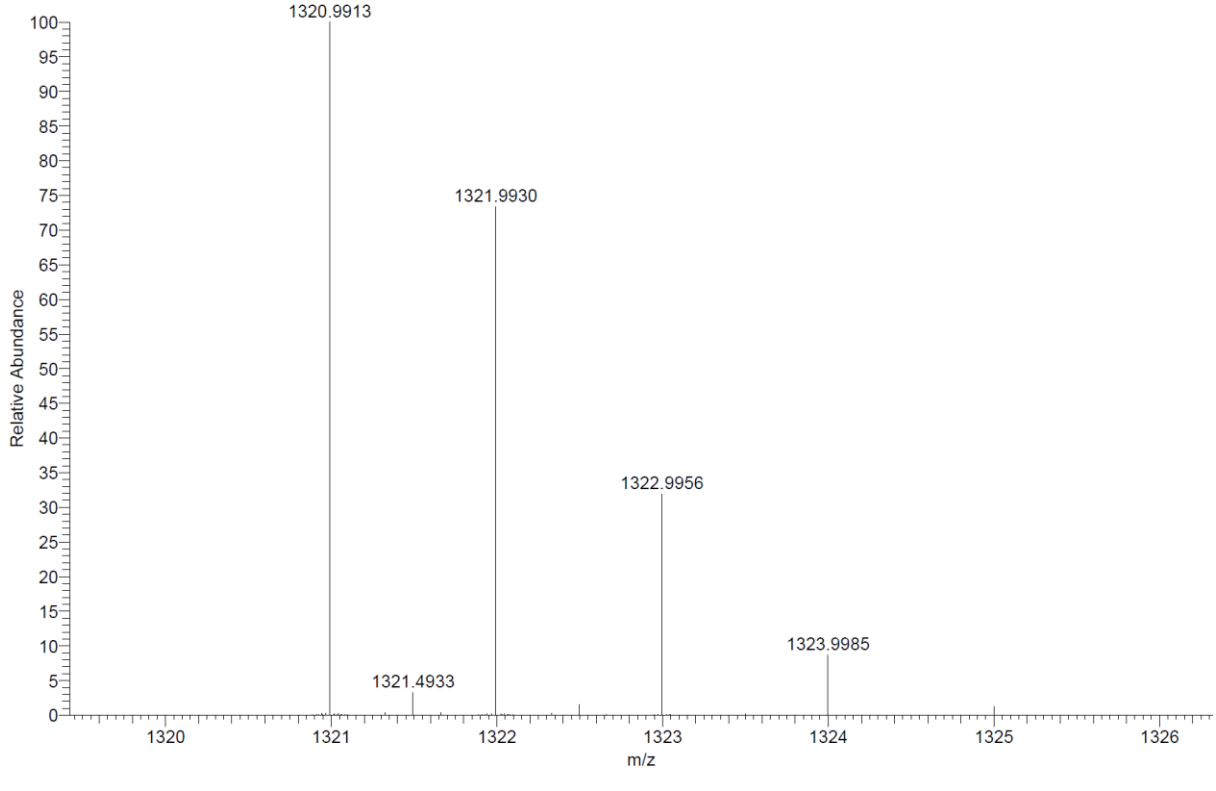

KkLlKLLKLLL (HP4) was obtained as white solid after preparative RP-HPLC (42.6 mg, 38.3%). Analytical RP-HPLC: t_R = 1.74 min (A/D 100:0 to 0:100 in 3.5 min, λ = 214 nm). MS (ESI+): $C_{66}H_{128}N_{16}O_{11}$ calc./obs. 1321.99/1322.00 Da $[M+H]^+$.

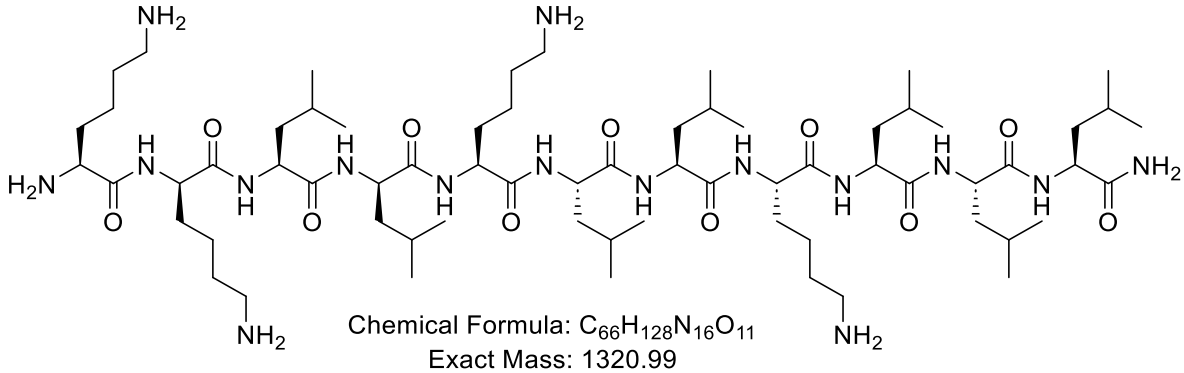

Analytical HPLC-MS data:

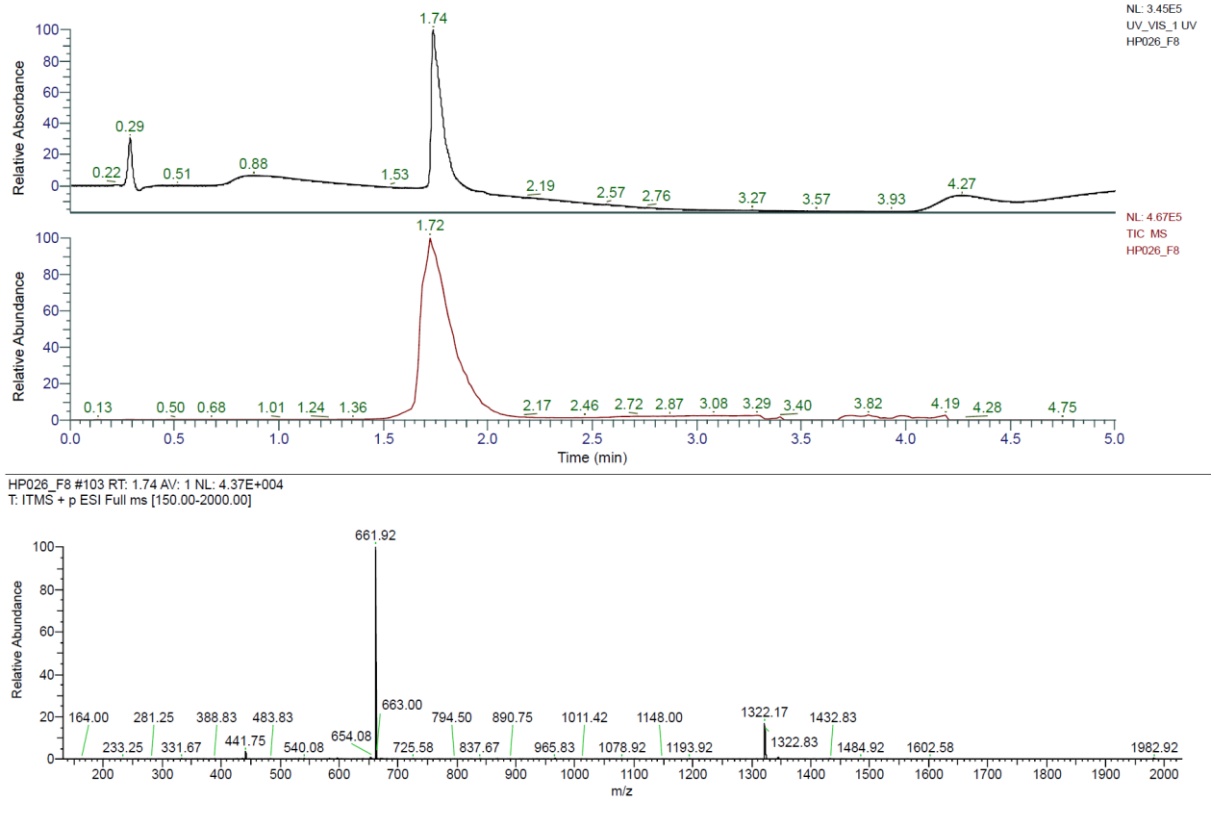

HRMS spectra:

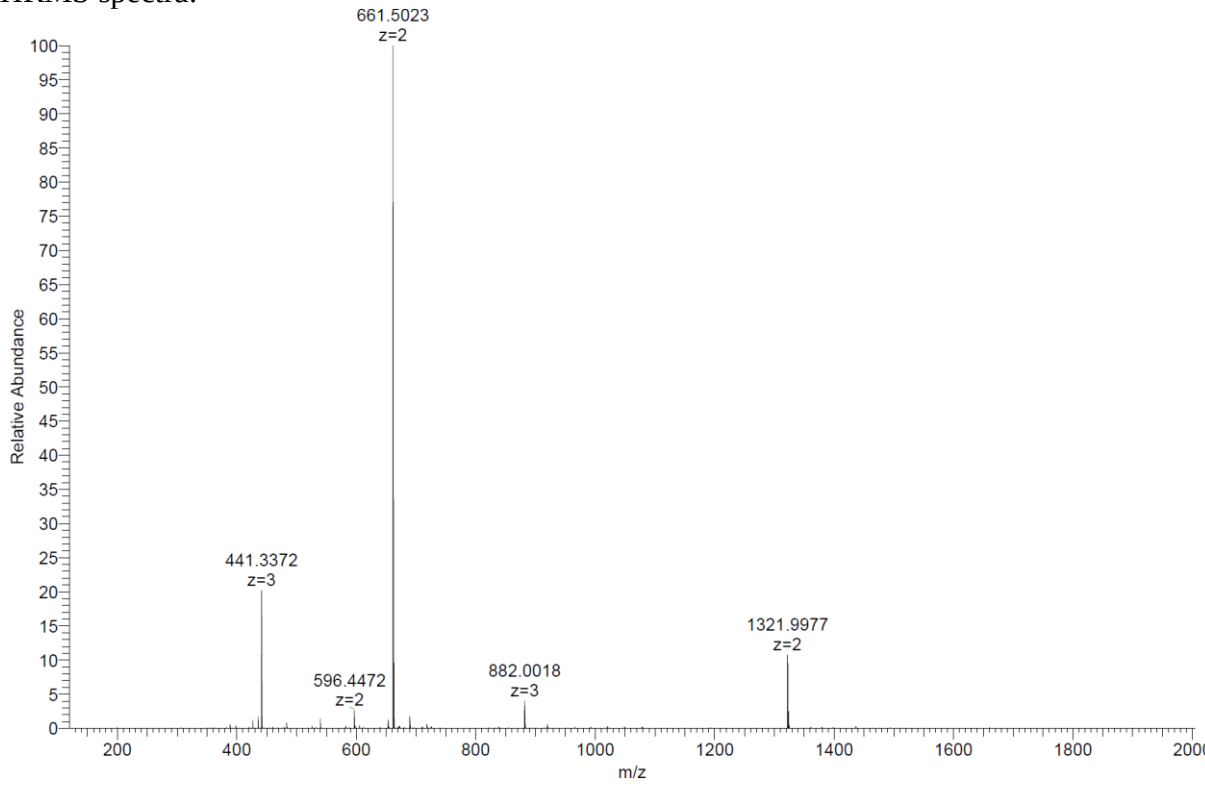

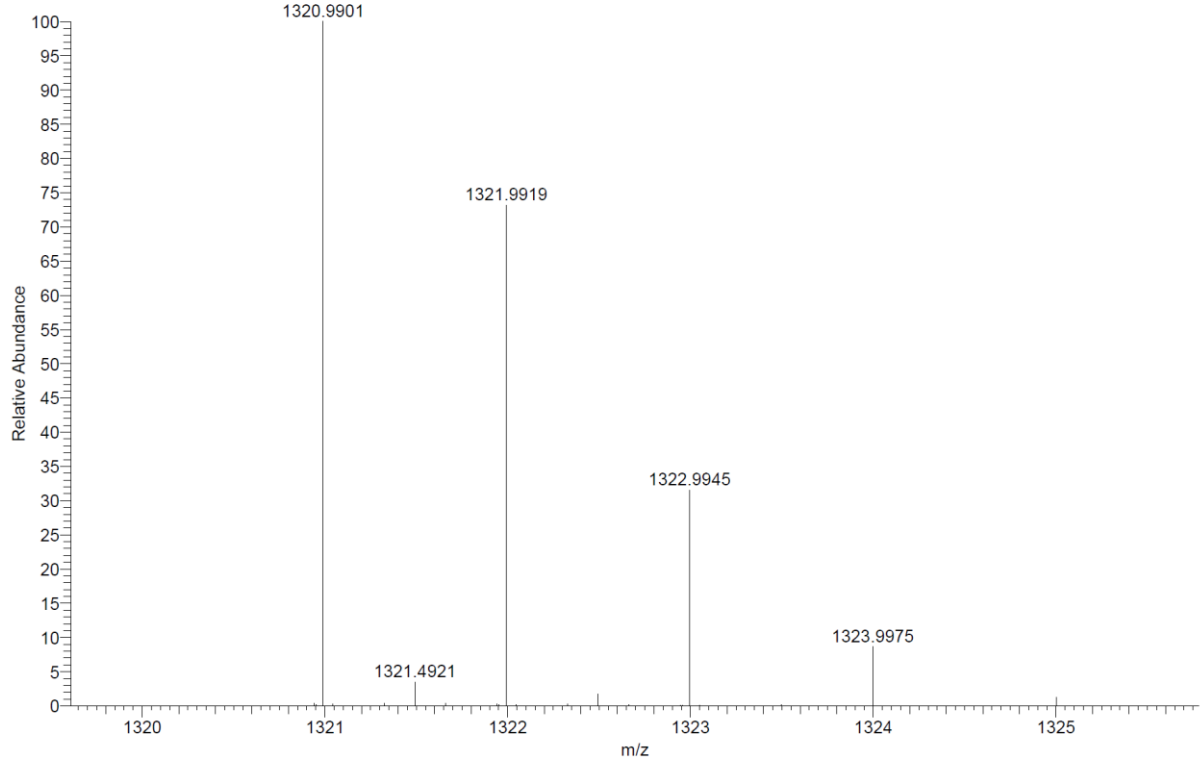

kKLLKLLKLLl (HP5) was obtained as white solid after preparative RP-HPLC (49.1 mg, 44.2%). Analytical RP-HPLC: t_R = 1.65 min (A/D 100:0 to 0:100 in 3.5 min, λ = 214 nm). MS (ESI+): $C_{66}H_{128}N_{16}O_{11}$ calc./obs. 1321.99/1322.00 Da $[M+H]^+$.

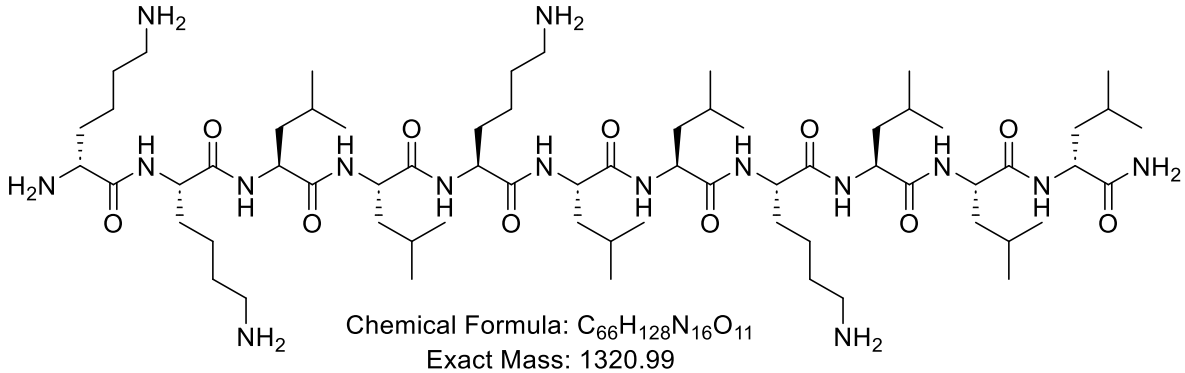

Analytical HPLC-MS data:

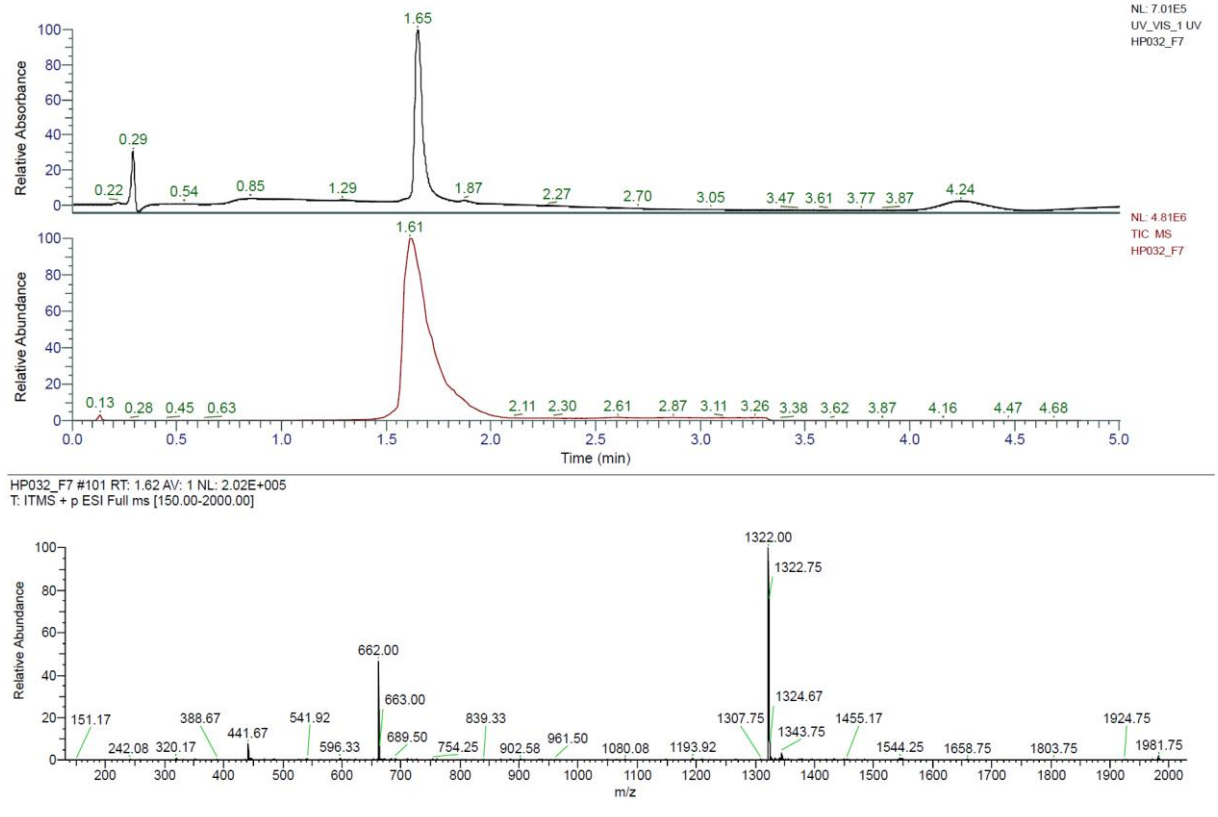

HRMS spectra:

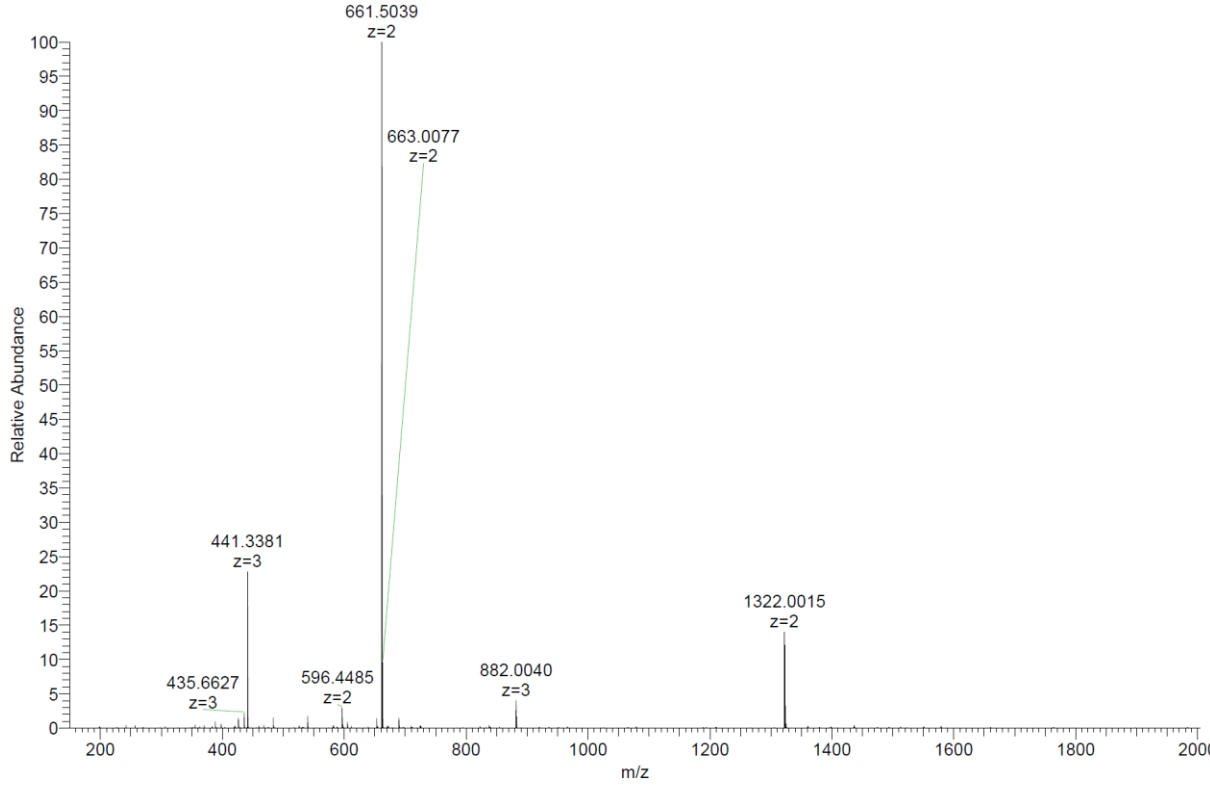

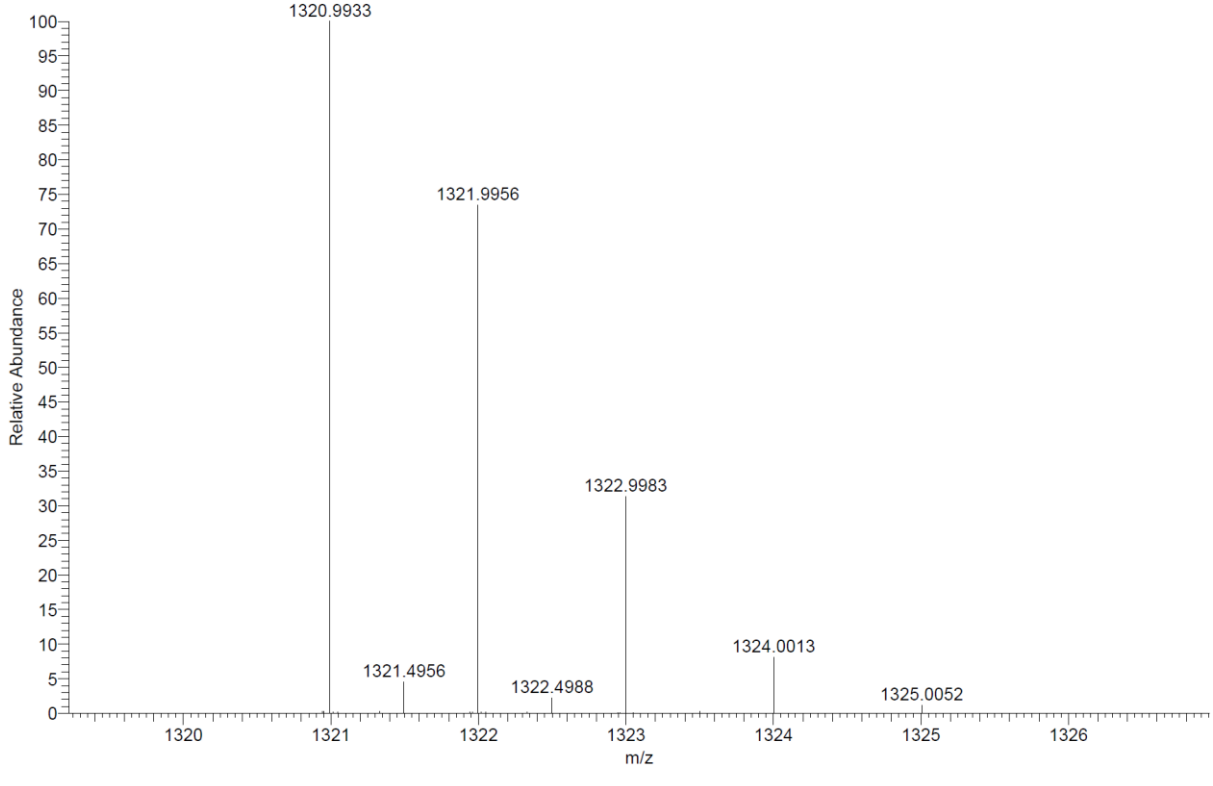

KKLLKllKLLL (HP6) was obtained as white solid after preparative RP-HPLC (49.3 mg, 44.4%). Analytical RP-HPLC: t_R = 1.53 min (A/D 100:0 to 0:100 in 3.5 min, λ = 214 nm). MS (ESI+): $C_{66}H_{128}N_{16}O_{11}$ calc./obs. 1321.99/1322.00 Da $[M+H]^+$.

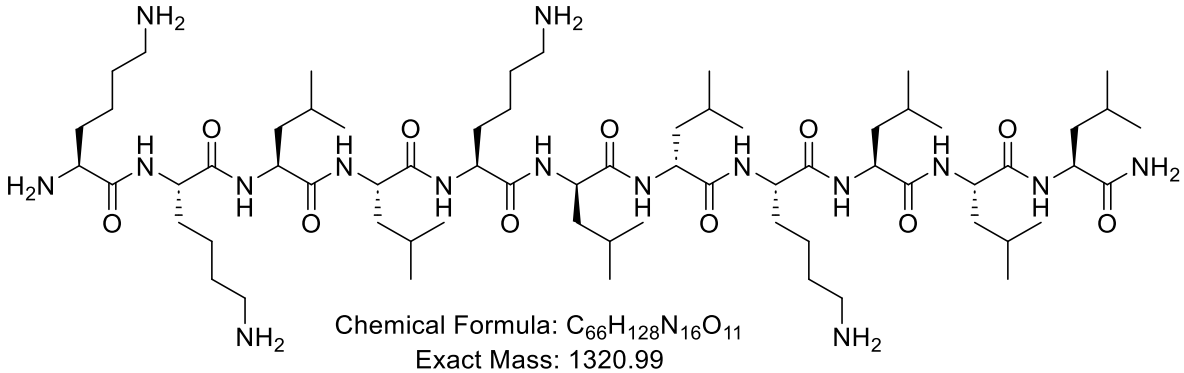

Analytical HPLC-MS data:

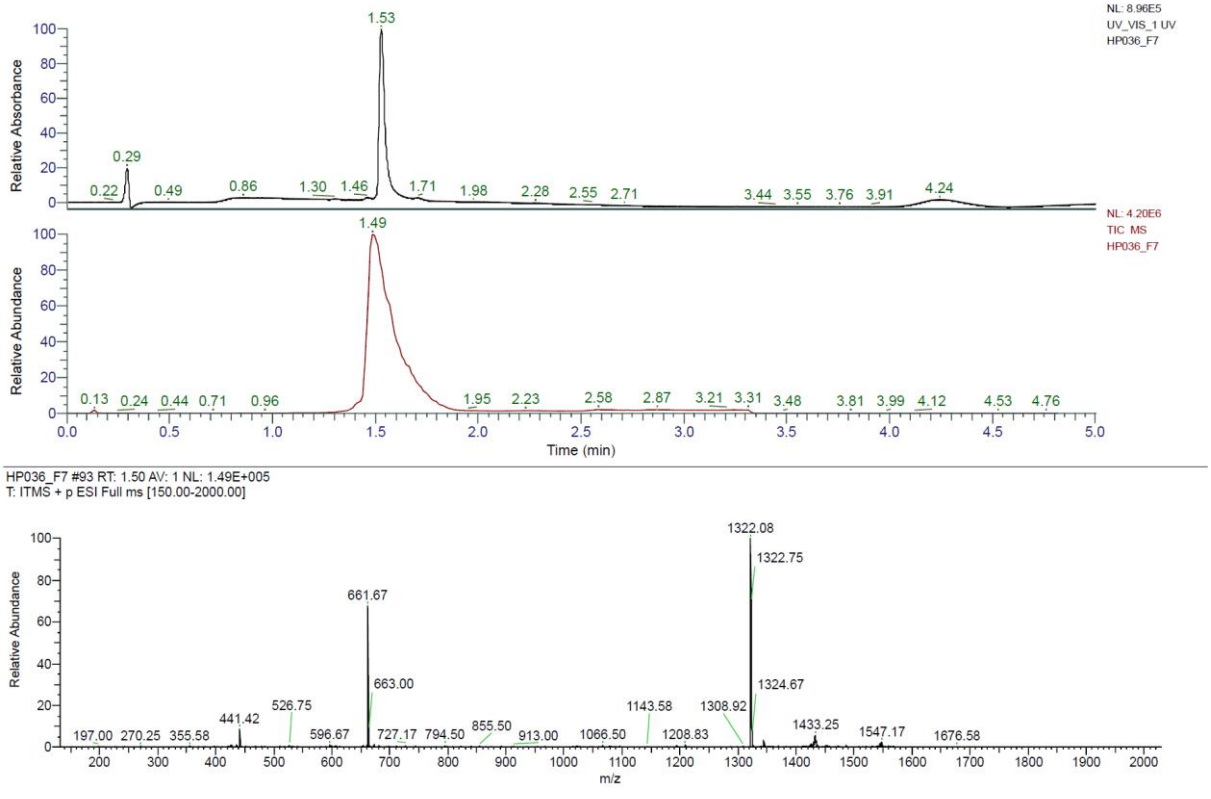

HRMS spectra:

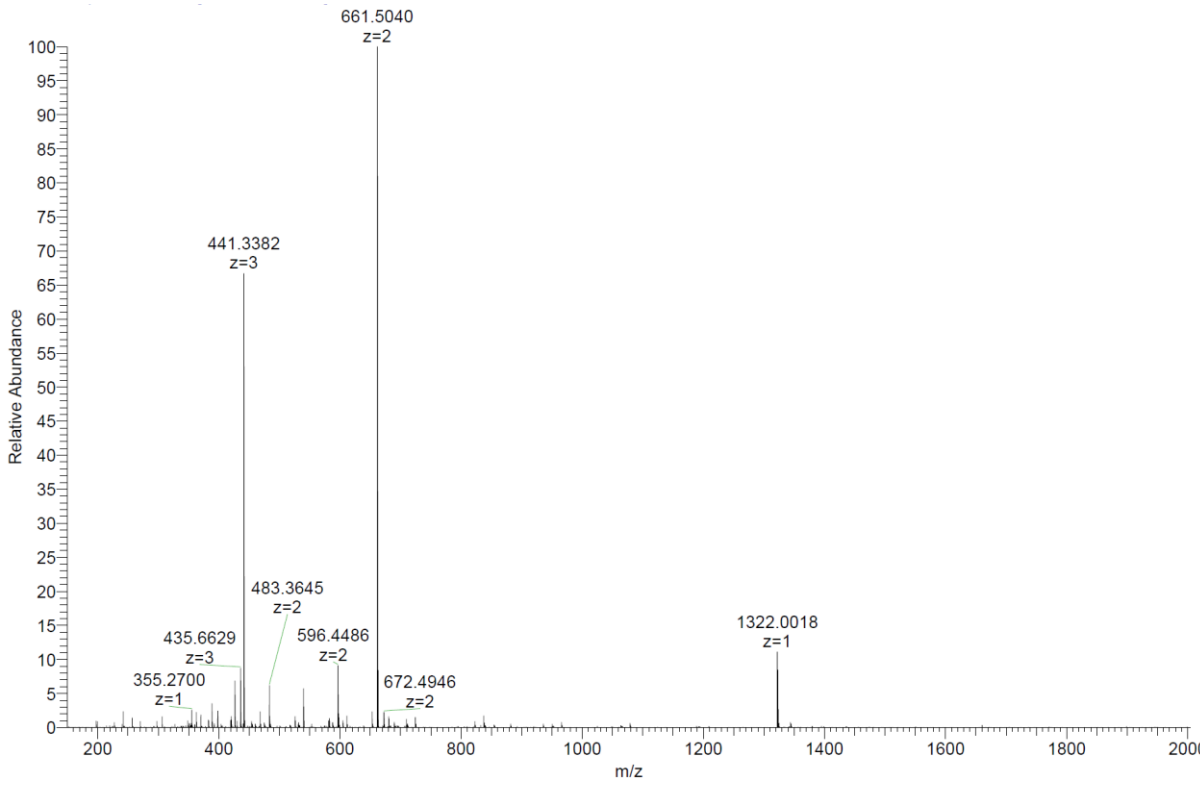

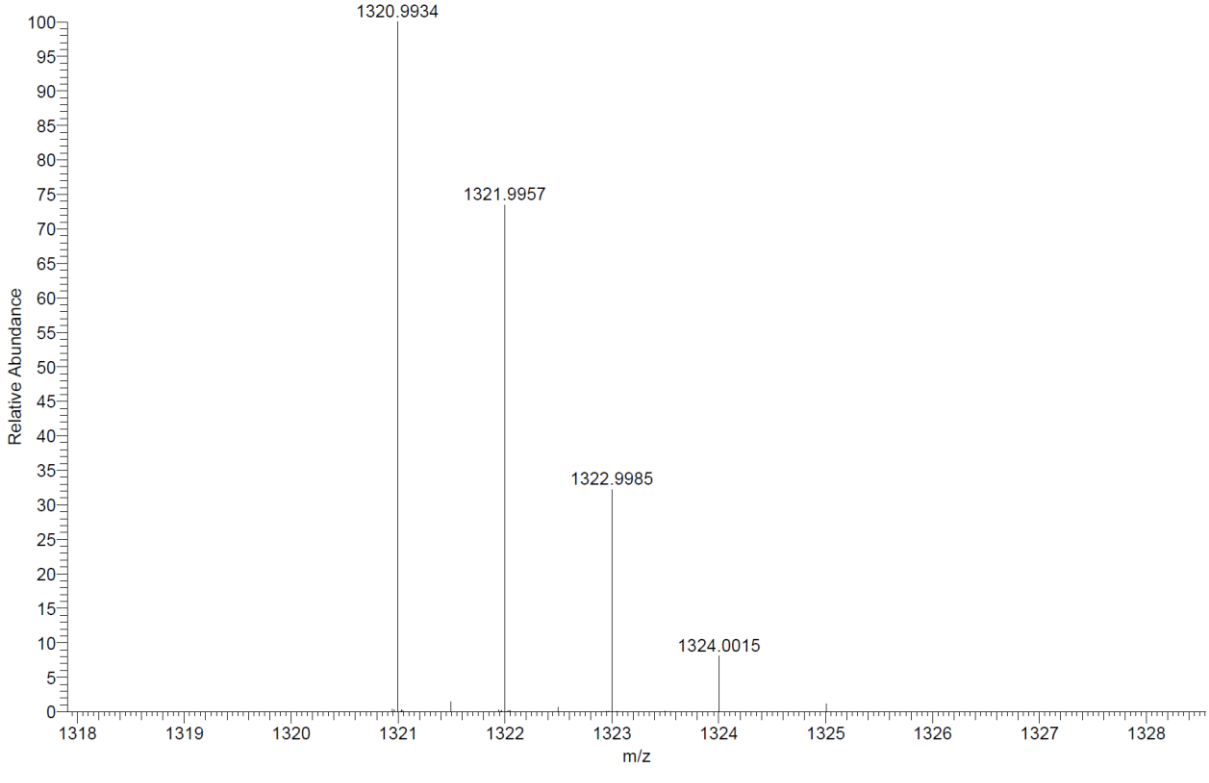

kkLLKLLKLLl (HP7) was obtained as white solid after preparative RP-HPLC (60.6 mg, 54.5%). Analytical RP-HPLC: t_R = 1.62 min (A/D 100:0 to 0:100 in 3.5 min, λ = 214 nm). MS (ESI+): $C_{66}H_{128}N_{16}O_{11}$ calc./obs. 1321.99/1322.00 Da $[M+H]^+$.

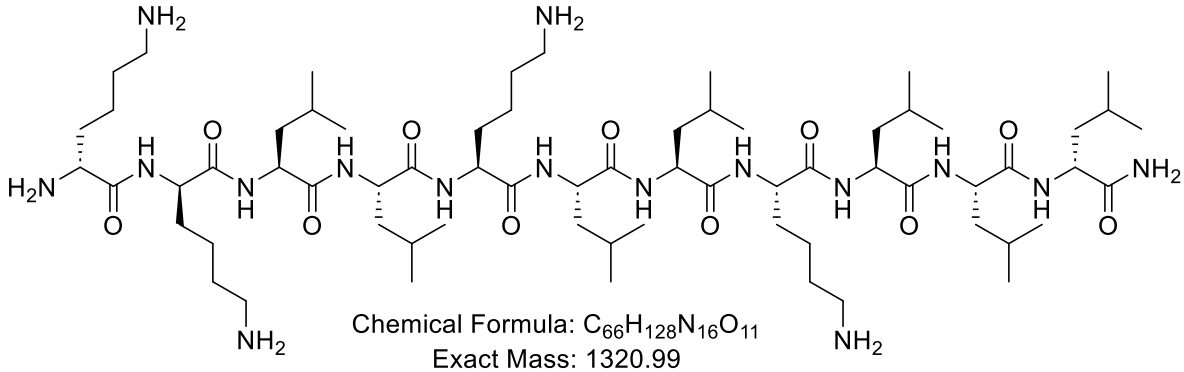

Analytical HPLC-MS data:

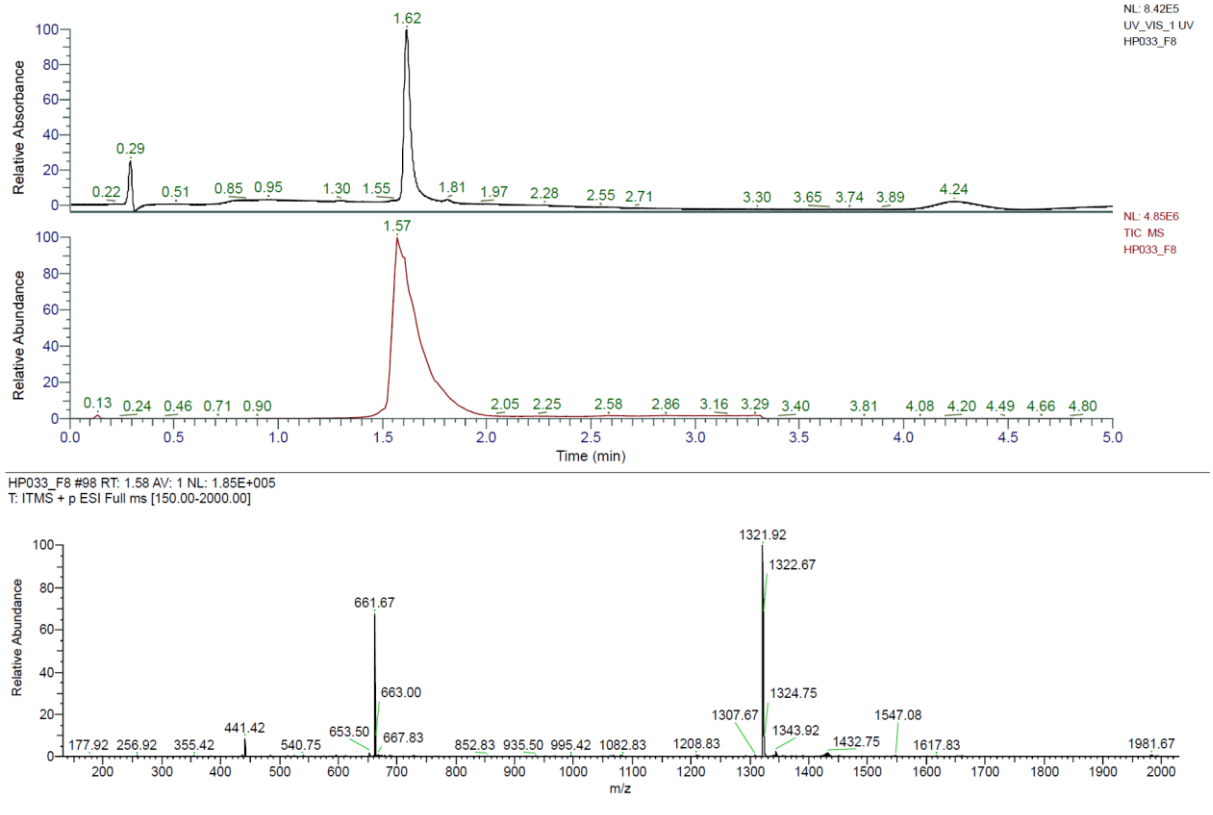

HRMS spectra:

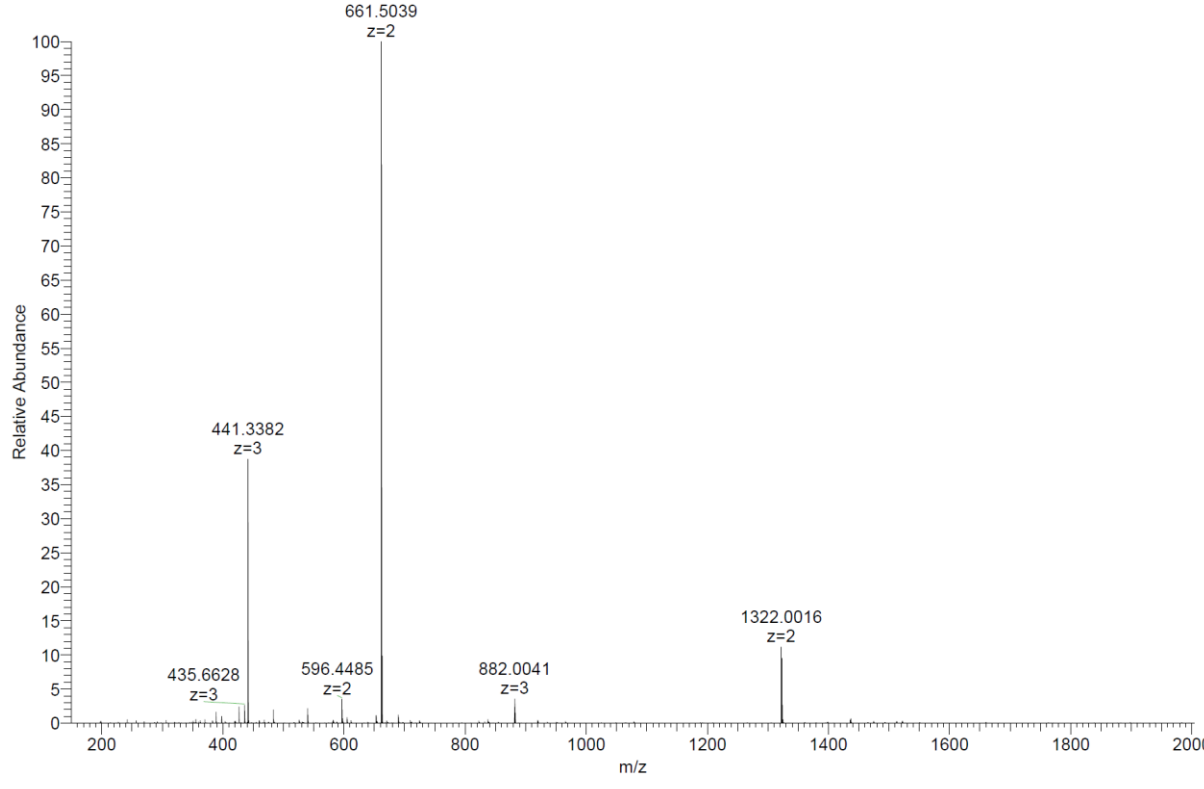

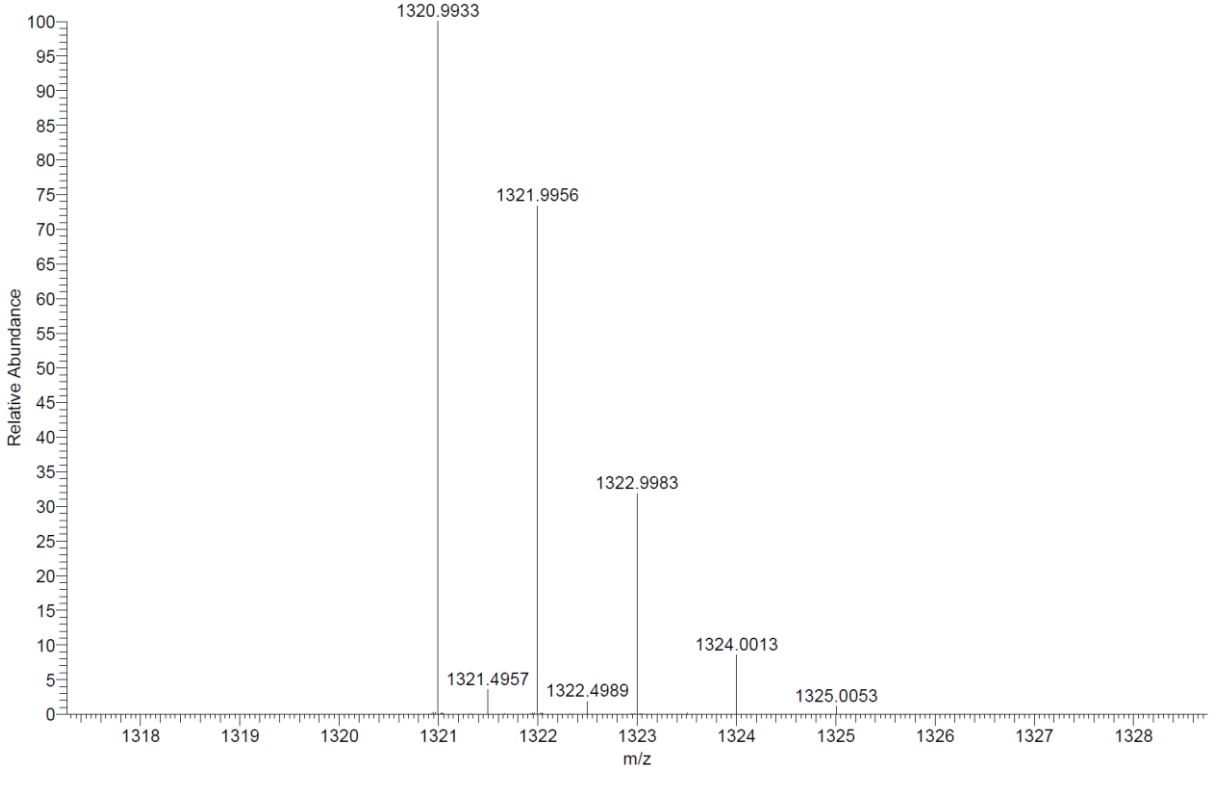

KkllKLLKLLL (HP8) was obtained as white solid after preparative RP-HPLC (46.9 mg, 42.2%). Analytical RP-HPLC: t_R = 1.63 min (A/D 100:0 to 0:100 in 3.5 min, λ = 214 nm). MS (ESI+): $C_{66}H_{128}N_{16}O_{11}$ calc./obs. 1321.99/1322.00 Da $[M+H]^+$.

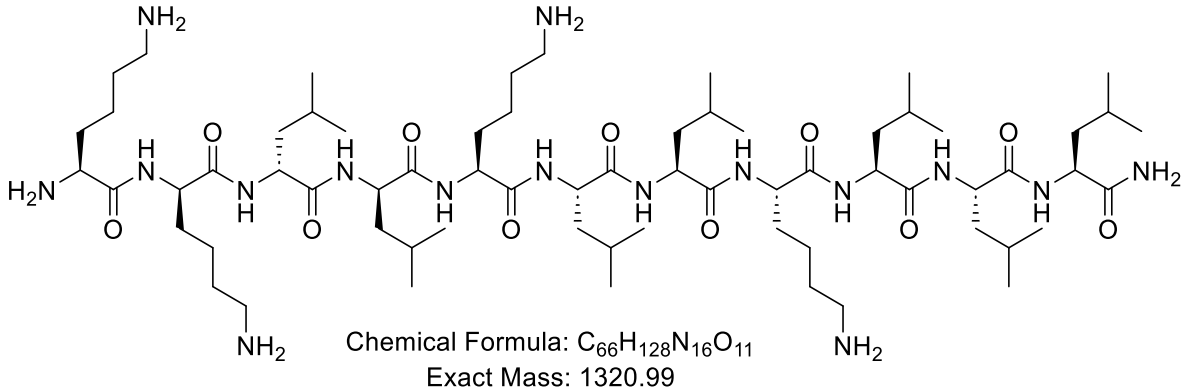

Analytical HPLC-MS data:

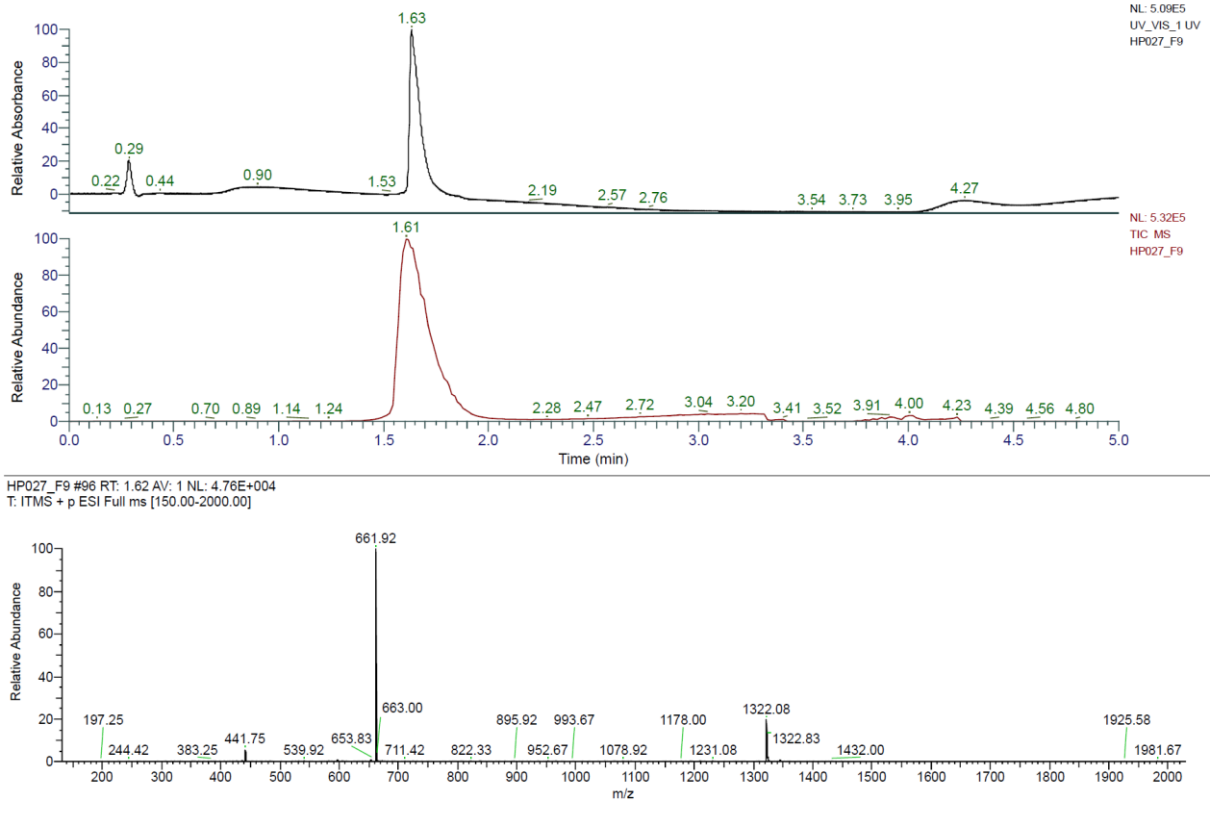

HRMS spectra:

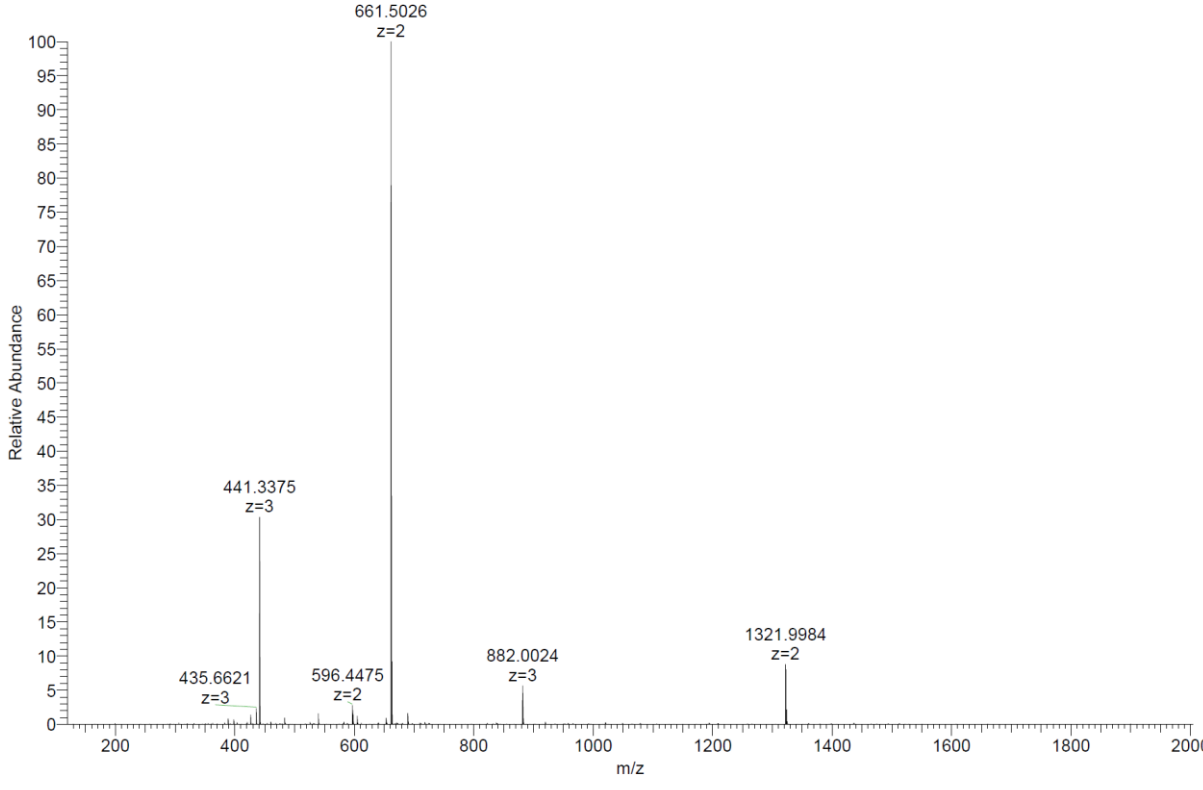

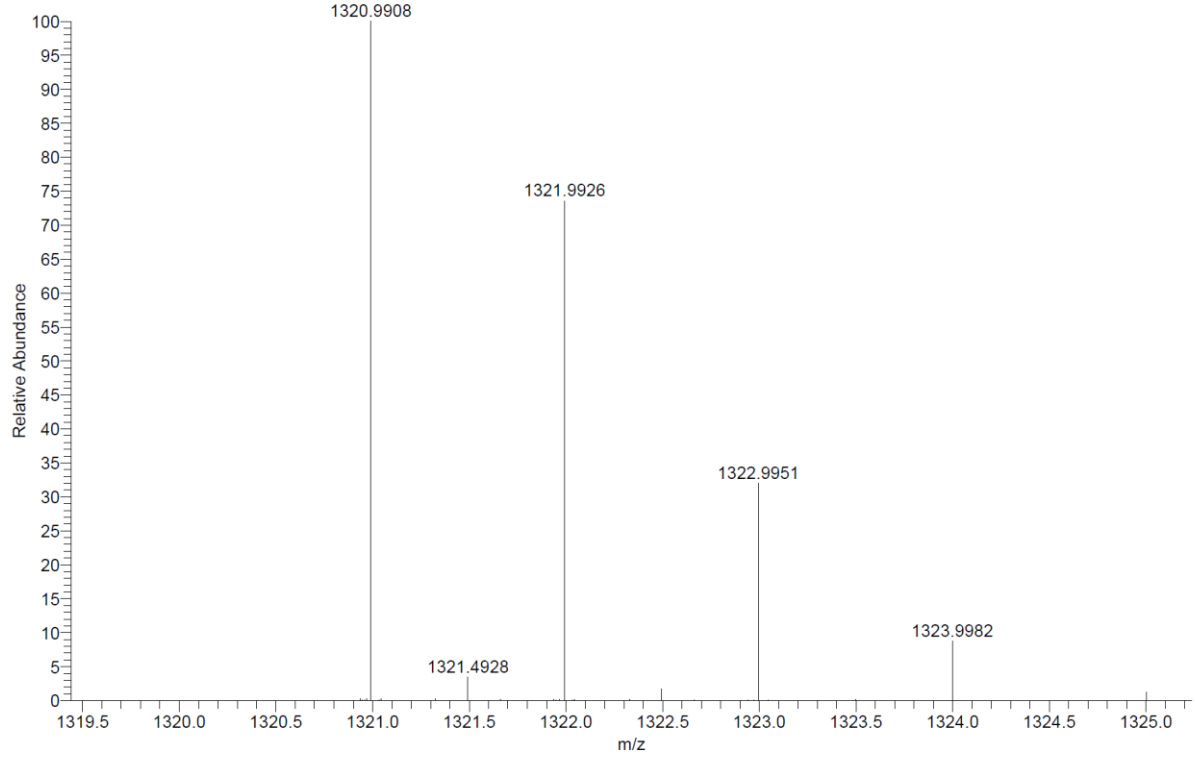

KKLLkllKLLL (HP9) was obtained as white solid after preparative RP-HPLC (63.9 mg, 57.5%). Analytical RP-HPLC: t_R = 1.52 min (A/D 100:0 to 0:100 in 3.5 min, λ = 214 nm). MS (ESI+): $C_{66}H_{128}N_{16}O_{11}$ calc./obs. 1321.99/1322.00 Da $[M+H]^+$.

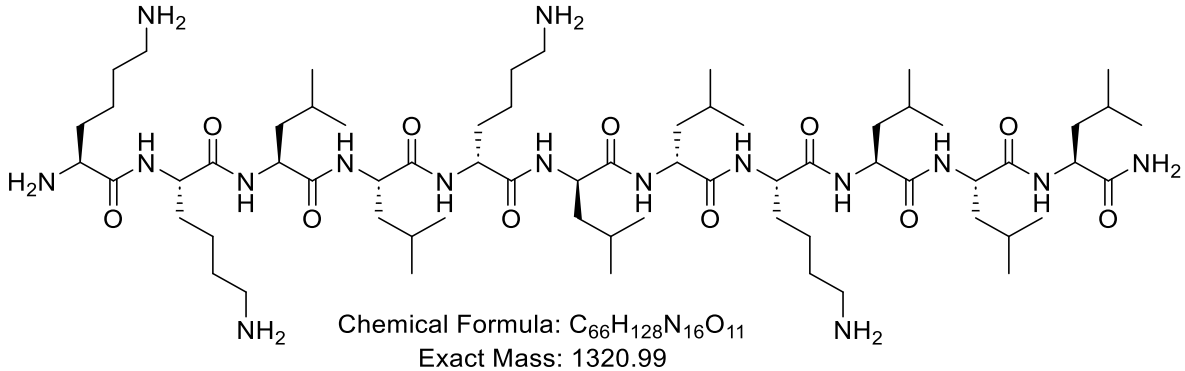

Analytical HPLC-MS data:

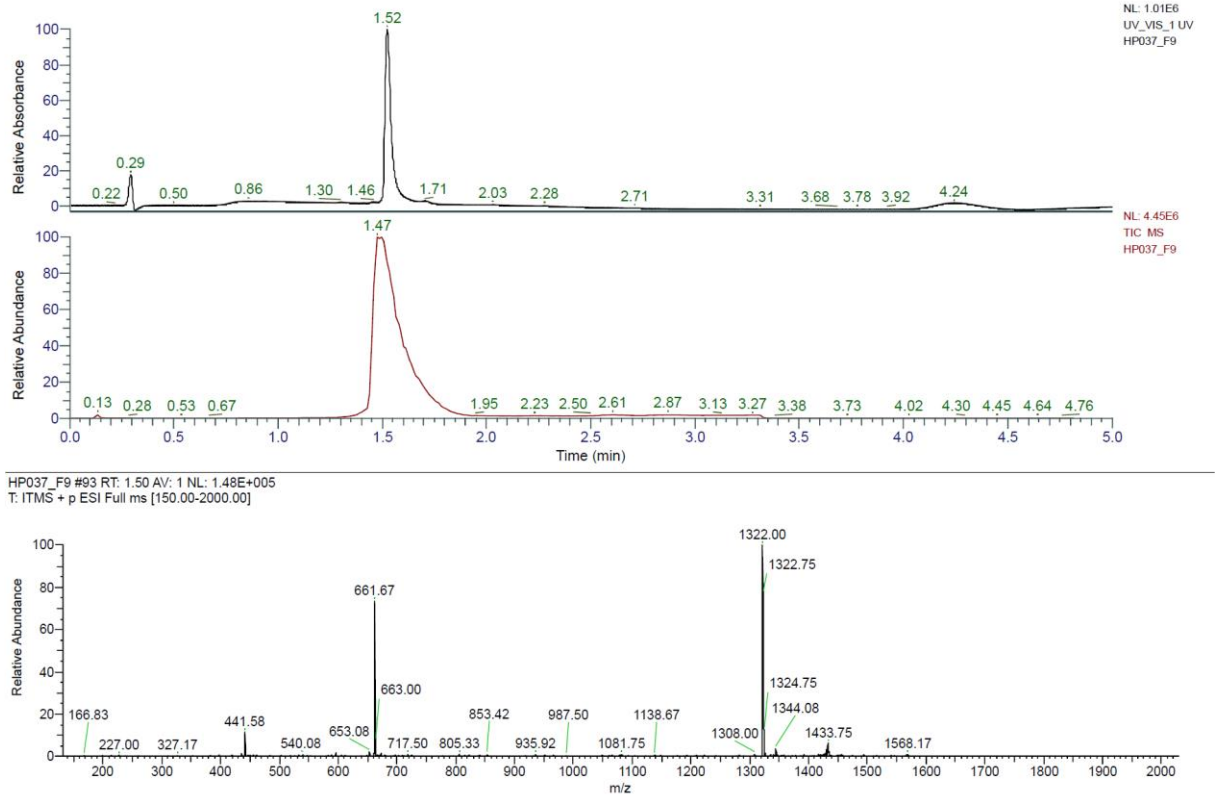

HRMS spectra:

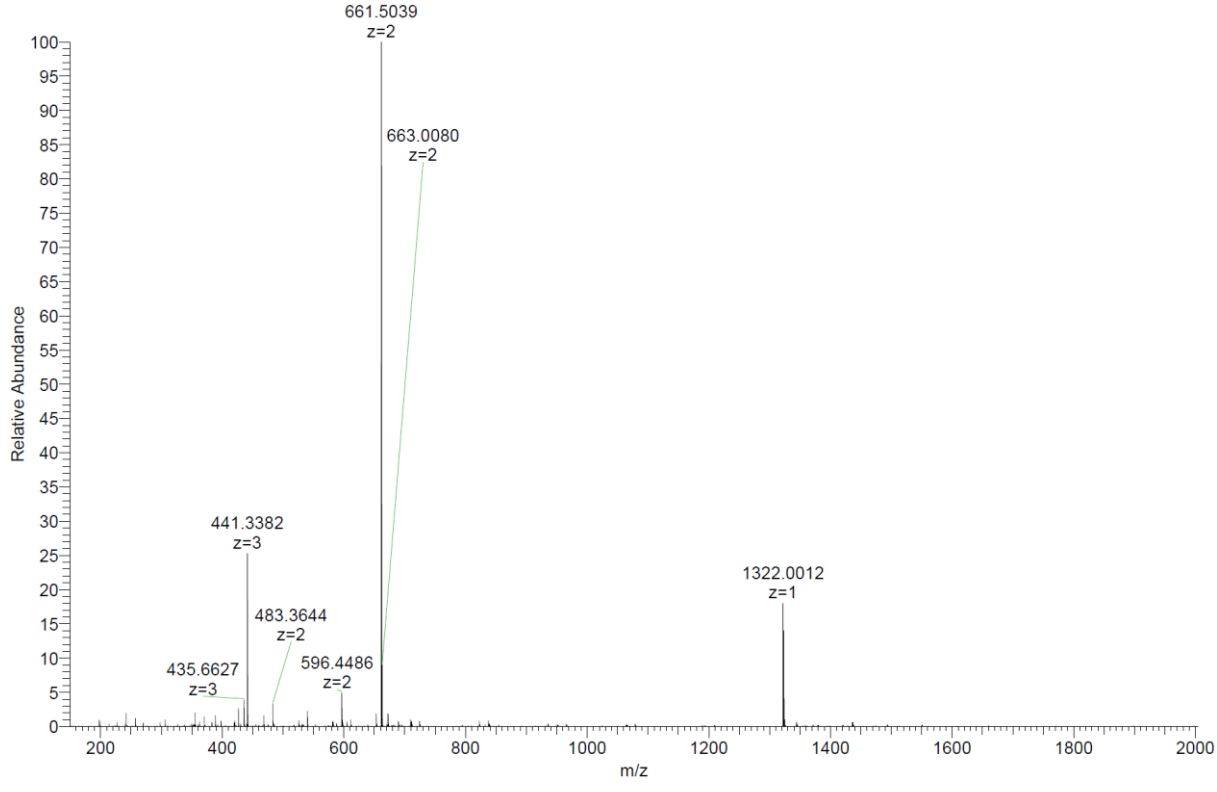

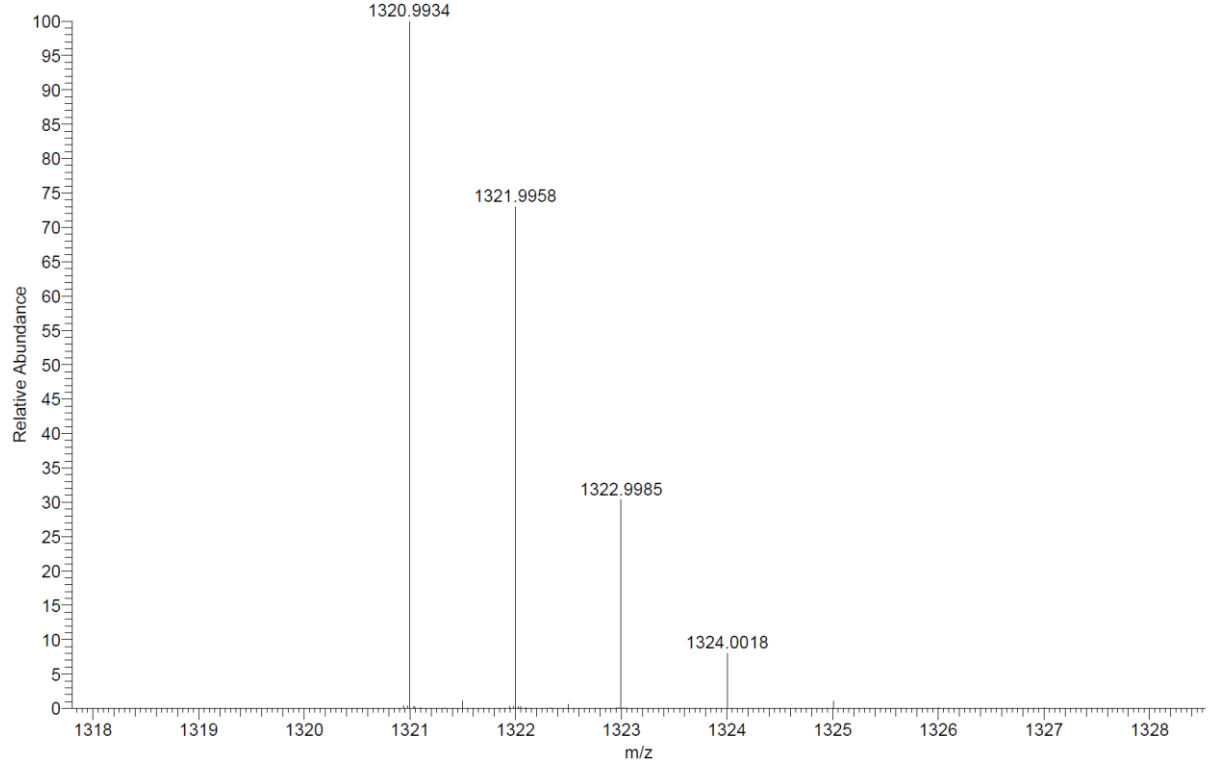

kkLLkLLKLLL (HP10) was obtained as white solid after preparative RP-HPLC (50.0 mg, 45.0%). Analytical RP-HPLC: t_R = 1.60 min (A/D 100:0 to 0:100 in 3.5 min, λ = 214 nm). MS (ESI+): $C_{66}H_{128}N_{16}O_{11}$ calc./obs. 1321.99/1322.00 Da $[M+H]^+$.

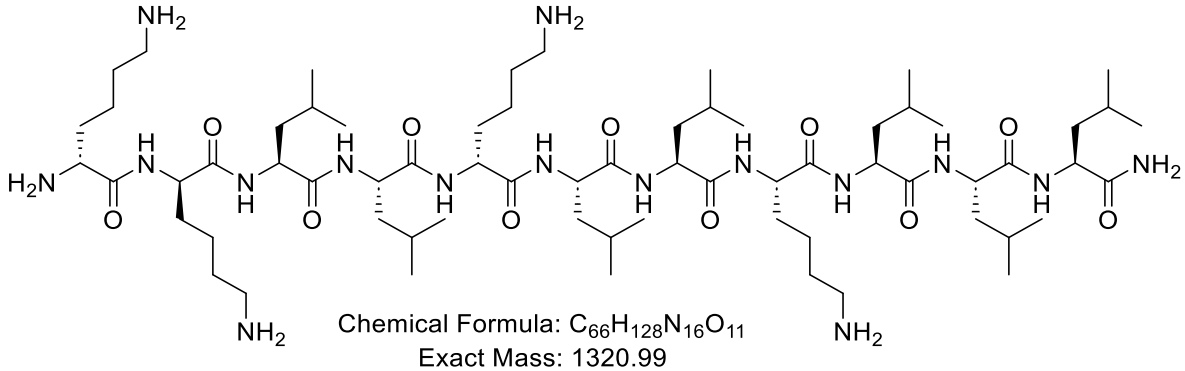

Analytical HPLC-MS data:

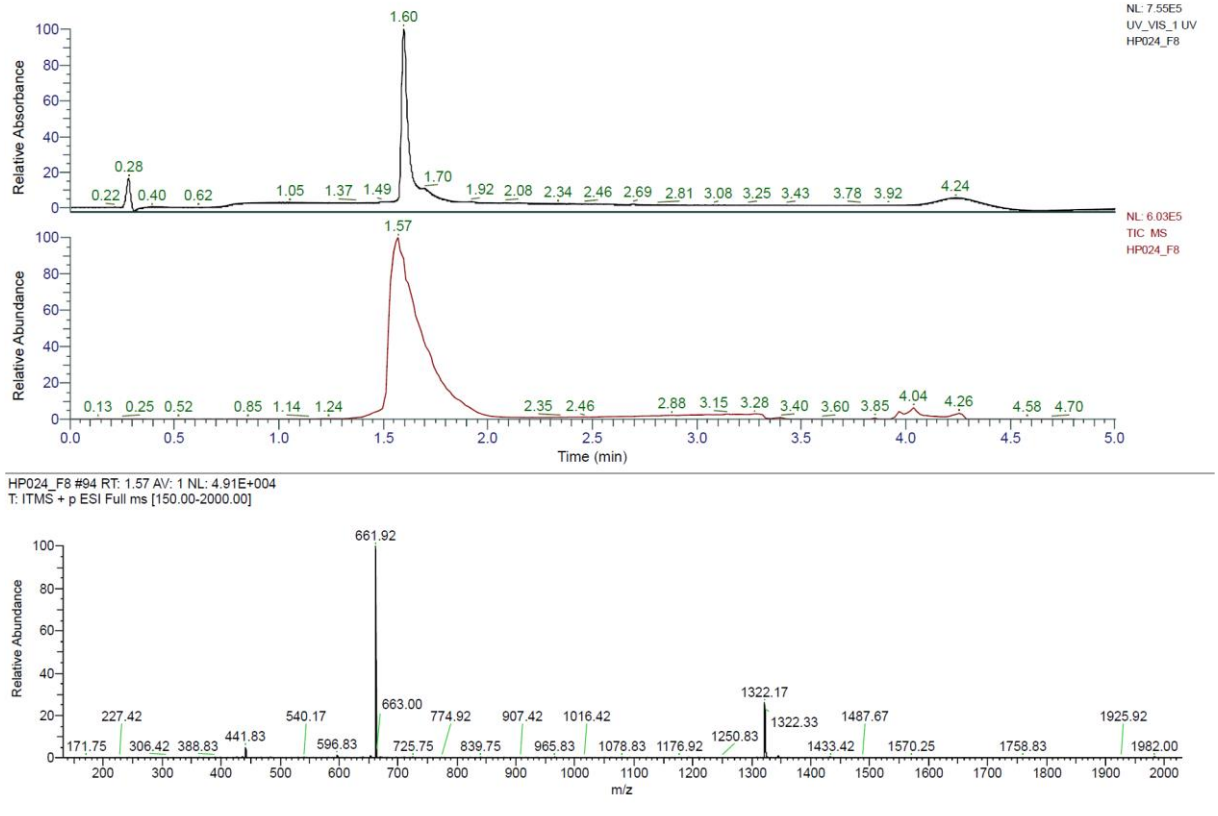

HRMS spectra:

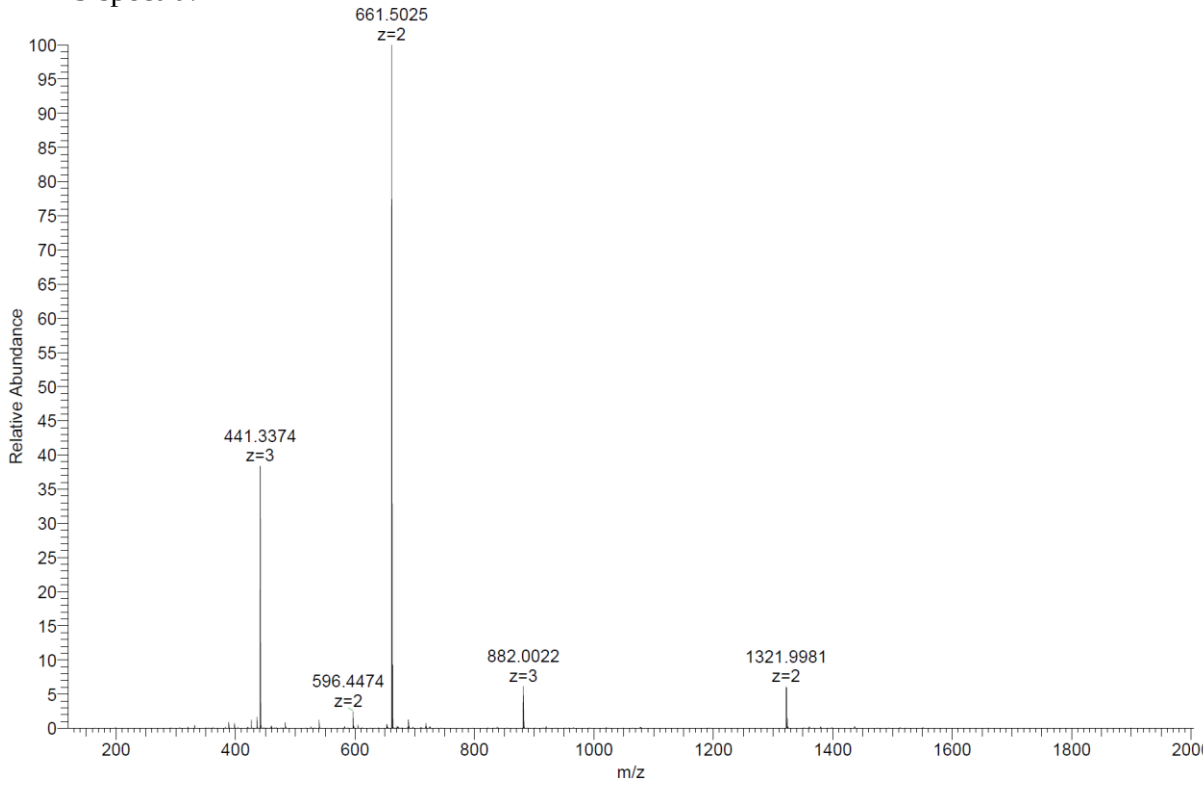

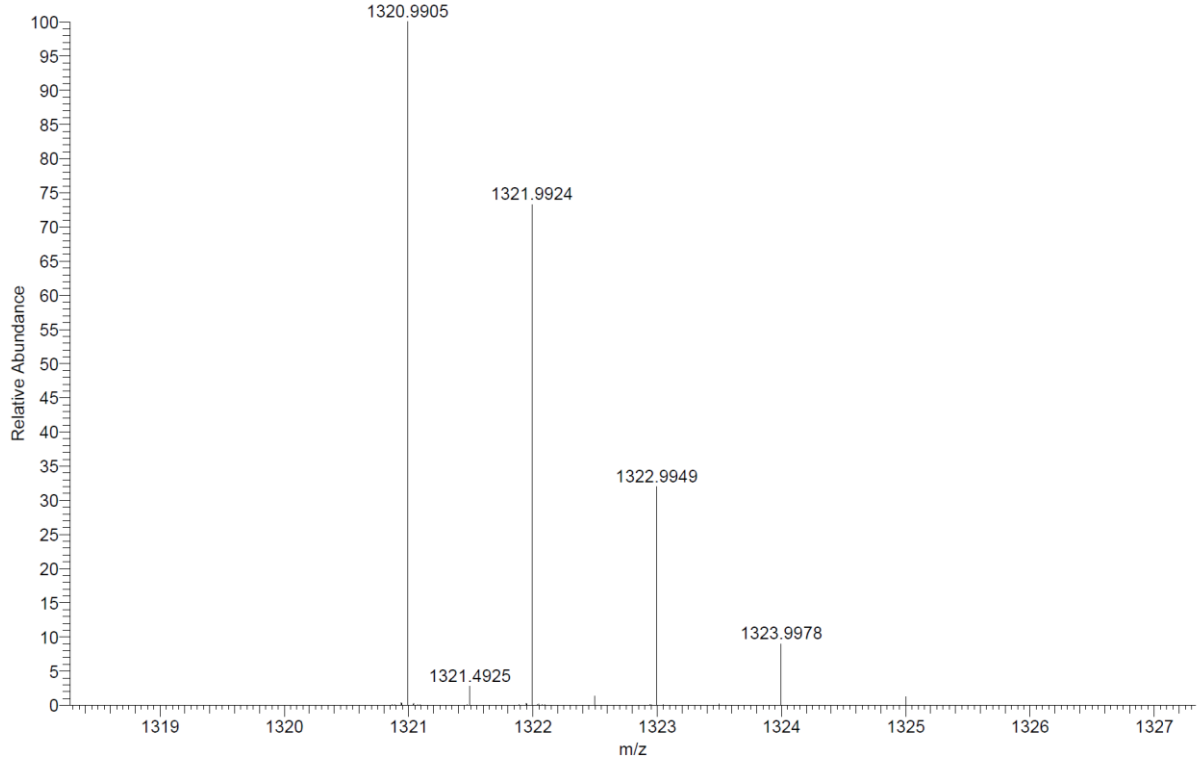

KkllKLlKLLL (HP11) was obtained as white solid after preparative RP-HPLC (31.5 mg, 35.4%). Analytical RP-HPLC: t_R = 1.60 min (A/D 100:0 to 0:100 in 3.5 min, λ = 214 nm). MS (ESI+): $C_{66}H_{128}N_{16}O_{11}$ calc./obs. 1321.99/1322.00 Da $[M+H]^+$.

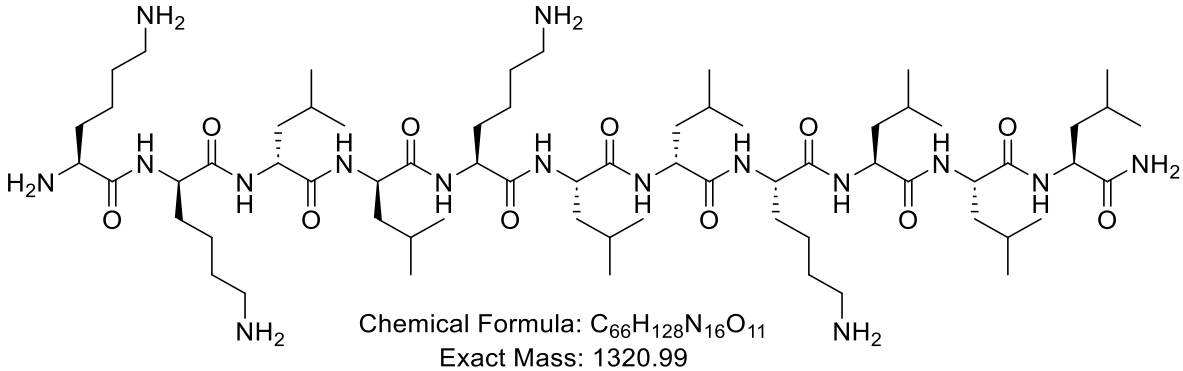

Analytical HPLC-MS data:

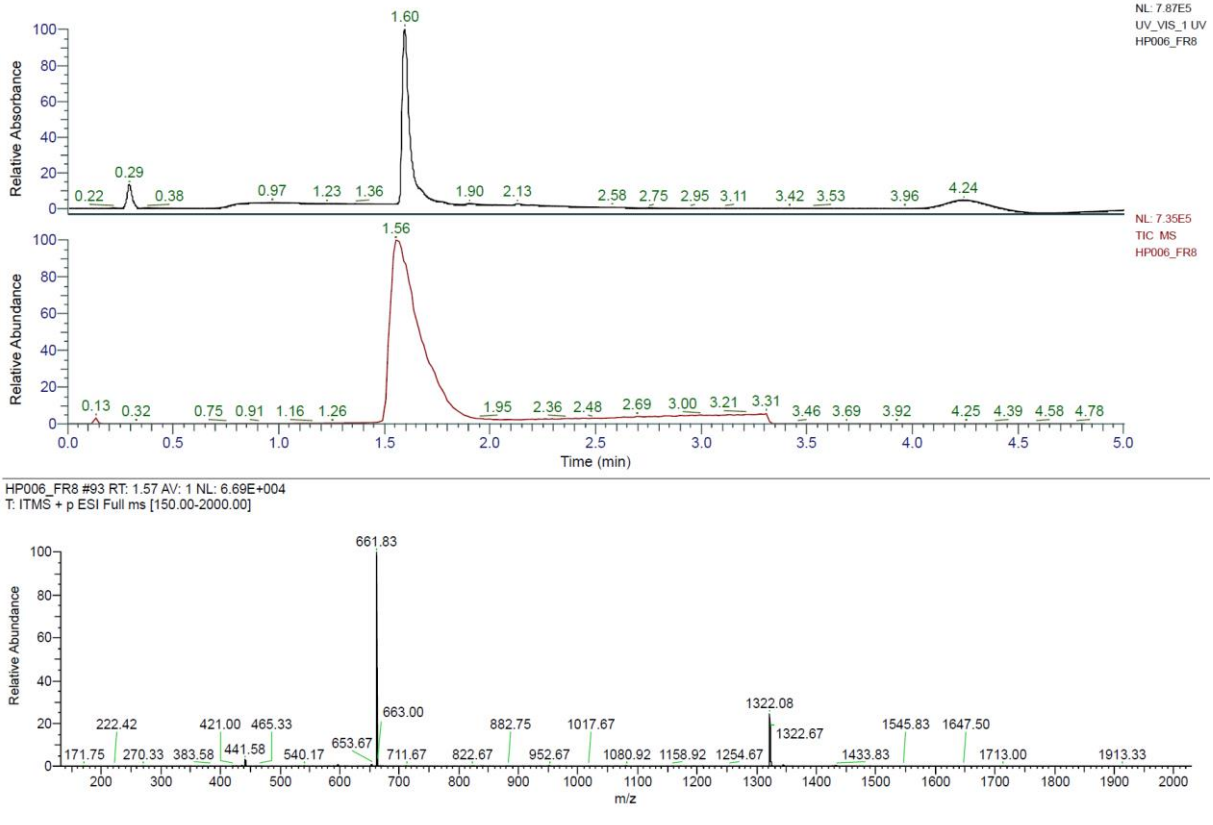

HRMS spectra:

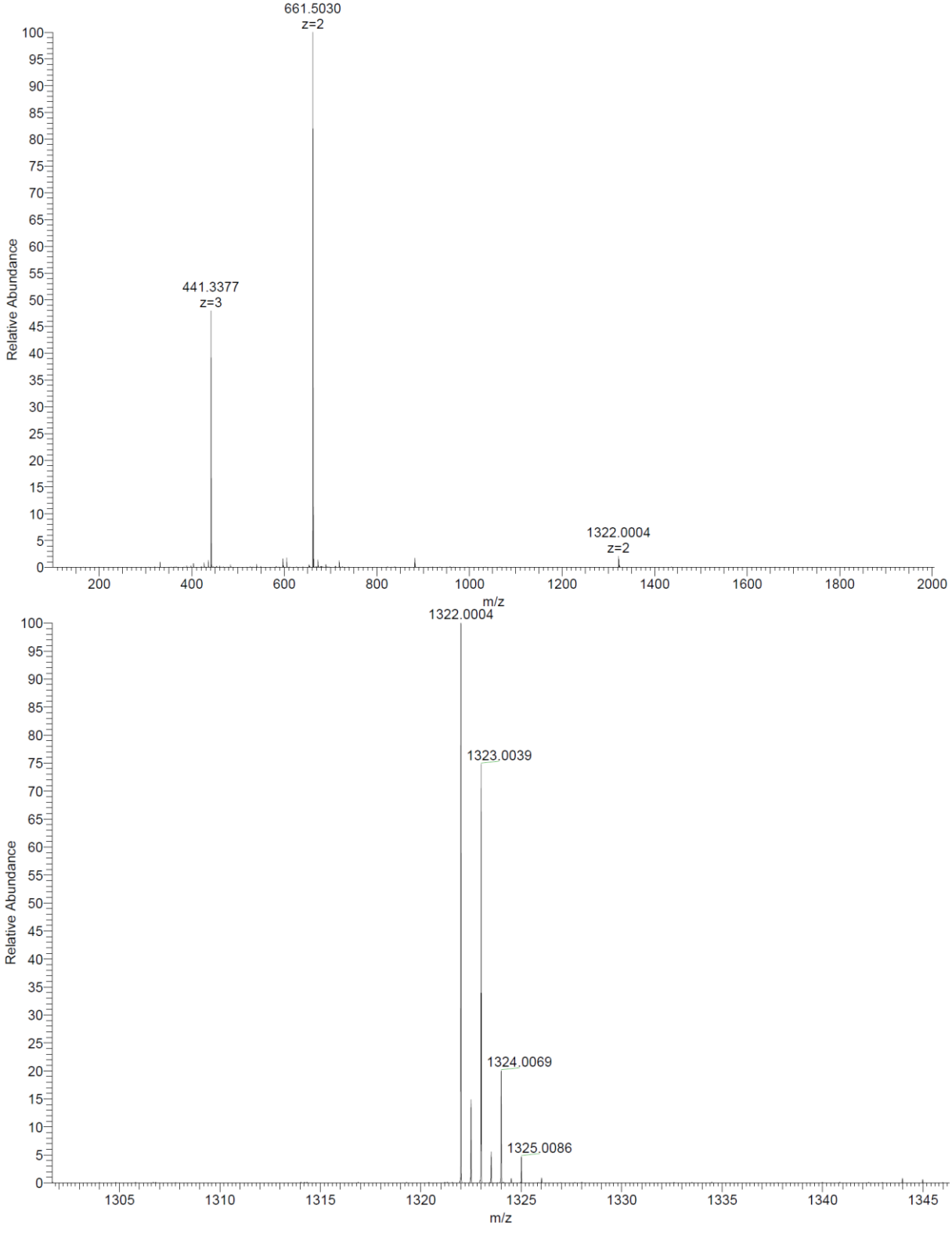

KkllKlLKLLL (HP12) was obtained as white solid after preparative RP-HPLC (26.8 mg, 30.1%). Analytical RP-HPLC: t_R = 1.60 min (A/D 100:0 to 0:100 in 3.5 min, λ = 214 nm). MS (ESI+): $C_{66}H_{128}N_{16}O_{11}$ calc./obs. 1321.99/1322.00 Da $[M+H]^+$.

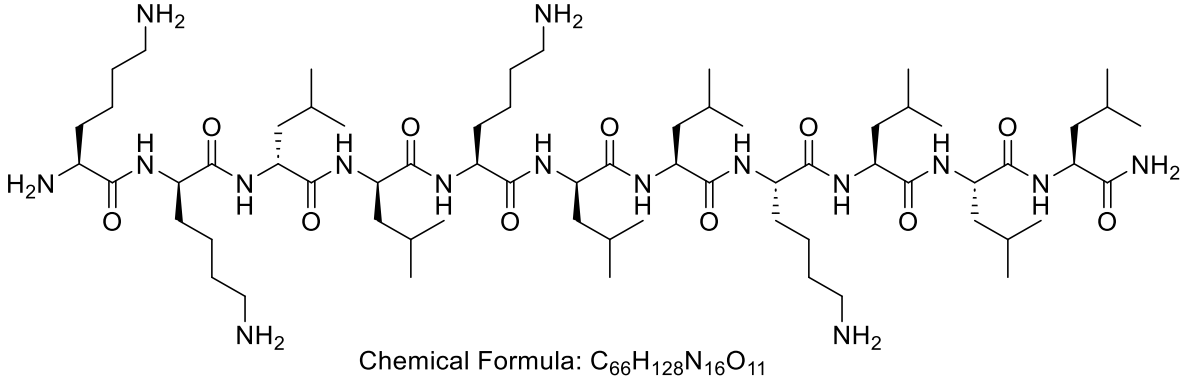

Chemical Formula: $C_{66}H_{128}N_{16}O_{11}$
Exact Mass: 1320.99
Molecular Weight: 1321.85

Analytical HPLC-MS data:

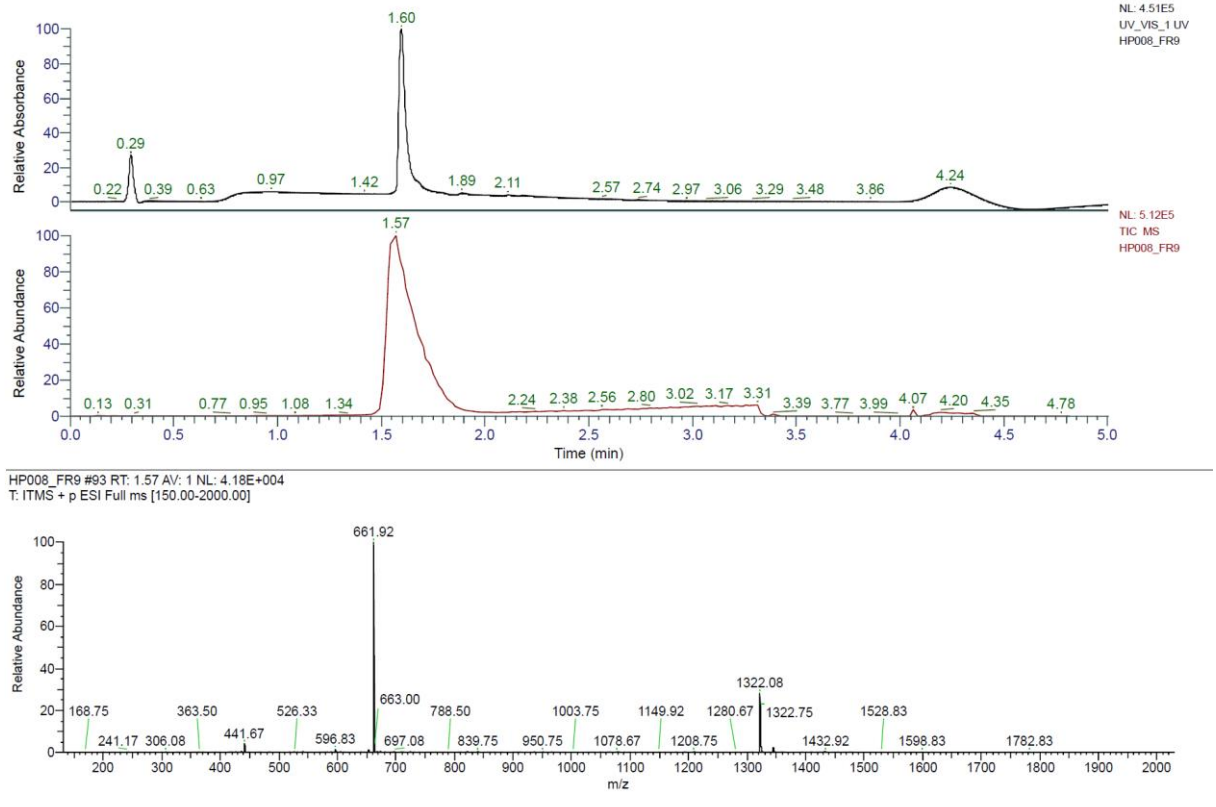

HRMS spectra:

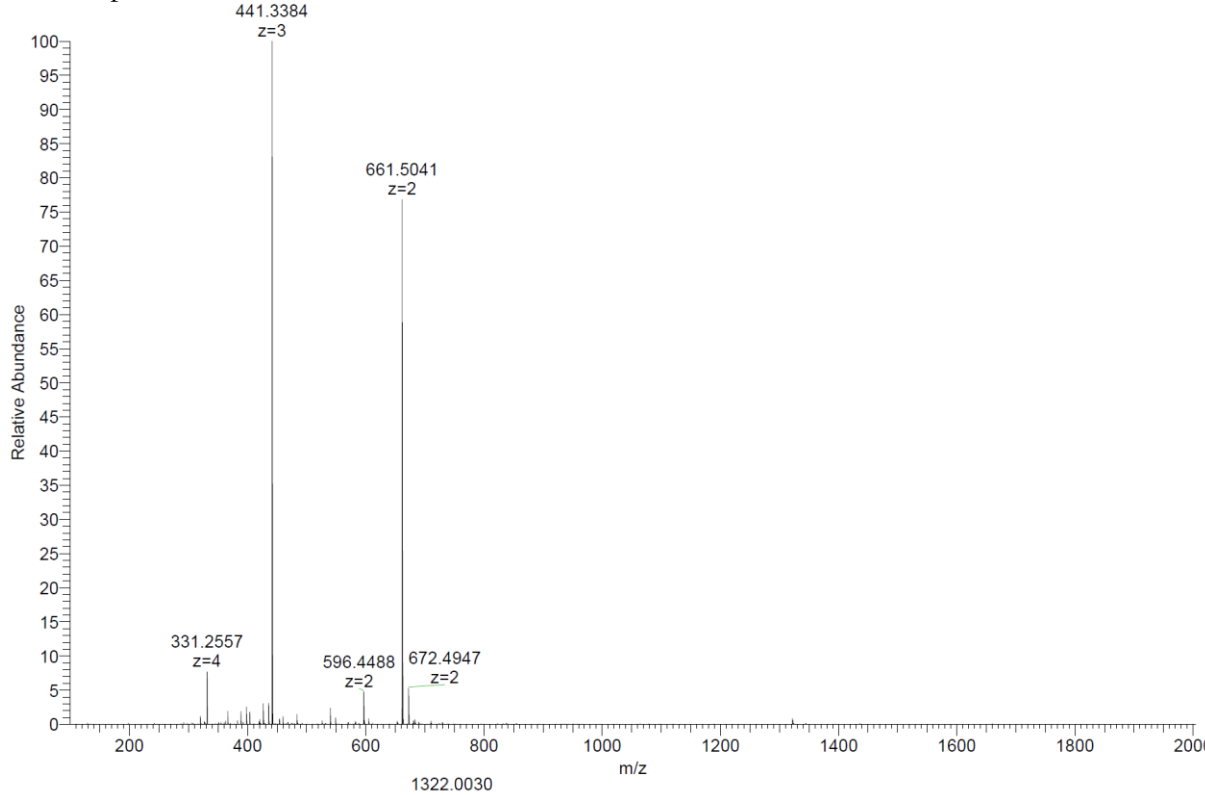

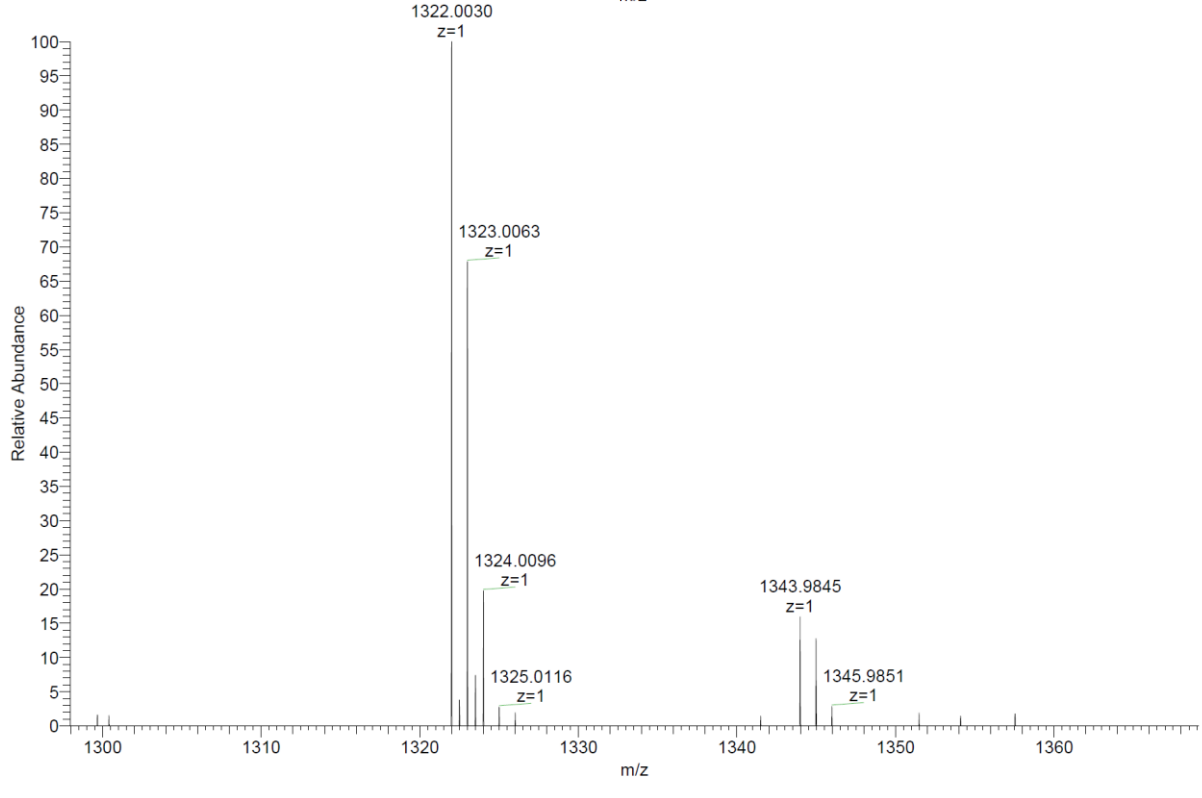

KKLLkllkLLL (HP13) was obtained as white solid after preparative RP-HPLC (37.4 mg, 42.1%). Analytical RP-HPLC: t_R = 1.53 min (A/D 100:0 to 0:100 in 3.5 min, λ = 214 nm). MS (ESI+): $C_{66}H_{128}N_{16}O_{11}$ calc./obs. 1321.99/1322.00 Da $[M+H]^+$.

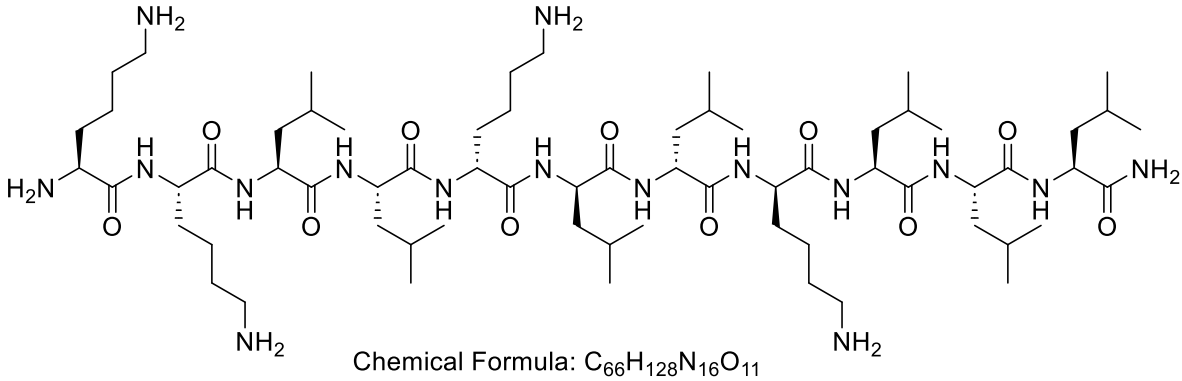

Chemical Formula: $C_{66}H_{128}N_{16}O_{11}$
Exact Mass: 1320.99
Molecular Weight: 1321.85

Analytical HPLC-MS data:

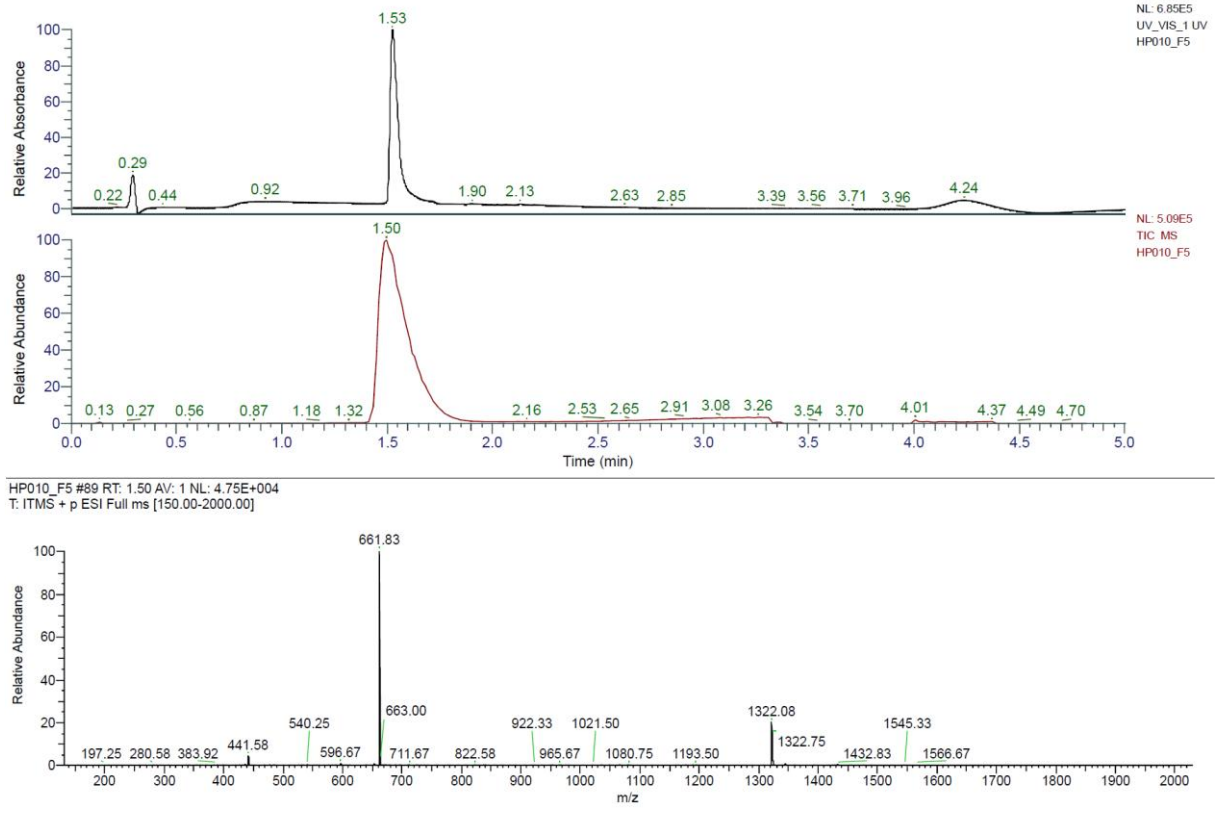

HRMS spectra:

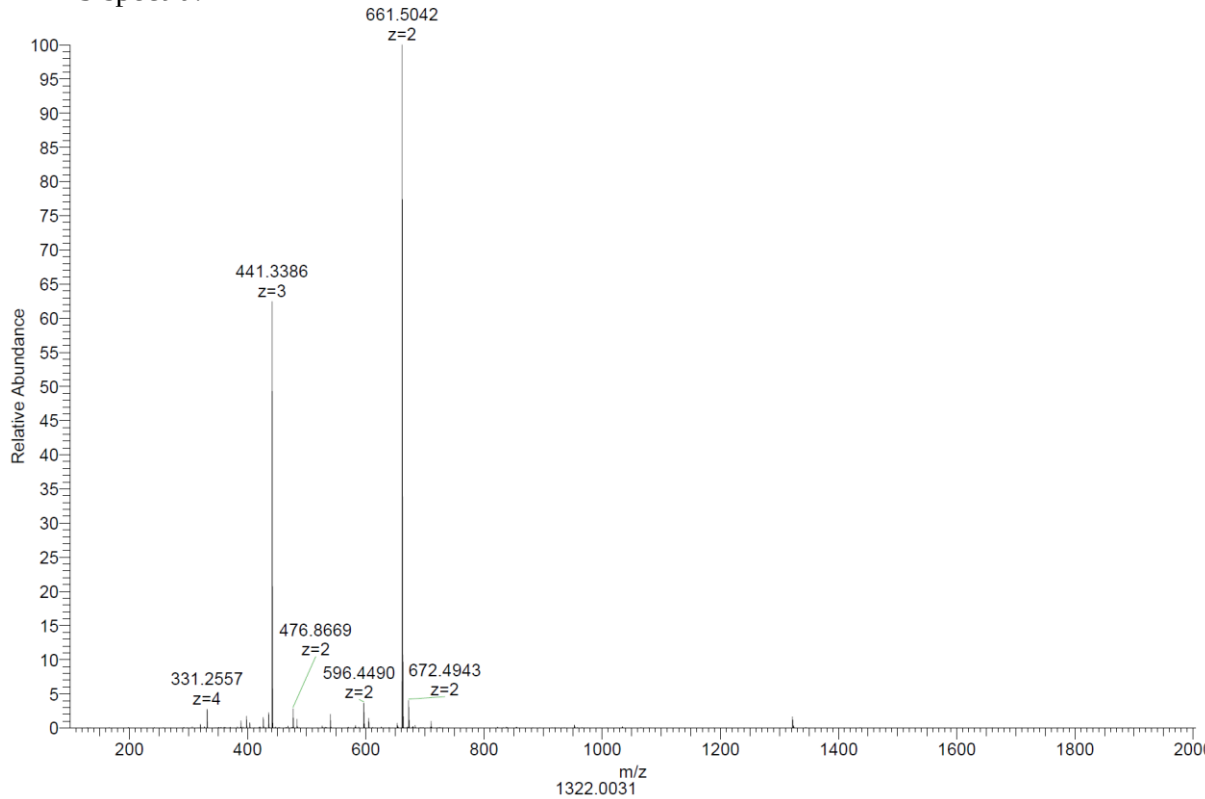

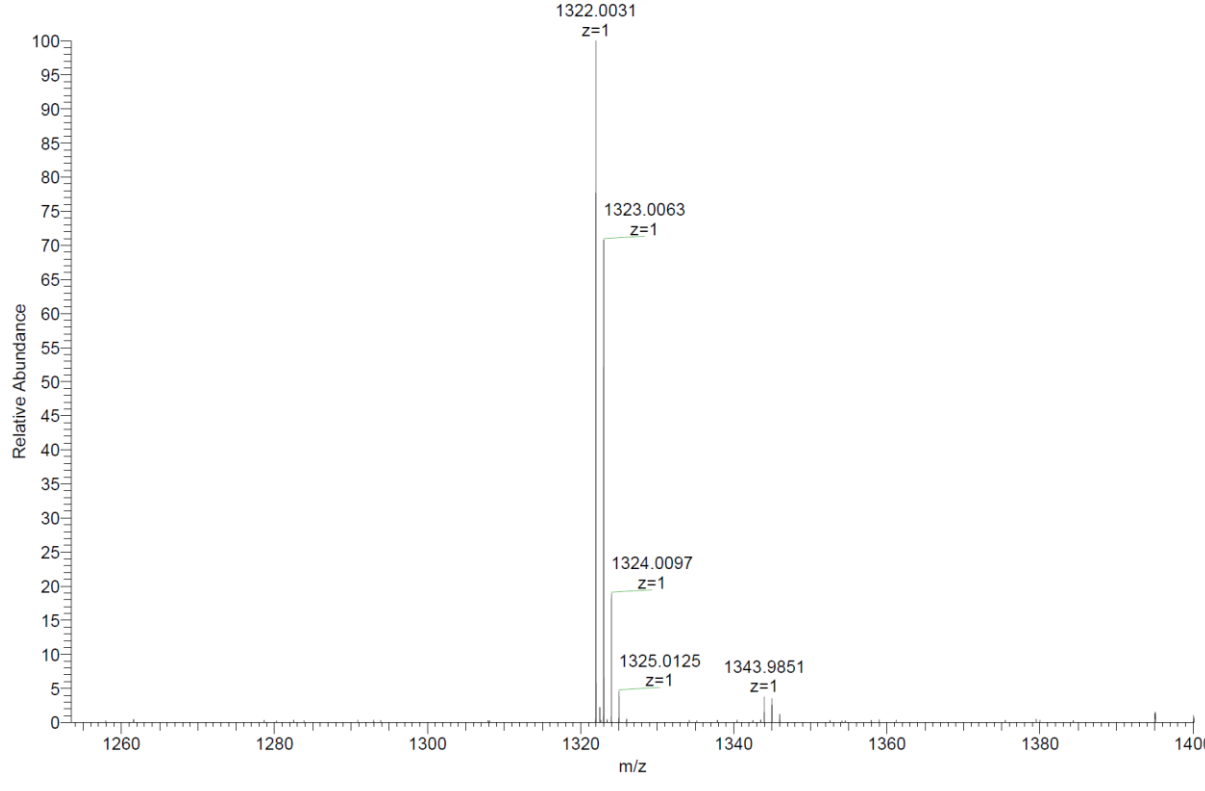

KKllKllKLLL (HP14) was obtained as white solid after preparative RP-HPLC (33.7 mg, 37.9%). Analytical RP-HPLC: t_R = 1.53 min (A/D 100:0 to 0:100 in 3.5 min, λ = 214 nm). MS (ESI+): $C_{66}H_{128}N_{16}O_{11}$ calc./obs. 1321.99/1322.00 Da $[M+H]^+$.

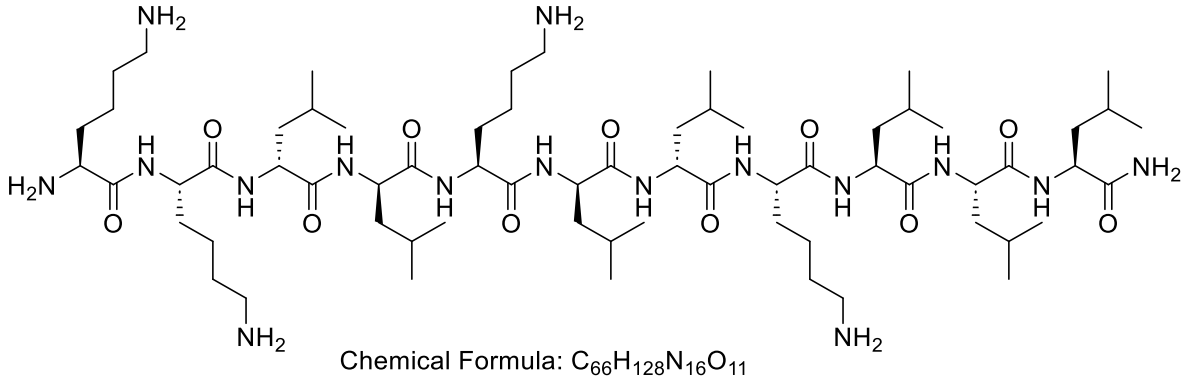

Chemical Formula: $C_{66}H_{128}N_{16}O_{11}$
Exact Mass: 1320.99
Molecular Weight: 1321.85

Analytical HPLC-MS data:

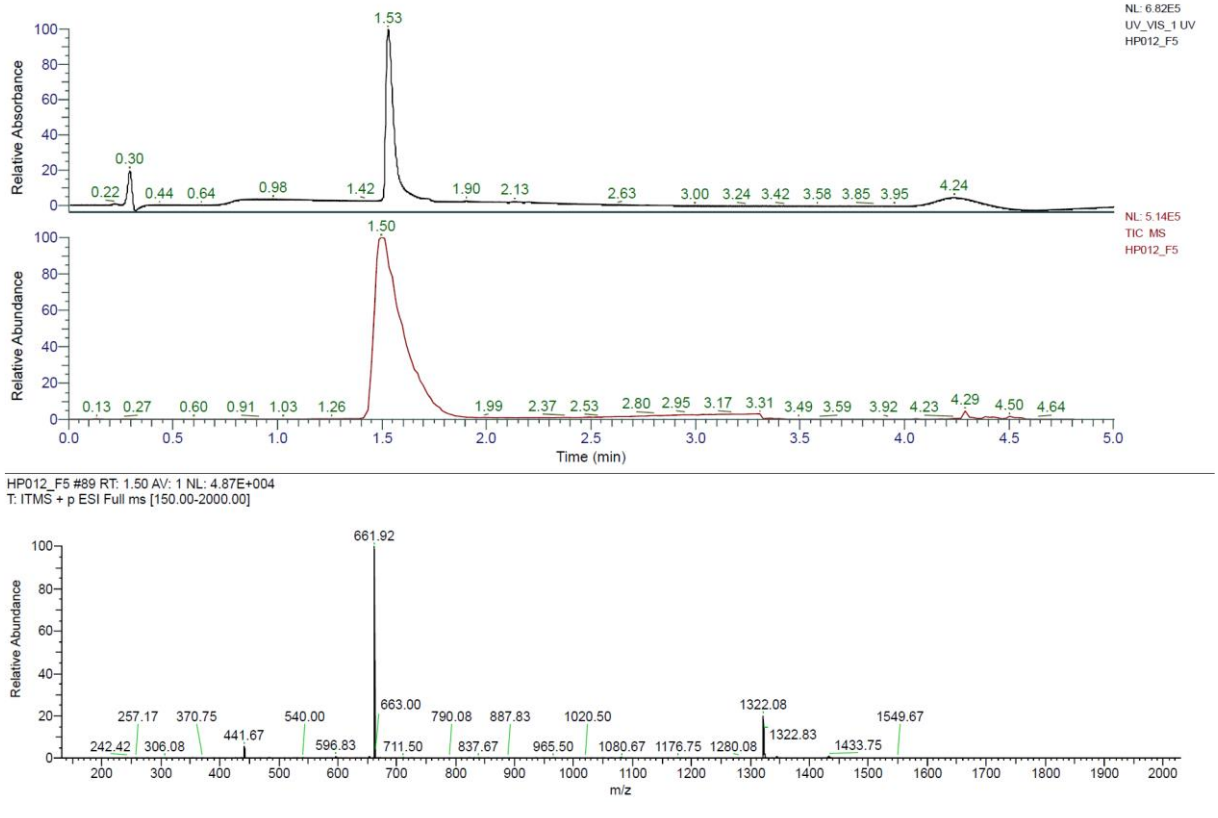

HRMS spectra:

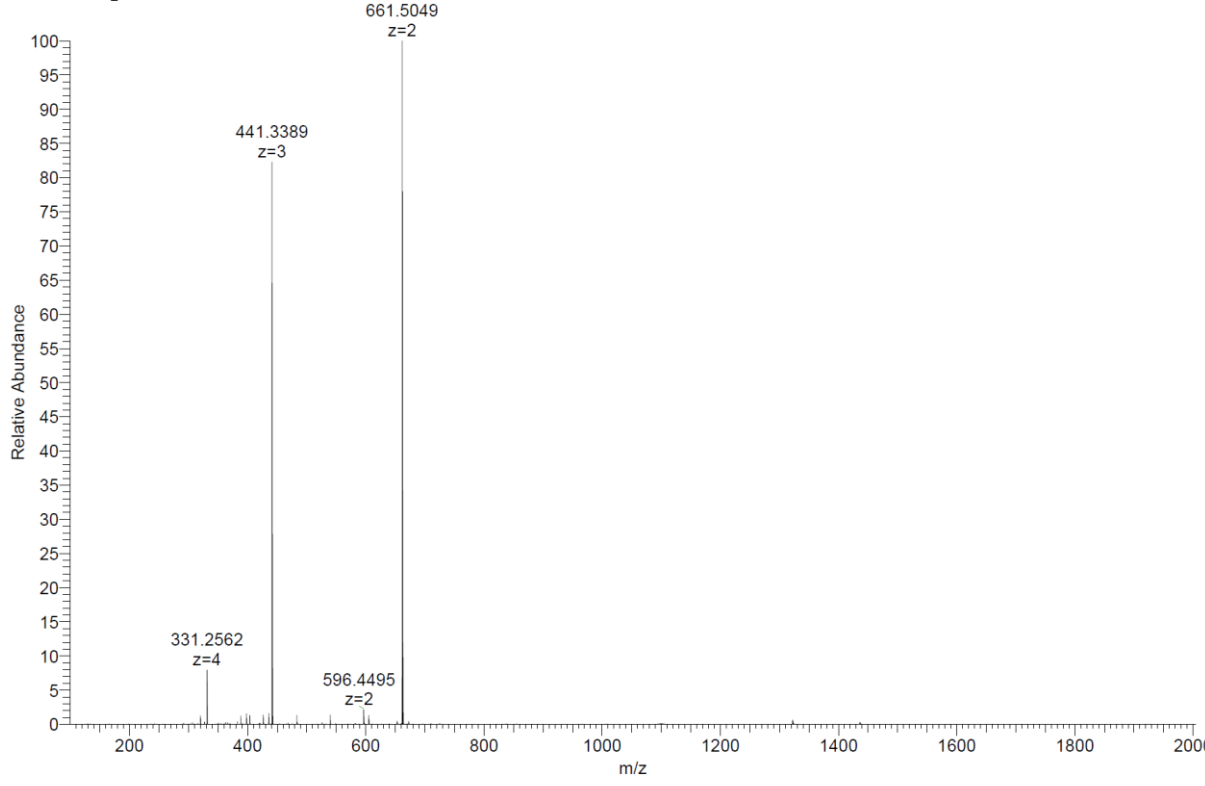

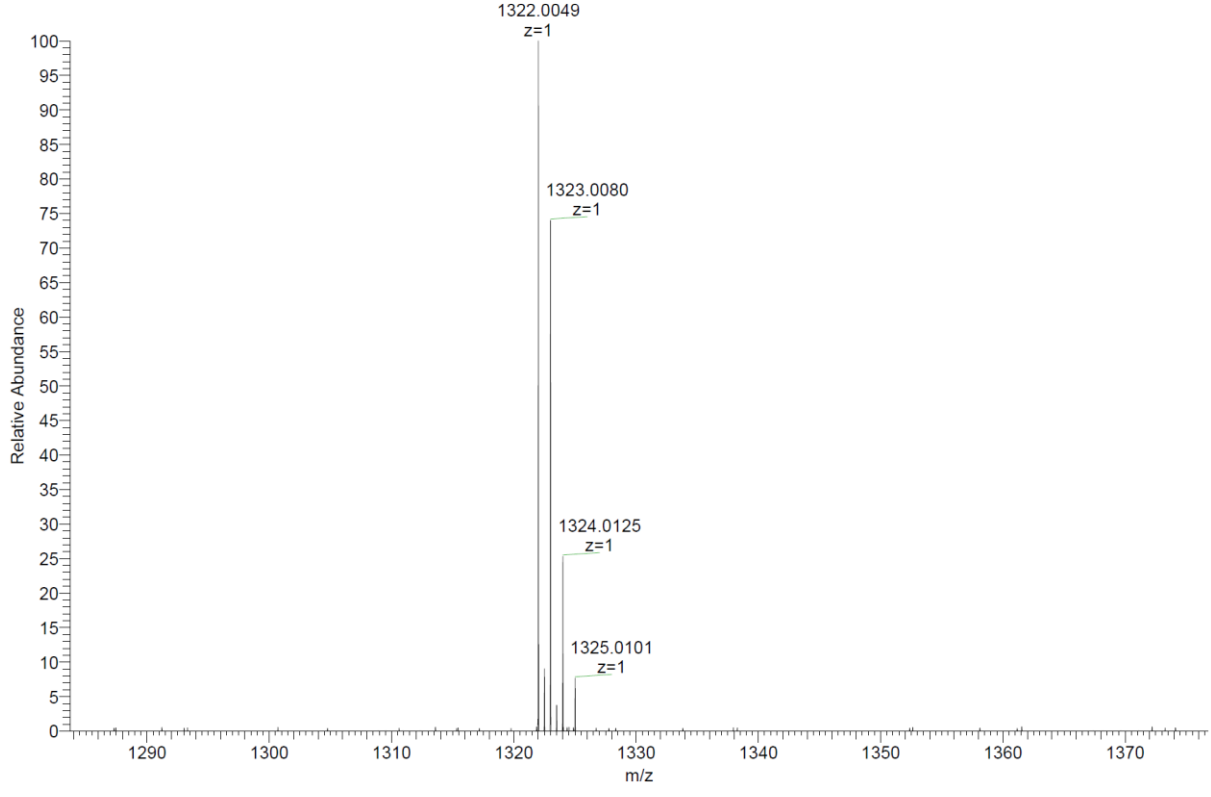

KKlKlLkLlLL (HP15) was obtained as white solid after preparative RP-HPLC (34.5 mg, 38.8%). Analytical RP-HPLC: t_R = 1.60 min (A/D 100:0 to 0:100 in 3.5 min, λ = 214 nm). MS (ESI+): $C_{66}H_{128}N_{16}O_{11}$ calc./obs. 1321.99/1322.00 Da $[M+H]^+$.

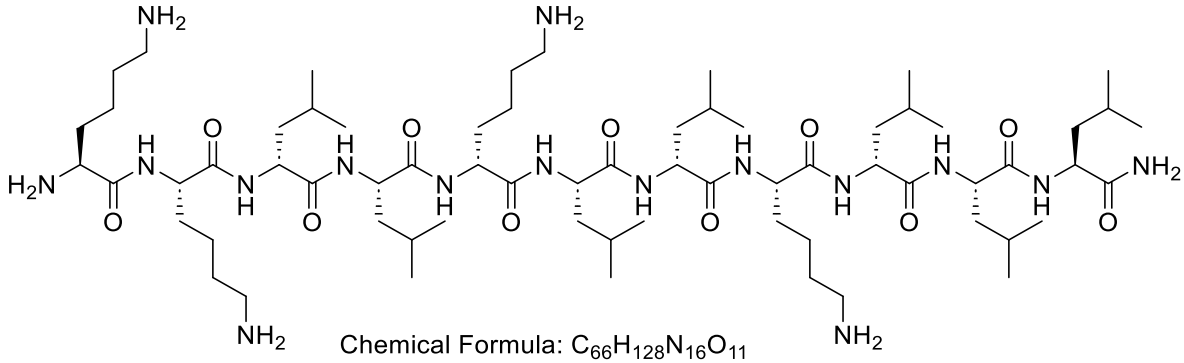

Analytical HPLC-MS data:

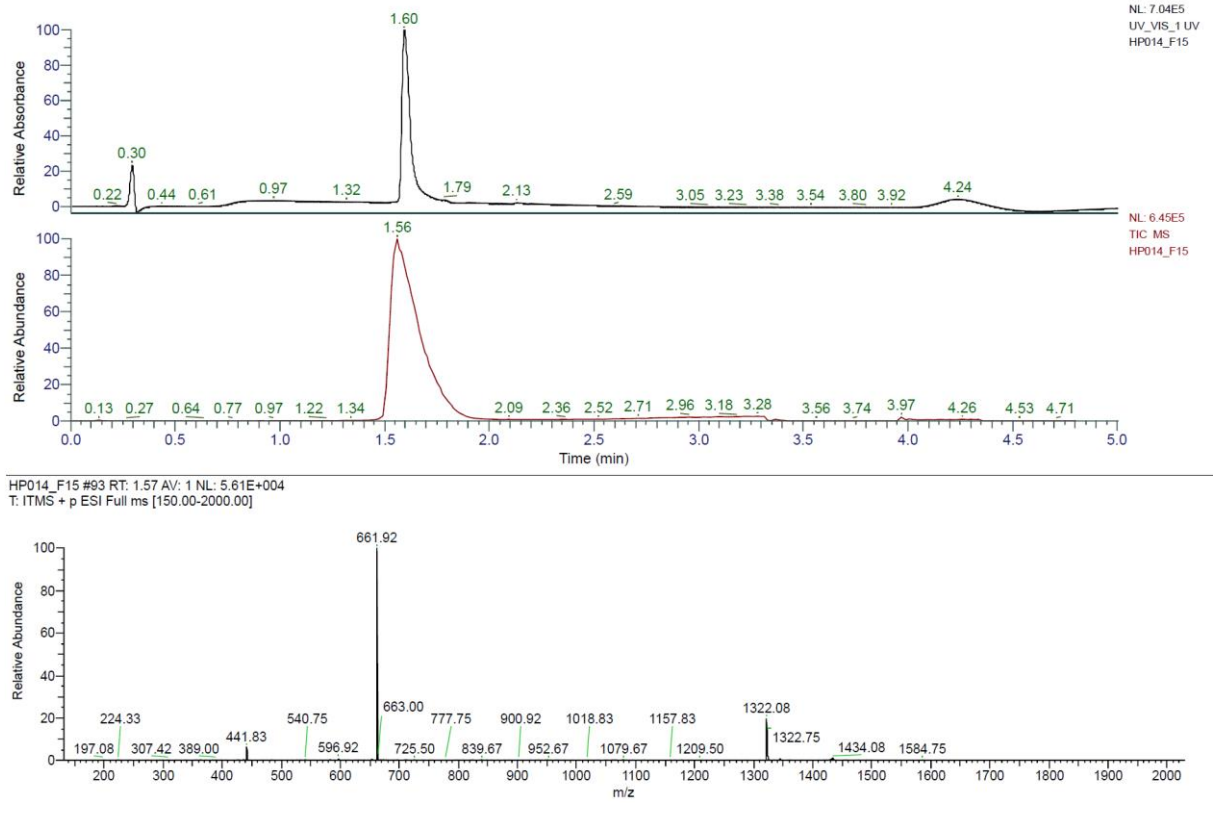

HRMS spectra:

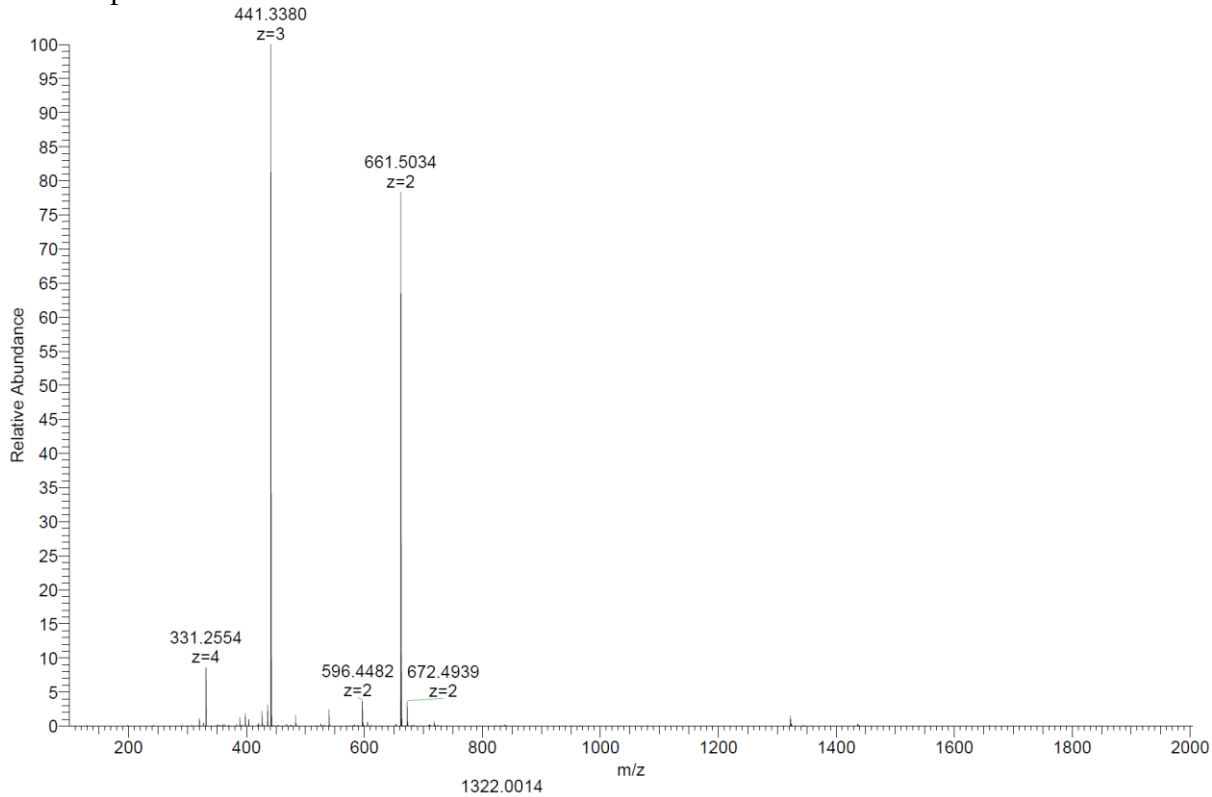

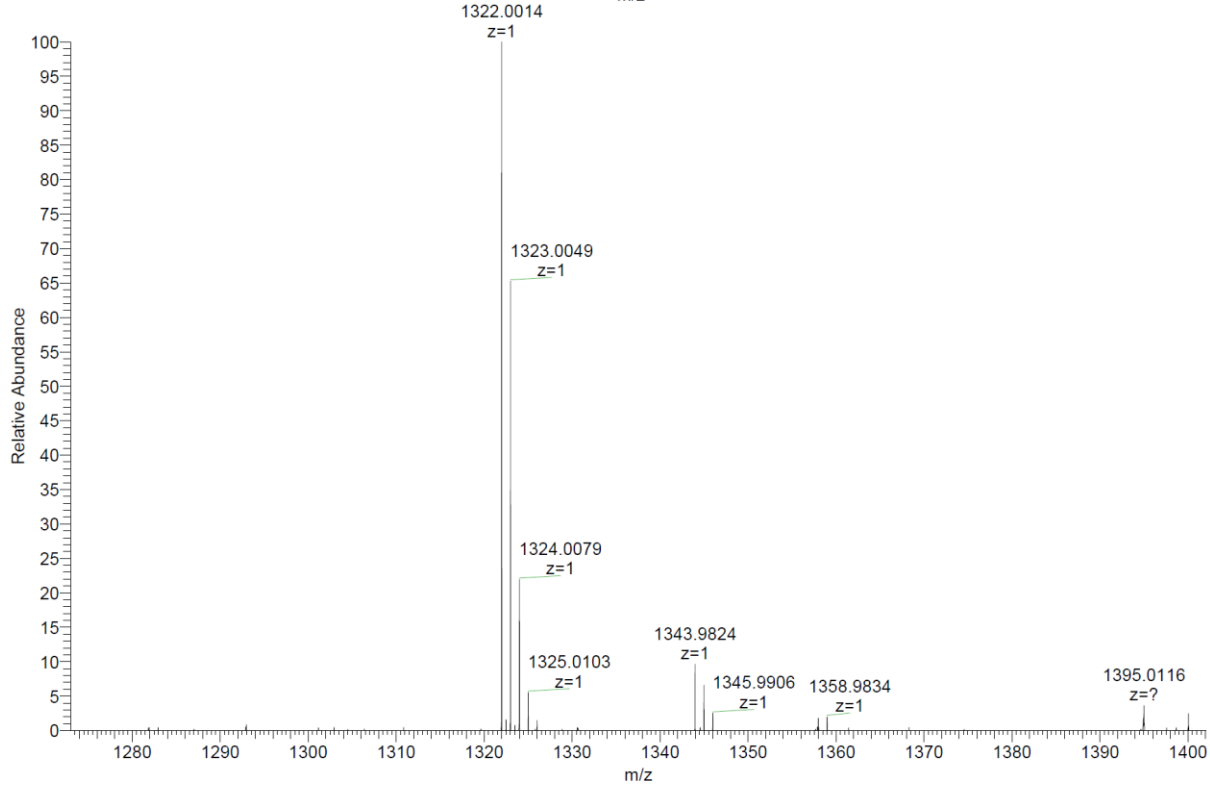

KKLlkLLklLL (HP16) was obtained as white solid after preparative RP-HPLC (16.0 mg, 18.0%). Analytical RP-HPLC: t_R = 1.59 min (A/D 100:0 to 0:100 in 3.5 min, λ = 214 nm). MS (ESI+): $C_{66}H_{128}N_{16}O_{11}$ calc./obs. 1321.99/1322.00 Da $[M+H]^+$.

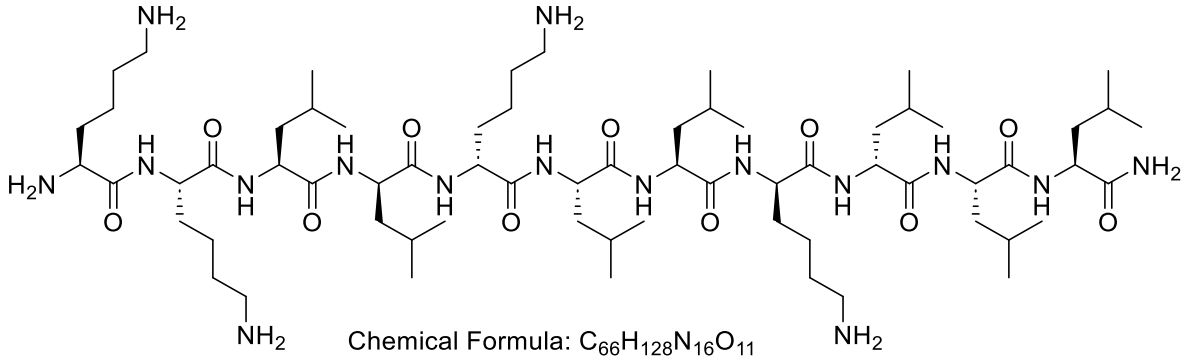

Analytical HPLC-MS data:

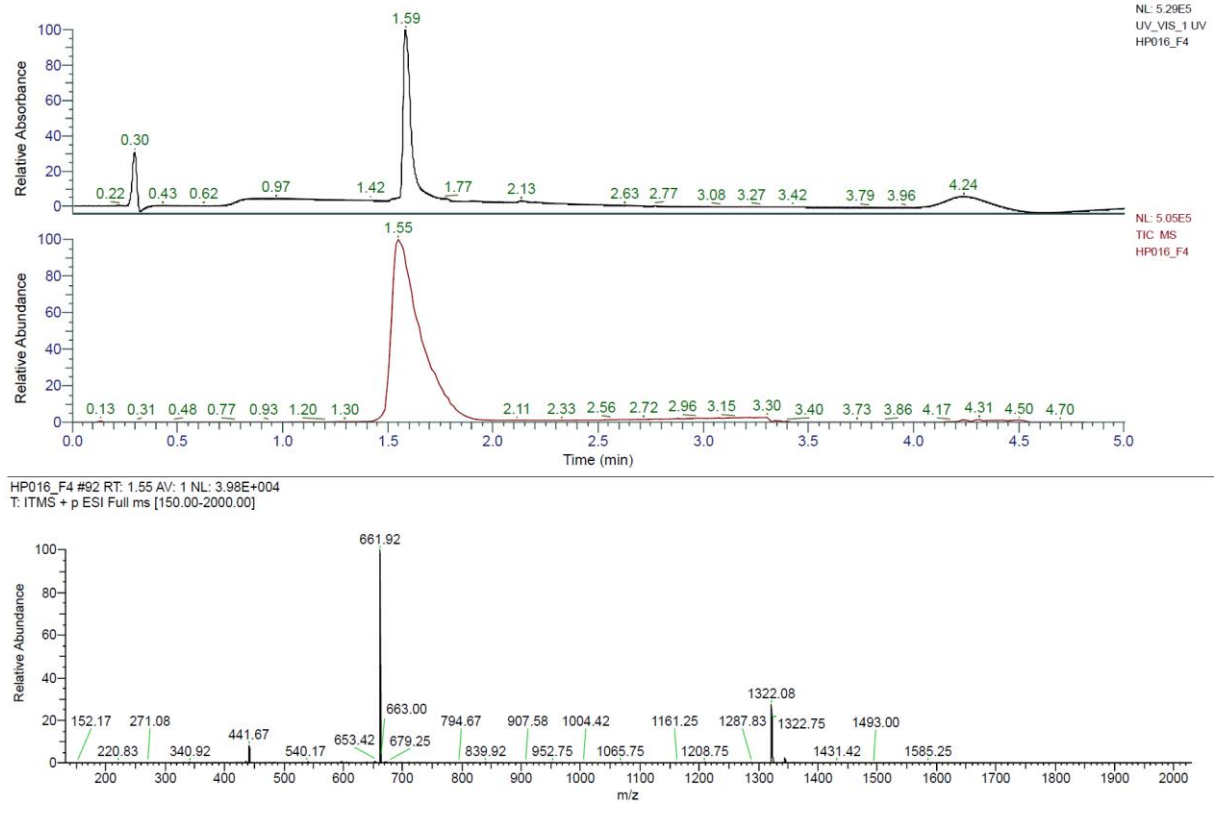

HRMS spectra:

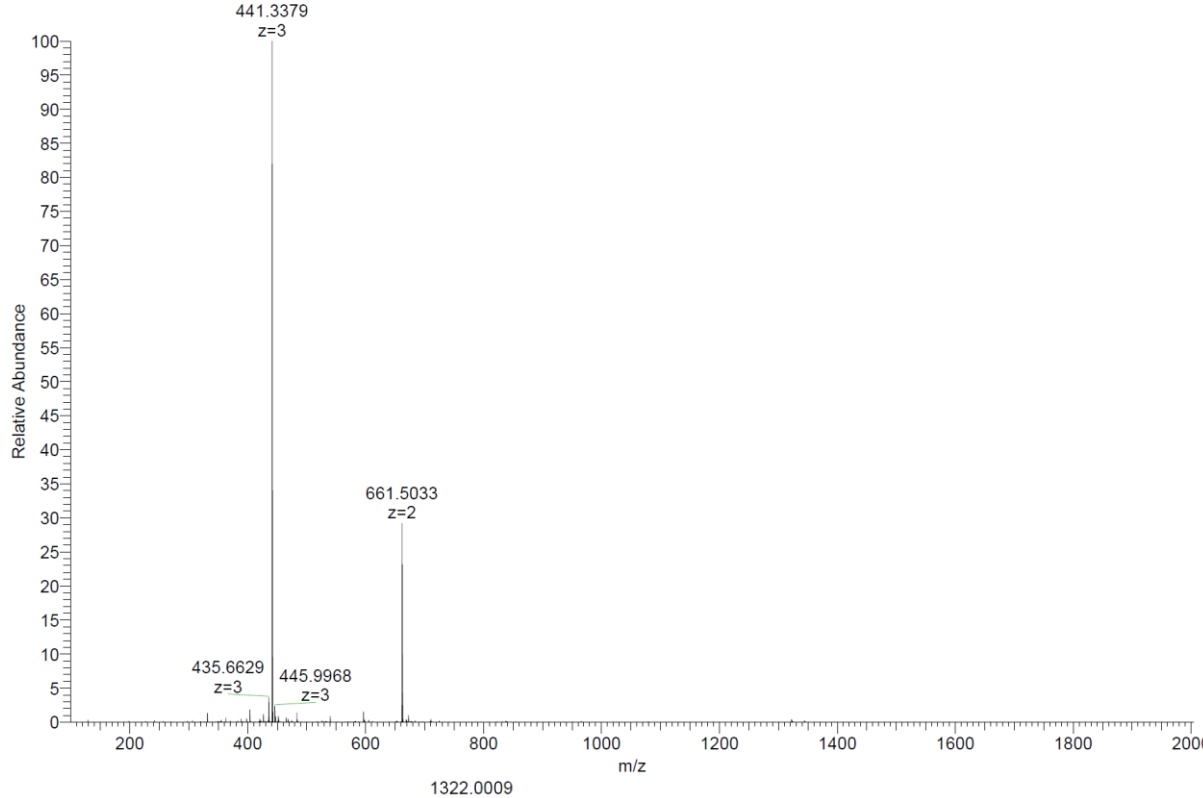

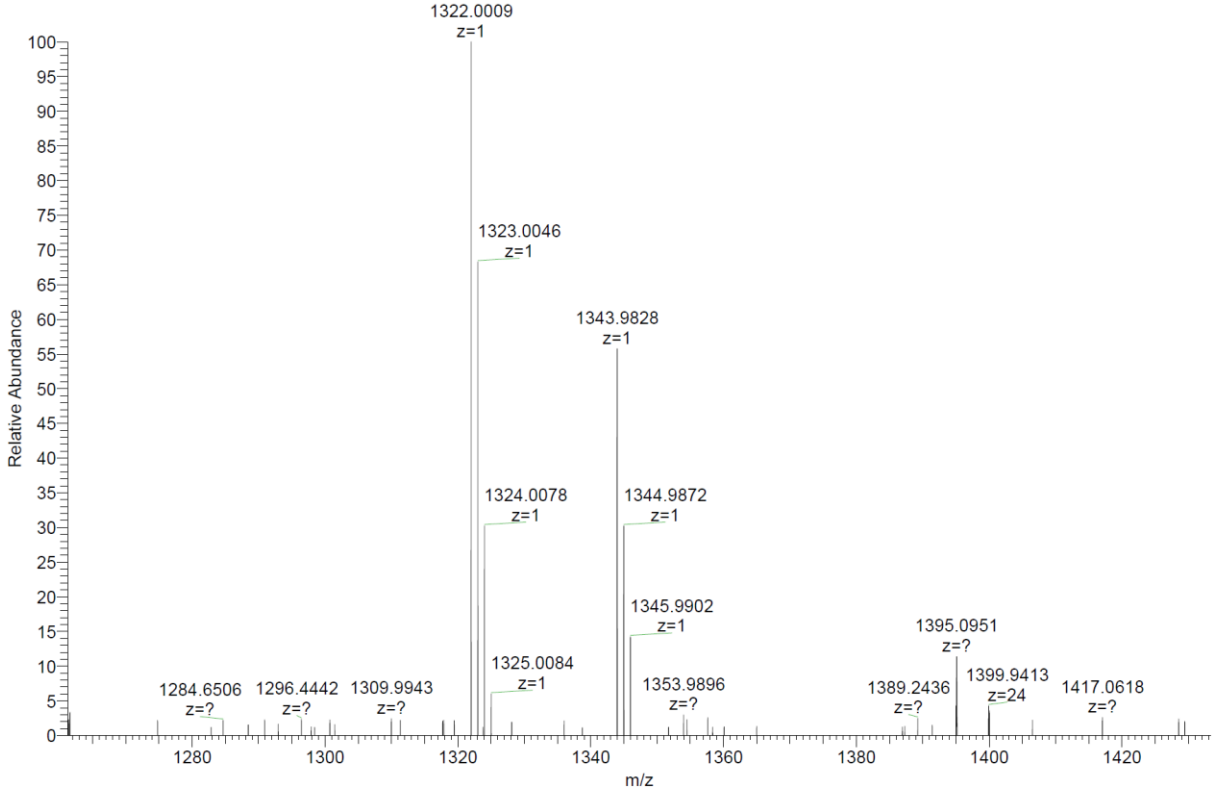

KklLKLLKllL (HP17) was obtained as white solid after preparative RP-HPLC (29.0 mg, 26.1%). Analytical RP-HPLC: t_R = 1.61 min (A/D 100:0 to 0:100 in 3.5 min, λ = 214 nm). MS (ESI+): $C_{66}H_{128}N_{16}O_{11}$ calc./obs. 1321.99/1322.00 Da $[M+H]^+$.

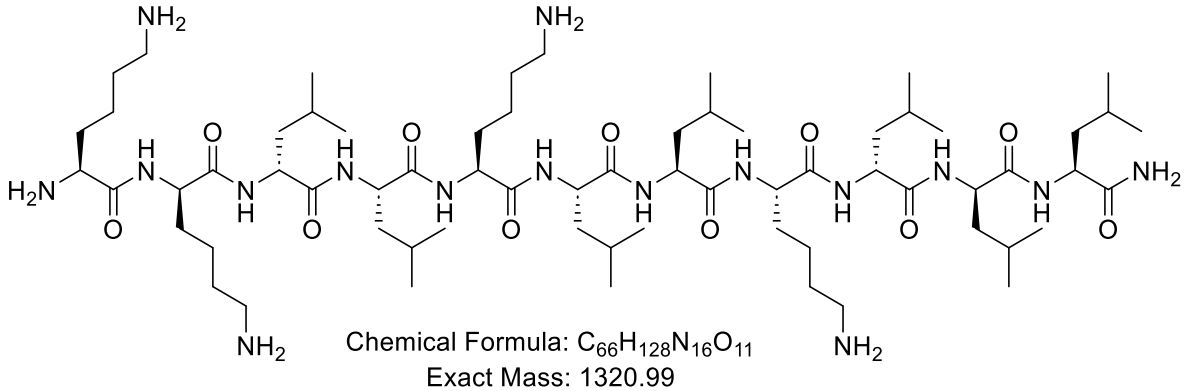

Analytical HPLC-MS data:

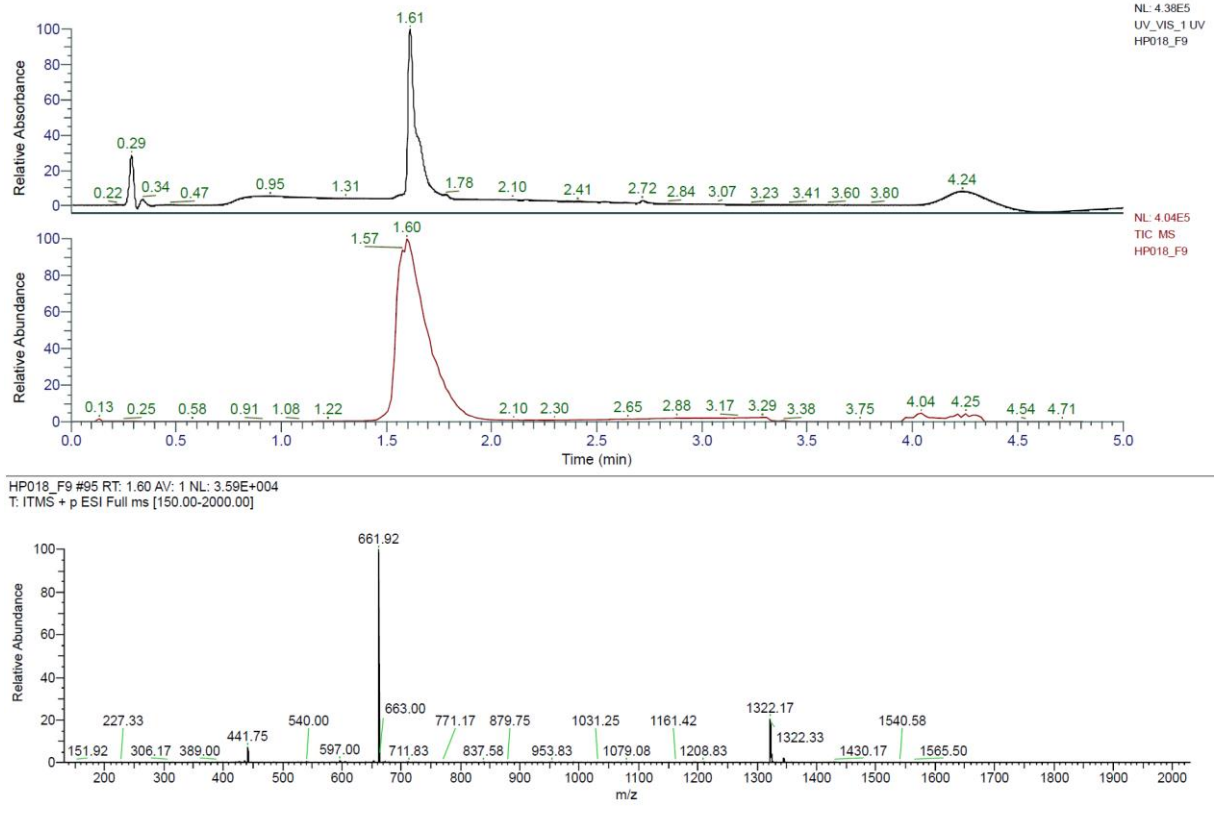

HRMS spectra:

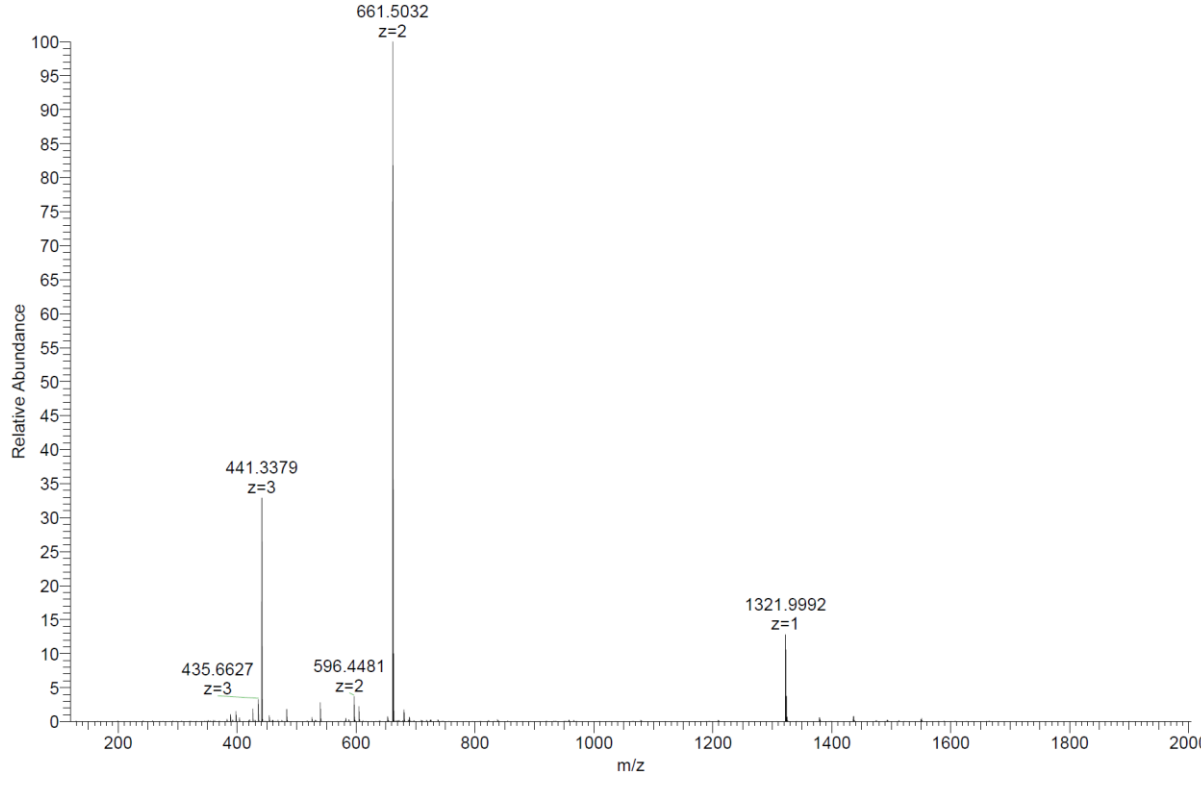

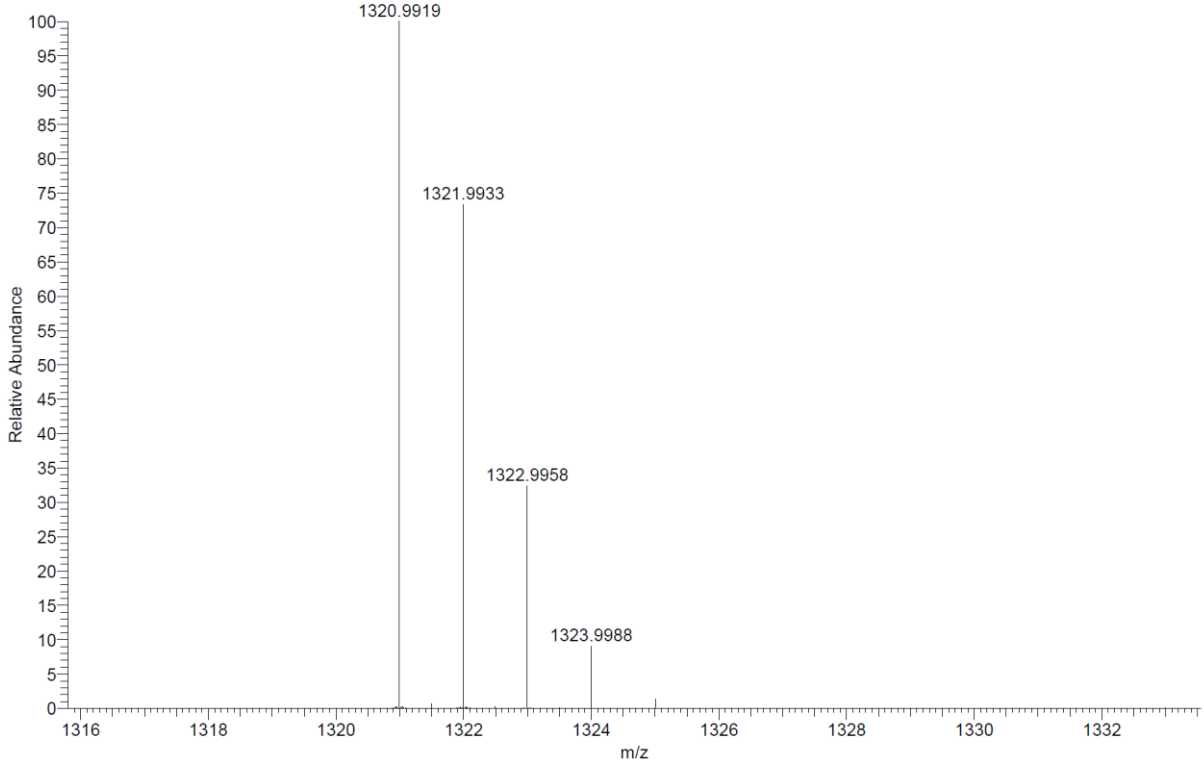

kkLLKLLKLll (HP18) was obtained as white solid after preparative RP-HPLC (36.3 mg, 32.7%). Analytical RP-HPLC: t_R = 1.58 min (A/D 100:0 to 0:100 in 3.5 min, λ = 214 nm). MS (ESI+): $C_{66}H_{128}N_{16}O_{11}$ calc./obs. 1320.99/1320.99 Da [M].

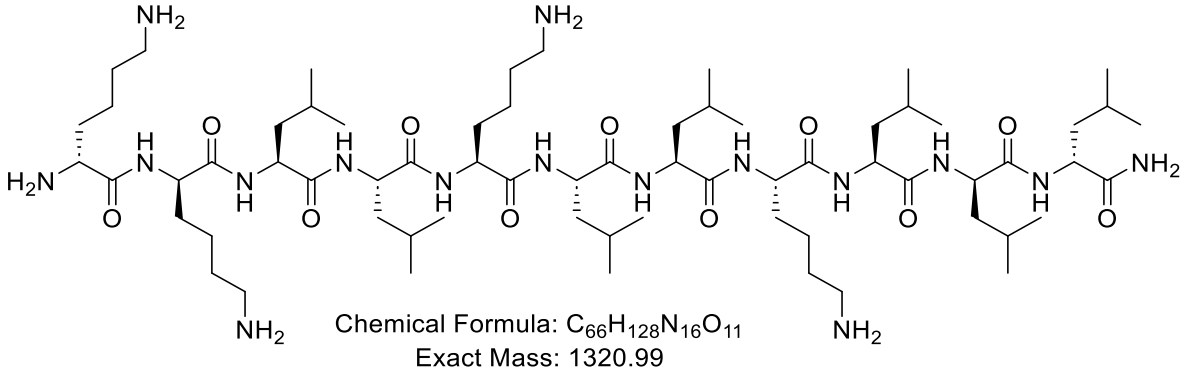

Analytical HPLC-MS data:

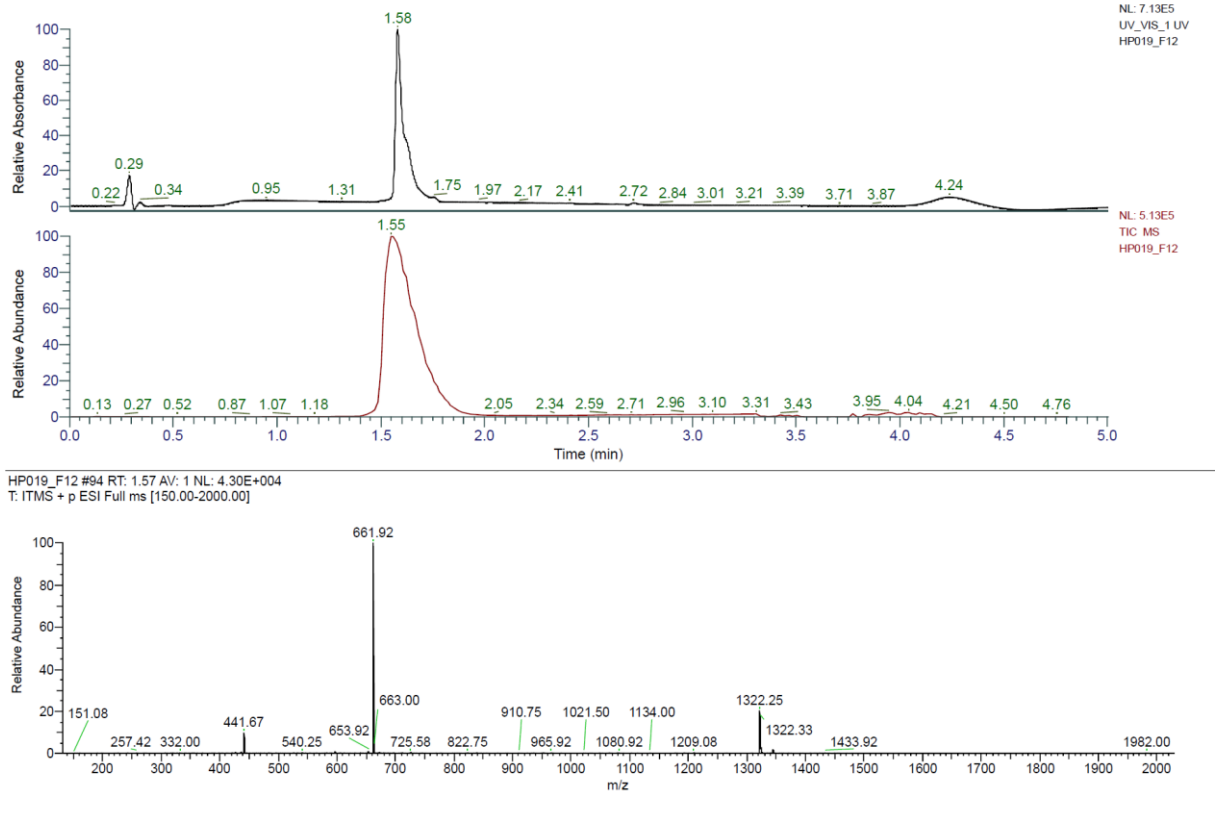

HRMS spectra:

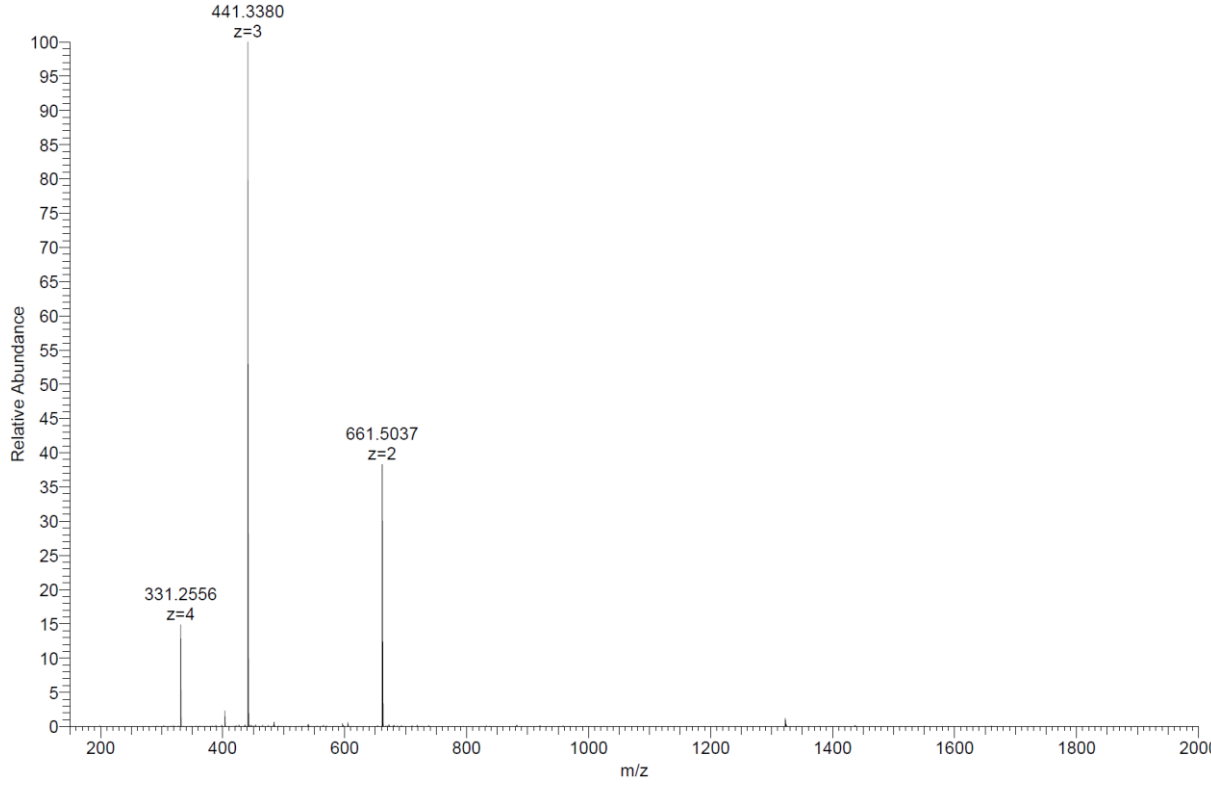

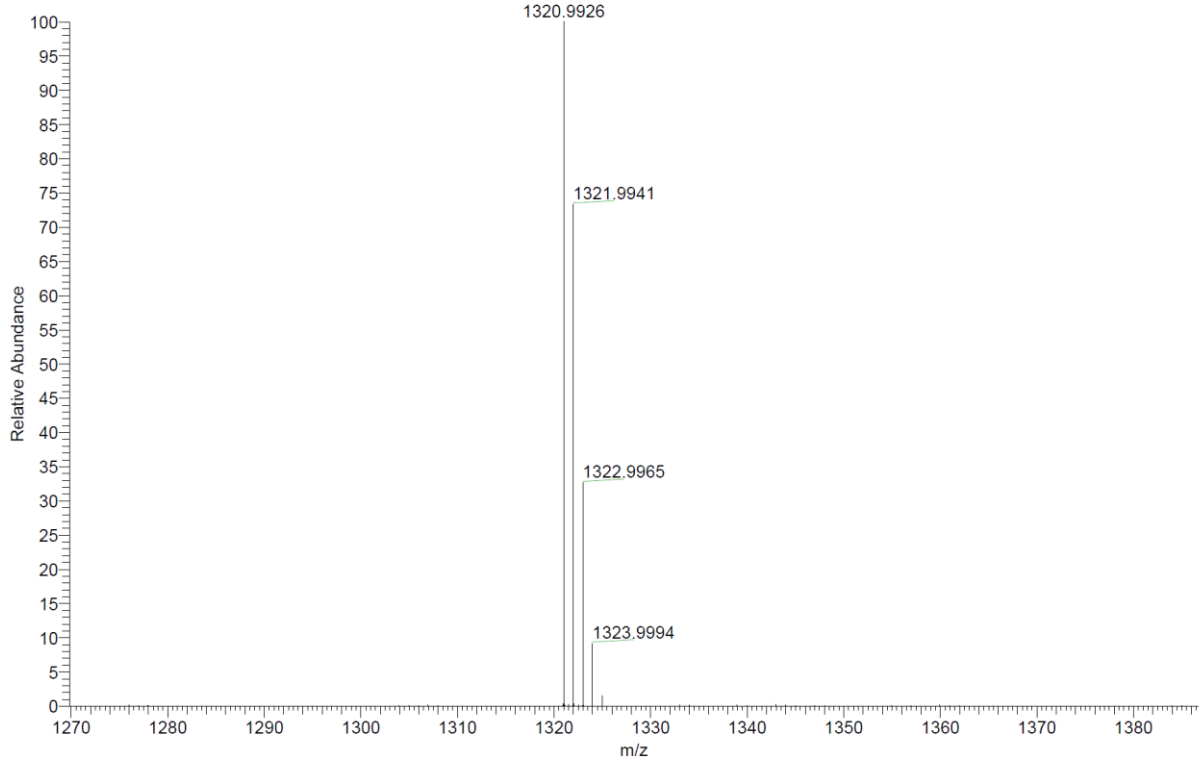

kkLLkLLKLLl (HP19) was obtained as white solid after preparative RP-HPLC (53.0 mg, 47.7%). Analytical RP-HPLC: t_R = 1.56 min (A/D 100:0 to 0:100 in 3.5 min, λ = 214 nm). MS (ESI+): $C_{66}H_{128}N_{16}O_{11}$ calc./obs. 1321.99/1322.00 Da $[M+H]^+$.

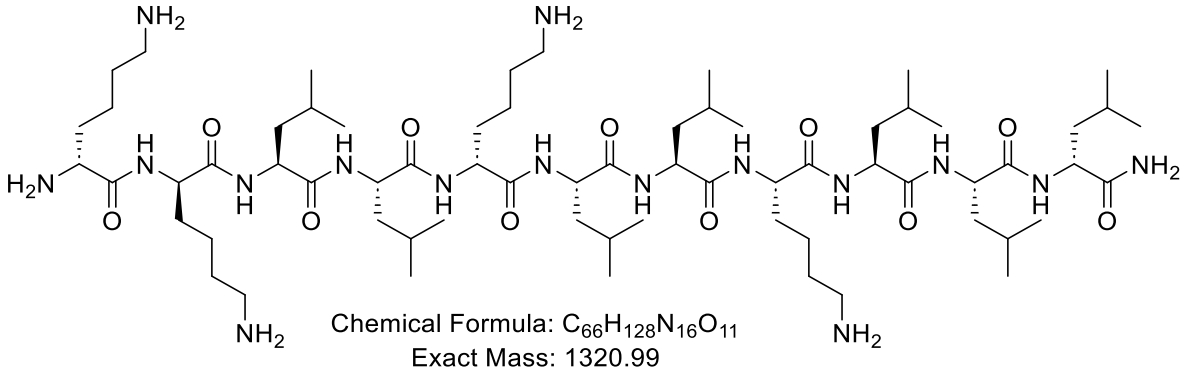

Analytical HPLC-MS data:

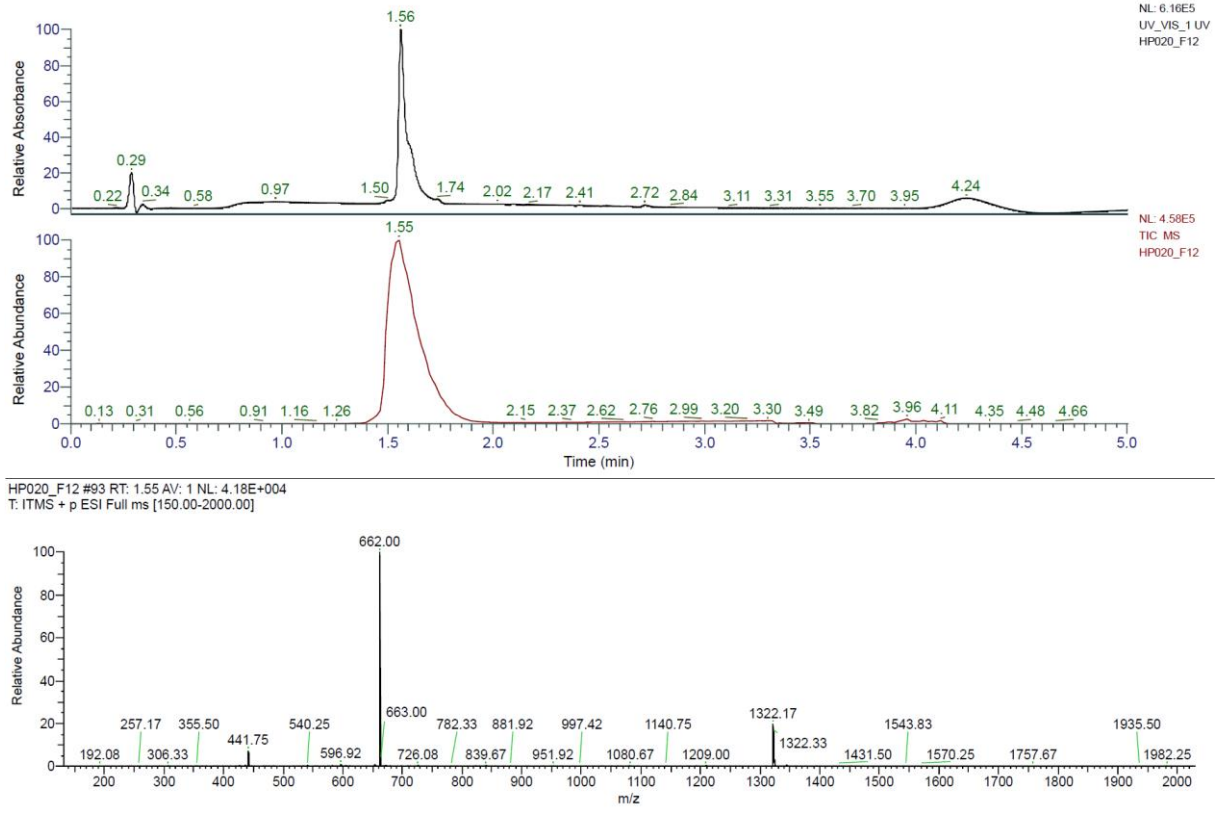

HRMS spectra:

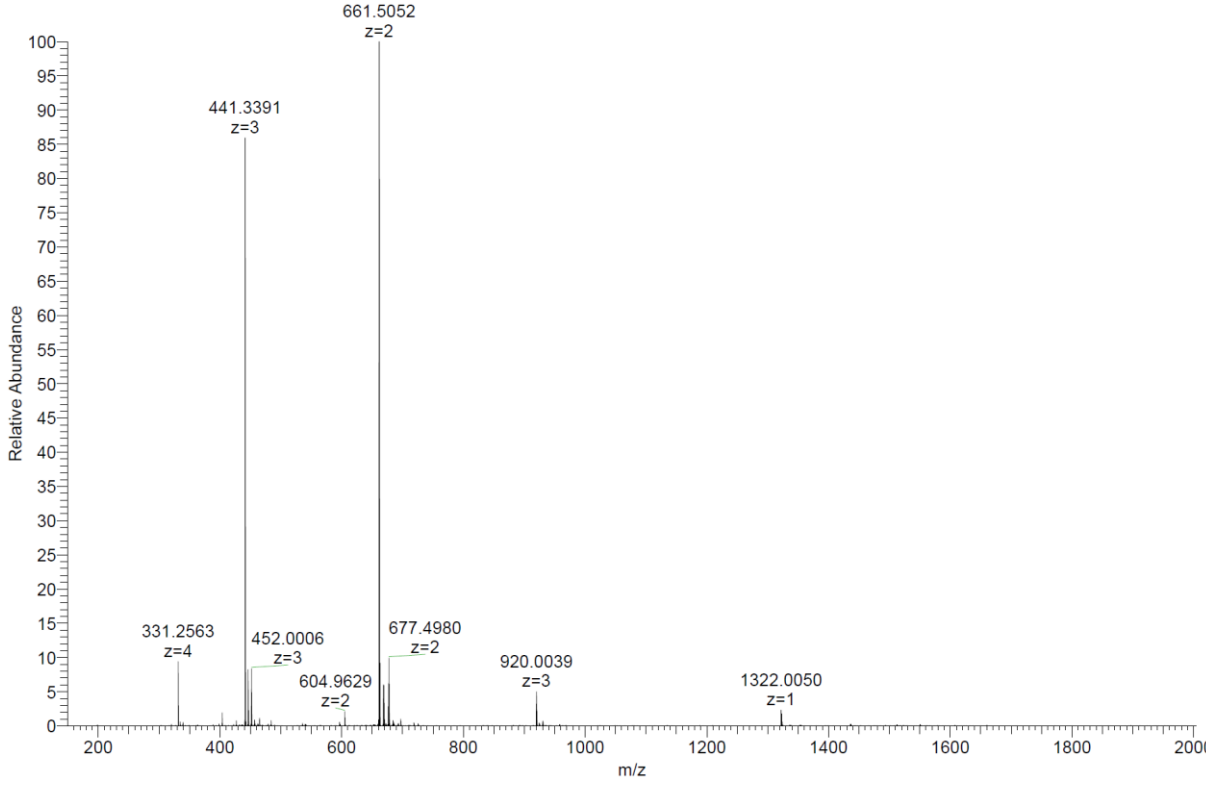

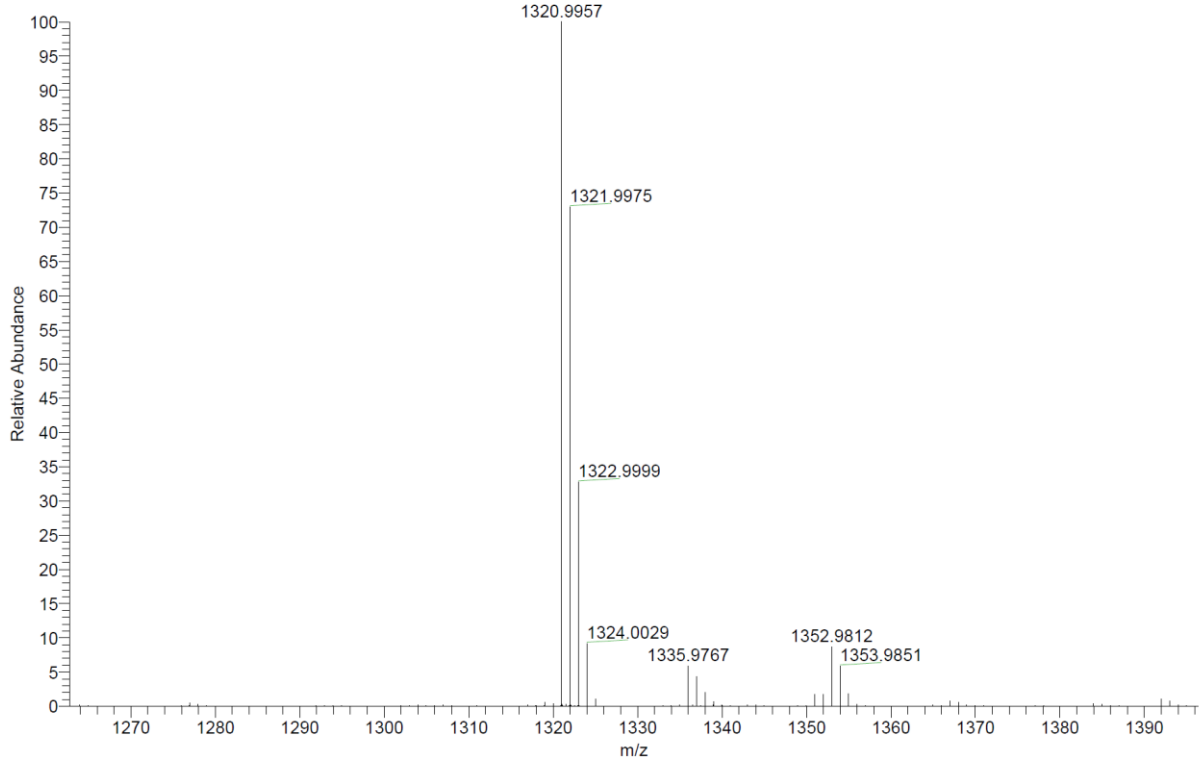

KKllKLLklLL (HP20) was obtained as white solid after preparative RP-HPLC (51.4 mg, 46.3%). Analytical RP-HPLC: t_R = 1.52 min (A/D 100:0 to 0:100 in 3.5 min, λ = 214 nm). MS (ESI+): $C_{66}H_{128}N_{16}O_{11}$ calc./obs. 1321.99/1322.00 Da $[M+H]^+$.

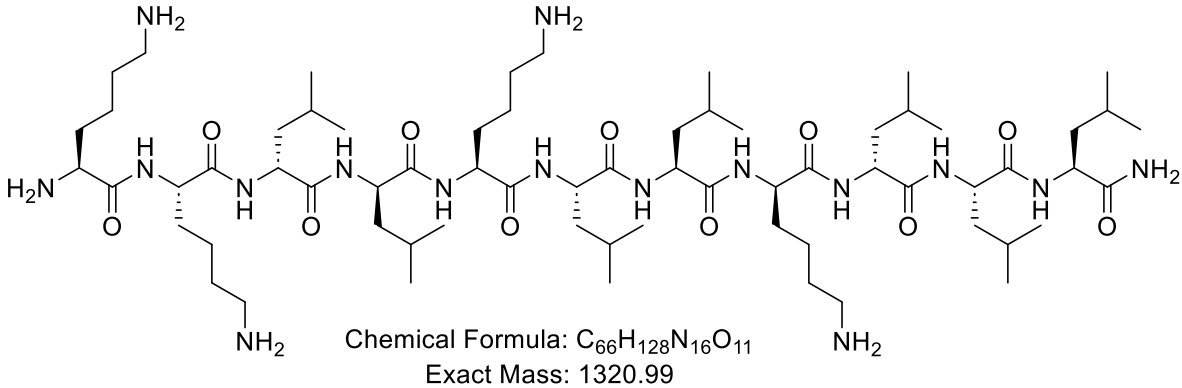

Analytical HPLC-MS data:

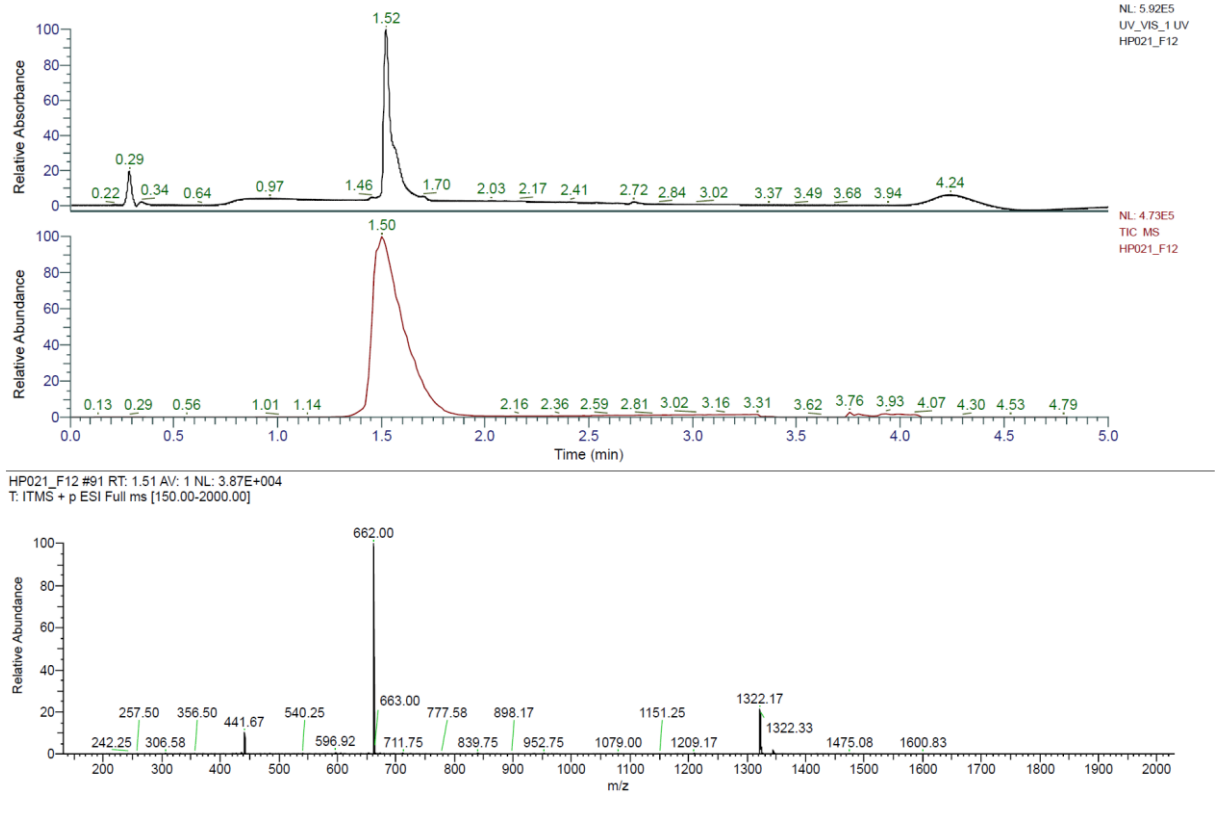

HRMS spectra:

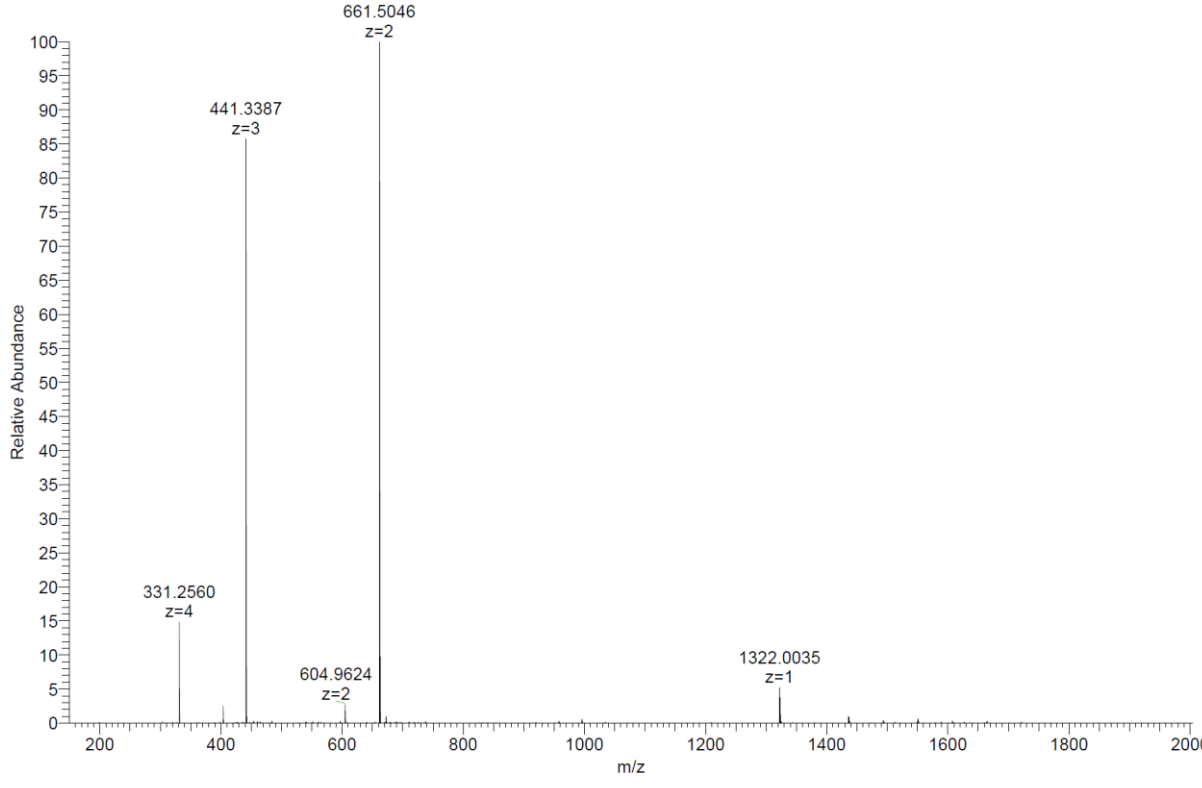

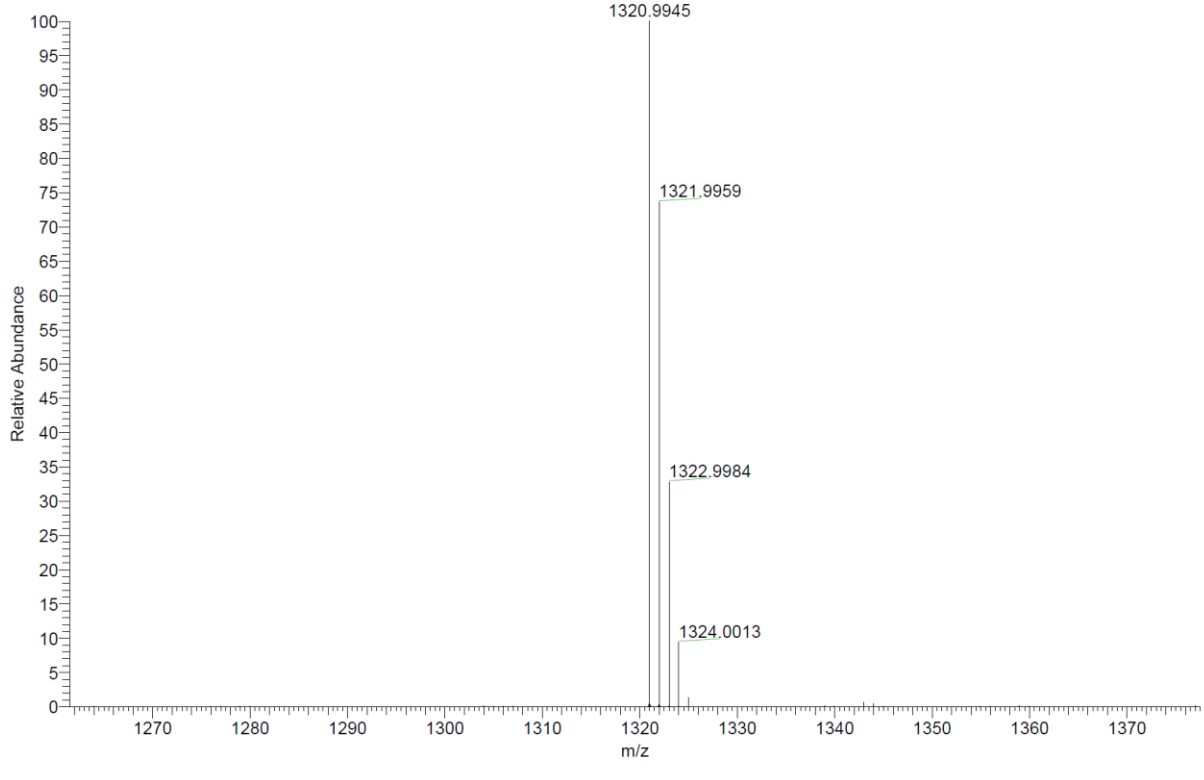

KklLKlLKlLL (HP21) was obtained as white solid after preparative RP-HPLC (64.2 mg, 65.7%). Analytical RP-HPLC: t_R = 1.60 min (A/D 100:0 to 0:100 in 3.5 min, λ = 214 nm). MS (ESI+): $C_{66}H_{128}N_{16}O_{11}$ calc./obs. 1321.99/1322.00 Da $[M+H]^+$.

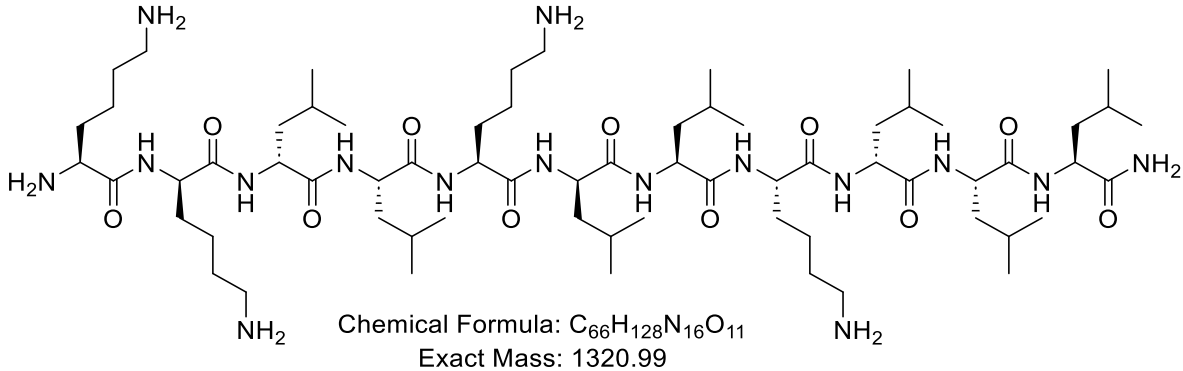

Analytical HPLC-MS data:

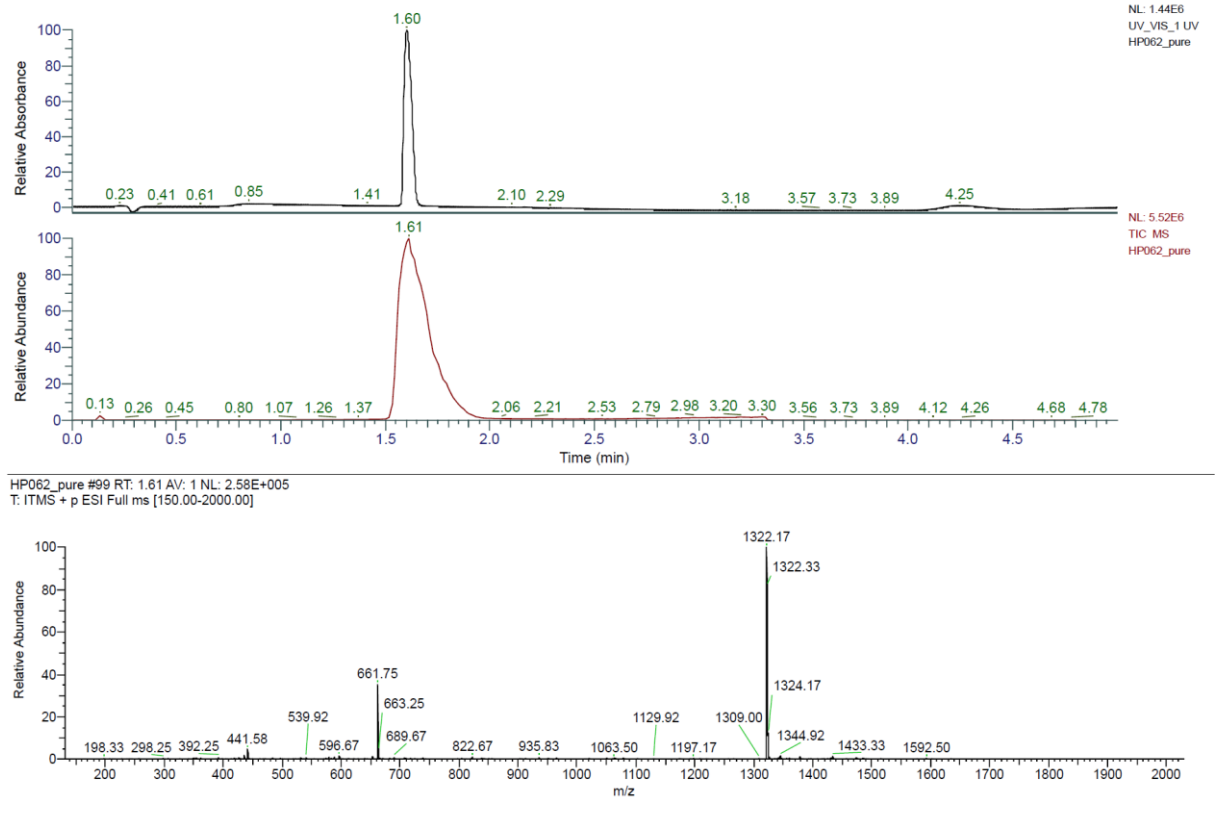

HRMS spectra:

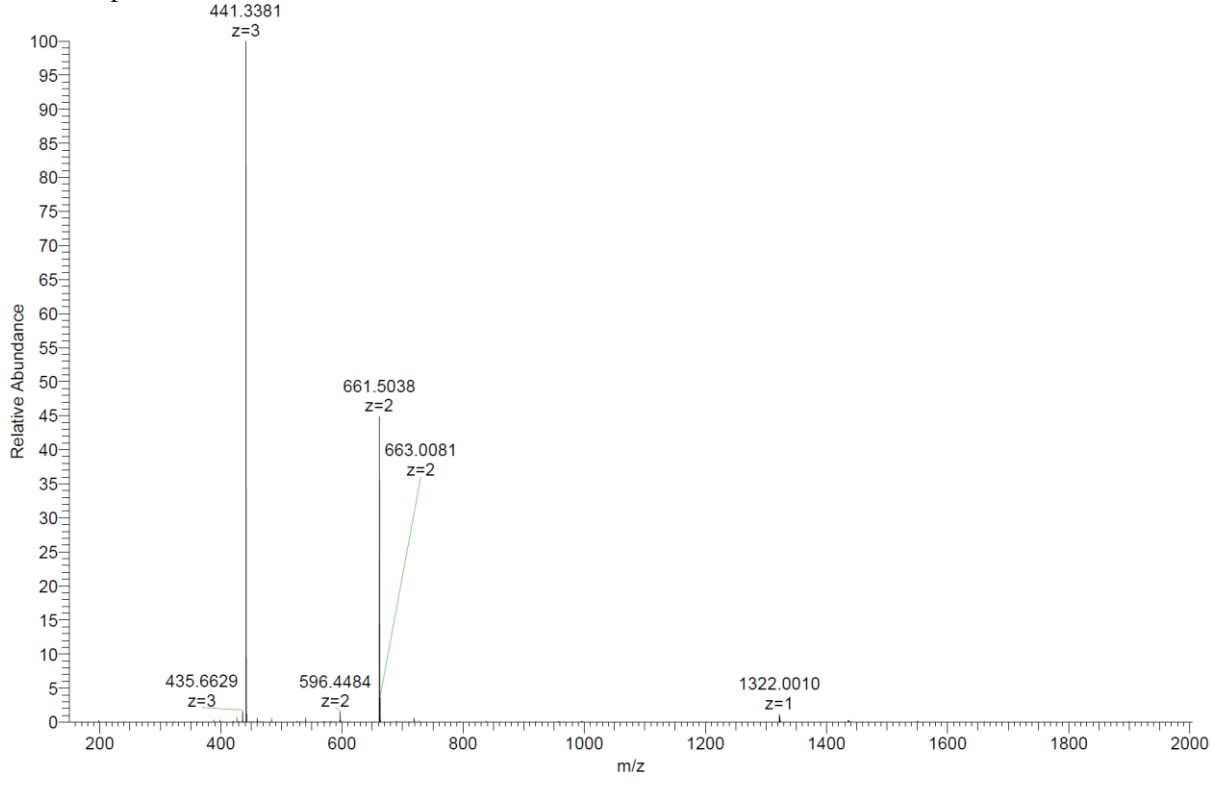

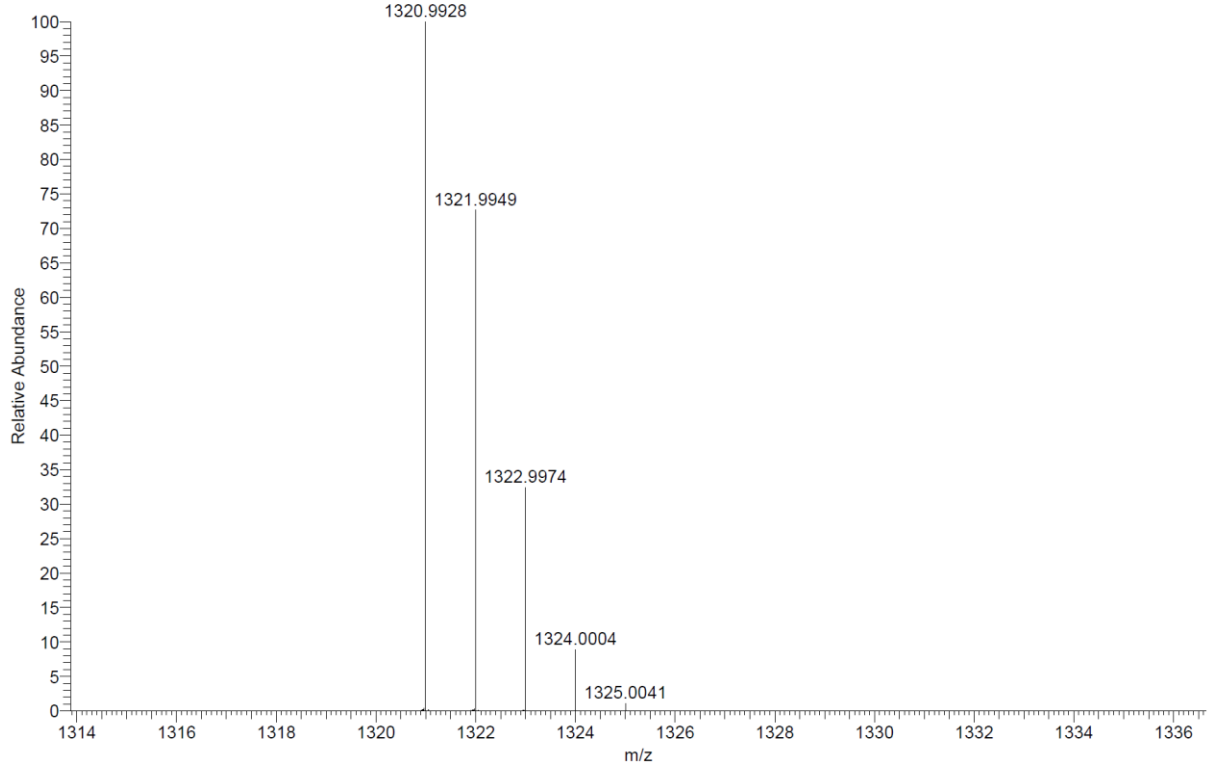

KKllKLlKLlL (HP22) was obtained as white solid after preparative RP-HPLC (45.9 mg, 46.9%). Analytical RP-HPLC: t_R = 1.55 min (A/D 100:0 to 0:100 in 3.5 min, λ = 214 nm). MS (ESI+): $C_{66}H_{128}N_{16}O_{11}$ calc./obs. 1321.99/1322.00 Da $[M+H]^+$.

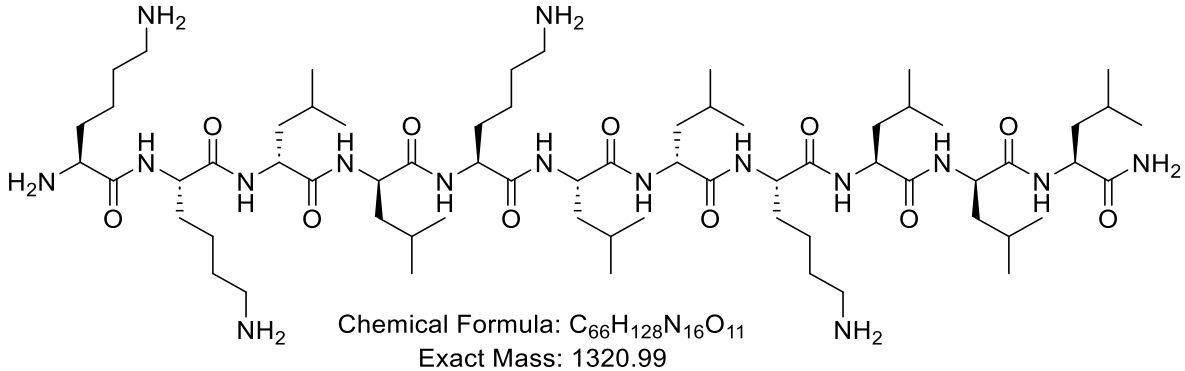

Analytical HPLC-MS data:

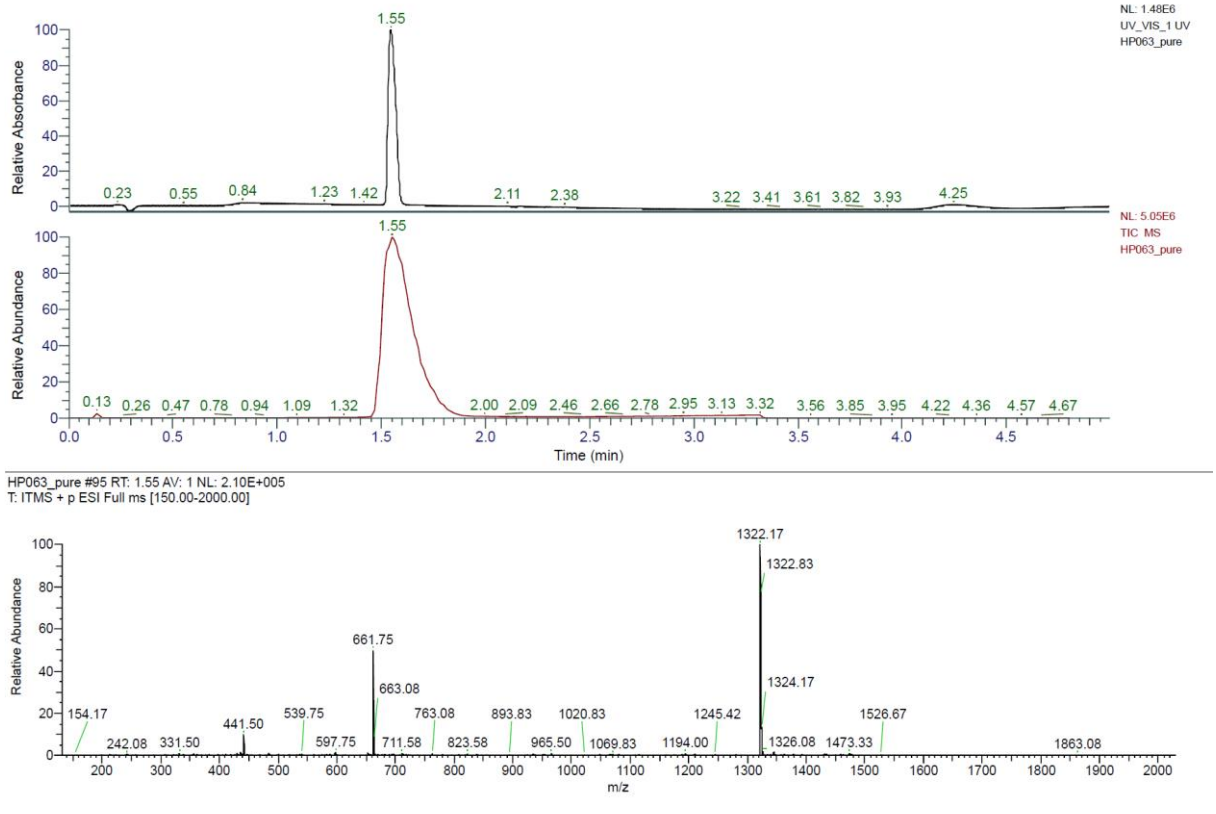

HRMS spectra:

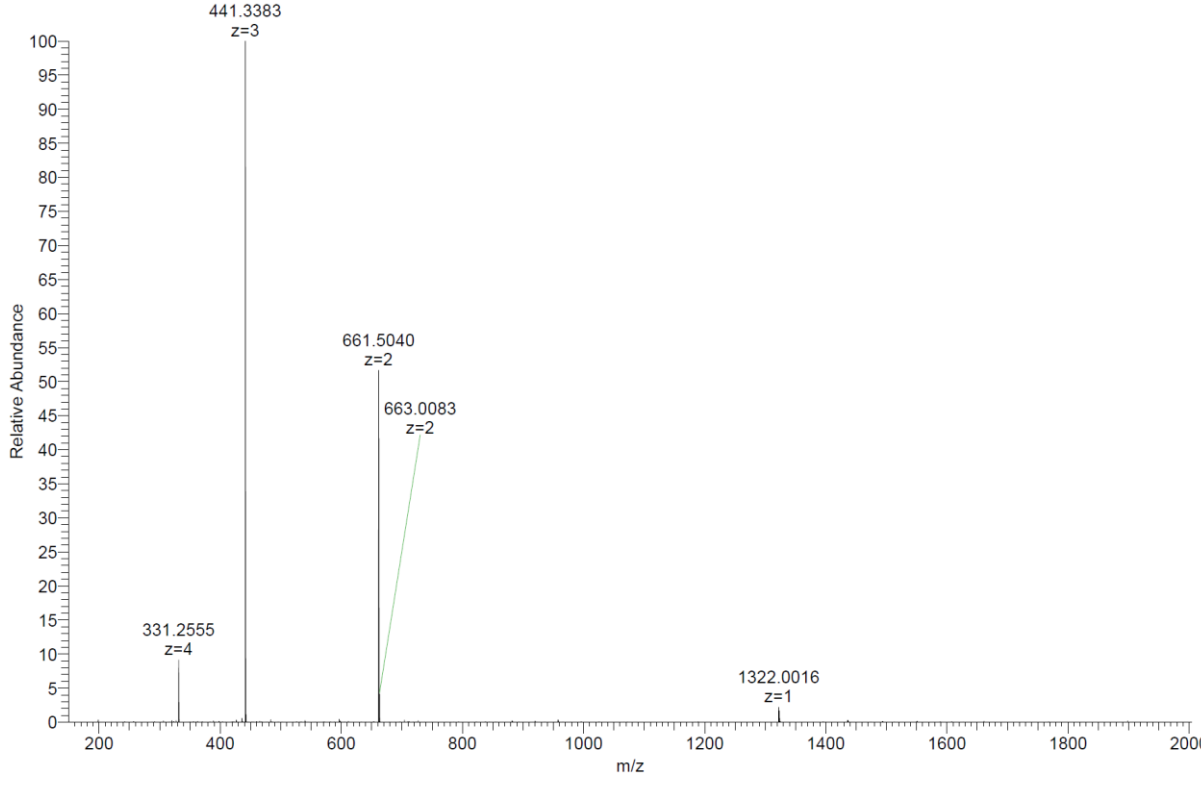

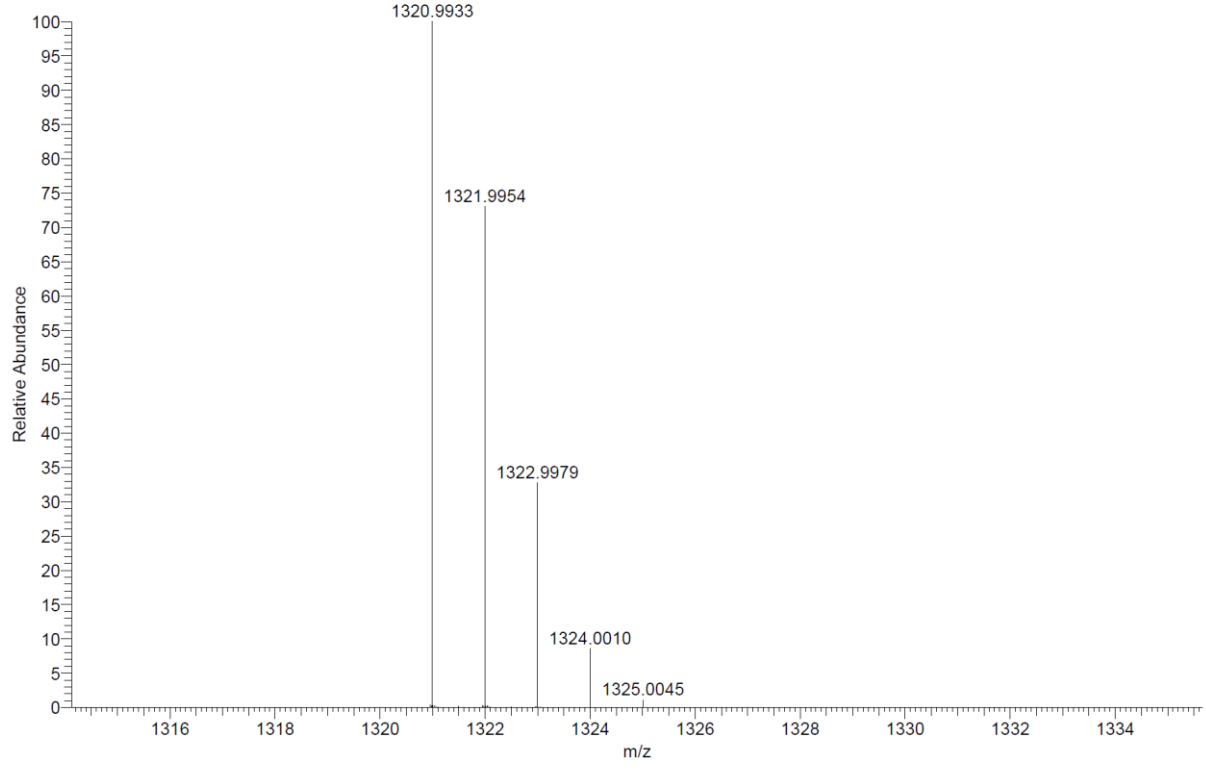

KKLlkLLkLLl (HP23) was obtained as white solid after preparative RP-HPLC (64.7 mg, 66.2%). Analytical RP-HPLC: t_R = 1.56 min (A/D 100:0 to 0:100 in 3.5 min, λ = 214 nm). MS (ESI+): $C_{66}H_{128}N_{16}O_{11}$ calc./obs. 1321.99/1322.00 Da $[M+H]^+$.

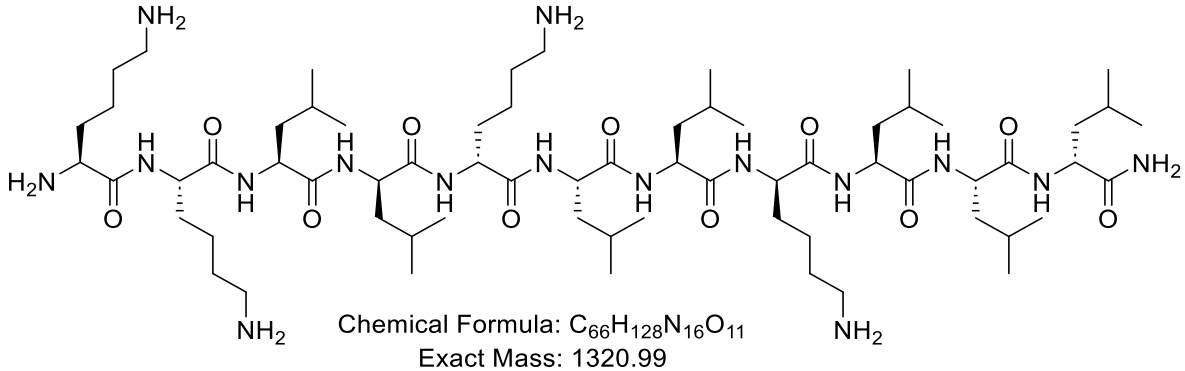

Analytical HPLC-MS data:

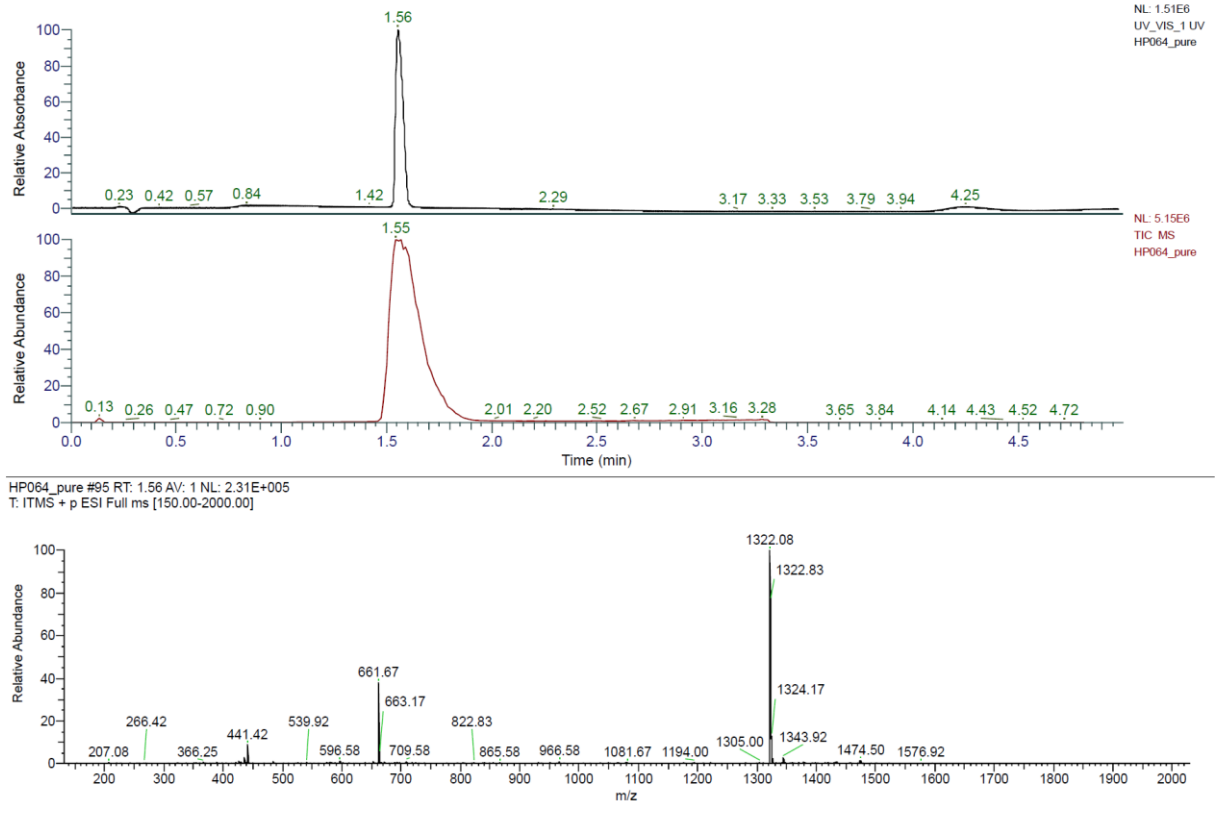

HRMS spectra:

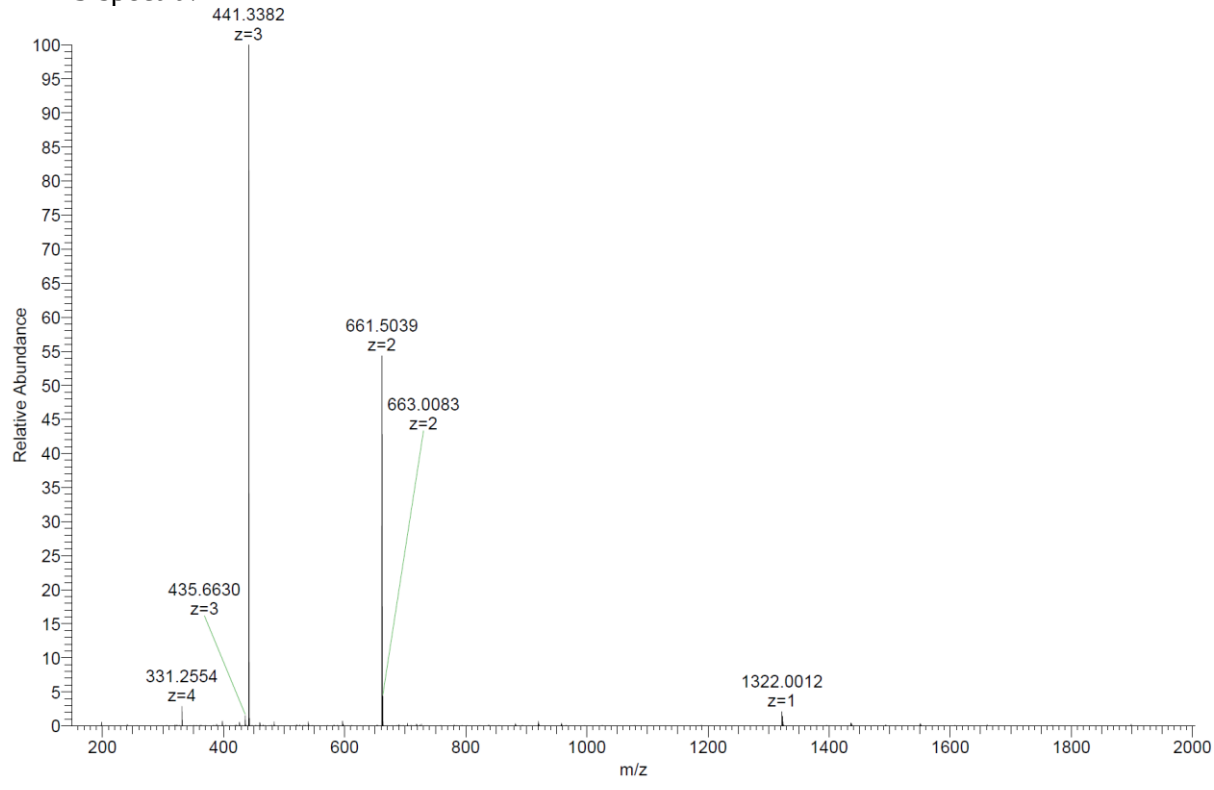

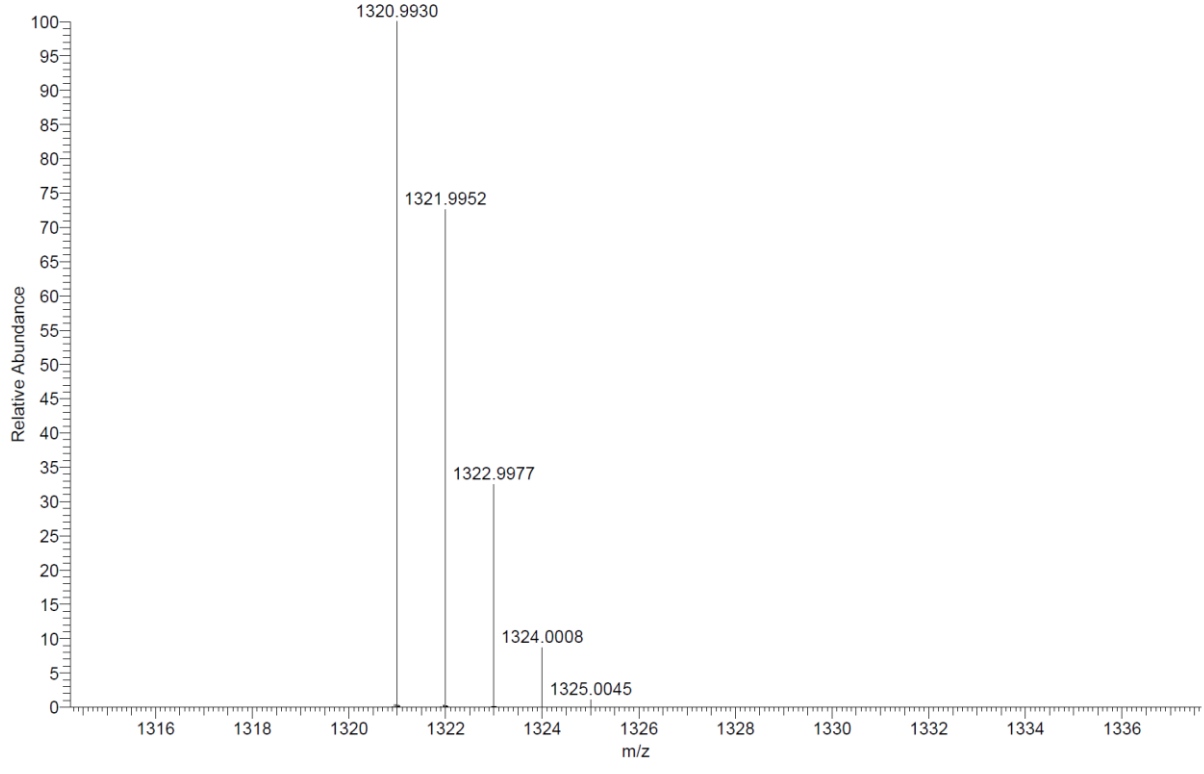

KkLlKllKLLL (HP24) was obtained as white solid after preparative RP-HPLC (54.7 mg, 49.2%). Analytical RP-HPLC: t_R = 1.56 min (A/D 100:0 to 0:100 in 3.5 min, λ = 214 nm). MS (ESI+): $C_{66}H_{128}N_{16}O_{11}$ calc./obs. 1321.99/1322.00 Da $[M+H]^+$.

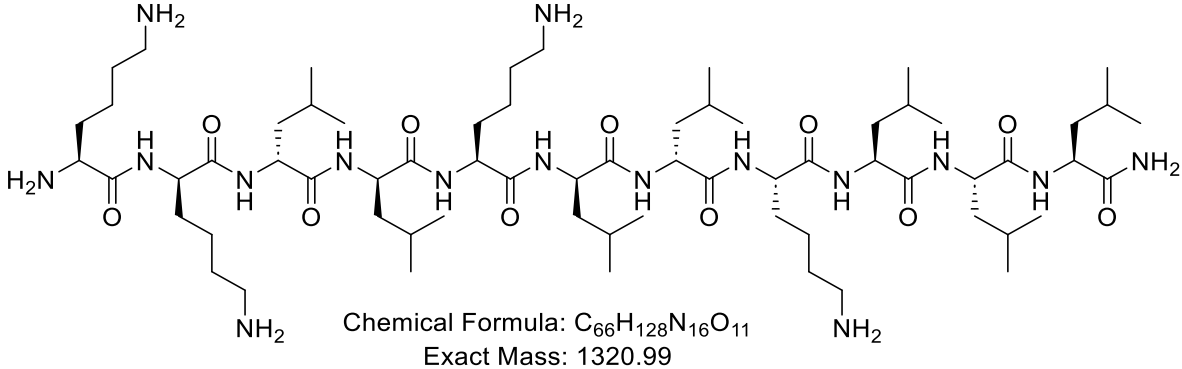

Analytical HPLC-MS data:

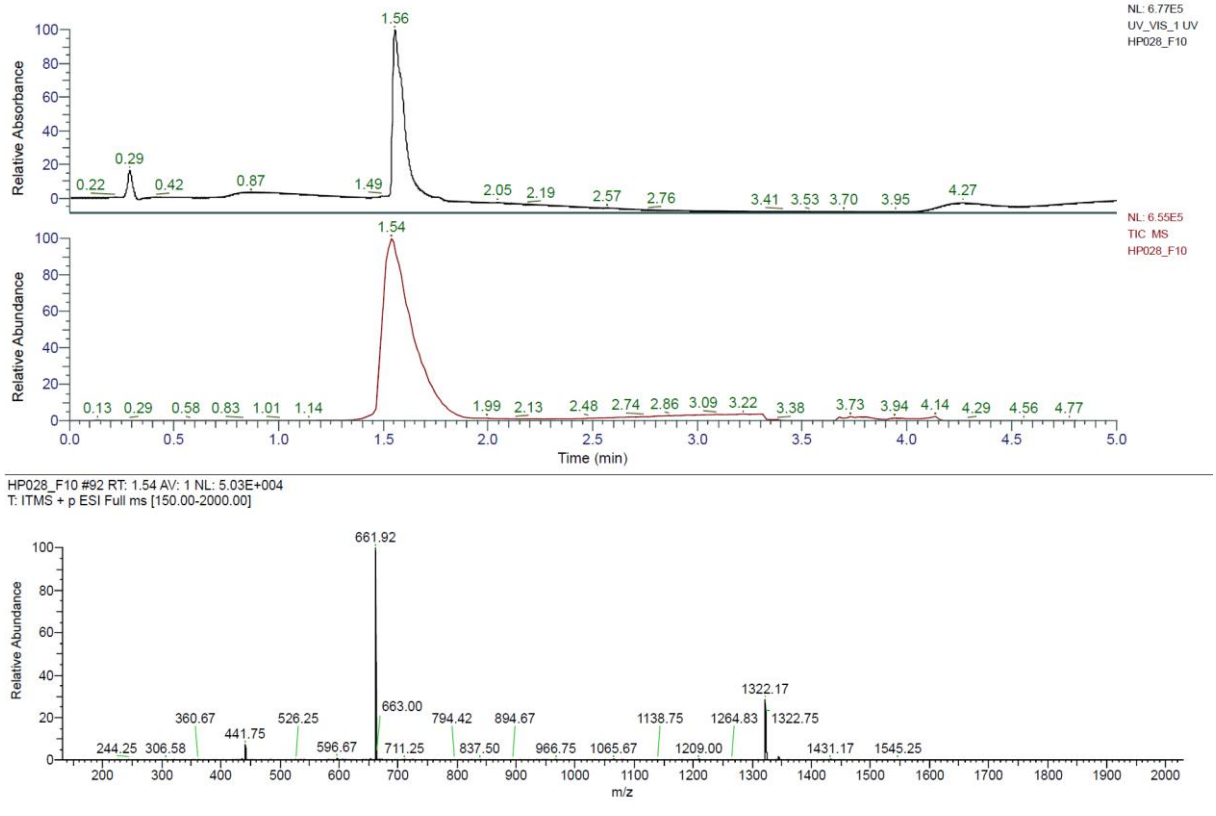

HRMS spectra:

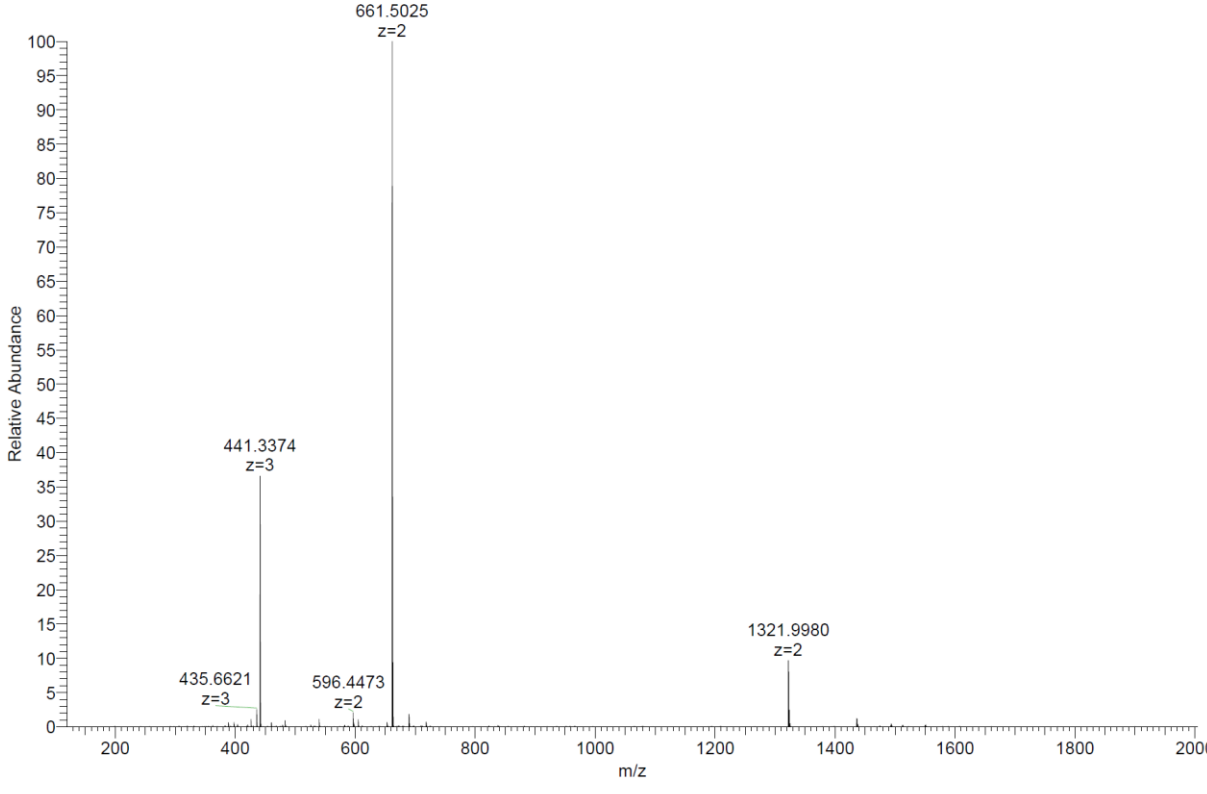

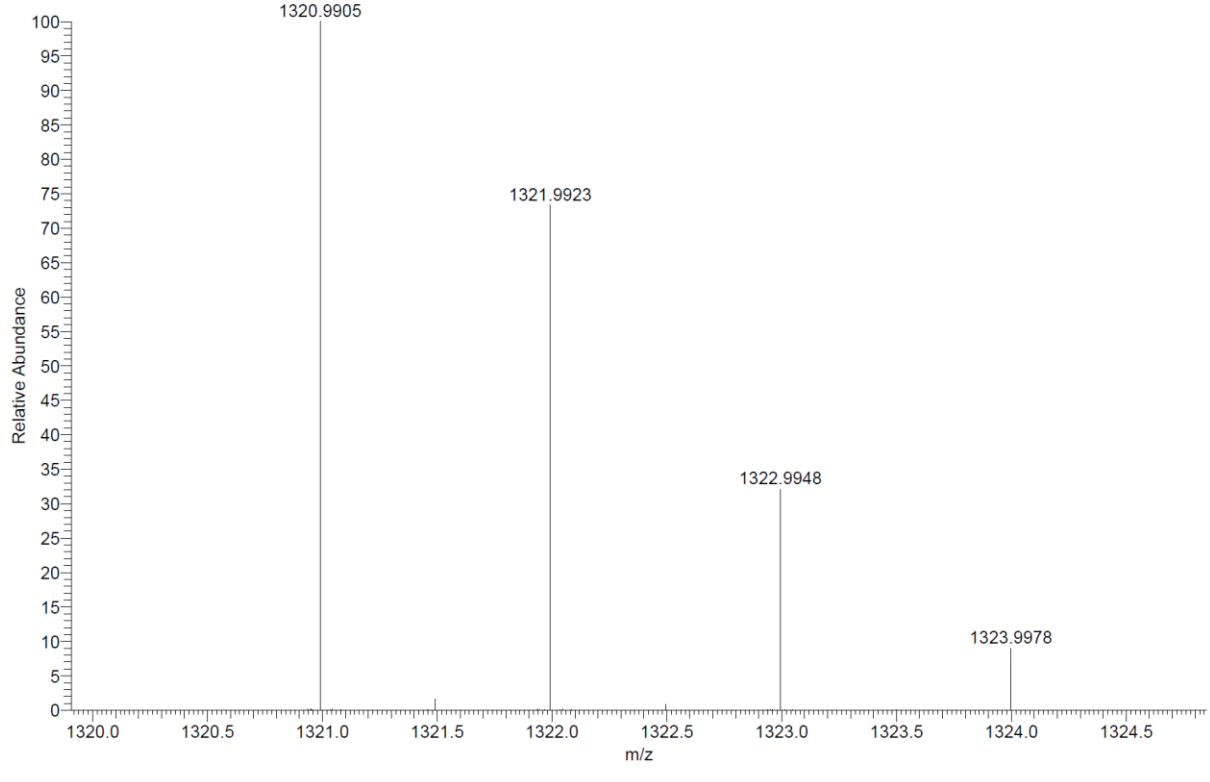

KKllKllKlLL (HP25) was obtained as white solid after preparative RP-HPLC (38.8 mg, 34.9%). Analytical RP-HPLC: t_R = 1.55 min (A/D 100:0 to 0:100 in 3.5 min, λ = 214 nm). MS (ESI+): $C_{66}H_{128}N_{16}O_{11}$ calc./obs. 1321.99/1322.00 Da $[M+H]^+$.

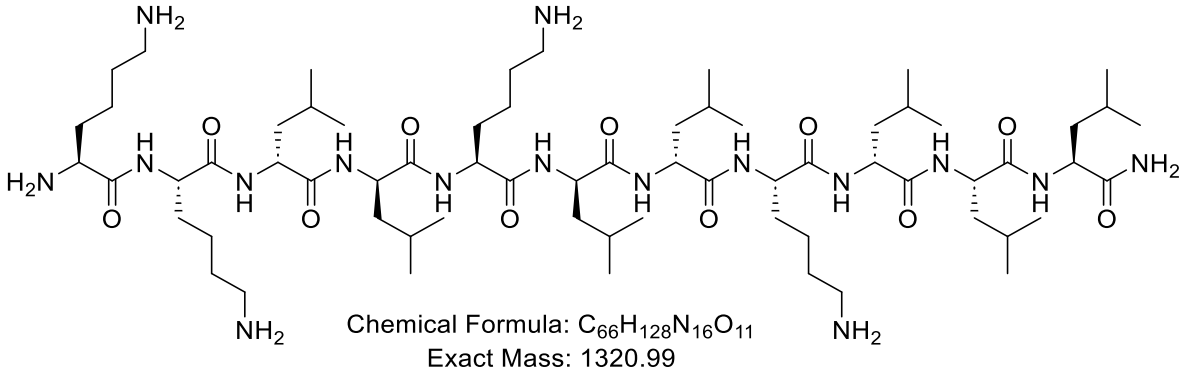

Analytical HPLC-MS data:

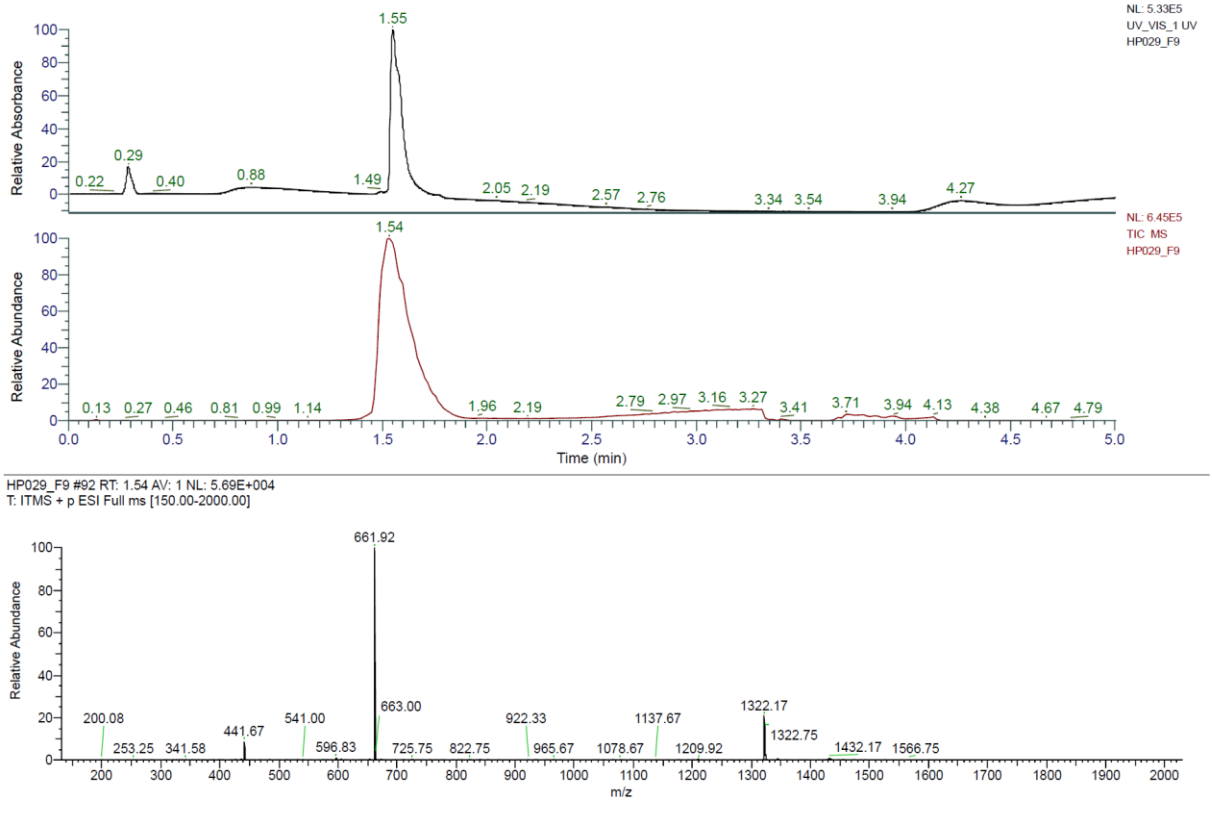

HRMS spectra:

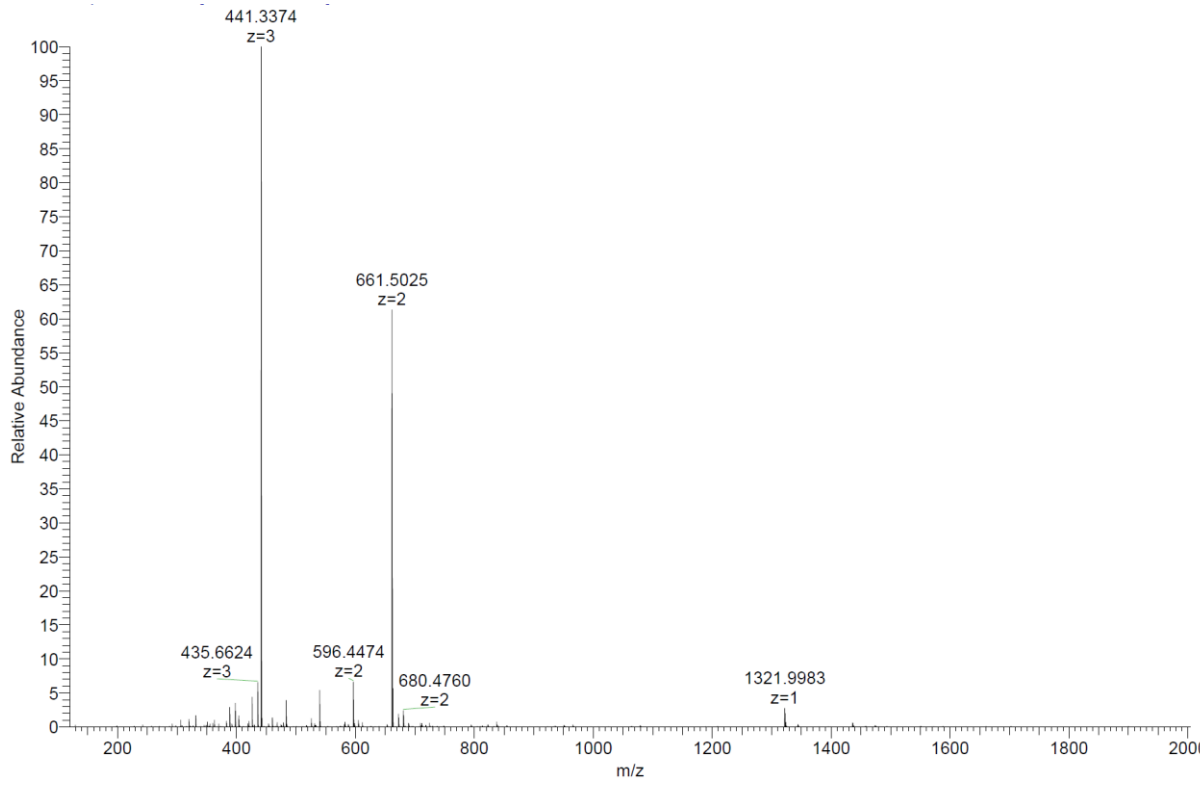

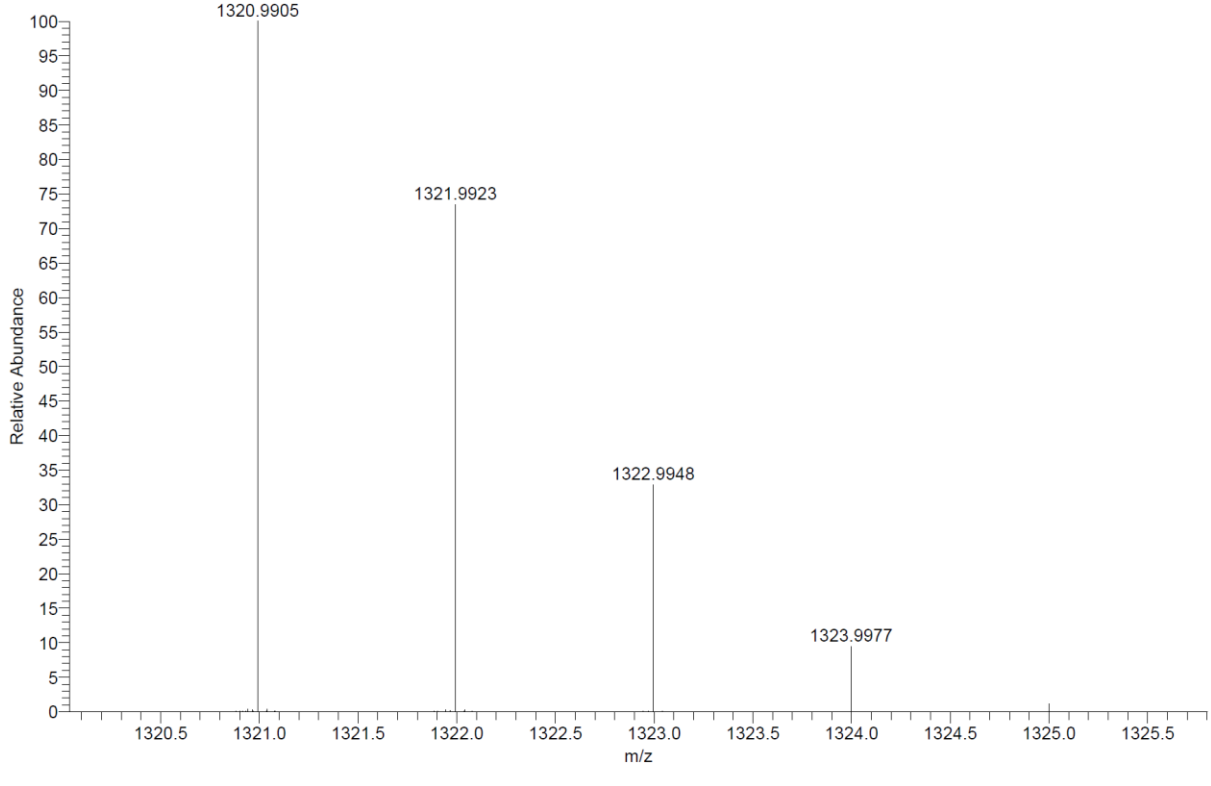

kkLLkLLKLll (HP26) was obtained as white solid after preparative RP-HPLC (52.6 mg, 47.3%). Analytical RP-HPLC: t_R = 1.57 min (A/D 100:0 to 0:100 in 3.5 min, λ = 214 nm). MS (ESI+): $C_{66}H_{128}N_{16}O_{11}$ calc./obs. 1321.99/1322.00 Da $[M+H]^+$.

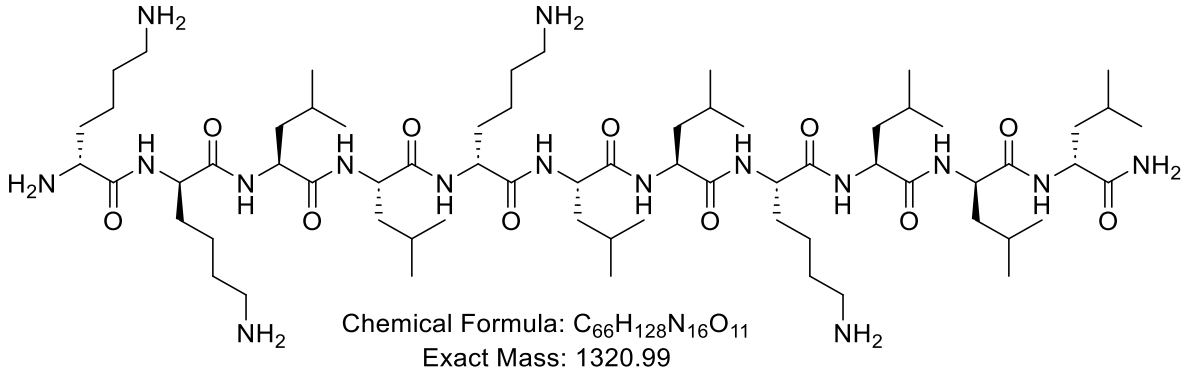

Analytical HPLC-MS data:

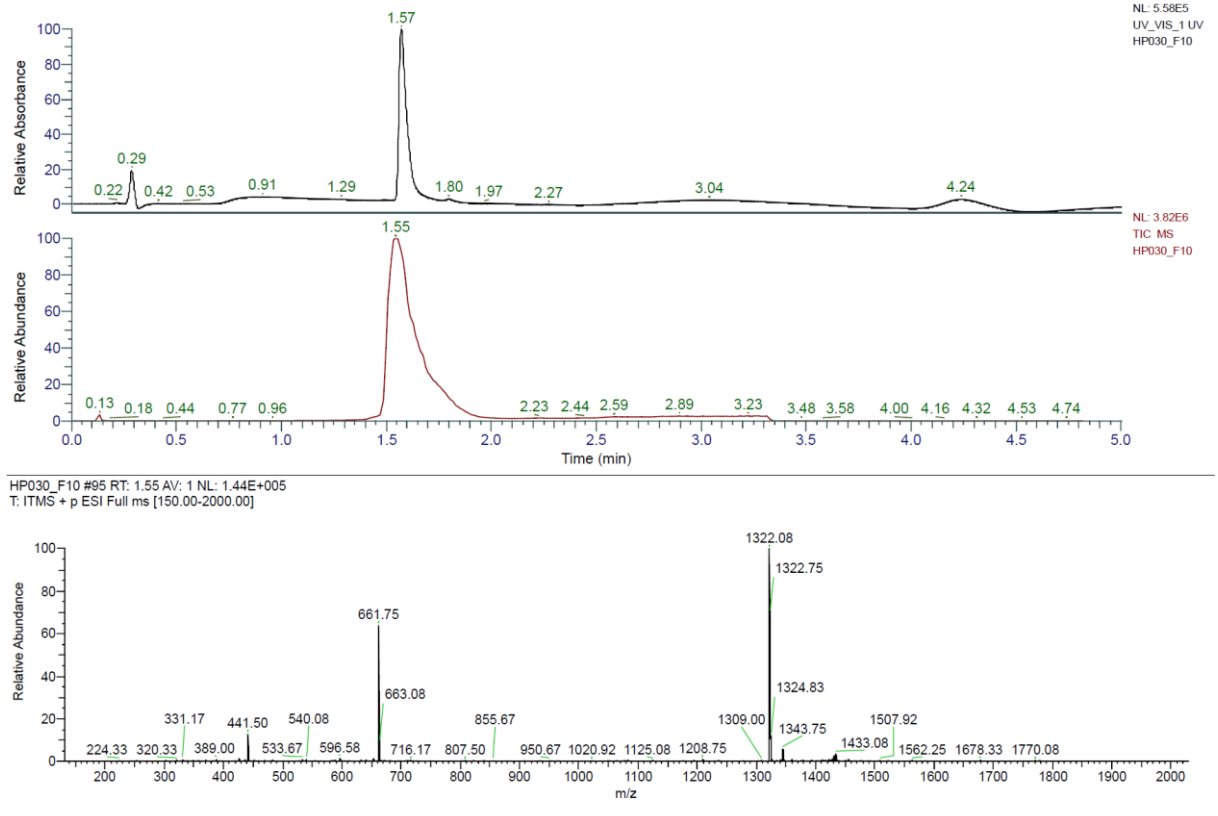

HRMS spectra:

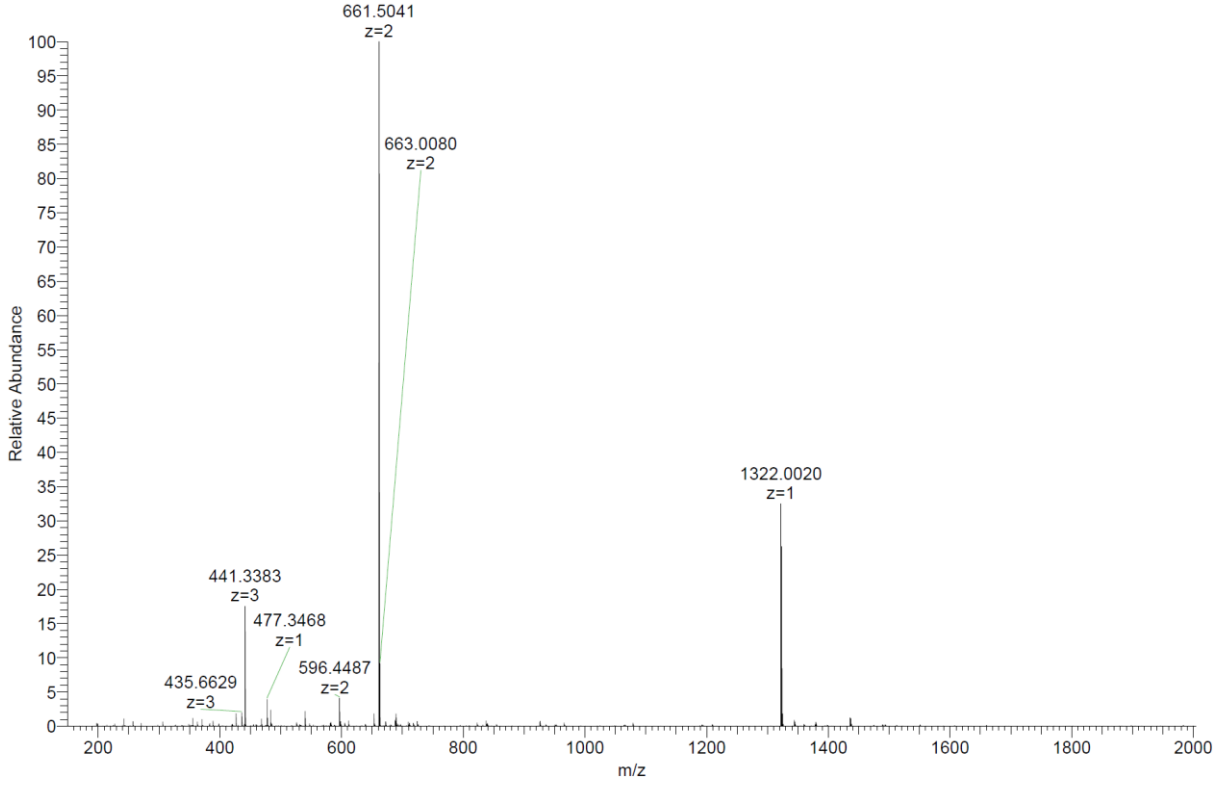

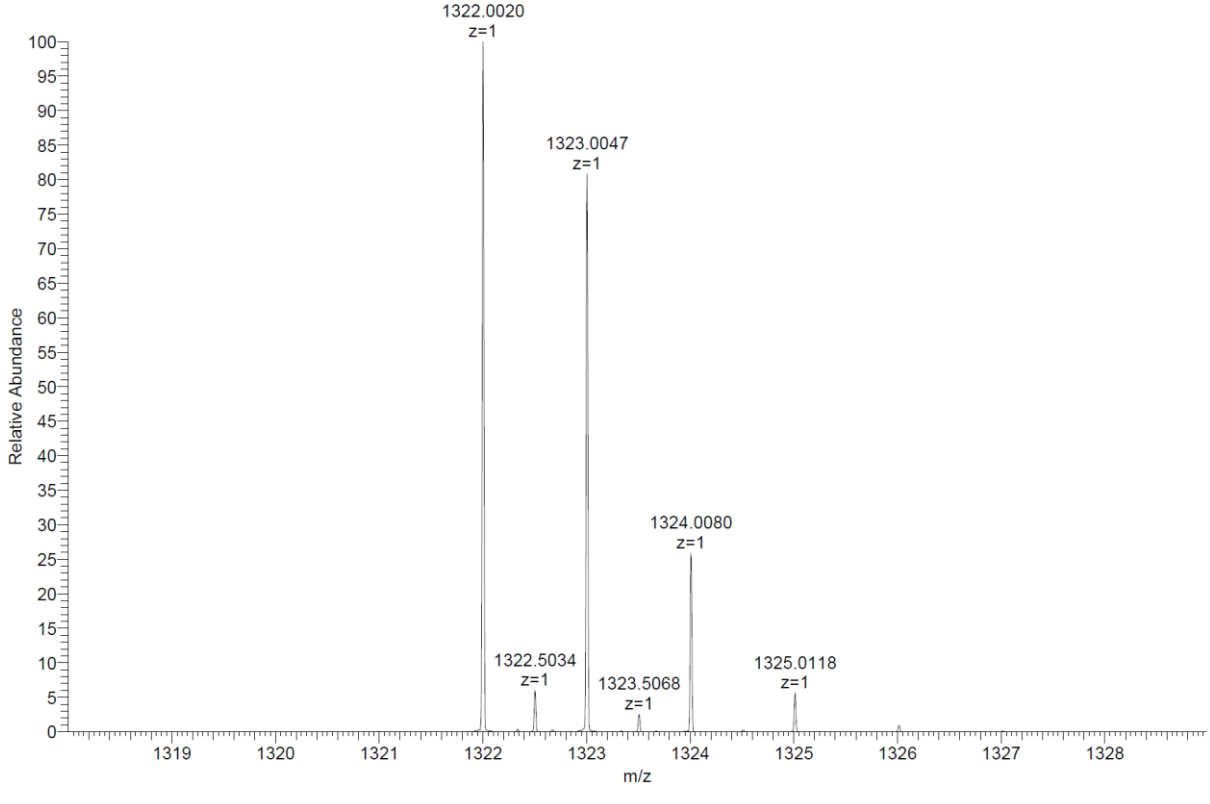

kkLLkLLkLLl (HP27) was obtained as white solid after preparative RP-HPLC (53.7 mg, 48.3%). Analytical RP-HPLC: t_R = 1.54 min (A/D 100:0 to 0:100 in 3.5 min, λ = 214 nm). MS (ESI+): $C_{66}H_{128}N_{16}O_{11}$ calc./obs. 1321.99/1322.00 Da $[M+H]^+$.

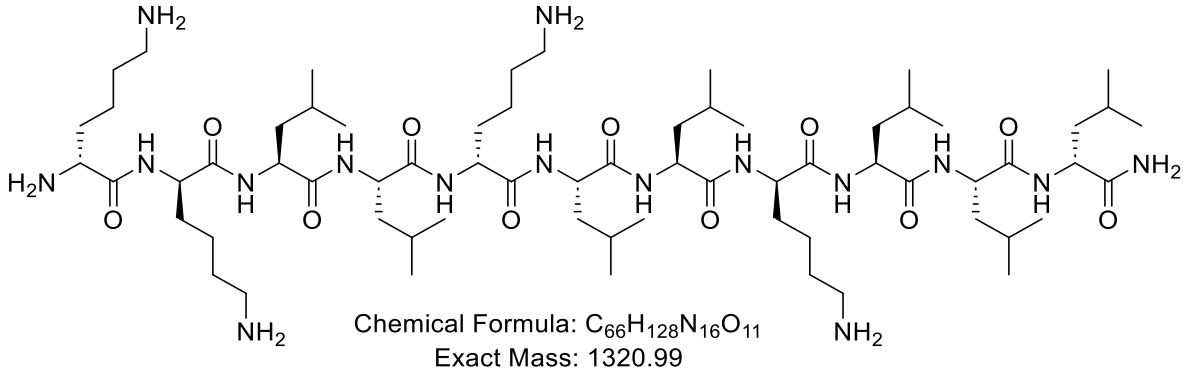

Analytical HPLC-MS data:

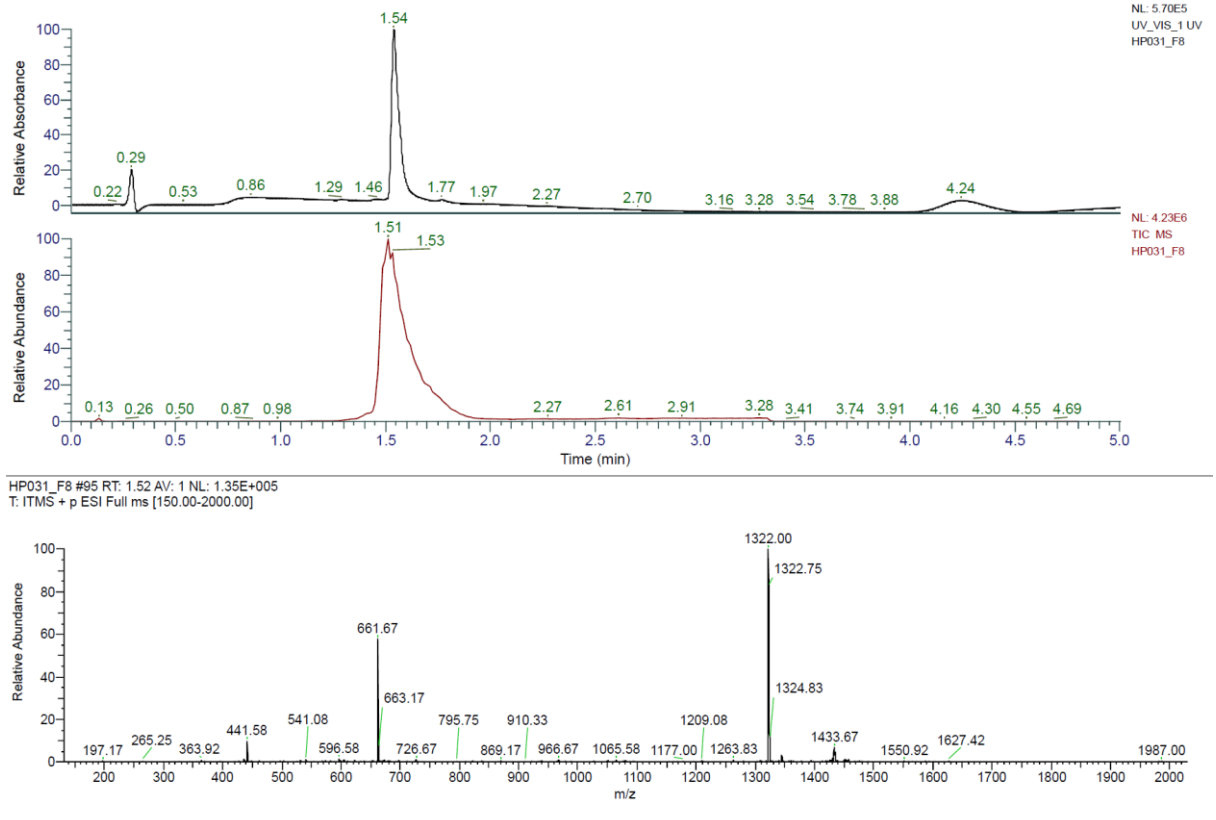

HRMS spectra:

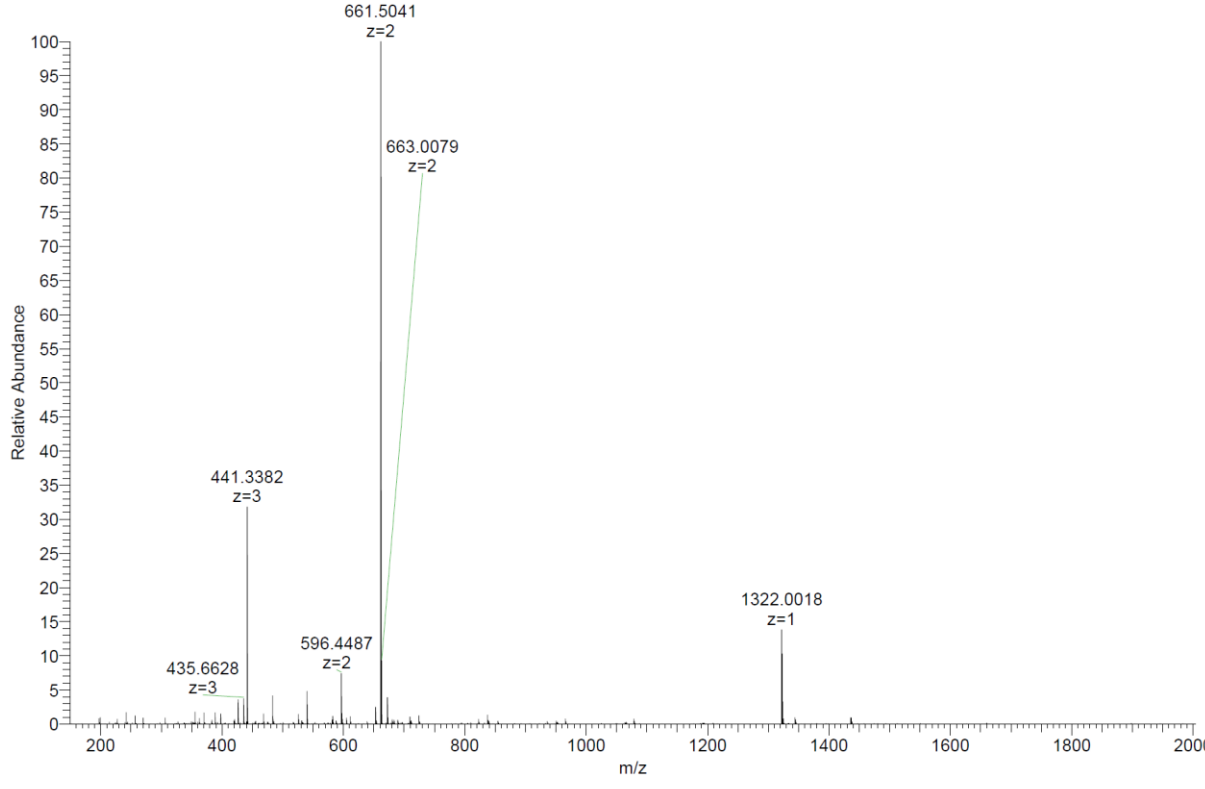

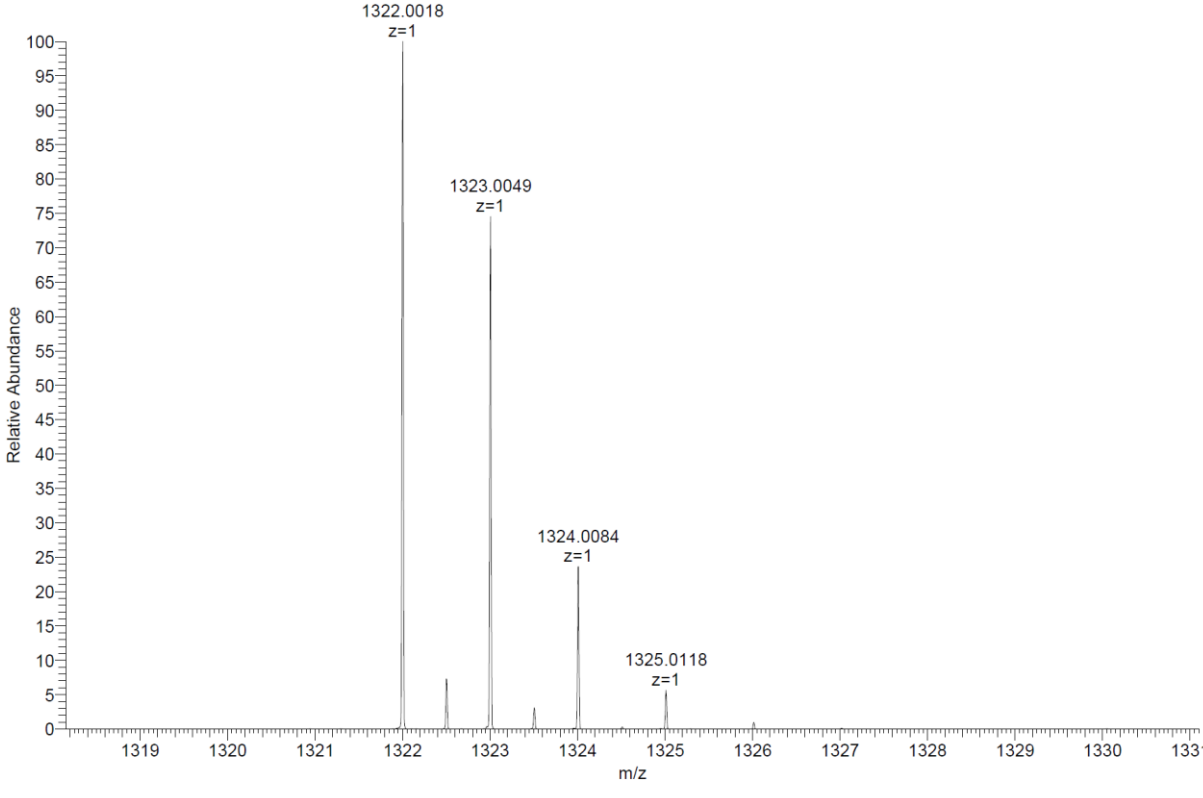

kKLLkllKLLl (HP28) was obtained as white solid after preparative RP-HPLC (45.6 mg, 41.0%). Analytical RP-HPLC: t_R = 1.55 min (A/D 100:0 to 0:100 in 3.5 min, λ = 214 nm). MS (ESI+): $C_{66}H_{128}N_{16}O_{11}$ calc./obs. 1321.99/1322.00 Da $[M+H]^+$.

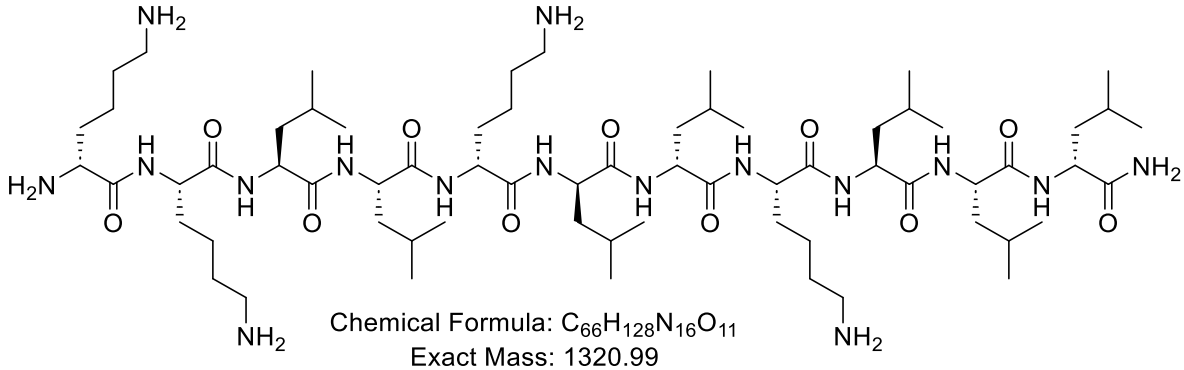

Analytical HPLC-MS data:

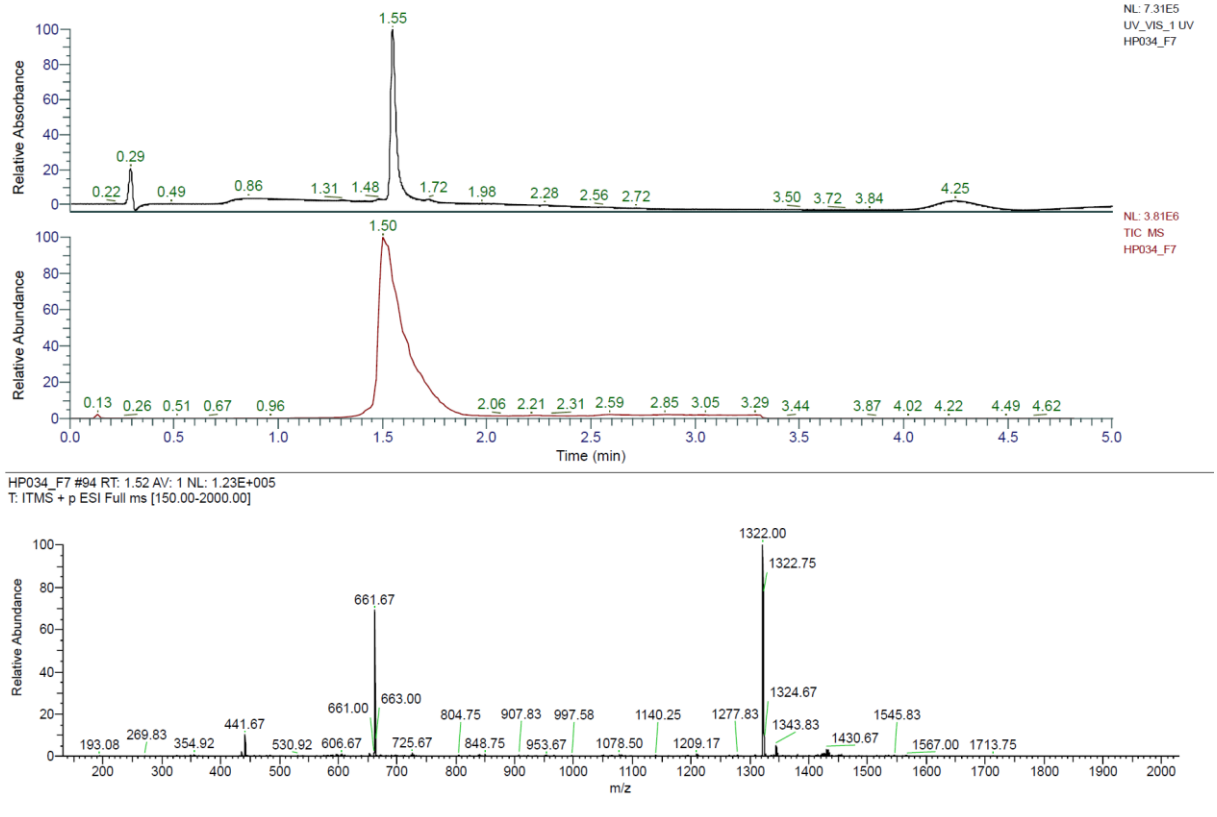

HRMS spectra:

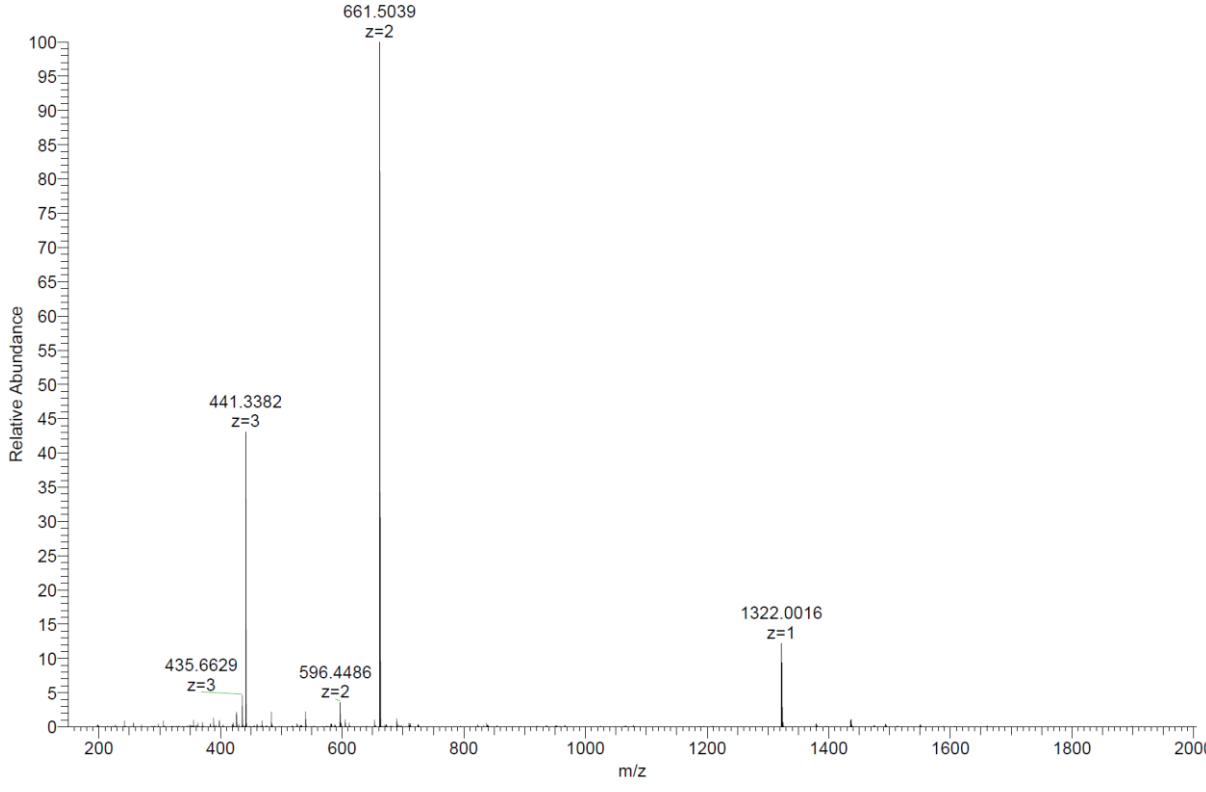

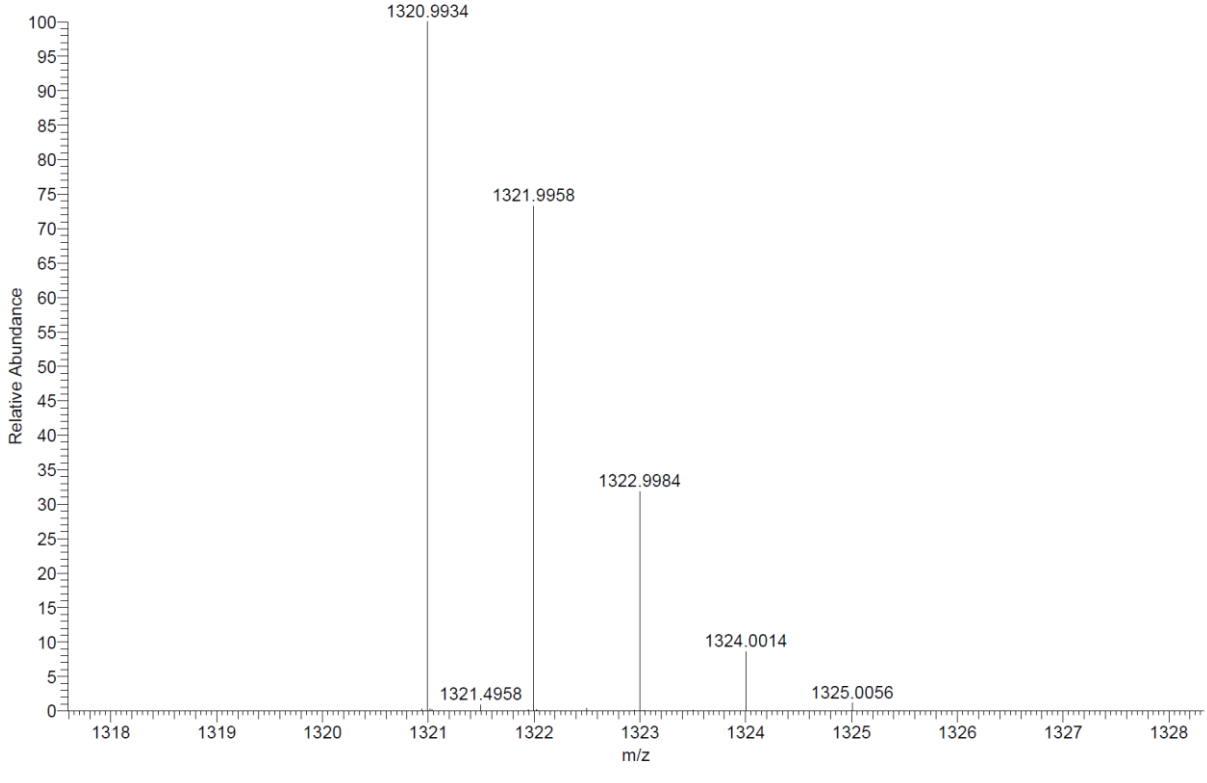

KKLlkllkLLL (HP29) was obtained as white solid after preparative RP-HPLC (59.3 mg, 53.4%). Analytical RP-HPLC: t_R = 1.58 min (A/D 100:0 to 0:100 in 3.5 min, λ = 214 nm). MS (ESI+): $C_{66}H_{128}N_{16}O_{11}$ calc./obs. 1321.99/1322.00 Da $[M+H]^+$.

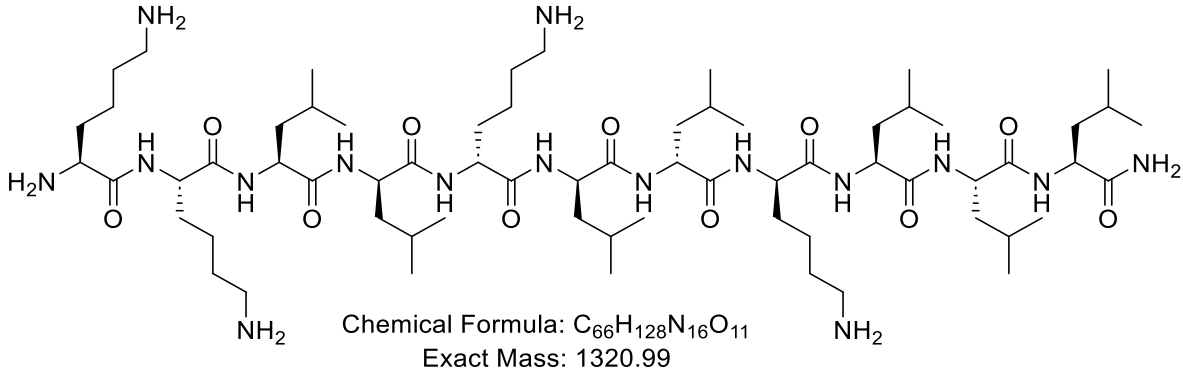

Analytical HPLC-MS data:

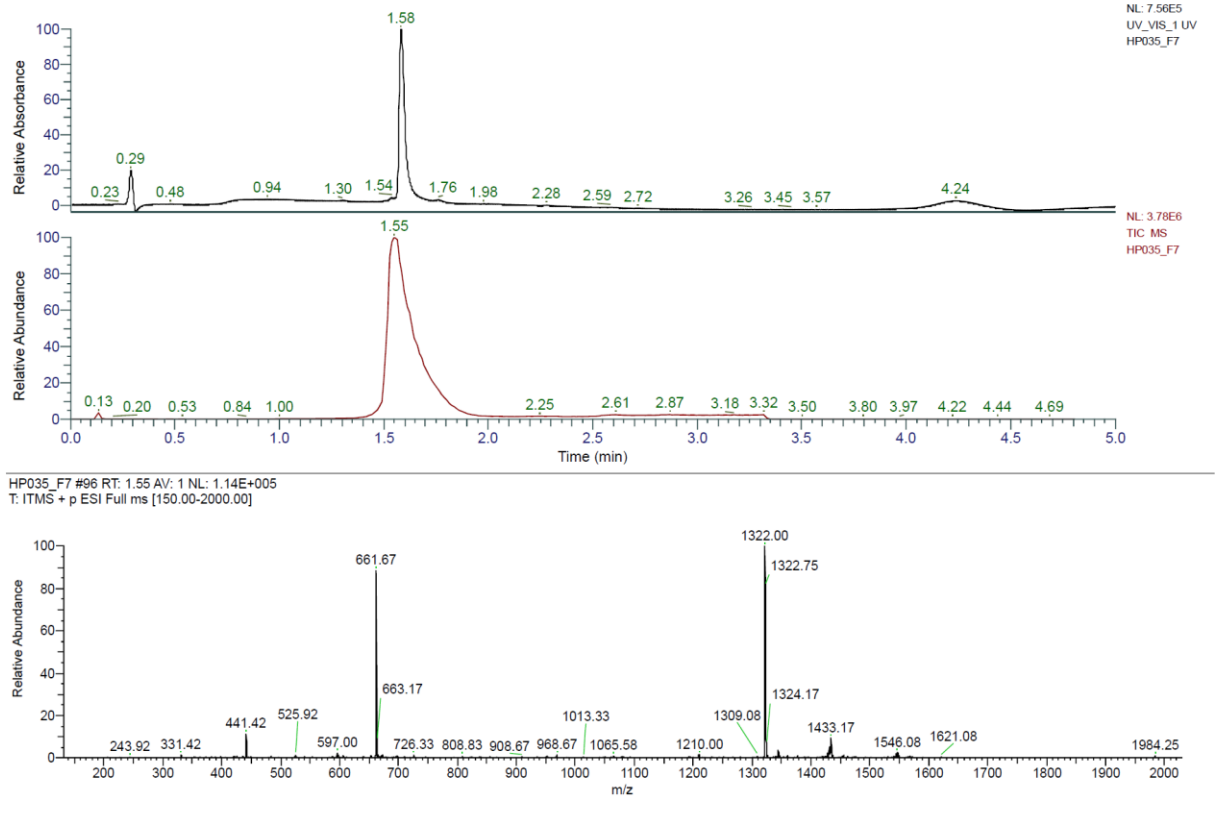

HRMS spectra:

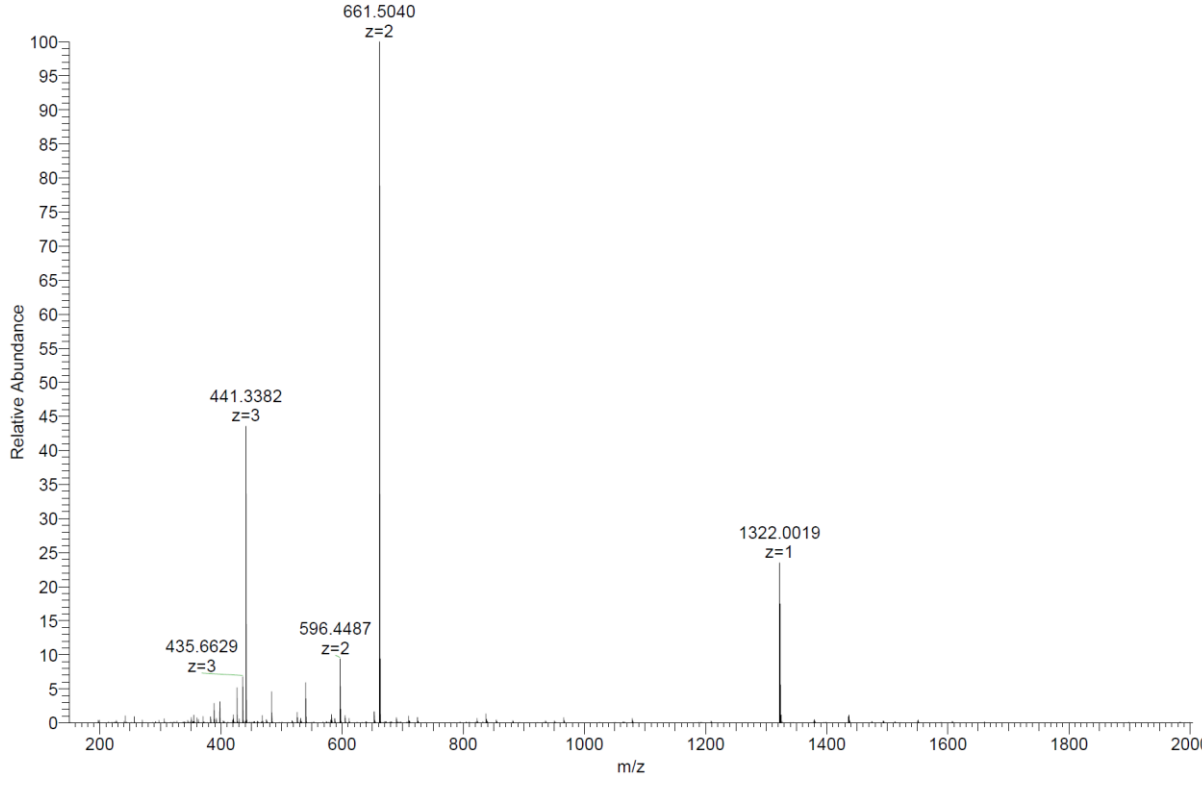

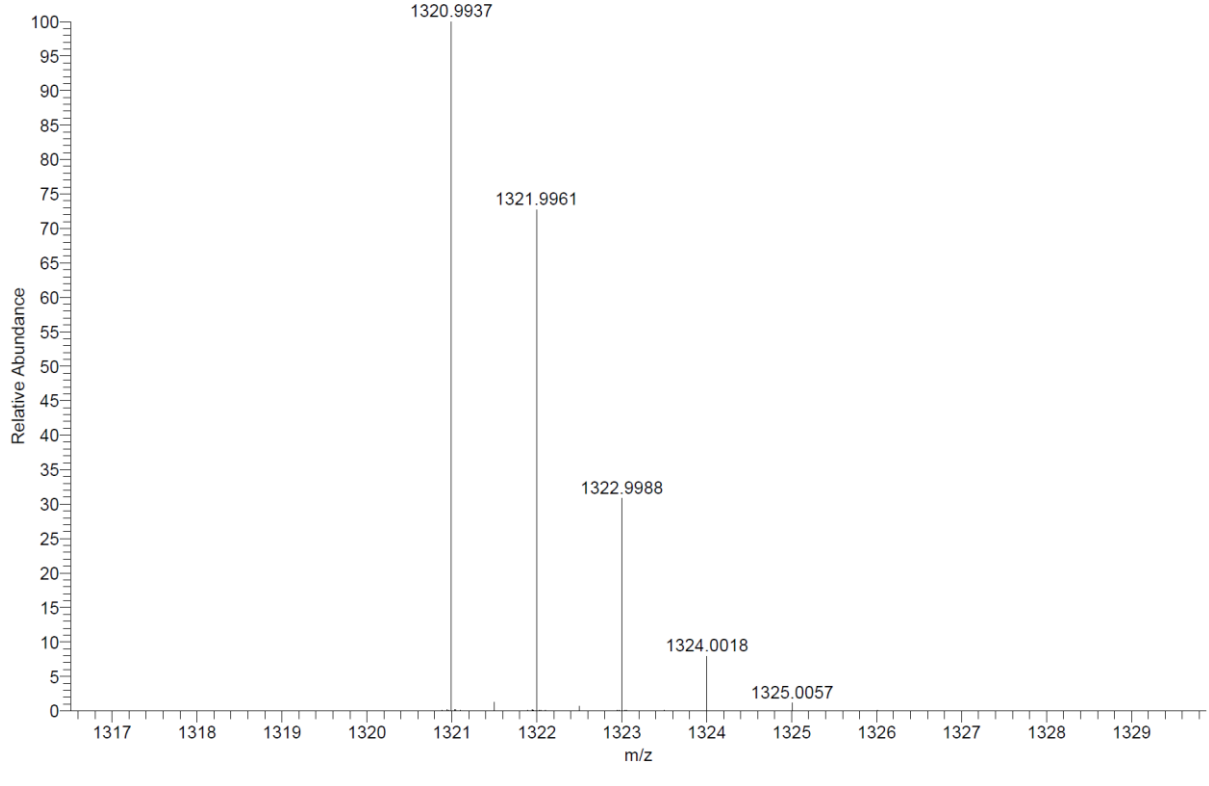

KkLlKlLkLlL (HP30) was obtained as white solid after preparative RP-HPLC (35.7 mg, 32.1%). Analytical RP-HPLC: t_R = 1.57 min (A/D 100:0 to 0:100 in 3.5 min, λ = 214 nm). MS (ESI+): $C_{66}H_{128}N_{16}O_{11}$ calc./obs. 1321.99/1322.00 Da $[M+H]^+$.

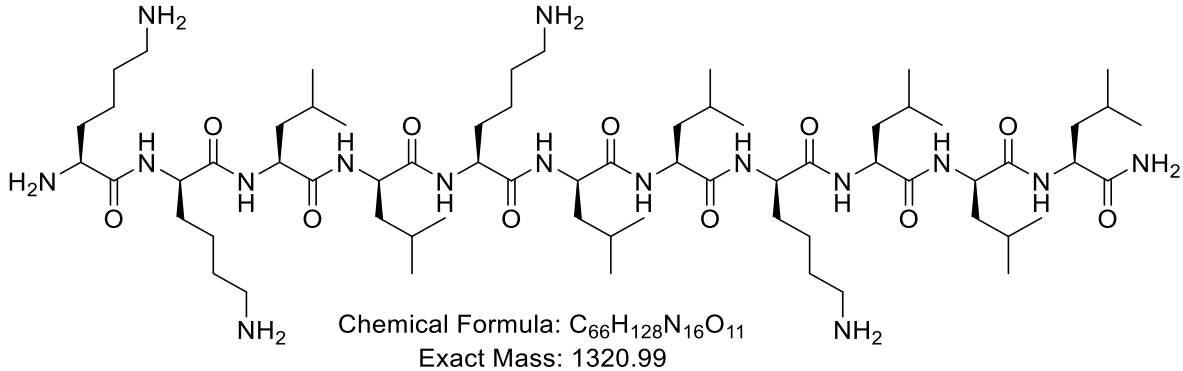

Analytical HPLC-MS data:

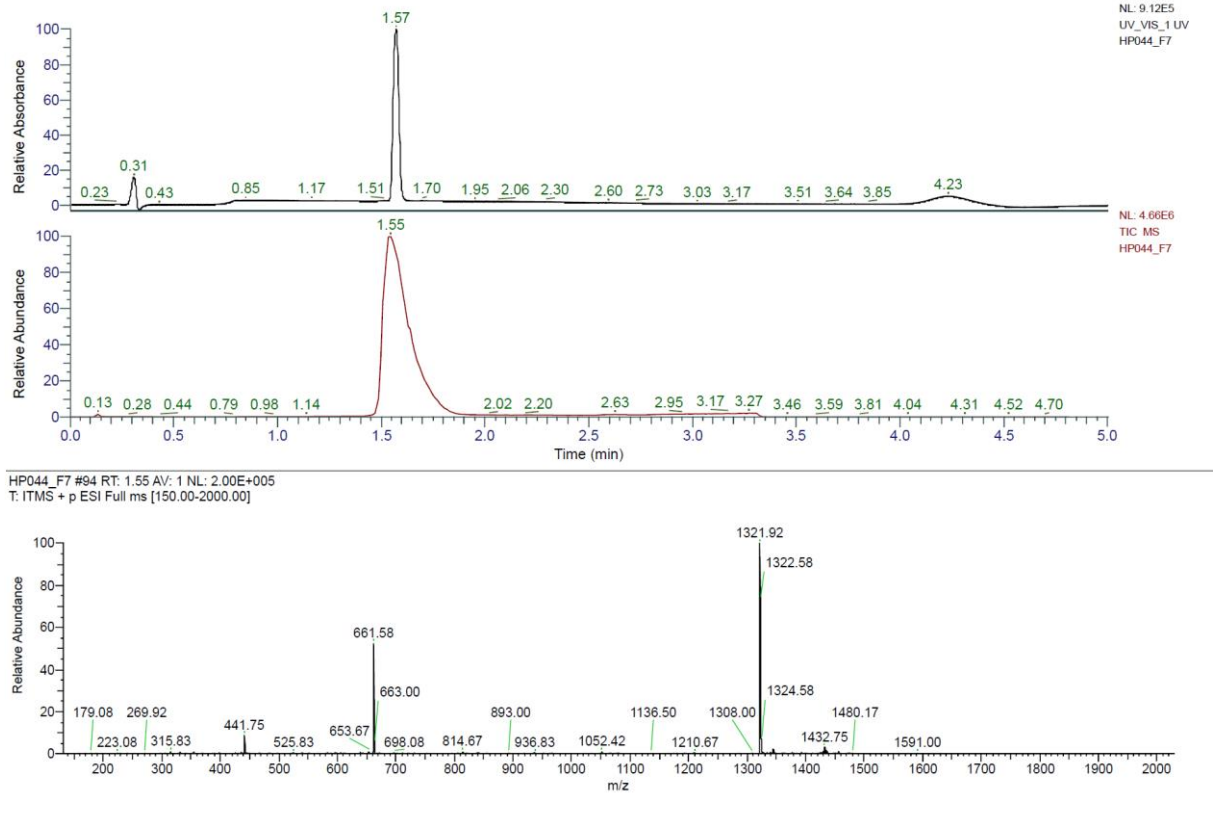

HRMS spectra:

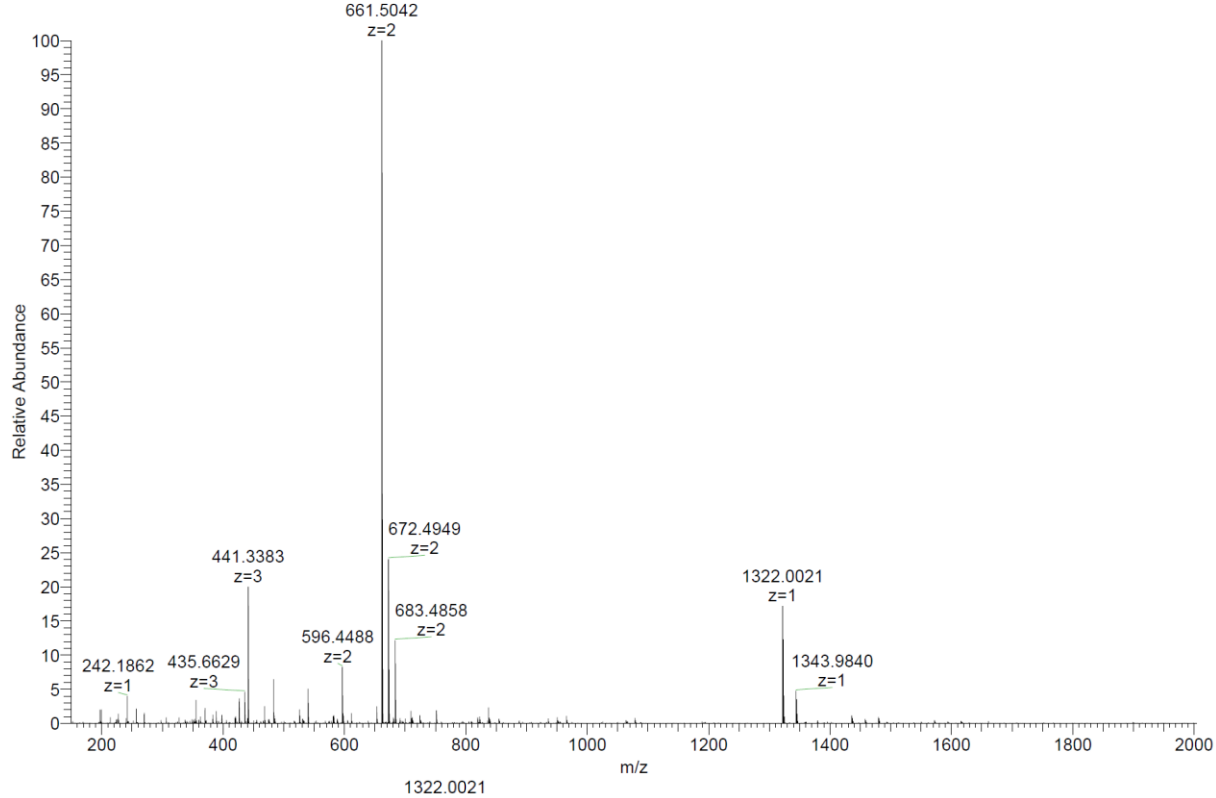

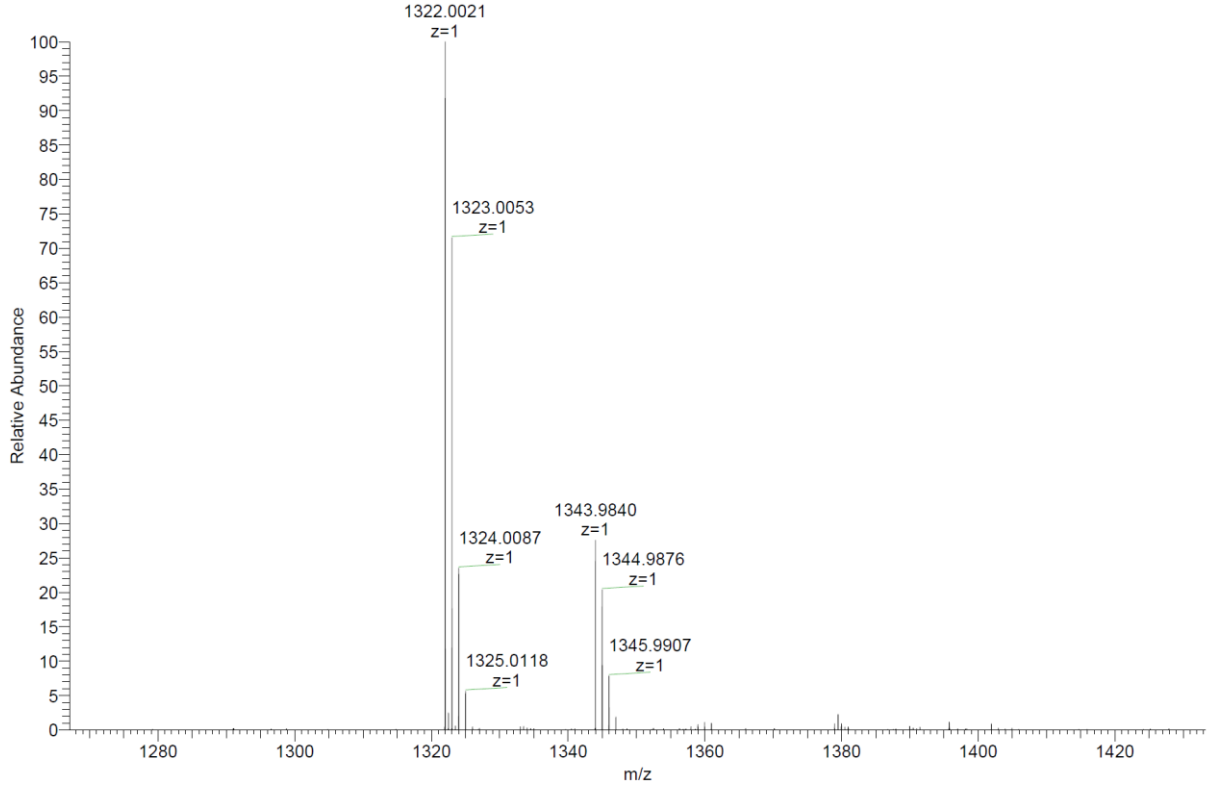

kKlLkLlKlLl (HP31) was obtained as white solid after preparative RP-HPLC (45.3 mg, 40.8%). Analytical RP-HPLC: t_R = 1.57 min (A/D 100:0 to 0:100 in 3.5 min, λ = 214 nm). MS (ESI+): $C_{66}H_{128}N_{16}O_{11}$ calc./obs. 1321.99/1322.00 Da $[M+H]^+$.

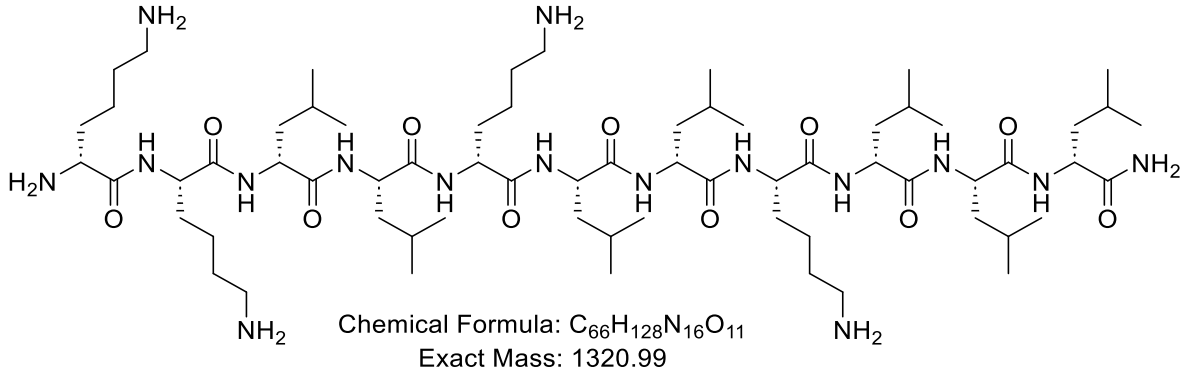

Analytical HPLC-MS data:

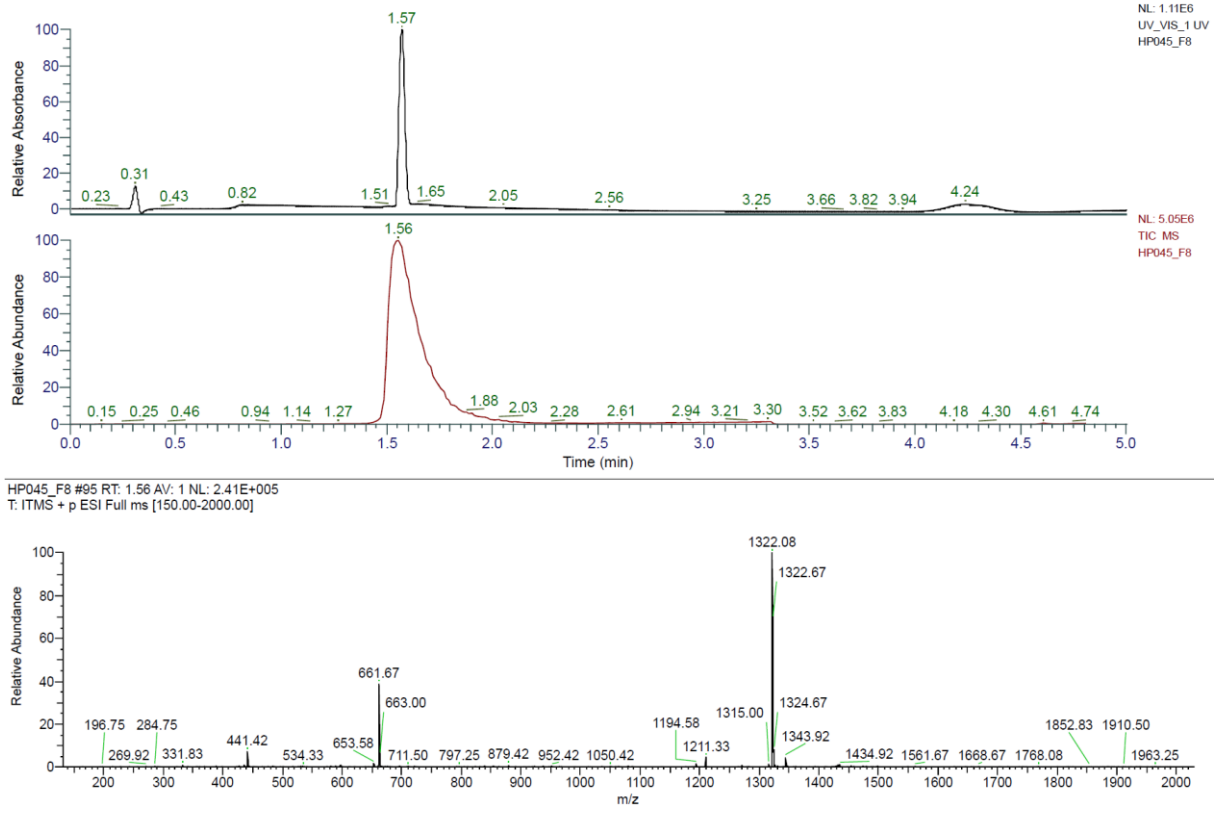

HRMS spectra:

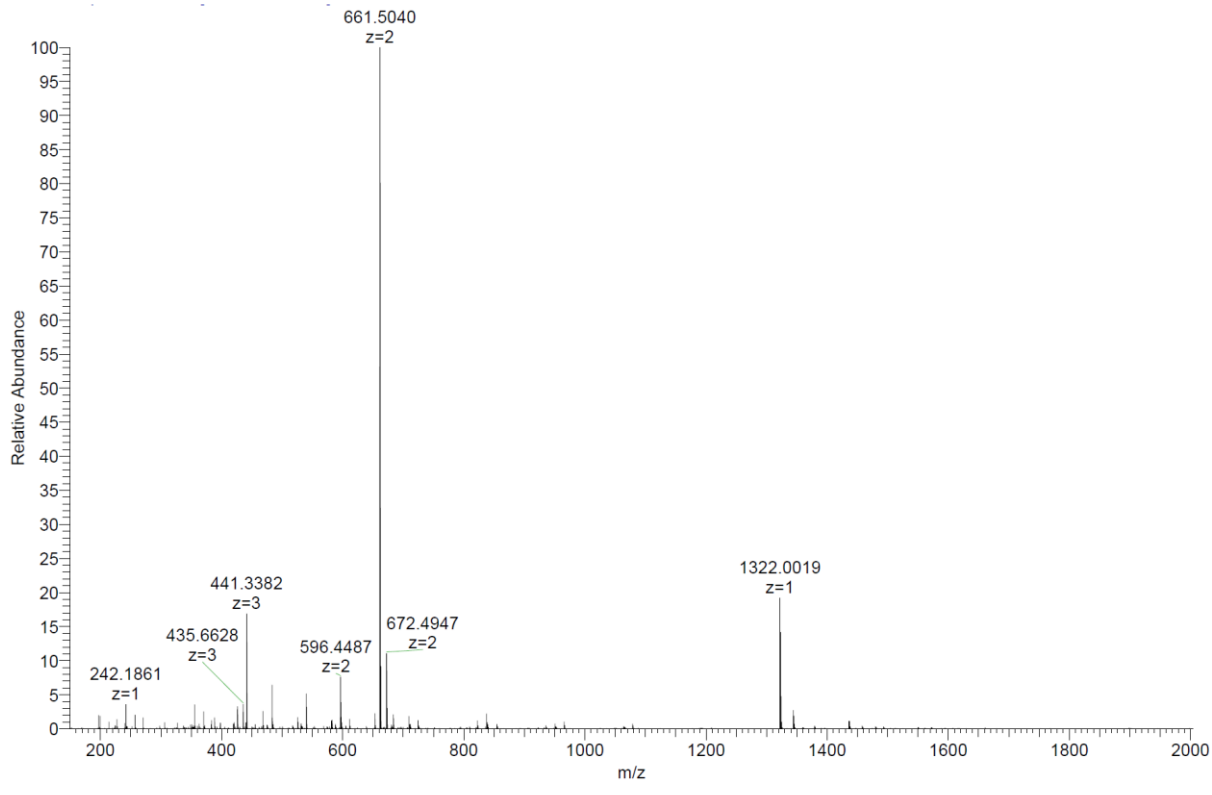

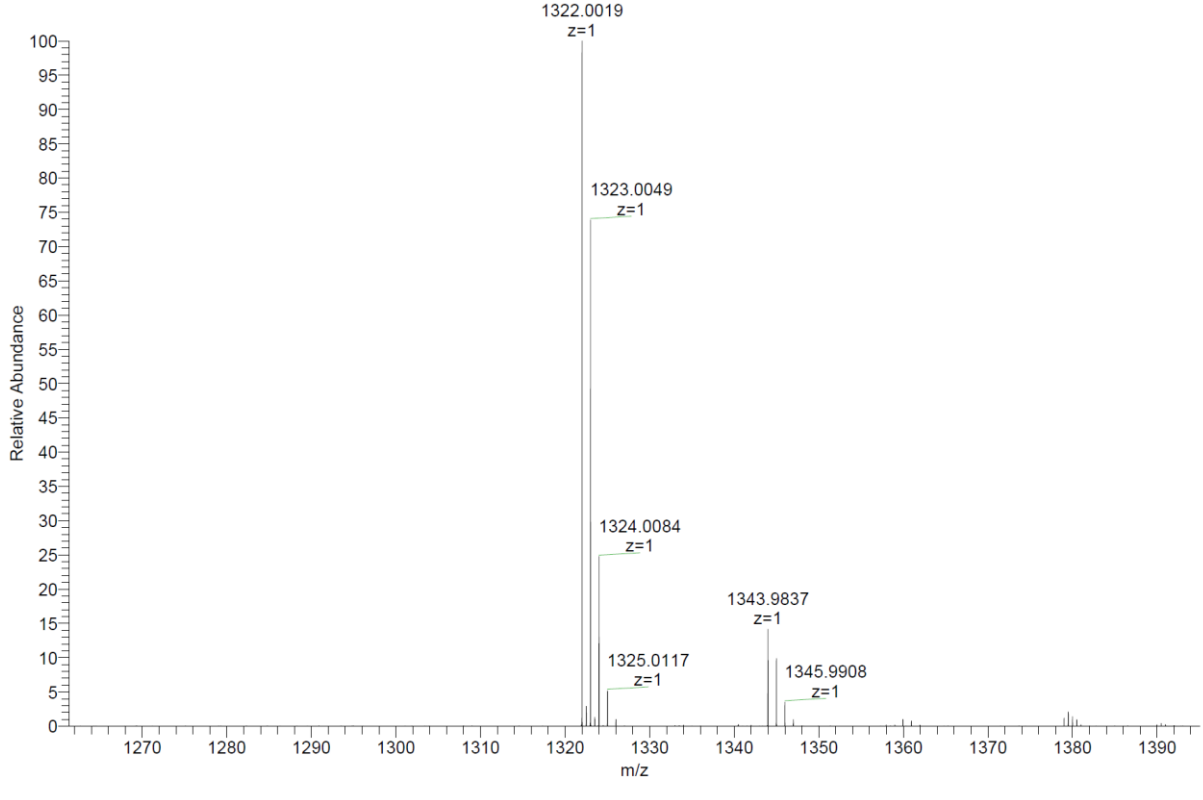

RRLLRLLRLLL (HP32) was obtained as white solid after preparative RP-HPLC (32.5 mg, 27.5%). Analytical RP-HPLC: t_R = 1.64 min (A/D 100:0 to 0:100 in 3.5 min, λ = 214 nm). MS (ESI+): $C_{66}H_{128}N_{24}O_{11}$ calc./obs. 1434.02/1434.03 Da $[M+H]^+$.

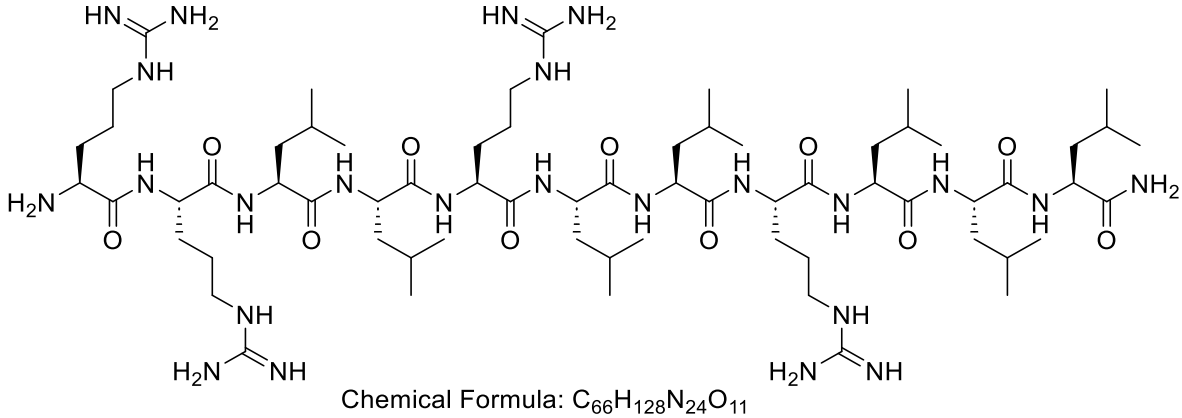

Chemical Formula: $C_{66}H_{128}N_{24}O_{11}$
Exact Mass: 1433.02
Molecular Weight: 1433.91

Analytical HPLC-MS data:

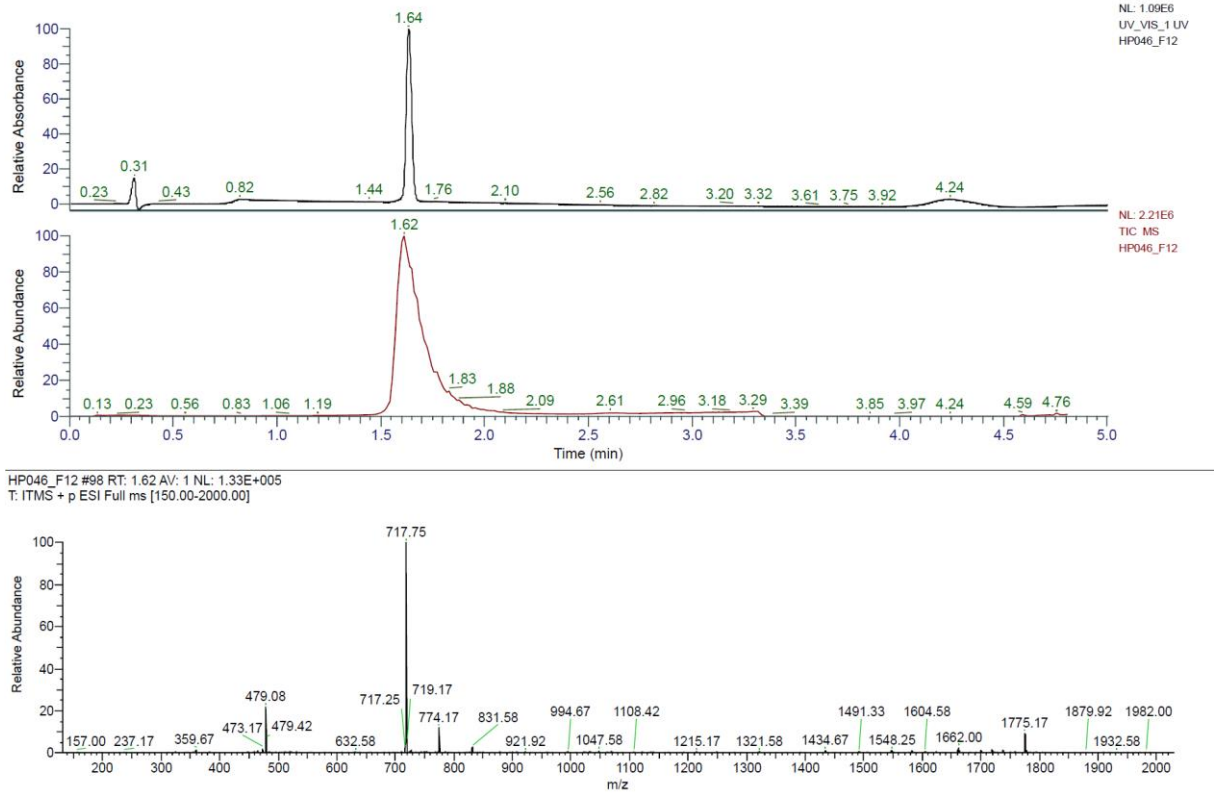

HRMS spectra:

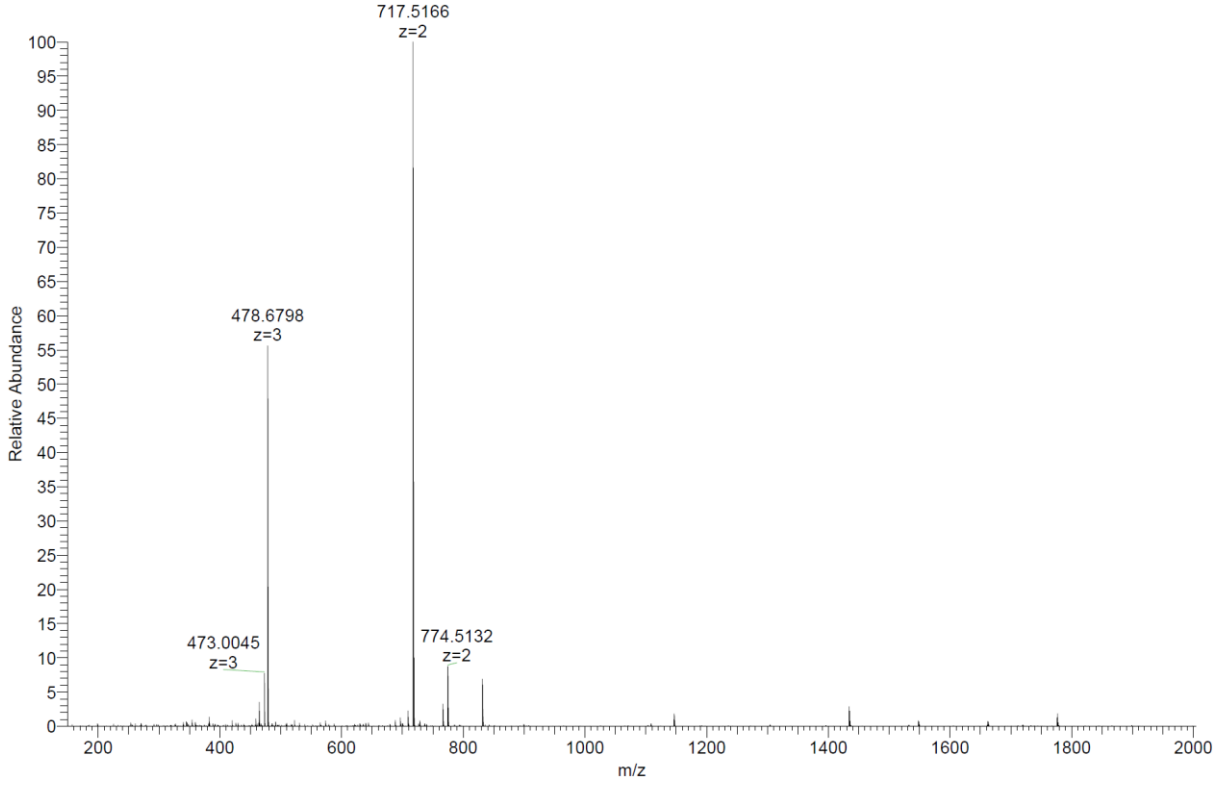

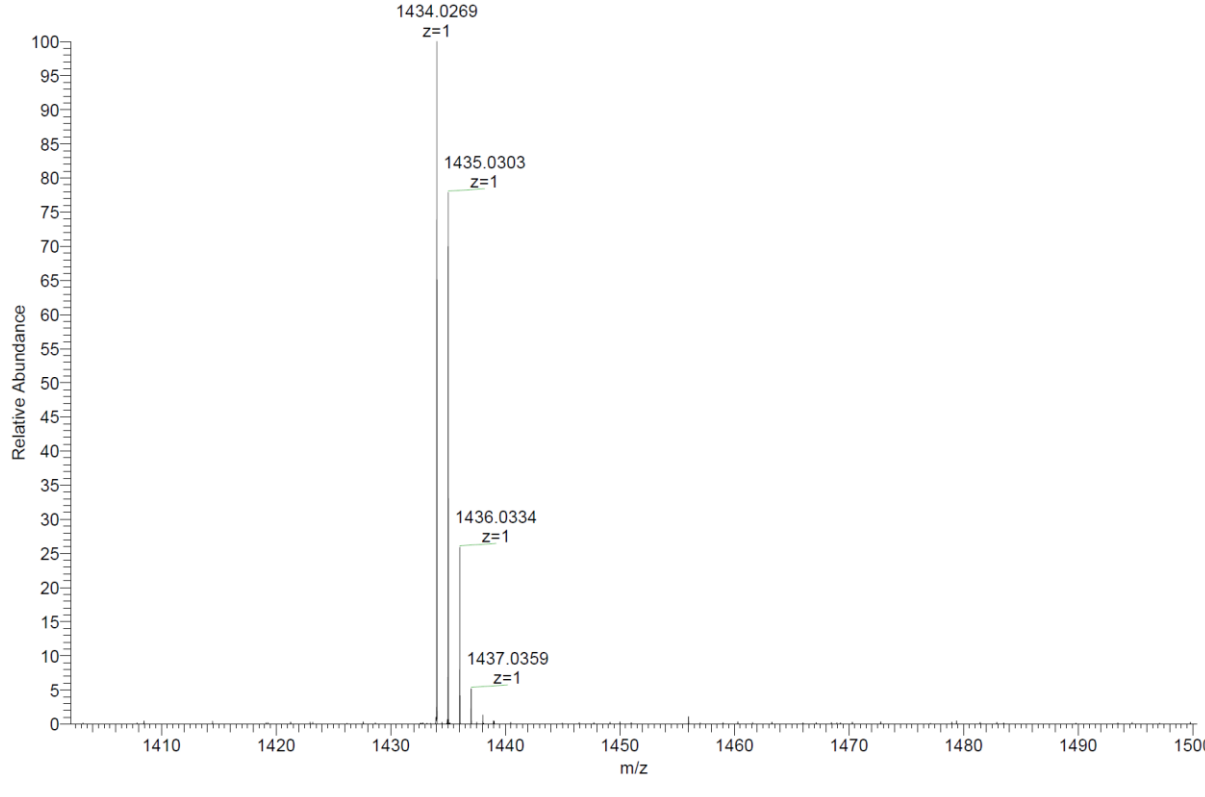

rrLLrLLrLLL (HP33) was obtained as white solid after preparative RP-HPLC (44.3 mg, 37.5%). Analytical RP-HPLC: t_R = 1.52 min (A/D 100:0 to 0:100 in 3.5 min, λ = 214 nm). MS (ESI+): $C_{66}H_{128}N_{24}O_{11}$ calc./obs. 1434.02/1434.03 Da $[M+H]^+$.

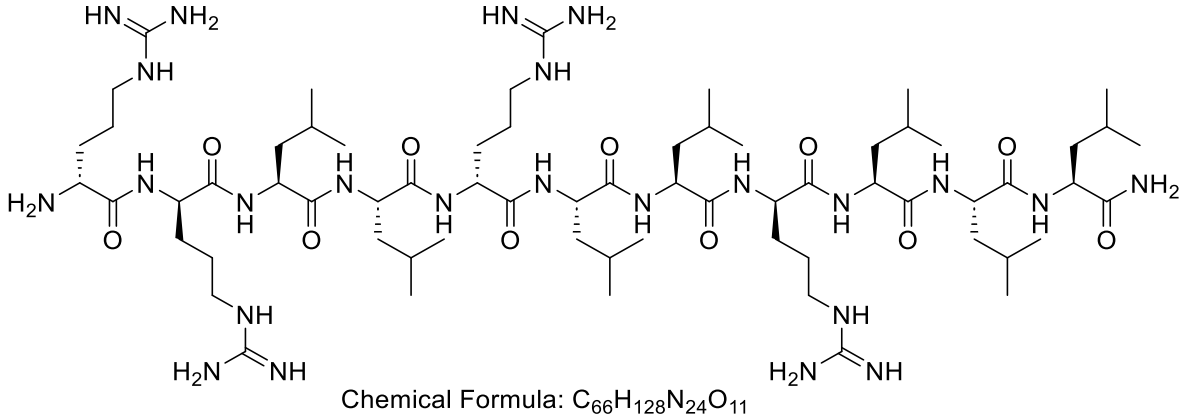

Chemical Formula: $C_{66}H_{128}N_{24}O_{11}$
Exact Mass: 1433.02
Molecular Weight: 1433.91

Analytical HPLC-MS data:

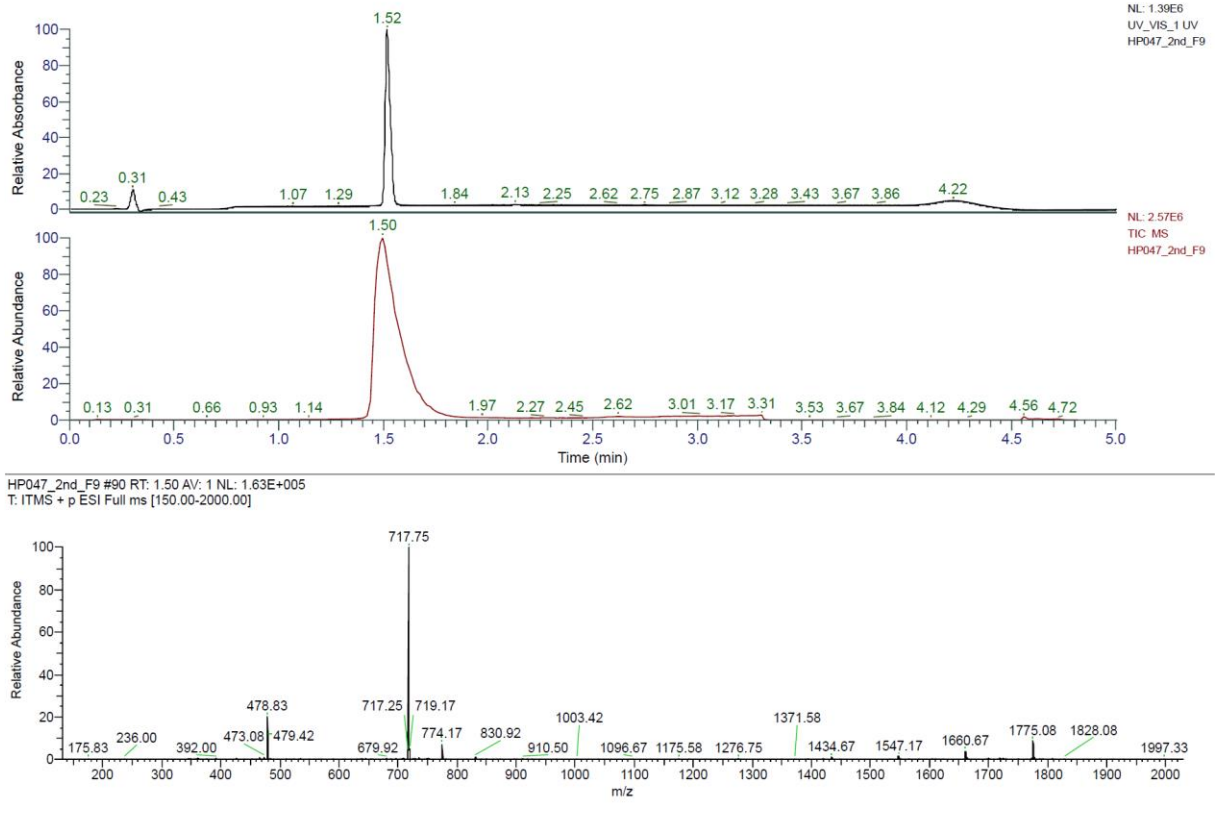

HRMS spectra:

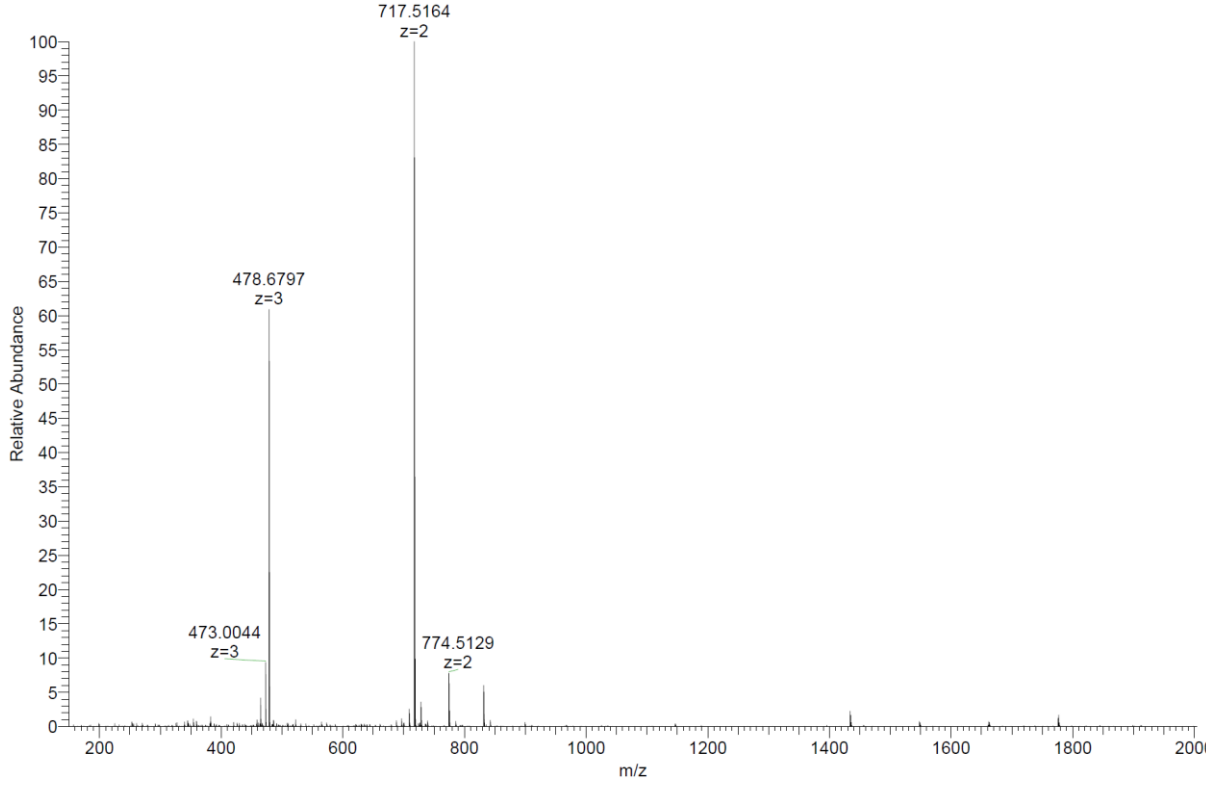

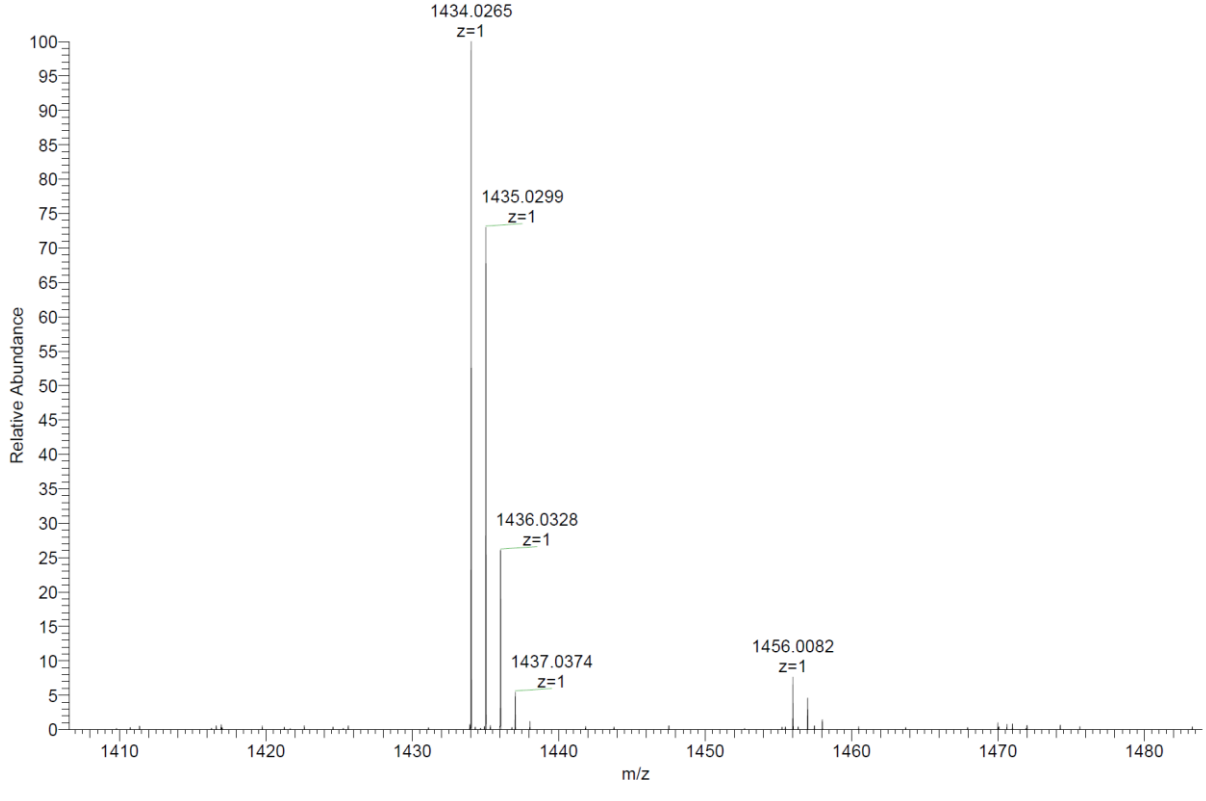

KKIIKIIKIII (HP34) was obtained as white solid after preparative RP-HPLC (35.1 mg, 31.6%). Analytical RP-HPLC: t_R = 1.44 min (A/D 100:0 to 0:100 in 3.5 min, λ = 214 nm). MS (ESI+): $C_{66}H_{128}N_{16}O_{11}$ calc./obs. 1321.99/1322.00 Da $[M+H]^+$.

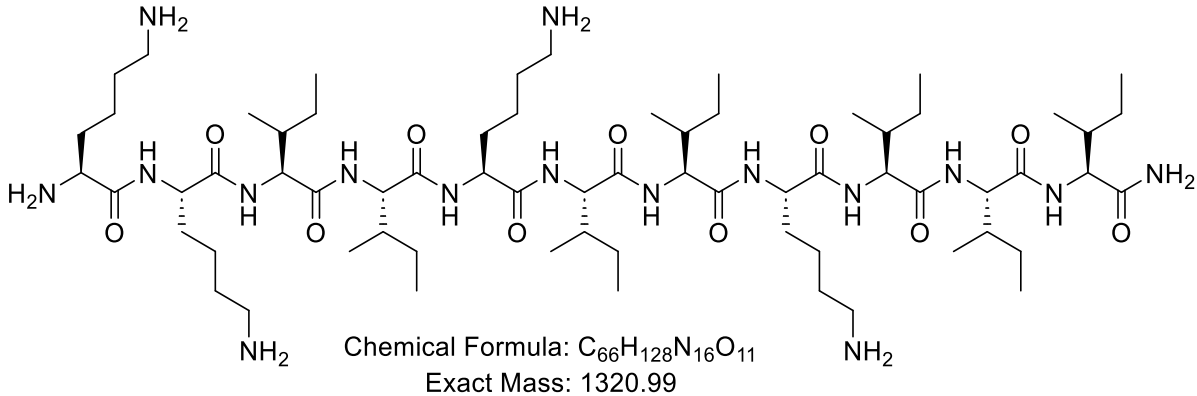

Analytical HPLC-MS data:

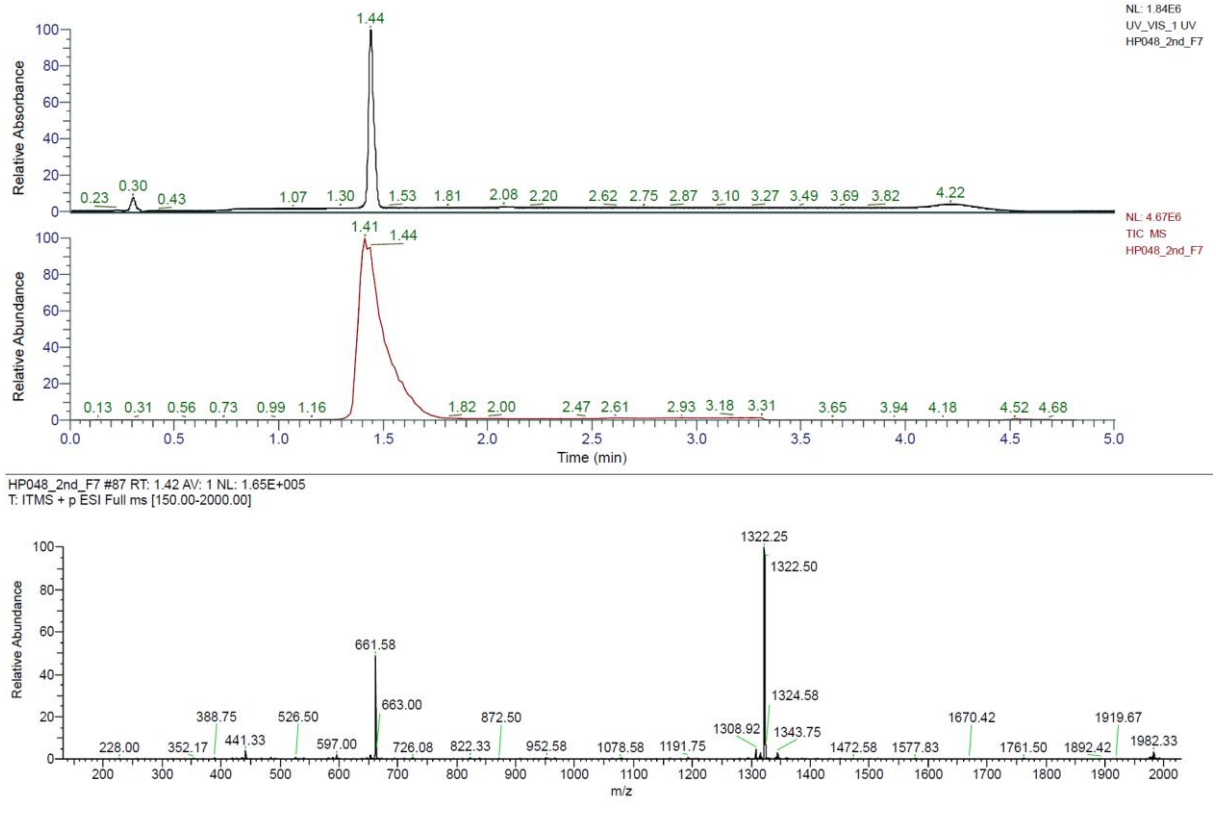

HRMS spectra:

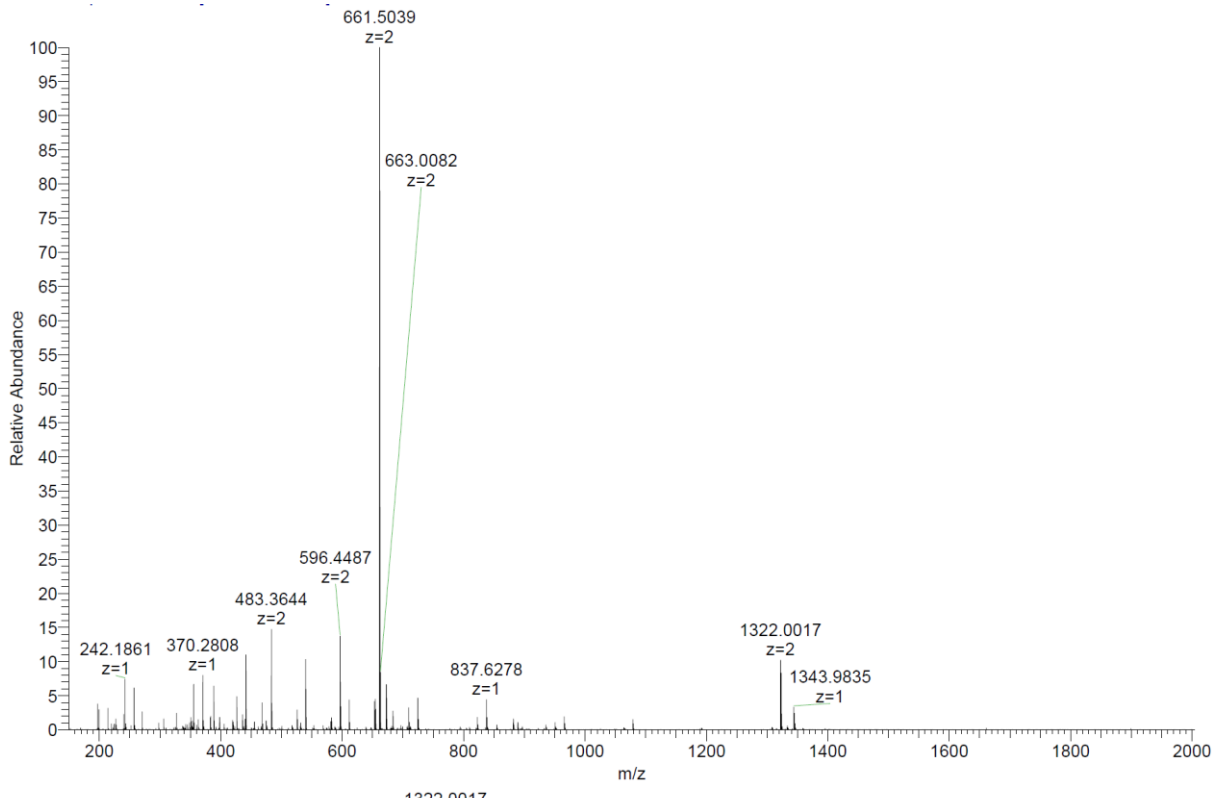

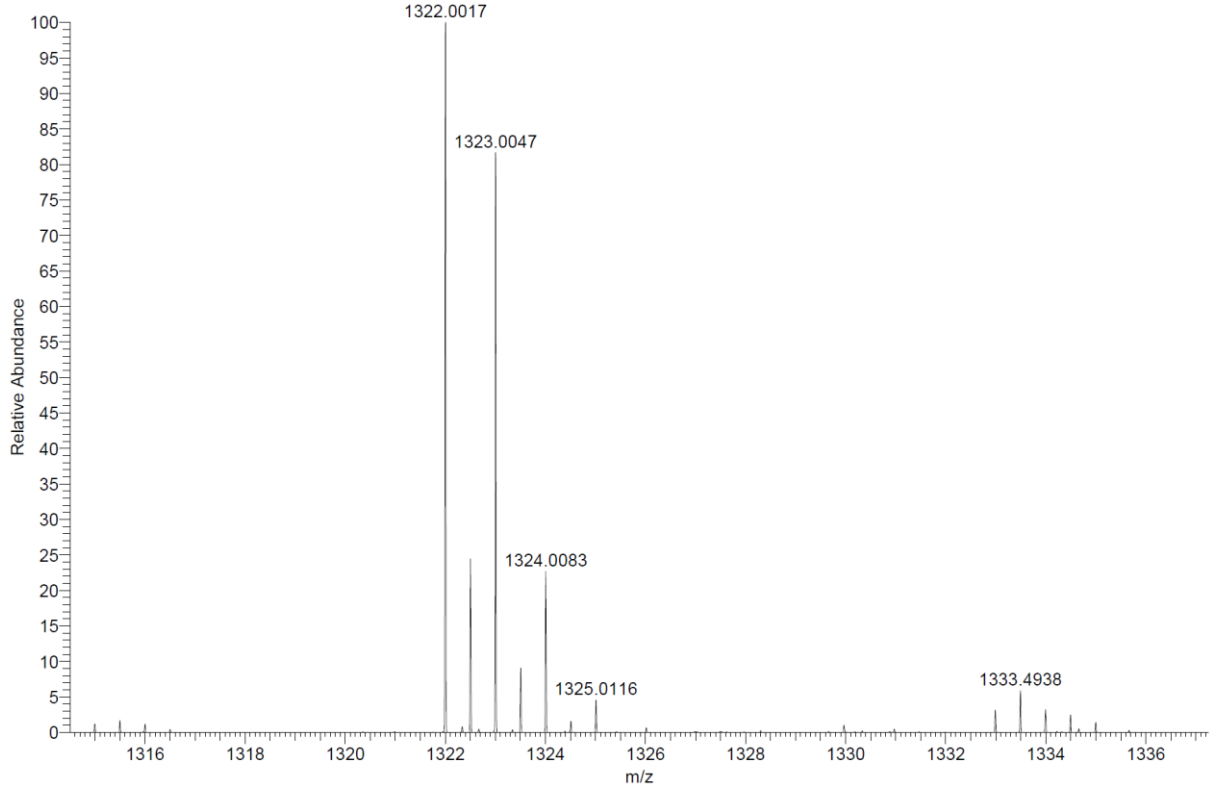

kkIIkIIkIII (HP35) was obtained as white solid after preparative RP-HPLC (29.3 mg, 26.4%). Analytical RP-HPLC: t_R = 1.36 min (A/D 100:0 to 0:100 in 3.5 min, λ = 214 nm). MS (ESI+): $C_{66}H_{128}N_{16}O_{11}$ calc./obs. 1321.99/1322.00 Da $[M+H]^+$.

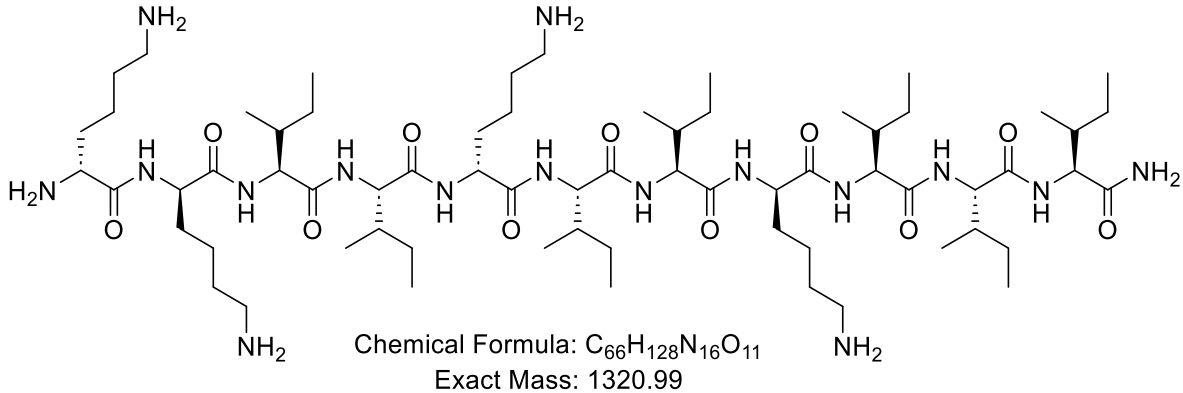

Analytical HPLC-MS data:

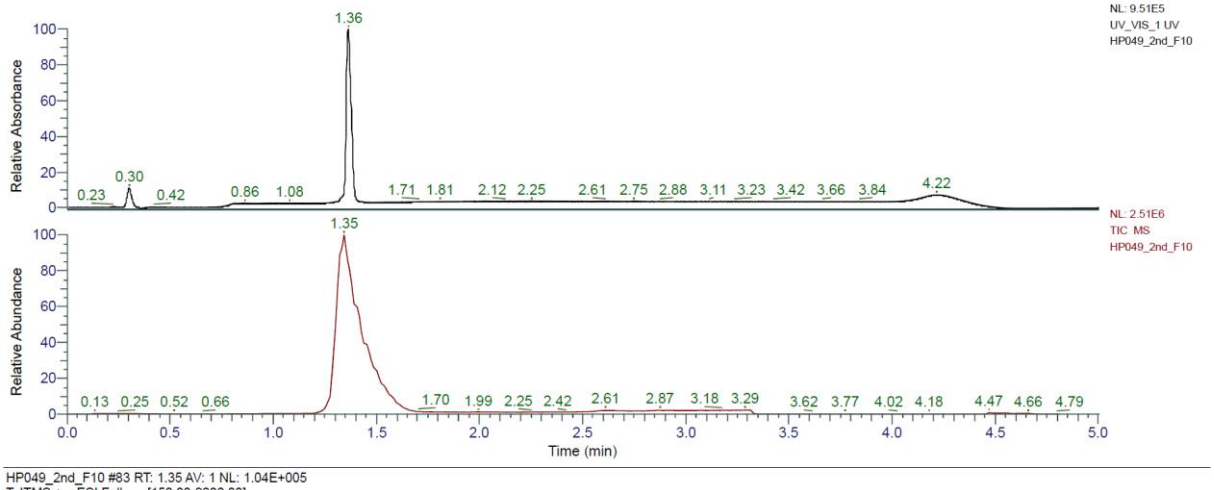

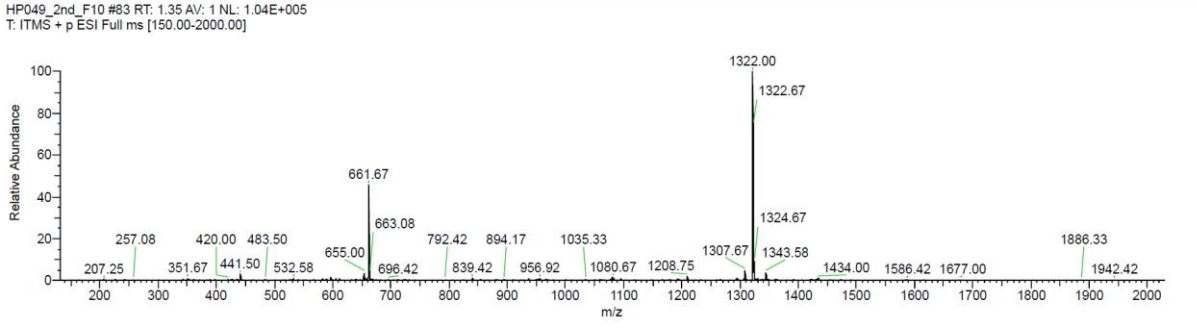

HRMS spectra:

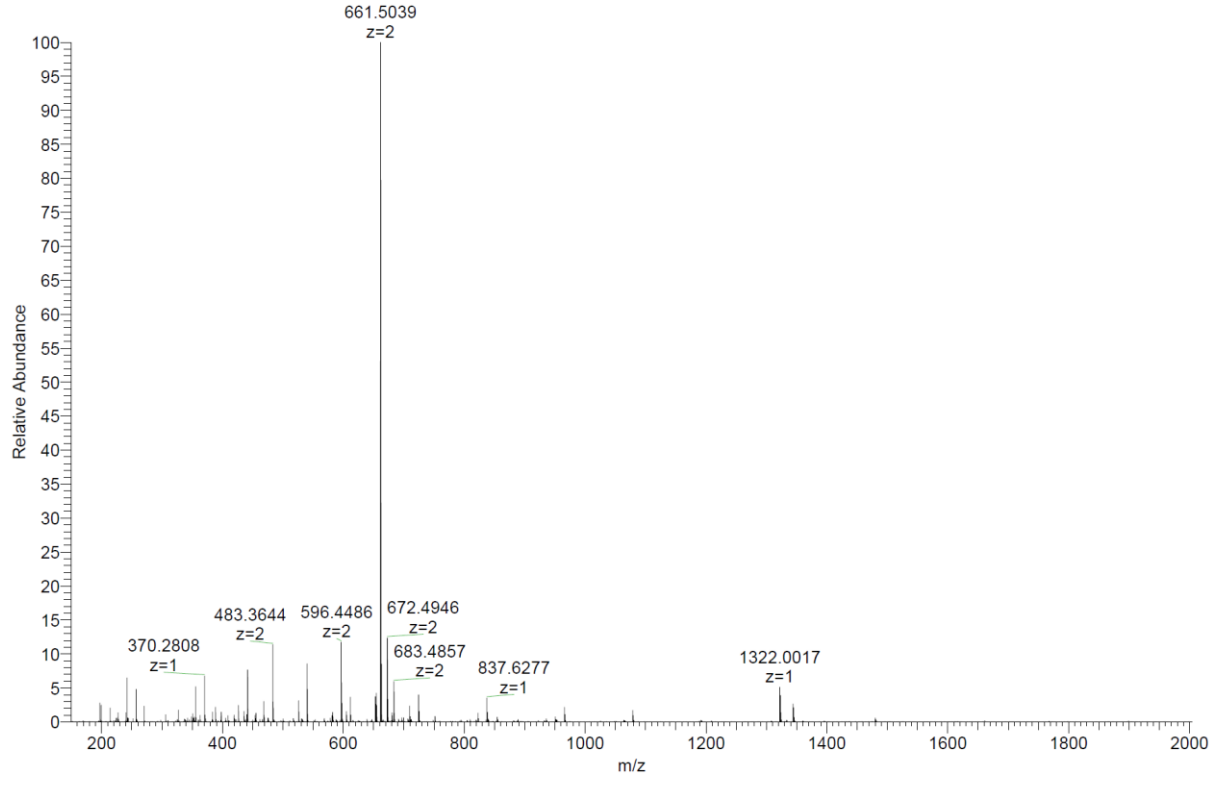

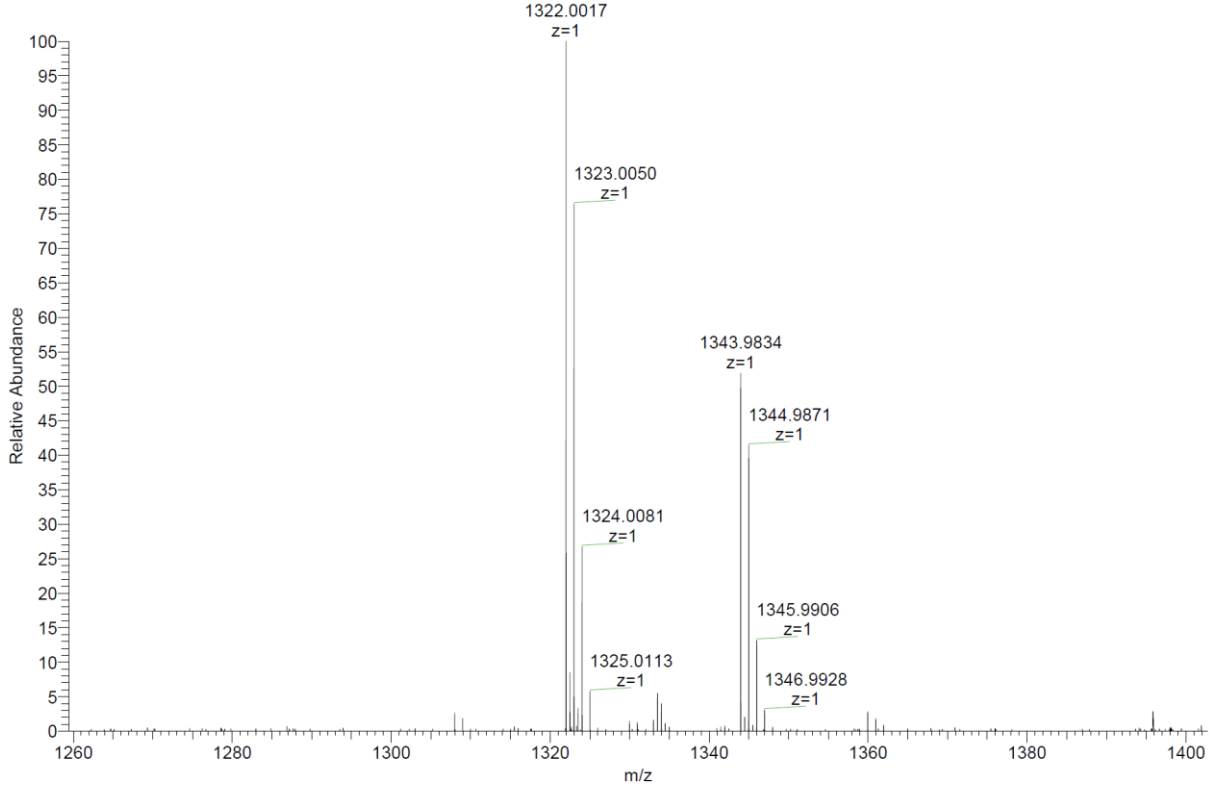

RRIIRIIRIII (HP36) was obtained as white solid after preparative RP-HPLC (7.7 mg, 6.5%). Analytical RP-HPLC: t_R = 1.47 min (A/D 100:0 to 0:100 in 3.5 min, λ = 214 nm). MS (ESI+): $C_{66}H_{128}N_{24}O_{11}$ calc./obs. 1434.02/1434.03 Da $[M+H]^+$.

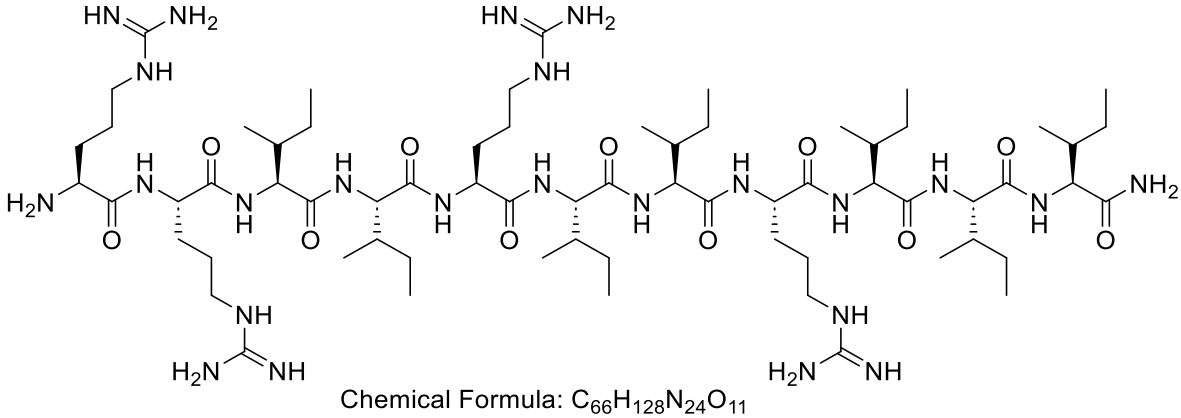

Chemical Formula: $C_{66}H_{128}N_{24}O_{11}$
Exact Mass: 1433.02
Molecular Weight: 1433.91

Analytical HPLC-MS data:

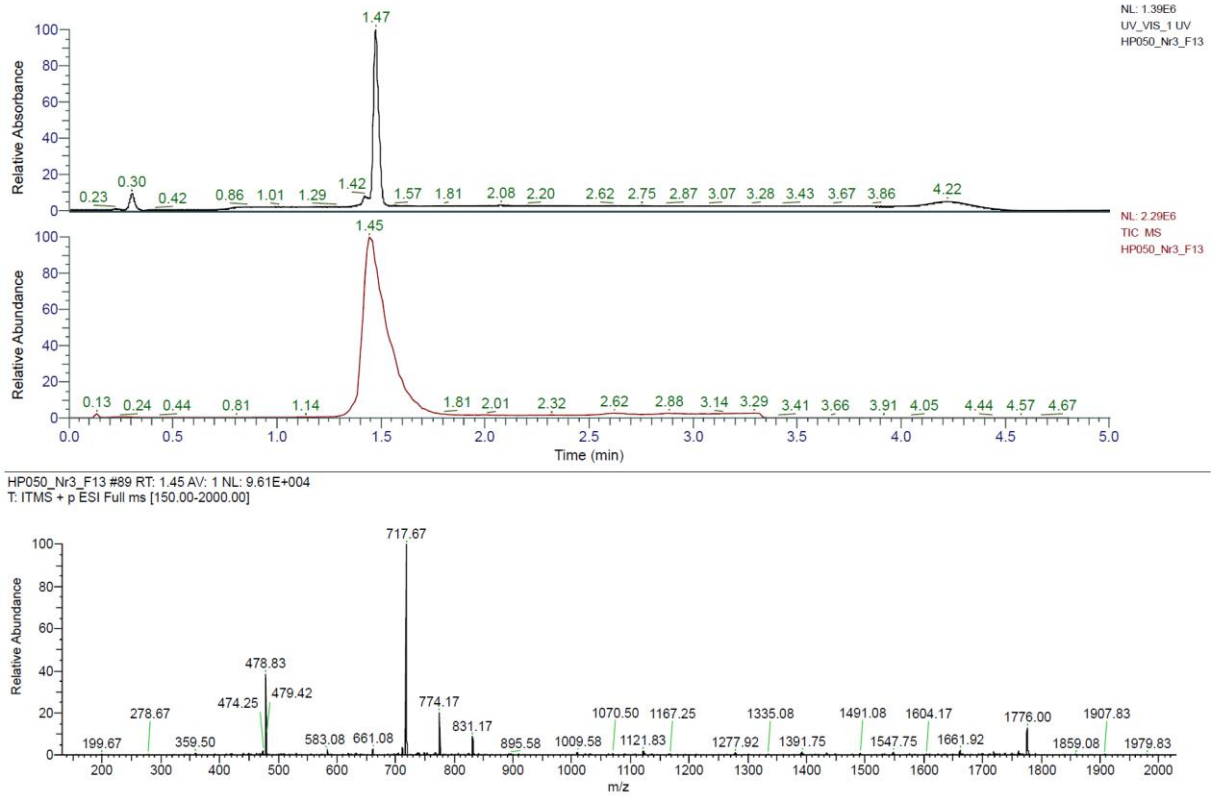

HRMS spectra:

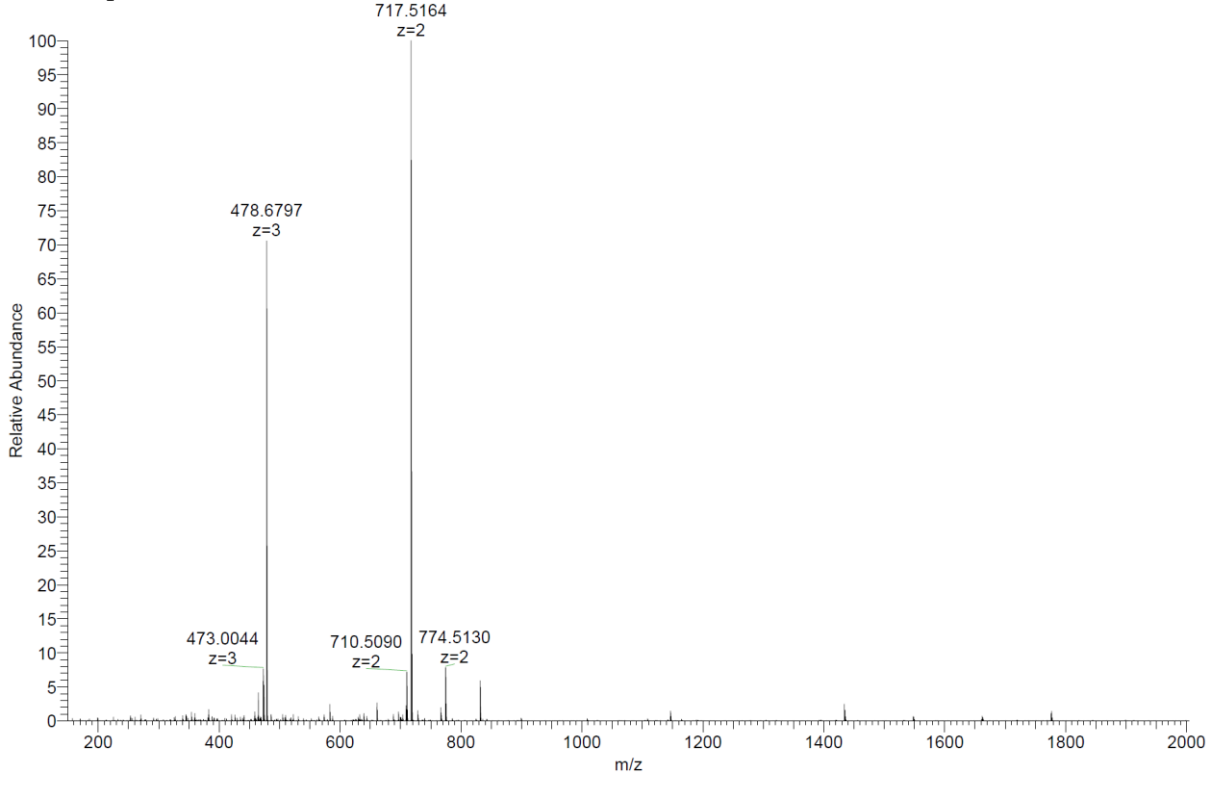

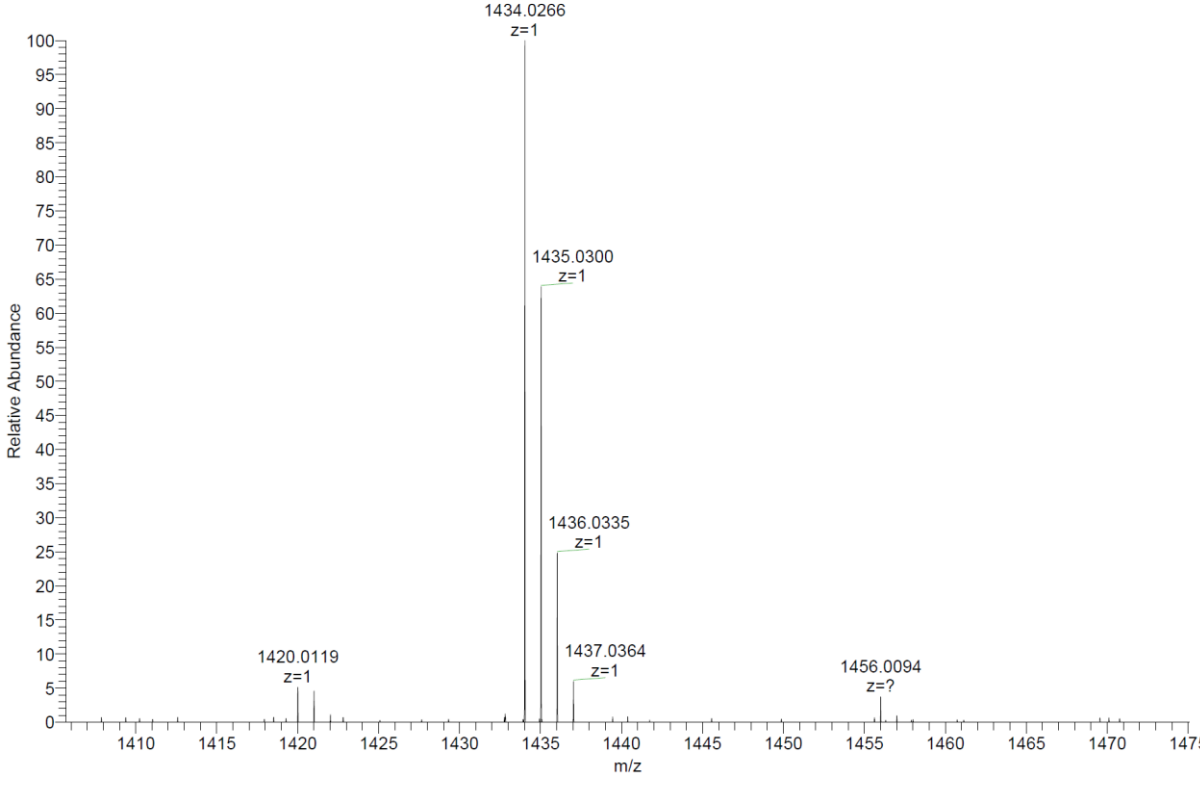

rrIIrIIrIII (HP37) was obtained as white solid after preparative RP-HPLC (38.7 mg, 32.8%). Analytical RP-HPLC: t_R = 1.68 min (A/D 100:0 to 0:100 in 3.5 min, λ = 214 nm). MS (ESI+): $C_{66}H_{128}N_{24}O_{11}$ calc./obs. 1434.02/1434.03 Da $[M+H]^+$.

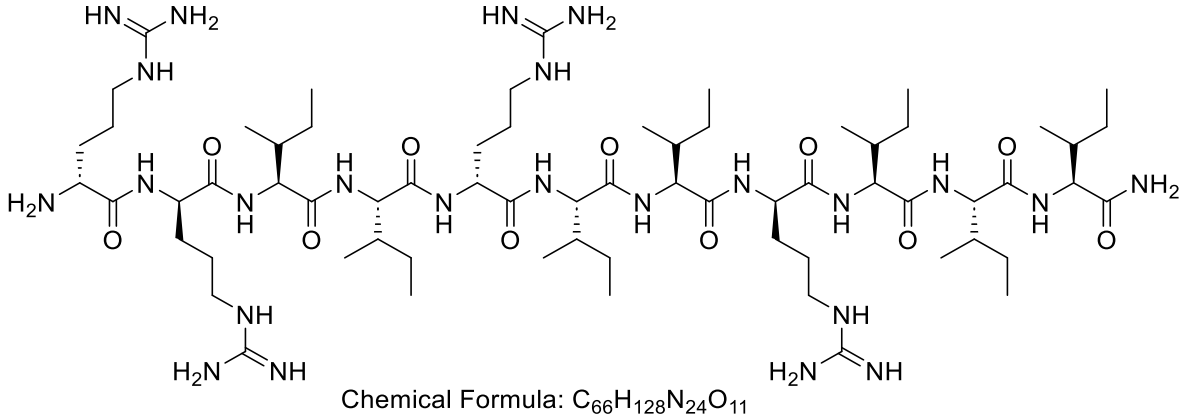

Chemical Formula: $C_{66}H_{128}N_{24}O_{11}$
Exact Mass: 1433.02
Molecular Weight: 1433.91

Analytical HPLC-MS data:

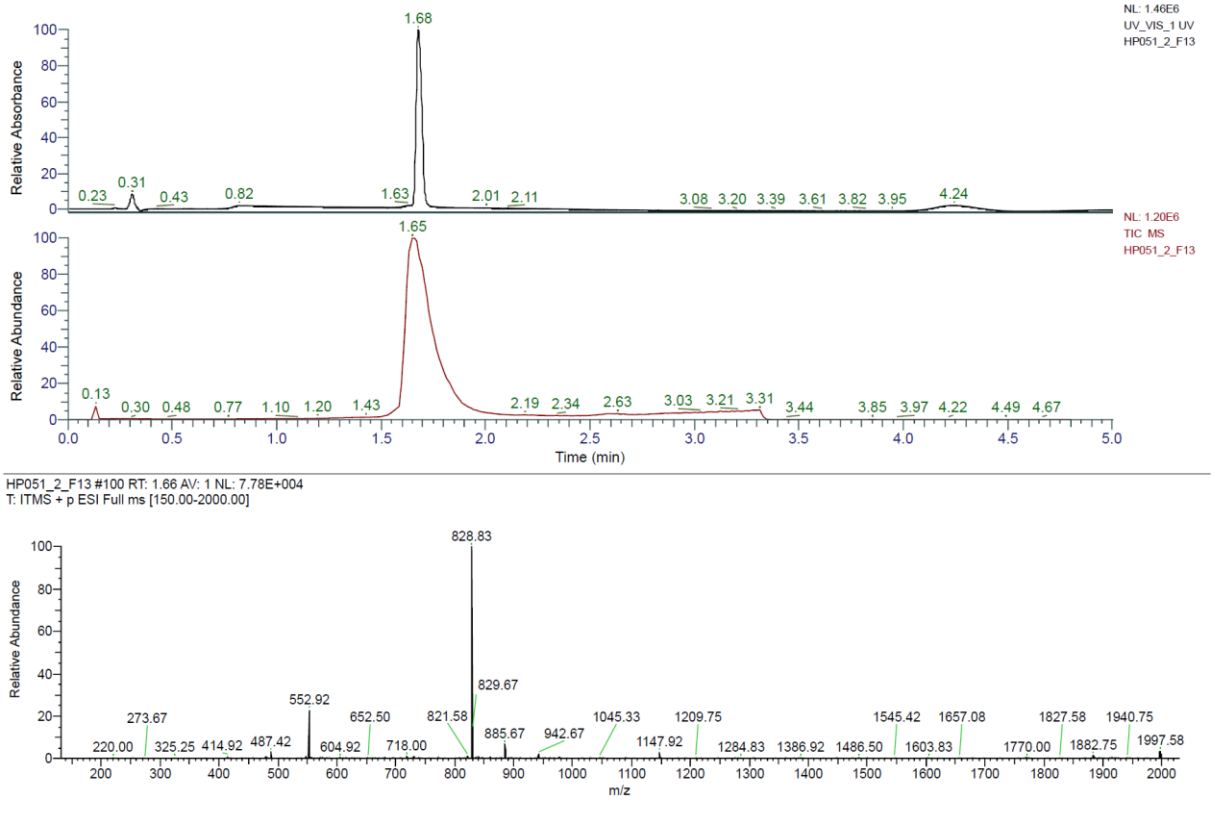

HRMS spectra:

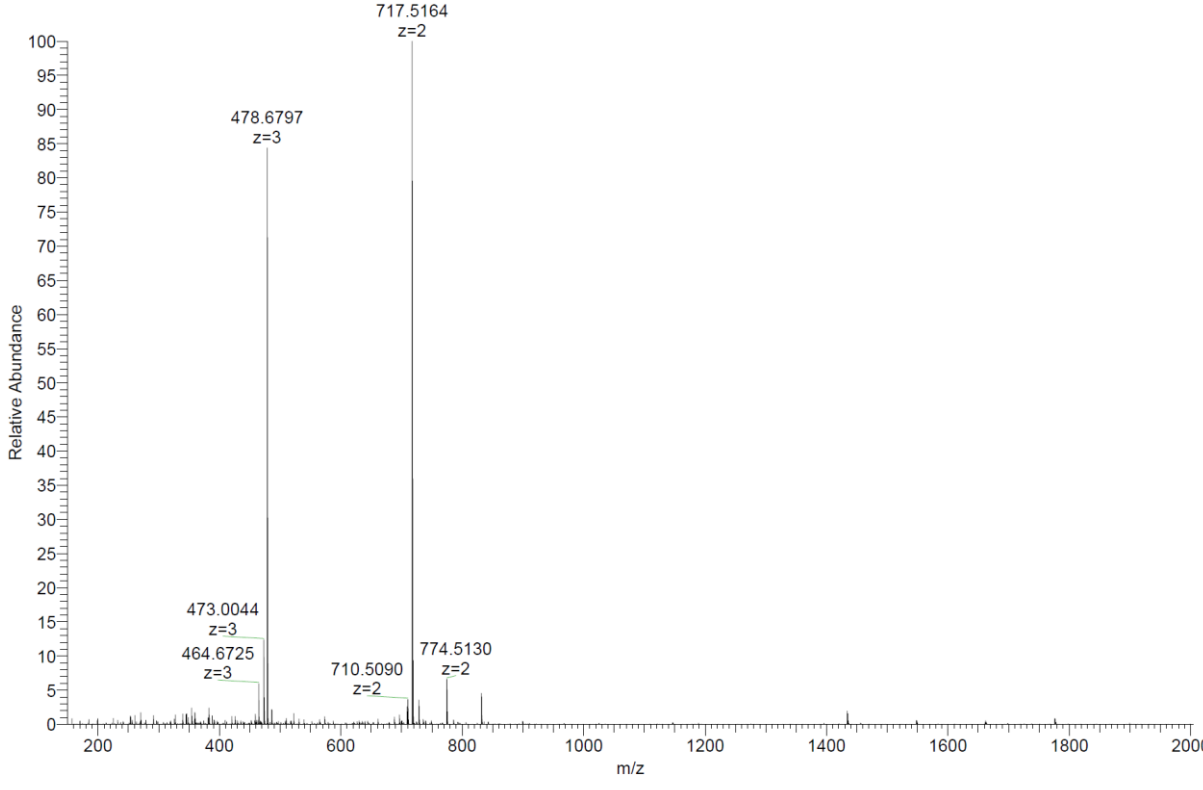

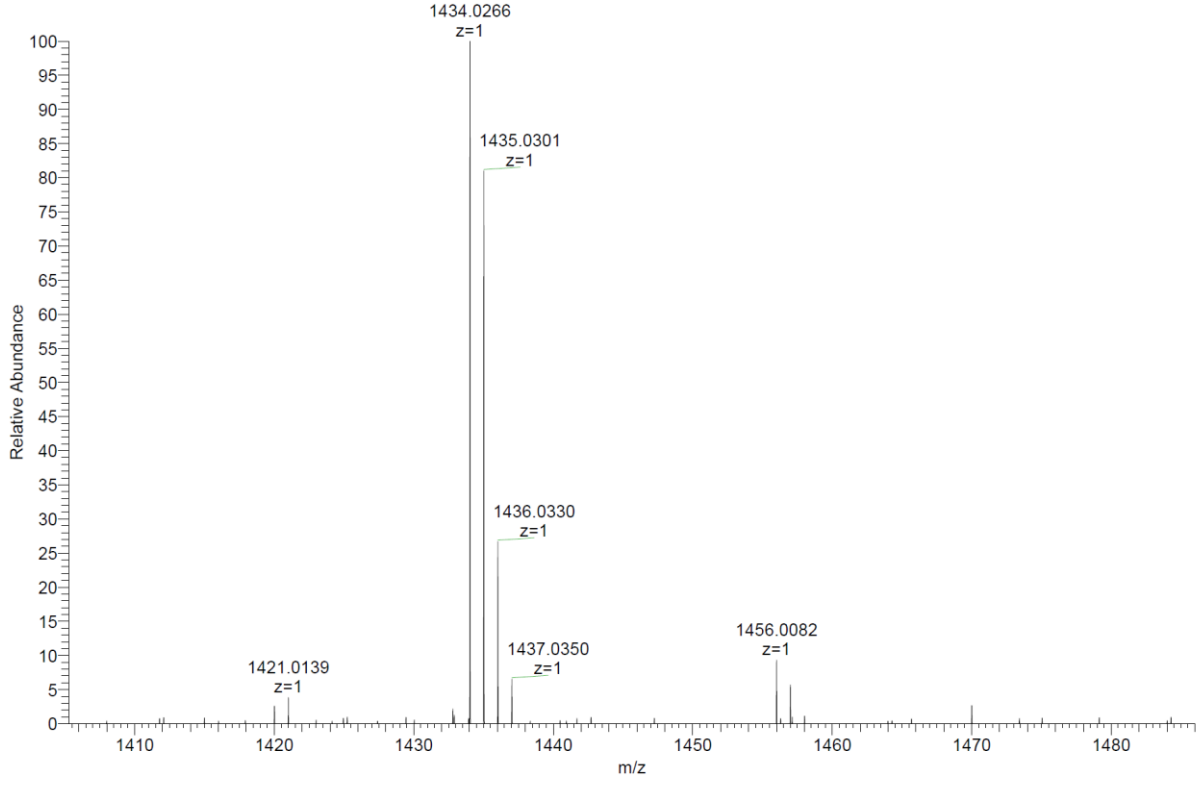

KKLLKLLKLLLKKLLKLLKLLL (2ln65) was obtained as white solid after preparative RP-HPLC (119.3 mg, 38.3%). Analytical RP-HPLC: t_R = 2.38 min (A/D 100:0 to 0:100 in 3.5 min, λ = 214 nm). MS (ESI+): $C_{132}H_{253}N_{31}O_{22}$ calc./obs. 2625.96/2625.97 Da $[M+H]^+$.

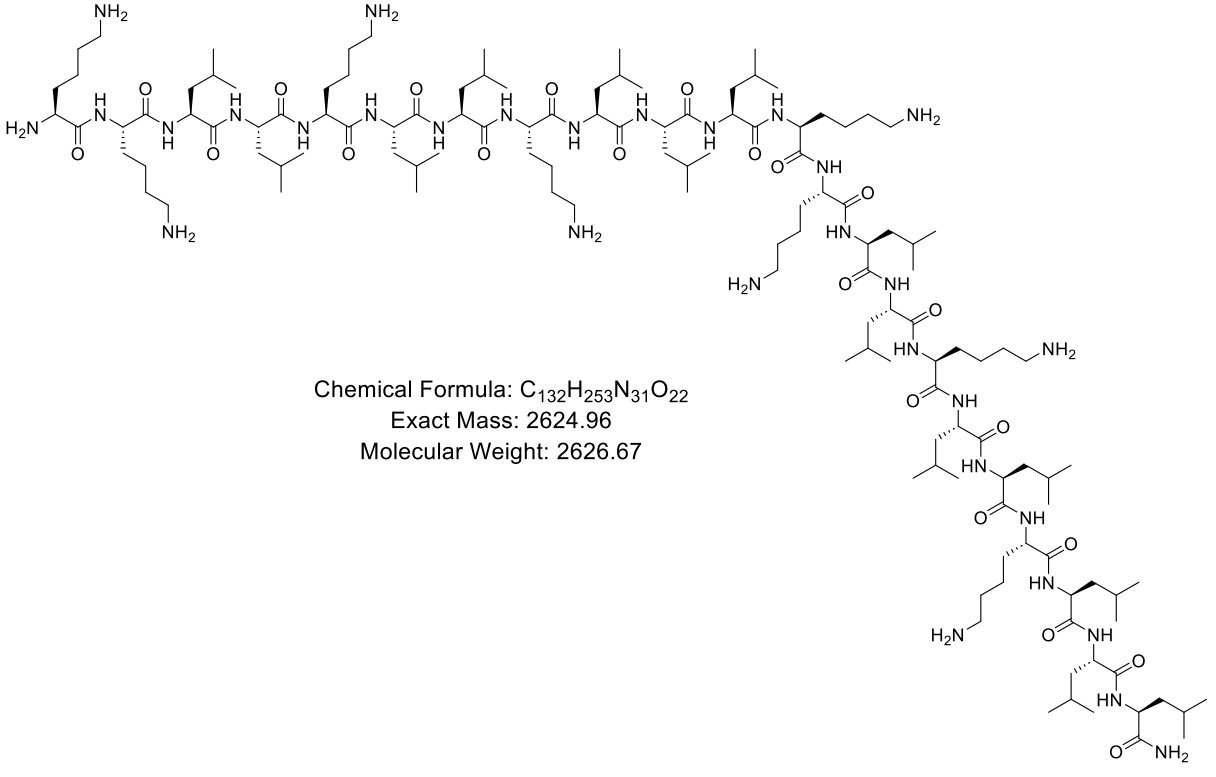

Chemical Formula: $C_{132}H_{253}N_{31}O_{22}$
Exact Mass: 2624.96
Molecular Weight: 2626.67

Analytical HPLC-MS data:

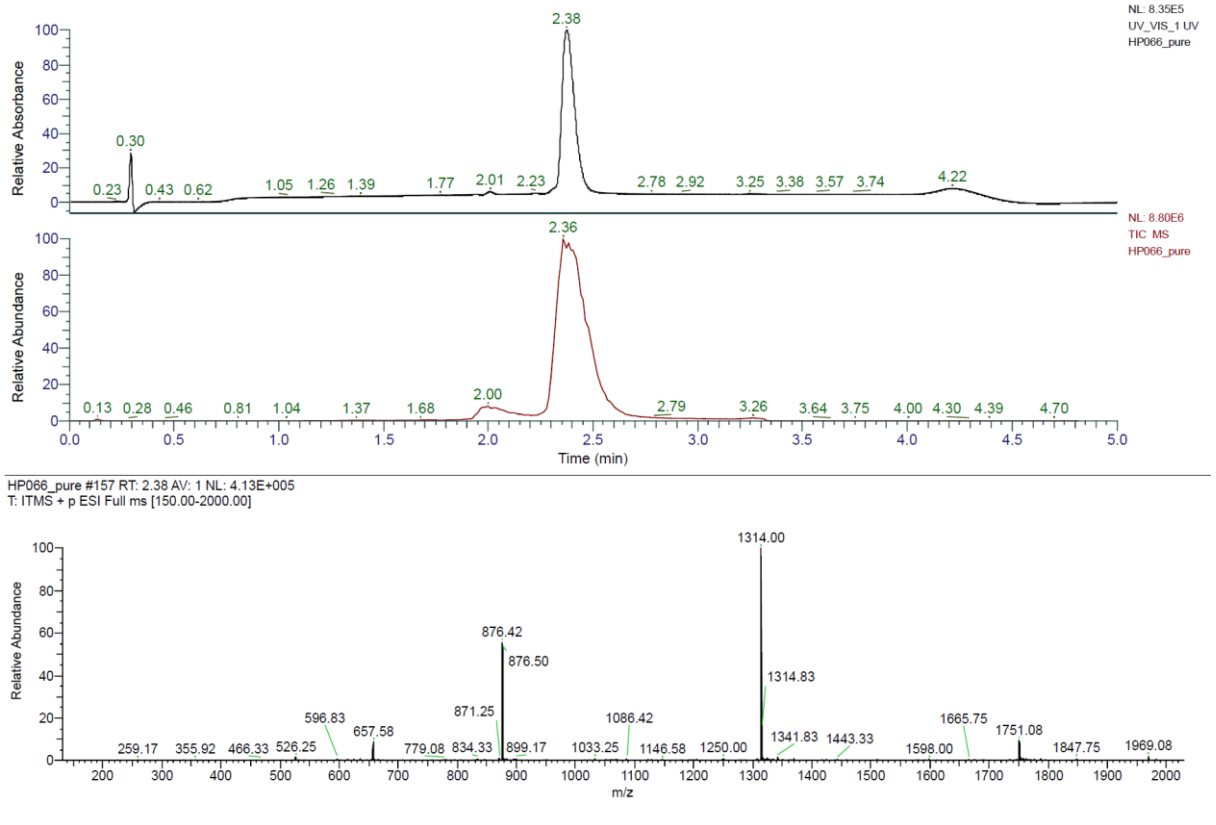

HRMS spectra:

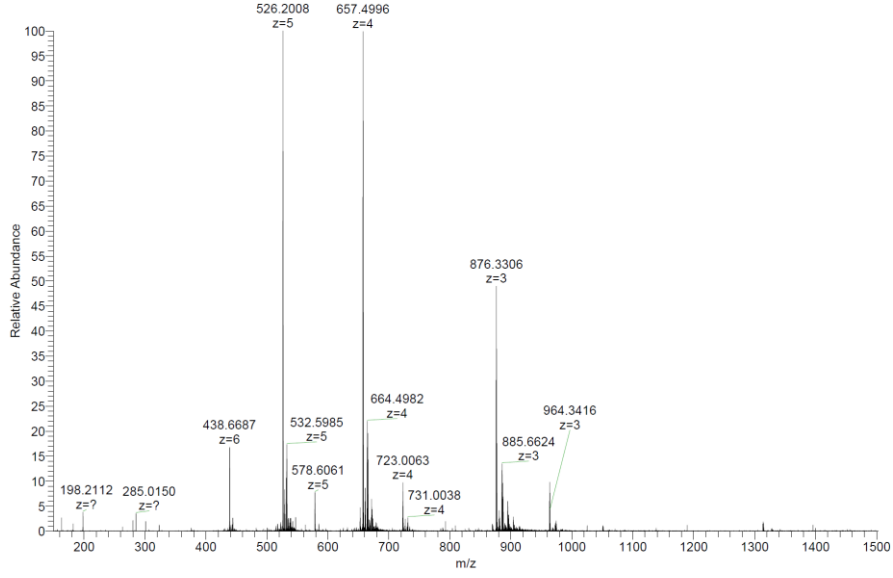

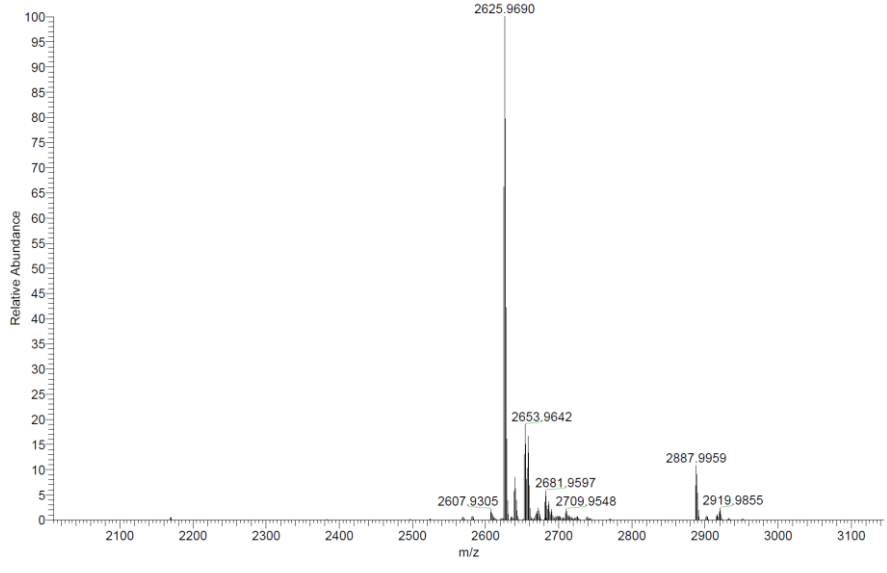

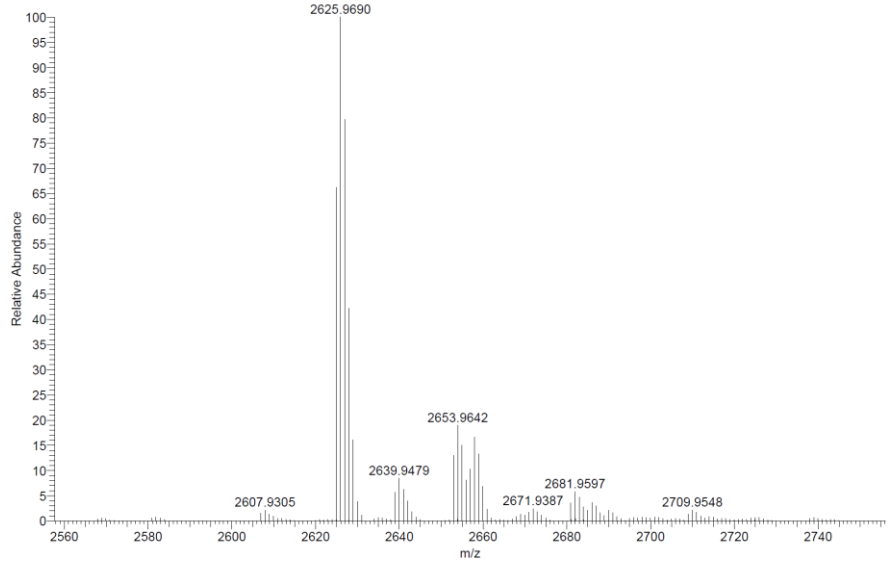

kkLLkLLkLLLkkLLkLLkLLL (2ln69) was obtained as white solid after preparative RP-HPLC (85.8 mg, 27.6%). Analytical RP-HPLC: t_R = 1.85 min (A/D 100:0 to 0:100 in 3.5 min, λ = 214 nm). MS (ESI+): $C_{132}H_{253}N_{31}O_{22}$ calc./obs. 2625.96/2625.97 Da $[M+H]^+$.

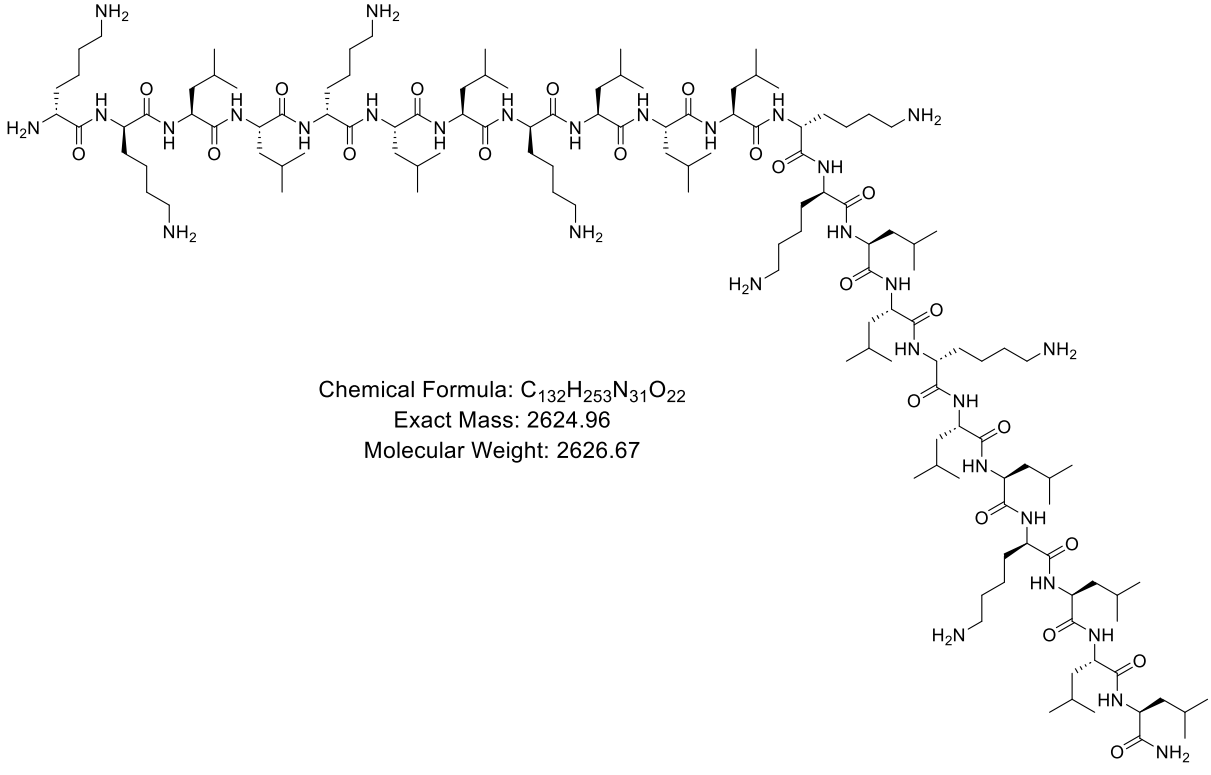

Chemical Formula: $C_{132}H_{253}N_{31}O_{22}$
Exact Mass: 2624.96
Molecular Weight: 2626.67

Analytical HPLC-MS data:

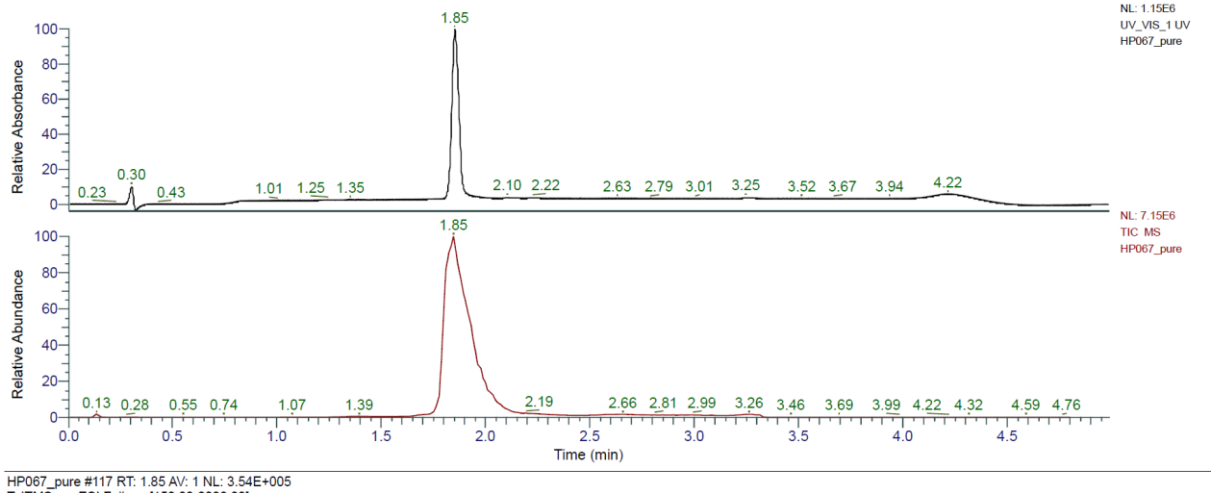

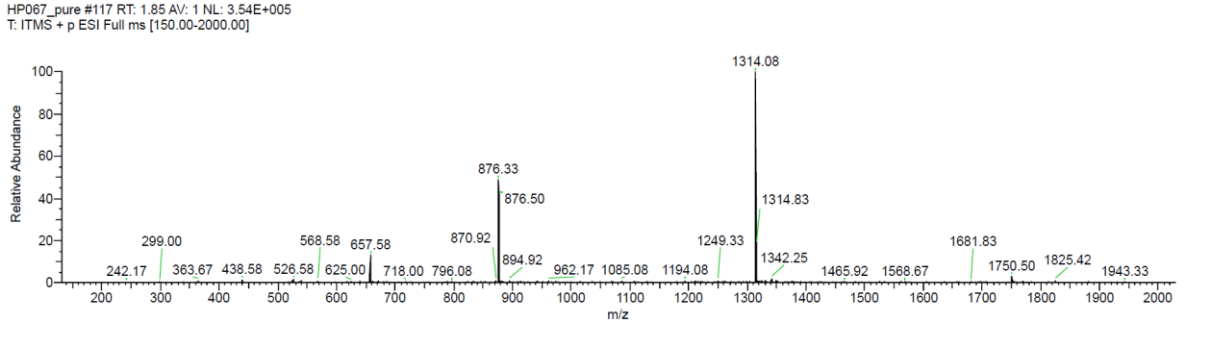

HRMS spectra:

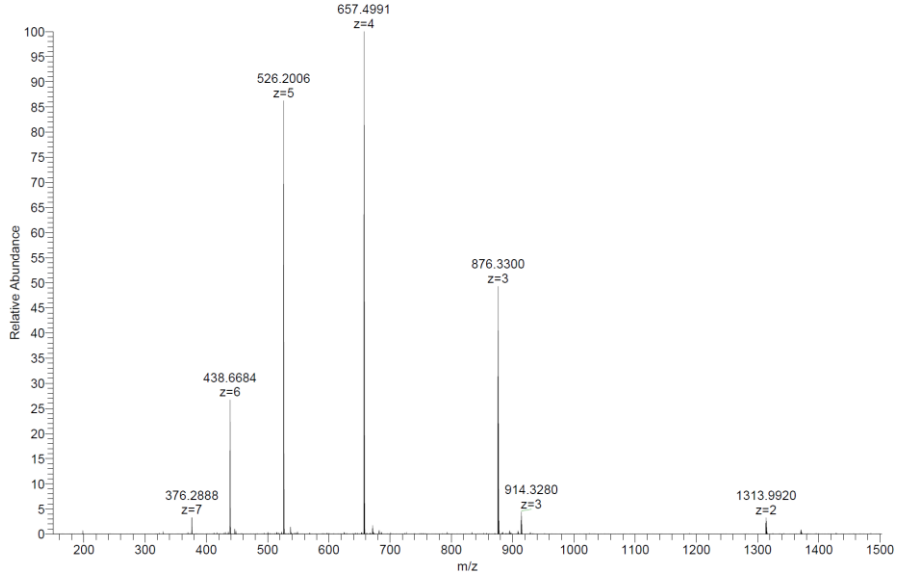

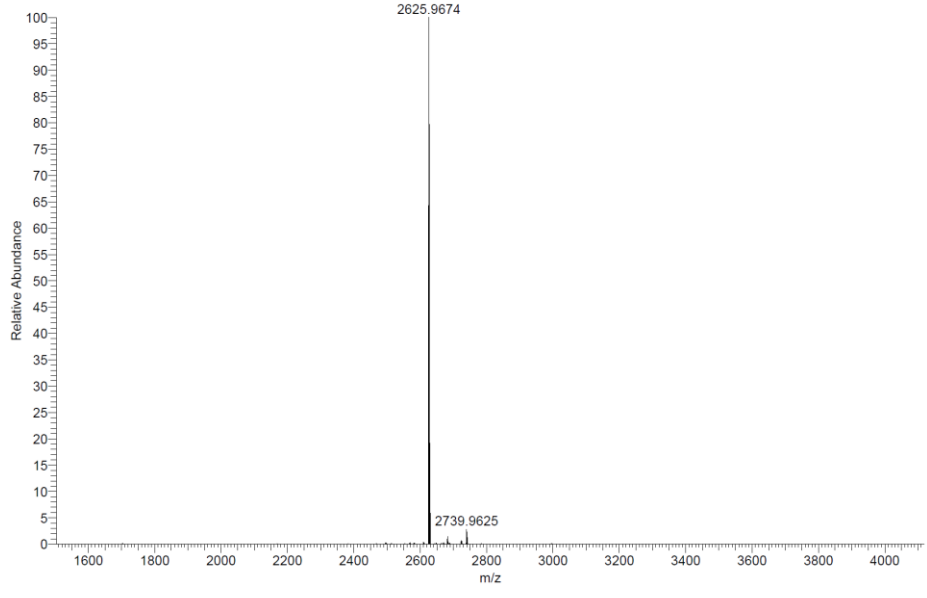

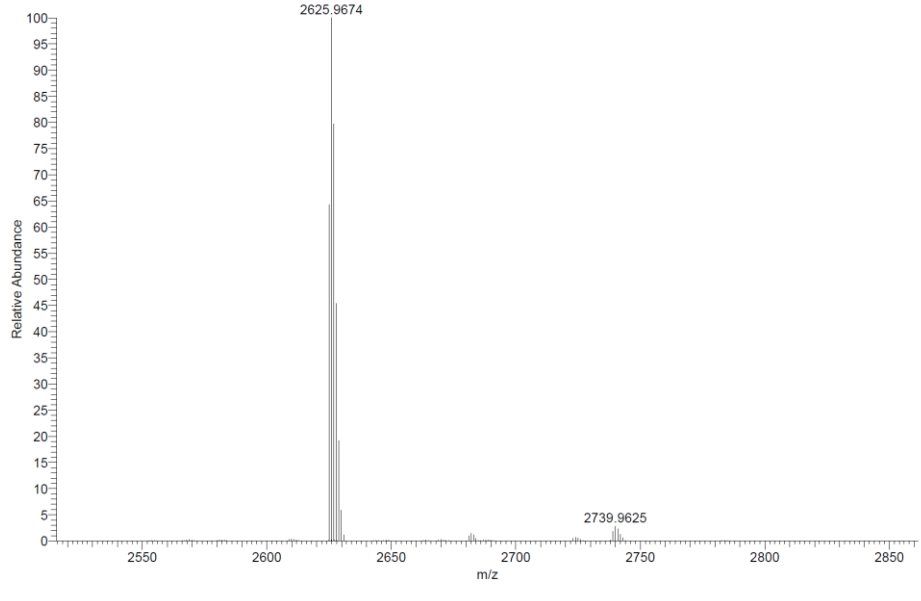

(*)KkLLKLLKLLL (FHP1) was obtained as white solid after preparative RP-HPLC (2.9 mg, 3.9%). Analytical RP-HPLC: t_R = 1.76 min (A/D 100:0 to 0:100 in 3.5 min, λ = 214 nm). MS (ESI+): $C_{66}H_{128}N_{16}O_{11}$ calc./obs. 1511.06/1511.07 Da $[M+2H]^{2+}$.

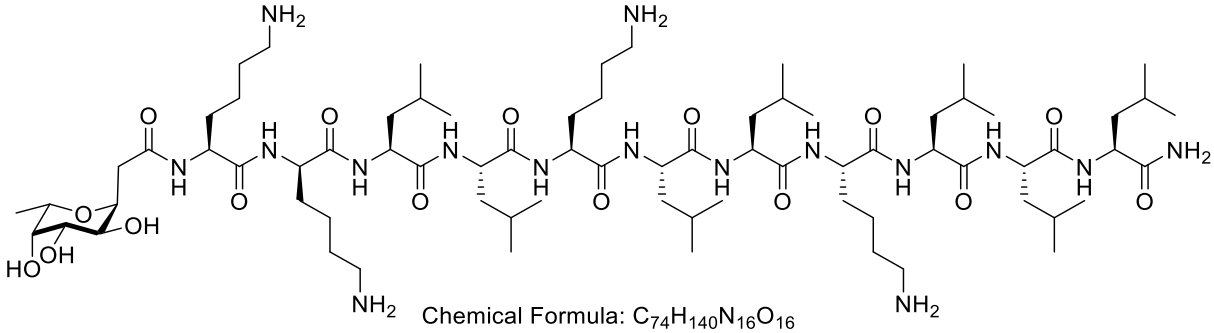

Analytical HPLC-MS data:

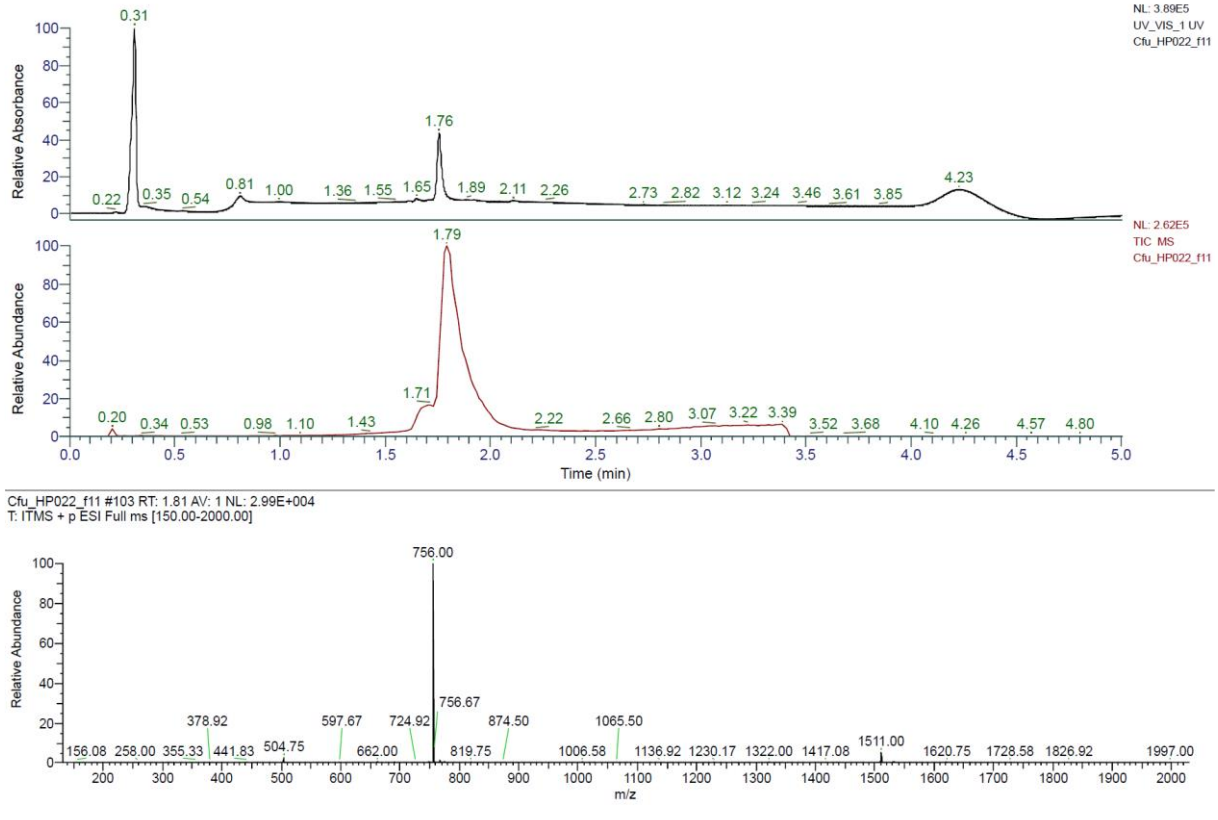

HRMS spectra:

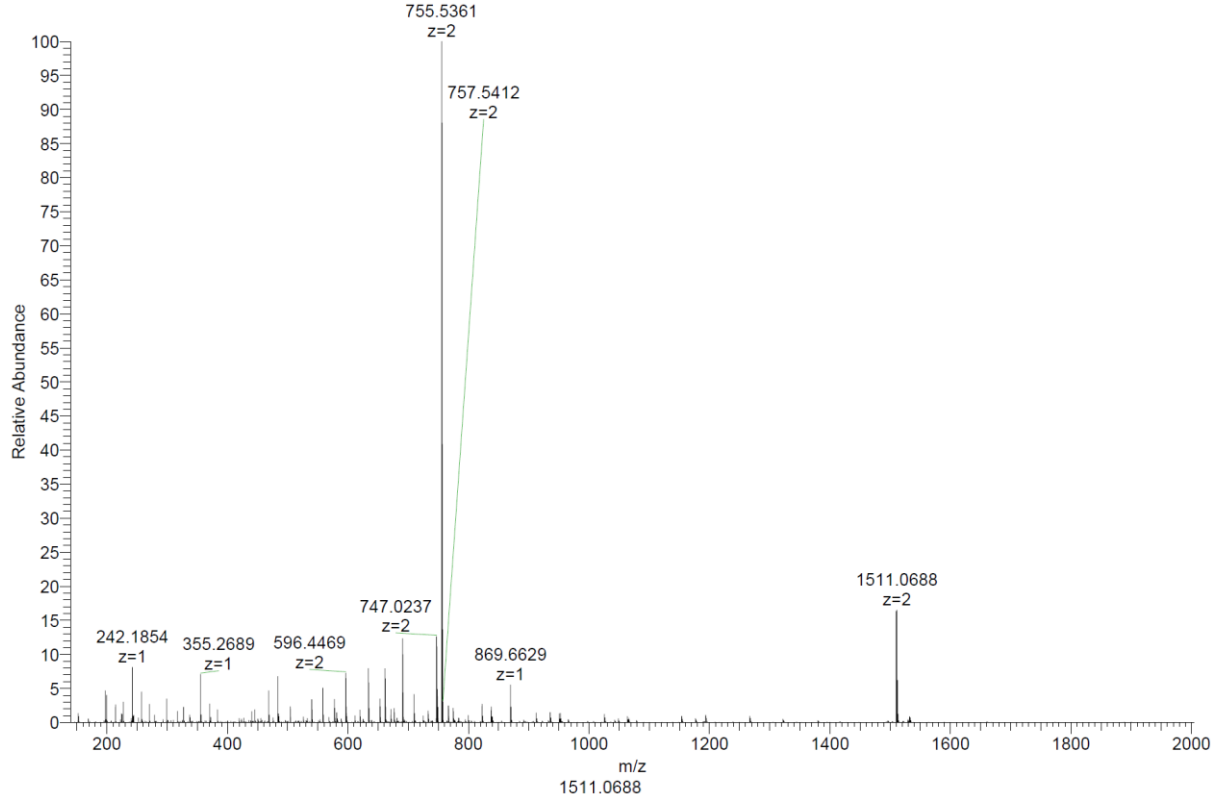

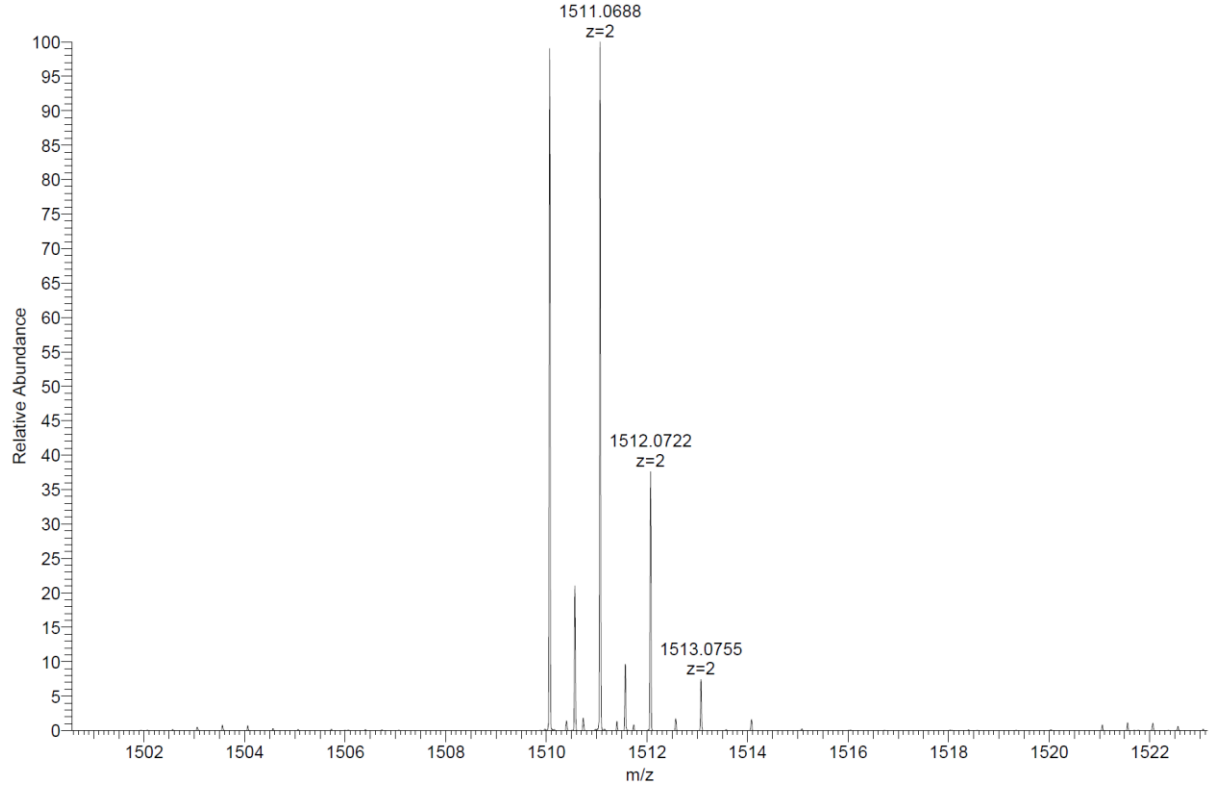

(*)kkLLKLLKLLL (FHP2) was obtained as white solid after preparative RP-HPLC (0.6 mg, 0.8%). Analytical RP-HPLC: t_R = 1.73 min (A/D 100:0 to 0:100 in 3.5 min, λ = 214 nm). MS (ESI+): $C_{66}H_{128}N_{16}O_{11}$ calc./obs. 1510.06/1510.07 Da $[M+H]^+$.

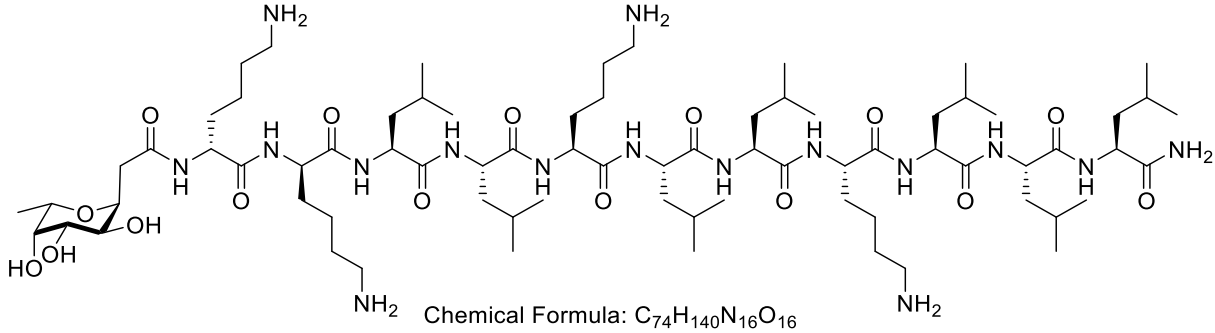

Analytical LC-MS data:

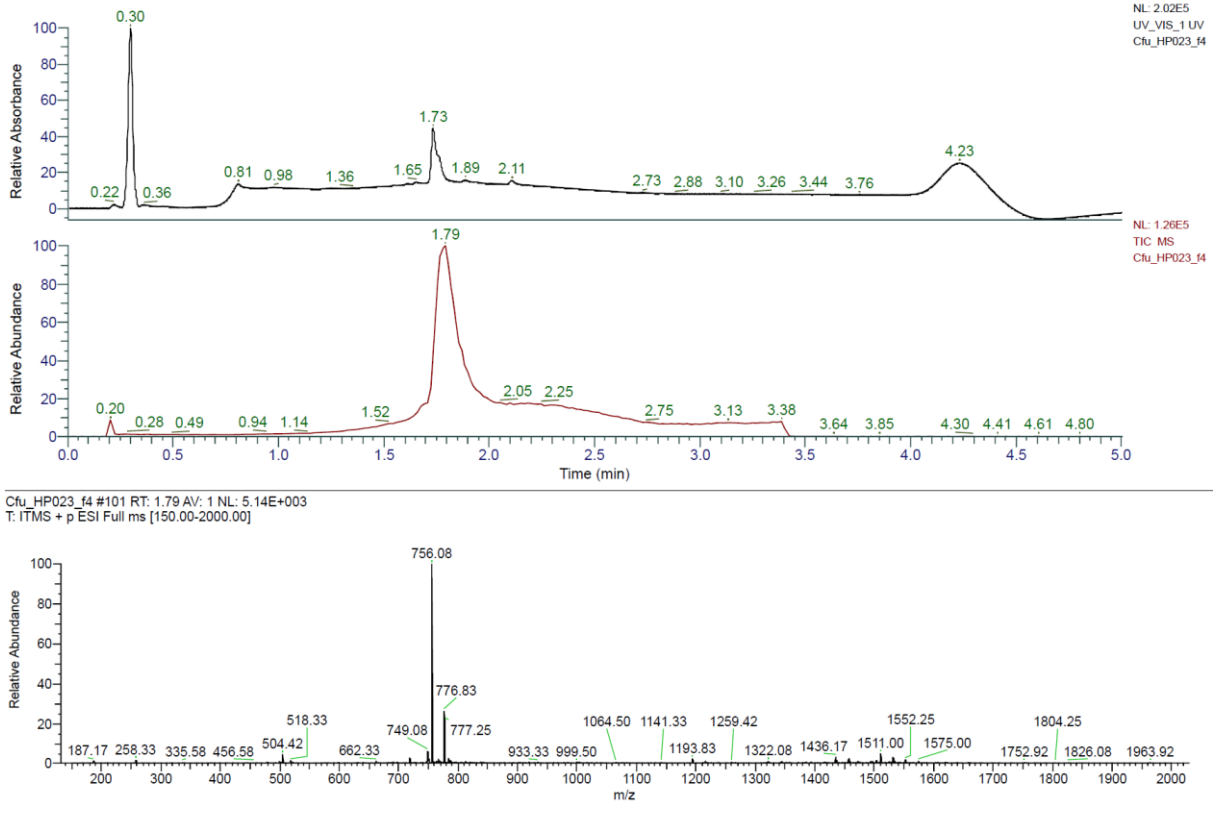

HRMS spectra:

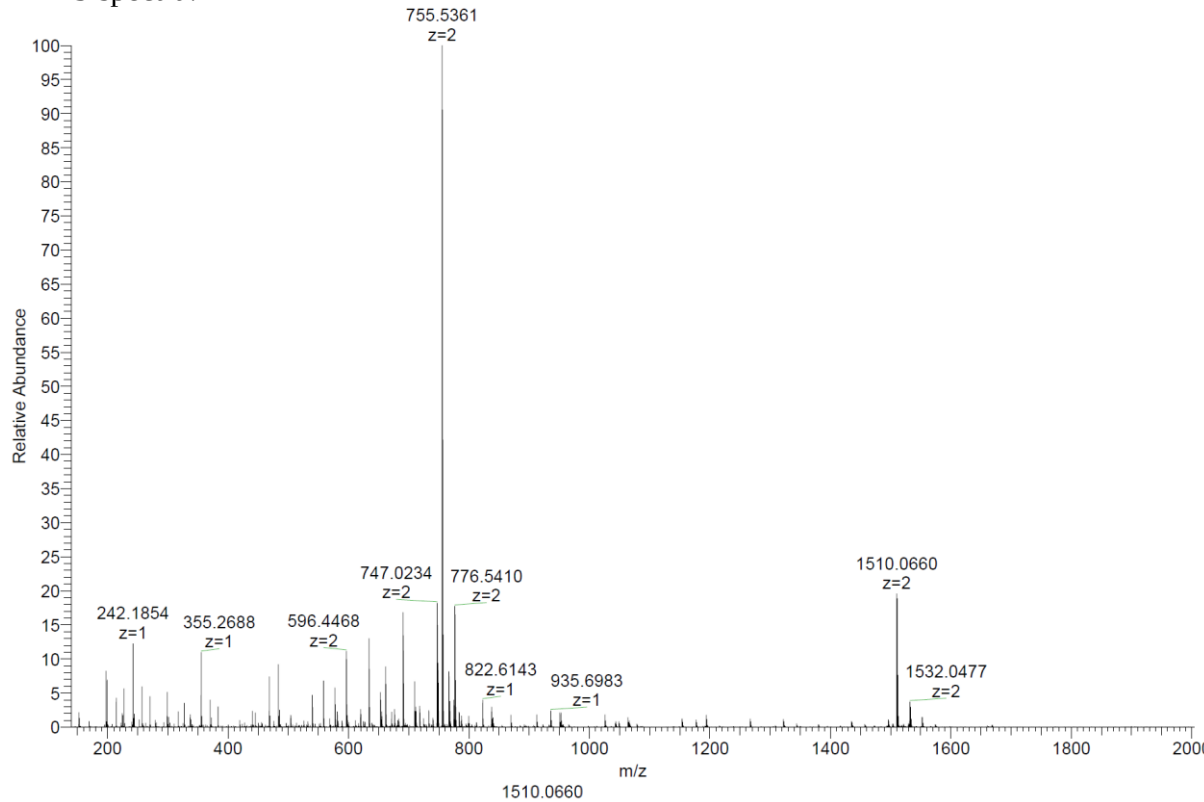

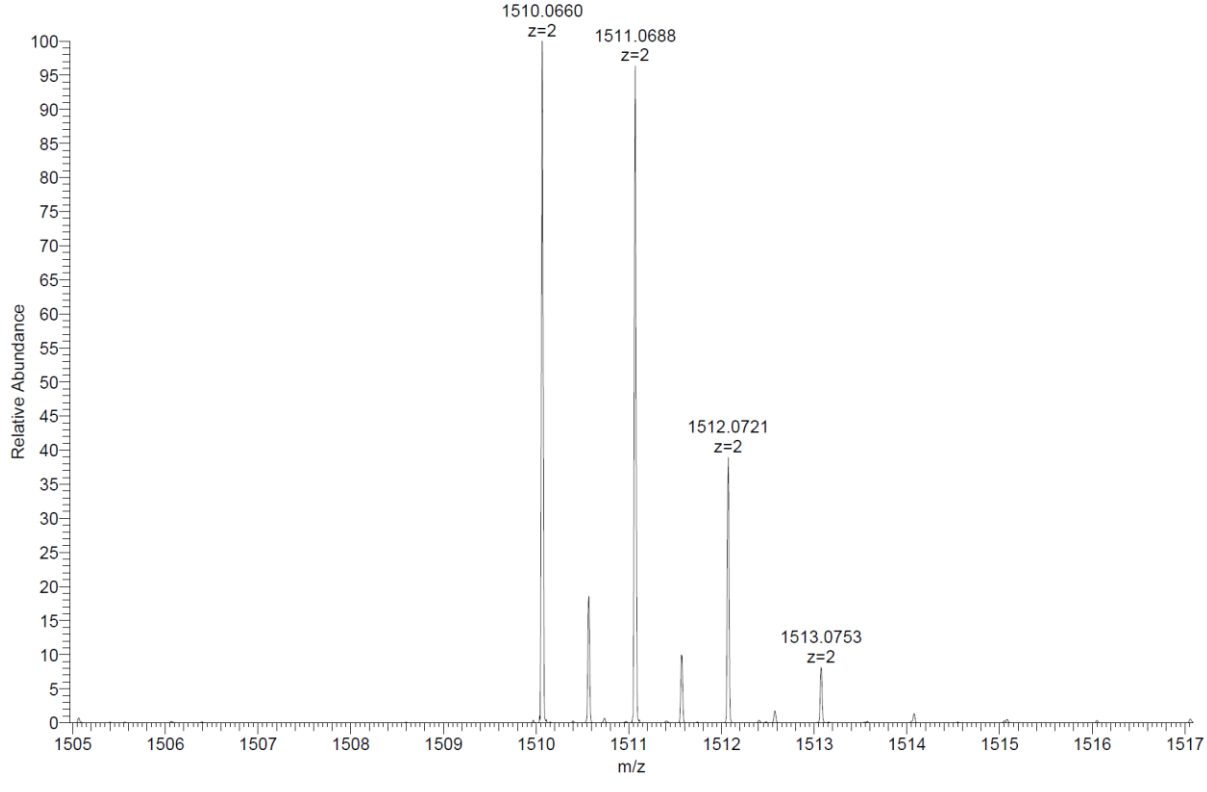

(*)KkLLkLLKLLL (FHP3) was obtained as white solid after preparative RP-HPLC (5.0 mg, 6.8%). Analytical RP-HPLC: t_R = 1.67 min (A/D 100:0 to 0:100 in 3.5 min, λ = 214 nm). MS (ESI+): $C_{66}H_{128}N_{16}O_{11}$ calc./obs. 1510.06/1510.07 Da $[M+H]^+$.

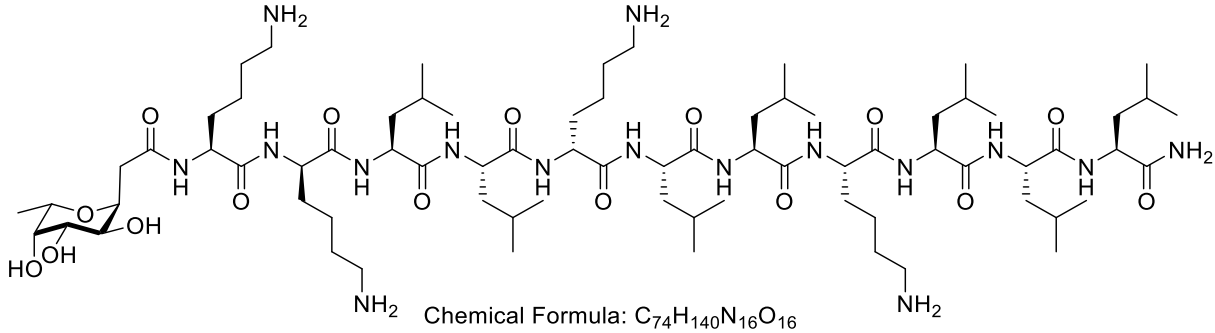

Analytical LC-MS data:

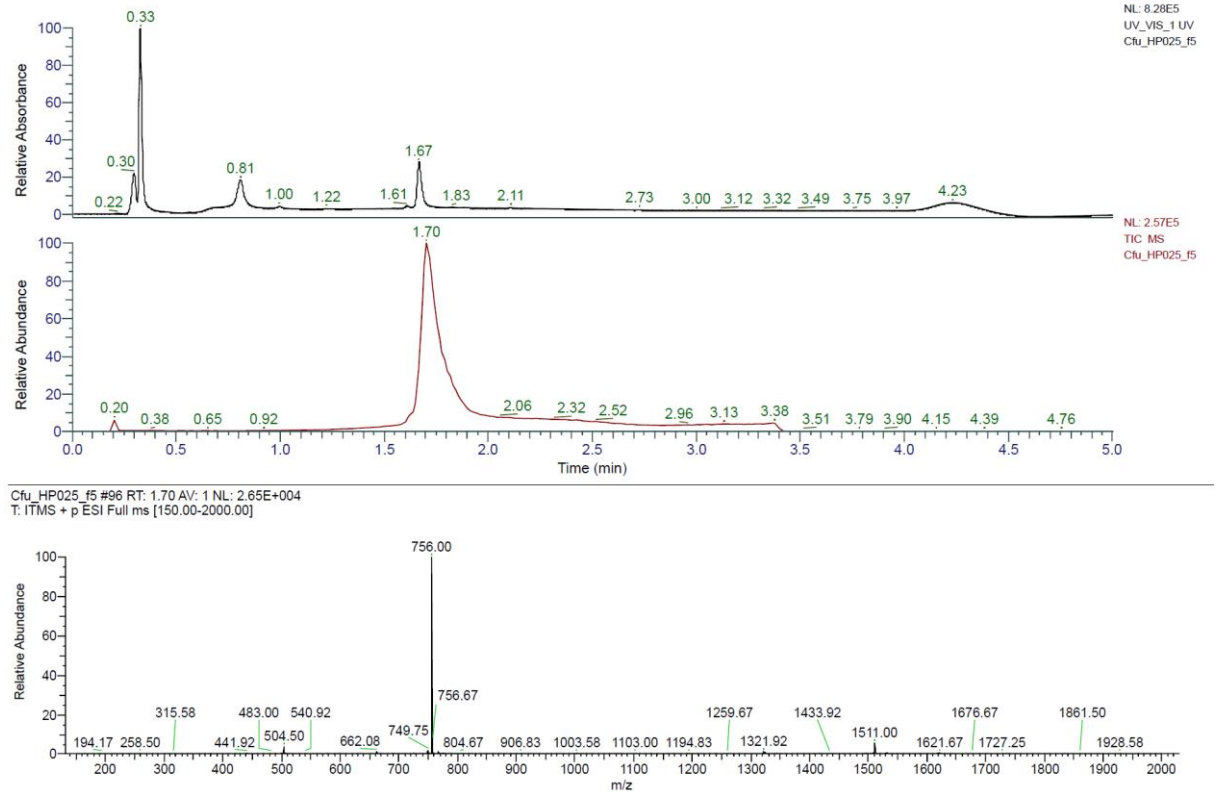

HRMS spectra:

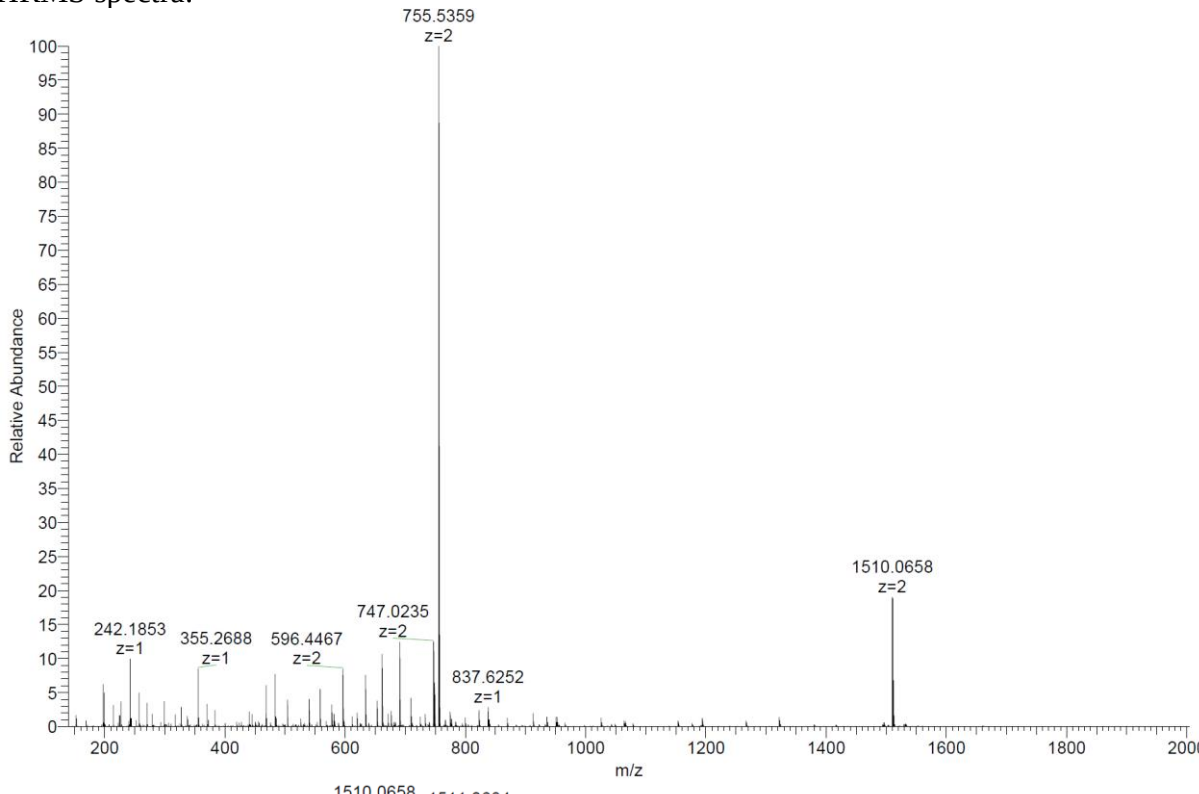

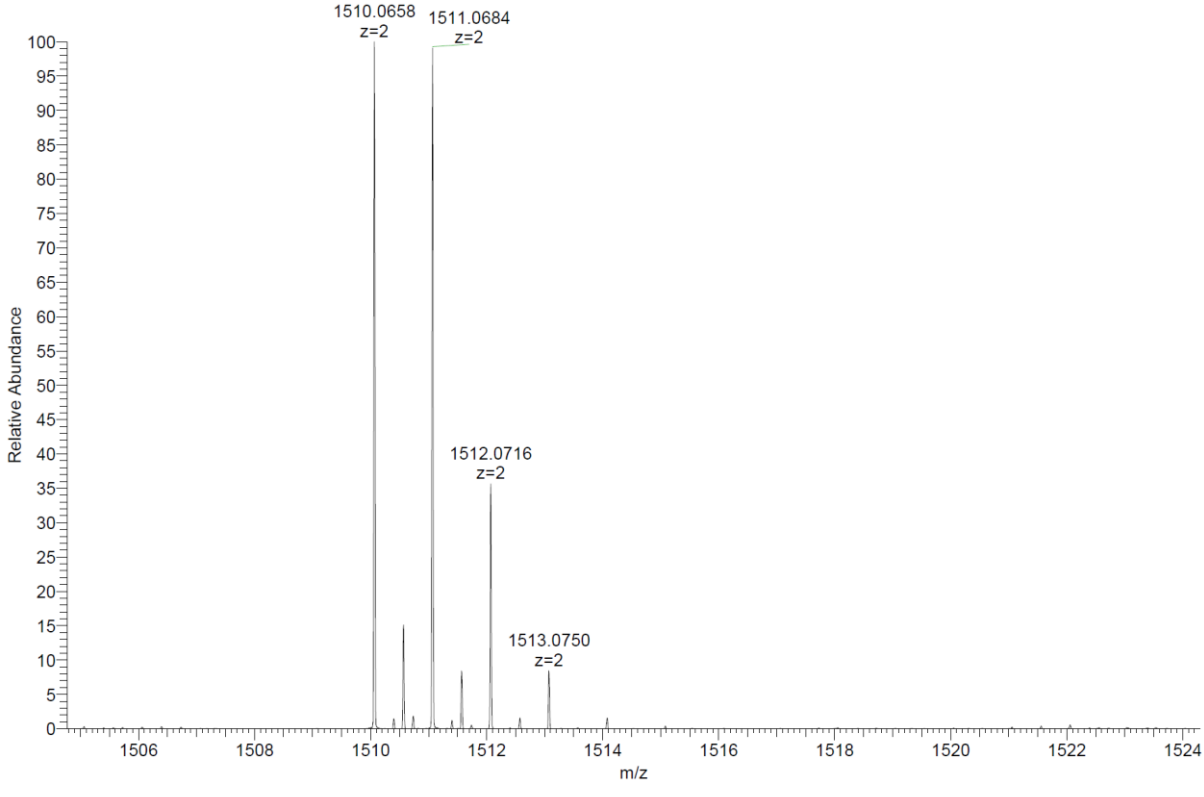

(*)KkLlKLLKLLL (FHP4) was obtained as white solid after preparative RP-HPLC (4.5 mg, 6.1%). Analytical RP-HPLC: t_R = 1.74 min (A/D 100:0 to 0:100 in 3.5 min, λ = 214 nm). MS (ESI+): $C_{66}H_{128}N_{16}O_{11}$ calc./obs. 1510.06/1510.07 Da $[M+H]^+$.

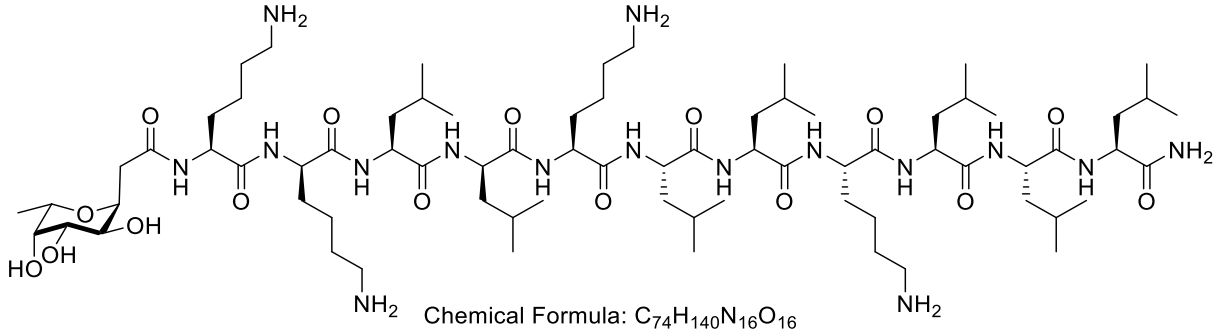

Analytical LC-MS data:

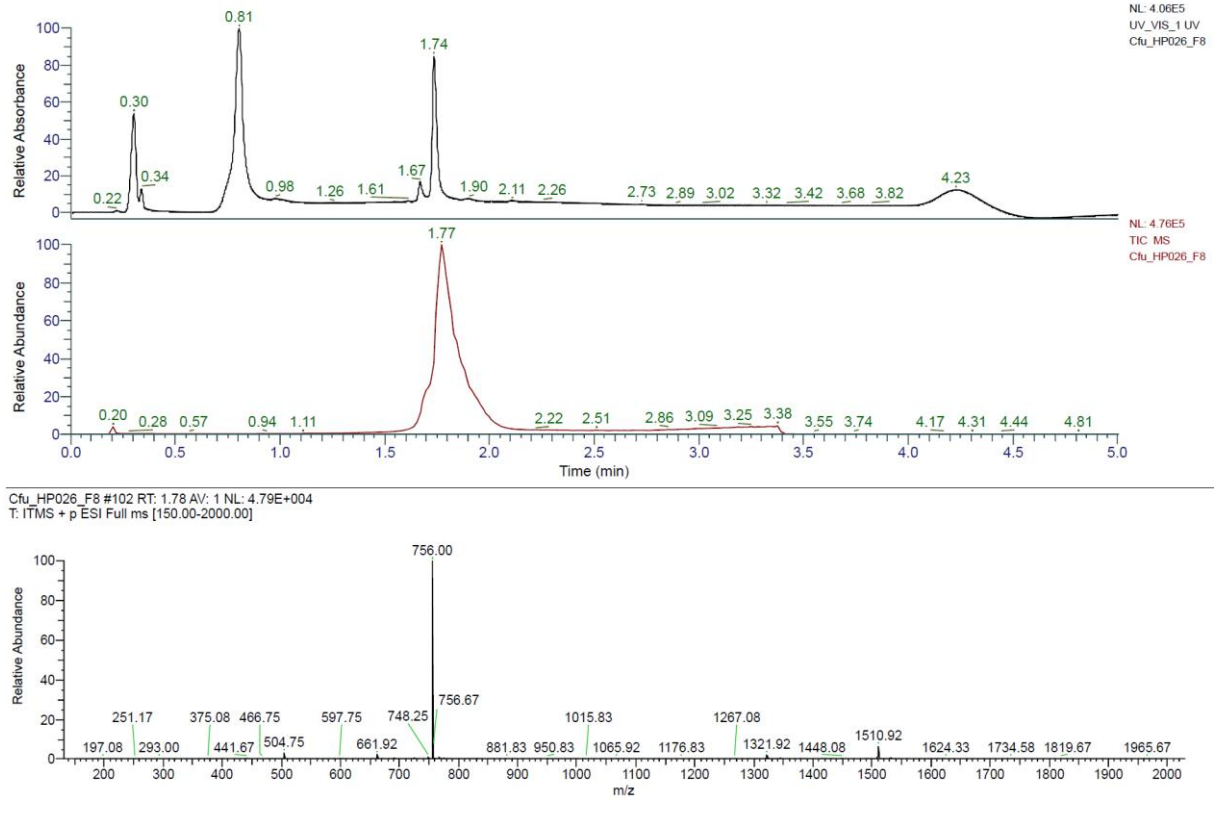

HRMS spectra:

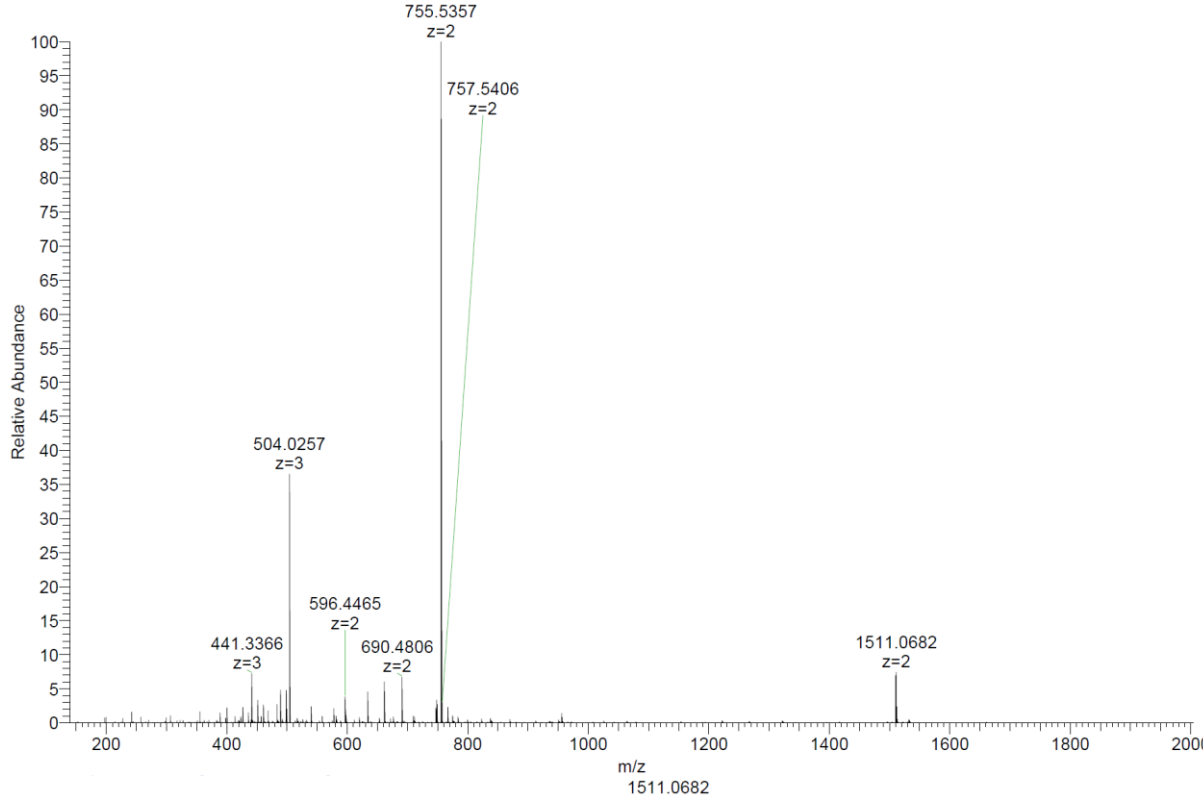

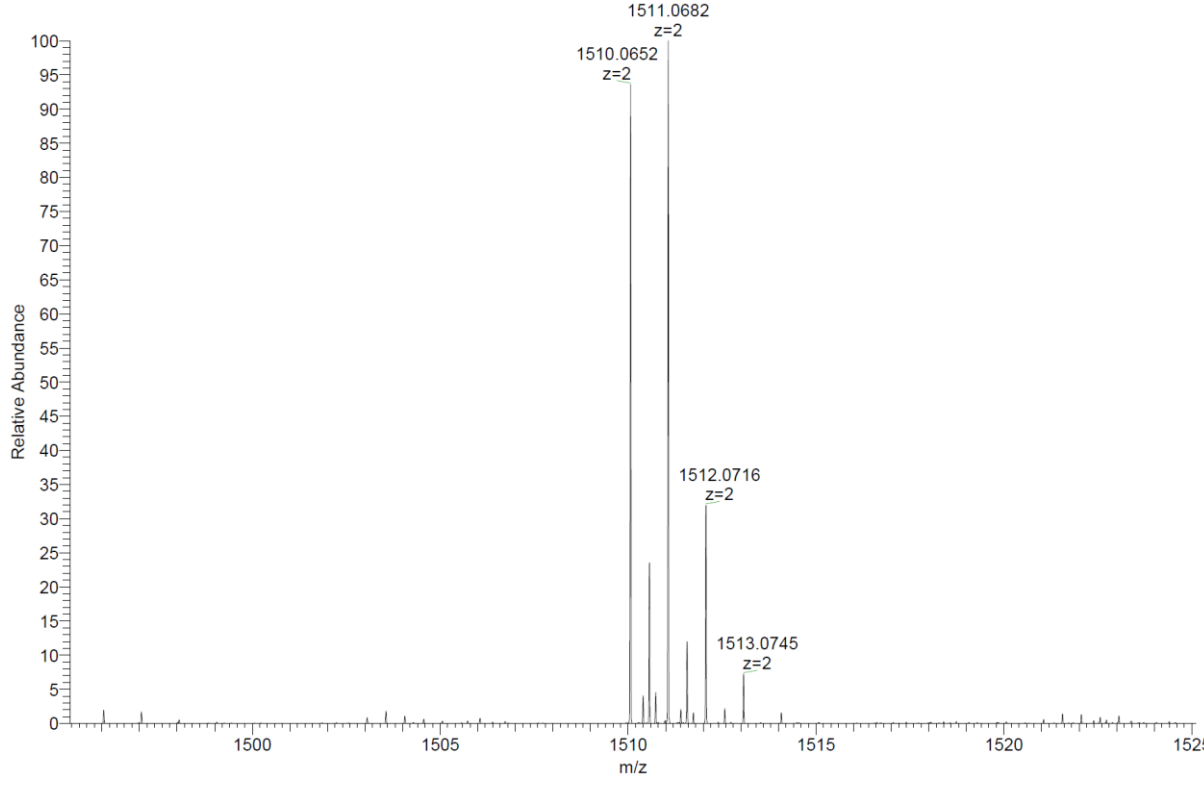

(*)kKLLKLLKLLl (FHP5) was obtained as white solid after preparative RP-HPLC (4.3 mg, 5.8%). Analytical RP-HPLC: t_R = 1.66 min (A/D 100:0 to 0:100 in 3.5 min, λ = 214 nm). MS (ESI+): $C_{66}H_{128}N_{16}O_{11}$ calc./obs. 1510.06/1510.07 Da $[M+H]^+$.

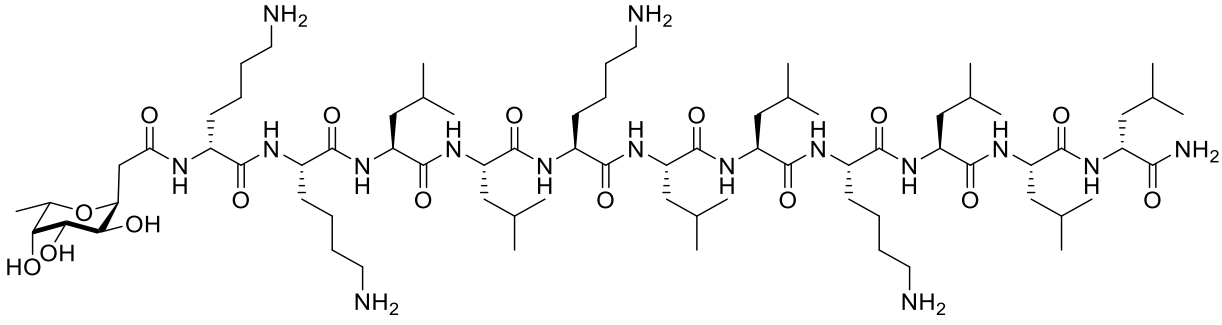

Chemical Formula: $C_{74}H_{140}N_{16}O_{16}$
Exact Mass: 1509.06
Molecular Weight: 1510.03

Analytical HPLC-MS data:

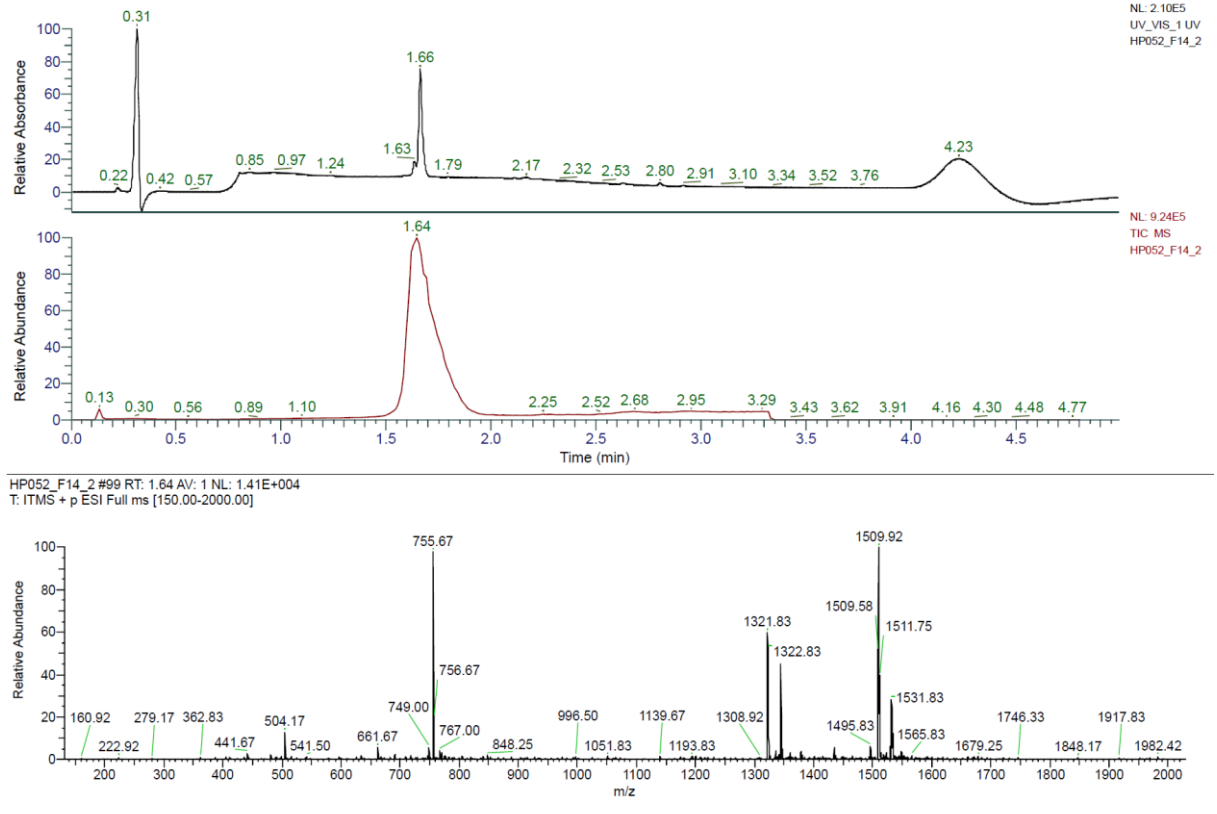

HRMS spectra:

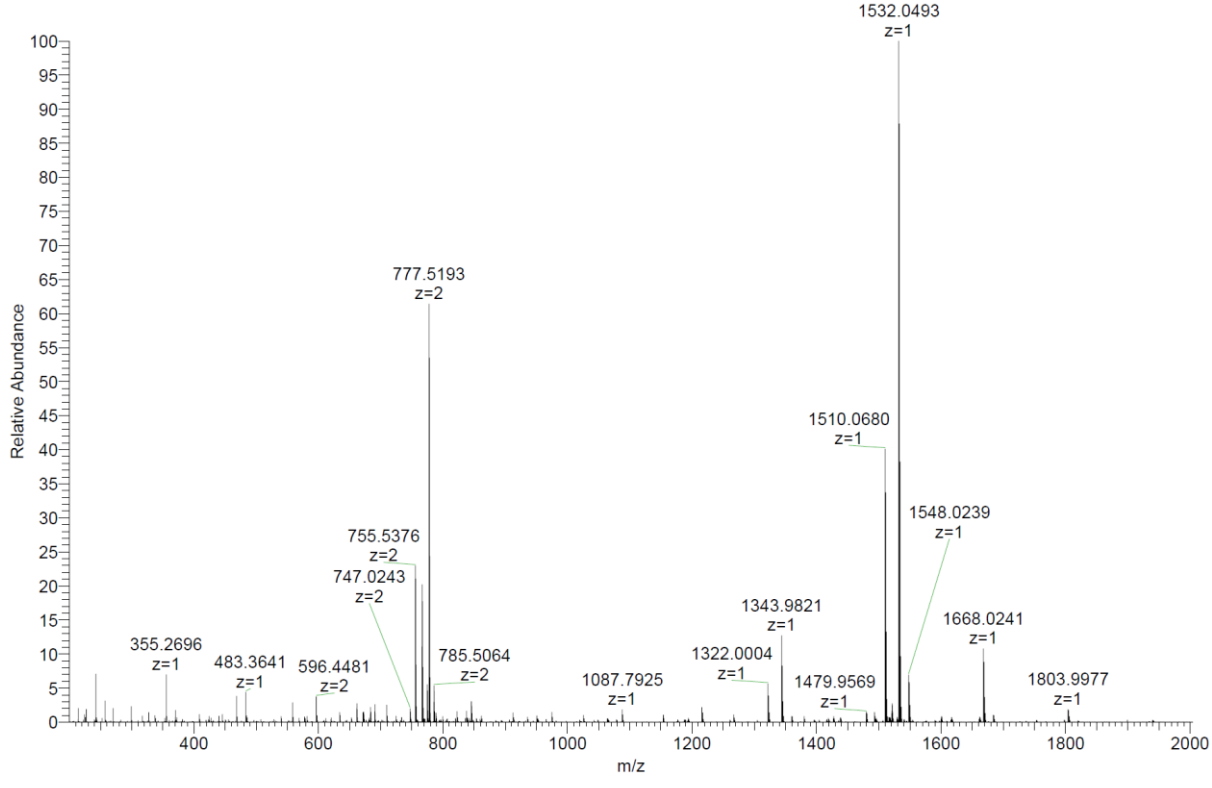

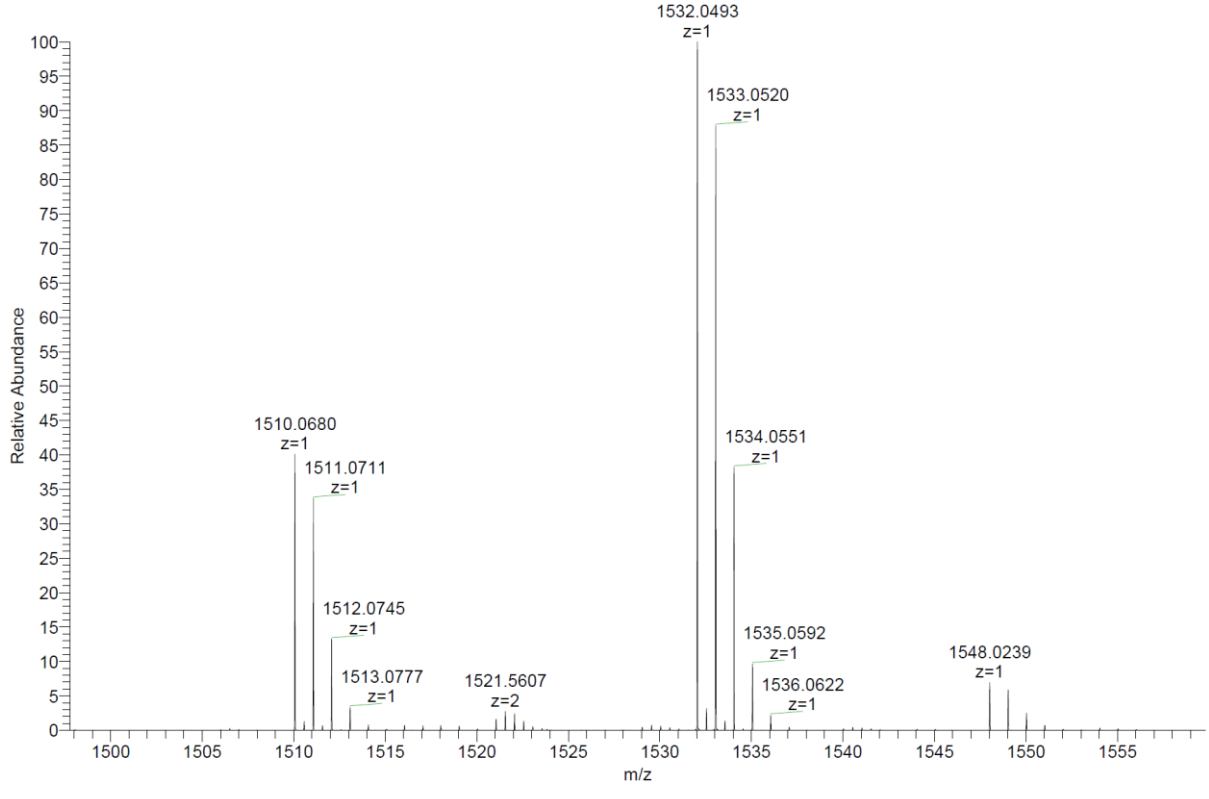

(*)kkLLKLLKLLl (FHP7) was obtained as white solid after preparative RP-HPLC (3.4 mg, 4.6%). Analytical RP-HPLC: t_R = 1.63 min (A/D 100:0 to 0:100 in 3.5 min, λ = 214 nm). MS (ESI+): $C_{74}H_{140}N_{16}O_{16}$ calc./obs. 1510.06/1510.07 Da $[M+H]^+$.

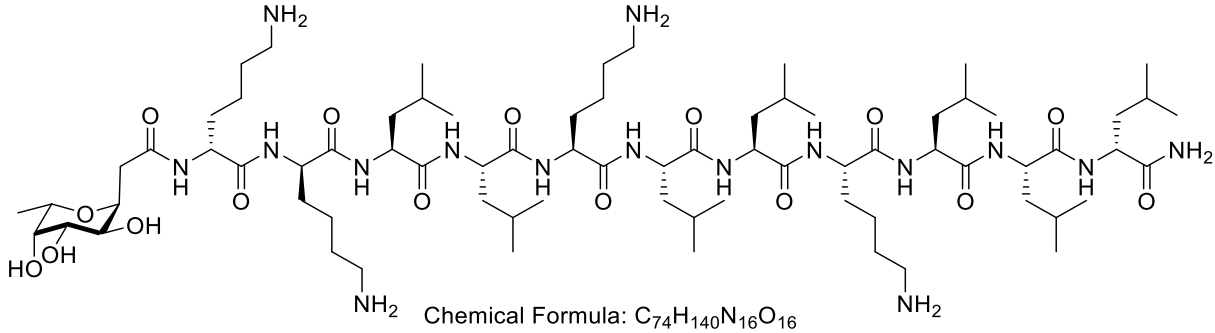

Analytical LC-MS data:

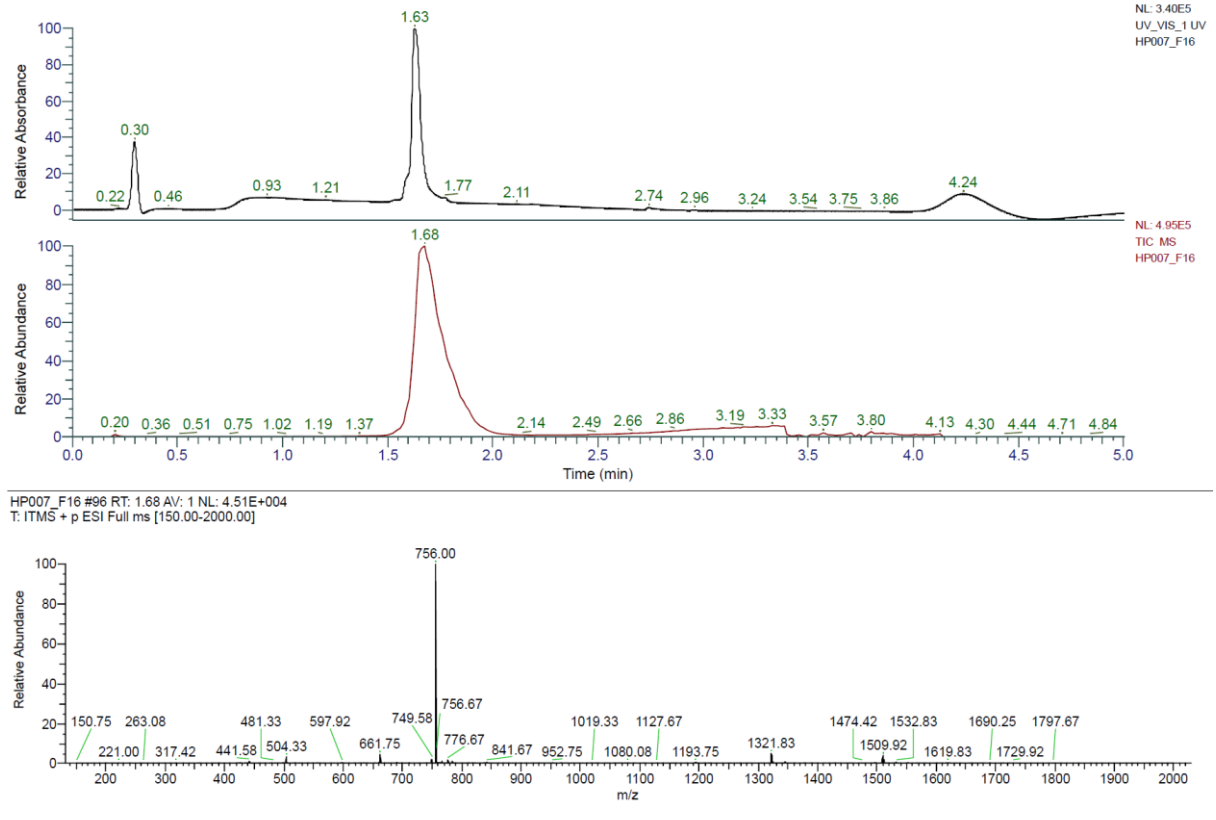

HRMS spectra:

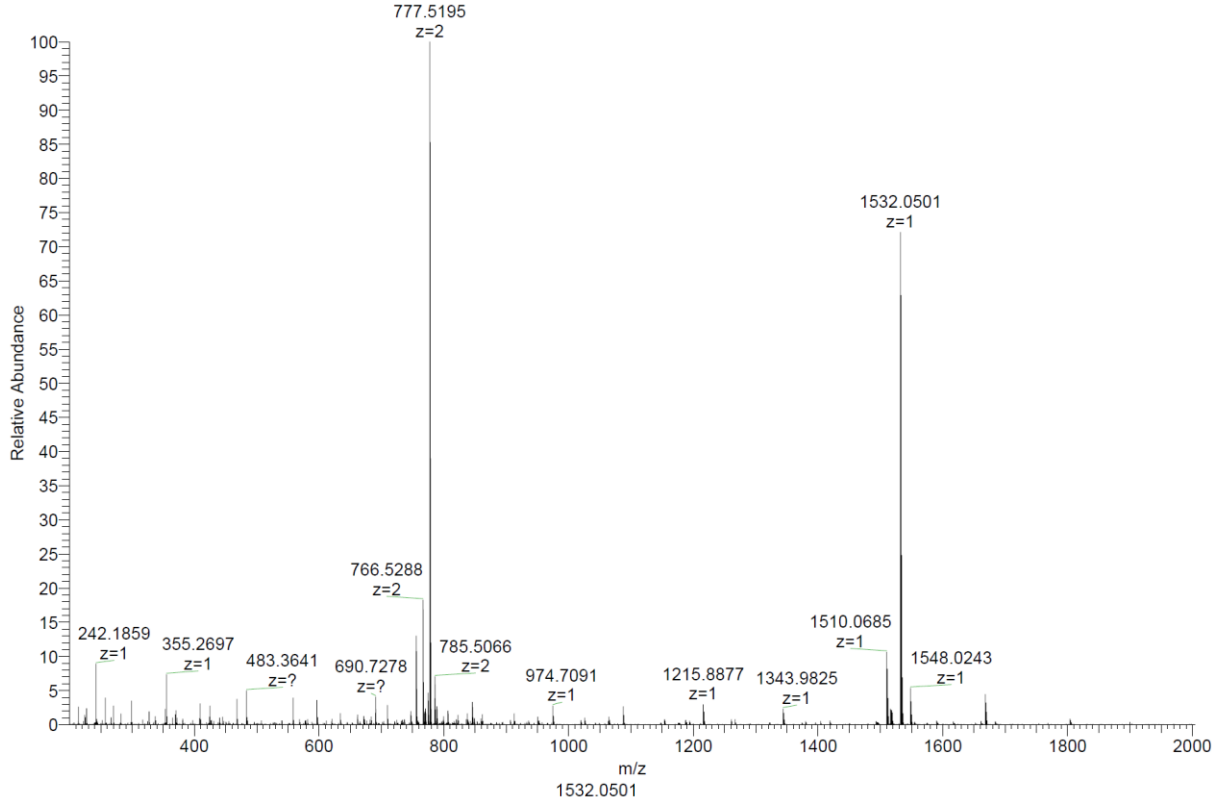

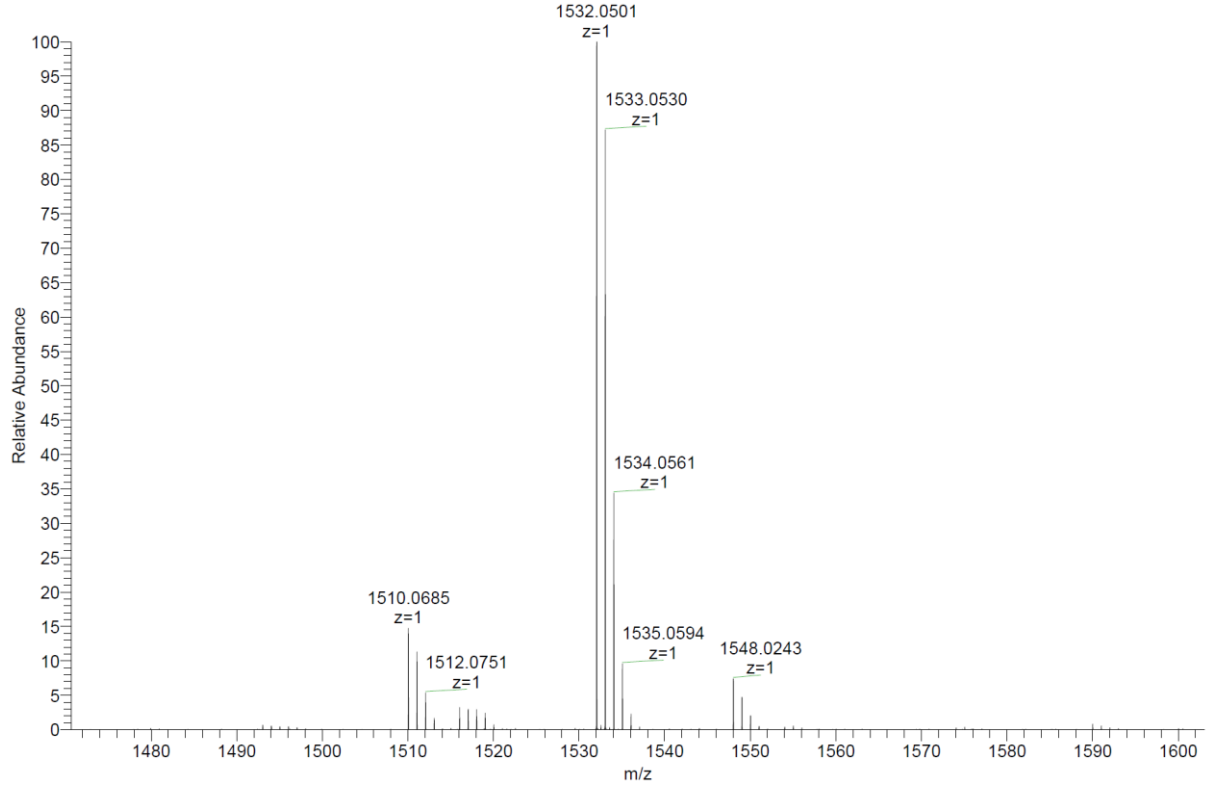

(*)KkllKLLKLLL (FHP8) was obtained as white solid after preparative RP-HPLC (5.7 mg, 7.7%). Analytical RP-HPLC: t_R = 1.63 min (A/D 100:0 to 0:100 in 3.5 min, λ = 214 nm). MS (ESI+): $C_{74}H_{140}N_{16}O_{16}$ calc./obs. 1510.06/1510.06 Da $[M+H]^+$.

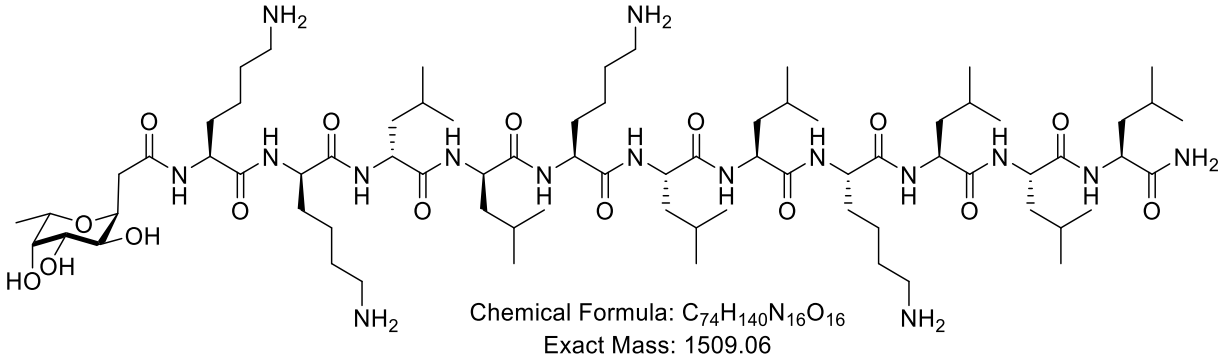

Analytical HPLC-MS data:

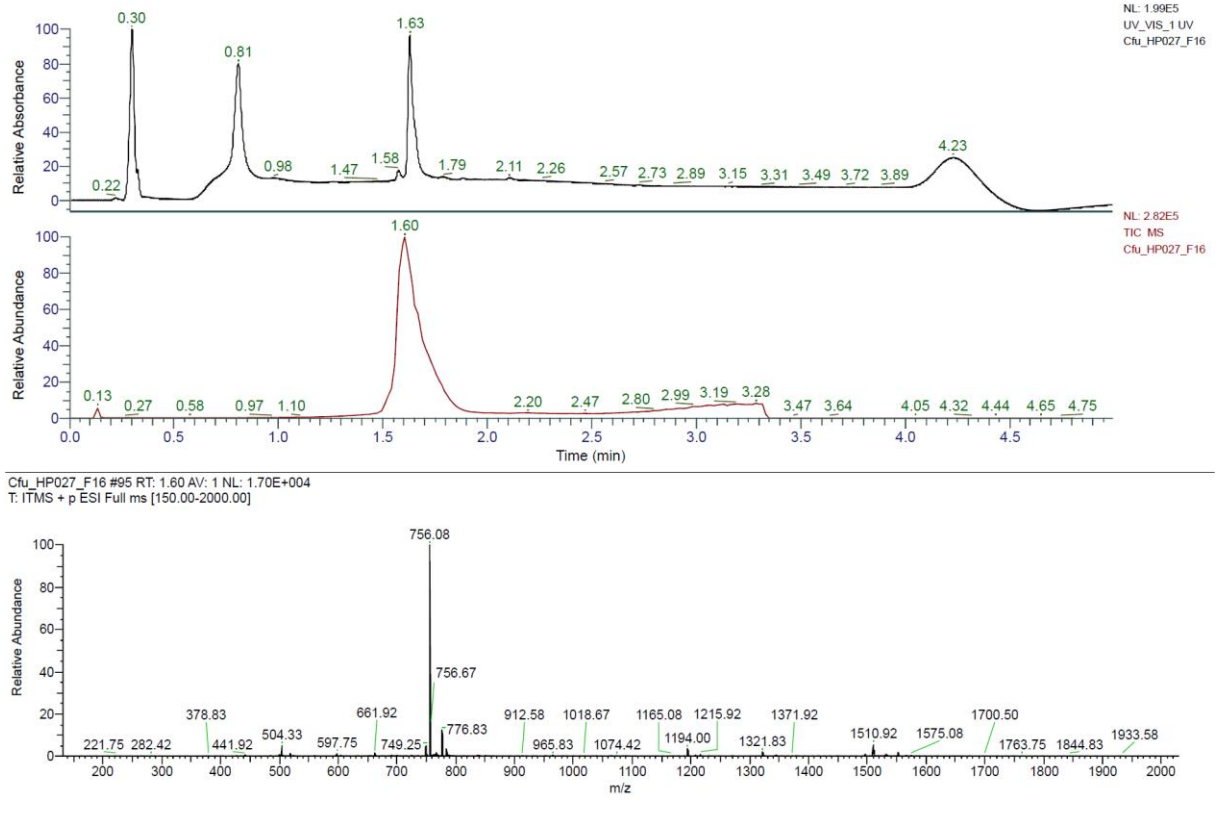

HRMS spectra:

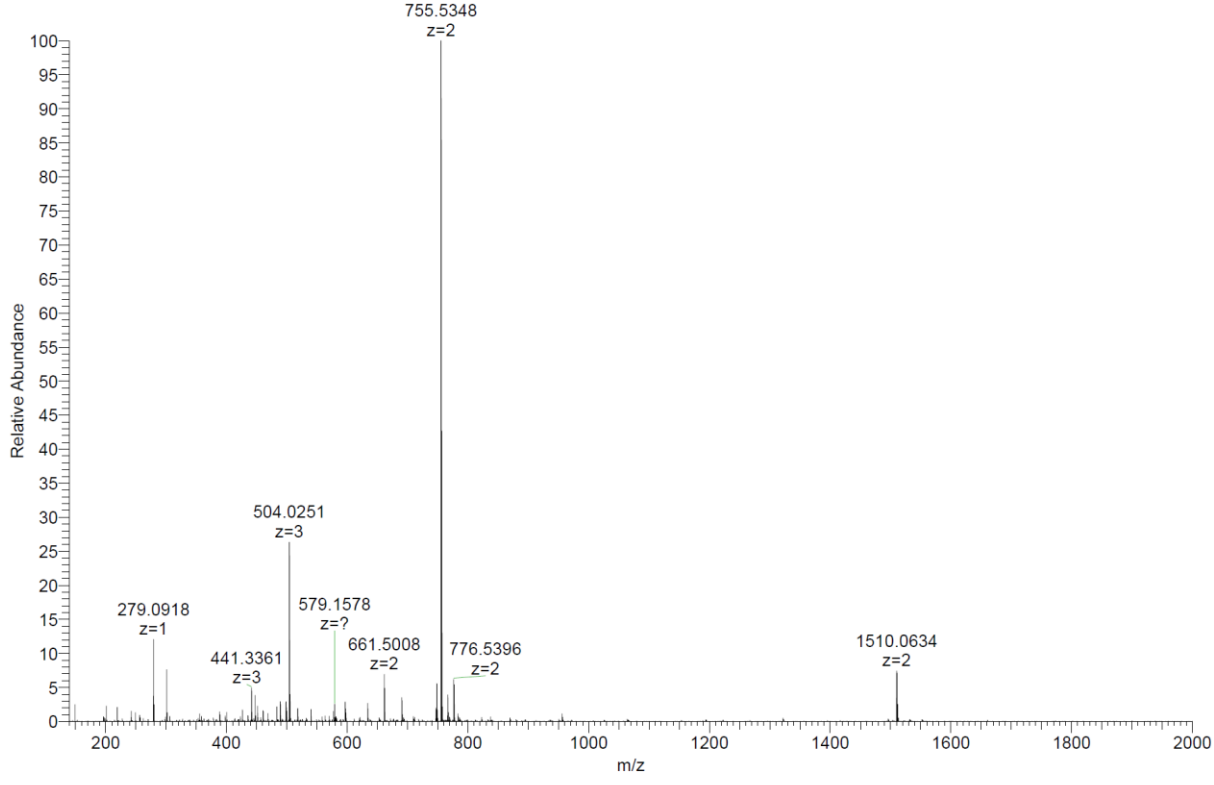

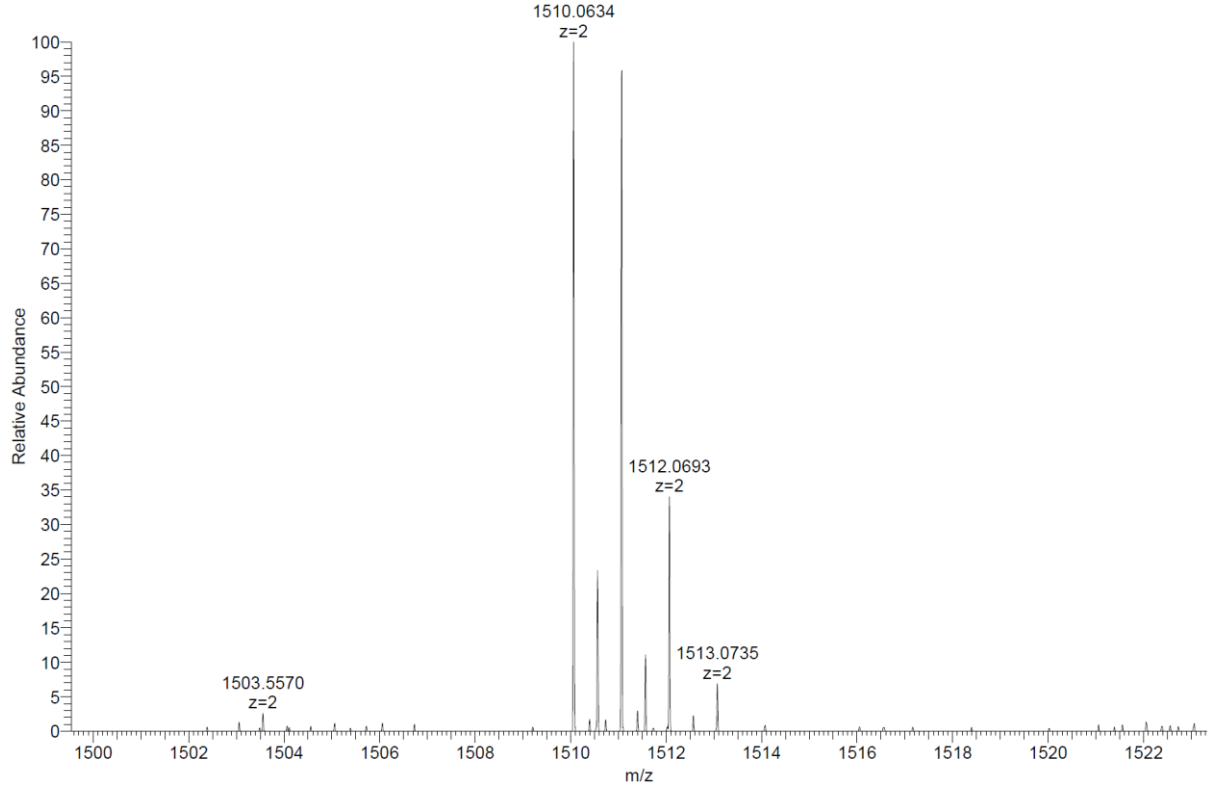

(*)kkLLkLLKLLL (FHP10) was obtained as white solid after preparative RP-HPLC (4.0 mg, 5.4%). Analytical RP-HPLC: t_R = 1.67 min (A/D 100:0 to 0:100 in 3.5 min, λ = 214 nm). MS (ESI+): $C_{74}H_{140}N_{16}O_{16}$ calc./obs. 1510.06/1510.07 Da $[M+H]^+$.

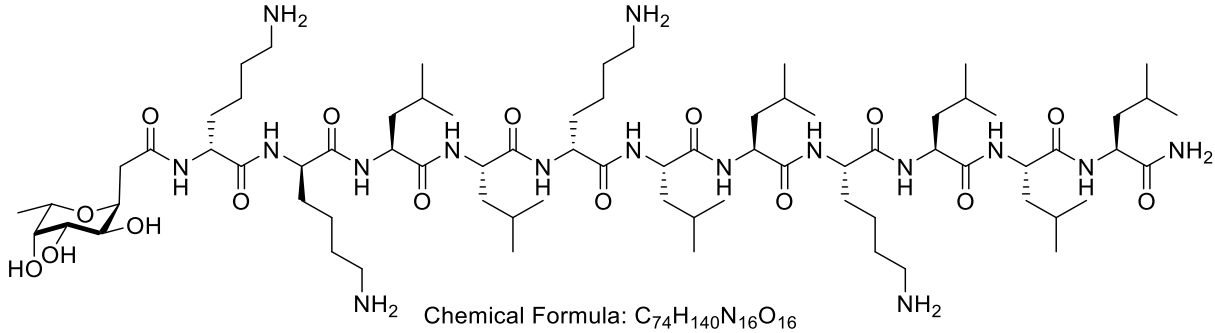

Analytical LC-MS data:

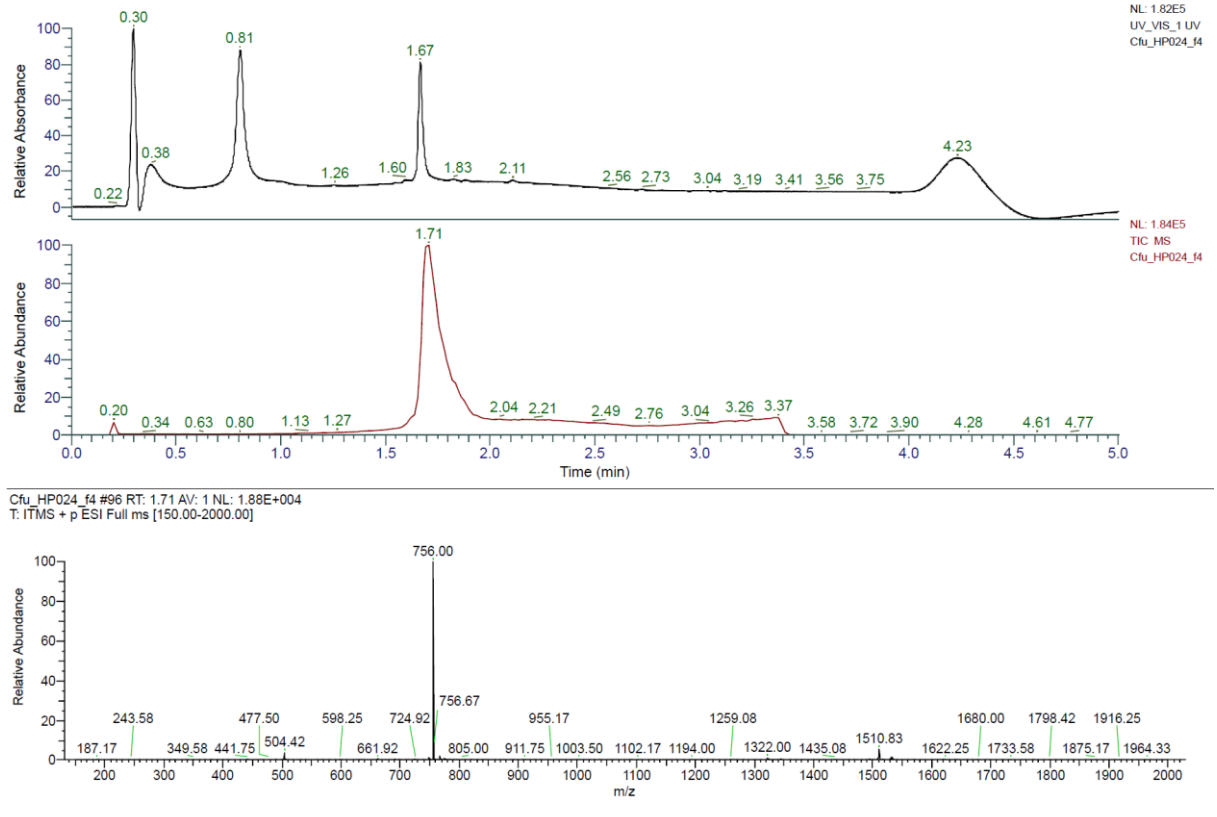

HRMS spectra:

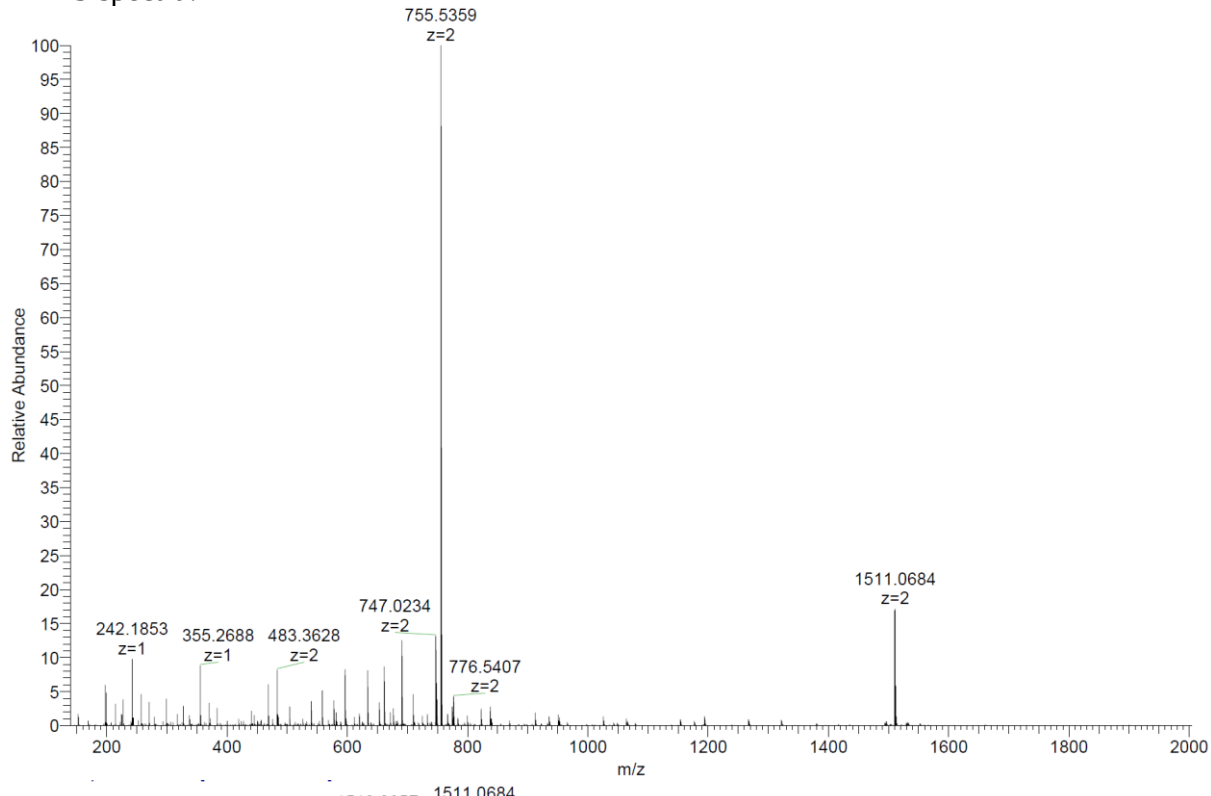

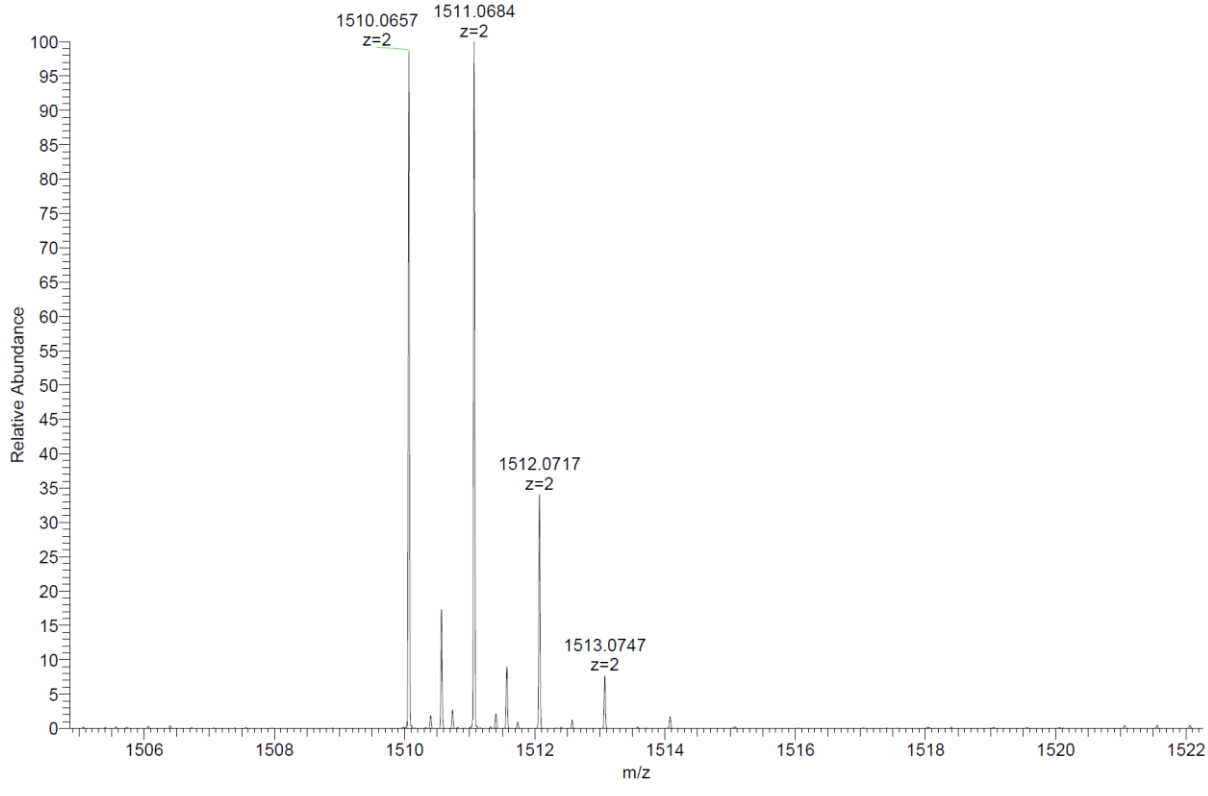

(*)KkllKLlKLLL (FHP11) was obtained as white solid after preparative RP-HPLC (16.9 mg, 17.2%). Analytical RP-HPLC: t_R = 1.63 min (A/D 100:0 to 0:100 in 3.5 min, λ = 214 nm). MS (ESI+): $C_{74}H_{140}N_{16}O_{16}$ calc./obs. 1510.06/1510.07 Da $[M+H]^+$.

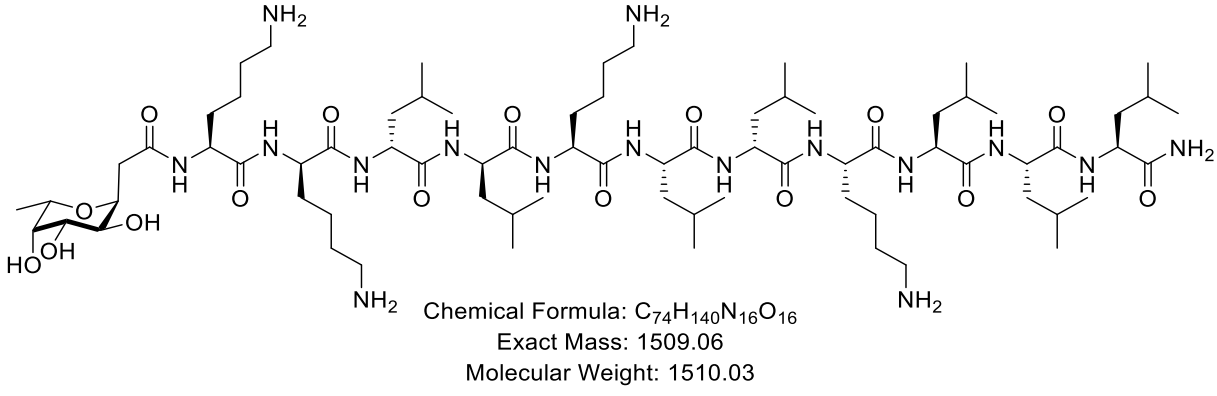

Analytical LC-data:

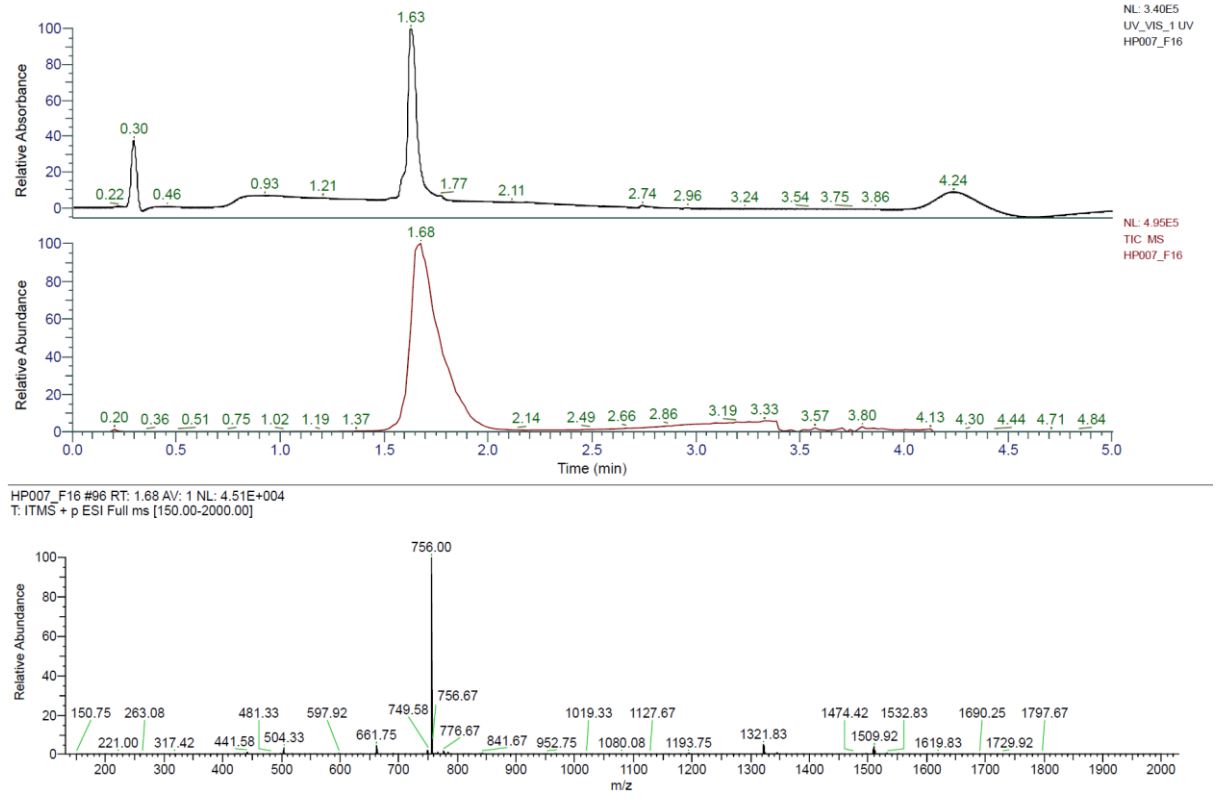

HRMS spectra:

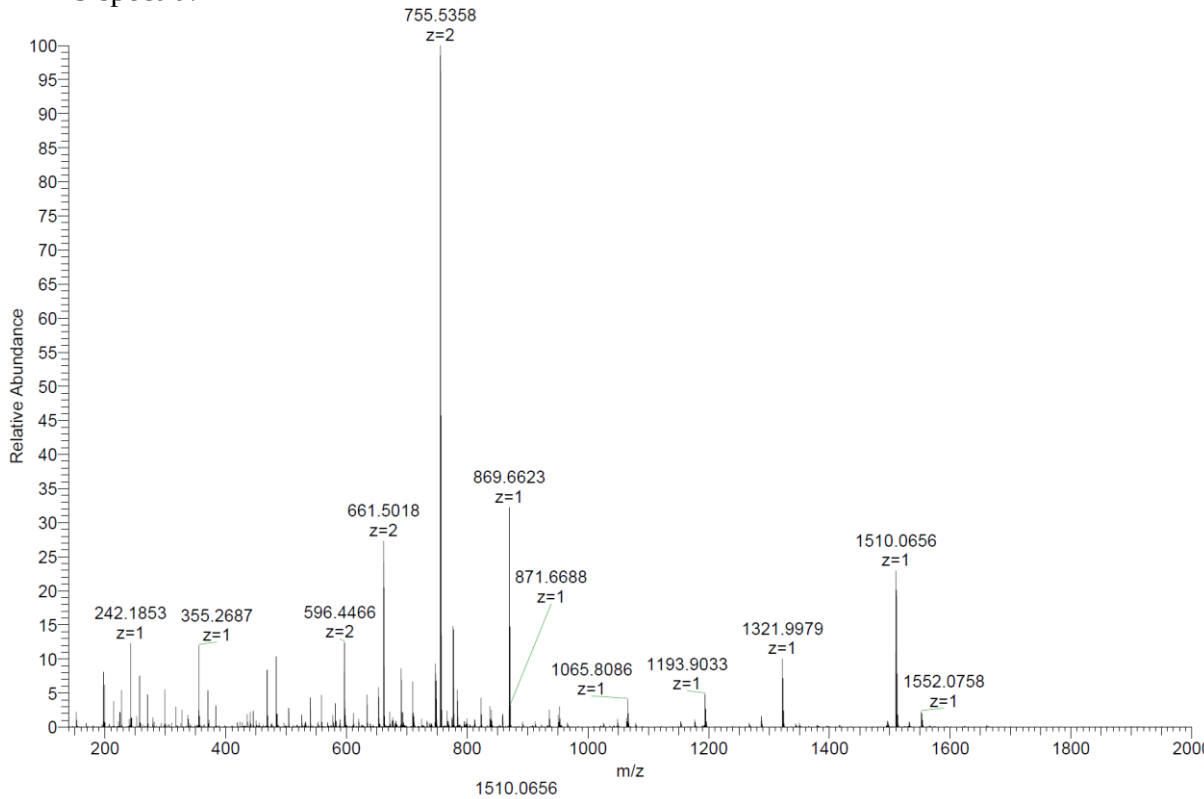

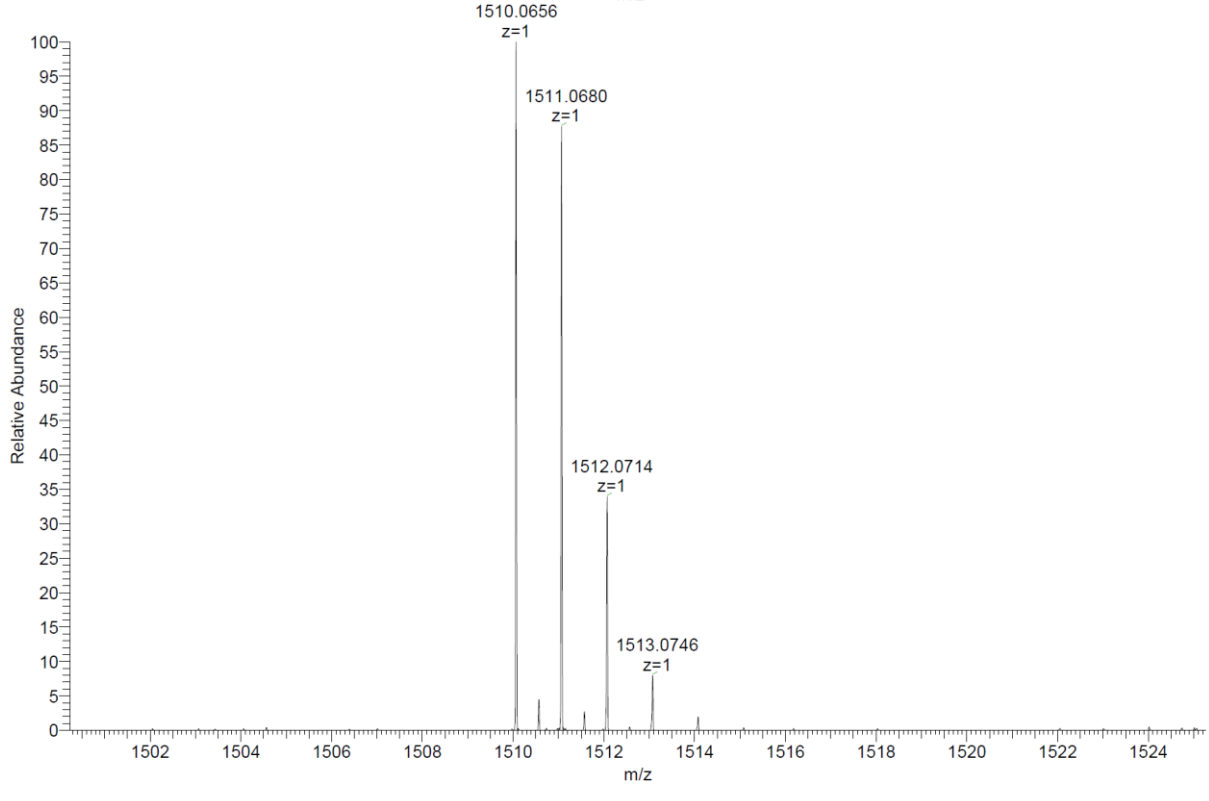

(*)KkLlKlLkLlL (FHP30) was obtained as white solid after preparative RP-HPLC (9.0 mg, 12.2%). Analytical RP-HPLC: t_R = 1.62 min (A/D 100:0 to 0:100 in 3.5 min, λ = 214 nm). MS (ESI+): $C_{66}H_{128}N_{16}O_{11}$ calc./obs. 1510.06/1510.07 Da $[M+H]^+$.

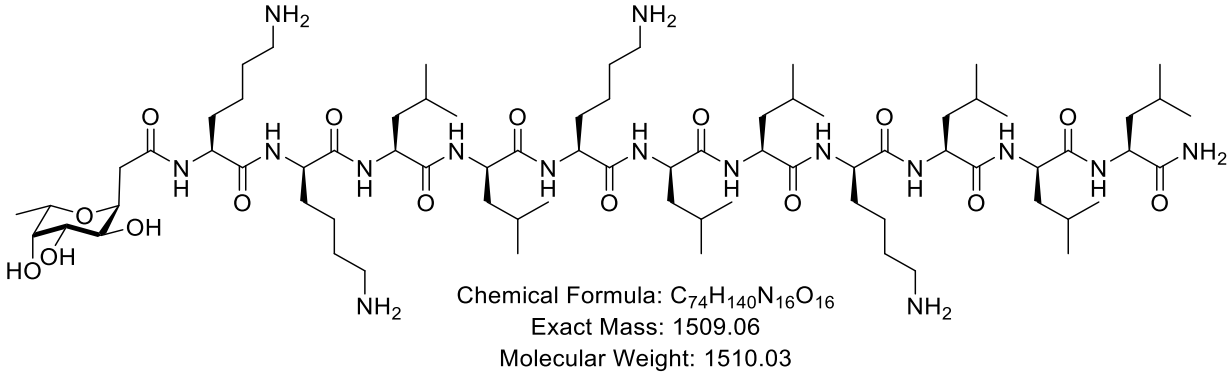

Analytical HPLC-MS data:

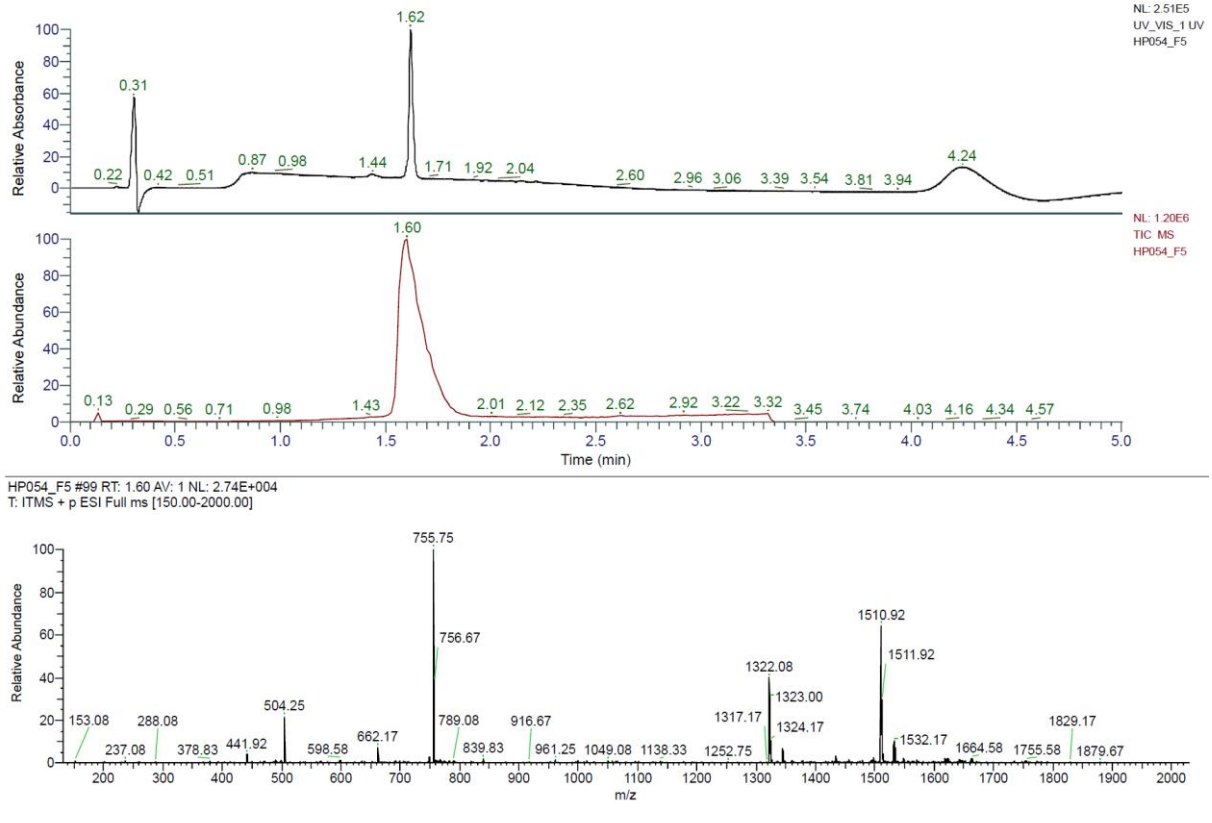

HRMS spectra:

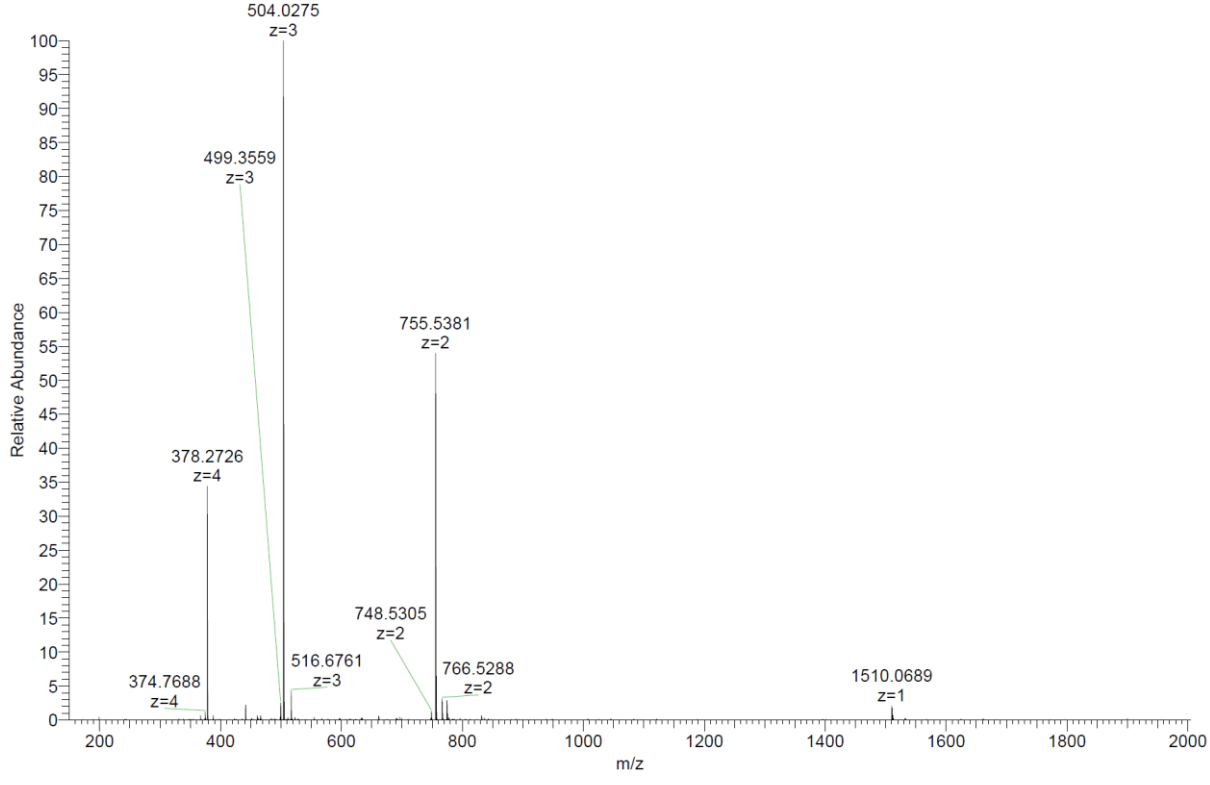

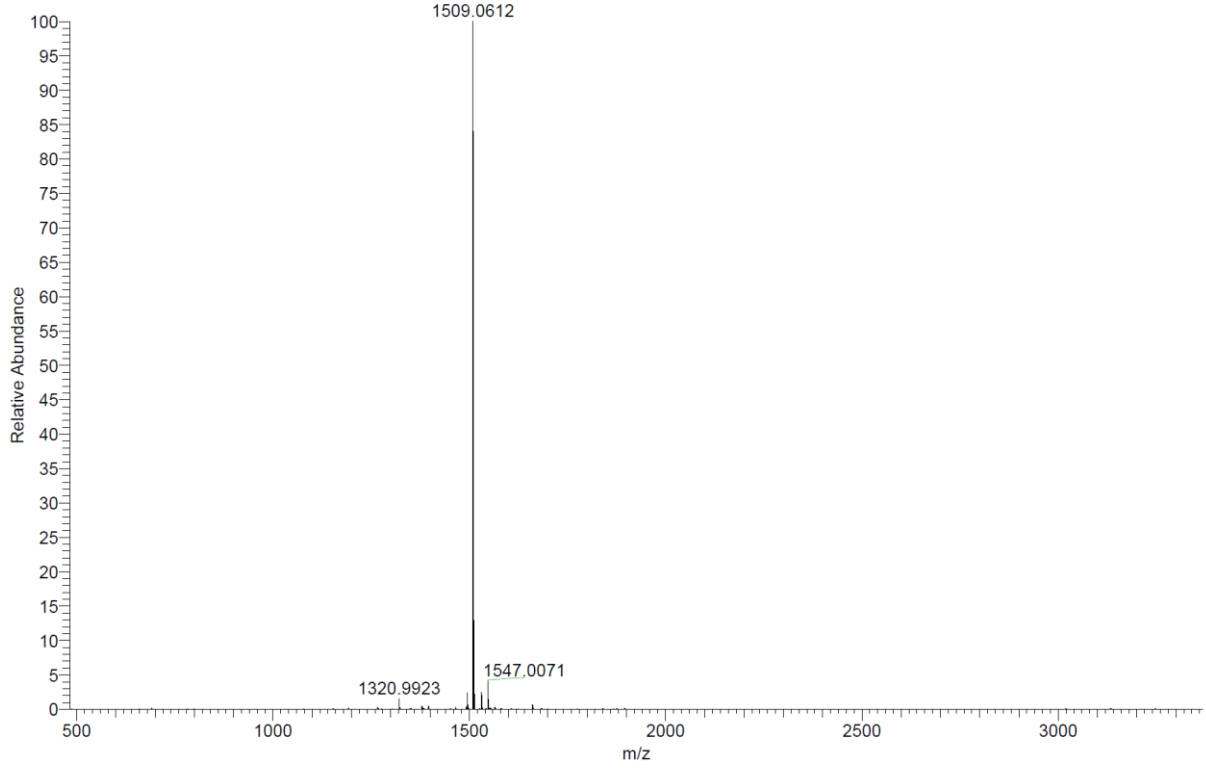

(*)kKlLkLlKlLl (FHP31) was obtained as white solid after preparative RP-HPLC (5.7 mg, 7.7%). Analytical RP-HPLC: t_R = 1.62 min (A/D 100:0 to 0:100 in 3.5 min, λ = 214 nm). MS (ESI+): $C_{66}H_{128}N_{16}O_{11}$ calc./obs. 1510.06/1510.07 Da $[M+H]^+$.

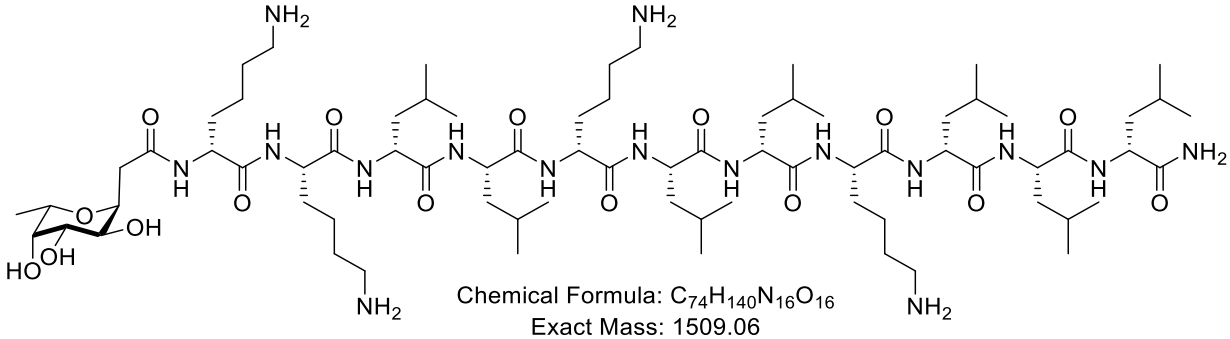

Analytical HPLC-MS data:

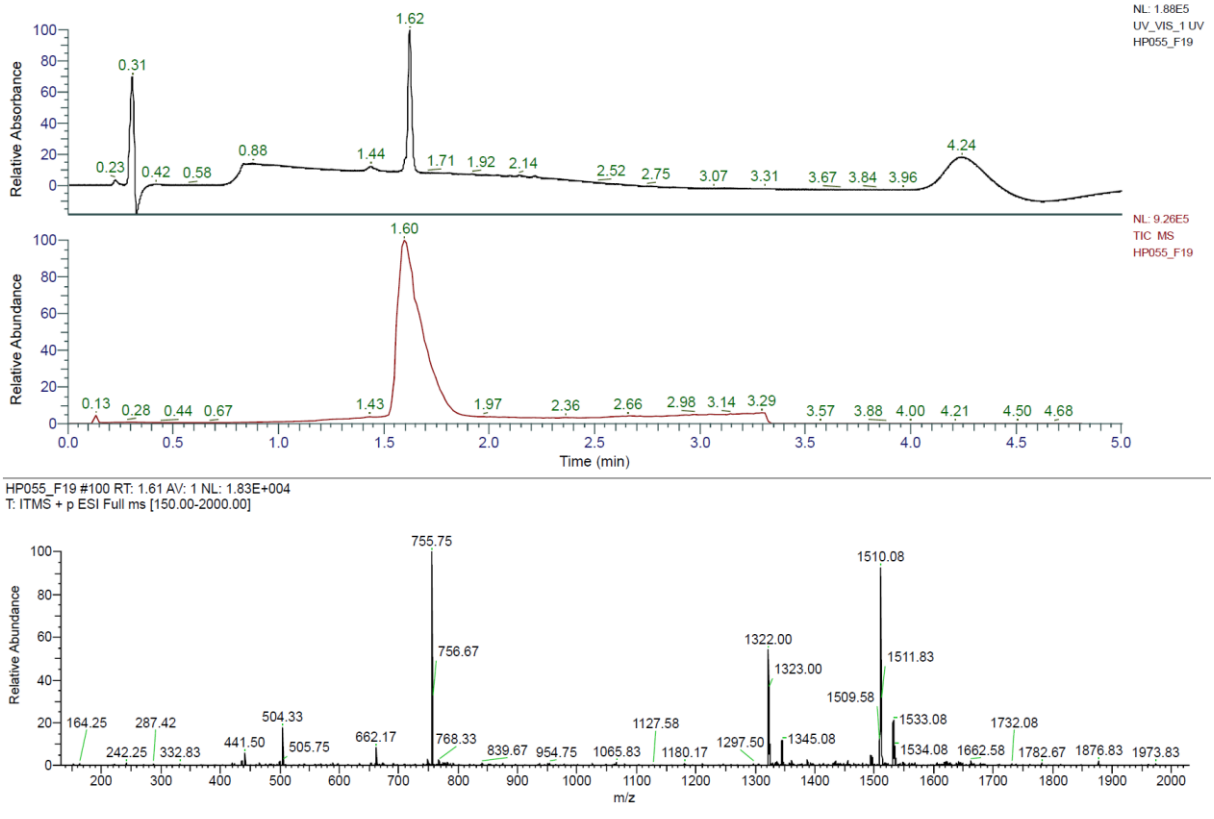

HRMS spectra:

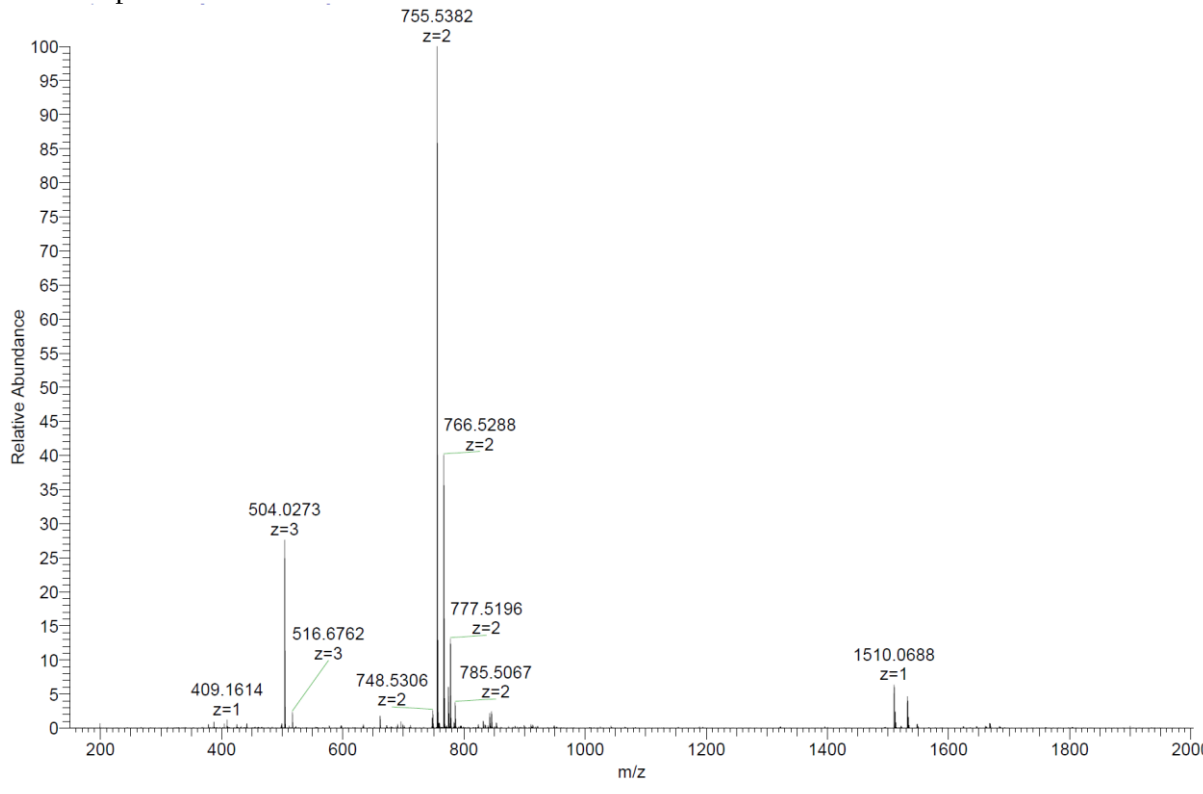

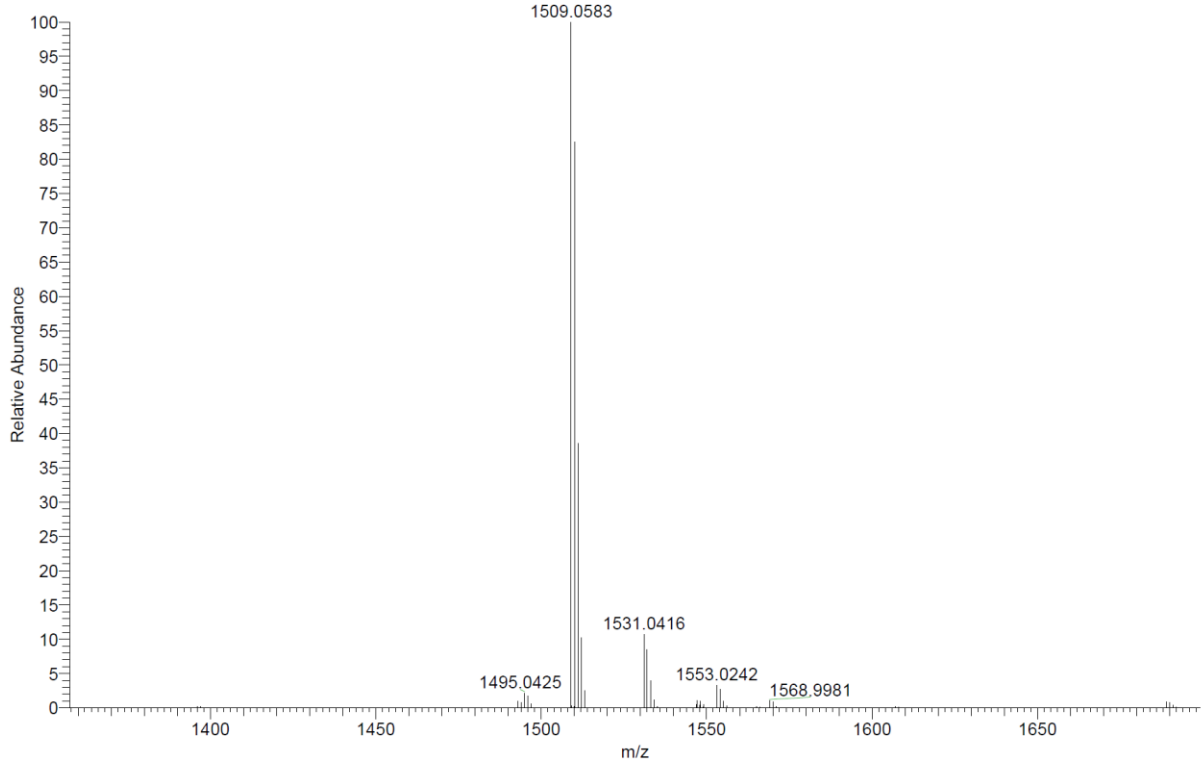

(*)RRLLRLLRLLL (FHP32) was obtained as white solid after preparative RP-HPLC (5.7 mg, 7.3%). Analytical RP-HPLC: t_R = 1.79 min (A/D 100:0 to 0:100 in 3.5 min, λ = 214 nm). MS (ESI+): $C_{74}H_{140}N_{24}O_{16}$ calc./obs. 1621.09/1621.09/ Da [M].

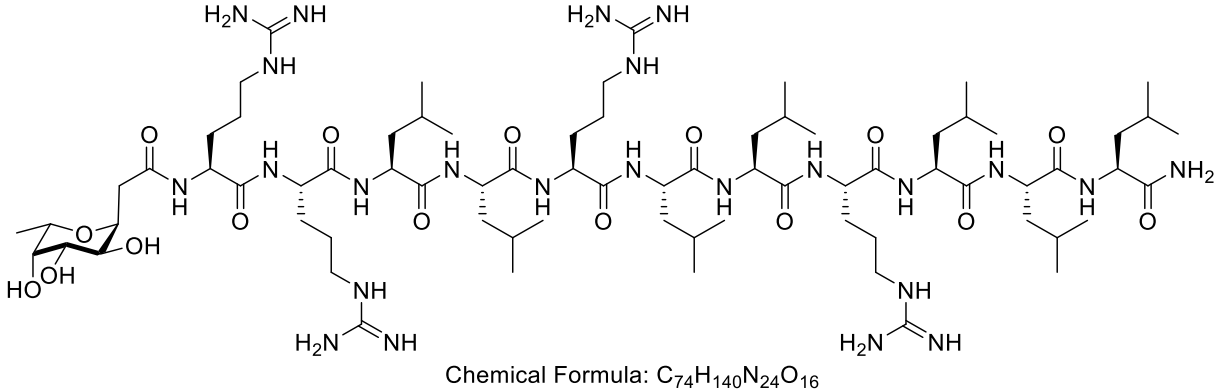

Chemical Formula: $C_{74}H_{140}N_{24}O_{16}$
Exact Mass: 1621.09
Molecular Weight: 1622.09

Analytical LC-MS data:

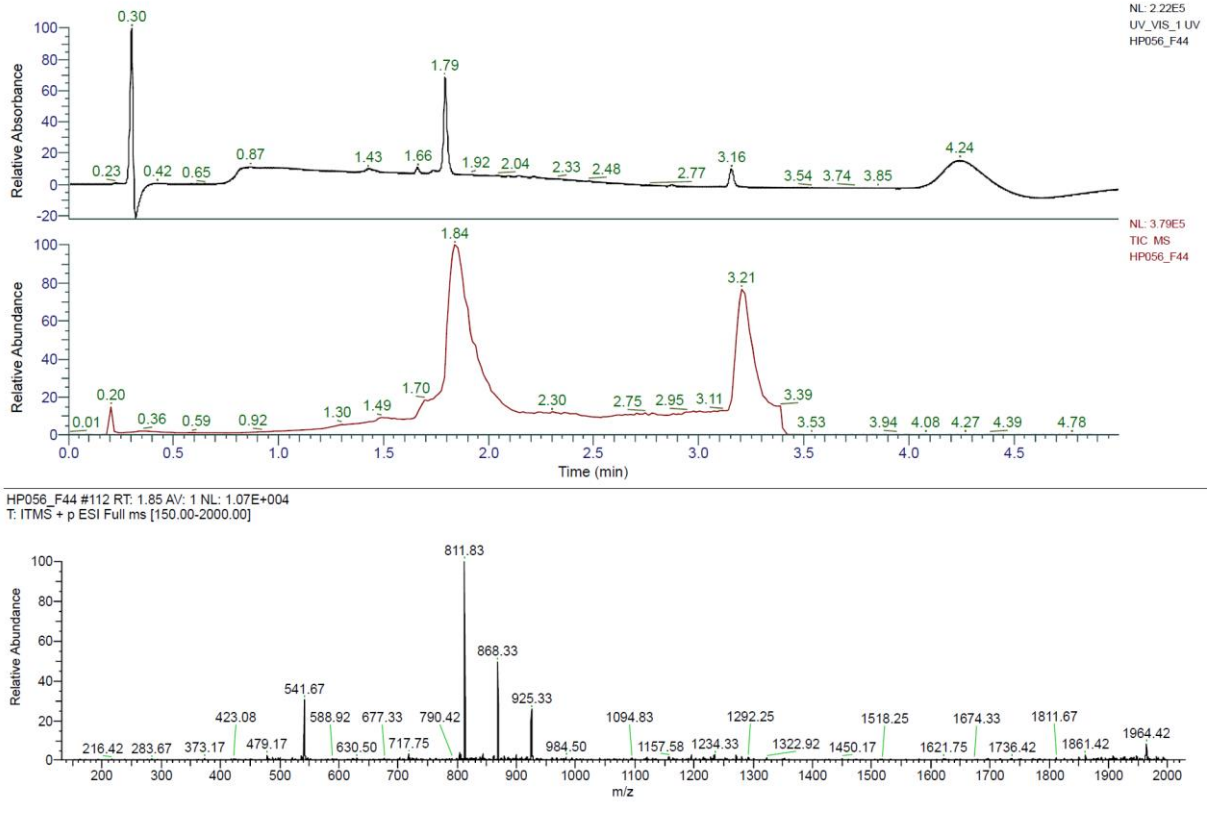

HRMS spectra:

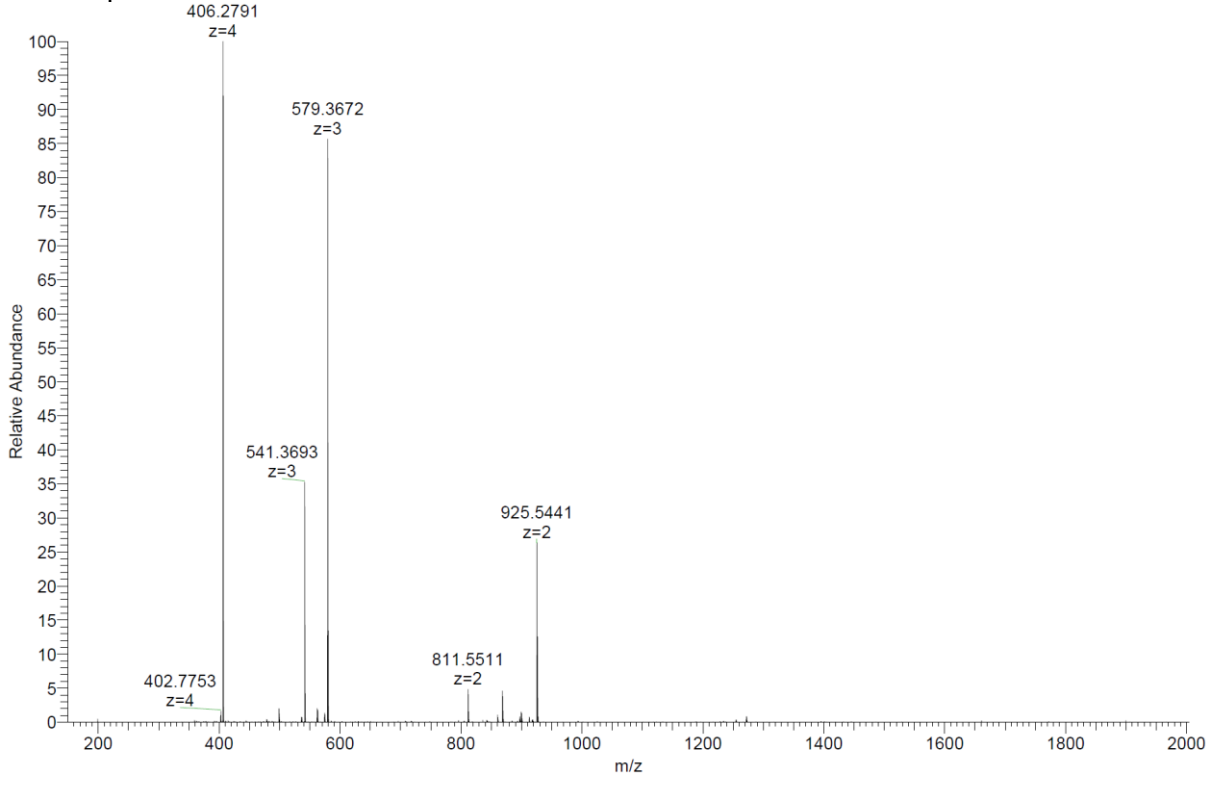

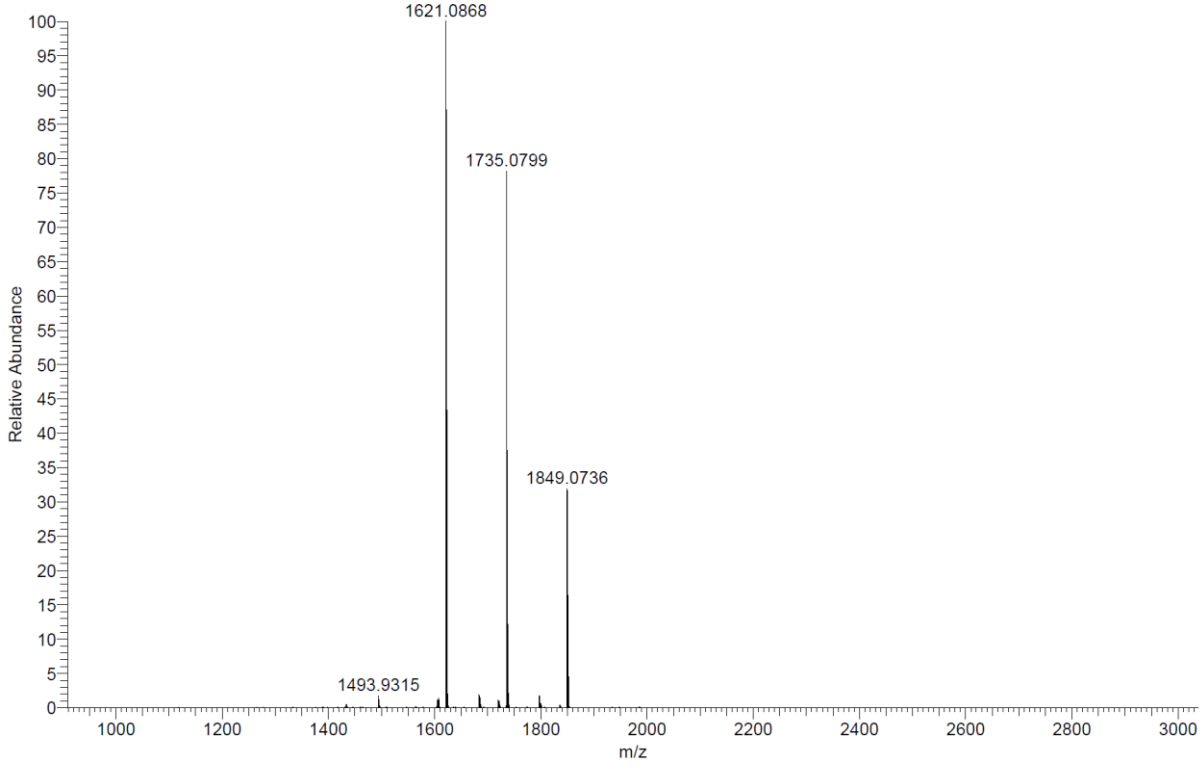

(*)RRLLRLLRLLL (FHP33) was obtained as white solid after preparative RP-HPLC (2.5 mg, 3.2%). Analytical RP-HPLC: t_R = 1.62 min (A/D 100:0 to 0:100 in 3.5 min, λ = 214 nm). MS (ESI+): $C_{74}H_{140}N_{24}O_{16}$ calc./obs. 1621.09/1621.09 Da [M].

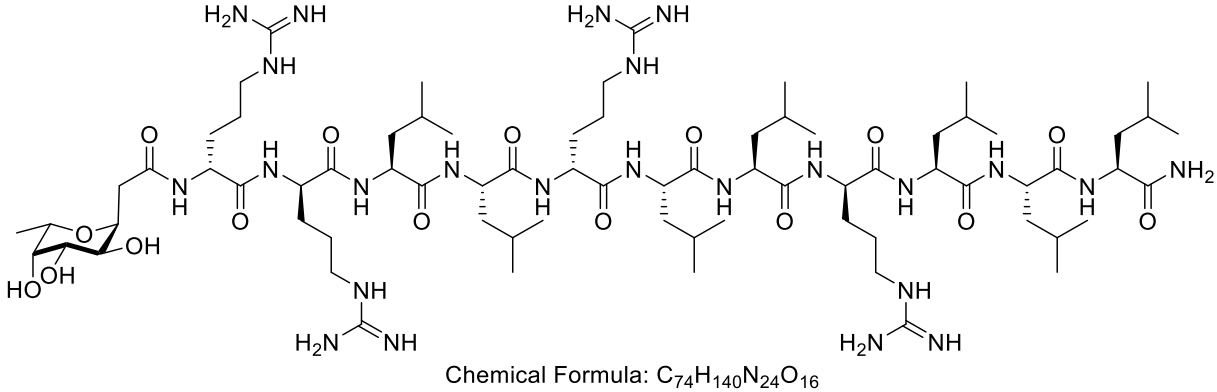

Chemical Formula: $C_{74}H_{140}N_{24}O_{16}$
Exact Mass: 1621.09
Molecular Weight: 1622.09

Analytical LC-MS:

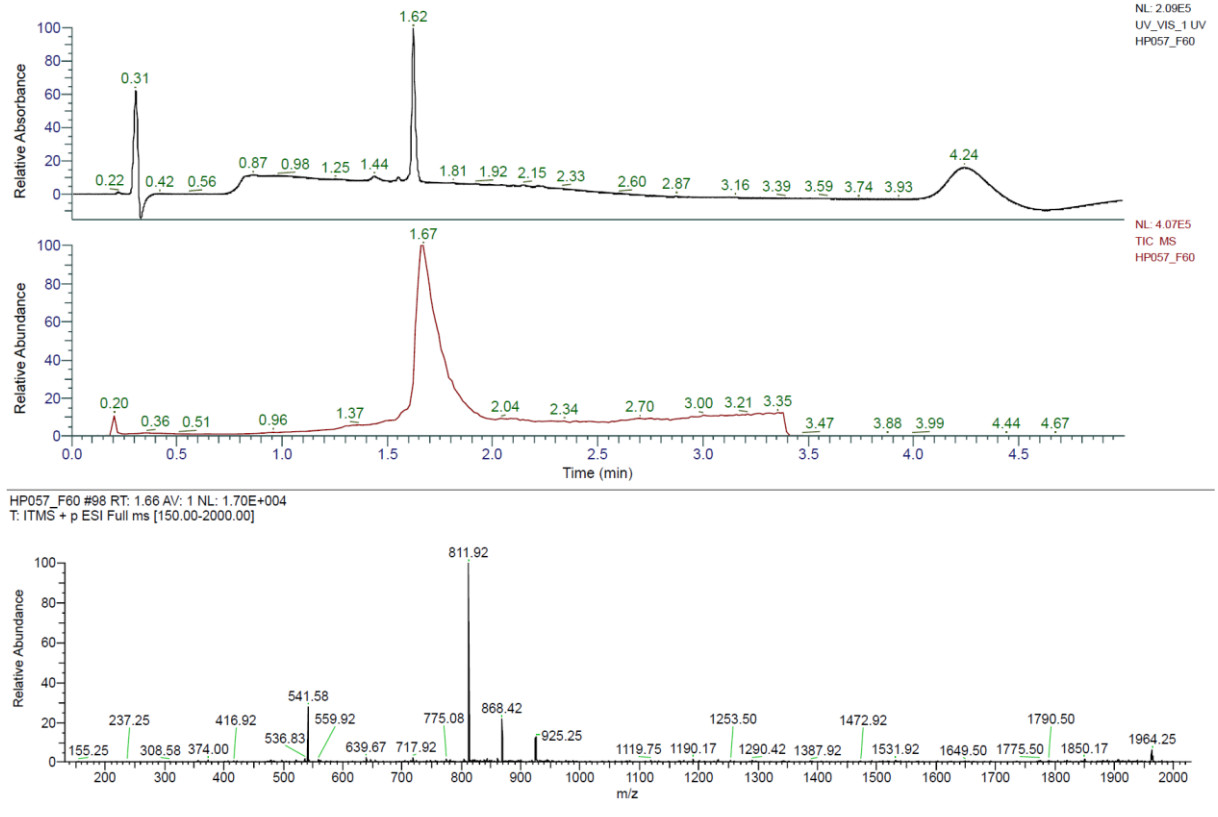

HRMS spectra:

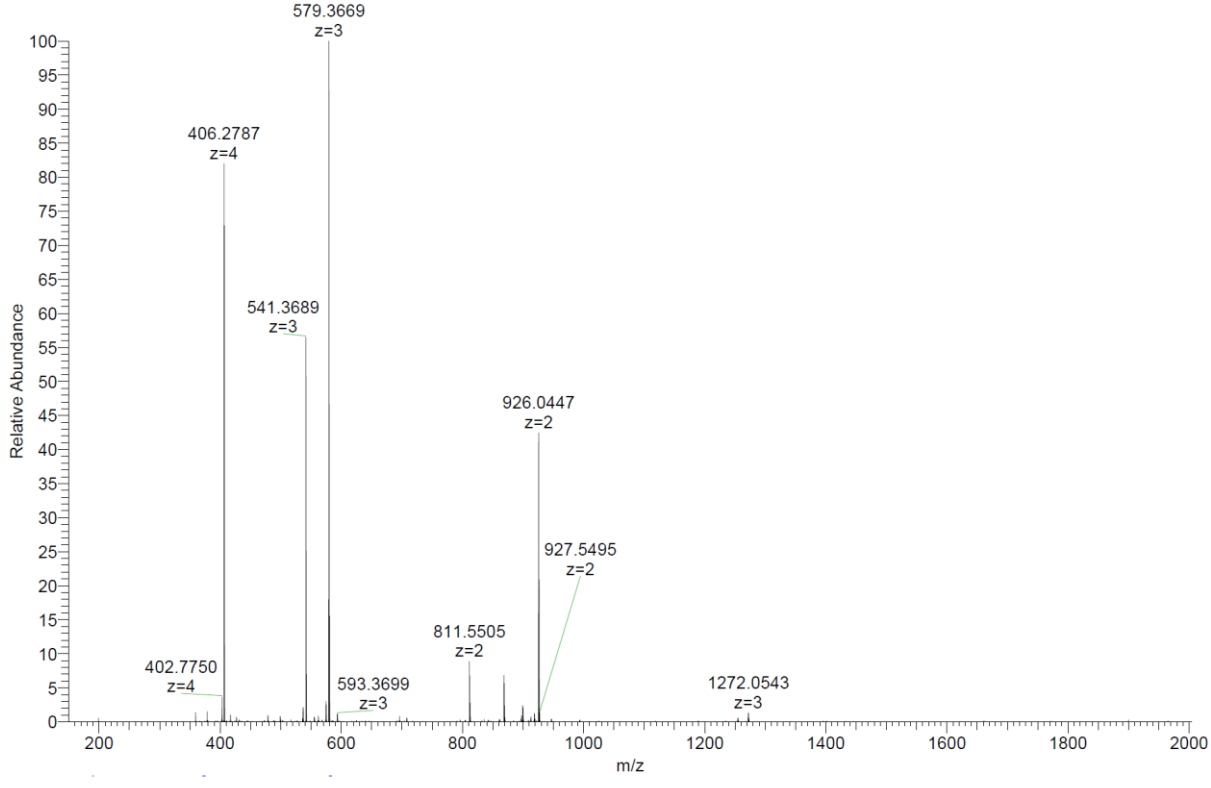

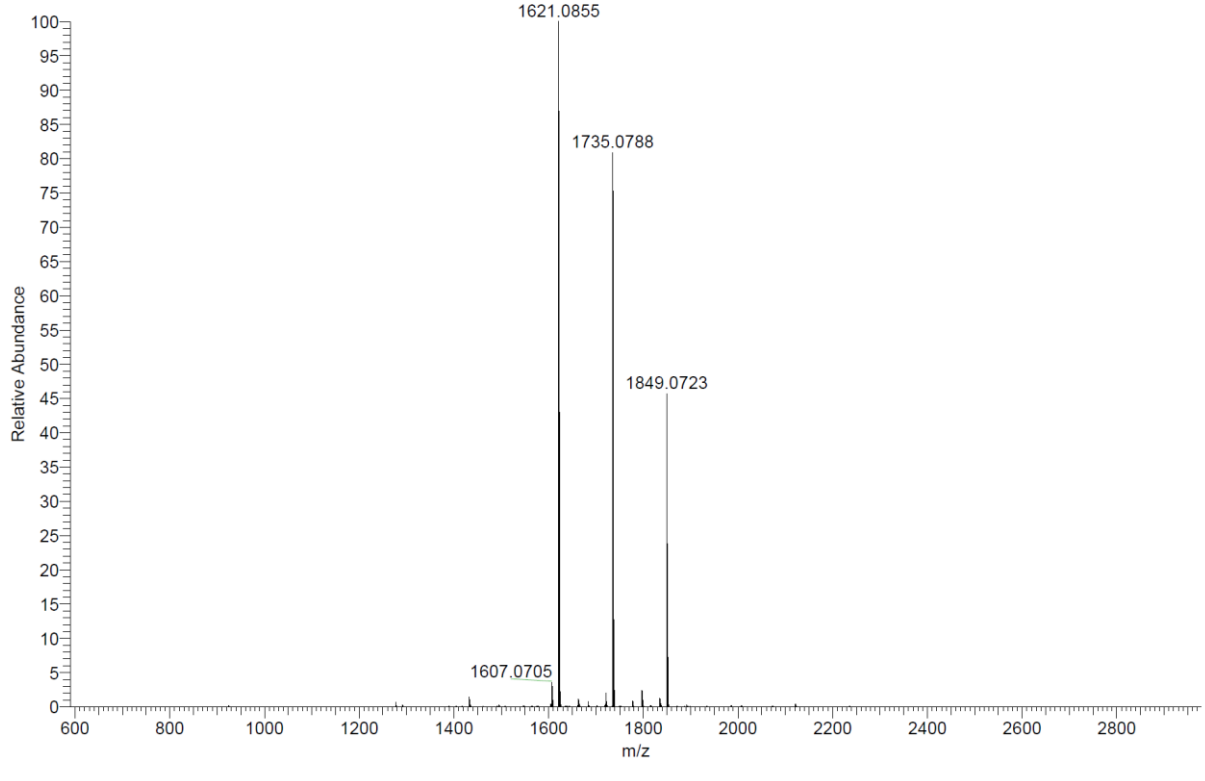

8.3 SI for Mixed-chirality design of existing α-helical AMPs

Circular dichroism

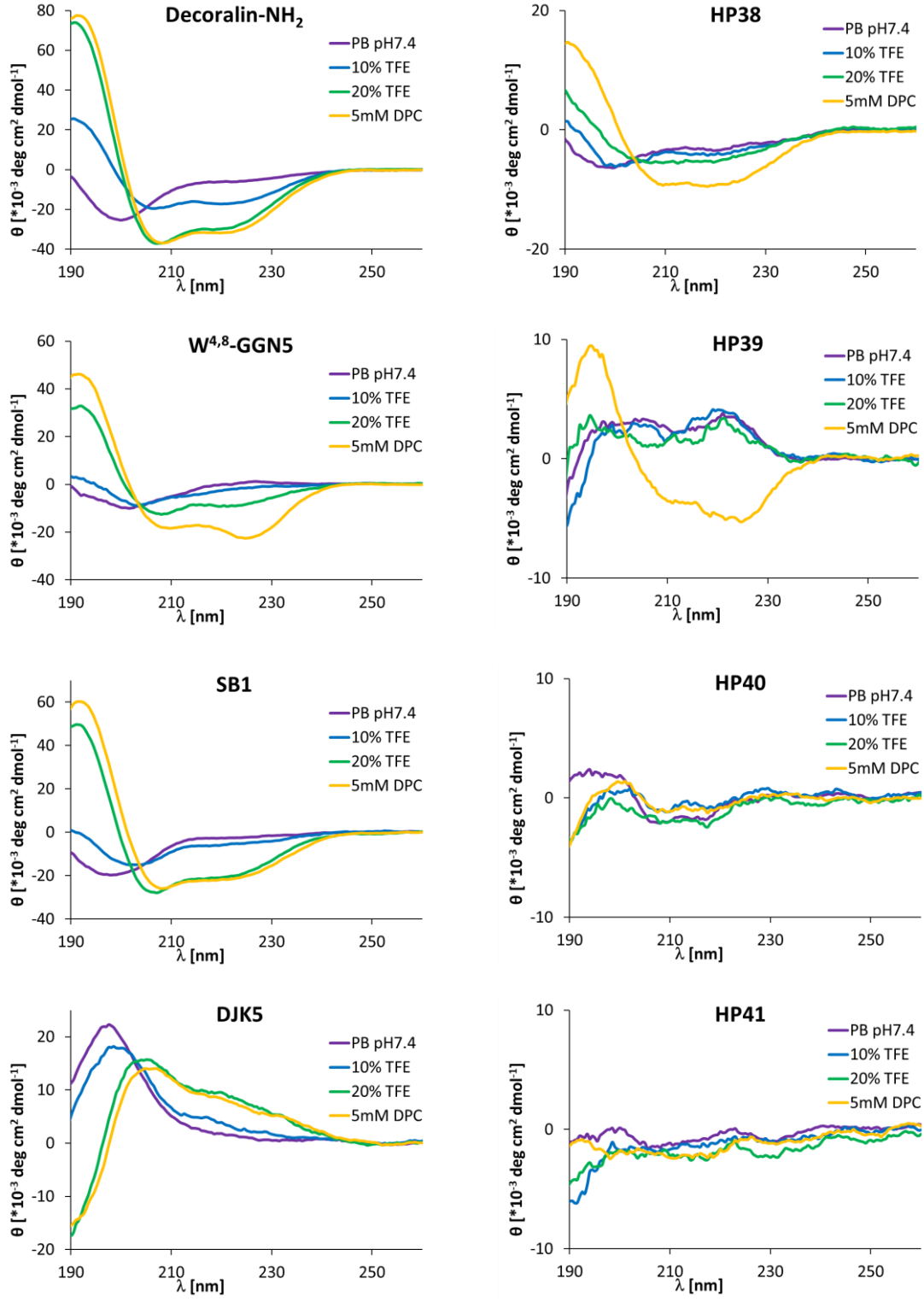

Figure S3.1: Circular dichroism spectra of linear peptides at 0.100 mg/mL in 7 mM phosphate buffer pH 7.4 with different amount of TFE and 5 mM DPC.

Table S3.1: Dichroweb analysis of linear peptides.

Cpd.	Sequence [a)]	CD α/β/t/u (%) [b)]			
		PB Buffer	10% TFE	20% TFE	5 mM DPC
Decoralin-NH_2	SLLSLIRKLIT	17/20/26/37	45/9/20/26	75/2/12/11	84/2/10/4
HP38	slLSlIRkLIT	10/33/24/33	12/22/24/32	15/31/22/32	26/25/20/29
$W^{4,8}$-GGN5	FLGWLFKWASK	10/31/24/35	14/31/24/31	43/15/19/23	77/1/5/17
HP39	flGWlFKwASK	8/40/24/28	9/38/23/30	10/39/23/28	28/24/19/29
SB1	KYKKALKKAKLL	13/25/25/37	22/22/24/32	66/2/15/17	78/2/13/7
HP40	kYkkALkkAkLL	8/40/21/31	6/38/23/33	7/38/24/31	7/38/23/32
DJK5	vqwrairvrvir	12/23/26/39	11/27/25/37	27/18/24/31	29/18/27/26
HP41	VQWrAIrVrVIr	11/38/20/31	8/36/23/33	10/36/24/30	7/37/24/32

[a)] One letter code for amino acids. D- amino acids are in lower. [b)] CD spectra were recorded at 0.100 mg/mL in aqueous 7 mM phosphate buffer pH 7.4 with addition of 0, 10 and 20% TFE or 5 mM DPC. The primary CD spectra were analyzed using Dichroweb and the percentages of α-helical (α), β-sheet (β), turns (t) and unordered (u) signals were extracted. The Contin-LL method and reference set 4 were used.[178]

Vesicle leakage assay

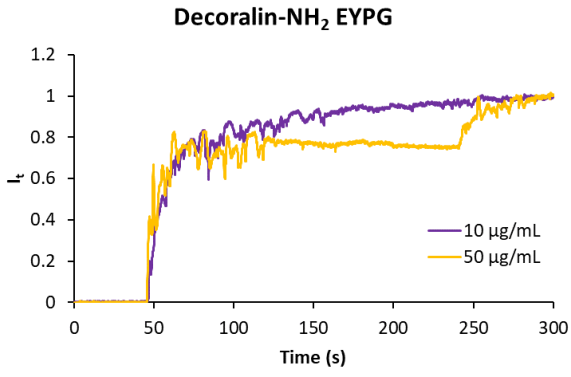

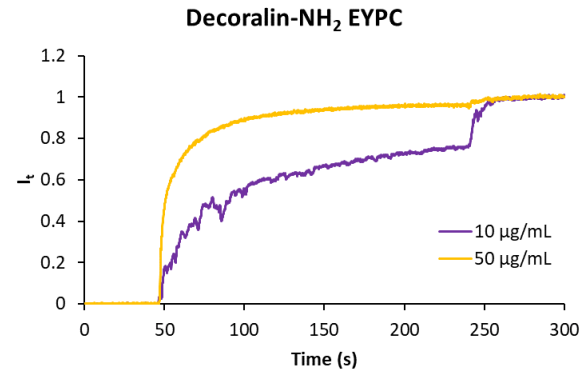

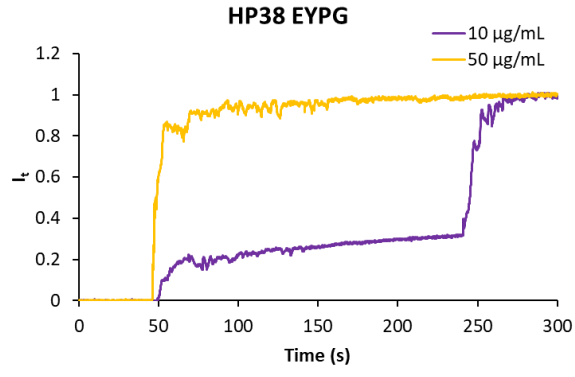

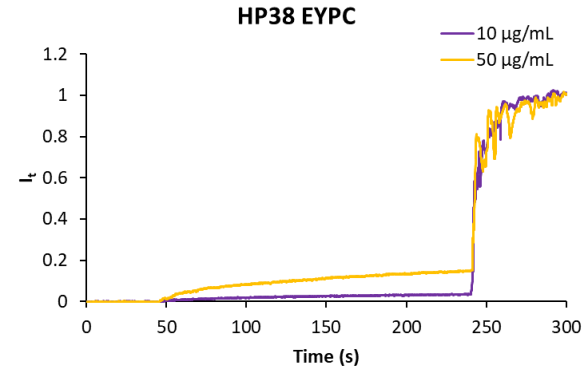

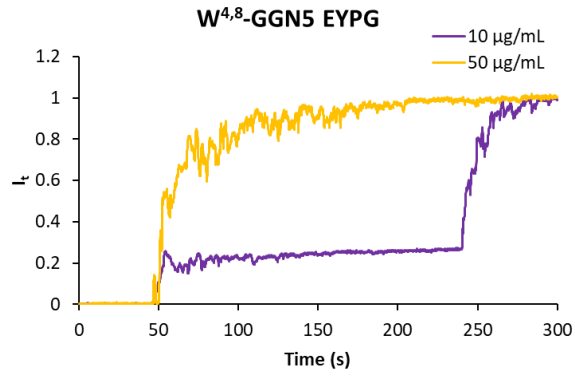

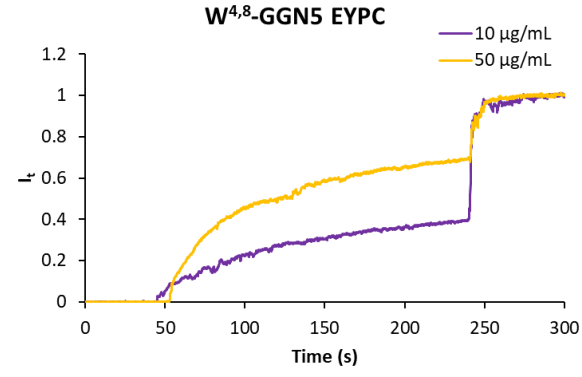

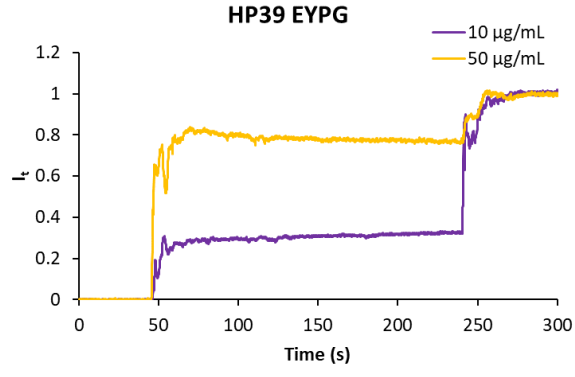

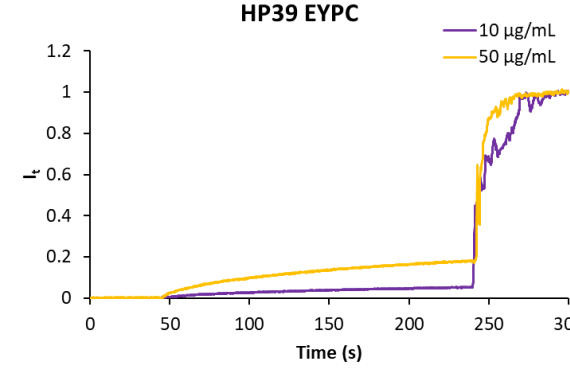

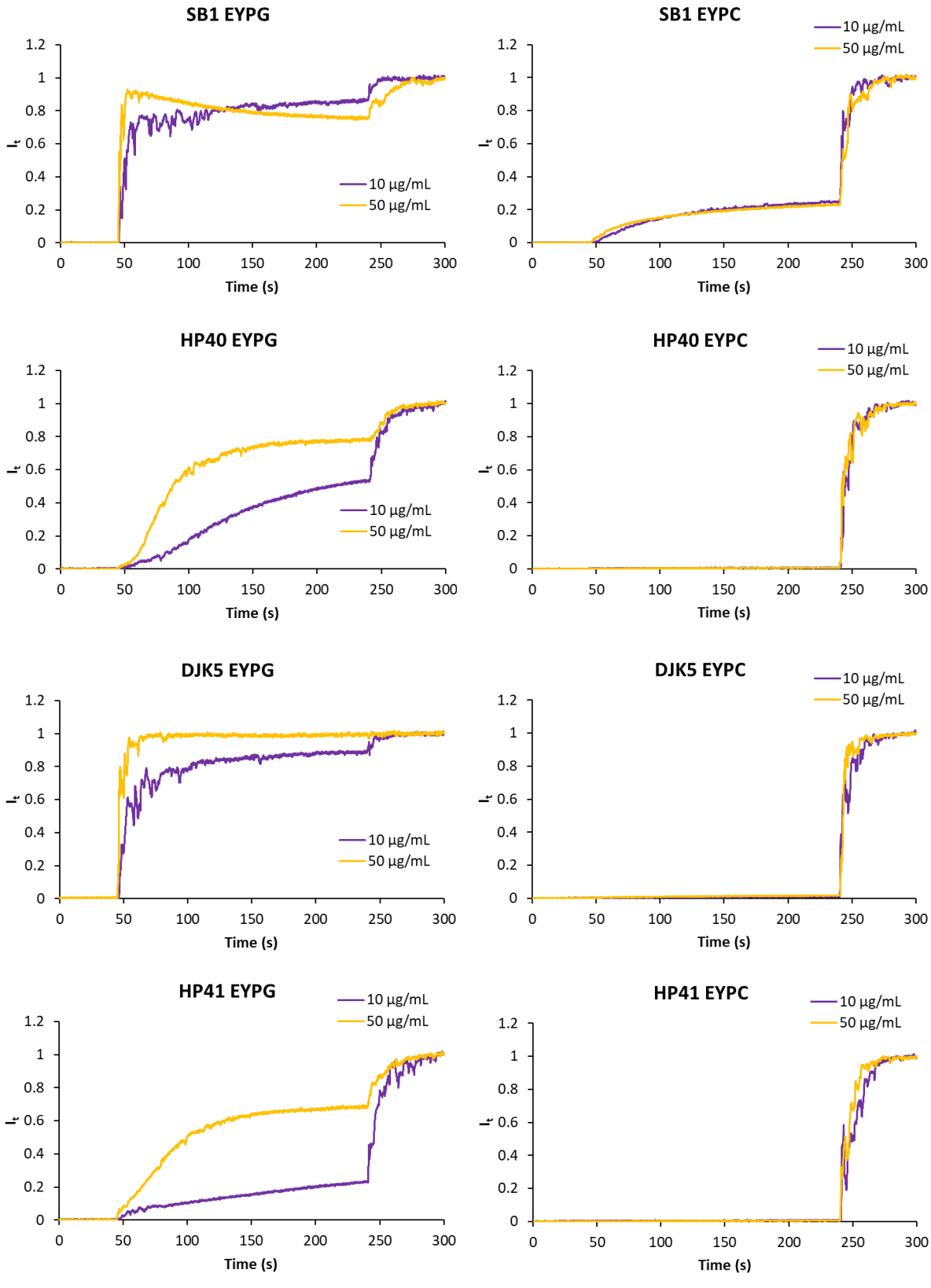

Figure S3.2: Vesicle leakage experiments using 5(6)-carboxyfluorescein induced by peptides. EYPG and EYPC vesicles were suspended in buffer (10 mM Tris, 107 mM NaCl, pH 7.4) and the indicated concentration of the compound was added after 45 seconds. After 240 seconds 30 µL of Triton X-100 1.2% was added for full release of the fluorescein.

HPLC and HRMS data

SLLSLIRKLIT (Decoralin-NH_2) was obtained as white solid after preparative RP-HPLC (40.6 mg, 31.1%). Analytical RP-HPLC: t_R = 1.85 min (A/D 100:0 to 0:100 in 3.5 min, λ = 214 nm). MS (ESI+): $C_{58}H_{110}N_{16}O_{14}$ calc./obs. 1255.84/1255.85 Da $[M+H]^+$.

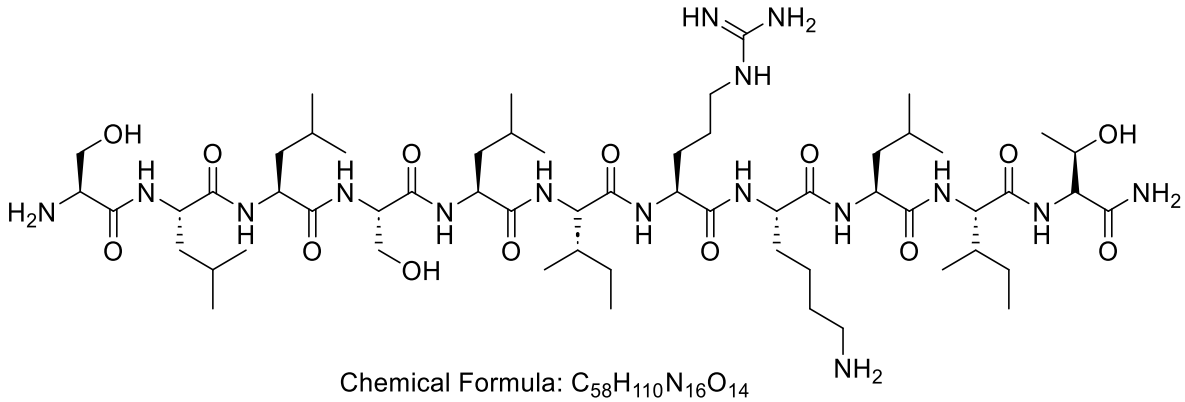

Chemical Formula: $C_{58}H_{110}N_{16}O_{14}$
Exact Mass: 1254.84
Molecular Weight: 1255.62

Analytical HPLC-MS data:

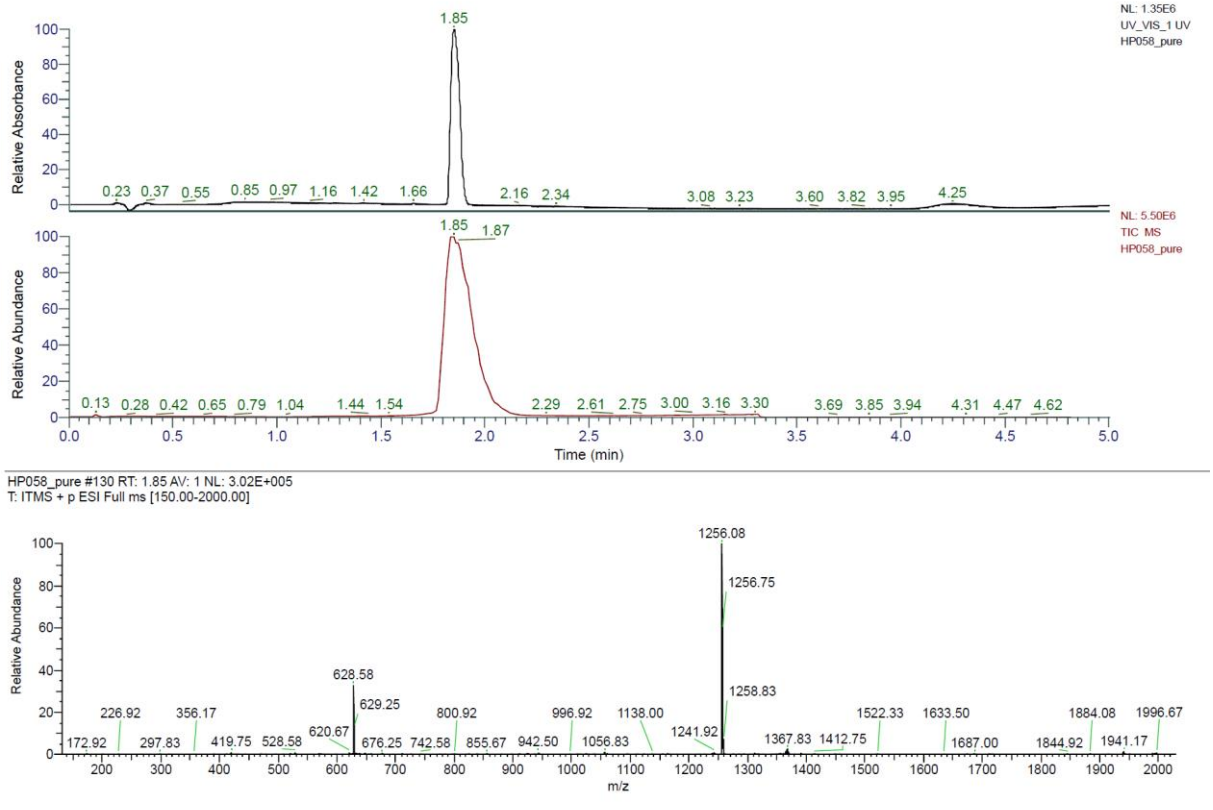

HRMS spectra:

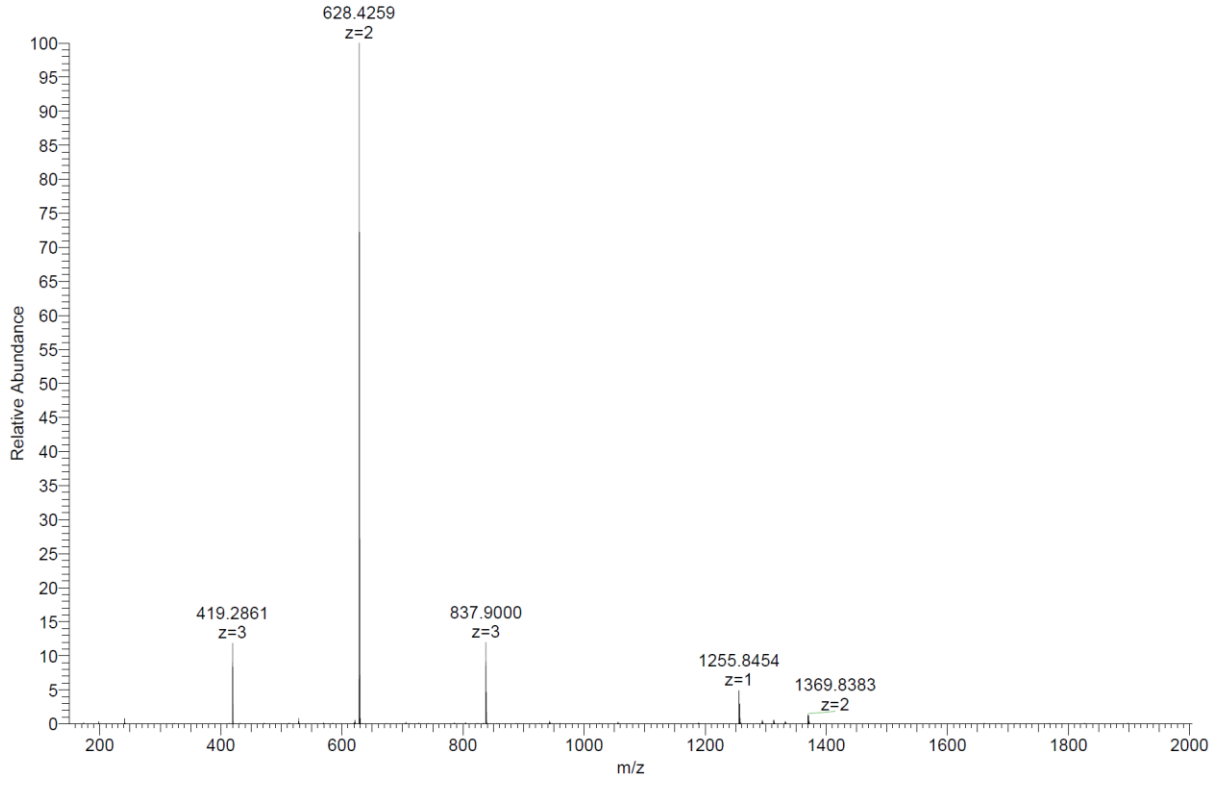
628.4259
z=2
419.2861
z=3
837.9000
z=3
1255.8454
z=1
1369.8383
z=2
Relative Abundance
m/z

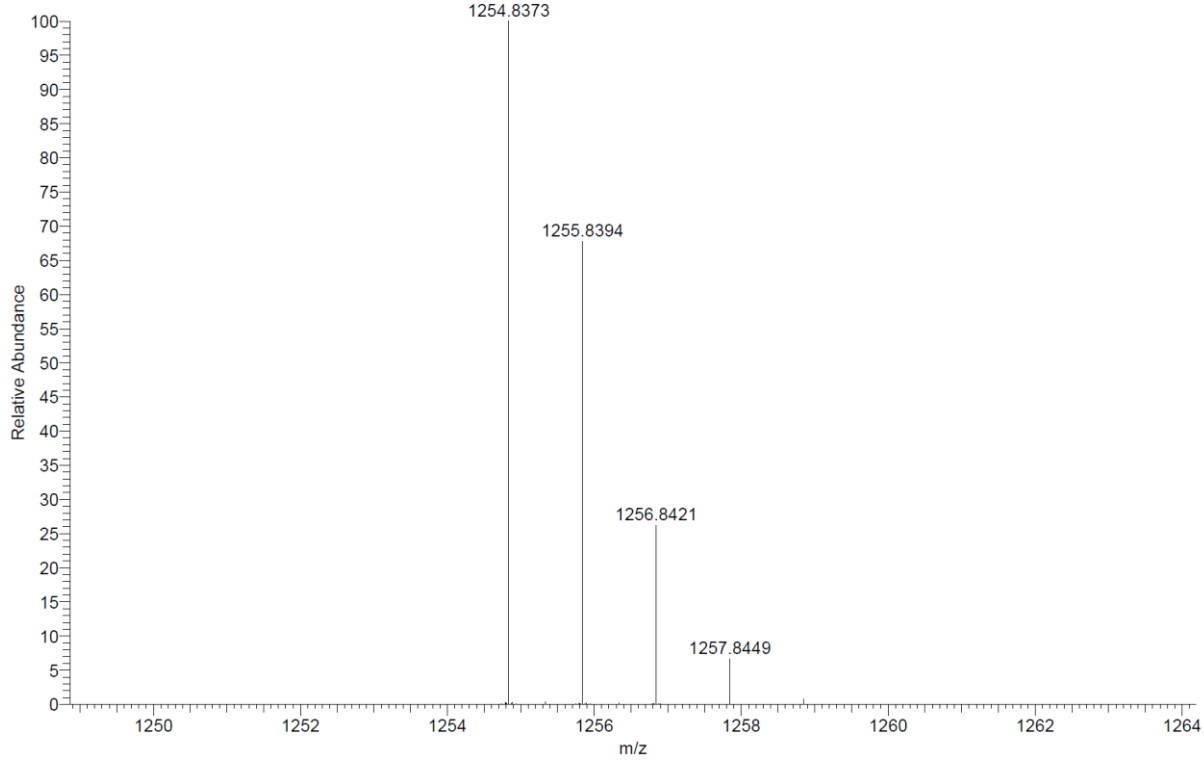
1254.8373
1255.8394
1256.8421
1257.8449
Relative Abundance
m/z

slLSlIRkLIT (HP38) was obtained as white solid after preparative RP-HPLC (39.8 mg, 42.9%). Analytical RP-HPLC: t_R = 1.60 min (A/D 100:0 to 0:100 in 3.5 min, λ = 214nm). HRMS (ESI+): $C_{58}H_{110}N_{16}O_{14}$ calc./obs. 1255.84/1255.85 Da $[M+H]^+$.

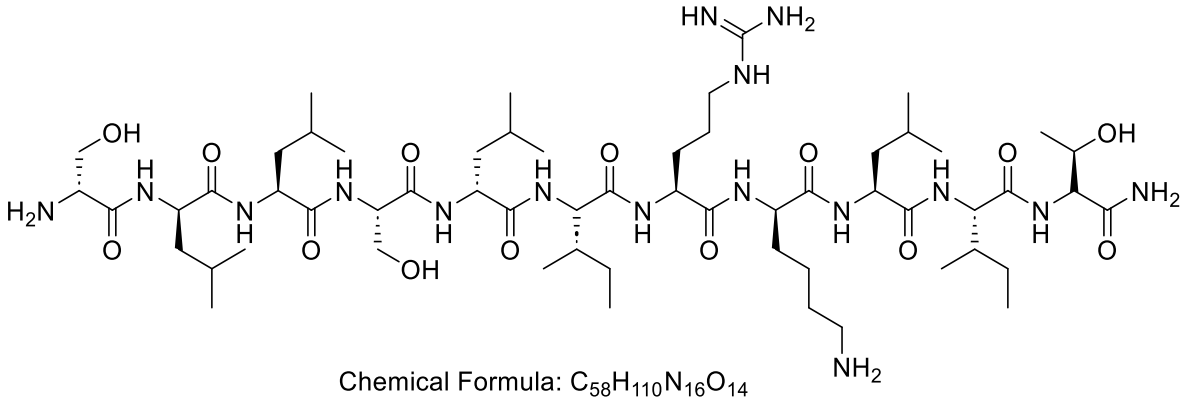

Chemical Formula: $C_{58}H_{110}N_{16}O_{14}$
Exact Mass: 1254.84
Molecular Weight: 1255.62

Analytical HPLC-MS data:

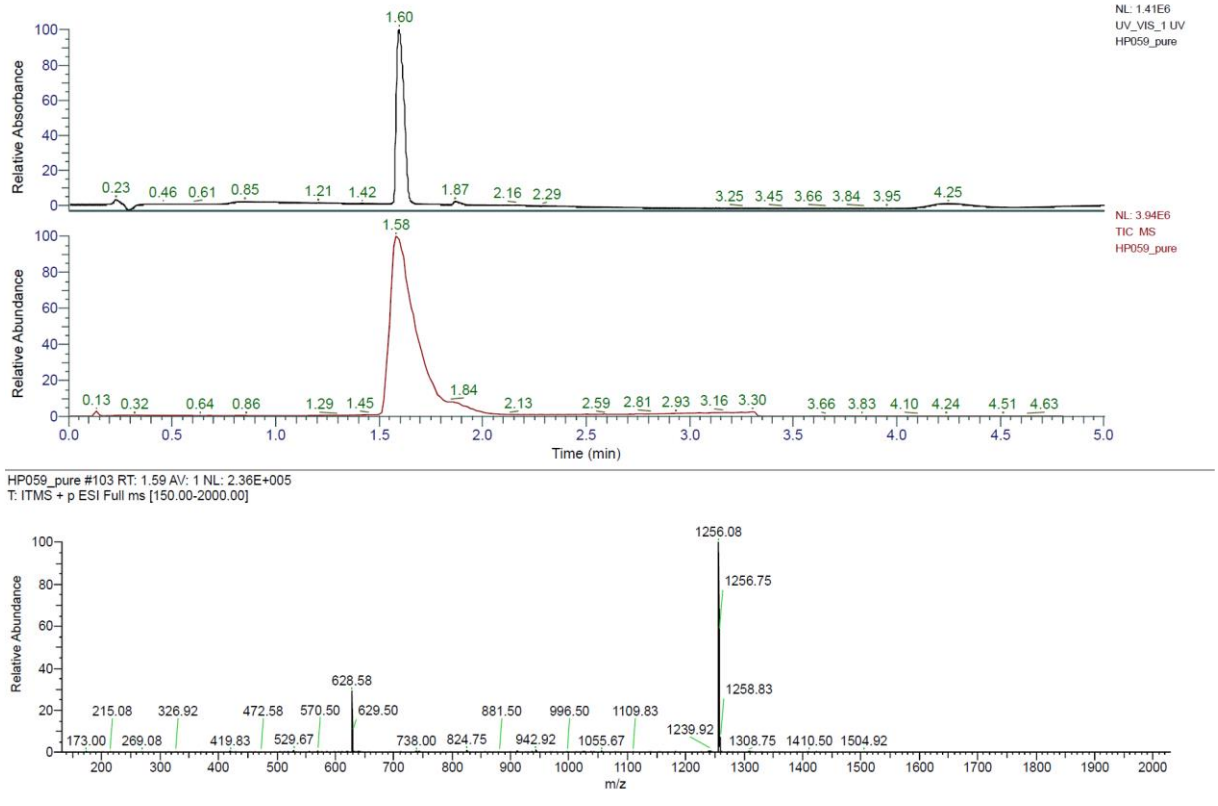

HRMS spectra:

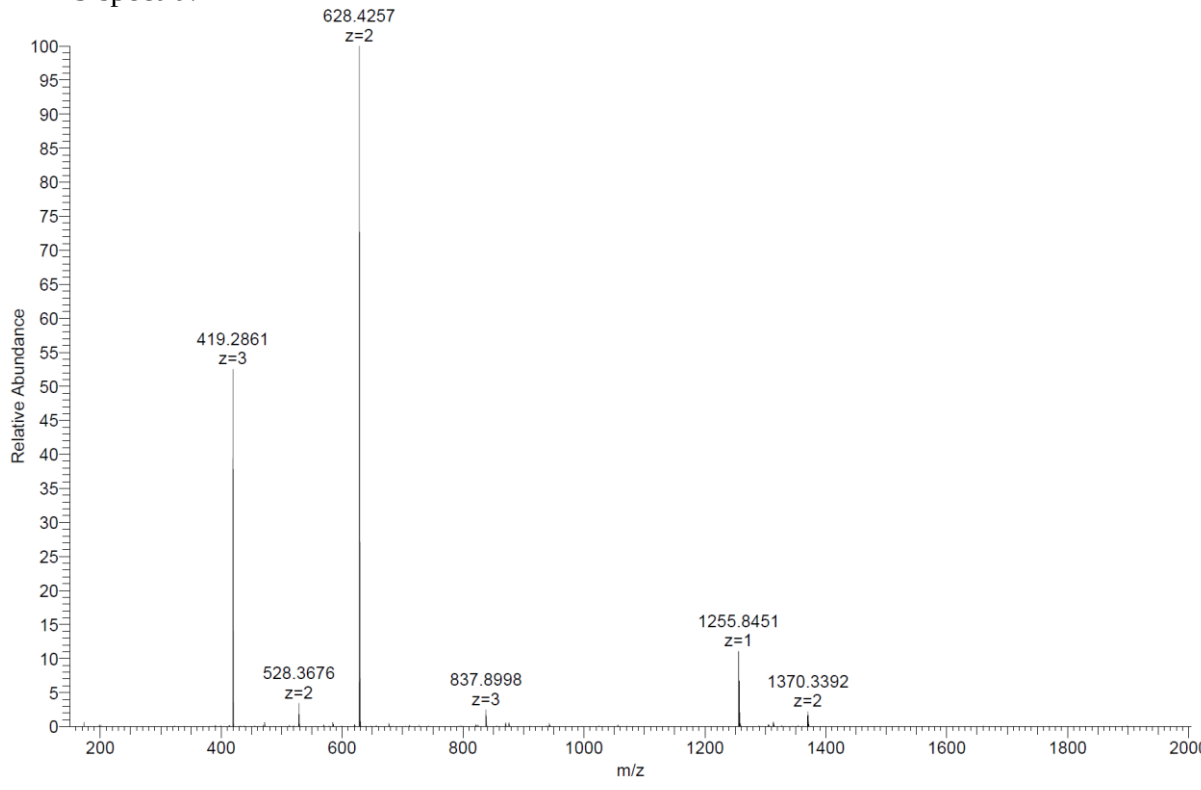

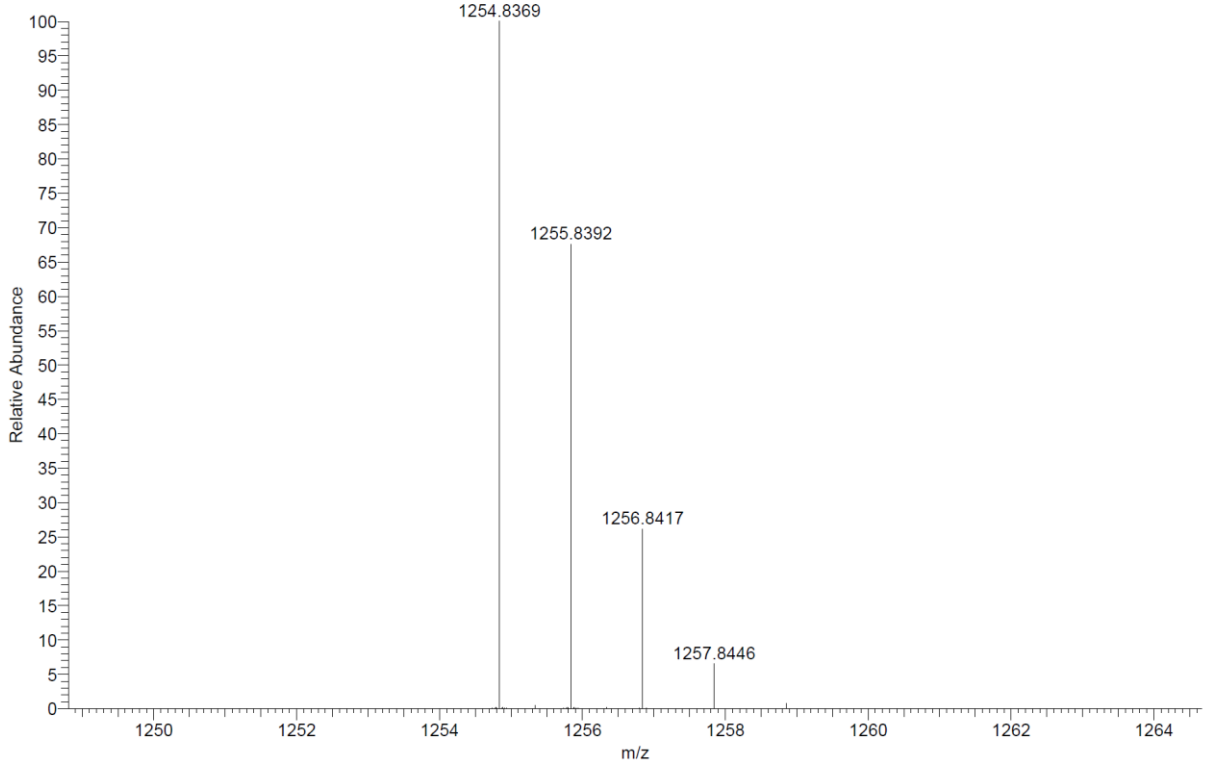

FLGWLFKWASK ($W^{4,8}$-GGN5) was obtained as white solid after preparative RP-HPLC (52.8 mg, 49.0%). Analytical RP-HPLC: t_R = 1.65 min (A/D 100:0 to 0:100 in 3.5 min, λ = 214nm). HRMS (ESI+): $C_{72}H_{100}N_{16}O_{12}$ calc./obs. 1381.77/1381.78 Da $[M+H]^+$.

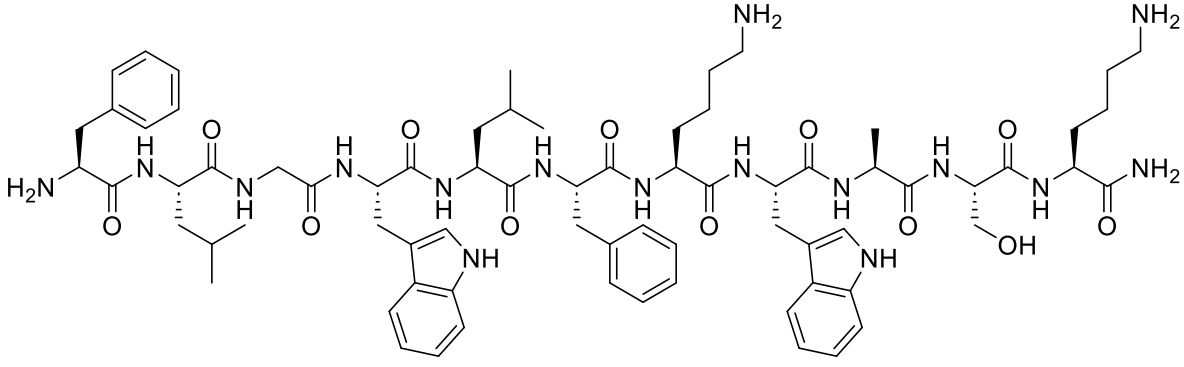

Chemical Formula: $C_{72}H_{100}N_{16}O_{12}$
Exact Mass: 1380.77
Molecular Weight: 1381.69

Analytical HPLC-MS data:

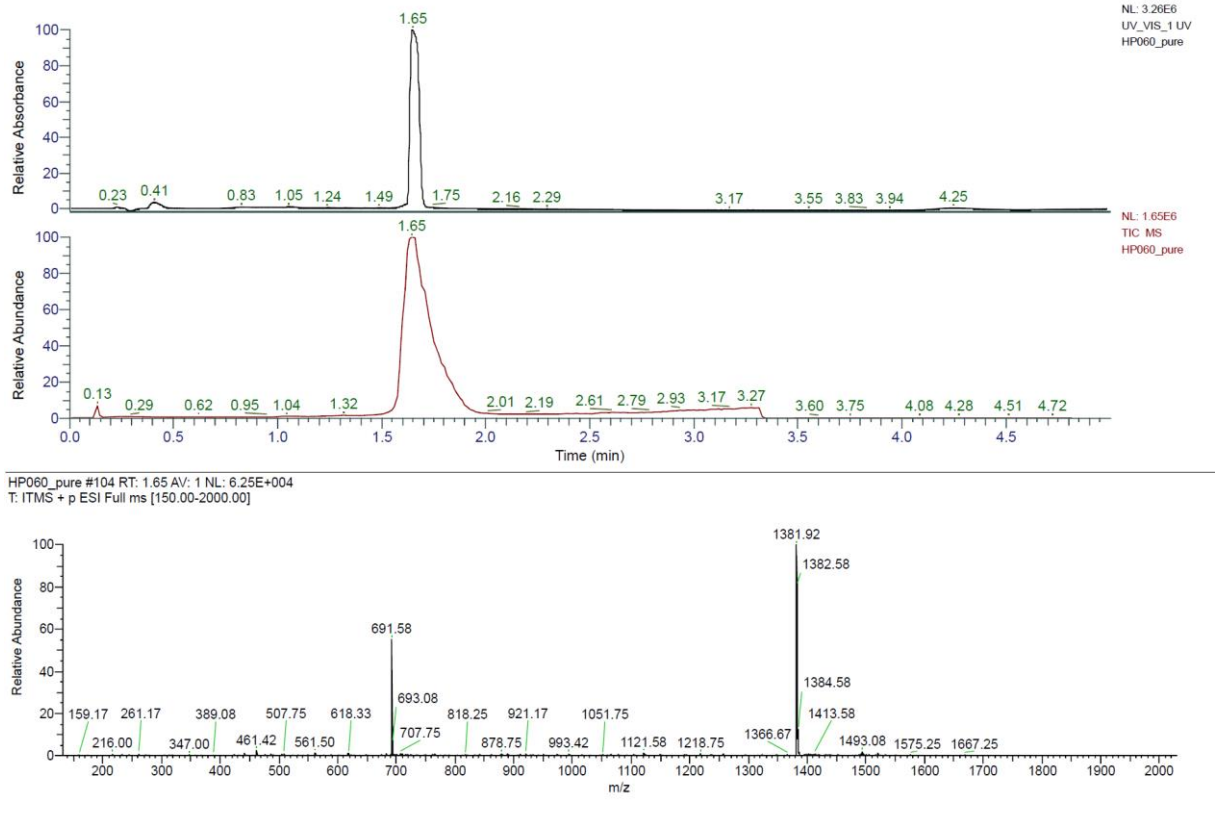

HRMS spectra:

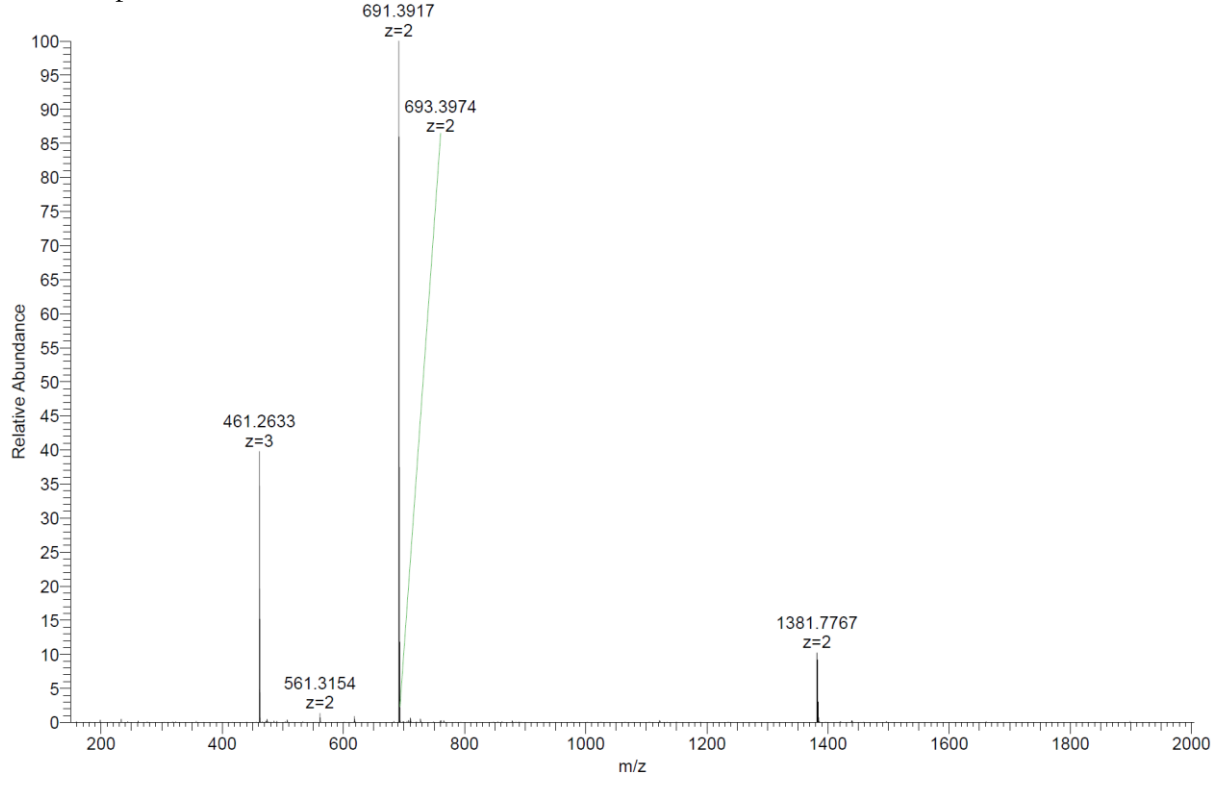

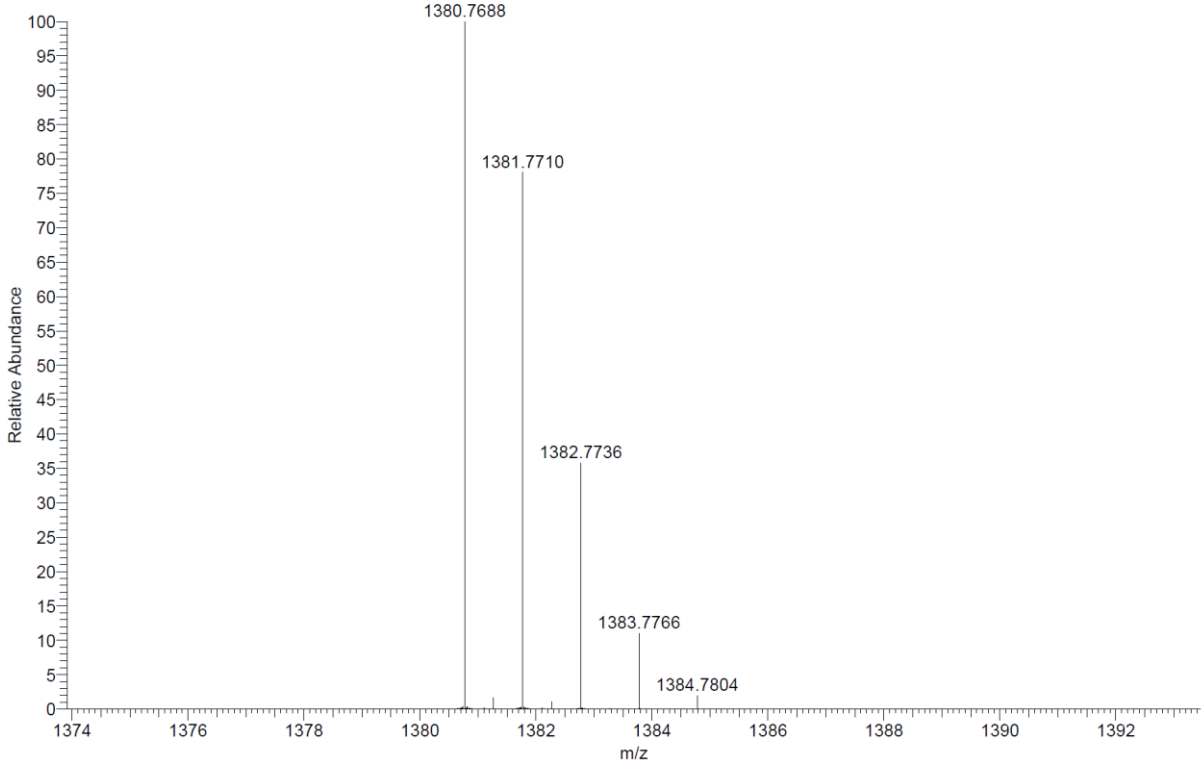

flGWlFKwASK (HP39) was obtained as white solid after preparative RP-HPLC (55.6 mg, 51.6%). Analytical RP-HPLC: t_R = 1.63 min (A/D 100:0 to 0:100 in 3.5 min, λ = 214nm). MS (ESI+): $C_{72}H_{100}N_{16}O_{12}$ calc./obs. 1381.77/1381.78 Da $[M+H]^+$.

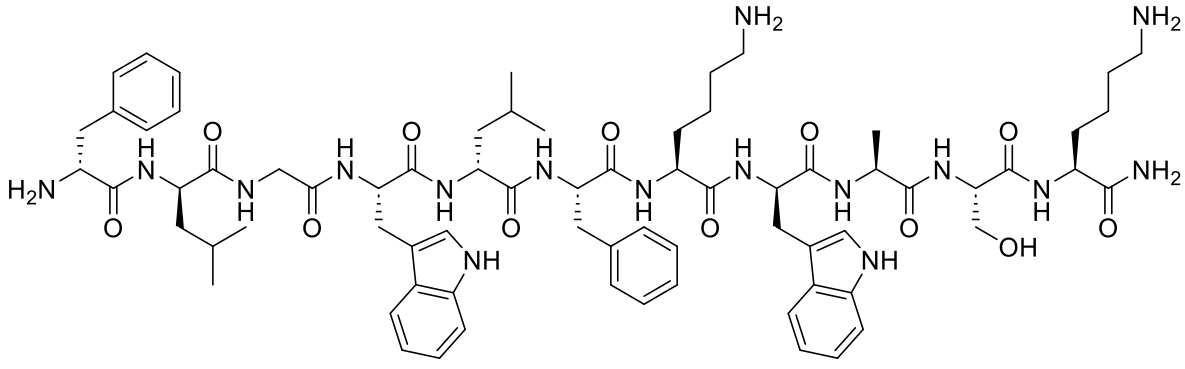

Chemical Formula: $C_{72}H_{100}N_{16}O_{12}$
Exact Mass: 1380.77
Molecular Weight: 1381.69

Analytical HPLC-MS data:

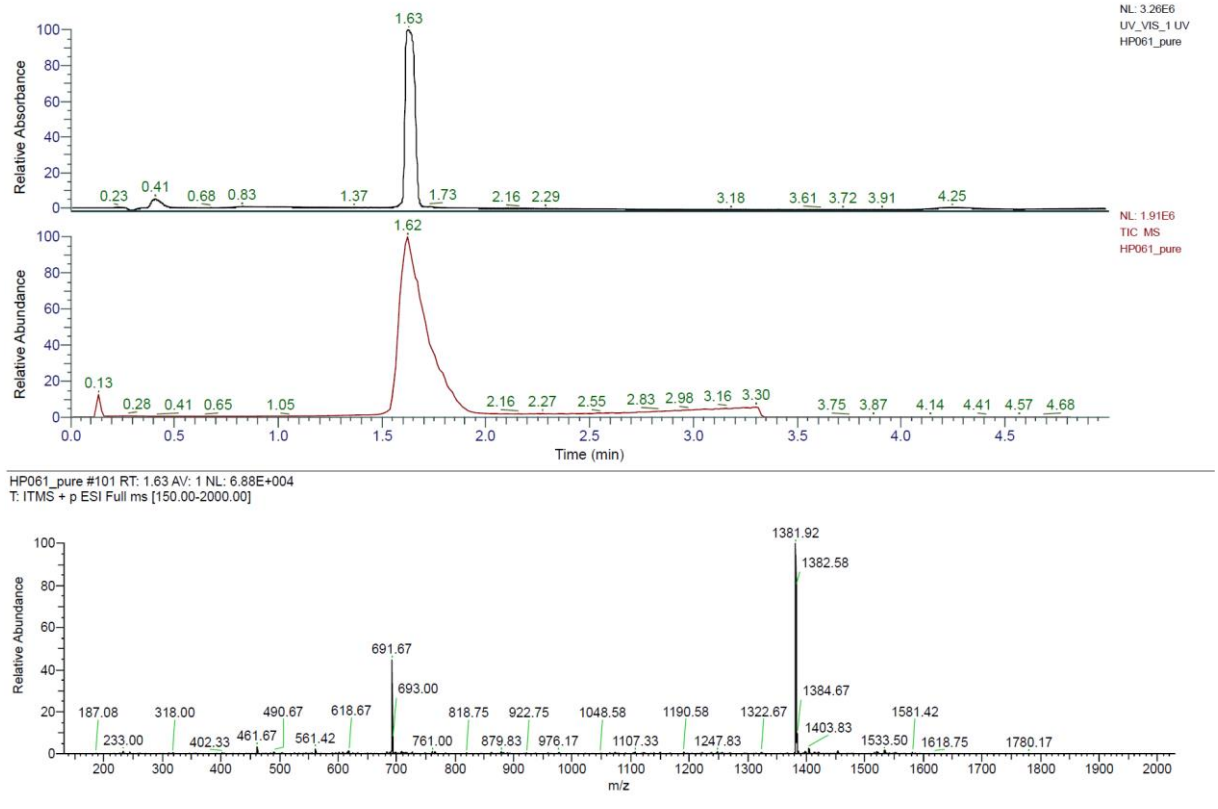

HRMS spectra:

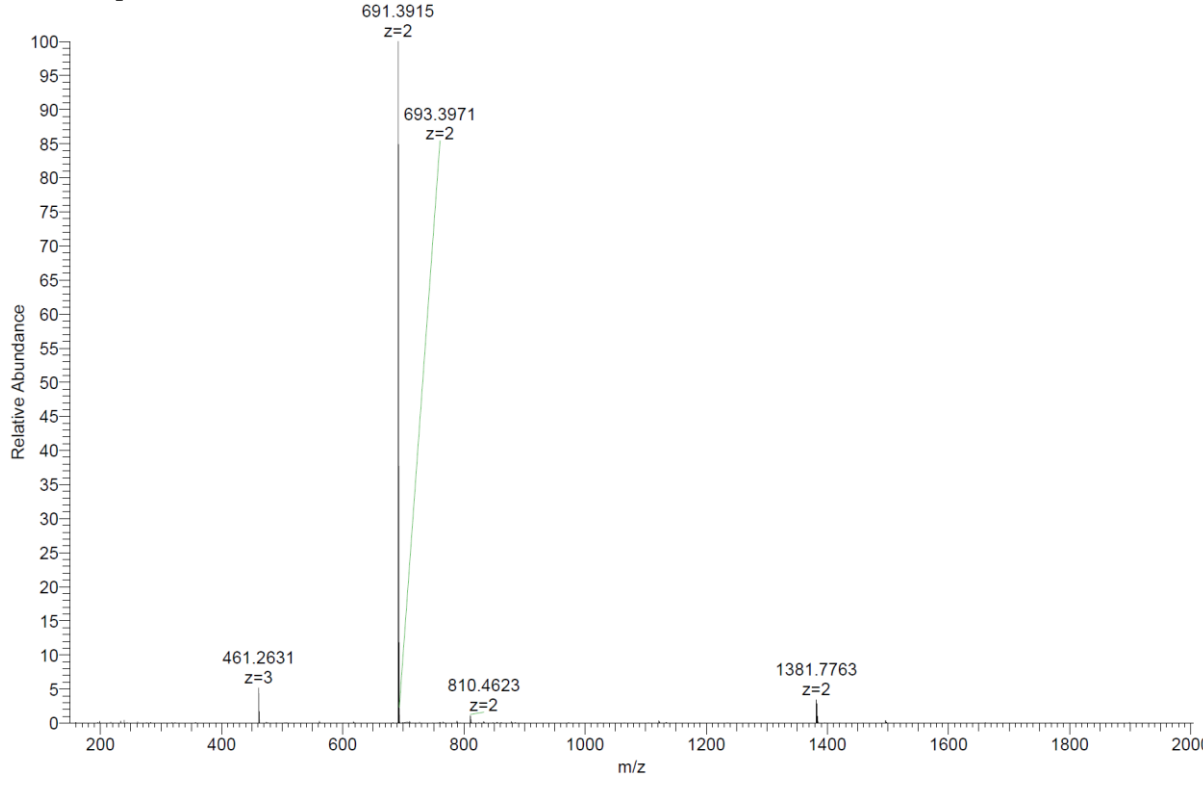

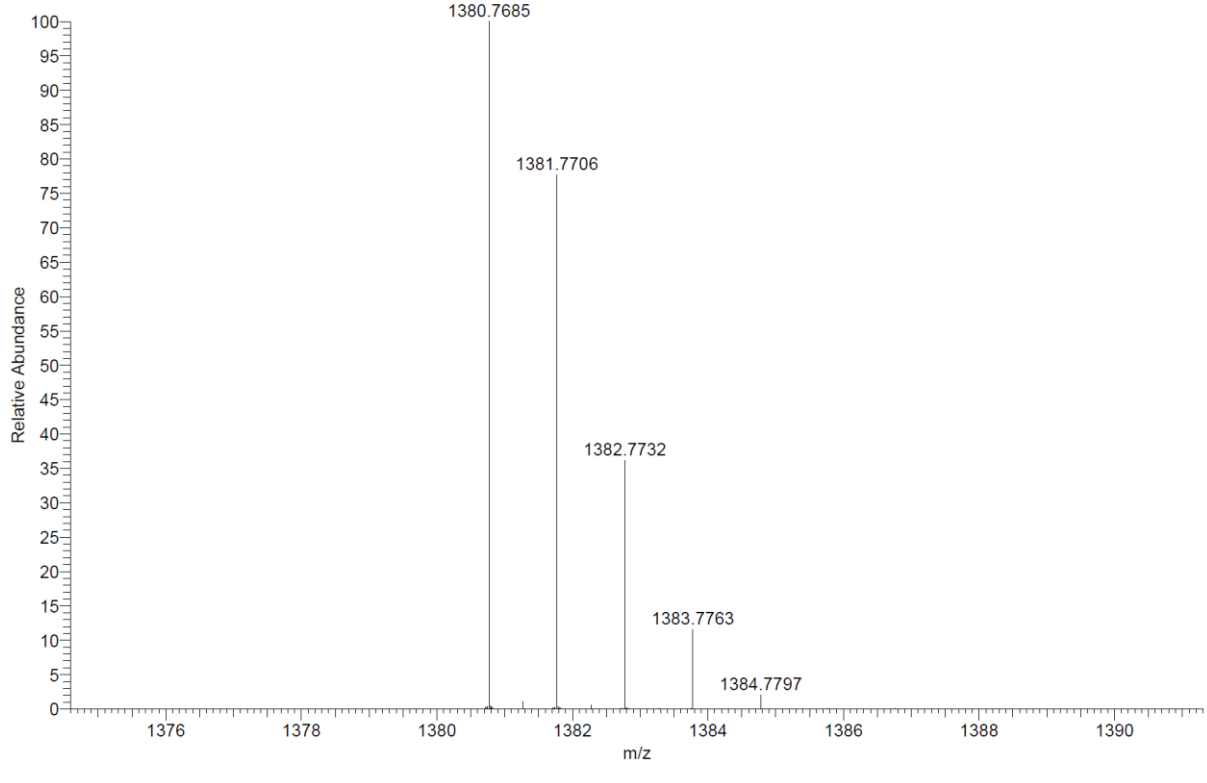

KYKKALKKLAKLL (SB1) was obtained as white solid after preparative RP-HPLC (87.6 mg, 44.7%). Analytical RP-HPLC: t_R = 1.35 min (A/D 100:0 to 0:100 in 3.5 min, λ = 214nm). MS (ESI+): $C_{75}H_{138}N_{20}O_{14}$ calc./obs. 1544.07/1544.07 Da $[M+H]^+$.

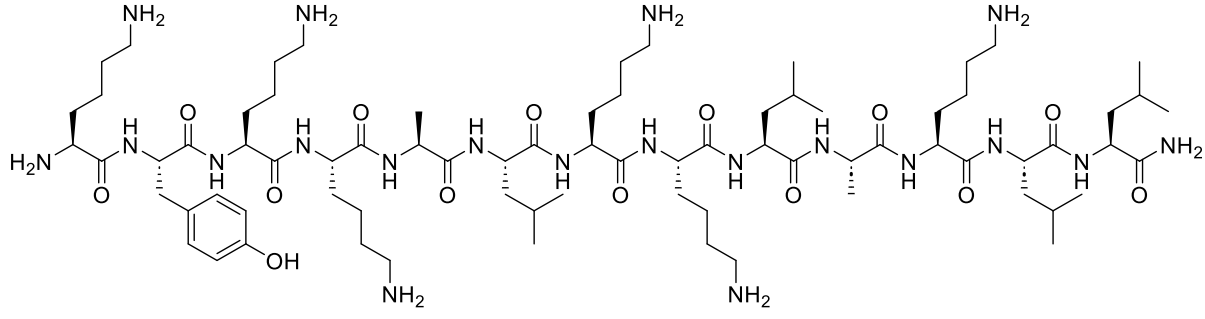

Chemical Formula: $C_{75}H_{138}N_{20}O_{14}$
Exact Mass: 1543.07
Molecular Weight: 1544.06

Analytical HPLC-MS data:

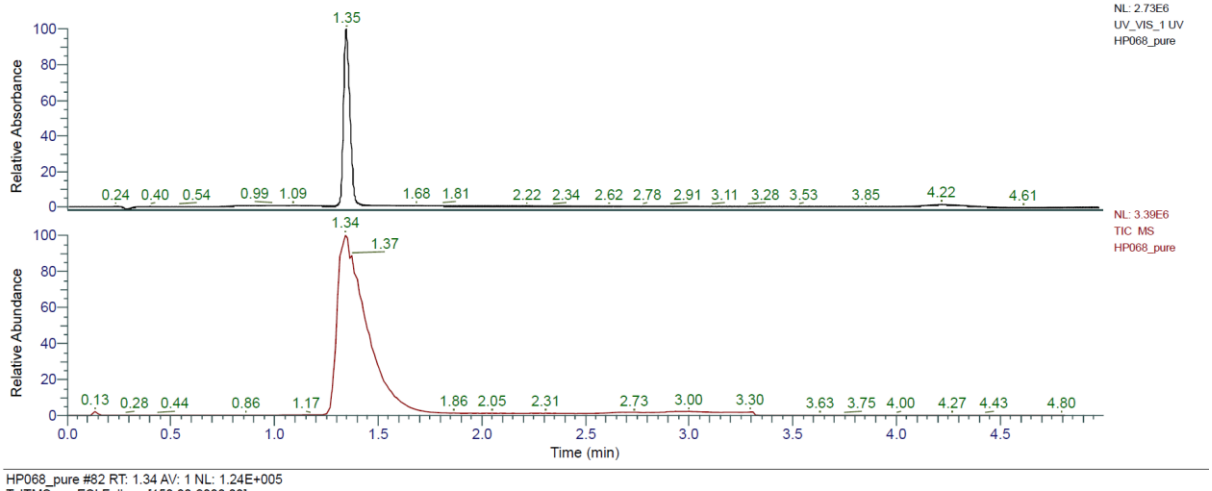

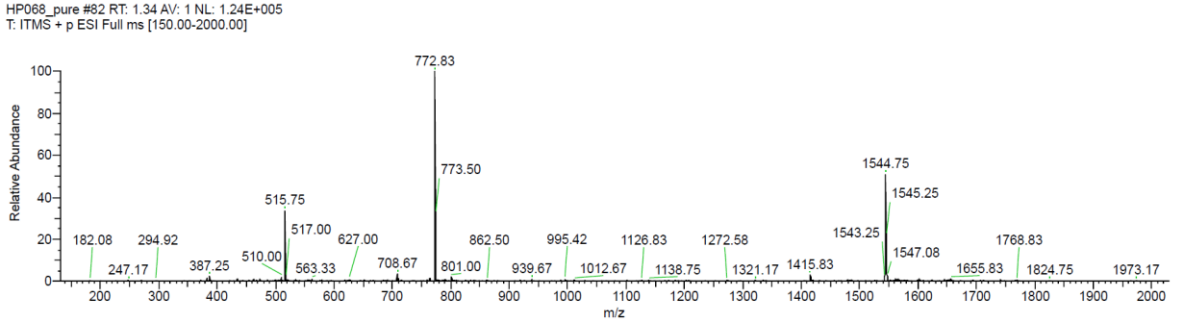

HRMS spectra:

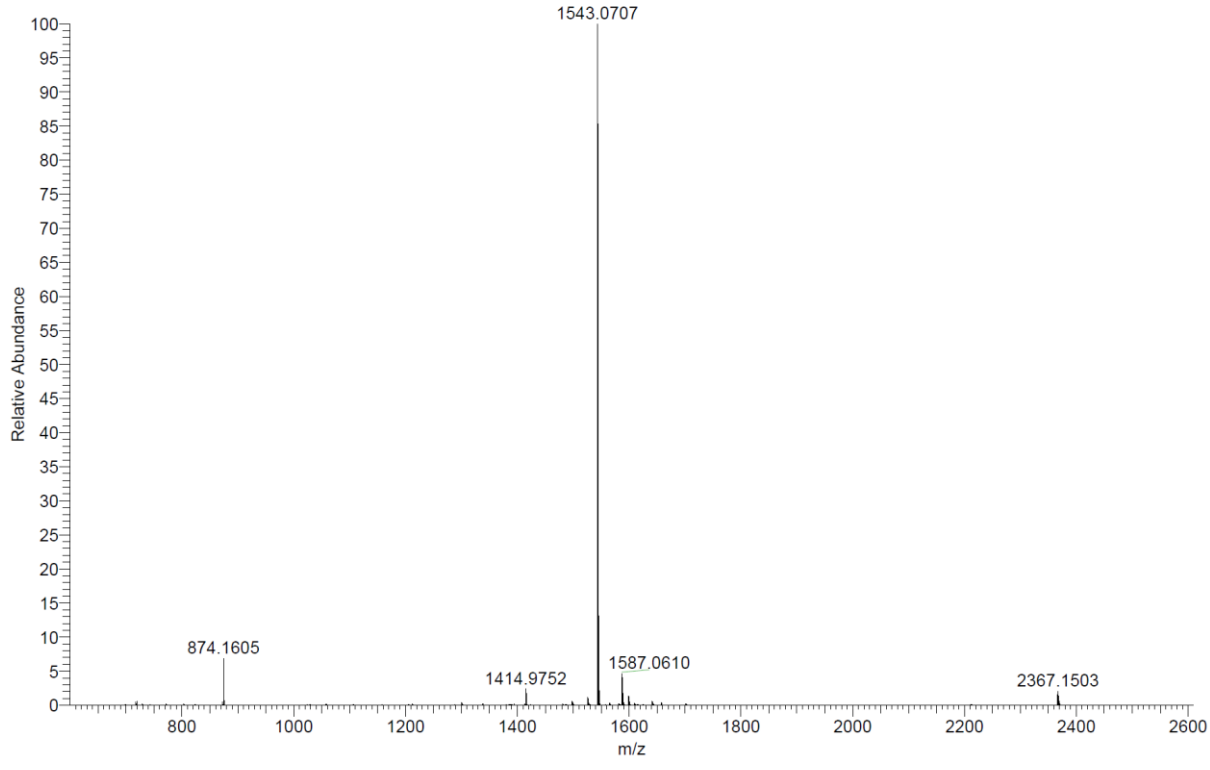

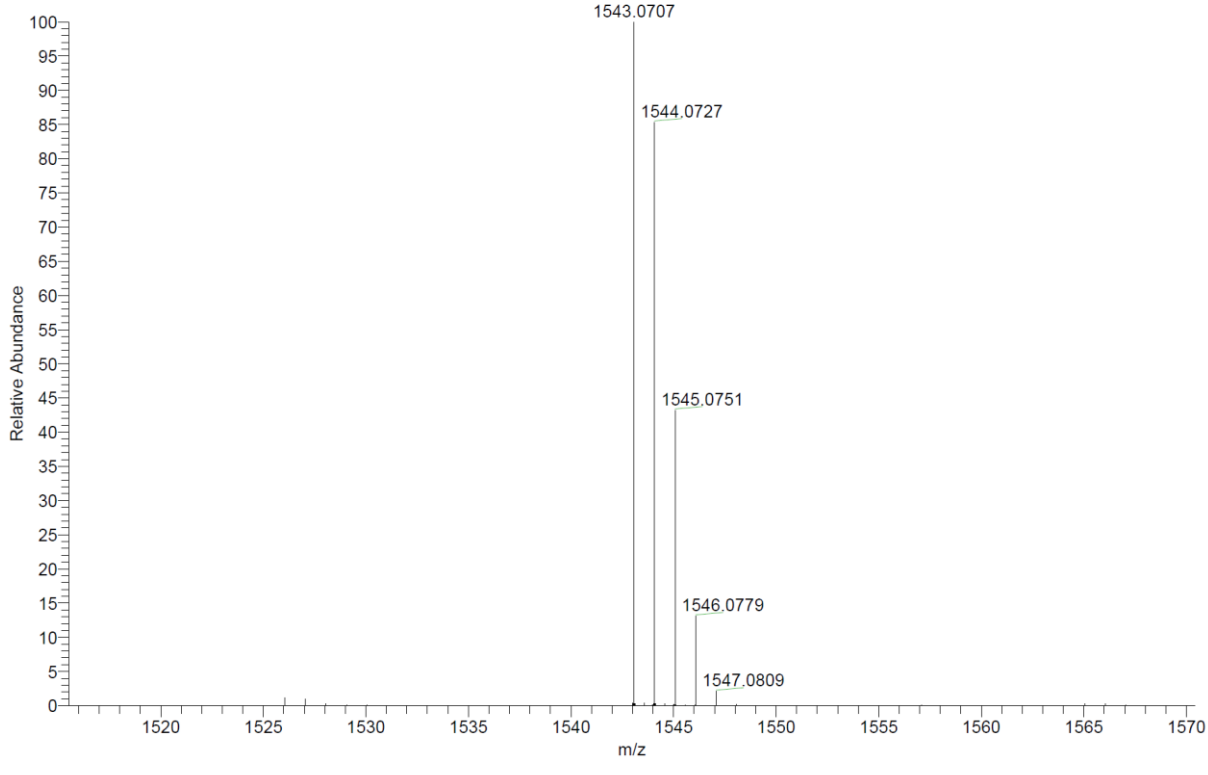

kYkkALkkLAkLL (HP40) was obtained as white solid after preparative RP-HPLC (78.0 mg, 39.8%). Analytical RP-HPLC: t_R = 1.27 min (A/D 100:0 to 0:100 in 3.5 min, λ = 214nm). MS (ESI+): $C_{75}H_{138}N_{20}O_{14}$ calc./obs. 1544.07/1544.07 Da $[M+H]^+$.

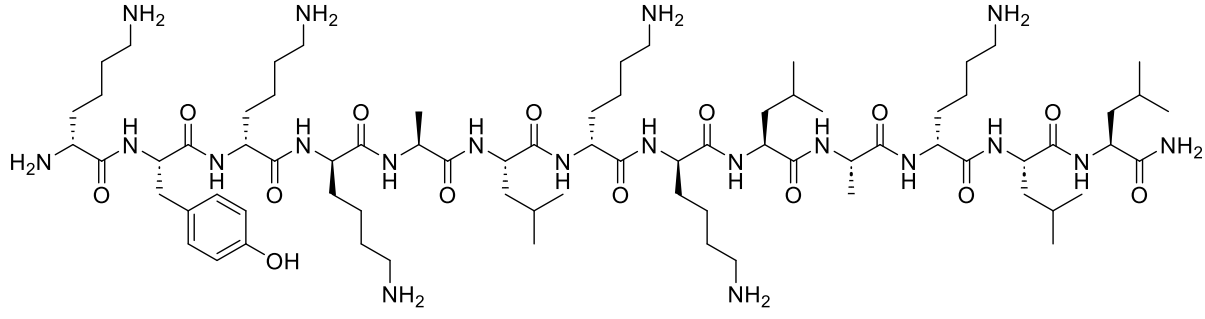

Chemical Formula: $C_{75}H_{138}N_{20}O_{14}$
Exact Mass: 1543.07
Molecular Weight: 1544.06

Analytical HPLC-MS data:

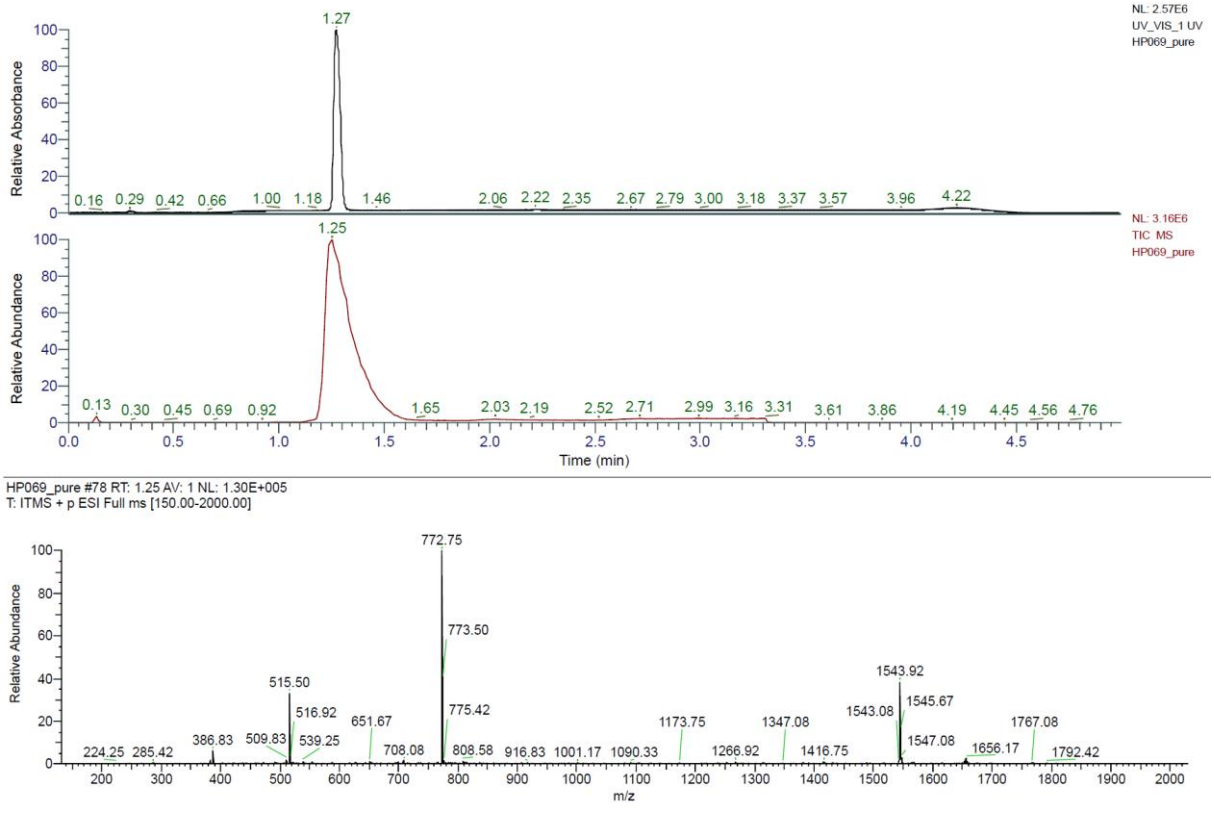

HRMS spectra:

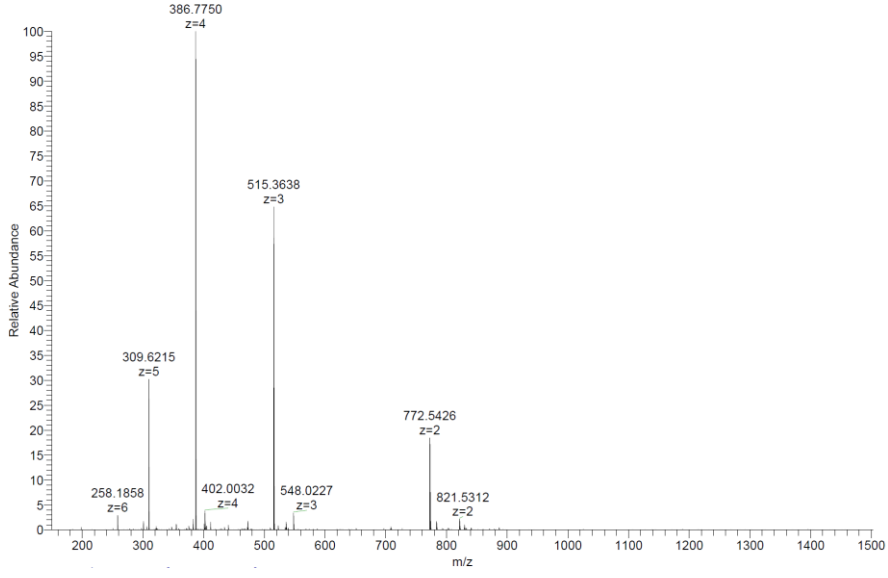

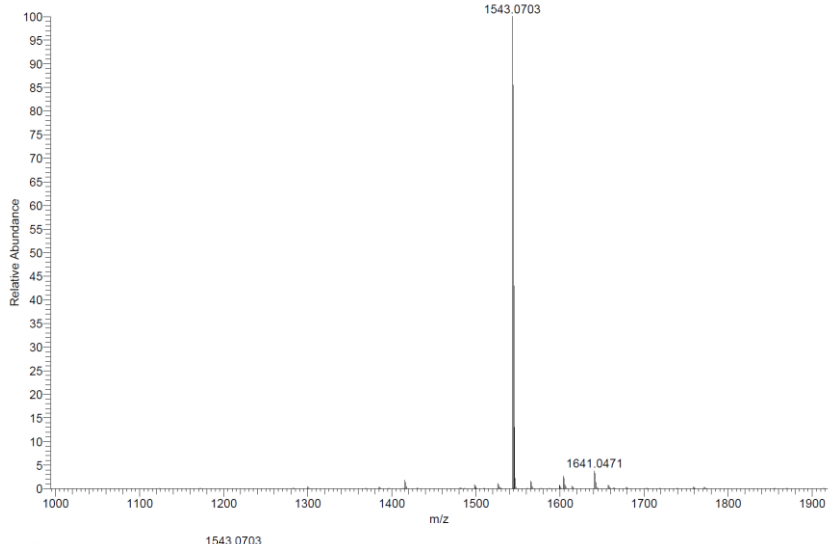

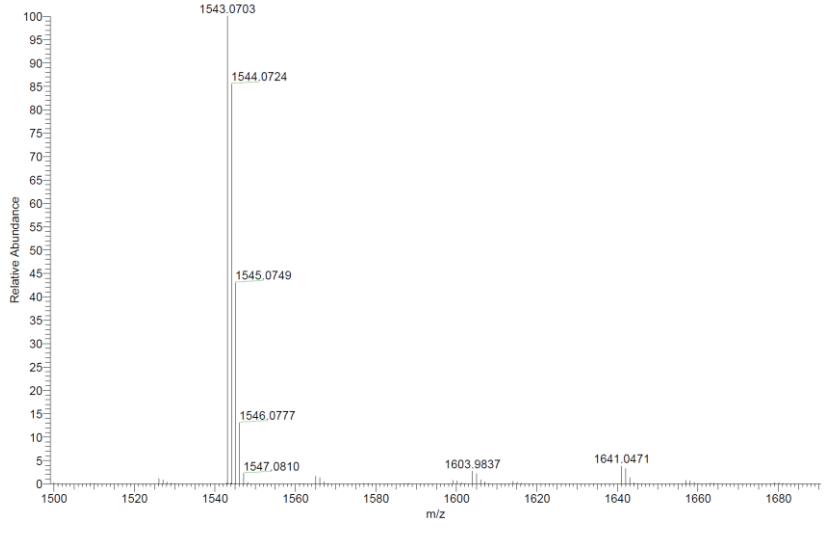

vqwrairvrvir (DJK5) was obtained as white solid after preparative RP-HPLC (47.3 mg, 26.8%). Analytical RP-HPLC: t_R = 1.33 min (A/D 100:0 to 0:100 in 3.5 min, λ = 214nm). MS (ESI+): $C_{70}H_{123}N_{27}O_{13}$ calc./obs. 1550.98/1550.98 Da $[M+H]^+$.

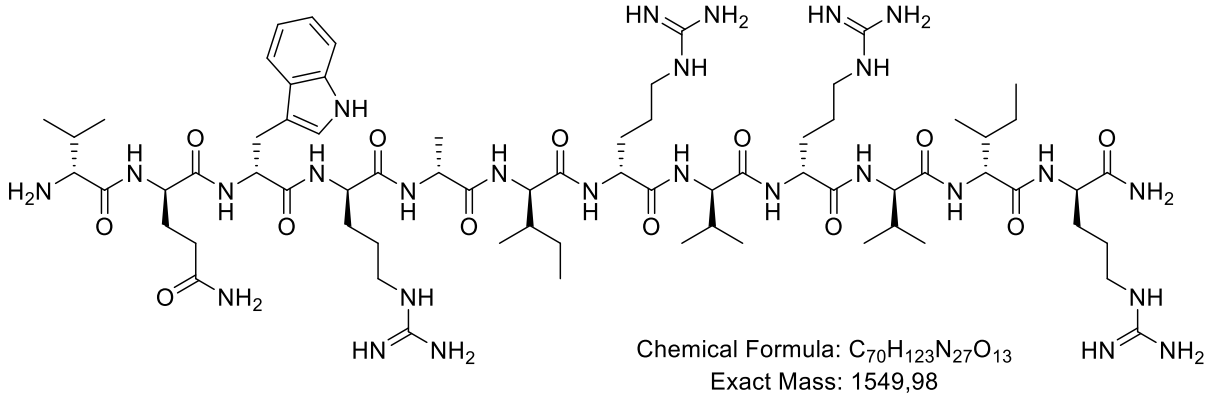

Chemical Formula: $C_{70}H_{123}N_{27}O_{13}$
Exact Mass: 1549,98
Molecular Weight: 1550,93

Analytical HPLC-MS data:

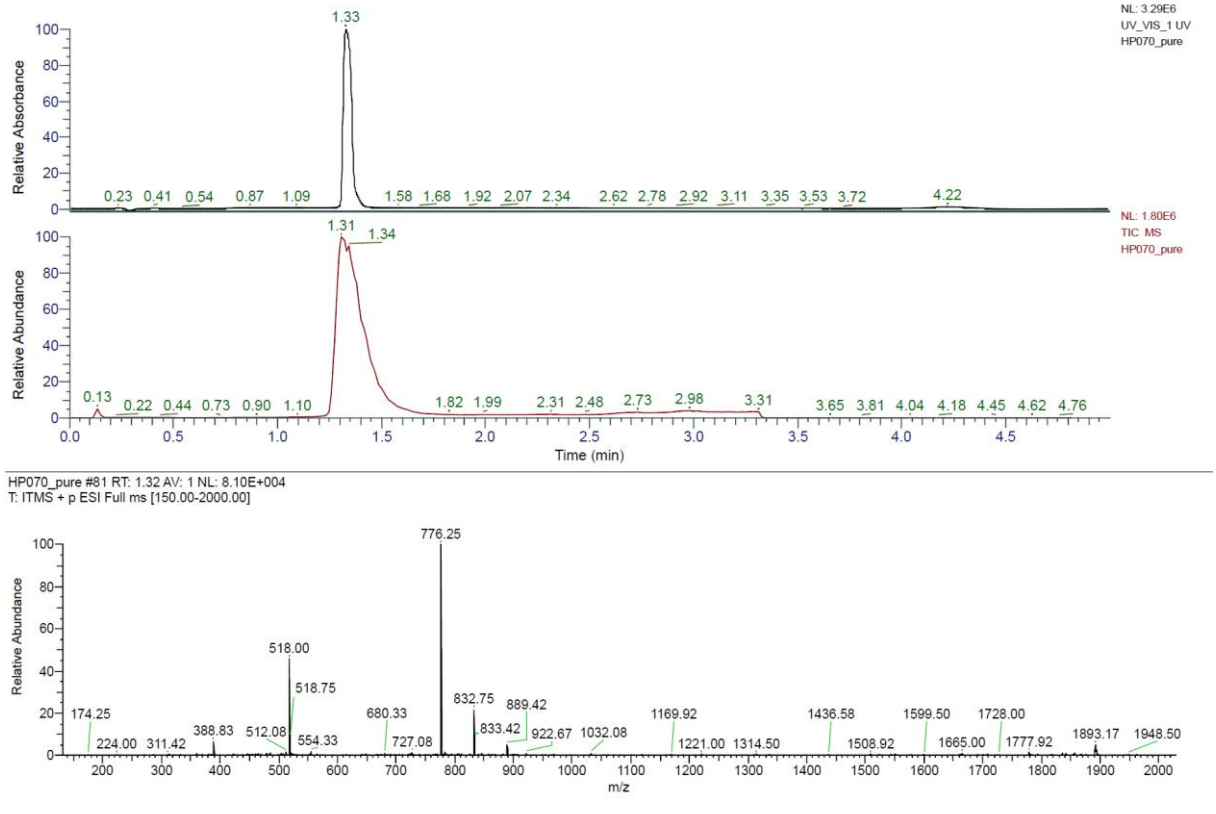

HRMS spectra:

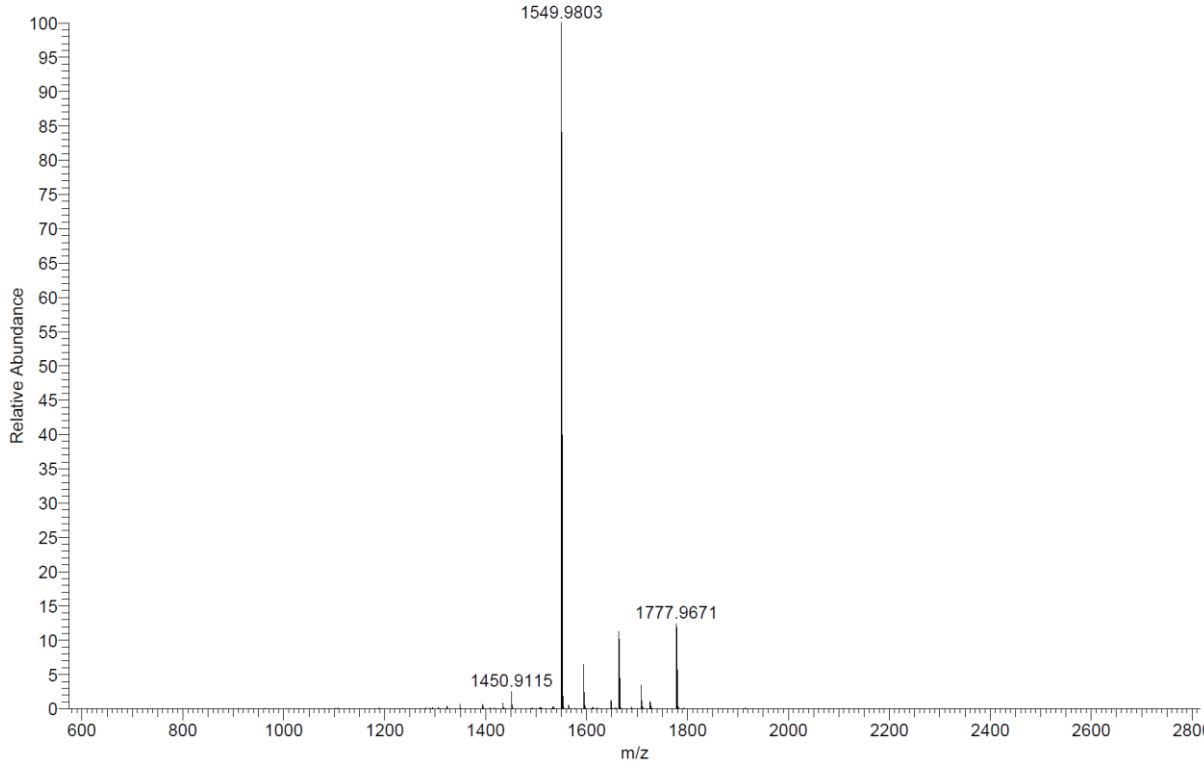

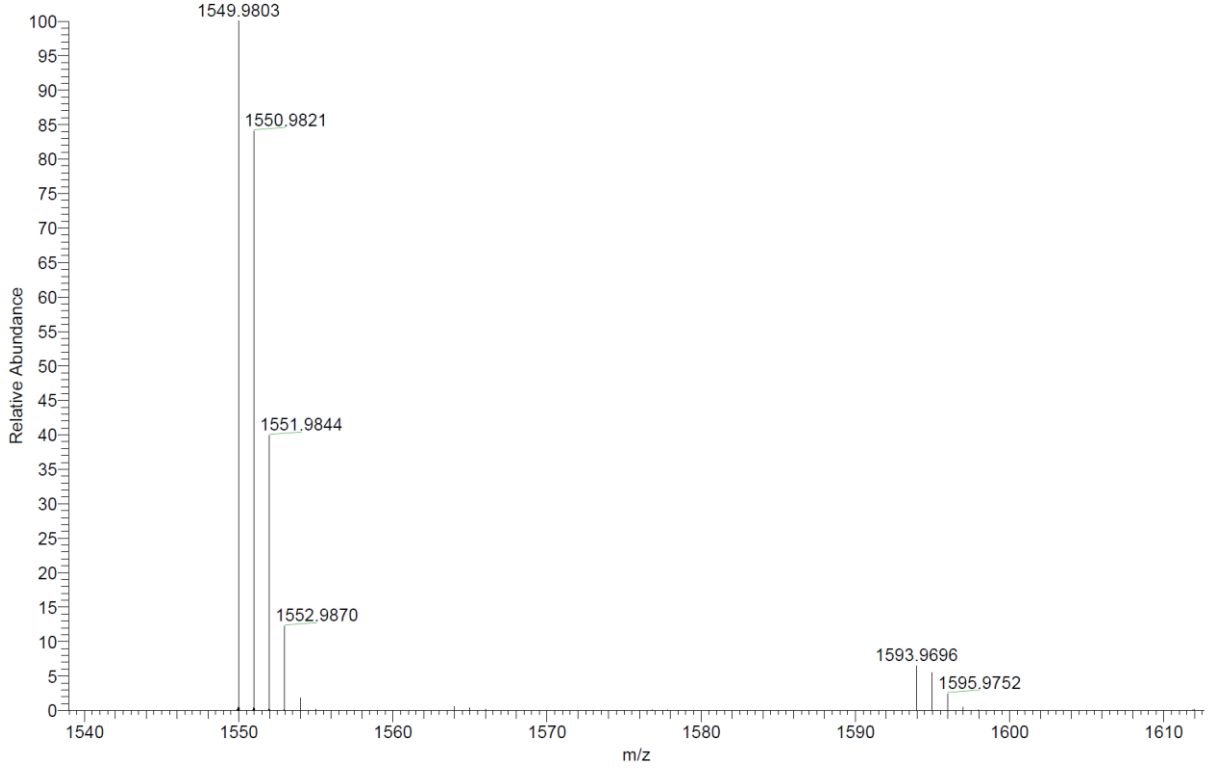

VQWrAIrVrVIr (HP41) was obtained as white solid after preparative RP-HPLC (64.3 mg, 36.4%). Analytical RP-HPLC: t_R = 1.26 min (A/D 100:0 to 0:100 in 3.5 min, λ = 214nm). MS (ESI+): $C_{70}H_{123}N_{27}O_{13}$ calc./obs. 1550.98/1550.98 Da $[M+H]^+$.

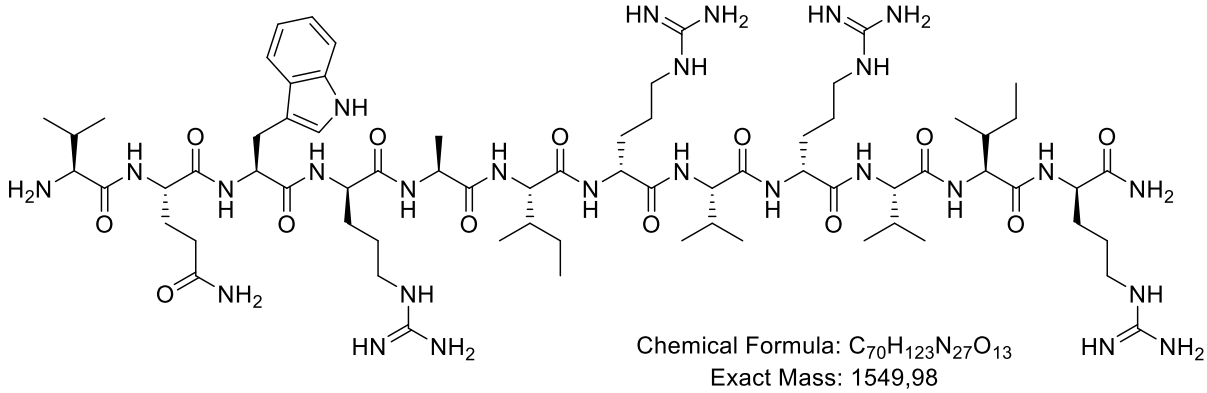

Analytical HPLC-MS data:

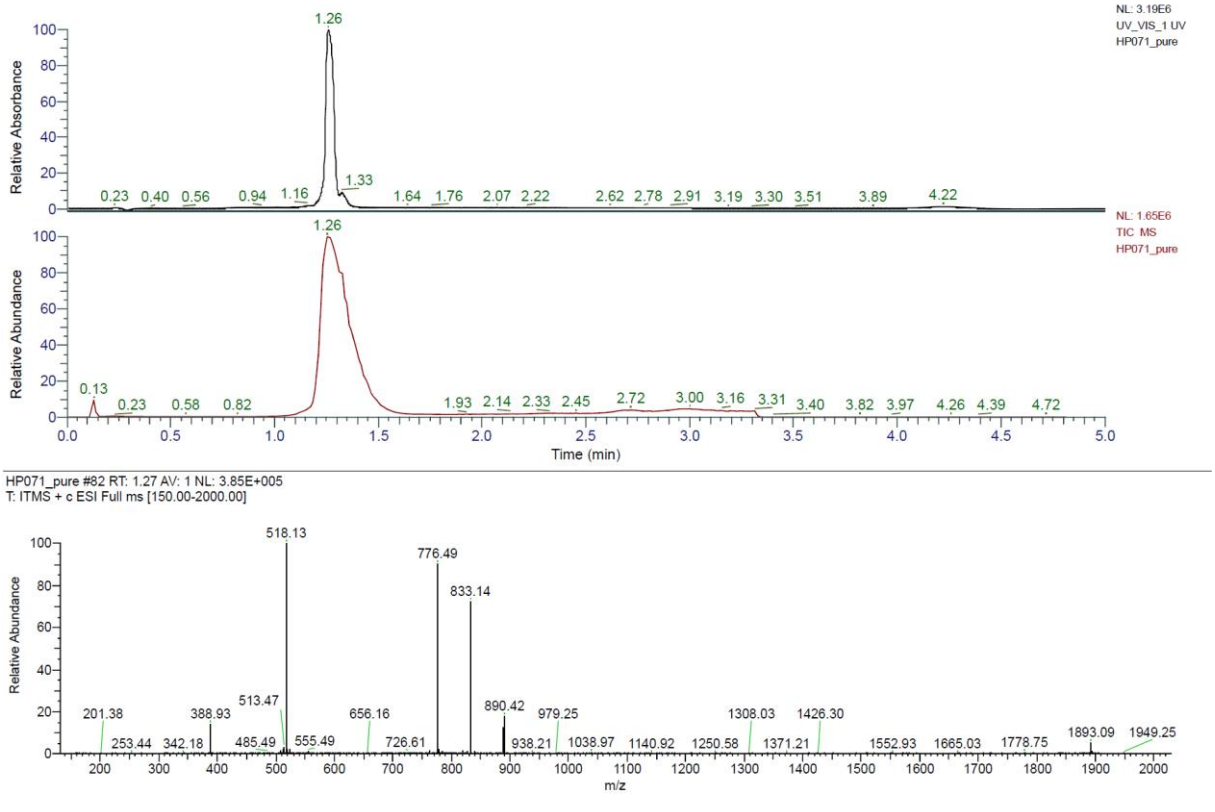

HRMS spectra:

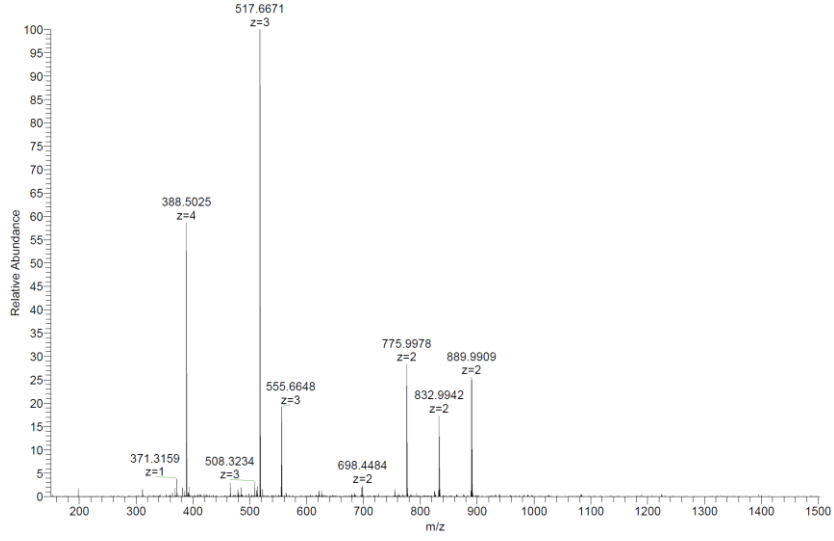

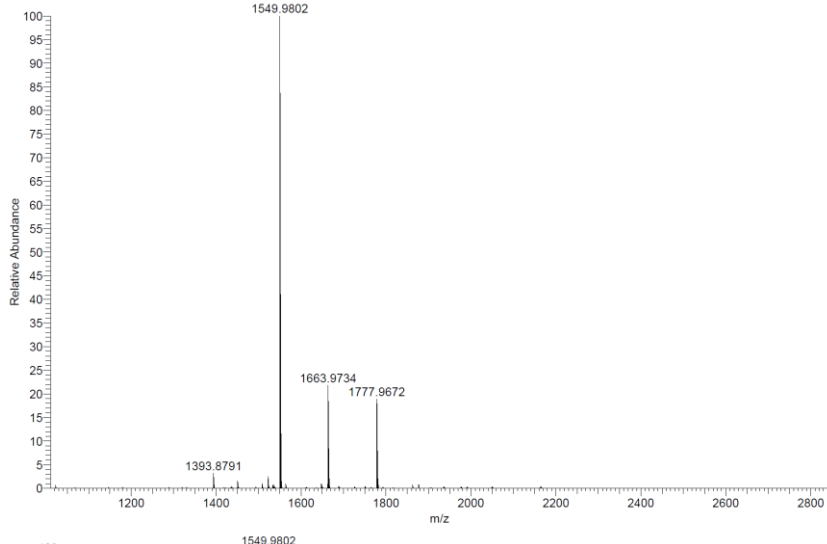

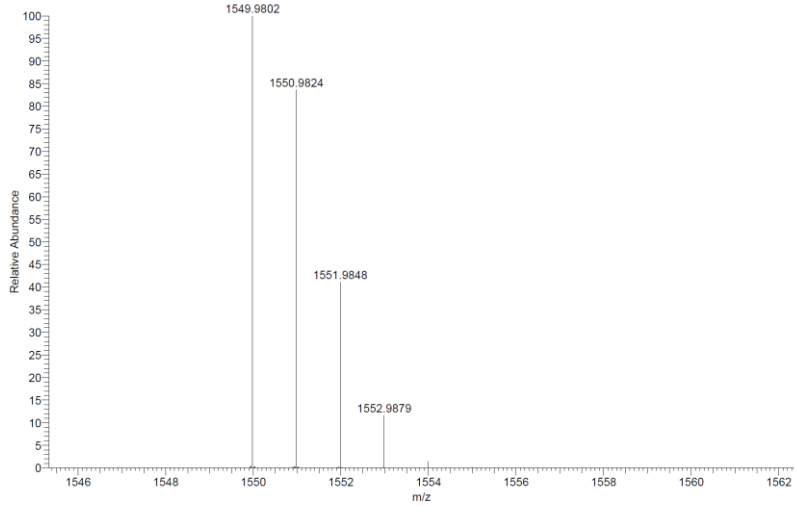

8.4 SI for Dipropylamine for 9-Fluorenylmethylcarbonyl (Fmoc) Deprotection with Reduced Aspartimide Formation in Solid-Phase Peptide Synthesis

Peptide synthesis

Solid Phase Peptide Synthesis of linear peptides. All linear peptides were synthesized using standard 9-fluorenylmethoxycarbonyl (Fmoc) Solid Phase Peptide Synthesis under nitrogen bubbling. All peptides were synthesized using Rink Amide LL resin (0.26-0.29 mmol/g) except for Bivaluridin for which Wang resin (1.2 mmol/g) was used. Resin was firstly deprotected twice for one minute and four minutes using the corresponding deprotection cocktail. For each amino acid, a double coupling was performed (2 × 8 minutes) using for each coupling 3 mL of 0.2 M of the corresponding Fmoc protected amino acid in DMF, 1.5 mL of 0.5 M Oxyma in DMF and 2 mL of 0.5 M DIC in DMF. Double deprotection steps (1 and 4 minutes) were achieved using the corresponding deprotection solution.

For **Bivalirudin**, first amino acid coupling was performed with addition of DMAP (0.2 eq.).

For **Afamelanotide**, the acetylation of N-terminus performed on-beads using a solution of 775 µL acetic anhydride, 500 µL DIPEA in 5 mL DMF (twice 30 minutes at room temperature).

For syntheses at 90 °C, coupling times were 2 × 4 minutes and deprotection times were 0.5 and 2.5 minutes.

Solid Phase Peptide Synthesis of G1KL. All peptide dendrimers were synthesized using standard 9-fluorenylmethoxycarbonyl (Fmoc) Solid Phase Peptide Synthesis under nitrogen bubbling using Rink Amide LL resin (0.26-0.29 mmol/g). Branching points consisted of Fmoc-Lys(Fmoc)-OH to obtained two free amines (α and ε) after Fmoc deprotection. Syntheses were performed as described above.

Solid Phase Peptide Synthesis of G2KL Syntheses of **G2KL** were performed at room temperature with the same reagents as described above in stirred syringes. Double deprotections were performed during 2 × 10 minutes. Double coupling was performed during 2 ×1 hour for the three first amino acids and the first generation, and a triple coupling was performed (3 × 1 hour) for the second generation residues.

Solid Phase Peptide Synthesis of G3KL. For syntheses performed at 60 °C, double deprotections was performed during 1 and 4 minutes and double coupling was performed during 2 × 8 minutes for the three first amino acids and first generation. For the second generation, triple deprotection (1, 2 and 4 minutes) and a quadruple coupling (4 × 8 minutes) were

performed. From the last branching lysine, quadruple deprotection (2, 4, 2 and 4 minutes) and 7 couplings of 8 minutes were performed.

Syntheses at room temperature with the same reagents as described above in stirred syringes. Double deprotections were performed during 2 × 10 minutes. For the three first amino acids and first generation, double coupling was performed during 2 × 1 hour. For the second generation, a triple coupling was performed during 3 × 1 hour. For the last generation (two last amino acids), quintuple coupling was performed during 5 × 1 hour.

Cleavage from resin. After the SPPS, peptide dendrimers were cleaved from the resin at room temperature using 7 mL of a mixture trifluoroacetic acid/triisopropylsilane/mQ water (TFA/TIS/H_2O) with the corresponding ratios 94/5/1 except for Hexapeptide **5** for which a 7 mL TFA /TIS /DODT/ H_2O mixture with the corresponding ratios 94/2.5/2.5/1 for three hours. Peptides were then precipitated using approximatively 25 mL of cold terbutylmethyl ether and centrifuged 10 minutes at 4400 rpm. Supernatant was removed and peptides were dried with argon before lyophilization and/or purification and LC-MS/HRMS analyses. All peptides were obtained as TFA salts.

Fmoc deprotection in solution. 50 mg of Fmoc-Lys(Boc)-OH, Fmoc-Phe-OH or Fmoc-PEG-OH were dissolved in the corresponding deprotection condition in a total volume of 500 µL. Deprotection conditions used in DMF were 20% v/v piperidine, 25% v/v dipropylamine, 5% w/v piperazine + 2% v/v DBU, 2% v/v DBU, 25%% v/v dipropylamine + 3% w/v piperazine, 25% v/v diethylamine, 25% v/v diisopropylamine and 25% diisobutylamine. Reaction mixtures were stirred during 30 minutes at room temperature. After the reaction and for each condition, 10 µL were diluted in MeCN for a final volume of 1 mL. All samples were analyzed by analytical RP-HPLC-MS using solvents B (100 mQ water + 0.1% formic acid) and C (90% MeCN + 10% mQ water + 0.1% formic acid) with a gradient 100% B to 100% C in 5 or 7 minutes.

^{1}H NMR data acquisition. ^{1}H NMR spectra were recorded on a Bruker Avance 300 spectrometer (300 MHz) at room temperature. Peptides analyzed by ^{1}H NMR were purified using preparative RP-HPLC prior to data acquisition. Spectra analyses were performed using MestReNova v14.2.1. See supporting information for measured spectra.

Table S4.1: Extended SPPS yields of peptide dendrimers and linear peptides using various Fmoc deprotection conditions.

Cpd. Sequence [a)]	**Deprotection condition** [b)]	**Crude purity** [c)] **%**	**Crude yield** [d)] **%**	**Isolated yield** [f)] **%**	**MS calc/obs (g/mol)**
Hexapeptide **1**	20% PPR, 60 °C	83 (17 / 0)	46.6	4.5	693.39/693.39
VKDGYI	20% PPR + 0.25 M Oxyma, 60 °C	93 (7 / 0)	22.1	n.d.	693.39/693.39
	20% PPR + 0.5 M Oxyma, 60 °C	93 (6 / 1)	16.8	n.d.	693.39/693.39
	5% PZ + 2% DBU, 60 °C	0 (0 / 100)	0	n.d.	693.39/-
	5% PZ + 2% DBU + 0.25 M HOBt, 60 °C	56 (27 / 17)	9.2	n.d.	693.39/693.39
	5% PZ + 2% DBU + 0.5 M HOBt, 60 °C	94 (5 / 1)	10.4	n.d.	693.39/693.39
	5% PZ + 2% DBU + 0.25 M Oxyma, 60 °C	76 (22 / 2)	16.3	n.d.	693.39/693.39
	5% PZ + 2% DBU + 0.5 M Oxyma, 60 °C	86 (13 / 1)	21.8	n.d.	693.39/693.39
	2% DBU, 60 °C	52 (25 / 23)	25.7	n.d.	693.39/693.39
	20% DPA, 60 °C	95 (5 / 0)	49.3	n.d.	693.39/693.39
	20% DPA + 0.5 M Oxyma, 60 °C	93 (6 / 1)	45.4	n.d.	693.39/693.39
	25% DPA, 60 °C	96 (4 / 0)	52.9	16.0	693.39/693.39
	25% DEA, 50 °C	86 (7 / 7)	43.4	n.d.	693.39/693.39
	25% DEA, 60 °C	89 (8 / 3)	45.7	n.d.	693.39/693.39
	25% DBA, 60 °C	93 (4 / 3)	52.1	n.d.	693.39/693.39
	25% DIBA, 60 °C	0 (0 / 100)	0	n.d.	693.39/-
	20% PPR, 90 °C	70 (20 / 10)	28.4	n.d.	693.39/693.39
	25% DPA, 90 °C	78 (11 / 11)	33.5	n.d.	693.39/693.39
Hexapeptide **2**	20% PPR, 60 °C	67 (32 / 1)	40.9	n.d.	593.30/593.30
GDGAKF	25% DPA, 60 °C	84 (8 / 8)	49.2	n.d.	593.30/593.30
Hexapeptide **3**	20% PPR, 60 °C	84 (8 / 8)	40.3	n.d.	792.47/792.47
VKDRYI	25% DPA, 60 °C	90 (4 / 6)	43.4	n.d.	792.47/792.47
Hexapeptide **4**	20% PPR, 60 °C	96 (3 / 1)	50.6	n.d.	693.36/693.39
GDRAKF	25% DPA, 60 °C	99 (0 / 1)	62.5	n.d.	693.36/693.39
Hexapeptide **5**	20% PPR, 60 °C	90 (5 / 5)	53.1	n.d.	739.37/739.38
VKDCYI	25% DPA, 60 °C	88 (4 / 8)	48.0	n.d.	739.37/739.38
Hexapeptide **6**	20% PPR, 60 °C	97 (1 / 2)	54.7	n.d.	707.40/707.41
VKDAYI	25% DPA, 60 °C	96 (1 / 3)	51.3	n.d.	707.40/707.41
Hexapeptide **7**	20% PPR, 60 °C	98 (0 / 2)	47.7	n.d.	707.40/707.41
VKEGYI	5% PZ + 2% DBU, 60 °C	99 (0 / 1)	52.4	n.d.	707.40/707.41
	20% DPA, 60 °C	98 (0 / 2)	44.3	n.d.	707.40/707.41
	20% DPA + 0.5M Oxyma, 60 °C	94 (0 / 6)	50.0	n.d.	707.40/707.41
Afamelanotide	20% PPR, 60 °C	46	69.8	16.8	1646.84/1646.84
Ac-SYSNleEHfRWGKPV	25% DPA, 60 °C	50	45.1	9.9	1646.84/1646.84
Bivalirudin	20% PPR, 60 °C	77	n.d.	46.3	2179.99/2179.99
fPRPGGGGNGDFEEIPEEYL [a)]	25% DPA, 60 °C	77	n.d.	38.7	2179.99/2179.99
	20% PPR, 90 °C	28	6.6	n.d.	2179.99/2179.99
	25% DPA, 90 °C	25	4.6	n.d.	2179.99/2179.99
G1KL	20% PPR, 60 °C	90	72.5	n.d.	869.66/869.66
$(KL)_2KKL$	5% PZ + 2% DBU, 60 °C	97	26.2	n.d.	869.66/869.66
	20% DIPA, 60 °C	0	0	n.d.	869.66/-
	20% DIPA + 1% DBU, 60 °C	86	35.6	n.d.	869.66/869.66
	20% DPA, 60 °C	78	35.2	n.d.	869.66/869.66
	20% DPA + 1% DBU, 60 °C	85	34.0	n.d.	869.66/869.66
	25% DPA, 60 °C	88	64.5	n.d.	869.66/869.66
G2KL	20% PPR, r.t.	79	64.9	n.d.	2090.57/2090.56
$(KL)_4(KKL)_2KKL$	5% PZ + 2% DBU, r.t.	74	53.9	n.d.	2090.57/2090.56
	20% DPA, r.t.	82	42.2	n.d.	2090.57/2090.56
	25% DPA, r.t.	80	46.4	n.d.	2090.57/2090.56
G3KL	20% PPR, 60 °C	74	46.8	n.d.	4532.38/4532.39
$(KL)_8(KKL)_4(KKL)_2KKL$	25% DPA, 60 °C	N/A [e)]	N/A [e)]	n.d.	4532.38/4532.39
	25% DPA (+ 1% DBU last generation), 60 °C	N/A [e)]	N/A [e)]	n.d.	4532.38/4532.39
	2% DBU, 60 °C	70	48.4	n.d.	4532.38/4532.39
	20% PPR, r. t.	78	40.5	n.d.	4532.38/4532.37
	25% DPA, r. t.	29	12.3	n.d.	4532.38/4532.37

[a)] One letter code for amino-acids, D- amino acids in lower case, K indicates branching L- lysine, C-termini are carboxamide except for Bivalirudin which is carboxyl. Ac =acetyl group, Nle = norleucine. [b)] SPPS was carried out in DMF using Oxyma/DIC as coupling reagents and the indicated base for Fmoc removal. PPR = Piperidine, PZ = Piperazine, DBU = 1,8-diazabicyclo[5.4.0]undec-7-ene, DPA = Dipropylamine, DIPA = Diisopropylamine, DEA = Diethylamine, DBA = Dibutylamine, DIBA = Diisobutylamine. Percentages (%) are in w/v in case of PZ and in v/v otherwise. [c)] Crude purity for hexapeptides **1-7** is given as follow: % desired product (% aspartimide or glutarimide / % other byproducts). The crude product after resin cleavage was precipitated, washed and dried, and analyzed by analytical HPLC to determine the percentage of desired product, aspartimide and other byproducts. [d)] Crude yield is calculated as followed: (crude mass / molecular weight of desired peptide) / (mass of resin × resin loading) × % of desired product content in crude. [e)] Not applicable. Peak integration was not possible in cases of **G3KL**, 25% DPA and 25% DPA + 1% DBU for the last generation, 60 °C due to byproducts / impurities in the crude but traces of desired compounds were observed by HRMS (see Supporting Information). [f)] Isolated yields were calculated after preparative RP-HPLC purification according to the amount of resin and its indicated loading. n.d. = not determined.

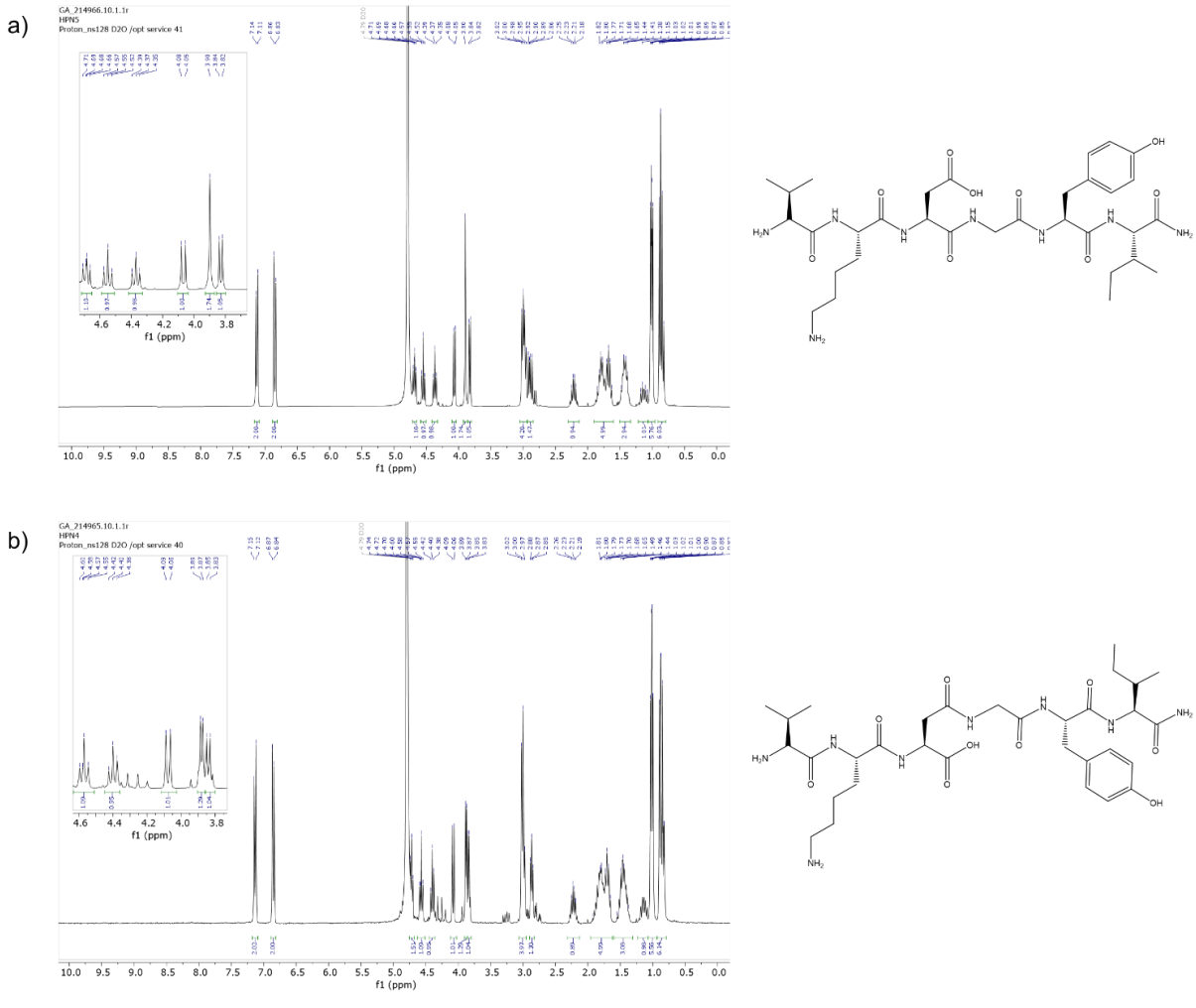

Figure S4.1: [1]H NMR spectra and structures of a) Hexapeptide **1** synthesized using 25% DPA as deprotection reagent and b) VKD(β)YI. Procedure is detailed in section 4 and assignments can be found in sections 5.2 (Hexapeptide **1** – 25% DPA) and 5.3 (VKD(β)YI).

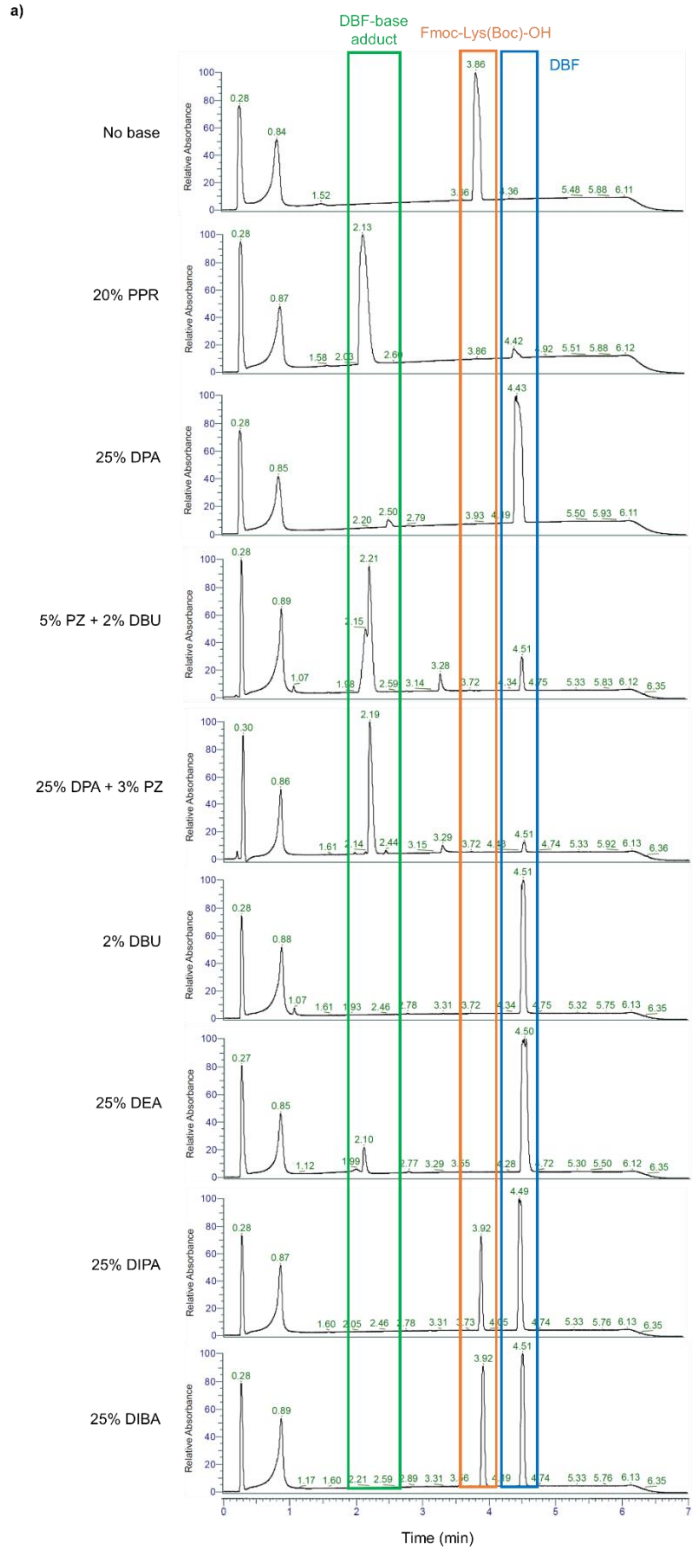
a)
DBF-base adduct
Fmoc-Lys(Boc)-OH
DBF
No base
20% PPR
25% DPA
5% PZ + 2% DBU
25% DPA + 3% PZ
2% DBU
25% DEA
25% DIPA
25% DIBA
Relative Absorbance
Time (min)

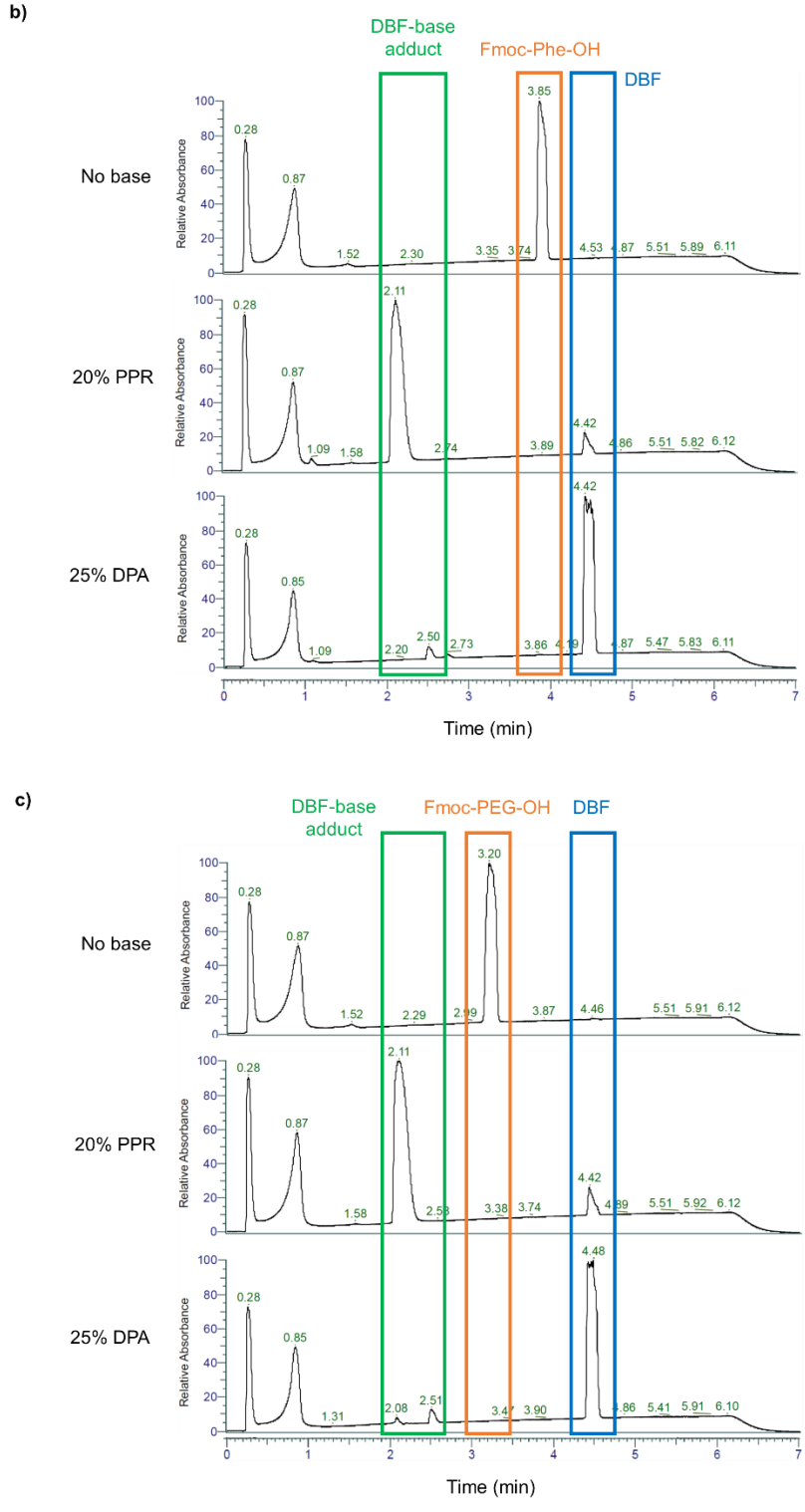

Figure S4.2: (previous page and above) Fmoc deprotection in DMF at room temperature during 30 minutes of a) Fmoc-Lys(Boc)-OH (t_R = 3.86-3.92 min), b) Fmoc-Phe-OH (t_R = 3.85 min) and c) Fmoc-PEG-OH (t_R = 3.20 min). DBF-PPR adduct (t_R = 2.11-2.13 min), DBF-PZ adduct (t_R = 2.19-2.21 min) DBF-DPA adduct (t_R = 2.50-2.51 min), DBF-DEA adduct (t_R = 2.10 min) and DBF (t_R = 4.42-4.51 min) can be observed. Deprotection was carried out at r.t. during 30 min. DBF = dibenzofulvene, PPR = Piperidine, DPA = Dipropylamine, PZ = Piperazine, DBU = 1,8-diazabicyclo[5.4.0]undec-7-ene, DEA = diethylamine, DIPA = Diisopropylamine, DIBA = Diisobutylamine. Procedure is detailed in section 3.

Compounds characterization

Hexapeptide 1 (VKDGYI)

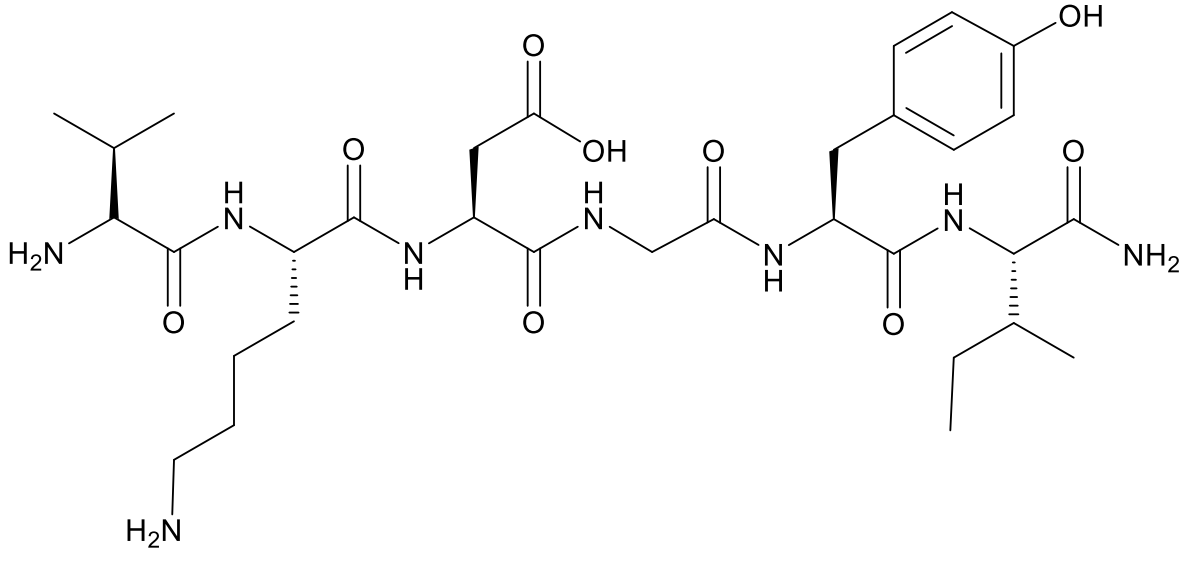

Chemical Formula: $C_{32}H_{52}N_8O_9$
Exact Mass: 692,39
Molecular Weight: 692,82

VKDGYI (20% v/v Piperidine, 60°C) was obtained as as white solid after preparative RP-HPLC (3.2 mg, 4.5%). Crude analysis: Analytical RP-HPLC: t_R = 1.92 min (A/D 100:0 to 0:100 in 7.00 min, λ = 214nm). HRMS (ESI+): $C_{32}H_{52}N_8O_9$ calc./obs. 693.39/693.39 Da $[M+H]^+$.

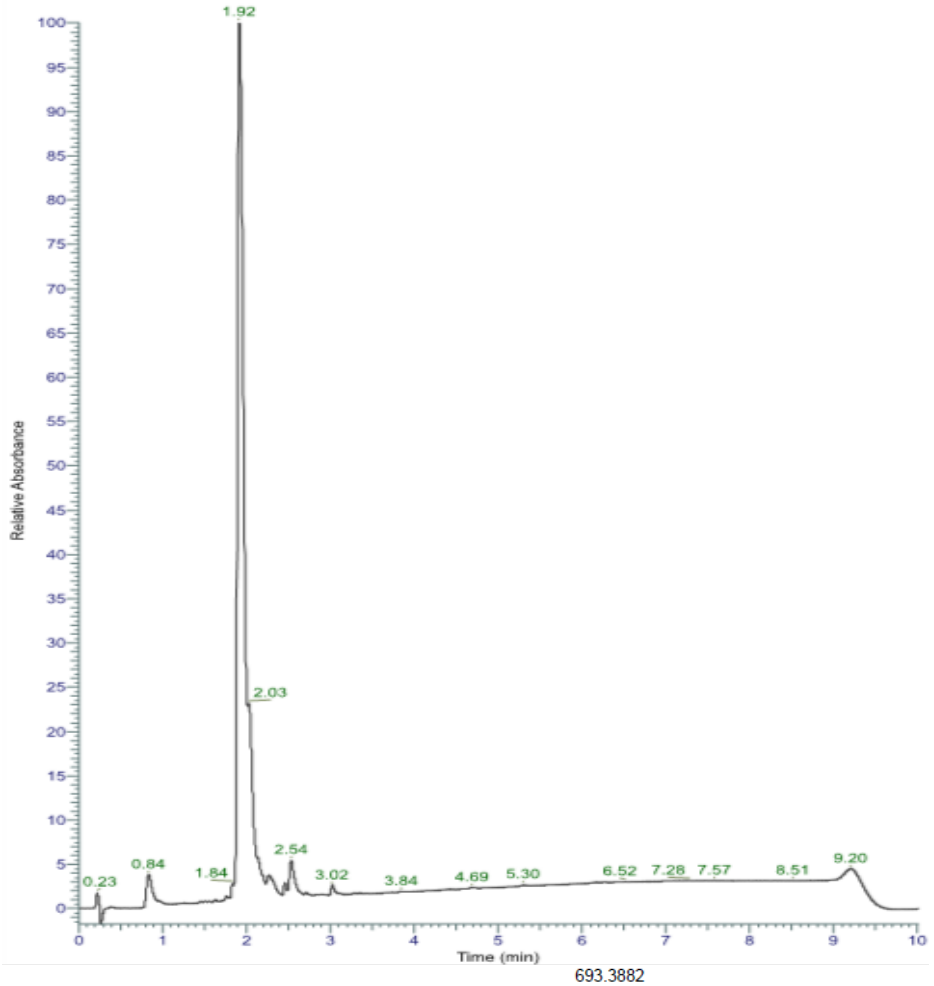

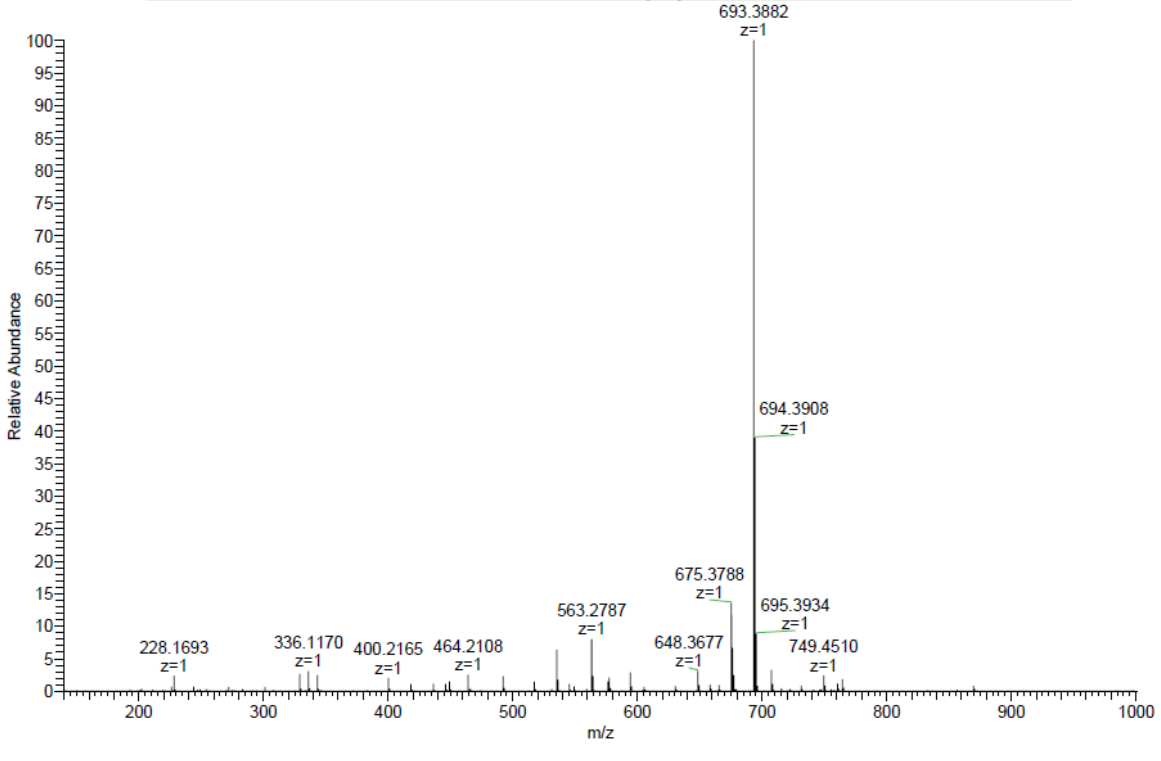

VKDGYI (20% v/v Piperidine + 0.25 M Oxyma, 60°C) was obtained as crude white solid after lyophilization (14.2 mg, 22.1%). Analytical RP-HPLC: t_R = 1.91 min (A/D 100:0 to 0:100 in 7.00 min, λ = 214nm). HRMS (ESI+): $C_{32}H_{52}N_8O_9$ calc./obs. 693.39/693.39 Da $[M+H]^+$.

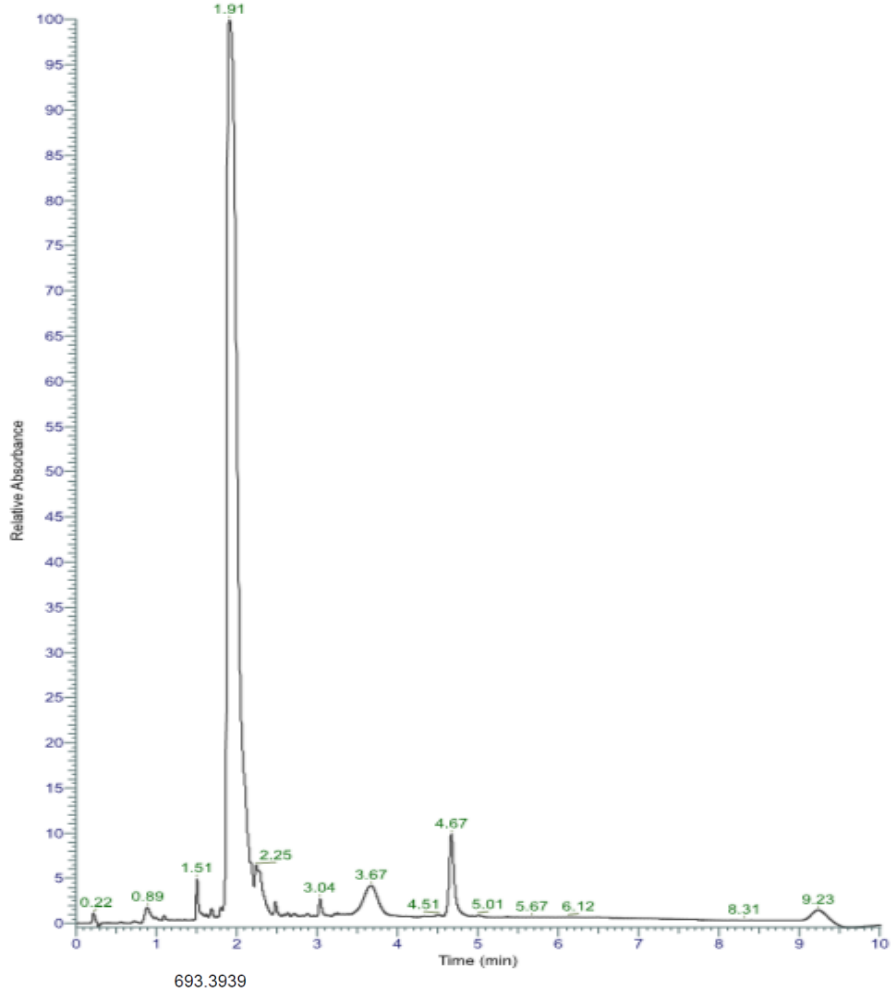

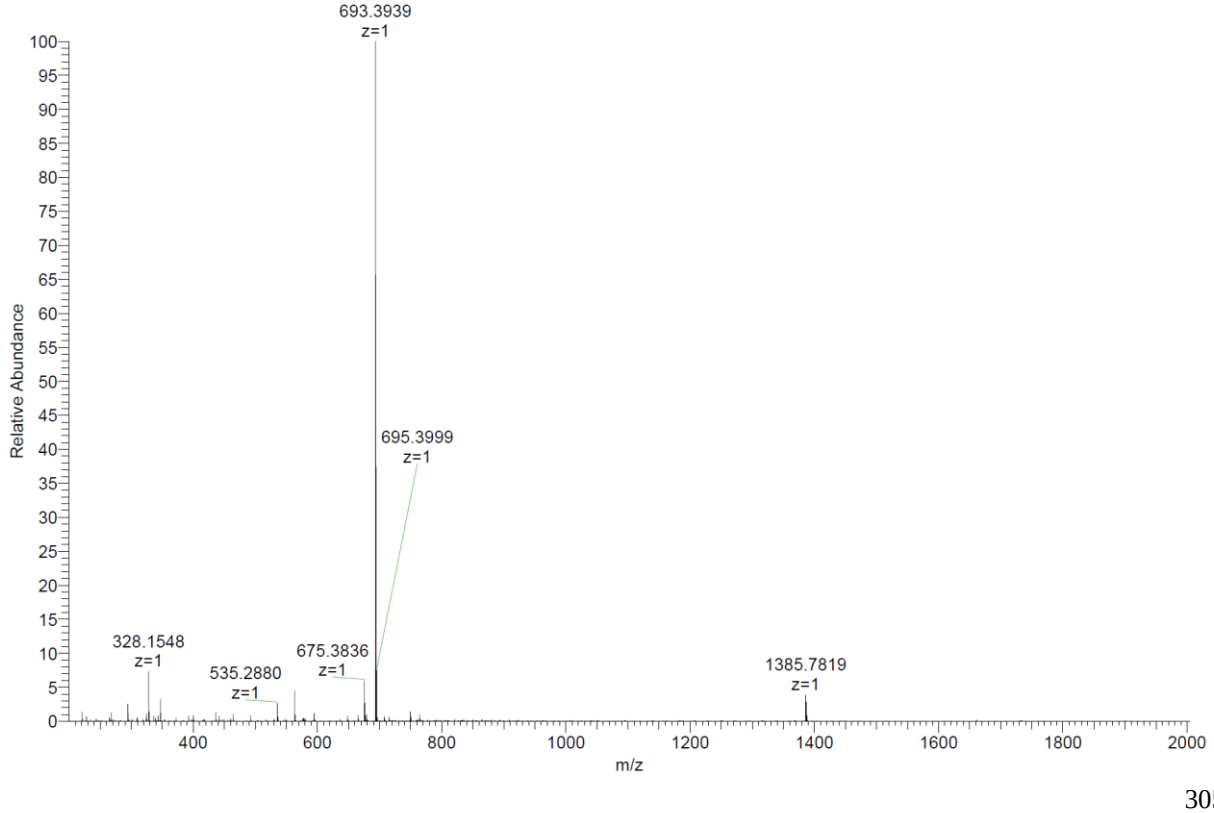

VKDGYI (20% v/v Piperidine + 0.5 M Oxyma, 60°C) was obtained as crude white solid after lyophilization (10.8 mg, 16.8%). Analytical RP-HPLC: t_R = 1.99 min (A/D 100:0 to 0:100 in 7.00 min, λ = 214nm). HRMS (ESI+): $C_{32}H_{52}N_8O_9$ calc./obs. 693.39/693.39 Da $[M+H]^+$.

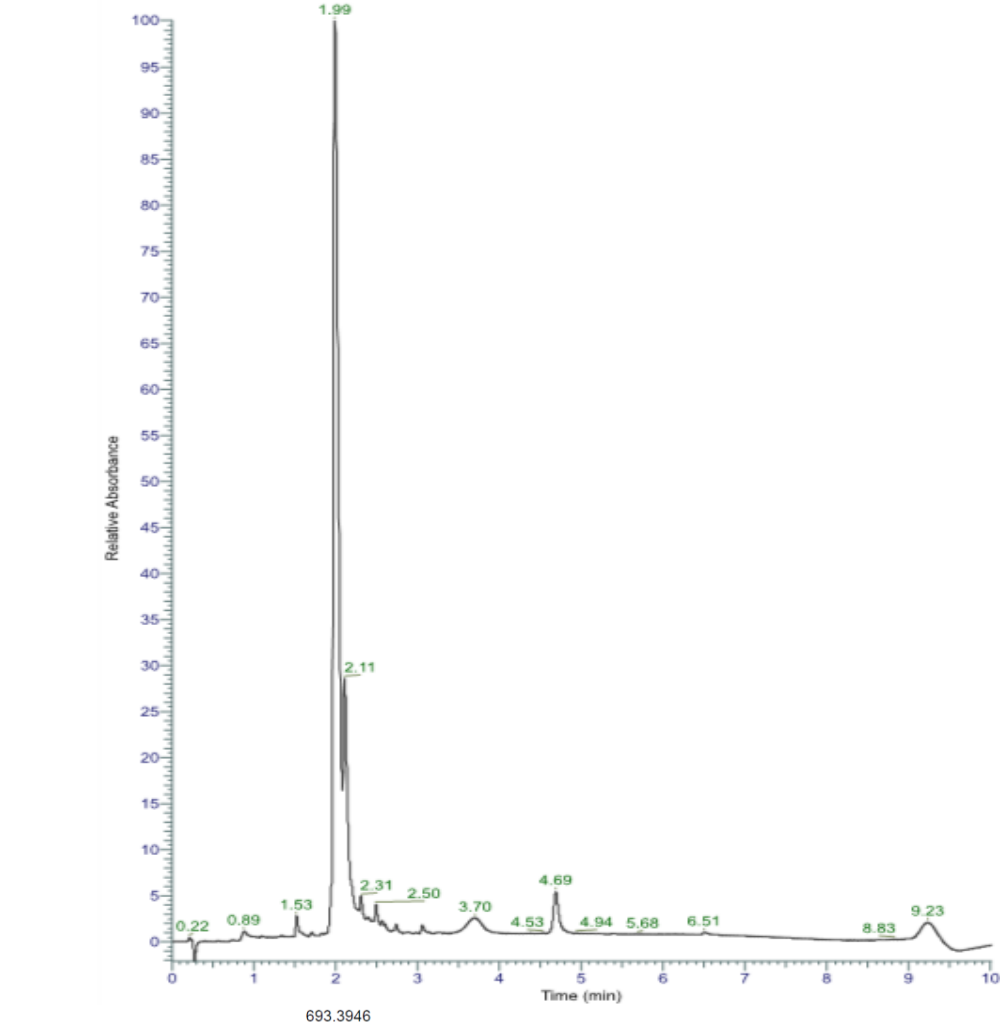

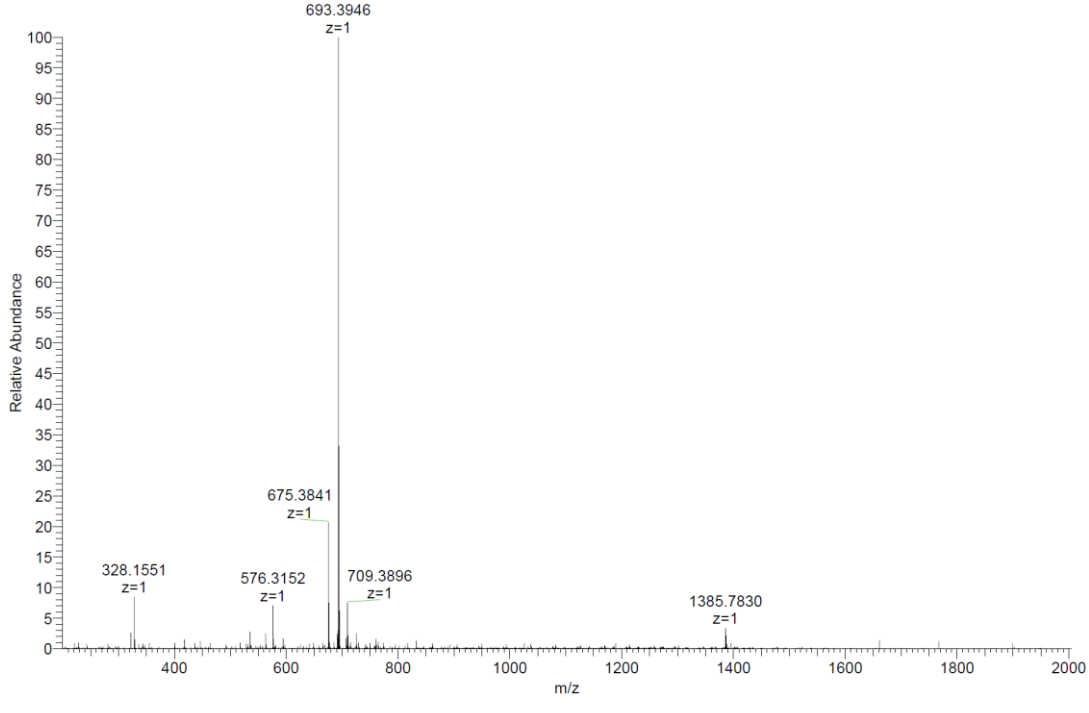

VKDGYI (5% w/v Piperazine + 2% v/v DBU, 60°C) was obtained as crude white solid after lyophilization (5.7 mg, 0.0%). Analytical RP-HPLC: t_R = - min (A/D 100:0 to 0:100 in 7.00 min, λ = 214nm). HRMS (ESI+): $C_{32}H_{52}N_8O_9$ calc./obs. 693.39/- Da $[M+H]^+$. (No compound observed).

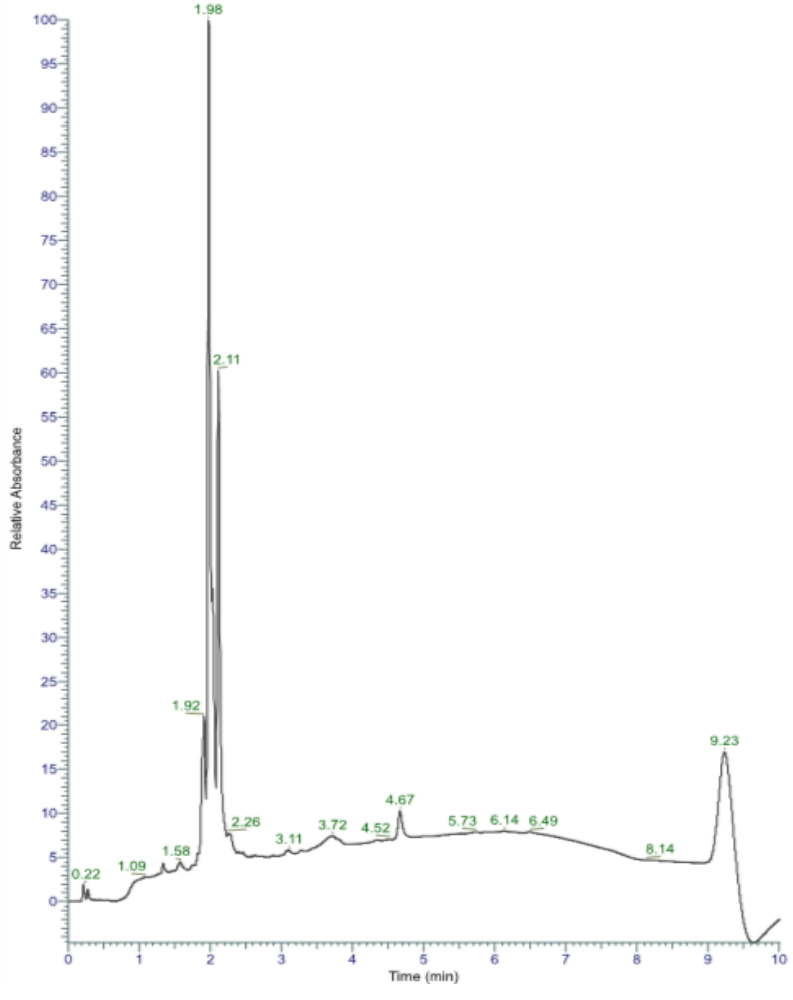

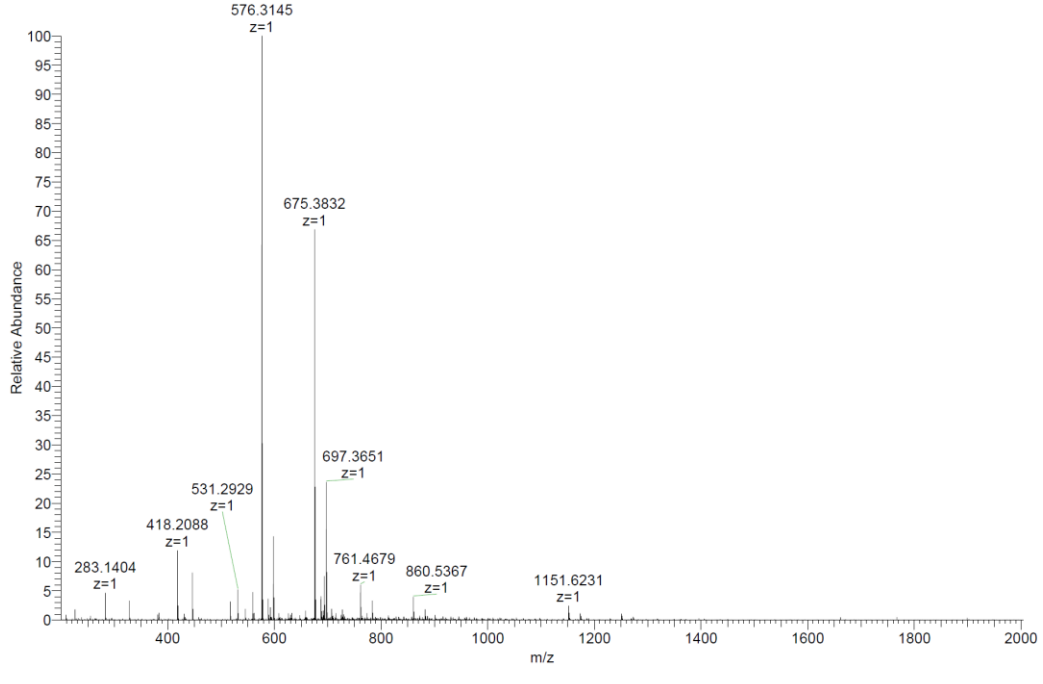

VKDGYI (5% w/v Piperazine + 2% v/v DBU + 0.25 M HOBt, 60°C) was obtained as crude white solid after lyophilization (9.8 mg, 9.2%). Analytical RP-HPLC: t_R = 2.01 min (A/D 100:0 to 0:100 in 7.00 min, λ = 214nm). HRMS (ESI+): $C_{32}H_{52}N_8O_9$ calc./obs. 693.39/693.39 Da $[M+H]^+$.

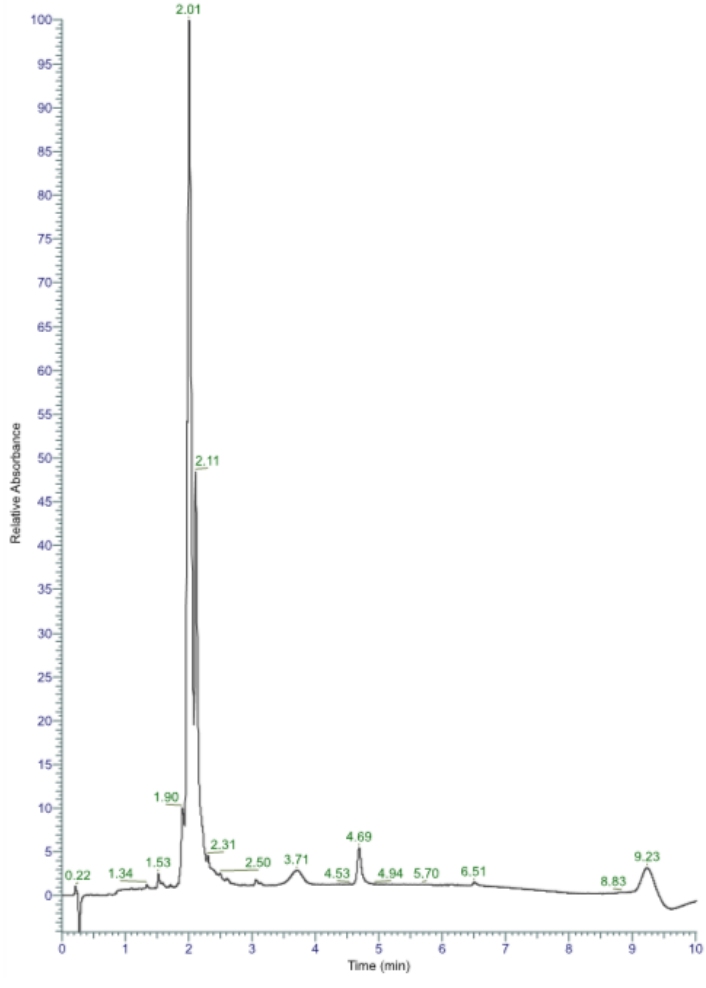

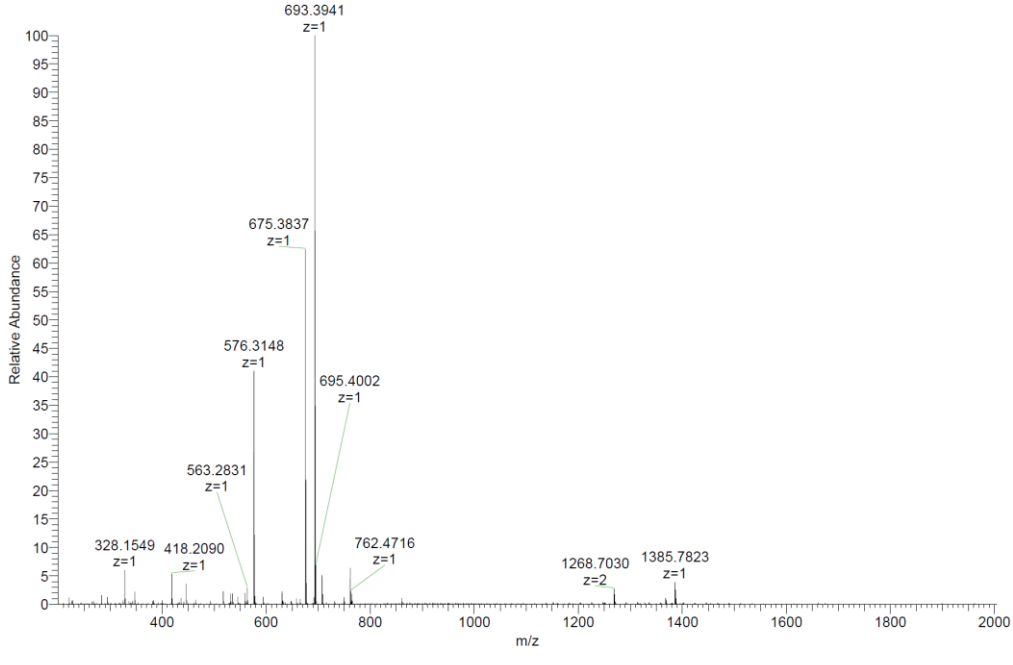

VKDGYI (5% w/v Piperazine + 2% v/v DBU + 0.5 M HOBt, 60°C) was obtained as crude white solid after lyophilization (6.6 mg, 10.4%). Analytical RP-HPLC: t_R = 1.92 min (A/D 100:0 to 0:100 in 7.00 min, λ = 214nm). HRMS (ESI+): $C_{32}H_{52}N_8O_9$ calc./obs. 693.39/693.39 Da $[M+H]^+$.

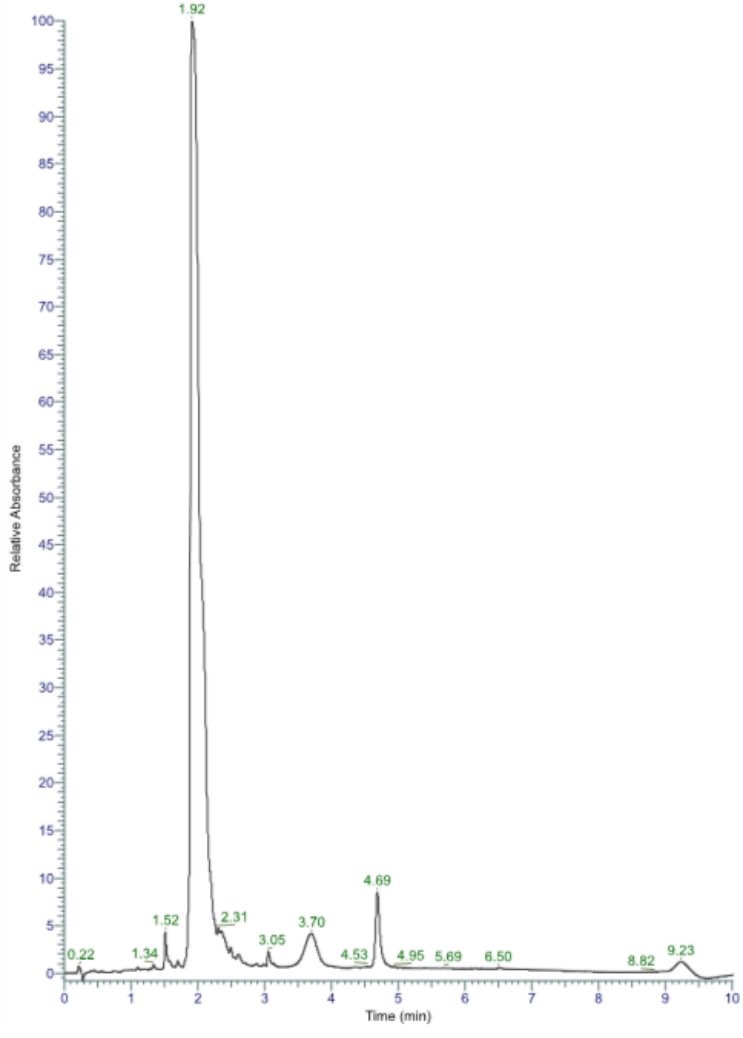

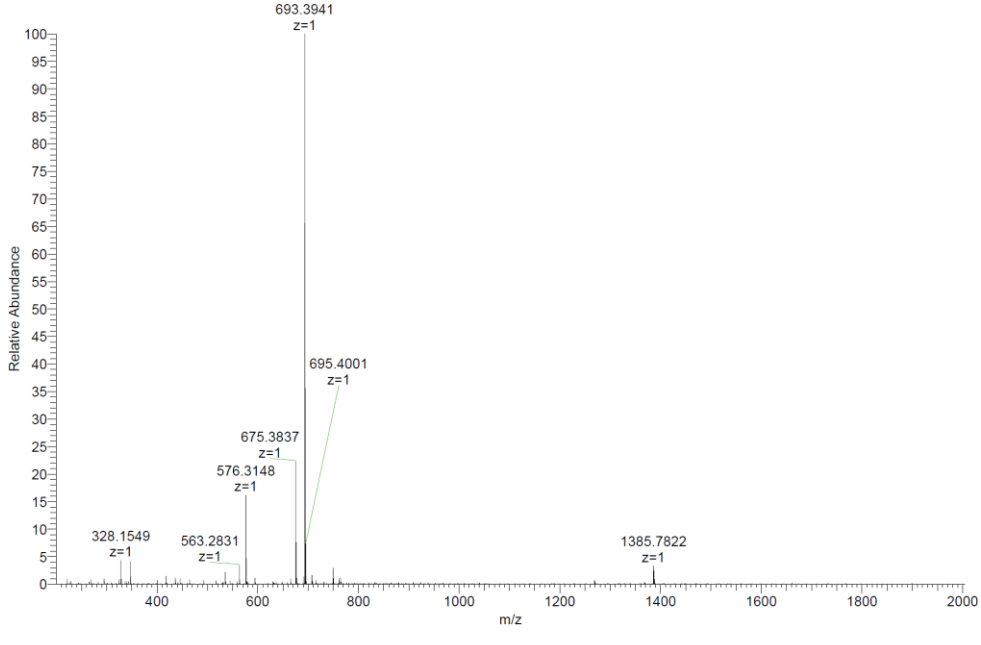

VKDGYI (5% w/v Piperazine + 2% v/v DBU + 0.25 M Oxyma, 60°C) was obtained as crude white solid after lyophilization (12.8 mg, 16.3%). Analytical RP-HPLC: t_R = 1.93 min (A/D 100:0 to 0:100 in 7.00 min, λ = 214nm). HRMS (ESI+): $C_{32}H_{52}N_8O_9$ calc./obs. 693.39/693.39 Da $[M+H]^+$.

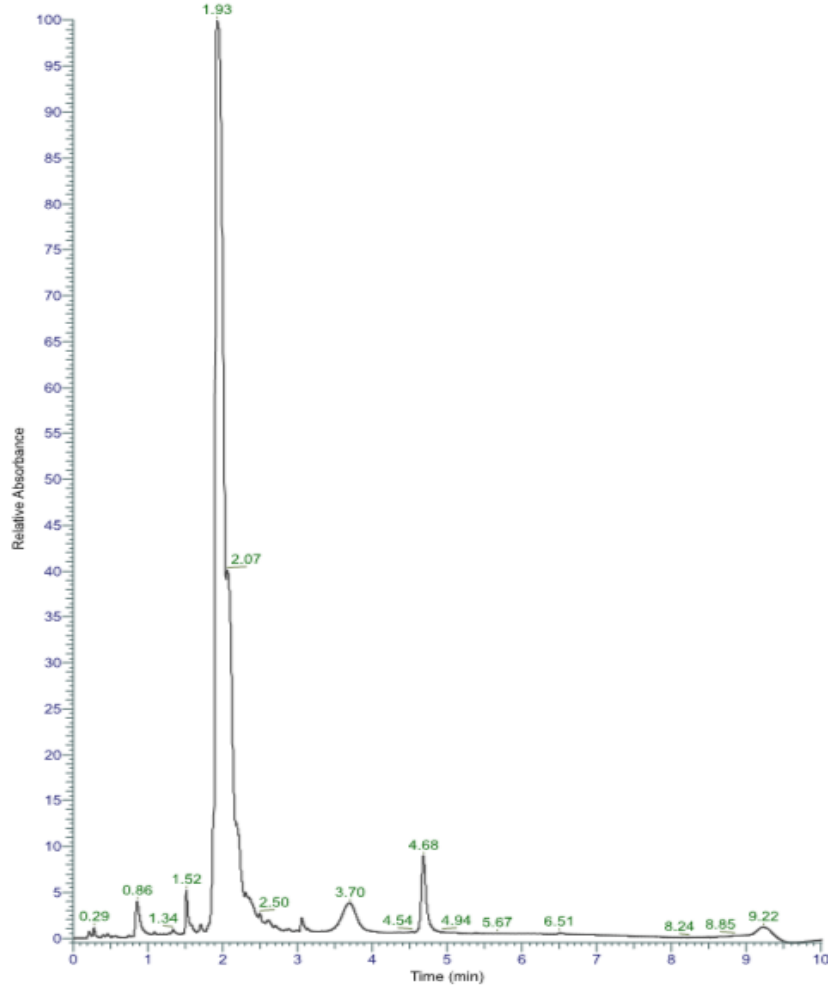

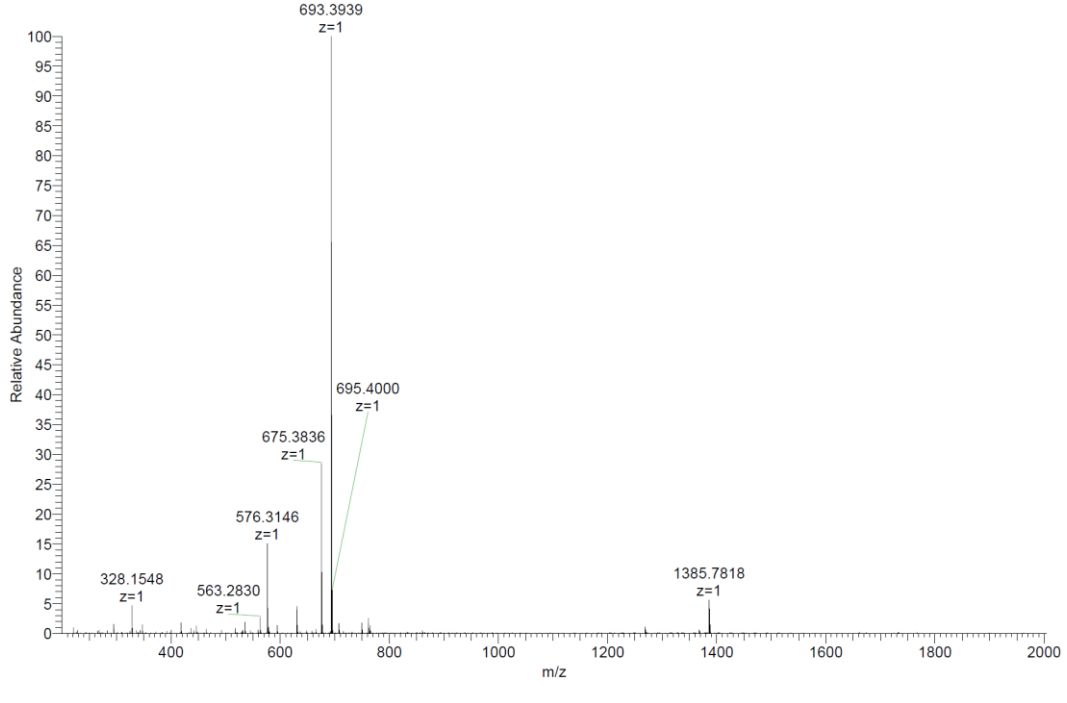

VKDGYI (5% w/v Piperazine + 2% v/v DBU + 0.5 M Oxyma, 60°C) was obtained as crude white solid after lyophilization (15.2 mg, 21.8%). Analytical RP-HPLC: t_R = 1.97 min (A/D 100:0 to 0:100 in 7.00 min, λ = 214nm). HRMS (ESI+): $C_{32}H_{52}N_8O_9$ calc./obs. 693.39/693.39 Da $[M+H]^+$.

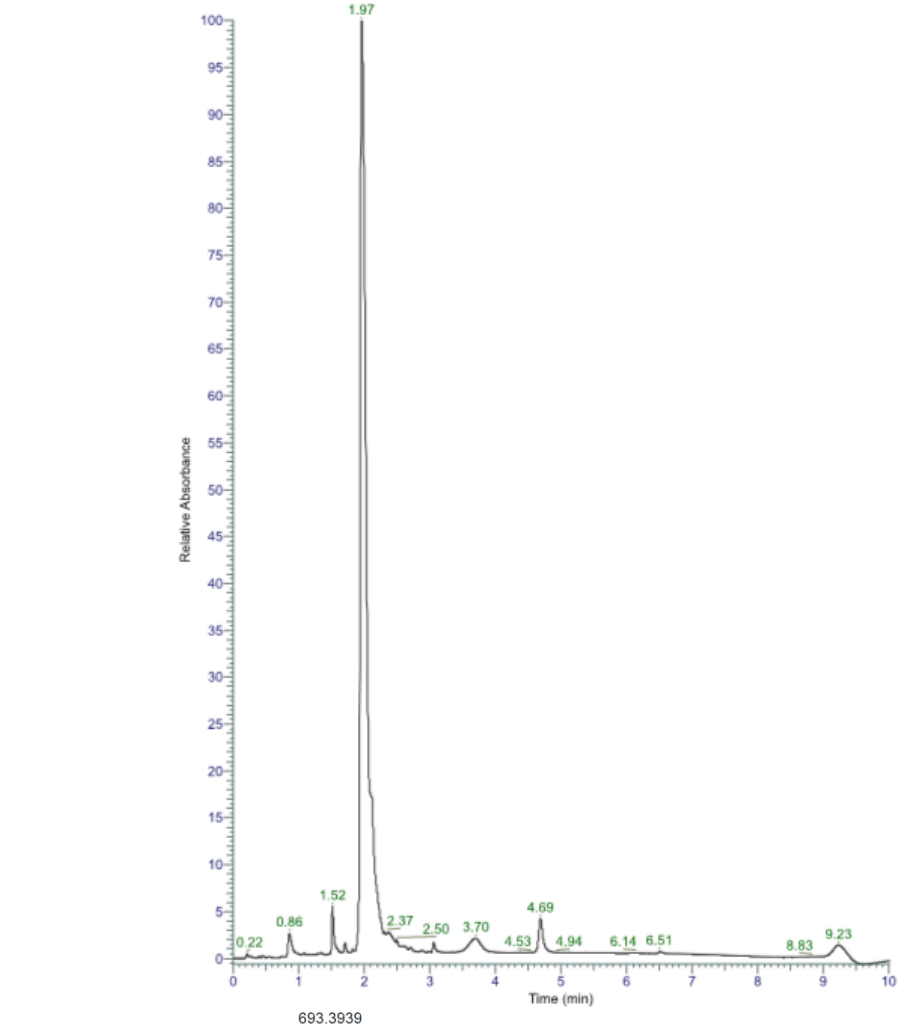

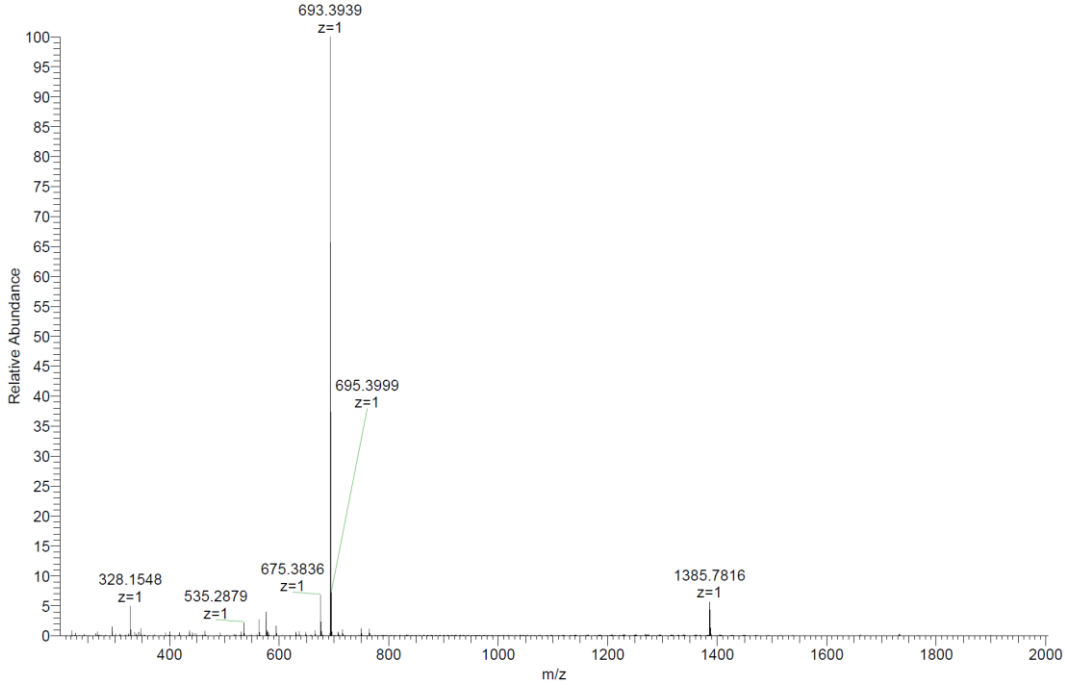

VKDGYI (2% v/v DBU, 60°C) was obtained as crude white solid after lyophilization (36.6 mg, 25.7%). Analytical RP-HPLC: t_R = 2.05 min (A/D 100:0 to 0:100 in 7.00 min, λ = 214nm). HRMS (ESI+): $C_{32}H_{52}N_8O_9$ calc./obs. 693.39/693.39 Da $[M+H]^+$.

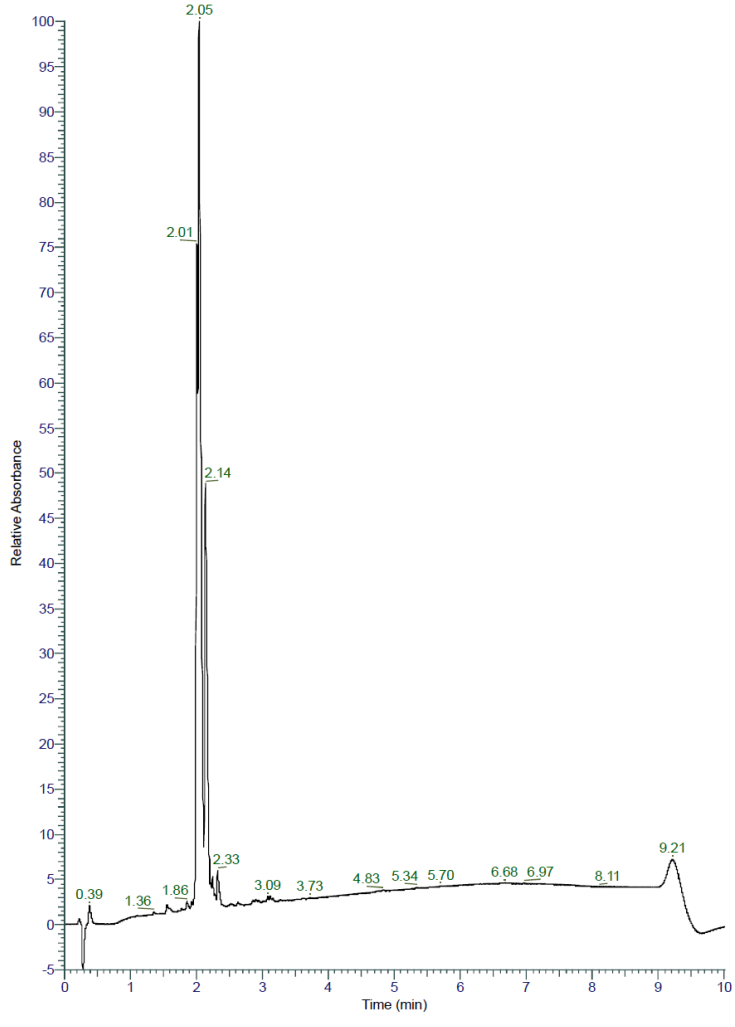

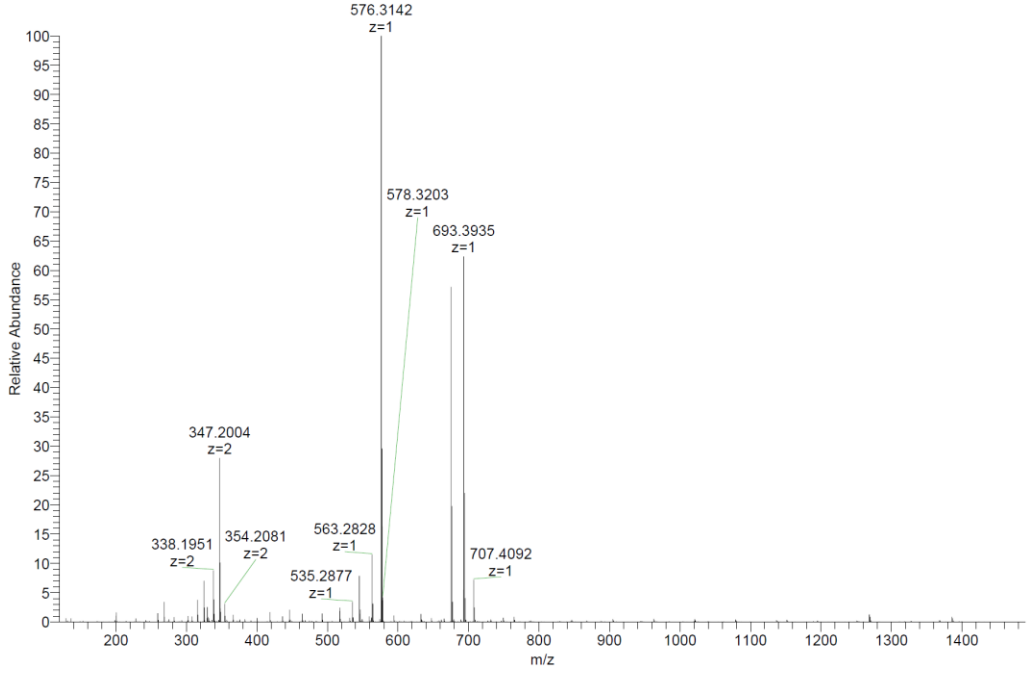

VKDGYI (20% v/v Dipropylamine, 60°C) was obtained as crude white solid after lyophilization (37.3 mg, 49.3%). Analytical RP-HPLC: t_R = 1.84 min (A/D 100:0 to 0:100 in 7.00 min, λ = 214nm). HRMS (ESI+): $C_{32}H_{52}N_8O_9$ calc./obs. 693.39/693.39 Da $[M+H]^+$.

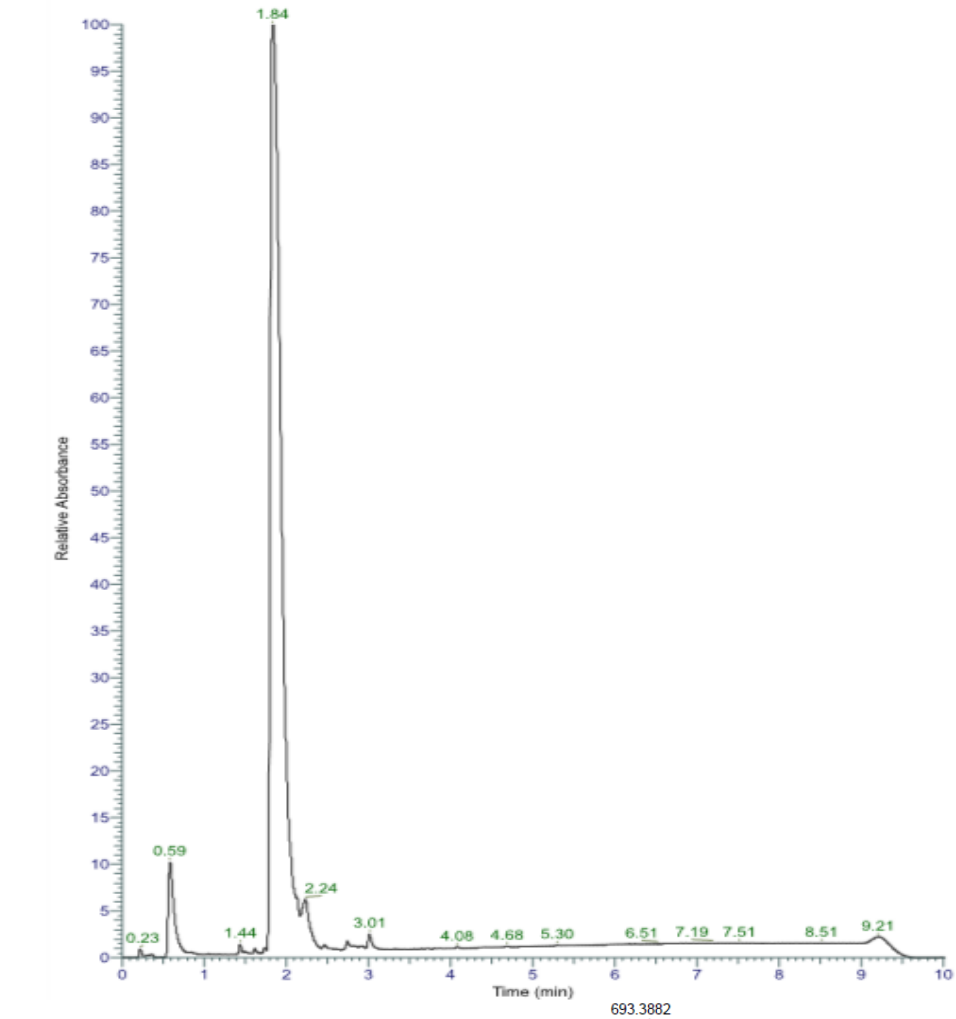

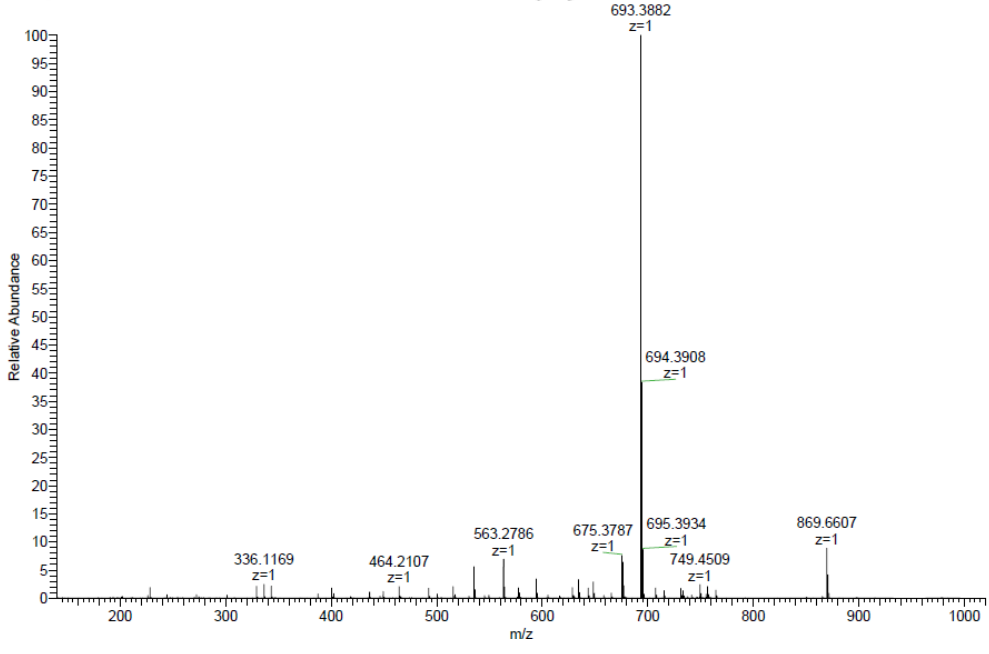

VKDGYI (25% v/v Dipropylamine, 60°C) was obtained as as white solid after preparative RP-HPLC (11.5 mg, 16.0%). Analytical RP-HPLC: t_R = 1.20 min (A/D 100:0 to 0:100 in 3.50 min, λ = 214nm). MS (ESI+): $C_{32}H_{52}N_8O_9$ calc./obs. 693.39/693.42 Da $[M+H]^+$.

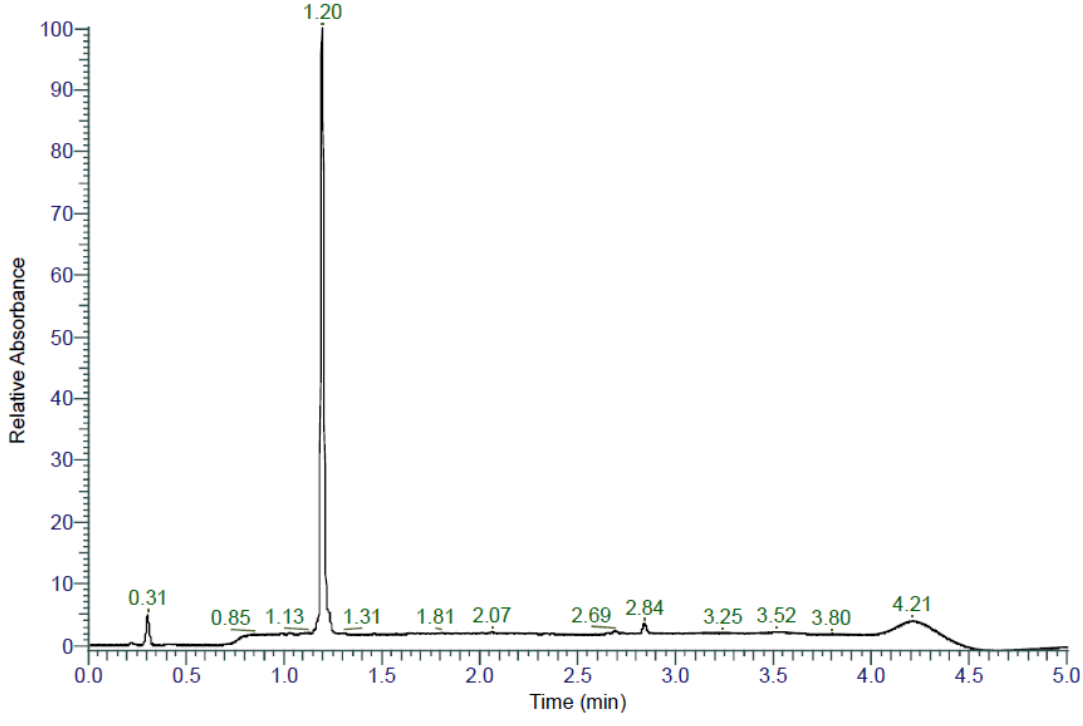

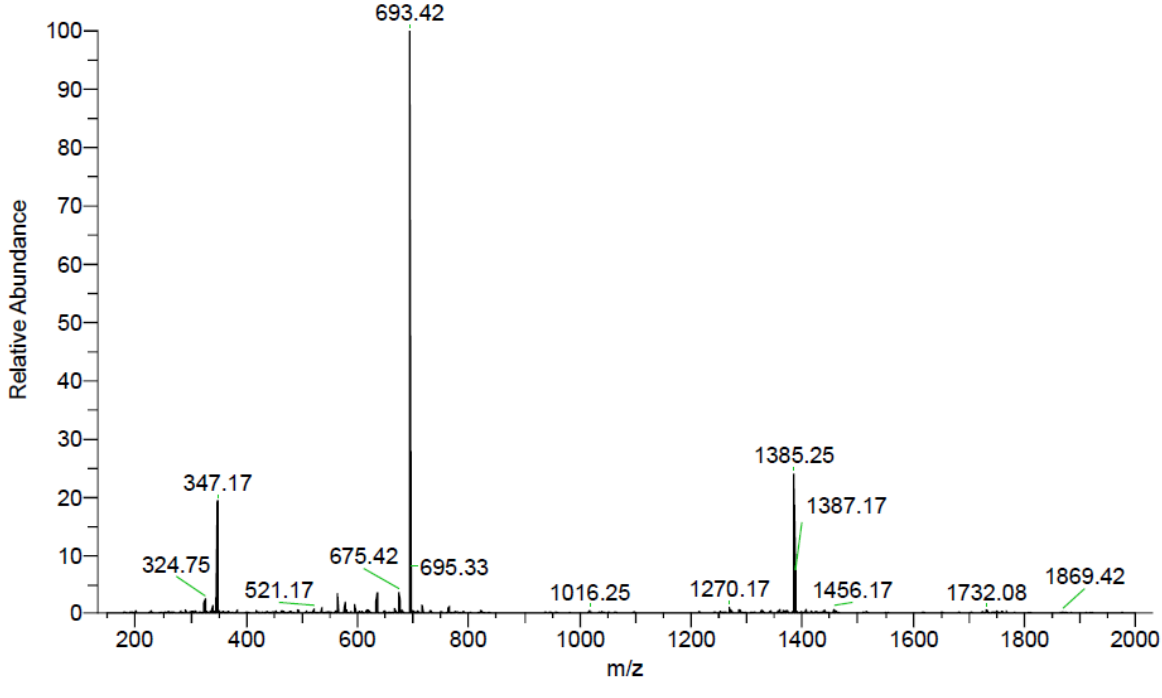

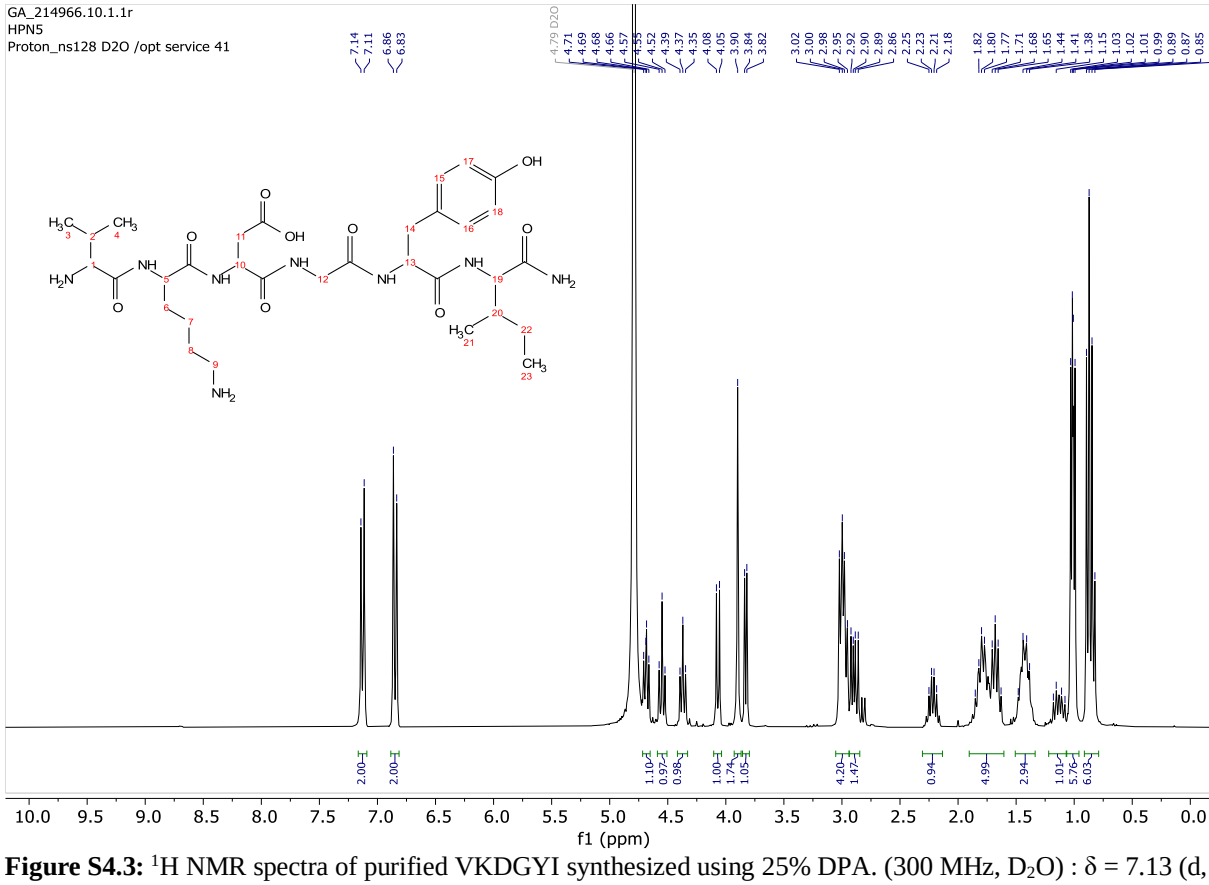

Figure S4.3: ^{1}H NMR spectra of purified VKDGYI synthesized using 25% DPA. (300 MHz, D_2O) : δ = 7.13 (d, *J* = 8.5 Hz, 2H, C(15 and 16)), 6.85 (d, *J* = 8.5 Hz, 2H, C(17 and 18)), 4.69 (t, 1H, C(13)), 4.55 (t, *J* = 7.6 Hz, 1H, C(10)), 4.37 (t, *J* = 7.2 Hz, 1H, C(5)), 4.07 (d, *J* = 7.9 Hz, 1H, C(19)), 3.90 (s, 2H, C(12)), 3.83 (d, *J* = 5.8 Hz, 1H, C(1)), 3.02 – 2.86 (m, 6H, C(9, 11 and 14)), 2.28 – 2.15 (m, 1H, C(20)), 1.82 – 1.65 (m, 6H, C(6, 8 and 22)), 1.51 – 1.35 (m, 3H, C(2 and 7)), 1.01 (dd, *J* = 7.0, 4.3 Hz, 6H, C(21 and 23)), 0.89 – 0.82 (m, 6H, C(3 and 4)).

VKDGYI (25% v/v Dipropylamine, 60°C) crude: Analytical RP-HPLC: t_R = 1.96 min (A/D 100:0 to 0:100 in 7.00 min, λ = 214nm). HRMS (ESI+): $C_{32}H_{52}N_8O_9$ calc./obs. 693.39/693.39 Da $[M+H]^+$.

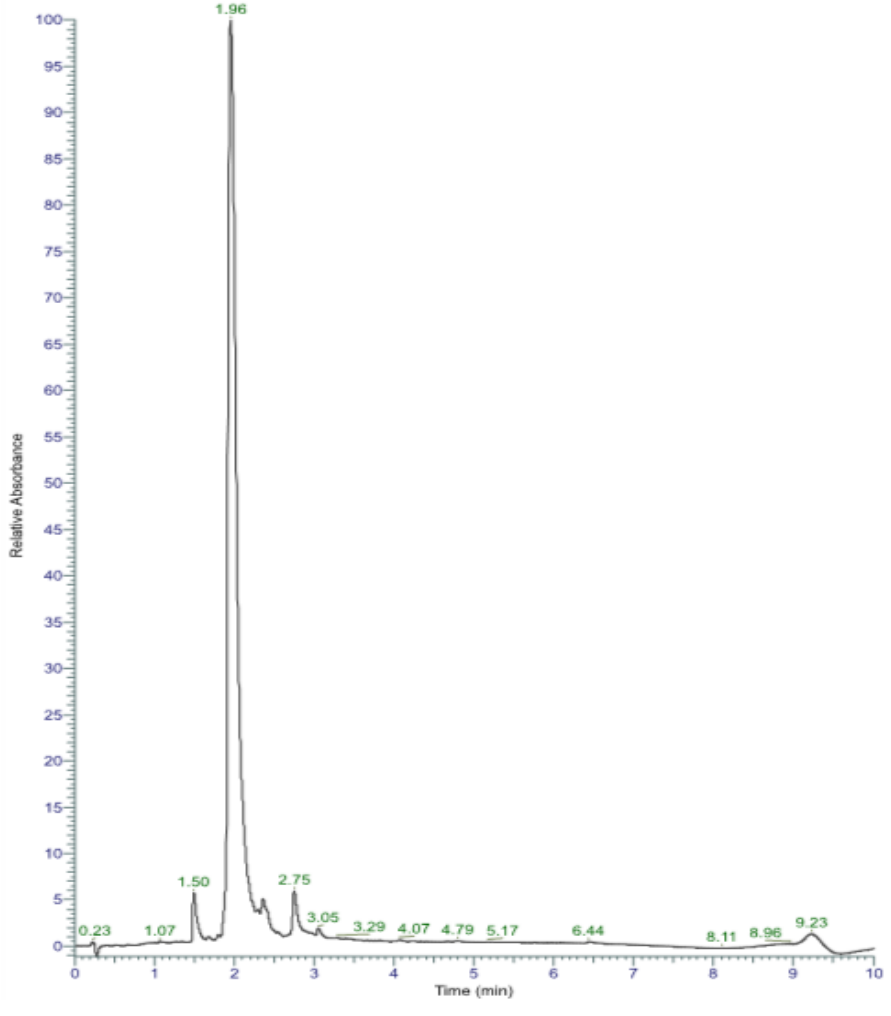

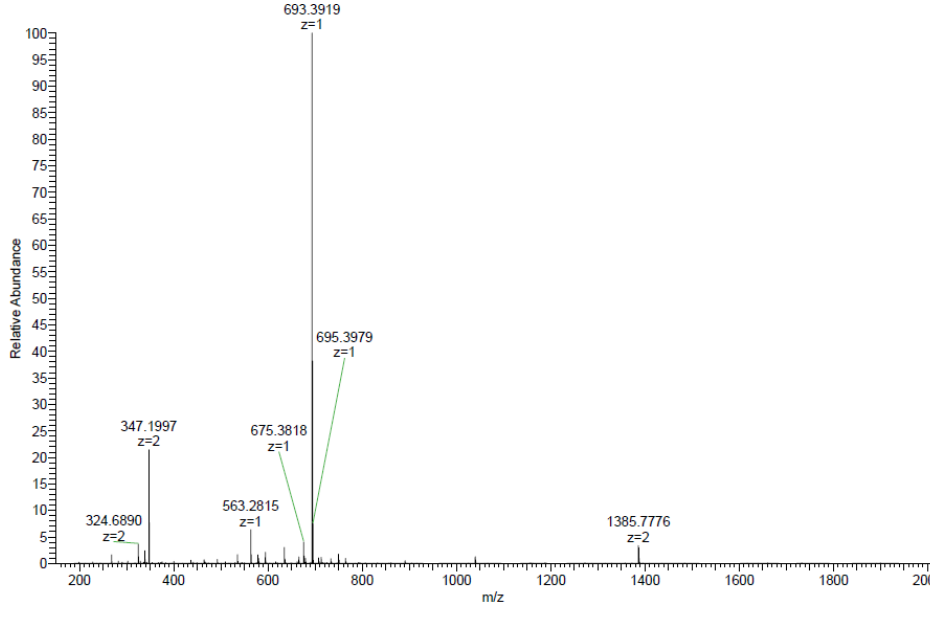

VKDGYI (20% v/v Dipropylamine + 0.5 M Oxyma, 60°C) was obtained as crude white solid after lyophilization (35.1 mg, 45.4%). Analytical RP-HPLC: t_R = 1.92 min (A/D 100:0 to 0:100 in 7.00 min, λ = 214nm). HRMS (ESI+): $C_{32}H_{52}N_8O_9$ calc./obs. 693.39/693.39 Da $[M+H]^+$.

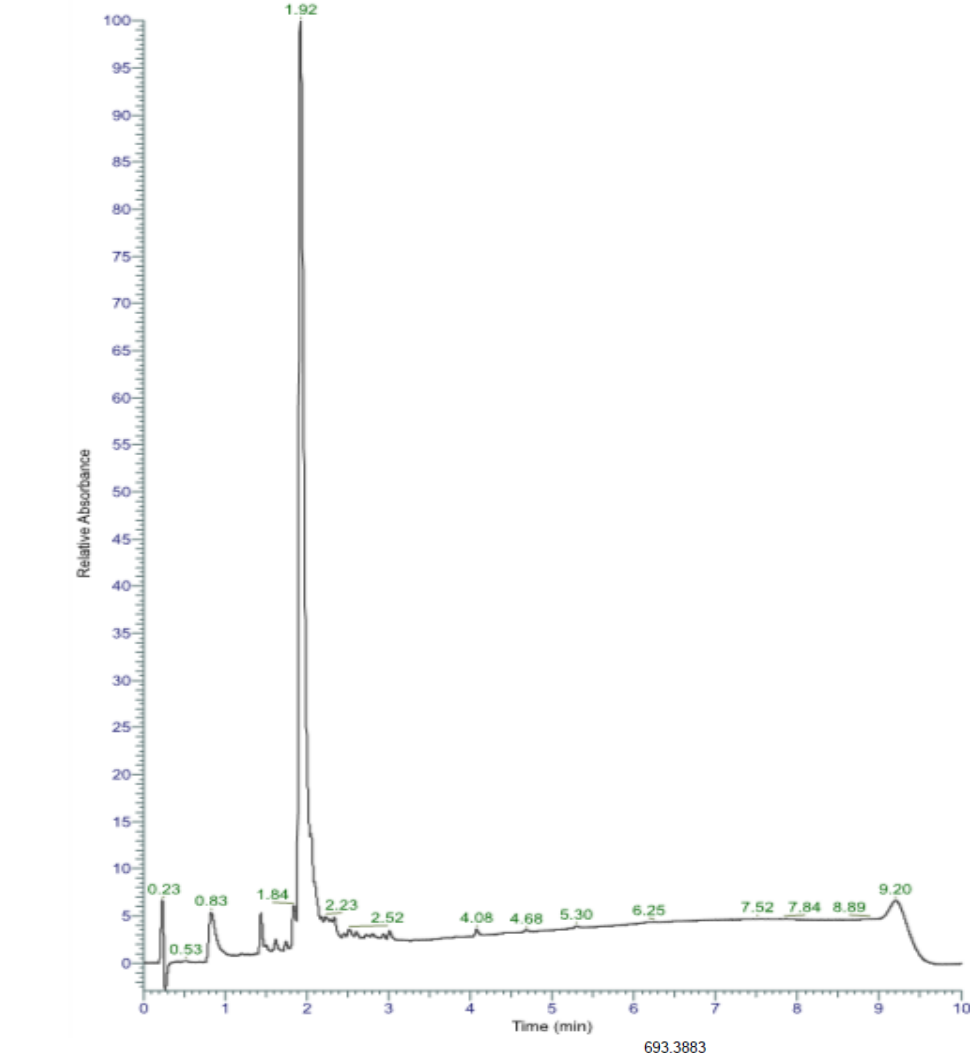

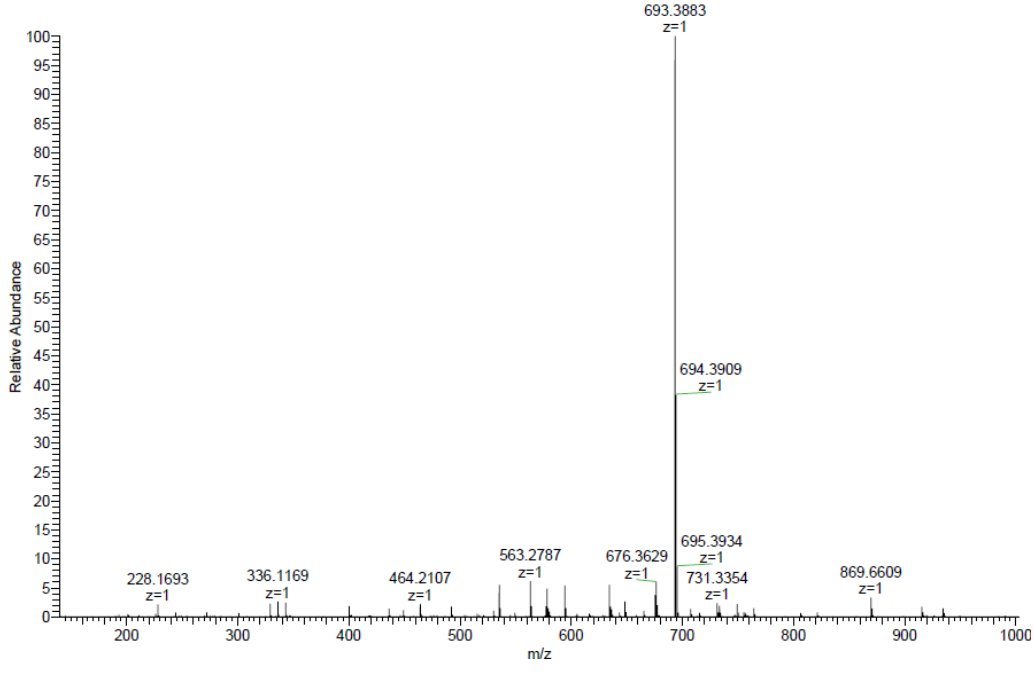

VKDGYI (25% v/v Diethylamine, 50°C) was obtained as crude white solid after lyophilization (40.5 mg, 43.4%). Analytical RP-HPLC: t_R = 1.98 min (A/D 100:0 to 0:100 in 7.00 min, λ = 214nm). HRMS (ESI+): $C_{32}H_{52}N_8O_9$ calc./obs. 693.39/693.39 Da $[M+H]^+$.

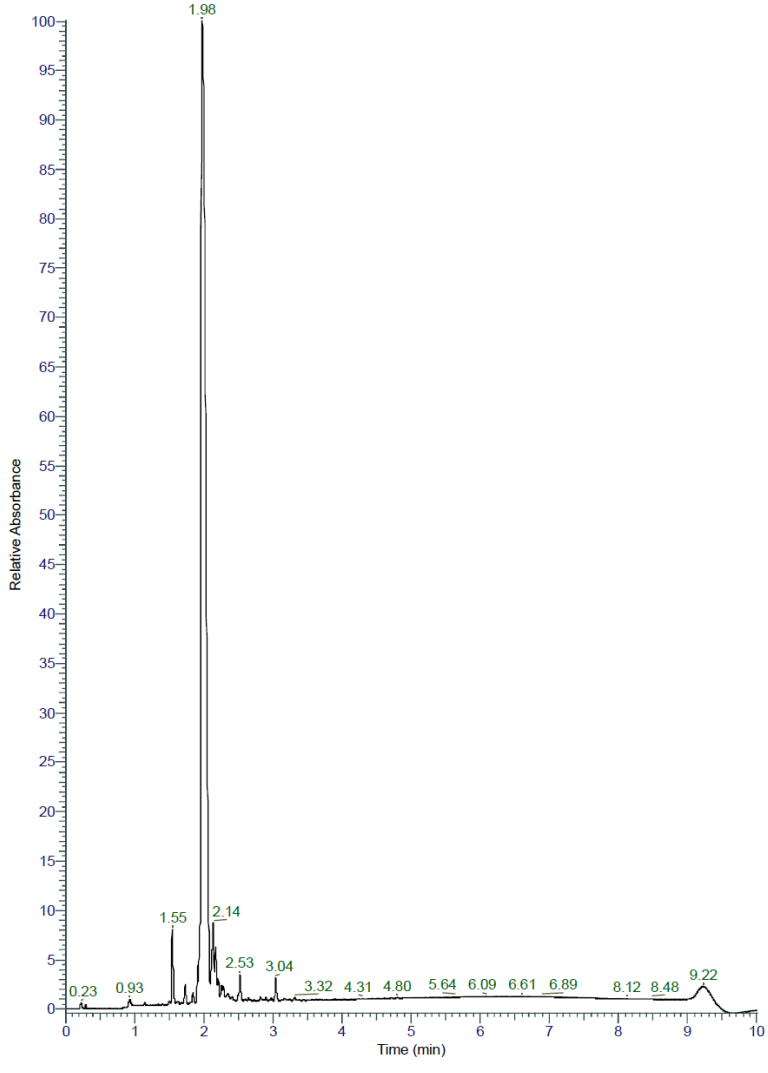

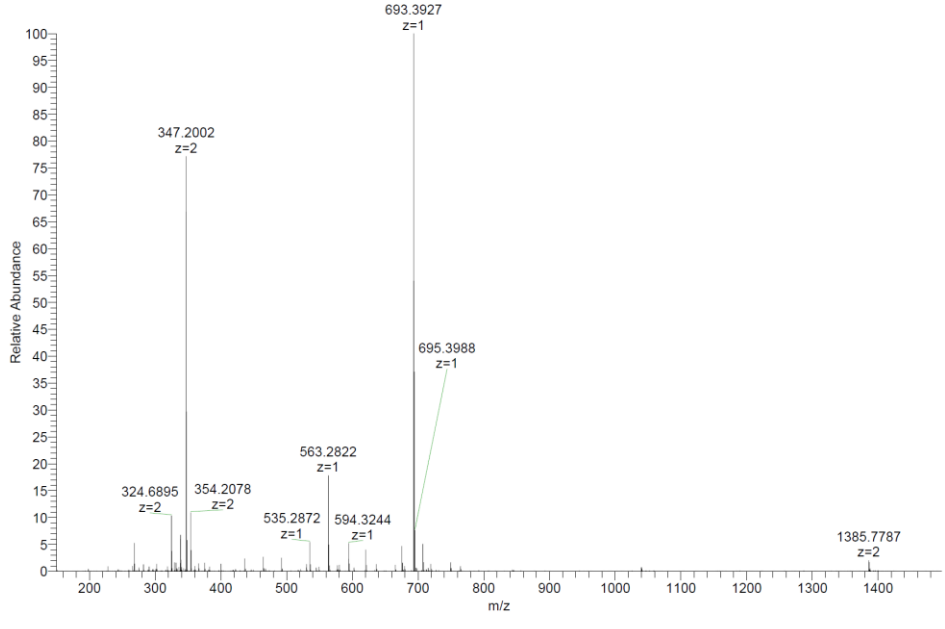

VKDGYI (25% v/v Diethylamine, 60°C) was obtained as crude white solid after lyophilization (40.7 mg, 45.7%). Analytical RP-HPLC: t_R = 2.04 min (A/D 100:0 to 0:100 in 7.00 min, λ = 214nm). HRMS (ESI+): $C_{32}H_{52}N_8O_9$ calc./obs. 693.39/693.39 Da $[M+H]^+$.

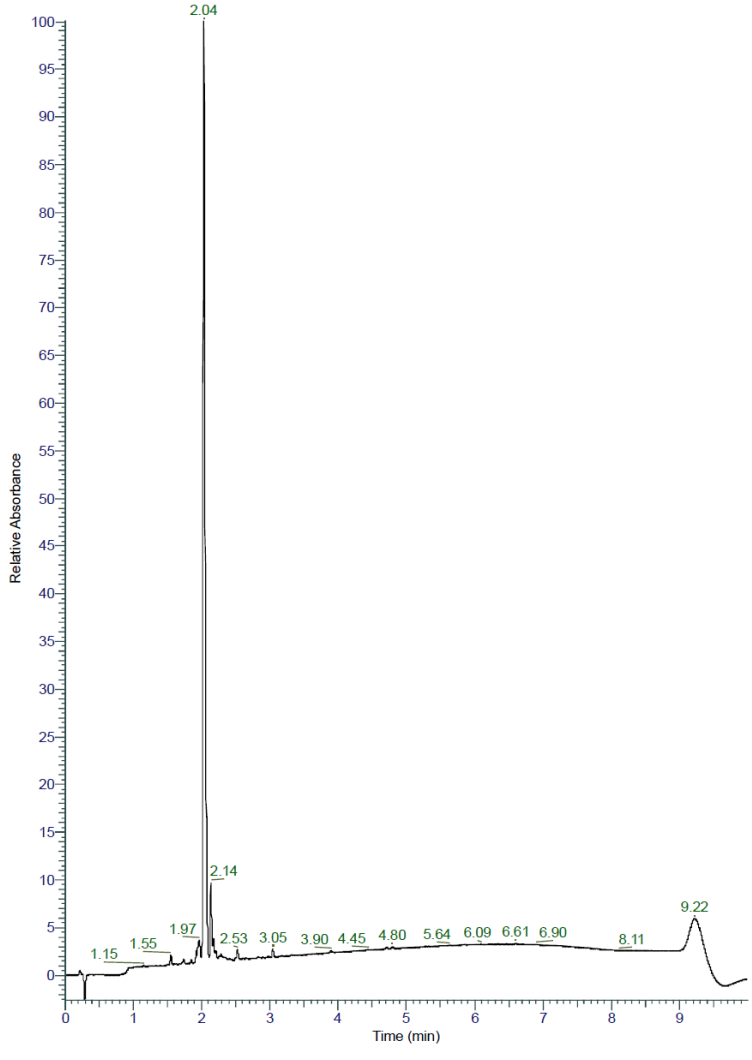

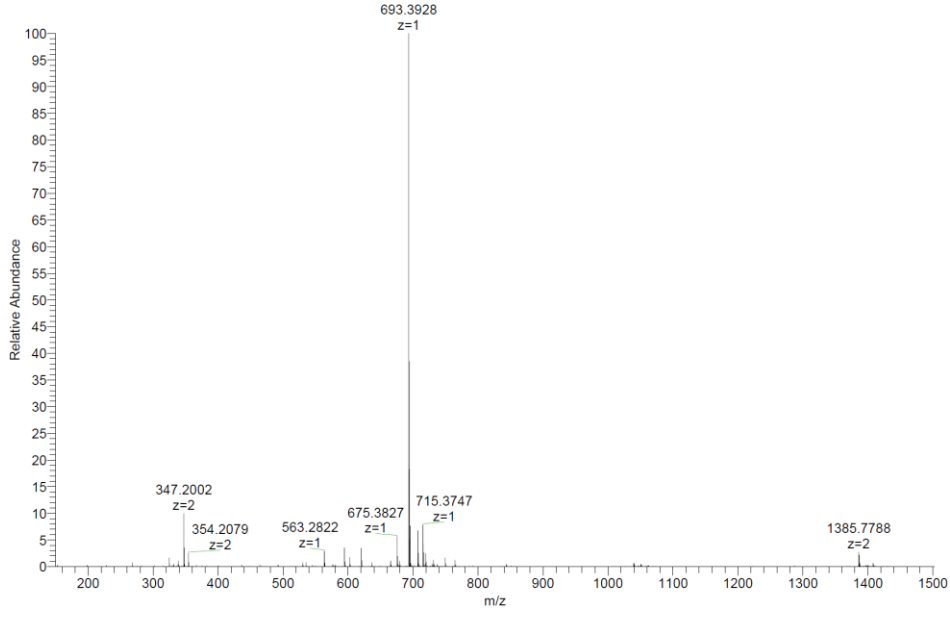

VKDGYI (25% v/v Dibutylamine, 60°C) was obtained as crude white solid after lyophilization (45.1 mg, 52.1%). Analytical RP-HPLC: t_R = 2.02 min (A/D 100:0 to 0:100 in 7.00 min, λ = 214nm). HRMS (ESI+): $C_{32}H_{52}N_8O_9$ calc./obs. 693.39/693.39 Da $[M+H]^+$.

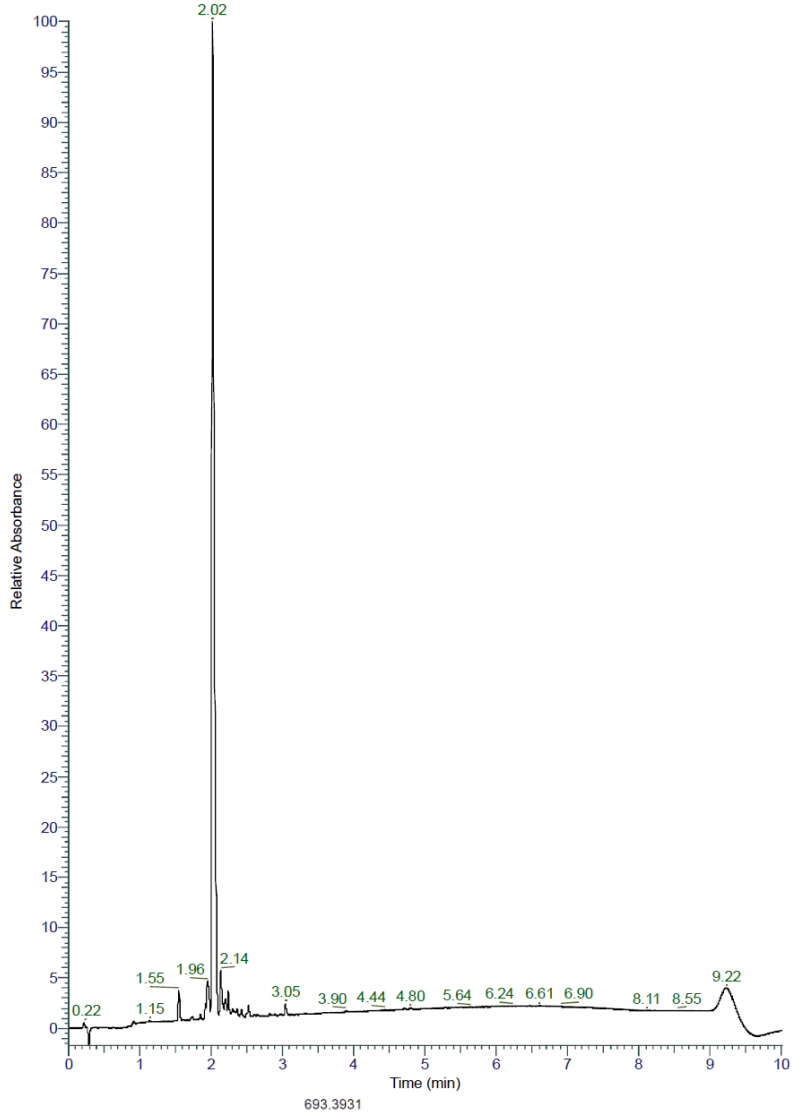

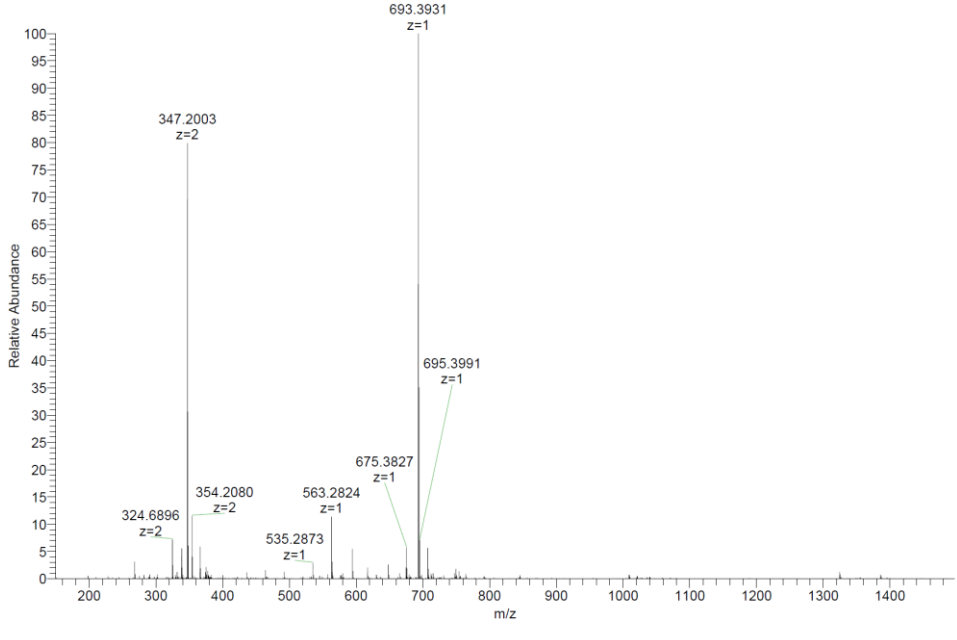

VKDGYI (25% v/v Diisobutylamine, 60°C) was obtained as crude white solid after lyophilization (0.4 mg, 0.0%). Analytical RP-HPLC: t_R = - min (A/D 100:0 to 0:100 in 7.00 min, λ = 214nm). HRMS (ESI+): $C_{32}H_{52}N_8O_9$ calc./obs. 693.39/- Da $[M+H]^+$ (no compound observed).

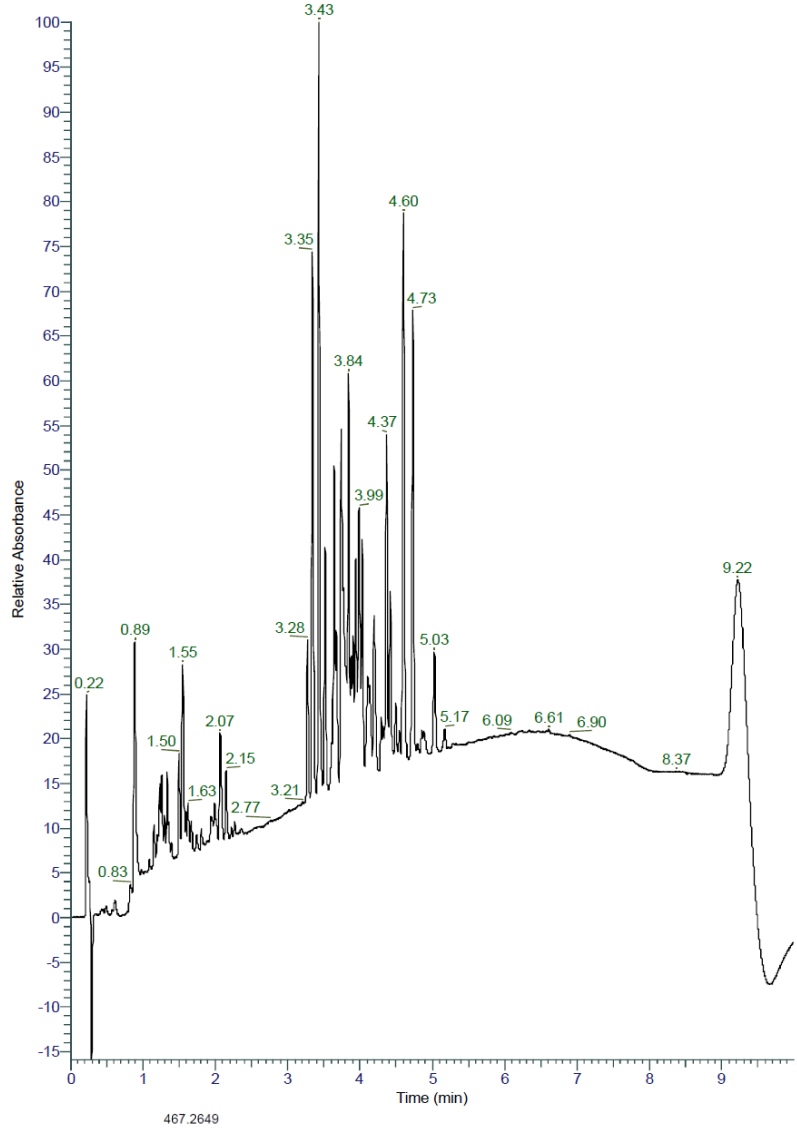

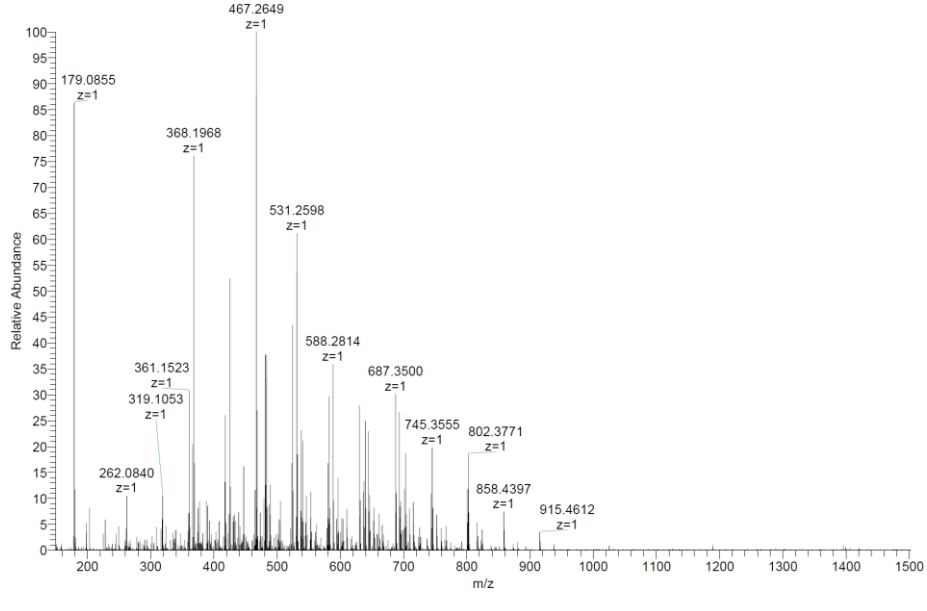

VKDGYI (20% v/v Piperidine, 90°C) was obtained as crude white solid after lyophilization (22.8 mg, 28.4%). Analytical RP-HPLC: t_R = 1.99 min (A/D 100:0 to 0:100 in 7.00 min, λ = 214nm). HRMS (ESI+): $C_{32}H_{52}N_8O_9$ calc./obs. 693.39/693.39 Da $[M+H]^+$.

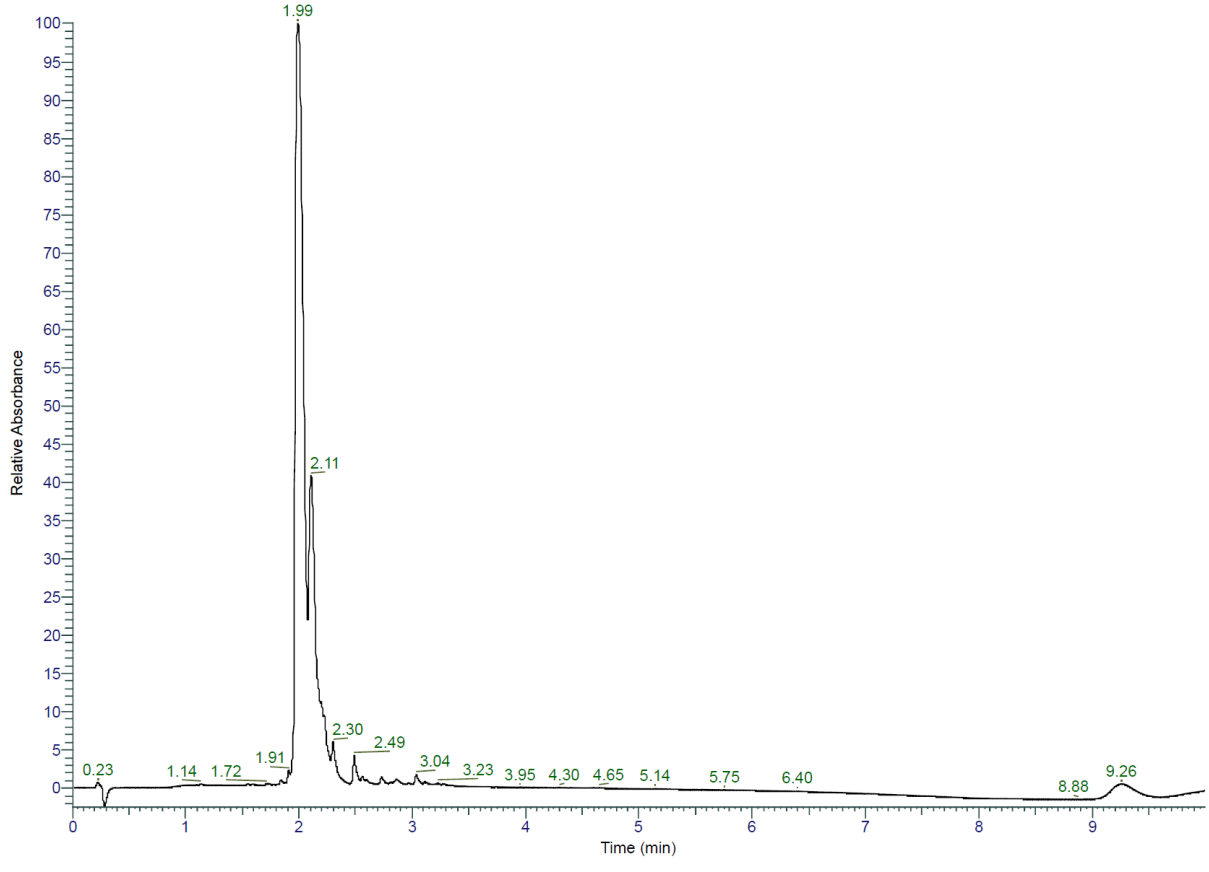

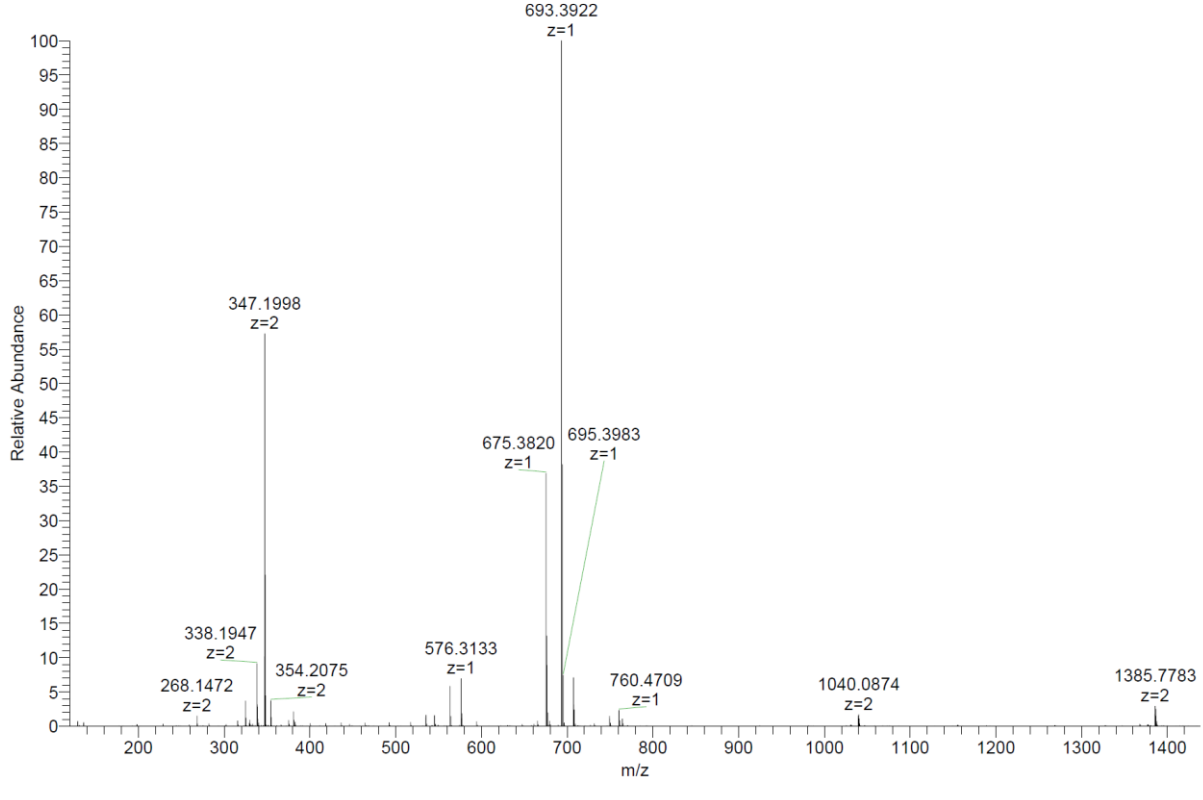

VKDGYI (25% v/v Dipropylamine, 90°C) was obtained as crude white solid after lyophilization (26.8 mg, 33.5%). Analytical RP-HPLC: t_R = 2.01 min (A/D 100:0 to 0:100 in 7.00 min, λ = 214nm). HRMS (ESI+): $C_{32}H_{52}N_8O_9$ calc./obs. 693.39/693.39 Da $[M+H]^+$.

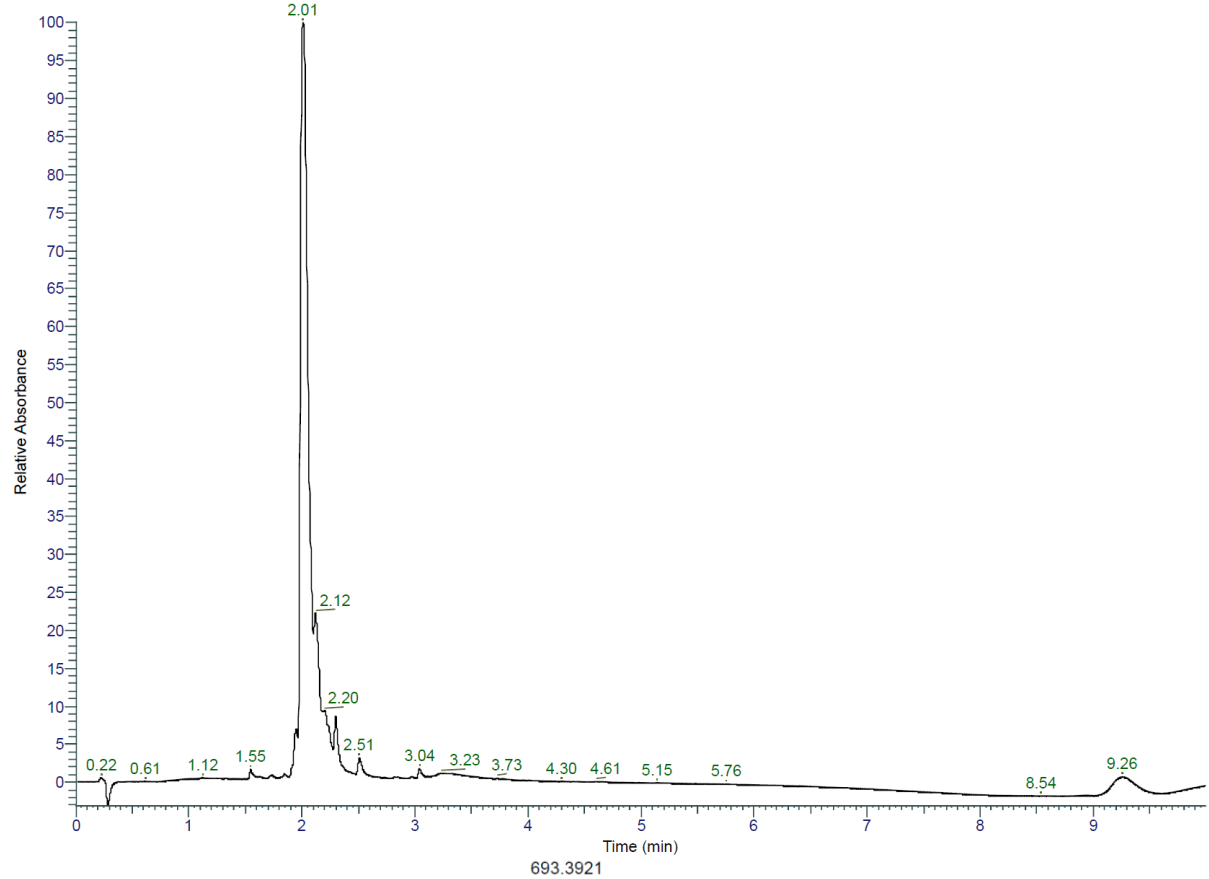

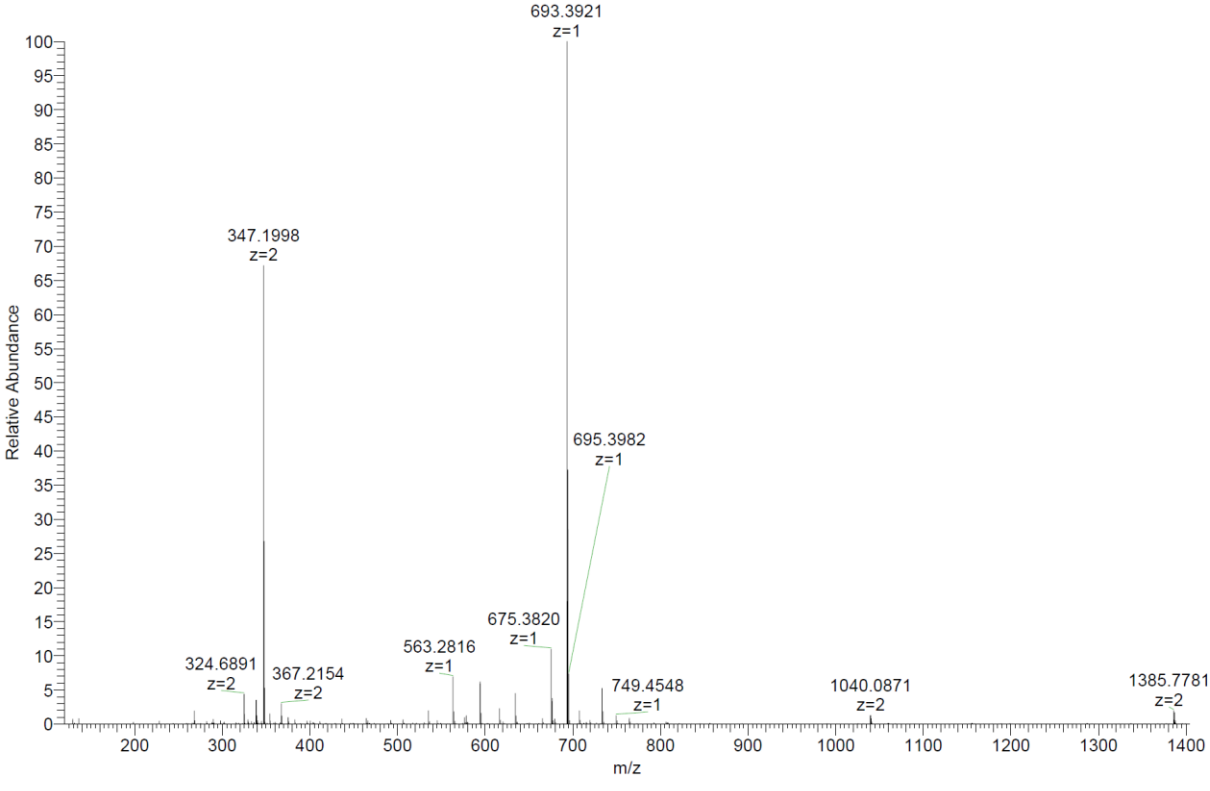

Hexappetide 1β (VKD(β)GYI)

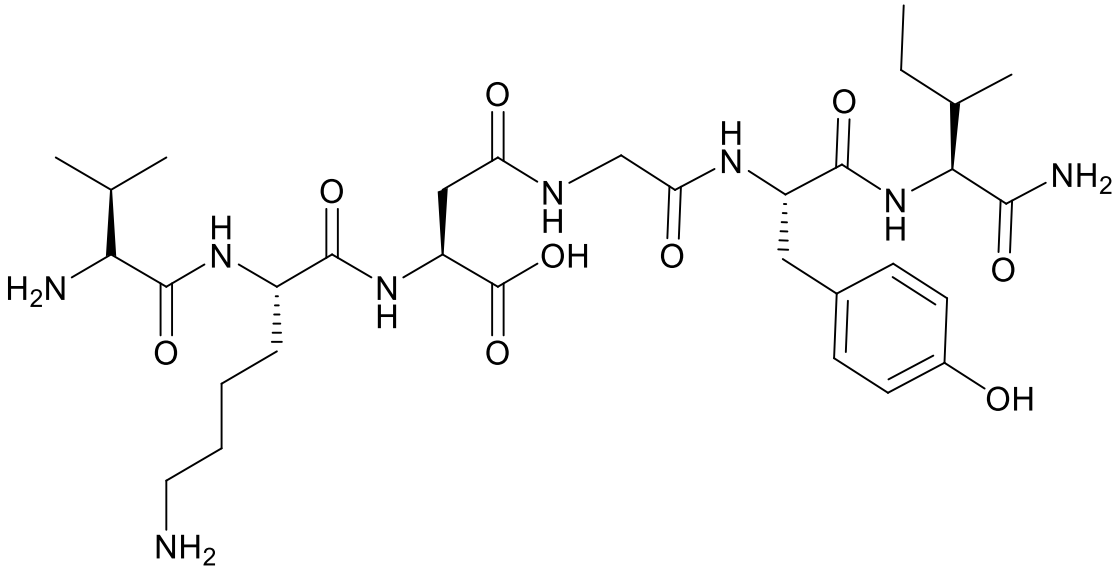

Chemical Formula: $C_{32}H_{52}N_8O_9$
Exact Mass: 692,39
Molecular Weight: 692,82

VKD(β)GYI was obtained as white solid after preparative RP-HPLC (6.4 mg, 14.2%). Analytical RP-HPLC: t_R = 1.19 min (A/D 100:0 to 0:100 in 3.50 min, λ = 214nm). MS (ESI+): $C_{32}H_{52}N_8O_9$ calc./obs. 693.39/693.42 Da $[M+H]^+$.

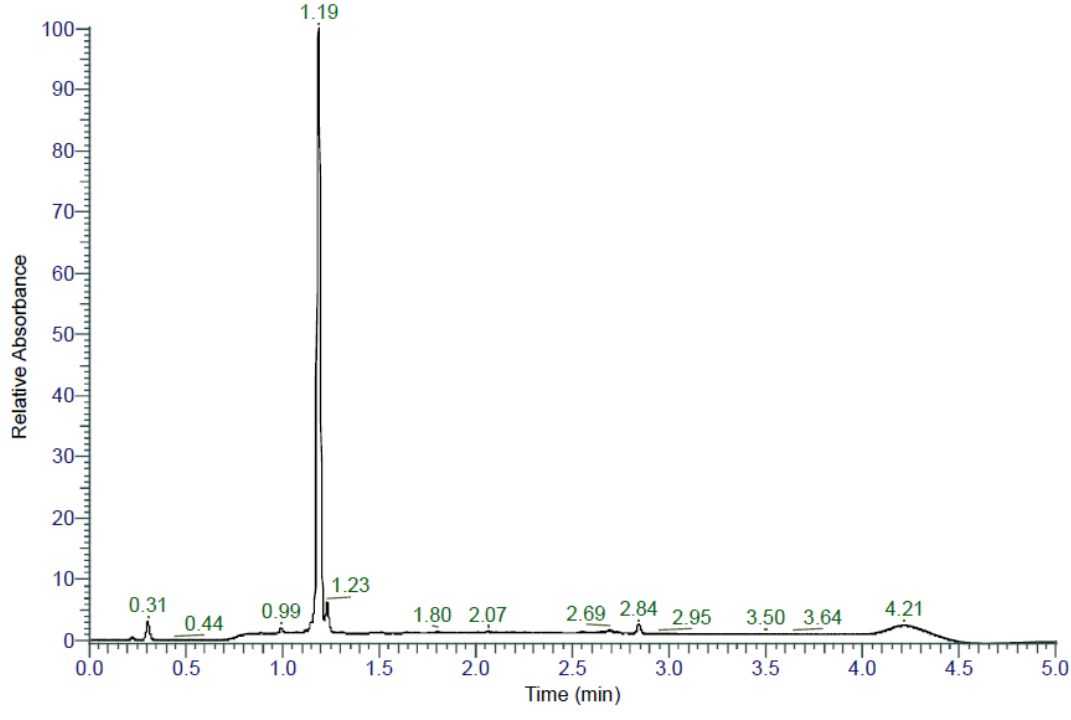

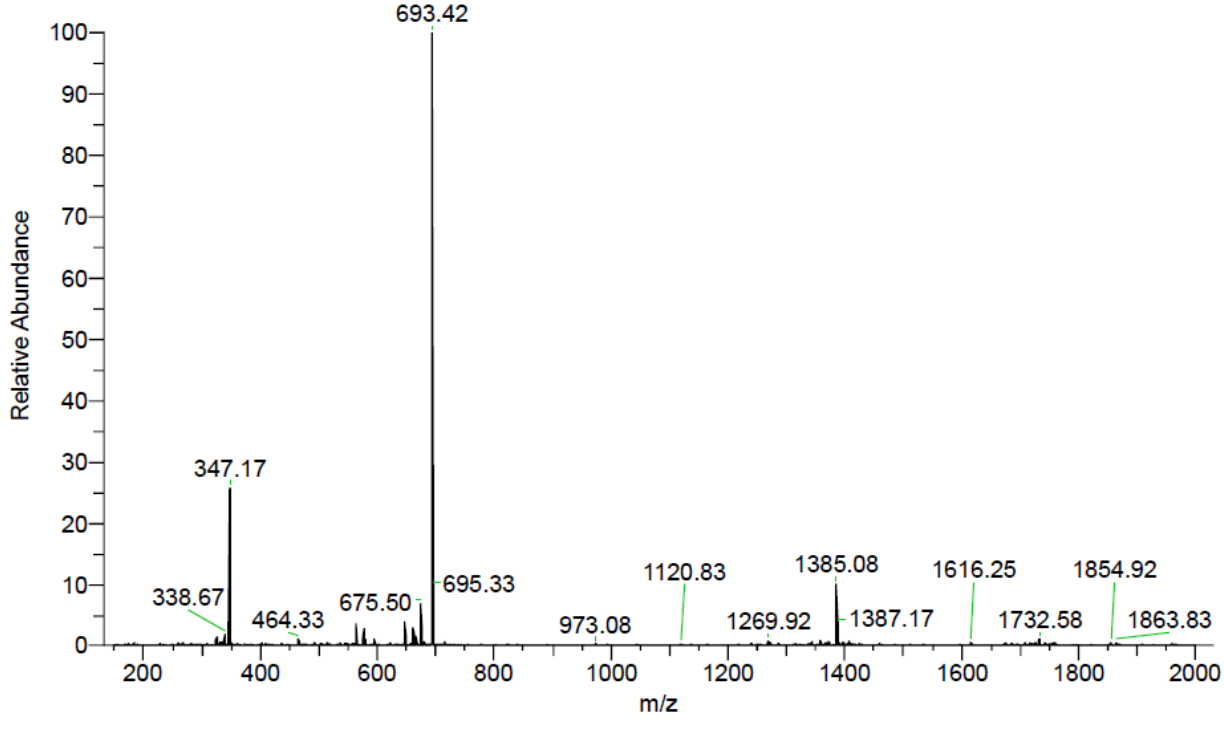

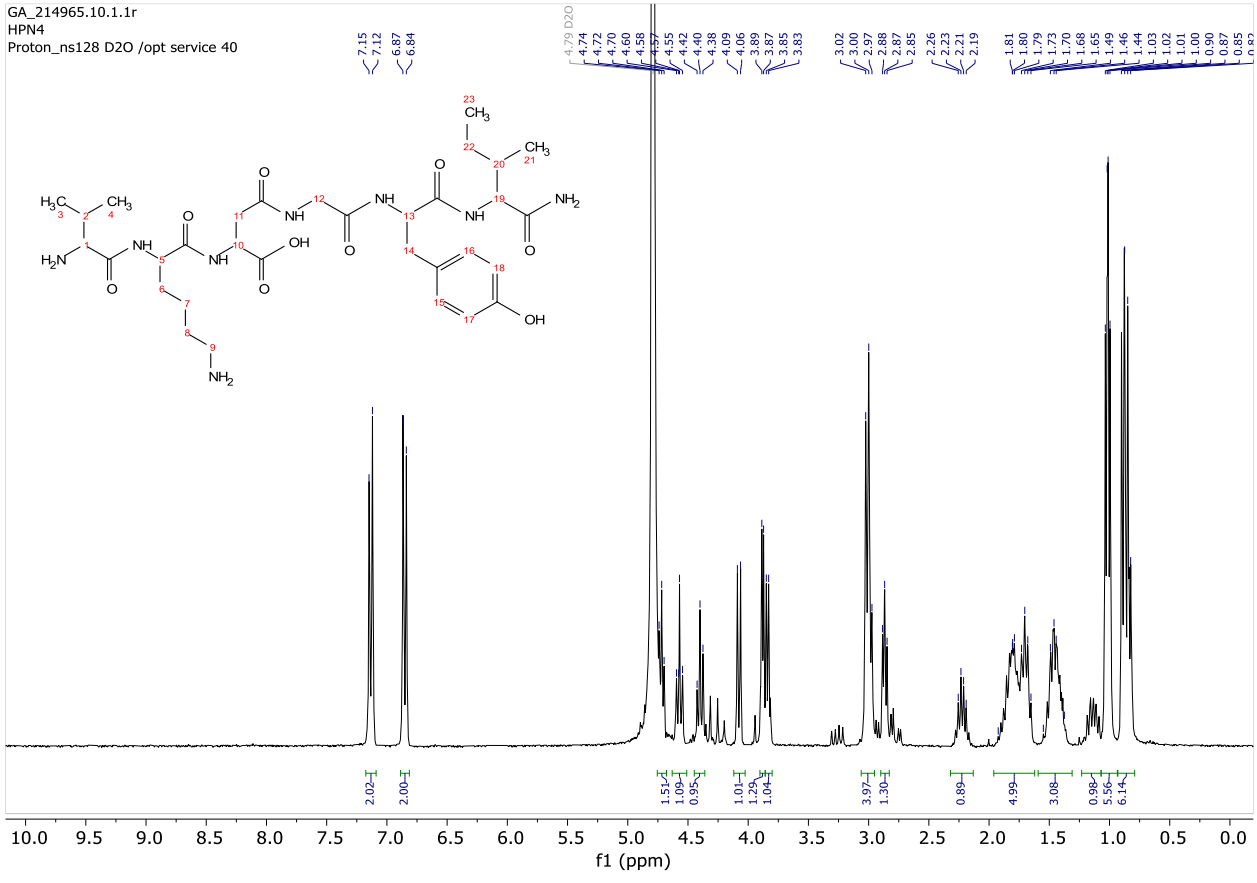

Figure S4.4: ^{1}H NMR spectra of purified VKD(β)GYI (300 MHz, D_2O) : δ = 7.13 (d, *J* = 8.6 Hz, 2H, C(15 and 16)), 6.85 (d, *J* = 8.6 Hz, 2H, C(17 and 18)), 4.72 (t, 1H, C(13)), 4.57 (t, *J* = 7.5 Hz, 1H, C(10)), 4.40 (t, *J* = 7.3 Hz, 1H, C(5)), 4.08 (d, *J* = 7.9 Hz, 1H, C(19)), 3.86 (m, 3H, C(1 and 12)), 3.00 (m, 4H, C(11 and 14)), 2.87 (t, *J* = 5.6 Hz, 2H, C(9)), 2.29 – 2.16 (m, 1H, C(20)), 1.84 – 1.62 (m, 6H, C(6, 8 and 22)), 1.49 – 1.44 (m, 3H, C(2 and7)), 1.02 (dd, *J* = 7.0, 4.6 Hz, 6H, C(21 and 23)), 0.93 – 0.79 (m, 6H, C(3 and 4)).

Hexapeptide 2 (GDGAKF)

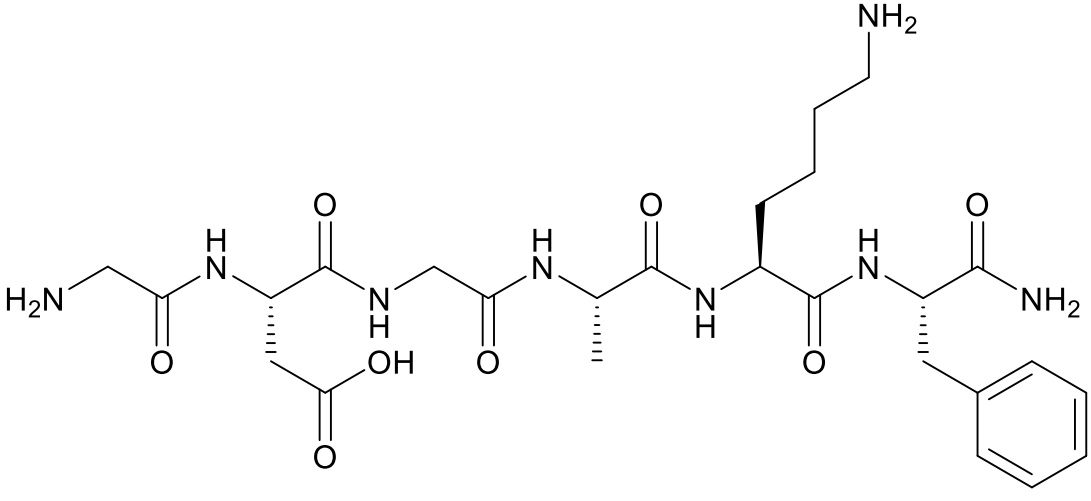

Chemical Formula: $C_{26}H_{40}N_8O_8$
Exact Mass: 592,30
Molecular Weight: 592,65

GDGAKF (20% v/v Piperidine, 60°C) was obtained as crude white solid after lyophilization (40.6 mg, 40.9%). Analytical RP-HPLC: t_R = 1.75 min (A/D 100:0 to 0:100 in 7.00 min, λ = 214nm). HRMS (ESI+): $C_{26}H_{40}N_8O_8$ calc./obs. 593.30/593.30 Da $[M+H]^+$.

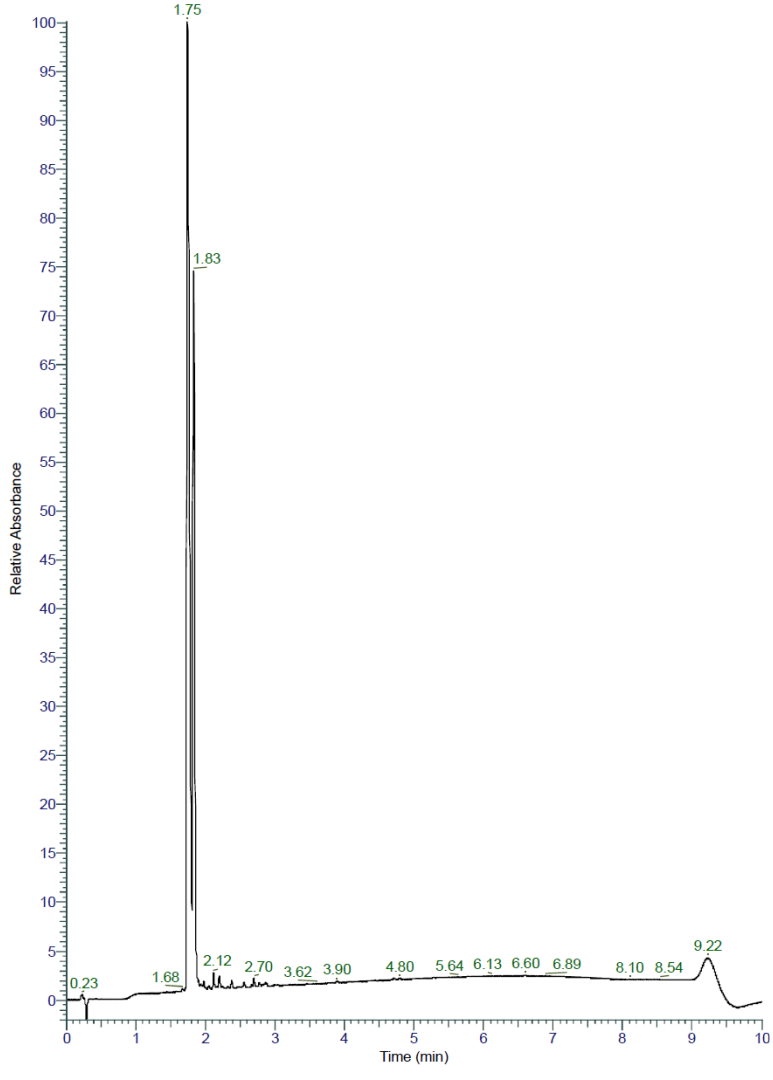

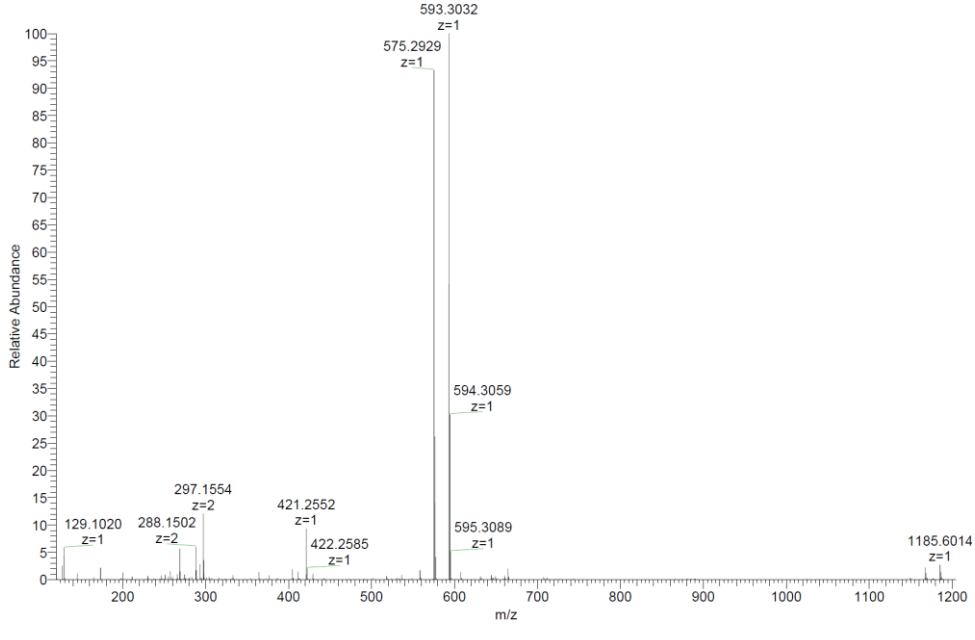

GDGAKF (25% v/v Dipropylamine, 60°C) was obtained as crude white solid after lyophilization (38.9 mg, 49.2%). Analytical RP-HPLC: t_R = 1.76 min (A/D 100:0 to 0:100 in 7.00 min, λ = 214nm). HRMS (ESI+): $C_{26}H_{40}N_8O_8$ calc./obs. 593.30/593.30 Da $[M+H]^+$.

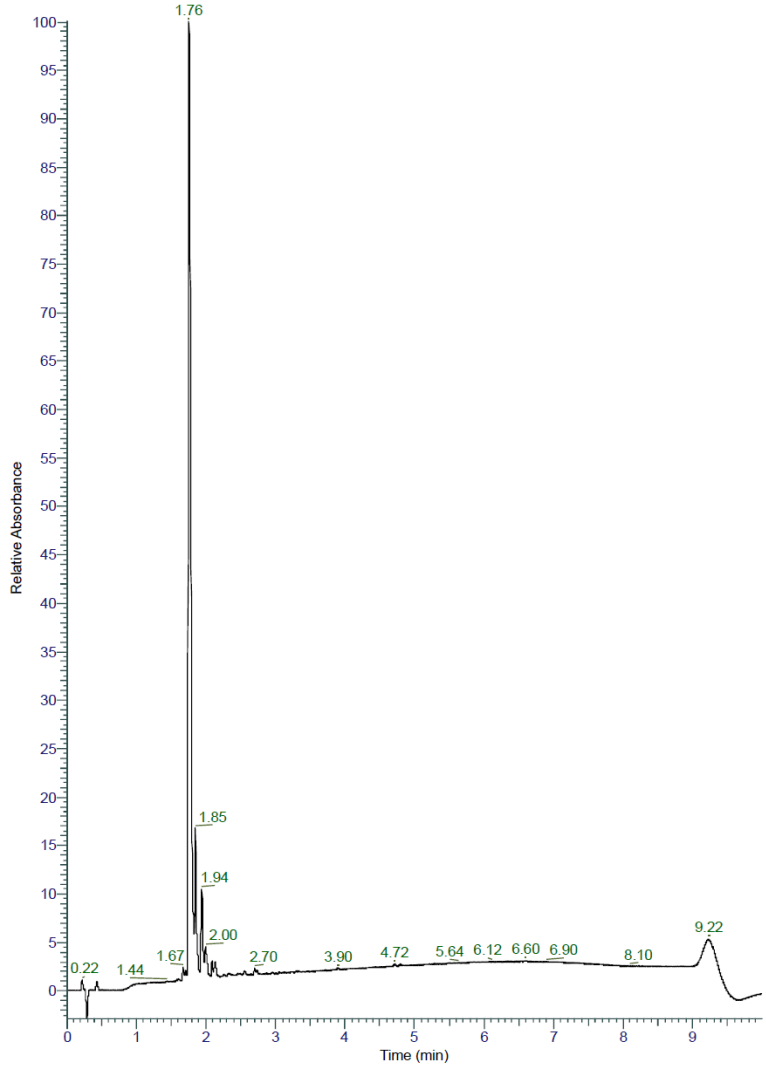

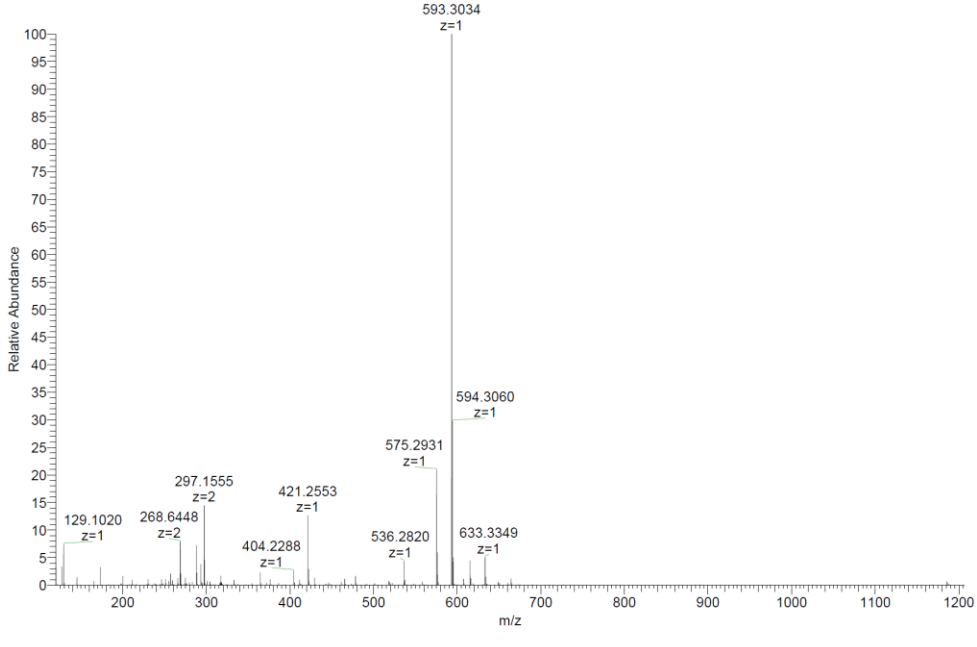

Hexapeptide 3 (VKDRYI)

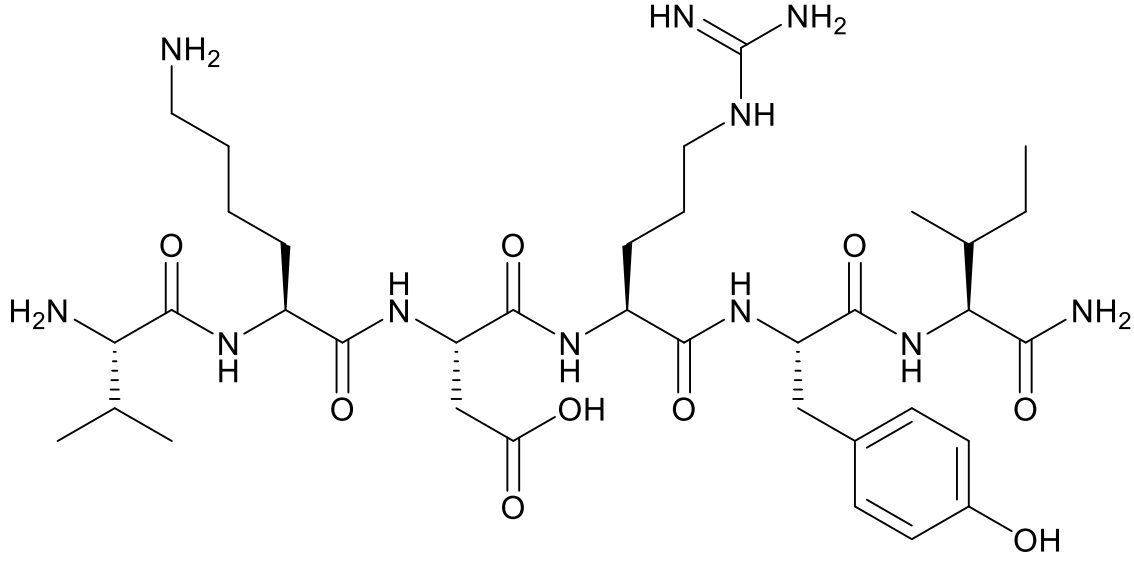

Chemical Formula: $C_{36}H_{61}N_{11}O_9$
Exact Mass: 791,47
Molecular Weight: 791,95

VKDRYI (20% v/v Piperidine, 60°C) was obtained as crude white solid after lyophilization (44.0 mg, 40.3%). Analytical RP-HPLC: t_R = 1.99 min (A/D 100:0 to 0:100 in 7.00 min, λ = 214nm). HRMS (ESI+): $C_{36}H_{61}N_{11}O_9$ calc./obs. 792.47/792.47 Da $[M+H]^+$.

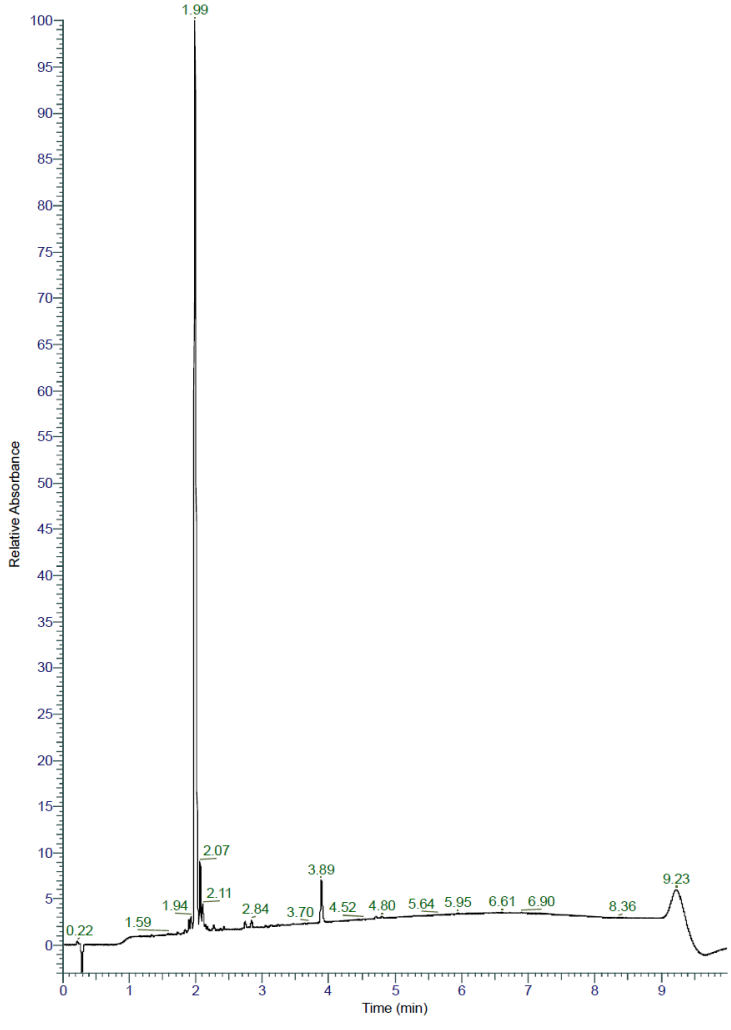

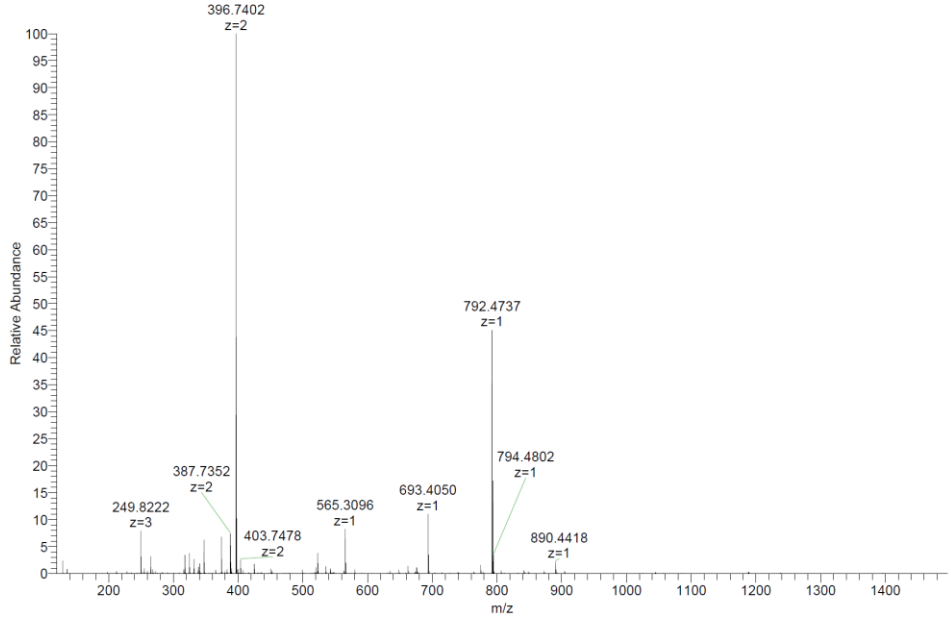

VKDRYI (25% v/v Dipropylamine, 60°C) was obtained as crude white solid after lyophilization (44.2 mg, 43.4%). Analytical RP-HPLC: t_R = 2.00 min (A/D 100:0 to 0:100 in 7.00 min, λ = 214nm). HRMS (ESI+): $C_{36}H_{61}N_{11}O_9$ calc./obs. 792.47/792.47 Da $[M+H]^+$.

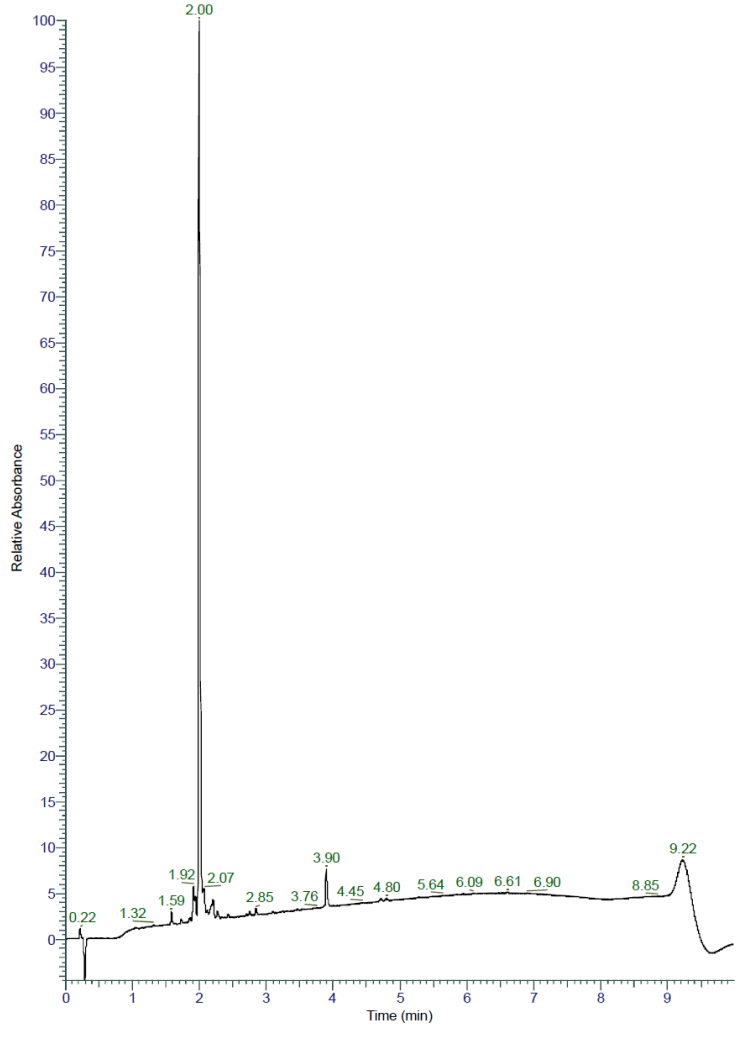

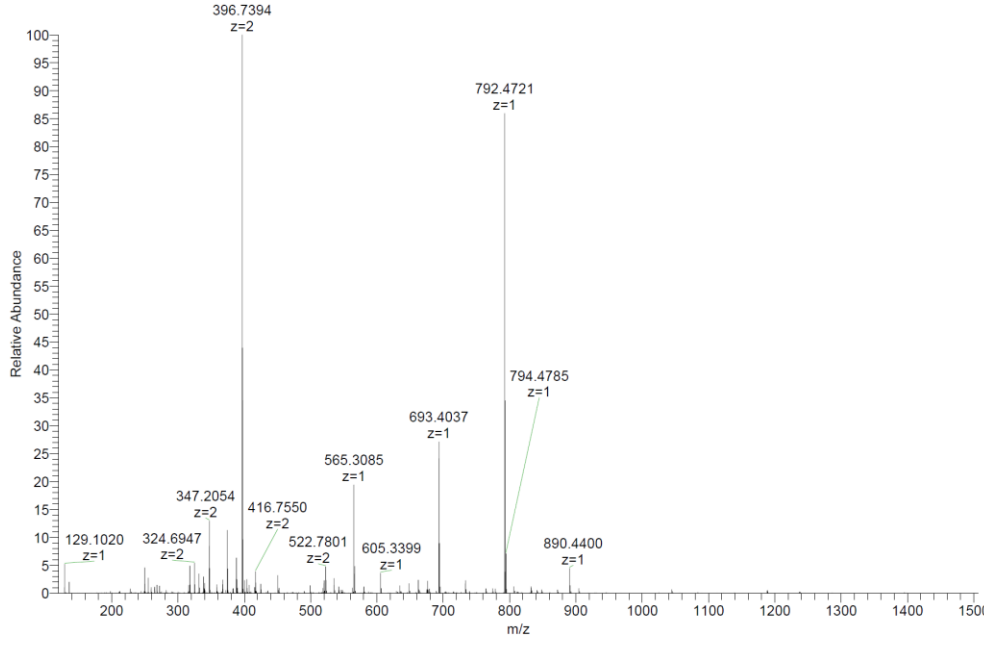

Hexapeptide 4 (GDRAKF)

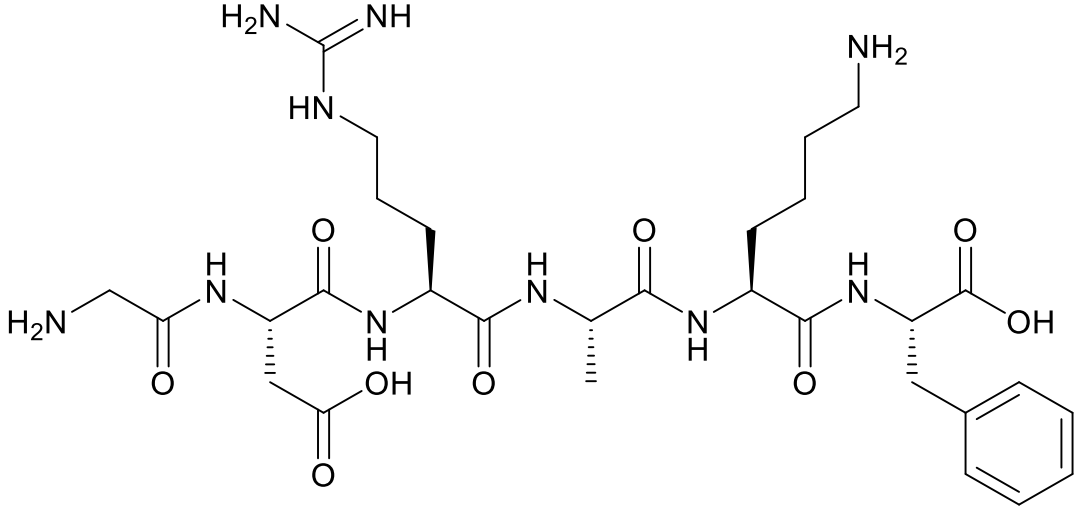

Chemical Formula: $C_{30}H_{48}N_{10}O_9$
Exact Mass: 692,36
Molecular Weight: 692,78

GDRAKF (20% v/v Piperidine, 60°C) was obtained as crude white solid after lyophilization (44.2 mg, 50.6%). Analytical RP-HPLC: t_R = 1.84 min (A/D 100:0 to 0:100 in 7.00 min, λ = 214nm). HRMS (ESI+): $C_{30}H_{48}N_{10}O_9$ calc./obs. 693.36/693.39Da $[M+H]^+$.

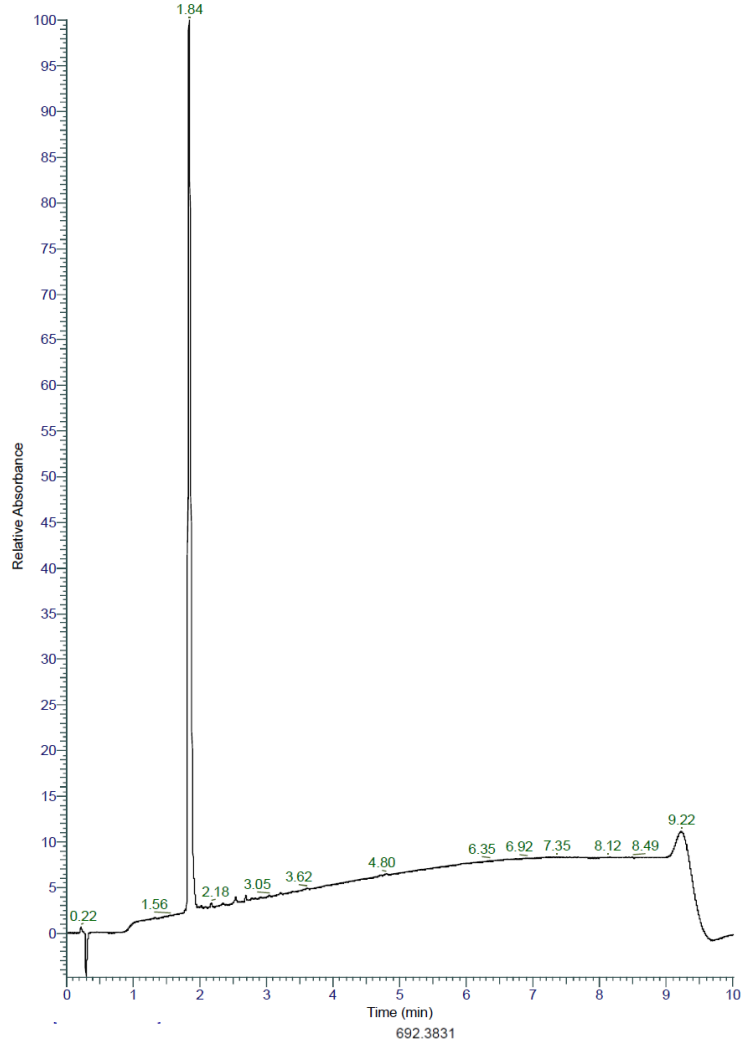

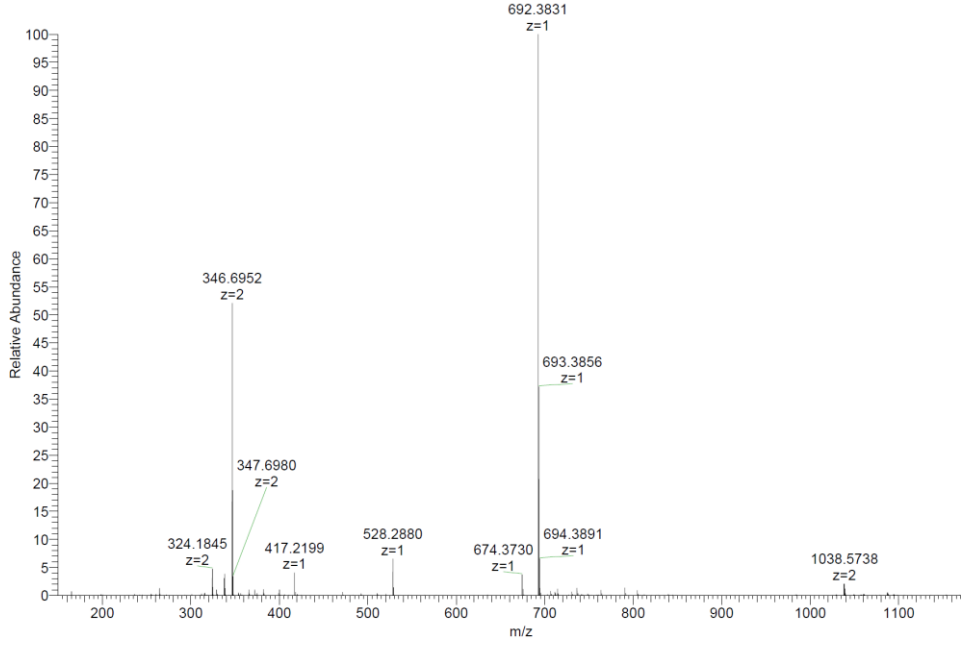

GDRAKF (25% v/v Dipropylamine, 60°C) was obtained as crude white solid after lyophilization (52.9 mg, 62.5%). Analytical RP-HPLC: t_R = 1.86 min (A/D 100:0 to 0:100 in 7.00 min, λ = 214nm). HRMS (ESI+): $C_{30}H_{48}N_{10}O_9$ calc./obs. 693.36/693.39Da $[M+H]^+$.

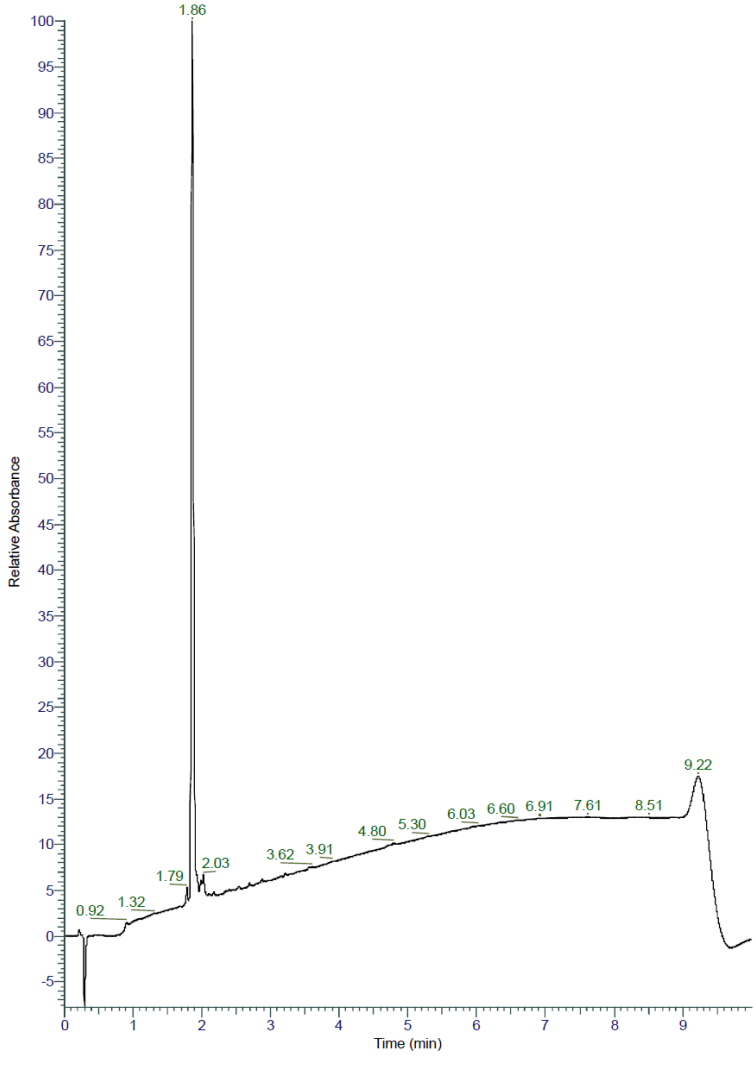

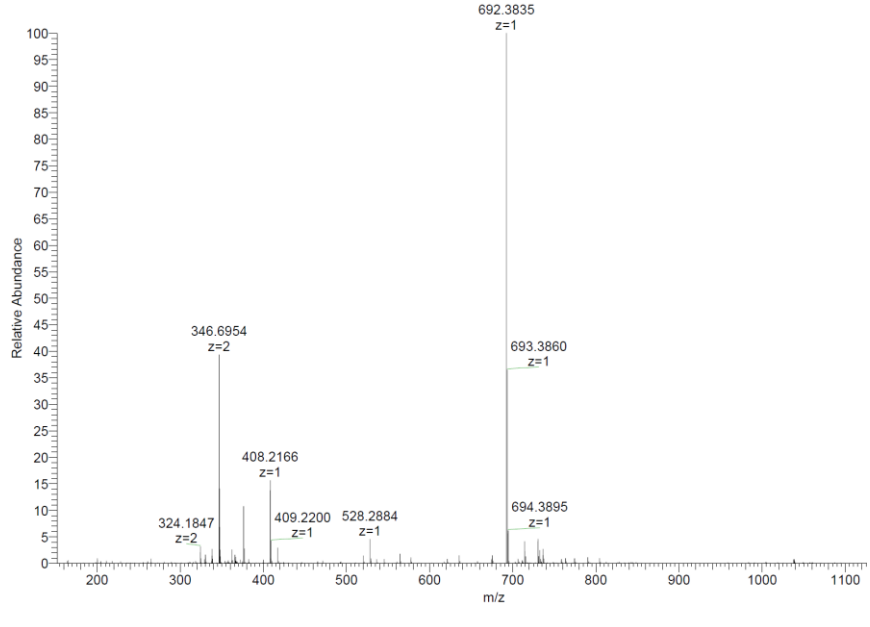

Hexapeptide 5 (VKDCYI)

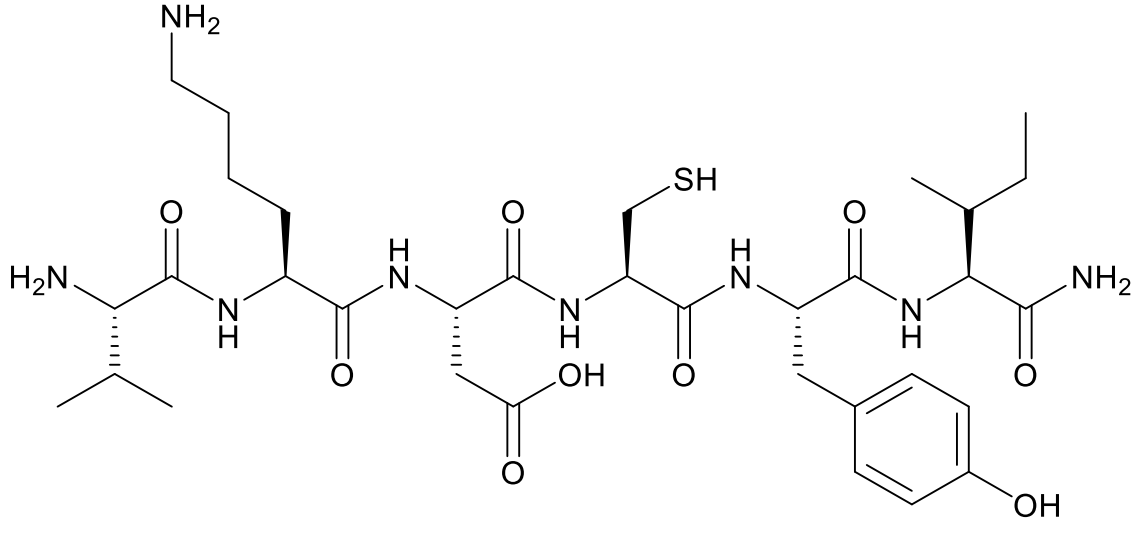

Chemical Formula: $C_{33}H_{54}N_8O_9S$
Exact Mass: 738,37
Molecular Weight: 738,90

VKDCYI (20% v/v Piperidine, 60°C) was obtained as crude white solid after lyophilization (46.2 mg, 53.1%). Analytical RP-HPLC: t_R = 2.23 min (A/D 100:0 to 0:100 in 7.00 min, λ = 214nm). HRMS (ESI+): $C_{33}H_{54}N_8O_9S$ calc./obs. 739.37/739.38 Da $[M+H]^+$.

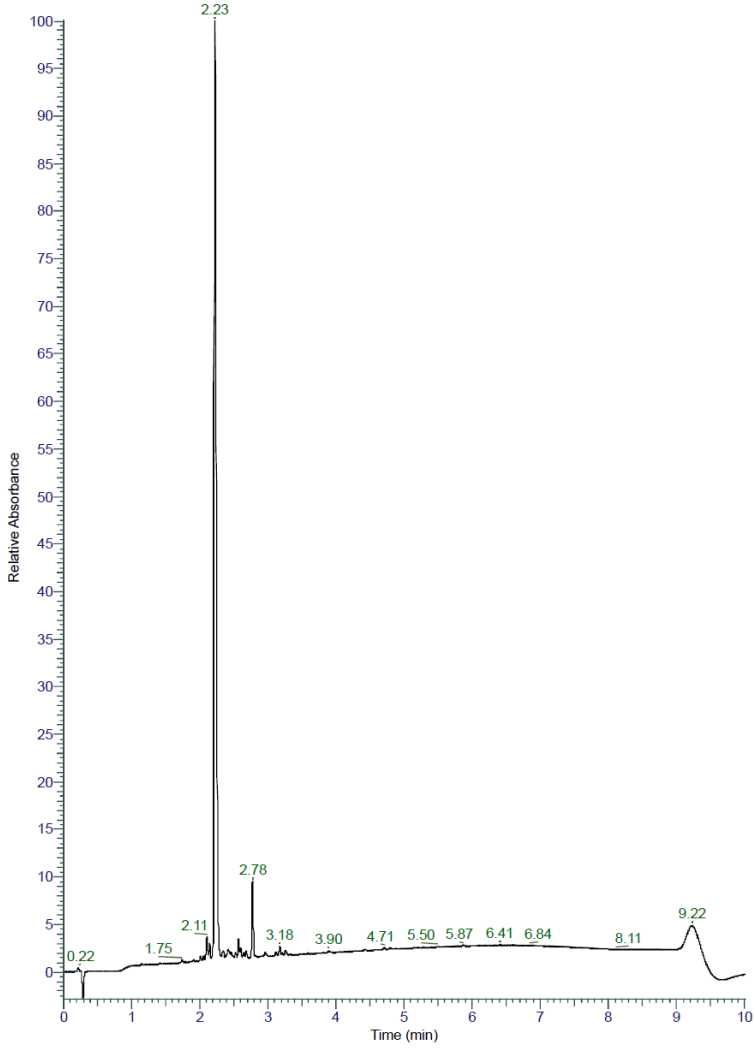

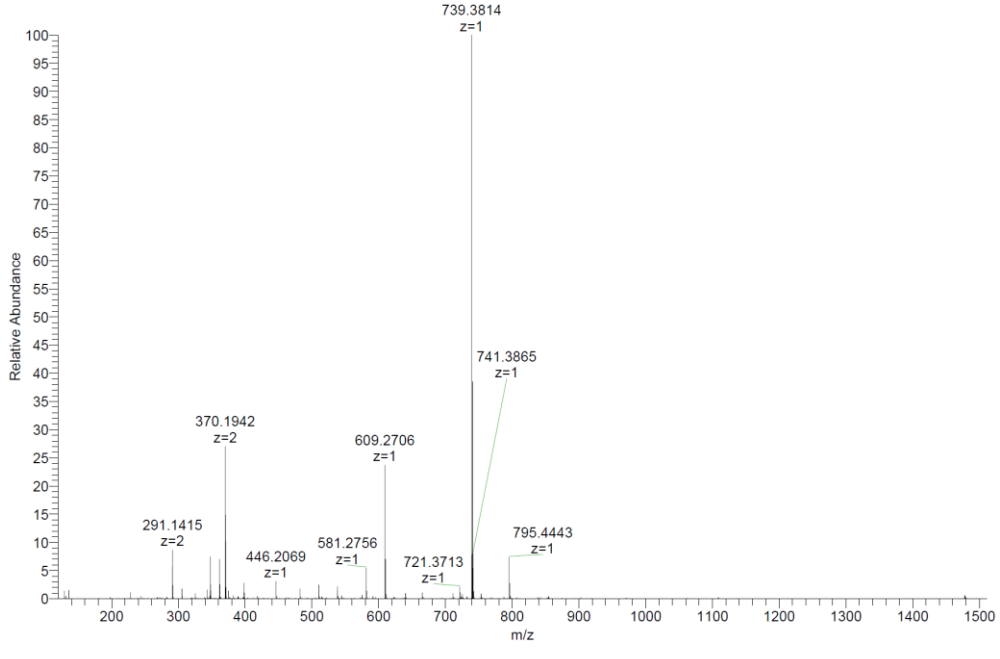

VKDCYI (25% v/v Dipropylamine, 60°C) was obtained as crude white solid after lyophilization (42.7 mg, 48.0%). Analytical RP-HPLC: t_R = 2.23 min (A/D 100:0 to 0:100 in 7.00 min, λ = 214nm). HRMS (ESI+): $C_{33}H_{54}N_8O_9S$ calc./obs. 739.37/739.38 Da $[M+H]^+$.

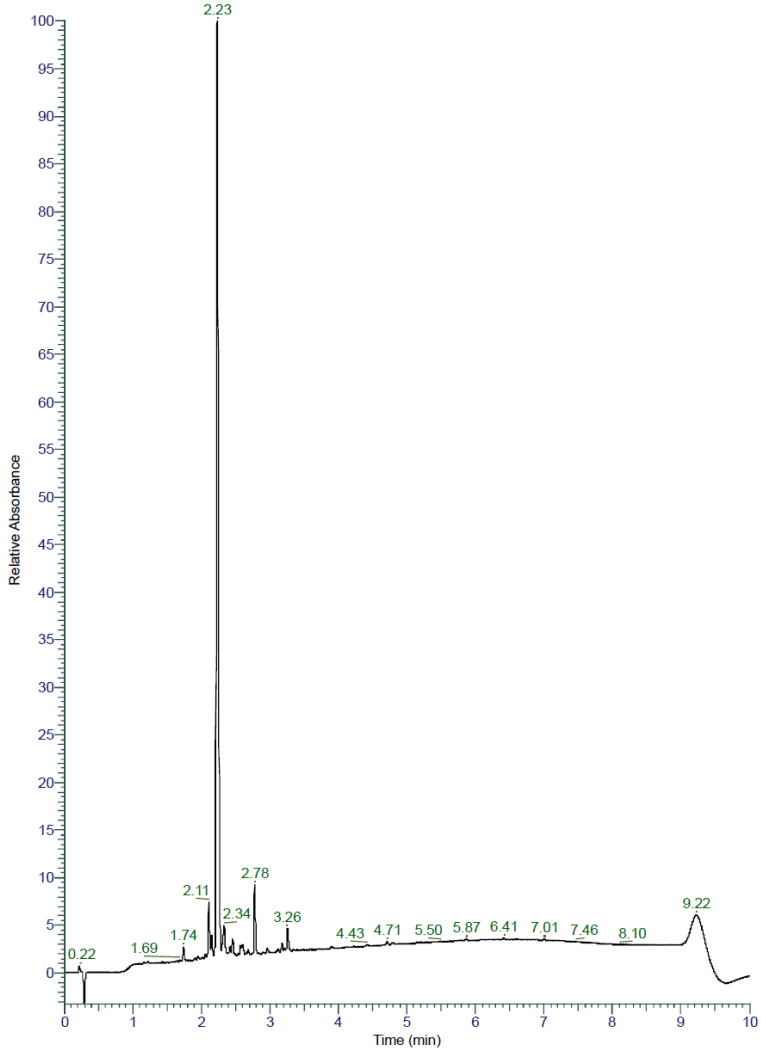

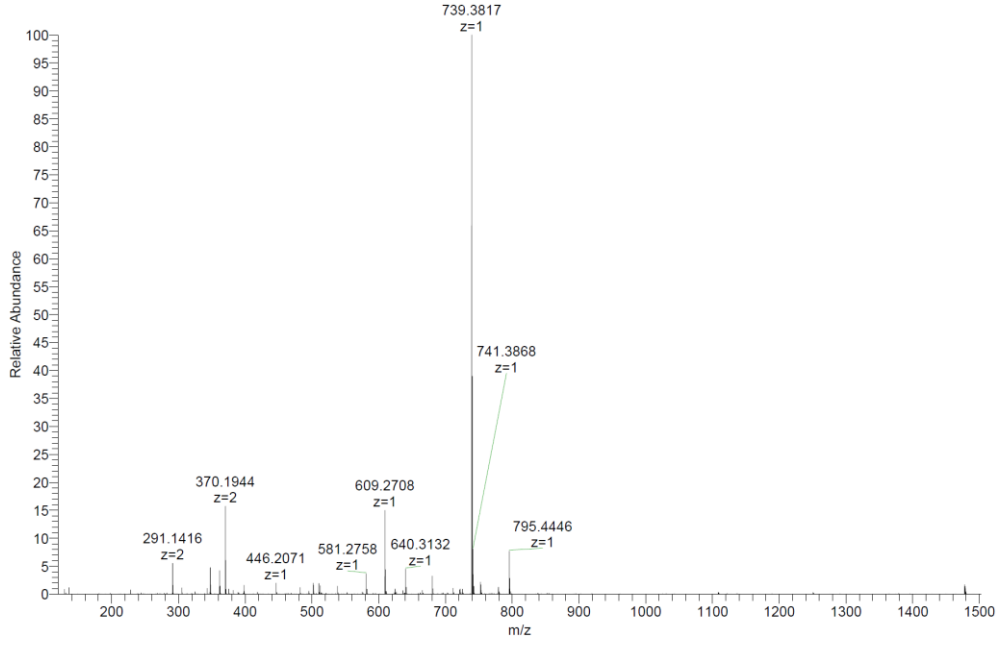

Hexapeptide 6 (VKDAYI)

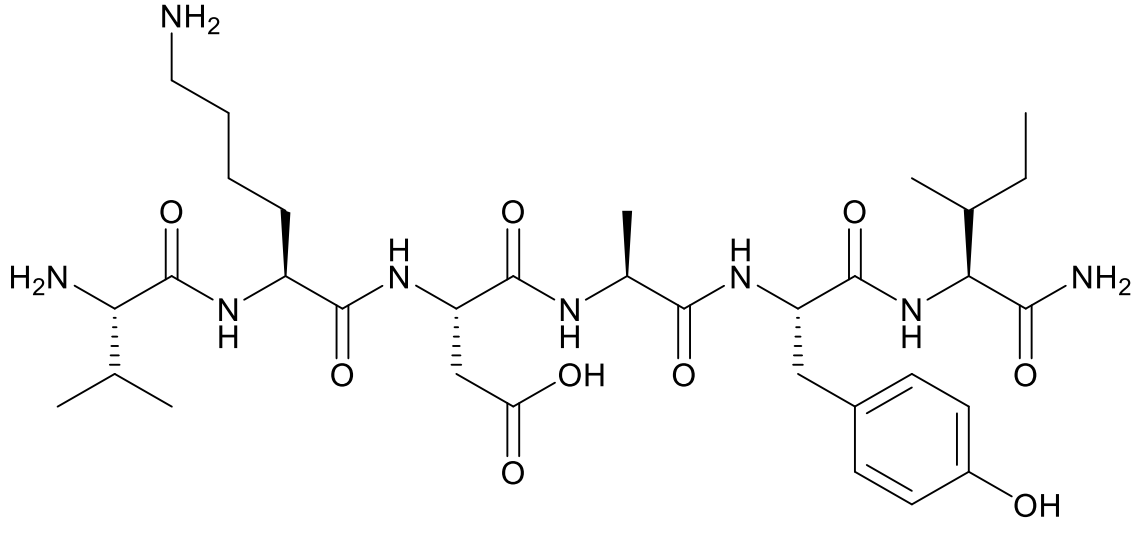

Chemical Formula: $C_{33}H_{54}N_8O_9$
Exact Mass: 706,40
Molecular Weight: 706,84

VKDAYI (20% v/v Piperidine, 60°C) was obtained as crude white solid after lyophilization (42.7 mg, 54.7%). Analytical RP-HPLC: t_R = 2.09 min (A/D 100:0 to 0:100 in 7.00 min, λ = 214nm). HRMS (ESI+): $C_{33}H_{54}N_8O_9$ calc./obs. 707.40/707.41 Da $[M+H]^+$.

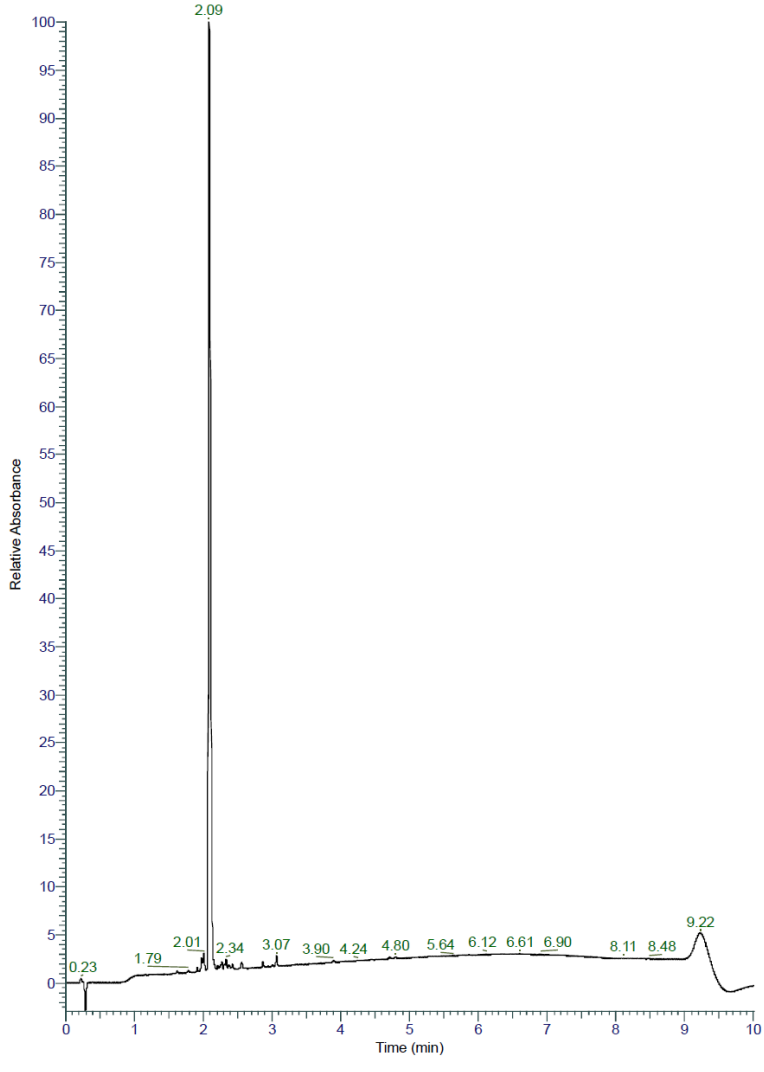

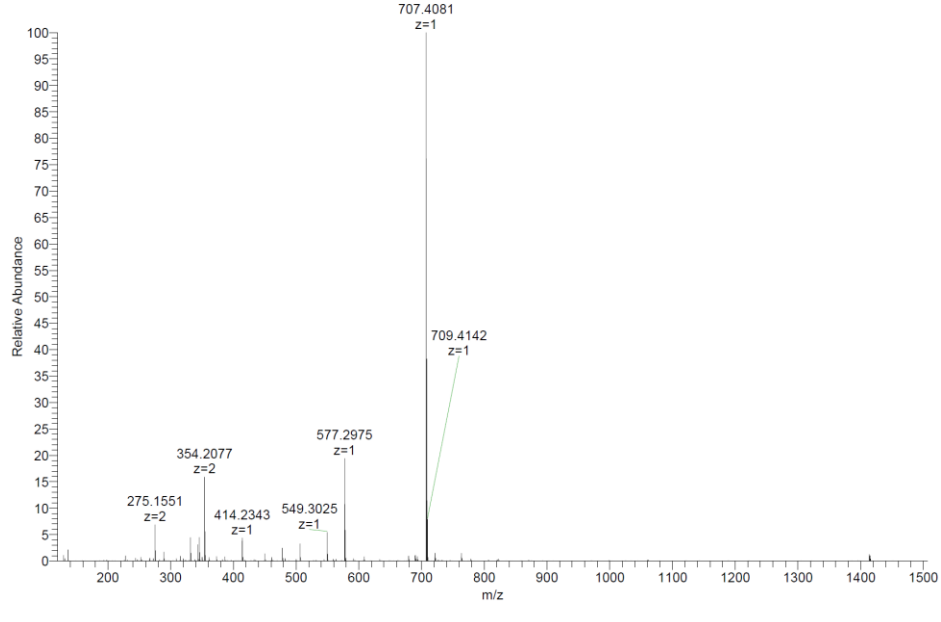

VKDAYI (25% v/v Dipropylamine, 60°C) was obtained as crude white solid after lyophilization (40.4 mg, 51.3%). Analytical RP-HPLC: t_R = 2.09 min (A/D 100:0 to 0:100 in 7.00 min, λ = 214nm). HRMS (ESI+): $C_{33}H_{54}N_8O_9$ calc./obs. 707.40/ Da $[M+H]^+$.

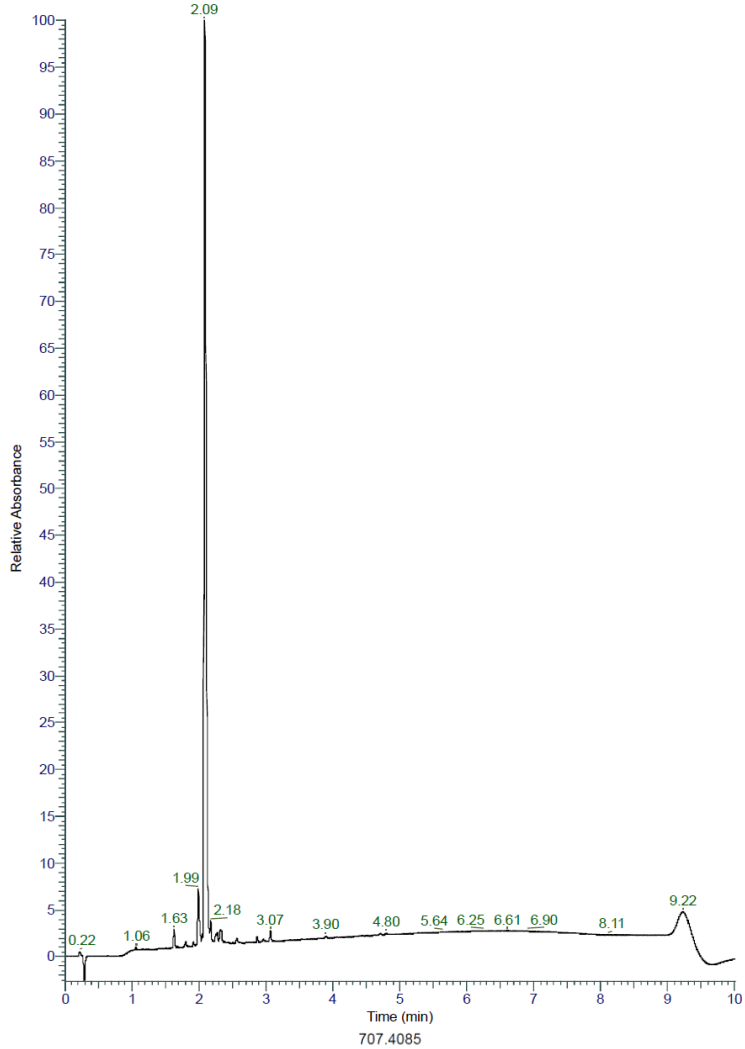

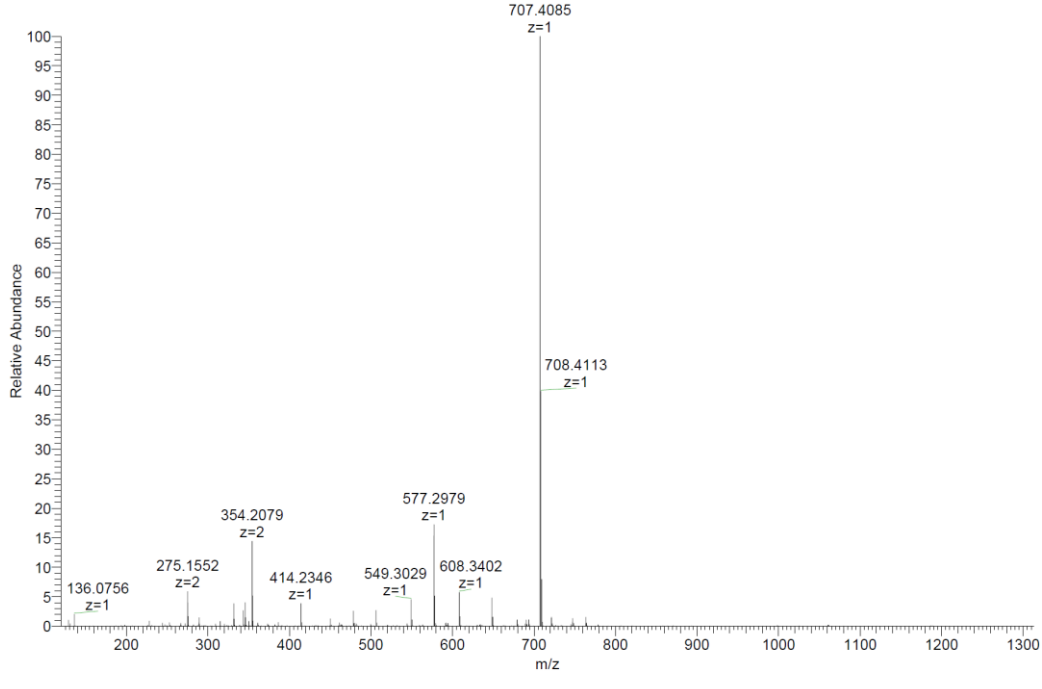

Hexapeptide 7 (VKEGYI)

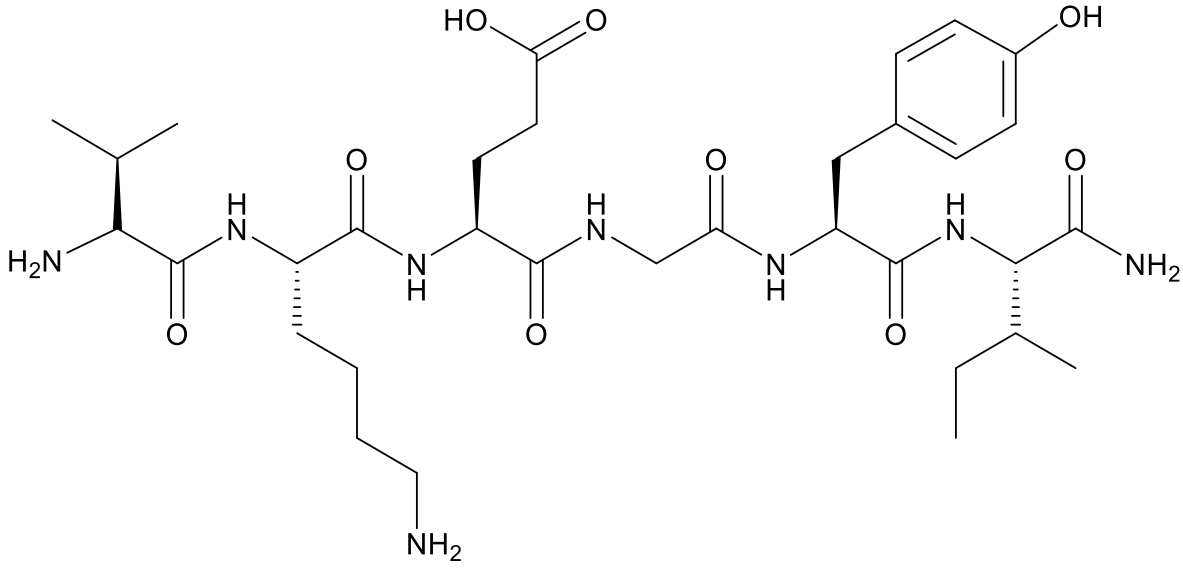

Chemical Formula: $C_{33}H_{54}N_8O_9$
Exact Mass: 706,40
Molecular Weight: 706,84

VKEGYI (20% v/v Piperidine, 60°C) was obtained as crude white solid after lyophilization (34.8 mg, 47.7%). Analytical RP-HPLC: t_R = 1.99 min (A/D 100:0 to 0:100 in 7.00 min, λ = 214nm). HRMS (ESI+): $C_{33}H_{54}N_8O_9$ calc./obs. 707.40/707.41 Da $[M+H]^+$.

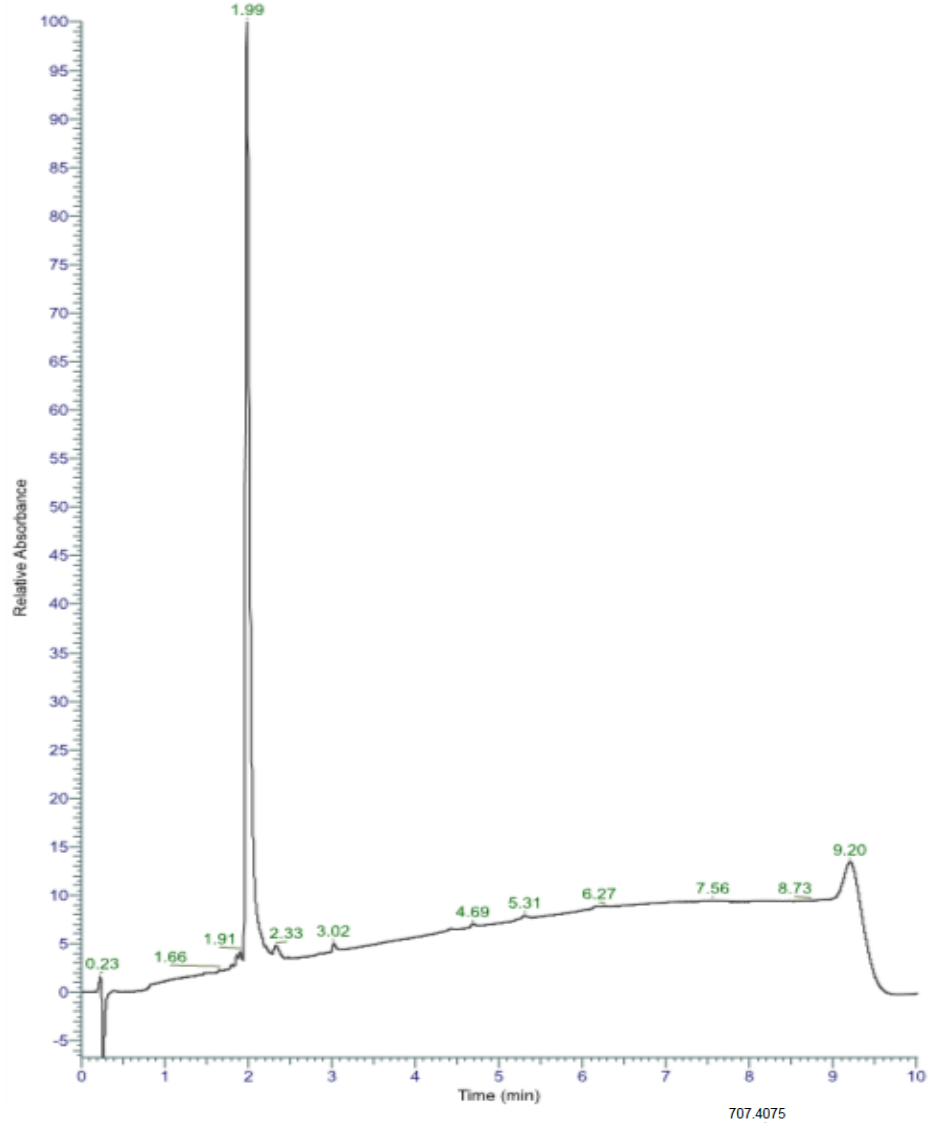

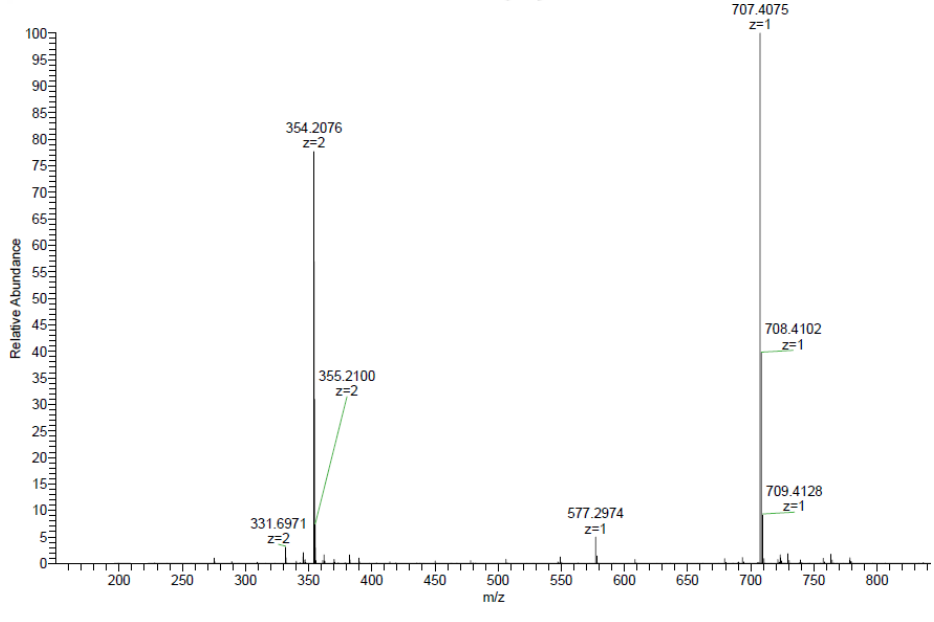

VKEGYI (5% w/v Piperazine + 2% v/v DBU, 60°C) was obtained as crude white solid after lyophilization (38.2 mg, 52.4%). Analytical RP-HPLC: t_R = 1.90 min (A/D 100:0 to 0:100 in 7.00 min, λ = 214nm). HRMS (ESI+): $C_{33}H_{54}N_8O_9$ calc./obs. 707.40/707.41 Da $[M+H]^+$.

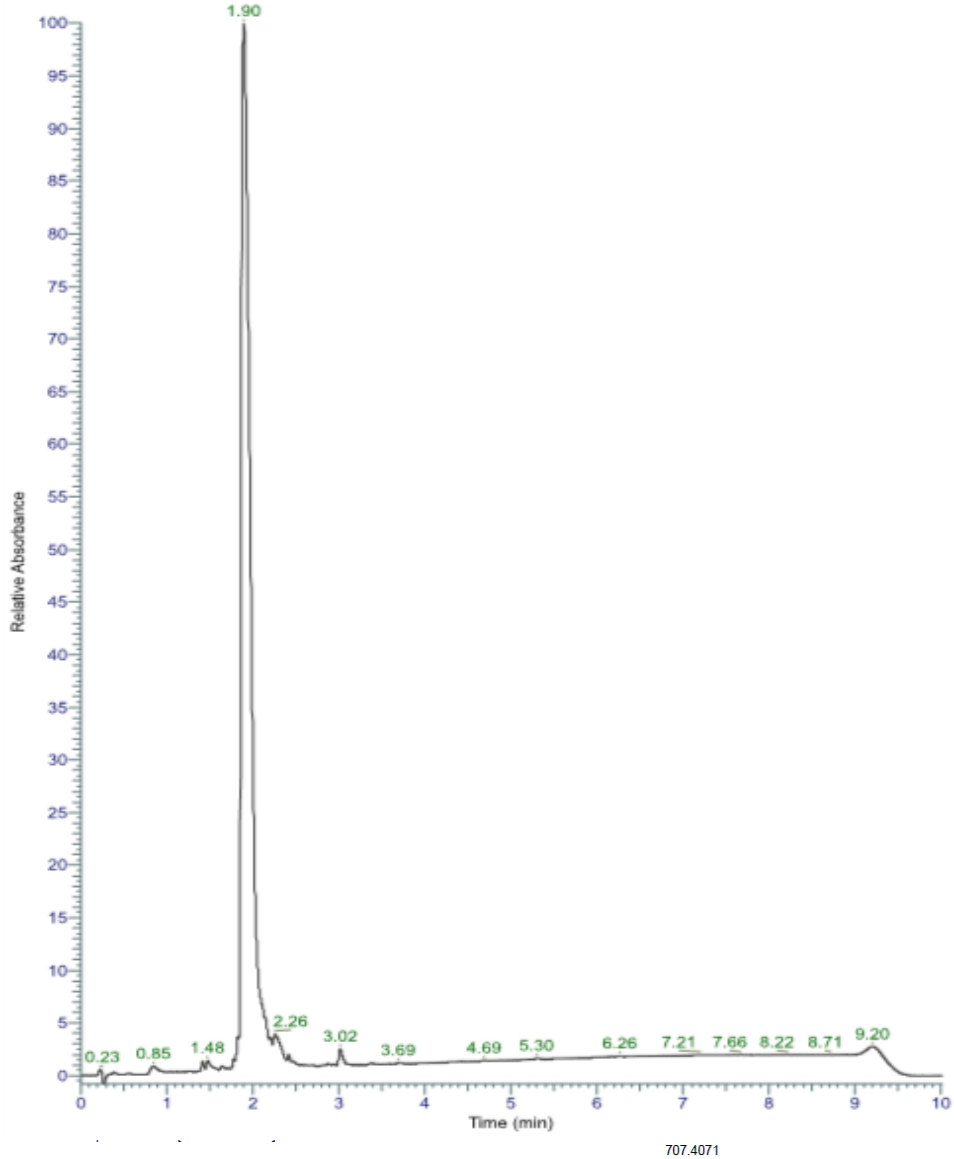

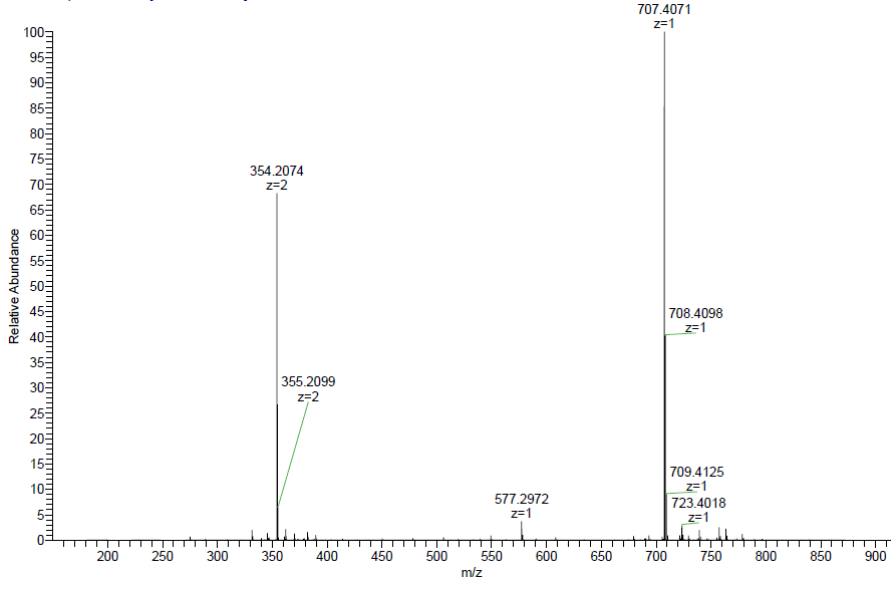

VKEGYI (20% v/v Dipropylamine, 60°C) was obtained as crude white solid after lyophilization (32.3 mg, 44.3%). Analytical RP-HPLC: t_R = 1.98 min (A/D 100:0 to 0:100 in 7.00 min, λ = 214nm). HRMS (ESI+): $C_{33}H_{54}N_8O_9$ calc./obs. 707.40/707.41 Da $[M+H]^+$.

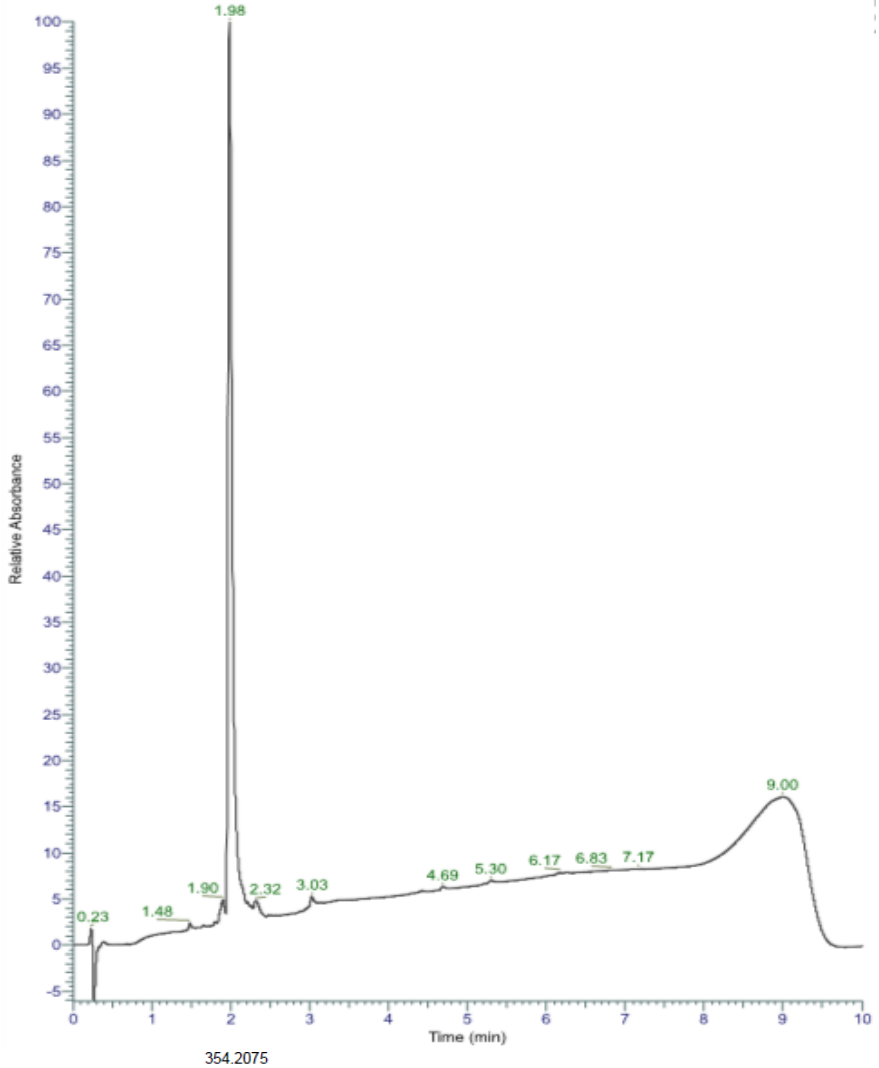

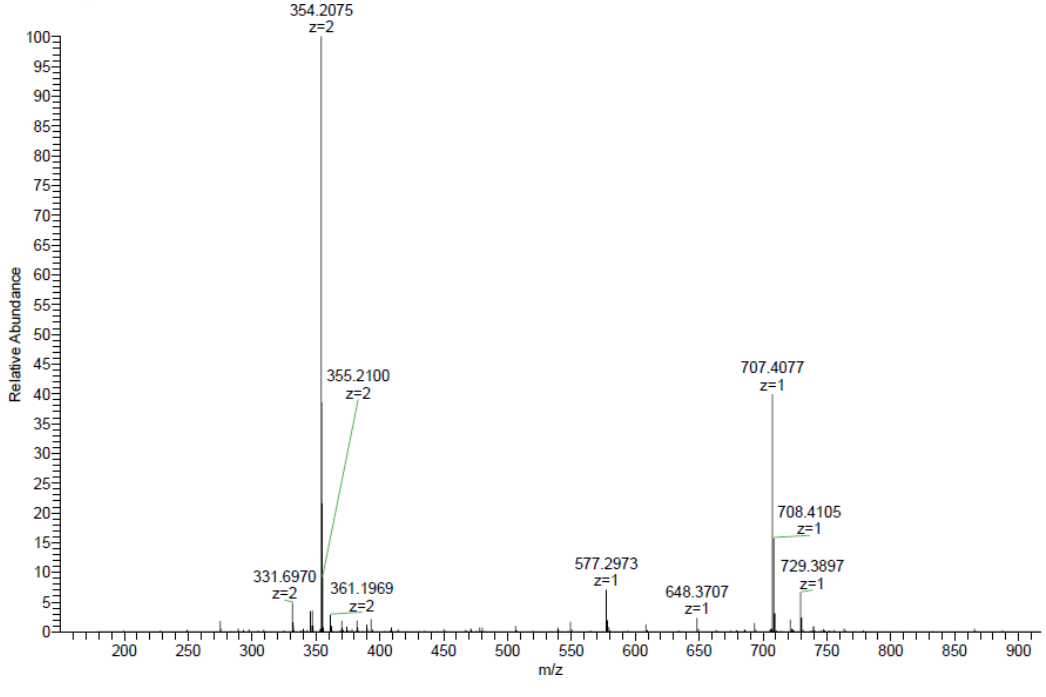

VKEGYI (20% v/v Dipropylamine + 0.5 M Oxyma, 60°C) was obtained as crude white solid after lyophilization (36.5 mg, 50.0%). Analytical RP-HPLC: t_R = 1.93 min (A/D 100:0 to 0:100 in 7.00 min, λ = 214nm). HRMS (ESI+): $C_{33}H_{54}N_8O_9$ calc./obs. 707.40/707.41 Da $[M+H]^+$.

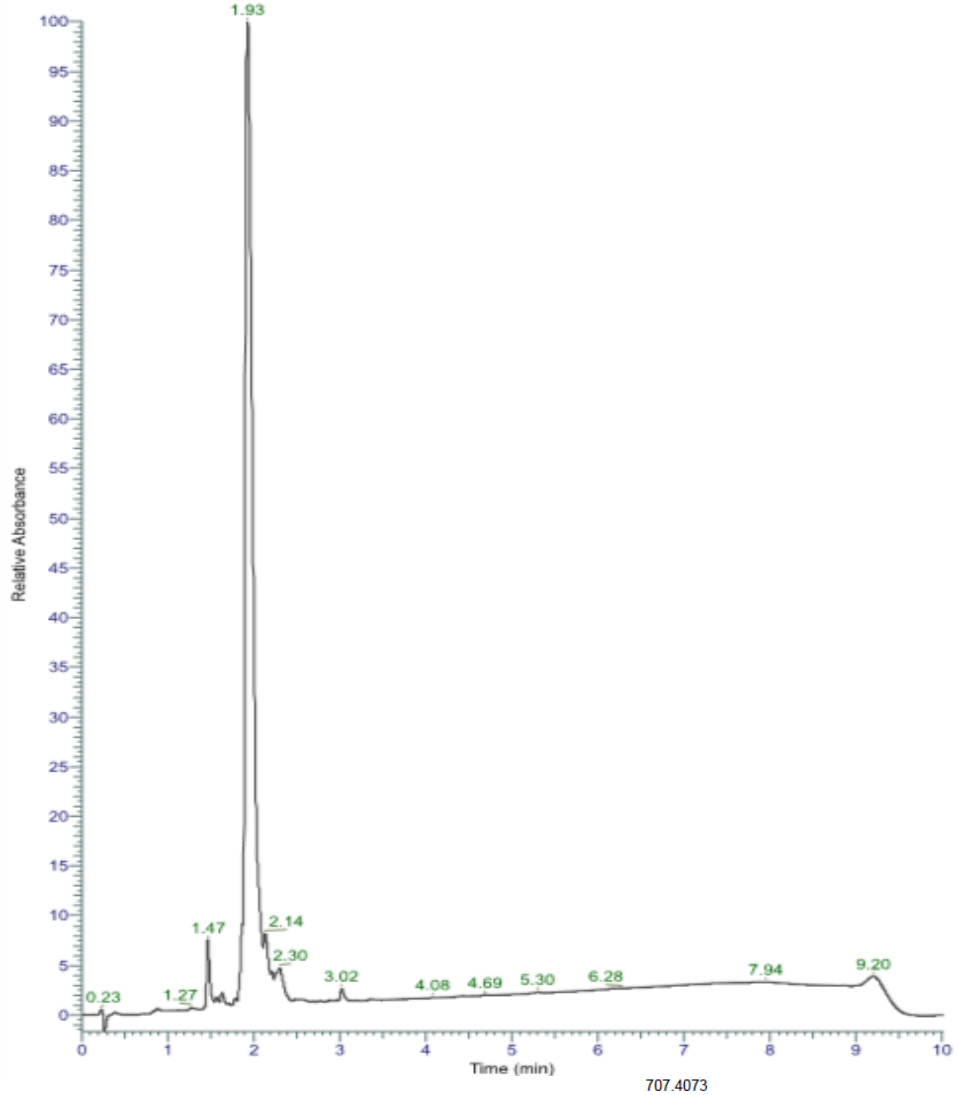

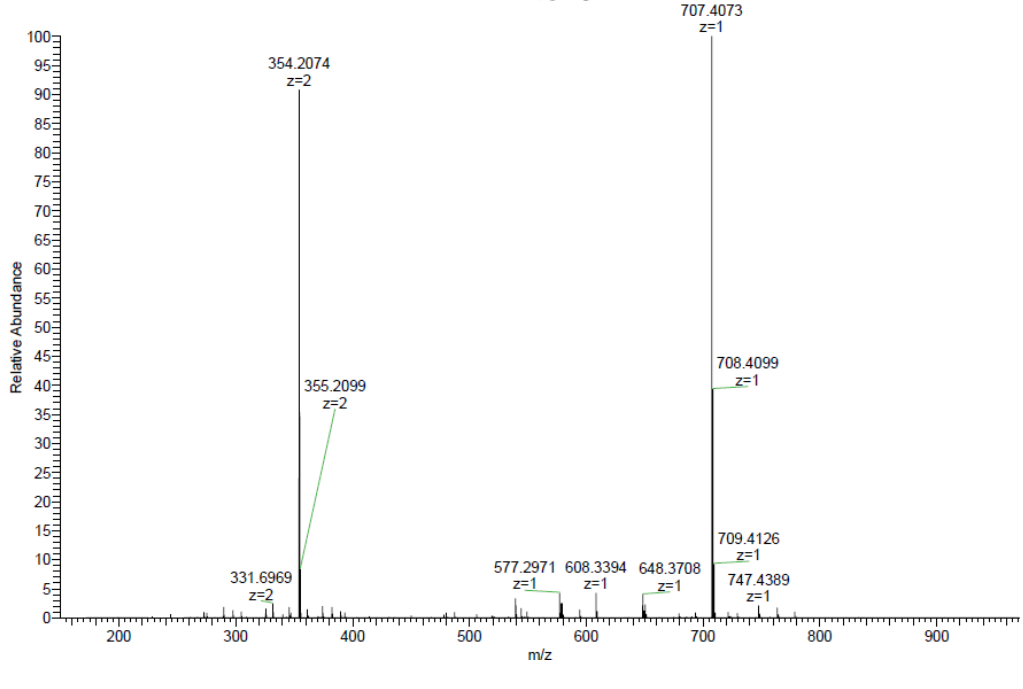

Afamelanotide (Ac-SYSNleEHfRWGKPV-NH_2)

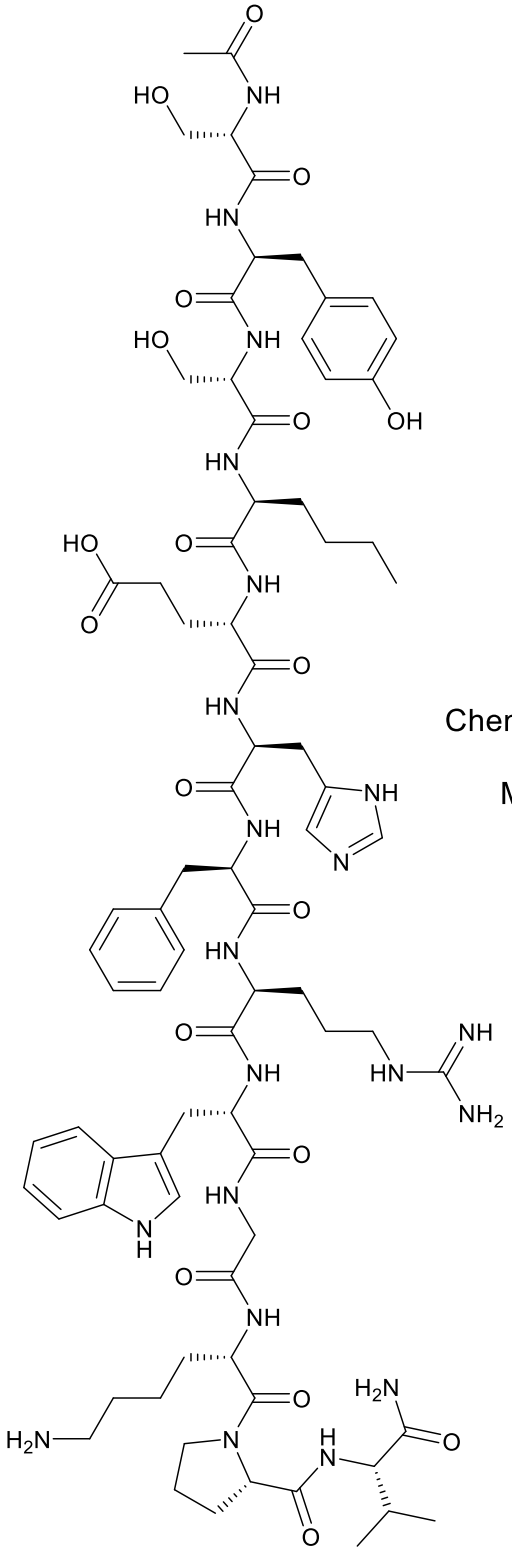

Chemical Formula: $C_{78}H_{111}N_{21}O_{19}$
Exact Mass: 1645,84
Molecular Weight: 1646,87

Afamelanotide (20% v/v Piperidine, 60°C) was obtained as foamy white solid after preparative RP-HPLC (21.6 mg, 16.8%). Analytical RP-HPLC: t_R = 1.43 min (A/D 100:0 to 0:100 in 3.50 min, λ = 214nm). HRMS (ESI+): $C_{78}H_{111}N_{21}O_{19}$ calc./obs. 1646.84/1646.84 Da $[M+H]^+$.

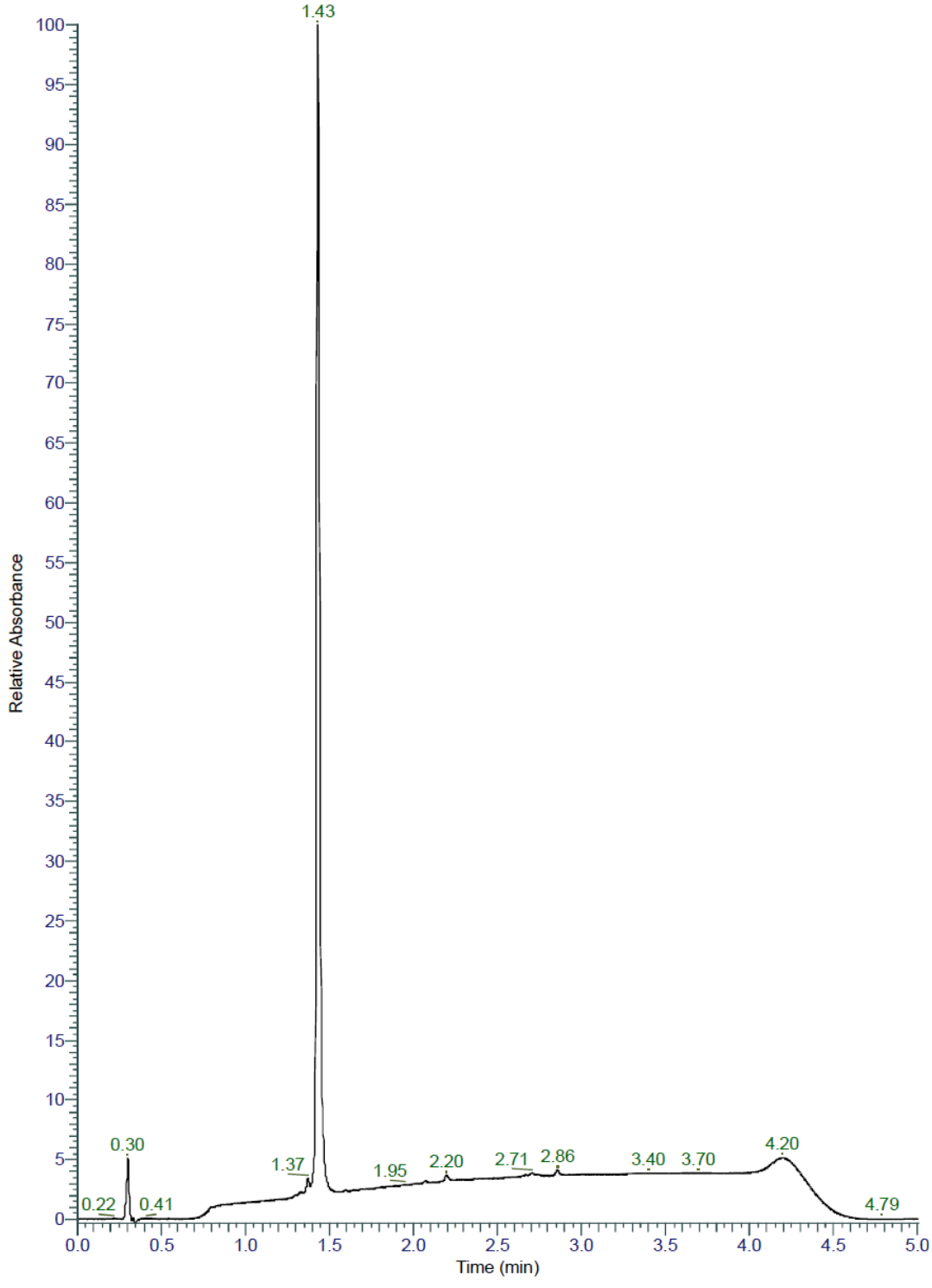

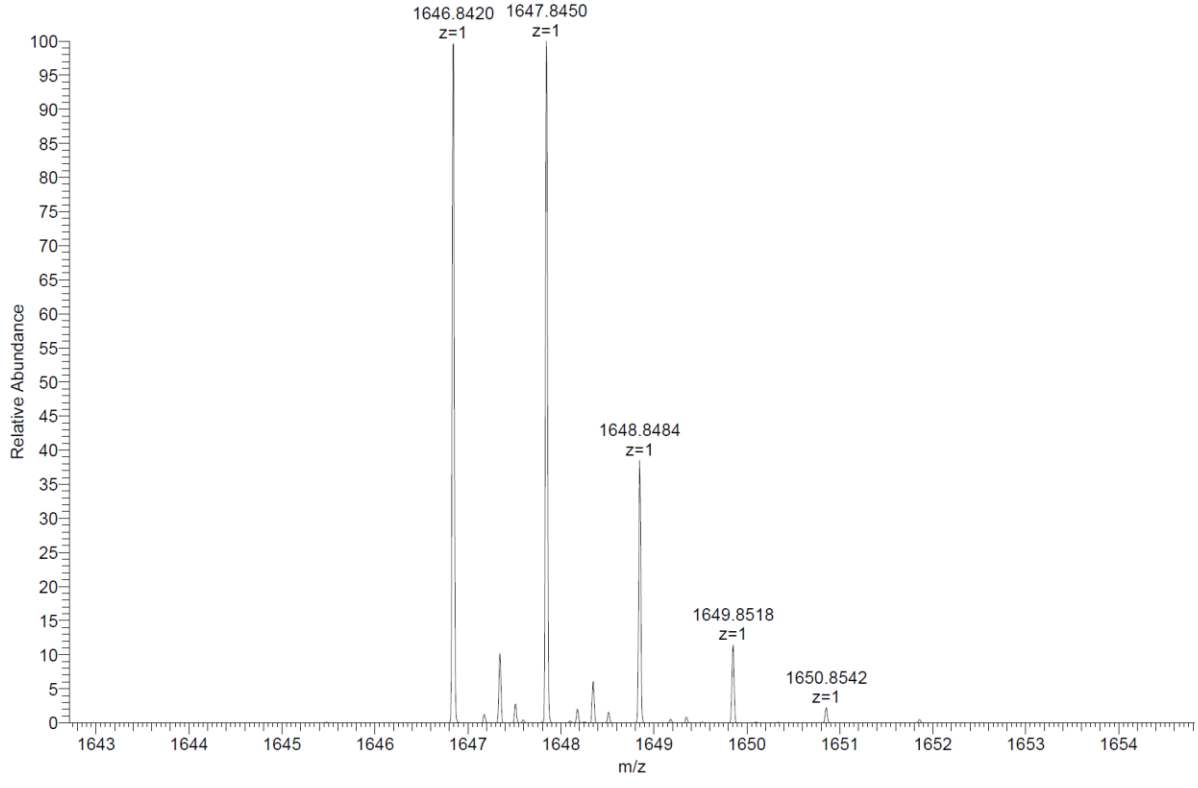
1646.8420
z=1
1647.8450
z=1
1648.8484
z=1
1649.8518
z=1
1650.8542
z=1
Relative Abundance
m/z

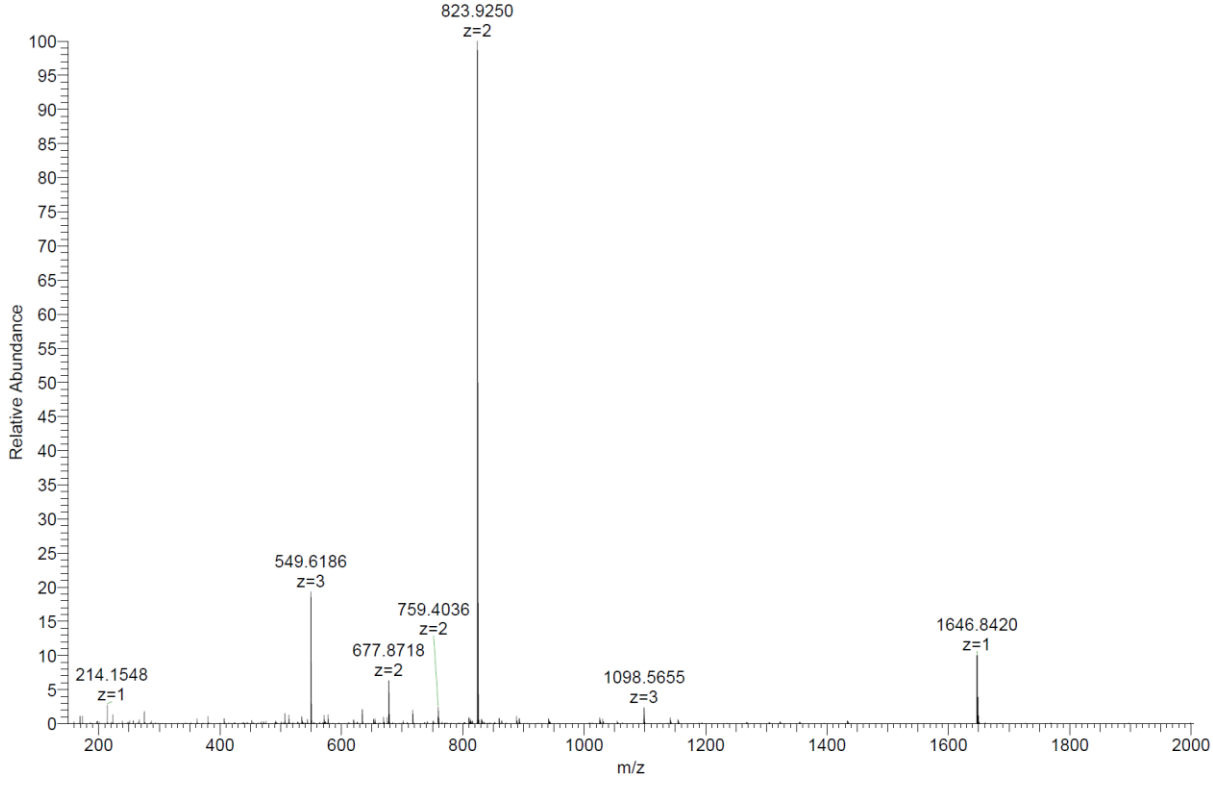
823.9250
z=2
549.6186
z=3
759.4036
z=2
677.8718
z=2
214.1548
z=1
1098.5655
z=3
1646.8420
z=1
Relative Abundance
m/z

Afamelanotide (25% v/v Dipropylamine, 60°C) was obtained as foamy white solid after preparative RP-HPLC (12.7 mg, 9.9%). Analytical RP-HPLC: t_R = 1.44 min (A/D 100:0 to 0:100 in 3.50 min, λ = 214nm). HRMS (ESI+): $C_{78}H_{111}N_{21}O_{19}$ calc./obs. 1646.84/1646.84 Da $[M+H]^+$.

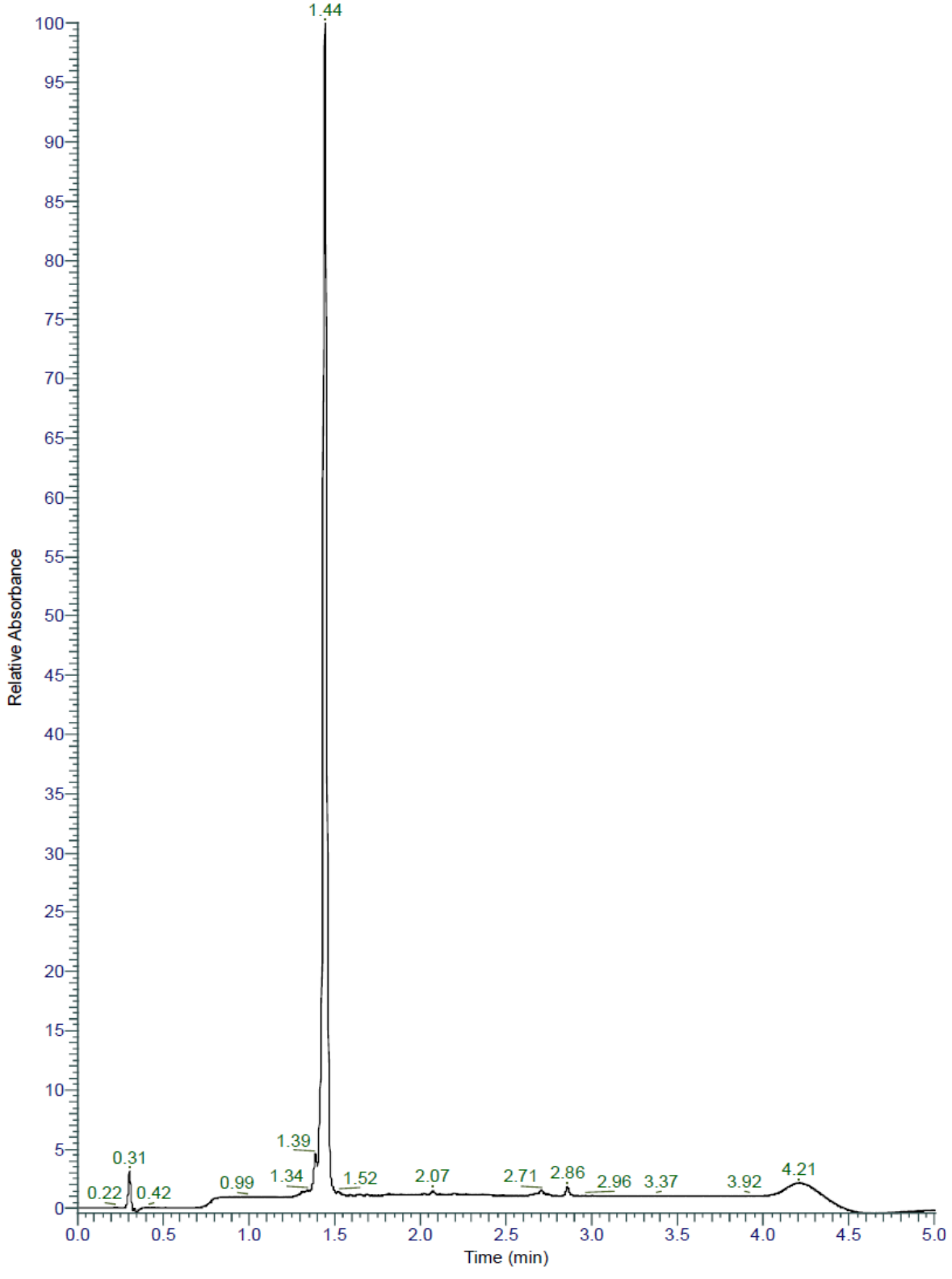

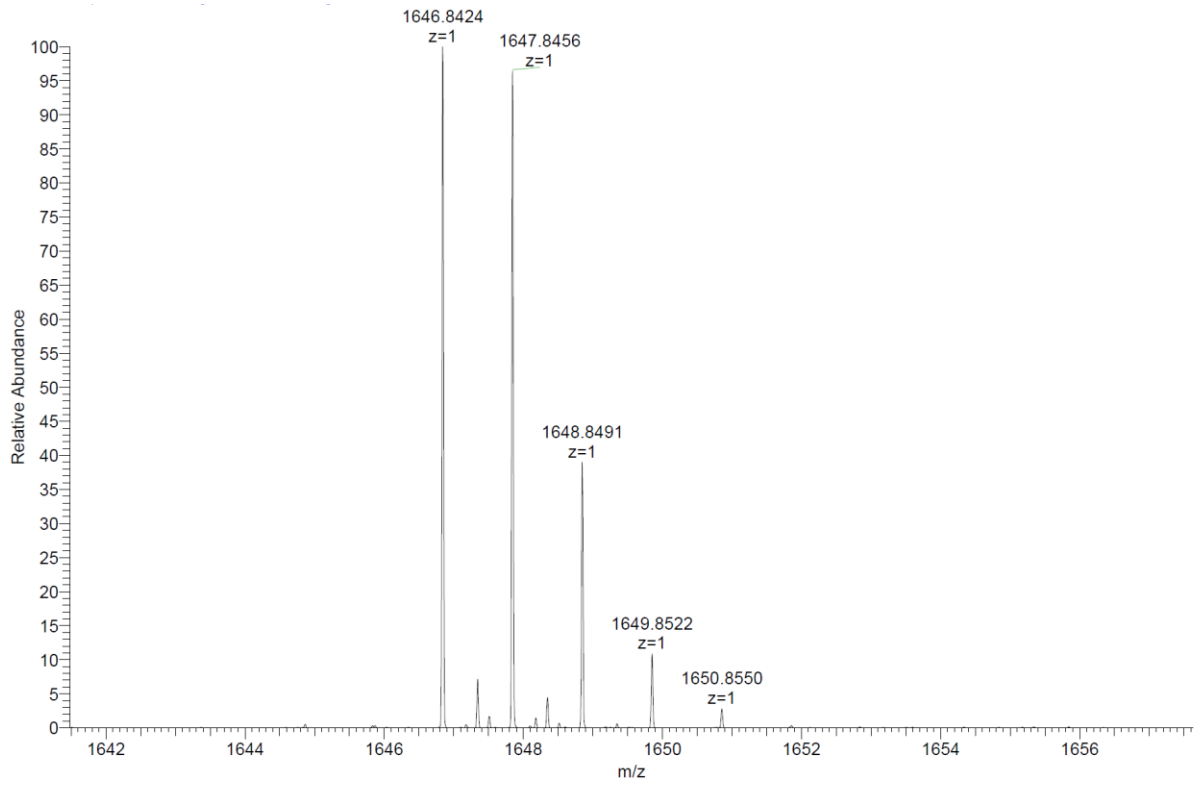
1646.8424
z=1
1647.8456
z=1
1648.8491
z=1
1649.8522
z=1
1650.8550
z=1
Relative Abundance
m/z

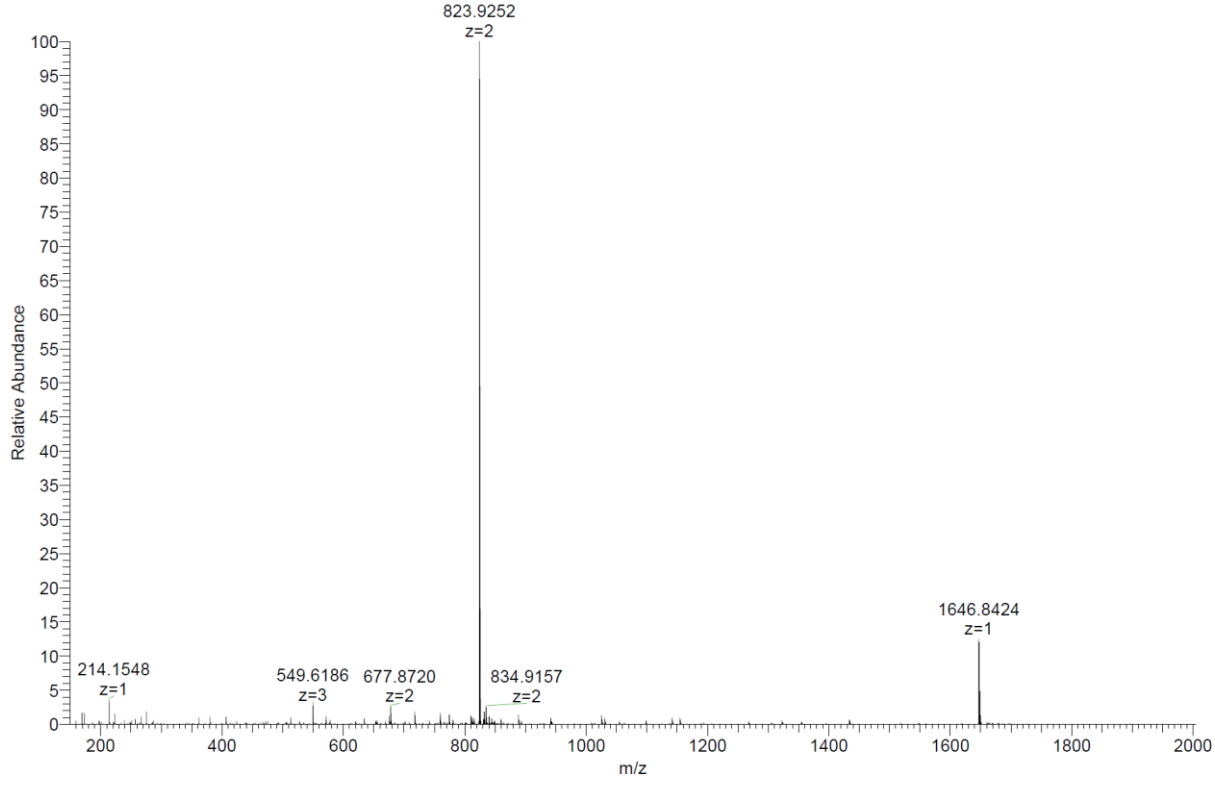
823.9252
z=2
1646.8424
z=1
214.1548
z=1
549.6186
z=3
677.8720
z=2
834.9157
z=2
Relative Abundance
m/z

Bivaluridin (fPRPGGGGNGDFEEIPEEYL-OH)

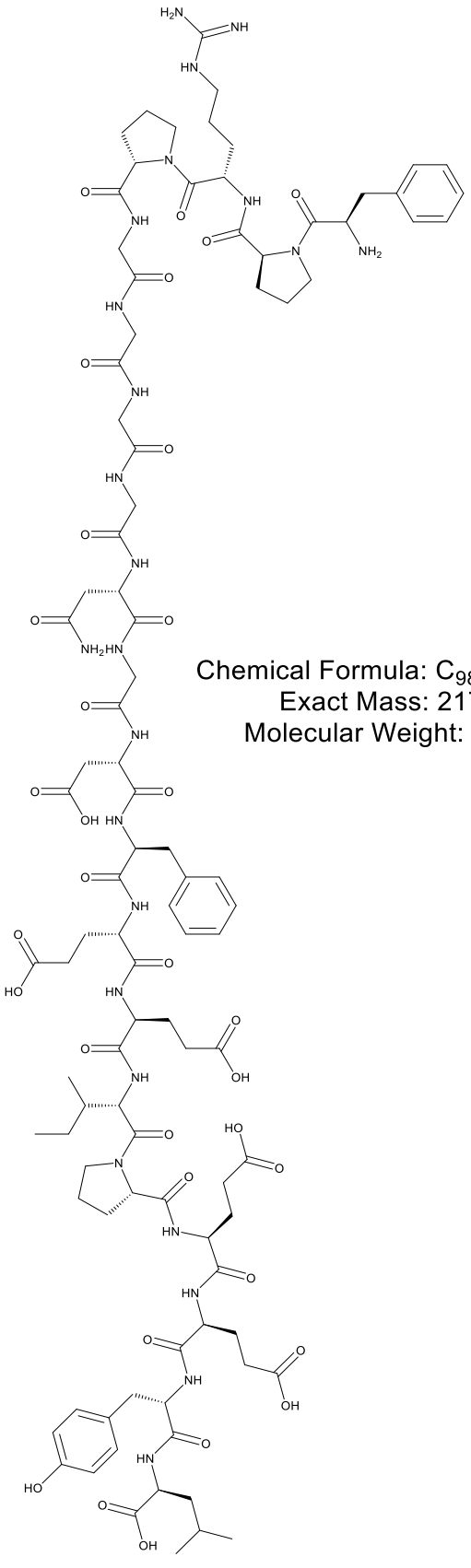

Chemical Formula: $C_{98}H_{138}N_{24}O_{33}$
Exact Mass: 2178,99
Molecular Weight: 2180,32

Bivaluridin (20% v/v Piperidine, 60°C) was obtained as foamy white solid after preparative RP-HPLC (111.6 mg, 46.3%). Analytical RP-HPLC: t_R = 1.52 min (A/D 100:0 to 0:100 in 3.50 min, λ = 214nm). HRMS (ESI+): $C_{98}H_{138}N_{24}O_{33}$ calc./obs. 2179.99/2179.99 Da $[M+H]^+$.

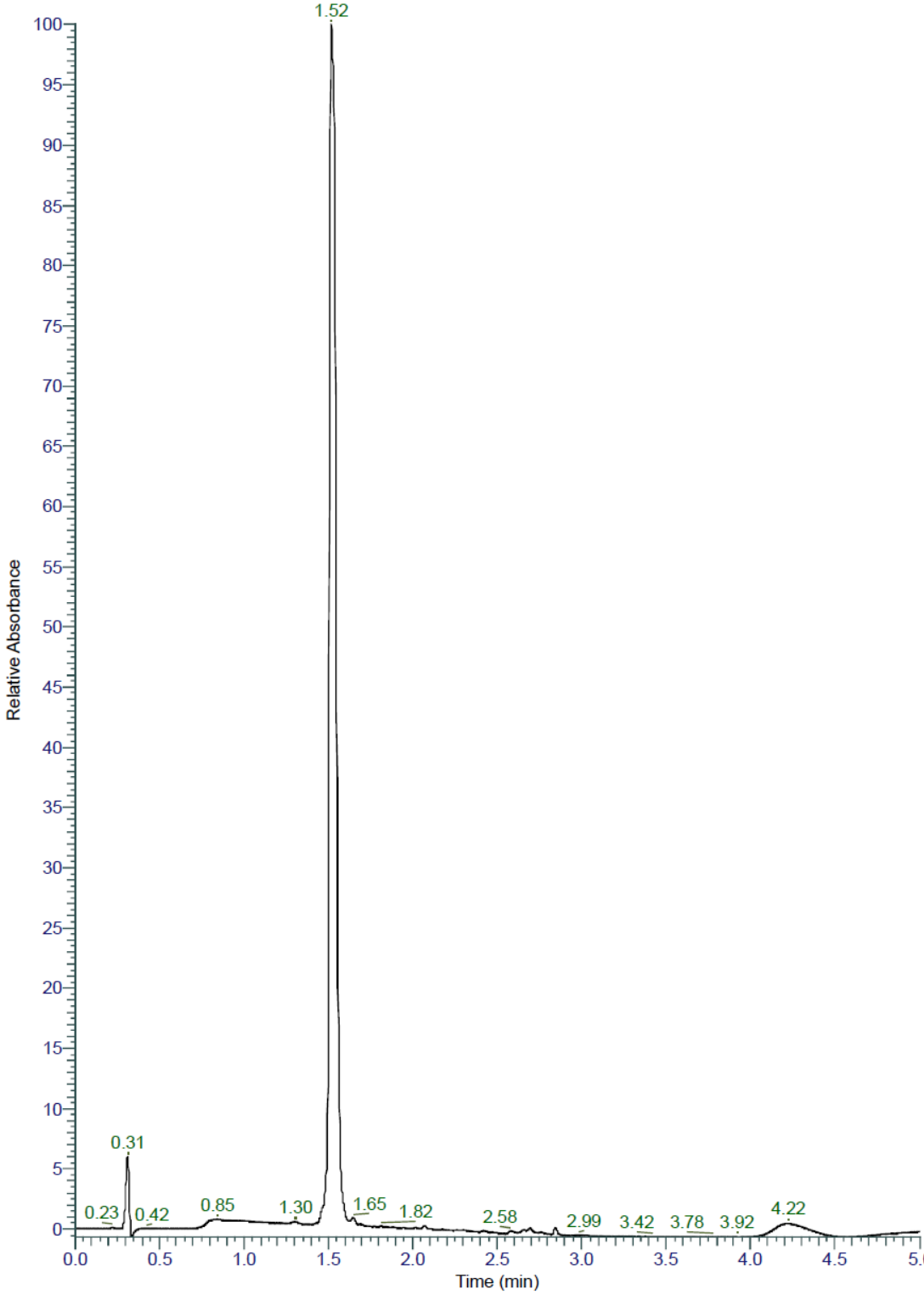

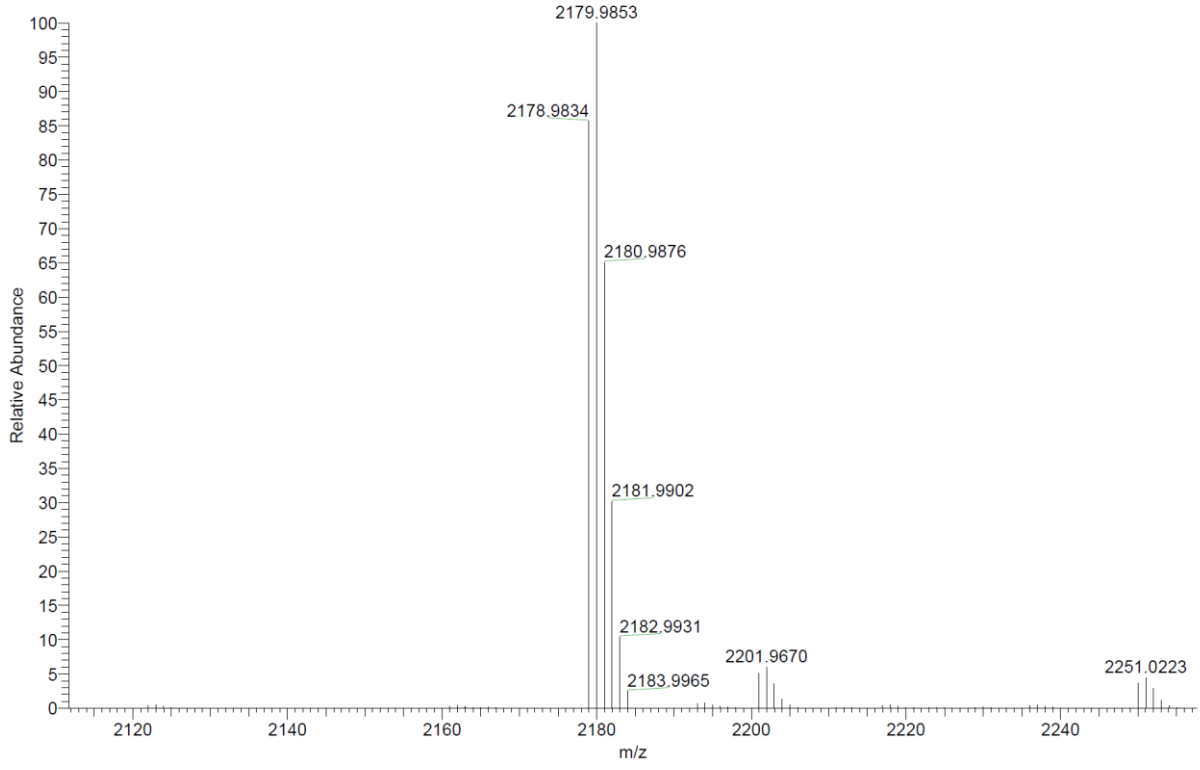
2179.9853
2178.9834
2180.9876
2181.9902
2182.9931
2201.9670
2183.9965
2251.0223
Relative Abundance
m/z

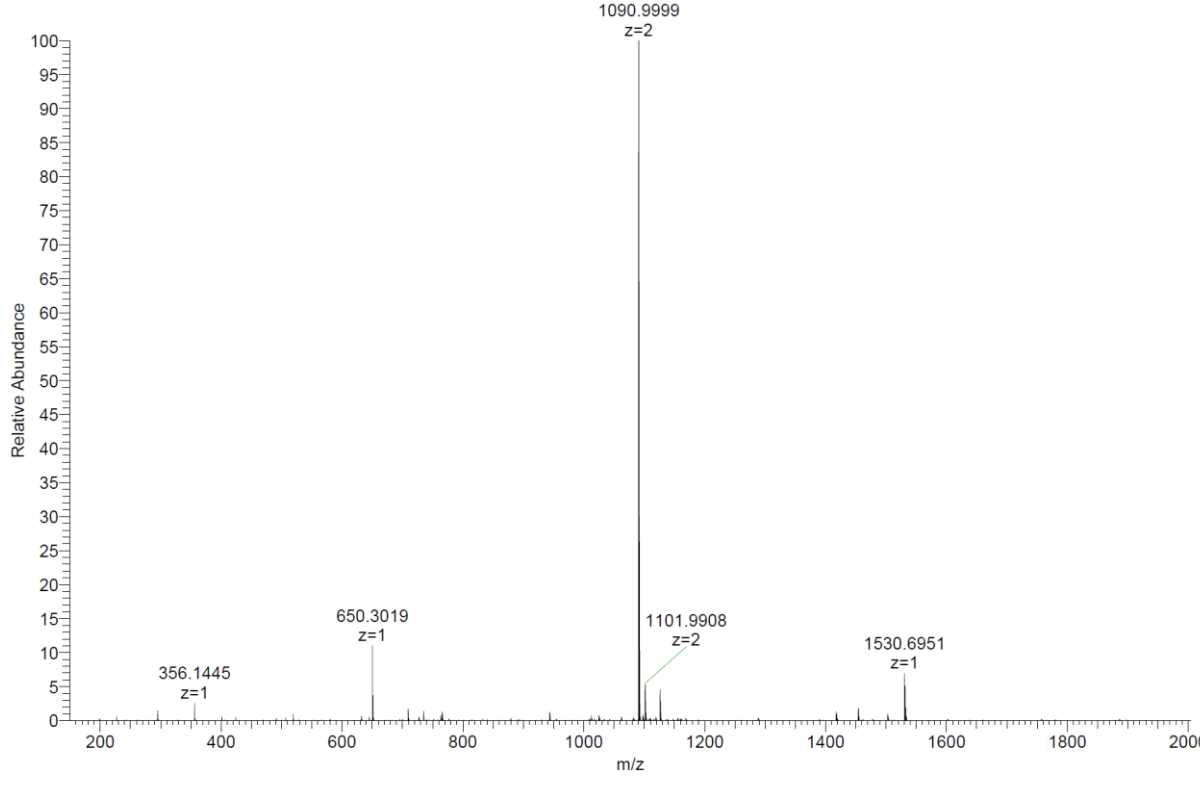
1090.9999
z=2
650.3019
z=1
1101.9908
z=2
1530.6951
z=1
356.1445
z=1
Relative Abundance
m/z

Bivaluridin (25% v/v Dipropylamine, 60°C) was obtained as foamy white solid after preparative RP-HPLC (93.3 mg, 38.7%). Analytical RP-HPLC: t_R = 1.52 min (A/D 100:0 to 0:100 in 3.50 min, λ = 214nm). HRMS (ESI+): $C_{98}H_{138}N_{24}O_{33}$ calc./obs. 2179.99/2179.99 Da $[M+H]^+$.

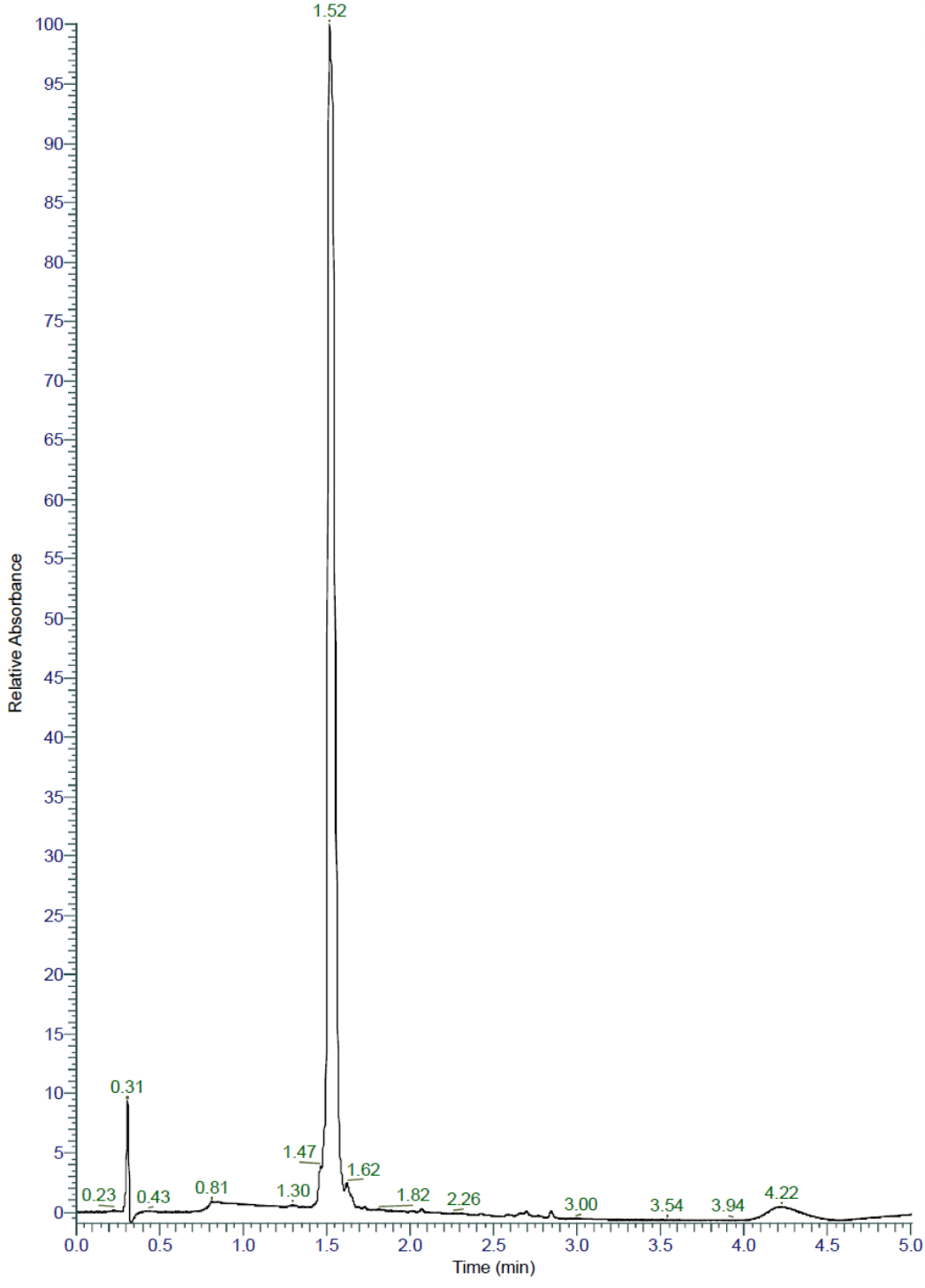

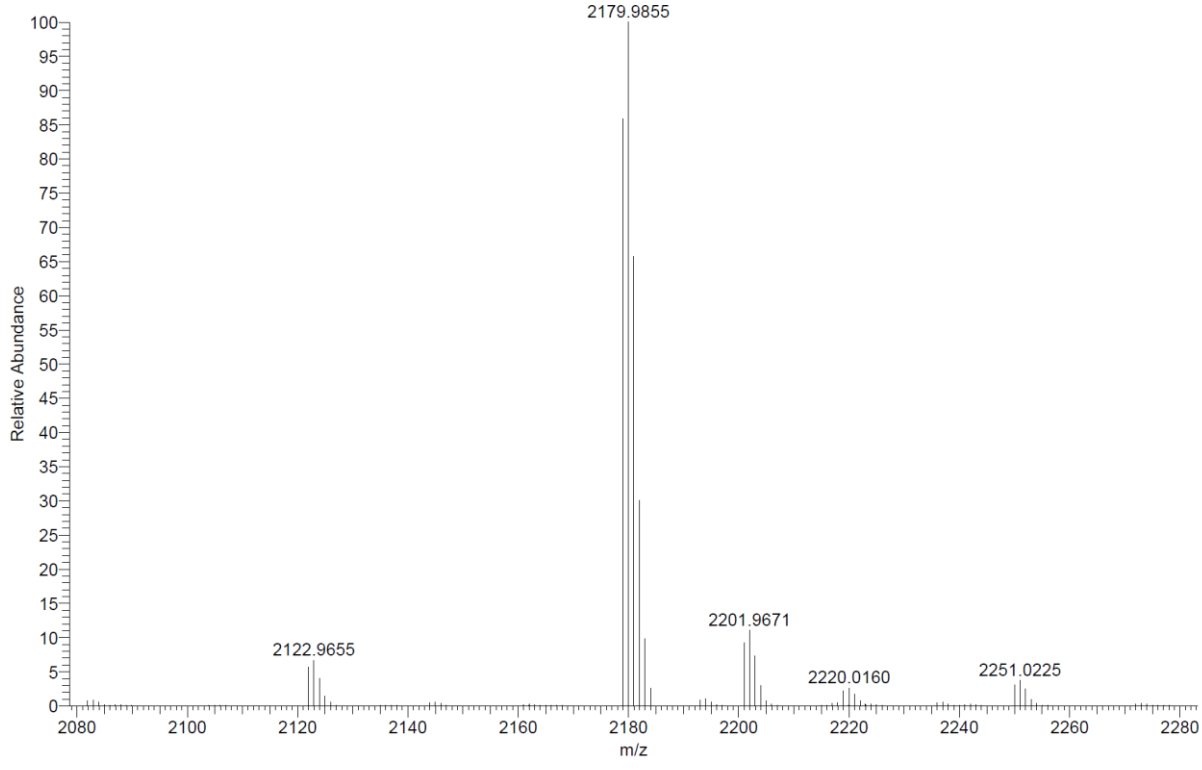
2179.9855
2201.9671
2122.9655
2220.0160
2251.0225
Relative Abundance
m/z

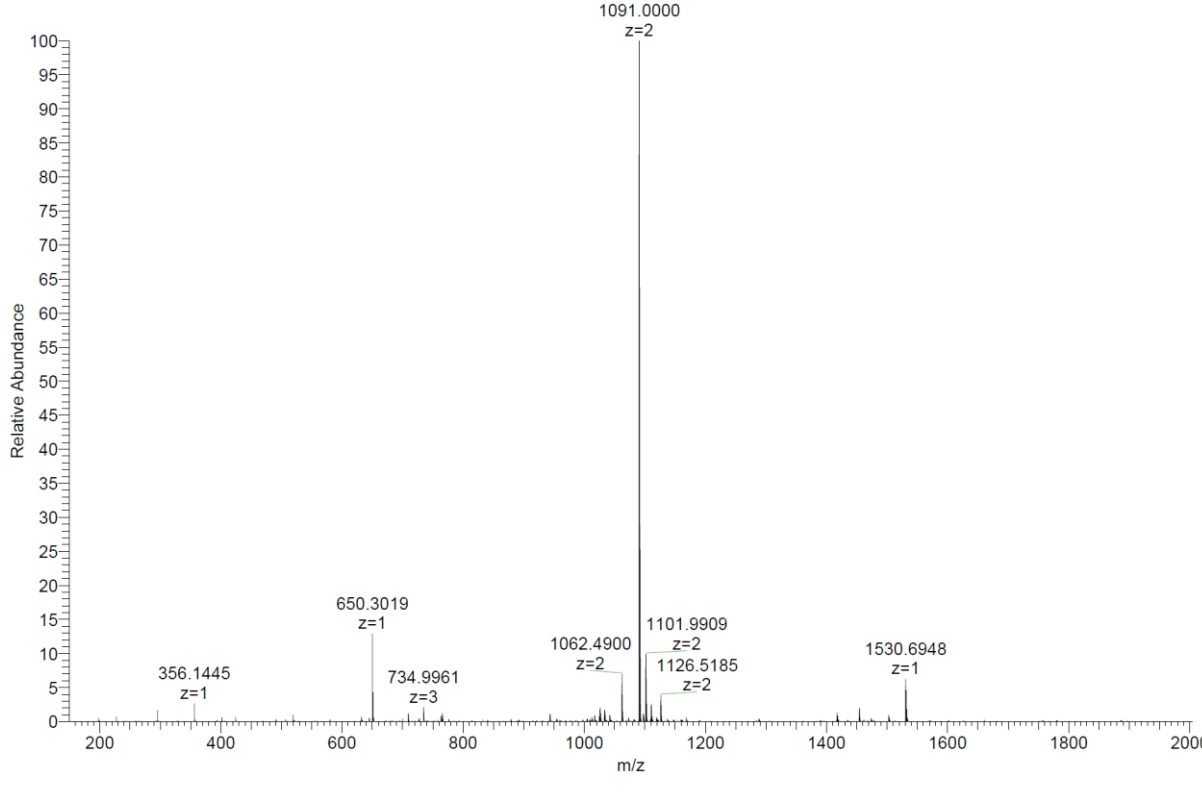
1091.0000
z=2
650.3019
z=1
1101.9909
z=2
1062.4900
z=2
1126.5185
z=2
1530.6948
z=1
356.1445
z=1
734.9961
z=3
Relative Abundance
m/z

Bivaluridin (20% v/v Piperidine, 90°C) was obtained as foamy white solid after lyophilization (57.2 mg, 6.6%). Analytical RP-HPLC: t_R = 3.17 min (A/D 100:0 to 0:100 in 7.00 min, λ = 214nm). HRMS (ESI+): $C_{98}H_{138}N_{24}O_{33}$ calc./obs. 2179.99/2179.99 Da $[M+H]^+$.

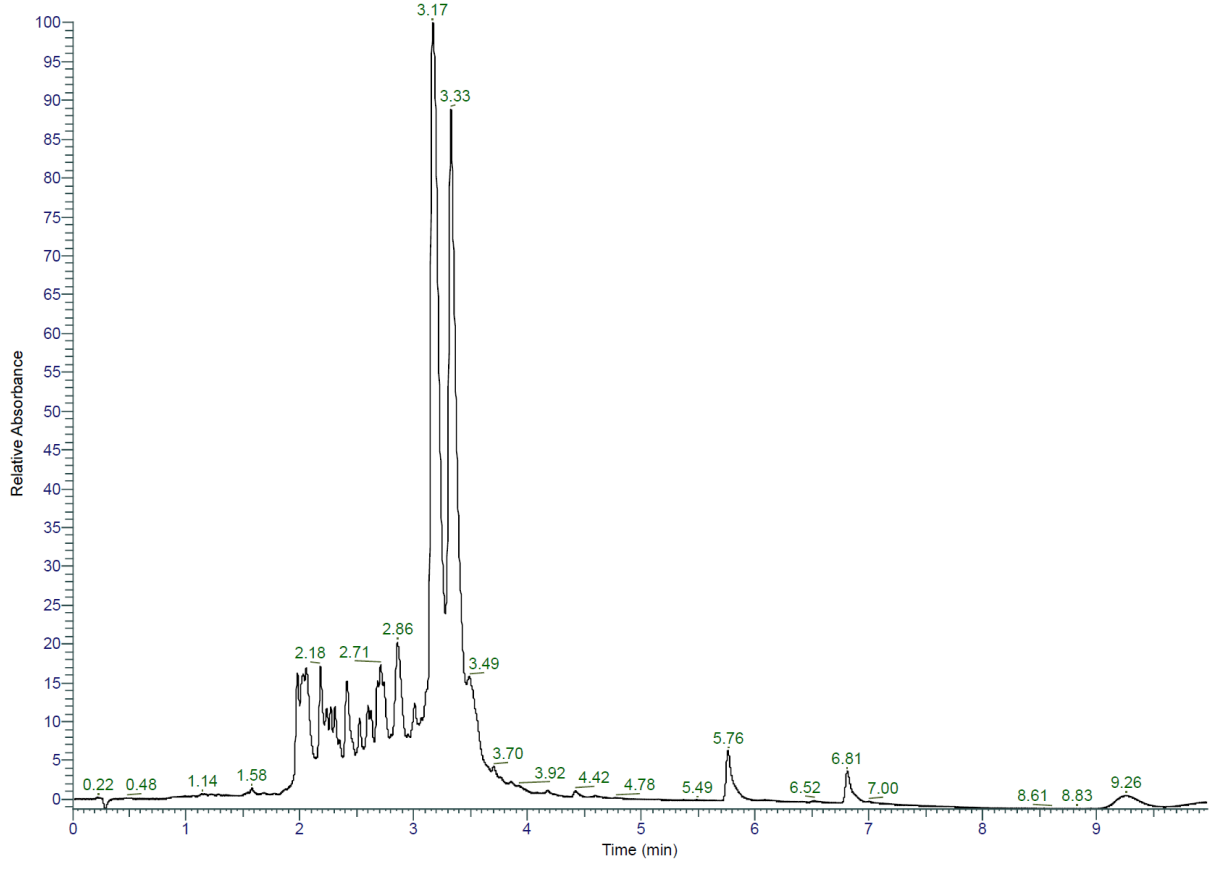

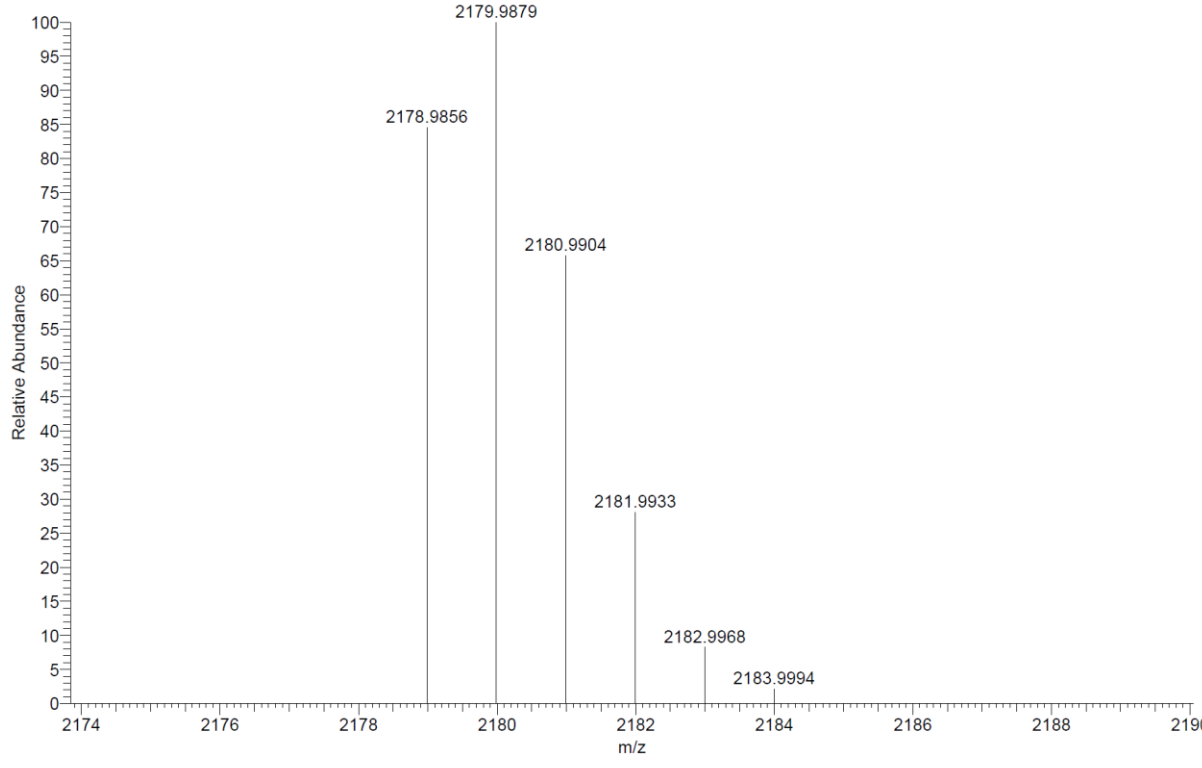
2179.9879
2178.9856
2180.9904
2181.9933
2182.9968
2183.9994
Relative Abundance
m/z
100
95
90
85
80
75
70
65
60
55
50
45
40
35
30
25
20
15
10
5
0
2174
2176
2178
2180
2182
2184
2186
2188
2190

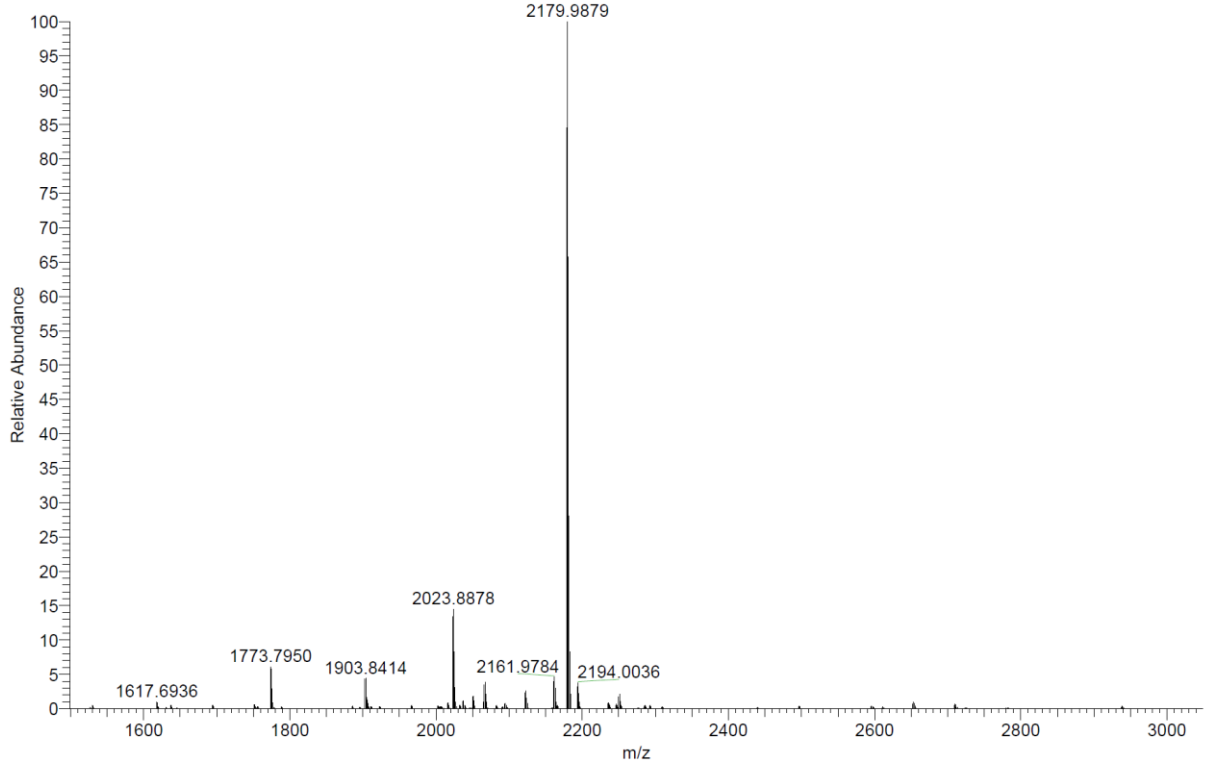
2179.9879
2023.8878
1773.7950
1903.8414
2161.9784
2194.0036
1617.6936
Relative Abundance
m/z
100
95
90
85
80
75
70
65
60
55
50
45
40
35
30
25
20
15
10
5
0
1600
1800
2000
2200
2400
2600
2800
3000

Bivaluridin (25% v/v Dipropylamine, 90°C) was obtained as foamy white solid after lyophilization (39.5 mg, 4.6%). Analytical RP-HPLC: t_R = 3.19 min (A/D 100:0 to 0:100 in 7.00 min, λ = 214nm). HRMS (ESI+): $C_{98}H_{138}N_{24}O_{33}$ calc./obs. 2179.99/2179.99 Da $[M+H]^+$.

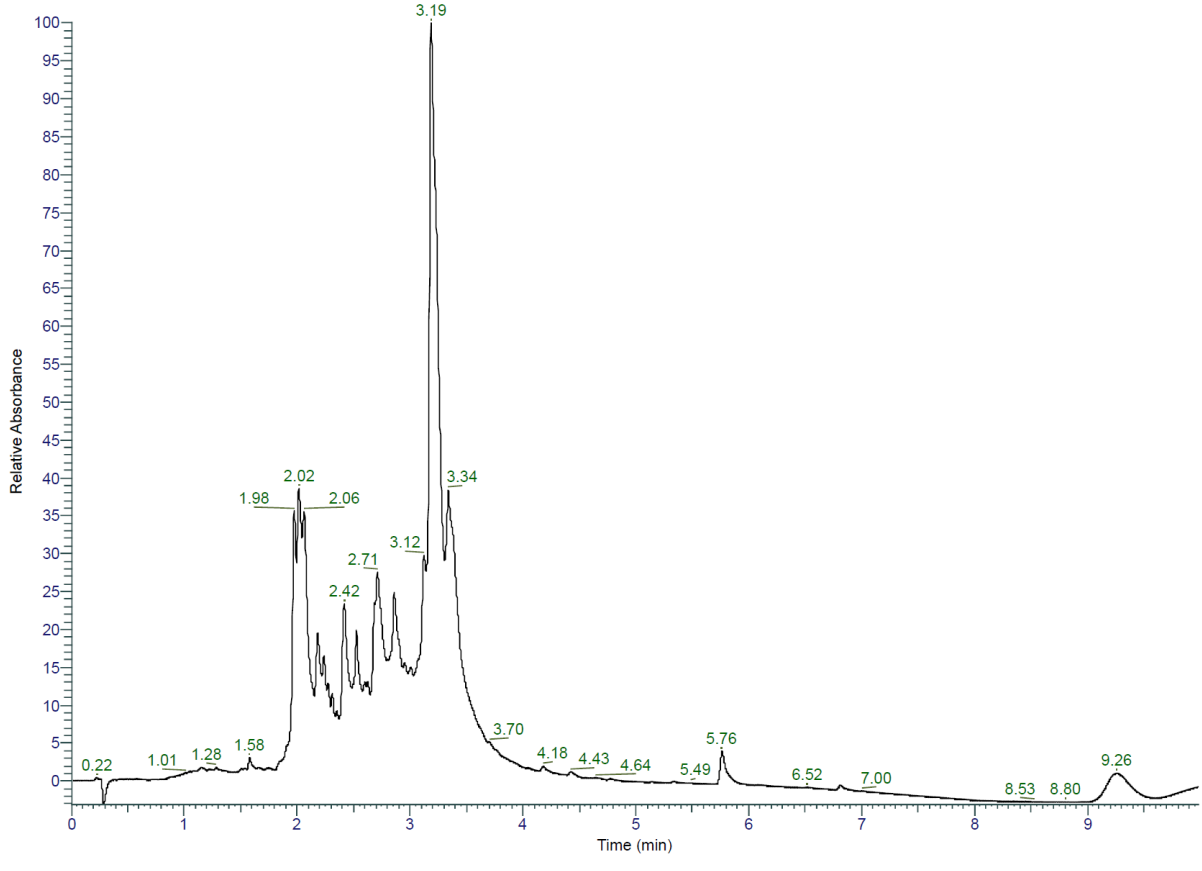

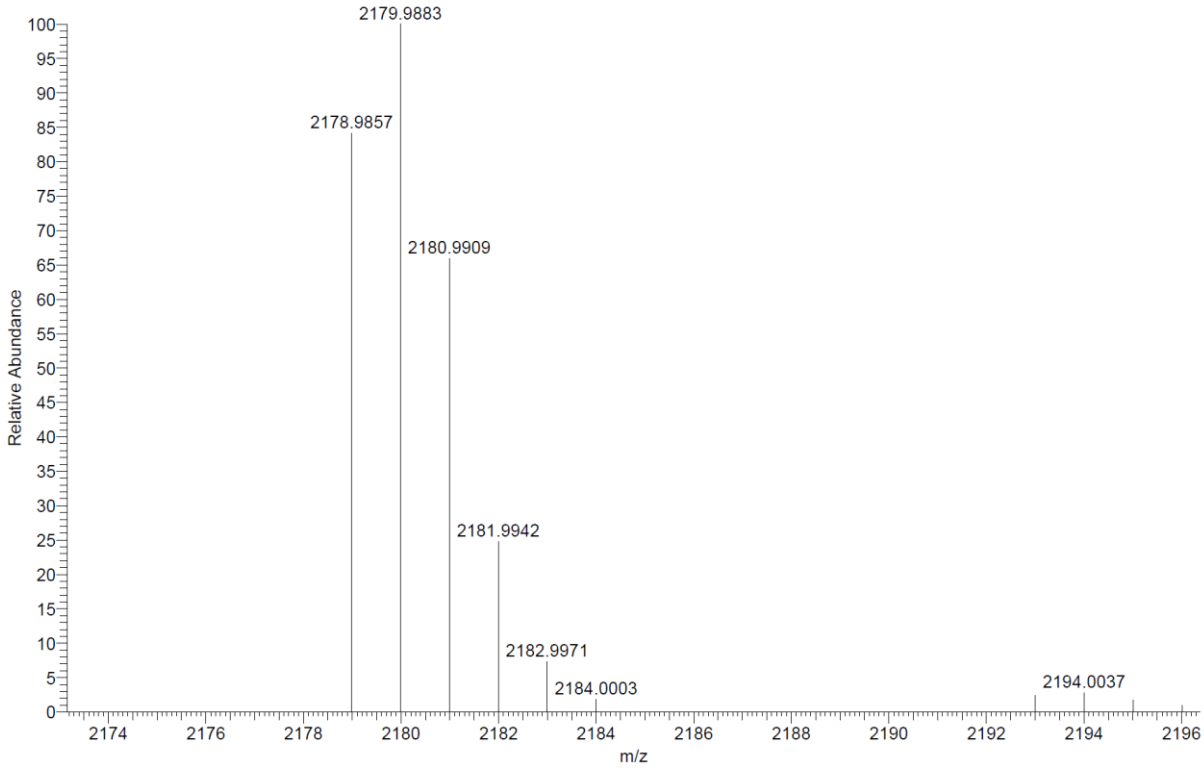
2179.9883
2178.9857
2180.9909
2181.9942
2182.9971
2184.0003
2194.0037
Relative Abundance
m/z

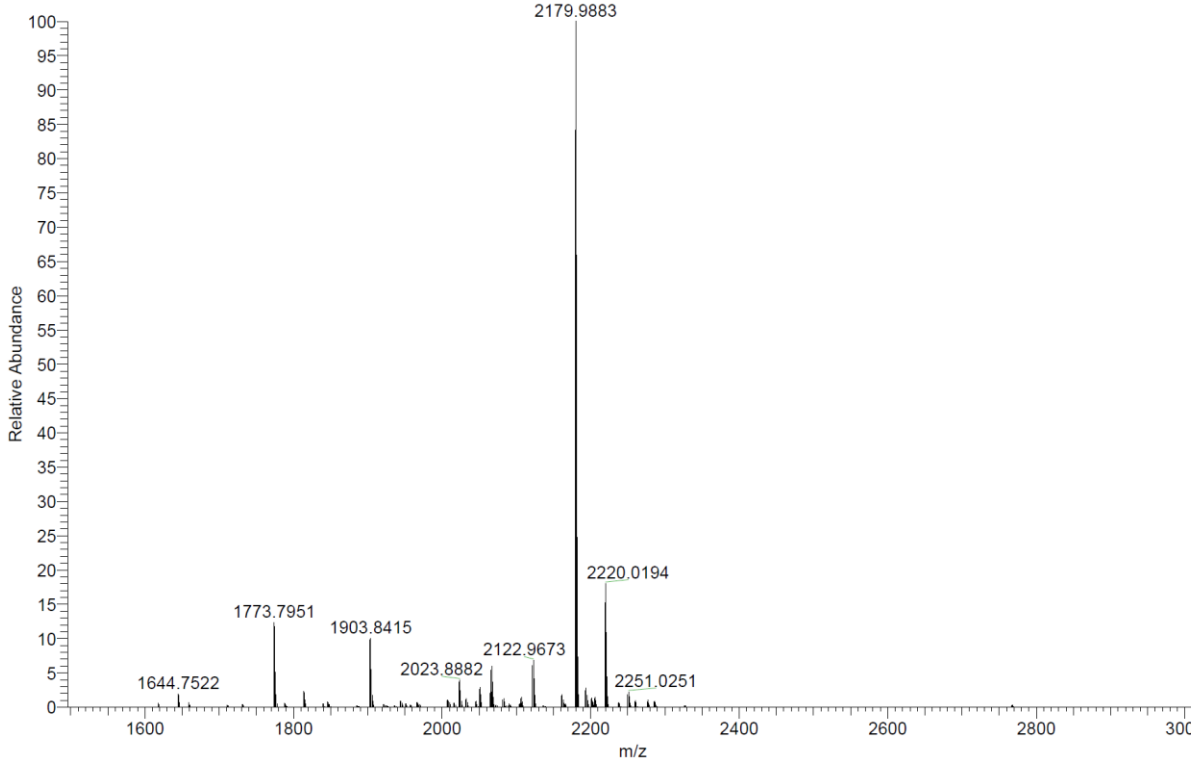
2179.9883
2220.0194
1773.7951
1903.8415
2122.9673
2023.8882
1644.7522
2251.0251
Relative Abundance
m/z

G1KL ((KL)$_2$*K*KL)

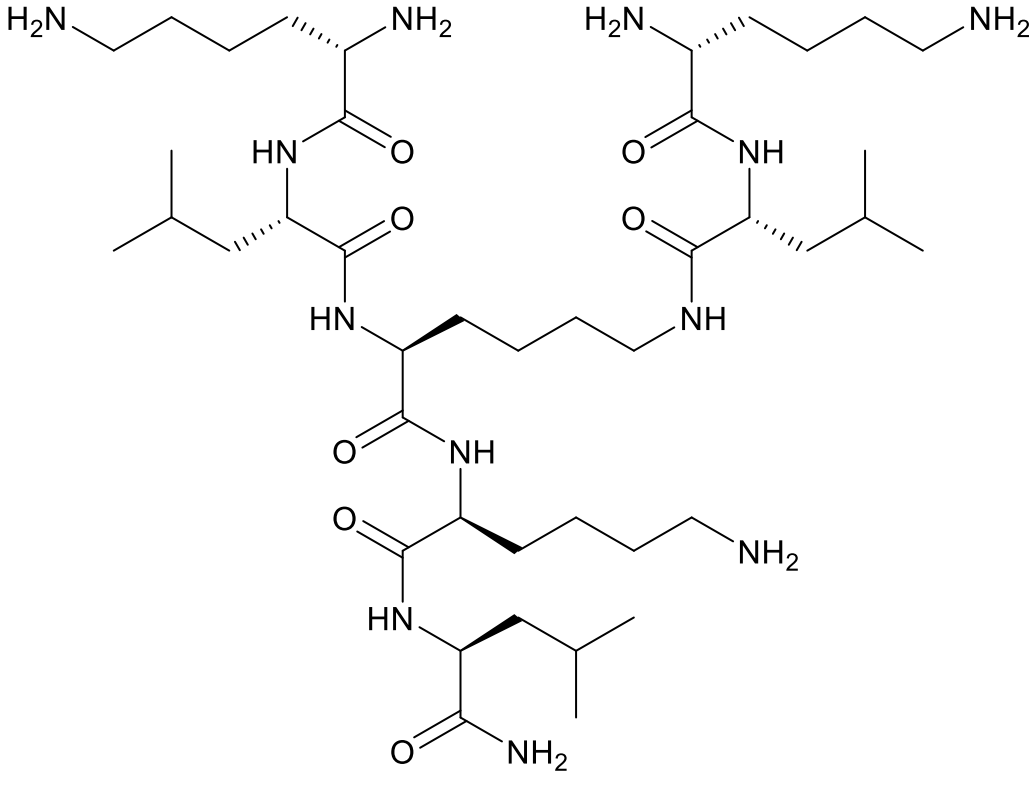

Chemical Formula: $C_{42}H_{84}N_{12}O_7$
Exact Mass: 868,66
Molecular Weight: 869,21

G1KL (20% v/v Piperidine, 60°C) was obtained as crude white solid after lyophilization (90.5 mg, 72.5%). Analytical RP-HPLC: t_R = 2.11 min (A/D 100:0 to 0:100 in 7.00 min, λ = 214nm). HRMS (ESI+): $C_{42}H_{84}N_{12}O_7$ calc./obs. 869.66/869.66 Da $[M+H]^+$.

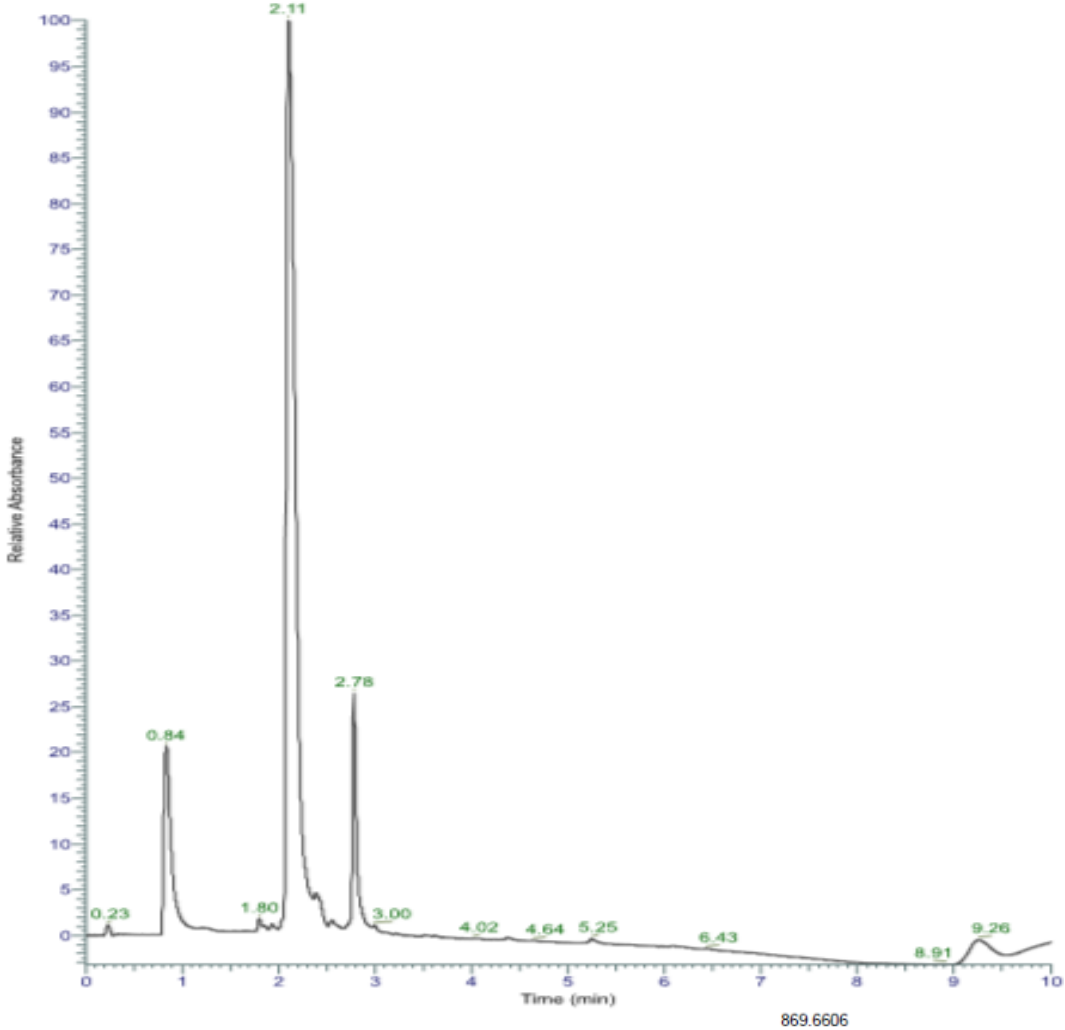

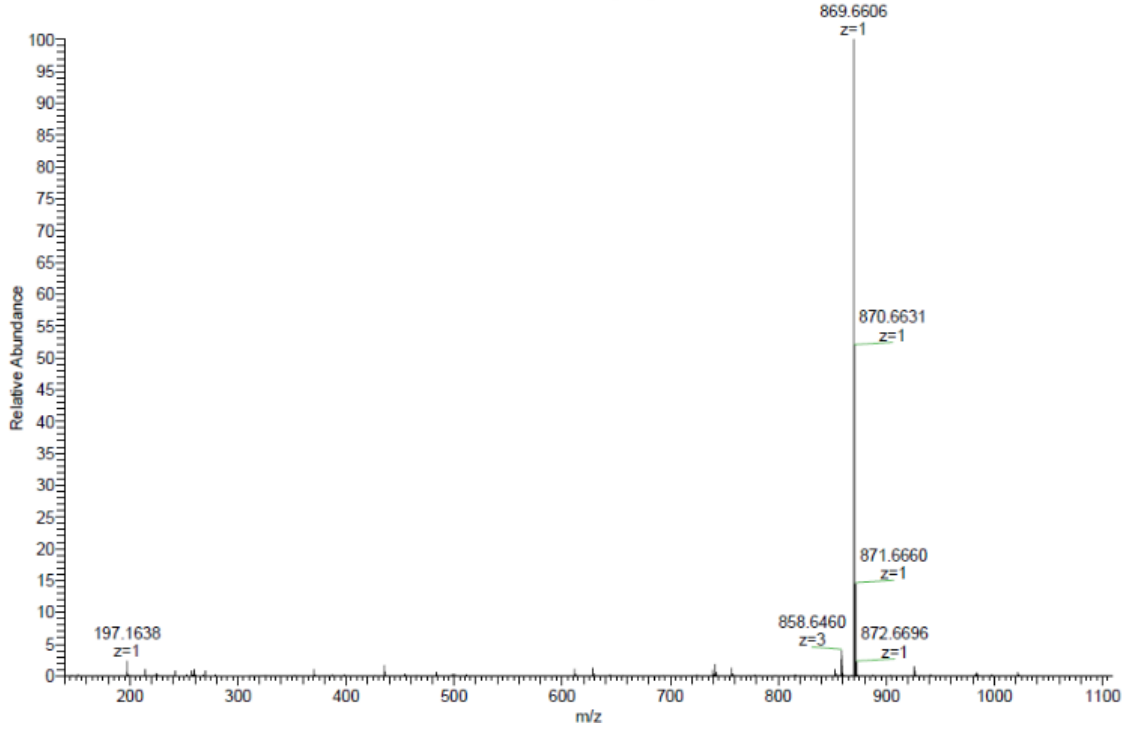

G1KL (5% w/v Piperazine + 2% v/v DBU, 60°C) was obtained as crude white solid after lyophilization (30.4 mg, 26.2%). Analytical RP-HPLC: t_R = 1.85 min (A/D 100:0 to 0:100 in 7.00 min, λ = 214nm). HRMS (ESI+): $C_{42}H_{84}N_{12}O_7$ calc./obs. 869.66/869.66 Da $[M+H]^+$.

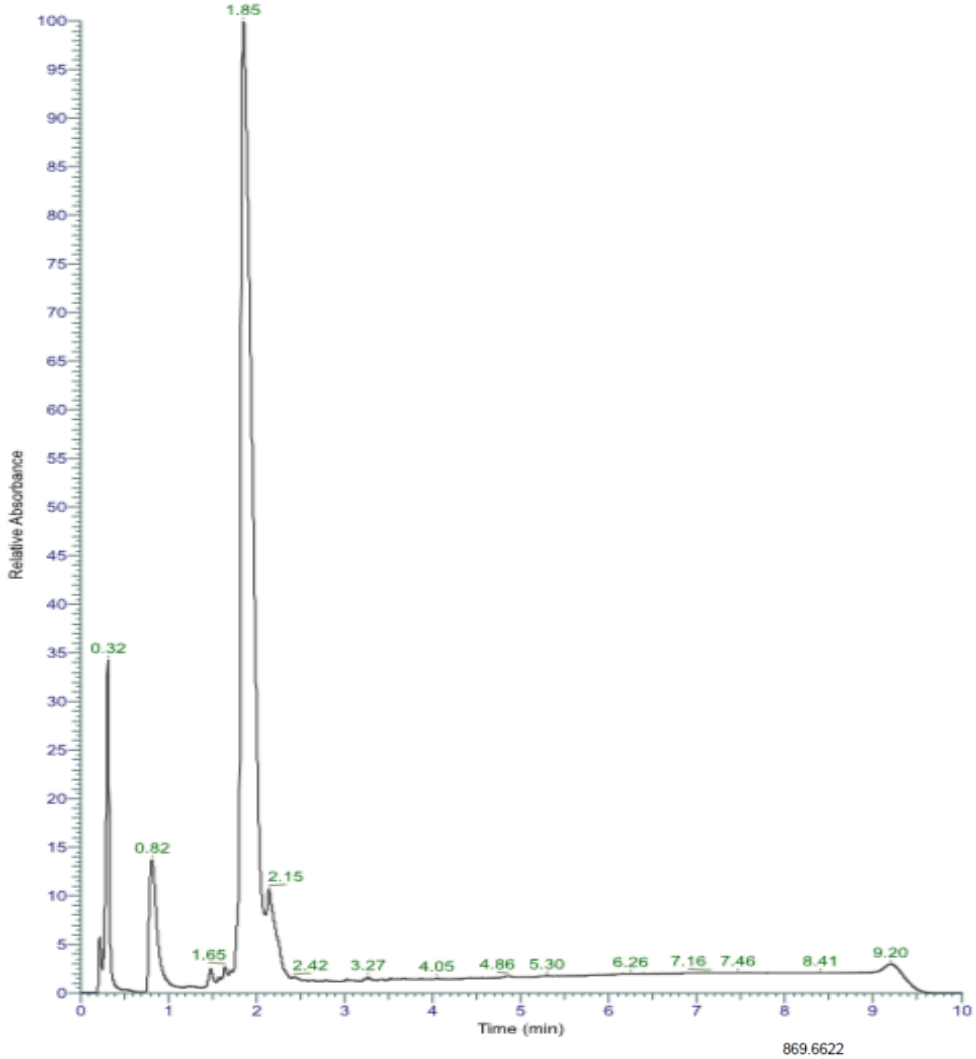

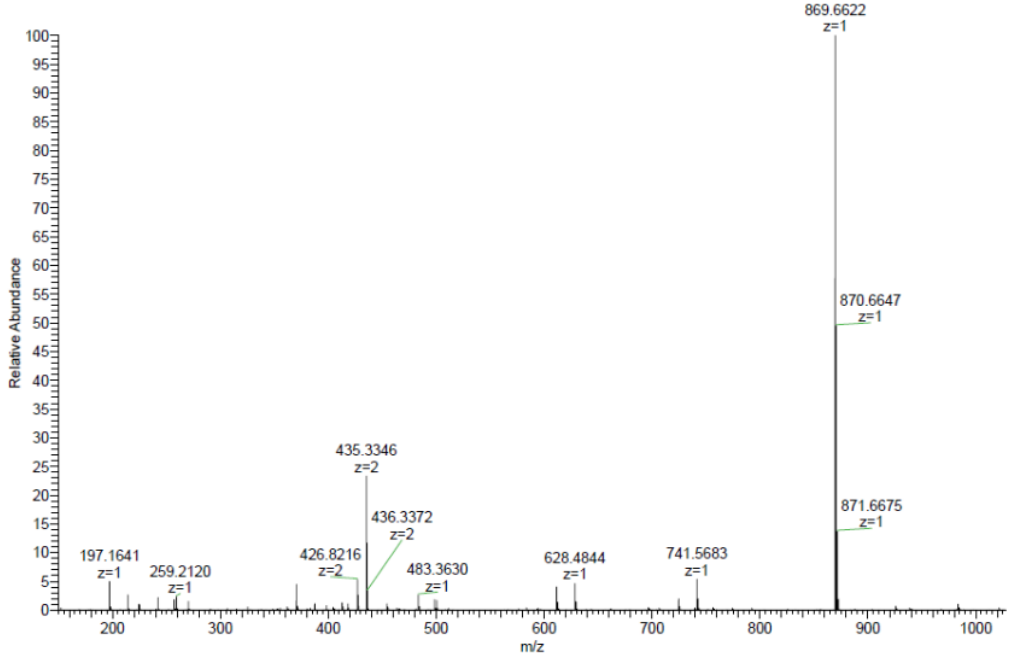

G1KL (20% v/v Diisopropylamine, 60°C) was obtained as crude white solid after lyophilization (0.3 mg, 0.0%). Analytical RP-HPLC: t_R = - min (A/D 100:0 to 0:100 in 7.00 min, λ = 214nm). HRMS (ESI+): $C_{42}H_{84}N_{12}O_7$ calc./obs. 869.66/869.66 Da $[M+H]^+$.

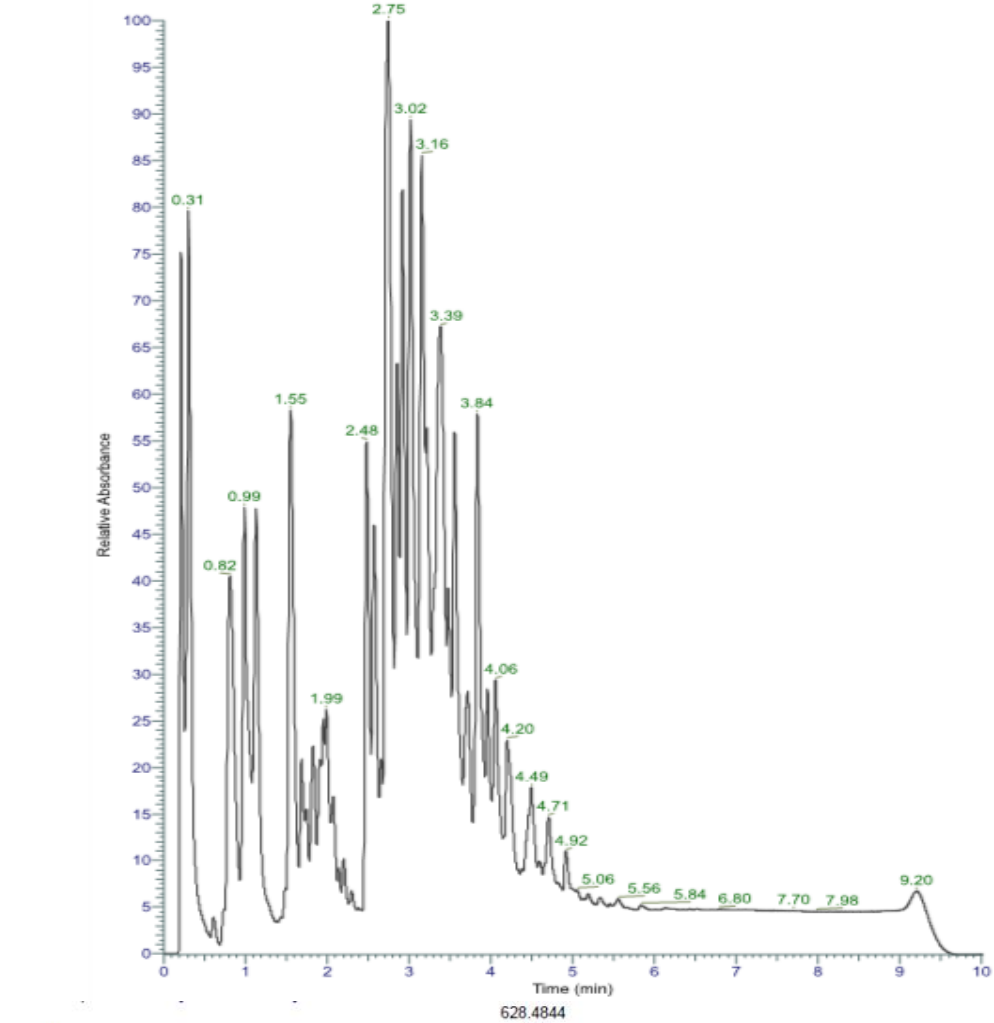

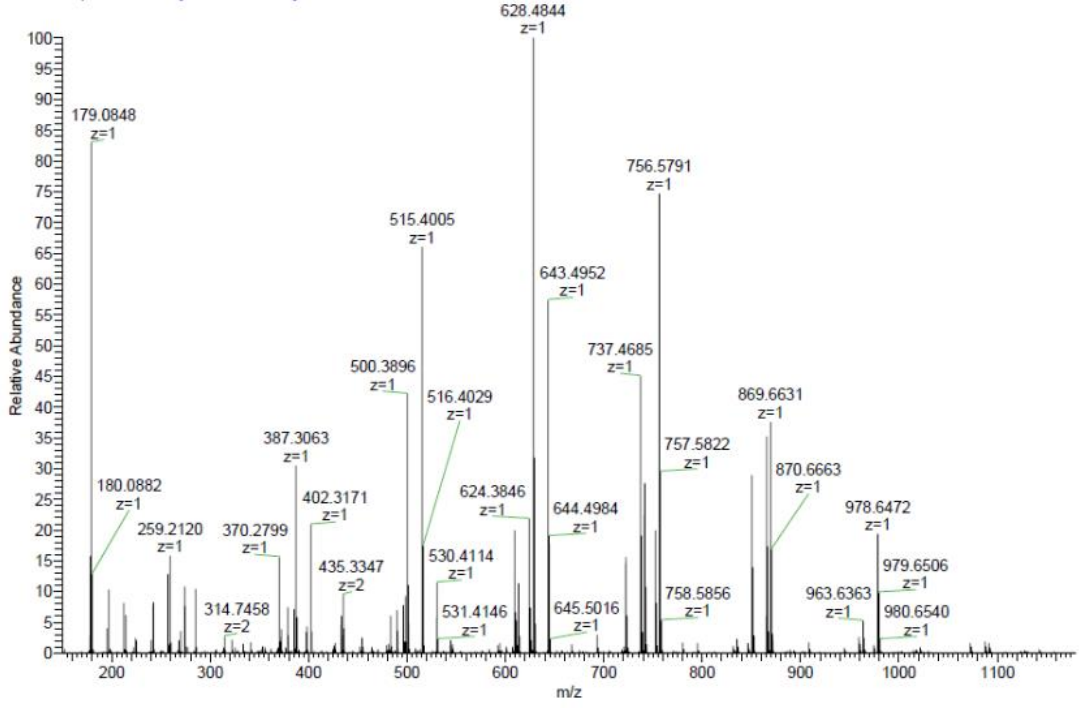

G1KL (20% v/v Diisopropylamine + 1% v/v DBU, 60°C) was obtained as crude white solid after lyophilization (38.8 mg, 35.6%). Analytical RP-HPLC: t_R = 1.81 min (A/D 100:0 to 0:100 in 7.00 min, λ = 214nm). HRMS (ESI+): $C_{42}H_{84}N_{12}O_7$ calc./obs. 869.66/869.66 Da $[M+H]^+$.

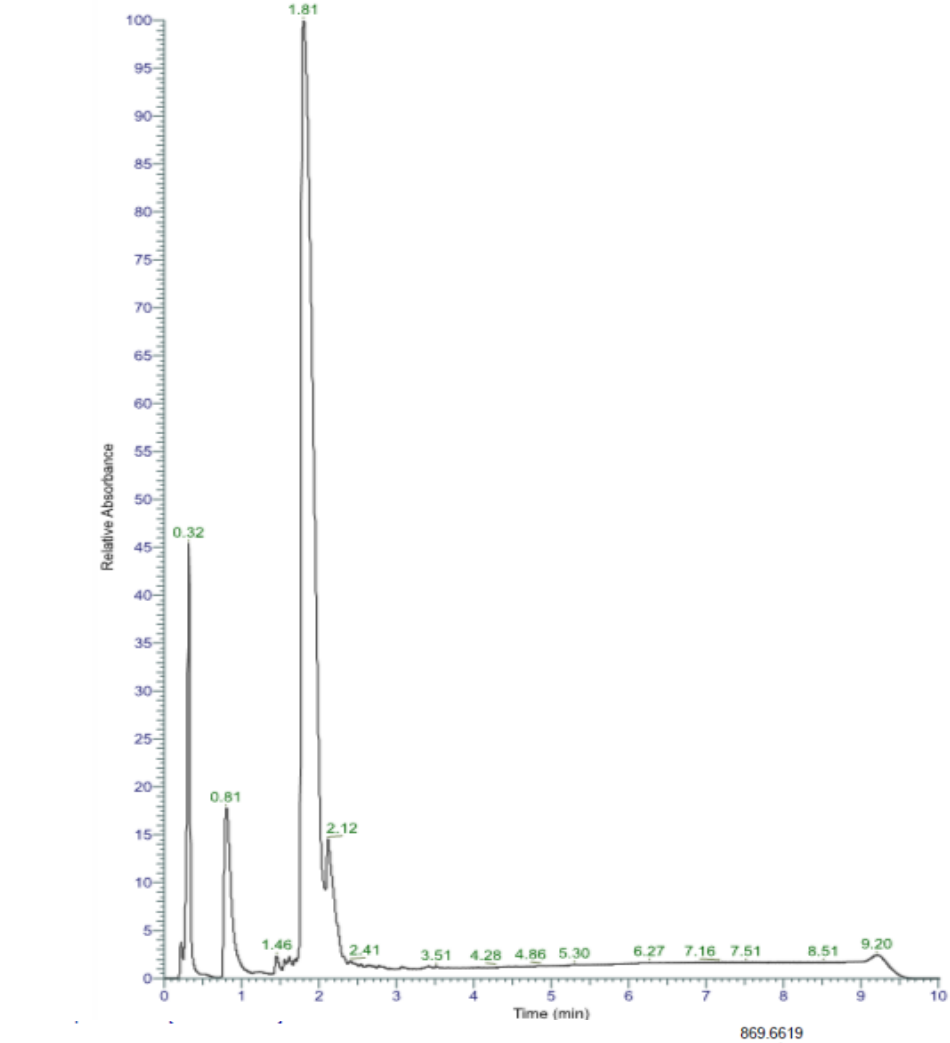

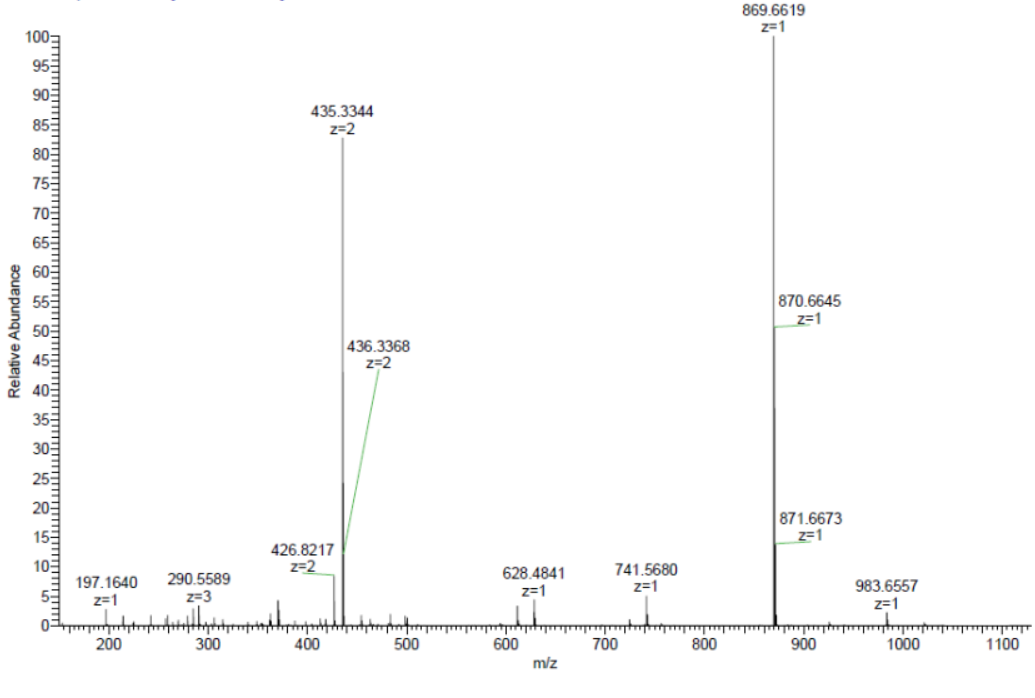

G1KL (20% v/v Dipropylamine, 60°C) was obtained as crude white solid after lyophilization (42.2 mg, 35.2%). Analytical RP-HPLC: t_R = 1.79 min (A/D 100:0 to 0:100 in 7.00 min, λ = 214nm). HRMS (ESI+): $C_{42}H_{84}N_{12}O_7$ calc./obs. 869.66/869.66 Da $[M+H]^+$.

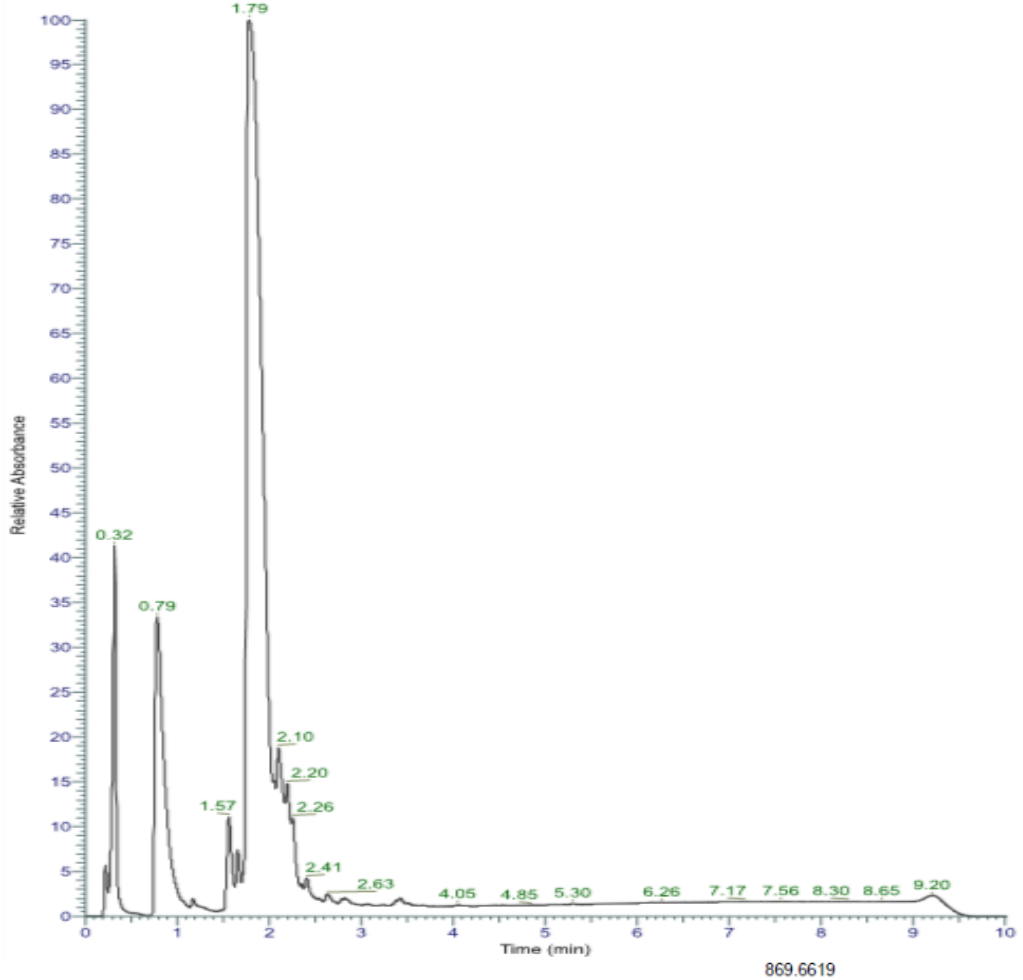

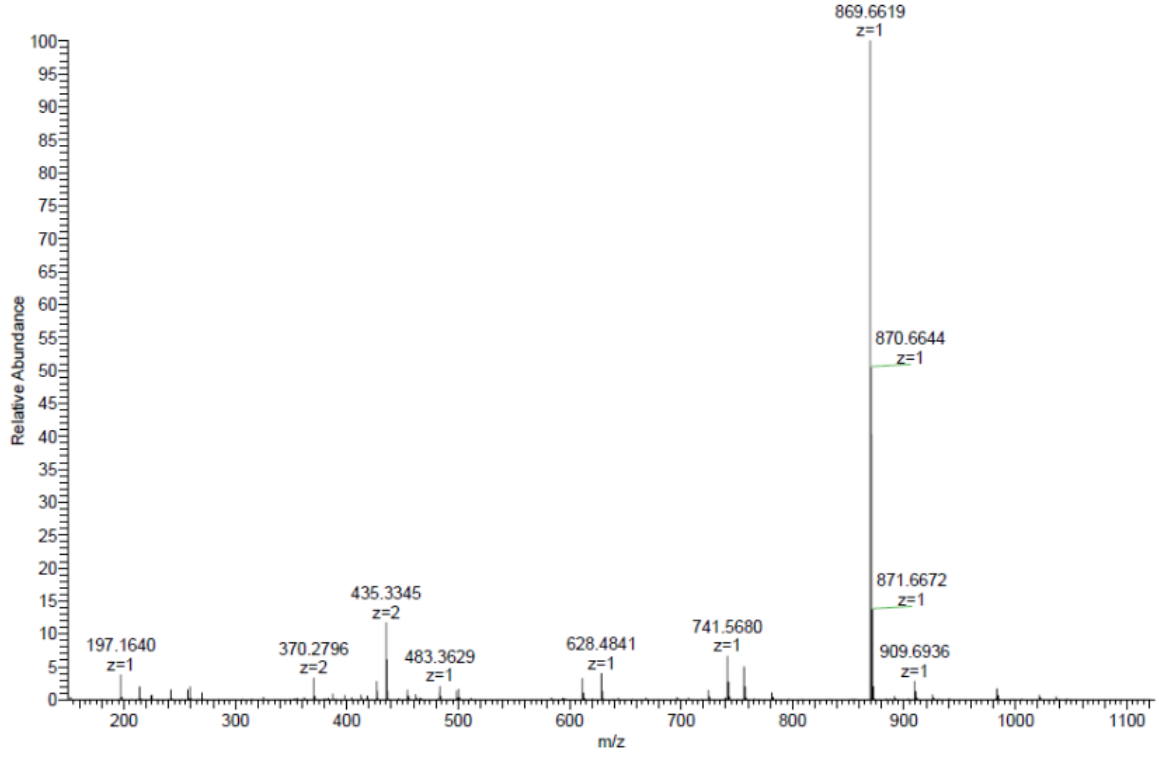

G1KL (20 v/v Dipropylamine + 1% v/v DBU, 60°C) was obtained as crude white solid after lyophilization (37.4 mg, 34.0%). Analytical RP-HPLC: t_R = 1.83 min (A/D 100:0 to 0:100 in 7.00 min, λ = 214nm). HRMS (ESI+): $C_{42}H_{84}N_{12}O_7$ calc./obs. 869.66/869.66 Da $[M+H]^+$.

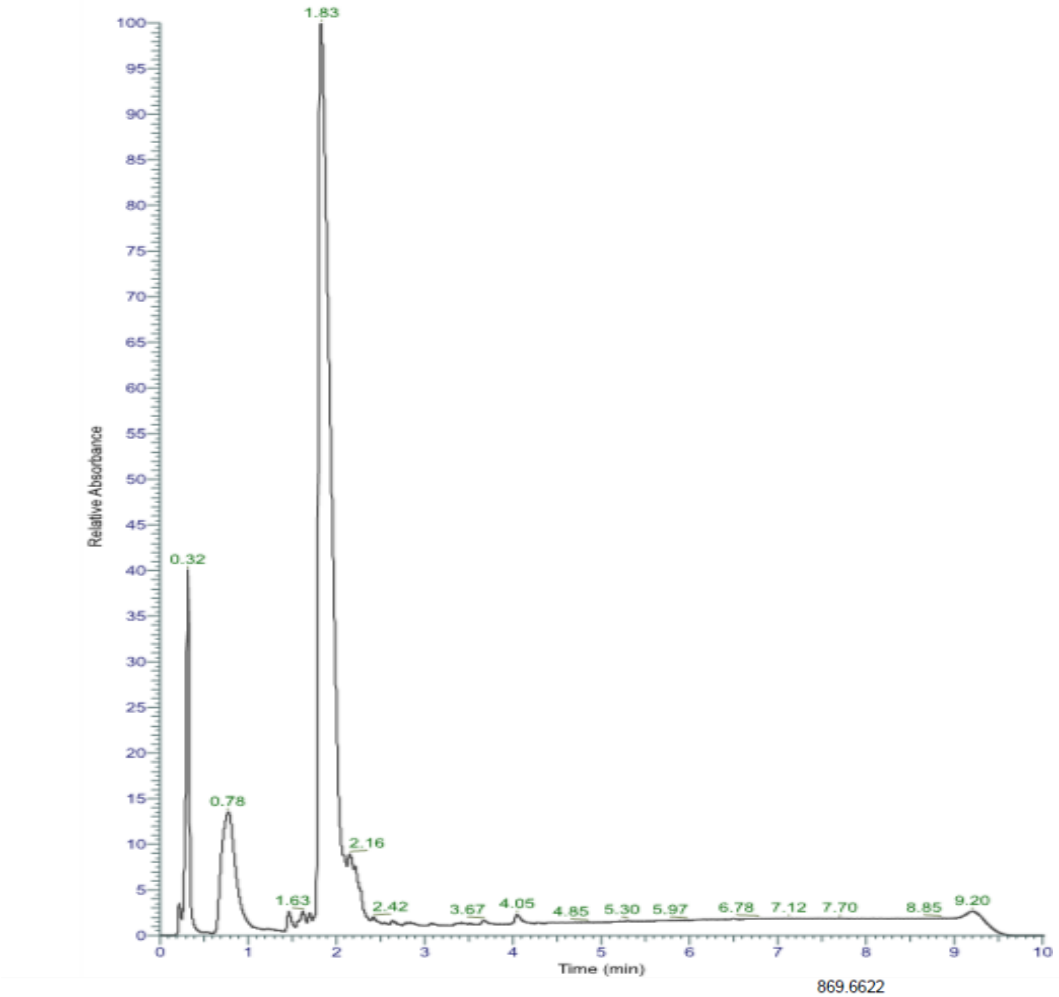

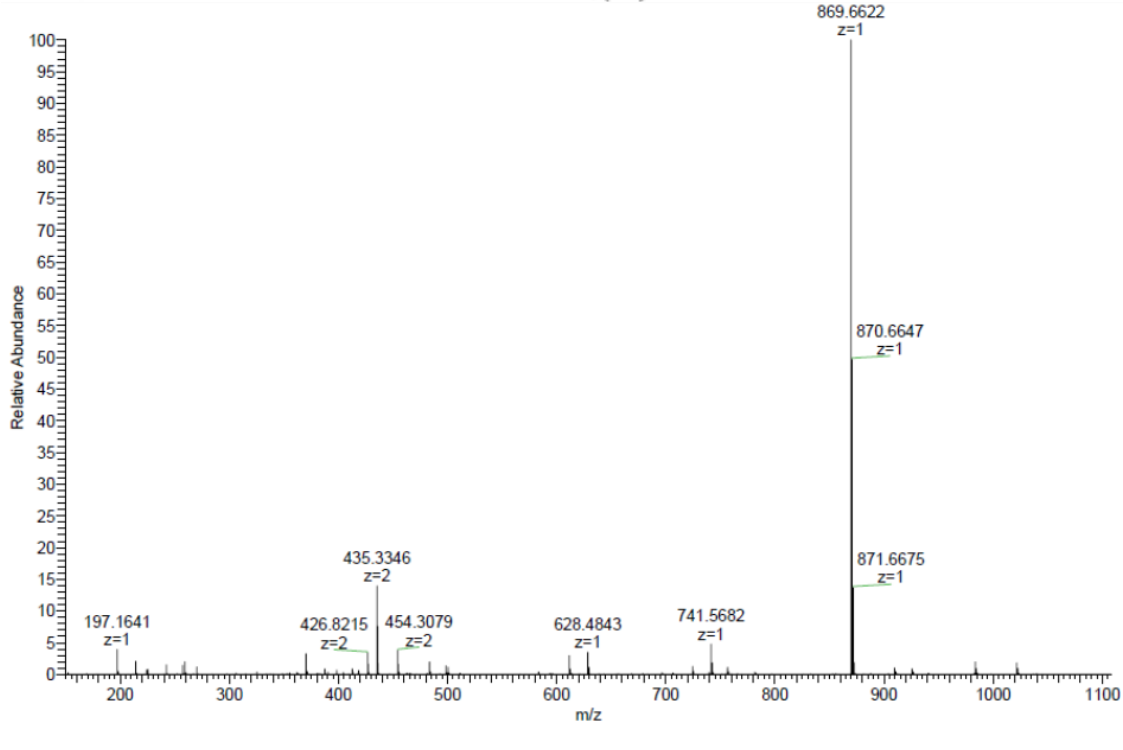

G1KL (25 v/v Dipropylamine, 60°C) was obtained as crude white solid after lyophilization (82.4 mg, 64.5%). Analytical RP-HPLC: t_R = 1.88 min (A/D 100:0 to 0:100 in 7.00 min, λ = 214nm). HRMS (ESI+): $C_{42}H_{84}N_{12}O_7$ calc./obs. 869.66/869.66 Da $[M+H]^+$.

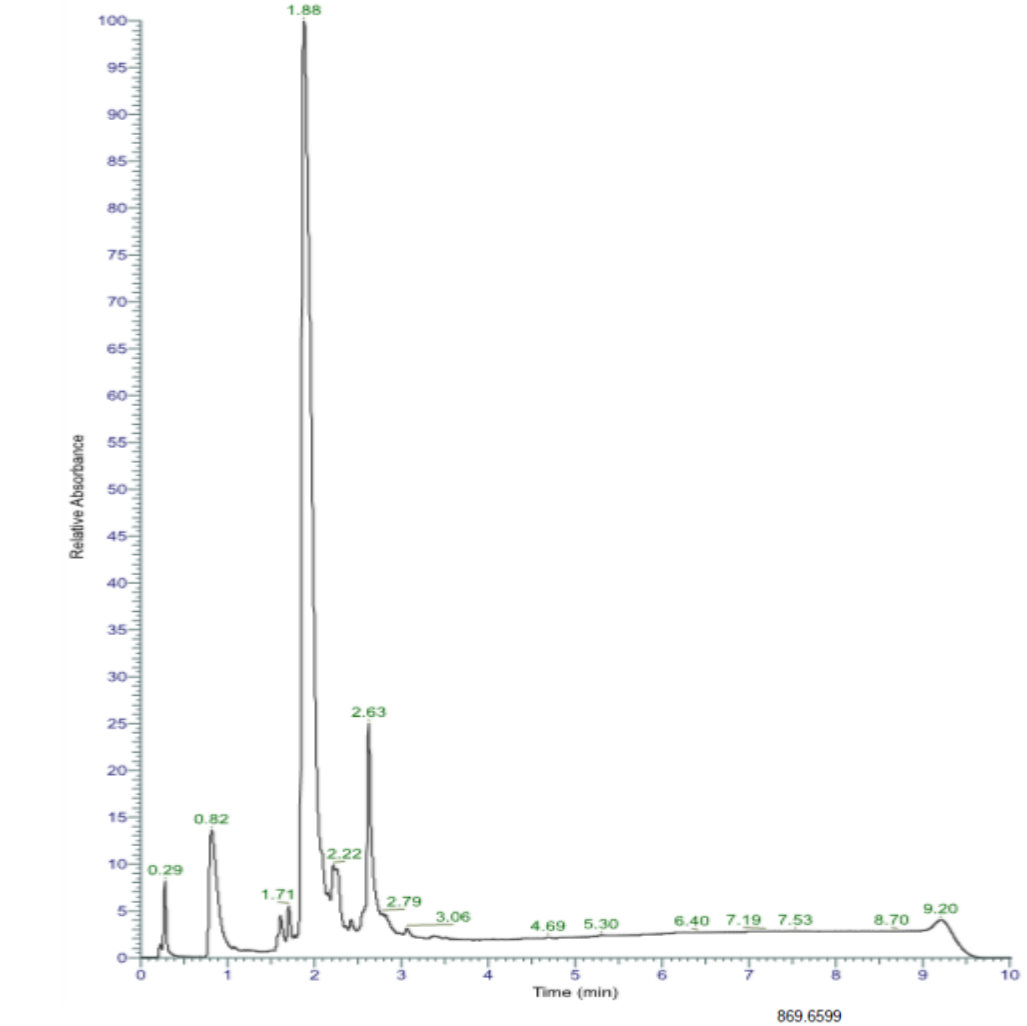

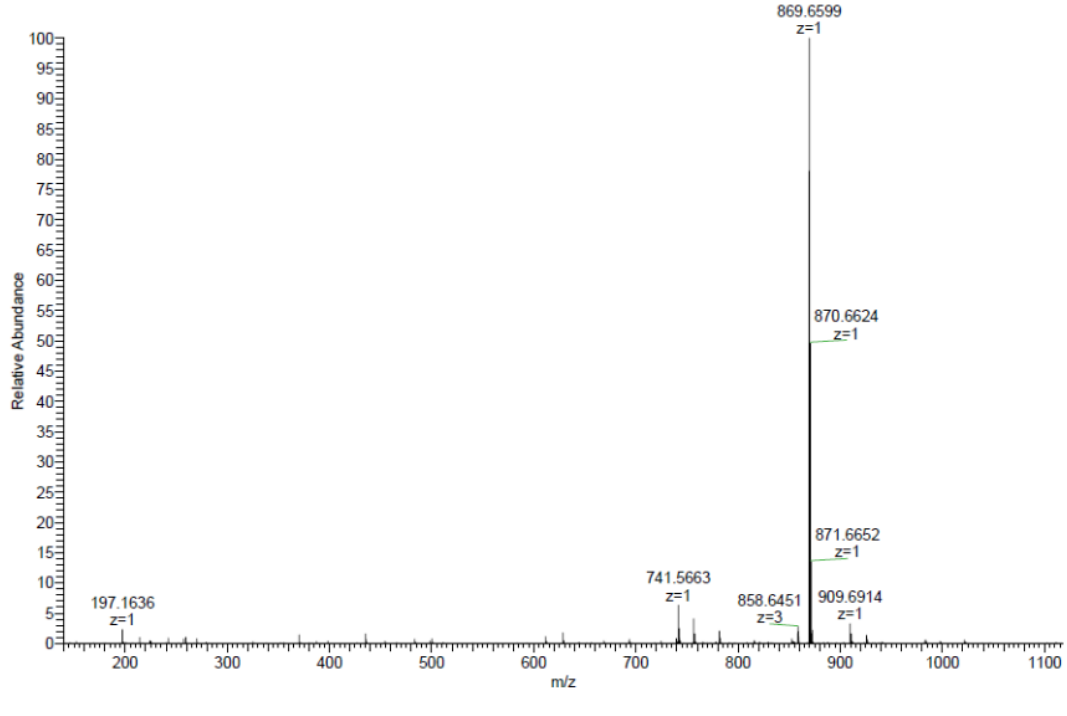

G2KL ((KL)$_4$(*K*KL)$_2$*K*KL)

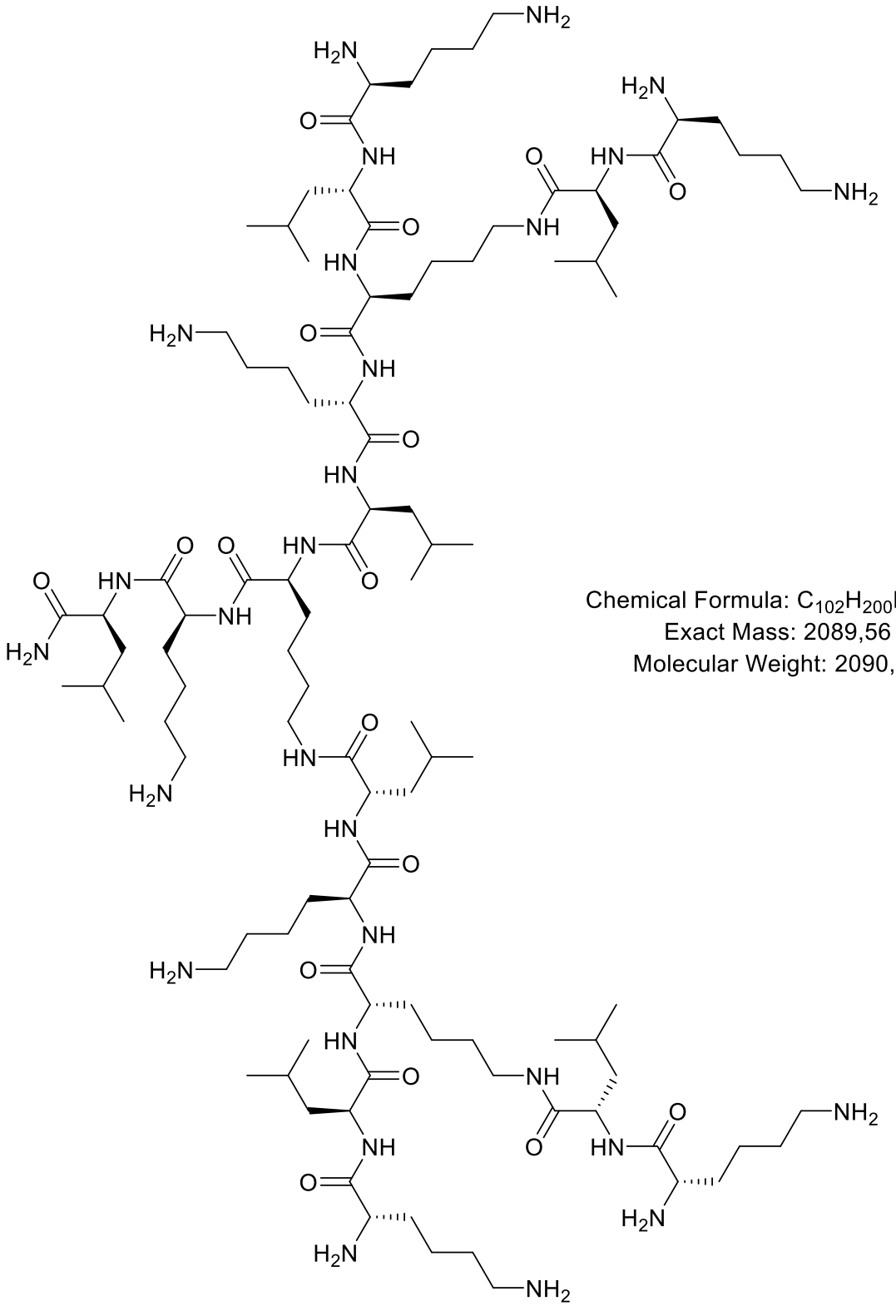

Chemical Formula: $C_{102}H_{200}N_{28}O_{17}$
Exact Mass: 2089,56
Molecular Weight: 2090,90

G2KL (20% v/v Piperidine, r. t.) was obtained as crude white solid after lyophilization (214.4 mg, 64.9%). Analytical RP-HPLC: t_R = 2.35 min (A/D 100:0 to 0:100 in 7.00 min, λ = 214nm). HRMS (ESI+): $C_{102}H_{200}N_{28}O_{17}$ calc./obs. 2090.56/2090.56 Da $[M+H]^+$.

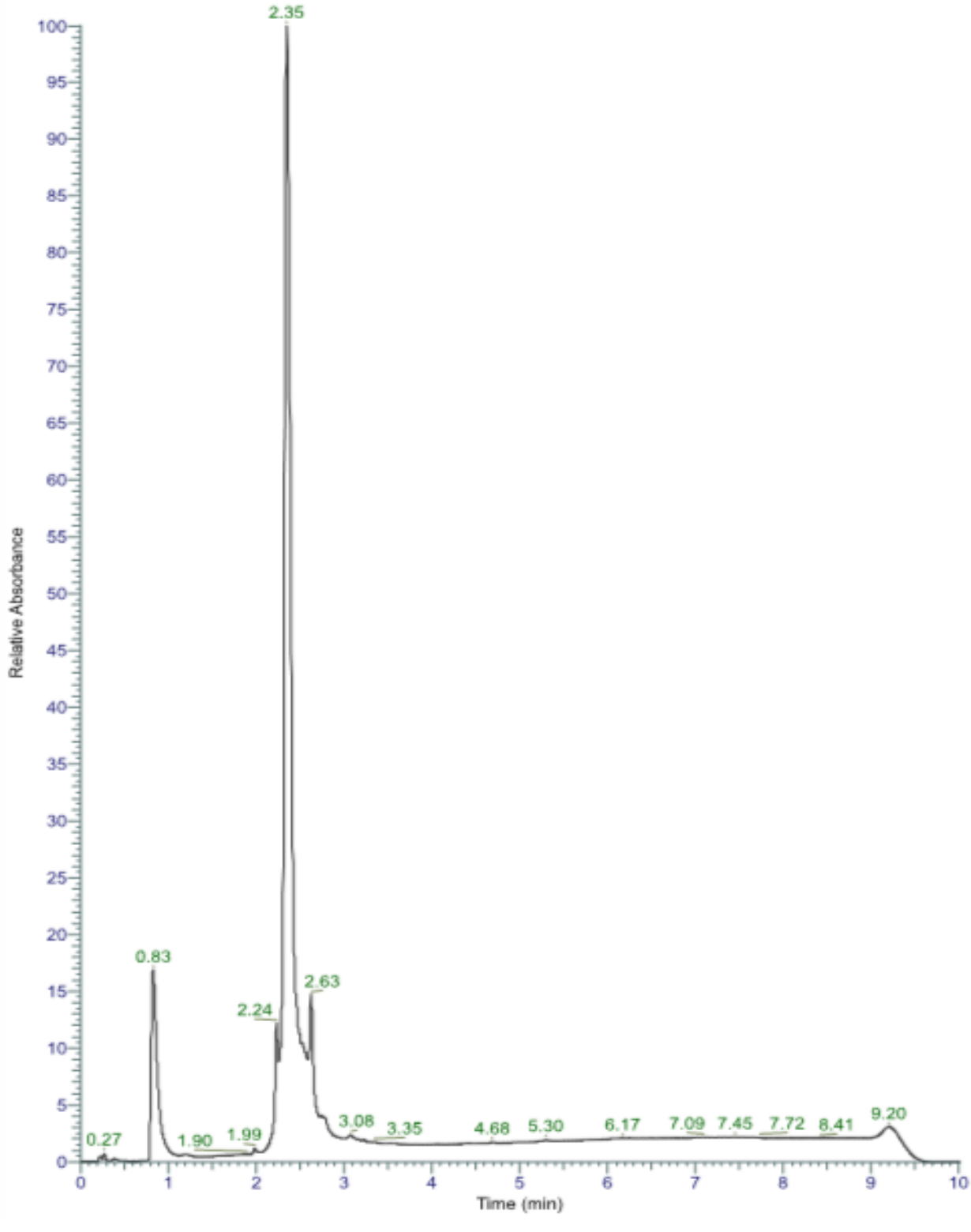

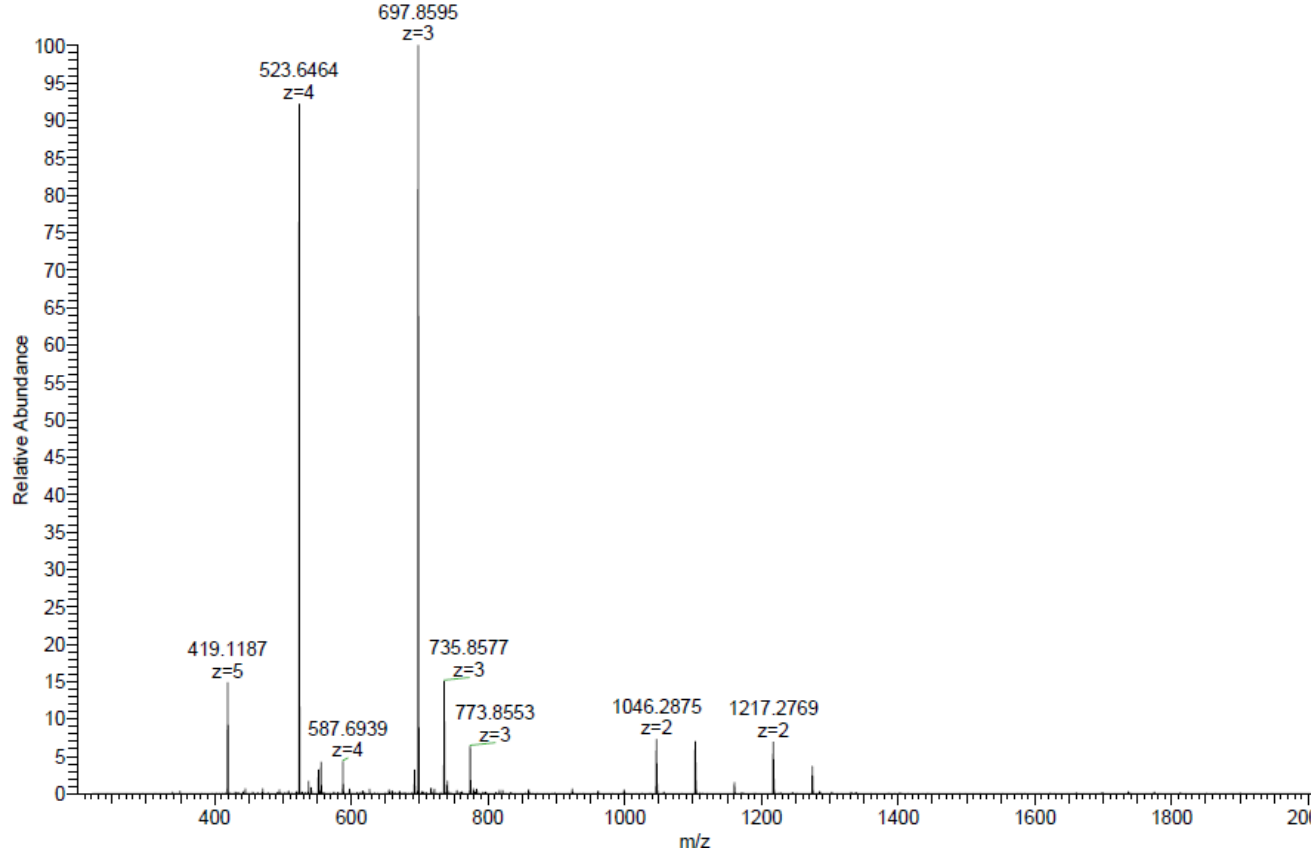
697.8595
z=3
523.6464
z=4
419.1187
z=5
735.8577
z=3
773.8553
z=3
587.6939
z=4
1046.2875
z=2
1217.2769
z=2
Relative Abundance
m/z

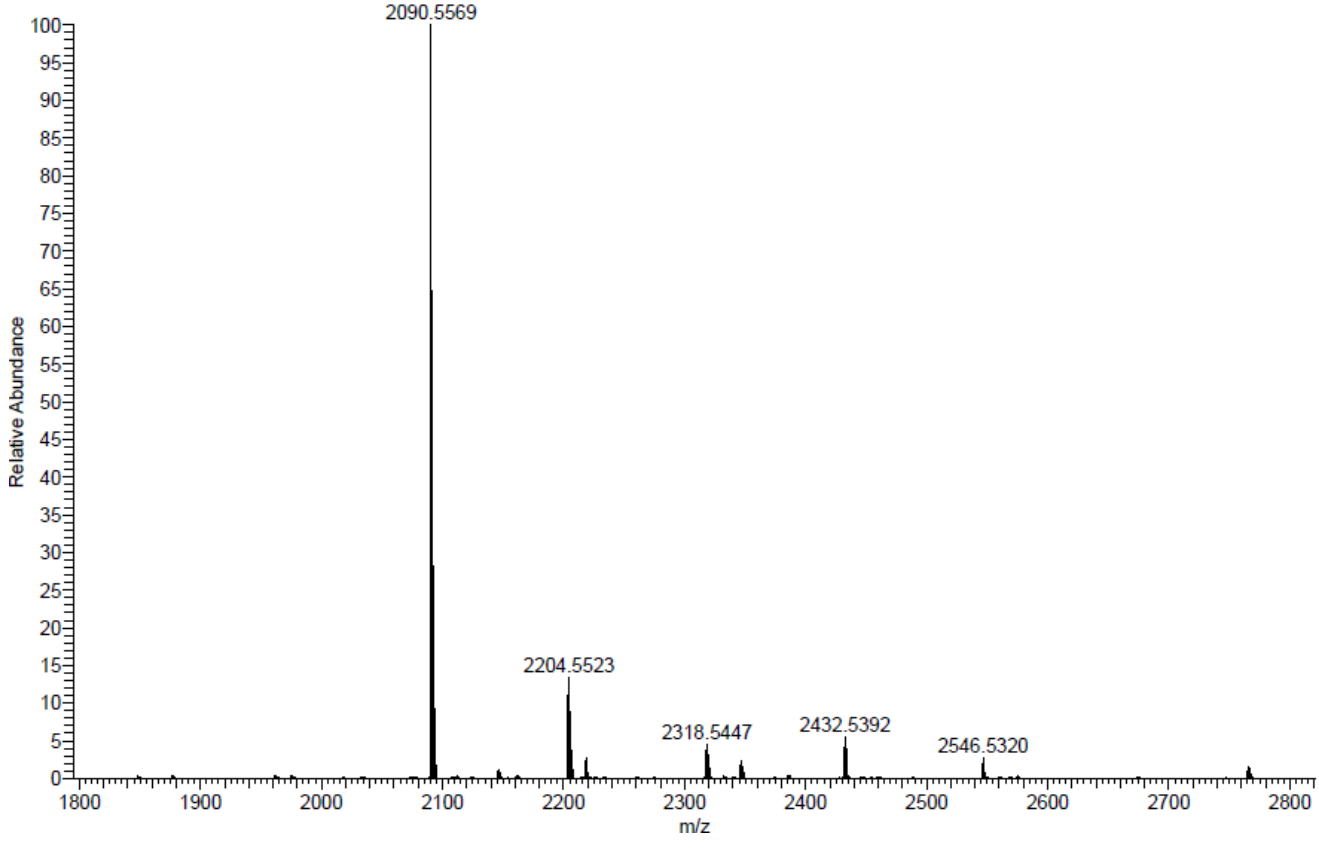
2090.5569
2204.5523
2318.5447
2432.5392
2546.5320
Relative Abundance
m/z

G2KL (5% w/v Piperazine + 2% DBU, r. t.) was obtained as crude white solid after lyophilization (189.9 mg, 53.9%). Analytical RP-HPLC: t_R = 2.32 min (A/D 100:0 to 0:100 in 7.00 min, λ = 214nm). HRMS (ESI+): $C_{102}H_{200}N_{28}O_{17}$ calc./obs. 2090.56/2090.56 Da $[M+H]^+$.

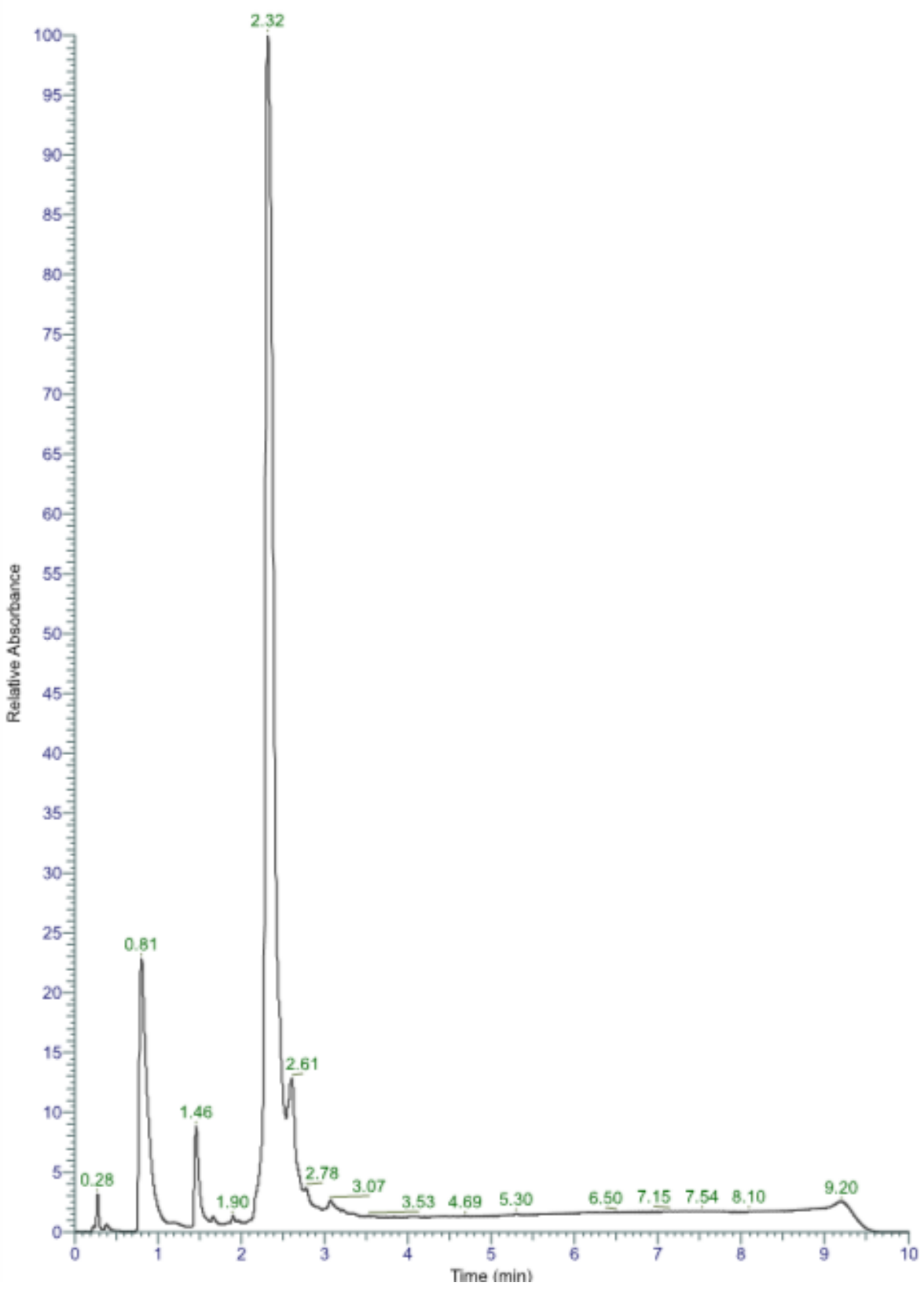

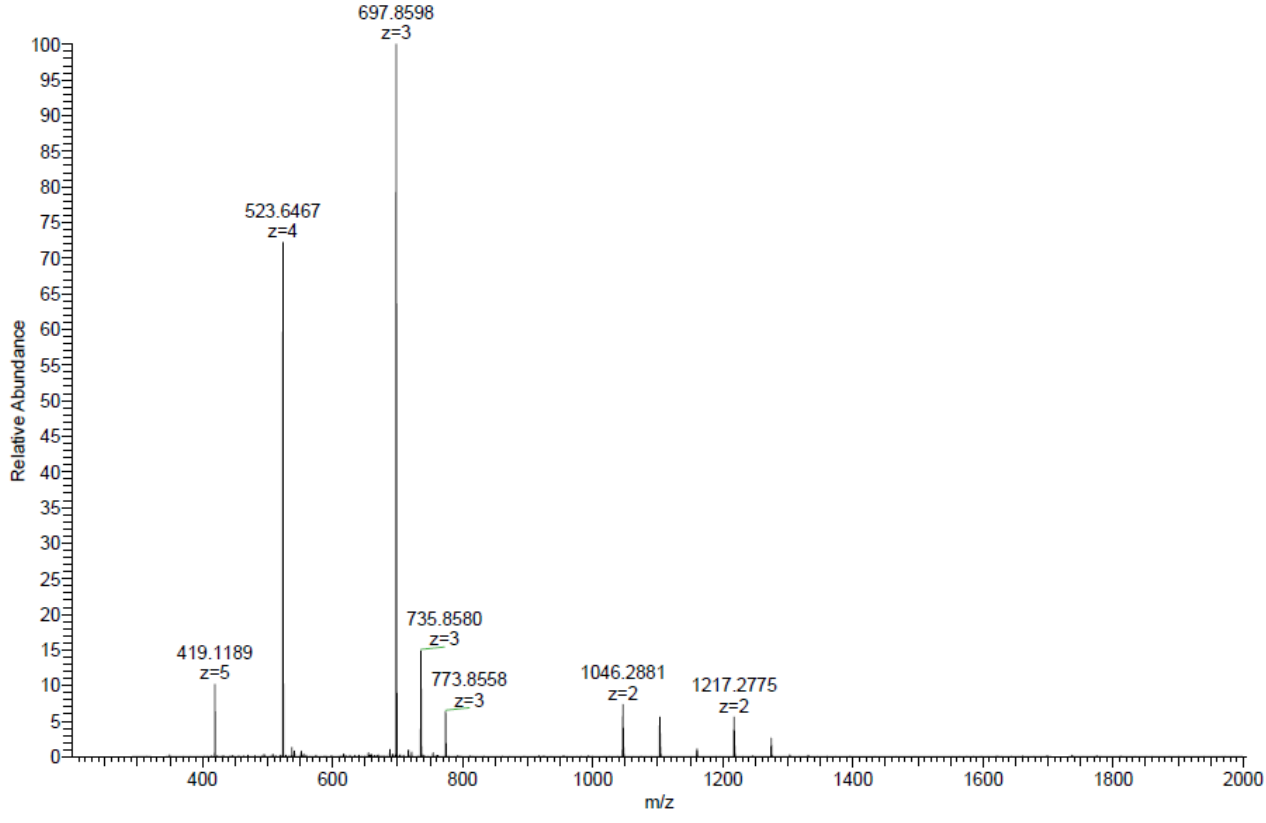
697.8598
z=3
523.6467
z=4
735.8580
z=3
419.1189
z=5
773.8558
z=3
1046.2881
z=2
1217.2775
z=2
Relative Abundance
m/z

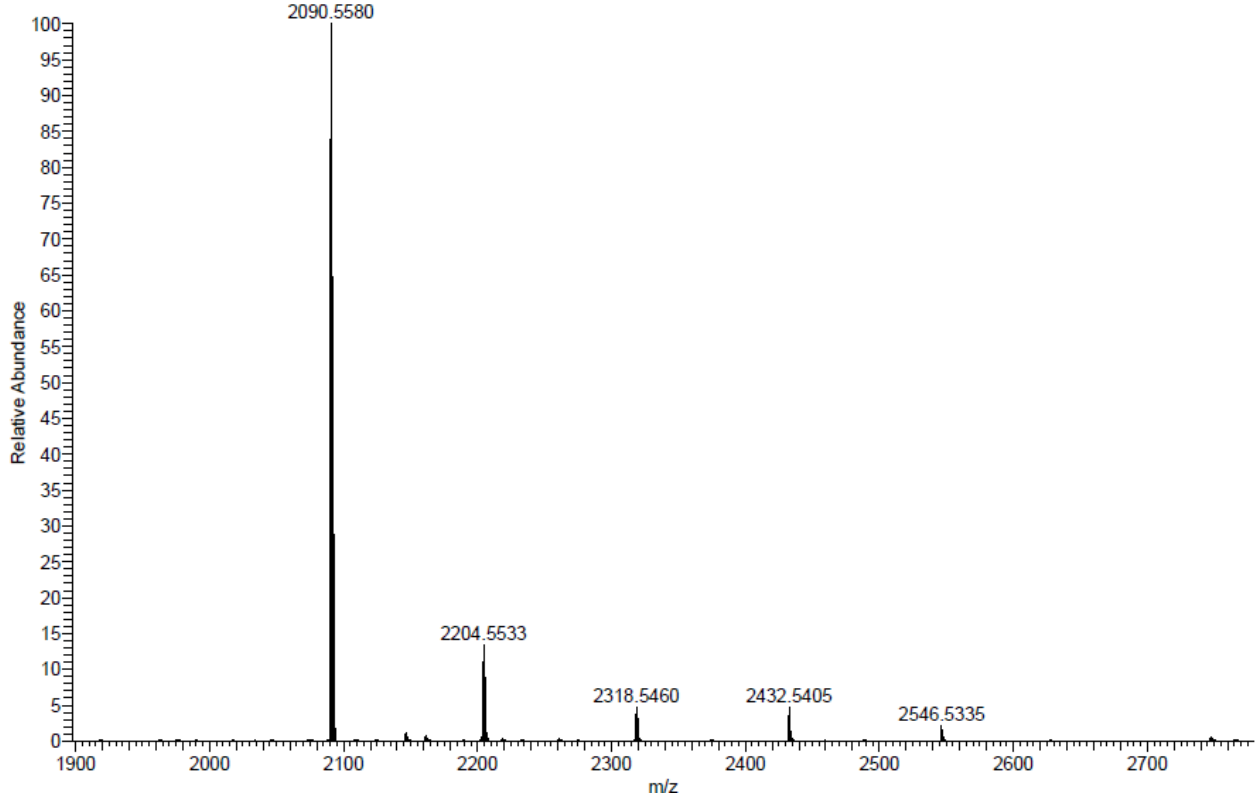
2090.5580
2204.5533
2318.5460
2432.5405
2546.5335
Relative Abundance
m/z

G2KL (20% v/v Dipropylamine, r. t.) was obtained as crude white solid after lyophilization (134.4 mg, 42.2%). Analytical RP-HPLC: t_R = 2.40 min (A/D 100:0 to 0:100 in 7.00 min, λ = 214nm). HRMS (ESI+): $C_{102}H_{200}N_{28}O_{17}$ calc./obs. 2090.56/2090.56 Da $[M+H]^+$.

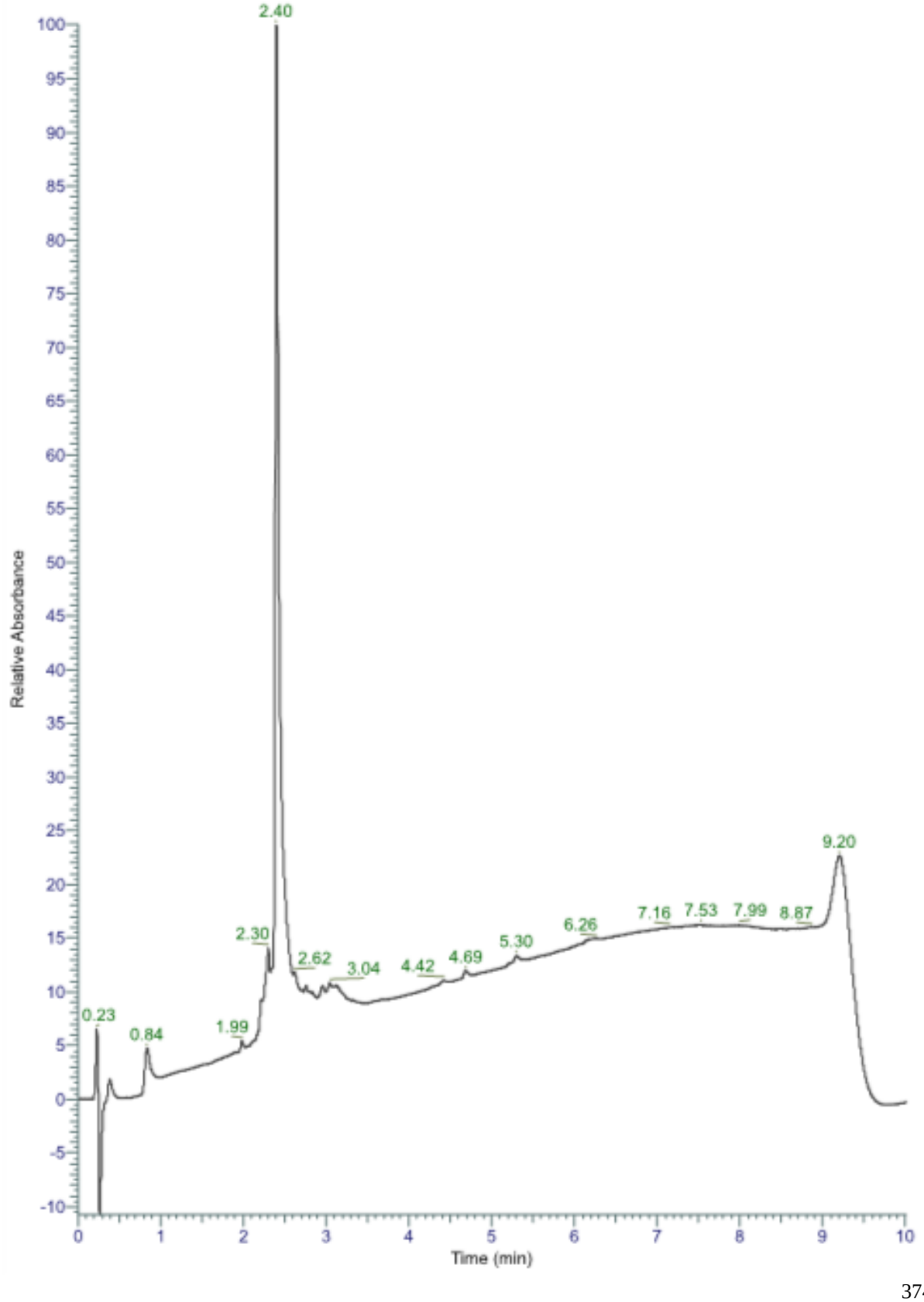

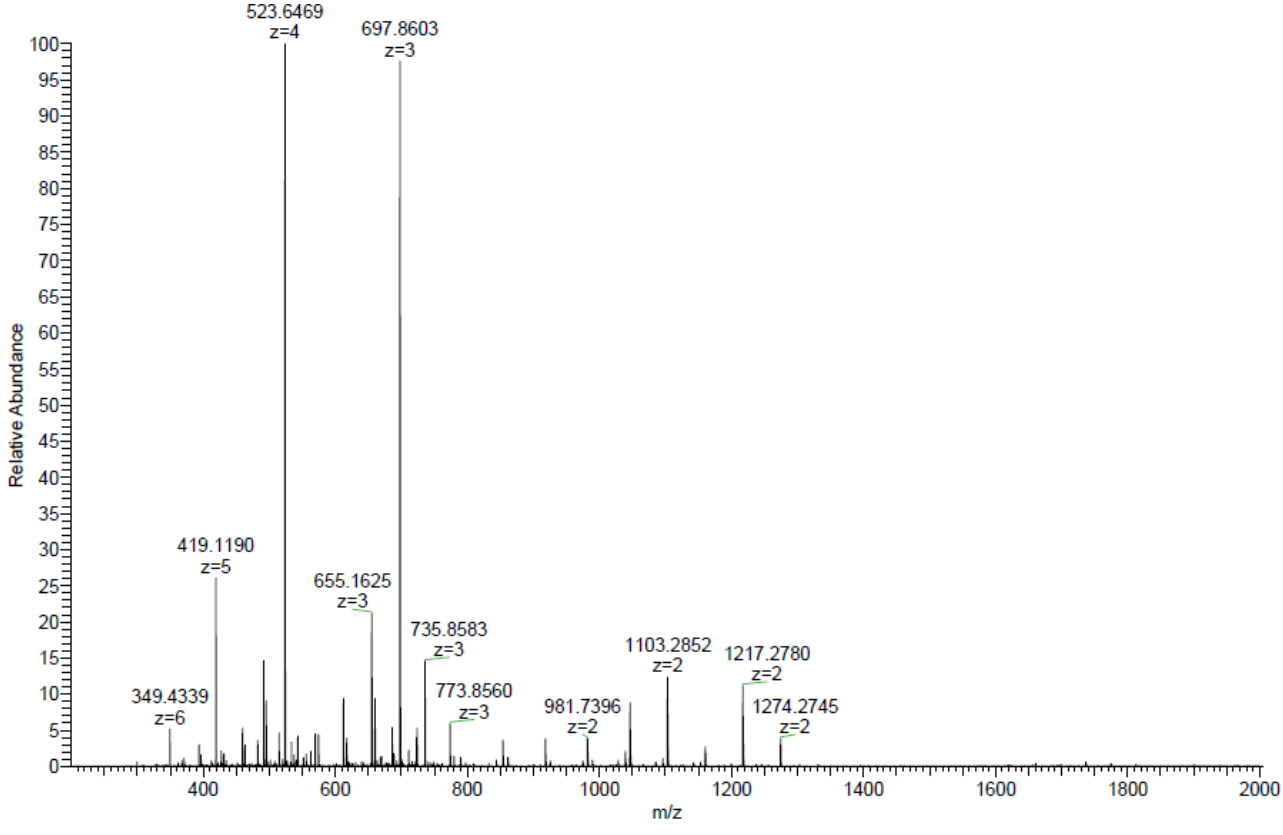
523.6469
z=4
697.8603
z=3
419.1190
z=5
655.1625
z=3
735.8583
z=3
1103.2852
z=2
1217.2780
z=2
773.8560
z=3
349.4339
z=6
981.7396
z=2
1274.2745
z=2
Relative Abundance
m/z

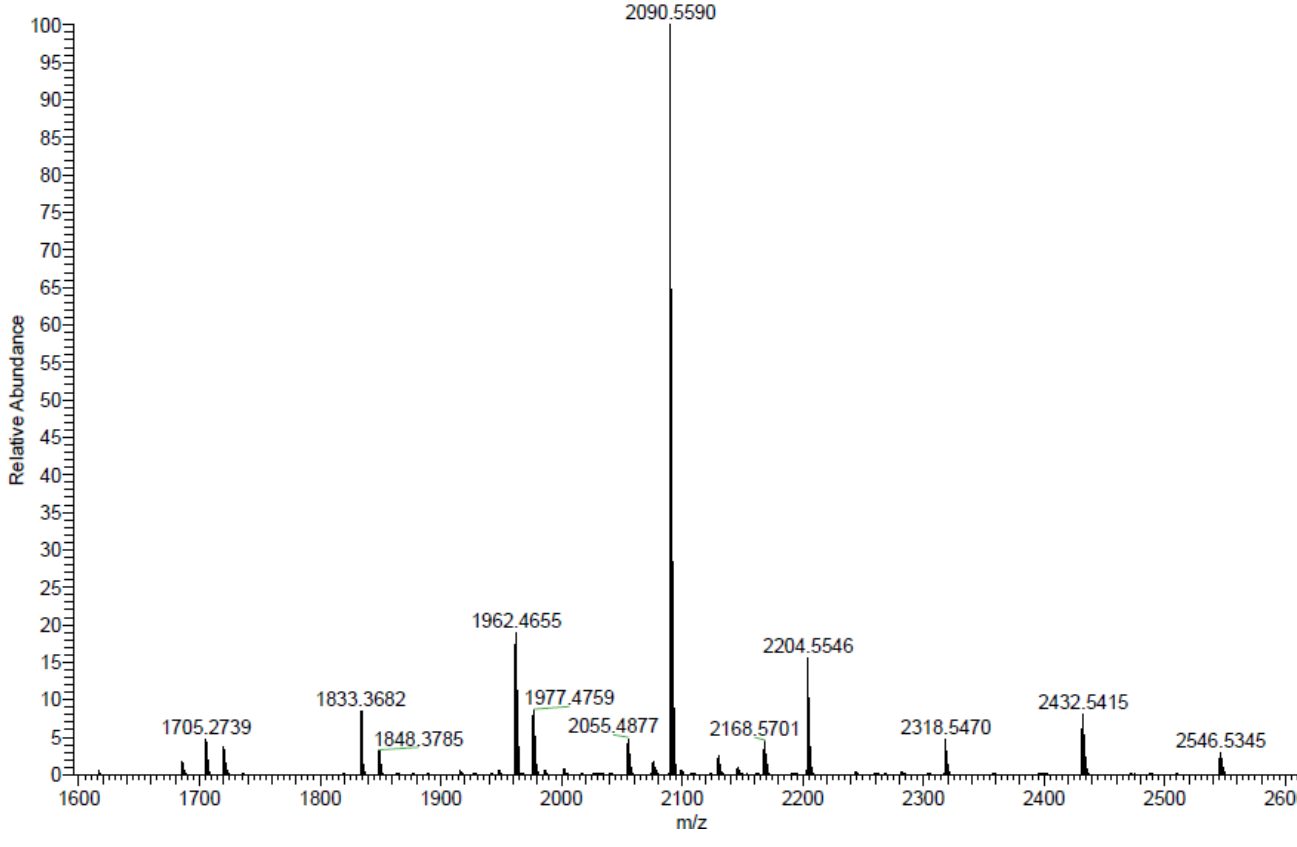
2090.5590
1962.4655
2204.5546
1833.3682
1977.4759
2432.5415
1705.2739
2055.4877
2168.5701
2318.5470
1848.3785
2546.5345
Relative Abundance
m/z

G2KL (25% v/v Dipropylamine, r. t.) was obtained as crude white solid after lyophilization (151.4 mg, 46.4%). Analytical RP-HPLC: t_R = 2.38 min (A/D 100:0 to 0:100 in 7.00 min, λ = 214nm). HRMS (ESI+): $C_{102}H_{200}N_{28}O_{17}$ calc./obs. 2090.56/2090.56 Da $[M+H]^+$.

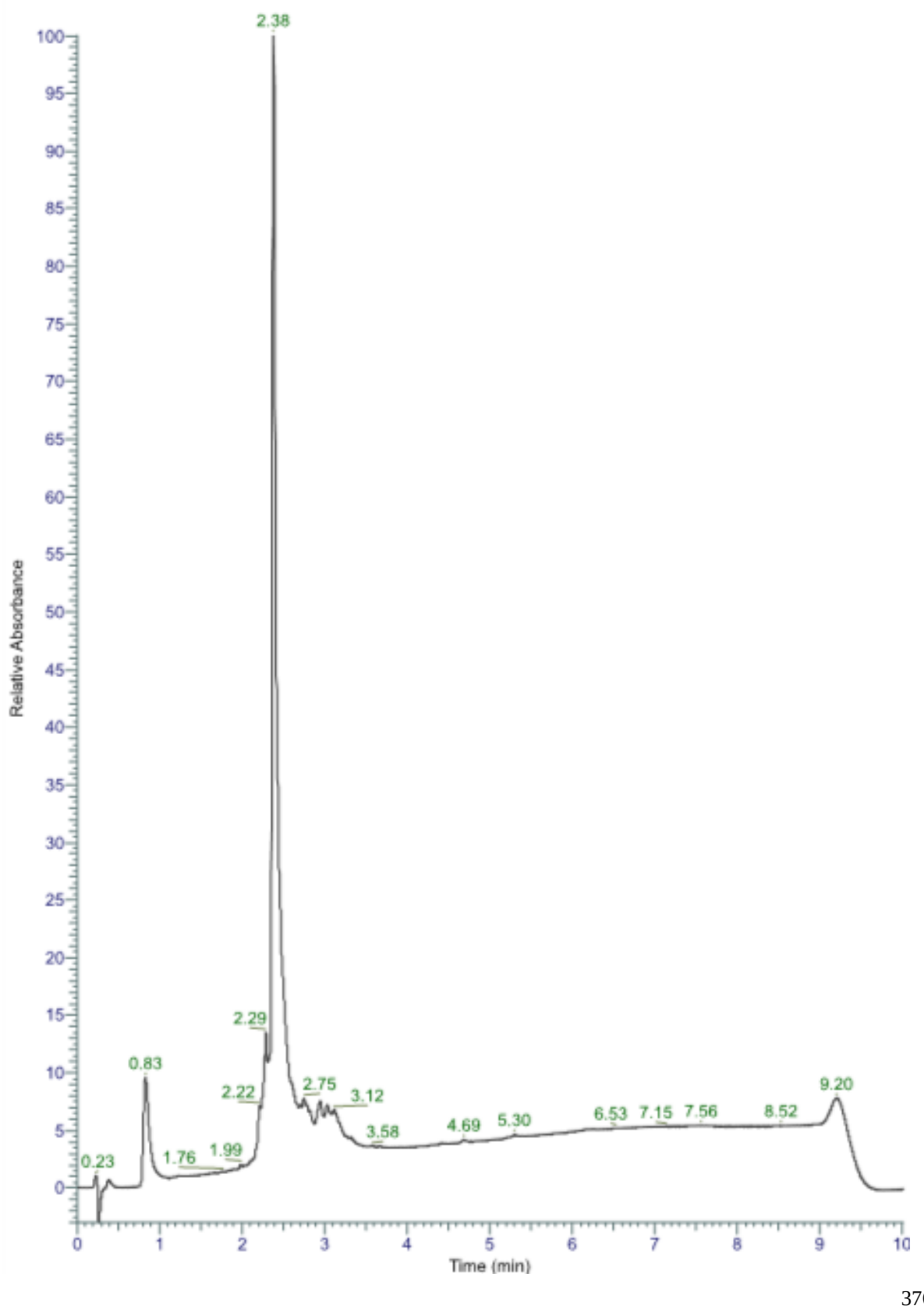

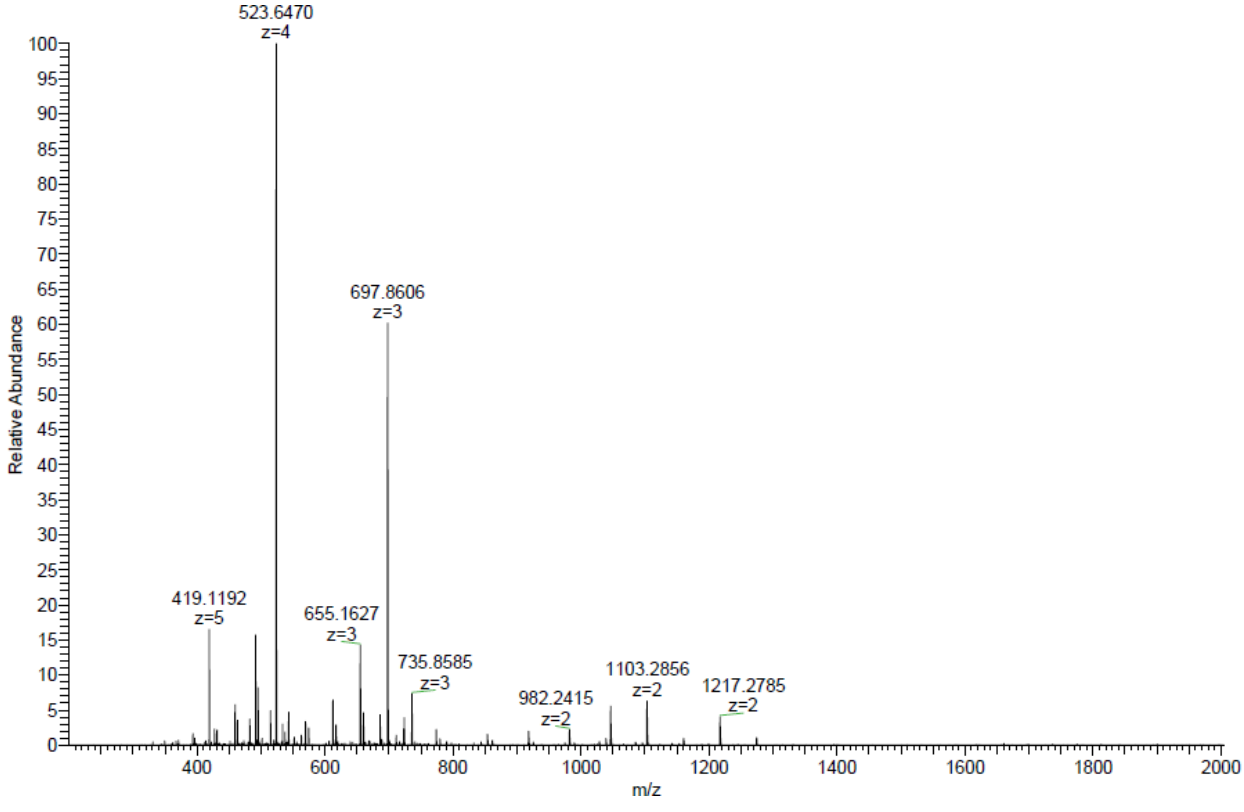
523.6470
z=4
697.8606
z=3
419.1192
z=5
655.1627
z=3
735.8585
z=3
982.2415
z=2
1103.2856
z=2
1217.2785
z=2
Relative Abundance
m/z

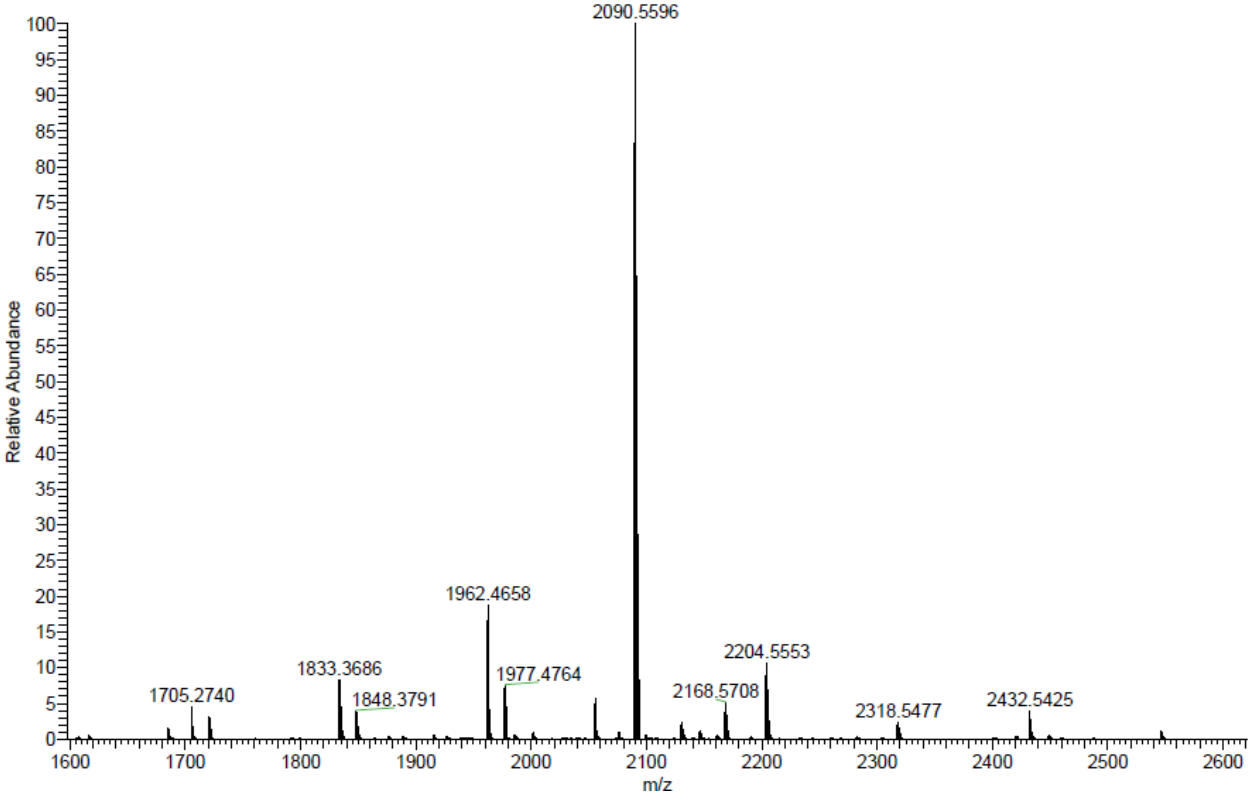
2090.5596
1962.4658
2204.5553
1833.3686
1977.4764
1705.2740
1848.3791
2168.5708
2318.5477
2432.5425
Relative Abundance
m/z

G3KL ((KL)$_8$(*K*KL)$_4$(*K*KL)$_2$*K*KL)

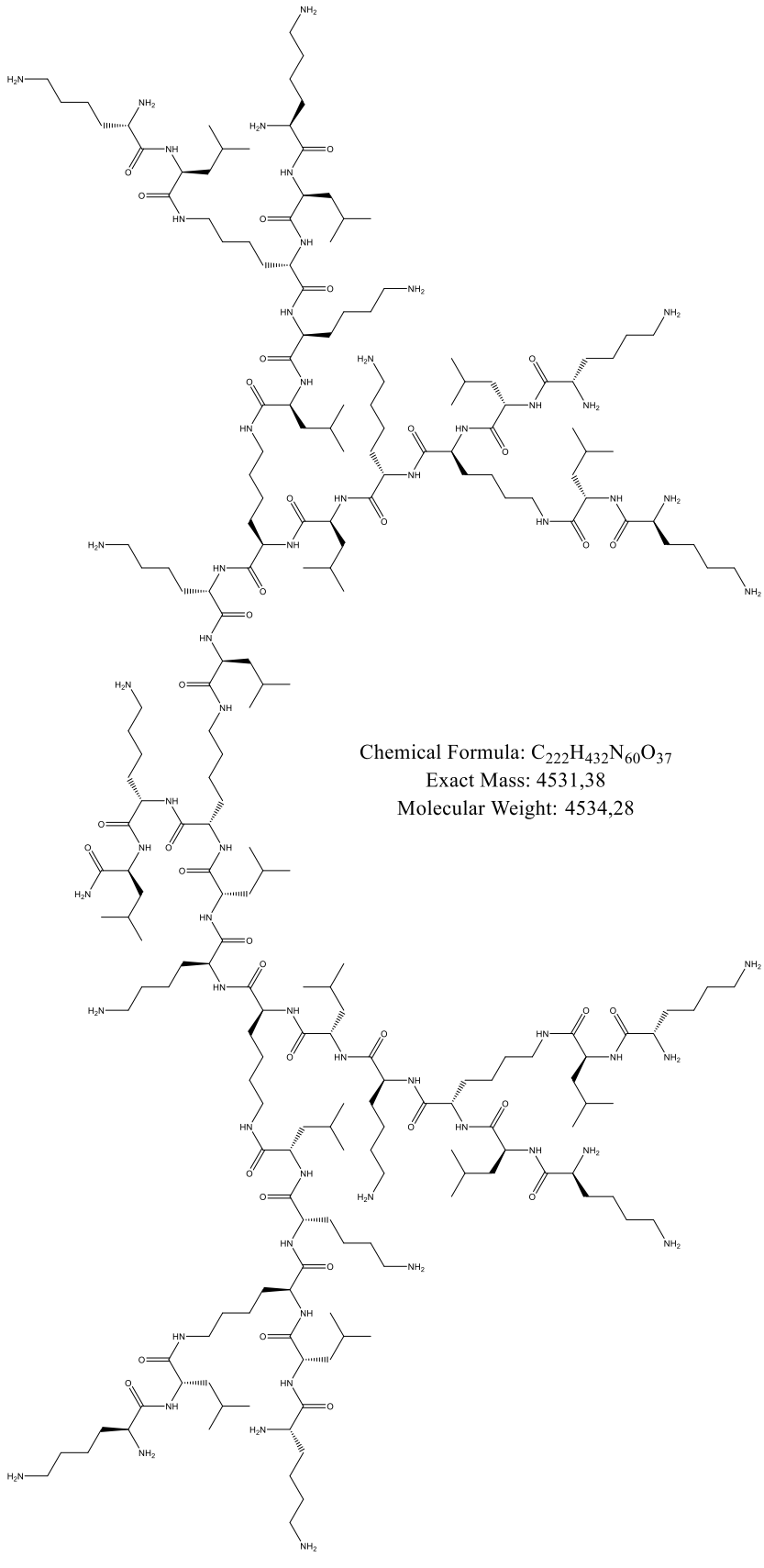

Chemical Formula: $C_{222}H_{432}N_{60}O_{37}$
Exact Mass: 4531,38
Molecular Weight: 4534,28

G3KL (20% v/v Piperidine, 60°C) was obtained as crude white solid after lyophilization (366.6 mg, 46.8%). Analytical RP-HPLC: t_R = 2.77 min (A/D 100:0 to 0:100 in 7.00 min, λ = 214nm). HRMS (ESI+): $C_{222}H_{432}N_{60}O_{37}$ calc./obs. 4532.38/4532.39 Da $[M+H]^+$.

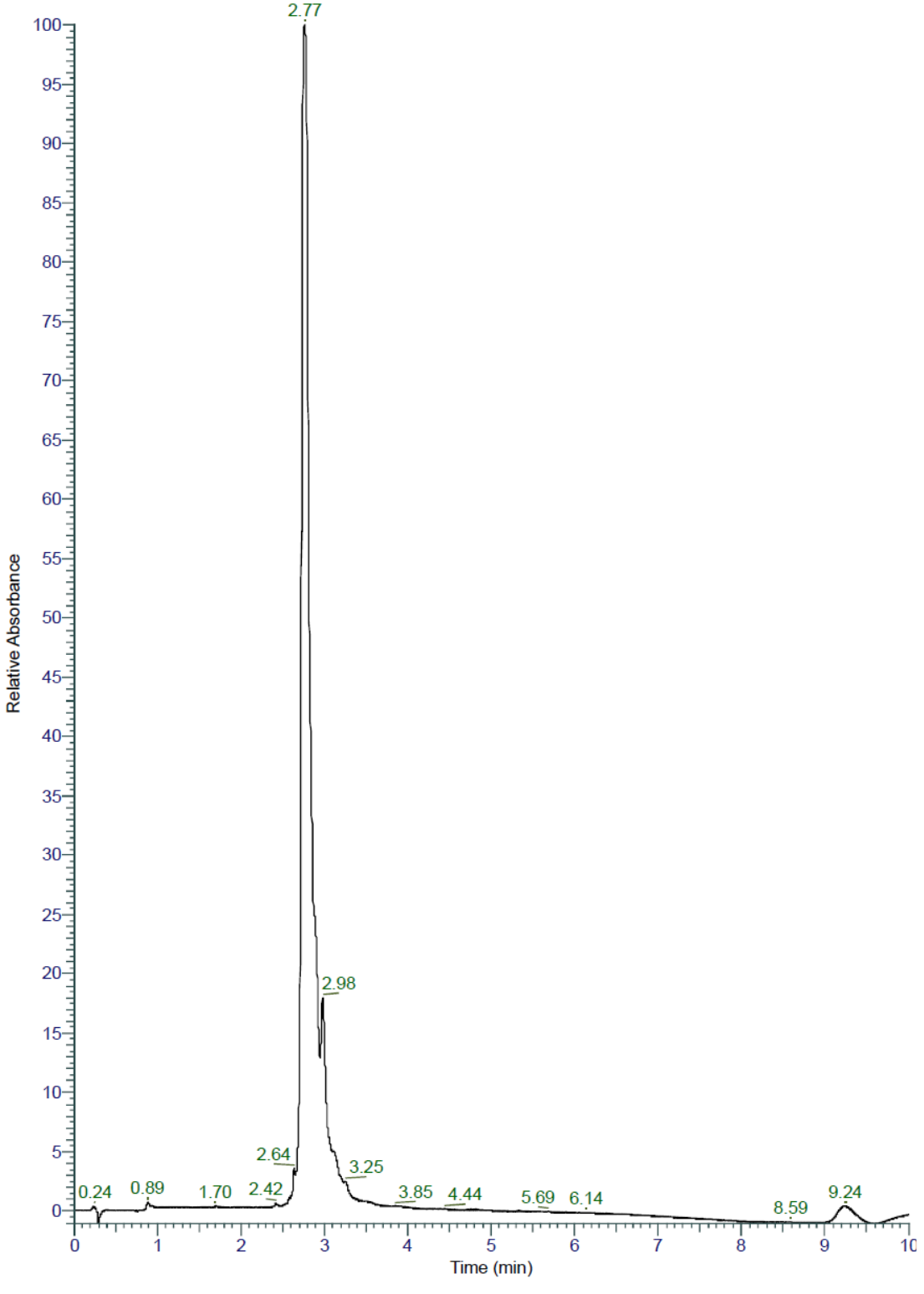

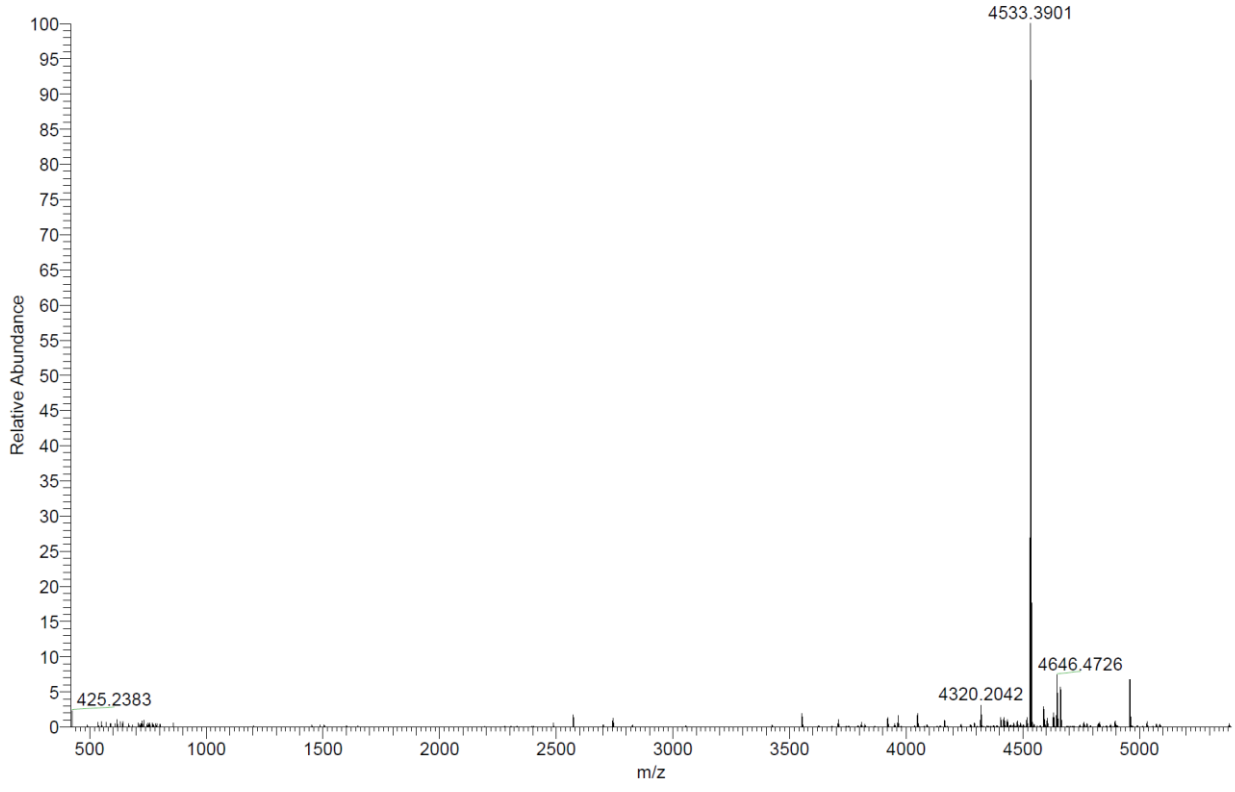
4533.3901
4646.4726
4320.2042
425.2383
Relative Abundance
m/z

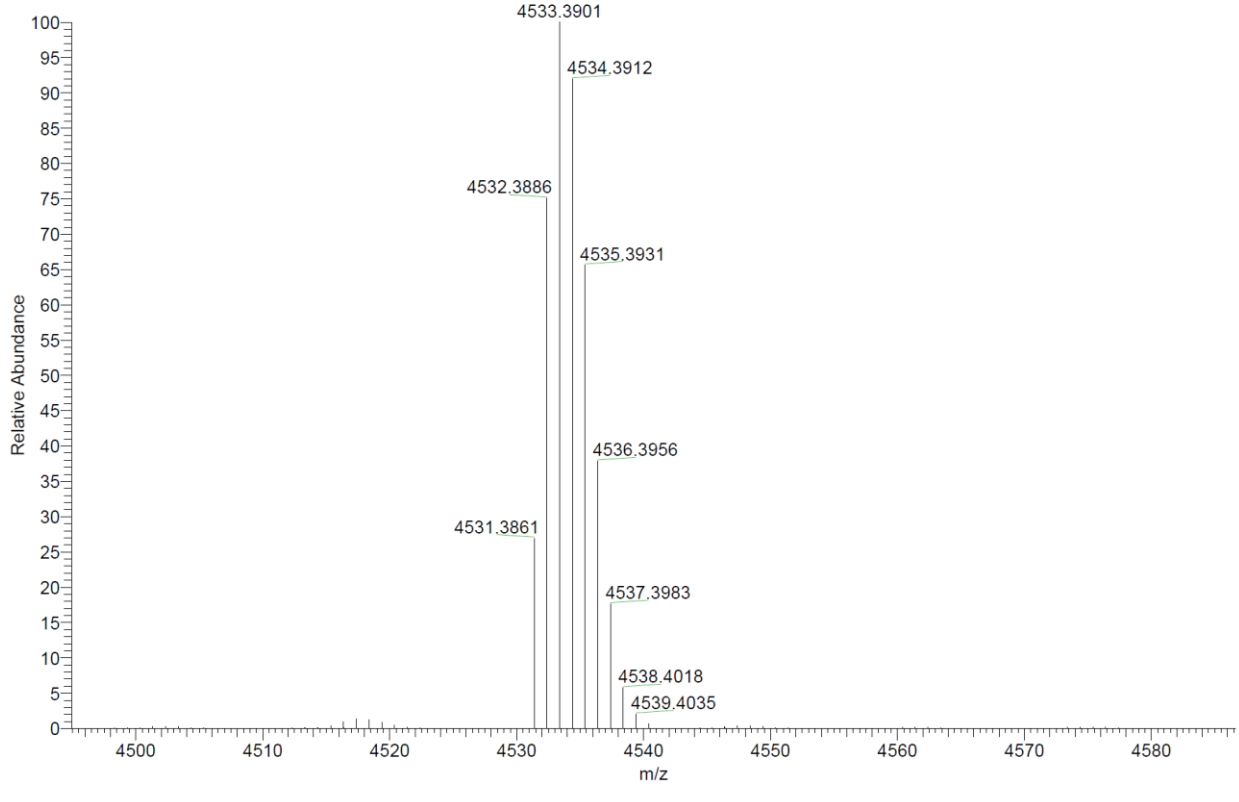
4533.3901
4534.3912
4532.3886
4535.3931
4536.3956
4531.3861
4537.3983
4538.4018
4539.4035
Relative Abundance
m/z

G3KL (25% v/v Dipropylamine, 60°C) was obtained as crude white solid after lyophilization (255.1 mg, n.d.). Analytical RP-HPLC: t_R = 2.79 min (A/D 100:0 to 0:100 in 7.00 min, λ = 214nm). HRMS (ESI+): $C_{222}H_{432}N_{60}O_{37}$ calc./obs. 4532.38/4532.39 Da $[M+H]^+$.

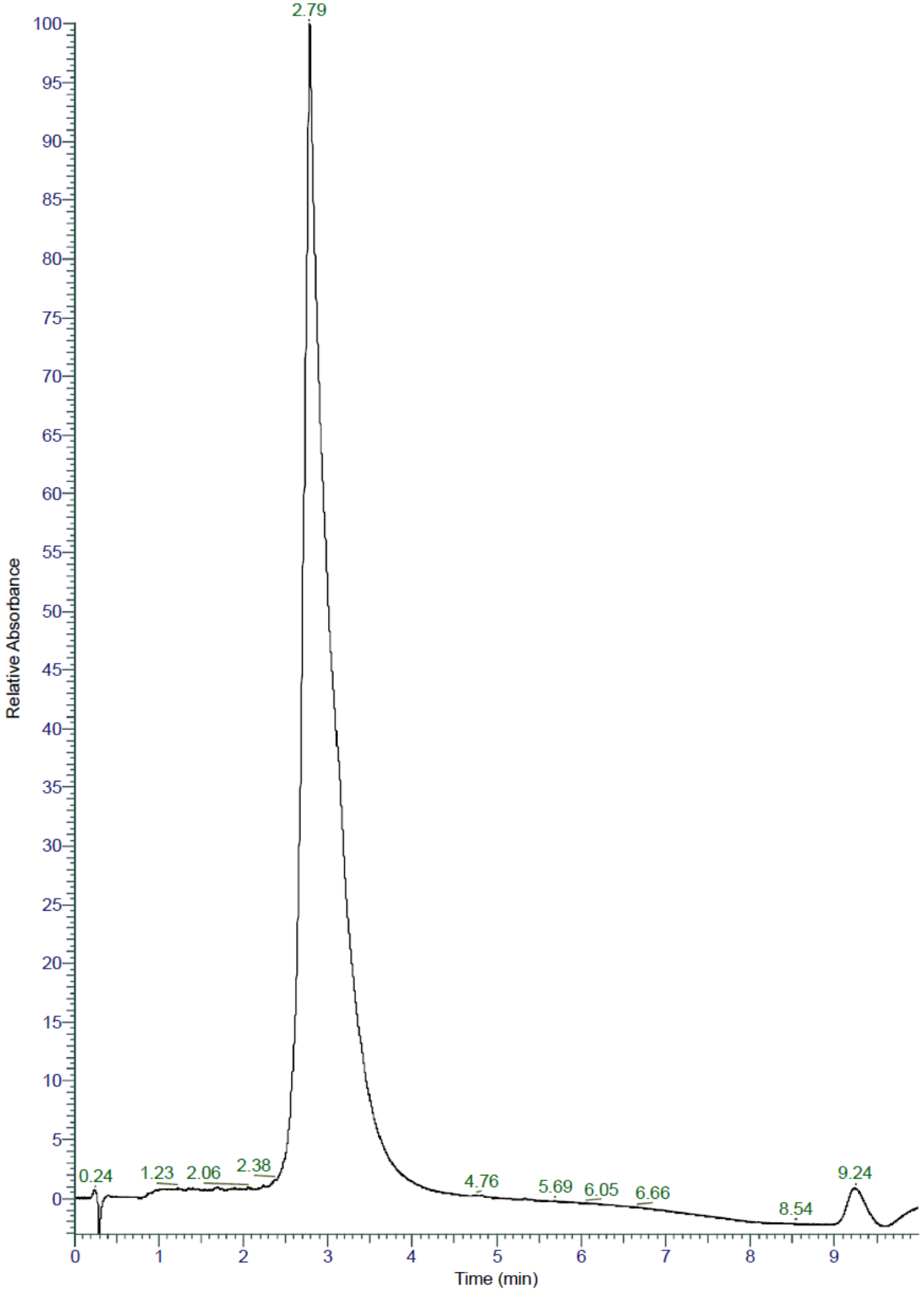

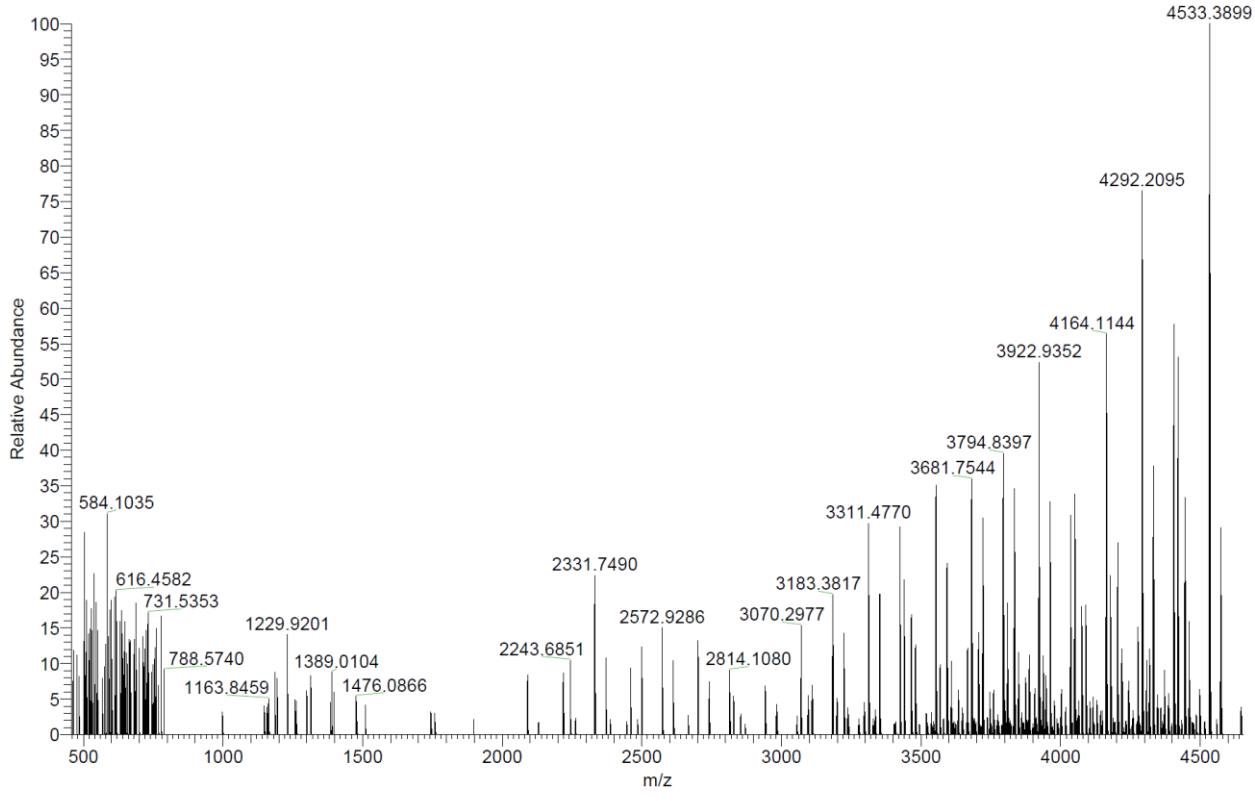
Relative Abundance
m/z
4533.3899
4292.2095
4164.1144
3922.9352
3794.8397
3681.7544
3311.4770
3183.3817
3070.2977
2814.1080
2572.9286
2331.7490
2243.6851
1476.0866
1389.0104
1229.9201
1163.8459
788.5740
731.5353
616.4582
584.1035

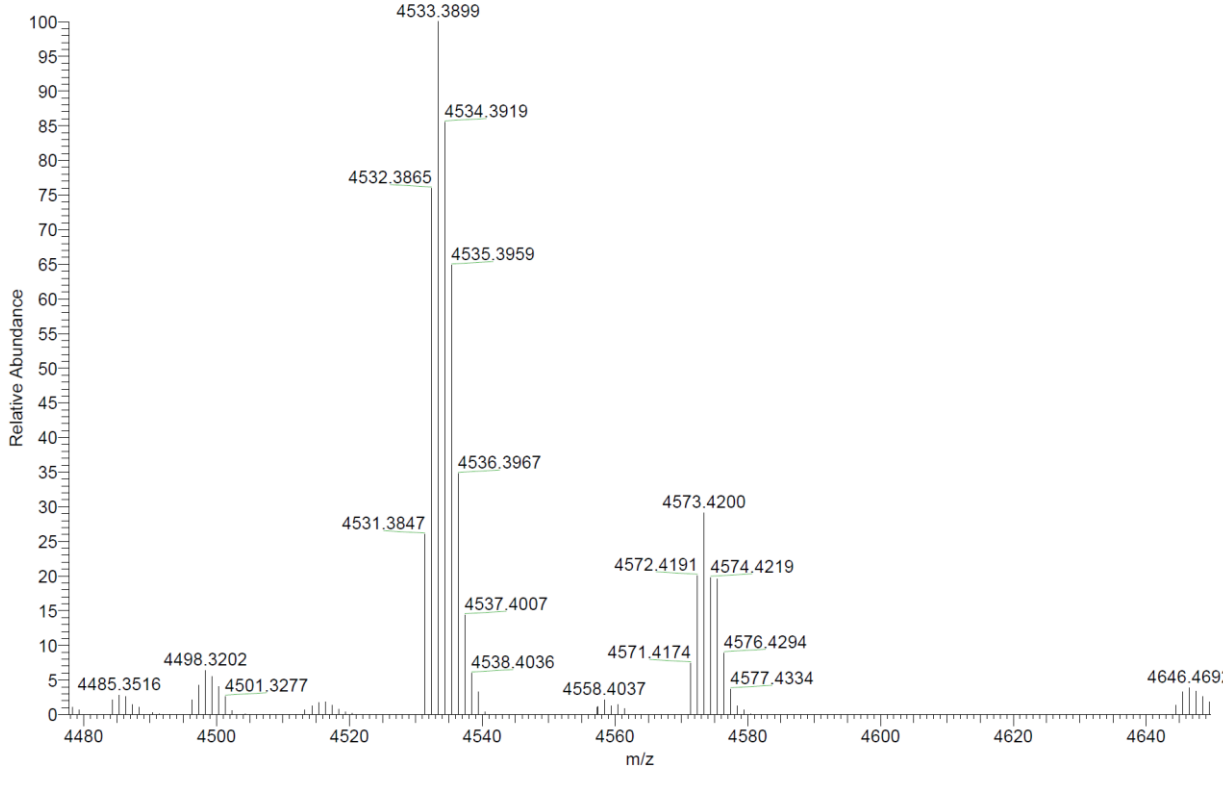
Relative Abundance
m/z
4533.3899
4534.3919
4532.3865
4535.3959
4536.3967
4573.4200
4531.3847
4572.4191
4574.4219
4537.4007
4576.4294
4571.4174
4538.4036
4577.4334
4498.3202
4485.3516
4501.3277
4558.4037
4646.4692

G3KL (25% v/v Dipropylamine (+ 1% v/v DBU for the last generation), 60°C) was obtained as crude white solid after lyophilization (252.0 mg, n.d.). Analytical RP-HPLC: t_R = 2.79 min (A/D 100:0 to 0:100 in 7.00 min, λ = 214nm). HRMS (ESI+): $C_{222}H_{432}N_{60}O_{37}$ calc./obs. 4532.38/4532.39 Da $[M+H]^+$.

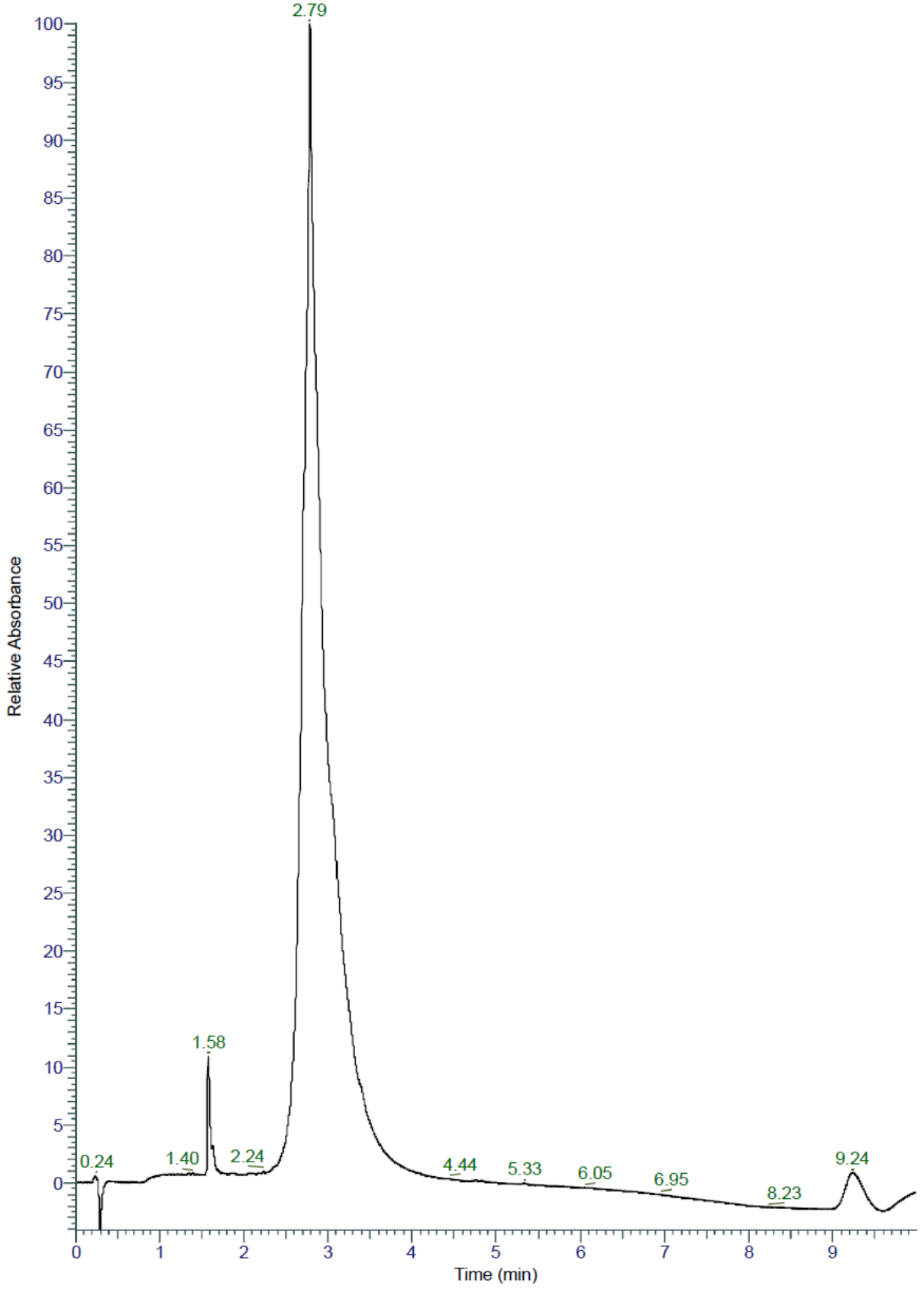

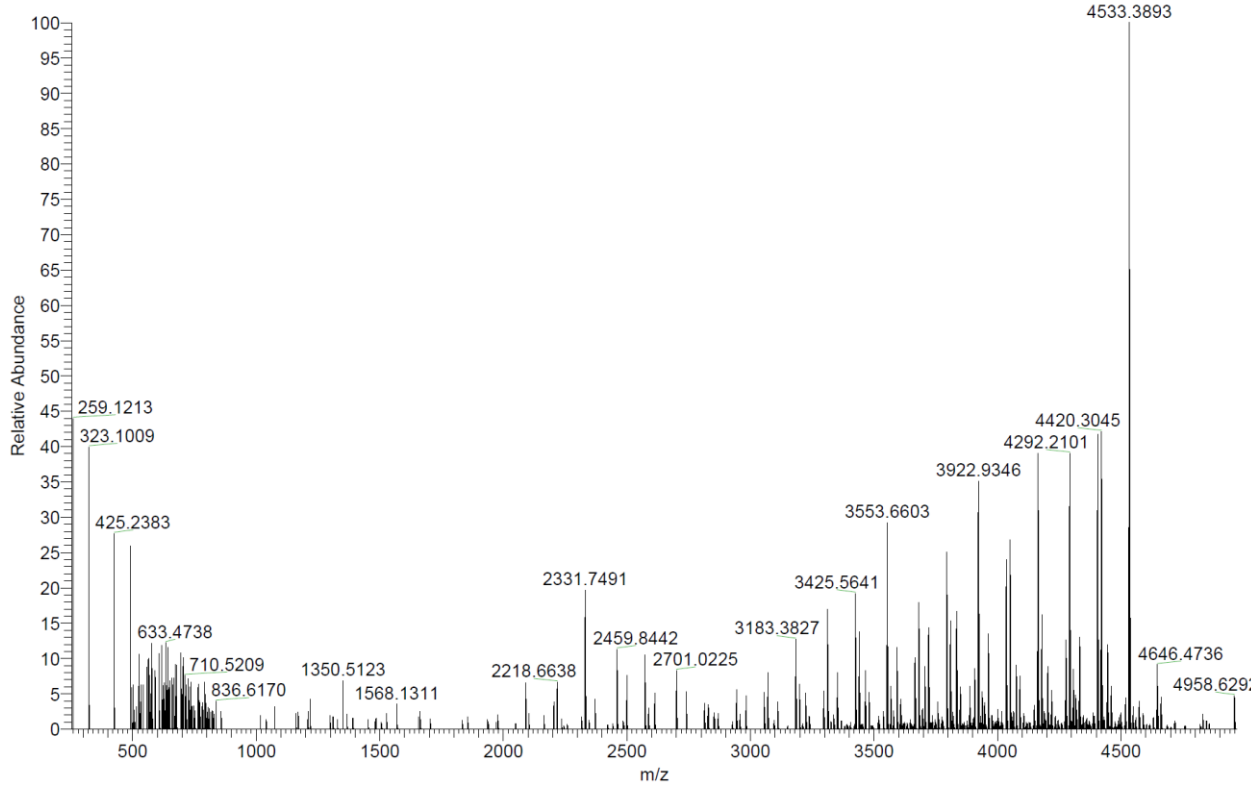
Relative Abundance
m/z
4533.3893
259.1213
323.1009
425.2383
633.4738
710.5209
836.6170
1350.5123
1568.1311
2218.6638
2331.7491
2459.8442
2701.0225
3183.3827
3425.5641
3553.6603
3922.9346
4292.2101
4420.3045
4646.4736
4958.6292

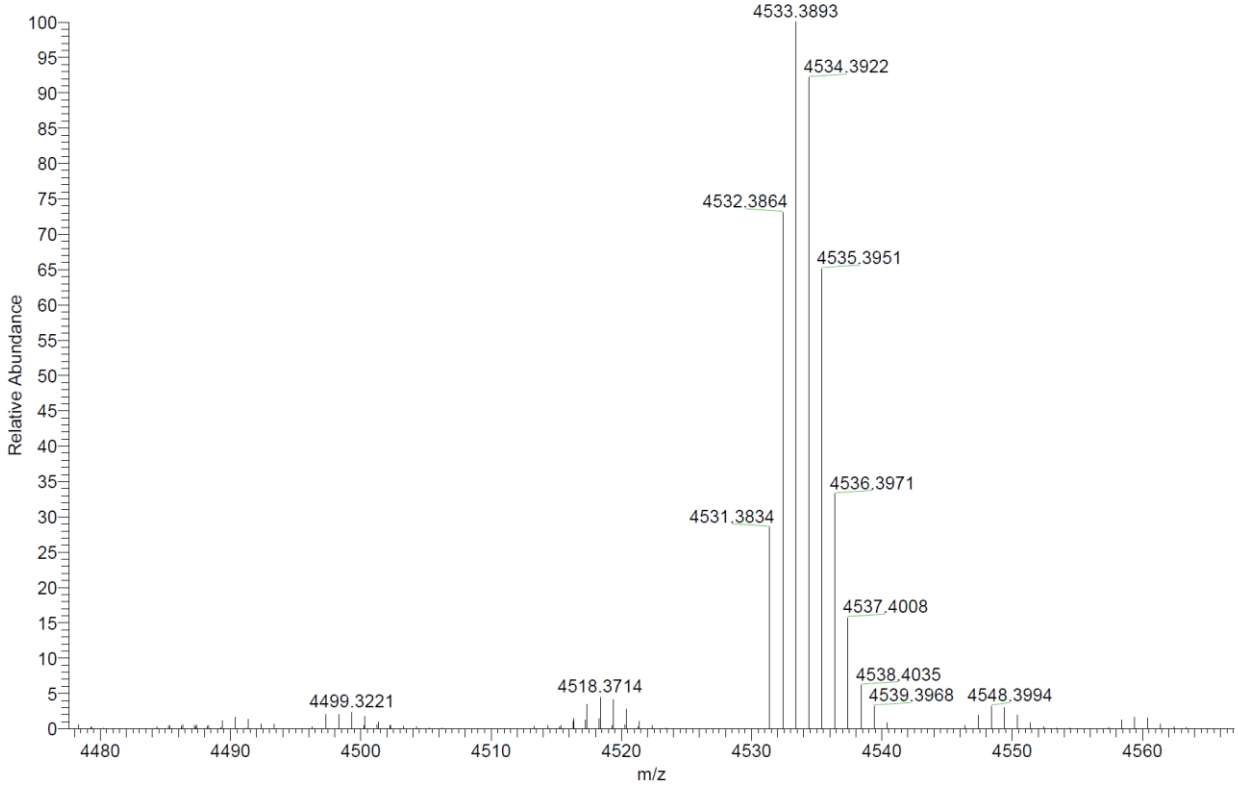
Relative Abundance
m/z
4533.3893
4534.3922
4532.3864
4535.3951
4536.3971
4531.3834
4537.4008
4538.4035
4539.3968
4548.3994
4518.3714
4499.3221

G3KL (2% v/v DBU, 60°C) was obtained as crude white solid after lyophilization (400.6 mg, 48.4%). Analytical RP-HPLC: t_R = 2.75 min (A/D 100:0 to 0:100 in 7.00 min, λ = 214nm). HRMS (ESI+): $C_{222}H_{432}N_{60}O_{37}$ calc./obs. 4532.38/4532.39 Da $[M+H]^+$.

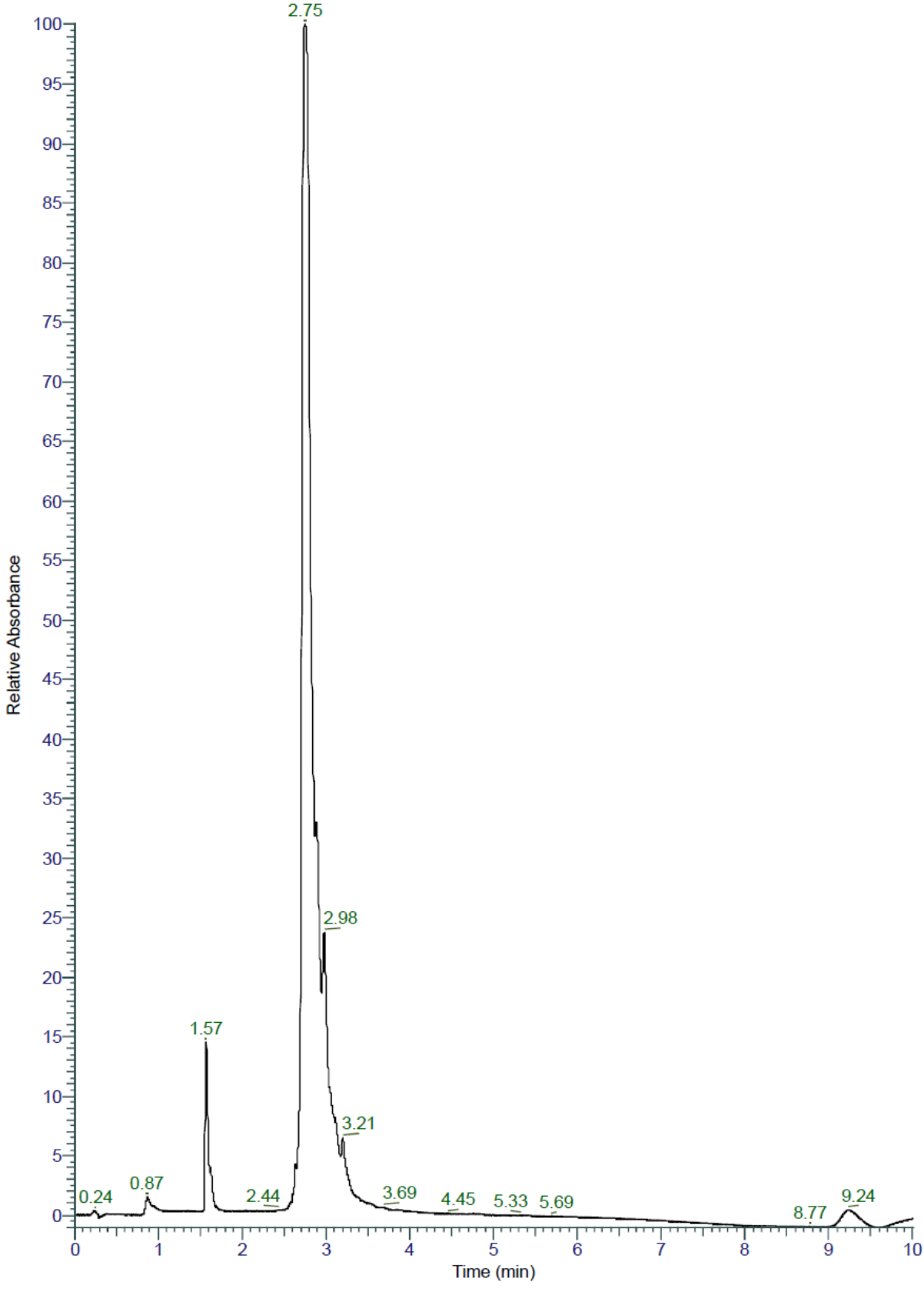

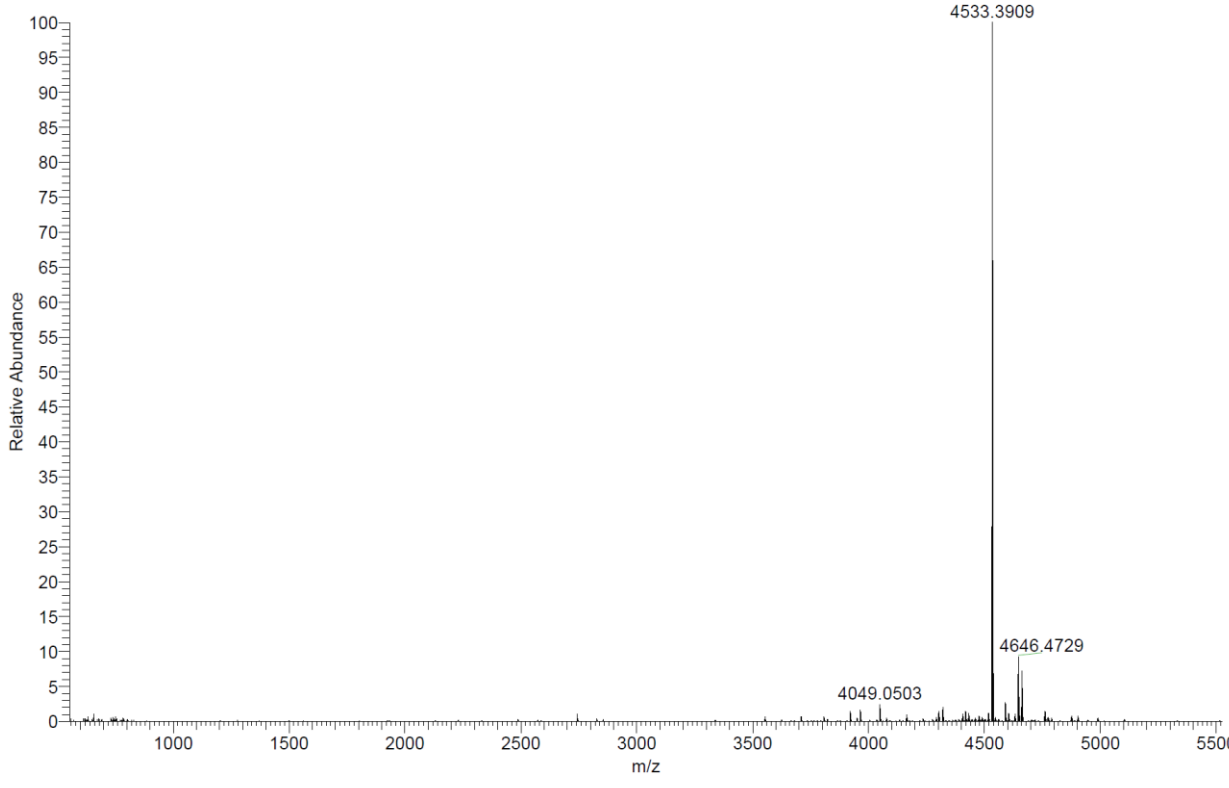
4533.3909
4646.4729
4049.0503
Relative Abundance
m/z

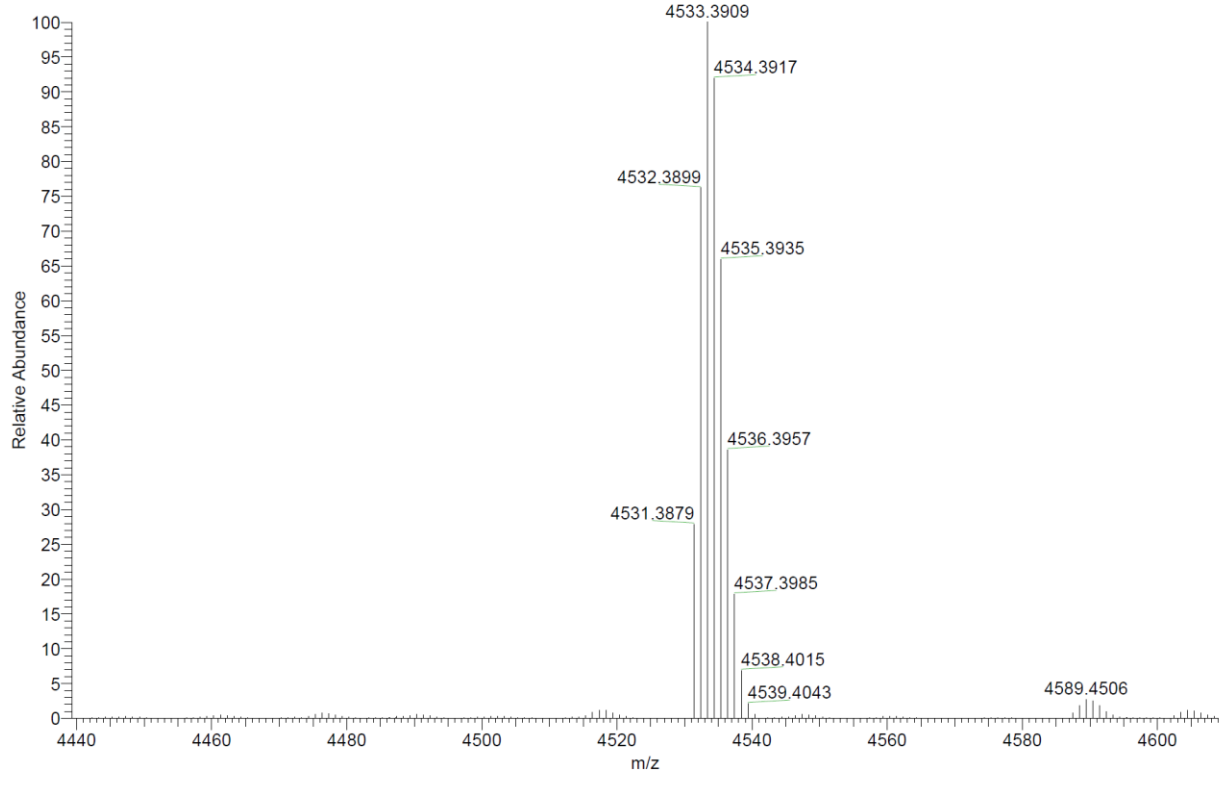
4533.3909
4534.3917
4532.3899
4535.3935
4536.3957
4531.3879
4537.3985
4538.4015
4539.4043
4589.4506
Relative Abundance
m/z

G3KL (20% v/v Piperidine, r.t.) was obtained as crude white solid after lyophilization (301.2 mg, 40.5%). Analytical RP-HPLC: t_R = 2.68 min (A/D 100:0 to 0:100 in 7.00 min, λ = 214nm). HRMS (ESI+): $C_{222}H_{432}N_{60}O_{37}$ calc./obs. 4532.38/4532.39 Da $[M+H]^+$.

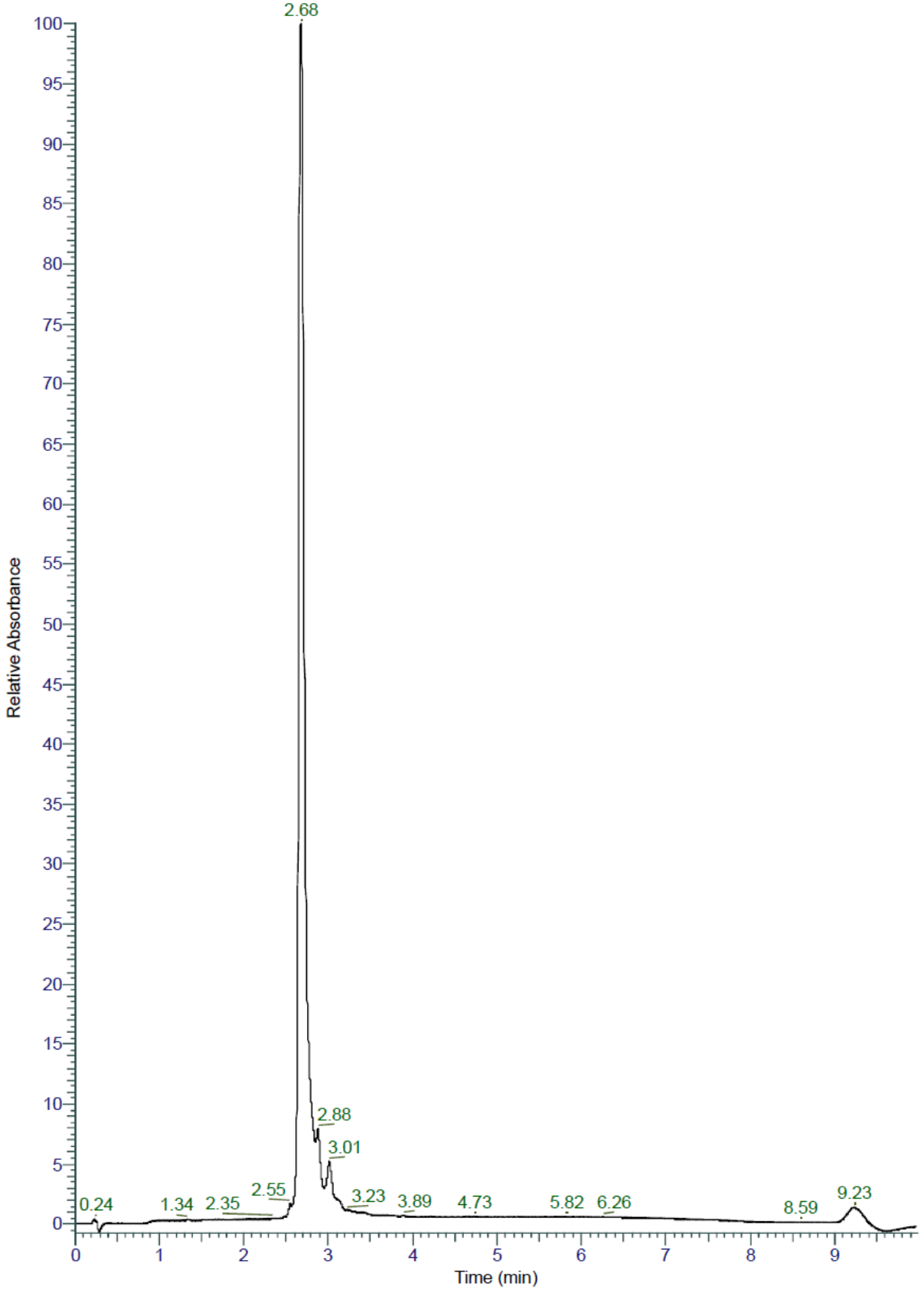

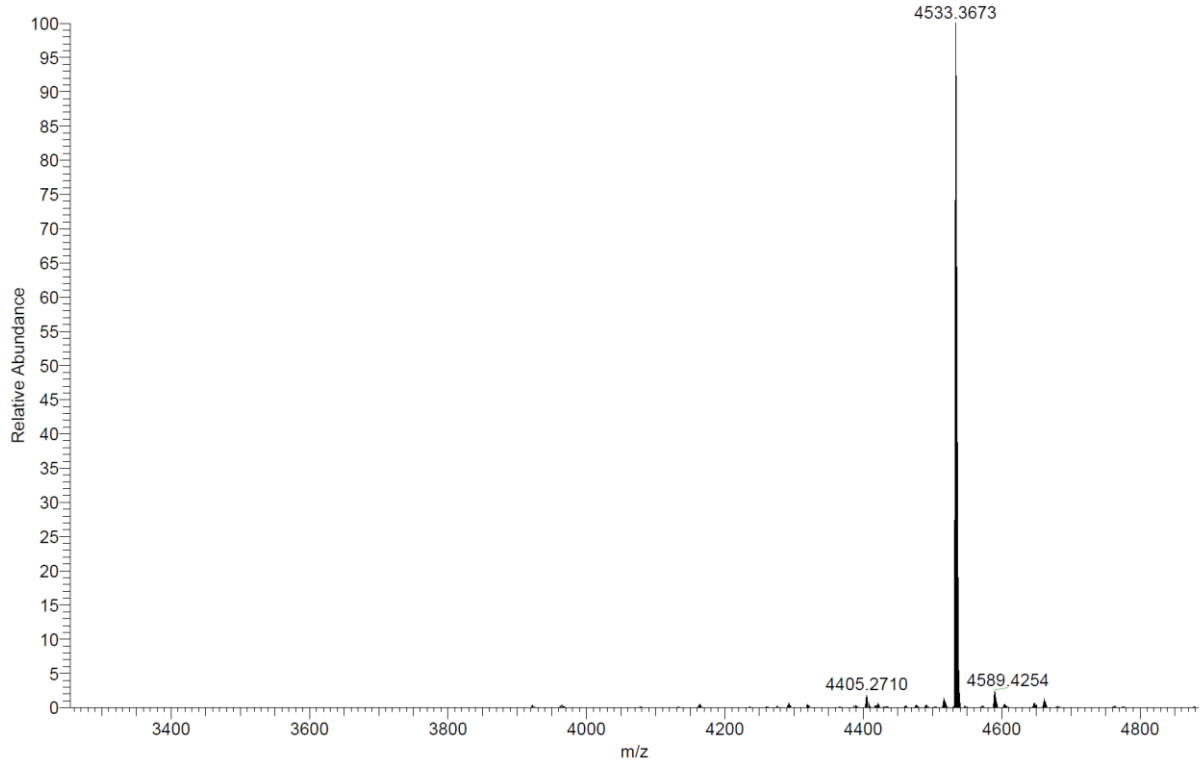
4533.3673
4405.2710
4589.4254
Relative Abundance
m/z

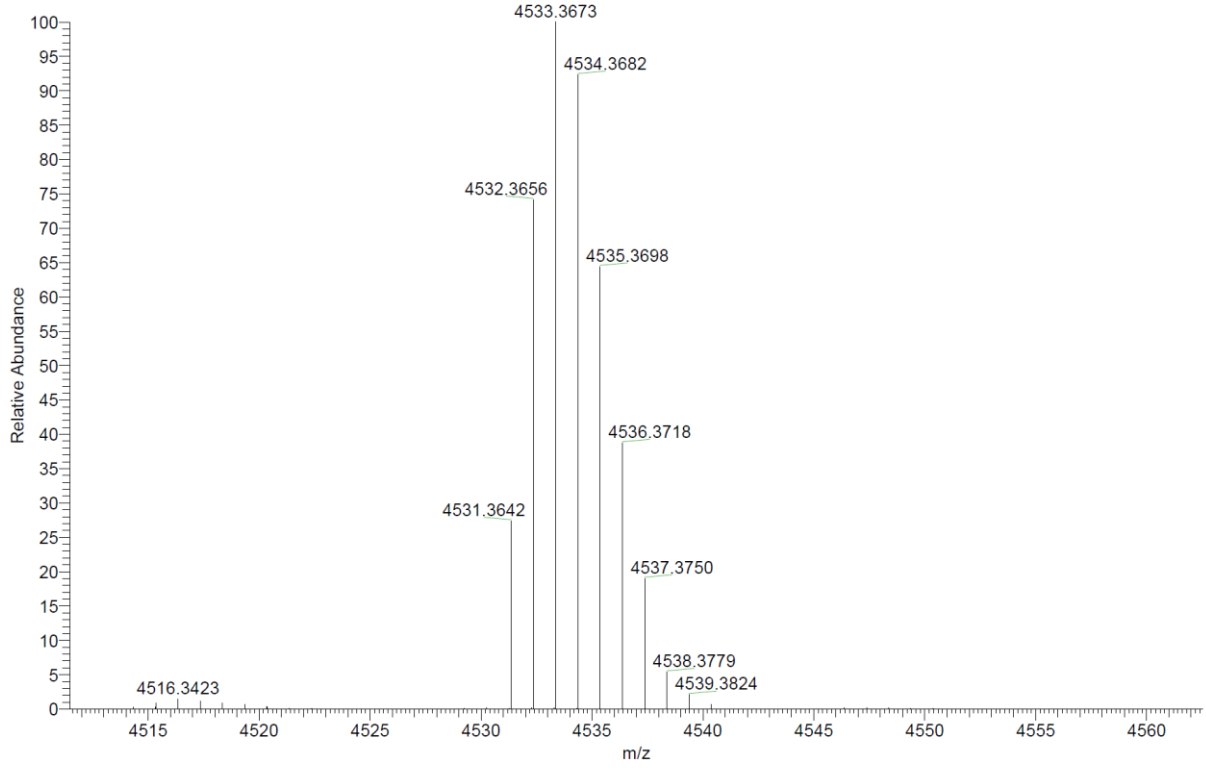
4533.3673
4534.3682
4532.3656
4535.3698
4536.3718
4531.3642
4537.3750
4538.3779
4539.3824
4516.3423
Relative Abundance
m/z

G3KL (25% v/v Dipropylamine, r.t.) was obtained as crude white solid after lyophilization (249.7 mg, 12.3%). Analytical RP-HPLC: t_R = 2.71 min (A/D 100:0 to 0:100 in 7.00 min, λ = 214nm). HRMS (ESI+): $C_{222}H_{432}N_{60}O_{37}$ calc./obs. 4532.38/4532.39 Da $[M+H]^+$.

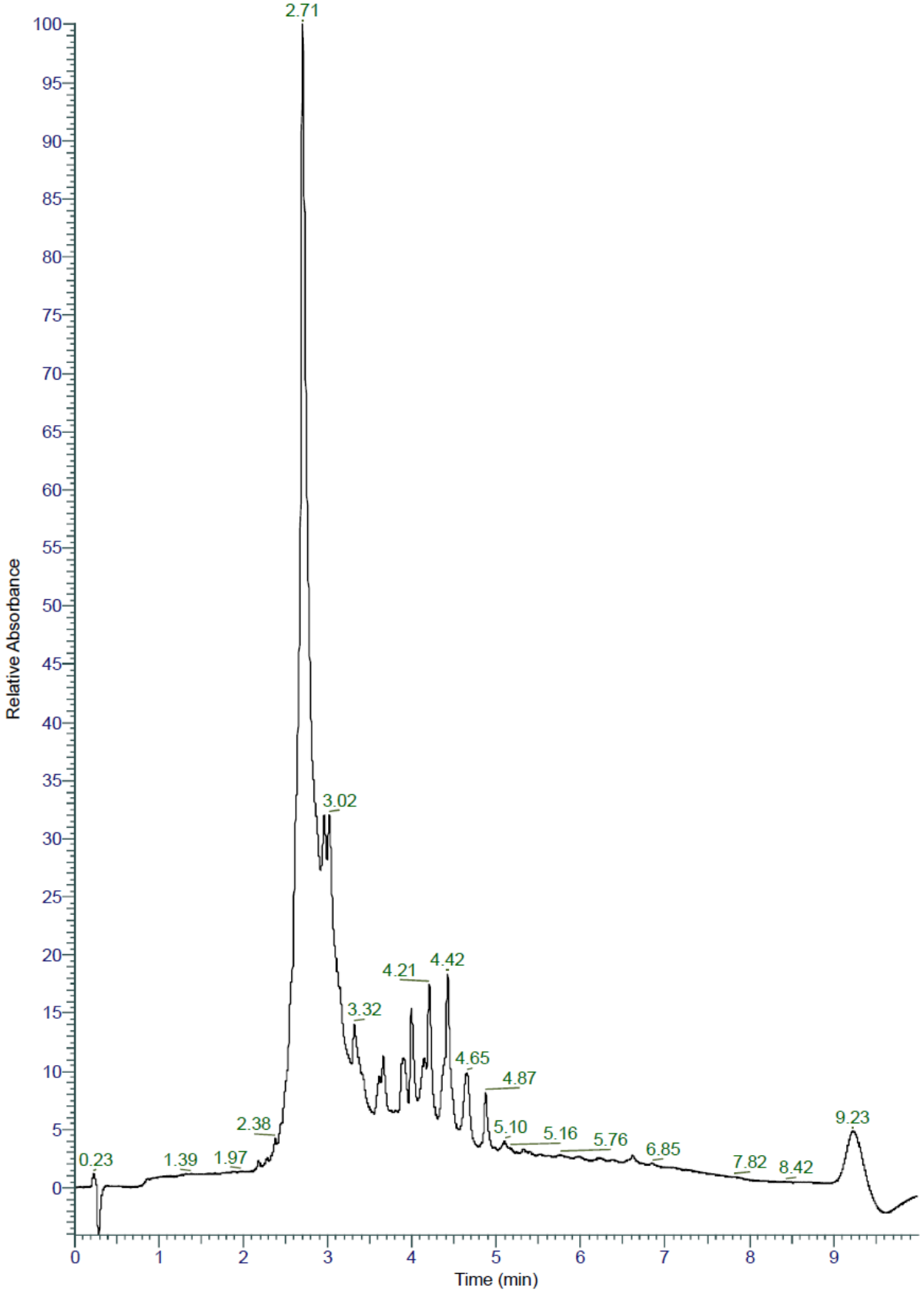

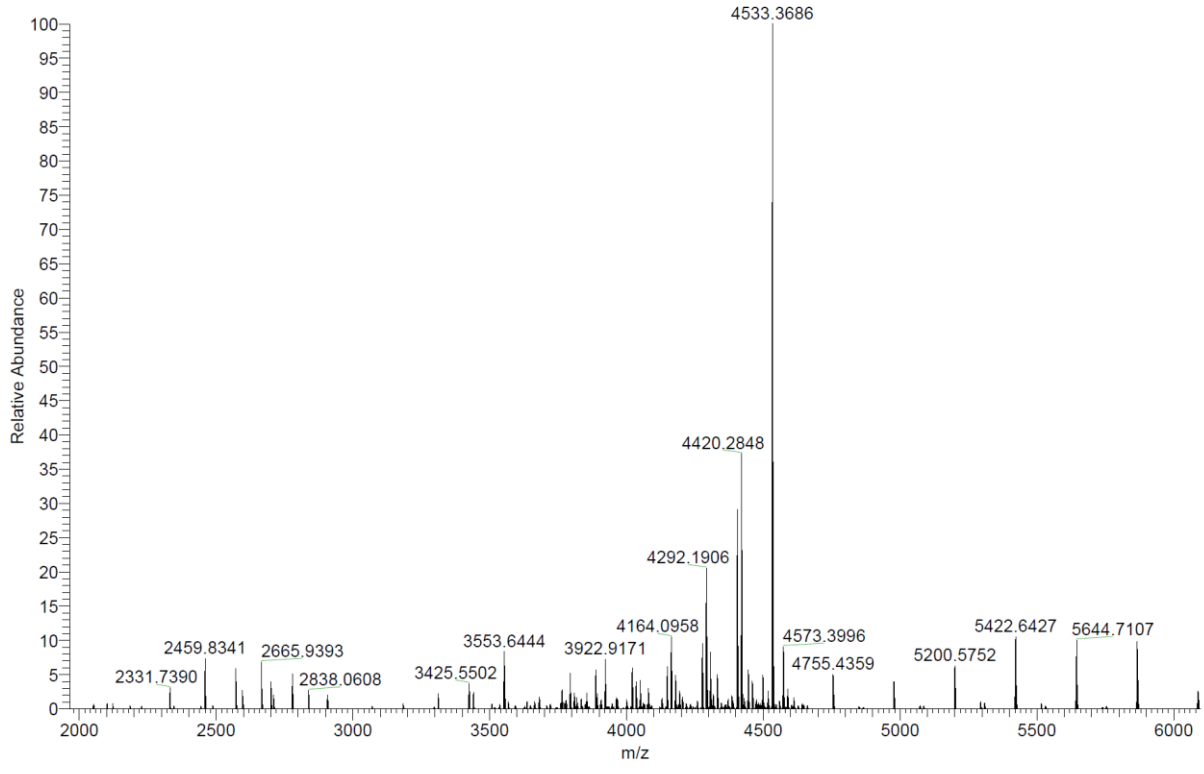
4533.3686
4420.2848
4292.1906
4164.0958
4573.3996
4755.4359
5422.6427
5644.7107
5200.5752
3553.6444
3922.9171
2459.8341
2665.9393
2331.7390
2838.0608
3425.5502
Relative Abundance
m/z

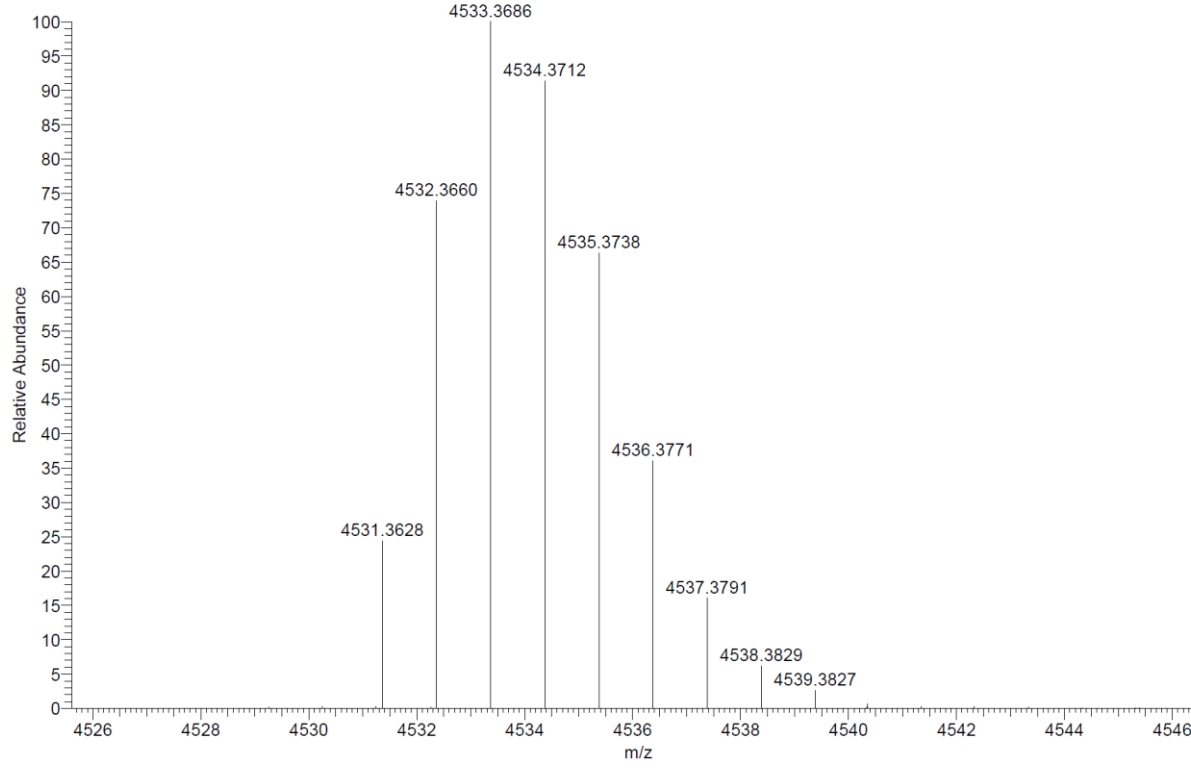
4533.3686
4534.3712
4532.3660
4535.3738
4536.3771
4531.3628
4537.3791
4538.3829
4539.3827
Relative Abundance
m/z

8.5 SI for Submonomer synthesis of antimicrobial inverse polyamidoamines

Synthesis of Tfa protected amine

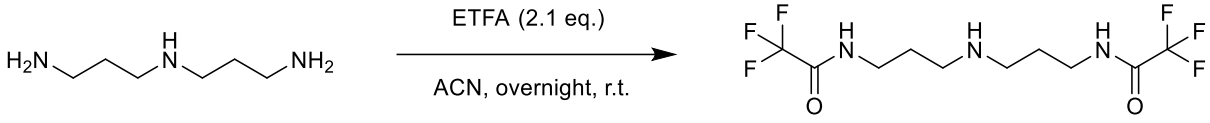

Bis(aminopropyl)amine (26.5 mL, 25 g) was diluted in 200 mL acetonitrile (> 99.9% pure) in a 500 mL round bottom flask. ethyltrifuoroacetate (ETFA, 47.5 mL, 2.1 eq.) was slowly added to the reaction flask. The reaction mixture was stirred at room temperature overnight. The next day, remaining ETFA and acetonitrile were evaporated at 60 °C, 10 mbar during two hours to obtain the crude product. The obtained yellowish oily material (49.2 g, 80%) was analyzed by NMR (^{1}H, ^{13}C) and analytical reverse-phase HPLC-MS.

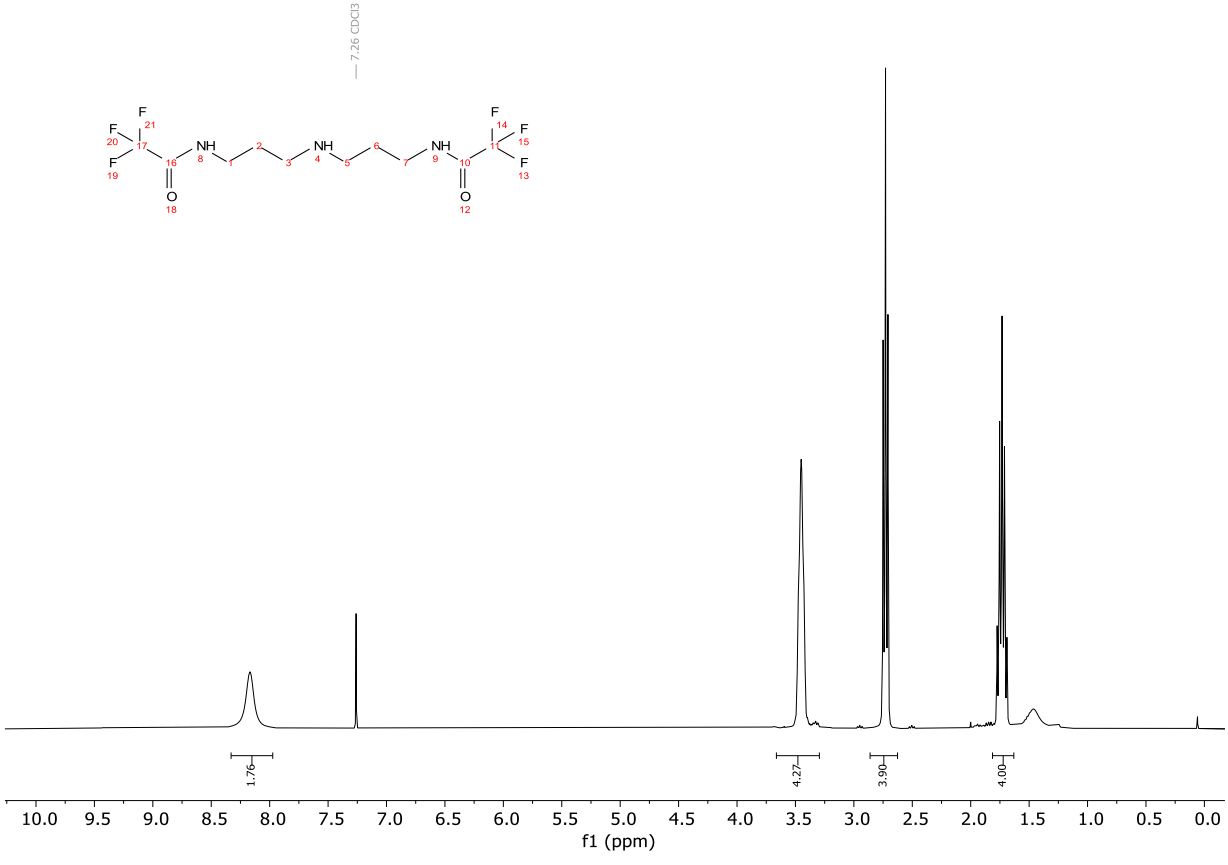

Figure S5.1: ^{1}H NMR spectra (300 MHz, $CDCl_3$) of *N*,*N*-bis(3-trifluoroacetylaminopropyl)amine. δ = 8.33 – 7.97 (m, 2H, N8 and N9), 3.45 (q, *J* = 5.2 Hz, 4H, C1 and C7), 2.73 (t, *J* = 6.2 Hz, 4H, C3 and C5), 1.73 (p, *J* = 6.3 Hz, 4H, C2 and C6).

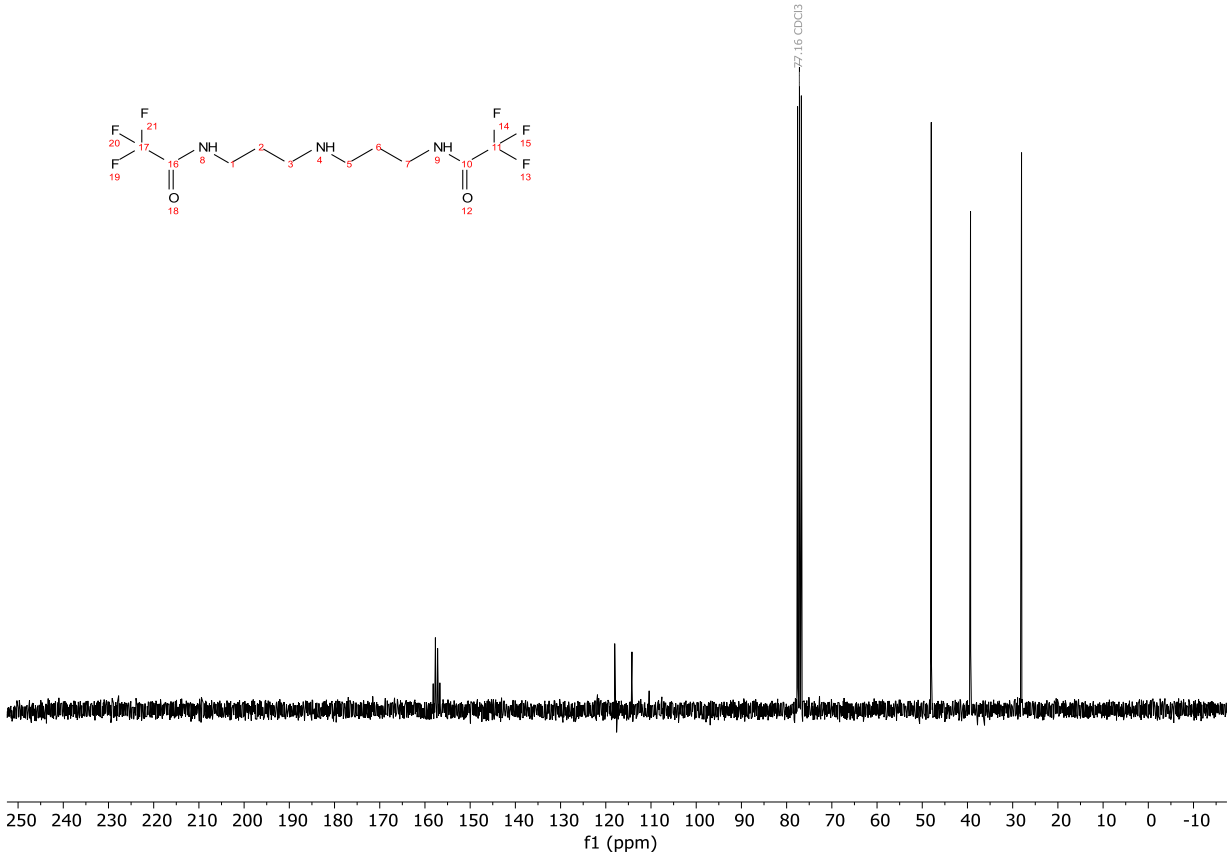

Figure S5.2: ^{13}C NMR spectra (75 MHz, $CDCl_3$) of *N*,*N*-bis(3-trifluoroacetylaminopropyl)amine. δ = 157.44 (q, *J* = 37.0 Hz, C10 and C16), 116.12 (d, *J* = 287.8 Hz, C11 and C17), 48.00 (s, C32 and C5), 39.32 (s, C1 and C7), 28.04 (s, C2 and C6).

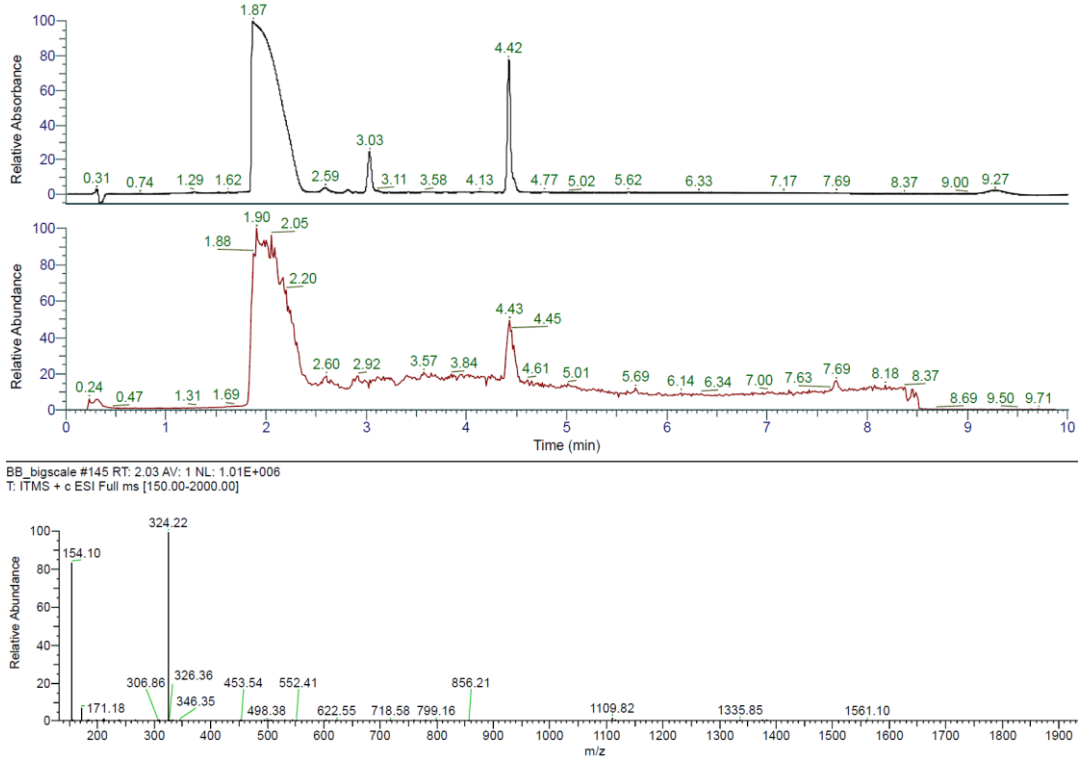

Figure S3: HPLC-MS spectra of *N*,*N*-bis(3-trifluoroacetylaminopropyl)amine. Biprotected product: t_R = 1.87 min. Triprotected product: t_R = 4.42 min.

Deprotection of trifluoroacetyl protecting groups

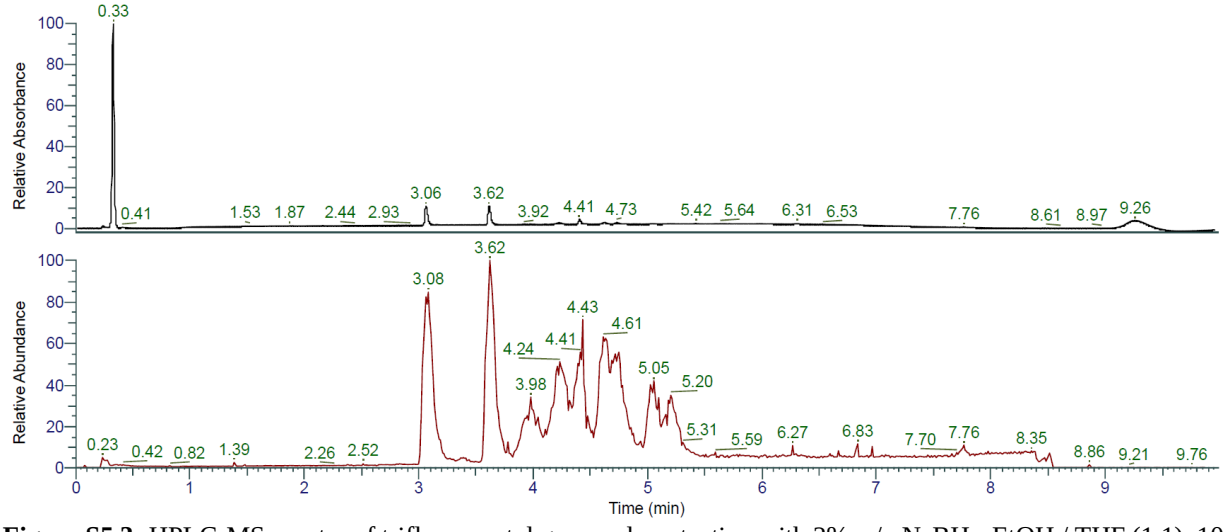

Figure S5.3: HPLC-MS spectra of trifluoroacetyl groups deprotection with 2% w/v $NaBH_4$, EtOH / THF (1:1), 10 min, 60 °C (entry **1** of Table 1). Retention times: fully deprotected product: t_R = 3.06 min, monoprotected product: t_R = 3.62 min, biprotected product: t_R = 4.41 min (A/D 100:0 to 0:100 in 7.00 min, λ = 214 nm).

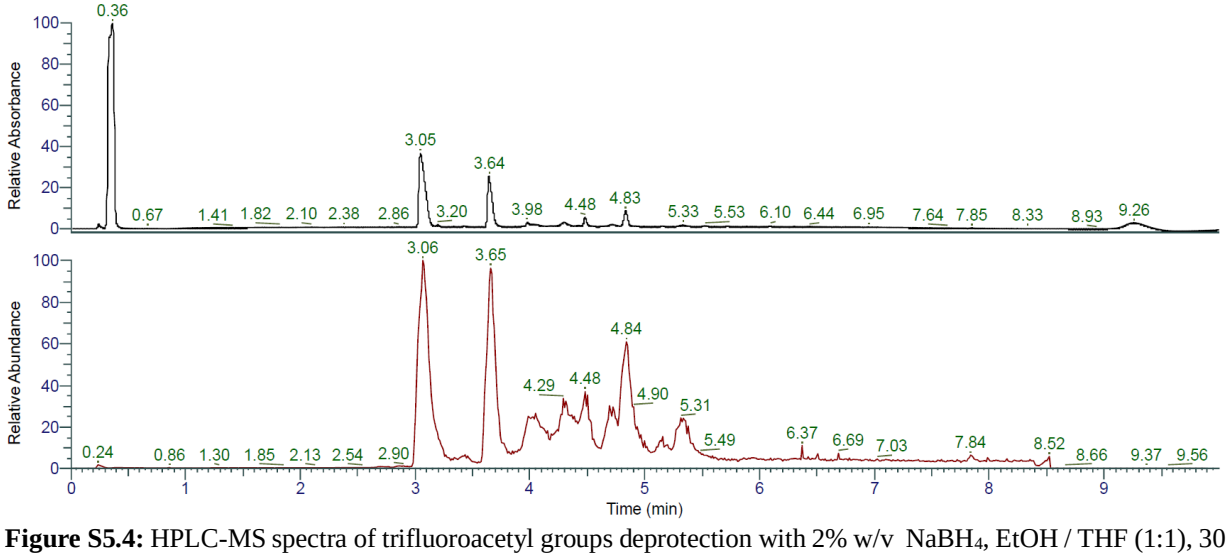

Figure S5.4: HPLC-MS spectra of trifluoroacetyl groups deprotection with 2% w/v $NaBH_4$, EtOH / THF (1:1), 30 min, r. t. (entry **2** of Table 1). Retention times: fully deprotected product: t_R = 3.05 min, monoprotected product: t_R = 3.64 min, biprotected product: t_R = 4.48 min (A/D 100:0 to 0:100 in 7.00 min, λ = 214 nm).

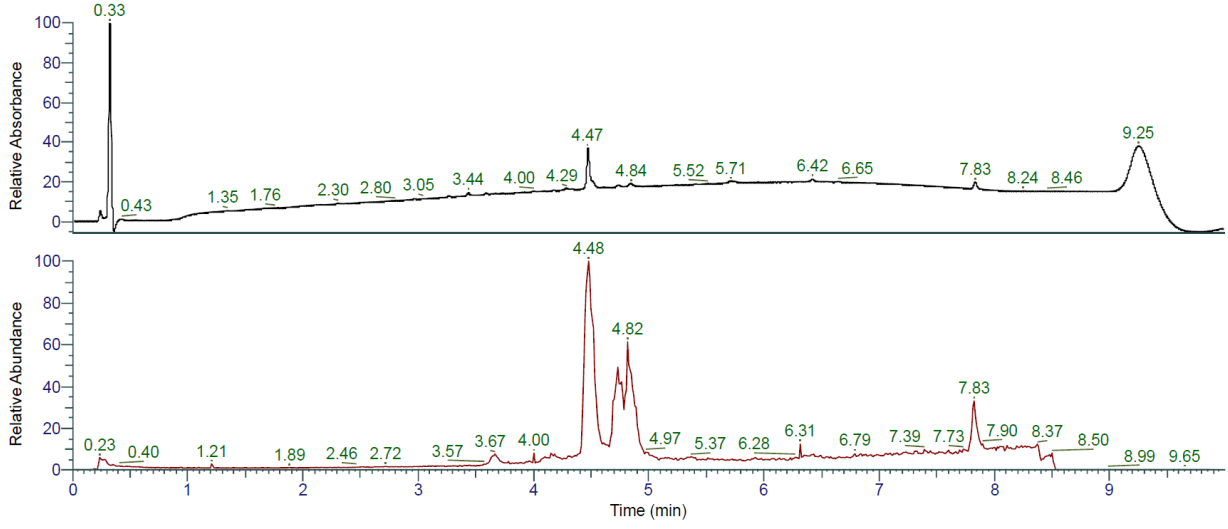

Figure S5.5: HPLC-MS spectra of trifluoroacetyl groups deprotection with 0.2 M NaOH, DMF / H_2O (1:1), 10 min, 60 °C (entry **3** of Table 1). Retention times: biprotected product: t_R = 4.47 min (A/D 100:0 to 0:100 in 7.00 min, λ = 214 nm).

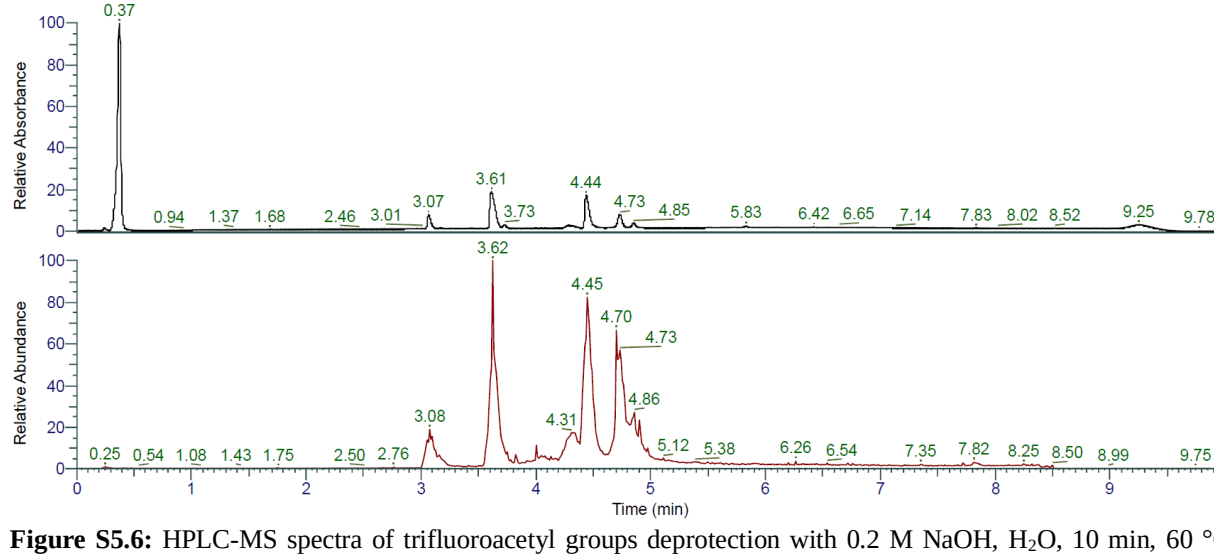

Figure S5.6: HPLC-MS spectra of trifluoroacetyl groups deprotection with 0.2 M NaOH, H_2O, 10 min, 60 °C (entry **4** of Table 1). Retention times: fully deprotected product: t_R = 3.07 min, monoprotected product: t_R = 3.61 min, biprotected product: t_R = 4.44 min (A/D 100:0 to 0:100 in 7.00 min, λ = 214 nm).

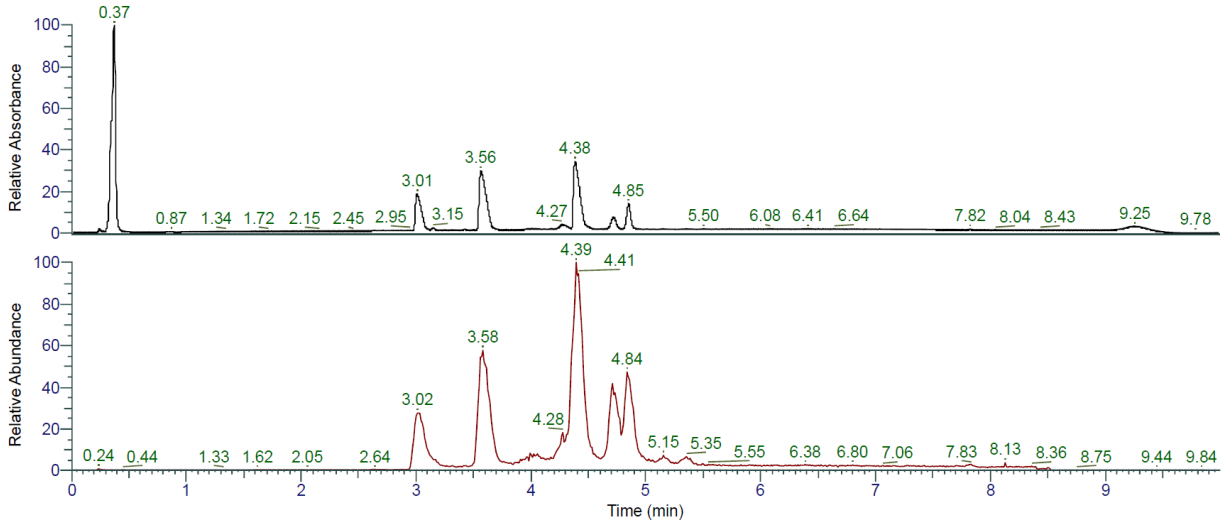

Figure S5.7: HPLC-MS spectra of trifluoroacetyl groups deprotection with 0.2 M LiOH, H_2O, 30 min, 60 °C (entry **5** of Table 1). Retention times: fully deprotected product: t_R = 3.01 min, monoprotected product: t_R = 3.56 min, biprotected product: t_R = 4.38 min (A/D 100:0 to 0:100 in 7.00 min, λ = 214 nm).

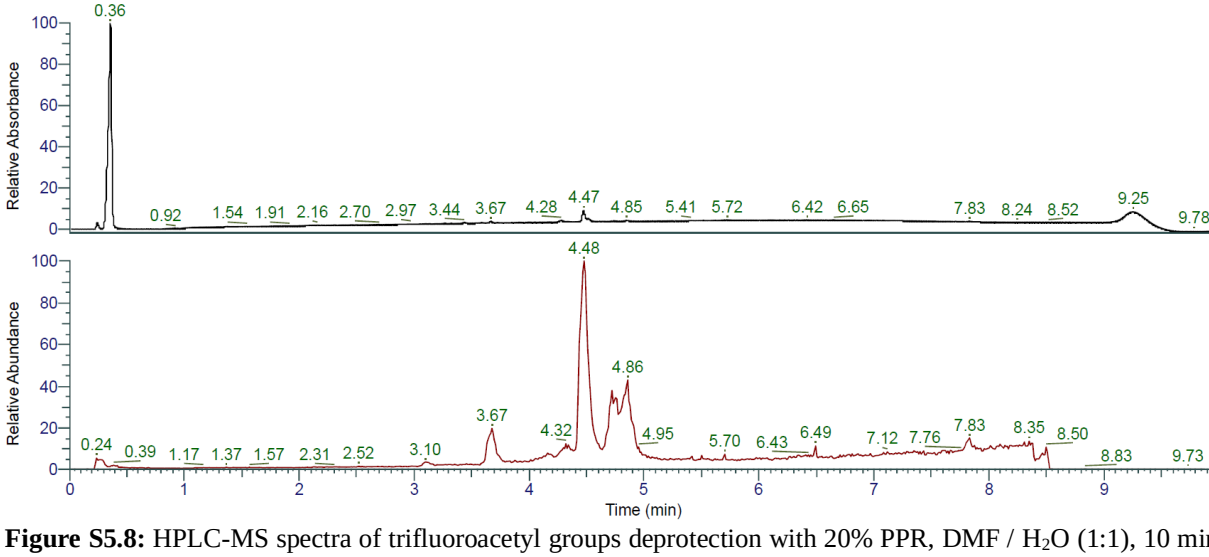

Figure S5.8: HPLC-MS spectra of trifluoroacetyl groups deprotection with 20% PPR, DMF / H_2O (1:1), 10 min, 60 °C (entry **6** of Table 1). Retention times: biprotected product: t_R = 4.47 min (A/D 100:0 to 0:100 in 7.00 min, λ = 214 nm).

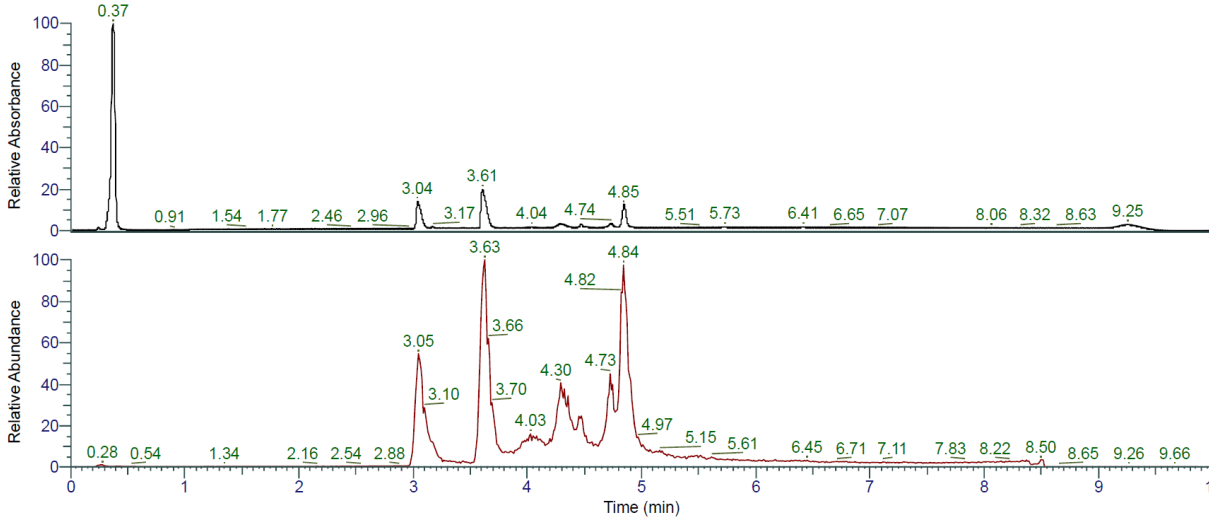

Figure S5.9: HPLC-MS spectra of trifluoroacetyl groups deprotection with 20% PPR, H_2O, 10 min, 60 °C (entry **7** of Table 1). Retention times: fully deprotected product: t_R = 3.04 min, monoprotected product: t_R = 3.61 min (A/D 100:0 to 0:100 in 7.00 min, λ = 214 nm).

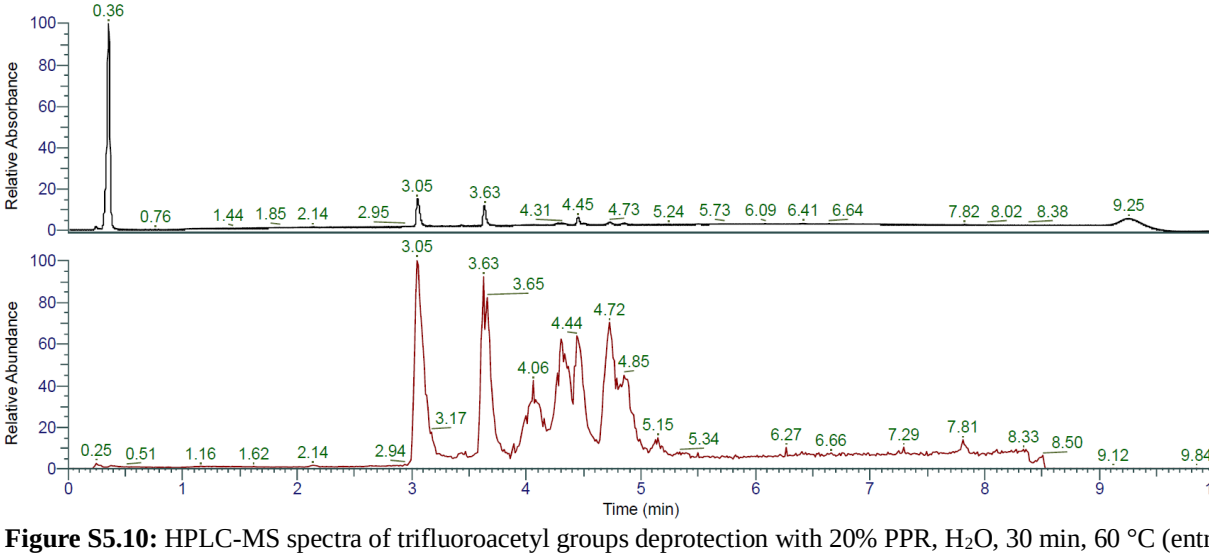

Figure S5.10: HPLC-MS spectra of trifluoroacetyl groups deprotection with 20% PPR, H_2O, 30 min, 60 °C (entry **8** of Table 1). Retention times: fully deprotected product: t_R = 3.05 min, monoprotected product: t_R = 3.63 min, biproducted product: t_R = 4.45 min (A/D 100:0 to 0:100 in 7.00 min, λ = 214 nm).

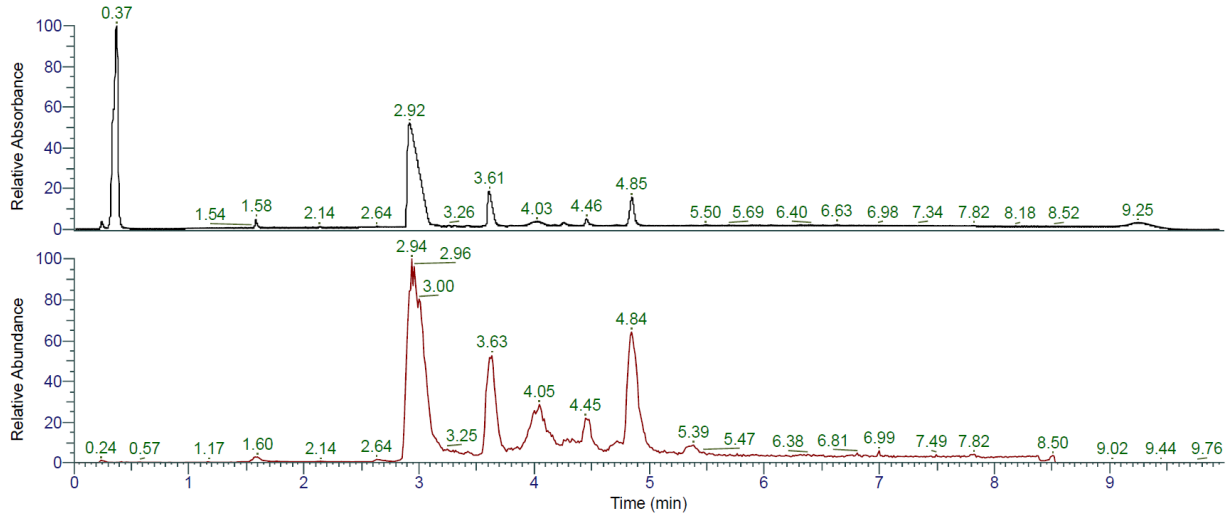

Figure S5.11: HPLC-MS spectra of trifluoroacetyl groups deprotection with 20% PPR, H_2O, 2 x 30 min, 60 °C (entry **9** of Table 1). Retention times: fully deprotected product: t_R = 2.92 min, monoprotected product: t_R = 3.61 min, biproducted product: t_R = 4.46 min (A/D 100:0 to 0:100 in 7.00 min, λ = 214 nm).

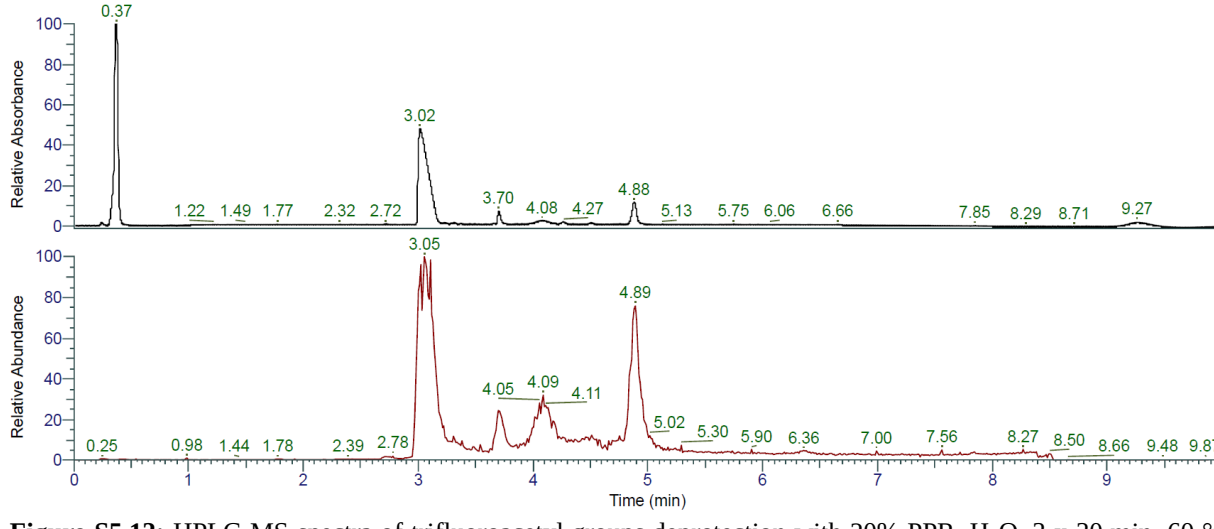

Figure S5.12: HPLC-MS spectra of trifluoroacetyl groups deprotection with 20% PPR, H_2O, 3 x 30 min, 60 °C (entry **10** of Table 1). Retention times: fully deprotected product: t_R = 3.02 min, monoprotected product: t_R = 3.70 min (A/D 100:0 to 0:100 in 7.00 min, λ = 214 nm).

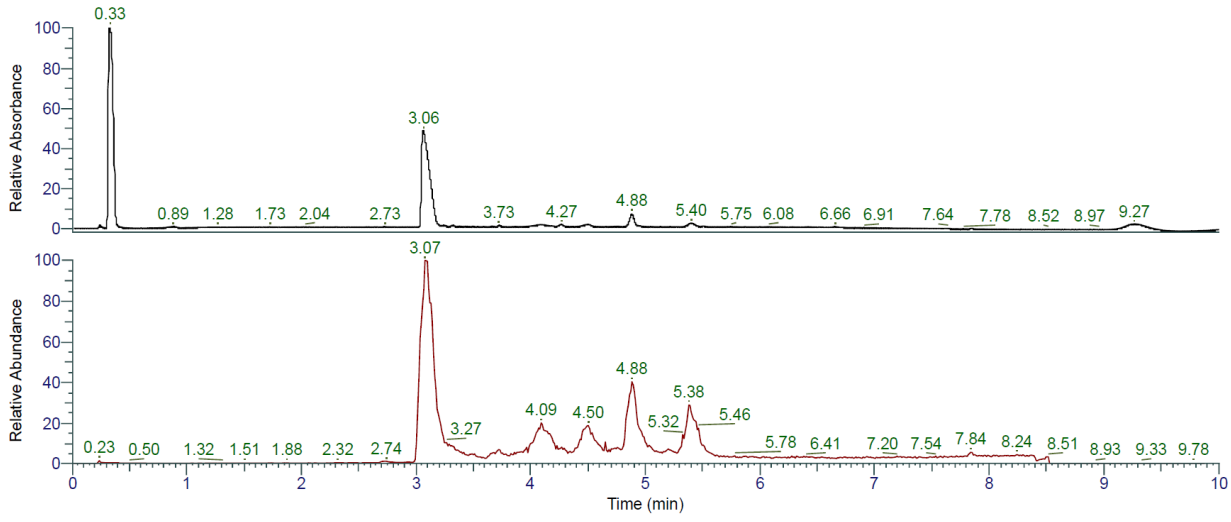

Figure S5.13: HPLC-MS spectra of trifluoroacetyl groups deprotection with 20% PPR, H_2O, 4 x 30 min, 60 °C (entry **11** of Table 1). Retention times: fully deprotected product: t_R = 3.06 min (A/D 100:0 to 0:100 in 7.00 min, λ = 214 nm).

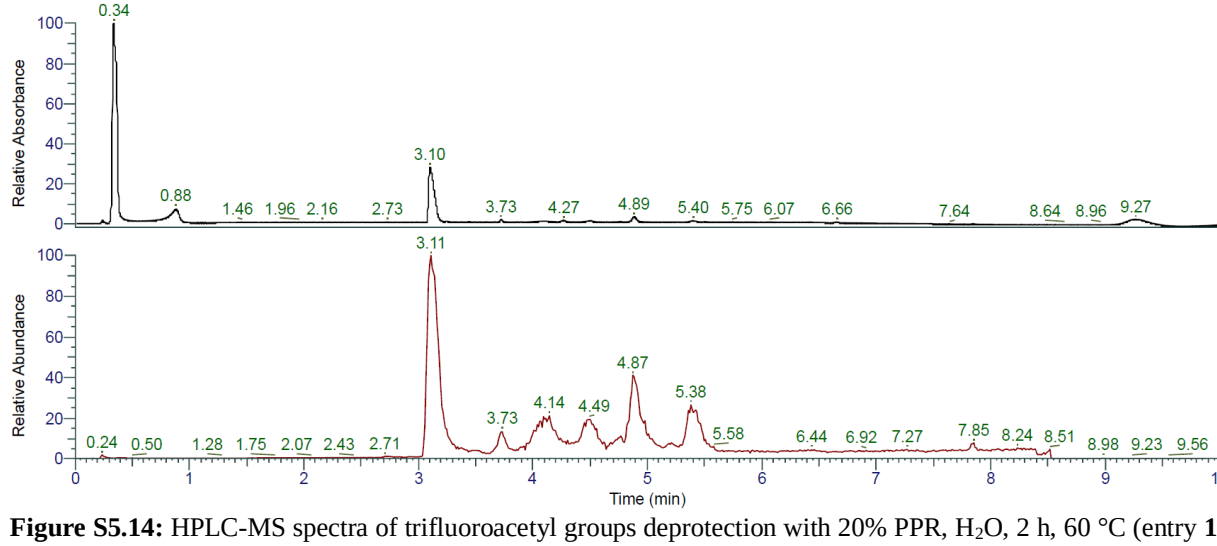

Figure S5.14: HPLC-MS spectra of trifluoroacetyl groups deprotection with 20% PPR, H_2O, 2 h, 60 °C (entry **12** of Table 1). Retention times: fully deprotected product: t_R = 3.10 min, monoprotected product: t_R = 3.73 min, biprotected product: t_R = 4.51 min (A/D 100:0 to 0:100 in 7.00 min, λ = 214 nm).

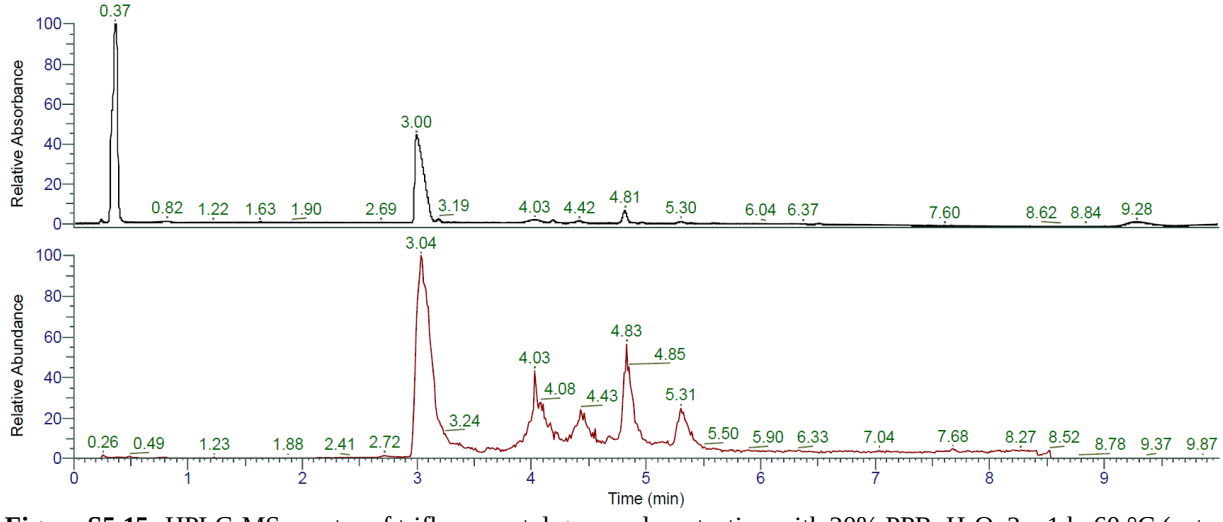

Figure S5.15: HPLC-MS spectra of trifluoroacetyl groups deprotection with 20% PPR, H_2O, 2 x 1 h, 60 °C (entry **13** of Table 1). Retention times: fully deprotected product: t_R = 3.00 min (A/D 100:0 to 0:100 in 7.00 min, λ = 214 nm).

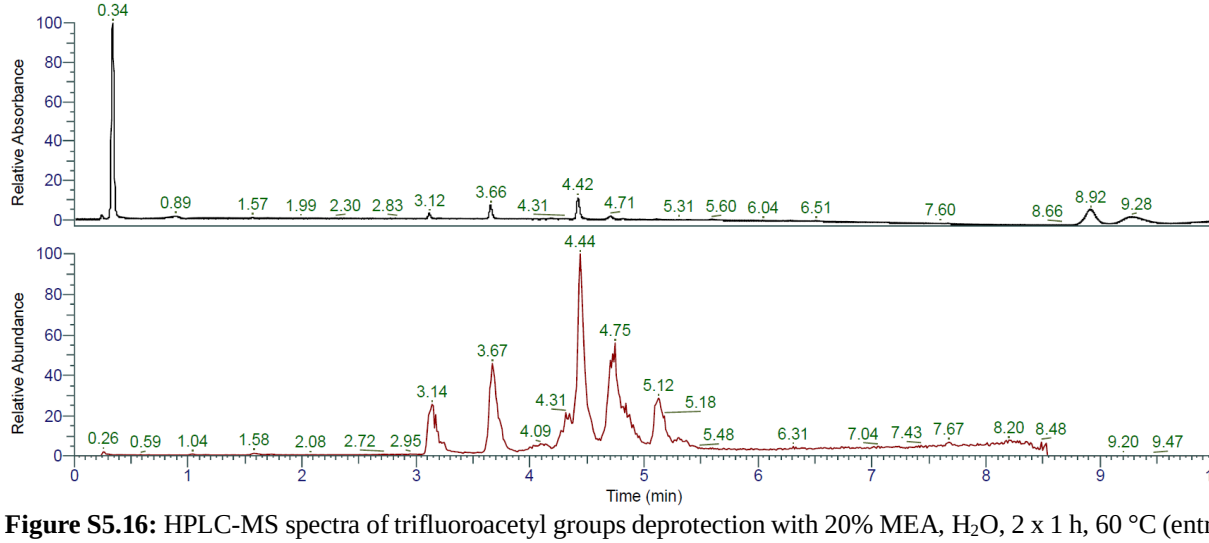

Figure S5.16: HPLC-MS spectra of trifluoroacetyl groups deprotection with 20% MEA, H_2O, 2 x 1 h, 60 °C (entry **14** of Table 1). Retention times: fully deprotected product: t_R = 3.00 min (A/D 100:0 to 0:100 in 7.00 min, λ = 214 nm).

i-PAMAMs synthesis

Table S5.1: Number of couplings depending on the number of branches.

Number of branches	1	2	4	8	16
Number of amino acid and $BrCH_2CO_2H$ couplings	2	2	4	6	8

All the iPAMAMs syntheses were performed under nitrogen bubbling at 60 °C. For each amino acid an $BrCH_2CO_2H$ coupling, 5 eq. building block (3 mL of a 0.11 M solution in DMF), 5 eq. Oxyma (1.5 mL of a 0.22 M solution in DMF) and 6 eq. of DIC (2 mL of a 0.20 M solution in DMF) were premixed before adding it to the resin. Equivalents are relative to the loading resin. Resin was washed twice with 6 mL DMF between each coupling, and three times after the last one.

Nucleophilic substitution of bromide by *N*,*N*-bis(3-trifluoroacetylaminopropyl)amine with the same procedure independently from the number of branches. 3 mL of building block solution containing 10 eq. in DMF relative to the number of bromine was added and the mixture was stirred under nitrogen bubbling during 15 min. Resin was washed three times with 6 mL DMF before repeating the reaction. After the second repetition, resin was washed five times with 6 mL DMF.

Tfa deprotection was performed twice one hour with an aqueous 20% PPR v/v solution (6-8 mL). After one hour, solution was removed and reaction was performed a second time. After the second repetition, resin was washed five times with 6 mL DMF and three times with 3 mL MeOH before checking the deprotection with a micro-cleavage.

Antimicrobial evaluation of i-PAMAMs

Table S5.2: Antimicrobial activity of i-PAMAMs measured in full MH medium at pH 7.4 and 8.5.

Cpd.	**MIC (µg/mL)**									
	P. aeruginosa PAO1		*K. pneumoniae* NCTC418		*A. baumannii* ATCC19606		*E. coli* W3110		*S. aureus* COL	
	pH 7.4	pH 8.5	pH 7.4	pH 8.5	pH 7.4	pH 8.5	pH 7.4	pH 8.5	pH 7.4	pH 8.5
1a	>32	>32	>32	>32	>32	>32	>32	>32	>32	>32
1b	>32	>32	>32	>32	>32	>32	>32	>32	>32	>32
2a	>32	>32	>32	>32	>32	>32	>32	>32	>32	>32
2b	>32	>32	>32	>32	>32	>32	>32	>32	>32	>32
3a	>32	>32	>32	>32	>32	>32	>32	>32	>32	32
3b	>32	>32	>32	>32	>32	>32	>32	>32	>32	>32
4a	>32	>32	>32	>32	>32	>32	>32	32	>32	16-32
4b	>32	>32	>32	>32	>32	>32	>32	>32	>32	>32
Pol B	0.5	0.5	0.25	0.5	0.25	0.25	<0.125	0.5	>16	2
Vancomycin	>16	>16	>16	>16	>16	>16	>16	>16	0.5	1

[a)] Minimum Inhibitory Concentrations were determined after incubation in full MH broth pH 7.4 and 8.5 for 16-20 h at 37 °C.

iPAMAMs characterization

***Bag*LLLL (1a)** was obtained as white solid after preparative RP-HPLC (18.0 mg, 27.8%). Analytical RP-HPLC: t_R = 3.03 min (A/D 100:0 to 0:100 in 7.0 min, λ = 214 nm). MS (ESI+): $C_{32}H_{64}N_8O_5$ calc./obs. 641.50/641.56 Da $[M+H]^+$.

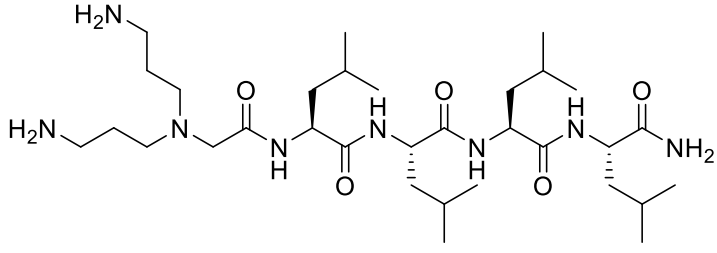

Chemical Formula: $C_{32}H_{64}N_8O_5$
Exact Mass: 640,50
Molecular Weight: 640,92

Analytical HPLC-MS data:

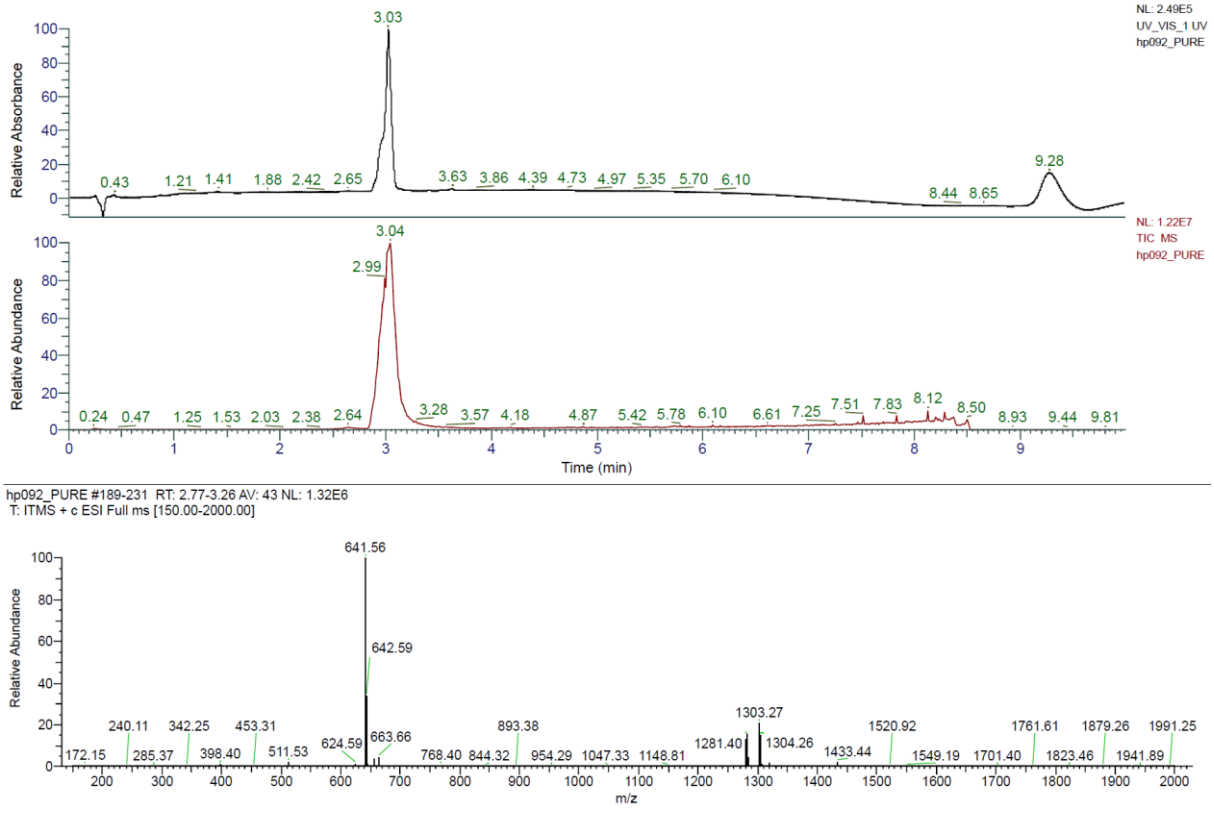

HRMS spectra:

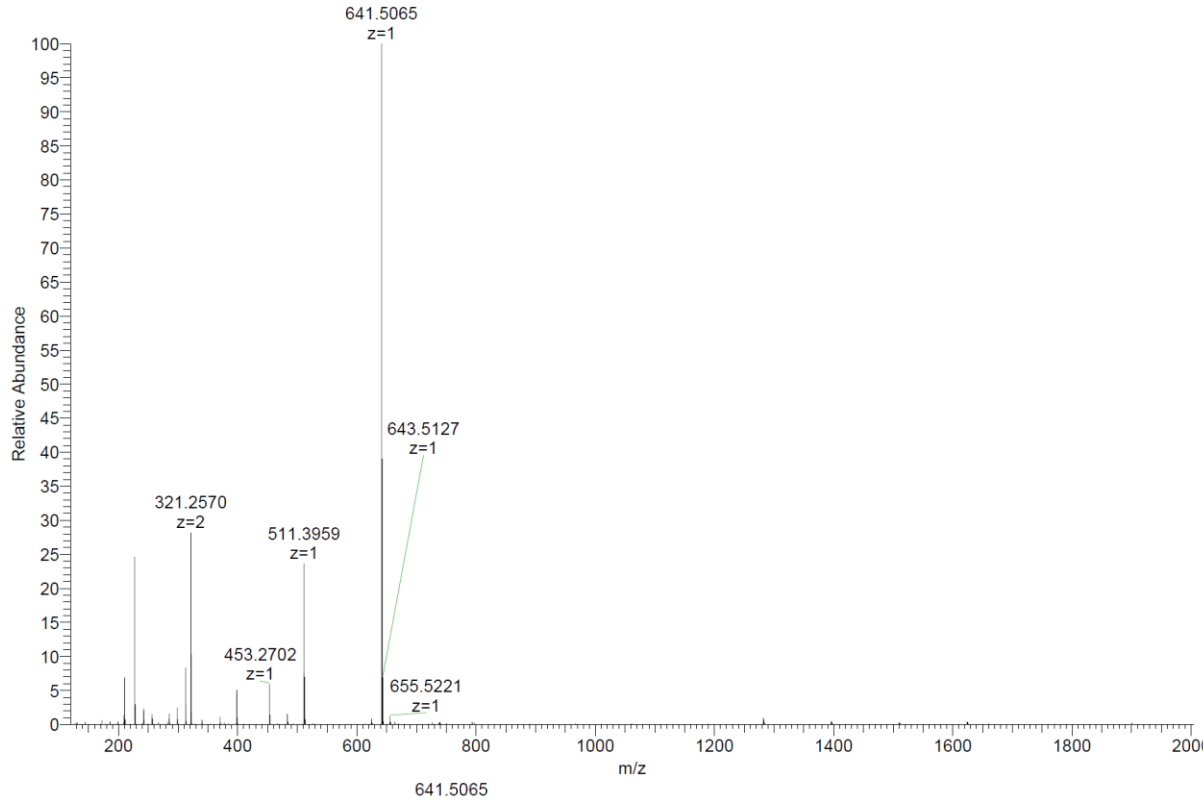

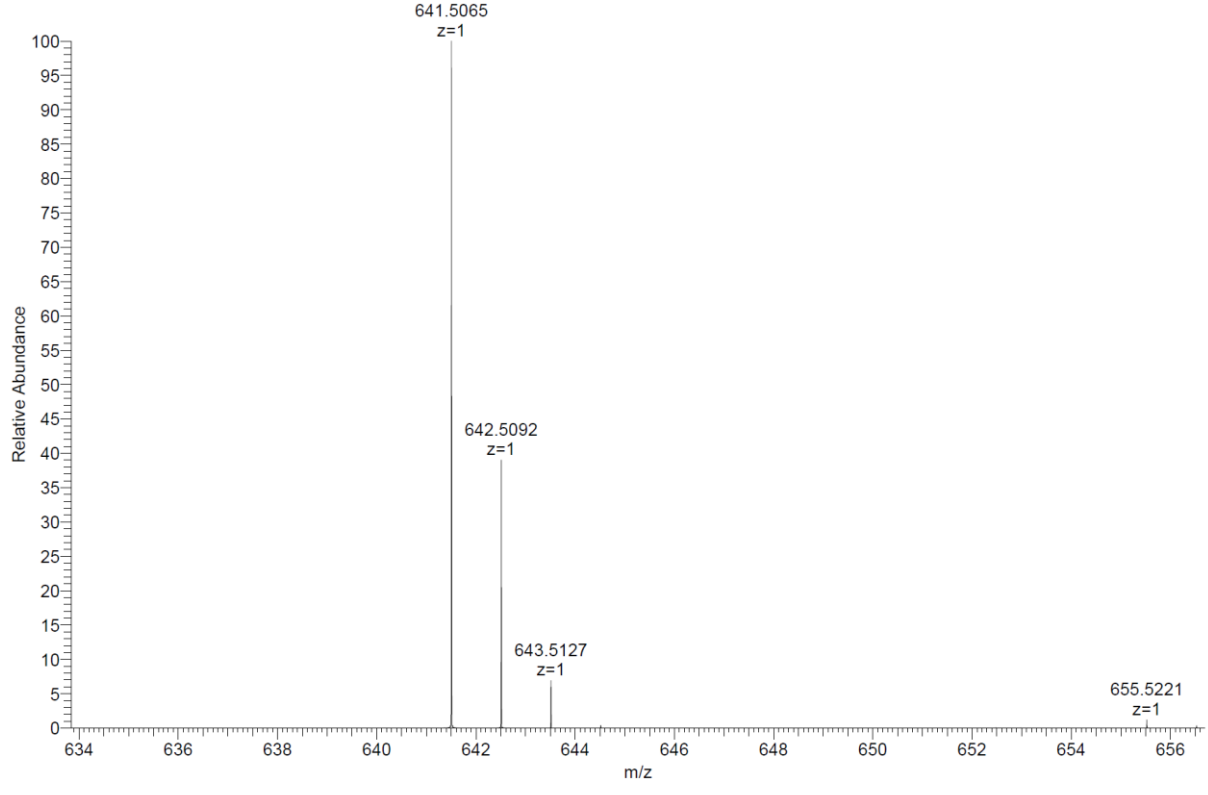

G_2*Bag*LLLL (1b) was obtained as white solid after preparative RP-HPLC (14.8 mg, 20.4%). Analytical RP-HPLC: t_R = 2.99 min (A/D 100:0 to 0:100 in 7.0 min, λ = 214 nm). MS (ESI+): $C_{36}H_{70}N_{10}O_7$ calc./obs. 755.54/755.55 Da $[M+H]^+$.

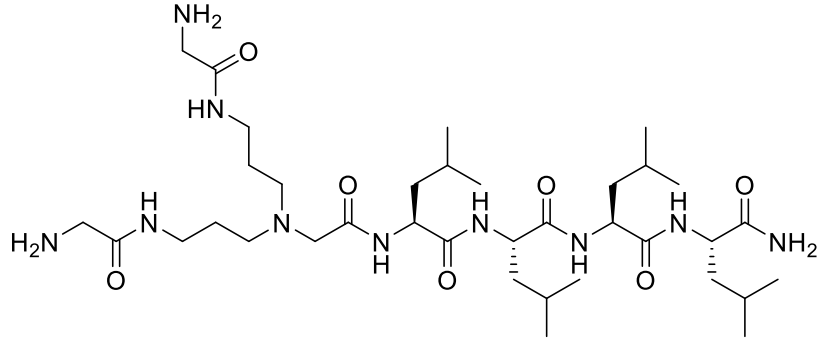

Chemical Formula: $C_{36}H_{70}N_{10}O_7$
Exact Mass: 754,54
Molecular Weight: 755,02

Analytical HPLC-MS data:

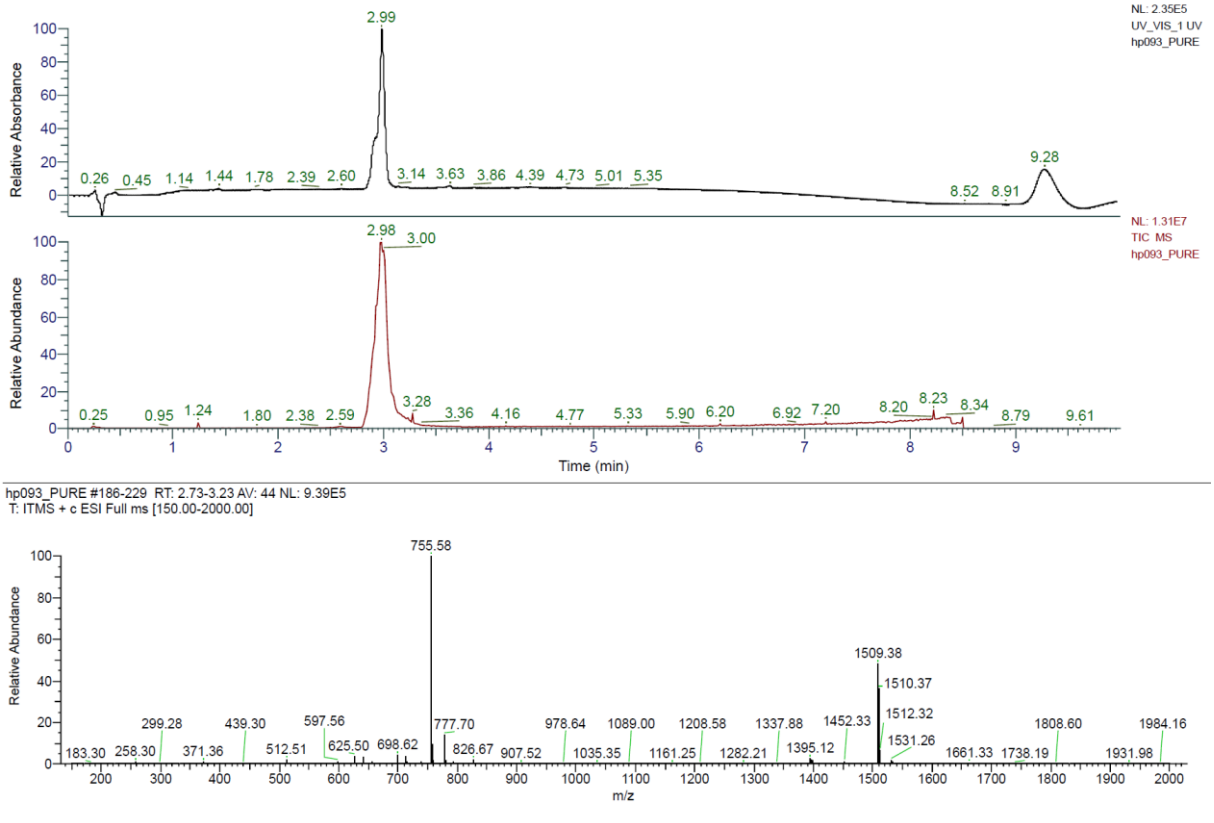

HRMS spectra:

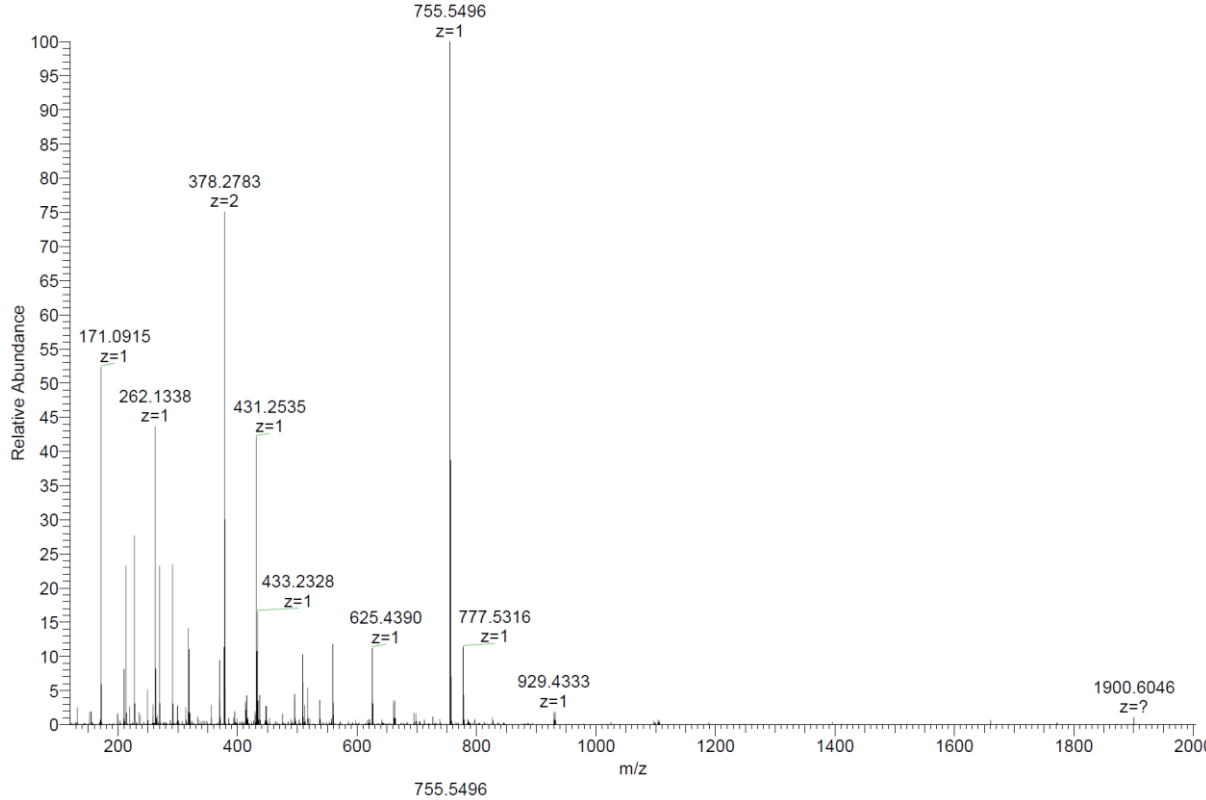

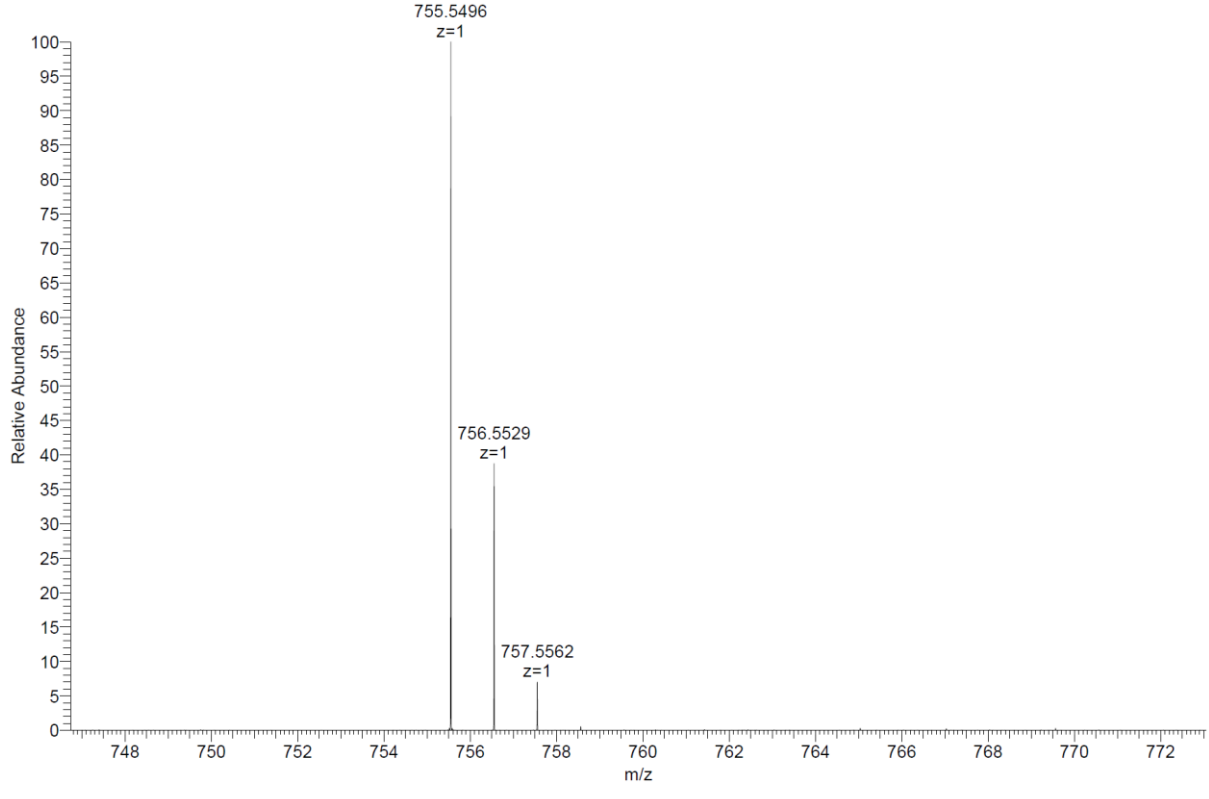

***Bag*$_2$*Bag*LLLL (2a)** was obtained as white solid after preparative RP-HPLC (22.7 mg, 19.3%). Analytical RP-HPLC: t_R = 2.65 min (A/D 100:0 to 0:100 in 7.0 min, λ = 214 nm). MS (ESI+): $C_{48}H_{98}N_{14}O_7$ calc./obs. 983.77/983.78 Da $[M+H]^+$.

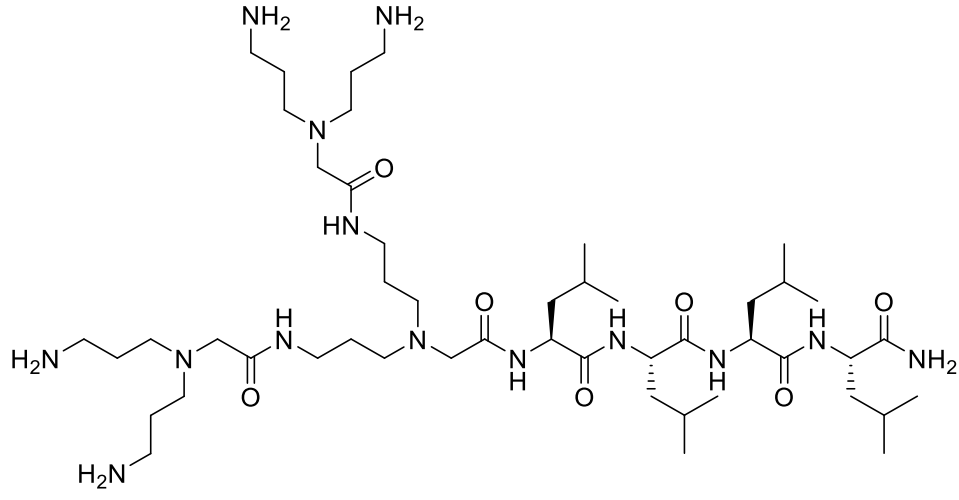

Chemical Formula: $C_{48}H_{98}N_{14}O_7$
Exact Mass: 982,77
Molecular Weight: 983,40

Analytical HPLC-MS data:

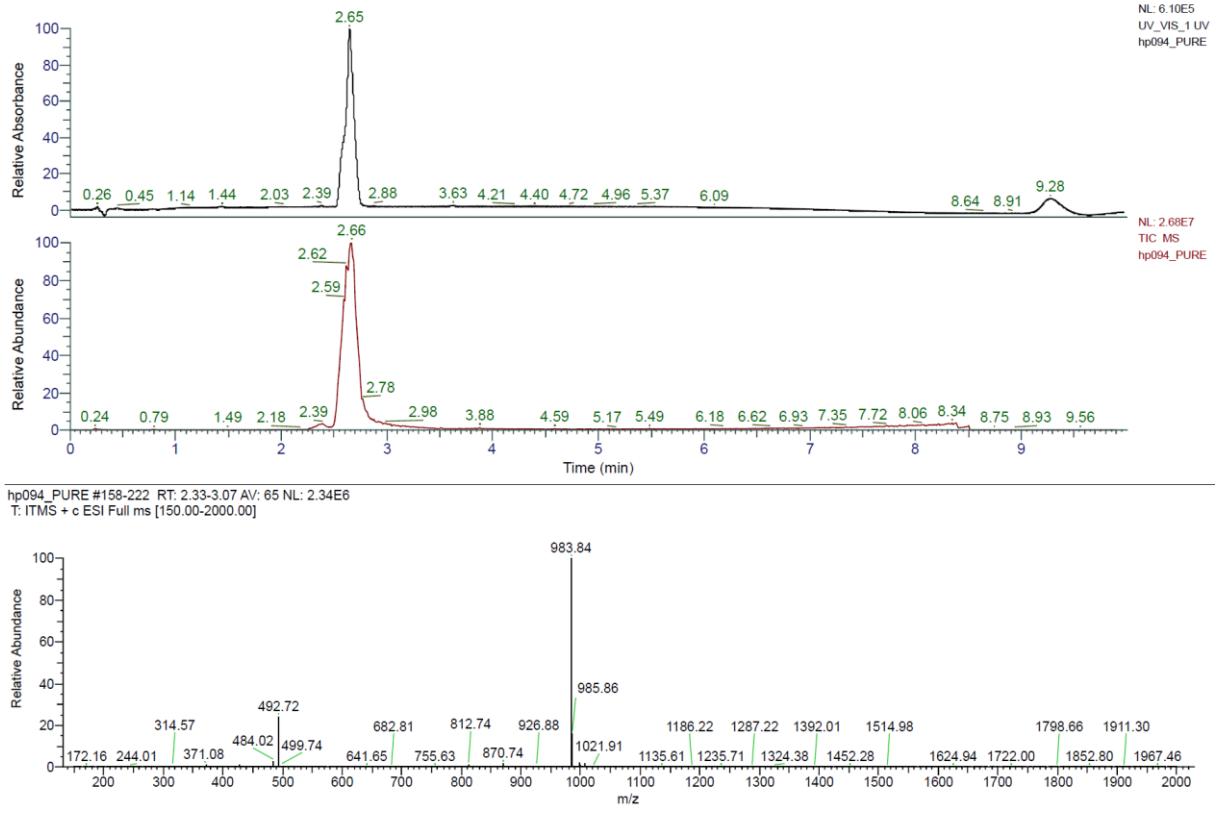

HRMS spectra:

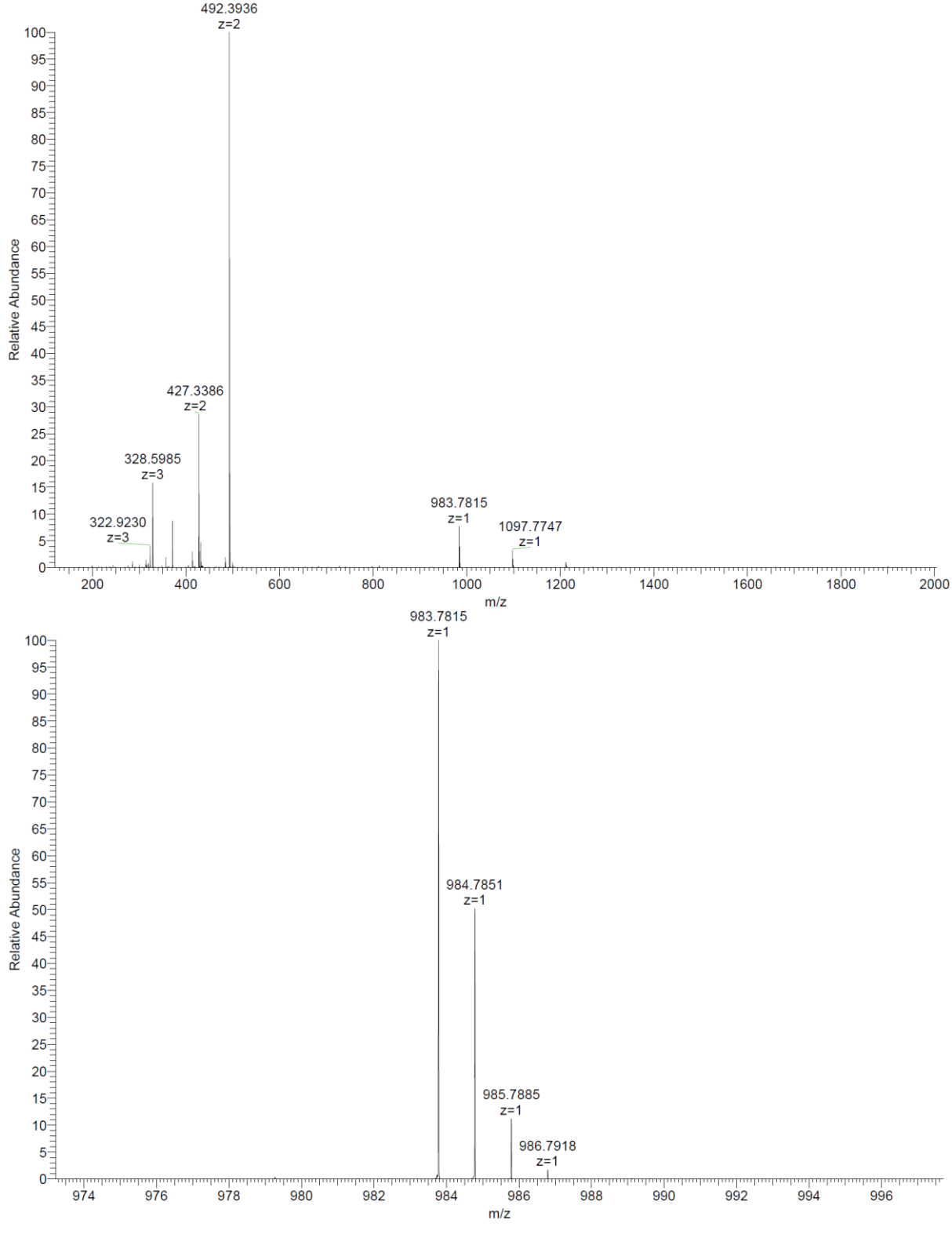

G$_4$*Bag*$_2$*Bag*LLLL (2b) was obtained as white solid after preparative RP-HPLC (11.5 mg, 8.7%). Analytical RP-HPLC: t_R = 2.61 min (A/D 100:0 to 0:100 in 7.0 min, λ = 214 nm). MS (ESI+): $C_{56}H_{110}N_{18}O_{11}$ calc./obs. 1210.86/1211.87 Da $[M+H]^+$.

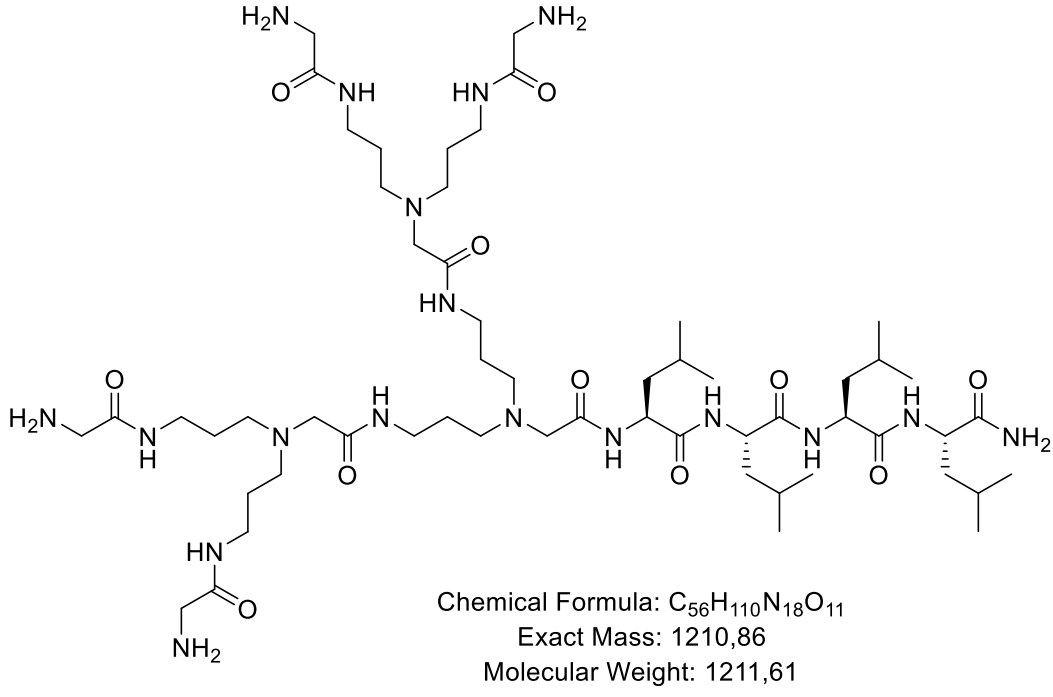

Analytical HPLC-MS data:

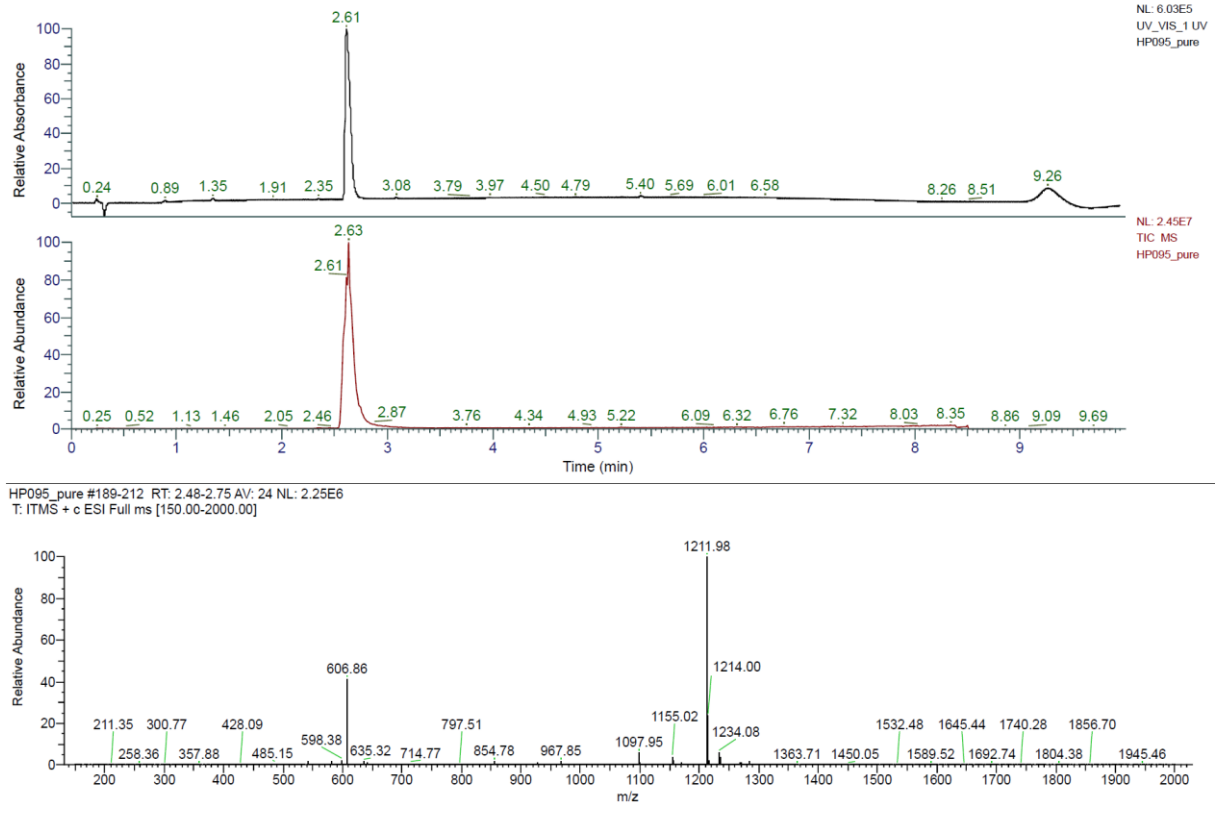

HRMS spectra:

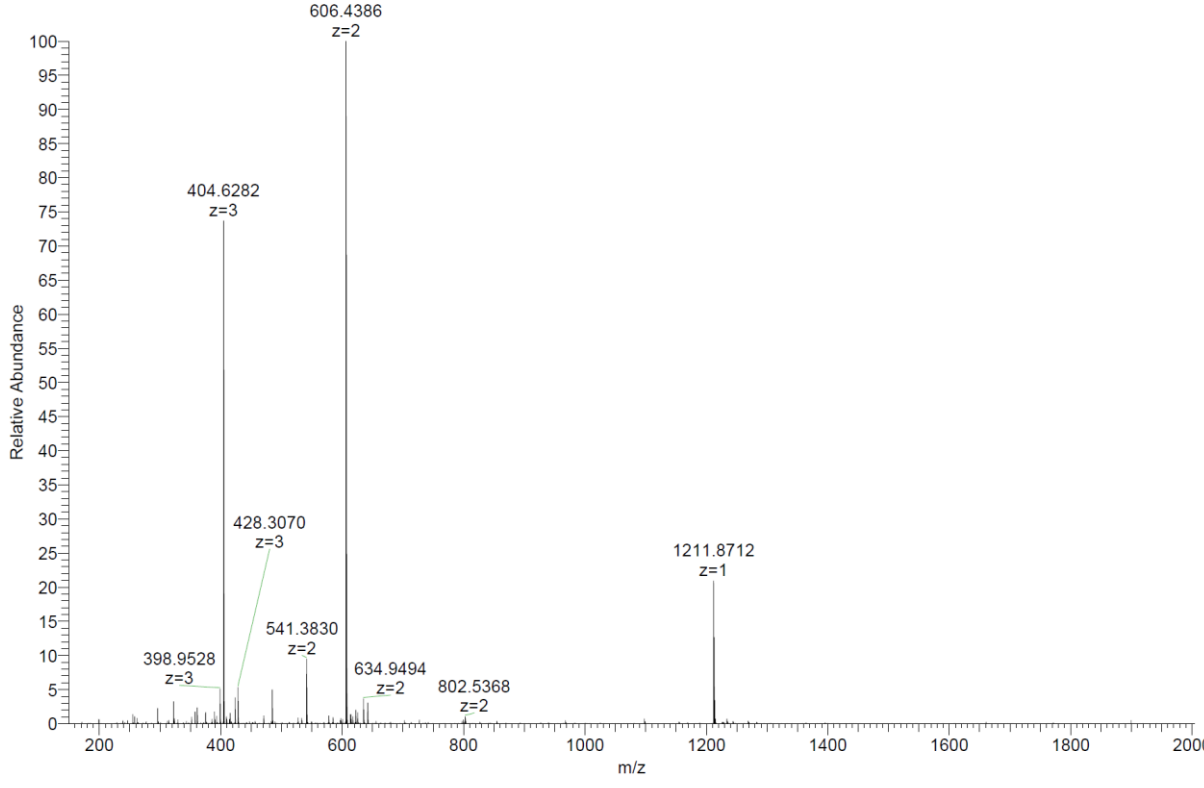

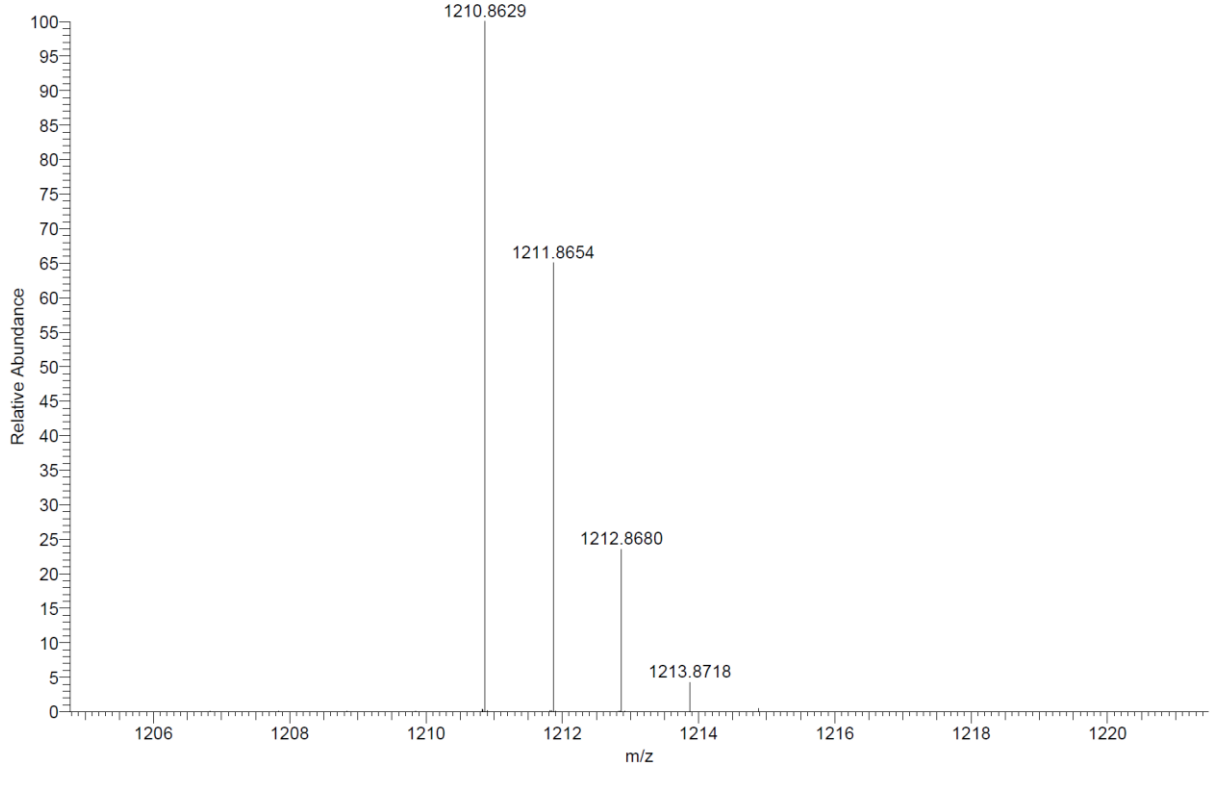

***Bag*$_4$*Bag*$_2$*Bag*LLLL (3a)** was obtained as sticky crystals after preparative RP-HPLC (12.5 mg, 5.6%). Analytical RP-HPLC: t_R = 2.42 min (A/D 100:0 to 0:100 in 7.0 min, λ = 214 nm). MS (ESI+): $C_{80}H_{166}N_{26}O_{11}$ calc./obs. 1667.32/1667.33 Da $[M+H]^+$.

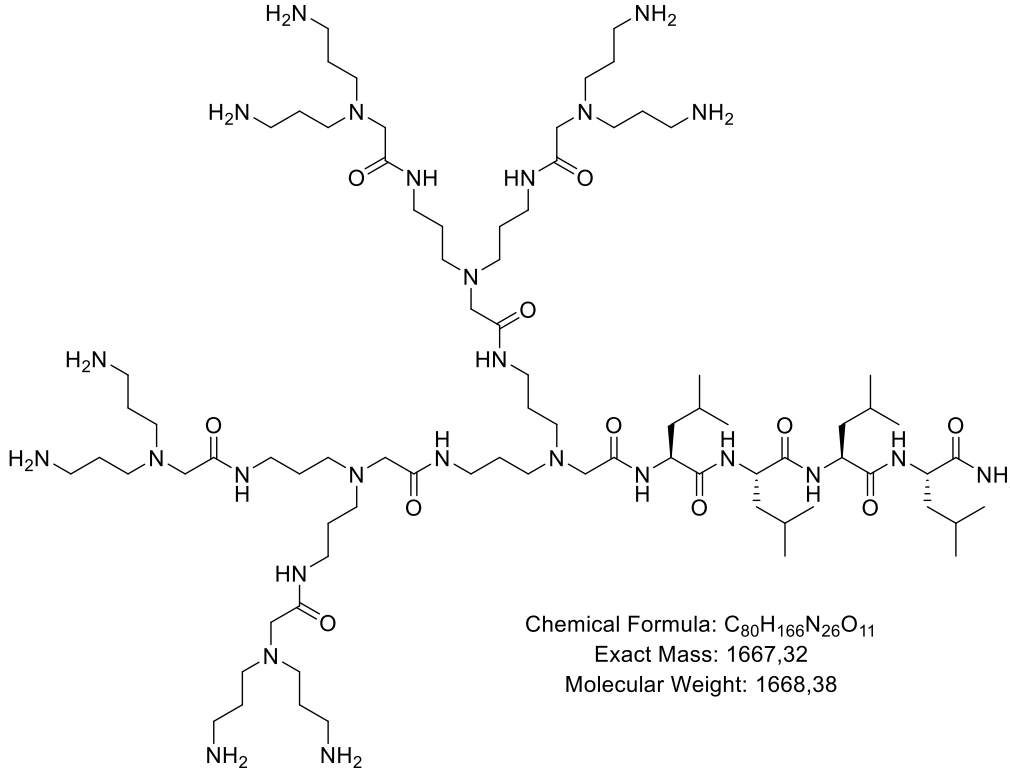

Analytical HPLC-MS data:

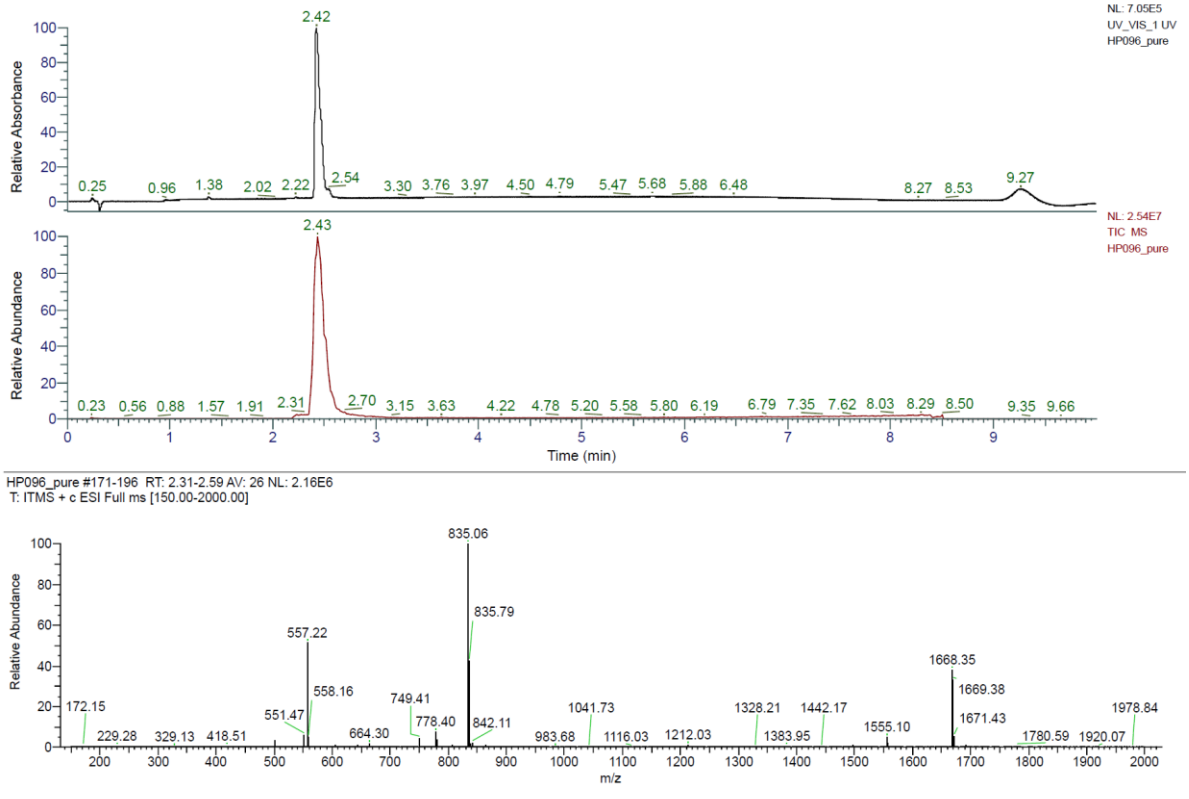

HRMS spectra:

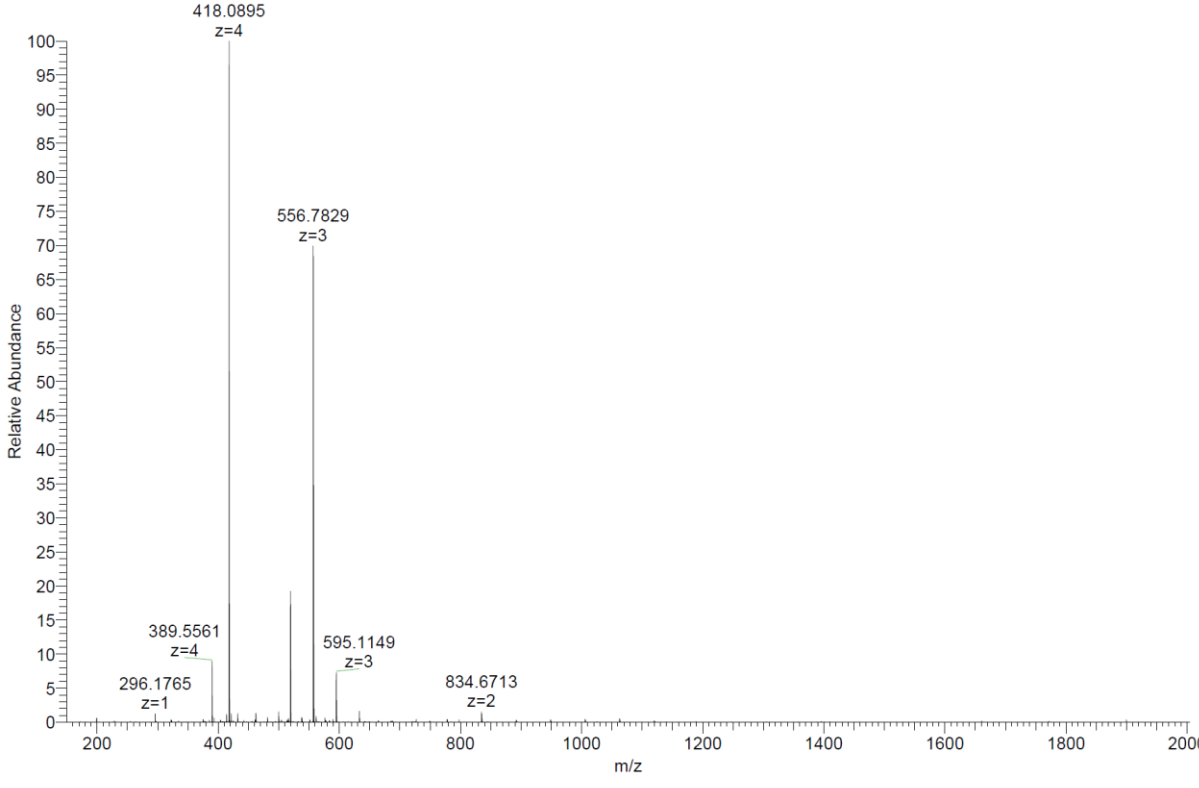

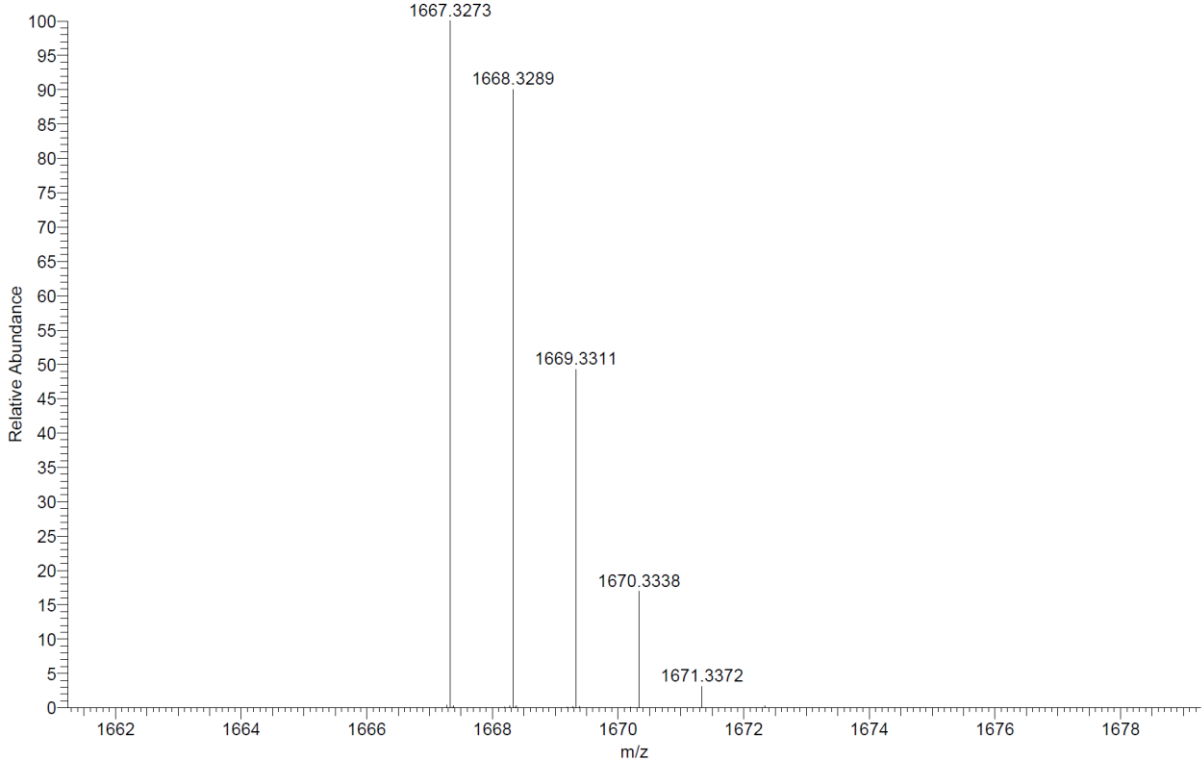

G$_8$*Bag*$_4$*Bag*$_2$*Bag*LLLL (3b) was obtained as sticky crystals after preparative RP-HPLC (15.8 mg, 6.2%). Analytical RP-HPLC: t_R = 2.33 min (A/D 100:0 to 0:100 in 7.0 min, λ = 214 nm). MS (ESI+): $C_{96}H_{190}N_{34}O_{19}$ calc./obs. 2124.49/2124.50 Da $[M+H]^+$.

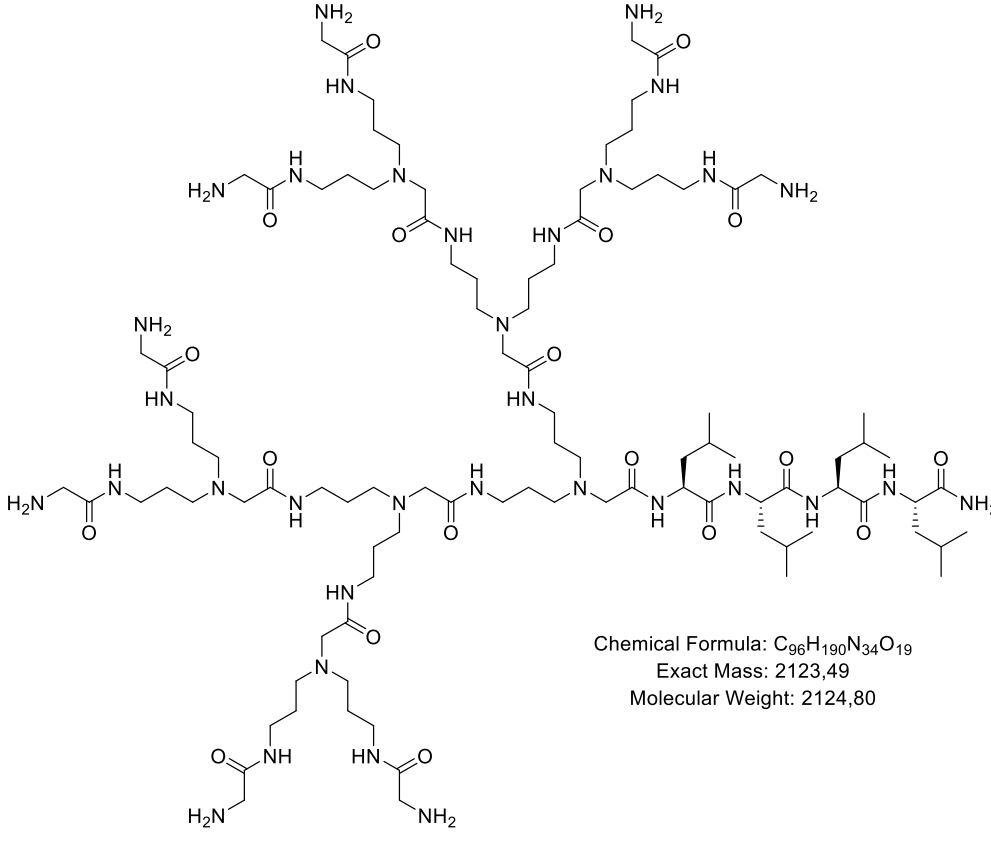

Analytical HPLC-MS data:

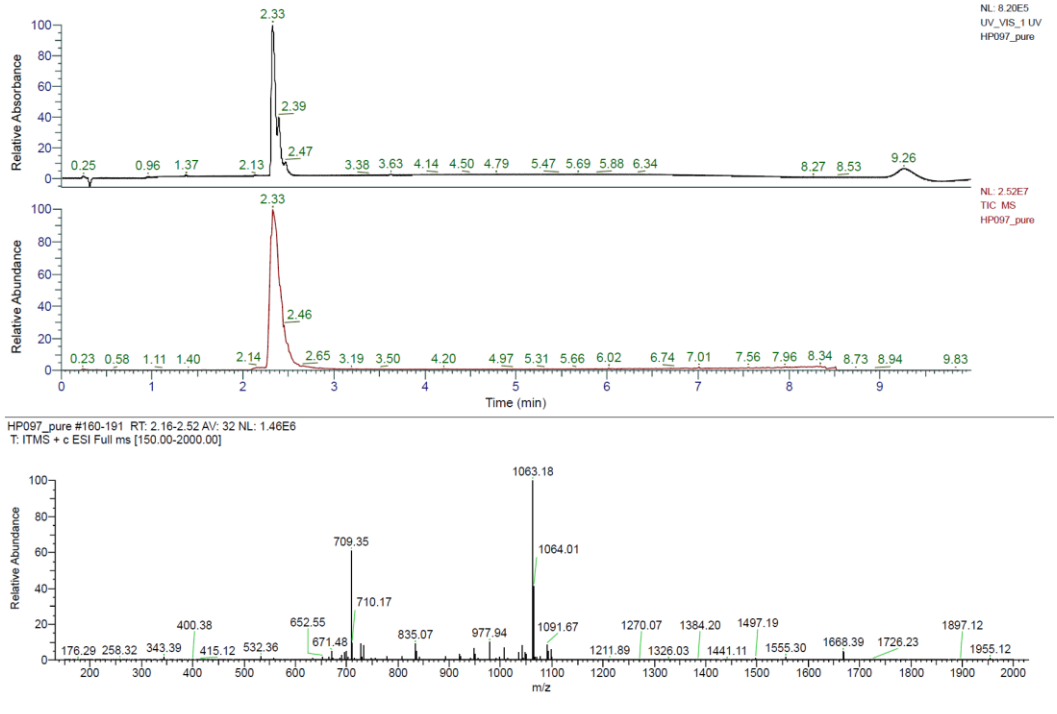

HRMS spectra:

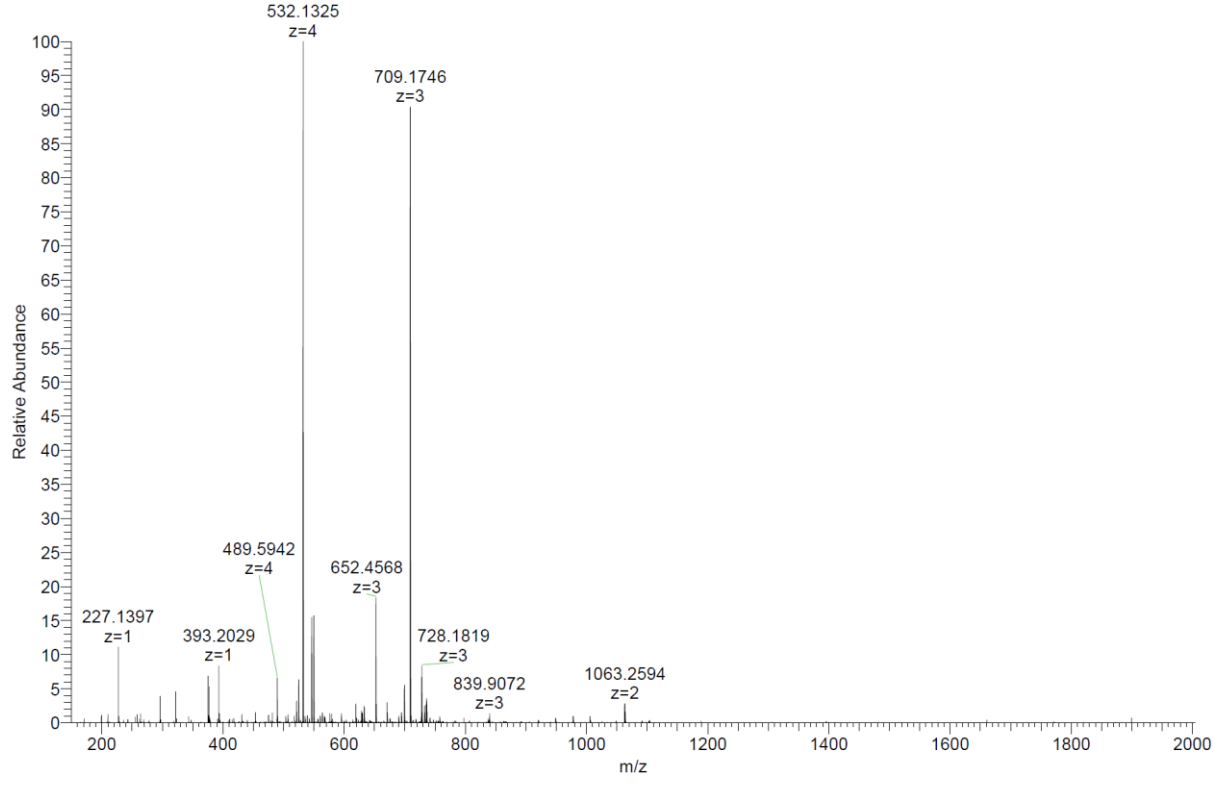

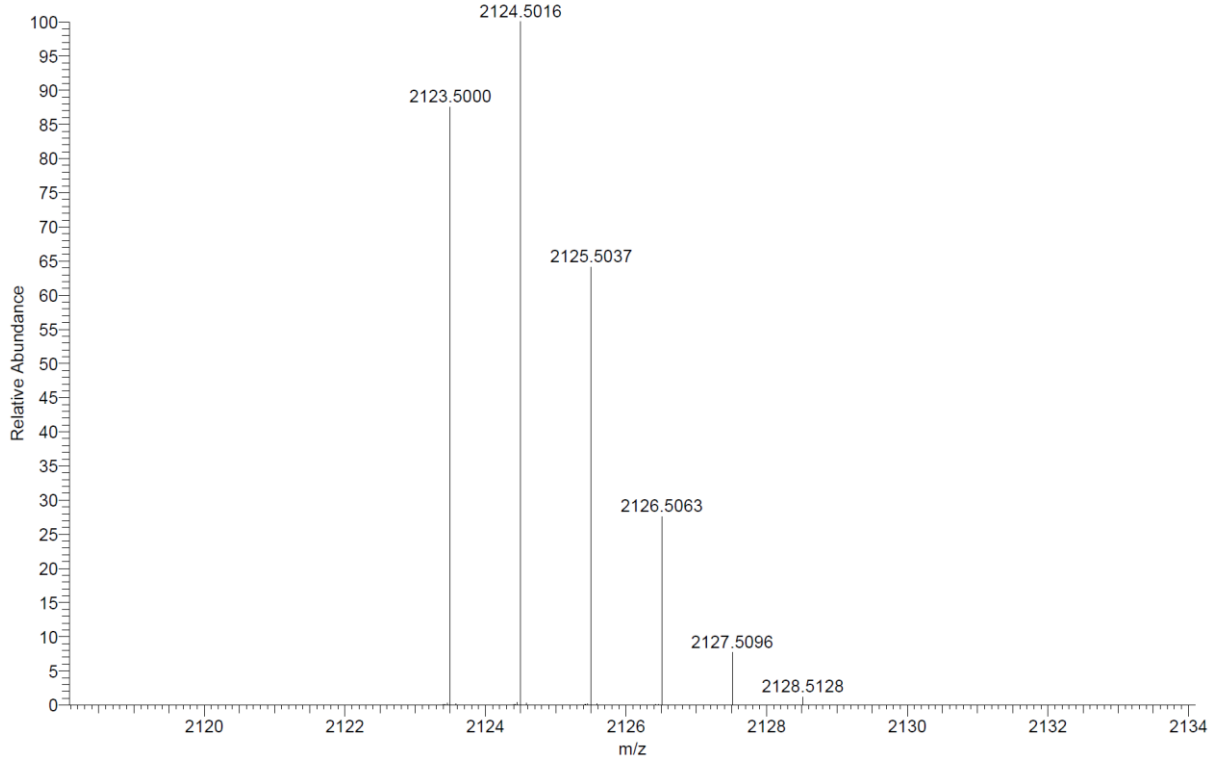

***Bag*$_8$*Bag*$_4$*Bag*$_2$*Bag*LLLL (4a)** was obtained as sticky crystals after preparative RP-HPLC (12.4 mg, 2.9%). Analytical RP-HPLC: t_R = 2.21 min (A/D 100:0 to 0:100 in 7.0 min, λ = 214 nm). MS (ESI+): $C_{144}H_{302}N_{50}O_{19}$ calc./obs. 3038.42/3038.43 Da $[M+H]^+$.

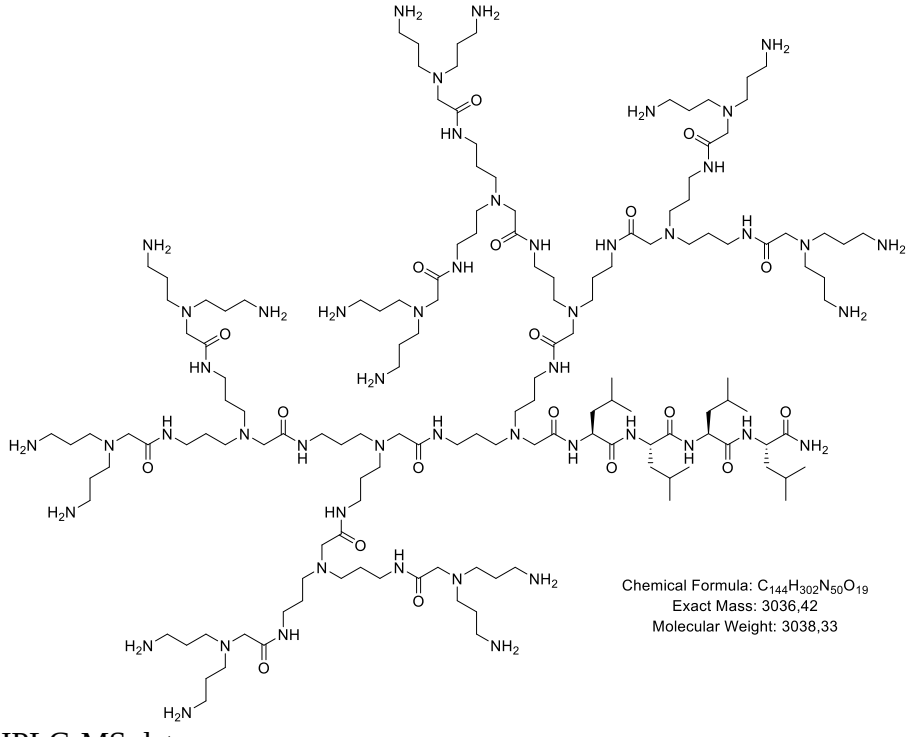

Analytical HPLC-MS data:

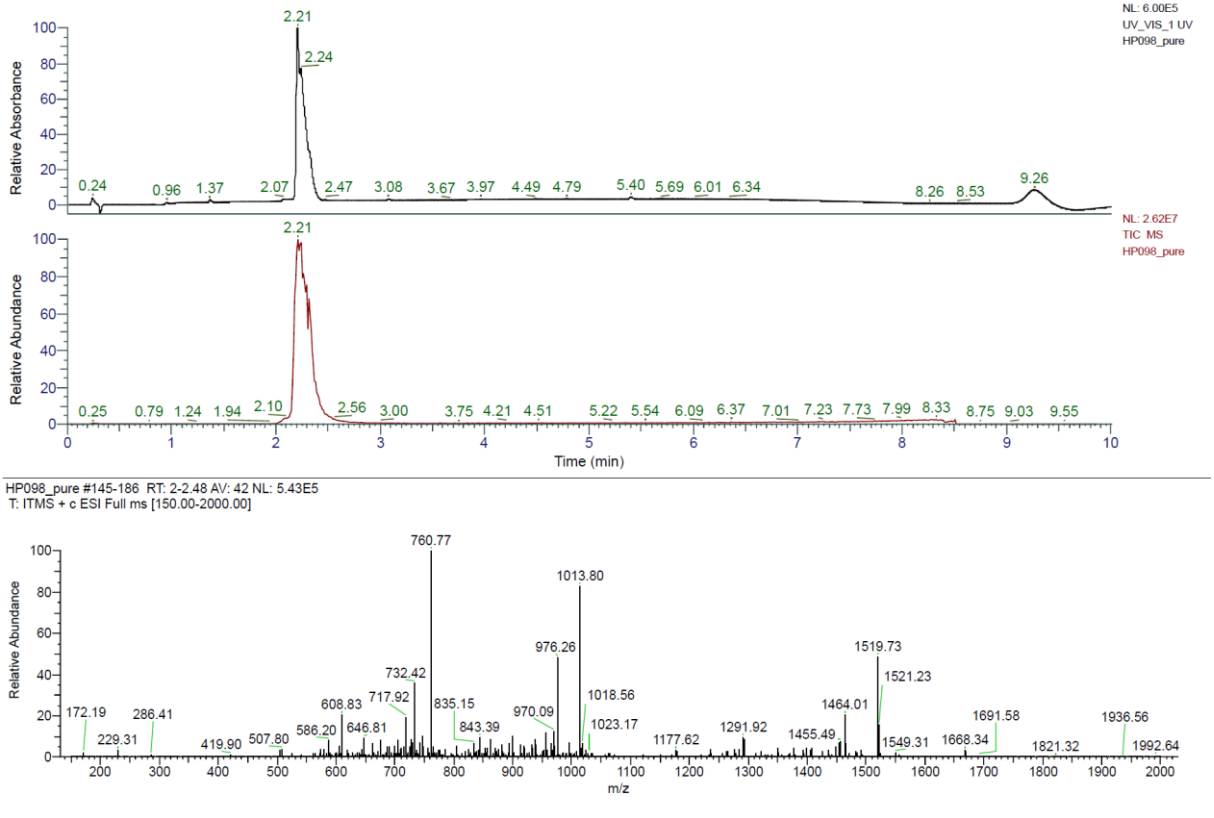

HRMS spectra:

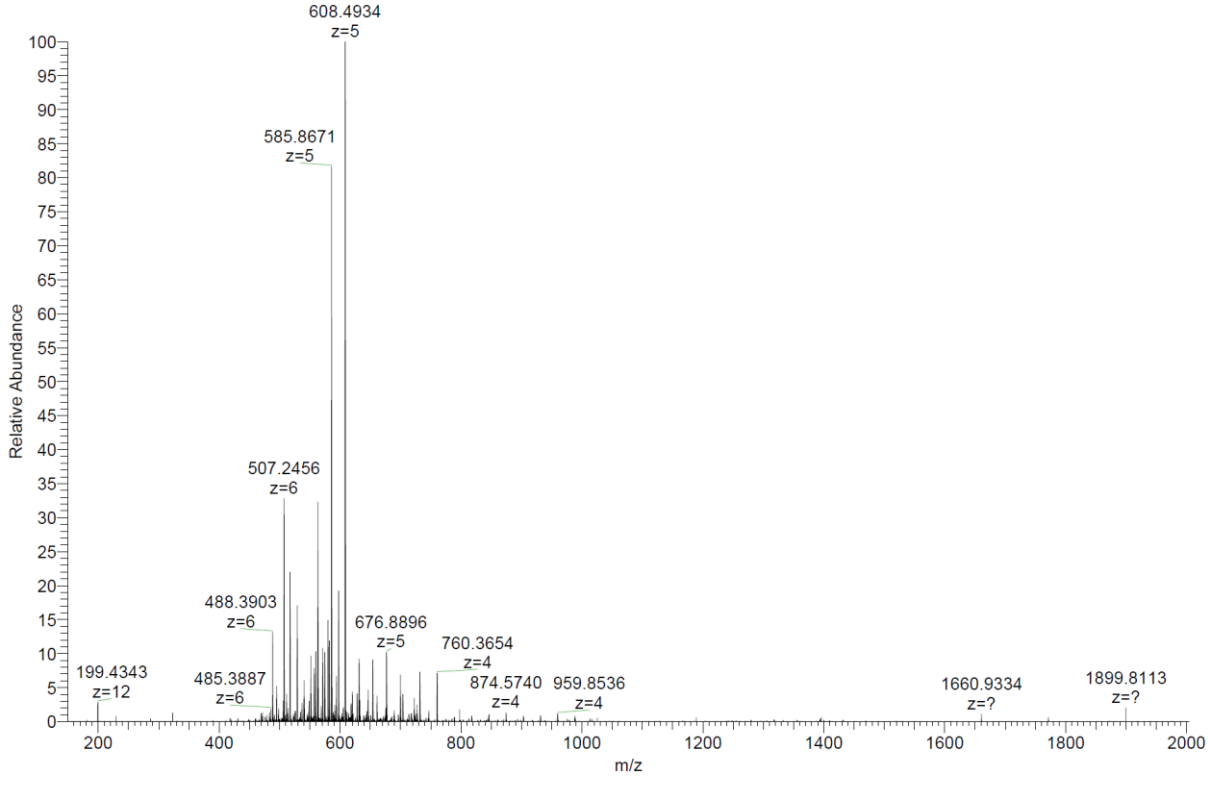

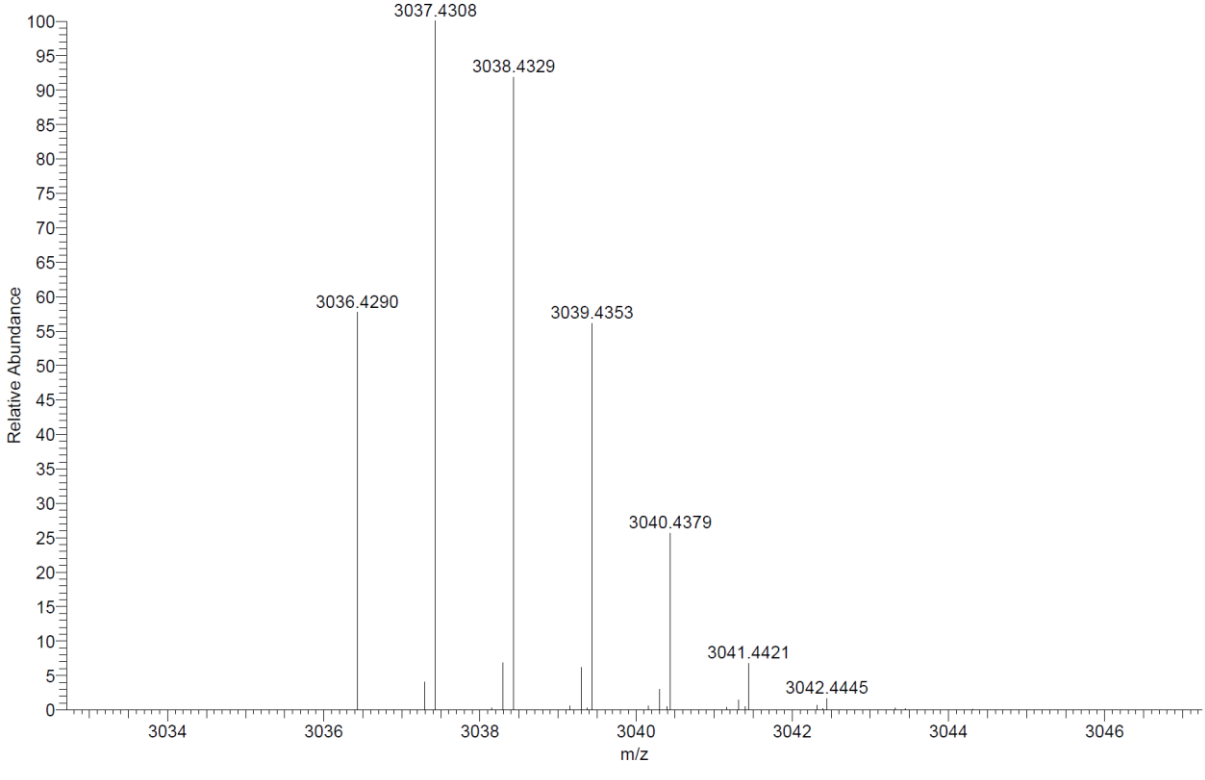

G$_{16}$*Bag*$_{8}$*Bag*$_{4}$*Bag*$_{2}$*Bag*LLLL (4b) was obtained as sticky crystals after preparative RP-HPLC (6.1 mg, 1.2%). Analytical RP-HPLC: t_R = 2.13 min (A/D 100:0 to 0:100 in 7.0 min, λ = 214 nm). MS (ESI+): $C_{176}H_{350}N_{66}O_{35}$ calc./obs. 3949.76/3949.78 Da $[M+H]^+$.

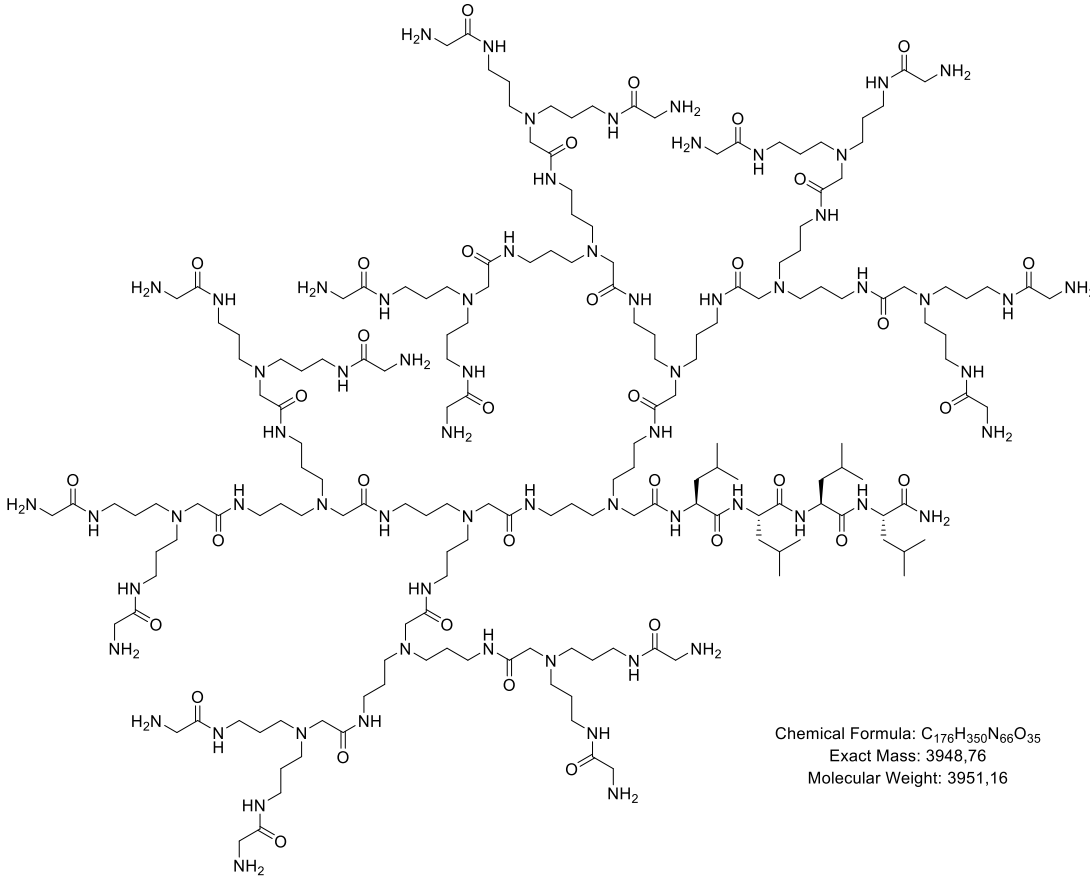

Analytical HPLC-MS data:

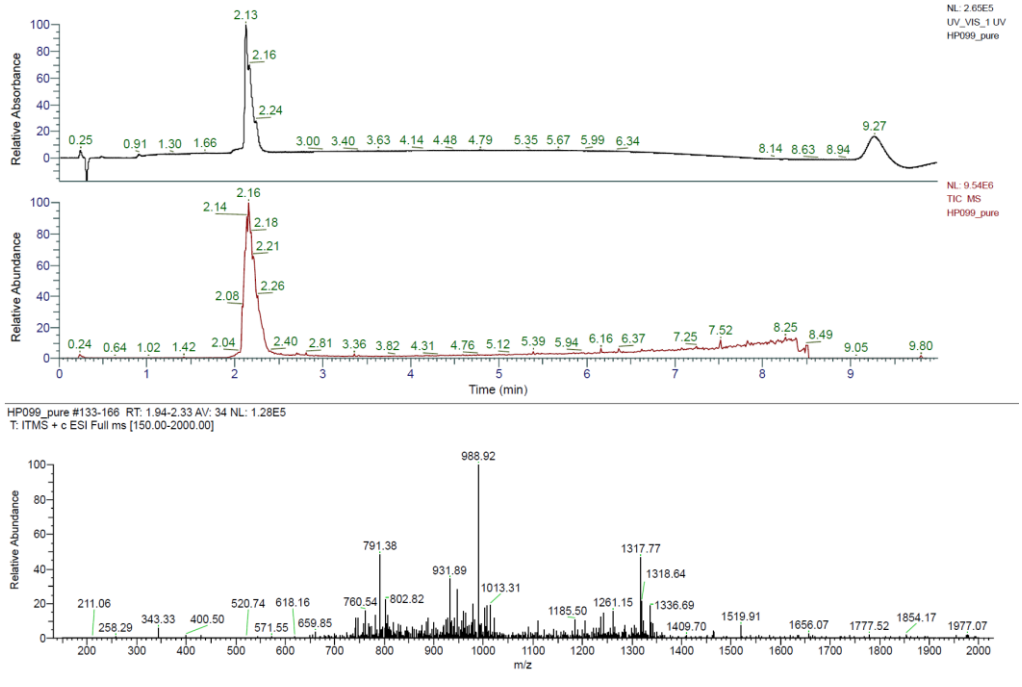

HRMS spectra: